Advances in Experimental Medicine and Biology 1239

Lynne M. Coluccio *Editor*

Myosins

A Superfamily of Molecular Motors

Second Edition

Springer

Advances in Experimental Medicine and Biology

Volume 1239

Advances in Experimental Medicine and Biology provides a platform for scientific contributions in the main disciplines of the biomedicine and the life sciences. This series publishes thematic volumes on contemporary research in the areas of microbiology, immunology, neurosciences, biochemistry, biomedical engineering, genetics, physiology, and cancer research. Covering emerging topics and techniques in basic and clinical science, it brings together clinicians and researchers from various fields.

Advances in Experimental Medicine and Biology has been publishing exceptional works in the field for over 40 years, and is indexed in SCOPUS, Medline (PubMed), Journal Citation Reports/Science Edition, Science Citation Index Expanded (SciSearch, Web of Science), EMBASE, BIOSIS, Reaxys, EMBiology, the Chemical Abstracts Service (CAS), and Pathway Studio.

2018 Impact Factor: 2.126.

More information about this series at http://www.springer.com/series/5584

Lynne M. Coluccio
Editor

Myosins

A Superfamily of Molecular Motors

Second Edition

Springer

Editor
Lynne M. Coluccio
Department of Physiology & Biophysics
Boston University School of Medicine
Boston, MA, USA

ISSN 0065-2598 ISSN 2214-8019 (electronic)
Advances in Experimental Medicine and Biology
ISBN 978-3-030-38061-8 ISBN 978-3-030-38062-5 (eBook)
https://doi.org/10.1007/978-3-030-38062-5

Preface

In the years since publication in 2008 of *Myosins: A Superfamily of Molecular Motors*, considerable new strides have been made in understanding the structure and function of myosin motors. In particular, the application of advanced cell imaging approaches, the development of new animal models, the availability of new crystal structures, and the discovery of isoform-specific inhibitors have propelled the field forward. This volume addresses the current state of our collective knowledge regarding myosin structure and function. The chapters are written by internationally recognized experts in molecular motors. It is a testament to the importance of this endeavor that authors of chapters in the 2008 volume who were asked to contribute to this new volume all enthusiastically agreed. In addition, new authors were effortlessly recruited to cover new areas including the more recently discovered myosins XVI, XVIII, and XIX, myosin inhibitors, and the structural basis for cargo binding. The hope is that this volume will serve as a reference for both investigators and students and stimulate new research on this amazing family of motor molecules. I am sincerely grateful to the contributors who made this volume possible. It has been my privilege and pleasure to work with each of them. I would also like to thank Gonzalo Cordova from Springer Nature BV, Dordrecht, for the opportunity to edit this book. The careful editing by Springer staff members is greatly appreciated.

Boston, MA, USA
October 2019

Lynne M. Coluccio

Contents

Contributors

Rebecca Adikes Department of Biochemistry and Cell Biology, 401 Life Sciences Building, Stony Brook University, Stony Brook, NY, USA

Toshio Ando Nano Life Science Institute (WPI NanoLSI), Kanazawa University, Kanazawa, Japan

Martin Bähler Institute for Molecular Cell Biology, Westfälische Wilhelms-Universität Münster, Münster, Germany

Inna A. Belyantseva National Institute on Deafness and Other Communication Disorders, National Institutes of Health, Section on Human Genetics, Bethesda, MD, USA

Jennifer L. Bocanegra Department of Biochemistry, University of Washington, Seattle, WA, USA

Beáta Bugyi Department of Biophysics, Medical School, University of Pecs, Pecs, Hungary

Folma Buss Cambridge Institute for Medical Research, University of Cambridge, The Keith Peters Building, Cambridge, UK

Urszula Cichoń Department of Biochemistry and Molecular Biology, The University of Chicago, Chicago, IL, USA

Lynne M. Coluccio Department of Physiology & Biophysics, Boston University School of Medicine, Boston, MA, USA

Adam Fineberg Physical and Theoretical Chemistry Laboratory (PTCL), Department of Chemistry, University of Oxford, Oxford, UK

Karine Frénal Microbiologie Fondamentale et Pathogénicité, UMR 5234, University of Bordeaux and CNRS, Bordeaux Cedex, France

Thomas B. Friedman Laboratory of Molecular Genetics, National Institute on Deafness and Other Communication Disorders, Porter Neuroscience Research Center, National Institutes of Health, Bethesda, MD, USA

Gregory I. Frolenkov Department of Physiology, University of Kentucky College of Medicine, Lexington, KY, USA

Peter J. Hanley Institute of Molecular Cell Biology, Westfalian Wilhelms University Münster, Münster, Germany

Wilma A. Hofmann Department of Physiology and Biophysics, Jacobs School of Medicine and Biomedical Sciences, University at Buffalo, Buffalo, NY, USA

Anne Houdusse Institut Curie, CNRS, Paris Cedex 05, France

Nikolas Hundt Department of Cellular Physiology, Ludwig-Maximilians-Universität München, Munich, Germany

John Kendrick-Jones MRC Laboratory of Molecular Biology, Cambridge, UK

András Kengyel Department of Biophysics, Medical School, University of Pecs, Pecs, Hungary

Noriyuki Kodera Nano Life Science Institute (WPI NanoLSI), Kanazawa University, Kanazawa, Japan

Aarti Krishnan Department of Microbiology and Molecular Medicine, Faculty of Medicine, University of Geneva, Geneva, Switzerland

Sharissa L. Latham The Kinghorn Cancer Centre, Garvan Institute of Medical Research, Darlinghurst, NSW, Australia
St Vincent's Clinical School, Faculty of Medicine, UNSW Sydney, Darlinghurst, NSW, Australia

Jianchao Li Division of Cell, Developmental and Integrative Biology, School of Medicine, South China University of Technology, Guangzhou, China

Ivan V. Maly Department of Physiology and Biophysics, Jacobs School of Medicine and Biomedical Sciences, State University of New York, Buffalo, NY, USA

Dietmar J. Manstein Hannover Medical School, Institute for Biophysical Chemistry, Fritz-Hartmann Center for Molecular Medicine, Hannover, Germany

Thomas O'Loughlin Cambridge Institute for Medical Research, University of Cambridge, The Keith Peters Building, Cambridge, UK

Thomas D. Pollard Department of Molecular, Cellular and Developmental Biology, Department of Molecular Biophysics and Biochemistry, Department of Cell Biology, Yale University, New Haven, CT, USA

Matthias Preller Hannover Medical School, Institute for Biophysical Chemistry, Hannover, Germany
German Electron Synchrotron (DESY), Hamburg, Germany

Omar A. Quintero Department of Biology, University of Richmond, Richmond, VA, USA

Julien Robert-Paganin Institut Curie, CNRS, Paris Cedex 05, France

Ronald S. Rock Department of Biochemistry and Molecular Biology, The University of Chicago, Chicago, IL, USA

Alicja Santos Department of Biochemistry and Molecular Biology, The University of Chicago, Chicago, IL, USA

Rasmus R. Schröder Cryo Electron Microscopy, BioQuant, Medical Faculty, Heidelberg University, Heidelberg, Germany

James R. Sellers Laboratory of Molecular Physiology, National Heart, Lung, and Blood Institute, National Institutes of Health, Bethesda, MD, USA

Yauhen Shauchuk Faculty of Biotechnology, University of Wrocław, Wrocław, Poland

Dominique Soldati-Favre Department of Microbiology and Molecular Medicine, Faculty of Medicine, University of Geneva, Geneva, Switzerland

H. Lee Sweeney Department of Pharmacology & Therapeutics, College of Medicine, University of Florida, Gainesville, FL, USA

Manuel H. Taft Institute for Biophysical Chemistry, Hannover Medical School, Hannover, Germany

Yasuharu Takagi Laboratory of Molecular Physiology, Center for Cell and Developmental Biology, National Heart, Lung, and Blood Institute (NHLBI), National Institutes of Health (NIH), Bethesda, MD, USA

Hiroshi Tokuo Department of Physiology & Biophysics, Boston University School of Medicine, Boston, MA, USA

Kevin C. Vavra Department of Biochemistry and Molecular Biology, The University of Chicago, Chicago, IL, USA

Veith Vollmer Institute of Molecular Cell Biology, Westfalian Wilhelms University Münster, Münster, Germany

Mingjie Zhang Division of Life Science, State Key Laboratory of Molecular Neuroscience, Hong Kong University of Science and Technology, Kowloon, Hong Kong, China
Center of Systems Biology and Human Health, School of Science and Institute for Advanced Study, Hong Kong University of Science and Technology, Kowloon, Hong Kong, China

Introduction

1

Lynne M. Coluccio

Abstract

This book, a collection of chapters written by some of the leading researchers in the field of molecular motors, highlights the current understanding of the structure, molecular mechanism, and cellular roles of members of the myosin superfamily. Here, I briefly review the discovery of the first myosin motor, skeletal muscle myosin-II, and preview the contents of subsequent chapters.

Keywords

Myosin · Actin · Skeletal muscle

1.1 Historical Perspective

Myosins are a remarkable superfamily of actin-based motor proteins that use the energy derived from ATP hydrolysis to translocate actin filaments and to produce force. The first myosin to be discovered and the one against which all subsequently identified myosins have been compared is the myosin-II responsible for skeletal muscle contraction. The history of skeletal muscle myosin-II's discovery and how early biochemical studies revealed the molecular mechanism of muscle contraction were documented in an excellent article written by the late Andrew Szent-Györgyi (Szent-Györgyi 2004). Briefly, skeletal muscle myosin-II was identified over 150 years ago when Kühne extracted from muscle exposed to high salt a protein that he called myosin (Kühne 1864). It was not until many years later, however, that myosin was recognized as the ATPase responsible for muscle contraction (Engelhardt and Ljubimowa 1939). In 1942 (Albert) Szent-Györgi and co-workers showed that overnight extraction of muscle tissue in high salt yielded threads that contracted with the addition of ATP (Szent-Györgyi 2004). They determined that this extract actually consisted of two proteins, and shortly after, Straub purified from this extract a protein that was responsible along with myosin for the observed contraction and named it actin (Straub 1942).

In the next decade Huxley and Hanson showed that in skeletal muscle thick myosin-containing filaments interdigitate with thin actin-containing filaments (Hanson and Huxley 1953), and by 1954 Huxley and colleagues proposed the sliding filament mechanism in which thick filaments slide past thin filaments to cause muscle contraction (Huxley and Niedergerke 1954; Huxley and Hanson 1954). Within 3 years, Huxley had proved the validity of the sliding filament model after developing a technique that allowed his direct observation with electron microscopy of

L. M. Coluccio (✉)
Department of Physiology & Biophysics, Boston University School of Medicine, Boston, MA, USA
e-mail: coluccio@bu.edu

L. M. Coluccio (ed.), *Myosins*, Advances in Experimental Medicine and Biology 1239,
https://doi.org/10.1007/978-3-030-38062-5_1

both the thick and thin filaments and cross-bridges projecting from the thick filaments to the thin filaments in thin sections of muscle (Huxley 1957).

Subsequently, biochemical analyses of proteolytic fragments and electron microscopy studies led to the recognition of muscle myosin as a hexamer consisting of two heavy chains, two regulatory light chains, and two essential light chains. Each heavy chain contains an N-terminal globular "head" domain containing ATP- and actin-binding sites and a C-terminal α-helical coiled-coil "tail" domain involved in dimerization. Myosin molecules associate via their tail domains to form bipolar filaments. When cleaved by chymotrypsin, the myosin heavy chain yields two fragments, heavy meromyosin (HMM), which contains the globular heads and a portion of the α-helical tail, and light meromyosin (LMM), which contains the remainder of the C-terminal tail. HMM can be further cleaved by papain to yield subfragment 1 (S1) consisting of an individual globular head with its light chains, and subfragment 2 (S2), a portion of the myosin tail region (Lowey et al. 1969). S1 is capable of supporting the translocation of actin filaments *in vitro* (Toyoshima et al. 1987; Manstein et al. 1989). In addition to skeletal muscle contraction, isoforms of this "two-headed" myosin, which became known as myosin-II or "conventional" myosin, would be recognized as also responsible for cardiac and smooth muscle contraction. Subsequently, three myosin-II isoforms, non-muscle myosin-IIA, non-muscle myosin-IIB, and non-muscle myosin-IIC (NMIIA, NMIIB, and NMIIC, respectively), were also found in non-muscle cells (Maruta and Korn 1977a, b; Pollard et al. 1978), where we now know that they play key roles in multiple processes including cytokinesis, cell migration, cell adhesion, and tissue morphogenesis (Wang et al. 2011; Heissler and Manstein 2013).

In 1973 Pollard and Korn isolated from the soil amoeba *Acanthamoeba castellanii* a protein with actin-activated ATPase activity (Pollard and Korn 1973a, b). Unlike myosin-II, which is a dimer of two heavy chains of ~200 kDa each, this molecule consisted of a single relatively small heavy chain of ~125 kDa and did not form filaments. Although the protein was named myosin-I because it was the first myosin to be isolated from *Acanthamoeba*, the name is appropriate because it was also the first single-headed and thus, the first "unconventional" myosin, to be identified (Mooseker and Foth 2008). With the identification in the early 1980s of a 110-kDa polypeptide and calmodulin complex from intestinal epithelial cells with myosin-like properties (Matsudaira and Burgess 1979, 1982; Howe and Mooseker 1983; Collins and Borysenko 1984; Verner and Bretscher 1985; Coluccio and Bretscher 1987) called brush border myosin-I (Mooseker and Coleman 1989) and today termed Myo1a (Gillespie et al. 2001), it became apparent that expression of class I myosins was not restricted to lower organisms.

By the late 1980s and early 1990s other unconventional members of the myosin superfamily, e.g., myosin-III (Montell and Rubin 1988) and myosin-V (Mercer et al. 1991; Espreafico et al. 1992), were identified, and within 10 years 18 classes of myosins had been identified by phylogenetic analyses (Berg et al. 2001). By 2007 35 different classes of myosins had been identified by phylogenetic analyses of motor domain sequences from 328 organisms (Odronitz and Kollmar 2007). With the exception of myosins-I and -II, the remaining classes were assigned Roman numerals in the order in which the sequences were reported (Mooseker and Foth 2008); however, this nomenclature has not been strictly adopted and individual isoforms are often denoted with Arabic numbers (e.g., myosin-5a vs. myosin-Va). Humans express 40 myosin genes representing 12 classes of myosins (class I, II, III, V, VI, VII, IX, X, XV, XVI, XVIII, and XIX) (Foth et al. 2006; Odronitz and Kollmar 2007), and a single cell can express multiple classes and splice forms of myosins.

Members of the myosin superfamily typically consist of a motor, or head, domain with ATP-binding and actin-binding sites, a light chain-binding, or neck, domain containing one or more IQ motifs, which bind calmodulin or a calmodulin-like light chain, and a C-terminal tail region that contains one or more of several motifs

involved in diverse functions such as dimerization, membrane binding, or cargo binding (for reviews, see (Mooseker and Foth 2008; Batters and Veigel 2016; Heissler and Sellers 2016; Masters et al. 2017)). The different myosin classes modulate a variety of actin-based functions including vesicle transport, cell migration, cell-substrate interactions, maintenance of cortical tension, phagocytosis, endocytosis, secretion, transcription, chromatin movement, and chromatin remodeling. Importantly, myosin dysfunction is associated with diseases including cardiomyopathies, deafness, blindness, kidney disease and neurological defects.

In the intervening years since the first edition of *Myosins: a superfamily of molecular motors* was published in 2008, we have learned much regarding myosin structure and function and the effects of myosin dysfunction. This second edition is designed to present a current view of the structure and function of members of the myosin superfamily and the techniques used to examine them.

1.2 Myosin Structure

The report of the first crystal structure of a myosin motor domain over 25 years ago (Rayment et al. 1993) opened the door to a major scientific initiative lasting to the present day devoted to understanding the conformational changes in the myosin motor domain that accompany the myosin power stroke. The current state of knowledge is detailed in Chap. 2 by Sweeney, Houdusse and Robert-Paganin.

Importantly, the C-terminal tail regions of myosins mediate the interaction of myosins with specific cargoes including other proteins and lipids, thus allowing myosins to participate in a variety of cellular processes. The structural basis for cargo binding is the subject of Chap. 3 by Li and Zhang.

Cryo-electron microscopy images of actomyosin and reconstructed 3D density maps of actomyosin in the presence and absence of nucleotide have been instrumental in understanding how myosins interact with actin filaments. This is reviewed in Chap. 4 by Schröder.

Recently, several small molecules that target the motor domain of specific myosins and inhibit myosin function have been identified. The discovery of these small effector molecules is giving new insight into the roles of myosins and present the possibility of their clinical use in diseases associated with myosin malfunction. Several classes of small inhibitors and their binding to myosin motor domains are described in Chap. 5 by Manstein and Preller.

1.3 Analyzing Myosin Motor Function

The use of single-molecule microscopy approaches including optical trapping, *f*luorescence *i*maging at *o*ne *n*anometer *a*ccuracy (FIONA), and interferometric scattering microscopy (iSCAT) has shed considerable light on the molecular mechanism of myosin motors. In Chap. 6, Takagi, Hundt and Fineberg elucidate the theory behind these sophisticated approaches and their application.

An exciting and notable moment in the study of myosins was the demonstration in 2010 that the movement of myosin-V as it walked along an actin filament could be captured by high-speed atomic force microscopy (HS-AFM). How myosin movement can be visualized with HS-AFM and an analysis of myosin-V movement are the focus of Chap. 7 by Kodera and Ando.

The two-headed class V myosin, myosin-Va, is arguably the best-characterized of the unconventional myosins, and multiple approaches including single-particle analyses, transient kinetics, optical trapping and FIONA studies were used to demonstrate its ability to walk processively along an actin filament taking 36-nm steps. In Chap. 8 Sellers and Takagi explain how myosin-Va's movement along actin was determined.

A central determinant of myosin movement is the actin tracks along which myosin motors move. Actin filaments are diverse in large part due to the plethora of actin-binding proteins present in cells that regulate actin activity including its organization into bundles and networks.

How actin tracks affect myosin motility is addressed by Santos, Shauchuk, Cichoń, Vavra and Rock in Chap. 9.

1.4 Cellular Roles for Myosins

Multiple classes of myosins including myosins-I, -II, -V, -VI, -X, -XVI and -XVIII are found in the nucleus where they participate in critical nuclear functions including transcription, chromatin dynamics, and chromosome movement. Myosin function in the nucleus is detailed in Chap. 10 by Maly and Hofmann.

Cytokinesis, the physical separation of the cytoplasm of one cell into two daughter cells, is a fundamental part of cell division. In Chap. 11 Pollard describes the evidence for myosin-II as the myosin motor responsible for cytokinesis, the organization of myosin-II filaments during cytokinesis, how the contractile ring is formed, and the mechanisms of force generation.

The multiple myosins that are expressed in vertebrates mediate normal cellular events that support physiological functions, so it is not surprising that defects in myosin expression and/or function result in disease. In Chap. 12, I address the association of myosins with human diseases including cardiomyopathies, cancer, glomerulosclerosis, and infectious disease.

In particular, considerable progress has been made in revealing the role of myosins in the sensory epithelia of the inner ear and how defects in myosins cause hearing loss. Friedman, Belyantseva and Frolenkov discuss the role of myosins in hearing in Chap. 13.

Some unique myosins are expressed in the intracellular parasites *Toxoplasma* and *Plasmodium* where in cooperation with actin filaments they participate in cellular events including motility, invasion and egress from infected cells. Insight into these less well known myosins and their function is found in Chap. 14 by Frénal, Krishnan and Soldati-Favre.

Binding sites for adaptor proteins and cargo are responsible for targeting of myosin motors to specific subcellular localizations. Several adaptor proteins have been successfully identified for myosin-VI by multiple methods. In Chap. 15 O'Loughlin, Kendrick-Jones and Buss discuss myosin-VI adaptor proteins, the methods used to identify them, and what their identification says about possible roles for myosin-VI in the cell. Attention is given to proximity-based proteomic strategies such as BioID (biotin identification), which is being used to identify larger transient motor-adaptor-cargo complexes for further insight into myosin-VI function.

Class IX myosins are both motor molecules and signaling molecules. By means of a unique GTPase-activating protein (RhoGAP) motif in the tail domain, myosins-IX negatively regulate Rho signaling, which is critical to organization of the actin cytoskeleton and actomyosin II contractility. Myosins-IX contribute to cell morphology, cell migration, cell-cell junctions, and membrane trafficking. Hanley, Vollmer and Bähler discuss the unique biochemical features of class IX myosins and their cellular roles in Chap. 16.

Myosin-X has a clear role in filopodia formation and cell migration, and increased expression of myosin-X is found in certain cancers. The physiological and pathological functions of Myo10, including its role in malignant melanoma, are the subject of Chap. 17 by Tokuo.

1.5 The More Recently Discovered Myosins

Three chapters introduce three different myosin classes about which too little was known 12 years ago to justify inclusion in the first volume. Although more recently discovered, evidence already is building that these myosins also play critical roles in cells and that like other myosins, their dysfunction leads to disease.

Two class XVI myosins are expressed in vertebrates: Myo16a, a tail-less isoform found in the cytoplasm, and Myo16b, a full-length isoform that localizes to the cytoplasm and nucleus. Interestingly, peak expression of myosin XVI is in neural tissues in late embryonic-early postnatal development and deletion of the *MYO16* gene, nuclear polymorphism in or adjacent to the

MYO16 gene, or altered expression patterns of Myo16 protein have been found in patients with neuropsychiatric disorders suggesting the importance of myosin XVI in normal neuronal development. The structure and function of myosin XVI are the subject of Chap. 18 by Kengyel and Bugyi.

Class XVIII myosins are highly divergent and consist of two isoforms, Myo18A and Myo18B; they are closely related to myosin-II. Interestingly, class XVIII myosins appear to lack ATPase activity suggesting that rather than functioning as actin-based motors, myosins-XVIII, which have been localized to such diverse places as the leading edge and the Golgi apparatus, may play structural roles. In Chap. 19, Taft and Latham provide insight into the current state of our knowledge of these myosins.

Myosin-XIX is a widely-expressed motor that associates through a MyMOMA motif in its tail domain with the outer mitochondrial membrane and mediates mitochondria transport. Insight into the structure and function of myosin-XIX is the subject of Chap. 20 by Bocanegra, Adikes, and Quintero.

Acknowledgments It is my great pleasure to acknowledge and thank the international team of scientists whose hard work made this book possible. I have no doubt that the fruits of your efforts will serve as important resources for both scientists and students alike. I thank Gonzalo Cordova, Springer-Dordrecht, for the opportunity to edit this book and the able assistance of the editorial team at Springer-Dordrecht for its production. The studies in my laboratory are supported by NIH grant GM111615.

References

Batters C, Veigel C (2016) Mechanics and activation of unconventional myosins. Traffic 17:860–871. https://doi.org/10.1111/tra.12400

Berg JS, Powell BC, Cheney RE (2001) A millennial myosin census. Mol Biol Cell 12(4):780–794

Collins JH, Borysenko CW (1984) The 110,000-dalton actin- and calmodulin-binding protein from intestinal brush border is a myosin-like ATPase. J Biol Chem 259(22):14128–14135

Coluccio LM, Bretscher A (1987) Calcium-regulated cooperative binding of the microvillar 110K-calmodulin complex to F-actin: formation of decorated filaments. J Cell Biol 105(1):325–333

Engelhardt WA, Ljubimowa MN (1939) Myosine and adenosinetriphosphatase. Nature 144:668–669

Espreafico EM, Cheney RE, Matteoli M, Nascimento AA, De Camilli PV, Larson RE, Mooseker MS (1992) Primary structure and cellular localization of chicken brain myosin-V (p 190), an unconventional myosin with calmodulin light chains. J Cell Biol 119(6):1541–1557

Foth BJ, Goedecke MC, Soldati D (2006) New insights into myosin evolution and classification. Proc Natl Acad Sci U S A 103:3681–3686

Gillespie PG, Albanesi JP, Bahler M, Bement WM, Berg JS, Burgess DR, Burnside B, Cheney RE, Corey DP, Coudrier E, de Lanerolle P, Hammer JA, Hasson T, Holt JR, Hudspeth AJ, Ikebe M, Kendrick-Jones J, Korn ED, Li R, Mercer JA, Milligan RA, Mooseker MS, Ostap EM, Petit C, Pollard TD, Sellers JR, Soldati T, Titus MA (2001) Myosin-I nomenclature. J Cell Biol 155(5):703–704. https://doi.org/10.1083/jcb.200110032

Hanson J, Huxley HE (1953) Structural basis of cross-striations in muscle. Nature 172:530–532

Heissler SM, Manstein DJ (2013) Nonmuscle myosin-2: mix and match. Cell Mol Life Sci 70(1):1–21. https://doi.org/10.1007/s00018-012-1002-9

Heissler SM, Sellers JR (2016) Kinetic adaptations of Myosins for their diverse cellular functions. Traffic 17:839–859. https://doi.org/10.1111/tra.12388

Howe CL, Mooseker MS (1983) Characterization of the 110-kdalton actin-calmodulin-, and membrane-binding protein from microvilli of intestinal epithelial cells. J Cell Biol 97(4):974–985

Huxley HE (1957) The double array of filaments in cross-striated muscle. J Biophys Biochem Cytol 3(5):631–648

Huxley H, Hanson J (1954) Changes in the cross-striations of muscle during contraction and stretch and their structural interpretation. Nature 173(4412):973–976

Huxley AF, Niedergerke R (1954) Structural changes in muscle during contraction. Interference microscopy of living muscle fibers. Nature 173:971–978

Kühne W (1864) Untersuchungen über das Protoplasma und die Contractilität. Verlag von Wilhelm Engelmann, Leipzig

Lowey S, Slayter HS, Weeds AG, Baker H (1969) Substructure of the myosin molecule. I Subfragments of myosin by enzymic degradation. J Mol Biol 42(1):1–29

Manstein DJ, Ruppel KM, Spudich JA (1989) Expression and characterization of a functional myosin head fragment in Dictyostelium discoideum. Science, NY 246(4930):656–658

Maruta H, Korn ED (1977a) Acanthamoeba myosin II. J Biol Chem 252(18):6501–6509

Maruta H, Korn ED (1977b) Purification from Acanthamoeba castellanii of proteins that induce gelation and syneresis of F-actin. J Biol Chem 252(1):399–402

Masters TA, Kendrick-Jones J, Buss F (2017) Myosins: domain organisation, motor properties, physiological

roles and cellular functions. Handb Exp Pharmacol 235:77–122. https://doi.org/10.1007/164_2016_29

Matsudaira PT, Burgess DR (1979) Identification and organization of the components in the isolated microvillus cytoskeleton. J Cell Biol 83(3):667–673

Matsudaira PT, Burgess DR (1982) Organization of the cross-filaments in intestinal microvilli. J Cell Biol 92(3):657–664

Mercer JA, Seperack PK, Strobel MC, Copeland NG, Jenkins NA (1991) Novel myosin heavy chain encoded by murine dilute coat colour locus [published erratum appears in nature 1991 Aug 8;352(6335):547]. Nature 349 (6311):709–713

Montell C, Rubin GM (1988) The Drosophila ninaC locus encodes two photoreceptor cell specific proteins with domains homologous to protein kinases and the myosin heavy chain head. Cell 52(5):757–772

Mooseker MS, Coleman TR (1989) The 110-kD protein-calmodulin complex of the intestinal microvillus (brush border myosin I) is a mechanoenzyme. J Cell Biol 108(6):2395–2400

Mooseker MS, Foth BJ (2008) The structural and functional diversity of the myosin family of actin-based molecular motors. In: Coluccio LM (ed) Myosins: a superfamily of molecular motors, Proteins and cell regulation, vol 7. Springer, Dordrecht, pp 1–34

Odronitz F, Kollmar M (2007) Drawing the tree of eukaryotic life based on the analysis of 2,269 manually annotated myosins from 328 species. Genome Biol 8(9):R196

Pollard TD, Korn ED (1973a) *Acanthamoeba* myosin. I. Isolation from *Acanthamoeba castellanii* of an enzyme similar to muscle myosin. J Biol Chem 248(13):4682–4690

Pollard TD, Korn ED (1973b) *Acanthamoeba* myosin. II. Interaction with actin and with a new cofactor protein required for actin activation of Mg^{2+} adenosine triphosphatase activity. J Biol Chem 248(13):4691–4697

Pollard TD, Stafford WF, Porter ME (1978) Characterization of a second myosin from Acanthamoeba castellanii. J Biol Chem 253(13):4798–4808

Rayment I, Rypniewski WR, Schmidt-Bäse K, Smith R, Tomchick DR, Benning MM, Winkelmann DA, Wesenberg G, Holden HM (1993) Three-dimensional structure of myosin subfragment-1: a molecular motor [see comments]. Science NY 261(5117):50–58

Straub FB (1942) Actin. Studies from the Institute of Medical Chemistry University Szegeb II

Szent-Györgyi AG (2004) The early history of the biochemistry of muscle contraction. J Gen Physiol 123:631–641

Toyoshima YY, Kron SJ, McNally EM, Niebling KR, Toyoshima C, Spudich JA (1987) Myosin subfragment-1 is sufficient to move actin filaments in vitro. Nature 328(6130):536–539

Verner K, Bretscher A (1985) Microvillus 110K-calmodulin: effects of nucleotides on isolated cytoskeletons and the interaction of the purified complex with F-actin. J Cell Biol 100:1455–1465

Wang A, Ma X, Conti MA, Adelstein RS (2011) Distinct and redundant roles of the non-muscle myosin II isoforms and functional domains. Biochem Soc Trans 39(5):1131–1135. https://doi.org/10.1042/BST0391131

Myosin Structures

2

H. Lee Sweeney, Anne Houdusse, and Julien Robert-Paganin

Abstract

Directed movements on actin filaments within the cell are powered by molecular motors of the myosin superfamily. On actin filaments, myosin motors convert the energy from ATP into force and movement. Myosin motors power such diverse cellular functions as cytokinesis, membrane trafficking, organelle movements, and cellular migration. Myosin generates force and movement via a number of structural changes associated with hydrolysis of ATP, binding to actin, and release of the ATP hydrolysis products while bound to actin. Herein we provide an overview of those structural changes and how they relate to the actin-myosin ATPase cycle. These structural changes are the basis of chemo-mechanical transduction by myosin motors.

Keywords

Myosin · Structure · Molecular motor · ATPase · Force generation

H. L. Sweeney (✉)
Department of Pharmacology & Therapeutics, College of Medicine, University of Florida, Gainesville, FL, USA
e-mail: lsweeney@ufl.edu

A. Houdusse · J. Robert-Paganin
Institut Curie, CNRS, Paris Cedex 05, France
e-mail: anne.houdusse@curie.fr

2.1 Myosin Classes

There are more than 40 known classes of myosin, all of which follow the blueprint in Fig. 2.1a (Foth et al. 2006). Of these, there are 13 myosin classes that are expressed in mammals. The first myosin that was discovered was that isolated from the thick filaments of muscle (see Chap. 1) and is now referred to as myosin II, or conventional myosin. The nonmuscle isoform of class II myosin is found in nearly all eukaryotic cells. It is the motor that powers cytokinesis (Chap. 11).

Some classes of the myosin family of motor proteins can move cargoes as single (two-headed) molecules. The first demonstration of this was with myosin V (Mehta et al. 1999), which is known to be a processive vesicle trafficking motor (see Chaps. 7 and 8), analogous to kinesin moving vesicles on a microtubule. The term processivity implies that these two-headed motor proteins can move along the actin filament (in the case of myosin V or myosin VI) or along a microtubule (in the case of kinesin) in a manner in which one head is always bound to the filament. If both heads ever dissociate simultaneously, then the motor and cargo diffuse away. While this is optimal for moving a cargo with a small number of motors, this is not the design of a myosin motor that is optimized for muscle. In the case of many motors working together in an asynchro-

L. M. Coluccio (ed.), *Myosins*, Advances in Experimental Medicine and Biology 1239,
https://doi.org/10.1007/978-3-030-38062-5_2

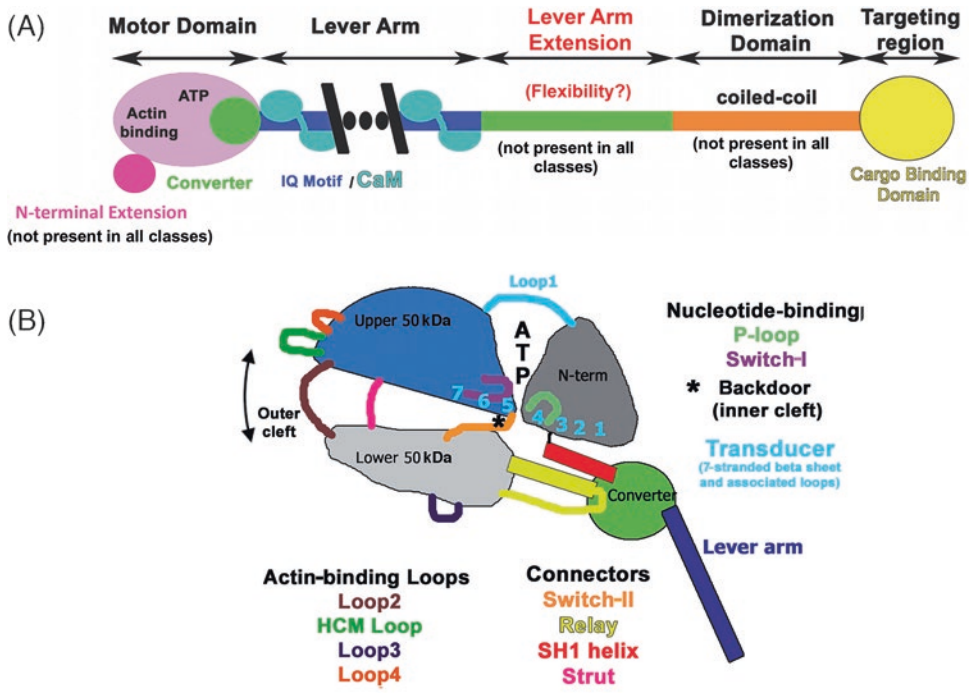

Fig. 2.1 Structural organization of myosin motors. (**a**) Blueprint for the myosin superfamily. The motor domain contains the ATP-hydrolysis site as well as the actin-binding interface. Several classes of myosins have an extension prior to the motor domain (N-terminal extension), including one splice form of class XVIII myosins. The C-terminus of the motor domain contains the converter subdomain, which amplifies rearrangements in the motor and is the first component of the lever arm. The lever arm contains a number of calmodulin (CaM)/light chain-binding sites. Extensions of the lever arm are varied; class VII and X contain single stable alpha helices (SAHs). Class XVIII myosin has a lever arm like that of class II myosins, with an essential (ELC) and regulatory (RLC) light chain. Parallel coiled coils appear in class II, V, and XVIII myosins. An anti-parallel coiled coil is found in class X myosin and likely will be found in other classes. The cargo-targeting region is the most variable of all regions and differs considerably between each class. (**b**) Structural elements of the myosin motor domain. A schematic diagram illustrates the positions of the four subdomains and connectors of the myosin motor domain. Subdomains are colored as follows: N-terminal (dark grey), upper 50-kDa (blue), lower 50-kDa (light grey) and converter (green). The actin-binding site is composed of actin-binding loops as well as a helix-loop-helix region of the lower 50-kDa subdomain. Thus, the binding site contains elements of both the upper and lower 50-kDa subdomains, which are separated by a large cleft. While the outer cleft region corresponds to the surface of the molecule that binds to actin, the inner cleft is near the **switch-II** connector, at a position close to the position where the gamma-phosphate of ATP is bound. (A movement of switch-II opens a backdoor (∗) to release phosphate upon actin binding at the beginning of the power stroke). The central beta-sheet is part of the transducer region (cyan) that plays a critical role in closing the cleft during the power stroke on actin. This affects the relative position of two elements of the nucleotide-binding site, namely the **P-loop** (which is part of the N-terminal subdomain) and **switch-I** (which is part of the Upper 50-kDa subdomain), and thus controls the release of MgADP from the active site. While the ADP is held in the P-loop, Mg^{2+} and ADP must indeed interact with switch-I for strong binding. Rearrangements within the motor domain are transmitted to the lever arm by rotation of the most mobile of the subdomains, the converter, which is connected to the rest of the motor domain by two highly deformable connectors: the Relay and the SH1 helix

nous manner, as in the sarcomeres of striated muscles, a much shorter duration of actin interaction under low loads (low duty ratio) allows for much higher velocities and power output.

2.2 Myosin Design

Myosin, via its cyclic interactions with actin filaments, is a superfamily of molecular motor proteins that powers movement on actin filaments

in all eukaryotic cells. The different classes of myosin motors provide for a number of types of cellular functions, as reviewed in Chaps. 11, 12, and 15. All known myosin superfamily members follow the blueprint shown in Fig. 2.1a. The myosin head can be subdivided into the motor domain, which is the actin-activated ATPase and a subdomain of the head, known as the converter, which in combination with an extended helix containing a variable number of consensus calmodulin or calmodulin-like light chain-binding sites, forms the myosin "lever arm". The lever arm amplifies the movements within the myosin motor domain. For some classes of myosins the lever arm is extended by regions of higher flexibility, which could be important for their functions in cells. The lever arm is followed by a region of coiled coil in two-headed myosins, and may contain sequences that act as elements for protein folding. Lastly is the targeting domain, which binds the myosin to its cellular target. The myosin motor domain itself can be divided into a number of subdomains, as diagramed in Fig. 2.1b.

All myosin motors are ATPases that hydrolyze ATP when not bound to actin, but only slowly release the hydrolysis products, MgADP and inorganic phosphate (P_i), unless the myosin binds to an F-actin filament. Once myosin does bind to F-actin, the binding catalyzes the release of P_i, followed by the release of Mg and ADP, before rebinding ATP, which dissociates the myosin from actin, allowing hydrolysis to occur again, and the cycle to repeat. The structural changes required to allow hydrolysis bring about a large movement of the myosin lever arm. This movement is reversed when the products are released while the myosin head is bound to actin. The movement of the lever arm on actin is known as the myosin power stroke, and generates force and movement. The movement of the lever arm that is associated with hydrolysis is known as the recovery stroke, and involves a rapid isomerization with a low free energy barrier. While all classes of myosin have the same basic kinetic cycle, the rates of transition between the states are highly variable. This allows myosin motors to be "kinetically tuned" for a variety of cellular functions by not only altering the rate that they proceed through the ATPase cycle, but also by changing the relative amount of the cycle that the myosin motor spends in strong actin-binding (force-generating) states. [See De La Cruz and Ostap 2004 for review.] The ratio of the occupancy of the strong states to the occupancy of the weak + dissociated + strong states is known as the the duty ratio.

The IQ motifs with associated calmodulins/light chains are generally thought to function as a lever arm for the myosin motor. Altering the length of the lever arm will change the step size of the myosin movement, as well as alter the ratio between speed of movement and ATP consumed. The lever arm region of some myosin classes, such as myosin X (Myo10), is extended by a single, stable alpha-helix that follows the IQ motifs, and for myosin VI, a three-helix bundle unfolds to form a lever arm extension when two myosin VI monomers dimerize. The compliance of these lever arms is likely quite variable and may be critical for the cellular functions of different myosin classes.

All but one class of myosins that have been studied move towards the (+)-end (barbed end) of an actin filament. Class VI myosin (Myo6) moves in the opposite direction (i.e., towards the (−)-end of the actin filament) as compared to other classes (Wells et al. 1999). Myo6 achieves this reversal of directionality by repositioning the lever arm, as shown in Fig. 2.2. The most conserved feature within the myosin superfamily is the motor domain itself. The differences that do exist within the motor domains of myosin are primarily restricted to additions/deletions at the N-terminus of the motor, and to variations in surface loops, many of which interact with actin. Myo6 is an exception to this with two unique insertions within the motor domain. One of the Myo6 inserts, insert 2, reverses the directionality of the motor by repositioning the lever arm (Figs. 2.1 and 2.2), while insert 1 alters ATP binding under load. Both of these adaptations are to optimize processive movements in the reverse direction [see Sweeney and Houdusse 2010a for review].

Perhaps the least conserved myosin feature is the C-terminus of the myosin molecule. While all two-headed myosins contain a coiled coil following the light chain-binding region, the most C-terminal region is different in each class of

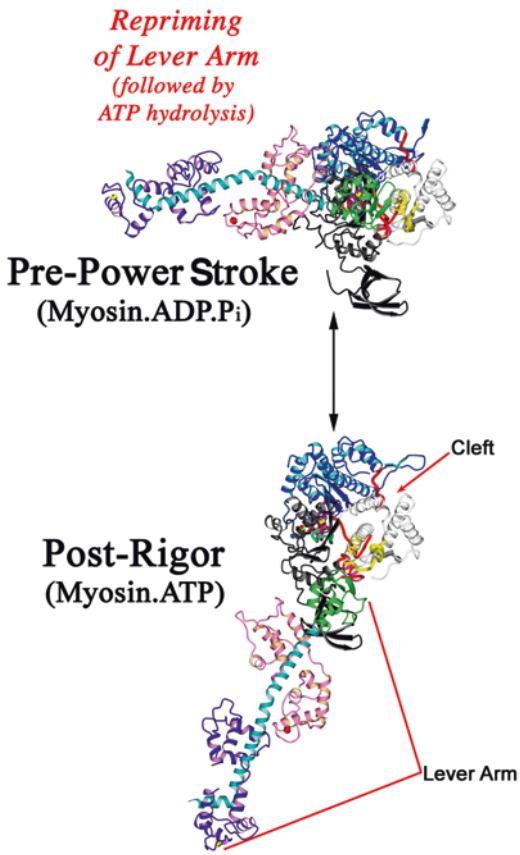

Fig. 2.2 The recovery stroke. The first two high-resolution crystal structures of the myosin head represented the states of myosin that exist in a rapid equilibrium in the absence of actin. The first of the structures (below) is the post-rigor structure, and was the state represented in the original chicken Myo2 structure of Rayment et al. (1993). The structure has been seen for myosin II with ADP, ATP, ATP analogues or no nucleotide at the active site. Depicted is the scallop striated muscle Myo2 post-rigor (PR) structure with MgADP at the active site (1SR6). ATP cannot be hydrolyzed in this state. This is the state created when ATP binds to myosin and dissociates it from the actin-myosin complex. Above the post-rigor state is the pre-power stroke state (PPS; 1QVI). This state is formed by structural rearrangements of the post-rigor state involving a movement of switch-I and a kinking of the switch-II helix that moves the lever arm to a primed position so that it is positioned for the next power stroke on actin. It is the state in which ATP is hydrolyzed to form ADP and inorganic phosphate, which are both trapped in the active site and only slowly released unless the myosin binds to actin

myosin, likely due to its role in cargo binding (see Chap. 3). Only the myosin II class (Myo2) appears to have a C-terminal coiled coil domain that promotes filament formation, although class XVIII myosin (Myo18) has a C-terminal region that promotes tetramer formation.

2.3 Myosin Structures: The Recovery Stroke

The first high-resolution myosin structure was of the entire head fragment of chicken fast skeletal myosin (Rayment et al. 1993). This first structure was initially referred to as a near-rigor state as it fit well into cryo-EM maps of skeletal muscle myosin in rigor. It later was recognized that the state corresponds to the ATP state populated after MgATP binds to and dissociates myosin from actin. (Although the crystals did not contain nucleotide, a sulfate was coordinated at the active site.) The actin-myosin complex with no nucleotide bound is known as the rigor state. The term comes from rigor mortis, which is the stiffening of skeletal muscle as the tissue dies, due to the irreversible actin and myosin cross-linking once ATP is depleted. Once it was realized that the initial structure corresponded to the state that is formed when ATP binds to the rigor state, triggering detachment from actin, the state became known as the post-rigor state. This state has now been crystallized for a number of myosin classes and all structures are quite similar (Table 2.1).

Two key features of the myosin motor mechanism were predicted by the first high-resolution myosin post-rigor structure (Fig. 2.2). First, the presence of a large cleft (so called 50-kDa cleft; see Figs. 2.1b and 2.2) in the middle of the head that ran from the nucleotide-binding site to the actin interface caused Rayment et al. (1993) to suggest that the cleft likely closes when myosin loses its hydrolysis products upon strong binding to actin. Indirect evidence from electron microscopy combined with image reconstruction, as well as fluorescent probes located in the cleft, supported this prediction (Volkman et al. 2000;

Table 2.1 List of myosin crystal structures by structural state

State in ATPase cycle	Genus and species	Myosin class	PDB accession number
Post-rigor	*Gallus gallus*	Myosin II	1MYS
	Dictyostelium	Myosin II	1MMD
	Scallop striated	Myosin II	1SR6
	Gallus gallus	Myosin V	1W7J
	Gallus gallus	Myosin V	1W7J
	Sus scrofa	Myosin VI	2VAS / 2VB6
	Homo sapiens/Homo sapiens/Bos taurus	Cardiac M2	4DB1 4P7H 6FSA
	Plasmodium falciparum	Myosin XIV	6I7D
Pre-power stroke	*Dictyostelium*	Myosin II (Myo2)	1VOM
	Gallus gallus	SMMII (SM Myo2)	1BR1
	Scallop striated	Myosin II (Myo2)	1QVI
	Dictyostelium MyoE	Myosin I (Myo1)	1LKX
	Sus scrofa	Myosin VI (Myo6)	2 V26
	Homo sapiens	Myosin Ic	4BYF
	Homo sapiens	Myosin Vc	4ZG4
	Homo sapiens	Myosin X	5I0H/5I0I
	Homo sapiens	NMIIc	5I4E
	Bos taurus	Cardiac Myo2	5N6A
	Toxoplasma	Myosin XIV	6DUE
	Plasmodium falciparum	Myosin XIV	6I7E
Phosphate release	*Sus scrofa*	Myosin VI (Myo6)	4PFO/4PJM/4PJN/
Rigor-like	*Gallus gallus*	Myosin V (Myo5)	1OE9/1W7I
	Squid	Myosin II (Myo2)	2AKA
	Pig	Myo6	2BKH/2BKI
	Squid	Myo2	3I5G
	Rattus norvegicus	Myosin Ib (Myo1b)	4 L79
	Homo sapiens	NMIIb (NMMyo2b)	4PD3
	Drosophila melanogaster	*Embryonic Myo2*	5W1A
	Plasmodium falciparum	Myosin XIV (Myo14)	6I7D
Intermediate recovery stroke	*Sus scrofa*	Myo6	5O2L

Yengo et al. 1999). The later high-resolution structure of the myosin V (Myo5) motor without nucleotide (described below) demonstrated how this cleft closes (Coureux et al. 2003).

The second striking feature and prediction of the Rayment structure focused on the myosin light chains. The light chains (which are members of the calmodulin superfamily) were bound to the C-terminal portion of the heavy chain, which formed an extended alpha helix. It appeared that this region formed a lever arm that could likely amplify small movements within the motor domain. This came to be known as the swinging lever arm hypothesis (Holmes and Geeves 1999) and has been validated by a number of lines of experimental evidence (Holmes and Geeves 1999; Huxley et al. 2006; Tyska and Warshaw 2002).

The second structural state that was seen at high resolution was of a state that allows hydrolysis of ATP and traps the hydrolysis products in the active site (Fisher et al. 1995; Dominguez et al. 1998). It is known as the pre-power stroke state (Figs. 2.2 and 2.3) and revealed the structural

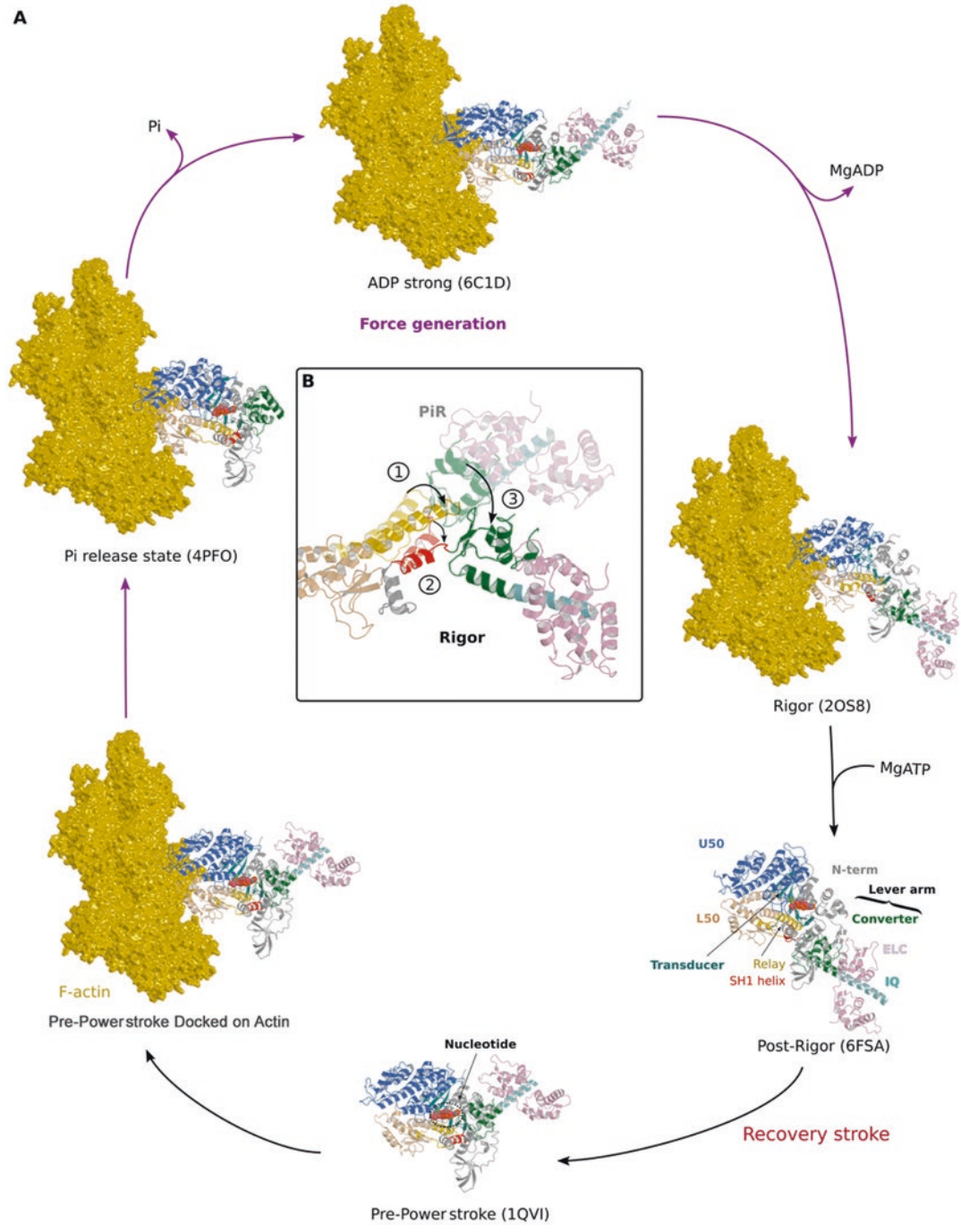

Fig. 2.3 Actin-activated ATPase cycle of myosin superfamily. (**a**) The ATPase cycle with known structures. The known transitions within the actin-myosin force-generating ATPase cycle depicting the different biochemical states along with the structural states (with PBD accession numbers) solved by X-ray crystallography and/or cryo-electron microscopy. When the myosin is detached from actin, it is in the post-rigor state (PR) bound to ATP. ATP hydrolysis along with the lever arm priming occur in the transition to the pre-power stroke state (PPS), which is able to dock on the actin filament with a low affinity. Actin-driven conformational changes allow first the release of the Pi when the Pi release state (P_iR) is formed, which allows a rapid movement of the lever arm

changes necessary for lever arm priming and ATP hydrolysis (Fisher et al. 1995; Dominguez et al. 1998; Houdusse et al. 2000). In this structure, switch-II rearranges from its post-rigor conformation in order to position water in the active site for hydrolysis of ATP to generate ADP and inorganic phosphate. This switch-II movement requires kinking of the helix that follows switch-II (part of the Relay in Fig. 2.1b). and repositioning of the subdomains in a manner that leads to a movement of the converter subdomain and thus the lever arm. This structure fully launched the swinging lever arm hypothesis (Holmes and Geeves 1999).

The movement of the lever arm associated with the re-priming, or recovery stroke in the absence of actin, correlated quite well with the measured size of the power stroke on actin (Fig. 2.2). However, the two states involved in the recovery stroke were obviously not the actin-bound states that generate force and the movement of the power stroke. The power stroke on actin begins with a rearrangement of the pre-power stroke (PPS) conformation so that it can bind to actin and ends with the rigor state that ATP disrupts when it forms the post-rigor state. As described below, the lever arm position in post-rigor, following detachment from actin, is in approximately the same position as in rigor, and the lever arm position in the phosphate release state (presented below) is similar to the position in the pre-power stroke structure. This accounts for the close correspondence of the amplitude of the lever arm movement in the recovery stroke with the size of the power stroke on actin.

Another early line of evidence in support of the lever arm hypothesis as the generator of movements by myosin is that the one class of myosins that moves in the reverse direction (Wells et al. 1999), class VI myosins (Myo6), does so largely by reversal of the lever arm position with respect to the converter (Ménétrey et al. 2005). However, there are additional specialized adaptations to optimize this reverse movement (Ménétrey et al. 2007; Mukherjea et al. 2009; Sweeney et al. 2007). The motor domain itself is that of a plus-end directed myosin other than these adaptations, and in fact replacement of the Myo6 lever arm with a Myo5 lever arm results in plus-end directed movement (Park et al. 2007).

Comparison of the known myosin structures show that the myosin motor domain is functionally made up of four major subdomains (Fig. 2.1b) that are linked by four flexible structural connectors that are highly conserved in sequence (Houdusse et al. 1999). The connectors are found at the periphery of the subdomains and can readily change conformation, in coordination with the movement of the subdomains relative to one another. Among these subdomains, the converter (which leads directly to the lever arm) has by far the greatest potential for movement since it is connected to the lower 50-kDa and N-terminal subdomains by only two deformable connectors (the relay and the SH1 helix, respectively). Thus, the converter functions as an amplifier of movements of the subdomains, which are further amplified by the rest of the myosin lever arm. Internal coupled rearrangements of the subdomains allow direct communication among the nucleotide-binding site, the actin-binding interface, and the lever arm (Sweeney and Houdusse 2010b). Coupling between the actin- and nucleotide-binding sites is mediated via the large cleft between the upper and lower 50-kDa subdomains, which separates the actin-binding interface in two distinct sites and communicates with the γ-phosphate pocket via a connector called switch-II (see Fig. 2.1b). In the pre-power stroke state, partial closure of the 50-kDa cleft involves only the inner part of the cleft (near switch-II) trapping the hydrolyzed phosphate (Fisher et al. 1995). In the nucleotide-free myosin V rigor-like

Fig. 2.3 (continued) and cleft closure to form the ADP strong state. A small lever arm swing coupled to relative movements of switch-I and the P-loop results in the release of MgADP and formation of the rigor state. ATP can then bind to the empty active site of myosin, recruiting a movement of switch-I that is coupled to a re-opening of the actin-binding cleft. This weakens the binding with actin, which allows the myosin to detach from the actin filament and to re-enter a new cycle. (**b**) The power stroke on actin. During the transition between the phosphate-release state (P_iR) and the rigor states, movements of the relay helix (1; *yellow*) and a piston-like movement of the SH1 helix (2; *red*) are coupled to the swing of the lever arm (3)

state, the outer cleft and the inner cleft are totally closed generating a new actin-binding interface that has a high affinity for actin (Coureux et al. 2003).

2.4 Myosin Structures: The Power Stroke

The power stroke begins with stereo-specific binding to actin that must create at least a subset of the actin-myosin interactions that will be maintained throughout the power stroke. Once this interface forms and the large cleft in the myosin at the actin-binding interface begins to close, the lever arm can swing, driving the power stroke. At the same time, the initial actin-bound state must create a means of allowing phosphate to escape from the active site, where it is trapped in the pre-power stroke state.

A structural state of Myo6 appears to fulfill these requirements. The structure was trapped in the absence of actin, but it demonstrates how the initial binding of myosin in the pre-power stroke state may cause the myosin interface with actin to rearrange, opening an escape route for the trapped phosphate (Llinas et al. 2015). In this structure, there has been a rotation of the lower 50-kDa subdomain coupled to a switch-II movement that creates an escape tunnel for the inorganic phosphate, without any significant movement of the lever arm, as compared to the PPS state. Once the phosphate is no longer trapped at the active site, the actin-interface can further rearrange, likely closing the cleft near actin, which is coupled to a large movement of the lever arm. At some point, the movement of the lever arm and closure of the actin-binding cleft must result in closing of the phosphate tunnel, as it no longer exists in the Rigor state discussed below. Blocking re-entry of the phosphate to the active site would make the reaction essentially irreversible.

This interpretation of what is referred to as the Myo6 phosphate-release (P_iR) state has resulted in significant controversy, due to the fact that release of phosphate into the solution is not detected until after lever arm movement is detected. Studies on muscle fibers suggest that force generation, and thus strong actin binding, occurs prior to phosphate release (Dantzig et al. 1992). However, this interpretation of the data has recently been brought in question (Stehle 2017). Nonetheless, the initial component of force production does not require lever arm movement, but does require that myosin bind to actin, which must precede phosphate release. In the phosphate-release state the movement of the lower 50-kDa subdomain coupled to a rearrangement of switch-II creates the actin-binding interface and in doing so opens an escape route for phosphate. If all that is necessary for the initiation of lever arm movement coupled to cleft closure is for phosphate to leave the active site, then the phosphate may not appear in solution until after the lever arm movement begins, given that there must be a delay between leaving the active site, entering the phosphate tunnel and then appearing in solution (Houdusse and Sweeney 2016). In fact, a rapid cleft closure coupled to lever arm movement once the phosphate leaves the active site would ensure the near irreversibility of the transition in the absence of load, assuming that at some point these rearrangements lead to closure of the phosphate tunnel. Load on the myosin that prevents lever arm movement, and presumably the completion of cleft closure, can allow phosphate to re-enter the active site, promoting isomerization back to the pre-power stroke state and detachment from actin.

The power stroke on actin ends when myosin has completed its lever arm swing and has released MgADP, forming the actin-myosin rigor complex. A structure of Myo5 revealed details of the rigor structure of myosin, albeit not bound to actin. It shows major rearrangements of the subdomains, leading to a movement of switch-I relative to the P-loop to weaken nucleotide binding, as well as closure of the actin-binding cleft in this final rigor state. However, as compared to the post-rigor state, the lever arm position appears to be similar. Thus, there is no reversal of the lever arm swing when ATP binds to myosin attached to actin to induce dissociation. What was not deduced from the initial myosin structures was that the subdomain movements associated with closing the cleft requires reliev-

ing a nucleotide binding-induced distortion of the seven-stranded β-sheet and associated loops (including the much-studied loop 1) and linkers (what we refer to as the "transducer" region of the myosin motor) underlying the nucleotide pocket (Coureux et al. 2003). This allows a relative movement of the N-terminal and upper 50-kDa subdomains and the associated elements of the nucleotide-binding site (P-loop and switch-I, see Figs. 2.1b and 2.3). This leads to release of the MgADP and an additional movement of the lever arm (beyond the main power stroke), resulting in the nucleotide-free (rigor) structure (Wulf et al. 2016).

While there are now multiple rigor-like structures that have been obtained (Table 2.1), only the Myo5 rigor structure has a completely closed cleft and well fits the rigor head density of cryo-EM maps of myosin-decorated actin (Wulf et al. 2016), such as those depicted in Chap. 4. This may be due to non-conserved interactions within the closed cleft of Myo5 that stabilize the closed cleft conformation (Coureux et al. 2003). ATP dissociates this rigor structure from actin by reopening the actin-binding cleft and thus weakening the interaction between myosin and actin. When MgATP binds to the rigor conformation of myosin, it induces a distortion of the seven-stranded β-sheet in order to position switch-I close enough to the P-loop to allow coordination of the MgATP. This regenerates the post-rigor confirmation of myosin, which rapidly detaches from actin, completing the ATP-consuming, force-generating cycle.

There are no high-resolution structures of the states/transitions that occur between the phosphate-release state, which is the first force-bearing actin-bound myosin state and the rigor structure that is the final actin-bound state. There is a cryo-EM structure of the state that strongly binds both ADP and actin (Wulf et al. 2016), and represents the state and the end of the main power stroke. Its features are discussed in Chap. 4.

Further movement of the lever occurs when MgADP is released, forming the rigor state and completing the power stroke on actin. This is an important transition for many myosins not in the generation of force, but in maintenance of force. Until MgADP is released, the myosin cannot rapidly detach from actin. Thus, this final component of the lever arm swing is highly load dependent. By altering the equilibrium between the strong MgADP-binding state and rigor, the myosin can be tuned to be more or less load dependent, and more suited to being an anchor on actin than for movement on actin (Laakso et al. 2008).

2.5 Correlation Between Structural and Kinetic States

High-resolution crystal structures of the myosin head with various nucleotides bound have thus provided direct visualization of the myosin motor in four distinct conformational states, as shown in Figs. 2.2 and 2.3. Understanding the chemo-mechanical coupling in the myosin motor requires assigning structural states to the distinct steps of the actin-myosin ATPase cycle characterized by kinetic studies. Of the high-resolution myosin structural states described above, the first two (post-rigor and pre-power stroke) can bind only weakly to actin. The post-rigor structure is the state represented in the original chicken myosin II structure of Rayment et al. (1993). ATP cannot be hydrolyzed in this state. In the overall actin-myosin ATPase cycle (see Fig. 2.3), it is the state created when ATP binds to myosin and dissociates it from the actin-myosin complex. The second state that was crystallized (Fisher et al. 1995; Dominguez et al. 1998) is known as the pre-power stroke state (formerly called the transition state). This state is formed by structural rearrangements of the post-rigor state, and is the state in which ATP is hydrolyzed to form ADP and inorganic phosphate. It has been referred to as the closed state, since there is partial cleft closure in this state, as well as trapping of the inorganic phosphate upon hydrolysis (Yount et al. 1995). There is rapid, reversible isomerization between these states, indicating that there is a low free energy change between them.

The pre-power stroke structures crystallized when either ATP or ATP analogs are bound to myosin show that ATP hydrolysis requires inter-

actions between switch-II and the γ-phosphate that result in the closure of the γ-phosphate pocket, preventing phosphate release. To avoid steric hindrance, the rigid conformation of switch-II in this state must be coupled with precise conformations of both the relay and the SH1 helix that leads to a primed position for the converter and the lever arm, characteristic of the pre-power stroke conformation of the myosin head. Site-directed mutagenesis studies confirmed that this conformation is essential for ATP hydrolysis and is preceded by a lever arm movement (Suzuki et al. 1998). Hydrolysis of ATP in the myosin motor is thus coupled to the priming of the lever arm. Trapping of the phosphate explains the stability of the pre-power stroke conformation until actin binding favors an isomerization that allows phosphate release. This underlies the low intrinsic ATPase activity of myosin in the absence of actin (Lymn and Taylor 1971).

The existence of an initial actin-binding state on myosin that can be detached by phosphate has long been described from muscle physiology experiments, and may be equivalent to a state that was described by Sleep and Hutton (1980). While the interpretation of the phosphate-release state (**P_iR**) is controversial, kinetic data support its assignment as this initial force-generating state, prior to lever arm movement. Amino acid substitutions that place bulky residues inside the myosin cleft near the actin interface greatly slow a kinetic transition that is monitored by the rate of pyrene-quenching of actin (so called weak-to-strong transition), but have no impact on phosphate release (Llinas et al. 2015). It is not clear if such mutations will slow or prevent lever arm movements, since this has not been measured. There is a drug, omecamtiv mercarbil, that can bind to cardiac myosin and prevent (or greatly slow) lever arm movement, but allows (and even accelerates) phosphate release (Rohde et al. 2017; Woody et al. 2018) (see Chap. 5). Thus, it would appear that formation of the state that releases phosphate precedes both the movement of the lever arm and complete closure of the actin-binding cleft of myosin.

The confusion surrounding the interpretation of the phosphate state results from the fact that while the rates of phosphate release and lever arm swing are both fast, the lever arm swing appears faster if unconstrained. However, if one views the critical transition that gates the lever arm swing as phosphate leaving the active site and entering the phosphate tunnel, and not the appearance of phosphate in solution, then the movement of the lower 50-kDa domain on actin that is coupled to the switch-II conformational change that creates the phosphate tunnel, is the initial rapid transition that precedes lever arm swing or phosphate release into the solution. Following the isomerization from the PPS state to the PiR state on actin, phosphate release into solution and lever arm swing precede in parallel.

The next kinetic transition that we can measure following the lever arm swing is the quenching of the pyrene probe that has been used to label Cys-374 of actin (Coates et al. 1985). This has been referred to as the weak-to-strong transition and indeed likely monitors the final closure of the actin-binding cleft and formation of the Strong ADP state on actin. Since the probe is not within the actin-myosin interface, it likely indicates that the complete closure of the myosin cleft near actin requires a rearrangement of the actin subdomains. It is also clear that this closure on actin destroys the phosphate tunnel preventing access of phosphate in solution to the active site. What is not clear is exactly how much of the actin-binding cleft closure occurs prior to the pyrene-quenching step and at what point the phosphate-binding tunnel is no longer accessible. There is likely some compliance in the coupling between the lever arm position and cleft closure on actin, but it is clear that preventing the complete swing of the lever arm (power stroke) can prevent formation of the strong ADP state (and presumably pyrene-actin quenching) and can keep the phosphate tunnel open. This allows phosphate in solution to re-enter the active site and to drive the transition back toward the PPS state.

Thus, the power stroke may largely occur prior to complete closure of the actin-binding cleft and is completed with formation of the strong ADP-bound state of myosin on actin. It may be that the closure of the cleft near actin is also complete with the formation of the strong ADP interface. Indeed, cryo-EM reconstruction of Myo5 in strong ADP and rigor can detect no significant changes in the actin-myosin interface during this transition (Wulf et al. 2016). While it is clear that during the transition from the initial force generating state (phosphate-release state) to the strong ADP-binding state the large swing of the lever arm that comprises the power stroke occurs and is coupled to closure of the actin-binding cleft, we currently have no detailed knowledge of the structural changes within the motor that allow this to happen.

As already discussed above, Myo5 has been crystallized in a "rigor" state in the absence of actin (Coureux et al. 2003). The kinetic tuning that allows Myo5 to predominately populate strong binding actin states in the presence of ATP likely involves changes in the cleft and transducer region that favor cleft closure in the absence of nucleotide even in the absence of actin. In contrast to skeletal myosin II, nucleotide-free Myo5 does not undergo any temperature-dependent conformational changes when it binds to actin (Coureux et al. 2003). Based on this and on a number of other important structural changes, the nucleotide-free structure of Myo5 likely represents the conformation of the myosin motor domain when it is bound to actin in rigor, with the likely exception of the surface loops that contribute to the actin-binding interface. Cryo-EM reconstructions support this assertion (Chap. 4).

2.6 Future Challenges

All of the crystal structures obtained to date are by nature without any strain imposed on the molecule, other than the internal strain generated by nucleotide binding. This leaves us with no real insights as to how the motor conformations are altered by load, which is of course what the motor is designed to move against. Applying load to the force-generating myosin heads will manifest in distortions of compliant regions of the motor itself. EM reconstructions have allowed the direct visualization (at low resolution) of the consequences of strain imposed by one myosin head on the other in the case of a single two-headed Myo5 molecule walking on actin (Walker et al. 2000; Oke et al. 2010). High speed AFM studies also visualized changes in lever arm position, but in real time (Uchihashi et al. 2012; Kodera and Ando 2014) (see Chap. 7). In this case, the elements that are notably distorted by the strain are the lever arm itself and the position of the converter. These structures, along with the transducer, are likely the major source of compliance within the myosin motor itself. Because of different crystal packing conditions (for example, see Ménétrey et al. 2012), we have been able to observe that the most mobile of the subdomains is the converter, due to compliant regions adjacent to the converter subdomain. This may be the primary or even sole source of compliance in the coupling between the actin-binding site and the lever arm.

While we have generated considerable insights in the mechanism of force production on actin from two high-resolution structures of myosin in the absence of actin (P_iR and Rigor structures), ultimately a detailed structural understanding of the subdomain rearrangements and actin-binding loop rearrangements during the state transitions of the force-generating cycle on actin can only come from high-resolution structural studies of myosin bound to actin. For X-ray studies, this will require small fragments of F-actin that can be co-crystallized with myosin trapped in distinct states of the cycle. It is likely that the general scheme of internal conformational changes within the motor domain throughout the cycle is relatively conserved among myosin classes. Whether essential elements in the actin-binding loops are conserved to produce the power stroke cannot be predicted. However, the variability of these loops suggests that they may give rise to

different actin interactions for different myosin classes that both position the motor somewhat differently on actin as well as differentially tune the kinetic transitions.

References

Coates JH, Criddle AH, Geeves MA (1985) Pressure-relaxation studies of pyrene-labelled actin and myosin subfragment-1 from rabbit skeletal muscle. Biochem 232:351–356

Coureux P-D, Wells AL, Ménétrey J, Yengo CM, Morris CA, Sweeney HL, Houdusse A (2003) The structure of myosin V motor without bound nucleotide. Nature 425:419–423

Dantzig JA, Goldman YE, Millar NC, Lacktis J, Homsher E (1992) Reversal of the cross-bridge force-generating transition by photogeneration of phosphate in rabbit psoas muscle fibres. J Physiol 451:247–278

De La Cruz EM, Ostap EM (2004) Relating biochemistry and function in the myosin superfamily. Curr Opin Cell Biol 16:61–67

Dominguez R, Freyzon Y, Trybus KM, Cohen C (1998) Crystal structure of a vertebrate smooth muscle myosin motor domain and its complex with the essential light chain: visualization of the pre-power stroke state. Cell 94:559–571

Fisher AJ, Smith CA, Thoden JB, Smith R, Sutoh K, Holden HM, Rayment I (1995) X-ray structures of the myosin motor domain of Dictyostelium discoideum complexed with MgADP.BeFx and MgADP.AlF4-. Biochemistry 34:8960–8972

Foth BJ, Goedecke MC, Soldati D (2006) New insights into myosin evolution and classification. Proc Natl Acad Sci U S A 103:3681–3686

Holmes KC, Geeves MA (1999) Structural mechanism of muscle contraction. Annu Rev Biochem 68:687–728

Houdusse A, Sweeney HL (2016) How myosin generates force on actin filaments. Trends Biochem Sci 41:989–997

Houdusse A, Kalabokis VN, Himmel D, Szent-Gyorgyi AG, Cohen C (1999) Atomic structure of scallop myosin subfragment S1 complexed with MgADP: a novel conformation of the myosin head. Cell 97:459–470

Houdusse A, Szent-Györgyi AG, Cohen C (2000) Three conformational states of scallop myosin S1. Proc Natl Acad Sci U S A 97:11238–11243

Huxley H, Reconditi M, Stewart A, Irving T (2006) X-ray interference studies of crossbridge action in muscle contraction: evidence from quick releases. J Mol Biol 363:743–761

Kodera N, Ando T (2014) The path to visualization of walking myosin V by high-speed atomic force microscopy. Biophys Rev 6(3–4):237–260

Laakso JM, Lewis JH, Shuman H, Ostap EM (2008) Myosin I can act as a molecular force sensor. Science 321:133–136

Llinas P, Isabet T, Song L, Ropars V, Zong B, Benisty H, Sirigu S, Morris C, Kikuti C, Safer D, Sweeney HL, Houdusse A (2015) How actin initiates the motor activity of myosin. Dev Cell 33(4):401–412

Lymn RW, Taylor EW (1971) Mechanism of adenosine triphosphate hydrolysis by actomyosin. Biochemistry 10:4617–4624

Mehta AD, Rock RS, Rief M, Spudich JA, Mooseker MS, Cheney RE (1999) Myosin V is a processive actin-based motor. Nature 400:590–593

Ménétrey J, Bahloul A, Wells AL, Yengo CM, Morris CA, Sweeney HL, Houdusse A (2005) The structure of the myosin VI motor reveals the mechanism of directionality reversal. Nature 435:779–785

Ménétrey J, Llinas P, Mukherjea M, Sweeney HL, Houdusse A (2007) The structural basis for the large powerstroke of myosin VI. Cell 131:300–308

Ménétrey J, Isabet T, Ropars V, Mukherjea M, Pylypenko O, Liu X, Perez J, Vachette P, Sweeney HL, Houdusse AM (2012) Processive steps in the reverse direction require uncoupling of the Lead head lever arm of myosin VI. Mol Cell 48:75–86

Mukherjea M, Llinas P, Kim HJ, Travaglia M, Safer D, Ménétrey J, Franzini-Armstrong C, Selvin PR, Houdusse A, Sweeney HL (2009) Myosin VI dimerization triggers an unfolding of a three-helix bundle in order to extend its reach. Mol Cell 35:305–315

Oke OA, Burgess SA, Forgacs E, Knight PJ, Sakamoto T, Sellers JR, White H, Trinick J (2010) Influence of lever structure on myosin 5a walking. Proc National Acad Sci 107:2509–2514

Park H, Li A, Chen LQ, Houdusse A, Selvin PR, Sweeney HL (2007) The unique insert at the end of the myosin VI motor is the sole determinant of directionality. Proc Natl Acad Sci U S A 104:778–783

Rayment I, Rypniewski WR, Schmidt-Bäde K, Smith R, Tomchick DR, Benning MM, Winkelmann DA, Wesenberg G, Holden HM (1993) Three-dimensional structure of myosin subfragment-1: a molecular motor. Science 261:50–58

Rohde JA, Thomas DD, Muretta JM (2017) Heart failure drug changes the mechanoenzymology of the cardiac myosin powerstroke. Proc Natl Acad Sci U S A 114:E1796–E1804

Sleep JA, Hutton RL (1980) Exchange between inorganic phosphate and adenosine 5′-triphosphate in the medium by actomyosin subfragment 1. Biochemistry 19:1276–1283

Stehle R (2017) Force responses and sarcomere dynamics of cardiac myofibrils induced by rapid changes in [pi]. Biophys J 112:356–367

Suzuki Y, Yasunaga T, Ohkura R, Wakabayashi T, Sutoh K (1998) Swing of the lever arm of a myosin motor at the isomerization and phosphate-release steps. Nature 396:380–383

Sweeney HL, Houdusse A (2010a) Myosin VI rewrites the rules for myosin motors. Cell 141:573–582

Sweeney HL, Houdusse A (2010b) Structural and functional insights into the myosin motor mechanism. Annu Rev Biophys 39:539–557

Sweeney HL, Park H, Zong AB, Yang Z, Selvin PR, Rosenfeld SS (2007) How myosin VI coordinates its heads during processive movement. EMBO J 26:2682–2692

Tyska MJ, Warshaw DM (2002) The myosin power stroke. Cell Motil Cytoskeleton 51:1–15

Uchihashi T, Kodera N, Ando T (2012) Guide to video recording of structure dynamics and dynamic processes of proteins by high-speed atomic force microscopy. Nat Protoc 7(6):1193–1206

Volkman N, Hanein D, Ouyang G, Trybus KM, DeRosier DJ, Lowey S (2000) Evidence for cleft closure in actomyosin upon ADP release. Nat Struct Biol 7:1147–1155

Walker ML, Burgess SA, Sellers JR, Wang F, Trinick J, Knight PJ (2000) Two-headed binding of a Processive myosin to F-actin. Nature 405:804–807

Wells AL, Lin AW, Chen L-Q, Safer D, Cain SM, Hasson T, Carragher BO, Milligan RA, Sweeney HL (1999) Myosin VI is an actin-based motor that moves backwards. Nature 401:505–508

Woody MS, Greenberg MJ, Barua B, Winkelmann DA, Goldman YE, Ostap EM (2018) Positive cardiac inotrope omecamtiv mecarbil activates muscle despite suppressing the myosin working stroke. Nat Commun 9:3838

Wulf SF, Ropars V, Fujita-Becker S, Oster M, Hofhaus G, Trabuco LG, Pylypenko O, Sweeney HL, Houdusse AM, Schröder RR (2016) Force-producing ADP state of myosin bound to actin. Proc Natl Acad Sci U S A 113:E1844–E1852

Yengo CM, Chrin L, Rovner AS, Berger CL (1999) Intrinsic tryptophan fluorescence identifies specific conformational changes at the actomyosin interface upon actin binding and ADP release. Biochemistry 38:14515–14523

Yount RG, Lawson D, Rayment I (1995) Is myosin a "back door" enzyme? Biophys J 68:44S–47S

Cargo Binding by Unconventional Myosins

3

Jianchao Li and Mingjie Zhang

Abstract

Unconventional myosins are a large superfamily of actin-based molecular motors that use ATP as fuel to generate mechanical motions/forces. The distinct tails in different unconventional myosin subfamilies can recognize various cargoes including proteins and lipids. Thus, they can play diverse roles in many biological processes such as cellular trafficking, mechanical supports, force sensing, etc. This chapter focuses on some recent advances on the structural studies of how unconventional myosins specifically bind to cargoes with their cargo-binding domains.

Keywords

Unconventional myosins · Myosin cargo-binding domain · Cargo recognition · Cargo transport

3.1 Introduction

Myosin family proteins typically contain three major parts: a motor or head domain responsible for actin-filament binding and ATP hydrolysis, an IQ-motif-containing neck region for movement amplification, and additional N- or C-terminal tails (Block 1996; Ruppel and Spudich 1996; Krendel and Mooseker 2005). Myosins can be generally grouped into two major categories, namely conventional myosin-II with their C-terminal tails containing a characteristic long coiled-coil for bipolar filament formation (e.g. muscle myosins), and unconventional myosins with diverse tails (Krendel and Mooseker 2005; Hartman et al. 2011; Hartman and Spudich 2012; Howard 1997; Huxley 1998; Geeves and Holmes 1999; Vale 1999; Berg et al. 2001). The human genome contains 24 unconventional myosins that can be classified into 11 subfamilies according to their domain structures in the tail region (Foth et al. 2006).

The specific domains in each unconventional myosin subfamily enable them to perform distinct functions (Hartman et al. 2011; Lu et al. 2014; Li et al. 2016b). Many well-defined

J. Li (✉)
Division of Cell, Developmental and Integrative Biology, School of Medicine, South China University of Technology, Guangzhou, China
e-mail: lijch@scut.edu.cn

M. Zhang
Division of Life Science, State Key Laboratory of Molecular Neuroscience, Hong Kong University of Science and Technology,
Kowloon, Hong Kong, China

Center of Systems Biology and Human Health, School of Science and Institute for Advanced Study, Hong Kong University of Science and Technology,
Kowloon, Hong Kong, China
e-mail: mzhang@ust.hk

L. M. Coluccio (ed.), *Myosins*, Advances in Experimental Medicine and Biology 1239,
https://doi.org/10.1007/978-3-030-38062-5_3

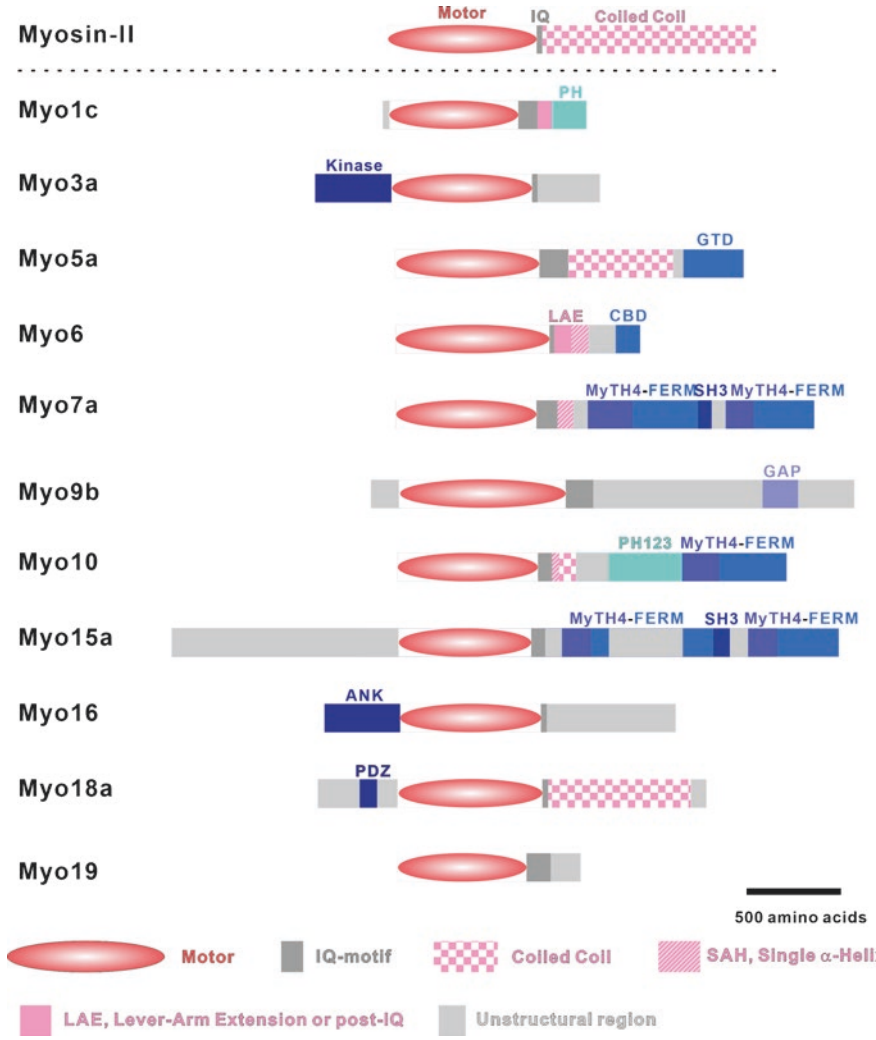

Fig. 3.1 Schematic representations showing the domain organizations of human myosins. The conserved motor domains are colored in salmon and the diverse cargo binding domains are colored in cyan or blue

domains are found in unconventional myosins (Fig. 3.1). For example, some myosins contain well-known protein-protein interacting domains like the SH3 (Src homology 3) domain in myosin-I, myosin-VII and myosin-XV; the MyTH4-FERM (myosin tail homology 4; band 4.1, ezrin, radixin, moesin) tandems in myosin-VII, myosin-X and myosin-XV; the PDZ (PSD-95, Dlg, ZO-1) domain in myosin-XVIII; and the ANK (ankyrin) repeats in myosin-XVI. Some myosins contain lipid-binding domains like the PH (pleckstrin homology) domains in myosin-I and myosin-X, and some myosins even contain an additional catalytic domain like the kinase domain in myosin-III and the GAP (GTPase activating protein) domain in myosin-IX. There are also specific domains only found in myosins, including the globular tail domain (GTD) in myosin-V and the helical cargo-binding domain (HCBD) and cargo-binding domain (CBD) in myosin-VI. Besides these well-folded domains, some myosins also contain long intrinsically disordered regions, such as the C-terminal tails of myosin-III, myosin-XVI and myosin-XIX, and the large N-terminal extension in myosin-XV.

Unconventional myosins have been reported to function in many biological processes. Myosins-I, -V, and -VI are involved in vesicle

trafficking events such as exocytosis, endocytosis and intracellular actin filament-based vesicle transport (Hammer and Sellers 2012; McConnell and Tyska 2010; Tumbarello et al. 2013). Myosin-III, -VII, -X and -XV are shown to be critical for development and maintenance of actin-based protrusions such as stereocilia, microvilli and filopodia (Hasson et al. 1995; Berg and Cheney 2002; Les Erickson et al. 2003; Belyantseva et al. 2005; Crawley et al. 2014). Despite their involvements in various biological processes, the functions of unconventional myosins are majorly divided into two: cellular transportation and dynamic tethering. These functions all depend on the specific binding of target proteins or lipid membranes to myosins which in turn facilitates their precise subcellular localization and function (Hartman et al. 2011).

Growing numbers of studies, especially high-resolution structural studies in recent years, have greatly advanced our knowledge towards understanding the mechanistic basis of how myosins can recognize specific cargoes via their distinct tails. Here we attempt to summarize these findings.

3.2 Myosins Participate in Diverse Biological Processes via Binding to Various Cargoes

3.2.1 Myosin-V Subfamily Binds to Various Cargoes Using Their Globular Tail Domain

The myosin-V subfamily is one of the best characterized cargo-transporting myosins (Hammer and Sellers 2012; Langford 2002; Sellers and Veigel 2006; Taylor 2007; Titus 1997). It contains all the typical elements required for cargo transportation along actin filaments: a motor or head domain for energy generation, a lever arm for movement amplification, a coiled-coil for dimerization, and a globular tail domain for cargo loading (Fig. 3.2a) (Trybus 2008).

The myosin-V subfamily is also one of the three most ancient myosin subfamilies (the other two are myosin-I and myosin-II) and found in nearly all eukaryotes (Reck-Peterson et al. 2000). Yeast (e.g., Baker's yeast *Saccharomyces cerevisiae*) contains two class V myosins (Myo2p and Myo4p), while humans contain three members (Myo5a, Myo5b and Myo5c). Yeast Myo2p/Myo4p have been shown to be responsible for transporting organelles such as vacuoles, peroxisomes and secretory vesicles (Schott et al. 1999; Catlett et al. 2000). Similarly, mammalian Myo5a/Myo5b/Myo5c not only transport organelles along actin-filaments, but also tether them to actin (Hammer and Sellers 2012).

The C-terminal globular tail domain (GTD) recognizes a broad range of cargoes, which is essential for myosins to carry out diverse functions. Although the GTD from yeast myosin-V and mammalian myosin-V only share ~20% sequence identity, the overall folding is highly similar to each other as shown by the several high-resolution structures of the cargo-free mammalian and yeast GTDs (Heuck et al. 2010; Nascimento et al. 2013; Pylypenko et al. 2013; Velvarska and Niessing 2013; Wei et al. 2013; Tang et al. 2019; Shi et al. 2014). They both form a helical bundled structure with two subdomains connected by a long helix and stabilized by another long C-terminal extended loop. The only subtle difference between yeast and mammalian GTDs comes from the subdomain I. The two termini in mammalian GTD form antiparallel β-strands, whereas those in yeast GTD form antiparallel α-helices (Fig. 3.2) (Wei et al. 2013).

A few binding sites have been identified in mammalian GTDs by structural studies (Fig. 3.2b, c). The most frequently used binding site is located at subdomain I between α4 and α7 and binds to the so-called GTBM (globular tail-binding motif) from a number of proteins. These proteins include melanophilin (MLPH, related to melanosome transport), granuphilin (Gran, related to secretory granules transport) and spire homolog 1/2 (Spir1/2, an actin nucleator) (Pylypenko et al. 2013, 2016; Wei et al. 2013). Though with slightly different detailed binding modes, the structures of Myo5a/MLPH and Myo5a/Spir2 complexes reveal a common feature required for specific GTBM/GTD interaction (Pylypenko et al. 2016): a few hydrophobic residues sandwiched by positively- and

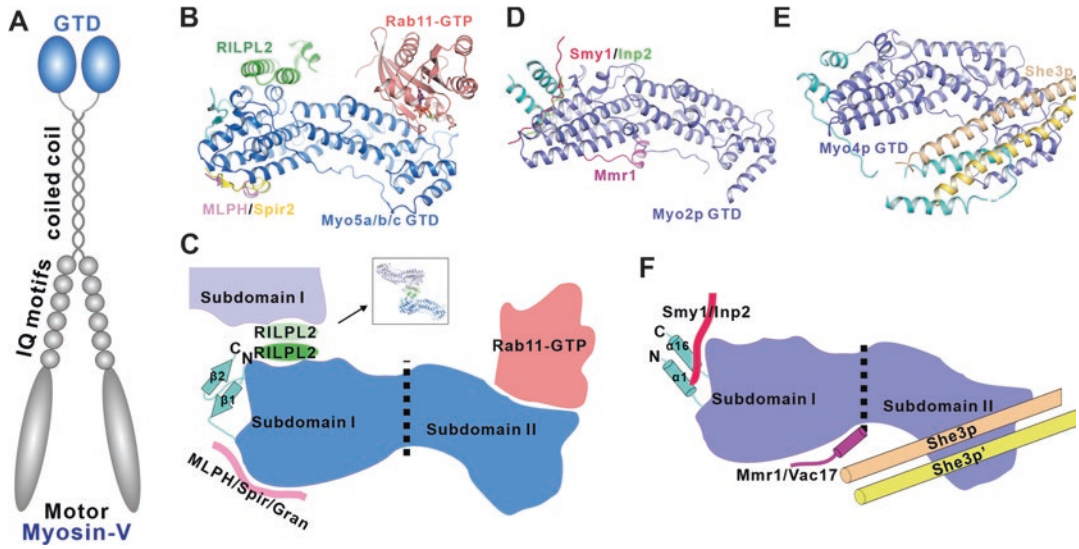

Fig. 3.2 Myosin-V GTD can recognize diverse cargoes. (**a**) Domain architecture of Myosin-V. (**b**) Structures of Myo5a/Myo5b GTD in complex with MLPH (PDB: 4KP3), Spir2 (PDB: 5JCY), RILPL2 (PDB: 4KP3) and GTP bound Rab11 (PDB: 4LWZ). The GTDs in these structures are aligned together and only the one in PDB: 4KP3 is shown for simplicity. (**c**) Schematic model showing the positions of three cargo binding sites in Myo5a/Myo5b/Myo5c. (**d**) Structures of yeast Myo2p GTD in complex with MIS of Smy1 (PDB: 6IXQ), Inp2 (PDB: 6IXR) and Mmr1 (PDB: 6IXP). The GTDs in these structures are aligned together and only the one in PDB: 6IXP is shown for simplicity. (**e**) Structures of yeast Myo4p GTD in complex with She3p (PDB: 4LL8). (**f**) Schematic model showing the positions of three cargo binding sites in yeast Myo2p/Myo4p

negatively-charged residues in the N- and C-termini, respectively. Another binding site located at subdomain I, on the opposite side of the GTBM binding site, is responsible for RILPL2 (Rab interacting lysosomal protein-like 2) binding (Wei et al. 2013). RILPL2 is also a binding partner of vesicle adaptor Rab protein (Cantalupo et al. 2001). Biochemical and structural studies showed that RILPL2 coiled-coil region can form a 2:2 complex with GTD of Myo5a but not Myo5b or Myo5c, and dimerization of RILPL2 is indispensable for complex formation (Wei et al. 2013). Besides the recognition of Rab-binding partners, mammalian myosin-V can also directly bind to Rab proteins. High-resolution structures show that both GDP- and GTP-bound Rab11 bind to Myo5a/Myo5b GTD subdomain II (Pylypenko et al. 2013, 2016), the only binding located in subdomain II that has currently been identified.

The cargo recognition mechanisms of yeast Myo2p/Myo4p GTD are also extensively studied (Shi et al. 2014; Tang et al. 2019), and three binding sites have been revealed (Fig. 3.2d–f). One is found in Myo2p GTD subdomain I shared by the MIS (Myo2-interacting site) of Smy1 and Inp2, which are cargo proteins for polarization of secretory vesicles and peroxisome transport, respectively (Tang et al. 2019). The yeast GTD-specific antiparallel helices (α1/α16) are critical for adopting the extended structures of Smy1/Inp2 MIS. The structure of Myo2p in complex with Mmr1 (mitochondria receptor Myo2 receptor-related protein 1) reveals another binding site in Myo2p GTD (Tang et al. 2019). Although with no high-resolution complex structure available, mutagenesis experiments confirmed that this binding site is shared by another cargo protein called Vac17, a vacuole-related protein. The third binding site is for Myo4p to recognize She3p (swi5p-dependent HO expression 3), a protein that links Myo4p to messenger ribonucleoprotein particles (mRNPs) (Shi et al. 2014). The coiled-coil dimer of She3p binds to Myo4p GTD at subdomain II, forming a 2:1 complex (Fig. 3.2e).

Interestingly, there is little overlap between the binding sites identified in mammalian Myo5a/Myo5b/Myo5c and yeast Myo2p/Myo4p. These findings highlight the extremely high capacity of myosin-V to recognize a large number of cargoes. Moreover, the distinct binding sites in yeast and mammalian myosin-V may also suggest that motor/cargo proteins coevolve with each other during evolution.

3.2.2 Myosin VI Contains Two Regions for Cargo Binding

The myosin-VI subfamily contains only one member, Myo6 (Buss et al. 2004). In contrast to the other unconventional myosins, which travel towards the plus end of actin filaments, Myo6 is the only one that moves to the minus end due to a specific insertion in its motor domain (Wells et al. 1999; Rock et al. 2001; Menetrey et al. 2005). The tail of Myo6 contains two consecutively arranged regions for cargo binding: an N-terminal helical cargo-binding domain (HCBD) and a more distal C-terminal cargo binding domain (CBD) (Fig. 3.3a).

The Myo6 CBD is of great interest as it has been shown to undergo cargo binding-induced dimerization (Spudich et al. 2007; Yu et al. 2009). The cargo-free form of Myo6 CBD exists as a stable monomer as shown by biochemical and structural studies. Unexpectedly, binding to the monomeric cargo protein Dab2 (Disabled homolog 2, an endocytic adaptor protein) converts both molecules into a stable 2:2 complex (Fig. 3.3b) (Yu et al. 2009). In this complex structure, no direct contacts are observed between the two Myo6 CBDs, suggesting that CBD dimerization is solely mediated by its cargo adaptor Dab2. This cargo-induced dimerization is suggested to be a possible mechanism to facilitate the processive movement along actin filaments towards the minus end. Other reported cargoes of Myo6 CBD like LMTK2 (Lemur tyrosine kinase 2) are not known to dimerize the motor (Chibalina et al. 2007). Therefore, Myo6, upon binding to these

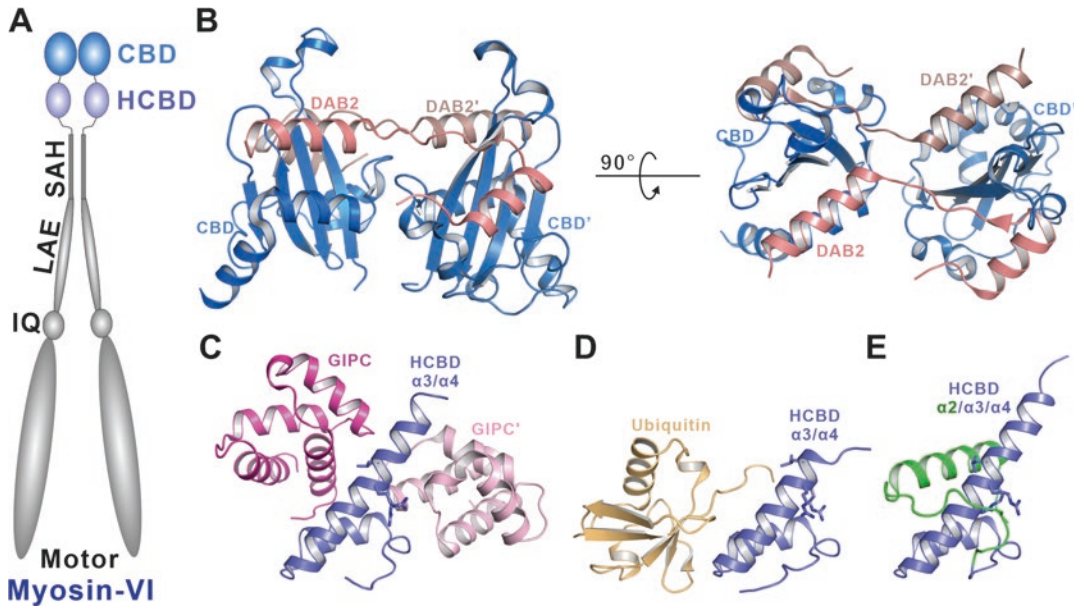

Fig. 3.3 Cargo recognition mechanisms of Myo6 CBD and HCBD. (**a**) Domain architecture of Myosin-VI. (**b**) Structure of Myo6 CBD/Dab2 complex (PDB: 3H8D) showing the cargo binding induced formation of 2:2 complex. (**c**) Structure of Myo6 HCBD/GIPC complex (PDB: 5V6E) showing the potential of oligomer formation. (**d**) NMR structure model of Myo6 HCBD/Ubiquitin complex (PDB: 2N13) showing that the Ubiquitin binding site overlaps with the GIPC binding site in HCBD. (**e**) NMR structure model of long isoforms of Myo6 HCBD (PDB: 2N12) showing that α2 helix sterically hinders the binding of GIPC/Ubiquitin

cargoes, may not function as a dimeric processive transporter but a monomeric tether.

Great research interests have been developed focusing on a region of ~130 residues located between the CBD and the putative SAH (He et al. 2016; Wollscheid et al. 2016; Shang et al. 2017; Hu et al. 2018). This region is composed of five α-helices, thus here referred to as HCBD. The α-helix immediately preceding the CBD contains an Arg-Arg-Leu ("RRL") motif which is important for binding to NDP52 (nuclear dot protein 52), TAX1BP1 (TRAF6-binding protein), OPTN (optineurin) and GIPC (GAIP-interacting protein C terminus) (Sahlender et al. 2005; Morriswood et al. 2007; Spudich et al. 2007). Crystal structures of Myo6/GIPC1 and Myo6/GIPC2 complexes reveal a higher order oligomerization state of the complex (Shang et al. 2017), mediated by two interfaces between Myo6 HCBD and GIPCs GH2 domains (Fig. 3.3c). The previously identified "RRL" motif is involved in both interfaces. This oligomeric complex formation provides an explanation of how GIPC1 and Myo6 can cluster cell surface receptors into clathrin-coated pits (Hasson 2003). The same HCBD region can also bind to K63-linked ubiquitin, as shown by the NMR (nuclear magnetic resonance) structure of Myo6/K63-ubiquitin complex (Fig. 3.3d) (He et al. 2016). The Myo6/K63-ubiquitin interface partially overlaps with one of the Myo6/GIPCs interfaces, suggesting that the binding is mutually exclusive. Although with no high-resolution structures, it is expected that Myo6 HCBD will adopt a similar conformation to recognize other binders like NDP52, TAX1BP1 and OPTN; and all these binders may also be mutually exclusive (He et al. 2016; Shang et al. 2017; Hu et al. 2018).

Alternative splicing adds to the complexity of the cargo-recognition mechanism of Myo6 HCBD. Myo6 CBD has 3 isoforms: the α2-containing long isoforms 1 and 3, and the α2-missing short isoform 2 (Buss et al. 2001; Tomatis et al. 2013; Wollscheid et al. 2016). These splicing variants have different cargo-binding specificities: the longer isoforms can bind to clathrin via α2, whereas the short isoform binds to GIPCs, NDP52, TAX1BP1 and OPTN. More interestingly, although the long isoforms also contain the "RRL" motif, they are unable to bind the latter four cargoes. Comparing the atomic structures of the longer Myo6 HCBD isoform and the Myo6 HCBD/cargo complex, it is clearly demonstrated that the additional α2 helix sterically hinders K63-ubiquitin or GIPCs binding (Fig. 3.3e). This thus provides the structural basis for differential cargo selection between the long and short isoforms (He et al. 2016; Wollscheid et al. 2016; Shang et al. 2017).

3.2.3 Diverse Cargo Recognition Mechanisms of MyTH4-FERM Tandem Containing Myosins

Another group of unconventional myosins contain MyTH4-FERM tandems in their tails. MyTH4-FERM containing myosins are also widespread in the eukaryotic kingdom and can even be found in unicellular amoebae of *Dictyostelium discoideum* (Dd) (Foth et al. 2006; Petersen et al. 2016; Planelles-Herrero et al. 2016; Kollmar 2006; Weck et al. 2017). Three subfamilies are found in humans: myosin-VII (Myo7a and Myo7b), myosin-X and myosin-XV. These myosins are characterized by the MyTH4-FERM tandem, a supramodule formed by a MyTH4 domain and a FERM domain. MyTH4 domain is found not only in myosins but also in several other proteins such as PLEKHH (pleckstrin homology domain-containing family H, also known as MAX-1) (Huang et al. 2002), ArhGAP39 (Rho GTPase-activating protein 39) (Lundstrom et al. 2004), as well as a plant kinesin KCBP (kinesin-like calmodulin binding protein) (Reddy and Reddy 1999), but the function of this domain is not yet clearly understood. The FERM domain is a well-studied protein-protein interaction module and is found in many proteins including a number of cytoskeletal-associated proteins like ezrin, talin, etc., (Chishti et al. 1998; Tepass 2009; Frame et al. 2010; Moleirinho et al. 2013).

The myosin-VII subfamily comprises the first identified MyTH4-FERM-containing myosins (Gibson et al. 1995; Hasson et al. 1995; Well et al. 1995, 1996). Mutations in the Myo7a gene are closely related to an inherited disease called Usher Syndrome. Patients with Usher Syndrome suffer from blindness and deafness. There are

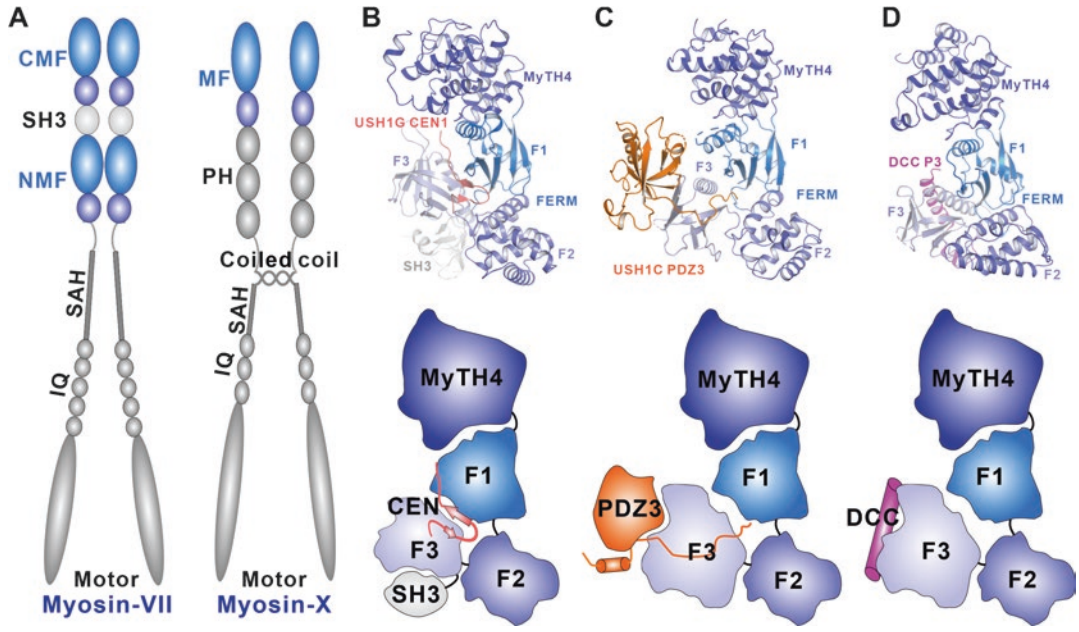

Fig. 3.4 Diverse cargo recognition mechanisms of MyTH4-FERM tandems in unconventional myosins. (**a**) Domain architectures of Myosin-VII (left) and Myosin-X (right). (**b**–**d**) Structures (top) and schematic models (bottom) of Myo7a/USH1G complex (PDB: 3PVL, *panel* **b**), Myo7b/USH1C complex (PDB: 5XBF, *panel* **c**) and Myo10/DCC complex (PDB: 3PZD, *panel* **d**)

two vertebrate paralogs in the myosin-VII subfamily, namely Myo7a and Myo7b (Chen et al. 2001). Both members have a pair of MyTH4-FERM tandems in their tails with a SH3 domain in between (Fig. 3.4a, left). Recent studies have demonstrated that both motors are essential for the development and maintenance of actin-based protrusions (Myo7a in hair cell stereocilia and Myo7b in brush border microvilli) (Lefevre et al. 2008; Crawley et al. 2014). They are both central components of the tip-link complexes by binding to the CEN region of USH1G/ANKS4B using their N-terminal MyTH4-FERM (NMF) and to the PDZ3 domain of USH1C using their C-terminal MyTH4-FERM domain (CMF) (Wu et al. 2011; Crawley et al. 2014, 2016 Li et al. 2016a, 2017; Yu et al. 2017). Structures of Myo7a NMF/USH1G CEN and Myo7b NMF/ANKS4B CEN complexes reveal an unexpected binding mode for FERM domains (Fig. 3.4b). The N-terminal part of the CEN region (CEN1) in USH1G/ANKS4B snugly sits in the center of the clover-leaf-shaped FERM domain, making contacts with all three lobes. And the C-terminal part of the CEN region (CEN2) is proposed to bind to a positively-charged surface within the MyTH4 domain, as suggested by the sparse densities in electron density maps of both complex structures (Wu et al. 2011; Li et al. 2016a). Binding of CEN2 to the MyTH4 domain is the only structural evidence showing that the MyTH4 domain can serve as a protein-binding module. The CMFs of Myo7a/Myo7b also use the clover-leaf center in their FERM domain for protein binding as shown by the high-resolution structures of Myo7a/USH1C and Myo7b/USH1C complexes (Fig. 3.4c) (Li et al. 2017; Yu et al. 2017). The very C-terminal tail of USH1C inserts into a positively-charged pocket formed by the three lobes. In addition, the PDZ3 domain of USH1C loosely attaches onto the F3 lobe of CMF. Both the NMF- and CMF-mediated interactions, together with the extremely strong association between USH1C and USH1G/ANKS4B (K_d of 1–3 nM), are believed to stabilize the Myo7a/USH1C/USH1G and Myo7b/USH1C/ANKS4B tripartite complexes and contribute to the proper function of stereocilia and microvilli.

The tail of Myo15 is structurally homologous to that of myosin-VII where a pair of MyTH4-FERM tandems are separated by a SH3 domain (Liang et al. 1999), although there is a ~370-residue insertion within the F1 domain of myosin-XV NMF. Not only are the domain organizations similar, these two motors also share similar functions. Myo7a together with its binding partners USH1G and USH1C forms the upper tip-link density (UTLD) in stereocilia, a protein dense region at the base of the tip-link (Bahloul et al. 2010; Grati and Kachar 2011). On the other end of the tip-link at the adjacent stereocilium, there is another protein dense region called the lower tip-link density (LTLD) (Furness and Hackney 1985; Kachar et al. 2000). It is reported that Myo15, whirlin and Eps8 interact with each other in this region (Manor et al. 2011; Zampini et al. 2011). Whirlin and USH1C are both multiple PDZ domain containing scaffold proteins (Verpy et al. 2000; Mburu et al. 2003). Given the high similarity in the two components, it will be interesting to know whether the structural organization of Myo15/Whirlin/Eps8 tripartite complex resembles that of Myo7a/USH1C/USH1G or Myo7b/USH1C/ANKS4B.

Myo10 differs from the other MyTH4-FERM-containing myosins in that it only contains one MyTH4-FERM tandem (Fig. 3.4a, right). Despite this difference, Myo10 is also reported to be enriched in actin-based protrusions especially filopodial structures in various tissues, and it plays important roles in many developmental processes such as neurogenesis and angiogenesis (Kerber and Cheney 2011). Like the MyTH4-FERM tandems in Myo7a/Myo7b, Myo10 MyTH4-FERM serves as a cargo-binding domain. Myo10 MyTH4-FERM can bind to the axon guidance receptor DCC (deleted in colorectal cancer) and regulate axon pathfinding in neurons. In the crystal structure of Myo10/DCC complex (Hirano et al. 2011; Wei et al. 2011), the C-terminal tail of DCC forms a short helix and binds to the α/β groove of the FERM domain F3 lobe, representing a novel target recognition mode of the FERM domain (Fig. 3.4d). It is noted that, this α/β groove is used in other FERM/targets binding. For example, the FERM domains from ERM family members (Ezrin/Radixin/Moesin) bind to a β-strand forming a "GTY" motif, as seen in the structures of Radixin/ICAM-2 and Moesin/Crumbs (Hamada et al. 2003; Wei et al. 2015); the Merlin FERM domain uses this groove to interact with the β-hairpin of DCAF FBD (FERM-binding domain) (Li et al. 2014). Myo10 MyTH4-FERM has also been implicated in the binding of other targets. Co-sedimentation and pull-down experiments concluded that the MyTH4 domain is required for microtubule binding mainly through charge-charge interactions provided by the positively-charged surface of MyTH4 domain and the acidic tails of α- and β-tubulins (Hirano et al. 2011; Planelles-Herrero et al. 2016); pull-down assay showed that the FERM domain is sufficient to bind the cytoplasmic tail of β5 integrin (Hirano et al. 2011). High-resolution structures will be needed to illustrate the molecular basis of these interactions.

Atomic structures of these MyTH4-FERM domains alone or in complex with their cargoes in the past decade have greatly advanced our understanding of this special group of myosins. By comparing all the structures of MyTH4-FERM, noticeable subdomain movements are present, although the overall architectures are more or less the same. This is likely due to the relatively low sequence homology between different MyTH4-FERM domains (20%–30% sequence identities). The differences in relative subdomain positions and presence of amino acids on exposed surfaces may dictate the diverse target recognition modes.

3.2.4 Myosin-IX Contains an Enzymatically Active RhoGAP Domain for Small GTPase RhoA

Myosin-IX and myosin-III are special because they both contain another enzymatically-active domain in addition to the motor domain and are therefore known as motorized signaling molecules (Bahler 2000). Myosin-IX subfamily members contain a RhoGAP (GTPase-activating pro-

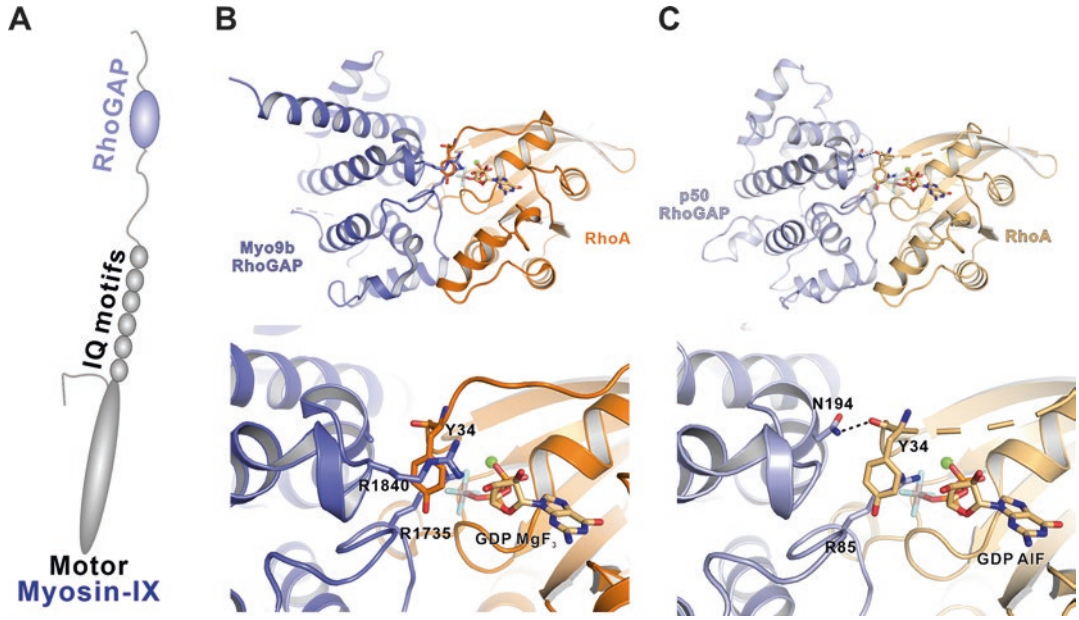

Fig. 3.5 Myosin-IX RhoGAP domain uses an unusual mechanism to catalyze small GTPase RhoA hydrolysis. (**a**) Domain architecture of Myosin-IX. (**b**) Structure of Myo9b/RhoA complex (PDB: 5HPY) showing the dual arginine fingers catalytic mechanism. (**c**) Structure of P50-RhoGAP/RhoA complex (PDB: 1TX4) showing the canonical catalytic mechanism

tein for Rho GTPases) domain, while members of the myosin-III subfamily contain a kinase domain.

The vertebrate myosin-IX subfamily contains two members, Myo9a and Myo9b (Reinhard et al. 1995; Chieregatti et al. 1998). The RhoGAP domain in their tails has been shown to promote GTP hydrolysis of the small GTPase RhoA (Fig. 3.5a, b) (Wirth et al. 1996), and thus converts it from an active GTP-bound state to an inactive GDP-bound state. RhoA is an important modulator of the actin cytoskeleton (Etienne-Manneville and Hall 2002), and Myo9a/Myo9b have been implicated to function in actin filament dynamics (van den Boom et al. 2007; Saczko-Brack et al. 2016). Myo9a is highly expressed in developing and adult brain tissues and plays roles in regulating neuronal morphology and function. Defects in Myo9a are associated with neurological diseases like the congenital myasthenic syndromes (O'Connor et al. 2016). Myo9b is detected in many different tissues including lung, liver, spleen, as well as the immune system. Myo9b is related to a number of immune disorders such as celiac disease and inflammatory bowel disease (Nunez et al. 2007). And it has recently been reported to be involved in Slit/ROBO signaling-mediated lung cancer suppression by interacting with the intracellular domain of ROBO (Kong et al. 2015). The function of the myosin-IX RhoGAP domain on RhoA is conserved during evolution. HUM-7, the *C. elegans* homolog of myosin-IX, was recently reported to modulate RHO-1 (the ortholog of RhoA in *C. elegans*) in embryonic morphogenesis (Wallace et al. 2018).

The catalytic activity of the RhoA GAP domain usually requires an arginine finger and a conserved auxiliary asparagine (Fig. 3.5c). The arginine finger inserts into the nucleotide-binding pocket as well as binds to the P-loop, and is thus essential for GAP activity. The auxiliary asparagine is another conserved polar residue in the majority of RhoGAP domains. It stabilizes the effector loop by making a hydrogen bond with the backbone of a tyrosine residue (Tyr34 in RhoA) from switch I (Rittinger et al. 1997a, b).

However, the absence of this conserved auxiliary asparagine residue in the Myo9a/Myo9b RhoGAP domain is contradictory to the well-characterized GAP activity towards RhoA, indicating that there must be an unknown catalytic mechanism for this RhoGAP domain. The structure of the Myo9b/RhoA complex elicits how this works (Fig. 3.5b) (Yi et al. 2016). The arginine finger performs a similar function in Myo9b RhoGAP. Surprisingly, although the asparagine residue is missing, another arginine residue interacts with the aromatic ring of Tyr34 to stabilize the switch I loop, compensating the function of the canonical asparagine. Therefore, this dual-arginine-finger mechanism enables the enzyme to accelerate RhoA GTP hydrolysis.

3.2.5 Myosin-III Uses the Intrinsically Disordered Sequences for Cargo Binding

Myosin-III is another enzymatic myosin. It contains an evolutionary-conserved Ser/Thr kinase domain at its very N-terminus, preceding the motor domain. It was reported that the kinase domain can regulate the ATPase activity by autophosphorylating the motor domain. The first myosin-III called NinaC (neither inactivation nor afterpotential C) was identified in *Drosophila* photoreceptors by genetic screening for essential genes involved in phototransduction (Montell and Rubin 1988). Myo3a and Myo3b, expressed mainly in vertebrate retina and cochlea, are the two members of the vertebrate myosin-III subfamily and have partially redundant functions in vertebrate visual and auditory systems (Dose and Burnside 2000).

In contrast to the above-mentioned unconventional myosins that contain well-folded domains in the tails, no folded domains are predicted to exist in the tails of NinaC, Myo3a and Myo3b (Fig. 3.6a). Instead, these tails are predicted to be intrinsically disordered. Nevertheless, vertebrate Myo3a/Myo3b still shares a highly-conserved stretch of sequences known as THDI (tail homology domain I), which is later confirmed to interact with an actin-bundling protein, Espin1 (Dose et al. 2003; Salles et al. 2009; Merritt et al. 2012). Besides, there are two other conserved regions specific in Myo3a, one N-terminal to THDI and responsible for MORN4 binding, and the other at the very C-terminus (referred to as THDII, tail homology domain II) and responsible for direct actin binding (thus also known as ABM, actin binding motif) (Fig. 3.6a).

Sequence analysis and structural characterizations together demonstrate that the THDI in Myo3a/Myo3b tails contains a pair of consecutive motifs capable of strongly binding to Espin1 ANK repeats (Liu et al. 2016). Espin1 is encoded by the gene *Espin*, the isoforms of which are shown to be expressed in a number of F-actin rich protrusions like hair cell stereocilia, brush border microvilli and Purkinje cell dendritic spines (Bartles et al. 1996). All these isoforms can use their common C-terminal actin bundling domain (ABD) to bundle actin filaments. Espin1 is the longest isoform that contains N-terminal ANK repeats, a well-known protein binding module. The binding of ARB1&2 motifs of Myo3a/Myo3b results in a Myo3a/Myo3b:$(Espin1)_2$ complex. Each motif forms an extended structure and lies in the inner groove of the ANK repeats (Fig. 3.6b, c), a binding mode that is also seen in other ANK repeats/targets binding such as Ankyrin R/B/G, RFXANK (Xu et al. 2012; Wang et al. 2014). Fluorescence imaging-based studies and transmission electron microscopy (TEM) studies demonstrate that the cross-linking of Espin1 by the two repeating motifs of Myo3a/Myo3b significantly promote the actin bundling activity of Espin1, leading to higher-order bundles (Liu et al. 2016).

In addition to THDI, Myo3a specifically contains another highly conserved region that can bind strongly to MORN4 (referred to as MBD for MORN4 binding domain) (Mecklenburg et al. 2015). MORN4 contains four MORN repeats, which were named after their proposed function as "Membrane Occupation and Recognition Nexus" when first found in the pro-

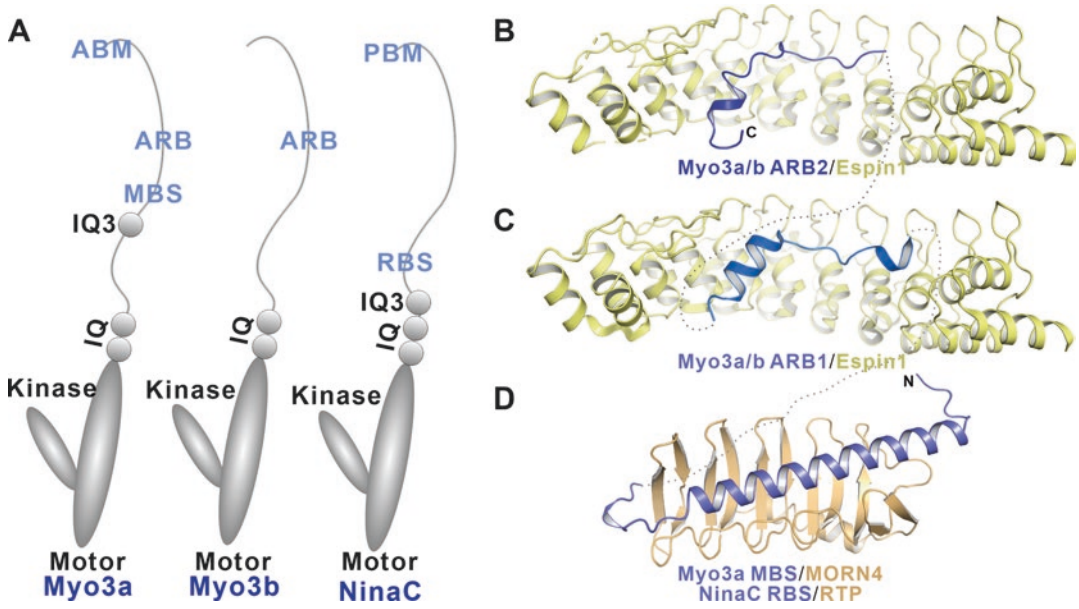

Fig. 3.6 Myosin-III subfamily bind to their cargoes using their intrinsically disordered tails. (**a**) Domain architectures of Myosin-III subfamily showing the intrinsically disordered tails. (**b**, **c**) Structures of the two consecutive ARBs (ARB1, PDB: 5ET1, *panel* **b**; ARB2, PDB: 5ET0, *panel* **c**) of Myo3b in complex with Espin1 ANK repeats. (**d**) Structure of Myo3a MBD/MORN4 complex (PDB: 6JLE) showing that MORN4 uses the conserved U-shaped groove to interact with Myo3a

tein junctophilin (Takeshima et al. 2000). The structure of Myo3a/MORN4 complex reveals that Myo3a MBD forms an elongated α-helix to interact with the hydrophobic U-shaped groove of the single-layered β-sheet formed by the MORN repeats of MORN4 (Fig. 3.6d) (Li et al. 2019). Consistently, biochemical and structural characterizations show that NinaC and Retinophilin (RTP), the *Drosophila* orthologs of Myo3a and MORN4, form a tightly-associated complex (Mecklenburg et al. 2010; Venkatachalam et al. 2010), although there is only very low sequence homology between Myo3a MBD and NinaC RBD (short for RTP binding domain). This structural finding implies that MORN repeats from other proteins like SETD7 (a lysine methyltransferase) and junctophilins (the tethering proteins between the plasma membrane and sarcoplasmic/endoplasmic reticulum membranes) may also be used to bind to their target proteins to execute their distinct functions (Takeshima et al. 2000; Wilson et al. 2002).

3.2.6 Myosins Can Target to Plasma Membranes or Vesicles via Direct Lipid Binding

In addition to protein cargoes, some myosins can also directly bind to lipid molecules. Examples include the three consecutive PH domains in class X myosins and the extended PH domain in class I myosins (Fig. 3.7a).

N-terminal to the MyTH4-FERM tandem in Myo10's tail are three PH domains arranged in an unusual way. The first PH domain is split into two halves in the β3/β4 loop by the second PH domain. Split PH domain arrangements are also seen in proteins like α-syntrophin, phospholipase Cγ and Rho kinase, etc. (Yan et al. 2005, 2008; Wen et al. 2006). The Myo10 $PH1_N$-PH2-$PH1_C$ forms a structural supramodule as shown by its crystal structure (Fig. 3.7b) (Lu et al. 2011). Biochemical data together with structural analysis confirm that the PH2 domain can specifically bind to phosphatidylinositol (3,4,5)-triphosphate [$PI(3,4,5)P_3$], whereas the PH1 domain displays

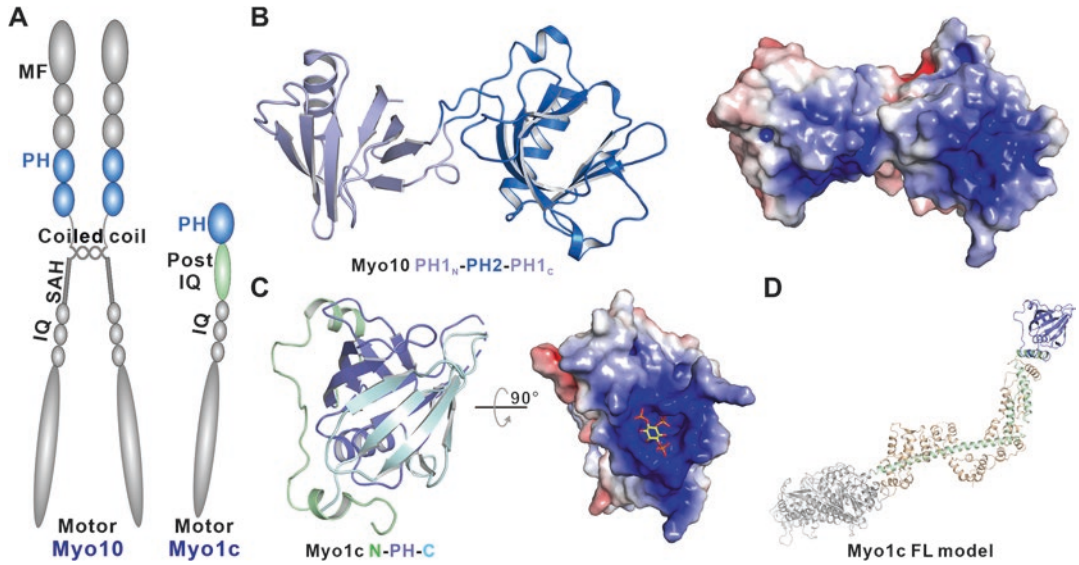

Fig. 3.7 Myosin-X and Myosin-I can bind to phospholipid with their PH domains. (**a**) Domain architectures of Myosin-X (left) and Myosin-I (right) showing the positions of PH domains in their tails. (**b**) Ribbon representation and surface electrostatic potential of the Myo10 $PH1_N$-PH2-$PH1_C$ structure (PDB: 3TFM) showing the supramodule formation of the split PH domains for synergistic lipid binding. (**c**) Ribbon representation and surface electrostatic potential of the extended PH domain in Myo1c (PDB: 4R8G). The PI(4,5)P is modeled to indicate the phospholipid binding pocket. (**d**) Ribbon diagram of a modeled full-length Myo1c structure in complex with three copies of CaM. The full-length structure was generated by combining the structure of the Myo1b motor domain (PDB: 4L79) and the structure of the Myo1c neck-tail domain (PDB: 4R8G)

no specificity for lipid molecules. More interestingly, the crystal structure shows that the lipid-binding pockets of PH1 and PH2 face the same site, supporting a model in which PH2 is responsible for specifically selecting $PI(3,4,5)P_3$ while PH1 functions to enhance the avidity of the tandem. This selective and strong lipid binding makes Myo10 a faithful interpreter of PI3 kinase activation signals. Together with its ability to bind other transmembrane receptors (e.g., netrin receptor DCC, integrin) by the C-terminal MyTH4-FERM tandem (Hirano et al. 2011; Wei et al. 2011), Myo10 can integrate both signals in regulating its cellular localization and motor activities and play a critical role in biological processes like promoting filopodia elongation (Kerber and Cheney 2011).

Myosin-I is another subfamily of unconventional myosins that contains a PH domain in its C-terminal tail. The myosin-I subfamily was the first unconventional myosin subfamily to be identified and has been shown to be single headed (Pollard and Korn 1973), in sharp contrast to conventional myosin-II. Myosin-I is the largest unconventional myosin subfamily and humans contain eight members (McIntosh and Ostap 2016). These members are involved in numerous physiological processes. For example, Myo1a is important in brush border microvilli assembly (Tyska et al. 2005); Myo1b participates in intracellular trafficking by regulating membrane remodeling in the *trans*-Golgi network (Almeida et al. 2011); Myo1c plays roles in sound perception, glucose uptake, podocyte formation and polarity maintenance in epithelial cells (Bose et al. 2002; Holt et al. 2002; Arif et al. 2011; Fan et al. 2012; Tiwari et al. 2013; Tokuo and Coluccio 2013); Myo1d is critical in left-right axis determination during development (Juan et al. 2018; Saydmohammed et al. 2018; Tingler et al. 2018); and Myo1e, Myo1f, and Myo1g have been shown to be essential in the immune system (Giron-Perez et al. 2019). The study of the lipid-binding properties of myosins-I dates back nearly 30 years (Adams and Pollard 1989; Miyata et al. 1989; Hayden et al. 1990), but the

existence of PH domains was not recognized until 2006 (Hokanson et al. 2006). The crystal structure of the entire neck-tail region of Myo1c in complex with calmodulin (CaM) clearly confirms that the C-terminus of Myo1c contains an extended PH domain, i.e., a canonical PH-domain fold with an N-terminal α-helical and C-terminal β-sheet extension (Fig. 3.7c) (Lu et al. 2015). This extended PH domain is tightly associated with the CaM bound post-IQ region, making the entire tail of Myo1c an integrated structural unit. Unlike Myo10 PH2, the Myo1c PH domain is not a lipid-specific binder but has preferences towards phospholipids with phosphates at the 4- or 5-position (Hokanson and Ostap 2006). Moreover, structural studies demonstrate that its lipid-binding pocket is fully accessible to lipid membrane, with no steric hindrance by the extensions. The role of the extension sequence is still unknown, but it can possibly serve as a protein cargo-binding site given the high sequence conservation during evolution.

As a single-headed myosin, it is unclear whether Myo1c can act as a cargo transporter along actin filament. Combining the high-resolution structures of the motor domain and the entire neck-tail region of Myo1c gives us an opportunity to build the first atomic model of full length Myo1c (Munnich et al. 2014; Shuman et al. 2014; Lu et al. 2015). The model suggests that Myo1c adopts a rigid conformation (Fig. 3.7d). With its C-terminal PH domain binding to lipid membrane and N-terminal motor domain binding to actin filament, we propose that Myo1c may serve as a molecular tether to bridge the plasma membrane and the cytoskeleton. More intriguingly, structural and biochemical data suggest that when the Ca^{2+} concentration is increased (e.g., the cells are stimulated), CaM binding on Myo1c leads to a dramatic structural rearrangement whereby the neck and post-IQ region becomes unstructured. The loss of rigidity induced by the increase in Ca^{2+} concentration will further lower the mechanical load of the motor, and finally lead to the dissociation of the motor from actin filaments (McConnell and Tyska 2010; Lu et al. 2015). This then breaks the linkage between the plasma membrane and the cytoskeleton and eventually releases tension, a process probably related to the adaptation mechanism in the hair cells of our auditory system (Gillespie and Muller 2009; Batters et al. 2004).

3.3 Conclusions and Perspectives

Due to the structural and biochemical studies in the most recent 10 years, our understanding of the cargo-recognition mechanisms of unconventional myosins has reached an unprecedented level. For the majority of human unconventional myosins, we already have atomic structures of the cargo-binding domains either alone or with at least one cargo bound. Even for some myosins, the structures of the cargo-binding domain in complex with various cargoes (e.g., myosin-V) are also available. We believe that the number of structures will continue growing.

Now with more and more structural information in hand, research into myosin cargo binding will reach another level. Cargo binding is precisely regulated to achieve the highly organized motion in cellular environment. Research is needed to understand how reversible cargo loading and unloading is regulated at certain times and locations. Moreover, accumulating evidence shows that cargo binding is not a passive behavior but can actively affect the motor. For example, myosin-V is reported to be autoinhibited when no cargo is loaded. Binding to cargoes like MLPH can release its autoinhibition and thus activate the motor. Such cargo binding-induced activation may also exist in other myosins such as Myo7a, Myo10. Elucidating how these myosins are autoinhibited and how cargo binding can release the autoinhibition will be another direction to follow in the future. Another exciting direction of future research is to further understand the mechanistic basis of diseases caused by mutations of myosins and to search for therapeutic methods for treating these diseases.

Acknowledgments We thank Dr. Zhe Feng of the M. Z. laboratory for critical reading and editing. Research described in this work from our laboratory was supported

by grants from RGC of Hong Kong (16149516 and many completed ones) to M.Z. We thank many of our past members of the laboratory for their contributions to the work described in this piece. We apologize to the authors whose papers have not been cited due to limited space of this review chapter. M.Z. is a Kerry Holdings Professor in Science and a Senior Fellow of IAS at HKUST.

References

Adams RJ, Pollard TD (1989) Binding of myosin-I to membrane-lipids. Nature 340(6234):565–568. https://doi.org/10.1038/340565a0

Almeida CG, Yamada A, Tenza D, Louvard D, Raposo G, Coudrier E (2011) Myosin 1b promotes the formation of post-Golgi carriers by regulating actin assembly and membrane remodelling at the trans-Golgi network. Nat Cell Biol 13(7):779–789. https://doi.org/10.1038/ncb2262

Arif E, Wagner MC, Johnstone DB, Wong HN, George B, Pruthi PA, Lazzara MJ, Nihalani D (2011) Motor protein Myo1c is a podocyte protein that facilitates the transport of slit diaphragm protein Neph1 to the podocyte membrane. Mol Cell Biol 31(10):2134–2150. https://doi.org/10.1128/MCB.05051-11

Bahler M (2000) Are class III and class IX myosins motorized signalling molecules? Biochim Biophys Acta 1496(1):52–59. https://doi.org/10.1016/S0167-4889(00)00008-2

Bahloul A, Michel V, Hardelin JP, Nouaille S, Hoos S, Houdusse A, England P, Petit C (2010) Cadherin-23, myosin VIIa and harmonin, encoded by Usher syndrome type I genes, form a ternary complex and interact with membrane phospholipids. Hum Mol Genet 19(18):3557–3565. https://doi.org/10.1093/hmg/ddq271

Bartles JR, Wierda A, Zheng L (1996) Identification and characterization of espin, an actin-binding protein localized to the F-actin-rich junctional plaques of Sertoli cell ectoplasmic specializations. J Cell Sci 109(Pt 6):1229–1239

Batters C, Arthur CP, Lin A, Porter J, Geeves MA, Milligan RA, Molloy JE, Coluccio LM (2004) Myo1c is designed for the adaptation response in the inner ear. EMBO J 23(7):1433–1440. https://doi.org/10.1038/sj.emboj.7600169

Belyantseva IA, Boger ET, Naz S, Frolenkov GI, Sellers JR, Ahmed ZM, Griffith AJ, Friedman TB (2005) Myosin-XVa is required for tip localization of whirlin and differential elongation of hair-cell stereocilia. Nat Cell Biol 7(2):148–156. https://doi.org/10.1038/ncb1219

Berg JS, Cheney RE (2002) Myosin-X is an unconventional myosin that undergoes intrafilopodial motility. Nat Cell Biol 4(3):246–250. https://doi.org/10.1038/ncb762

Berg JS, Powell BC, Cheney RE (2001) A millennial myosin census. Mol Biol Cell 12(4):780–794. https://doi.org/10.1091/mbc.12.4.780

Block SM (1996) Fifty ways to love your lever: myosin motors. Cell 87(2):151–157. https://doi.org/10.1016/S0092-8674(00)81332-X

Bose A, Guilherme A, Robida SI, Nicoloro SMC, Zhou QL, Jiang ZY, Pomerleau DP, Czech MP (2002) Glucose transporter recycling in response to insulin is facilitated by myosin Myo1c. Nature 420(6917):821–824. https://doi.org/10.1038/Nature01246

Buss F, Arden SD, Lindsay M, Luzio JP, Kendrick-Jones J (2001) Myosin VI isoform localized to clathrin-coated vesicles with a role in clathrin-mediated endocytosis. EMBO J 20(14):3676–3684. https://doi.org/10.1093/emboj/20.14.3676

Buss F, Spudich G, Kendrick-Jones J (2004) Myosin VI: cellular functions and motor properties. Annu Rev Cell Dev Biol 20:649–676. https://doi.org/10.1146/annurev.cellbio.20.012103.094243

Cantalupo G, Alifano P, Roberti V, Bruni CB, Bucci C (2001) Rab-interacting lysosomal protein (RILP): the Rab7 effector required for transport to lysosomes. EMBO J 20(4):683–693. https://doi.org/10.1093/emboj/20.4.683

Catlett NL, Duex JE, Tang F, Weisman LS (2000) Two distinct regions in a yeast myosin-V tail domain are required for the movement of different cargoes. J Cell Biol 150(3):513–526. https://doi.org/10.1083/jcb.150.3.513

Chen ZY, Hasson T, Zhang DS, Schwender BJ, Derfler BH, Mooseker MS, Corey DP (2001) Myosin-VIIb, a novel unconventional myosin, is a constituent of microvilli in transporting epithelia. Genomics 72(3):285–296. https://doi.org/10.1006/geno.2000.6456

Chibalina MV, Seaman MN, Miller CC, Kendrick-Jones J, Buss F (2007) Myosin VI and its interacting protein LMTK2 regulate tubule formation and transport to the endocytic recycling compartment. J Cell Sci 120 (Pt 24):4278–4288. https://doi.org/10.1242/jcs.014217

Chieregatti E, Gartner A, Stoffler HE, Bahler M (1998) Myr 7 is a novel myosin IX-RhoGAP expressed in rat brain. J Cell Sci 111(Pt 24):3597–3608

Chishti AH, Kim AC, Marfatia SM, Lutchman M, Hanspal M, Jindal H, Liu SC, Low PS, Rouleau GA, Mohandas N, Chasis JA, Conboy JG, Gascard P, Takakuwa Y, Huang SC, Benz EJ Jr, Bretscher A, Fehon RG, Gusella JF, Ramesh V, Solomon F, Marchesi VT, Tsukita S, Tsukita S, Hoover KB et al (1998) The FERM domain: a unique module involved in the linkage of cytoplasmic proteins to the membrane. Trends Biochem Sci 23(8):281–282. https://doi.org/10.1016/S0968-0004(98)01237-7

Crawley SW, Shifrin DA Jr, Grega-Larson NE, McConnell RE, Benesh AE, Mao S, Zheng Y, Zheng QY, Nam KT, Millis BA, Kachar B, Tyska MJ (2014) Intestinal brush border assembly driven by protocadherin-based intermicrovillar adhesion. Cell 157(2):433–446. https://doi.org/10.1016/j.cell.2014.01.067

Crawley SW, Weck ML, Grega-Larson NE, Shifrin DA Jr, Tyska MJ (2016) ANKS4B is essential for intermicrovillar adhesion complex formation. Dev Cell 36(2):190–200. https://doi.org/10.1016/j.devcel.2015.12.022

Dose AC, Burnside B (2000) Cloning and chromosomal localization of a human class III myosin. Genomics 67(3):333–342. https://doi.org/10.1006/geno.2000.6256

Dose AC, Hillman DW, Wong C, Sohlberg L, Lin-Jones J, Burnside B (2003) Myo3A, one of two class III myosin genes expressed in vertebrate retina, is localized to the calycal processes of rod and cone photoreceptors and is expressed in the sacculus. Mol Biol Cell 14(3):1058–1073. https://doi.org/10.1091/mbc.e02-06-0317

Etienne-Manneville S, Hall A (2002) Rho GTPases in cell biology. Nature 420(6916):629–635. https://doi.org/10.1038/nature01148

Fan Y, Eswarappa SM, Hitomi M, Fox PL (2012) Myo1c facilitates G-actin transport to the leading edge of migrating endothelial cells. J Cell Biol 198(1):47–55. https://doi.org/10.1083/jcb.201111088

Foth BJ, Goedecke MC, Soldati D (2006) New insights into myosin evolution and classification. Proc Natl Acad Sci U S A 103(10):3681–3686. https://doi.org/10.1073/pnas.0506307103

Frame MC, Patel H, Serrels B, Lietha D, Eck MJ (2010) The FERM domain: organizing the structure and function of FAK. Nat Rev Mol Cell Biol 11(11):802–814. https://doi.org/10.1038/nrm2996

Furness DN, Hackney CM (1985) Cross-links between stereocilia in the guinea-pig cochlea. Hear Res 18(2):177–188. https://doi.org/10.1016/0378-5955(85)90010-3

Geeves MA, Holmes KC (1999) Structural mechanism of muscle contraction. Annu Rev Biochem 68:687–728. https://doi.org/10.1146/annurev.biochem.68.1.687

Gibson F, Walsh J, Mburu P, Varela A, Brown KA, Antonio M, Beisel KW, Steel KP, Brown SDM (1995) A type-VII myosin encoded by the mouse deafness gene shaker-1. Nature 374(6517):62–64. https://doi.org/10.1038/374062a0

Gillespie PG, Muller U (2009) Mechanotransduction by hair cells: models, molecules, and mechanisms. Cell 139(1):33–44. https://doi.org/10.1016/j.cell.2009.09.010

Giron-Perez DA, Piedra-Quintero ZL, Santos-Argumedo L (2019) Class I myosins: highly versatile proteins with specific functions in the immune system. J Leukoc Biol 105(5):973–981. https://doi.org/10.1002/JLB.1MR0918-350RRR

Grati M, Kachar B (2011) Myosin VIIa and sans localization at stereocilia upper tip-link density implicates these Usher syndrome proteins in mechanotransduction. Proc Natl Acad Sci U S A 108(28):11476–11481. https://doi.org/10.1073/pnas.1104161108

Hamada K, Shimizu T, Yonemura S, Tsukita S, Tsukita S, Hakoshima T (2003) Structural basis of adhesion-molecule recognition by ERM proteins revealed by the crystal structure of the radixin-ICAM-2 complex. EMBO J 22(3):502–514. https://doi.org/10.1093/emboj/cdg039

Hammer JA 3rd, Sellers JR (2012) Walking to work: roles for class V myosins as cargo transporters. Nat Rev Mol Cell Biol 13(1):13–26. https://doi.org/10.1038/nrm3248

Hartman MA, Spudich JA (2012) The myosin superfamily at a glance. J Cell Sci 125 (Pt 7):1627–1632. https://doi.org/10.1242/jcs.094300

Hartman MA, Finan D, Sivaramakrishnan S, Spudich JA (2011) Principles of unconventional myosin function and targeting. Annu Rev Cell Dev Biol 27:133–155. https://doi.org/10.1146/annurev-cellbio-100809-151502

Hasson T (2003) Myosin VI: two distinct roles in endocytosis. J Cell Sci 116 (Pt 17):3453–3461. https://doi.org/10.1242/jcs.00669

Hasson T, Heintzelman MB, Santos-Sacchi J, Corey DP, Mooseker MS (1995) Expression in cochlea and retina of myosin VIIa, the gene product defective in Usher syndrome type 1B. Proc Natl Acad Sci U S A 92(21):9815–9819. https://doi.org/10.1073/pnas.92.21.9815

Hayden SM, Wolenski JS, Mooseker MS (1990) Binding of brush-border myosin-I to phospholipid-vesicles. J Cell Biol 111(2):443–451. https://doi.org/10.1083/jcb.111.2.443

He F, Wollscheid HP, Nowicka U, Biancospino M, Valentini E, Ehlinger A, Acconcia F, Magistrati E, Polo S, Walters KJ (2016) Myosin VI contains a compact structural motif that binds to ubiquitin chains. Cell Rep 14(11):2683–2694. https://doi.org/10.1016/j.celrep.2016.01.079

Heuck A, Fetka I, Brewer DN, Huls D, Munson M, Jansen RP, Niessing D (2010) The structure of the Myo4p globular tail and its function in ASH1 mRNA localization. J Cell Biol 189(3):497–510. https://doi.org/10.1083/jcb.201002076

Hirano Y, Hatano T, Takahashi A, Toriyama M, Inagaki N, Hakoshima T (2011) Structural basis of cargo recognition by the myosin-X MyTH4-FERM domain. EMBO J 30(13):2734–2747. https://doi.org/10.1038/emboj.2011.177

Hokanson DE, Ostap EM (2006) Myo1c binds tightly and specifically to phosphatidylinositol 4,5-bisphosphate and inositol 1,4,5-trisphosphate. Proc Natl Acad Sci U S A 103(9):3118–3123. https://doi.org/10.1073/pnas.0505685103

Hokanson DE, Laakso JM, Lin T, Sept D, Ostap EM (2006) Myo1c binds phosphoinositides through a putative pleckstrin homology domain. Mol Biol Cell 17(11):4856–4865. https://doi.org/10.1091/mbc.E06-05-0449

Holt JR, Gillespie SKH, Provance DW, Shah K, Shokat KM, Corey DP, Mercer JA, Gillespie PG (2002) A chemical-genetic strategy implicates myosin-1c in adaptation by hair cells. Cell 108(3):371–381. https://doi.org/10.1016/S0092-8674(02)00629-3

Howard J (1997) Molecular motors: structural adaptations to cellular functions. Nature 389(6651):561–567. https://doi.org/10.1038/39247

Hu S, Wang Y, Gong Y, Liu J, Li Y, Pan L (2018) Mechanistic insights into recognitions of ubiquitin and myosin VI by autophagy receptor TAX1BP1. J Mol Biol 430(18 Pt B):3283–3296. https://doi.org/10.1016/j.jmb.2018.06.030

Huang X, Cheng HJ, Tessier-Lavigne M, Jin Y (2002) MAX-1, a novel PH/MyTH4/FERM domain cytoplas-

mic protein implicated in netrin-mediated axon repulsion. Neuron 34(4):563–576. https://doi.org/10.1016/S0896-6273(02)00672-4

Huxley A (1998) How molecular motors work in muscle. Nature 391(6664):239–240. https://doi.org/10.1038/34567

Juan T, Geminard C, Coutelis JB, Cerezo D, Poles S, Noselli S, Furthauer M (2018) Myosin1D is an evolutionarily conserved regulator of animal left-right asymmetry. Nat Commun 9(1):1942. https://doi.org/10.1038/s41467-018-04284-8

Kachar B, Parakkal M, Kurc M, Zhao Y, Gillespie PG (2000) High-resolution structure of hair-cell tip links. Proc Natl Acad Sci U S A 97(24):13336–13341. https://doi.org/10.1073/pnas.97.24.13336

Kerber ML, Cheney RE (2011) Myosin-X: a MyTH-FERM myosin at the tips of filopodia. J Cell Sci 124 (Pt 22):3733–3741. https://doi.org/10.1242/jcs.023549

Kollmar M (2006) Thirteen is enough: the myosins of Dictyostelium discoideum and their light chains. BMC Genomics 7:183. https://doi.org/10.1186/1471-2164-7-183

Kong R, Yi F, Wen P, Liu J, Chen X, Ren J, Li X, Shang Y, Nie Y, Wu K, Fan D, Zhu L, Feng W, Wu JY (2015) Myo9b is a key player in SLIT/ROBO-mediated lung tumor suppression. J Clin Invest 2015. https://doi.org/10.1172/JCI81673

Krendel M, Mooseker MS (2005) Myosins: tails (and heads) of functional diversity. Physiology (Bethesda) 20:239–251. https://doi.org/10.1152/physiol.00014.2005

Langford GM (2002) Myosin-V, a versatile motor for short-range vesicle transport. Traffic 3(12):859–865. https://doi.org/10.1034/j.1600-0854.2002.31202.x

Lefevre G, Michel V, Weil D, Lepelletier L, Bizard E, Wolfrum U, Hardelin JP, Petit C (2008) A core cochlear phenotype in USH1 mouse mutants implicates fibrous links of the hair bundle in its cohesion, orientation and differential growth. Development 135(8):1427–1437. https://doi.org/10.1242/Dev.012922

Les Erickson F, Corsa AC, Dose AC, Burnside B (2003) Localization of a class III myosin to filopodia tips in transfected HeLa cells requires an actin-binding site in its tail domain. Mol Biol Cell 14(10):4173–4180. https://doi.org/10.1091/mbc.E02-10-0656

Li Y, Wei Z, Zhang J, Yang Z, Zhang M (2014) Structural basis of the binding of Merlin FERM domain to the E3 ubiquitin ligase substrate adaptor DCAF1. J Biol Chem 289(21):14674–14681. https://doi.org/10.1074/jbc.M114.551184

Li J, He Y, Lu Q, Zhang M (2016a) Mechanistic basis of organization of the harmonin/USH1C-mediated brush border microvilli tip-link complex. Dev Cell 36(2):179–189. https://doi.org/10.1016/j.devcel.2015.12.020

Li J, Lu Q, Zhang M (2016b) Structural basis of cargo recognition by unconventional myosins in cellular trafficking. Traffic 17(8):822–838. https://doi.org/10.1111/tra.12383

Li J, He Y, Weck ML, Lu Q, Tyska MJ, Zhang M (2017) Structure of Myo7b/USH1C complex suggests a general PDZ domain binding mode by MyTH4-FERM myosins. Proc Natl Acad Sci U S A 114(19):E3776–E3785. https://doi.org/10.1073/pnas.1702251114

Li J, Liu H, Raval MH, Yengo CM, Liu W, Zhang M (2019) Structure of the MORN4/Myo3a tail complex reveals MORN repeats as protein binding modules. Structure 27(9):1366–1374.e3. https://doi.org/10.1016/j.str.2019.06.004

Liang Y, Wang A, Belyantseva IA, Anderson DW, Probst FJ, Barber TD, Miller W, Touchman JW, Jin L, Sullivan SL, Sellers JR, Camper SA, Lloyd RV, Kachar B, Friedman TB, Fridell RA (1999) Characterization of the human and mouse unconventional myosin XV genes responsible for hereditary deafness DFNB3 and shaker 2. Genomics 61(3):243–258. https://doi.org/10.1006/geno.1999.5976

Liu H, Li J, Raval MH, Yao N, Deng X, Lu Q, Nie S, Feng W, Wan J, Yengo CM, Liu W, Zhang M (2016) Myosin III-mediated cross-linking and stimulation of actin bundling activity of Espin. Elife 5. https://doi.org/10.7554/eLife.12856

Lu Q, Yu J, Yan J, Wei ZY, Zhang MJ (2011) Structural basis of the myosin X PH1(N)-PH2-PH1(C) tandem as a specific and acute cellular PI(3,4,5)P-3 sensor. Mol Biol Cell 22(22):4268–4278. https://doi.org/10.1091/mbc.E11-04-0354

Lu Q, Li J, Zhang M (2014) Cargo recognition and cargo-mediated regulation of unconventional myosins. Acc Chem Res 47(10):3061–3070. https://doi.org/10.1021/ar500216z

Lu Q, Li J, Ye F, Zhang M (2015) Structure of myosin-1c tail bound to calmodulin provides insights into calcium-mediated conformational coupling. Nat Struct Mol Biol 22(1):81–88. https://doi.org/10.1038/nsmb.2923

Lundstrom A, Gallio M, Englund C, Steneberg P, Hemphala J, Aspenstrom P, Keleman K, Falileeva L, Dickson BJ, Samakovlis C (2004) Vilse, a conserved Rac/Cdc42 GAP mediating Robo repulsion in tracheal cells and axons. Genes Dev 18(17):2161–2171. https://doi.org/10.1101/gad.310204

Manor U, Disanza A, Grati M, Andrade L, Lin H, Di Fiore PP, Scita G, Kachar B (2011) Regulation of stereocilia length by myosin XVa and whirlin depends on the actin-regulatory protein Eps8. Curr Biol 21(2):167–172. https://doi.org/10.1016/j.cub.2010.12.046

Mburu P, Mustapha M, Varela A, Weil D, El-Amraoui A, Holme RH, Rump A, Hardisty RE, Blanchard S, Coimbra RS, Perfettini I, Parkinson N, Mallon AM, Glenister P, Rogers MJ, Paige AJ, Moir L, Clay J, Rosenthal A, Liu XZ, Blanco G, Steel KP, Petit C, Brown SD (2003) Defects in whirlin, a PDZ domain molecule involved in stereocilia elongation, cause deafness in the whirler mouse and families with DFNB31. Nat Genet 34(4):421–428. https://doi.org/10.1038/ng1208

McConnell RE, Tyska MJ (2010) Leveraging the membrane – cytoskeleton interface with myosin-1. Trends

Cell Biol 20(7):418–426. https://doi.org/10.1016/j.tcb.2010.04.004

McIntosh BB, Ostap EM (2016) Myosin-I molecular motors at a glance. J Cell Sci 129(14):2689–2695. https://doi.org/10.1242/jcs.186403

Mecklenburg KL, Takemori N, Komori N, Chu B, Hardie RC, Matsumoto H, O'Tousa JE (2010) Retinophilin is a light-regulated phosphoprotein required to suppress photoreceptor dark noise in Drosophila. J Neurosci 30(4):1238–1249. https://doi.org/10.1523/JNEUROSCI.4464-09.2010

Mecklenburg KL, Freed SA, Raval M, Quintero OA, Yengo CM, O'Tousa JE (2015) Invertebrate and vertebrate class III myosins interact with MORN repeat-containing adaptor proteins. PLoS One 10(3):e0122502. https://doi.org/10.1371/journal.pone.0122502

Menetrey J, Bahloul A, Wells AL, Yengo CM, Morris CA, Sweeney HL, Houdusse A (2005) The structure of the myosin VI motor reveals the mechanism of directionality reversal. Nature 435(7043):779–785. https://doi.org/10.1038/nature03592

Merritt RC, Manor U, Salles FT, Grati M, Dose AC, Unrath WC, Quintero OA, Yengo CM, Kachar B (2012) Myosin IIIB uses an actin-binding motif in its espin-1 cargo to reach the tips of actin protrusions. Curr Biol 22(4):320–325. https://doi.org/10.1016/j.cub.2011.12.053

Miyata H, Bowers B, Korn ED (1989) Plasma-membrane-association of Acanthamoeba myosin-I. J Cell Biol 109(4):1519–1528. https://doi.org/10.1083/jcb.109.4.1519

Moleirinho S, Tilston-Lunel A, Angus L, Gunn-Moore F, Reynolds PA (2013) The expanding family of FERM proteins. Biochem J 452(2):183–193. https://doi.org/10.1042/BJ20121642

Montell C, Rubin GM (1988) The Drosophila ninaC locus encodes two photoreceptor cell specific proteins with domains homologous to protein kinases and the myosin heavy chain head. Cell 52(5):757–772. https://doi.org/10.1016/0092-8674(88)90413-8

Morriswood B, Ryzhakov G, Puri C, Arden SD, Roberts R, Dendrou C, Kendrick-Jones J, Buss F (2007) T6BP and NDP52 are myosin VI binding partners with potential roles in cytokine signalling and cell adhesion. J Cell Sci 120(Pt 15):2574–2585. https://doi.org/10.1242/jcs.007005

Munnich S, Taft MH, Manstein DJ (2014) Crystal structure of human myosin 1c – the motor in GLUT4 exocytosis: implications for Ca^{2+} regulation and 14-3-3 binding. J Mol Biol 426(10):2070–2081. https://doi.org/10.1016/j.jmb.2014.03.004

Nascimento AFZ, Trindade DM, Tonoli CCC, de Giuseppe PO, Assis LHP, Honorato RV, de Oliveira PSL, Mahajan P, Burgess-Brown NA, von Delft F, Larson RE, Murakami MT (2013) Structural insights into functional overlapping and differentiation among myosin V motors. J Biol Chem 288(47):34131–34145. https://doi.org/10.1074/jbc.M113.507202

Nunez C, Oliver J, Mendoza JL, Gomez-Garcia M, Pinero A, Taxonera C, Diaz-Rubio M, Lopez-Nevot MA, la Concha EG, Nieto A, Urcelay E, Martinez A, Martin J (2007) MYO9B polymorphisms in patients with inflammatory bowel disease. Gut 56(9):1321–1322. https://doi.org/10.1136/gut.2007.121905

O'Connor E, Topf A, Muller JS, Cox D, Evangelista T, Colomer J, Abicht A, Senderek J, Hasselmann O, Yaramis A, Laval SH, Lochmuller H (2016) Identification of mutations in the MYO9A gene in patients with congenital myasthenic syndrome. Brain 139 (Pt 8):2143–2153. https://doi.org/10.1093/brain/aww130

Petersen KJ, Goodson HV, Arthur AL, Luxton GW, Houdusse A, Titus MA (2016) MyTH4-FERM myosins have an ancient and conserved role in filopod formation. Proc Natl Acad Sci U S A 113(50):E8059–E8068. https://doi.org/10.1073/pnas.1615392113

Planelles-Herrero VJ, Blanc F, Sirigu S, Sirkia H, Clause J, Sourigues Y, Johnsrud DO, Amigues B, Cecchini M, Gilbert SP, Houdusse A, Titus MA (2016) Myosin MyTH4-FERM structures highlight important principles of convergent evolution. Proc Natl Acad Sci U S A 113(21):E2906–E2915. https://doi.org/10.1073/pnas.1600736113

Pollard TD, Korn ED (1973) Acanthamoeba myosin. I. Isolation from Acanthamoeba castellanii of an enzyme similar to muscle myosin. J Biol Chem 248(13):4682–4690

Pylypenko O, Attanda W, Gauquelin C, Lahmani M, Coulibaly D, Baron B, Hoos S, Titus MA, England P, Houdusse AM (2013) Structural basis of myosin V Rab GTPase-dependent cargo recognition. Proc Natl Acad Sci U S A 110(51):20443–20448. https://doi.org/10.1073/pnas.1314329110

Pylypenko O, Welz T, Tittel J, Kollmar M, Chardon F, Malherbe G, Weiss S, Michel CI, Samol-Wolf A, Grasskamp AT, Hume A, Goud B, Baron B, England P, Titus MA, Schwille P, Weidemann T, Houdusse A, Kerkhoff E (2016) Coordinated recruitment of Spir actin nucleators and myosin V motors to Rab11 vesicle membranes. Elife 5. https://doi.org/10.7554/eLife.17523

Reck-Peterson SL, Provance DW, Mooseker MS, Mercer JA (2000) Class V myosins. Biochim Biophys Acta 1496(1):36–51. https://doi.org/10.1016/S0167-4889(00)00007-0

Reddy VS, Reddy ASN (1999) A plant calmodulin-binding motor is part kinesin and part myosin. Bioinformatics 15(12):1055–1057. https://doi.org/10.1093/bioinformatics/15.12.1055

Reinhard J, Scheel AA, Diekmann D, Hall A, Ruppert C, Bahler M (1995) A novel type of myosin implicated in signalling by rho family GTPases. EMBO J 14(4):697–704

Rittinger K, Walker PA, Eccleston JF, Nurmahomed K, Owen D, Laue E, Gamblin SJ, Smerdon SJ (1997a) Crystal structure of a small G protein in complex with the GTPase-activating protein rhoGAP. Nature 388(6643):693–697. https://doi.org/10.1038/41805

Rittinger K, Walker PA, Eccleston JF, Smerdon SJ, Gamblin SJ (1997b) Structure at 1.65 A of RhoA and its GTPase-activating protein in complex with a transition-state analogue. Nature 389(6652):758–762. https://doi.org/10.1038/39651

Rock RS, Rice SE, Wells AL, Purcell TJ, Spudich JA, Sweeney HL (2001) Myosin VI is a processive motor with a large step size. Proc Natl Acad Sci U S A 98(24):13655–13659. https://doi.org/10.1073/pnas.191512398

Ruppel KM, Spudich JA (1996) Structure-function analysis of the motor domain of myosin. Annu Rev Cell Dev Biol 12:543–573. https://doi.org/10.1146/annurev.cellbio.12.1.543

Saczko-Brack D, Warchol E, Rogez B, Kross M, Heissler SM, Sellers JR, Batters C, Veigel C (2016) Self-organization of actin networks by a monomeric myosin. Proc Natl Acad Sci U S A 113(52):E8387–E8395. https://doi.org/10.1073/pnas.1612719113

Sahlender DA, Roberts RC, Arden SD, Spudich G, Taylor MJ, Luzio JP, Kendrick-Jones J, Buss F (2005) Optineurin links myosin VI to the Golgi complex and is involved in Golgi organization and exocytosis. J Cell Biol 169(2):285–295. https://doi.org/10.1083/jcb.200501162

Salles FT, Merritt RC Jr, Manor U, Dougherty GW, Sousa AD, Moore JE, Yengo CM, Dose AC, Kachar B (2009) Myosin IIIa boosts elongation of stereocilia by transporting espin 1 to the plus ends of actin filaments. Nat Cell Biol 11(4):443–450. https://doi.org/10.1038/ncb1851

Saydmohammed M, Yagi H, Calderon M, Clark MJ, Feinstein T, Sun M, Stolz DB, Watkins SC, Amack JD, Lo CW, Tsang M (2018) Vertebrate myosin 1d regulates left-right organizer morphogenesis and laterality. Nat Commun 9(1):3381. https://doi.org/10.1038/s41467-018-05866-2

Schott D, Ho J, Pruyne D, Bretscher A (1999) The COOH-terminal domain of Myo2p, a yeast myosin V, has a direct role in secretory vesicle targeting. J Cell Biol 147(4):791–808. https://doi.org/10.1083/jcb.147.4.791

Sellers JR, Veigel C (2006) Walking with myosin V. Curr Opin Cell Biol 18(1):68–73. https://doi.org/10.1016/j.ceb.2005.12.014

Shang G, Brautigam CA, Chen R, Lu D, Torres-Vazquez J, Zhang X (2017) Structure analyses reveal a regulated oligomerization mechanism of the PlexinD1/GIPC/myosin VI complex. Elife 6. https://doi.org/10.7554/eLife.27322

Shi H, Singh N, Esselborn F, Blobel G (2014) Structure of a myosin center dot adaptor complex and pairing by cargo. Proc Natl Acad Sci U S A 111(12):E1082–E1090. https://doi.org/10.1073/pnas.1401428111

Shuman H, Greenberg MJ, Zwolak A, Lin T, Sindelar CV, Dominguez R, Ostap EM (2014) A vertebrate myosin-I structure reveals unique insights into myosin mechanochemical tuning. Proc Natl Acad Sci U S A 111(6):2116–2121. https://doi.org/10.1073/pnas.1321022111

Spudich G, Chibalina MV, Au JS, Arden SD, Buss F, Kendrick-Jones J (2007) Myosin VI targeting to clathrin-coated structures and dimerization is mediated by binding to Disabled-2 and PtdIns(4,5)P2. Nat Cell Biol 9(2):176–183. https://doi.org/10.1038/ncb1531

Takeshima H, Komazaki S, Nishi M, Iino M, Kangawa K (2000) Junctophilins: a novel family of junctional membrane complex proteins. Mol Cell 6(1):11–22. https://doi.org/10.1016/S1097-2765(05)00005-5

Tang K, Li Y, Yu C, Wei Z (2019) Structural mechanism for versatile cargo recognition by the yeast class V myosin Myo2. J Biol Chem 294(15):5896–5906. https://doi.org/10.1074/jbc.RA119.007550

Taylor KA (2007) Regulation and recycling of myosin V. Curr Opin Cell Biol 19(1):67–74. https://doi.org/10.1016/j.ceb.2006.12.014

Tepass U (2009) FERM proteins in animal morphogenesis. Curr Opin Genet Dev 19(4):357–367. https://doi.org/10.1016/j.gde.2009.05.006

Tingler M, Kurz S, Maerker M, Ott T, Fuhl F, Schweickert A, LeBlanc-Straceski JM, Noselli S, Blum M (2018) A conserved role of the unconventional myosin 1d in laterality determination. Curr Biol 28(5):810–816. e813. https://doi.org/10.1016/j.cub.2018.01.075

Titus MA (1997) Motor proteins: myosin V – the multipurpose transport motor. Curr Biol 7(5):R301–R304. https://doi.org/10.1016/S0960-9822(06)00143-6

Tiwari A, Jung JJ, Inamdar SM, Nihalani D, Choudhury A (2013) The myosin motor Myo1c is required for VEGFR2 delivery to the cell surface and for angiogenic signaling. Am J Physiol Heart Circ Physiol 304(5):H687–H696. https://doi.org/10.1152/ajpheart.00744.2012

Tokuo H, Coluccio LM (2013) Myosin-1c regulates the dynamic stability of E-cadherin–based cell–cell contacts in polarized Madin–Darby canine kidney cells. Mol Biol Cell 24(18):2820–2833. https://doi.org/10.1091/mbc.E12-12-0884

Tomatis VM, Papadopulos A, Malintan NT, Martin S, Wallis T, Gormal RS, Kendrick-Jones J, Buss F, Meunier FA (2013) Myosin VI small insert isoform maintains exocytosis by tethering secretory granules to the cortical actin. J Cell Biol 200(3):301–320. https://doi.org/10.1083/jcb.201204092

Trybus KM (2008) Myosin V from head to tail. Cell Mol Life Sci 65(9):1378–1389. https://doi.org/10.1007/s00018-008-7507-6

Tumbarello DA, Kendrick-Jones J, Buss F (2013) Myosin VI and its cargo adaptors – linking endocytosis and autophagy. J Cell Sci 126 (Pt 12):2561–2570. https://doi.org/10.1242/jcs.095554

Tyska MJ, Mackey AT, Huang JD, Copeland NG, Jenkins NA, Mooseker MS (2005) Myosin-1a is critical for normal brush border structure and composition. Mol Biol Cell 16(5):2443–2457. https://doi.org/10.1091/mbc.e04-12-1116

Vale RD (1999) Millennial musings on molecular motors. Trends Cell Biol 9(12):M38–M42. https://doi.org/10.1016/S0962-8924(99)01665-7

van den Boom F, Dussmann H, Uhlenbrock K, Abouhamed M, Bahler M (2007) The myosin IXb motor activity targets the myosin IXb RhoGAP domain as cargo to sites of actin polymerization. Mol Biol Cell 18(4):1507–1518. https://doi.org/10.1091/mbc.e06-08-0771

Velvarska H, Niessing D (2013) Structural insights into the globular tails of the human type V myosins Myo5a, Myo5b, and Myo5c. PLoS One 8(12). https://doi.org/10.1371/journal.pone.0082065

Venkatachalam K, Wasserman D, Wang X, Li R, Mills E, Elsaesser R, Li HS, Montell C (2010) Dependence on a retinophilin/myosin complex for stability of PKC and INAD and termination of phototransduction. J Neurosci 30(34):11337–11345. https://doi.org/10.1523/JNEUROSCI.2709-10.2010

Verpy E, Leibovici M, Zwaenepoel I, Liu XZ, Gal A, Salem N, Mansour A, Blanchard S, Kobayashi I, Keats BJ, Slim R, Petit C (2000) A defect in harmonin, a PDZ domain-containing protein expressed in the inner ear sensory hair cells, underlies Usher syndrome type 1C. Nat Genet 26(1):51–55. https://doi.org/10.1038/79171

Wallace AG, Raduwan H, Carlet J, Soto MC (2018) The RhoGAP HUM-7/Myo9 integrates signals to modulate RHO-1/RhoA during embryonic morphogenesis in Caenorhabditis elegans. Development 145(23). https://doi.org/10.1242/dev.168724

Wang C, Wei ZY, Chen KY, Ye F, Yu C, Bennett V, Zhang MJ (2014) Structural basis of diverse membrane target recognitions by ankyrins. Elife 3. https://doi.org/10.7554/eLife.04353

Weck ML, Grega-Larson NE, Tyska MJ (2017) MyTH4-FERM myosins in the assembly and maintenance of actin-based protrusions. Curr Opin Cell Biol 44:68–78. https://doi.org/10.1016/j.ceb.2016.10.002

Wei Z, Yan J, Lu Q, Pan L, Zhang M (2011) Cargo recognition mechanism of myosin X revealed by the structure of its tail MyTH4-FERM tandem in complex with the DCC P3 domain. Proc Natl Acad Sci U S A 108(9):3572–3577. https://doi.org/10.1073/pnas.1016567108

Wei ZY, Liu XT, Yu C, Zhang MJ (2013) Structural basis of cargo recognitions for class V myosins. Proc Natl Acad Sci U S A 110(28):11314–11319. https://doi.org/10.1073/pnas.1306768110

Wei Z, Li Y, Ye F, Zhang M (2015) Structural basis for the phosphorylation-regulated interaction between the cytoplasmic tail of cell polarity protein crumbs and the actin-binding protein moesin. J Biol Chem 290(18):11384–11392. https://doi.org/10.1074/jbc.M115.643791

Weil D, Levy G, Sahly I, Levi-Acobas F, Blanchard S, El-Amraoui A, Crozet F, Philippe H, Abitbol M, Petit C (1996) Human myosin VIIA responsible for the Usher 1B syndrome: a predicted membrane-associated motor protein expressed in developing sensory epithelia. Proc Natl Acad Sci U S A 93(8):3232–3237. https://doi.org/10.1073/pnas.93.8.3232

Well D, Blanchard S, Kaplan J, Guilford P, Gibson F, Walsh J, Mburu P, Varela A, Levillers J, Weston MD, Kelley PM, Kimberling WJ, Wagenaar M, Leviacobas F, Largetpiet D, Munnich A, Steel KP, Brown SDM, Petit C (1995) Defective myosin VIIa gene responsible for Usher syndrome type 1b. Nature 374(6517):60–61. https://doi.org/10.1038/374060a0

Wells AL, Lin AW, Chen LQ, Safer D, Cain SM, Hasson T, Carragher BI, Milligan RA, Sweeney HL (1999) Myosin VI is an actin-based motor that moves backwards. Nature 401(6752):505–508. https://doi.org/10.1038/46835

Wen W, Yan J, Zhang M (2006) Structural characterization of the split pleckstrin homology domain in phospholipase C-gamma1 and its interaction with TRPC3. J Biol Chem 281(17):12060–12068. https://doi.org/10.1074/jbc.M600336200

Wilson JR, Jing C, Walker PA, Martin SR, Howell SA, Blackburn GM, Gamblin SJ, Xiao B (2002) Crystal structure and functional analysis of the histone methyltransferase SET7/9. Cell 111(1):105–115. https://doi.org/10.1016/S0092-8674(02)00964-9

Wirth JA, Jensen KA, Post PL, Bement WM, Mooseker MS (1996) Human myosin-IXb, an unconventional myosin with a chimerin-like rho/rac GTPase-activating protein domain in its tail. J Cell Sci 109(Pt 3):653–661

Wollscheid HP, Biancospino M, He F, Magistrati E, Molteni E, Lupia M, Soffientini P, Rottner K, Cavallaro U, Pozzoli U, Mapelli M, Walters KJ, Polo S (2016) Diverse functions of myosin VI elucidated by an isoform-specific alpha-helix domain. Nat Struct Mol Biol 23(4):300–308. https://doi.org/10.1038/nsmb.3187

Wu L, Pan LF, Wei ZY, Zhang MJ (2011) Structure of MyTH4-FERM domains in myosin VIIa tail bound to cargo. Science 331(6018):757–760. https://doi.org/10.1126/science.1198848

Xu C, Jin J, Bian C, Lam R, Tian R, Weist R, You L, Nie J, Bochkarev A, Tempel W, Tan CS, Wasney GA, Vedadi M, Gish GD, Arrowsmith CH, Pawson T, Yang XJ, Min J (2012) Sequence-specific recognition of a PxLPxI/L motif by an ankyrin repeat tumbler lock. Sci Signal 5(226):ra39. https://doi.org/10.1126/scisignal.2002979

Yan J, Wen W, Xu W, Long JF, Adams ME, Froehner SC, Zhang M (2005) Structure of the split PH domain and distinct lipid-binding properties of the PH-PDZ supramodule of alpha-syntrophin. EMBO J 24(23):3985–3995. https://doi.org/10.1038/sj.emboj.7600858

Yan J, Wen W, Chan LN, Zhang M (2008) Split pleckstrin homology domain-mediated cytoplasmic-nuclear localization of PI3-kinase enhancer GTPase. J Mol Biol 378(2):425–435. https://doi.org/10.1016/j.jmb.2008.02.052

Yi F, Kong R, Ren J, Zhu L, Lou J, Wu JY, Feng W (2016) Noncanonical Myo9b-RhoGAP accelerates RhoA

GTP hydrolysis by a dual-arginine-finger mechanism. J Mol Biol 428(15):3043–3057. https://doi.org/10.1016/j.jmb.2016.06.014

Yu C, Feng W, Wei ZY, Miyanoiri Y, Wen WY, Zhao YX, Zhang MJ (2009) Myosin VI undergoes cargo-mediated dimerization. Cell 138(3):537–548. https://doi.org/10.1016/j.cell.2009.05.030

Yu IM, Planelles-Herrero VJ, Sourigues Y, Moussaoui D, Sirkia H, Kikuti C, Stroebel D, Titus MA, Houdusse A (2017) Myosin 7 and its adaptors link cadherins to actin. Nat Commun 8:15864. https://doi.org/10.1038/ncomms15864

Zampini V, Ruttiger L, Johnson SL, Franz C, Furness DN, Waldhaus J, Xiong H, Hackney CM, Holley MC, Offenhauser N, Di Fiore PP, Knipper M, Masetto S, Marcotti W (2011) Eps8 regulates hair bundle length and functional maturation of mammalian auditory hair cells. PLoS Biol 9(4):e1001048. https://doi.org/10.1371/journal.pbio.1001048

The Structure of Acto-Myosin

4

Rasmus R. Schröder

Abstract

After several decades studying different acto-myosin complexes at lower and intermediate resolution – limited by the electron microscope instrumentation available then – recent advances in imaging technology have been crucial for obtaining a number of excellent high-resolution 3D reconstructions from cryo electron microscopy. The resolution level reached now is about 3–4 Å, which allows unambiguous model building of filamentous actin on its own as well as that of actin filaments decorated with strongly bound myosin variants. The interface between actin and the myosin motor domain can now be described in detail, and the function of parts of the interface (such as, e.g., the cardiomyopathy loop) can be understood in a mechanistical way. Most recently, reconstructions of actin filaments decorated with different myosins, which show a strongly bound acto-myosin complex also in the presence of the nucleotide ADP, have become available. The comparison of these structures with the nucleotide-free Rigor state provide the first mechanistic description of force sensing. An open question is still the initial interaction of the motor domain of myosin with the actin filament. Such weakly interacting states have so far not been the subject of microscopical studies, even though high-resolution structures would be needed to shed light on the initial steps of phosphate release and power stroke initiation.

Keywords

Acto-myosin complex · Strongly bound state · Weakly bound state · Force sensing · Cryo electron microscopy

4.1 Introduction

When considering "the structure of acto-myosin" two seemingly different meanings come to mind: in the first place we think about the mechanism of force generation and motility via the actin/myosin molecular motor system. The notion that the structure of the interacting complex of the motor protein myosin and its track, filamentous actin, will define function is evident, and ever since electron microscopists produced the first visualisation of the interactions of myosin with actin in a muscle sarcomere (cf. Fig. 4.1; Huxley 1957) structural biologists carried out work to understand different states of the crossbridge cycle at finer and finer detail.

R. R. Schröder (✉)
Cryo Electron Microscopy, BioQuant, Medical Faculty, Heidelberg University, Heidelberg, Germany
e-mail: rasmus.schroeder@bioquant.uni-heidelberg.de

L. M. Coluccio (ed.), *Myosins*, Advances in Experimental Medicine and Biology 1239,
https://doi.org/10.1007/978-3-030-38062-5_4

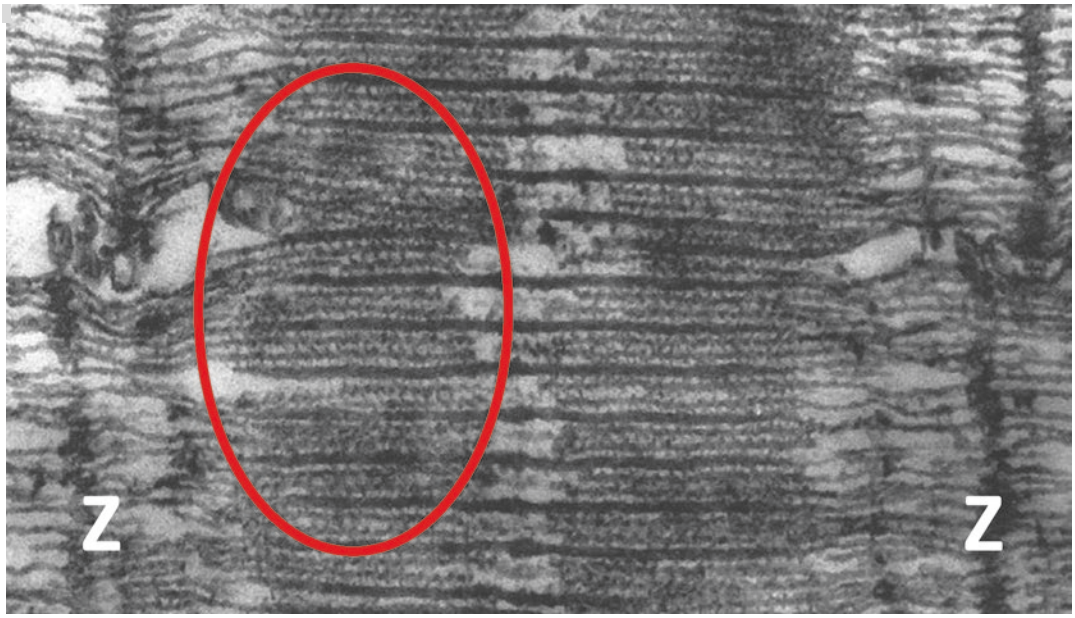

Fig. 4.1 Electron micrograph of an ultrathin section of chemically fixed, heavy metal stained, and resin embedded muscle sample. Note the sarcomere Z-lines and the area of overlapping thick and thin filaments (red circle). In the area one can clearly see the myosin motor domains as "crossbridges" between the filaments. Such micrographs represent the typical first visualization of the acto-myosin complex and are considered recently again – in their 3D tomogram flavour – a valuable source for information about crossbridge states (cf. Figs. 4.11, 4.12 and text Sect. 4.5). (Image adapted from Huxley 1957)

On the other hand, the phrase "acto-myosin" has for a long time been used by electron microscopists when talking about "decorated F-actin". This means purified filaments of either actin on its own, or sometimes as reconstituted or even native thin filaments with their tropomyosin and troponin components "decorated" with myosin sub-fragments where myosin binds strongly to the actin in its nucleotide-free Rigor state. This protein complex was for many years the only state of the crossbridge cycle accessible until crystals of myosin could finally be grown (Rayment et al. 1993a; Houdusse et al. 2000). "Decorated actin" was thus excessively studied, first by conventional electron microscopy via the so-called negative-staining technique, then since the 1990s by cryo electron microscopy. Typical reconstructions are shown in Fig. 4.2 illustrating some very early examples of this work (Moore et al. 1970; Milligan and Flicker 1987; Flicker et al. 1991).

As has happened often in structural biology, high-resolution structures from protein X-ray crystallography and not from electron microscopy have dominated the progress in our understanding of molecular functions. The common wisdom was that X-ray structures intrinsically have higher resolution and will give much more information than 3D reconstructions from electron micrographs. Acto-myosin has not been an exception from this rule, and X-ray crystallographers have produced a very large number of structures using nucleotide analogues, myosin mutants and/or unconventional myosins to produce a detailed picture of the possible conformational space of the motor domain on its own. What has been lacking for a long time was detailed information about the motor domain

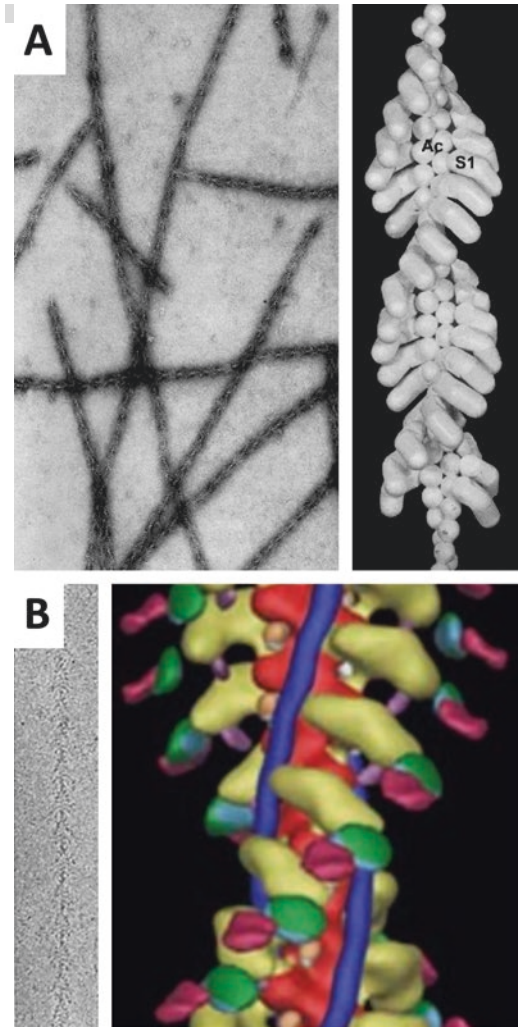

Fig. 4.2 Typical micrographs and 3D reconstructions from early myosin decorated F-actin in their nucleotide-free strong binding state, contrasted with negative stain (**a**), or embedded in a vitrified ice layer (**b**). In the case of the cryo electron microscopy sample (**b**), tropomyosin (blue in the 3D reconstruction) was present. (Images in (**a**) adapted from Moore et al. (1970), in (**b**) from Flicker et al. (1991))

interacting with its track F-actin. Despite numerous attempts to form a small enough acto-myosin complex, which might be in the correct binding conformation and able to form crystals (Dawson et al. 2003; Qu et al. 2018), to date there is not yet any crystallographic interaction structure.

This leaves the field still wide open for electron microscopy, which in recent years has developed from a medium-resolution technique, providing typical 1-nm resolution data, to a truly structural biology tool, contributing data at the 3–4-Å resolution level at present. Over the last 25 years advances in sample preparation, image processing, as well as development of new microscopes, detectors, and automated data collection have boosted the field (cf. review by Schröder 2015) resulting in the awarding of Nobel prizes to Dubochet, Frank, and Henderson (Cressey and Callaway 2017). In the last 2 years high-resolution structures of F-actin (3.1 Å, Chou and Pollard 2019) and myosin-decorated F-actin (3.7 Å, Mentes et al. 2018) have been published. They show very clearly that electron microscopy can now be used to study the mechanism of the actin-myosin motor system.

Figure 4.3 illustrates the crossbridge cycle of actin and myosin, indicating also which structural biology technique (X-ray crystallography or electron microscopy) might be most useful to obtain additional information in the future. In this chapter we will briefly look back at some earlier work, which already pointed out interesting questions, such as the mechanism for the actin-activation of myosin ATP hydrolysis or the coupling between nucleotide state and lever arm movement, also known as the power stroke. It is also interesting to see how the increase in resolution developed and fostered a completely new understanding of how the conformational changes connect to function. This will lead to an in-depth discussion of the highest resolution structure of decorated F-actin to date and its implications for the detailed description of the strongly interacting acto-myosin states. Here, we will not repeat the crystallographic results. They are described in detail in Chap. 2 by Sweeney and colleagues and also in a very recent review by Robert-Paganin et al. 2019. We will end the chapter by exploring some ideas regarding future microscopy studies, which should close the blind spots of both X-ray crystallography and static electron microscopy.

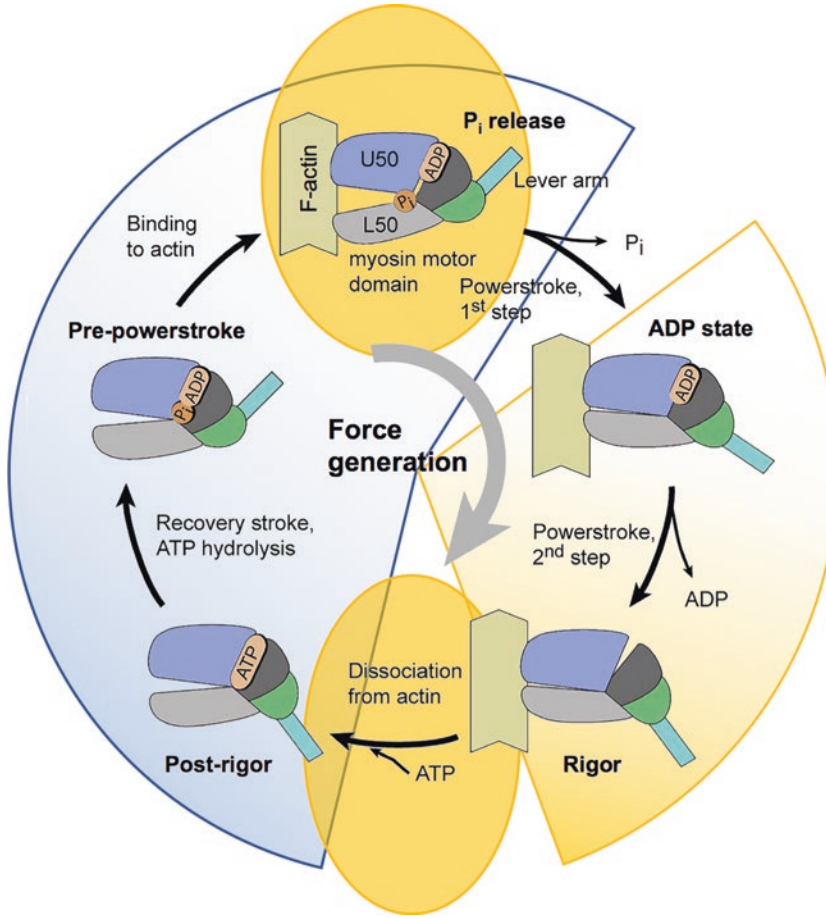

Fig. 4.3 Schematics of the acto-myosin crossbridge cycle. The background pie segments assign the states in the cycle to either X-ray crystallography (blue) or cryo electron microscopy (orange) as that technique, which is most commonly used to obtain structural information about that particular acto-myosin state. The two orange ellipses denote states, which might become accessible for cryo electron microscopy in the future (cf. also Sect. 4.5). (Image of the crossbridge cycle adapted from Wulf et al. 2016)

4.2 Studying the Canonical Acto-myosin State – The Strongly Bound Motor

As discussed above, electron microscopy was the natural technique to investigate the strongly bound states of myosin to F-actin (cf. Fig. 4.3, light orange background). At times when only skeletal myosins were examined, the nucleotide-free myosin state (Rigor) was studied, as no difference between an ADP-bound or nucleotide-free state could be observed at the resolution attainable then. Early work was satisfied with visualising the binding state with a first attempt to dock the quasi-molecular crystallographic structure into the reconstructed density, which was at a resolution level of about 20–30 Å (Flicker et al. 1991; Rayment et al. 1993b; Schröder et al. 1993). These models were in hindsight not very helpful as their definition of the actin-myosin interface was not good enough to draw detailed conclusions.

This situation changed when myosins other than skeletal muscle myosin 2 were explored. For example, two states were reported for smooth muscle myosin 2 (Whittaker et al. 1995) shown in Fig. 4.4a and for brush border myosin 1 (now myosin 1A; Myo1a) (Jontes et al. 1995). Besides

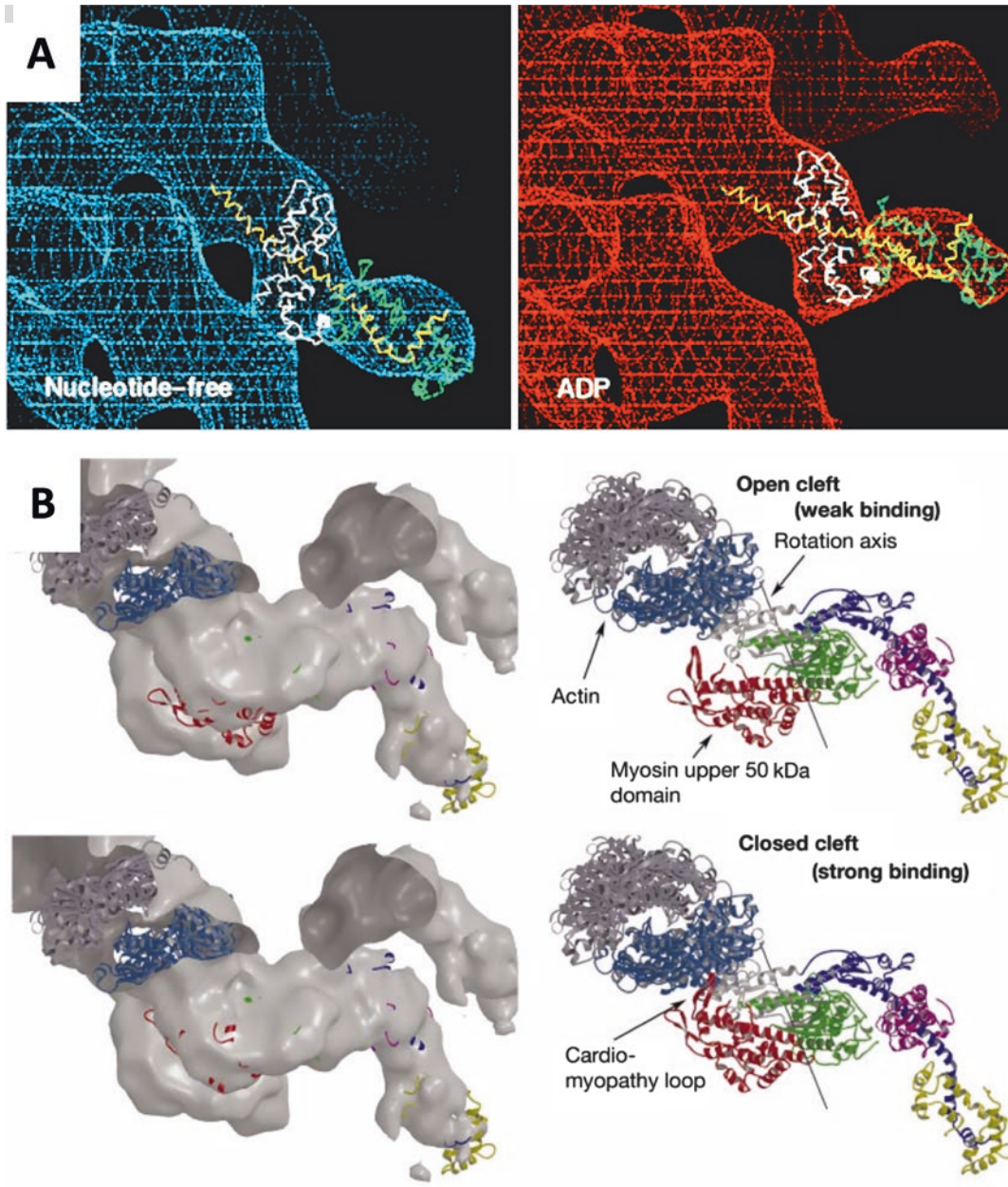

Fig. 4.4 (**a**) Low resolution helical reconstruction of F-actin decorated with the smooth muscle myosin 1 motor domain and its light chain, left in the nucleotide-free Rigor state, right in AM.ADP state. Images adapted from Whittacker et al. (Whittaker et al. 1995). Note the difference in the direction of the light chains pointing away from the F-actin axis. Together with work on brush border myosin 1 (Jontes et al. 1995), these were the first structural data indicating that the motor domain and its lever arm are in an intermediate power stroke position when ADP is still bound. Cf. Sect. 4.3 and the high-resolution work by Mentes et al. (2018), also Fig. 4.9. (**b**) Closure of the cleft in the upper 50 kDa motor domain upon strong binding to actin. Image from Holmes et al. (2003). The reconstruction of the acto-myosin complex at medium resolution provided a well-defined molecular envelope, which then allowed molecular fitting of the crystallographic model of skeletal myosin 2. To fit into the envelope the crystal structure had to be modified. The upper row shows the unmodified structure with the lower 50 kDa domain (grey) already docked to the actin surface. The lower row shows the fit with the closed cleft and both, upper and lower 50 kDa domain in a position forming the actin-myosin interface for the strongly bound complex

the conventional Rigor state, the ADP state was described, i.e., the strongly bound myosin where the nucleotide ADP is still bound. Such a nucleotide state can be populated for a number of myosins, e.g., myosin 5 (Wulf et al. 2016) and myosin 1B (Mentes et al. 2018) as will be discussed later. Interestingly, the reconstructions showed a clear difference in the direction the lever arm is pointing. In the Rigor state it swings slightly downwards towards the barbed end of the decorated filament, while the ADP state reveals a more upwards directed lever arm. These two states were also subsequently found in single-molecule mechanics experiments, identified as the two states in displacement graphs from optical trap studies (Veigel et al. 1999; Sellers and Veigel 2006).

in the middle of the 1990's it was already well anticipated from these experiments that the "strongly bound" state should come in different flavours and should be more populated in some myosins than others. This also indicates a correlation between existence of the ADP state and motor function. The existence of such a long-lived ADP state is today understood as a stopping point in the crossbridge cycle. In this state the myosin can sense force, e.g., strain pulling at the lever arm (cf. e.g., Chap. 8 by Sellers and Takagi as well as the discussion of the ADP high-resolution reconstructions below).

Another flavour of the strongly bound state is its function as a trigger for the power stroke. Rephrased in a more mechanistical way, the transition from a weakly to a strongly bound myosin must be the signal for the motor to start with the power stroke. This order of events is mandatory, as otherwise – in a decoupled scenario – part of the power stroke's effect would be lost. Myosin's sensing of its binding coordination upon binding to F-actin has been investigated in numerous studies, again using electron microscopy, but also myosin mutants, spectroscopic probes, and elaborate biochemical state preparations for X-ray crystallography. One of the first visualisations of a conformational change upon strong binding is illustrated in Fig. 4.4b (Holmes et al. 2003) where the closure of the cleft between the upper and lower 50-kDa domains was observed when trying to fit the original crystallographic skeletal myosin 2 model into a 3D reconstruction of decorated actin at about 14-Å resolution.

Unfortunately, this level of resolution was still not good enough to derive a detailed model of the molecular mechanisms, but it pointed to a number of hotspots in the myosin structure which were then studied with a number of different approaches.

4.3 Changing the Game – Cryo Electron Microscopy 2.0 and High-Resolution Reconstructions of the Nucleotide-Free Rigor State and ADP States

4.3.1 Pushing the Limits – Advances in Instrumentation and Image Processing

In the years from about 2010 new ideas and technical advances have changed electron microscopy. While progress in many details such as instrument stability and automated data collection had happened in secrecy, the appearance of novel reconstruction software (Scheres 2012) coincided with the availability and application of direct electron detectors (Campbell et al. 2012; Clough et al. 2014; McMullan et al. 2016) and put a spotlight on the possibility of obtaining high-resolution structures in the 3–4-Å resolution range by cryo electron microscopy (Kühlbrandt 2014).

This development is reflected in the boost of resolution for many reconstructions of F-actin and myosin-decorated F-actin or thin filaments over the years. Figs. 4.5 and 4.6 reflect the change in appearance and information content of the 3D reconstructions obtained. For myosin-decorated actin filaments (Fig. 4.5) representative reconstructions were published by Behrmann et al. (2012, 7.4 Å resolution, data found as EMD-1988 in EMDataResource.org), Fujii and Namba (2017, 5.2 Å, EMD-6664), and van der Ecken et al. (2016, 3.9 Å, EMD-8165), which illustrate also the limits of resolution imposed, e.g., by the

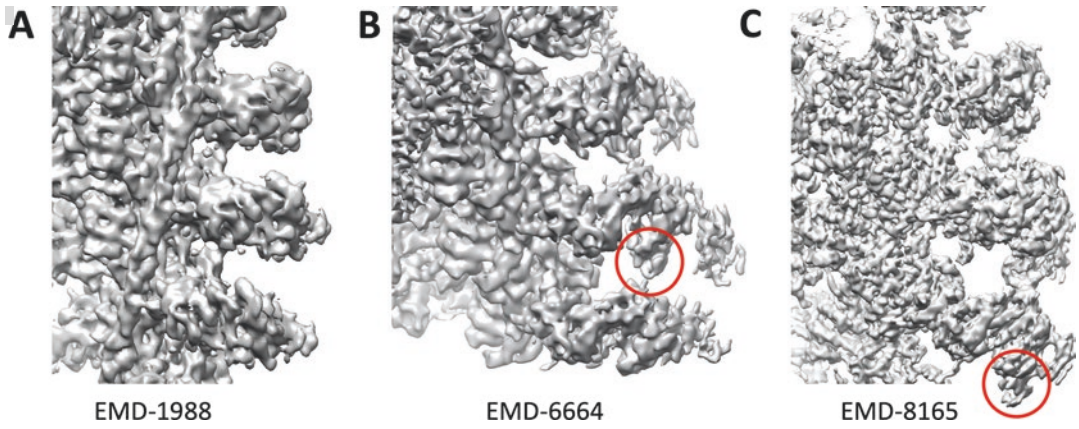

Fig. 4.5 Recent 3D helical reconstructions of actin filaments decorated with myosin subfragment-1 at increasing resolution: (**a**) 7.4 Å from Behrmann et al. (2012) including tropomyosin, data found as EMD-1988 in EMDataResource.org; (**b**) 5.2 Å from Fujii and Namba (2017) as pure F-actin, EMD-6664; (**c**) 3.9 Å from von der Ecken et al. (2016) including tropomyosin, EMD-8165. Note the different appearance of details with increasing resolution but also the likeness of the general fit of the binding motor domain. The red circle marks the N-terminal beta-barrel of myosin. (All maps are visualized using the graphics software USCF Chimera (Pettersen et al. 2004))

electron detectors used. Maybe the best comparison and most obvious effect is seen by the direct juxtaposition of a by then state-of-the-art "pre-revolution" F-actin reconstruction (Fujii et al. 2010) and the at present best published F-actin cryo electron microscopy reconstruction at about 3.1 Å resolution (Chou and Pollard 2019) as shown in Fig. 4.6.

That latter study included an interesting comparison of F-actin structures published over the years derived by different techniques ranging from X-ray diffraction on ordered gels to cryo electron microscopy. Again, the boost in resolution for microscopy is apparent, but also the differences in resolution, which correlate with details of data collection and data processing. Here, technologies proved a mixed bag, e.g., the use of electron energy filtering microscopy, which has been around for a long time but has been belittled, seems to improve resolution, while the recently hyped physical phase plates in their current implementation seem to deteriorate highest resolution. It will be interesting to see where cryo electron microscopy goes from there and which standard will emerge in the next years.

The newest reconstructions of F-actin provide a detailed analysis of the actin polymerization mechanism derived from the comparison of three reconstructions (AMPPNP, $ADPP_i$, ADP), all in the resolution range of 3.1–3.7 Å (Chou and Pollard 2019; cf. also Bradshaw and Paul 2019).

4.3.2 The 50-kDa Domain in Its Strongly Bound State and the Acto-myosin Interface

Quite a few high-resolution reconstructions have by now described the Rigor state of the myosin motor domain bound to F-actin alone (Mentes et al. 2018) or thin filaments without troponin (Behrmann et al. 2012; van der Ecken et al. 2016). In the overall structure of the Rigor complex, i.e., the orientation of myosin's motor domain at the surface of F-actin, there have been very few changes to earlier medium resolution data (cf. Fig. 4.4b, Holmes et al., 2003). In particular, the details about the closure of the deep cleft in the 50-kDa domain of myosin still hold. This closure changes the orientation of the so-called switch-1 with respect to the bound nucleotide (cf. Fig. 4.10 and also Chap. 2 on myosin structure by Sweeney and colleagues), thus weakening its binding interaction. The detailed

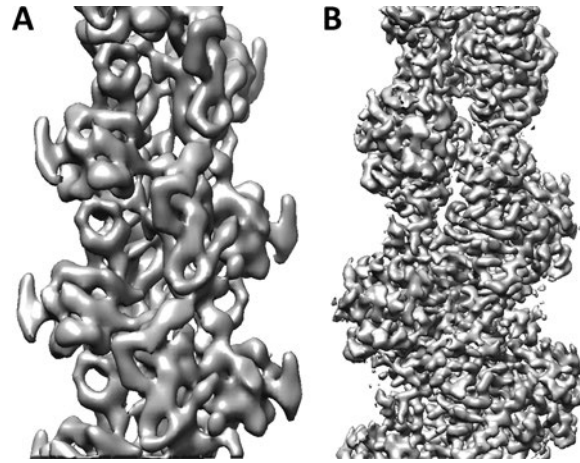

Fig. 4.6 Comparison of 3D reconstructions of filamentous actin before (**a**) and after (**b**) the "resolution revolution" originating from the use of movie correction made possible by the fast frame rates of Direct Electron Detectors. (**a**) from Fuji et al. (2010), data found as EMD-5168 in EMDataResource.org; (**b**) from Chou and Pollard (2019), EMD-7936. This direct comparison of the two reconstructed 3D maps illustrates the difference in information content and obvious detail when highest resolution (here 3.1 Å) is available. (All maps are visualized using the graphics software USCF Chimera (Pettersen et al. 2004))

amino acid interactions of this coordination vary slightly among the different reconstructions, but the general concept that the transition from a weakly to a strongly bound state of the acto-myosin interaction will affect nucleotide coordination and binding strength is still correct. Interestingly, the dissociation of the motor domain from the filament upon ATP binding must – in principle – reverse this step. That is, by recruiting switch-1 for nucleotide coordination, the cleft in the 50-kDa domain is forced to open and the motor domain dissociates from F-actin. As is described below, the weakly bound state upon formation of the acto-myosin binding complex and also the structures when myosin dissociates from the strongly bound complex are not known at present, and thus a molecular mechanism for this is not really known. But we can assume that the detailed interactions in myosin are not "symmetric", i.e., the sequence of steps when going through the crossbridge cycle is reflected in an order of structural changes not freely interchangeable. An example of such a directed change could be the coordination of the N-terminal extension of myosin with the lever arm now seen upon ADP release (cf. Fig. 4.9, Mentes et al. 2018). It has to be seen which other structures of the crossbridge cycle will be available in the future.

It should be mentioned that the structures by Behrmann et al. (2012) and van der Ecken et al. (2016) show additional details about the interactions of amino acids in the interface between myosin and actin. This gives new information regarding the effects of mutations in surface loops of actin and myosin interrupting the interface between myosin and actin and thus cause pathological effects, such as, e.g., familial cardiomyopathies.

4.3.3 The ADP-State of Myosin Strongly Bound to Actin – And What It Tells Us About Force Sensing

Two studies, albeit at different levels of resolution, lately compared the nucleotide-free myosin Rigor model with the conformation where the nucleotide ADP is bound. Wulf et al. (2016) used myosin 5 (myo5) for their reconstructions (ending up at about 6-8 Å resolution), while Mentes et al. (2018) used myosin 1b (Myo1b) reaching resolutions in the order of 3.2–4.1 Å. Figure 4.7

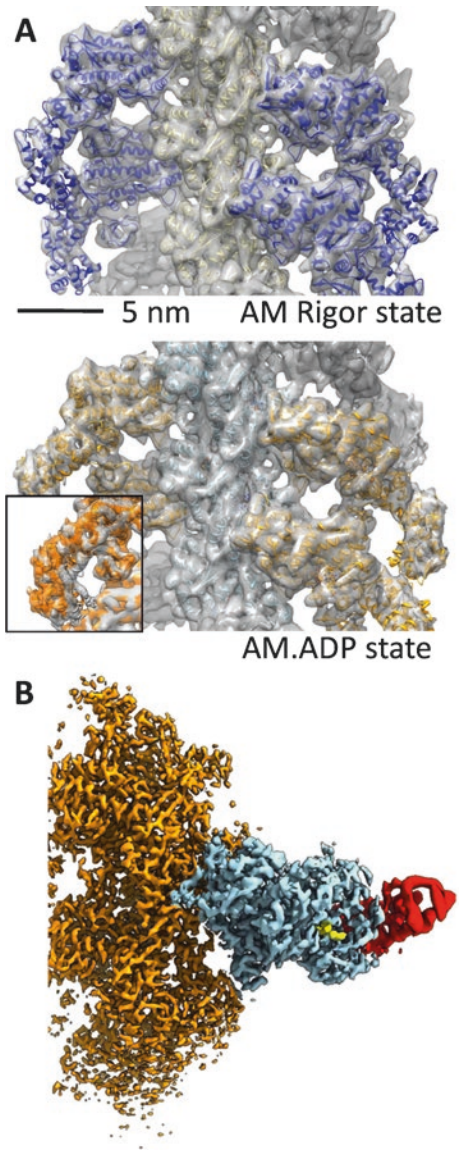

Fig. 4.7 Comparison of 3D reconstructions of F-actin decorated with myosin 5 (**a**) from Wulf et al. (2016) and F-actin 1B decorated with myosin (**b**) from Mentes et al. (2018). Note the difference in resolution (about 6 Å for (**a**), about 3.3 Å for (**b**)), equivalent to the situation for F-actin alone illustrated in Fig. 4.6. Both reconstructions are from samples in their AM.ADP states. (Pictures copyright by PNAS/United States National Academy of Science (US))

shows the general appearance of the reconstructions and focusses also on the central beta-sheet (the so-called transducer; Coureux et al. 2004). It was long speculated that this beta-sheet – together with other structural elements, in particular the N-terminal domain, which includes part of the beta-sheet – couples the lever arm to the nucleotide-binding site. And indeed, one of the more obvious changes between the ADP and Rigor state is the position of the lever arm and the bending and twisting of the transducer domain. In simple terms, pulling at the lever arm in opposite direction to its power stroke will also pull at the central beta-sheet (and other structural elements, see below) which leads to a lower probability of the ADP leaving the nucleotide-binding site. Conversely, when allowed to swing freely in its genuine power stroke direction, myosin changes its conformation such that ADP can rapidly leave the molecule.

This simple scheme can provide a first mechanistical model, e.g., for the coordination of heads in the processive walking of myosin 5 as well as the force sensing of a number of different myosins.

Mentes et al. (2018) in fact contribute a very detailed mechanistical model of how mechanical load prevents MgADP release and thus obstructs the transition from an intermediate acto-myosin-ADP state to the final Rigor state after the power stroke. Figure 4.8 (adapted from their original publication) illustrates the detailed changes of the molecular conformation when transitioning from (i) an AM.ADP state (denoted $AM.ADP^{A}$) with the lever arm not yet in a Rigor-like position to (ii) a second AM.ADP state which still has ADP bound, but the lever arm has already moved ($AM.ADP^{B}$), to (iii) the Rigor state. The definition of the second $AM.ADP^{B}$ state with its moved lever arm resulted from the classification of reconstructed data, i.e., while the majority of acto-myosin complexes were in the state $AM.ADP^{A}$, about 15% of the complexes included in the reconstruction had the lever arm almost in the Rigor position, but ADP was still present. This succession of states and their changes regarding the coordination of loop 5 and the N-terminal subdomain, as illustrated in Fig. 4.9, can be put together as a working hypothesis in the following mechanistical model: The swinging of the lever arm is coupled to the nucleotide, which is bound in the motor domain by the now

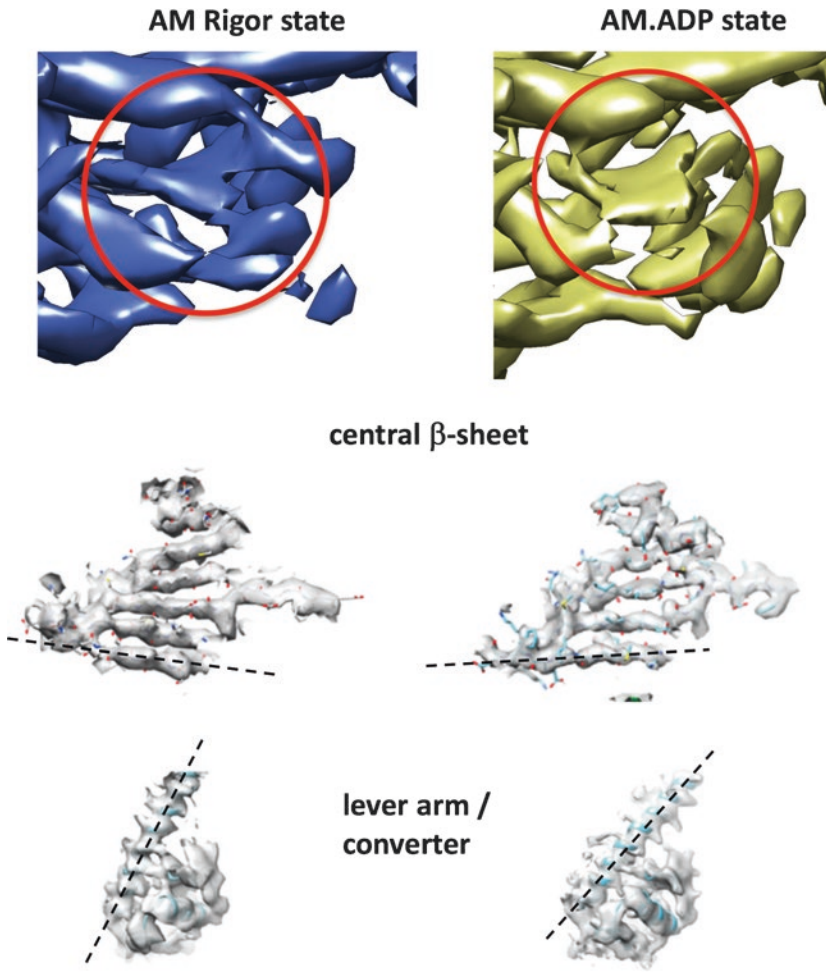

Fig. 4.8 The conformations of myosin's central beta-sheet in the nucleotide-free Rigor state and the AM.ADP state – where ADP is still bound in the nucleotide binding pocket (upper two rows; top row from Wulf et al. (2016) – beta strands in the sheet are not resolved at 6 Å resolution, while the strands are very well resolved in the reconstruction from Mentes et al. (2018) at 3.3 Å resolution. Note the distinct difference in the bending of the beta-sheet for the two different nucleotide states. The difference between Rigor and AM.ADP is also reflected in the direction of the lever arm, which is illustrated for the data from Mentes et al. (2018) (bottom row). (Pictures adapted from images in the cited publications in PNAS/United States National Academy of Science (US))

so-called N-terminal subdomain (which also includes part of the central beta-sheet). In the individual small figures in row D this subdomain is shown in blue, also including the N-terminal extension. While the latter coordinates with the subdomain in the AM.ADP state (aka AM.ADP^{A}, cf. Fig. 4.9 row C, note the different binding of the extension coloured in magenta), it starts to interact with the lever arm in the intermediate state (AM.ADP^{B}). Future studies (e.g., Molecular Dynamics calculations driving a transition among these three structures) may show what the energy landscape of these three structures looks like and why the conformational changes happen in the sequence observed now. It may be envisaged that pulling at the lever arm may allow the N-terminal extension to change its binding position with a higher probability and thus to weaken the otherwise stabilized AM.ADP^{A} state. In the rigor state this extension is then again coordinated to the lever arm. The important result of the work is the visualization of an existing intermediate state,

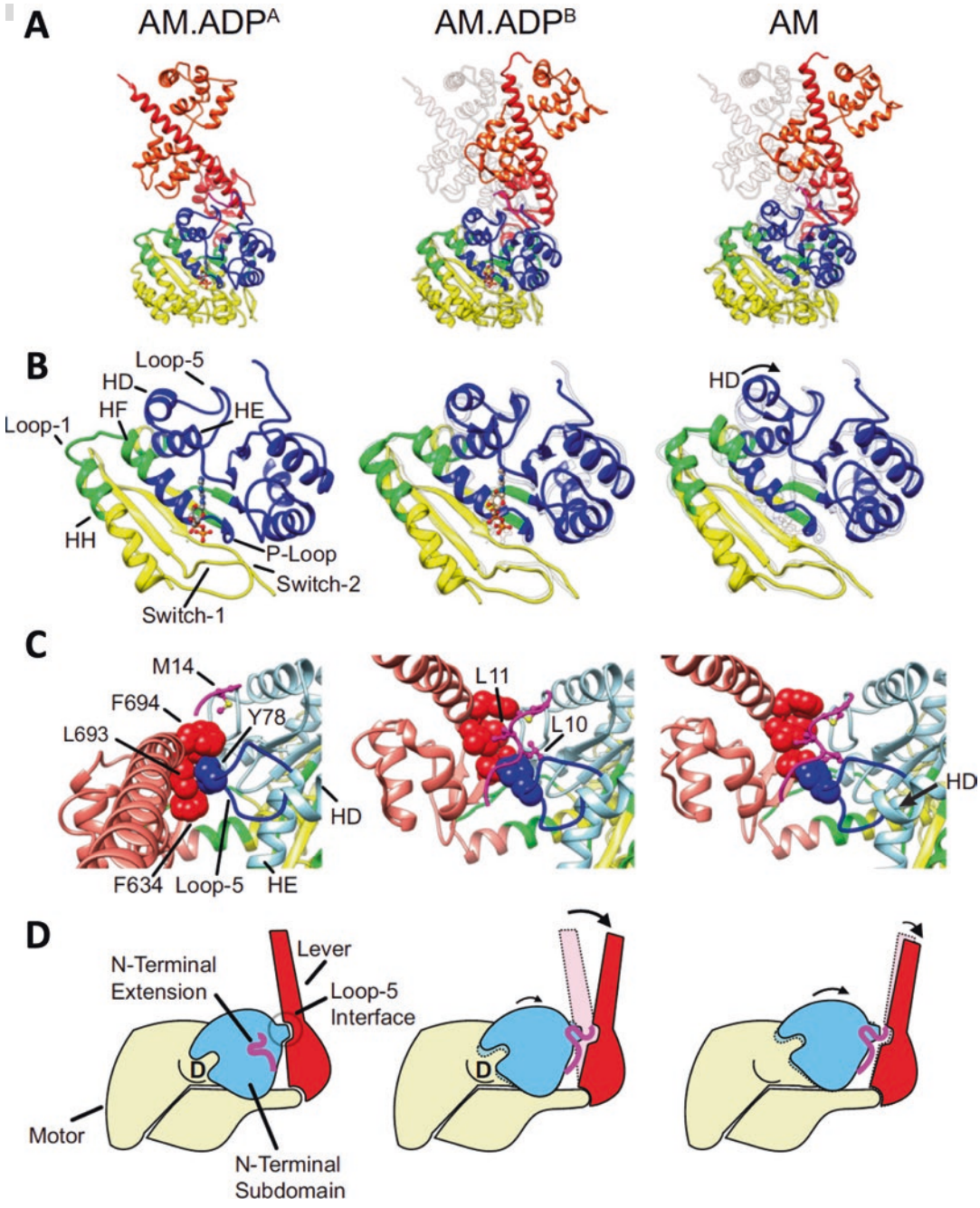

Fig. 4.9 Figure from Mentes et al. (2018) illustrating the detailed changes in lever arm direction and coordination of the N-terminal subdomain/N-terminal extension in the different states AM.ADP^{A}, AM.ADP^{B}, and Rigor (AM). The two ADP states were found in the ensemble of recorded ADP acto-myosin filaments, with the majority (85%) of complexes in the AM.ADP^{A} form. AM.ADP^{B} is supposed to be an intermediate with the lever arm already swinging into the usual direction of the Rigor state. (**a**) shows the general conformation of nucleotide binding pocket, central beta-sheet, N-terminal domain (blue) and lever arm (red). (**b**) shows details of the nucleotide binding site, and (**c**) illustrates the corresponding conformations for the N-terminal extension (magenta) interacting either with the N-terminal domain or the lever arm. These changes are combined with a large change of the coordination of loop-5 and the swinging of the lever arm into its Rigor direction. (**d**) Schematic models for the three discussed states. (Picture copyright by PNAS/United States National Academy of Science (US))

which shows the changes of the coordination of the N-terminal extension.

It should be mentioned here that for myosin 6 (Wells et al. 1999) mechanisms for force sensing were discussed as well (Gurel et al. 2017), but they were not based on any structural data of acto-myosin at that level of resolution.

4.4 Putting All the Information Together – The Crossbridge Cycle

By combining all the crystallographic, spectroscopic and microscopic data, one can compile a detailed description of states and transitions of the motor's crossbridge cycle. The best compilation to date is given in Fig. 4.10, adapted from a recent review by Robert-Paganin et al. (2019; cf. also Chap. 2 on myosin structure by Sweeney and colleagues).

Two details of this crossbridge cycle scheme are noteworthy: At present we have no experimental evidence for a defined structure after the first, non-stereospecific initial association of the ADP.P_i-loaded pre-power stroke myosin. However, there must be a transition to a specific binding of the lower and upper 50-kDa domain, which initiates a sequence of conformational changes leading to the power stroke. The second point then concerns the structure of this specific binding, which can be imagined as a somewhat open conformation as proposed by Robert-Paganin et al. (2019) or already with a further closed cleft as proposed e.g., by Behrmann et al. (2012). Experimental evidence for such details is not overwhelming as all the modelling is based on crystallographic states of myosin on its own. It is most likely that these conformations – which *a priori* only describe possible states in free myosin's conformational space – will also be used by myosin when interacting with actin. But we have to remember that there are no interpretable structural data for any weakly bound acto-myosin states (cf. below). Considering the evidence for other states and transitions in the crossbridge cycle, in particular our detailed understanding of the transition between AM.ADP and the Rigor state, it seems not irrelevant to wait for more structural data of such weakly bound complexes. Whether this will be crystallographic data or reconstructions from cryo electron microscopy has to be seen, but certainly both will help to shed more light onto the details of the initial binding of myosin to actin, phosphate release and the initiation of the lever arm swing with its transition to the above discussed AM.ADP^{A} state.

4.5 The Future of the Field – Chasing the Weakly Bound Acto-myosin States

Very little progress has been reported on crystallizing any acto-myosin complex, and the small steps, e.g., efforts to stop actin from polymerizing resulting in formation of a small, F-actin-like oligomer (Qu et al. 2018; Dawson et al. 2003), should not be overinterpreted. However, after the success of cryo electron microscopy described so far in analyzing more or less ordered complexes – and also watching the advances of classification and sorting of states applied in other fields of biomedical research – one should reconsider the possibilities of advanced sample preparation.

As is well known from stop-flow kinetic experiments, rapid mixing is one possible way to populate transient states. In the case of electron microscopy this could be translated into a rapid mixing and freeze experiment. In this experiment a myosin suspension with gold nanoparticles is sprayed onto an electron microscopy grid that is already covered by a thin film of a suspension of actin filaments. The grid is quick-frozen milliseconds after spraying, so that the mixing time is very short. The gold nanoparticles in the myosin solution are used as markers that the myosin spray has actually hit the sample. Figure 4.11a from Walker et al. (1999) shows a vitrified ice layer with two such nanoparticles and two F-actin filaments, which do not show the typical arrowhead appearance of well-ordered myosin decorated F-actin filaments (cf. Figs. 4.2 and 4.3), but look like myosin randomly interacting with the filament. This indicates that myosin might not yet be bound in a stereospecific way, which makes it

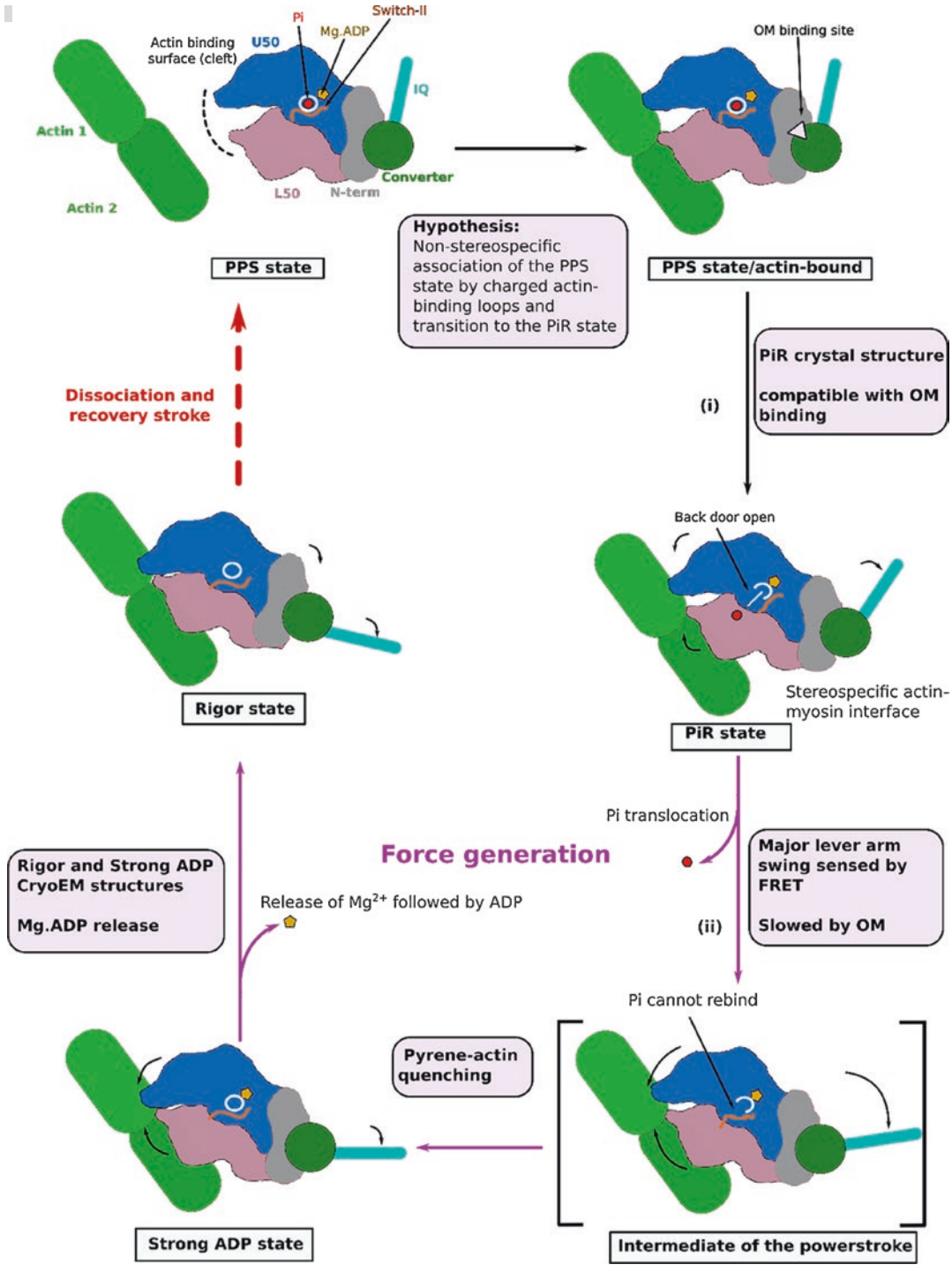

Fig. 4.10 Schematic of the crossbridge cycle proposing a detailed structural and mechanistic model for the different states of the myosin motor domain. This detailed model has very recently been proposed in Robert-Paganin et al. (2019), cf. also chapter 2 on the structure of myosin in this book. (Picture copyright by American Chemical Society (US))

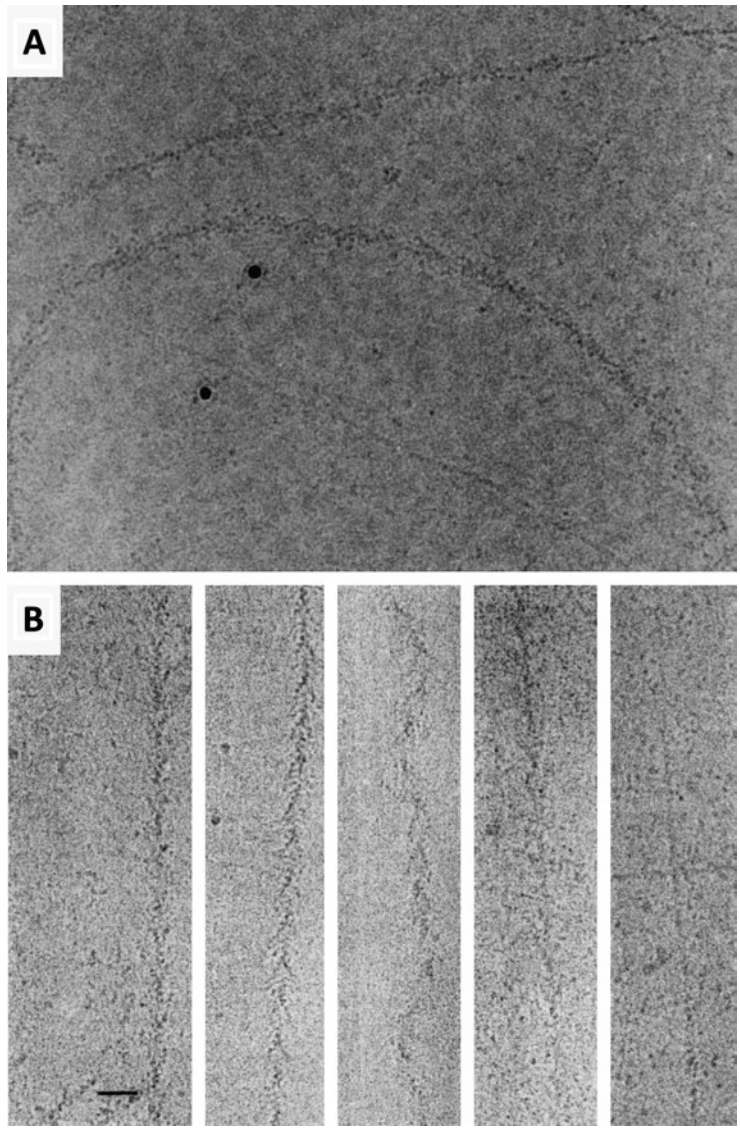

Fig. 4.11 Capturing dynamic states of the acto-myosin complex, which are intermediates in the crossbridge cycle (cf. Fig. 4.3, states marked by orange ellipses). (**a**) nucleotide-free myosin subfragment-S1 sprayed onto a suspension of F-actin and then quick-frozen to stop binding reaction in an early/intermediate weak binding state. Picture from Walker et al. (1999), copyright by PNAS/United States National Academy of Science (US). Note the disordered appearance of the myosin molecules interacting with F-actin. Conventionally, i.e. some more time after mixing, myosin would form nicely ordered "arrowheads" as shown in Fig. 4.2. The data are consistent with the hypothesis that the initial coordination of myosin molecules upon actin binding is non-stereospecific. However, it should be noted that the experiments shown here are in the absence of nucleotide, i.e., they are not identical to the initial binding of myosin in an ADP.P_i state. (**b**) Time-resolved dissociation of myosin subfragment-1 from F-actin (Ménétret et al. 1991). In this experiment flash-photolysis of caged-AMPPNP was used, which slows down nucleotide binding and complex dissociation and thus allows to freeze intermediate states. Freezing delay after flashing (left to right): no flashing, 20 ms, 30 ms, 80 ms, 2 s. Scale bar 35.5 nm. Note the curly appearance of the intermediates at 30 ms delay time, which may indicate breaking of the helical symmetry of the F-actin filament by the still interacting myosin molecules. (Picture from Ménétret et al. (1991), copyright by Elsevier)

likely that such myosins are attached in a weakly binding state – as desired.

The lack of symmetry, which is in contrast to what would be expected from a well-ordered decoration, makes image processing complicated for such samples. In principle, a single-particle approach could be applied if myosin molecules were only sparsely attached to the filament. Then, the F-actin backbone could be used for aligning the molecules, while classification might sort a wider distribution of motor domain attachment geometries. If enough molecules are selected even averaging the molecules to higher resolution might be feasible. Such an approach needs to be repeated with modern microscopes and direct electron detectors. It may help to visualize the first interactions of the motor domain with F-actin and to find out what conformation of the 50-kDa cleft is adopted (cf. Fig. 4.9 and discussion above). An additional interesting detail is exposed by Fig. 4.10a: While a cooperative effect for strong binding of myosin to actin has been described many times (e.g., Prochniewicz et al. 1996), it seems as if the weakly bound states could prime the filament for motor domain binding, too. While two actin filaments seem to be covered by myosin to a rather high degree, another filament is still completely bare. This is a surprising observation, which might indicate that already for non-stereospecific interactions myosin molecules can link adjacent actin monomers, e.g., bridge them with different attachment geometries of the lower and upper 50-kDa domain with a still reasonably open cleft. This is all speculation at this point, but this discussion should awaken interest in more dynamic sample preparation experiments and high-resolution image processing of micrographs from such samples.

Another experiment exploring a dynamic sample preparation technique is illustrated in Fig. 4.11b, which shows the detachment of motor domains from filamentous actin. In this experiment (Ménétret et al. 1991) flash-photolysis of ATP or AMPPNP was used to add nucleotide just milliseconds before rapid freezing. While ATP leads to a rapid detachment of myosin from F-actin, AMPPNP slows down this process and "intermediates" of the detachment process can be followed. In Fig. 4.10b a succession of filament appearances from left (no free nucleotide is added) to right (freezing 2 s after AMPPNP release) is shown. In itself the detachment process is certainly less exciting to study as we cannot expect further insight into the power stroke mechanism. One aspect of the process is the appearance of "curly" filaments, which could be explained by a local symmetry breaking of the actin helical symmetry when individual motor domains are detaching. This is interesting, as helical symmetry of actin filaments does indeed change when proteins bind to actin; a very large symmetry change was discovered by McGough et al. (1997) for cofilin binding to actin. But on a smaller scale this is also observed for the acto-myosin complex as decorated filamentous actin. Chou and Pollard (2019) report a consistent 27.4-Å axial repeat/ −166.6° helical turn for their different F-actin reconstructions, while actin filaments decorated with myosin 5 (Wulf et al. 2016) showed similar axial repeats at a larger helical turn (−167.1 to −167.4°) as refined by an iterative helical reconstruction process (Egelman 2007). Recently, work by Huehn et al. (2018) on cofilin-decorated filaments demonstrated that the change in symmetry of the filaments occurs quite localized at the boundary between decorated and bare filament areas. In that particular case the change in helical symmetry is quite large resulting in a helical turn of −162.1° (McGough et al. 1997; Galkin et al. 2011).

While information about the mechanism of the motor might not be derived from these observations they might help to better understand the dynamics of actin and how different conformations of the filament might be adopted.

Finally, a more complex approach to the visualization of weakly bound states – and in fact all the states in the myosin crossbridge cycle – should be discussed: cryo electron tomography on sarcomeres of vitrified muscle samples. It is possible to quick-freeze contracting muscle fibers (Taylor et al. 1999), and Figs. 4.12 and 4.13 show different views of 3D tomographic reconstructions of ultrathin sections of freeze-substituted and plastic-embedded muscle (Wu et al. 2010, 2012). While there is no doubt that such a sample prepa-

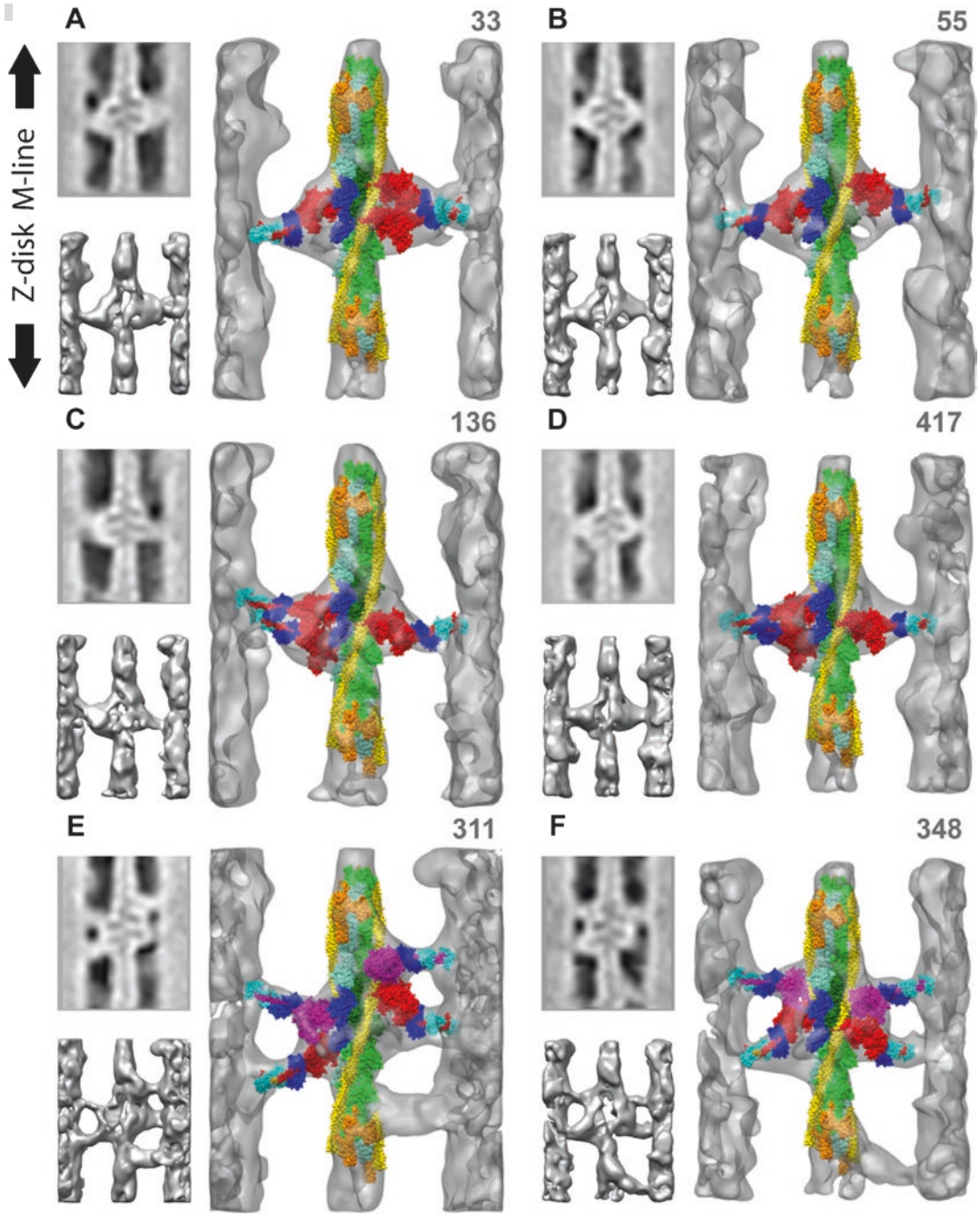

Fig. 4.12 Conventional electron tomography of ultrathin plastic sections of quick-frozen muscle after freeze substitution. Picture from Wu et al. (2010), copyright by PLOS, US. The 3D rendering illustrates different classes of interaction motives found for the crossbridges between thick and thin filaments (cf. also Fig. 4.2). These motives are found after classification and averaging of corresponding motives in 3D. This averaging procedure reduces noise considerably, permitting an initial attempt of docking myosin motor domains into the reconstructed densities

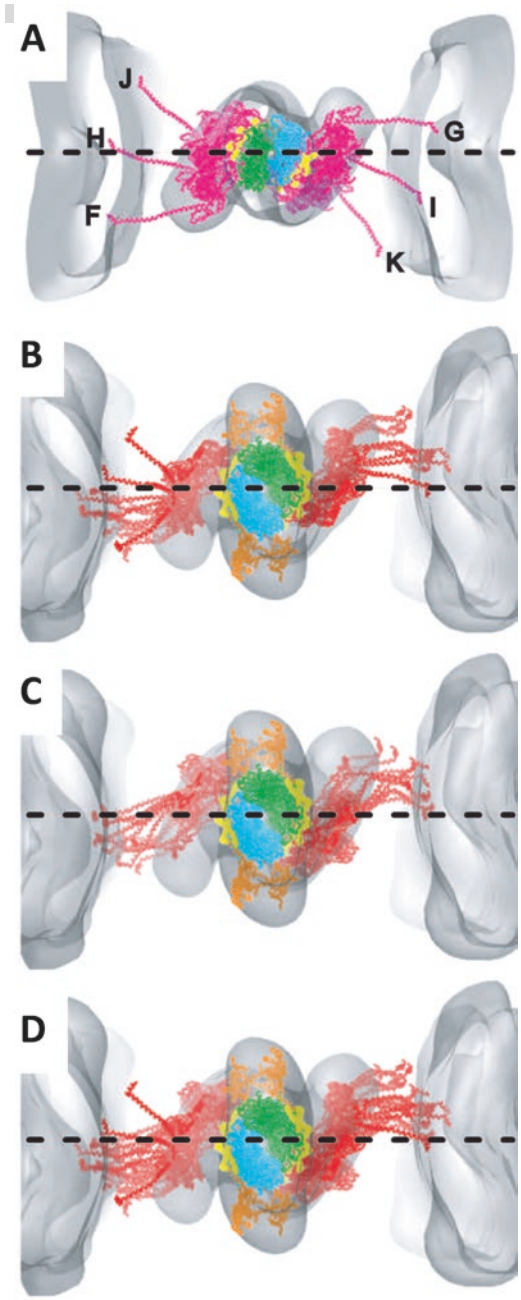

Fig. 4.13 Distribution of possible orientations of the myosin motor domain and lever arm fitted into cross-bridge densities of electron tomograms from muscle fibre sections (prepared as in Fig. 4.12). (**a**–**d**) Different distributions of orientation for different interaction motives as seen in Fig. 4.12. (Picture from Wu et al. (2010), copyright by PLOS, US)

ration comes with quite severe fixation, staining, and embedding artifacts, it is still surprising at what level of detail such tomograms can be interpreted. They can certainly not satisfy the need for high-resolution structures, but they do illustrate a possible roadmap to high-resolution structures. What has to be developed next is a routine workflow to prepare cryo samples of sarcomeres for cryo electron tomography. Focused ion beam milling of cellular samples has been developed in recent years (Schaffer et al. 2017) as well as cryo lamella lift out from larger samples (Schaffer et al. 2019). If a really large number of tomograms from such lamella can be recorded, then classifications similar to those discussed in Taylor et al. (2019) might result in many different states of the myosin motor domains. When bringing these states into the correct successive order such work might provide us with movie-like data of all possible structures of actin and myosin and the acto-myosin complex in the crossbridge cycle.

References

Behrmann E, Müller M, Penczek PA, Mannherz HG, Manstein DJ, Raunser S (2012) Structure of the rigor actin-tropomyosin-myosin complex. Cell 150:327–338

Bradshaw M, Paul DM (2019) After the revolution: how is Cryo-EM contributing to muscle research? J Muscle Res Cell M 40:93–98

Campbell MG, Cheng A, Brilot AF, Moeller A, Lyumkis D, Veesler D, Pan J, Harrison SC, Potter CS, Carragher B, Grigorieff N (2012) Movies of ice-embedded particles enhance resolution in electron cryo-microscopy. Structure 20:1823–1828. https://doi.org/10.1016/j.str.2012.08.026

Chou SZ, Pollard TD (2019) Mechanism of actin polymerization revealed by cryo-EM structures of actin filaments with three different bound nucleotides. Proc Natl Acad Sci U S A 116:4265–4274

Clough RN, Moldovan G, Kirkland A (2014) Direct detectors for electron microscopy. J Phys Conf Ser 522:012046. https://doi.org/10.1088/1742-6596/522/1/012046

Coureux PD, Sweeney HL, Houdusse A (2004) Three myosin V structures delineate essential features of chemo-mechanical transduction. EMBO J 23:4527–4537

Cressey D, Callaway E (2017) Cryo-electron microscopy wins chemistry Nobel. Nature 550:167. https://doi.org/10.1038/nature.2017.22738

Dawson JF, Sablin EP, Spudich JA, Fletterick RJ (2003) Structure of an F-actin trimer disrupted by gelsolin and implications for the mechanism of severing. J Biol Chem 278:1229–1238

Egelman EH (2007) The iterative helical real space reconstruction method: surmounting the problems posed by real polymers. J Struct Biol 157:83–94

Flicker PF, Milligan RA, Applegate D (1991) Cryo-electron microscopy of S1-decorated actin filaments. Adv Biophys 27:185–196

Fujii T, Namba K (2017) Structure of actomyosin rigour complex at 5.2 Å resolution and insights into the ATPase cycle mechanism. Nat Commun 8:13969. https://doi.org/10.1038/ncomms13969

Fujii T, Iwane AH, Yanagida T, Namba K (2010) Direct visualization of secondary structures of F-actin by electron cryomicroscopy. Nature 467:724–728. https://doi.org/10.1038/nature09372

Galkin VE, Orlova A, Kudryashov DS, Solodukhin A, Reisler E, Schröder GF, Egelman EH (2011) Remodeling of actin filaments by ADF/cofilin proteins. Proc Natl Acad Sci U S A 108:20568–20572. https://doi.org/10.1073/pnas.1110109108

Gurel PS, Kim LY, Ruijgrok PV, Omabegho T, Bryant Z, Alushin GM (2017) Cryo-EM structures reveal specialization at the myosin VI-actin interface and a mechanism of force sensitivity. Elife 6:e31125. https://doi.org/10.7554/eLife.31125

Holmes KC, Angert I, Kull FJ, Jahn W, Schröder RR (2003) Electron cryo-microscopy shows how strong binding of myosin to actin releases nucleotide. Nature 425:423–427

Houdusse A, Szent-Gyorgyi AG, Cohen C (2000) Three conformational states of scallop myosin S1. Proc Natl Acad Sci U S A 97:11238–11243

Huehn A, Cao W, Elam WA, Liu X, De La Cruz EM, Sindelar CV (2018) The actin filament twist changes abruptly at boundaries between bare and cofilin-decorated segments. J Biol Chem 293:5377–5383. https://doi.org/10.1074/jbc.AC118.001843

Huxley HE (1957) The double array of filaments in cross-striated muscle. J Biophys Biochem Cytol 3:631–648

Jontes JD, Wilson-Kubalek EM, Milligan RA (1995) A 32 degree tail swing in brush border myosin I on ADP release. Nature 378:751–753

Kühlbrandt W (2014) The resolution revolution. Science 343:1443–1444

McGough A, Pope B, Chiu W, Weeds A (1997) Cofilin changes the twist of F-actin: implications for actin filament dynamics and cellular function. J Cell Biol 138:771–781

McMullan G, Faruqi AR, Henderson R (2016) Direct electron detectors. Methods Enzymol 579:1–17. https://doi.org/10.1016/bs.mie.2016.05.056

Ménétret JF, Hofmann W, Schröder RR, Rapp G, Goody RS (1991) Time-resolved cryo-electron microscopic study of the dissociation of actomyosin induced by photolysis of photolabile nucleotides. J Mol Biol 219:139–144

Mentes A, Huehn A, Liu X, Zwolak A, Dominguez R, Shuman H, Ostap EM, Sindelaar CV (2018) High-resolution cryo-EM structures of actin-bound myosin states reveal the mechanism of myosin force sensing. Proc Natl Acad Sci U S A 15:1292–1297

Milligan RA, Flicker EE (1987) Structural relationships of actin, myosin, and tropomyosin revealed by cryo-electron microscopy. J Cell Biol 105:29–39

Moore PB, Huxley HE, DeRosier DJ (1970) Three-dimensional reconstruction of F-actin, thin filaments and decorated thin filaments. J Mol Biol 50:279–295

Pettersen EF, Goddard TD, Huang CC, Couch GS, Greenblatt DM, Meng EC, Ferrin TE (2004) UCSF Chimera – a visualization system for exploratory research and analysis. J Comput Chem 25:1605–1612

Prochniewicz E, Zhang Q, Janmey PA, Thomas DD (1996) Cooperativity in F-actin: binding of gelsolin at the barbed end affects structure and dynamics of the whole filament. J Mol Biol 260:756–766

Qu Z, Fujita-Becker S, Ballweber E, Ince S, Herrmann C, Schroeder RR, Mannherz HG (2018) Interaction of isolated cross-linked short actin oligomers with the skeletal muscle myosin motor domain. FEBS J 285:1715–1729. https://doi.org/10.1111/febs.14442

Rayment I, Rypniewski WR, Schmidt-Bäse K, Smith R, Tomchick DR, Benning MM, Winkelmann DA, Wesenberg G, Holden HM (1993a) Three-dimensional structure of myosin subfragment-1: a molecular motor. Science 261:50–58

Rayment I, Holden HM, Whittaker M, Yohn CB, Lorenz M, Holmes KC, Milligan RA (1993b) Structure of the actin-myosin complex and its implications for muscle contraction. Science 261:58–65

Robert-Paganin J, Pylypenko O, Kikuti C, Sweeney HL, Houdusse A (2019) Force generation by myosin motors: a structural perspective. Chem Rev. https://doi.org/10.1021/acs.chemrev.9b00264. [Epub ahead of print]

Schaffer M, Mahamid J, Engel BD, Laugks T, Baumeister W, Plitzko JM (2017) Optimized cryo-focused ion beam sample preparation aimed at in situ structural studies of membrane proteins. J Struct Biol 197:73–82. https://doi.org/10.1016/j.jsb.2016.07.010

Schaffer M, Pfeffer S, Mahamid J, Kleindiek S, Laugks T, Albert S, Engel BD, Rummel A, Smith AJ, Baumeister W, Plitzko JM (2019) A cryo-FIB lift-out technique enables molecular-resolution cryo-ET within native Caenorhabditis elegans tissue. Nat Methods 16:757–762. https://doi.org/10.1038/s41592-019-0497-5

Scheres SHW (2012) RELION: implementation of a Bayesian approach to cryo-EM structure determination. J Struct Biol 180:519–530

Schröder RR (2015) Advances in electron microscopy: a qualitative view of instrumentation development for macromolecular imaging and tomography. Arch Biochem Biophys 581:25–38. https://doi.org/10.1016/j.abb.2015.05.010

Schröder RR, Manstein DJ, Jahn W, Holden H, Rayment I, Holmes KC, Spudich JA (1993) Three-dimensional

atomic model of F-actin decorated with Dictyostelium myosin S1. Nature 364:171–174

Sellers JR, Veigel C (2006) Walking with myosin V. Curr Opin Cell Biol 18:68–73

Taylor KA, Schmitz H, Reedy MC, Goldman YE, Franzini-Armstrong C, Sasaki H, Tregear RT, Poole K, Lucaveche C, Edwards RJ, Chen LF, Winkler H, Reedy MK (1999) Tomographic 3D reconstruction of quick-frozen, Ca^{2+}-activated contracting insect flight muscle. Cell 99:421–431

Taylor KA, Rahmani H, Edwards RJ, Reedy MK (2019) Insights into actin-myosin interactions within muscle from 3D electron microscopy. Int J Mol Sci 20:E1703. https://doi.org/10.3390/ijms20071703

Veigel C, Coluccio LM, Jontes JD, Sparrow JC, Milligan RA, Molloy JE (1999) The motor protein myosin-I produces its working stroke in two steps. Nature 398:530–533

von der Ecken J, Heissler SM, Pathan-Chhatbar S, Manstein DJ, Raunser S (2016) Cryo-EM structure of a human cytoplasmic actomyosin complex at near-atomic resolution. Nature 534:724–728

Walker M, Zhang XZ, Jiang W, Trinick J, White HD (1999) Observation of transient disorder during myosin subfragment-1 binding to actin by stopped-flow fluorescence and millisecond time resolution electron cryomicroscopy: evidence that the start of the cross-bridge power stroke in muscle has variable geometry. Proc Natl Acad Sci U S A 96:465–470

Wells AL, Lin AW, Chen LQ, Safer D, Cain SM, Hasson T, Carragher BO, Milligan RA, Sweeney HL (1999) Myosin VI is an actin-based motor that moves backwards. Nature 401:505–508

Whittaker M, Wilson-Kubalek EM, Smith JE, Faust L, Milligan RA, Sweeney HL (1995) A 35-A movement of smooth muscle myosin on ADP release. Nature 378:748–751

Wu S, Liu J, Reedy MC, Tregear RT, Winkler H, Franzini-Armstrong C, Sasaki H, Lucaveche C, Goldman YE, Reedy MK, Taylor KA (2010) Electron tomography of cryofixed, isometrically contracting insect flight muscle reveals novel actin-myosin interactions. PLoS One 5:e12643. https://doi.org/10.1371/journal.pone.0012643

Wu S, Liu J, Reedy MC, Perz-Edwards RJ, Tregear RT, Winkler H, Franzini-Armstrong C, Sasaki H, Lucaveche C, Goldman YE, Reedy MK, Taylor KA (2012) Structural changes in isometrically contracting insect flight muscle trapped following a mechanical perturbation. PLoS One 7:e39422. https://doi.org/10.1371/journal.pone.0039422

Wulf SF, Ropars V, Fujita-Becker S, Oster M, Hofhaus G, Trabuco LG, Pylypenko O, Sweeney HL, Houdusse AM, Schröder RR (2016) Force-producing ADP state of myosin bound to actin. Proc Natl Acad Sci U S A 113:E1844–E1852. https://doi.org/10.1073/pnas.1516598113

Small Molecule Effectors of Myosin Function

5

Dietmar J. Manstein and Matthias Preller

Abstract

Several small molecule effectors of myosin function that target the motor domains of myosin classes I, II, V, and VI have been identified. Four distinct binding sites in the myosin motor domain have been reported with unique properties and mechanisms of action. This chapter describes the structural basis and activities of known small molecule effectors that allosterically target the myosin motor domain.

Keywords

Actin · Allostery · Enzyme · Motility · Myosin · Small molecule effectors

5.1 Introduction

The superfamily of myosin motors has emerged as an attractive target for the modulation of their physiological function by small molecule effectors. To date, at least 14 types of allosteric small molecule effectors of the myosin heavy chain have been reported (Fig. 5.1). Small effector molecules that inhibit or activate the function of well-defined myosin isoforms do not only have great potential for the development of new therapeutics and the targeted modulation of dysfunctional myosins and myosin-related diseases, but have proven to be invaluable tools for the investigation of cytoskeletal processes in cellular systems.

A major challenge for a specific modulation of distinct myosin isoforms is the ubiquitous occurrence of these motor proteins in the human body and in important pathogens. Myosin isoforms can be grouped into at least 35 myosin classes (Foth et al. 2006; Odronitz and Kollmar 2007) with diverse and prominent roles for a wide range of intracellular processes. Myosins are involved in processes such as muscle contraction, intracellular transport, tethering, signaling and cell division, as well as organization of the cytoskeleton. The human genome contains more than 40 genes that encode myosin isoforms from 12 different classes – myosin classes I, II, III, V, VI, VII, IX, X, XV, XVI, XVIII, and XIX (Berg et al. 2001; Kollmar and Mühlhausen 2017). Structurally, myosins feature broad diversities in their tail

D. J. Manstein (✉)
Hannover Medical School, Institute for Biophysical Chemistry and Division of Structural Biochemistry, Fritz Hartmann Centre for Medical Research, Hannover, Germany
e-mail: manstein.dietmar@mh-hannover.de

M. Preller
Hannover Medical School, Institute for Biophysical Chemistry, Hannover, Germany
e-mail: preller.matthias@mh-hannover.de

L. M. Coluccio (ed.), *Myosins*, Advances in Experimental Medicine and Biology 1239,
https://doi.org/10.1007/978-3-030-38062-5_5

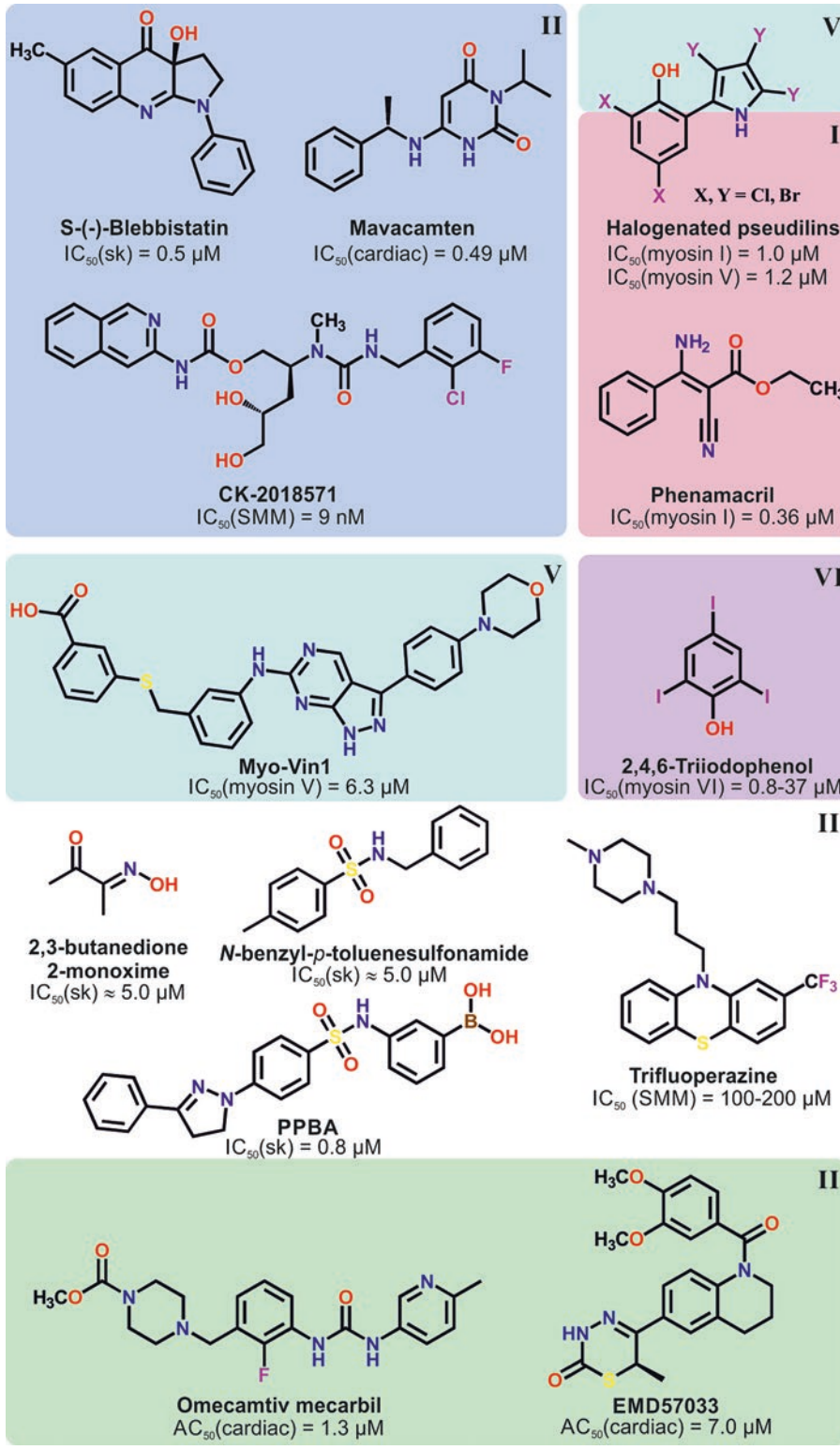

Fig. 5.1 Schematic overview of known allosteric small molecule effectors of myosin function. The small molecule effectors are grouped according to their specificities. Color code: blue = class II myosin inhibitors, red = class I myosin inhibitors, cyan = class V myosin inhibitors, purple = class VI myosin inhibitors, white = no particular specificities defined, however inhibition of myosin II is reported in the literature, green = class II myosin activators. Determined potencies of the inhibitors or activators are given as IC_{50} or AC_{50} values

regions, which are designed for cargo transport and interactions with other components of the cell, while the catalytically active motor domain is largely conserved across the myosinome. The approximately 80 kDa motor domain harbors the active site and the actin-binding region. Polar actin filaments (F-actin) serve as tracks for the directional movement of myosin motors. Several small molecule effectors have been shown to preferentially affect the generic myosin motor domain of specific isoforms. Compounds with well-defined specificity profiles serve currently as lead compounds for the development of treatments of myosin-associated diseases, in particular heart failure and hypertrophic cardiomyopathy (www.clinicaltrials.gov, identifiers NCT01300013, NCT01786512, NCT02929329, NCT02329184, NCT03470545, NCT0376855). Together, the ability of small effector molecules to exert their effect on certain myosin isoforms and the identification of at least four allosteric binding sites in the myosin motor domain illustrate the druggability of members of the myosin superfamily.

The specific modulation of individual myosin isoforms within the scope of the common "one-target-one-disease" paradigm, also known as Paul Ehrlich's magic bullet (Strebhardt and Ullrich 2008), can provide innovative access to major human diseases that are currently difficult to treat. The major focus of ongoing pharmaceutical research programs lies on diseases affecting skeletal, smooth and cardiac muscle performance (Spudich 2014; Greenberg 2016; Varian and Tang 2017; Kaplinsky and Mallarkey 2018). However, strong links have also been established between major human pathologies and cytoskeletal myosin motors (see Chap. 12). Changes in the abundance, functional competence, and regulation of cytoskeletal myosin isoforms can play causal roles in the development of neurodegenerative disorders (Nadif Kasri and Van Aelst 2008; Hur et al. 2011; Ma and Adelstein 2014), diabetes (Charlton et al. 1997; Papadaki et al. 2018), various forms of cancer, with at least seven classes of myosins participating in tumorigenesis and cancer proliferation (Li et al. 2016b), viral, bacterial, and parasitic infections (Xiong et al. 2015; Cymerys et al. 2016; Cowman et al. 2017; Tan et al. 2019), and drug addiction (Young et al. 2015; Volkow and Morales 2015). The identification of specific small molecule effectors that change the function of the associated myosin isoforms in a well-defined manner can provide means to cure or at least treat the affected patients. These diseases are however complex, with diverse causative factors, versatile mechanisms to adapt to altered conditions and drug treatments, and several groups of myosin isoforms displaying functional redundancy. Therefore, analogous to the multitarget drug discovery concept (Roth et al. 2004; Morphy and Rankovic 2005; Keith et al. 2005; Ramsay et al. 2018), which yielded promising applications in various areas, such as e.g. multikinase inhibitors, accounting for the majority of the approved kinase inhibitor agents (Cohen and Alessi 2013), the development of multimyosin drugs has the potential to yield compounds with improved therapeutic potency and superior safety profiles.

This chapter will review the current status of small molecule effectors of myosin function, and focus on compounds that allosterically target the myosin motor domain.

Four classes of myosins, classes I, II, V, and VI, were shown to be affected by small effector molecules. The first part of this chapter will outline the structural basis underlying the modulating effect of the small molecules. How do the effector molecules bind to their target myosins; what factors determine their isoform specificity; and what is the structural mechanism behind their modulating effect? The second part will elaborate on the specificity of the small molecule effectors towards myosin isoforms or classes, in particular associated diseases, and their application in scientific studies of the function of myosins in the cell. Finally, allosteric modulation triggered by protein-protein interactions will be discussed in the third part. While the small molecule effectors in general either increase or reduce ATP turnover, motor function or force development of myosins, they can modulate the motor properties of myosins in an even more intricate manner by affecting specific substeps of the mechanochemical cycle. Myosins share a

common motor cycle with actin-detached and -attached states that go along with large conformational changes in the myosin motor domain.

5.2 Binding Sites of Small Molecule Effectors in the Myosin Motor Domain

Structural studies have so far revealed four distinct allosteric binding pockets in the myosin motor domain for small molecule effectors (Allingham et al. 2005; Fedorov et al. 2009; Preller et al. 2011b; Sirigu et al. 2016; Planelles-Herrero et al. 2017). These binding pockets share a primarily hydrophobic nature but with both apolar and polar residues contributing to the interaction with the small molecule effectors. The binding pockets are found in regions that are known to be important for mechanochemical coupling between critical remote sites in the motor domain.

During myosin motor activity, ATP binding, hydrolysis, and release of hydrolysis products are coupled to large scale rearrangements of structural elements that affect actin binding and the position of the lever arm. An actomyosin ATPase cycle that associates chemical changes affecting the nucleotide with large-scale conformational changes was first proposed by Lymn and Taylor (Lymn and Taylor 1971) and further extended over time by the introduction of additional substrates, contributing to myosin function (Preller and Manstein 2017). Critical structural elements or regions of the myosin motor domain that determine the state and the properties of the myosin motor domain include the actin-binding cleft, the central seven-stranded β-sheet, also known as the transducer, the relay helix, the SH1/SH2-region, the converter domain together with the adjacent lever arm, and the active site elements switch-1, switch-2, and the P-loop. To briefly recapture the actomyosin ATPase cycle, starting with the nucleotide-free, strongly actin-bound rigor state of myosin, the motor domain features a closed actin-binding cleft, which is responsible for the favorable and strong interaction with the actin filament. The converter and lever arm in this state are in the down position, the relay helix is straight, and the transducer is twisted. Binding of ATP leads to small-scale rearrangements in the active site, the associated opening of the actin-binding cleft, and the dissociation of the myosin motor domain from the actin filament. This ATP-bound state is referred to as the post-rigor state with the converter and lever arm still in the down position. In addition to the coupling between the active site and the actin-binding cleft, conformational changes in the active site are coupled via the transducer, the relay helix, the SH1/SH2-region, and the converter domain to a swinging of the lever arm. Subsequent to ATP-induced actin detachment, the converter domain rotates from the down to the up position, a process also known as the recovery stroke of myosin, which primes the lever arm for force generation. The recovery stroke includes structural changes in the central β-sheet, which untwists and a bending of the long relay helix, which in turn is coupled to repositioning of the SH1/SH2-region to allow the converter being rotated. The recovery stroke is suggested to follow a stepwise seesaw mechanism (Fischer et al. 2005; Kintses et al. 2008) leading to the catalytically competent pre-power stroke state, in which ATP is hydrolyzed to ADP and P_i. Hydrolysis leads to a relaxation of binding constraints in the active site. As a consequence of conformational changes that are coupled to the subsequent opening of the active site, the myosin reattaches to the actin filament by closing of the actin-binding cleft, which together with the release of the inorganic phosphate initiates twisting of the central β-sheet, straightening of the relay helix, and finally the power stroke, which drives the converter and lever arm from the up position back to the down position. In the last substep of the cycle, ADP is released from myosin and drives the motor domain back to the rigor state. ATP binding starts a new round of the ATPase cycle (Geeves et al. 2005; Houdusse and Sweeney 2016).

The four identified allosteric binding sites for blebbistatin, the series of halogenated pseudilins, CK-571, and omecamtiv mecarbil involve structural elements that have been shown to play a crucial role in the coupling mechanisms within

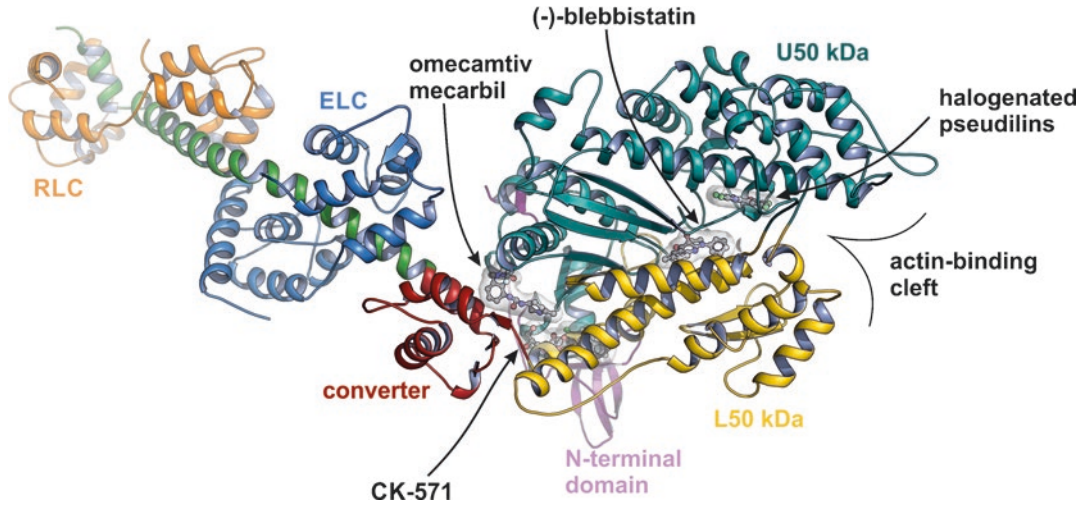

Fig. 5.2 Overview of the four identified allosteric binding pockets in the myosin motor domain of small molecule effectors, mapped to the crystal structure of myosin II. The binding sites were determined by co-crystallization of myosin in complex with (−)-blebbistatin (pdb 1yv3), halogenated pseudilins (pdb 2jhr, 2xo8, 2xel), CK-571 (pdb 5 t45), and OM (pdb 5n69). Subdomains and critical structural elements of the motor domain are color coded and labeled in the diagram

the myosin motor domain (Fig. 5.2). The binding site for blebbistatin directly involves active site switch-2 residues as well as residues of the relay helix and the actin-binding cleft, explaining the effect of blebbistatin on the actomyosin interaction and product release. Halogenated pseudilins bind approximately 7.5 Å apart from the blebbistatin site near actin-binding residues at the top of the cleft. Their binding involves residues of loop 2 and the strut loop of myosin, which were shown to support coupling between the active site state and the actin-binding region. CK-571 binding involves residues of the SH1/SH2-region and the relay helix, thereby inhibiting the coupling between ATP hydrolysis and converter rotation. Omecamtiv mecarbil involves extensive interactions with the N-terminal subdomain and the converter, in addition to contacts with the relay helix and the transducer. The clustering of allosteric binding pockets at critical intersections of the communication pathways in the motor domain brings up the question whether further effector molecules and binding pockets can be identified along the pathways that couple distant sites in the myosin motor domain and how differences between myosin isoforms can be exploited to support the development of potent and specific small molecule myosin effectors (Table 5.1).

5.2.1 Binding Site at the Apex of the Actin-Binding Cleft (Blebbistatin Site)

Blebbistatin was identified as a potent inhibitor of skeletal myosin II and nonmuscle myosin II isoforms in 2003 (Straight et al. 2003) and was the first myosin inhibitor whose structural mechanism was determined using X-ray crystallography (Allingham et al. 2005). The small molecule effector inhibits myosin II isoforms with half maximal inhibitory concentration (IC_{50}) values between 0.5 and 80 μM, while myosins from classes I, V, and X have $IC_{50} > 150$ μM (Limouze et al. 2004). Blebbistatin is a 1-phenyl-2-pyrrolidinone derivative possessing a tricyclic core scaffold (A-, B-, and C-rings) and a D-ring phenyl substituent, as well as a chiral stereocenter bearing a hydroxy group. Blebbistatin was found to bind to a primarily hydrophobic pocket in the myosin motor domain, adjacent to the γ-phosphate sensor loops (switch-1, switch-2,

Table 5.1 Summary of the properties of known allosteric small molecule effectors of the myosin motor domain

Effector	Target (potency)	Binding site	Mechanism of action	References
2,3-butanedione 2-monoxime (BDM)	Skeletal muscle myosin II ($K_i \approx 5$ mM)	n.d.	ATPase rate and force production decreased Inhibition of P_i release and stabilization of the weakly actin-bound Myosin•ADP•P_i state	Higuchi and Takemori (1989), Herrmann et al. (1992), and Mckillop et al. (1994)
N-benzyl-p-toluenesulfonamide (BTS)	Muscle myosin II ($IC_{50} \approx 5$ μM)	n.d.	In vitro gliding motility, force production and ATPase rate inhibited Actin-myosin interaction weakened and P_i release suppressed	Cheung et al. (2002) and Shaw et al. (2003)
Trifluoperazine (TFP)	Smooth, nonmuscle, skeletal muscle myosin II, myosin V ($IC_{50} \approx 40$–75 μM)	n.d.	ATPase rate and in vitro gliding motility inhibited Myosin light chains are removed at higher concentrations (1–2 mM)	Patel et al. (2000) and Sellers et al. (2003)
3-[4-(3-phenyl-2-pyrazolin-1-yl) benzene-1-sulfonylamido] phenylboronic acid (PPBA)	Skeletal muscle myosin II ($K_i \approx 0.8$ μM)	n.d.	Initially reported to operate competitively Shown to inhibit myosin allosterically by stabilizing a ternary myosin•PPBA•nucleotide complex	Hiratsuk (1994) and Hiratsuka (2006)
(−)-Blebbistatin and Blebbistatin analogs	Skeletal and nonmuscle myosin II ($IC_{50} = 0.5$–2 μM)	Allosteric binding site at the apex of the large actin-binding cleft (PDB: 1yv3, 3bz7, 3bz8, 3bz9, 3mjx)	Myosin trapped in a weak actin-binding pre-power stroke ADP•P_i state P_i release inhibited	Straight et al. (2003), Limouze et al. (2004), Kovács et al. (2004), Allingham et al. (2005), and Lucas-Lopez et al. (2008)
CK2018571 (CK-571)	Smooth muscle myosin II ($IC_{50} = 9$ nM)	Allosteric binding site between SH1/SH2 region and the relay helix	Myosin trapped in an intermediate state of the recovery stroke, reduced ATP hydrolysis and actin affinity	Sirigu et al. (2016)
Mavacamten (MYK-463)	Cardiac myosin II ($IC_{50} = 0.3$ μM)	n.d.	Reduced ATPase function and weak-to-strong transition Stabilization of an autoinhibited super-relaxed state	Green et al. (2016) and Kawas et al. (2017)
MyoVin-1	MyosinV ($K_i = 6.3$ μM)	n.d.	ATPase rate decreased ADP release inhibited	Islam et al. (2010)

(continued)

Table 5.1 (continued)

Effector	Target (potency)	Binding site	Mechanism of action	References
Halogenated pseudilins (Pentabromopseudilin (PBP), Pentachloropseudilin (PClP), Tribromodichloropseudilin (TBDClP))	PBP: Myosin-5a (IC_{50} = 1.2 μM) PClP: Myosin-1 (IC_{50} = 1.0 μM) TBDClP: Myosin-2 (IC_{50} = 47.2 μM)	Allosteric binding site close to the actin-binding region and the apex of the large internal cleft about 16 Å away from the active site (PDB: 2XO8, 2XEL, 2JHR)	ATP binding, hydrolysis and ADP dissociation inhibited, as well as coupling between actin and nucleotide binding sites reduced Active site is affected through a signal relay path as well as global protein dynamics	Fedorov et al. (2009), Chinthalapudi et al. (2011) and Preller et al. (2011a, b)
Phenamacril	*Fusarium spp.* Myosin I (IC_{50} = 0.36 μM)	n.d.	ATPase rate and motility decreased	Wollenberg et al. (2019)
2,4,6-Triiodophenol (TIP)	Myosin-6 (K_{i1} = 0.8 μM and K_{i2} = 37 μM)	n.d.	ATPase activity reduced	Heissler et al. (2012)
EMD57033	Cardiac myosin II (AC_{50} = 7.0 μM)	n.d.	ATP hydrolysis increased, improved coupling between the active site and actin-binding region, increased actin affinity Protection against thermal denaturation and heat stress	Radke et al. (2014)
Omecamtiv mecarbil (OM)	Cardiac myosin-2 (EC_{50} = 2.3 μM)	Allosteric binding site bridging the converter domain, the relay helix and the N-terminal domain	Transition from weak to strong actin-bound state accelerated and P_i release rate increased	Morgan et al. (2010), Malik et al. (2011), and Planelles-Herrero et al. (2017)

n.d. = not determinded

P-loop) of the active site, at the apex of the actin-binding cleft (Allingham et al. 2005) (Fig. 5.3). In the crystal structure (pdb: 1yv3), numerous hydrophobic interactions of blebbistatin and *Dictyostelium discoideum* (*Dd*) myosin II are formed with residues of the U50 linker, a loop following β7-strand (Tyr261 and Leu262), residues of the relay helix (Phe466, Glu467, Ile471, and Thr474), and residues of the W-helix (Val630, Tyr634, Glu637, and Leu641), which contribute largely to the high binding affinity of blebbistatin. In addition, three direct hydrogen bonds stabilize the binding pose of blebbistatin in the allosteric myosin pocket: a hydrogen bond of the chiral hydroxy group with the main chain amide group of Gly240, a residue directly following switch-1, and a hydrogen bond with the main chain carbonyl oxygen of Leu262, as well as a hydrogen bond of the carbonyl oxygen of blebbistatin with switch-2 residue Ser456. The interactions of the chiral hydroxy group with both Leu262 and Gly240 are critical for the effective binding and inhibition of myosin by the S-(−)-enantiomer of blebbistatin. The R-(+)-

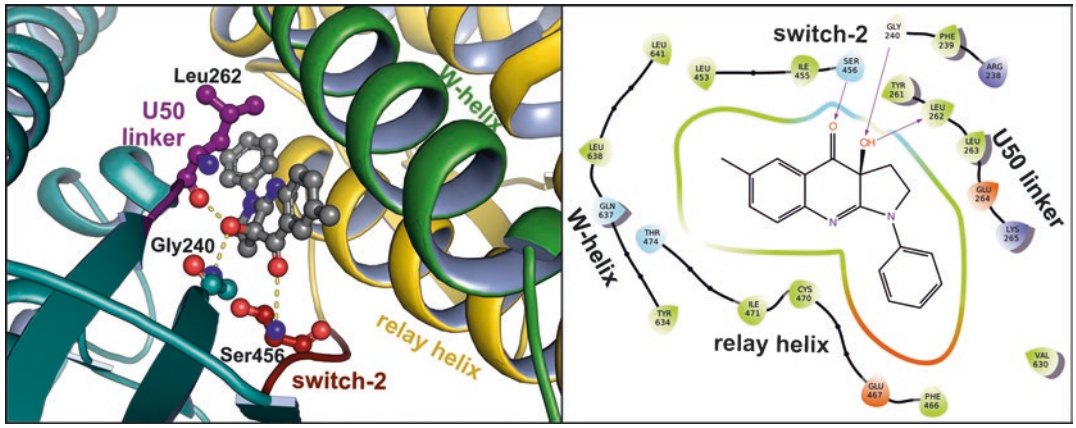

Fig. 5.3 Binding site of (−)-blebbistatin in the motor domain of *Dd* myosin II in the pre-power stroke state at the apex of the actin-binding cleft (pdb 1yv3) and 2-dimensional interaction diagram, showing the favorable non-covalent interactions of blebbistatin with polar and hydrophobic residues of the myosin binding pocket. Color code: purple arrows = hydrogen bonds, blue amino acids = positively charged residues, red amino acids = negatively charged residues, green amino acids = hydrophobic residues, cyan amino acids = polar residues, white amino acid = glycine residues

enantiomer, which is not capable of forming hydrogen bonds with Leu262 and Gly240, has no detectable effect on myosin (Straight et al. 2003).

As mentioned before, blebbistatin is reported to show a clear specificity for conventional class II myosins over unconventional myosins, particularly from classes I, V, and X (Limouze et al. 2004). The structural basis for this specificity was established around the interacting residues Ser456, Thr474, Tyr634, and Glu637, which were found to show the highest degree of variability among myosin isoforms (Allingham et al. 2005). A crucial role was demonstrated for residue Ser456. This amino acid is part of the γ-phosphate-sensing switch-2 with its consensus sequence DIXGFE, with X being an alanine or serine in conventional class II myosins but a bulky, aromatic tyrosine or phenylalanine in most unconventional myosins, including classes I, V, and X. Mutational studies, replacing the native alanine residue at this position in smooth muscle and nonmuscle myosin II by bulkier amino acids, such as phenylalanine, tyrosine, tryptophan, arginine, or glutamate, resulted in a loss of blebbistatin's inhibitory potency against these mutated myosins (Zhang et al. 2017). Additionally, the adjacent residue Ile455 has been suggested to be responsible for the blebbistatin insensitivity of wildtype *Drosophila melanogaster* (*Dm*) nonmuscle myosin II, which possesses a methionine at that particular position. However, blebbistatin is able to inhibit mutant *Dm* nonmuscle myosin II, in which the methionine is replaced by an isoleucine, and loses its potency to inhibit mutant *Hs* nonmuscle myosin II, when isoleucine is exchange to methionine (Zhang et al. 2017).

Structural rearrangements of the side chains of Leu262 and Tyr634 by approximately 4.5 Å and 3 Å are required to accommodate blebbistatin in its binding pocket, suggesting an induced fit mechanism (Allingham et al. 2005). Through its direct interactions with the switch-2 motif and further structural elements of the actin-binding cleft, blebbistatin affects switch-1 and switch-2 opening-closing movements of the active site, and thus coupling with the actin-binding region. Blebbistatin traps the myosin motor domain in an actin-detached pre-power stroke state, impairing P_i release and actin-binding cleft closure, thereby the transition to the force-generating, strongly actin-bound states. The co-crystallized structure of blebbistatin bound to *Dd* myosin II in the pres-

ence of the non-hydrolyzable ATP transition state analogue ADP·VO_4 highly resembles other *Dd* myosin II pre-power stroke state structures that were obtained in the presence of transition state ATP analogues. Interestingly, the structure of myosin in the presence of ADP and blebbistatin was reported to adopt a previously unobserved structural state, priming the converter and lever arm for the power stroke, while at the same time not affecting actin filament interaction (Takács et al. 2010). The low-resolution electron microscopy structure of this myosin II·ADP·blebbistatin complex was interpreted as the start-of-power stroke state, prior to force generation, similar to proposed structural models of the start-of-power stroke state (Preller and Holmes 2013), and showed that in the presence of ADP, blebbistatin blocks switch-2 opening, thereby priming the lever arm. However, switch-1 opening can occur, which is coupled to the closure of the actin-binding cleft and a concomitant increase in actin affinity. The binding site and pose of blebbistatin has been confirmed by co-crystallization of A-ring derivatives, where the position of the methyl group at the A-ring was modified, and which bind identically to the myosin motor domain (Lucas-Lopez et al. 2008).

5.2.2 Binding Site at the Top of the Actin-Binding Cleft (Pseudilin Site)

Halogenated pseudilins are a class of marine alkaloids with a 2-phenylpyrrole scaffold that was shown to inhibit different classes of myosins and myosin-dependent cellular processes with IC_{50} values in the low micromolar range (Fedorov et al. 2009; Chinthalapudi et al. 2011; Preller et al. 2011b; Martin et al. 2014). Structural analysis revealed that the halogenated pseudilins bind to an allosteric binding pocket in the myosin motor domain at the top of the actin-binding cleft, close to the actin-binding region, about 7.5 Å apart from the blebbistatin-binding site and 16 Å from the active site (Fedorov et al. 2009). The binding pocket is primarily formed by two helices of the U50 kDa domain, the strut loop, and loop 2 (Fig. 5.4). It is open to the actin-binding cleft as well as the protein surface, giving access for the halogenated pseudilins to enter the binding site.

In the crystal structures of *Dd* myosin II co-crystallized with three different halogenated pseudilins (pdb 2jhr, 2xo8, 2xel), the small molecule inhibitors bind to the allosteric pocket

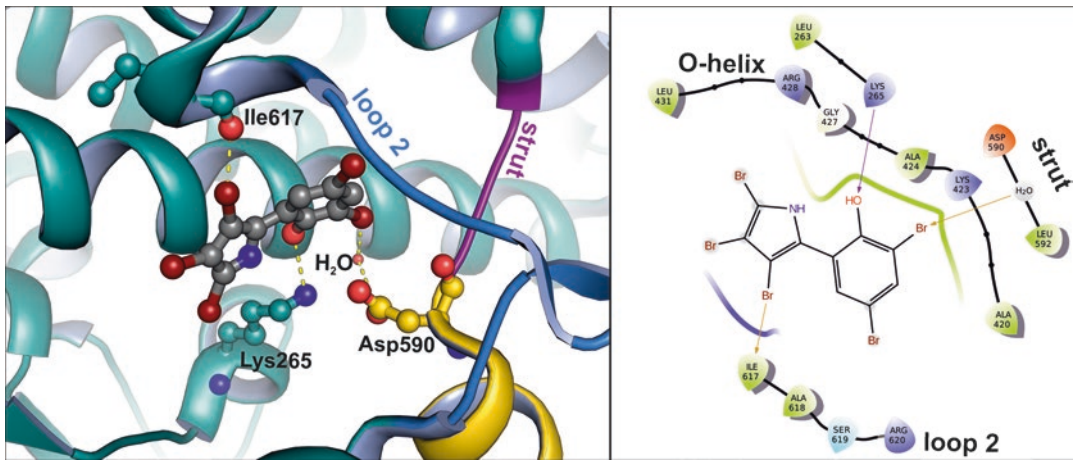

Fig. 5.4 Binding site of the halogenated pseudilin pentabromopseudilin in the motor domain of *Dd* myosin II in the pre-power stroke state at the top of the actin-binding cleft (pdb 2jhr) and 2-dimensional interaction diagram, showing the favorable interactions of pentabromopseudilin with the myosin residues. Color code: purple arrows = hydrogen bonds, orange arrows = halogen bonds, blue amino acids = positively charged residues, red amino acids = negatively charged residues, green amino acids = hydrophobic residues, cyan amino acids = polar residues, white amino acid = glycine residues

through both hydrogen bonds and numerous hydrophobic interactions with residues, including Lys265, Ala420, Ala424, Arg428, Leu431, Asp590, Ile617, and Ala618. A particularly important role has been suggested for the interaction with Lys265, which is hydrogen bonded either to the hydroxy group or the amine group of the halogenated pseudilins. Upon binding of the small molecule inhibitors, the side chain of Lys265 reorients by up to 3.5 Å as compared to myosin structures in the same structural state and without bound pseudilin. This interaction leads to a cascade of small rearrangements of residue side chains along the so-called signal relay pathway, thereby affecting the active site and preventing the proper positioning of the lytic water molecule for an in-line attack of the ATP's γ-phosphate (Chinthalapudi et al. 2011; Preller et al. 2011b). Mutational studies, replacing this lysine residue, confirmed the importance of this residue for myosin inhibition by halogenated pseudilins, since mutant *Dd* myosin II in which Lys265 is replaced by alanine becomes insensitive to pseudilins (Behrens et al. 2017). In addition, the mutational study revealed that this conserved Lys265 is a key residue in the coupling pathway between the active site and the actin-binding region (Behrens et al. 2017). Similar roles for the coupling between actin-binding region and active site have been earlier demonstrated for the strut loop and loop 2 (Geeves et al. 2005). Kinetic analysis of the inhibitory effect of halogenated pseudilins on myosin revealed that the pseudilins reduce the coupling between the active site and the actin-binding region, which can be rationalized by the direct interaction of the small molecule effectors with Lys265 as well as the strut loop and loop 2. Additionally, the pseudilins affect the active site, through the signal relay pathway, which correlates with the experimentally determined effect of halogenated pseudilins on ATP binding and hydrolysis, as well as ADP dissociation.

The three crystallized pseudilin derivatives were found to adopt slightly different binding poses within the allosteric binding pocket (Preller et al. 2011b). Depending on the halogen substituents, the pseudilins show specificities towards certain myosin classes. While highly chlorinated pseudilins exhibit their strongest effect on class I myosins, highly brominated pseudilins preferentially affect class V myosins. Pseudilins with mixed halogenations do not feature any preference for myosin classes. These specificity behaviors of the pseudilins are strongly correlated with differences in the polarities and physicochemical properties of the allosteric binding pocket in different myosin isoforms and classes (Preller et al. 2011b).

5.2.3 Binding Site Between the SH1/SH2 Region and the Relay Helix (CK-571 Site)

The third known allosteric binding site for a small molecule effector in the myosin motor domain is the binding pocket of the smooth muscle myosin II-specific inhibitor CK-2018571 (CK-571) (Sirigu et al. 2016). CK-571 inhibits smooth muscle myosin II with a high potency ($IC_{50} \sim 9$ nM) and kinetically traps the myosin in an ATP-bound, actin-detached intermediate state of the recovery stroke. Hence, in contrast to the crystal structures of myosin II with blebbistatin or halogenated pseudilins, which both are crystallized in the pre-power stroke state, the smooth muscle myosin II·CK-571 structure (pdb 5t45) has similarities with post-rigor state structures, featuring an open actin-binding cleft and the converter and lever arm in the down position. However, other critical structural elements, such as the central β-sheet or switch-2, are found in intermediate conformations between the post-rigor and pre-power stroke states.

The identified allosteric binding pocket for CK-571 is located between the SH1-helix and the relay helix in the myosin motor domain, 22 Å apart from the active site (Fig. 5.5). Interestingly, this pocket is not accessible either in the post-rigor or the pre-power stroke state of myosin, and is suggested to only open during the recovery stroke (Sirigu et al. 2016). Binding of CK-571 is primarily mediated by hydrophobic interactions with residues of the N-terminal domain (Asp88,

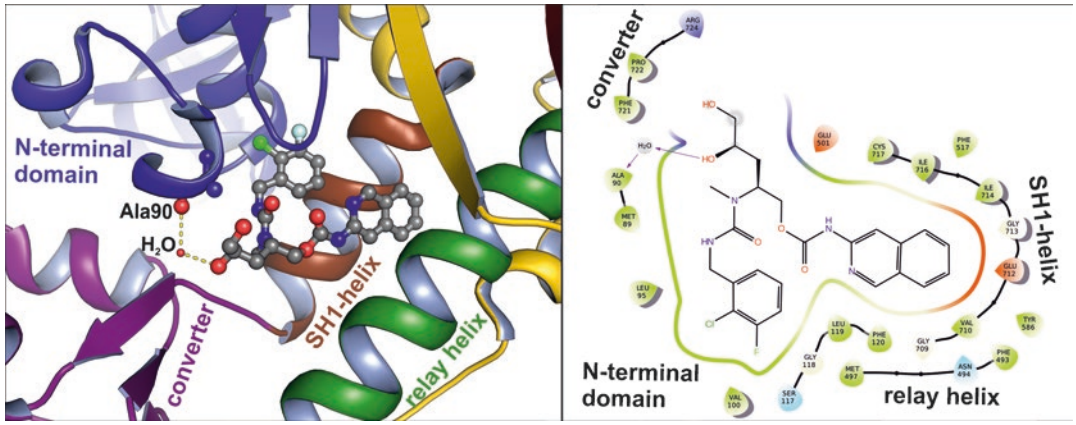

Fig. 5.5 Binding site of CK-571 in the motor domain of smooth muscle myosin II in an intermediate state between post-rigor and pre-power stroke states, between the SH1/SH2-region and the relay helix (pdb 5t45) and 2-dimensional interaction diagram, showing the favorable interactions of CK-571 with the myosin residues. Color code: purple arrow = hydrogen bonds, blue amino acids = positively charged residues, red amino acids = negatively charged residues, green amino acids = hydrophobic residues, cyan amino acids = polar residues, white amino acid = glycine residues

Met89, Ala90, Leu95, Val100, Ser117, Gly118, Leu119, and Phe120), relay helix (Phe493, Asn494, Met497, and Glu501), SH1-helix (Gly709, Val710, Glu712, Gly713, Ile716, and Cys717), and converter domain (Pro722 and Arg724). In the crystal structure with smooth muscle myosin II, no attractive hydrogens bonds were detected between CK-571 and myosin. The structural basis for the inhibition of smooth muscle myosin II by CK-571 has been attributed to the trapping of the myosin motor domain in an intermediate state, resembling the post-rigor state, by interfering with the required conformational changes of the relay helix and the SH1-helix, which in turn prevents myosin from transitioning through the recovery stroke and adopting the catalytically active pre-power stroke state. This effect is similar to the reported consequences of cold-sensitive single-point mutations G680A and G680 V in the SH1-helix, which were shown via kinetic and structural analyses to freeze the mutated myosin in a state similar to the post-rigor state, impairing myosin motor function (Preller et al. 2011a). Small-angle X-ray scattering experiments confirmed that CK-571-bound myosin preferentially adopts such an intermediate post-rigor-like structure. Particularly switch-2 appears affected by CK-571. Marked differences between the CK-571 intermediate state and the wild type post-rigor state have been suggested for the catalytically important switch-2, which is no longer able to close around the ATP γ-phosphate to position the lytic water for the hydrolysis reaction (Sirigu et al. 2016).

All residues of the binding pocket, which are involved in interaction with CK-571, are highly conserved within the class II myosins, preventing establishment of the structural basis for the specificity behavior of CK-571 towards smooth muscle myosin II over other members of the myosin class II.

5.2.4 Binding Site at the L50 kDa – Converter Interface (OM Site)

Omecamtiv mecarbil (OM), earlier denoted as CK-1827452, is a diaryl-urea-based small molecule activator of cardiac myosin II, which is currently in phase 3 clinical trials as a treatment of systolic heart failure. OM was shown to specifically bind to the cardiac myosin motor domain with an affinity of 1.3 μM, and to accelerate the transition rate of the β-cardiac myosin II motor domain into actin-bound, force-generating states (Malik et al. 2011). The co-crystallized

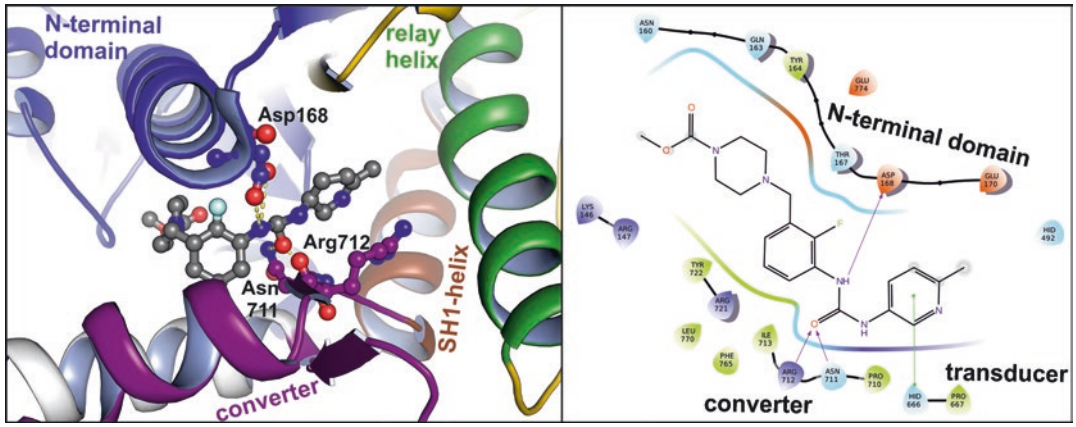

Fig. 5.6 Binding site of OM in the motor domain of cardiac myosin II in the pre-power stroke state at the L50 kDa – converter interface (pdb 5n69) and 2-dimensional interaction diagram, showing the favorable interactions of OM with the myosin residues. Color code: purple arrow = hydrogen bonds, green line = π-π-stacking, blue amino acids = positively charged residues, red amino acids = negatively charged residues, green amino acids = hydrophobic residues, cyan amino acids = polar residues, white amino acid = glycine residues

high-resolution structure of cardiac myosin II in complex with OM has been solved in two different structural states, with controversial results and binding positions (Winkelmann et al. 2015; Planelles-Herrero et al. 2017). However, the determined kinetic mechanism of action of OM on cardiac myosin II (Malik et al. 2011; Liu et al. 2015; Swenson et al. 2017), as well as binding studies using isothermal calorimetry, and low-resolution solution structural analysis by small angle X-ray scattering (Sirigu et al. 2016) indicate a preference of OM for cardiac myosin II states directly prior to the power stroke and at the end of the recovery stroke, with the converter and lever arm in the up position, i.d. the pre-power stroke state.

The high-resolution structure of cardiac myosin II in complex with OM, crystallized in the pre-power stroke state (pdb 5n69), reveals a binding pocket for OM that is located approximately 31 Å apart from the active site, at a coupling hot spot in the motor domain, critical for regulation of the converter domain and the lever arm swing, and hence for force production (Sirigu et al. 2016) (Fig. 5.6). All structural elements that are directly involved in binding OM play a role in communication between the active site and the force-generating lever arm swing. OM binds to a pocket of predominantly hydrophobic nature. One side of the pocket is built by the converter domain, and only existent if the converter domain together with the lever arm is in the up position, as in the pre-power stroke. Indeed, comparison of crystal structures in the same state, however in the presence and absence of OM, showed, that OM is required to fully close the binding pocket by pulling the converter closer to itself. Hence, OM seems to bind through an induced fit mechanism to the cardiac myosin II motor domain, and stabilize states with the lever arm in the up position, primed for the power stroke. Local rearrangements were found surrounding the bound OM, mostly involving residues of the converter domain. Hydrophobic interactions stabilize OM in the pocket and are formed with residues of the N-terminal domain (Lys146, Arg147, Asn160, Gln163, Tyr164, Thr167, and Asp168), the relay helix (His492), the third β-strand of the central transducer (His666), and the converter domain (Pro710, Ile713, Arg721, Tyr726, Phe765, and Leu770). In addition, polar interactions are found with Asp168, Asn711, Arg712, and the urea moiety of OM, as well as potentially Tyr164 and Glu774, and the piperazine ring of OM. The OM-mediated formation of this tight interaction network leads to a stabilization of motor domain conformations with the converter and lever arm in the up position. This leads to an associated

shift of the ensemble of conformers to states where most motor domains are primed for rebinding to actin and the force-generating power stroke (Sirigu et al. 2016). Earlier studies using a photoreactive benzophenone derivative of OM suggested already this critical hot spot and particularly interactions with the N-terminal domain, as the photo-reactive OM derivative was found to crosslink to Ser148 in the N-terminal domain (Malik et al. 2011). Myosin isoform-specific differences in the interacting residues have been attributed to the high specificity of OM within class II towards cardiac myosin II, including Tyr164, one of the hydrogen bonded residues, which is a serine in smooth muscle myosin II and a phenylalanine in skeletal myosin II isoforms, His666, which is replaced by a threonine residue in smooth muscle myosin II, Asn711, which is a serine in skeletal muscle myosin, and Ile713, which is replaced by a valine residue in skeletal muscle myosin. Other residues of the binding pocket that show variations between the different myosin isoforms include Asp168, His492, and Arg712.

As mentioned before, several reported experiments indicate that OM preferentially acts on force-generating myosin states with the lever arm in the up position: (1) according to kinetic studies, OM has an impact on the equilibrium of ATP hydrolysis and lever arm priming, shifting it towards intermediate states with bound ADP·P_i prior to power stroke (Liu et al. 2015), (2) measurements of the binding affinity of OM to different myosin states revealed a 20-fold higher affinity towards the pre-power stroke state (in the presence of the non-hydrolysable nucleotide analogue ADP·VO_4 that traps myosin in the intermediate state) as compared to post-rigor state (in the presence of ADP) (Sirigu et al. 2016), (3) in solution, cardiac myosin II in the presence of OM preferentially adopts a conformation that closely resembles the pre-power stroke as determined by small-angle X-ray scattering (Sirigu et al. 2016).

The structural mechanism for OM activation of cardiac myosin function seems to be a stabilization of the pre-power stroke state with OM supporting the interaction of the relay helix, the N-terminal domain, and the converter domain, and thereby the priming of the lever arm in the up position. This increased population of catalytically competent states leads to an elevated number of myosin motor domain with bound ADP·P_i, which possess a higher affinity for actin filament. The rebinding of actin filaments rapidly releases P_i and allows force production. This postulated mechanism is compatible with the findings that OM reduces the ATP activity in the absence of actin (basal ATPase activity) (Malik et al. 2011; Liu et al. 2015; Swenson et al. 2017), due to the increased population of ADP·P_i states.

5.3 Myosin Classes Targeted by Small Molecule Effectors

5.3.1 Preference Towards Conventional Myosins (Class II)

5.3.1.1 Small Molecule Inhibitors of Myosin II

One of the first identified myosin II inhibitor was 2,3-butanedione monoxime (BDM) (Higuchi and Takemori 1989; Mckillop et al. 1994). BDM binds with a low affinity of $K_i \approx 5$ mM to skeletal muscle myosin II, inhibiting myosin ATPase activity in a noncompetitive and reversible manner (Herrmann et al. 1992). Despite the high concentrations required to inhibit myosin II, BDM was used widely in studies of myosin II function in cellular systems. However, the applicability of BDM as a general myosin II inhibitor is limited due to controversially discussed uncertainties about the specificity of BDM towards skeletal muscle myosin II and possible inhibitory effects on other myosin classes and isoforms, such as nonmuscle myosin II, class I, V, and VI myosins (Cramer and Mitchison 1995; Ostap 2002). In addition, BDM was found to affect many other non-myosin proteins (Sellin and McArdle 1994), including acetylcholinesterase (Wilson and Ginsburg 1955), potassium channels (Schlichter et al. 1992; Lopatin and Nichols 1993), L-type calcium channels (Ferreira et al. 1997), serine

and threonine phosphorylation (Stapleton et al. 1998), and myosin II light-chain kinase (Siegman et al. 1994).

Targeted screening of a chemical library led to the identification of *N*-benzyl-*p*-toluene sulfonamide (BTS) as a reversible small molecule inhibitor of fast muscle myosin II with IC_{50} values of ~5 μM for fast skeletal muscle myosin II (Cheung et al. 2002). According to nucleotide competition experiments, it was suggested that BTS binds noncompetitively to the myosin motor domain. BTS was shown to inhibit contraction and force production in skeletal muscle fibers, and possesses 100-fold specificity towards fast skeletal muscle myosin II over other class II isoforms, including slow skeletal muscle myosin II, cardiac myosin II, platelet myosin II, and nonmuscle myosin II (Cheung et al. 2002).

The antipsychotic drug trifluoperazine (TFP) was reported to inhibit the myosin II ATPase activity and motility at concentrations of 100–200 μM (Sellers et al. 2003). TFP was known earlier as an efficient calmodulin antagonist that leads to removal of the regulatory light chains of smooth muscle myosins (Trybus et al. 1994; Yang and Sweeney 1995) and scallop striated muscle myosins (Patel et al. 2000) at concentrations in the millimolar range.

3-[4-(3-pheny-2-pyrazolin-1-yl) benzene-1-sulfonylamido]-phenylboronic acid (PPBA) is a fluorescent dye that was initially surmised to competitively inhibit skeletal myosin II function with a submicromolar potency ($K_i \approx 0.8$ μM) (Hiratsuka 1994). However, this was later revised and PPBA was suggested to bind to the nucleotide-bound myosin motor domain and act through an allosteric mechanism (Hiratsuka 2006). On the basis of manual fitting the structure of PPBA to the crystal structure of *Dd* myosin II, a hydrophobic pocket distant from the active site was speculated to be the binding site of PPBA, with direct interactions of the small molecule inhibitor and Phe472.

In contrast to the small molecule inhibitors described above, blebbistatin and blebbistatin derivatives are well characterized small molecule myosin inhibitors that exhibit marked specificities towards class II myosins with no or weak activities on class I, V, and X myosins (Limouze et al. 2004). The highest IC_{50} of 0.5 μM was determined for skeletal muscle myosin II, while cardiac myosin II and nonmuscle myosin II isoforms are affected in the range of 1–10 μM. Larger variations of the potencies of blebbistatin for smooth muscle myosin II are reported ranging from 3 to 80 μM. The myosin II-specific small molecule inhibitors have been applied in numerous studies to reveal the physiological and pathological role of myosin II isoforms in biological processes, including the spatiotemporal control of cytokinesis (Straight et al. 2003), control of cell migration and antigen capture in dendritic cells (Chabaud et al. 2015), regulation of detrusor contractility in partial bladder outlet obstruction (Zhang et al. 2011), and in optical mapping of the heart (Swift et al. 2012). Hence, blebbistatin and its derivatives have advanced to front line research tools for studying myosin-dependent processes. The mechanism as well as the structural basis of myosin inhibition by blebbistatin has been determined (Ramamurthy et al. 2004; Kovács et al. 2004; Allingham et al. 2005). However, blebbistatin has several drawbacks that interfere with its general use, such as phototoxicity and -instability, high fluorescence, cytotoxic effects, and poor solubility. Therefore, comprehensive optimizations of blebbistatin were carried out, particularly centering on derivatizations of the A- and D-ring of blebbistatin to improve the physicochemical properties and the inhibitory potency of the small molecules (Képiró et al. 2014; Várkuti et al. 2016; Verhasselt et al. 2017a, b, c; Roman et al. 2018; Rauscher et al. 2018). As a reminder, blebbistatin has a tricyclic tetrahydropyrroloquinolinone scaffold forming the A-, B-, and C-rings, and a phenyl ring, the D-ring, linked to the pyrrole (C-ring) nitrogen. A-ring modifications had minor or negative impacts on the properties and potencies of the small molecule blebbistatin derivatives (Lucas-Lopez et al. 2008; Verhasselt et al. 2017c). However, superior physicochemical properties or potencies were observed for modifications of the D-ring at the meta- or para-position of the phenyl ring (Rauscher et al. 2018). Addition of small polar functional groups, particularly *para*-nitro

and *para*-amino, as well as *meta*-hydroxy or *meta*-nitro groups improved the photosensitivity, hence the structural stability of the small molecules, and the solubility, while at the same time leading to a reduced phototoxicity and fluorescence (Képiró et al. 2014; Várkuti et al. 2016; Verhasselt et al. 2017b). Such optimized scaffolds potentially open the way for safer use of these compounds in scientific studies of myosin-dependent processes and for directed targeting of myosin II-associated diseases.

CK-2018571 (CK-571) is a small molecule inhibitor that was identified by high-throughput screenings and chemical modification to target smooth muscle myosin II and muscle contraction for potential use in associated diseases, including asthma and chronic obstructive pulmonary disease (Sirigu et al. 2016). Co-crystallization of CK-571 with smooth muscle myosin II confirmed the allosteric mechanism of CK-571. Considerable specificities within myosin class II were observed for CK-571 with high potency towards smooth muscle myosin II (IC_{50} = 9 nM), and 280-fold and 1255-fold lower potencies against cardiac myosin II and skeletal muscle myosin II, as well as 8.5-fold lower potency for the closely related nonmuscle myosin II. The small molecule inhibitor interferes with ATP hydrolysis and actin reattachment by trapping the myosin in an ATP-bound intermediate state of the recovery stroke (Sirigu et al. 2016). *In vivo* experiments verify the relaxing effect of CK-571 on different smooth muscle tissues and decreased force production in stimulated skinned artery rings. Concentrations in the range of 1 μM were required to relax skinned and intact tissue. In addition, CK-571 was shown to inhibit methacholine-induced bronchoconstriction in naïve dogs with comparable effect as obtained with albuterol, as the clinically-relevant β2-adrenergic agonist, highlighting the therapeutic potential of CK-571 (Sirigu et al. 2016).

The recently identified small molecule inhibitor of cardiac myosin II mavacamten (MYK-461) shows potent inhibitory effects on the ATPase function of cardiac myosin II (IC_{50} = 0.3–0.7 μM) and the weak-to-strong transition of myosin (Green et al. 2016; Kawas et al. 2017). Mavacamten was developed specifically to target mutated cardiac myosins, a prime cause for hypertrophic cardiomyopathy (HCM) and is currently tested in phase 3 clinical trials for treatment of HCM. The cardiac myosin inhibitor reduces phosphate release as well as the myosin duty ratio – the fraction of the time myosin stays strongly bound to the actin filament (Kawas et al. 2017). Mavacamten has additionally been suggested to stabilize an autoinhibited super-relaxed state with markedly reduced ATPase activity, which might be common for a fraction of healthy cardiac myosins, and which is prevented by HCM mutations in the cardiac myosin heavy chain (Rohde et al. 2018; Anderson et al. 2018). In transgenic mice harboring heterozygous mutations in β-cardiac myosin, mavacamten improved cardiac function, as evidenced from reduced fractional shortening and left ventricular hypertrophy, myocyte disarray and fibrosis (Green et al. 2016). Additionally, a clinical feline model of HCM treated with mavacamten displayed an improved sarcomere contractility and relieved left ventricular outflow tract obstruction (Stern et al. 2016).

5.3.1.2 Pharmacological Chaperones

Myosin family members are among the most abundant proteins in our bodies. All of our movement, each step and every heartbeat, requires the force and tension-generating action of myosins. These activities subject myosins to physical stress that, together with the extremes of pH and temperature found in the cell, can lead to the formation of roadblock-like, strongly-bound complexes of "dead" myosin motors with actin filament tracks (Murphy and Spudich 1999). Even a slight increase in the occurrence of such roadblocks can trigger catastrophic consequences in actomyosin-rich organs. Here, the restoration of normal myosin homeostasis by pharmacological chaperones promises to provide an efficient means of interfering with the progression of an acute crisis and to support long-term stabilization of patients (Radke et al. 2014; Wustman et al. 2014).

The thiadiazenone EMD57033 is a cardiotonic agent that enhances both systolic and diastolic function in failing hearts at minimal

energetic cost (Solaro et al. 1993; Senzaki et al. 2000). The well-known effects of EMD57033 as an inotropic Ca^{2+} sensitizer and activator of cardiac actomyosin (Ferroni et al. 1991; Beier et al. 1991; Gambassi et al. 1993) are fully explained by an EMD57033-mediated shift in the duty-ratio and their consequences on thin-filament regulation (Radke et al. 2014). EMD57033 binds with an affinity of 7.3 μM to an allosteric pocket in the β-cardiac myosin II motor domain and protects myosin against heat stress and thermal denaturation (Radke et al. 2014). Addition of the compound to heat-inactivated β-cardiac myosin results in refolding and reactivation of ATPase and motile activities. Moreover, in heat-stressed cardiomyocytes expression of the stress-marker atrial natriuretic peptide is suppressed by EMD 57033. Thus, EMD 57033 displays a much wider spectrum of activities than those previously associated with small, drug-like compounds (Radke et al. 2014). Current efforts by our groups have led to the discovery of further thiadiazenones that act as pharmacological chaperones for β-cardiac myosin. We see the greatest potential for the therapeutic use of pharmacological chaperones in the area of cardiac and cytoskeletal myosin II isoforms.

5.3.2 Preference Towards Unconventional Class I Myosins

Two small molecule inhibitors of class I myosins have been described in the literature with clear isoform or even species specificities. The fully chlorinated marine antibiotic pentachloropseudilin (PClP) inhibits the enzymatic and motor function of myosin I in a reversible manner with IC_{50} values in the range of 1–5 μM for mammalian class I myosins (Chinthalapudi et al. 2011). PClP shows largely effects on most tested myosin I isoforms in the low micromolar range, and 20- to 90-fold higher potencies as compared to class II und V myosins. In addition, even at 100 μM concentrations, PClP does not inhibit human myosin VI or myosin VII isoforms. Comparative structural studies attributed the specificity of highly chlorinated halogenated pseudilins, such as PClP, to the isoform-specific differences in polarity of the allosteric binding pocket in the myosin motor domain (Preller et al. 2011b). PClP is active in cells and tissue and was shown to induce comparable effects in HeLa cells at low micromolar concentrations as observed with myosin IC knockdown cells, resulting in abnormalities in lysosome morphology and distribution (Chinthalapudi et al. 2011). Above concentrations of 25 μM, PClP showed cytotoxic effects on the HeLa cells. Hence, PClP was used as a tool compound for studying myosin I functions in cellular systems. Selective inhibition of myosin I by PClP demonstrated the role of class I myosins in autophagosome-lysosome fusion (Brandstaetter et al. 2014), as well as a critical function of myosin I in the maintenance and formation of blastodisc morphology, cell-division and dynamics as well as distribution of lipid droplets within the blastodisc in early zebrafish embryos (Gupta et al. 2017). Additionally, both PClP and the related myosin class V-specific pentabromopseudilin were used to elucidate that changes in cell shape, apical contraction, and cell intercalation highly depend on myosin II function, whereas myosin I and myosin V are involved in the assembly of supercellular cable-like myosin II structures at cell junctions that mediate primitive streak formation (Rozbicki et al. 2015).

The second class I-specific myosin inhibitor is the cyanoacrylate-based compound phenamacril, a well-known fungicide, whose direct inhibitory effect on *Fusarium graminearum* myosin I has recently been described and characterized (Zhang et al. 2015; Wollenberg et al. 2019). Phenamacril reversibly inhibits the ATPase activity and *in vitro* motility of *Fusarium graminearum* and *Fusarium avenaceum* myosin I with potencies up to IC_{50} = 0.36 μM but does not affect the related *Fusarium solani* myosin I, nor human myosin IC or class I and II isoforms of the slime mold *D. discoideum*. Phenamacril is an environmentally-friendly fungicide that is widely used in regulation of cereal infections by fungi of the *Fusarium* family in China (Li et al. 2008). Docking experi-

ments predicted the binding site of phenamacril to be in the actin-binding cleft of myosin, in proximity of the binding pockets of halogenated pseudilins or blebbistatin, which correlates with identified mutations in the myosin motor domain that are implicated in resistance development of the fungi against phenamacril (Li et al. 2016a; Hou et al. 2018).

5.3.3 Preference Towards Unconventional Class V Myosins

Based on the concept of privileged chemical scaffolds that were derived from known bioactive compounds, particularly kinase inhibitors (Peters et al. 2006), a search for class V-specific myosin inhibitors was performed and yielded the small molecule inhibitor of myosin V, based on a pyrazolopyrimidine scaffold, Myo-Vin1 (Islam et al. 2010). Myo-Vin1 demonstrates a preference for class V myosins, which are inhibited in the low micromolar range ($IC_{50} \approx 6$ μM), over skeletal muscle and nonmuscle myosin II isoforms, which are not affected at concentrations up to 50 μM. In addition, no inhibition of many representative kinases was observed at 100 μM compound concentrations.

Highly brominated members of the halogenated pseudilin family of small molecule myosin inhibitors, such as pentabromopseudilin (PBP), were identified as potent and reversible inhibitors with specificities towards class V myosins over class I and II myosins (Fedorov et al. 2009). Halogenated pseudilins were initially reported as marine alkaloids with antitumor and phytotoxic activities, and effects on 12- and 15-human lipoxygenases (Ohri et al. 2005). *In vitro*, PBP potently affects the enzymatic ATPase activity and the motor function of myosin V with IC_{50} values of 1.2 μM for chicken myosin VA, as well as isometric tension development and unloaded shortening velocity in muscle. Cellular studies have shown that the phenotypic effect of PBP on mitochondrial fragmentation closely resembles the phenotype observed with mutant yeast, leading to an impaired expression of myosin V (Fedorov et al. 2009).

5.3.4 Preference Towards Unconventional Class VI Myosins

Myosin VI has been shown to play a critical role in migration, metastasis, and tumorigenesis of cancer cells (Yoshida et al. 2004; Dunn et al. 2006). In addition, strong links have been made between mutations in myosin VI and diseases such as hypertrophic cardiomyopathy (Mohiddin et al. 2004), Snell's Waltzer deafness and nonsyndromic hearing loss (Melchionda et al. 2001). There is only a single small molecule effector of class VI myosins reported to date: 2,4,6-triiodophenol inhibits human myosin VI actin-activated ATPase activity following a biphasic behavior with a $K_{i,1}$ of 0.8 μM, contributing 37% to the inhibition, and a second $K_{i,2}$ of 37 μM, contributing 63% to the inhibition (Heissler et al. 2012). This biphasic behavior, observed in the inhibition assays, was interpreted as the binding to two independent binding sites in the myosin VI motor domain. However, no structural data are currently available to support the existence of two binding sites for 2,4,6-triiodophenol. No effect of 2,4,6-triiodophenol on the ATPase activity of *Dd* myosin ID, human nonmuscle myosin IIC, or porcine β-cardiac myosin II were observed up to concentrations of 50 μM of the small molecule effector, hence 2,4,6-triiodophenol seems to show a preferential binding and inhibition of class VI myosins (Heissler et al. 2012). 2,4,6-Triiodophenol was earlier shown to possess nonsteroid anti-inflammatory effects by inhibiting leukotriene B4 synthesis (Trocóniz et al. 2006). Accompanying live-cell studies confirmed the inhibitory effect of 2,4,6-triiodophenol on the physiological function of myosin VI during the final stages of the secretory pathway, with a comparable efficiency as myosin VI knockdown, indicating an IC_{50} of 1.6 μM (Heissler et al. 2012).

5.4 Allosteric Modulation by Protein-Protein Interactions

Myosins are multifunctional enzymes that typically function within the framework of supramolecular complexes whose function is regulated and modulated by multiple allosteric trigger events. In addition to the binding of small effector molecules, allosteric trigger events include post-translational modifications, protein-protein interactions, and disease-causing mutations. Thus, allosteric trigger events are contributed by more than 100 gene products encoding actin- and myosin-binding proteins (Dos Remedios et al. 2003; Winder and Ayscough 2005), hundreds of post-translational modifications for which actin and actin-binding proteins are major targets (Li et al. 2015; Terman and Kashina 2013), and well over 100 disease causing mutations affecting core components of actin-dependent contractile complexes (Richard et al. 2003; Goebel and Laing 2009; Ampe and Van Troys 2017; Marian and Braunwald 2017). This brings up the question of how we can address the resulting functional and regulatory complexity. The answer is to address one complex at a time in a stringently defined state, to be complete in the analysis of the individual components, to report the results using the correct nomenclature, and to develop and refine structure-based models that explain the changes brought about by individual allosteric perturbations. The availability of highly sensitive, rapid, and quantitative analytical methods, high-resolution structures of complexes composed of F-actin-Tpm (tropomyosin) cofilaments and myosin motor domains (A-Tpm-M), the stringent use of an unambiguous systematic protein nomenclature, and the increasing performance of computational approaches will help to unravel the complexity and to move programs for the identification of small allosteric effectors of myosin function to a new level. The following paragraph describes the need for and the advantages of such an approach using thin filament regulation by Tpm as an example.

Tpm form a large family of double-stranded alpha-helical coiled-coil actin-binding proteins that play a key role in regulating the interaction of actin filaments with both sarcomeric myosin and cytoskeletal myosin isoforms (Schaub and Ermini 1969; Galińska-Rakoczy et al. 2008; Meiring et al. 2018; Manstein et al. 2019). Over 40 Tpm isoforms are produced by alternate promoter selection and splicing of four different genes – *TPM1–4*. The resulting types of A-Tpm co-polymers show remarkably little functional redundancy (Bryce et al. 2003; Tojkander et al. 2011; Gateva et al. 2017). Modelling, which is based on structural and kinetic analysis of A-M-Tpm-complexes and their individual components (Behrmann et al. 2012; Münnich et al. 2014a, b; von der Ecken et al. 2015; Hundt et al. 2016; Ecken et al. 2016; Chinthalapudi et al. 2017; Pathan-Chhatbar et al. 2018), predicts that the mechanism by which Tpm isoforms support cytoskeletal functions differs fundamentally from the regulatory role described for sarcomeric Tpm isoforms. In the cytoskeletal environment, the higher duty-ratio of the interacting myosin isoforms and the absence of a mechanism for the stringent synchronization of different types and classes of myosin motors are predicted to keep Tpm permanently in an "open" state on F-actin. This means that myosins can always interact with A-Tpm cofilaments. In the absence of a "blocked" state, the contribution of Tpm to the stereospecific interaction surface with myosin has three distinct consequences. A widely accepted consequence is the function of a gatekeeper that favours the interaction between certain combinations of myosin and Tpm isoforms while inhibiting others (Coulton et al. 2010; Gunning et al. 2015; Moore et al. 2016; Manstein and Mulvihill 2016; Gateva et al. 2017). The second, equally well-accepted consequence is the cooperative behaviour of actomyosin in the presence of Tpm. Here, it is well known that in the presence of bare F-actin the activation of ATP turnover by myosin subfragment-1 (S1) is linear as a function of added S1, yet becomes sigmoidal when Tpm is present (Lehrer and Morris 1982; Moraczewska et al. 1999; Tobacman 2008). Tpm inhibits the actomyosin ATPase at low S1:F-actin ratios and activates the ATPase at moderate to high S1:F-actin ratios more strongly than bare actin filaments. Inhibition and activation by Tpm are greatest

when troponin and Ca^{2+} are present, but strong cooperative behaviour is also observed with the cytoskeletal isoforms in the absence of troponin (Lehrer and Morris 1982, 1984). The third consequence is a Tpm isoform-dependent change in key enzymatic parameters of the myosin motor. The Tpm isoform defines the rate of ATP turnover, the duty-ratio, thermodynamic coupling, maximal velocity, and strain-sensitivity of product release steps (Hundt et al. 2016; Gateva et al. 2017; Pathan-Chhatbar et al. 2018). Accordingly, motor activity is geared towards slower or faster movement, tension holding, or active constriction. The elucidation of the exact role of individual Tpm isoforms, the mechanisms that are responsible for the sorting of the different isoforms, and the temporal and spatial control of complex formation and turnover are arguably amongst the most important tasks in cell biology. The profound and diverse Tpm-mediated changes in myosin motor activity challenge current concepts and call for their revision by a classification system in which myosin motor function is not only classified on the basis of the interaction with bare F-actin. In the context of small allosteric effectors of myosin motor activity, the terms activator and inhibitor should be best avoided or at least more systematically defined. An appropriate definition needs to reflect protein context, physiological function, changes in apparent actin affinity in the presence of ATP, maximal ATP-turnover in the absence and presence of F-actin, maximal velocity, cooperativity, duty ratio, and stall force.

Acknowledgments This work was supported by grants from Deutsche Forschungsgemeinschaft to D.J.M (MA1081-22/1) and M.P (PR1478-2/1).

References

Allingham JS, Smith R, Rayment I (2005) The structural basis of blebbistatin inhibition and specificity for myosin II. Nat Struct Mol Biol 12:378–379. https://doi.org/10.1038/nsmb908

Ampe C, Van Troys M (2017) Mammalian actins: isoform-specific functions and diseases. Handb Exp Pharmacol 235:1–37. https://doi.org/10.1007/164_2016_43

Anderson RL, Trivedi DV, Sarkar SS et al (2018) Deciphering the super relaxed state of human β-cardiac myosin and the mode of action of mavacamten from myosin molecules to muscle fibers. Proc Natl Acad Sci 115:E8143–E8152. https://doi.org/10.1073/PNAS.1809540115

Behrens VA, Münnich S, Adler-Gunzelmann G et al (2017) The conserved lysine-265 allosterically modulates nucleotide- and actin-binding site coupling in myosin-2. Sci Rep 7:7650. https://doi.org/10.1038/s41598-017-07933-y

Behrmann E, Müller M, Penczek PA et al (2012) Structure of the rigor actin-tropomyosin-myosin complex. Cell 150:327–338. https://doi.org/10.1016/J.CELL.2012.05.037

Beier N, Harting J, Jonas R et al (1991) The novel cardiotonic agent EMD 53 998 is a potent "calcium sensitizer". J Cardiovasc Pharmacol 18:17–27

Berg JS, Powell BC, Cheney RE (2001) A millennial myosin census. Mol Biol Cell 12:780–794. https://doi.org/10.1091/mbc.12.4.780

Brandstaetter H, Kishi-Itakura C, Tumbarello DA et al (2014) Loss of functional MYO1C/myosin 1c, a motor protein involved in lipid raft trafficking, disrupts autophagosome-lysosome fusion. Autophagy 10:2310–2323. https://doi.org/10.4161/15548627.2014.984272

Bryce NS, Schevzov G, Ferguson V et al (2003) Specification of actin filament function and molecular composition by tropomyosin isoforms. Mol Biol Cell 14:1002–1016. https://doi.org/10.1091/mbc.e02-04-0244

Chabaud M, Heuzé ML, Bretou M et al (2015) Cell migration and antigen capture are antagonistic processes coupled by myosin II in dendritic cells. Nat Commun 6:7526. https://doi.org/10.1038/ncomms8526

Charlton MR, Balagopal P, Nair KS (1997) Skeletal muscle myosin heavy chain synthesis in type 1 diabetes. Diabetes 46:1336–1340. https://doi.org/10.2337/diab.46.8.1336

Cheung A, Dantzig JA, Hollingworth S et al (2002) A small-molecule inhibitor of skeletal muscle myosin II. Nat Cell Biol 4:83–88. https://doi.org/10.1038/ncb734

Chinthalapudi K, Taft MH, Martin R et al (2011) Mechanism and specificity of pentachloropseudilin-mediated inhibition of myosin motor activity. J Biol Chem 286:29700–29708. https://doi.org/10.1074/jbc.M111.239210

Chinthalapudi K, Heissler SM, Preller M et al (2017) Mechanistic insights into the active site and allosteric communication pathways in human nonmuscle myosin-2C. Elife 6:1–24. https://doi.org/10.7554/eLife.32742

Cohen P, Alessi DR (2013) Kinase drug discovery – what's next in the field? ACS Chem Biol 8:96–104. https://doi.org/10.1021/cb300610s

Coulton AT, East DA, Galinska-Rakoczy A et al (2010) The recruitment of acetylated and unacetylated tropomyosin to distinct actin polymers permits the discrete regulation of specific myosins in fission yeast. J Cell Sci 123:3235–3243. https://doi.org/10.1242/JCS.069971

Cowman AF, Tonkin CJ, Tham WH, Duraisingh MT (2017) The molecular basis of erythrocyte invasion by malaria parasites. Cell Host Microbe 22:232–245. https://doi.org/10.1016/j.chom.2017.07.003

Cramer LP, Mitchison TJ (1995) Myosin is involved in postmitotic cell spreading. J Cell Biol 131:179–189. https://doi.org/10.1083/jcb.131.1.179

Cymerys J, SŁonska A, Skwarska J, Banbura MW (2016) Function of myosin during entry and egress of equid herpesvirus type 1 in primary murine neurons. Acta Virol 60:410–416. https://doi.org/10.4149/av_2016_04_410

Dos Remedios CG, Chhabra D, Kekic M et al (2003) Actin binding proteins: regulation of cytoskeletal microfilaments. Physiol Rev 83:433–473. https://doi.org/10.1152/physrev.00026.2002

Dunn TA, Chen S, Faith DA et al (2006) A novel role of myosin VI in human prostate cancer. Am J Pathol 169:1843–1854. https://doi.org/10.2353/AJPATH.2006.060316

Fedorov R, Böhl M, Tsiavaliaris G et al (2009) The mechanism of pentabromopseudilin inhibition of myosin motor activity. Nat Struct Mol Biol 16:80–88. https://doi.org/10.1038/nsmb.1542

Ferreira G, Artigas P, Pizarro Gustavo Brum G (1997) Butanedione Monoxime promotes voltage-dependent inactivation of L-type calcium channels in heart. Effects on gating currents. J Mol Cell Cardiol 29:777–787. https://doi.org/10.1006/JMCC.1996.0321

Ferroni C, Hano O, Ventura C et al (1991) A novel positive inotropic substance enhances contractility without increasing the Ca^{2+} transient in rat myocardium. J Mol Cell Cardiol 23:325–331. https://doi.org/10.1016/0022-2828(91)90068-W

Fischer S, Windshügel B, Horak D et al (2005) Structural mechanism of the recovery stroke in the myosin molecular motor. Proc Natl Acad Sci U S A 102:6873–6878. https://doi.org/10.1073/pnas.0408784102

Foth BJ, Goedecke MC, Soldati D (2006) New insights into myosin evolution and classification. Proc Natl Acad Sci 103:3681–3686. https://doi.org/10.1073/pnas.0506307103

Galińska-Rakoczy A, Engel P, Xu C et al (2008) Structural basis for the regulation of muscle contraction by troponin and tropomyosin. J Mol Biol 379:929–935. https://doi.org/10.1016/J.JMB.2008.04.062

Gambassi G, Capogrossi MC, Klockow M, Lakatta EG (1993) Enantiomeric dissection of the effects of the inotropic agent, EMD 53998, in single cardiac myocytes. Am J Physiol 264:H728–H738. https://doi.org/10.1152/ajpheart.1993.264.3.H728

Gateva G, Kremneva E, Reindl T et al (2017) Tropomyosin isoforms specify functionally distinct actin filament populations in vitro. Curr Biol 27:705–713. https://doi.org/10.1016/J.CUB.2017.01.018

Geeves MA, Fedorov R, Manstein DJ (2005) Molecular mechanism of actomyosin-based motility. Cell Mol Life Sci 62:1462–1477. https://doi.org/10.1007/s00018-005-5015-5

Goebel HH, Laing NG (2009) Actinopathies and myosinopathies: Mini-symposium: Protein aggregate myopathies. Brain Pathol 19:516–522. https://doi.org/10.1111/j.1750-3639.2009.00287.x

Green EM, Wakimoto H, Anderson RL et al (2016) A small-molecule inhibitor of sarcomere contractility suppresses hypertrophic cardiomyopathy in mice. Science 351:617–621. https://doi.org/10.1126/science.aad3456

Greenberg B (2016) Novel therapies for heart failure – where do they stand? Circ J 80:1882–1891. https://doi.org/10.1253/circj.CJ-16-0742

Gunning PW, Hardeman EC, Lappalainen P, Mulvihill DP (2015) Tropomyosin – master regulator of actin filament function in the cytoskeleton. J Cell Sci 128:2965–2974. https://doi.org/10.1242/jcs.172502

Gupta P, Martin R, Knölker H-J et al (2017) Myosin-1 inhibition by PClP affects membrane shape, cortical actin distribution and lipid droplet dynamics in early Zebrafish embryos. PLoS One 12:e0180301. https://doi.org/10.1371/journal.pone.0180301

Heissler SM, Selvadurai J, Bond LM et al (2012) Kinetic properties and small-molecule inhibition of human myosin-6. FEBS Lett 586:3208–3214. https://doi.org/10.1016/j.febslet.2012.07.014

Herrmann C, Wray J, Travers F, Barman T (1992) Effect of 2,3-butanedione monoxime on myosin and myofibrillar ATPases. An example of an uncompetitive inhibitor. Biochemistry 31:12227–12232. https://doi.org/10.1021/bi00163a036

Higuchi H, Takemori S (1989) Butanedione monoxime suppresses contraction and ATPase activity of rabbit skeletal muscle. J Biochem 105:638–643. https://doi.org/10.1093/oxfordjournals.jbchem.a122717

Hiratsuk T (1994) Nucleotide-induced closure of the ATP-binding pocket in myosin subfragment-1. J Biol Chem 269:27251–27257

Hiratsuka T (2006) The interaction of Phe472 with a fluorescent inhibitor bound to the complex of myosin subfragment-1 with nucleotide. Biochemistry 45:1234–1241. https://doi.org/10.1021/bi0513731

Hou Y-P, Qu X-P, Mao X-W et al (2018) Resistance mechanism of *Fusarium fujikuroi* to phenamacril in the field. Pest Manag Sci 74:607–616. https://doi.org/10.1002/ps.4742

Houdusse A, Sweeney HL (2016) How myosin generates force on actin filaments. Trends Biochem Sci 41:989–997

Hundt N, Steffen W, Pathan-Chhatbar S et al (2016) Load-dependent modulation of non-muscle myosin-2A function by tropomyosin 4.2. Sci Rep 6:20554. https://doi.org/10.1038/srep20554

Hur E-M, Yang IH, Kim D-H et al (2011) Engineering neuronal growth cones to promote axon regenera-

tion over inhibitory molecules. Proc Natl Acad Sci U S A 108:5057–5062. https://doi.org/10.1073/pnas.1011258108

Islam K, Chin HF, Olivares AO et al (2010) A myosin V inhibitor based on privileged chemical scaffolds. Angew Chem Int Ed 49:8484–8488. https://doi.org/10.1002/anie.201004026

Kaplinsky E, Mallarkey G (2018) Cardiac myosin activators for heart failure therapy: focus on omecamtiv mecarbil. Drugs Context 7:1–10. https://doi.org/10.7573/dic.212518

Kawas RF, Anderson RL, Bartholomew Ingle SR et al (2017) A small-molecule modulator of cardiac myosin acts on multiple stages of the myosin chemomechanical cycle. J Biol Chem 292:16571–16577. https://doi.org/10.1074/jbc.M117.776815

Keith CT, Borisy AA, Stockwell BR (2005) Multicomponent therapeutics for networked systems. Nat Rev Drug Discov 4:71–78. https://doi.org/10.1038/nrd1609

Képiró M, Várkuti BH, Végner L et al (2014) *para*-nitroblebbistatin, the non-cytotoxic and photostable myosin II inhibitor. Angew Chem Int Ed 53:8211–8215. https://doi.org/10.1002/anie.201403540

Kintses B, Yang Z, Málnási-Csizmadia A (2008) Experimental investigation of the seesaw mechanism of the relay region that moves the myosin lever arm. J Biol Chem 283:34121–34128. https://doi.org/10.1074/jbc.M805848200

Kollmar M, Mühlhausen S (2017) Myosin repertoire expansion coincides with eukaryotic diversification in the Mesoproterozoic era. BMC Evol Biol 17:211. https://doi.org/10.1186/s12862-017-1056-2

Kovács M, Tóth J, Hetényi C et al (2004) Mechanism of blebbistatin inhibition of myosin II. J Biol Chem 279:35557–35563. https://doi.org/10.1074/jbc.M405319200

Lehrer SS, Morris EP (1982) Dual effects of tropomyosin and troponin-tropomyosin on actomyosin subfragment 1 ATPase. J Biol Chem 257:8073–8080

Lehrer SS, Morris EP (1984) Comparison of the effects of smooth and skeletal tropomyosin on skeletal actomyosin subfragment 1 ATPase. J Biol Chem 259:2070–2072

Li H, Diao Y, Wang J et al (2008) JS399-19, a new fungicide against wheat scab. Crop Prot 27:90–95. https://doi.org/10.1016/J.CROPRO.2007.04.010

Li M, Ogilvie H, Ochala J, Artemenko K, Iwamoto H, Yagi N, Bergquist J, Larsson L (2015) Aberrant post-translational modifications compromise human myosin motor function in old age. Aging Cell 14:228–235. https://doi.org/10.1111/acel.12307

Li B, Zheng Z, Liu X et al (2016a) Genotypes and characteristics of phenamacril-resistant mutants in *Fusarium asiaticum*. Plant Dis 100:1754–1761. https://doi.org/10.1094/PDIS-02-16-0169-RE

Li Y-R, Yang W-X, Li Y-R, Yang W-X (2016b) Myosins as fundamental components during tumorigenesis: diverse and indispensable. Oncotarget 7:46785–46812. https://doi.org/10.18632/oncotarget.8800

Limouze J, Straight AF, Mitchison T, Sellers JR (2004) Specificity of blebbistatin, an inhibitor of myosin II. J Muscle Res Cell Motil 25:337–341. https://doi.org/10.1007/s10974-004-6060-7

Liu Y, White HD, Belknap B et al (2015) Omecamtiv mecarbil modulates the kinetic and motile properties of porcine β-cardiac myosin. Biochemistry 54:1963–1975. https://doi.org/10.1021/bi5015166

Lopatin AN, Nichols CG (1993) Block of delayed rectifier (DRK1) K^+ channels by internal 2,3-butanedione monoxime in Xenopus oocytes. Receptors Channels 1:279–286

Lucas-Lopez C, Allingham JS, Lebl T et al (2008) The small molecule tool (S)-(−)-blebbistatin: novel insights of relevance to myosin inhibitor design. Org Biomol Chem 6:2076. https://doi.org/10.1039/b801223g

Lymn RW, Taylor EW (1971) Mechanism of adenosine triphosphate hydrolysis by actomyosin. Biochemistry 10:4617–4624. https://doi.org/10.1021/bi00801a004

Ma X, Adelstein RS (2014) The role of vertebrate nonmuscle myosin II in development and human disease. BioArchitecture 4:88–102. https://doi.org/10.4161/bioa.29766

Malik FI, Hartman JJ, Elias KA et al (2011) Cardiac myosin activation: A potential therapeutic approach for systolic heart failure. Science 331:1439–1443. https://doi.org/10.1126/science.1200113

Manstein DJ, Mulvihill DP (2016) Tropomyosin-mediated regulation of cytoplasmic myosins. Traffic 17:872–877. https://doi.org/10.1111/tra.12399

Manstein DJ, Meiring JCM, Hardeman EC, Gunning PW (2019) Actin–tropomyosin distribution in non-muscle cells. J Muscle Res Cell Motil:1–12. https://doi.org/10.1007/s10974-019-09514-0

Marian AJ, Braunwald E (2017) Hypertrophic cardiomyopathy. Circ Res 121:749–770. https://doi.org/10.1161/CIRCRESAHA.117.311059

Martin R, Risacher C, Barthel A et al (2014) Silver(I)-catalyzed route to pyrroles: synthesis of halogenated pseudilins as allosteric inhibitors for myosin atpase and x-ray crystal structures of the protein-inhibitor complexes. European J Org Chem 2014:4487–4505. https://doi.org/10.1002/ejoc.201402177

Mckillop DFA, Fortune NS, Ranatunga KW, Geeves MA (1994) The influence of 2,3-butanedione 2-monoxime (BDM) on the interaction between actin and myosin in solution and in skinned muscle fibres. J Muscle Res Cell Motil 15:309–318. https://doi.org/10.1007/BF00123483

Meiring JCM, Bryce NS, Wang Y et al (2018) Co-polymers of actin and tropomyosin account for a major fraction of the human actin cytoskeleton. Curr Biol 28:2331–2337.e5. https://doi.org/10.1016/j.cub.2018.05.053

Melchionda S, Ahituv N, Bisceglia L et al (2001) MYO6, the human homologue of the gene responsible for deafness in Snell's waltzer mice, is mutated in autosomal dominant nonsyndromic hearing loss. Am J Hum Genet 69:635–640. https://doi.org/10.1086/323156

Mohiddin SA, Ahmed ZM, Griffith AJ et al (2004) Novel association of hypertrophic cardiomyopathy, sensorineural deafness, and a mutation in unconventional myosin VI (MYO6). J Med Genet 41:309–314. https://doi.org/10.1136/jmg.2003.011973

Moore JR, Campbell SG, Lehman W (2016) Structural determinants of muscle thin filament cooperativity. Arch Biochem Biophys 594:8–17. https://doi.org/10.1016/j.abb.2016.02.016

Moraczewska J, Nicholson-Flynn K, Hitchcock-DeGregori SE (1999) The ends of tropomyosin are major determinants of actin affinity and myosin subfragment 1-induced binding to F-actin in the open state. Biochemistry 38:15885–15892. https://doi.org/10.1021/bi991816j

Morgan BP, Muci A, Lu PP et al (2010) Discovery of omecamtiv mecarbil the first, selective, small molecule activator of cardiac myosin. ACS Med Chem Lett 1:472–477. https://doi.org/10.1021/ml100138q

Morphy R, Rankovic Z (2005) Designed multiple ligands. An emerging drug discovery paradigm. J Med Chem 48:6523–6543. https://doi.org/10.1021/JM058225D

Münnich S, Pathan-Chhatbar S, Manstein DJ (2014a) Crystal structure of the rigor-like human non-muscle myosin-2 motor domain. FEBS Lett 588:4754–4760. https://doi.org/10.1016/j.febslet.2014.11.007

Münnich S, Taft MH, Manstein DJ (2014b) Crystal structure of human myosin 1c—the motor in GLUT4 exocytosis: implications for Ca^{2+} regulation and 14-3-3 binding. J Mol Biol 426:2070–2081. https://doi.org/10.1016/j.jmb.2014.03.004

Murphy CT, Spudich JA (1999) The sequence of the myosin 50−20K loop affects myosin's affinity for actin throughout the actin−myosin ATPase cycle and its maximum ATPase activity. Biochemistry 38:3785–3792. https://doi.org/10.1021/BI9826815

Nadif Kasri N, Van Aelst L (2008) Rho-linked genes and neurological disorders. Pflügers Arch – Eur J Physiol 455:787–797. https://doi.org/10.1007/s00424-007-0385-1

Odronitz F, Kollmar M (2007) Drawing the tree of eukaryotic life based on the analysis of 2,269 manually annotated myosins from 328 species. Genome Biol 8:R196. https://doi.org/10.1186/gb-2007-8-9-r196

Ohri RV, Radosevich AT, James Hrovat K et al (2005) A Re(V)-catalyzed C−N bond-forming route to human lipoxygenase inhibitors. Org Lett 7:2501. https://doi.org/10.1021/OL050897A

Ostap EM (2002) 2,3-Butanedione monoxime (BDM) as a myosin inhibitor. J Muscle Res Cell Motil 23:305–308. https://doi.org/10.1023/A:1022047102064

Papadaki M, Holewinski RJ, Previs SB et al (2018) Diabetes with heart failure increases methylglyoxal modifications in the sarcomere, which inhibit function. JCI Insight 3. https://doi.org/10.1172/JCI.INSIGHT.121264

Patel H, Margossian SS, Chantler PD (2000) Locking regulatory myosin in the off-state with trifluoperazine. J Biol Chem 275:4880–4888. https://doi.org/10.1074/jbc.275.7.4880

Pathan-Chhatbar S, Taft MH, Reindl T et al (2018) Three mammalian tropomyosin isoforms have different regulatory effects on nonmuscle myosin-2B and filamentous β-actin in vitro. J Biol Chem 293:863–875. https://doi.org/10.1074/jbc.M117.806521

Peters U, Cherian J, Kim JH et al (2006) Probing cell-division phenotype space and Polo-like kinase function using small molecules. Nat Chem Biol 2:618–626. https://doi.org/10.1038/nchembio826

Planelles-Herrero VJ, Hartman JJ, Robert-Paganin J et al (2017) Mechanistic and structural basis for activation of cardiac myosin force production by omecamtiv mecarbil. Nat Commun 8:190. https://doi.org/10.1038/s41467-017-00176-5

Preller M, Holmes KC (2013) The myosin start-of-power stroke state and how actin binding drives the power stroke. Cytoskeleton 70:651–660. https://doi.org/10.1002/cm.21125

Preller M, Manstein DJ (2017) Myosin motors: structural aspects and functionality. In: Reference module in life sciences

Preller M, Bauer S, Adamek N et al (2011a) Structural basis for the allosteric interference of myosin function by reactive thiol region mutations G680A and G680V. J Biol Chem 286:35051–35060. https://doi.org/10.1074/jbc.M111.265298

Preller M, Chinthalapudi K, Martin R et al (2011b) Inhibition of myosin ATPase activity by halogenated pseudilins: A structure-activity study. J Med Chem 54:3675–3685. https://doi.org/10.1021/jm200259f

Radke MB, Taft MH, Stapel B et al (2014) Small molecule-mediated refolding and activation of myosin motor function. Elife 2014:1–19. https://doi.org/10.7554/eLife.01603

Ramamurthy B, Yengo CM, Straight AF et al (2004) Kinetic mechanism of blebbistatin inhibition of nonmuscle myosin IIB. Biochemistry 43:14832–14839. https://doi.org/10.1021/BI0490284

Ramsay RR, Popovic-Nikolic MR, Nikolic K et al (2018) A perspective on multi-target drug discovery and design for complex diseases. Clin Transl Med 7:3. https://doi.org/10.1186/s40169-017-0181-2

Rauscher AÁ, Gyimesi M, Kovács M, Málnási-Csizmadia A (2018) Targeting myosin by blebbistatin derivatives: optimization and pharmacological potential. Trends Biochem Sci 43:700–713. https://doi.org/10.1016/J.TIBS.2018.06.006

Richard P, Charron P, Carrier L et al (2003) Hypertrophic cardiomyopathy. Circulation 107:2227–2232. https://doi.org/10.1161/01.CIR.0000066323.15244.54

Rohde JA, Roopnarine O, Thomas DD, Muretta JM (2018) Mavacamten stabilizes an autoinhibited state of two-headed cardiac myosin. Proc Natl Acad Sci U S A 115:E7486–E7494. https://doi.org/10.1073/pnas.1720342115

Roman BI, Verhasselt S, Stevens CV (2018) Medicinal chemistry and use of myosin II inhibitor (S)-blebbistatin and its derivatives. J Med Chem 61:9410–9428. https://doi.org/10.1021/acs.jmedchem.8b00503

Roth BL, Sheffler DJ, Kroeze WK (2004) Magic shotguns versus magic bullets: selectively non-selective drugs for mood disorders and schizophrenia. Nat Rev Drug Discov 3:353–359. https://doi.org/10.1038/nrd1346

Rozbicki E, Chuai M, Karjalainen AI et al (2015) Myosin-II-mediated cell shape changes and cell intercalation contribute to primitive streak formation. Nat Cell Biol 17:397–408. https://doi.org/10.1038/ncb3138

Schaub MC, Ermini M (1969) Effect of bivalent cations on the adenosine triphosphatase of actomyosin and its modification by tropomyosin and troponin. Biochem J 111:777–783. https://doi.org/10.1042/bj1110777

Schlichter LC, Pahapill PA, Chung I (1992) Dual action of 2,3-butanedione monoxime (BDM) on K^+ current in human T lymphocytes. J Pharmacol Exp Ther 261

Sellers JR, Wang F, Chantler PD (2003) Trifluoperazine inhibits the MgATPase activity and in vitro motility of conventional and unconventional myosins. J Muscle Res Cell Motil 24:579–585. https://doi.org/10.1023/B:JURE.0000009969.04562.58

Sellin LC, McArdle JJ (1994) Multiple effects of 2,3-butanedione monoxime. Pharmacol Toxicol 74:305–313. https://doi.org/10.1111/j.1600-0773.1994.tb01365.x

Senzaki H, Isoda T, Paolocci N et al (2000) Improved mechanoenergetics and cardiac rest and reserve function of in vivo failing heart by calcium sensitizer EMD-57033. Circulation 101:1040–1048. https://doi.org/10.1161/01.CIR.101.9.1040

Shaw MA, Ostap EM, Goldman YE (2003) Mechanism of inhibition of skeletal muscle actomyosin by N-benzyl-p-toluenesulfonamide. Biochemistry 42:6128–6135. https://doi.org/10.1021/BI026964F

Siegman MJ, Mooers SU, Warren TB et al (1994) Comparison of the effects of 2,3-butanedione monoxime on force production, myosin light chain phosphorylation and chemical energy usage in intact and permeabilized smooth and skeletal muscles. J Muscle Res Cell Motil 15:457–472. https://doi.org/10.1007/BF00122119

Sirigu S, Hartman JJ, Planelles-Herrero VJ et al (2016) Highly selective inhibition of myosin motors provides the basis of potential therapeutic application. Proc Natl Acad Sci 201609342. https://doi.org/10.1073/pnas.1609342113

Solaro RJ, Gambassi G, Warshaw DM et al (1993) Stereoselective actions of thiadiazinones on canine cardiac myocytes and myofilaments. Circ Res 73:981–990. https://doi.org/10.1161/01.RES.73.6.981

Spudich JA (2014) Hypertrophic and dilated cardiomyopathy: four decades of basic research on muscle lead to potential therapeutic approaches to these devastating genetic diseases. Biophys J 106:1236–1249. https://doi.org/10.1016/J.BPJ.2014.02.011

Stapleton MT, Fuchsbauer CM, Allshire AP (1998) BDM drives protein dephosphorylation and inhibits adenine nucleotide exchange in cardiomyocytes. Am J Physiol Circ Physiol 275:H1260–H1266. https://doi.org/10.1152/ajpheart.1998.275.4.H1260

Stern JA, Markova S, Ueda Y et al (2016) A small molecule inhibitor of sarcomere contractility acutely relieves left ventricular outflow tract obstruction in feline hypertrophic cardiomyopathy. PLoS One 11:e0168407. https://doi.org/10.1371/journal.pone.0168407

Straight AF, Cheung A, Limouze J et al (2003) Dissecting temporal and spatial control of cytokinesis with a myosin II inhibitor. Science 299:1743–1747. https://doi.org/10.1126/science.1081412

Strebhardt K, Ullrich A (2008) Paul Ehrlich's magic bullet concept: 100 years of progress. Nat Rev Cancer 8:473–480. https://doi.org/10.1038/nrc2394

Swenson AM, Tang W, Blair CA et al (2017) Omecamtiv mecarbil enhances the duty ratio of human β-cardiac myosin resulting in increased calcium sensitivity and slowed force development in cardiac muscle. J Biol Chem 292:3768–3778. https://doi.org/10.1074/jbc.M116.748780

Swift LM, Asfour H, Posnack NG et al (2012) Properties of blebbistatin for cardiac optical mapping and other imaging applications. Pflügers Arch – Eur J Physiol 464:503–512. https://doi.org/10.1007/s00424-012-1147-2

Takács B, Billington N, Gyimesi M et al (2010) Myosin complexed with ADP and blebbistatin reversibly adopts a conformation resembling the start point of the working stroke. Proc Natl Acad Sci U S A 107:6799–6804. https://doi.org/10.1073/pnas.0907585107

Tan L, Yuan X, Liu Y et al (2019) Non-muscle myosin II: role in microbial infection and its potential as a therapeutic target. Front Microbiol 10:401. https://doi.org/10.3389/fmicb.2019.00401

Terman JR, Kashina A (2013) Post-translational modification and regulation of actin. Curr Opin Cell Biol 25:30–38. https://doi.org/10.1016/J.CEB.2012.10.009

Tobacman LS (2008) Cooperative binding of tropomyosin to actin. Springer, New York, pp 85–94

Tojkander S, Gateva G, Schevzov G et al (2011) A molecular pathway for myosin II recruitment to stress fibers. Curr Biol 21:539–550. https://doi.org/10.1016/j.cub.2011.03.007

Trocóniz IF, Zsolt I, Garrido MJ et al (2006) Dealing with time-dependent pharmacokinetics during the early clinical development of a new leukotriene B4 synthesis inhibitor. Pharm Res 23:1533–1542. https://doi.org/10.1007/s11095-006-0254-1

Trybus KM, Waller GS, Chatman TA (1994) Coupling of ATPase activity and motility in smooth muscle myosin is mediated by the regulatory light chain. J Cell Biol 124:963–969. https://doi.org/10.1083/jcb.124.6.963

Varian K, Tang WHW (2017) Therapeutic strategies targeting inherited cardiomyopathies. Curr Heart Fail Rep 14:321–330. https://doi.org/10.1007/s11897-017-0346-8

Várkuti BH, Képiró M, Horváth IÁ et al (2016) A highly soluble, non-phototoxic, non-fluorescent blebbistatin derivative. Sci Rep 6:26141. https://doi.org/10.1038/srep26141

Verhasselt S, Roman BI, Bracke ME, Stevens CV (2017a) Improved synthesis and comparative

analysis of the tool properties of new and existing D-ring modified (S)-blebbistatin analogs. Eur J Med Chem 136:85–103. https://doi.org/10.1016/J.EJMECH.2017.04.072

Verhasselt S, Roman BI, De Wever O et al (2017b) Discovery of (S)-3′-hydroxyblebbistatin and (S)-3′-aminoblebbistatin: polar myosin II inhibitors with superior research tool properties. Org Biomol Chem 15:2104–2118. https://doi.org/10.1039/C7OB00006E

Verhasselt S, Stevens CV, Van den broecke T et al (2017c) Insights into the myosin II inhibitory potency of A-ring-modified (S)-blebbistatin analogs. Bioorg Med Chem Lett 27:2986–2989. https://doi.org/10.1016/J.BMCL.2017.05.008

Volkow ND, Morales M (2015) The brain on drugs: from reward to addiction. Cell 162:712–725. https://doi.org/10.1016/J.CELL.2015.07.046

von der Ecken J, Müller M, Lehman W et al (2015) Structure of the F-actin–tropomyosin complex. Nature 519:114–117. https://doi.org/10.1038/nature14033

von der Ecken J, Heissler SM, Pathan-Chhatbar S et al (2016) Cryo-EM structure of a human cytoplasmic actomyosin complex at near-atomic resolution. Nature 534:724–728. https://doi.org/10.1038/nature18295

Wilson IB, Ginsburg S (1955) A powerful reactivator of alkylphosphate-inhibited acetylcholinesterase. Biochim Biophys Acta 18:168–170. https://doi.org/10.1016/0006-3002(55)90040-8

Winder SJ, Ayscough KR (2005) Actin-binding proteins. J Cell Sci 118:651–654. https://doi.org/10.1242/jcs.01670

Winkelmann DA, Forgacs E, Miller MT, Stock AM (2015) Structural basis for drug-induced allosteric changes to human β-cardiac myosin motor activity. Nat Commun 6:7974. https://doi.org/10.1038/ncomms8974

Wollenberg RD, Taft MH, Giese S et al (2019) Phenamacril is a reversible and noncompetitive inhibitor of Fusarium class I myosin. J Biol Chem 294:1328–1337. https://doi.org/10.1074/jbc.RA118.005408

Wustman BA, Steele JW, Sjoberg ER, Stevens AC (2014) Bringing dead proteins back to life. Elife 3:e02189. https://doi.org/10.7554/eLife.02189

Xiong D, Du Y, Wang H-B et al (2015) Nonmuscle myosin heavy chain IIA mediates Epstein-Barr virus infection of nasopharyngeal epithelial cells. Proc Natl Acad Sci U S A 112:11036–11041. https://doi.org/10.1073/pnas.1513359112

Yang Z, Sweeney HL (1995) Restoration of phosphorylation-dependent regulation to the skeletal muscle myosin regulatory light chain. J Biol Chem 270:24646–24649. https://doi.org/10.1074/jbc.270.42.24646

Yoshida H, Cheng W, Hung J et al (2004) Lessons from border cell migration in the Drosophila ovary: a role for myosin VI in dissemination of human ovarian cancer. Proc Natl Acad Sci U S A 101:8144–8149. https://doi.org/10.1073/pnas.0400400101

Young E, Briggs S, Miller C (2015) The actin cytoskeleton as a therapeutic target for the prevention of relapse to methamphetamine use. CNS Neurol Disord Drug Targets 14:731–737. https://doi.org/10.2174/1871527314666150529145531

Zhang X, Seftel A, DiSanto ME (2011) Blebbistain, a myosin II inhibitor, as a novel strategy to regulate detrusor contractility in a rat model of partial bladder outlet obstruction. PLoS One 6:e25958. https://doi.org/10.1371/journal.pone.0025958

Zhang C, Chen Y, Yin Y et al (2015) A small molecule species specifically inhibits Fusarium myosin I. Environ Microbiol 17:2735–2746. https://doi.org/10.1111/1462-2920.12711

Zhang H-M, Ji H-H, Ni T et al (2017) Characterization of blebbistatin inhibition of smooth muscle myosin and nonmuscle myosin-2. Biochemistry 56:4235–4243. https://doi.org/10.1021/acs.biochem.7b00311

6 Single-Molecule Biophysical Techniques to Study Actomyosin Force Transduction

Yasuharu Takagi, Nikolas Hundt, and Adam Fineberg

Abstract

Inside the cellular environment, molecular motors can work in concert to conduct a variety of important physiological functions and processes that are vital for the survival of a cell. However, in order to decipher the mechanism of how these molecular motors work, **single-molecule microscopy techniques** have been popular methods to understand the molecular basis of the emerging ensemble behavior of these motor proteins.

In this chapter, we discuss various single-molecule biophysical imaging techniques that have been used to expose the mechanics and kinetics of myosins. The chapter should be taken as a general overview and introductory guide to the many existing techniques; however, since other chapters will discuss some of these techniques more thoroughly, the readership should refer to those chapters for further details and discussions. In particular, we will focus on scattering-based single-molecule microscopy methods, some of which have become more popular in the recent years and around which the work in our laboratories has been centered.

Keywords

Single molecule microscopy techniques · *In vitro* actin gliding assay · Single molecule fluorescence microscopy (SMFM) · Optical trap or tweezer (OT) · Dark-field microscopy · Interferometric scattering (iSCAT)

Y. Takagi (✉)
Laboratory of Molecular Physiology, Center for Cell and Developmental Biology, National Heart, Lung, and Blood Institute (NHLBI), National Institutes of Health (NIH), Bethesda, MD, USA
e-mail: takagiy@mail.nih.gov

N. Hundt
Department of Cellular Physiology, Ludwig-Maximilians-Universität München, Munich, Germany
e-mail: nikolas.hundt@med.uni-muenchen.de

A. Fineberg
Physical and Theoretical Chemistry Laboratory (PTCL), Department of Chemistry, University of Oxford, Oxford, UK
e-mail: adam.fineberg@chem.ox.ac.uk

6.1 Why Use Single-Molecule Assays?

Single-molecule techniques have been employed in the actomyosin/cytoskeletal field for the last 30+ years. These methods have been very popular in this field, because it was generally difficult to decrypt the molecular details of how individual proteins function from ensemble or bulk measurements. In ensemble experiments, the measured variable is usually an average over the

L. M. Coluccio (ed.), *Myosins*, Advances in Experimental Medicine and Biology 1239,
https://doi.org/10.1007/978-3-030-38062-5_6

entire population of molecules. More critically, the observables are often large scale solution properties, such as light absorption, scattering, fluorescence and conductivity, which can change in response to a molecular behavior, but they do not visualize the molecular behavior itself. This limits the interpretation of the underlying mechanism. For instance, it would require some basic understanding of the system if an increase in light scattering of a solution of actin were to be interpreted as a polymerization into filaments. For myosins, it would require a large array of different experiments to conclude that a motor walks processively along actin filaments. Using single-molecule techniques, however, these mechanisms become immediately apparent. One can then even start to probe molecular behavior on a molecule-by-molecule basis, which allows the characterization of sub-populations and ultimately leads to the understanding of the resultant bulk behavior from a "bottom-up" perspective.

In recent decades or so, single-molecule techniques have become so advanced that dynamic behavior of proteins can be measured with angstrom level spatial resolution and micro-second temporal resolution. This information can be used to draw a detailed picture of how conformational changes are linked to enzymatic activity and in the case of molecular motors to directed force production. In combination with structural studies, single-molecule techniques can decipher molecular dynamics at the atomic level and make it possible to even understand design principles that can be used to build artificial molecular motors (Chen et al. 2012; Furuta et al. 2017; Furuta and Furuta 2018).

6.2 The Original Assays – Bead Motility and *in vitro* Actin Gliding Assays

To understand the advances in single-molecule microscopy techniques utilized in the actomyosin field, we have to first step back and discuss an ensemble microscopy assay that has become the "granddaddy of them all": the myosin motility assay.

Initial experiments to understand the mechanical activity of myosins used an assay geometry whereby native actin bundles (*i.e.,* polar actin cables of the alga *Nitella axillaris)* (Sheetz and Spudich 1983; Vale et al. 1984) or stereocilia from bullfrog sacculi and semicircular canals (Shepherd et al. 1990)) were adhered to a coverslip glass as tracks for myosins attached to large polystyrene beads, the motion of which could be followed under a microscope. An illustration of this assay is shown in Fig. 6.1. In the presence of ATP, these beads moved along the actin filament bundles in a processive unidirectional manner (Sheetz and Spudich 1983; Sheetz et al. 1986; Hynes et al. 1987). This bead motility assay was the first practical and quantitative assay to determine the motion of ensembles of myosins and was also used as a prototype system for future single-molecule assays in the late 1980's/early 1990's.

The second type of assay, the *in vitro* actin-gliding assay, was first shown to work by the Spudich group (Kron and Spudich 1986). Here, myosin motion was measured using a purified protein system (*in vitro*) in a chamber with essentially myosin, actin filaments and ATP. This was similar to the bead motility assay but used purified individual actin filaments instead of bundled actin filaments.

In this assay, flow cells were constructed with a microscope coverslip coated on one surface with either rabbit skeletal muscle myosin or *Dictyostelium discoideum* myosin. A mixture of fluorescent phalloidin-labeled actin filaments together with ATP was then infused into the flow cell. The motion of the fluorescently-labeled actin filaments, propelled by the surface-attached myosins, was observed using a microscope equipped with a wide-field fluorescence imaging modality (Fig. 6.2). Videos of the actin filaments' motion were saved on video-tapes for further analysis such as to determine actin filament lengths, velocities and distances traveled. More details on the assay can be found in a methodology paper by Kron et al. (1991).

In vitro actin gliding formed the basis of the single-molecule mechanical and kinetic assays, whereby a simplified system with only actin fila-

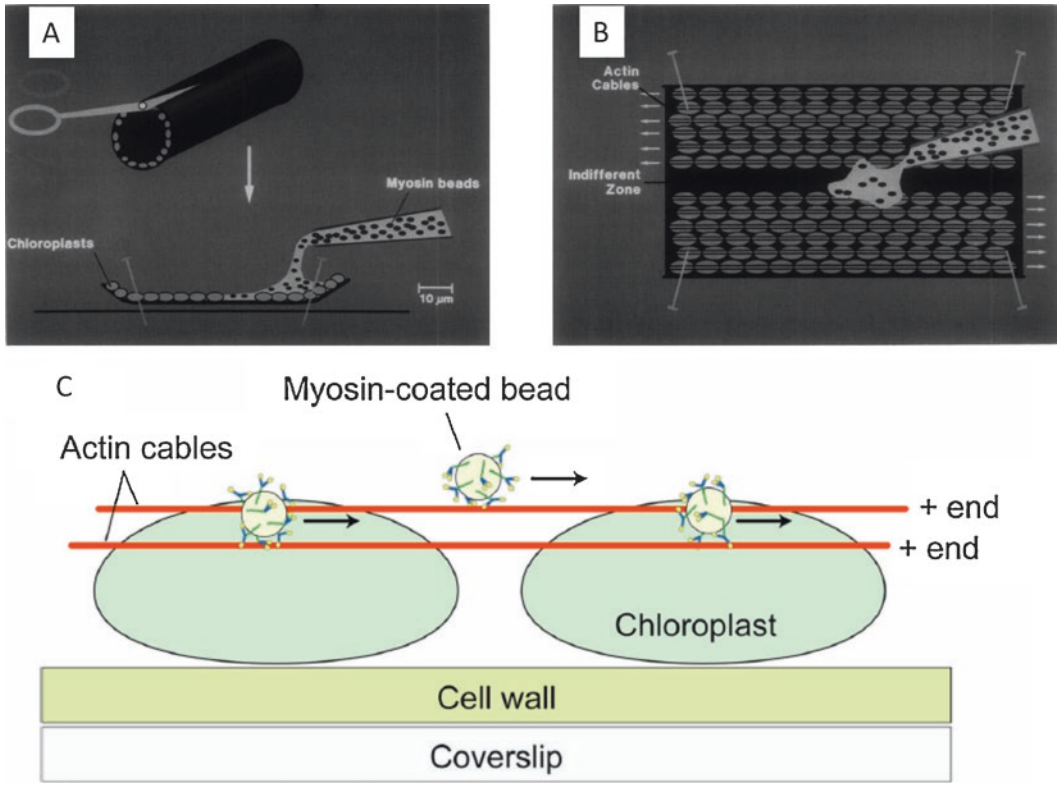

Fig. 6.1 Bead motility assay. (**a**) Diagram showing cutting of the cylindrical *Nitella* cell, pinning of the cut cell, and deposition of the myosin-attached beads. (**b**) Diagram showing the open cell from the top. Arrows indicate direction of movement of vesicular elements *in vivo*. Myosin-2-coated beads move in the same direction *in vitro*. (**c**) Diagram showing the motion of the myosin-2-coated beads on the actin cables. (Diagrams reproduced from Sheetz et al. 1986 and Kodera and Ando 2014. Copyright 1986 Elsevier BV)

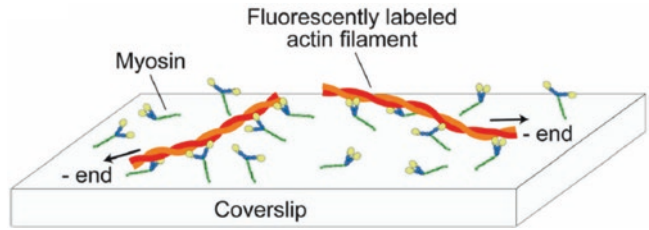

Fig. 6.2 *in vitro* actin gliding assay. Diagram illustrating the motion of the fluorescently-labeled actin filaments on a bed of myosins attached to the surface. (Diagram reproduced from Kodera and Ando 2014)

ments and myosin is reconstituted inside a microscope flow cell. Over time, advances in the theoretical understanding of the underlying processes have produced variations of this assay in which other actin-binding proteins apply loads to the propelled actin filaments by retarding their movement (Warshaw et al. 1990; Bing et al. 2000; Greenberg and Moore 2010; Aksel et al. 2015). This variation of the assay has been used to investigate the response of myosin ensembles to external forces.

In recent years, in order to quantitatively analyze *in vitro* actin gliding data, new programs such as FIESTA and FASTA have been devel-

oped (Ruhnow et al. 2011; Aksel et al. 2015) making analysis easier and more efficient. However, other "analog" motion analysis type modules have been utilized to quantify data in a similar fashion since the 1990's (Homsher et al. 1992; Sellers et al. 1993).

For measuring the mechanics of higher-order myosin macromolecular complexes such as myosin-2 assembled into bipolar filamentous structures, experiments have been performed by attaching native molluscan myosin-2 "thick filaments" onto a glass surface and measuring the actin filaments moving above them (Sellers and Kachar 1990). These experiments used a combination of differential interference contrast (DIC) and wide-field fluorescence microscopy to visualize the myosin thick filaments and actin, respectively. As expected from the bipolar structure of the myosin filament, the actin filaments were seen to move towards the center of the thick filaments. The study showed that the actin filaments moved on the myosin filament structure towards the center of the bare zone at a rate of ~9 μm s^{-1}. Contrary to this expected direction of motion, the authors also showed that the actin filaments can move from the center bare zone towards the outside of the bipolar myosin filament but at a slower velocity, ~1 μm s^{-1}. This result suggested that any given orientation of the actin filament could interact with any portion of the myosin filament and contribute to the force generation process. This assay topology has been used in a recent study of cardiac myosin-2 in the presence of a variety of wild-type and mutant cardiac myosin binding protein-C (Previs et al. 2012) to show how cardiac myosin-binding protein-C modulates cardiac contractility.

Myosin filament-based assays can also be used in an "inverted" geometry where the actin filaments are bound to the surface and the movement of the myosin filaments is observed. In recent years, such experiments have been performed with smooth, skeletal and cardiac myosin-2 (Brizendine et al. 2015; Brizendine et al. 2017), as well as non-muscle myosin-2A and myosin-2B filaments (Nagy et al. 2013; Melli et al. 2018) to decipher the molecular mechanism of force generation and motion of these filament complexes as a more physiological motile unit.

All of these "motor ensemble" *in vitro* motility assays developed in the 1980's-90's laid the foundation for the single-molecule microscopy assays performed in the following decades.

6.3 Early Days of Single-Molecule Fluorescence Assays

When light propagates through a medium such as a glass coverslip and encounters a medium of lower refractive index such as water or buffer, it is either refracted or reflected depending upon the angle of incidence and the difference in refractive indices of the two media. At the critical angle, *i.e.* ~62° for a glass/water interface, where light is totally internally reflected, an evanescent wave extends into the aqueous medium whose intensity falls exponentially with penetration depth (~100 nm), thus illuminating only a shallow volume above the interface.

This fluorescence technique, called **T**otal **I**nternal **R**eflection **F**luorescence (TIRF) microscopy, allows only the fluorophores that are very close to the interface to be excited without exciting the "background" fluorophores that are not reached by the evanescent wave. This technique achieves an increased signal-to-noise ratio of the intensity of fluorophores that are very close to the coverslip. Different optical paths, or methods, to accomplish TIRF microscopy have been described previously in Axelrod 2001 and Axelrod 2008, which can be referred to for more details (Fig. 6.3).

Single-molecule fluorescence measurements of myosins began with an article published in 1995 by the Yanagida group who used TIRF microscopy to visualize single molecules of skeletal muscle heavy meromyosin (HMM) labeled with a Cy3 dye and bound to a coverslip surface (Funatsu et al. 1995). The authors demonstrated that the fluorescence of the observed "myosin" spots disappeared in either one or two quantal steps of photobleaching, providing evidence that either one or two fluorophores were covalently

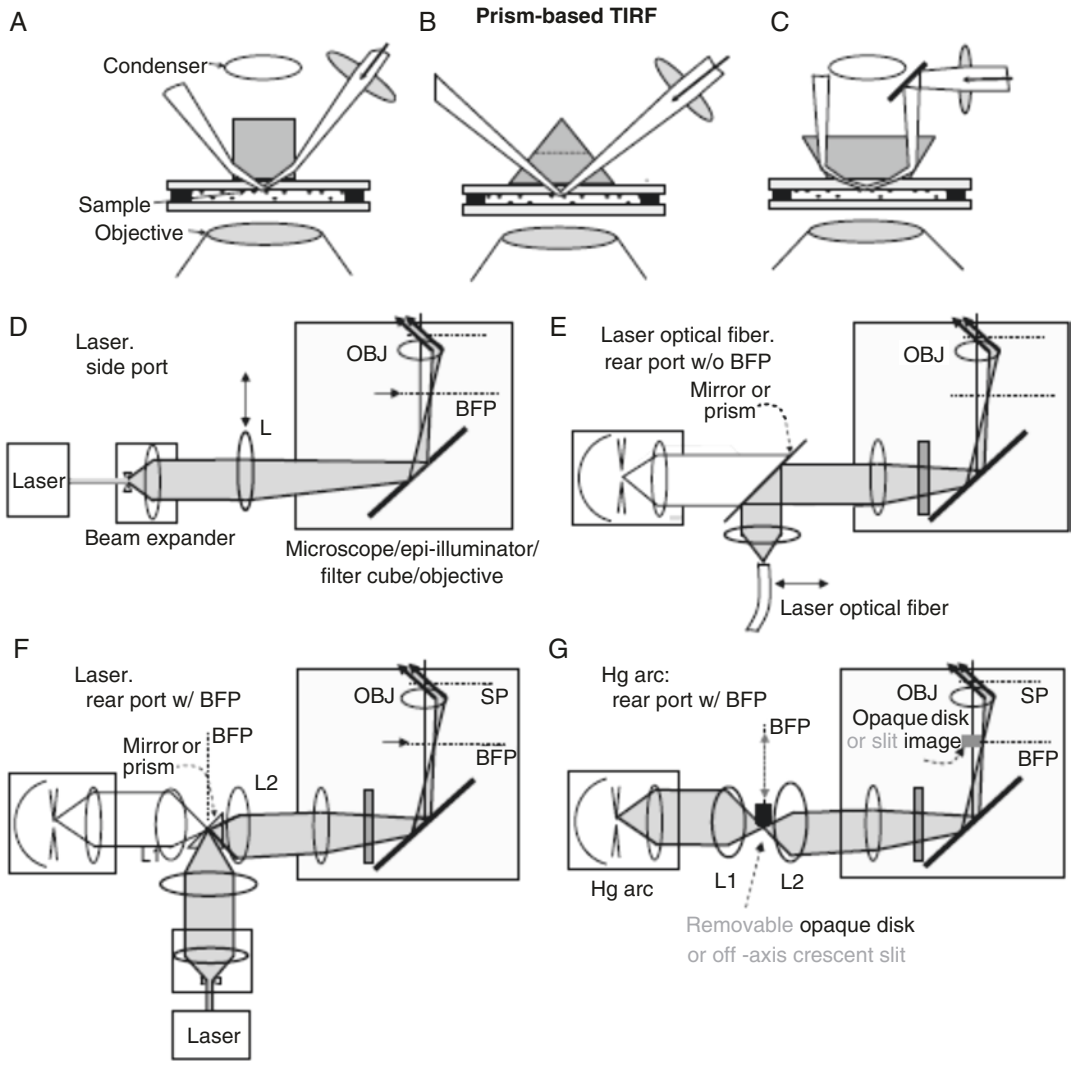

Fig. 6.3 TIRF microscopy examples. (**a**–**c**) Schematic illustrations of different types of prism-based TIRF microscopy. Sample chambers can be made as a "sandwich" with a lower glass coverslip, a spacer such as Teflon or double-sided sticky tape and a coverslip with sample which is mounted upside-down so that the sample faces downwards. The outer surface of the sample coverslip is put into contact with a prism through a film of immersion oil. (**d**–**g**) Schematic illustrations of different objective-type TIRF in an inverted microscope. (**d**) Laser illumination from the side port using a dichroic mirror cube facing towards the side port. The beam is focused onto the BFP at a radial position sufficient to lead to supercritical angle propagation at the coverslip. Transverse motion of L can be used to alter between epi-fluorescence and TIRF modes. (**e**) Laser illumination using an optical fiber, through the rear port. (**f**) Laser illumination using an equivalent BFP in some microscope systems to focus the beam. Another equivalent back focal plane sometimes marked as the aperture lane exists in some systems. (**g**) An arc lamp can be used for total internal reflection illumination, too. For more details on these schemes, please refer to Axelrod 2001 and Axelrod 2008. OBJ = objective lens, SP = sample plane, BFP = back focal plane, L = focusing lenses. (Diagram reproduced from Axelrod 2008. Copyright 2008 Elsevier BV)

bound to the molecule. Furthermore, they explored the binding and dissociation of Cy5-labeled ATP using TIRF microcopy and found that lifetimes of merging Cy3/Cy5 spots were consistent with the known kinetics of binding, hydrolysis and release of ATP by the myosin.

6.4 Single-Molecule Fluorescence Assays Using Enhanced Localization Techniques

The movement of processive molecular motors was commonly studied using the inverted geometry of the *in vitro* actin gliding assay, with the actin filaments bound to the surface of the image plane, such that the motion of these molecular motors could be observed. Rather than linking a large bead to myosins as in the early studies from the 80's described above, scientists created other methods to "tag" a protein with fluorescent probes so that the motion of the protein could be inferred from the motion of the attached marker. Genetically encoded fluorophores (such as green fluorescent protein (GFP) or enhanced GFP (eGFP)) (Snyder et al. 2004; Yildiz et al. 2004b), an accessory protein (i.e., calmodulin) attached to an organic dye (Forkey et al. 2003; Yildiz et al. 2004b; Sakamoto et al. 2005) or quantum dots (Qdots) (Warshaw et al. 2005; Ali et al. 2007) were a few examples of how researchers attached fluorophores to the myosin.

6.4.1 FIONA

At first, TIRF-based inverted single-molecule motility assays were used to measure only velocities and run lengths of individual myosins over actin filaments fixed to the surface (Sakamoto et al. 2000, 2003). However, the detailed translocation, or stepping, mechanism at the nanometer resolution was still unresolved using fluorescence techniques.

In microscopy, Abbe's law dictates that in order for two objects to be resolved they must be separated by a distance $\Delta x \geq \frac{\lambda}{2 \cdot NA}$, where λ is the wavelength of light and NA is the numerical aperture of the objective lens. This separation distance is thus typically around 200–350 nm for visible light ($\lambda \sim 400$–750 nm), which also defines the width of the imaged spots of the fluorophores or the so-called point spread function (PSF). In order to overcome this limit, a method was developed that used the shape of the PSF to localize fluorescent probes at higher precision than was dictated by Abbe's diffraction limit (Yildiz et al. 2003) and was applied to studying the detailed mechanics of myosin-5a translocation.

This method, named FIONA for ***F***luorescence ***I***maging at ***O***ne ***N***anometer ***A***ccuracy, allowed the specificity and sensitivity of single-molecule fluorescence with nanometer localization precision of the position of the fluorophore. The two-dimensional PSF of a fluorophore was observed such that sufficient photons (~5000–10,000) were collected per diffraction limited PSF of a single fluorophore. A Gaussian fit to the PSF was used to localize the average position of the fluorophore to approximately 1.5 nanometer accuracy.

The mathematical expression for this emission intensity distribution was described as a two-dimensional Gaussian in the form:

$$I(x,y) = I_{Background} + A \exp\left\{-\frac{1}{2}\left[\frac{x-x_0}{S_x}\right]^2 - \left[\frac{y-y_0}{S_y}\right]^2\right\}, \tag{6.1}$$

where $I_{Background}$ is the background intensity (or noise floor), x_0 and y_0 describe the coordinates of the center position of the fluorophore, and S_x and S_y are the standard deviations of the distribution in both directions.

The width, or the standard error of the mean, $\sigma^{\mu}_{x,y}$, of this distribution can be described as:

$$\sigma^{\mu}_{x,y} = \sqrt{\frac{S^2_{x,y}}{N_{Photons}} + \frac{a^2}{12 \cdot N_{Photons}} + \frac{8 \cdot \pi \cdot S^4_{x,y} \cdot b^2}{a^2 \cdot N_{Photons}}}, \tag{6.2}$$

where, $N_{Photons}$ is the number of collected photons, a is the pixel size of the image detector and b is the standard deviation of the background fluctuations (Thompson et al. 2002; Yildiz et al. 2003).

The first term in Eq. 6.2, $\frac{S^2_{x,y}}{N_{Photons}}$, is the photon noise; the second term, $\frac{a^2}{12 \cdot N_{Photons}}$, is the effect

of the pixel size of the detector; and the third term, $\frac{8 \cdot \pi \cdot S_{x,y}^4 \cdot b^2}{a^2 \cdot N_{Photons}}$, is the effect caused by background fluctuations. Thus, for a photon noise limited case – *i.e.,* when the noise in each pixel is dominated by photons originating from the particle being localized – the equation above can be reduced to show that the expression for the best estimate of the position of the fluorophore is:

$$\left(\Delta x\right)^2 = \frac{S_{x,y}^2}{N_{Photons}}, \tag{6.3}$$

where Δx is the error in localization, $S_{x,y}$ is the standard deviation of the point-spread function and $N_{Photons}$ is the number of photons collected. Thus, increasing the number of collected photons leads to lower localization uncertainty. In this case ~1.5 nm localization precision was achieved by collecting ~10,000 photons per diffraction limited spot, or fluorophore (Fig. 6.4).

This ability to achieve a high localization precision, together with the observation that certain fluorophores undergo blinking, was the starting point for imaging techniques later developed for use in cell biological studies such as photoactivated localization microscopy (PALM) (Betzig et al. 2006) and stochastic optical reconstruction microscopy (STORM) (Rust et al. 2006; Huang et al. 2008).

The results with myosin-5a using FIONA led to the development of a model in which the motor steps in a hand-over-hand motion, taking alternating step sizes between 37 + 2x and 37 − 2x nm, where x is the distance along the direction of motion between the dye and the midpoint between the two heads (Yildiz et al. 2003) (Fig. 6.5). The same "super-resolution" localization method has been applied to other cytoskeletal motor systems such as kinesin (Yildiz et al. 2004a) and dynein (Reck-Peterson et al. 2006).

6.4.2 Two Fluorophore Super-Resolution Fluorescence Imaging

With the development of FIONA, other single-molecule localization methods to determine distances have emerged such as ***S***ingle-molecule ***H***igh-***R***esolution ***Im***aging with ***P***hotobleaching (SHRImP) (Gordon et al. 2004) and ***NA***nometer-***L***ocalized ***M***ultiple ***S***ingle-molecule fluorescence microscopy (NALMS) (Qu et al. 2004). These methods were conceived to measure distances between two identical fluorophores in the range of 10–200 nm using photobleaching. Similarly, ***S***ingle-molecule ***H***igh ***RE***solution ***C***olocalization (SHREC) was developed to measure intramolecular distances using two different fluorophores (Churchman et al. 2005). Both SHRImP and SHREC have been used extensively to observe the stepping mechanics of myosin-5a and myosin-6 (Churchman et al. 2005; Warshaw et al. 2005; Balci et al. 2005). Figure 6.6 shows an example of a dual Qdot-labeled myosin-5a with head spacing of ~36 nm measured by the distances between the two Qdots, and step size of 72 nm calculated from tracking one Qdot over time.

6.4.3 *pol*TIRF

Nanometer measurements of intramolecular domain distances and stepping patterns have been extremely useful for understanding how motor proteins work. Moreover, detecting the rotational dynamics of myosins has been another direction for single-molecule fluorescence microscopy development that has advanced our understanding of the mechanisms behind force and motion generation in myosins. On this avenue, fluorescence polarization techniques have been used extensively to probe the angular changes of the lever arm domain of myosins during their enzymatic cycle. *pol*TIRF or ***pol***ar-

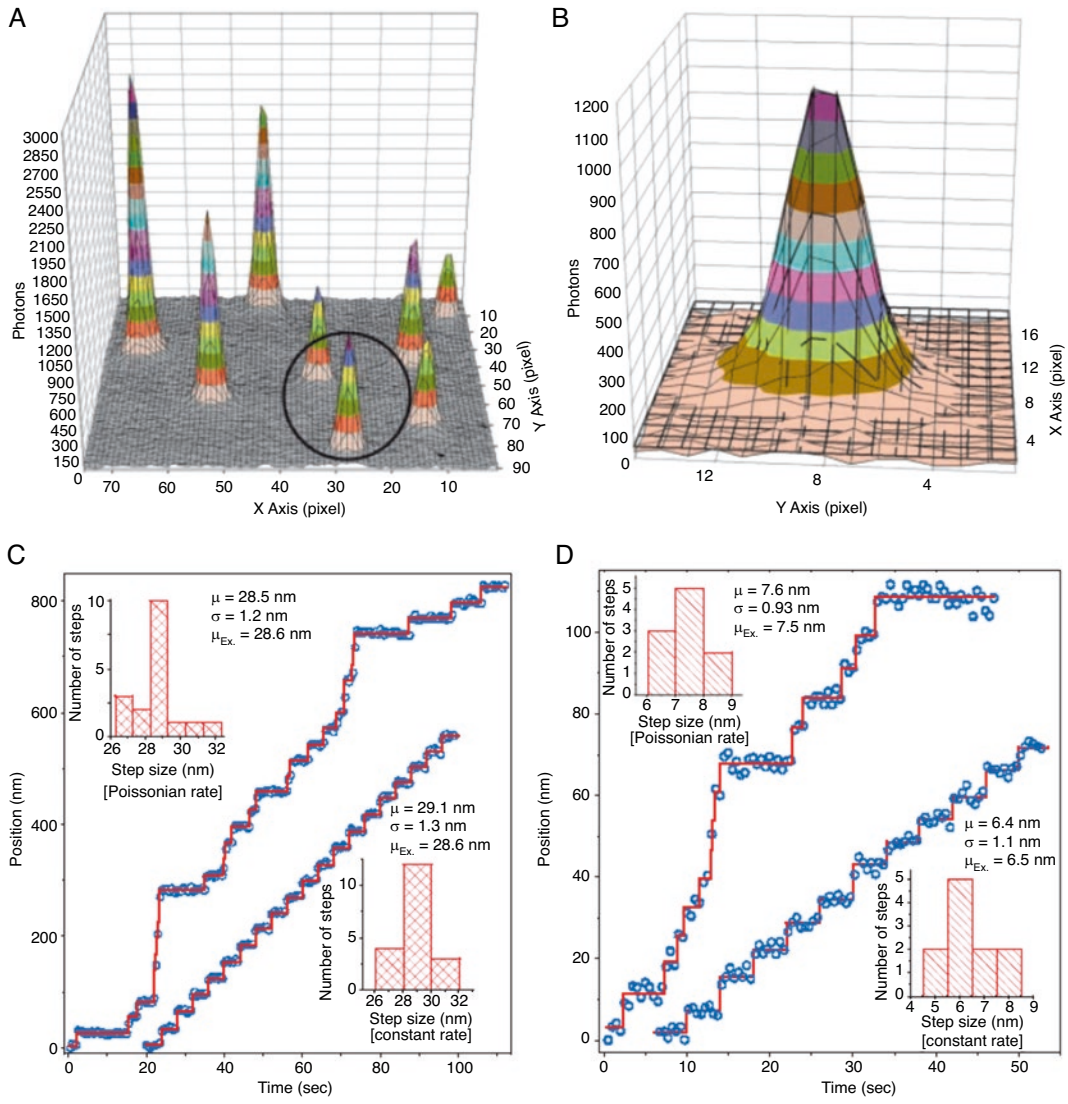

Fig. 6.4 FIONA example – Cy3. (**a**) Point-spread functions (PSF) of individual Cy3 molecules attached to a coverslip with 0.5 s integration time. (**b**) Gaussian fit to the PSF, with center position determined at 1.3 nm precision. Width of PSF is 287 nm. (**c** and **d**) Coverslip with Cy3 dye molecules were moved using the piezo-stage, using a constant or a Poisson distributed rate, while the PSF of the dyes were tracked. Precision is approximately 1 nm. (Diagram reproduced from Yildiz et al. 2003. Copyright 2003 Science/AAAS)

ization ***T***otal ***I***nternal ***R***eflection ***F***luorescence microscopy (Fig. 6.7) is an imaging modality that takes advantage of the polarized characteristic of the emission dipole of the fluorophore with respect to the excitation laser or incident light source. *pol*TIRF microscopy has been performed using a prism-type TIRF microscope arrangement, allowing complex combinations of multiple input laser paths and polarizations for fluorophore excitation in the field-of-view of the microscope. Emission of the fluorophores in different polarizations are monitored using avalanche photodiodes (APDs). Using this method, it was possible to measure the rotational motion of a fluorophore (bifunctional rhodamine) attached to the calmodulin on the lever arms of myosin-5 (Forkey et al. 2003) and myosin-6 (Sun et al. 2007), as well as myosin-10 (Sun et al.

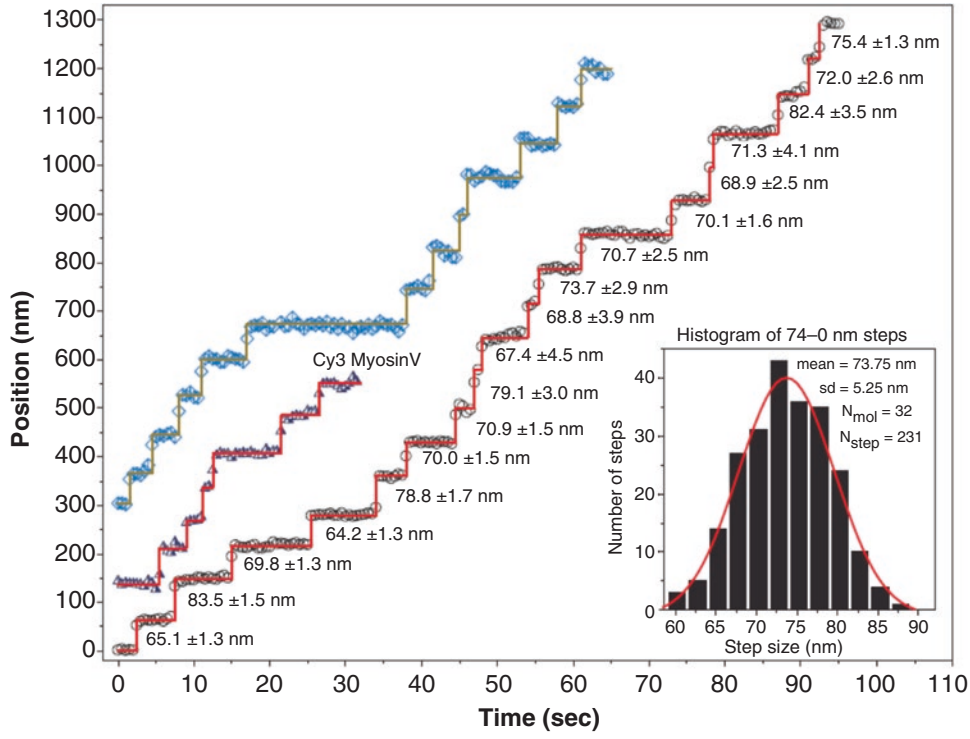

Fig. 6.5 FIONA example – Myosin-5a. Stepping trajectory of three different myosin-5a molecules, displaying ~74 nm steps since only one of the lever arms was labeled with a bifunctional rhodamine or Cy3 dye. Histogram of all steps (inset) confirms an average step size of ~74-nm. (Diagram reproduced from Yildiz et al. 2003. Copyright 2003 Science/AAAS)

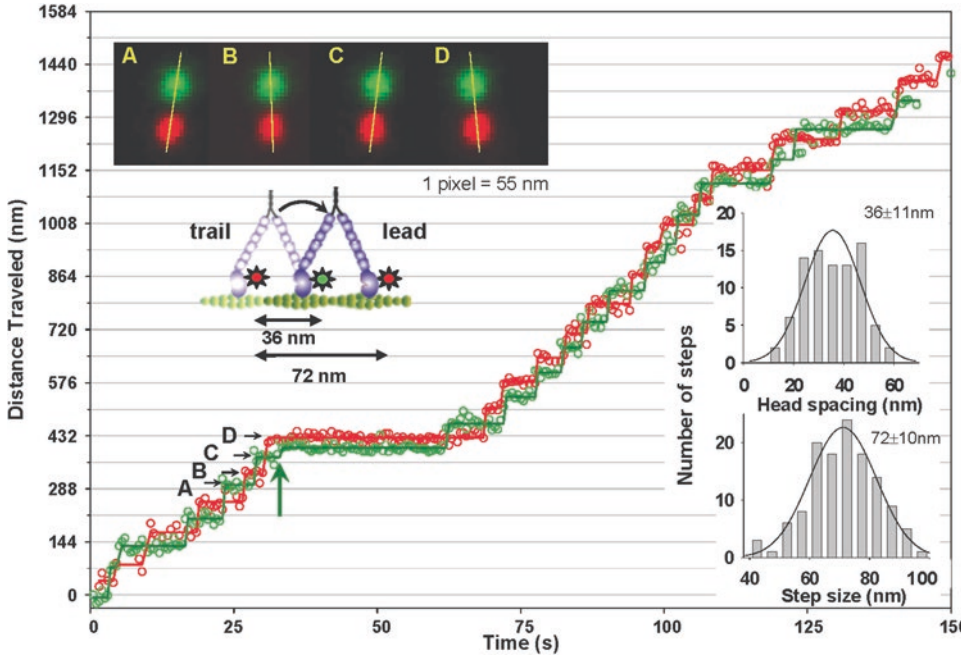

Fig. 6.6 SHREC – Myosin-5a with Qdots. Myosin-5a with a biotinylation site on the motor domain was labeled with Qdot 565 (Green) and Qdot 655 (Red). Upper left image shows the averaged Qdot images for the steps labeled **A** to **D** with the two-color images offset vertically for clarity. The yellow lines emphasize the alternating relative head positions. Inset histograms show inter-head spacing (~36 nm average) and step-size (~72 nm average). (Diagram reproduced from Warshaw et al. 2005. Copyright 2005 Elsevier BV)

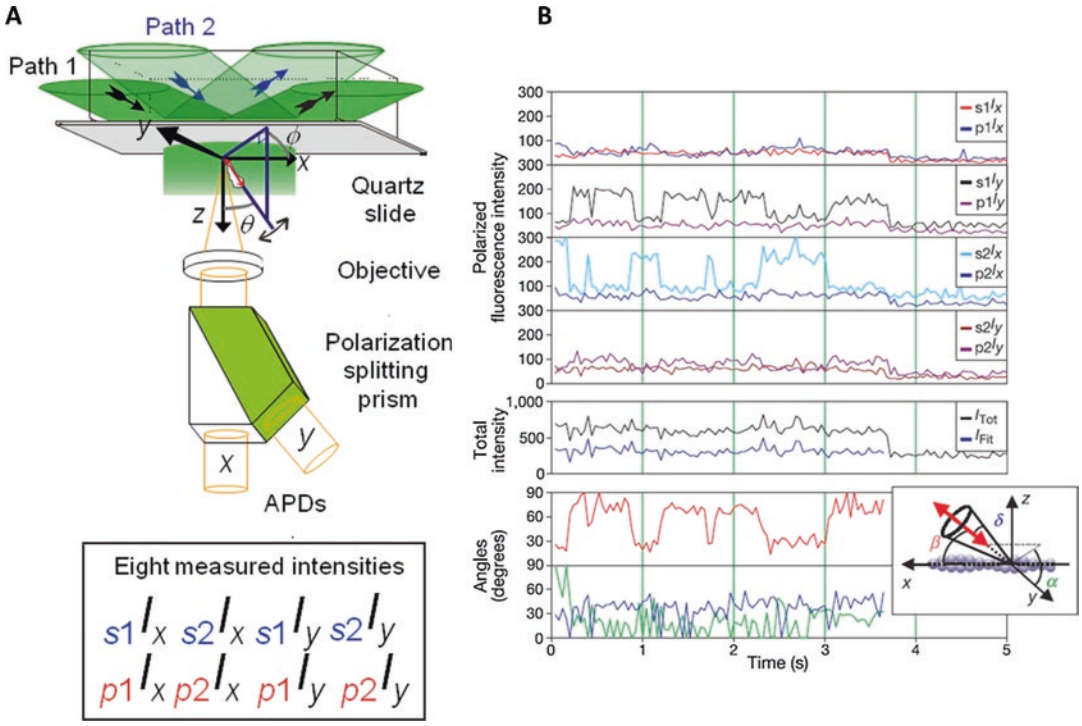

Fig. 6.7 *pol*TIRF-scheme and myosin-5a. (**a**) Scheme for single-molecule polTIRF setup. Dual path illumination of an input laser is used to create an evanescent wave at the sample surface using a prism –type TIRF microscope. Emission of a fluorophore is collected using an objective lens and passed through a polarization splitting prism. A pair of avalanche photodiodes is used to collect the x- and y-polarized fluorescent emissions. This configuration of the polTIRF allows collection of 8 different combinations of polarized excitation/emission intensities. Further analysis of these measurements allows interpretation of single-molecule rotational motion of the studied fluorophores. (Image from Rosenberg et al. 2005. Copyright 2005 American Chemical Society). (**b**) polTIRF data of a single molecule of myosin-5a labeled with a bifunctional rhodamine-labeled calmodulin moving along an actin filament. Polarized fluorescence intensities ($_{s\_}I_{\_}$ and $_{p\_}I_{\_}$; units = photocounts per 10 ms gate) and total intensity ($I_{\_}$; units = photocounts per 40 ms cycle) are shown (upper four graphs). The first subscripts, $_{s\_}$ and $_{p\_}$, describe the linear excitation polarizations along the x- and y- axes and the excitation polarizations approximately along the z-axis, respectively. The second subscripts represent the detection polarization in the x- and y-axes of the experimental coordinate system. Measurements are used to define the motion of the labeled calmodulin bound to myosin-5a during translocation *via* the β, α and δ angles (represented as red, green and blue; lower two graphs). The β angle shows two distinct angles of the probe, representing the tilting of the lever arm between two structural states. The inset (bottom right) defines these angles relative to the actin filament and the polTIRF apparatus coordinate systems as shown. (Images from Forkey et al. 2003. Copyright 2003 Nature Publishing Group)

2010). More details can be found in the following articles and reviews about this method (Forkey et al. 2000, 2003; Beausang et al. 2012, 2013).

6.4.4 DOPI

DOPI, or ***D***efocused ***O***rientation and ***P***osition ***I***maging, another twist on the single-molecule localization method (Toprak et al. 2006), was developed to quantify the rotational motion, or orientation, of a fluorescent probe while simultaneously measuring its position. The rotational orientation of the fluorophore was determined by imaging a defocused PSF (Fig. 6.8). By tracking the translational and rotational motion of a single bifunctional rhodamine probe attached to one of the calmodulins of the light-chain binding domain (LCBD) of myosin-5, it was found that the rhodamine probe dwelled in two distinct ori-

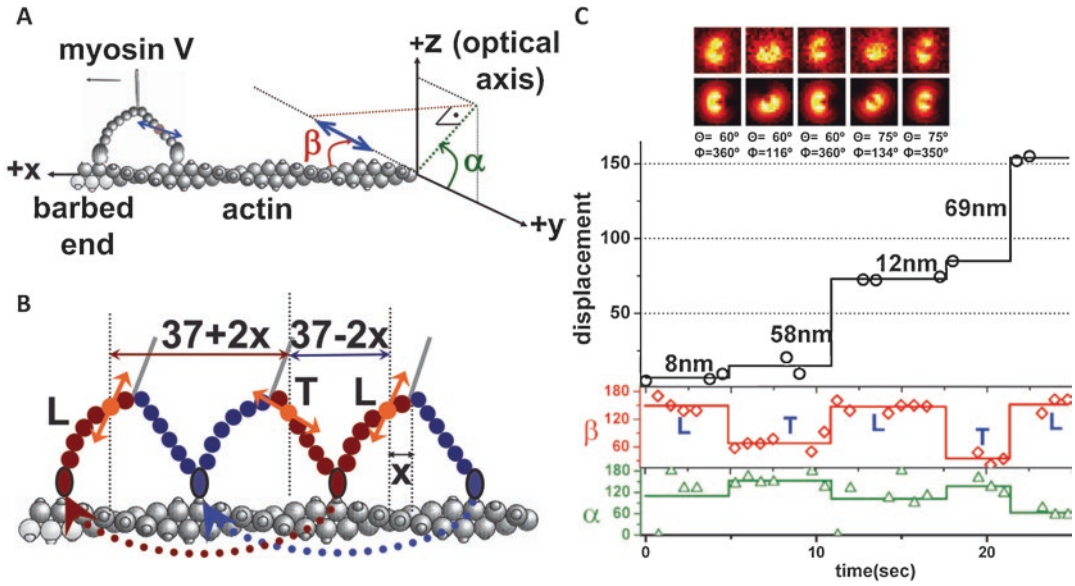

Fig. 6.8 DOPI – Myosin-5a. (**a**) Actin-based coordinate system used to analyze the relative motion of the dye attached to myosin-5a. (**b**) Cartoon of myosin-5 undergoing two steps, showing the tilting emission dipoles of the dye attached to one of its IQ motifs (orange arrow). (**c**) DOPI (3D orientation) and FIONA (displacement) data for single molecules of myosin-5a. Figures show data from two different myosin-5a molecules stepping on average 64–10 nm (first step – second step). The differences in stepping distances are due to the multiple positions where the labeled calmodulins can be bound on the lever arm. Upper panels are the images of the labeled myosin-5a. Second panel from top are the FIONA stepping data. Third and fourth from top show the β and α angles determined from fitting the images in the top panel. (Images from Toprak et al. 2006. Copyright 2006 National Academy of Sciences, USA)

entations. These dwells coincided with two distinct step sizes which could be explained by the asymmetric positioning of the calmodulin bound to one of the myosin-5 heavy chain's LCBD on the lever arm, which was then alternating between the leading and trailing position.

6.5 Scattering-Based Microscopy

The field has gained considerable insight into the molecular details of myosin stepping mechanisms from single-molecule fluorescence studies. However, some of the conformational transitions in myosins, such as the diffusive period of a detached motor domain during a processive walk, happen at the timescale of a few ms down to μs. Although fluorescence-based imaging has enabled the localization of single motors down to a precision of a nanometer (see FIONA), the fundamental physics of the fluorescent process eventually limit the achievable precision and time resolution as it becomes more and more difficult to capture a sufficient number of photons (Eq. 6.3). The maximum speed of the excitation-emission cycle of a fluorophore is dictated by its photophysics. Many fluorophores can also return to their ground-state without emitting a photon at all. Oxidative stress and photobleaching further hamper the quest for an ever-higher imaging speed that requires more and more incident light.

The process of light scattering is not affected by these fundamental limits of fluorescence, as the number of scattered photons simply scales with the number of incident photons. Theoretically, the detection in scattering is therefore only limited by the light intensity that can be directed onto the sample. In practice, however, scattering-based detection has a major disadvantage over fluores-

cence, which has probably been the main reason for its lower popularity. While the signal in fluorescence measurements is specifically generated by the fluorophore and all background signal is suppressed through optical filters, scattered light is produced by all species in a sample, which therefore all contribute to the detected signal. This makes it crucial for scattering-based single-molecule studies to have a strategy for removal of any unwanted background.

As mentioned in previous chapters, most single-molecule myosin experiments operate at a glass-water interface (Deniz et al. 2007). If light is directed onto such a sample, a glass-water interface will reflect 0.4% of the incident illumination (Hecht 1998). The light that is not reflected will then be scattered by any object with a different refractive index to the surrounding medium, in this case, the aqueous solution. The intensity, I_{det}, detected by the camera depends on the amplitudes of the reflected electric field including other background light, $\mathbf{E}_r$, and the scattered electric field, $\mathbf{E}_s$, as well as their relative phases φ:

$$I_{\text{det}} = \left|\mathbf{E}_r + \mathbf{E}_s\right|^2 = \left|\mathbf{E}_r\right|^2 + \left|\mathbf{E}_s\right|^2 + 2\left|\mathbf{E}_r\right|\left|\mathbf{E}_s\right|\cos\varphi \tag{6.4}$$

Equation (6.4) shows the three contributions to the detected intensity: the reference and background signal, $|\mathbf{E}_r|^2$, the scattering signal, $|\mathbf{E}_s|^2$, and an interference term, $2|\mathbf{E}_r||\mathbf{E}_s|\cos\varphi$.

To date, researchers have used two different scattering-based microscopic techniques to study myosin dynamics, dark-field (DF) microscopy and interferometric scattering microscopy (iSCAT).

Dark-field microscopes operate by reducing the background light, $|\mathbf{E}_r|^2$, so as to make the pure scattering signal, $|\mathbf{E}_s|^2$, the dominant term in Eq. (6.4). This produces a dark image with bright scattering objects.

Interferometric scattering microscopy, on the other hand, does not exclude all background light and uses the large signal from the glass-water interface as a reference field. For sufficiently small scatters, $|\mathbf{E}_s|^2$ becomes negligible and therefore the detected signal is the interference term, $2|\mathbf{E}_r||\mathbf{E}_s|\cos\varphi$, on top of a bright background, $|\mathbf{E}_r|^2$.

6.5.1 Dark-Field Microscopy

As early as 1903, scattering was used as a contrast mechanism to visualize colloidal gold particles (Siedentopf and Zsigmondy 1903). The pioneering researchers used a so-called "ultramicroscope" to collect light from a sample at a 90° angle from the illuminating beam path. This earliest example highlights the general principle of dark-field microscopy in which all background light is rejected while the pure scattering contribution is detected. In this regard, dark-field microscopy is technically similar to fluorescence microscopy, only the strategy of attenuating the background illumination has to be adjusted, since the scattered light is not spectrally shifted as it usually is in fluorescence.

In modern commercial dark-field microscopes, the illuminating light is usually focused onto the sample through a condenser (Gage 1920) as shown in Fig. 6.9a by which the light can be seamlessly shifted into and away from the detecting optic. This way the user can easily switch between bright- and dark-field imaging (Fig. 6.9a).

Other more recent strategies use laser beams that are coupled into the back focal plane of an objective and illuminate the sample in total internal reflection (Nishikawa et al. 2010; Ueno et al. 2010; Mickolajczyk and Hancock 2018). The illuminating beam in these setups is directed into the objective using perforated mirrors (Nishikawa et al. 2010; Ueno et al. 2010) or micro-mirrors (Mickolajczyk and Hancock 2018) that leave space for the scattering image to be picked up into the detecting beam path while excluding the illuminating light (Fig. 6.9b and c).

Revisiting Eq. (6.4), dark-field microscopy rejects all background light from the sample and collects the pure scattering signal, reducing the expression to:

$$I_{\text{det}} = \left|\mathbf{E}_s\right|^2 = \left|\mathbf{E}_i\right|^2 \cdot \left|s\right|^2, \tag{6.5}$$

where $\mathbf{E}_i$ is the electric field of incident light upon the sample and s is the complex scattering amplitude. As the scattering intensity is directly proportional to the intensity of the incident light,

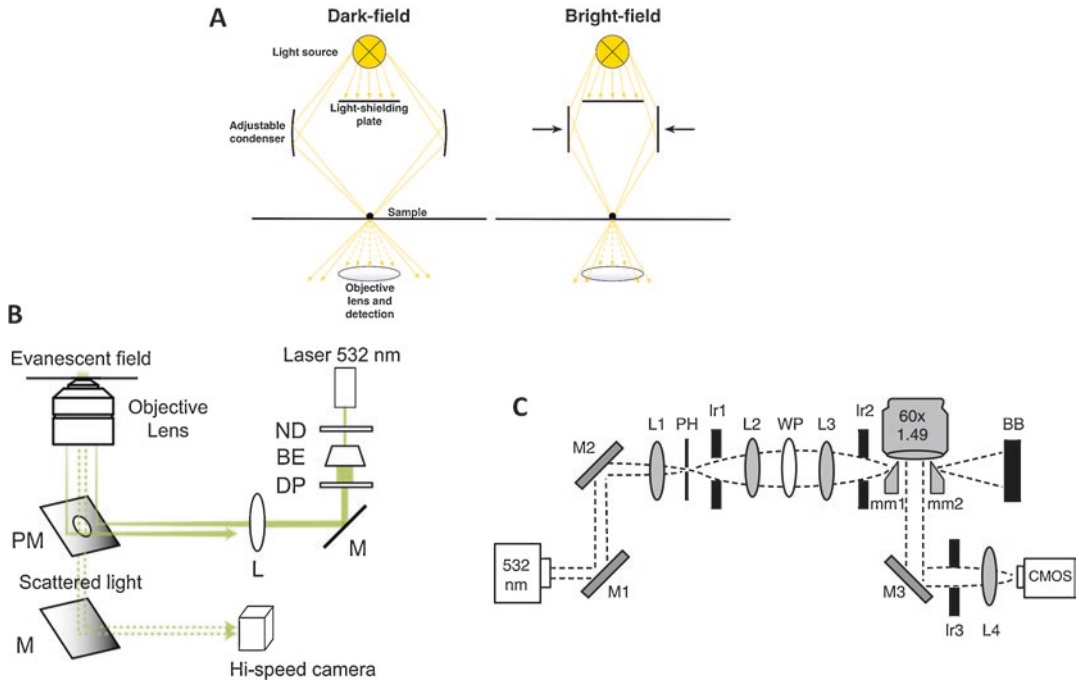

Fig. 6.9 Dark-field microscopy setups. (**a**) Schematic of commercial darkfield microscopes that are able to gradually switch between dark-field and bright-field by shifting the adjustable condenser. (**b**) TIRDF by Ueno et al. 2010 with perforated mirror (PM). ND = neutral-density filter, BE = beam expander, DP = diaphragm, M = mirror, L = lens. (**c**) Micro-mirror (mm) TIRDF by Mickolajczyk and Hancock 2018. M = mirror, L = lens, PH = pinhole, Ir = iris, WP = half-wave-plate, BB = beam blocker. (Images used with permission. Copyright 2010 Elsevier BV and Copyright 2018 Nature Springer)

the signal obtained from objects in dark-field microscopy can be arbitrarily increased through higher incident light intensities. Lasers help in this endeavor as they provide much higher photon fluxes than traditional non-coherent light sources.

Compared to the signal generated by fluorescent probes, however, the scattered light from most nano-objects has very low intensities. According to Mie theory (Mie 1908; Wriedt 2012), the scattering amplitude, s, of a spherical particle (diameter < 1.6λ) scales (Baron and Willeke 2001) as:

$$s \sim \varepsilon_m \pi \frac{d^3}{2} \frac{\varepsilon_p - \varepsilon_m}{\varepsilon_p + 2\varepsilon_m} \tag{6.6}$$

where ε_p and ε_m are the dielectric constants of the particle and its surrounding medium, respectively, and d is the particle diameter. This means that the detected scattering signal of a particle decreases rapidly with its size. Following from the two Eqs. (6.5) and (6.6), a particle that reduces its diameter by half will only generate 1/64th of the signal.

Most organic matter intrinsically has a very similar dielectric constant to aqueous solutions, which additionally exacerbates the detection of single protein molecules using scattering as a contrast mechanism. Therefore, it is common to attach a marker to the molecule of interest that is made from a material with stronger polarizability.

Gold nanoparticles have become very popular as molecular probes due to their surface plasmon resonance effect. If gold particles are smaller than the wavelength of light, their electrons can be displaced within the gold lattice by the electric field such that a dipole is generated (Fig. 6.10a). The positively-charged ions in the lattice generate a restoring force making the electrons behave like a harmonic oscillator (localized surface plas-

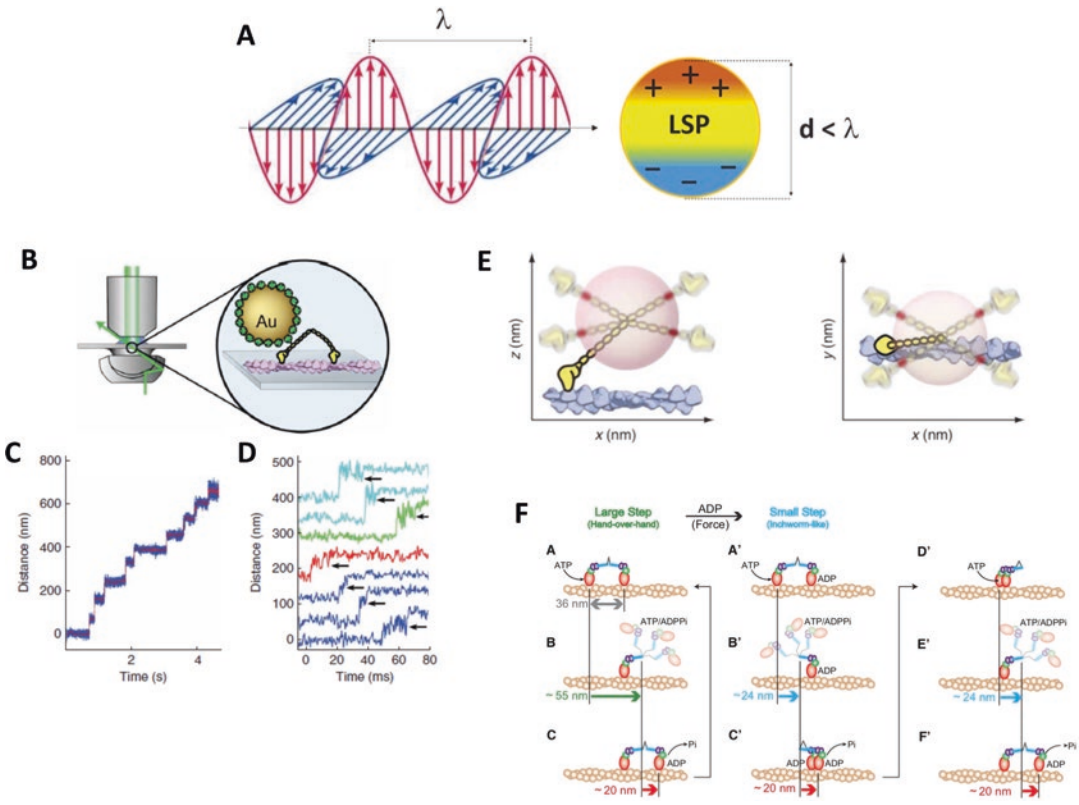

Fig. 6.10 Dark-field microscopy – Myosin-5a and myosin-6 experiments. (**a**) The electric field of light resonantly excites a localized surface plasmon (LSP) in a gold nanoparticle causing a strong scattering response. (Illustration from Amendola et al. 2017. Copyright 2017 IOP Publishing Ltd.) (**b**–**d**) Tracking the motion of the myosin-5 lever arm with millisecond time resolution. (**b**) A myosin-5 dimer is labeled with a gold nanoparticle on one of its lever arms through a biotin-streptavidin linkage. The myosin-5-gold conjugate walks along surface-immobilized actin. Light scattered by the gold particle is collected by the objective. (**c**) Sample data trace; 40 nm gold, 3 mM ATP. Frames were taken every 0.32 ms (blue); a 6.4 ms sliding average is shown in red. (**d**) Sample 49 nm substeps; 3125 Hz, 40 nm gold. The end of the substep is indicated by an arrow. Each color corresponds to an individual molecule. Note the increase in variance during the substep. (**e**) Dunn and Spudich swivel model how the observed increase in standard deviation for the gold location before each dwell can be explained. (Illustrations in **b**–**e** reproduced from Dunn and Spudich 2007. Copyright 2007 Nature Publishing Group). (**f**) Myosin-6 stepping model based on Qdot fluorescence and gold particle dark-field tracking experiment by the Yanagida laboratory. The myosin either steps in a hand-over-hand (left) or inchworm-like fashion (right). (Illustration from Nishikawa et al. 2010. Copyright 2010 Elsevier BV)

mon). The gold particles, therefore, act as "nano-antennas" with certain resonance frequencies, which depend on the surrounding medium and particle size, and they scatter light strongly at these frequencies (Amendola et al. 2017).

The strong scattering amplitude of gold particles has the additional advantage that their signal dominates over the background scattering in an aqueous sample and the species of interest can be equally well followed as a fluorescently-labelled molecule without any of the disadvantageous effects such as blinking and photobleaching that limit the achievable spatial and temporal resolution as discussed earlier.

The popularity of gold nanoparticles has led to the development of surface modification chemistry that enables the attachment of protein molecules to the gold particles. Thus, well-established biomolecular labelling methods for attaching the nanoparticles to the molecules of interest, such as through biotin-streptavidin or biotin/NeutrAvidin, are available.

Dunn and Spudich (Dunn and Spudich 2007) demonstrated the superiority of dark-field imag-

ing for the tracking of myosin motion in a study where they attached 40-nm gold particles to the lever arm of myosin-5 (Fig. 6.10b). Using this strategy, they could follow the conformational transitions of the motor during its processive runs at frame rates up to 3125 Hz, which enabled them to resolve the head motion in between the dwells on the actin filaments (Fig. 6.10c and d). They concluded that the detached head of myosin-5 freely pivots around the forward-leaning lever arm of the attached head before rebinding to the actin filament (Fig. 6.10e). They also noticed a lateral displacement of 4–8 nm of the detached head to the side of the actin filament axis (Fig. 6.10e), which they attributed to an off-axis contribution of the power stroke that could explain the observation that myosin-5 walks in a left-handed spiral (Ali et al. 2002). However, they argued that the size of the gold particle in this study could also have had a steric effect on the motor causing this displacement.

A similar study was conducted by Nishikawa and colleagues (Nishikawa et al. 2010) on myosin-6. They tracked 40 nm NeutrAvidin-coated gold particles attached to the biotinylated motor domain of an artificially dimerized myosin-6 construct with 2 nm localization precision at 37 μs time resolution. These experiments revealed a very distinct stepping behavior of the myosin in which the motor switches between a hand-over-hand and an inchworm-like mechanism. As the dark-field experiments allowed the observation of the detached state of the myosin head, the authors were able to determine the respective lever arm orientations during the two step types (Fig. 6.10f).

Even though dark-field microscopy appears to be a valuable alternative to fluorescence microscopy and provides a deeper mechanistic understanding of the studied molecular system, the technique has its limitations and pitfalls that should be mentioned here.

First of all, scattering-based measurements require a much more careful sample preparation as larger particles on the glass surface and in solution will have much greater impact on the background signatures than in fluorescence where the signal is specific to the labelled molecules.

As the above two examples show, it is possible to achieve nm spatial precision at μs temporal resolution with modern dark-field setups. In this time regime, however, the diffusional motion of the gold particle around its tether starts to be resolved and the ability to localize the myosin domain structure may be limited by this effect rather than by the localization precision for the gold itself. Therefore, it should be carefully considered what time scales are relevant for the chosen experiment and the average time window should be as long as possible when following a molecule's motion (Young and Kukura 2019).

A 40-nm gold particle is still a large marker compared to most fluorescent dyes (< 1 nm) or quantum dots (~10–20 nm), or even to the motor itself. This may reduce labelling efficiency or sterically interfere with the motor's conformational freedom. In order to minimally perturb the labelled protein, it would be desirable to use smaller nanoparticles or image entirely label-free. As discussed earlier, the strong scaling of the scattering signal with size makes it technically very challenging to achieve similar results with smaller nanoparticles.

Another scattering-based imaging technique called interferometric scattering microscopy circumvents the size scaling problem and enables high signal-to-noise, non-resonant imaging of smaller sized gold nanoparticles and even direct detection of native, unlabeled biomolecules.

6.5.2 Interferometric Scattering (iSCAT) Microscopy

If the goal is to image very small particles with a low scattering amplitude, pure scattering as a contrast mechanism quickly loses sensitivity. In this case, it is beneficial to include the background light that is rejected in dark-field microscopy. If we inspect Eq. (6.4) again, we find that the pure scattering term $|\mathbf{E}_s|^2$ becomes negligible for very small scatterers. However, the scattered light interferes with the background light and generates a signal defined by the third term $2|\mathbf{E}_r||\mathbf{E}_s|\cos\varphi$, which scales linearly with the par-

ticle volume and is therefore much more accessible than the pure scattering signal.

This principle has originally been realized by interference reflection microscopy (IRM) (Curtis 1964) or reflection interference contrast microscopy (RICM) (Ploem 1975). Its first biological application was to investigate the adhesion of cells to a glass substrate, because the technique proved useful to probe the optical path differences along membrane-water-glass interfaces (Curtis 1964; Limozin and Sengupta 2009). Later, less complex systems were chosen to enable more quantitative measurements (Rädler and Sackmann 1993; Rädler et al. 1995). These studies, however, did not achieve the signal-to-noise ratios required for nanoparticle detection. The advent of lasers finally enabled coherent illumination at much higher light intensities. A decade ago, the first laser-based setups, at this point called interferometric scattering (iSCAT) microscopes, were used to take non-fluorescent images of single quantum dots (Kukura et al. 2009a) and to track a virus particle diffusing on a lipid bilayer (Kukura et al. 2009b).

iSCAT's ability to track single particles with high spatial precision and temporal resolution makes it an ideal tool for myosin motility assays. A simple experimental setup is shown in Fig. 6.11a. A collimated laser beam from a diode laser is scanned over the sample by imaging a deflection from two orthogonal acousto-optic deflectors (AODs) producing a large, even illumination pattern. In order to separate the detection and illumination beam paths, a polarizing beam splitter (PBS) is used. It sends linearly polarized illumination through a quarter waveplate (QWP) and into the objective. The QWP circularly polarizes the light so upon reflection, the detected signal will be of an opposite handedness to the illumination and therefore converted by the QWP back into orthogonally linearly polarized light which is then reflected into the detection pathway by the PBS (Fig. 6.12). The image is captured by an sCMOS camera.

As with dark-field microscopy, myosin-5a was the first motor protein studied with iSCAT. The enhanced sensitivity of iSCAT makes it feasible to use smaller labels such as 20 nm gold nanoparticles, which minimize steric perturbation of the labeled motors. This allowed the Kukura group (Andrecka et al. 2015) to track 20 nm gold particles directly attached to the motor domain of myosin-5a without noticeably affecting its motion at 1 kHz frame rate and 4 nm localization precision (Fig. 6.11b–g). The reduced noise on the position of the detached head during myosin-5a's stepping cycle, compared to previous dark-field experiments, revealed that rather than undergoing a free 3D Brownian search, as suggested by the Dunn and Spudich study (Dunn and Spudich 2007), it occupies a spatially constrained state upon detachment of actin 40 nm off-axis and about 24 nm above the plane of actin. This result provided evidence that myosin-5 preserves the angle between its lever arms through structural constraints. It thereby reduces the degrees of freedom during its step which leads to a more directed and efficient 2-dimensionally constrained search for the next actin-binding site.

The study also observed a small rotation of the N-terminal part of the bound motor domain during its power stroke when the other head detaches. This is one of the only times a structural transition during the power stroke has been directly observed. The small rotation of the N-terminal domain during the power stroke, the constrained transient state of the unbound head together with results from a correlative fluorescence – iSCAT experiment (discussed later in this chapter) provide some interesting insight into how energy is transferred through myosin-5a's structure to lead to concerted, efficient, unidirectional motion.

A study by Ortega Arroyo and colleagues (Ortega Arroyo et al. 2014) has demonstrated that iSCAT-based imaging can even be used to visualize the motion of motor proteins without the need for external markers. Through careful removal of the static image background, the authors were able to extract the small scattering signal of native, single myosin-5a molecules (iSCAT contrast signal = 0.18%) and follow their movement along actin filaments in real time (Fig. 6.13a–e). The sensitivity was sufficiently high to reproduce the characteristic 37 nm step of the motor (Fig. 6.13e).

The sensitivity limit for label-free detection of proteins ultimately comes down to how much their signal can be raised above the measurement noise level. Assuming one can achieve purely

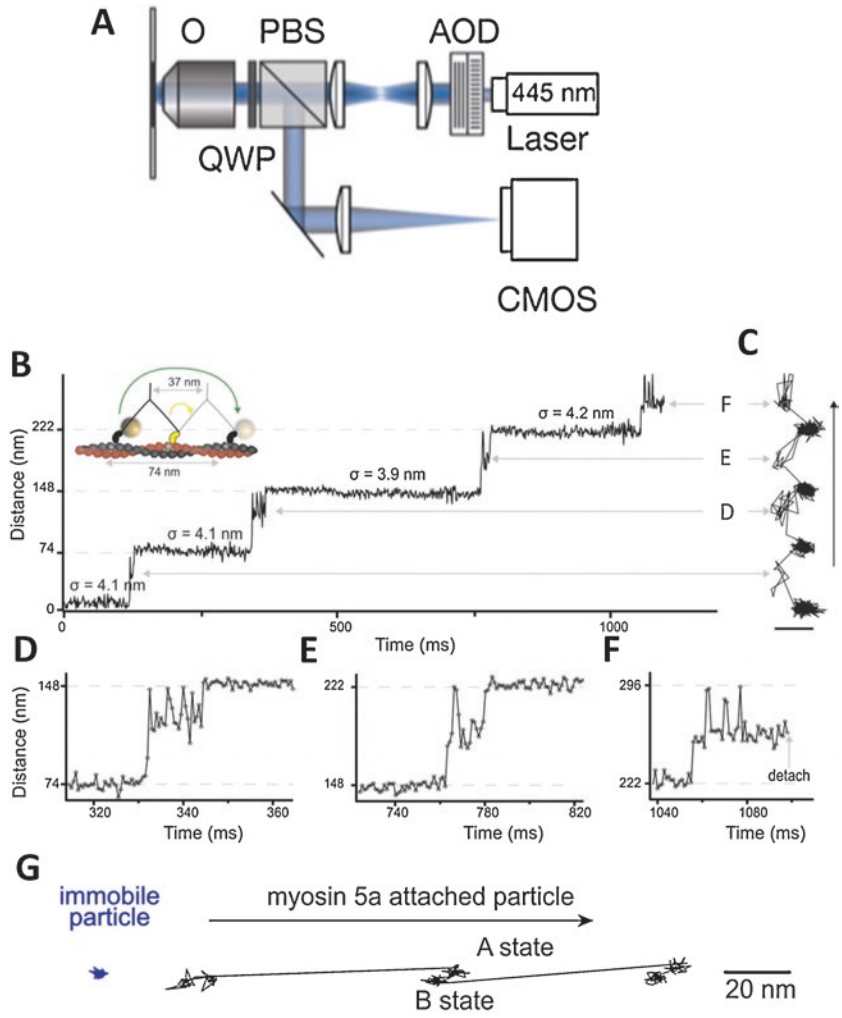

Fig. 6.11 iSCAT – Myosin-5a tracking. (**a**) Illustration of a simple iSCAT microscope. AOD = acousto-optical deflector, PBS = polarizing beam splitter, QWP = quarter-wave-plate, O = objective (Diagram reproduced from Ortega Arroyo et al. 2014.) (**b**–**g**) High-speed nanometric tracking of myosin-5 with iSCAT microscopy. (**b**) Distance traveled as a function of time for a single myosin-5 molecule biotinylated at the N-terminus and labeled with a 20 nm streptavidin-functionalized gold particle. The lateral localisation precision, σ, defined as the standard deviation of the positional fluctuations of the label while bound to actin is given above each of the actin-attached periods. Inset: schematic of gold-labeled myosin-5 stepping along actin. (**c**) Corresponding 2D-trajectory with the arrow indicating the direction of movement. (**d**–**f**) Close-up of the transient states indicated in B and C. ATP concentration: 10 μM. Scale bar: 50 nm. Imaging speed: 1000 frames/s. (**g**) Two states of the motor domain during myosin movement. Sample 2D trajectories for a 20 nm gold particle immobilised on the surface (left) and attached to the N-terminus of myosin-5a (right). The arrow indicates the direction of myosin movement. (Illustrations in B-G reproduced from Andrecka et al. 2015. Copyright 2015 eLife Science Publication)

shot-noise limited detection on a camera, which is possible using smart background removal strategies, the signal-to-noise ratio, (SNR), for a molecule is a function of its interferometric scattering contrast and the number of acquired photons, N.

$$\mathrm{SNR} = \frac{\text{iSCAT signal}}{\text{background fluctuations}} = \text{contrast}\sqrt{\mathrm{N}} \tag{6.7}$$

One strategy for improving the SNR is therefore to accumulate more photons from a sample,

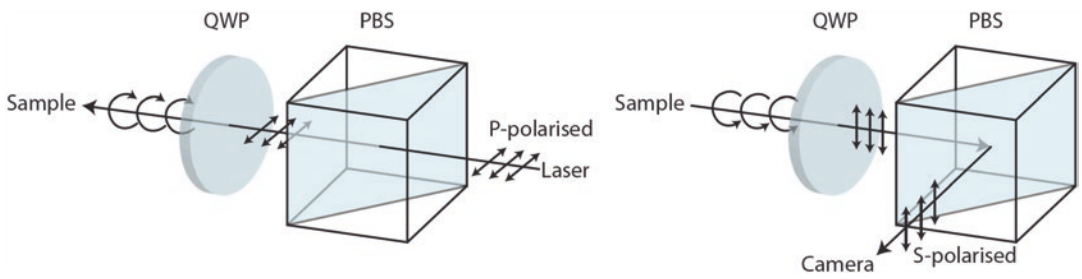

Fig. 6.12 Polarization-based separation of illuminating light from the detection path in iSCAT. (Top) S-polarized laser illumination is reflected by the polarizing beam splitter (PBS) and converted to circularly polarized light by the quarter waveplate (QWP). (Bottom) Reflected light from the sample returns with opposite handedness circularly polarised, is converted to p-polarized light by the QWP and transmitted by the PBS, effectively separating illumination and detection paths

i.e., measure at higher light intensities. Higher photon fluxes can be captured on cameras with high photon capacities and by distributing the signal over many frames and pixels. However, this approach has its limitations, especially because most cameras with high photon capacities have low quantum yields making them less efficient for collecting the incident light. It would require the detection of 10^8 photoelectrons to detect a signal that is 0.1% of the background illumination with an SNR of 10, but most cameras fail to provide a well capacity beyond 10^5 photoelectrons (Cole et al. 2017).

The alternative strategy would be to increase the contrast of a molecule while capturing the same number of photons. The iSCAT contrast of a particle is determined by the ratio between its signal, I_{det}, and the background intensity, I_{bkg}, which according to Eq. (6.4) is:

$$\begin{aligned}\text{contrast} &= \frac{I_{\text{det}}}{I_{bkg}} = \frac{|r|^2 + 2|r||s|\cos\varphi}{|r|^2} \\ &= 1 + \frac{2|s|\cos\varphi}{|r|},\end{aligned} \tag{6.8}$$

where $|r|^2$ is the reflectivity of the interface that provides the reference light. The contrast of a molecule can thus be increased by selectively reducing the amount of detected back-reflections from the sample. Technically, this is possible by making use of the fact that most of the signal from small scatterers is collected at high angles in the objective while the background light is evenly distributed over all angles of detection (typically the low numerical aperture of the objective) (Lee et al. 2011). By placing a partial reflective mirror into the back focal plane of the objective that attenuates the low numerical aperture contributions to the image, the contrast of scattering objects will be selectively enhanced (Cole et al. 2017; Liebel et al. 2017). This procedure does not by itself improve the SNR due to the concomitant loss of detected photons on the camera, but this can be compensated for by increasing the illumination intensity accordingly. The major advantage of this strategy is that by using the right combination of illumination intensity and reflectance of the mirror, cameras do not require extremely high well depths and the photons can be captured more efficiently. Figure 6.13f–h illustrates this approach schematically.

These recent technological advances in iSCAT microscopy have enabled high SNR, label-free imaging of proteins across most of the relevant size range. The ability to detect and accurately determine the interferometric contrast of individual proteins opens up another very exciting possibility. As most proteins have a very similar refractive index and specific volume, their contrast scales linearly with their mass (Piliarik and Sandoghdar 2014; Young et al. 2018). This can be used to generate mass spectra of protein samples in solution (Young et al. 2018). Since the contrast of each molecule can be determined very accurately, the size distributions obtained using this so-called mass photometry approach have better resolution than ensemble-based measurements

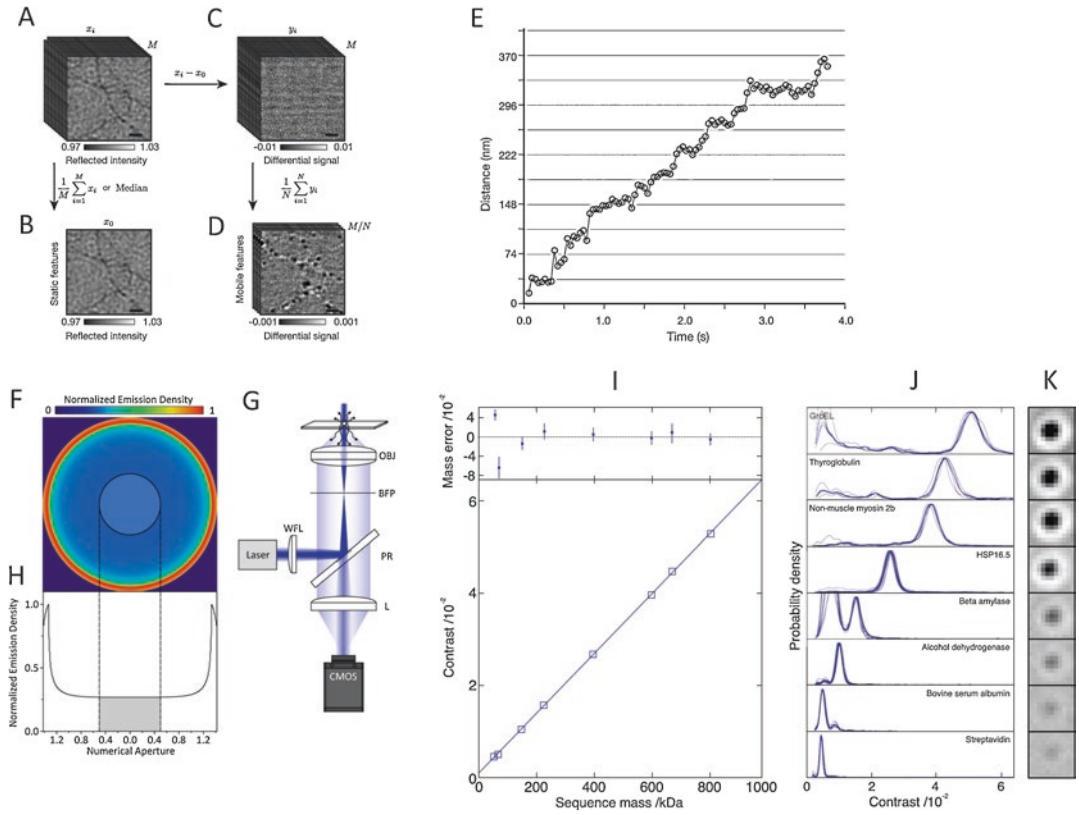

Fig. 6.13 Label-free iSCAT. (**a**–**d**) Interferometric scattering detection of myosin 5a HMM at the single-molecule level. (**a**) Sequence containing M iSCAT images, x_i, of actin filaments on a microscope cover glass in the presence of myosin-5a HMM. (**b**) An image containing purely stationary iSCAT features obtained by taking the median or averaging over the sequence of images in (**a**). (**c**) Sequence of M differential iSCAT images, y_i, obtained by subtracting the stationary iSCAT features from the image sequence in (**a**). (**d**) Time-averaged differential images generated by binning N = 170 consecutive frames together. Note the order-of-magnitude decrease in z-scale from (**c**) to (**d**). Scale bars: 1 μm (black line). (**e**) Distance traveled for a single myosin-5a molecule with contrast of 0.31% at 10 μM ATP concentration. Imaging speed: 1 kHz averaged to 25 Hz. (Illustrations in **a**–**e** reproduced from Ortega Arroyo et al. 2014. Copyright 2014 ACS Publication.) (**f**–**h**) Concept and experimental realization of numerical aperture filtered interferometric scattering microscopy (iSCAT). (**f**) Emission pattern of a nanoscopic scatterer at a glass−water interface emerging from the back aperture of a high-numerical-aperture (1.42) microscope objective for circularly polarized illumination. The semi-transparent circle indicates the region occupied by a partial reflector shown in the schematic experimental setup in **g** (**g**). Schematic of a numerical aperture-filtered iSCAT microscope. WFL = wide-field lens, BFP = back focal plane, OBJ = objective, PR = partial reflector, L = lens. (**h**) Emission density as a function of numerical aperture, with the gray area indicating the region attenuated by the partial reflector. (Illustrations in **f**–**h** reproduced from Cole et al. 2017. Copyright 2017 ACS Publication.) (**i**–**k**) Principle of iSCAT-based mass photometry. (**i**) Linear relationship between interferometric contrast and protein mass as determined using the standard proteins in **j** and **k**. (**j**) Size-distributions of the indicated standard proteins. (**k**) Exemplary point spread functions representing the protein peaks in **j**. (Diagrams in **i**–**k** modified from Young et al. 2018. Copyright 2018 Science)

like dynamic light scattering (DLS), size-exclusion chromatography (SEC) and analytical ultracentrifugation (AUC). Figure 6.13I-K illustrates this mass photometry approach, including the quality of data which can be achieved with this method.

Young et al. (2018) demonstrated that mass photometry can be used to investigate complex binding equilibria. In the future, the technique may therefore prove very useful to investigate the interaction of myosins with interaction partners, which has become a stronger effort in the field over the

past years. If mass sensitivity were combined with simultaneous single-particle tracking, iSCAT could become a very powerful tool for the investigation of reconstituted physiological myosin complexes and their motility entirely label-free.

6.6 Single-Molecule Force Measurements

6.6.1 Introduction

Considerable information about the functional principles of myosin motors has been extracted from single-molecule imaging methods. Only observing a motor, however, gives a superficial understanding of the way it works. The chemomechanical cycle of a myosin after all is designed to produce directed force that overcomes the random nature of processes in solution and facilitates coordinated motion in all living beings. A single myosin motor produces forces on the scale of pico-Newtons and displacements in the order of nanometers, but the sum of these small individual contributions can lead to macroscopic force production and displacements such as during muscle contraction.

If the goal is to understand the smallest components of a large-scale motor assembly on a molecular level and how force and motion are produced by its basic building blocks, it requires techniques that are sufficiently sensitive to detect pico-Newton forces and nanometer displacements that are able to interact with the motors under investigation.

The following sections will introduce a number of methods that have been employed in the myosin field to measure forces and displacements on a single-molecule level.

6.6.2 Glass Microneedles and ZnO Whisker Crystal Scanning Probe

The first force measurements of actomyosin interactions were performed using a thin glass microneedle (~300 nm in diameter) (Fig. 6.14a and b) made from a larger (1-mm diameter) glass rod. The needle-like extension was generated using a glass pipette puller (Kishino and Yanagida 1988) and had previously been used for microtubule sliding force measurements in flagella (Kamimura and Takahashi 1981). Biomolecules, such as actin or myosin, can be attached to the glass microneedle, and when an external force is applied, the microneedle will bend (Fig. 6.14a). Therefore, it can be used as a sensor for externally applied forces. The advantage of using a microneedle for force measurements is that it does not require any special optics, *i.e.,* microneedles can be combined with an existing microscope equipped with fluorescence optics. However, it does have its disadvantages, such as the fragility of the needles, and that every needle needs to be calibrated for use in force measurement. The time resolution achieved by using a microneedle can be up to ~1 ms by making it stiff and short (Ishijima et al. 1996), but drag forces imposed onto the needle make it inferior to other methods described later in this chapter.

Kishino and Yanagida (1988) measured the tensile strength of tetramethyl-rhodamine phalloidin-stabilized actin filaments (~110 pN), thin filaments (actin filaments decorated with tropomyosin and troponin) (~120 pN), as well as the force production by full-length rabbit skeletal muscle myosin-2 and the subfragment-1 (S1) actomyosin. They concluded that double-headed (*i.e.,* full-length) and single-headed proteins (*i.e.*, S1) generated ~0.2 pN force per head/motor domain. Note that these force values for individual motors were inferred from an ensemble experiment, whereby the force was measured with a microneedle attached to a single actin filament that was pulled by a "bed of myosins". The number of myosins attached to the surface in these studies was estimated based on the concentration used to coat the surface and used to calculate an "average" force from an individual molecule (Kishino and Yanagida 1988; Ishijima et al. 1991). A variation of the glass microneedle technique (Ishijima et al. 1994, 1996) was used later to probe single molecules of myosin-2 incorporated inside a "synthetic filament" composed of mostly tail domains of myosin-2.

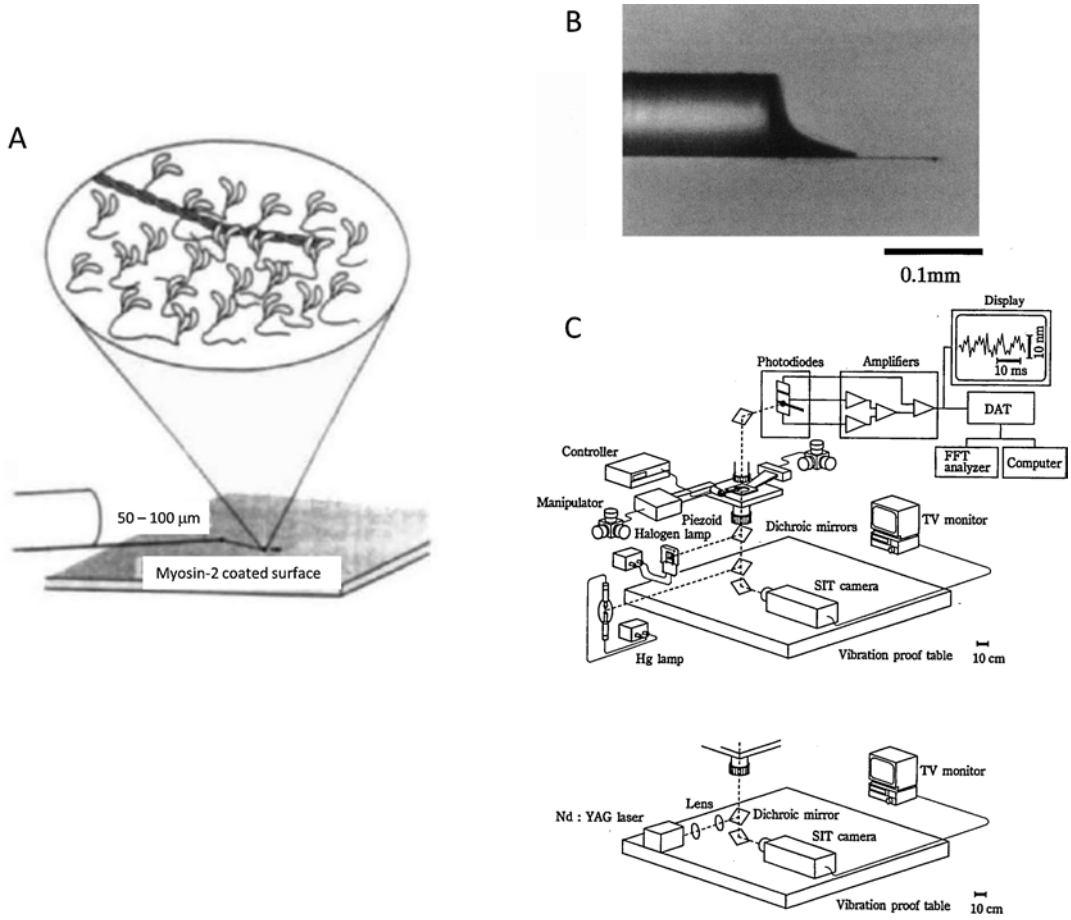

Fig. 6.14 Glass microneedle: actin and myosin-2. (**a**) Illustration of a glass microneedle assay. A single actin filament is attached to the end of the glass microneedle, ~50–100 μm long, and dragged along the myosin-2 coated surface. (**b**) Image of the glass microneedle using a dark-field microscope. (**c**) Schematic diagram of the high-resolution force and displacement measurement system using a microneedle transducer. (Diagrams reproduced from Ishijima et al. 1991, 1996. Copyright 1991 Nature Publishing Group and copyright 1996 Elsevier BV)

A zinc oxide (ZnO) crystal whisker scanning probe (Kitamura et al. 1999) was used as an improvement to the glass microneedle method, where a 5–7 μm long crystal with a 15 nm tip was used to attach a single S1 fragment of myosin-2 (Fig. 6.15). Rather than attaching an actin filament to a glass microneedle, actin was attached to a glass surface of an experimental chamber for this assay. This ZnO scanning probe instrument was also coupled to a TIRF microscope to allow a combination of force measurement using the ZnO scanning probe and fluorescence imaging to image the fluorescent myosin. The latter was used to ensure that the force measurements were taken with a single myosin on the tip. The study showed that a single S1 fragment of myosin-2 could take multiple, unidirectional, successive steps per actin encounter, varying from ~5 to ~30 nm, with an average step size of ~5.3 nm. These results indicated the possibility that the myosin head may be able to store energy from ATP hydrolysis and later release it productively in several packets of work. Measurements using an S1 fragment of myosin-5 was shown to behave similarly to make unidirectional, successive steps per actin encounter with an average step size of ~5.3 nm (Okada et al. 2007).

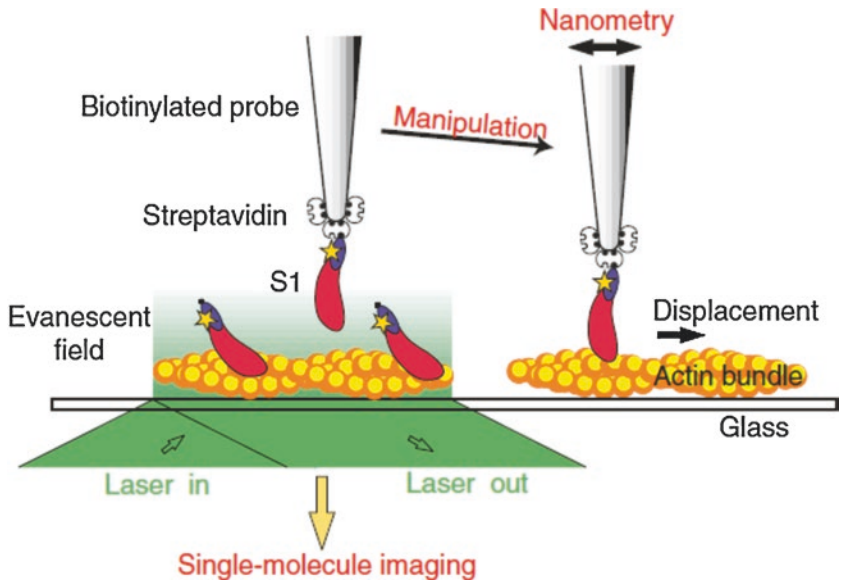

Fig. 6.15 ZnO whisker with myosin-2 subfragment-1 (S1) on tip. Scheme of the experiment is shown. A single myosin-2 S1 fragment, which was biotinlylated and labeled with a Cy3 dye, was attached to the tip of the ZnO whisker attached to a glass microneedle. Under TIRF illumination, the single myosin-2 S1 fragment can be manipulated onto the actin bundle while visualizing the Cy3 dye, and simultaneously, the ZnO whisker is used for nanometry to measure the force generation of a myosin-2 S1 in the presence of ATP. (Diagram reproduced from Kitamura et al. 1999. Copyright 1999 Nature Publishing Group.)

More details on the glass microneedle and ZnO crystal whisker scanning probe can be found in this methods article (Yanagida et al. 2011).

6.6.3 Atomic Force Microscopy

Atomic force microscopy (AFM) is another scanning probe microscopy method that has been used for decades for biophysical studies. AFM can be used for measuring forces and imaging molecules, as well as for manipulations.

In brief, AFM is dependent on the measurement of interactions between the sample surface and a probe, which is usually a thin tip. This tip is attached to a flexible cantilever that is bent as the tip interacts with the surface. There are different modes of how the tip can be used to probe. It can be brought into contact with the surface in order to sense a repelling force depending on the height of the surface. Alternatively, the tip can be held in close proximity and will experience attractive interactions. Another common method is to let the tip oscillate above the specimen. Detection of cantilever bending is detected via a laser focused onto the back of the cantilever and imaging the reflection of that laser beam on a photodiode. Changes in the position of the reflected laser beam on the photodiode are used to measure the interaction of the tip with the sample.

A basic scheme of an AFM is illustrated in Fig. 6.16 (Santos and Castanho 2004). The sample is attached to a piezo scanner, which can be moved at angstrom levels in order to generate an image of the surface topology at nm resolution. The AFM setup is usually coupled to an optical microscope for positioning the probe onto a field of interest.

As the bending of the cantilever is proportional to the interaction force between the tip and its substrate, the technique can also be used to measure forces. A traditional AFM detects forces between 10^{-7} and 10^{-12} N (Neuman and Nagy 2008).

The AFM is truly a useful method to measure forces of molecular interactions, however, due to the geometric constraints of how the AFM is set up with an optical microscope, it is hard to mea-

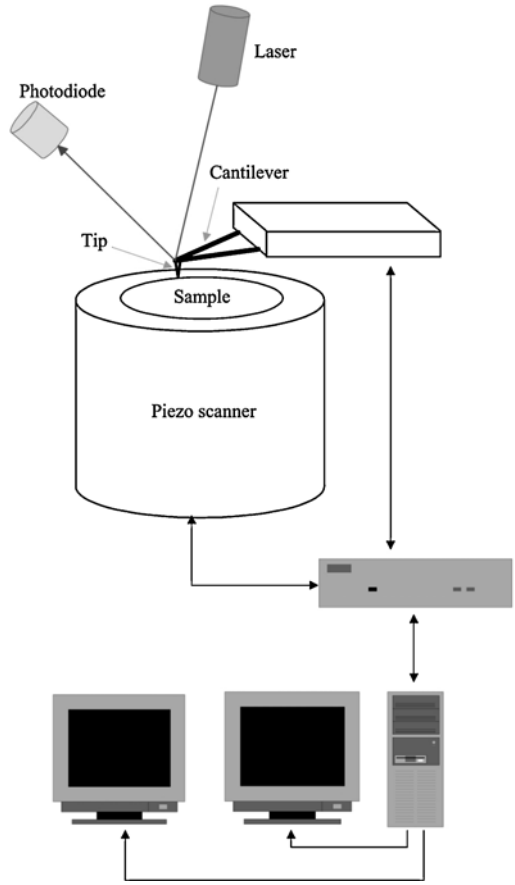

Fig. 6.16 Atomic force microscopy overview. A schematic representation of the components for an AFM setup. A cantilever with an "AFM tip" to probe the sample. Bending or twisting of the cantilever is detected by focusing a laser onto the cantilever face, opposite to the AFM tip. The reflection of the beam is focused onto a photodiode to detect forces in the range of 10^{-7} to 10^{-12} N. Scanning can be performed by moving the probe or the sample using a piezo-scanner, and usually with some variation of a feedback mechanism. Computer control is required for scanning as well as detection. (Diagram reproduced from Santos and Castanho 2004. Copyright 2004 Elsevier BV)

sure the mechanics or locomotion of a myosin. However, the method has been used to compare the elasticity of the tail domains of processive and non-processive myosin-5 at the single-molecule level (Nagy et al. 2009).

As mentioned above, an AFM can be used as a molecular imaging technique rather than for measuring forces between molecules. Technical advances in scanning speed and probing mechanism have led to the development of "high-speed" AFMs that achieve imaging speeds close to video rate. High-speed AFM has been used to directly observe single molecules of myosin-5 as they move on actin filaments, while actually resolving the structure of the protein (Kodera et al. 2010; Kodera and Ando 2018). The researchers in these studies were capable of visualizing myosin-5 translocation at ~7 frames-per-second (FPS) of a field-of-view (FOV) of ~100 × 100 nm^2, with a typical spatial resolution of ~2–3 nm in the lateral direction and ~0.15 nm in the vertical direction (Ando et al. 2013; Ando 2018). This incredible method, which is further discussed in Chap. 7 of this book, can be applied to studying many biomolecular systems, making it possible to directly watch motion and interactions at a molecular scale in action. It is a valuable tool that will surely be in the spotlight for many years in the single-molecule biophysics field (Ando 2014; Uchihashi and Scheuring 2018).

6.6.4 Optical Trap Measurements

The optical-trapping technique, invented by Arthur Ashkin in the mid 1970's, has been used widely in the biophysics field to study the detailed force-generating mechanism of molecular motors. Ashkin was one of three scientists who were awarded the 2018 Nobel prize in physics for creating groundbreaking tools from beams of light. Ashkin discovered that the momentum of light can be used as an extremely sensitive "trap" or "tweezers" to manipulate small particles.

Optical trapping started as "optical levitation" (Ashkin and Dziedzic 1975, 1985) whereby liquid droplets or particles could be trapped in air using the radiation pressure created by a laser beam. This is due to the fact that photons possess a momentum, p, that is dependent on their wavelength, and can be expressed as

$$|\vec{p}| = \frac{h}{\lambda}, \tag{6.9}$$

where h is the Planck constant. Thus, when a beam passes through a dielectric particle, such as a polystyrene bead with a refractive index (n) greater than the surrounding medium, it is

refracted away from the direction of the incident beam with a corresponding change in momentum of the laser. Due to conservation of momentum, there is an equal change in the momentum of the bead pointing into the opposite direction of the change in momentum of the laser beam. The momentum change leads to a force on the bead. The geometry of a laser focus is such that the net force on the particle directs it toward the center of the focus, where it will be trapped.

Another way to describe this effect is based on the particle's polarizability χ. The light's electric field induces an electric dipole moment $\boldsymbol{p}_{elec}$ in the particle, expressed as

$$\boldsymbol{p}_{elec} = \chi E \tag{6.10}$$

Thus, the force F on the particle in the electric field gradient of the light is

$$F = \boldsymbol{p}_{elec} \nabla E = \chi E \nabla E \tag{6.11}$$

This means that small particles will be drawn along the electric field intensity gradient, which pulls them into the focus of the beam. By focusing a beam of light to a diffraction limited spot, *i.e.,* with a high numerical aperture objective lens, one can create a large electric field gradient to effectively immobilize the particles.

Eventually, Ashkin found that this method could also be used to optically "trap" a dielectric particle in three dimensions in water (Ashkin et al. 1986). Following this finding, he published numerous papers putting forth the elementary steps to using optical traps as a quantitative tool to measure biological mechanics and kinetics. He first showed that the optical trapping technique could be applied to the trapping of viruses and bacteria (Ashkin and Dziedzic 1987) using a spatially filtered argon laser (wavelength = 5145 Å). He then changed the wavelength of the laser to an infra-red regime (1.06 μm neodymium-doped yttrium aluminum garnet, Nd:YAG) to minimize optical damage to live specimens and showed that the technique could be used to trap cells such as yeast and red blood cells (Ashkin et al. 1986) without altering their growth rate (for yeast), or flexibility and shape (for red blood cells). Furthermore, Ashkin showed that organelles inside the plant cytoplasm (Ashkin and Dziedzic 1989), as well as in amoebae (Ashkin et al. 1990), could be trapped to perform "laser surgery" to pick up structures inside cells or to measure escape forces of organelles/mitochondria that were suspected to move via microtubule-based motors, such as kinesin and dynein. An illustration of the early custom-made optical-trapping setup is shown as Fig. 6.17.

Apart from these cell-based applications, optical trapping allows for the manipulation of particles such as polystyrene or silica beads, which can be used as handles for proteins or other molecules. Unlike the microneedle transducer explained previously, the optical trap provides more freedom to manipulate these particles giving versatility to the assay geometry. Furthermore, the trapped particle with biomolecules attached exerts substantially lower drag force than the long microneedle due to the smaller particle size (*i.e.* 1 μm polystyrene beads).

While optical traps are useful as tools for the micromanipulation of small objects, they can be used as a very sensitive force sensor, too. At its simplest description, the optical trap functions as a very weak Hookean spring, which confines a particle within its three-dimensional potential well. The force F exerted on a displaced particle according to Hook's law is

$$F = -k \cdot x, \tag{6.12}$$

where k is the spring constant/optical trap stiffness and x is the displacement of the particle from the center of the optical trap. The force exerted on the trapped particle can be directly measured through its displacement if the trap stiffness is known. It is worth noting that this relationship only works for small distances from the trap center (~200–300 nm). Usually, either the bead image or the laser scattered by the trapped bead is monitored using a quadrant photo diode (Visscher et al. 1996) (Fig. 6.18).

6.6.4.1 Optical Trap Force Calibration

As the trap stiffness, k, depends on many different parameters like the objective's numerical aperture, the wavelength of the laser, the laser intensity and the refractive indices of particle and medium, its value is usually determined

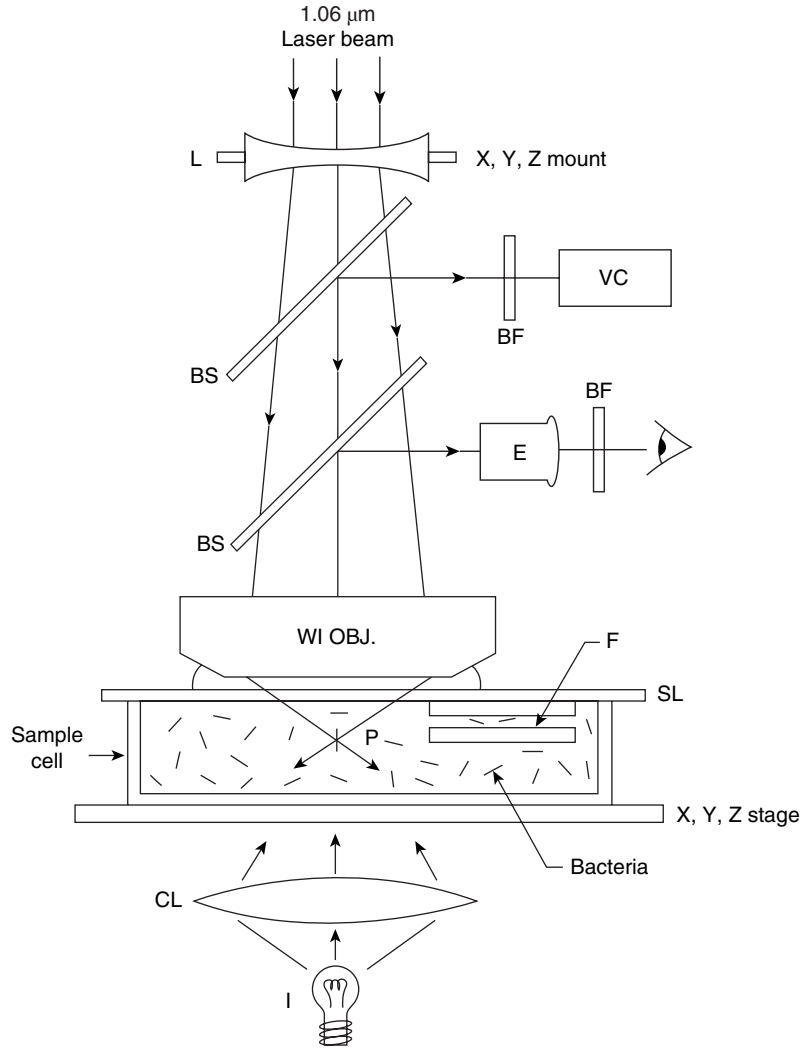

Fig. 6.17 Optical trapping overview. A schematic diagram of the combined high-resolution optical microscope and 1.06 mm infra-red laser trap for observing, manipulating and separating bacteria and other organisms. L = lens; BS = beam splitter; WI OBJ = 1.25 N.A. water immersion objective lens; CL = condenser lens. I = illuminator; E = eye piece; VC = video camera; P = trapping beam focused at point P. (Diagram reproduced from Ashkin et al. 1987. Copyright 1987 Nature Publishing Group)

empirically for a given particle/trap specimen. This procedure is referred to as a force calibration.

The simplest way of calculating the trap stiffness from a sample record of the statistical position fluctuations of a bead in a trap works through considering the equipartition theorem (Neuman and Block 2004), which predicts that the translational freedom of a particle in one dimension based on thermal fluctuations is $\frac{1}{2}k_bT$, where k_b is the Boltzmann constant and T is the absolute temperature. Without external perturbations, a bead in an optical trap will therefore fluctuate within the spring potential $\frac{1}{2}\, k < x^2 >$ up to values of $\frac{1}{2}k_bT$.

$$\frac{1}{2}kx^2 = \frac{1}{2}k_bT \tag{6.13}$$

$$\Leftrightarrow k = \frac{k_bT}{x^2} \tag{6.14}$$

The trap stiffness k can thus be directly calculated from the bead's mean squared displacement $<x^2>$. The disadvantage of this simple method is that the value of the trap stiffness depends on the accuracy of the displacement measurements, which are themselves determined through a calibration. Moreover, additional noise sources (e.g., localization noise, read noise from the position detector, drift) contribute to the value of $<x^2>$ and lead to an underestimation of the trap stiffness.

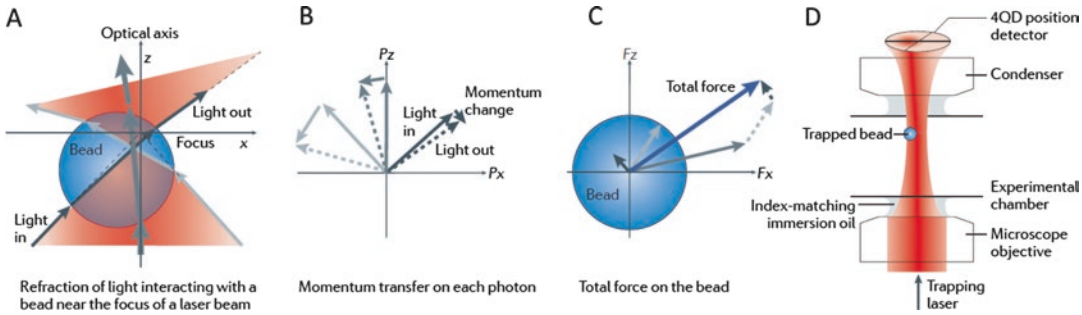

Fig. 6.18 Optical trapping ray diagrams and detection. (**a**) Ray optics sketch of light rays within a focused laser light illustrated in a red gradient. The laser is refracted through the bead that is trapped showing the three different gray light paths. The width of the gray arrows indicates the strength of the light intensity, which is highest through the optical axis. (**b**) Deflection of each photon results in a momentum change and a transfer of that momentum onto the bead. The arrows between the original photon momentum (solid lines) and the deflected photon momentum (dashed lines) illustrate the momentum transfer for each photon. (**c**) The total momentum transfer over time on all deflected photons from the three rays equals the force exerted onto the bead, shown in blue. (**d**) Position and force detection by back-focal-plane interferometry using a quadrant photodiode (4QD) placed after the microscope condenser so that it collects the deflected laser light and detects angular shifts in the transmitted trapping light. (Diagram reproduced from Veigel and Schmidt 2011. Copyright 2011 Nature Publishing Group)

Due to these shortcomings, it has become more common to determine the trap stiffness using the power spectrum of a bead's position fluctuations (Visscher et al. 1996; Gittes and Schmidt 1998; Neuman and Block 2004). This method does not require absolute position values to determine the trap stiffness. The Fourier transform or power-spectrum of the position fluctuations of an optically trapped bead usually shows a flat distribution at low frequencies (Fig. 6.19), which reflects the particle's restricted motion in the focused laser beam. The particle is not restricted by the trap at high frequencies resulting in an exponential decay of the power spectrum as usual for a freely diffusing particle (Fig. 6.19). This behavior is commonly described with a Lorentzian function.

$$S(f) = \frac{D}{\pi^2 \left(f_c^2 + f^2\right)}, \tag{6.15}$$

where $D = k_bT/\gamma$ is the diffusion coefficient for a spherical particle with the drag coefficient $\gamma = 6\pi\eta r$, the viscosity of the surrounding liquid, η, and the radius of the particle, r. The cut-off frequency (also called corner or roll-off frequency), f_c, is a characteristic frequency that describes where the spectrum drops off and depends on the trap stiffness, k, in the following way:

$$f_c = \frac{k}{2\pi\gamma} \tag{6.16}$$

The cut-off frequency, and thus the trap stiffness, can be determined by fitting the Lorentzian in Eq. (6.15) to an experimental power spectrum of the bead/trap combination that is meant to be calibrated.

The Lorentzian in Eq. (6.15) is an approximation that only holds when the sampling rate of the detection system is considerably higher than the cut-off frequency of the trapped bead, which ensures that the power spectrum can be determined reliably over a sufficient spectral frequency range. This may not be fulfilled when operating at high trap stiffness and the simple Lorentzian will systematically underestimate the cut-off frequency and thus the trap stiffness. Berg-Sørensen and Flyvbjerg (2004) have introduced an improved expression for the power spectrum that takes into account the frequency dependence of viscous drag on the particle and the effects of the sampling frequency and signal filtering during acquisition on the resulting experimental power spectrum. They provide a MATLAB routine that can be used to fit data

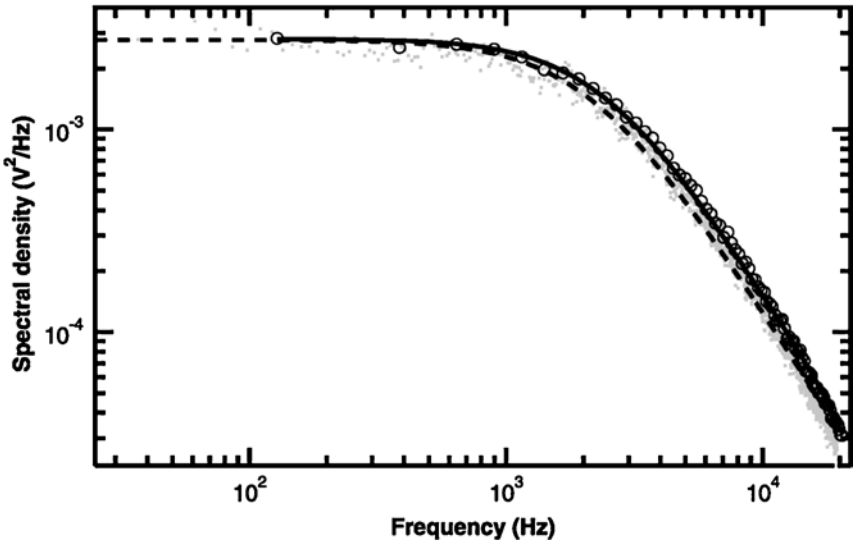

Fig. 6.19 Optical trap calibration. Power spectrum of a trapped bead. Power spectrum of a 0.5 μm polystyrene bead trapped 1.2 μm above the surface of the trapping chamber recorded with a position-sensitive detector (gray dots). The raw power spectrum was averaged over 256-Hz windows on the frequency axis (black circles) and fit (black line) to a Lorentzian function [Eq. (6.15)] corrected for the effects of the antialiasing filter, frequency-dependent hydrodynamic effects, and finite sampling frequency, as described by Berg-Sørensen and Flyvbjerg 2004. The cut-off frequency is 2.43 kHz, corresponding to a stiffness of 0.08 pN/nm. For comparison, the raw power spectrum was fit to an uncorrected Lorentzian function (dashed line), which returns a cut-off frequency of 2.17 kHz. Whereas the discrepancies are on the order 10% for a relatively weak trap, they generally become more important at higher cut-off frequencies. (Diagram reproduced from Neuman and Block 2004. Copyright 2004 AIP Publishing)

based on these more complicated considerations (Hansen et al. 2006). Figure 6.19 shows a comparison between a power spectrum fitted with a simple Lorentzian and the optimized routine. This method in general provides a more accurate estimate of the trap stiffness and has been implemented by more laboratories in the field in recent years.

6.6.4.2 Single-Bead Assay

In the late 1980's/early 1990's, the "bead motility" assay described earlier in this chapter was used to study the processive motion of single kinesin motors with an optical trap (Block et al. 1990; Svoboda et al. 1993). The concentration of the kinesin was titrated down to a regime where beads were very rarely bound with a single kinesin. This "single-bead" optical trapping assay (Fig. 6.20a) allowed the characterization of bead motion in an optical trap, such that the measurement was an output of the kinesin motion and force (Svoboda et al. 1993; Coppin et al. 1996). The kinesin attached to the bead was brought into close proximity of the microtubule and allowed to bind, then take multiple catalytic steps against the force of the optical trap until it either detached or stalled under force. These early experiments showed that kinesin is a processive motor that takes ~8 nm steps on microtubules. For myosins, it was not until the late 1990's/early 2000's that the single-bead optical trapping assay was used to characterize the mechanics and kinetics of myosin-5 (Rief et al. 2000), which was the first of the processive myosins to be discovered in 1993 (Cheney et al. 1993).

This single-bead assay to study the mechanics and kinetics of a processive molecular motor, such as kinesin, was useful since at least one of the motor domains of a processive motor is always attached to the track during its translocation process. However, this assay does not work well for non-processive motors, which briefly detach from the track. In the beginning, when optical trapping was used for myosins in the early

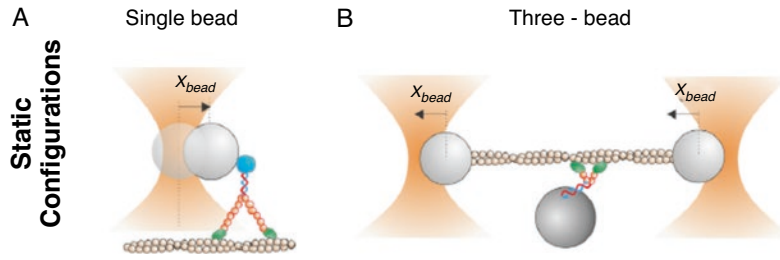

Fig. 6.20 Single-bead and three-bead assay schemes. (**a**) In a single-bead/trap configuration, the trap is static and the bead displacement, shown as X_{bead}, allows measurement of the molecular motor moving against the trap along a surface-bound track. If the optical trap force is higher than the stall force of the molecular motor, the protein will detach from the track and return back towards the center position of the trap. The single-bead configuration is useful for determining the mechanics of processive molecular motors. (**b**) In a three-bead assay, both optical traps are static with a track such as an actin filament in tension attached between the two beads. The molecular motor will exert motion against the track to displace the beads either closer to or further away, by X_{bead}, from the center of the trap due to the direction of force generation. The three-bead assay can be used to study the mechanics of both processive and non-processive molecular motors. (Diagram reproduced from Capitanio and Pavone 2013. Copyright 2013 Elsevier BV)

1990's, the only type of myosins discovered were non-processive ones. In order to study these non-processive myosins, a new geometry for the optical trapping assay needed to be developed.

6.6.4.3 Three-Bead Assay

Historically, for single-molecule actomyosin interactions, the "three-bead" assay (Finer et al. 1994; Molloy et al. 1995; Guilford et al. 1997) was developed to study the interactions, i.e., the power stroke and forces of non-processive myosins (Fig. 6.20b). Since non-processive myosins, such as skeletal muscle myosin-2 (Finer et al. 1994; Molloy et al. 1995; Guilford et al. 1997) or smooth muscle myosin-2 (Guilford et al. 1997; Lauzon et al. 1998; Tanaka et al. 2008), briefly detach from the actin filament every time they go through their enzymatic cycle, it would not be possible to use the single-bead assay (Block et al. 1990) as for processive motors, which can take multiple catalytic steps while at least one motor domain stays attached to the track. To overcome this limitation, the three-bead assay positioned the actin filament, suspended between two optically-trapped beads (a so-called actin filament "dumbbell"), above a third, usually larger, surface-bound bead sparsely coated with myosin used as a pedestal. In this geometry, when the myosin undergoes its enzymatic cycle and detaches briefly from the actin filament, the filament will remain in close proximity to the myosin such that it will quickly find the actin filament again. Data collection therefore becomes easy since many attachment/detachment processes of non-processive actomyosin interactions can be monitored within a short period of time. Parameters such as the size of the power stroke and the dwell/attachment times of unitary actomyosin interactions can be measured using this technique (Knight et al. 2001). Many studies have used the three-bead assay to measure the mechanics and kinetics of processive myosins as well (Mehta et al. 1999; Moore et al. 2001; Rock et al. 2001; Veigel et al. 2002, 2005; Purcell et al. 2005; Kad et al. 2008; Norstrom et al. 2010; Sellers and Veigel 2010; Watanabe et al. 2010; Takagi et al. 2014; Hundt et al. 2016; Gardini et al. 2018).

6.6.4.4 Load-Dependent Mechanics and Kinetics Using the Three-Bead Assay

Another beneficial attribute of the optical trap assay is that a load can be applied to the studied molecule in a controlled manner. Accordingly, measurements of how the kinetics of the motor's conformational transitions are altered by external force, or load, can be directly examined. Most optical trapping experiments are performed using a low stiffness (~0.01–0.03 pN/nm), so that the

displacement caused by an actomyosin interaction is measured under low load. This also greatly increases the signal-to-noise ratio of the detached *versus* the attached states of the actomyosin interactions, facilitating the separation of these states based on the variance or co-variance of the bead position signals.

In one variation of the experiment, the load on the myosin is altered using a "dynamic feedback" once an interaction between the myosin and actin filament is detected. This can be achieved by a fast change in laser power, which changes the trap stiffness, or by moving the actin filament with respect to the myosin.

Initial experiments using a dynamic feedback consisted of increasing and decreasing the laser power to mimic a situation whereby the myosin is undergoing a near-isometric condition (Finer et al. 1994; Molloy et al. 1995). An isometric condition in a single-molecule assay is one in which the relative positions, or strain, of single interacting myosin and actin molecules remain fixed by maintaining the position of one of the beads in a fixed position to reduce its motion. These methods revealed a distribution of isometric forces between 1–7 pN, with peaks centered around 2–3 pN.

Soon after these initial experiments, it was apparent that the end-compliance of the bead-actin attachments for the dumbbell assembly was highly non-linear (Dupuis et al. 1997; Mehta et al. 1997; Veigel et al. 1998) in the range of forces (~2 pN) previously applied. The problem with the three-bead assay is that if there is insufficient tension on the bead-actin connections in the dumbbell, the bead displacements and forces measured can be large underestimates of the actual displacements and forces produced by the molecular motor because some of the myosin motion is damped by the actin-bead-link compliance. Studies were performed to determine the connection stiffness of the bead-actin linkages by either looking at the limited correlated diffusion between motion of the two optically-trapped beads attached to the ends of a single actin filament (Mehta et al. 1997), or by moving one of the positions of the bead via the optical trap controlled by an electro-optical device (Dupuis et al. 1997; Veigel et al. 1998). From these experiments, it was determined that for the three-bead assay, it should be a routine to apply 4–6 pN of tension to the dumbbell to minimize measurement errors.

The method for determining the actin-bead link stiffness was also used to perform measurements on the stiffness of the actomyosin cross-bridge (Veigel et al. 1998). By driving one optical trap in a large-sinusoidal wave while keeping the other bead stationary (Fig. 6.21), it was possible to disentangle the stiffness of the myosin-actin link from that of the actin-bead connections. This way, crossbridge stiffnesses for single actin-myosin-2 interactions have been determined in the range of 1–2 pN/nm (Smith et al. 2001; Capitanio et al. 2006; Takagi et al. 2006; Lewalle et al. 2008). The method has also been used to determine the stiffness of other myosins such as myosin-5a (Veigel et al. 2002) and myosin-10 (Takagi et al. 2014).

Consequently, application of oscillations to the dumbbell complex in the three-bead assay has been a useful technique to also decrease the temporal limitation of detecting events (Veigel et al. 1998, 1999; Sellers and Veigel 2010; Nagy et al. 2013; Takagi et al. 2014; Hundt et al. 2016). The detection strategy of events, as described briefly earlier in this section, was based on the difference in thermal fluctuations between the detached and attached states. An initial attempt of this oscillatory method was a procedure using a small amplitude, 1 kHz sine wave onto one of the traps with an AOD to artificially increase the positional noise, or variance, which can then be detected at the other sensor bead. Due to the larger signal variance created, the relative decrease in the variance when the myosin attached to the actin filament was more pronounced and easier to detect. Using this method, binding events were therefore detected within ~1 ms. Furthermore, in combination with this oscillatory technique, a range of assisting and resisting loads was applied to a unitary actomyosin interaction within ~3 ms after detecting a binding event. This technique created a new avenue for both detection and load application using the three-bead assay in the studies of many myosins (Veigel et al. 1999). In recent

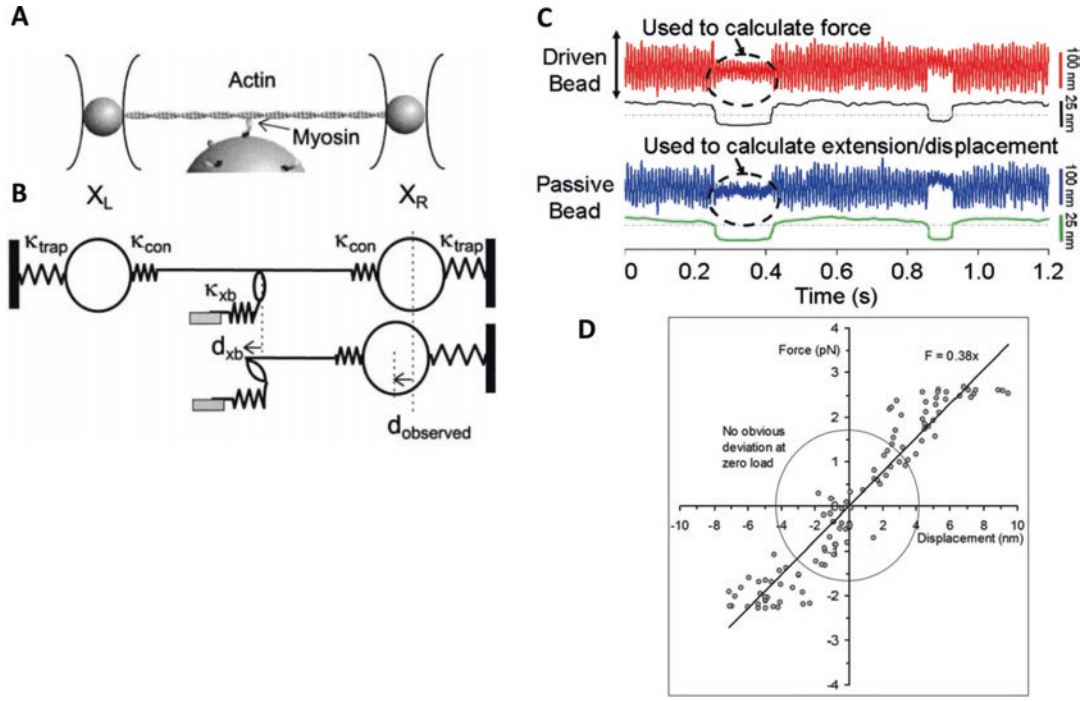

Fig. 6.21 Measuring the myosin stiffness using the three-bead assay. (**a**) The three-bead geometry scheme shown allows the manipulation of a taut actin filament strung between two optically-trapped beads to be positioned over the myosin, which is attached on a third larger bead on the surface of an experimental chamber. In this scheme, the position of the two beads, X_R and X_L, are monitored using a quadrant photodiode/detector. The three-bead geometry can be represented as a system of springs and masses, i.e., a mechanical system, as shown in (**b**). When a myosin attaches to the actin, the cross-bridge stiffness, κ_{xb}, is in series with the actin-to-bead connection stiffness, κ_{con}. These springs are also in parallel with the optical trap stiffness, κ_{trap}. The actual cross-bridge power stroke, d_{xb}, depending on the stiffness of these different springs, can be taken up by their compliance, and thus, the bead displacement observed (d_{obs}) could be an underestimate of the actual power stroke. A mechanical system allows interpretation of how the system reacts to different external loads, displacements and stiffnesses and can be a useful method to understand the mechanics of the three-bead assay. (**c**) The stiffness of a myosin-10 was measured using the output of the two quadrant photodiodes monitoring the two different optical traps. A large amplitude triangular wave (100 nm; 10 Hz) was applied to drive one of the optically-trapped beads back and forth, while simultaneously measuring the bead position at both ends of the actin filament. The difference in position between the bead held in the driven trap and the trap centroid was used to calculate the applied force, while the position of the bead on the other end of the actin filament allowed distortion of the acto-myosin-10 complex. Following a mathematical correction for the actin-bead connection compliance, force-extension diagrams were plotted. Force extension data in (**d**) show a stiffness of ~0.38 pN/nm for a single acto-myosin-10 complex. (Diagram reproduced from Veigel et al. 1998 and Takagi et al. 2014. Copyright 1998 Elsevier BV and copyright 2014 National Academy of Sciences, USA)

years, this method has been used to show that non-muscle myosin-2A requires a resisting load to be an efficient processive motor (Hundt et al. 2016), showing predominantly 5 nm forward steps and stall forces of ~4 pN.

As a variation of the three-bead assay with oscillations, a recently developed method called "**H**armonic **F**orce **S**pectroscopy" (HFS) (Sung et al. 2015) automatically and randomly applies sinusoidally varying loads to a single actomyosin interaction by moving the dumbbell complex with respect to the stage when attached to the myosin (Fig. 6.22). Published methods of harmonic force spectroscopy have applied sinusoids with an amplitude of 30–50 nm and frequencies between 100 and 200 Hz using a piezo-electric stage, while the actin dumbbell undergoes cycles of myosin binding and unbinding. Force-

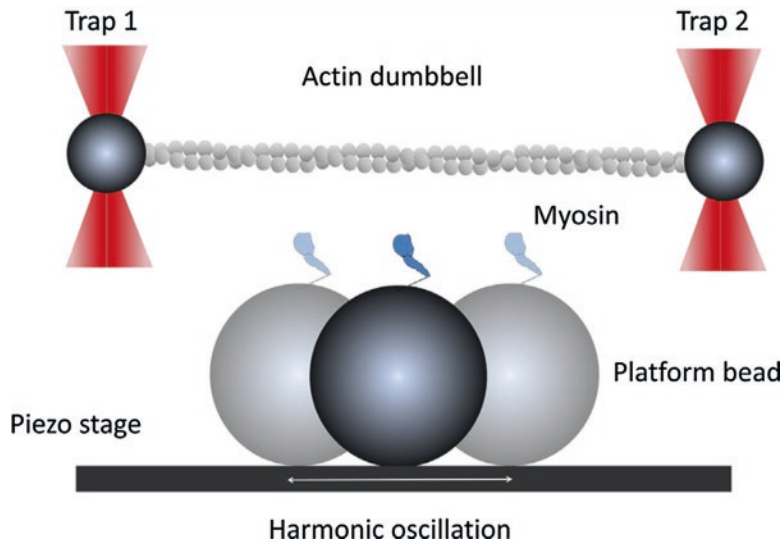

Fig. 6.22 Harmonic force spectroscopy (HFS). Using a standard, static, three-bead assay in concert with a simple harmonic oscillation introduced by the piezo-stage, HFS can be used to measure the load-dependent kinetics of molecular motor interactions without intricate feedback loops. (Diagram reproduced from Sung et al. 2017. Copyright 2017 Elsevier BV)

dependent kinetics of many β-cardiac myosin-2 mutation constructs have been studied in the past few years using this method (Liu et al. 2018). This technique appears to be a very useful variation to the three-bead assay, whereby this method also can be incorporated by moving the dumbbell complex using an electro-optical device, rather than the stage.

Innovative methods to incorporate a feedback system into the three-bead assay in order to decrease the end-compliance and to apply forces in different directions relative to the power stroke of the myosin have been developed over the years. In the previously described methods for measuring isometric forces, the actin filament moved significantly, and due to the limited tension applied to the dumbbell, the isometric forces measured were most likely an underestimate. To decrease the end-compliance, as well as to measure the isometric force, a feedback system that includes the whole dumbbell component in the feedback was developed (Takagi et al. 2006). In this feedback mode, an approach was taken to reduce and adjust the extent of actin motion at the moment of myosin binding. This method incorporated a procedure where one of the beads in the dumbbell was fixed in force by using an AOD while changing the position of the other bead. In this manner, the effective stiffness of the trap is increased, enabling testing of the effect of the stiffness on the developed force (Fig. 6.23b). The results showed that the force developed by unitary skeletal muscle actomyosin-2 interactions is considerably increased when the dynamic stiffness of the actin presented to the myosin molecules is increased. The authors showed that using this feedback mode, termed "isometric force clamp", the rate of load application can be altered, as fast as in the range of milliseconds or slower. Using a high gain feedback with a reaction time to apply dynamic load within ~1 ms, myosin-2 was shown to produce a range of forces between 2.5 pN and 17 pN with an average of ~6 pN, which was significantly higher than the earlier estimates in the 1–4 pN range (Finer et al. 1994; Molloy et al. 1995; Guilford et al. 1997). This single-molecule measurement of skeletal muscle myosin-2 force seems compatible with high-resolution muscle fiber measurements, which reported an estimate of ~6 pN per actomyosin crossbridge (Piazzesi et al. 2007).

Application of this method has also revealed novel features of myosin-1. In the presence of small loads, ~2 pN, the detachment of this myosin from actin filaments decreases by >75-fold, demonstrating that myosin-1 can transition from a low (<0.2) to a high (>0.9) duty ratio motor, supporting the motor's role as a molecular force sensor (Laakso et al. 2008). Furthermore, load-dependent kinetics differences within different

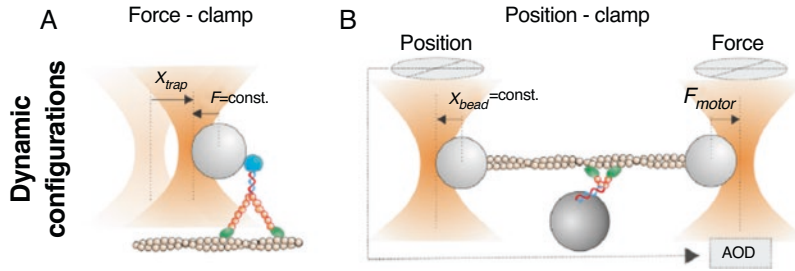

Fig. 6.23 Optical trapping feedback schemes. (**a**) Using a single-bead trapping geometry, a force clamp can be performed. In this case, a feedback loop is used to move the optical trap and keep the force on the trapped bead constant. The trap displacement, X_{trap}, measures the molecular motor motion under a force clamp. (**b**) A position clamp, also known as the isometric clamp, is performed by using the left bead as a "sensor" bead to detect the movement of the dumbbell and moving the right bead using an AOD to oppose the detected motion of the sensor bead, keeping it at its pre-determined position. The right bead therefore measures the actual force, F_{motor}, output by the molecular motor under isometric condition. (Diagram reproduced from Capitanio and Pavone 2013. Copyright 2013 Elsevier BV)

myosin-1 isoforms have been studied (Greenberg et al. 2012) as well as the role of the N-terminal domain in this load-dependence behavior of myosin-1s (Greenberg et al. 2015).

To measure force-dependent actomyosin kinetics and mechanics even faster than ~1 ms time resolution as achieved by the previously mentioned methods, ultrafast force-clamp spectroscopy has been used to apply constant loads with only a delay of ~10 μs (Capitanio et al. 2012; Capitanio and Pavone 2013). This system utilizes two separate AOD-driven feedbacks, one for each optical trap, to force-clamp the two beads at two different forces. Thus, within this feedback, a net constant force of +ΔF is applied to the dumbbell assembly, where the clamped force for one of the beads is −F, and the other F + ΔF. Different from previous methods, the dumbbell therefore moves against viscous drag at a constant velocity when the actin filament is not attached to the myosin, and by altering the direction of the net force, the dumbbell complex can move in a triangular wave, of ~+/−200 nm. Since the ultrafast force clamp is supposed to maintain the force between the dumbbell complex in the absence and presence of an attachment, the constant force of +ΔF is transferred to the myosin when it attaches to the actin, with a concomitant "stop" of the dumbbell movement (Fig. 6.24). Using this method, the Capitanio group showed that under resistive loads, ~5–10 nm power strokes usually followed binding after a short dwell time (0.2–1 ms). However, particularly short events (< 1 ms) did not exhibit any substantial power stroke. Furthermore, using a detailed analysis on the effect of applied load, a premature (< 5 ms) dissociation pathway was shown to be more populated as the force was increased, resulting in a working stroke that decreased with amount of load.

6.7 Simultaneous Methods

Some of the single-molecule methods described in this chapter have been combined to measure multiple parameters of myosin output, simultaneously. A couple of these attempts, which used a combination of different single-molecule techniques, are discussed as examples.

6.7.1 Optical Trapping and Fluorescence

The strengths of displacement and force measurements using optical trapping has been coupled to a single-molecule fluorescence detection scheme to visualize the nucleotide occupancy relative to motion of a single myosin (Ishijima

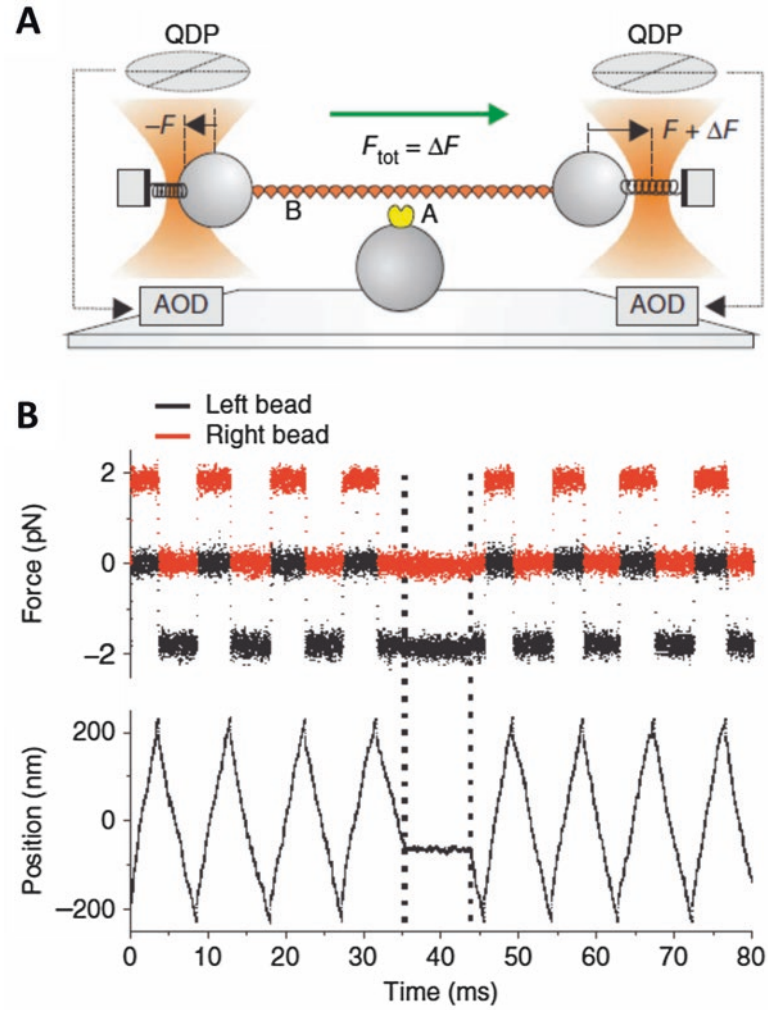

Fig. 6.24 Ultrafast force-clamp spectroscopy overview. (**a**) Schematic of the ultrafast force clamp spectroscopy relies on using two separate feedback systems to apply -F on the left optical trap and $F + \Delta F$ on the right optical trap such that molecule B, i.e., an actin filament, is under a total force of ΔF. Feedback operates on monitoring the force using a quadrant detector photodiodes (QDP), while moving the optical traps with an acousto-optic deflector (AOD). (**b**) Illustration of ΔF on the left (black) and right (red) beads. Within the ultrafast force-clamp feedback, the force is switched back and forth between $+\Delta F$ and $-\Delta F$ so that the bead-actin-bead complex oscillates within a confined distance of ±200 nm. When molecule A binds to B, the constant force is transferred to B, stopping the dumbbell motion as illustrated between the dotted black lines. (Diagram reproduced from Capitanio et al. 2012. Copyright 2012 Nature Publishing Group)

et al. 1998). This *tour de force* article coupled an optical trapping microscope capable of performing a modified three-bead assay together with a TIRF microscope (Fig. 6.25). In order to visualize a uniform TIRF image, glass surfaces were chemically etched to microfabricate "flat" pedestals that were ~ 7 μm wide and 1 μm deep. This study measured the force and displacement of a unitary, single-headed skeletal muscle myosin-2, while simultaneously observing a fluorescent nucleotide (Cy3-ATP) colocalized near the point of the acto-myosin interaction. Cy5 dyes were also used to visualize the actin filament within the three-bead assay, as well as the artificial thick filament made with a 1:1000 ratio of single-headed skeletal muscle myosin-2:skeletal muscle

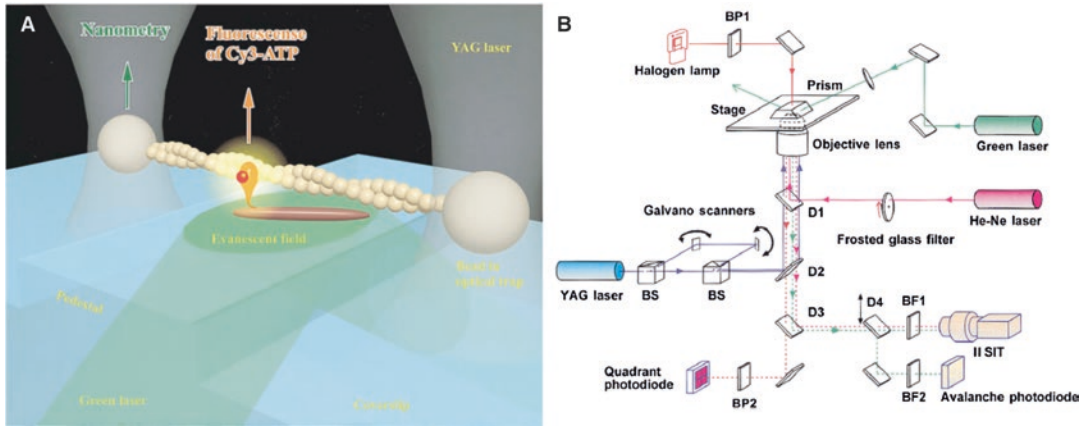

Fig. 6.25 Simultaneous optical trap/TIRF microscopy scheme. (**a**) Illustration of the assay at the specimen plane. Using a three-bead assay geometry an actin filament was brought into contact with a synthetic single-headed myosin-rod co-filament (myosin: rod ratio = 1:1000) attached to a pedestal microfabricated on the surface of the coverslip. TIRF microscopy was used to visualize Cy3-ATP as it associates and dissociates while the myosin undergoes its enzymatic cycle. (**b**) Optics layout of the optical trap/TIRF microscope. D = dichroic lenses; BS = beam splitter; BF = barrier filter; BP = band pass filters; II SIT = image intensified silicon intensifier target camera. More details can be found in the original article. (Diagram reproduced from Ishijima et al. 1998. Copyright 1998 Nature Publishing Group)

myosin-2 rods. This strategy of labeling both the actin filament and the synthetic co-filament of myosin-2 and rods, made controlling the angle of contact between the two individual filaments possible (~30°). This was done because previous studies had suggested that forces and displacements were strongly dependent on the angle between an actin filament and the myosin (Ishijima et al. 1994; Tanaka et al. 1998).

Interestingly, these measurements showed that force generation can happen several hundred milliseconds after the release of ADP from the myosin head, as if the myosin has a prolonged hysteresis or memory effect. This was an unusual finding which does not seem to fit any of the conventional kinetic mechanisms for myosin. Since nobody else has performed these simultaneous optical trapping and fluorescence measurements for myosins, it would be interesting to see if others obtain similar results in the future, and whether similar effects are observed with other classes of myosins.

6.7.2 Single-Molecule Fluorescence and iSCAT

A fluorescence channel has also been coupled into an iSCAT experiment in order to visualize two domains of myosin motors simultaneously. This, in practice, is a relatively simple modification in which a dichroic mirror is added into the illumination pathway. A blue laser is focused through a 500 mm lens into the back focal plane of the objective steered by two adjustable mirrors. The beam position can be displaced laterally by mounting one of the mirrors onto a translation stage in order to switch between epi-illumination and TIRF. Another dichroic mirror will separate the red-shifted emission from the illumination channel, and the image is passed through a filter and is focused onto an EMCCD. By using a red wavelength for the iSCAT channel, a fluorescence detection window in the green region can be used, ideal for molecules labelled with GFP. Using standard experimental techniques,

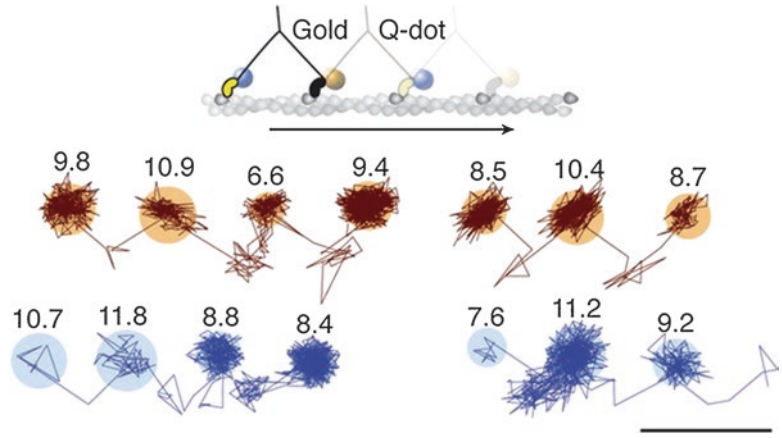

Fig. 6.26 Simultaneous iSCAT/TIRF microscopy of myosin-5a. One head was labeled with a 20 nm streptavidin-functionalized gold particle (red) and the other with a fluorescent quantum dot (blue). Reported values correspond to the standard deviation, σ, in the position of the bound state (nm) and the shaded regions encompass an area of 3σ. The traces are colored according to the label colors in the inset. ATP concentration: 10 μM. Scale bar: 100 nm. Imaging speed: 500 frames/s. (Diagram reproduced from Andrecka et al. 2015. Copyright 2015 eLife Science Publication)

the two channels can be temporally synchronized and spatially registered in order to achieve two truly correlated images.

This technique has been used effectively by the Kukura laboratory (Andrecka et al. 2015) to further understand the structural motion of myosin-5a (Fig. 6.26). Similar to the dual Qdot labeling strategy (Warshaw et al. 2005) employed previously for SHREC, they labelled both motor domains, one with a gold nanoparticle for scattering imaging and one with a Qdot for fluorescence imaging. Andrecka et al. observed that the spatially constrained transient state of the motor domain (discussed in detail in Chap. 8 in this book) occurred on the same side of the actin. This was the first evidence for a spinning compass-like gait of myosin-5a. This gait model would suggest that the cargo of myosin-5a should also rotate with each stride, or that some swivel in the myosin's structure alleviates the torsional strain that would be generated. Such a rotation has been measured before by the orientation of quantum rods attached to the myosin-5a tail, although in this work the source of the rotational movement was thought to be thermal (Ohmachi et al. 2012). The compass-like spinning motion may be an indication of how myosin-5a's structure helps facilitate and control the motion of the unbound head in a 1-dimensional arc to achieve a high specificity in finding the desired binding site, aiding unidirectional motion.

Andrecka et al. also simultaneously tracked one myosin-5a motor domain with the stalk domain. The motor domain was labelled with a gold nanoparticle and a C-terminal GFP was conjugated with a GFP booster nanobody as reported in Ries et al. 2012. The results showed that both the translocation of labeled motor domain and the small rotation of the N-terminus on the bound motor domain (again, discussed in more detail in Chap. 8) occurs synchronously with the translocation of the stalk. This provides evidence that the small-scale N-terminus transition observed is representative of the pre- to post-power stroke transition, a process previously unobserved. These experiments show that simultaneous observation of scattering and fluorescence can be a useful method to track the different domains of a molecular motor, facilitating understanding of how motions of different domains are coupled to each other.

6.8 Commercially Available Microscopes/Parts from Companies

Implementing single-molecule techniques into a laboratory with no previous background on the subject is a difficult and demanding task. The field is often very technology-driven. It therefore helps to understand and follow the trends and information relevant to single-molecule techniques in order to be innovative. However, single-molecule techniques are just a set of tools that can be used to answer the right question, if set in the right context.

The fact that many microscopes and instruments are commercially available these days helps newcomers to implement single-molecule measurements into their research. In this section, we list a number of companies and information (available in 2019) about "where to start" if one were interested in learning more about commercially available systems. Only a subset of existing companies is listed in this section.

Commercial Microscope Companies: Rather than building a microscope from scratch, it is sometimes beneficial to use a platform that already has a variety of imaging modalities built-in. The more established and well-known microscope companies have a variety of different types of microscopes that can be used to custom-build an instrument specific to your single-molecule investigations and needs. Furthermore, many of these companies also have "turn-key" solutions for single-molecule studies – for example, TIRF microscopes capable of single-molecule detection that have both hardware and software already pieced together to work effectively. Additionally, discussions with the application scientists and engineers from these companies with a thorough background and understanding of different microscopy techniques is a great way to learn about what types of microscope platforms are available from each company and which may be suitable for the single-molecule experiments one would like to perform.

Leica: https://www.leica-microsystems.com/
Nikon: https://www.microscope.healthcare.nikon.com/Products
Olympus: https://www.olympus-lifescience.com/en/
Zeiss: https://www.zeiss.com/microscopy/us/solutions/life-sciences.html

Single Molecule Microscope Frames: If one chooses to build a microscope from scratch, there are companies such as Edmund Optics, (https://www.edmundoptics.com/), Newport (https://www.newport.com/), OptoSigma (https://america.optosigma.com/?redirect_to=optosigma_us) and Thorlabs (https://www.thorlabs.com/) that sell both optics and opto-mechanical parts. An alternative is to start with a versatile microscope frame as a scaffold that can be modified according to the user's needs. These are usually compatible with other off-the-shelf components offered from the companies, making it possible to assemble a microscope like a LEGO-set.

Applied Scientific Instrumentation (ASI) - RAPID AUTOMATED MODULAR MICROSCOPE SYSTEM (RAMM): http://www.asiimaging.com/products/complete-system-solutions/rapid-automated-modular-microscope-ramm-system/
Mad City Labs - RM21™: http://www.madcitylabs.com/singlemolecule.html
Sigma Koki - Core Unit for Microscopy: https://www.global-optosigma.com/en_jp/Catalogs/pno/?from=page&pnoname=CUMS-GUIDE&ccode=&dcode=

Single Molecule Fluorescence Imaging: Companies, such Oxford Nanoimaging, also have built-in turn-key solutions to many types of single-molecule fluorescence techniques. The system called Nanoimager can be configured to perform single-molecule fluorescence imaging and single-molecule fluorescence resonance energy transfer (smFRET) microscopy. In addition, the system has imaging modalities that can be used for super-resolution imaging of cells, such as PALM, direct STORM, and structured illumination microscopy (SIM). The hardware system from Oxford Nanoimaging is packaged with data acquisition software, as well as a suite of analysis software.

Oxford Nanoimaging (ONI): https://oni.bio/

Interferometric Scattering Microscopy: For scattering-based single-molecule techniques such as iSCAT microscopy, Refeyn Ltd. has a turn-key system (Refeyn One^{MP}) that is capable of interferometric scattering mass photometry measurements. For dark-field scattering experiments, many of the large microscope companies provide dark-field condensers which are commercially available for their microscopes.

Refeyn Ltd.: https://www.refeyn.com/

Optical Trapping: A number of companies exists that provide commercial units specific for optical trapping. Some are fully integrated units, some are components that can be used to bolt onto existing microscopes, and some are modular kits that can be built to your specific optical-trapping needs.

Elliott Scientific: https://www.elliotscientific.com/Optical-Tweezers
IMPETUX: https://www.impetux.com/
JPK/Bruker: https://www.jpk.com/products/force-sensing-optical-tweezers-and-optical-trapping
LOT-QuantumDesign GmbH: https://lot-qd.de/en/products/life-sciences/optical-tweezers/product/optical-tweezers/
Lumicks: https://lumicks.com/
Meadowlark Optics: https://www.meadowlark.com/optical-tweezers-cube-p-120?mid=12
Molecular Machines & Industries (MMI): http://www.molecular-machines.com/single_cell_sorting_products/mmi_cellmanipulator_-_optical_tweezers/technology_55
Thorlabs Inc.: https://www.thorlabs.com/newgrouppage9.cfm?objectgroup_id=12442 or https://www.thorlabs.com/newgrouppage9.cfm?objectgroup_id=3959 or https://www.thorlabs.com/newgrouppage9.cfm?objectgroup_ID=6966

AFM: Atomic force microscopes are also commercially available. Some come as stand-alone units, and some can be attached/combined to a light microscope for simultaneous imaging modes.

JPK/Bruker: https://www.jpk.com/products/atomic-force-microscopy
Nanosurf: https://www.nanosurf.com/en/
Oxford Instruments/Asylum Research: https://afm.oxinst.com/
Research Institute of Biomolecule Metrology Co., Ltd. (RIBM): https://www.ribm.co.jp/

6.9 Conclusion

In this chapter, we discuss some of the single-molecule techniques that have been used to study myosins over the last three decades. Single-molecule techniques are truly advantageous tools that make it possible to decipher the molecular mechanisms of enzymatic activity and directed force production by molecular motors that cannot be easily assessed with ensemble techniques.

Many questions about different types of myosins have been challenged and answered using single-molecule approaches with considerable agreement among many laboratories. However, at the moment there is also considerable disagreement in the field concerning many of the myosins. Perhaps further enhancement of both the temporal and spatial resolution, as well as new ways of studying external parameters, such as load, with these single-molecule techniques may help resolve some of these experimental differences. Other single-molecule techniques such as magnetic tweezers (Seol and Neuman 2018), which have been used to study other molecular motors, but which have not been used to study myosins, may pave new avenues of myosin research and advance our understanding about these well-studied, yet still mysterious, molecular motors.

Acknowledgements We thank Dr. James R. Sellers (NHLBI, NIH) for critical reading of the chapter, as well as for helpful discussions and ideas. Y.T. was supported by the intramural funds from the NHLBI, NIH (Grant HL 004229). N.H. was supported by a DFG (German Research Foundation) research fellowship (HU 2462/1-1) and later by a DFG return grant (HU2462/3-1). A.F. was supported by a ERC starting investigator grant (nanoscope, 337757).

References

Aksel T, Choe Y, Sutton S, Ruppel KM, Spudich JA (2015) Ensemble force changes that result from human cardiac myosin mutations and a small-molecule effector. Cell Rep 11(6):910–920

Ali MY, Uemura S, Adachi K, Itoh H, Kinosita K Jr, Ishiwata S (2002) Myosin V is a left-handed spiral motor on the right-handed actin helix. Nat Struct Biol 9(6):464–467

Ali MY, Krementsova EB, Kennedy GG, Mahaffy R, Pollard TD, Trybus KM, Warshaw DM (2007) Myosin Va maneuvers through actin intersections and diffuses along microtubules. Proc Natl Acad Sci U S A 104(11):4332–4336

Amendola V, Pilot R, Frasconi M, Maragò OM, Iatì MA (2017) Surface plasmon resonance in gold nanoparticles: a review. J Phys Condens Matter 29(20):203002

Ando T (2014) High-speed AFM imaging. Curr Opin Struct Biol 28:63–68

Ando T (2018) High-speed atomic force microscopy and its future prospects. Biophys Rev 210(2):285–292

Ando T, Uchihashi T, Kodera N (2013) High-speed AFM and applications to biomolecular systems. Annu Rev Biophys 42:393–414

Andrecka J, Ortega Arroyo J, Takagi Y, de Wit G, Fineberg A, MacKinnon L, Young G, Sellers JR, Kukura P (2015) Structural dynamics of myosin 5 during processive motion revealed by interferometric scattering microscopy. elife 4. https://doi.org/10.7554/eLife.05413.

Ashkin A, Dziedzic JM (1975) Optical levitation of liquid drops by radiation pressure. Science 187(4181):1073–1075

Ashkin A, Dziedzic JM (1985) Observation of radiation-pressure trapping of particles by alternating light beams. Phys Rev Lett 54(12):1245–1248

Ashkin A, Dziedzic JM (1987) Optical trapping and manipulation of viruses and bacteria. Science 235(4795):1517–1520

Ashkin A, Dziedzic JM (1989) Internal cell manipulation using infrared laser traps. Proc Natl Acad Sci U S A 86(20):7914–7918

Ashkin A, Dziedzic JM, Bjorkholm JE, Steven C (1986) Observation of a single-beam gradient force optical trap for dielectric particles. Opt Lett 11:288–290

Ashkin A, Dziedzic JM, Yamane T (1987) Optical trapping and manipulation of single cells using infrared laser beams. Nature 330(6150):769–771

Ashkin A, Schütze K, Dziedzic JM, Euteneuer U, Schliwa M (1990) Force generation of organelle transport measured in vivo by an infrared laser trap. Nature 348(6299):346–348

Axelrod D (2001) Selective imaging of surface fluorescence with very high aperture microscope objectives. J Biomed Opt 6(1):6–13

Axelrod D (2008) Total internal reflection fluorescence microscopy. Methods Cell Biol 89:169–221

Balci H, Ha T, Sweeney HL, Selvin PR (2005) Interhead distance measurements in myosin VI via SHRImP support a simplified hand-over-hand model. Biophys J 89(1):413–417

Baron PA, Willeke K (2001) Aerosol measurement : principles, techniques, and applications, 2nd edn. Wiley, New York/Chichester, p 463

Beausang JF, Sun Y, Quinlan ME, Forkey JN, Goldman YE (2012) Orientation and rotational motions of single molecules by polarized total internal reflection fluorescence microscopy (polTIRFM). Cold Spring Harb Protoc:pii: pdb.top069344. https://doi.org/10.1101/pdb.top069344

Beausang JF, Shroder DY, Nelson PC, Goldman YE (2013) Tilting and wobble of myosin V by high-speed single-molecule polarized fluorescence microscopy. Biophys J 104(6):1263–1273

Berg-Sørensen K, Flyvbjerg H (2004) Power spectrum analysis for optical tweezers. Rev Sci Instrum 75:594–612

Betzig E, Patterson GH, Sougrat R, Lindwasser OW, Olenych S, Bonifacino JS, Davidson MW, Lippincott-Schwartz J, Hess HF (2006) Imaging intracellular fluorescent proteins at nanometer resolution. Science 313(5793):1642–1645

Bing W, Knott A, Marston SB (2000) A simple method for measuring the relative force exerted by myosin on actin filaments in the in vitro motility assay: evidence that tropomyosin and troponin increase force in single thin filaments. Biochem J 350:693–699

Block SM, Goldstein LS, Schnapp BJ (1990) Bead movement by single kinesin molecules studied with optical tweezers. Nature 348(6299):348–352

Brizendine RK, Alcala DB, Carter MS, Haldeman BD, Facemyer KC, Baker JE, Cremo CR (2015) Velocities of unloaded muscle filaments are not limited by drag forces imposed by myosin cross-bridges. Proc Natl Acad Sci U S A 112(36):11235–11240

Brizendine RK, Sheehy GG, Alcala DB, Novenschi SI, Baker JE, Cremo CR (2017) A mixed-kinetic model describes unloaded velocities of smooth, skeletal, and cardiac muscle myosin filaments in vitro. Sci Adv 3(12):eaao2267

Capitanio M, Pavone FS (2013) Interrogating biology with force: single molecule high-resolution measurements with optical tweezers. Biophys J 105(6):1293–1303

Capitanio M, Canepari M, Cacciafesta P, Lombardi V, Cicchi R, Maffei M, Pavone FS, Bottinelli R (2006) Two independent mechanical events in the interaction cycle of skeletal muscle myosin with actin. Proc Natl Acad Sci U S A 103(1):87–92

Capitanio M, Canepari M, Maffei M, Beneventi D, Monico C, Vanzi F, Bottinelli R, Pavone FS (2012) Ultrafast force-clamp spectroscopy of single molecules reveals load dependence of myosin working stroke. Nat Methods 9(10):1013–1019

Chen L, Nakamura M, Schindler TD, Parker D, Bryant Z (2012) Engineering controllable bidirectional molecular motors based on myosin. Nat Nanotechnol 7(4):252–256

Cheney RE, O'Shea MK, Heuser JE, Coelho MV, Wolenski JS, Espreafico EM, Forscher P, Larson RE, Mooseker MS (1993) Brain myosin-V is a two-headed unconventional myosin with motor activity. Cell 75(1):13–23

Churchman LS, Okten Z, Rock RS, Dawson JF, Spudich JA (2005) Single molecule high-resolution colocalization of Cy3 and Cy5 attached to macromolecules measures intramolecular distances through time. Proc Natl Acad Sci U S A 102(5):1419–14123

Cole D, Young G, Weigel A, Sebesta A, Kukura P (2017) Label-free single-molecule imaging with numerical-aperture-shaped interferometric scattering microscopy. ACS Photonics 4(2):211–216

Coppin CM, Finer JT, Spudich JA, Vale RD (1996) Detection of sub-8-nm movements of kinesin by high-resolution optical-trap microscopy. Proc Natl Acad Sci U S A 93(5):1913–1917

Curtis ASG (1964) The mechanism of adhesion of cells to glass. J Cell Biol 20(2):199–215

Deniz AA, Mukhopadhyay S, Lemke EA (2007) Single-molecule biophysics: at the interface of biology, physics and chemistry. J R Soc Interface 5(18):15–45

Dunn AR, Spudich JA (2007) Dynamics of the unbound head during myosin V processive translocation. Nat Struct Mol Biol 14(3):246–248

Dupuis DE, Guilford WH, Wu J, Warshaw DM (1997) Actin filament mechanics in the laser trap. J Muscle Res Cell Motil 18(1):17–30

Finer JT, Simmons RM, Spudich JA (1994) Single myosin molecule mechanics: piconewton forces and nanometre steps. Nature 368(6467):113–119

Forkey JN, Quinlan ME, Goldman YE (2000) Protein structural dynamics by single-molecule fluorescence polarization. Prog Biophys Mol Biol 74(1–2):1–35

Forkey JN, Quinlan ME, Shaw MA, Corrie JE, Goldman YE (2003) Three-dimensional structural dynamics of myosin V by single-molecule fluorescence polarization. Nature 422(6930):399–404

Funatsu T, Harada Y, Tokunaga M, Saito K, Yanagida T (1995) Imaging of single fluorescent molecules and individual ATP turnovers by single myosin molecules in aqueous solution. Nature 374(6522):555–559

Furuta K, Furuta A (2018) Re-engineering of protein motors to understand mechanisms biasing random motion and generating collective dynamics. Curr Opin Biotechnol 51:39–46

Furuta A, Amino M, Yoshio M, Oiwa K, Kojima H, Furuta K (2017) Creating biomolecular motors based on dynein and actin-binding proteins. Nat Nanotechnol 12(3):233–237

Gage SH (1920) Modern dark-field microscopy and the history of its development. Trans Am Microsc Soc 39(2):95

Gardini L, Heissler SM, Arbore C, Yang Y, Sellers JR, Pavone FS, Capitanio M (2018) Dissecting myosin-5B mechanosensitivity and calcium regulation at the single molecule level. Nat Commun 9(1):2844

Gittes F, Schmidt CF (1998) Interference model for back-focal-plane displacement detection in optical tweezers. Opt Lett 23(1):7–9

Gordon MP, Ha T, Selvin PR (2004) Single-molecule high-resolution imaging with photobleaching. Proc Natl Acad Sci U S A 101(17):6462–6465

Greenberg MJ, Moore JR (2010) The molecular basis of frictional loads in the in vitro motility assay with applications to the study of the loaded mechanochemistry of molecular motors. Cytoskeleton (Hoboken) 67:273–285

Greenberg MJ, Lin T, Goldman YE, Shuman H, Ostap EM (2012) Myosin IC generates power over a range of loads via a new tension-sensing mechanism. Proc Natl Acad Sci U S A 109(37):E2433–E2440

Greenberg MJ, Lin T, Shuman H, Ostap EM (2015) Mechanochemical tuning of myosin-I by the N-terminal region. Proc Natl Acad Sci U S A 112(26):E3337–E3344

Guilford WH, Dupuis DE, Kennedy G, Wu J, Patlak JB, Warshaw DM (1997) Smooth muscle and skeletal muscle myosins produce similar unitary forces and displacements in the laser trap. Biophys J 72(3):1006–1021

Hansen PM, Tolic-Nørrelykke IM, Flyvbjerg H, Berg-Sørensen K (2006) Tweezercalib 2.1: faster version of MatLab package for precise calibration of optical tweezers. Comput Phys Commun 175:572–573

Hecht E (1998) Optics, vol 1. Addison Wesley Longman, Boston

Homsher E, Wang F, Sellers JR (1992) Factors affecting movement of F-actin filaments propelled by skeletal muscle heavy meromyosin. Am J Phys 262(3 Pt 1):C714–C723

Huang B, Wang W, Bates M, Zhuang X (2008) Three-dimensional super-resolution imaging by stochastic optical reconstruction microscopy. Science 319(5864):810–813

Hundt N, Steffen W, Pathan-Chhatbar S, Taft MH, Manstein DJ (2016) Load-dependent modulation of non-muscle myosin-2A function by tropomyosin 4.2. Sci Rep 6:20554

Hynes TR, Block SM, White BT, Spudich JA (1987) Movement of myosin fragments in vitro: domains involved in force production. Cell 48(6):953–963

Ishijima A, Doi T, Sakurada K, Yanagida T (1991) Sub-piconewton force fluctuations of actomyosin in vitro. Nature 352(6333):301–306

Ishijima A, Harada Y, Kojima H, Funatsu T, Higuchi H, Yanagida T (1994) Single-molecule analysis of the actomyosin motor using nano-manipulation. Biochem Biophys Res Commun 199(2):1057–1063

Ishijima A, Kojima H, Higuchi H, Harada Y, Funatsu T, Yanagida T (1996) Multiple- and single-molecule analysis of the actomyosin motor by nanometer-piconewton manipulation with a microneedle: unitary steps and forces. Biophys J 70(1):383–400

Ishijima A, Kojima H, Funatsu T, Tokunaga M, Higuchi H, Tanaka H, Yanagida T (1998) Simultaneous obser-

vation of individual ATPase and mechanical events by a single myosin molecule during interaction with actin. Cell 92(2):161–171

Kad NM, Trybus KM, Warshaw DM (2008) Load and pi control flux through the branched kinetic cycle of myosin V. J Biol Chem 283(25):17477–17484

Kamimura S, Takahashi K (1981) Direct measurement of the force of microtubule sliding in flagella. Nature 293(5833):566–568

Kishino A, Yanagida T (1988) Force measurements by micromanipulation of a single actin filament by glass needles. Nature 334(6177):74–76

Kitamura K, Tokunaga M, Iwane AH, Yanagida T (1999) A single myosin head moves along an actin filament with regular steps of 5.3 nanometres. Nature 397(6715):129–134

Knight AE, Veigel C, Chambers C, Molloy JE (2001) Analysis of single-molecule mechanical recordings: application to acto-myosin interactions. Prog Biophys Mol Biol 77(1):45–72

Kodera N, Ando T (2014) The path to visualization of walking myosin V by high-speed atomic force microscopy. Biophys Rev 6(3–4):237–260

Kodera N, Ando T (2018) Direct imaging of walking myosin V by high-speed atomic force microscopy. Methods Mol Biol 1805:103–122

Kodera N, Yamamoto D, Ishikawa R, Ando T (2010) Video imaging of walking myosin V by high-speed atomic force microscopy. Nature 468(7320):72–76

Kron SJ, Spudich JA (1986) Fluorescent actin filaments move on myosin fixed to glass surface. Proc Natl Acad Sci U S A 83:6272–6276

Kron SJ, Toyoshima YY, Uyeda TQ, Spudich JA (1991) Assays for actin sliding movement over myosin-coated surfaces. Methods Enzymol 196:399–416

Kukura P, Celebrano M, Renn A, Sandoghdar V (2009a) Imaging a single quantum dot when it is dark. Nano Lett 9(3):926–929

Kukura P, Ewers H, Müller C, Renn A, Helenius A, Sandoghdar V (2009b) High-speed nanoscopic tracking of the position and orientation of a single virus. Nat Methods 6(12):923–927

Laakso JM, Lewis JH, Shuman H, Ostap EM (2008) Myosin I can act as a molecular force sensor. Science 321(5885):133–136

Lauzon AM, Tyska MJ, Rovner AS, Freyzon Y, Warshaw DM, Trybus KM (1998) A 7-amino-acid insert in the heavy chain nucleotide binding loop alters the kinetics of smooth muscle myosin in the laser trap. J Muscle Res Cell Motil 19(8):825–837

Lee KG, Chen XW, Eghlidi H, Kukura P, Lettow R, Renn A, Sandoghdar V, Götzinger S (2011) A planar dielectric antenna for directional single-photon emission and near-unity collection efficiency. Nat Photonics 5:166–169

Lewalle A, Steffen W, Stevenson O, Ouyang Z, Sleep J (2008) Single-molecule measurement of the stiffness of the rigor myosin head. Biophys J 94(6):2160–2169

Liebel M, Hugall JT, van Hulst NF (2017) Ultrasensitive label-free Nanosensing and high-speed tracking of single proteins. Nano Lett 17(2):1277–1281

Limozin L, Sengupta K (2009) Quantitative reflection interference contrast microscopy (RICM) in soft matter and cell adhesion. ChemPhysChem 10(16):2752–2768

Liu C, Kawana M, Song D, Ruppel KM, Spudich JA (2018) Controlling load-dependent kinetics of β-cardiac myosin at the single-molecule level. Nat Struct Mol Biol 25(6):505–514

Mehta AD, Finer JT, Spudich JA (1997) Detection of single-molecule interactions using correlated thermal diffusion. Proc Natl Acad Sci U S A 94(15):7927–7931

Mehta AD, Rock RS, Rief M, Spudich JA, Mooseker MS, Cheney RE (1999) Myosin-V is a processive actin-based motor. Nature 400(6744):590–593

Melli L, Billington N, Sun SA, Bird JE, Nagy A, Friedman TB, Takagi Y, Sellers JR (2018) Bipolar filaments of human nonmuscle myosin 2-a and 2-B have distinct motile and mechanical properties. Elife 7:pii: e32871

Mickolajczyk KJ, Hancock WO (2018) High-resolution single-molecule kinesin assays at kHz frame rates. Methods Mol Biol 1805:123–138

Mie G (1908) Beiträge zur Optik trüber Medien, speziell kolloidaler Metallösungen. Ann Phys 330(3):377–445

Molloy JE, Burns JE, Kendrick-Jones J, Tregear RT, White DC (1995) Movement and force produced by a single myosin head. Nature 378(6553):209–212

Moore JR, Krementsova EB, Trybus KM, Warshaw DM (2001) Myosin V exhibits a high duty cycle and large unitary displacement. J Cell Biol 155(4):625–635

Nagy A, Piszczek G, Sellers JR (2009) Extensibility of the extended tail domain of processive and nonprocessive myosin V molecules. Biophys J 97(12):3123–3131

Nagy A, Takagi Y, Billington N, Sun SA, Hong DK, Homsher E, Wang A, Sellers JR (2013) Kinetic characterization of nonmuscle myosin IIb at the single molecule level. J Biol Chem 288(1):709–722

Neuman KC, Block SM (2004) Optical trapping. Rev Sci Instrum 75(9):2787–2809

Neuman KC, Nagy A (2008) Single-molecule force spectroscopy: optical tweezers, magnetic tweezers and atomic force microscopy. Nat Methods 5(6):491–505

Nishikawa S, Arimoto I, Ikezaki K, Sugawa M, Ueno H, Komori T, Iwane AH, Yanagida T (2010) Switch between large hand-over-hand and small inchworm-like steps in myosin VI. Cell 142(6):879–888

Norstrom MF, Smithback PA, Rock RS (2010) Unconventional processive mechanics of non-muscle myosin IIB. J Biol Chem 285(34):26326–26334

Ohmachi M, Komori Y, Iwane AH, Fujii F, Jin T, Yanagida T (2012) Fluorescence microscopy for simultaneous observation of 3D orientation and movement and its application to quantum rod-tagged myosin V. Proc Natl Acad Sci U S A 109(14):5294–5298

Okada T, Tanaka H, Iwane AH, Kitamura K, Ikebe M, Yanagida T (2007) The diffusive search mechanism of processive myosin class-V motor involves directional

steps along actin subunits. Biochem Biophys Res Commun 354(2):379–384

Ortega Arroyo J, Andrecka J, Spillane KM, Billington N, Takagi Y, Sellers JR, Kukura P (2014) Label-free, all-optical detection, imaging, and tracking of a single protein. Nano Lett 14(4):2065–2070

Piazzesi G, Reconditi M, Linari M, Lucii L, Bianco P, Brunello E, Decostre V, Stewart A, Gore DB, Irving TC, Irving M, Lombardi V (2007) Skeletal muscle performance determined by modulation of number of myosin motors rather than motor force or stroke size. Cell 131(4):784–795

Piliarik M, Sandoghdar V (2014) Direct optical sensing of single unlabelled proteins and super-resolution imaging of their binding sites. Nat Commun 5:4495

Ploem JS (1975) Reflection-contrast microscopy as a tool for investigation of the attachment of living cells to a glass surface. Blackwell, Oxford

Previs MJ, Beck Previs S, Gulick J, Robbins J, Warshaw DM (2012) Molecular mechanics of cardiac myosin-binding protein C in native thick filaments. Science 337(6099):1215–1218

Purcell TJ, Sweeney HL, Spudich JA (2005) A force-dependent state controls the coordination of processive myosin V. Proc Natl Acad Sci U S A 102(39):13873–13878

Qu X, Wu D, Mets L, Scherer NF (2004) Nanometer-localized multiple single-molecule fluorescence microscopy. Proc Natl Acad Sci U S A 101(31):11298–11303

Rädler J, Sackmann E (1993) Imaging optical thicknesses and separation distances of phospholipid vesicles at solid surfaces. J Phys II 3:727–748

Rädler JO, Feder TJ, Strey HH, Sackmann E (1995) Fluctuation analysis of tension-controlled undulation forces between giant vesicles and solid substrates. Phys Rev E Stat Phys Plasmas Fluids Relat Interdiscip Topics 51(5):4526–4536

Reck-Peterson SL, Yildiz A, Carter AP, Gennerich A, Zhang N, Vale RD (2006) Single-molecule analysis of dynein processivity and stepping behavior. Cell 126(2):335–348

Rief M, Rock RS, Mehta AD, Mooseker MS, Cheney RE, Spudich JA (2000) Myosin-V stepping kinetics: a molecular model for processivity. Proc Natl Acad Sci U S A 97(17):9482–9486

Ries J, Kaplan C, Platonova E, Eghlidi H, Ewers H (2012) A simple, versatile method for GFP-based super-resolution microscopy via nanobodies. Nat Methods 9(6):582–584

Rock RS, Rice SE, Wells AL, Purcell TJ, Spudich JA, Sweeney HL (2001) Myosin VI is a processive motor with a large step size. Proc Natl Acad Sci U S A 98(24):13655–13659

Rosenberg SA, Quinlan ME, Forkey JN, Goldman YE (2005) Rotational motions of macro-molecules by single-molecule fluorescence microscopy. Acc Chem Res 38(7):583–593

Ruhnow F, Zwicker D, Diez S (2011) Tracking single particles and elongated filaments with nanometer precision. Biophys J 100(11):2820–2828

Rust MJ, Bates M, Zhuang X (2006) Sub-diffraction-limit imaging by stochastic optical reconstruction microscopy (STORM). Nat Methods 3(10):793–795

Sakamoto T, Amitani I, Yokota E, Ando T (2000) Direct observation of processive movement by individual myosin V molecules. Biochem Biophys Res Commun 272(2):586–590

Sakamoto T, Wang F, Schmitz S, Xu Y, Xu Q, Molloy JE, Veigel C, Sellers JR (2003) Neck length and processivity of myosin V. J Biol Chem 278(31):29201–29207

Sakamoto T, Yildiz A, Selvin PR, Sellers JR (2005) Step-size is determined by neck length in myosin V. Biochemistry 44(49):16203–16210

Santos NC, Castanho MA (2004) An overview of the biophysical applications of atomic force microscopy. Biophys Chem 107(2):133–149

Sellers JR, Kachar B (1990) Polarity and velocity of sliding filaments: control of direction by actin and of speed by myosin. Science 249(4967):406–408

Sellers JR, Veigel C (2010) Direct observation of the myosin-Va power stroke and its reversal. Nat Struct Mol Biol 17(5):590–595

Sellers JR, Cuda G, Wang F, Homsher E (1993) Myosin-specific adaptations of the motility assay 39:23–49

Seol Y, Neuman KC (2018) Combined magnetic tweezers and micro-mirror Total internal reflection fluorescence microscope for single-molecule manipulation and visualization. Methods Mol Biol 1665:297–316

Sheetz MP, Spudich JA (1983) Movement of myosin-coated fluorescent beads on actin cables in vitro. Nature 303(5912):31–35

Sheetz MP, Block SM, Spudich JA (1986) Myosin movement in vitro: a quantitative assay using oriented actin cables from Nitella. Methods Enzymol 134:531–544

Shepherd GM, Corey DP, Block SM (1990) Actin cores of hair-cell stereocilia support myosin motility. Proc Natl Acad Sci U S A 87(21):8627–8631

Siedentopf H, Zsigmondy R (1903) Über Sichtbarmachung und Groessenbestimmung ultramikroskopischer Teilchen, mit besonderer Anwendung auf Goldrubinglaesern. Annalen der Physik 10:1–39

Smith DA, Steffen W, Simmons RM, Sleep J (2001) Hidden-Markov methods for the analysis of single-molecule actomyosin displacement data: the variance-hidden-Markov method. Biophys J 81(5):2795–2816

Snyder GE, Sakamoto T, Hammer JA 3rd, Sellers JR, Selvin PR (2004) Nanometer localization of single green fluorescent proteins: evidence that myosin V walks hand-over-hand via Telemark configuration. Biophys J 87(3):1776–1783

Sun Y, Schroeder HW 3rd., Beausang JF, Homma K, Ikebe M, Goldman YE (2007) Myosin VI walks "wiggly" on actin with large and variable tilting. Mol Cell 28(6):954–964

Sun Y, Sato O, Ruhnow F, Arsenault ME, Ikebe M, Goldman YE (2010) Single-molecule stepping and

structural dynamics of myosin X. Nat Struct Mol Biol 17(4):485–491
Sung J, Nag S, Mortensen KI, Vestergaard CL, Sutton S, Ruppel K, Flyvbjerg H, Spudich JA (2015) Harmonic force spectroscopy measures load-dependent kinetics of individual human β-cardiac myosin molecules. Nat Commun 6:7931
Sung J, Mortensen KI, Spudich JA, Flyvbjerg H (2017) How to measure load-dependent kinetics of individual motor molecules without a force-clamp. Methods Enzymol 582:1–29
Svoboda K, Schmidt CF, Schnapp BJ, Block SM (1993) Direct observation of kinesin stepping by optical trapping interferometry. Nature 365(6448):721–727
Takagi Y, Homsher EE, Goldman YE, Shuman H (2006) Force generation in single conventional actomyosin complexes under high dynamic load. Biophys J 90(4):1295–1307
Takagi Y, Farrow RE, Billington N, Nagy A, Batters C, Yang Y, Sellers JR, Molloy JE (2014) Myosin-10 produces its power-stroke in two phases and moves processively along a single actin filament under low load. Proc Natl Acad Sci U S A 111(18):E1833–E1842
Tanaka H, Ishijima A, Honda M, Saito K, Yanagida T (1998) Orientation dependence of displacements by a single one-headed myosin relative to the actin filament. Biophys J 75(4):1886–1894
Tanaka H, Homma K, White HD, Yanagida T, Ikebe M (2008) Smooth muscle myosin phosphorylated at single head shows sustained mechanical activity. J Biol Chem 283(23):15611–15618
Thompson RE, Larson DR, Webb WW (2002) Precise nanometer localization analysis for individual fluorescent probes. Biophys J 82(5):2775–2783
Toprak E, Enderlein J, Syed S, McKinney SA, Petschek RG, Ha T, Goldman YE, Selvin PR (2006) Defocused orientation and position imaging (DOPI) of myosin V. Proc Natl Acad Sci U S A 103(17):6495–6499
Uchihashi T, Scheuring S (2018) Applications of high-speed atomic force microscopy to real-time visualization of dynamic biomolecular processes. Biochim Biophys Acta Gen Subj 1862(2):229–240
Ueno H, Nishikawa S, Iino R, Tabata KV, Sakakihara S, Yanagida T, Noji H (2010) Simple dark-field microscopy with nanometer spatial precision and microsecond temporal resolution. Biophys J 98(9):2014–2023
Vale RD, Szent-Gyorgyi AG, Sheetz MP (1984) Movement of scallop myosin on Nitella actin filaments: regulation by calcium. Proc Natl Acad Sci U S A 81(21):6775–6778
Veigel C, Schmidt CF (2011) Moving into the cell: single-molecule studies of molecular motors in complex environments. Nat Rev Mol Cell Biol 12(3):163–176
Veigel C, Bartoo ML, White DC, Sparrow JC, Molloy JE (1998) The stiffness of rabbit skeletal actomyosin cross-bridges determined with an optical tweezers transducer. Biophys J 75(3):1424–1438
Veigel C, Coluccio LM, Jontes JD, Sparrow JC, Milligan RA, Molloy JE (1999) The motor protein myosin-I produces its working stroke in two steps. Nature 398(6727):530–533
Veigel C, Wang F, Bartoo ML, Sellers JR, Molloy JE (2002) The gated gait of the processive molecular motor, myosin V. Nat Cell Biol 4(1):59–65
Veigel C, Schmitz S, Wang F, Sellers JR (2005) Load-dependent kinetics of myosin-V can explain its high processivity. Nat Cell Biol 7(9):861–869
Visscher K, Gross SP, Block SM (1996) Construction of multiple-beam optical traps with nanometer-resolution position sensing. IEEE J Sel Top Quantum Electron 2(4):1066–1076
Warshaw DM, Desrosiers JM, Work SS, Trybus KM (1990) Smooth muscle myosin cross-bridge interactions modulate actin filament sliding velocity in vitro. J Cell Biol 111:453–463
Warshaw DM, Kennedy GG, Work SS, Krementsova EB, Beck S, Trybus KM (2005) Differential labeling of myosin V heads with quantum dots allows direct visualization of hand-over-hand processivity. Biophys J 88(5):L30–L32
Watanabe TM, Iwane AH, Tanaka H, Ikebe M, Yanagida T (2010) Mechanical characterization of one-headed myosin-V using optical tweezers. PLoS One 5(8):e12224
Wriedt T (2012) In: Hergert W, Wriedt T (eds) Mie theory: a review, vol 169. Springer, Berlin/Heidelberg, pp 53–71
Yanagida T, Ishii Y, Ishijima A (2011) Single-molecule measurements using microneedles. Methods Mol Biol:143–159
Yildiz A, Forkey JN, McKinney SA, Ha T, Goldman YE, Selvin PR (2003) Myosin V walks hand-over-hand: single fluorophore imaging with 1.5-nm localization. Science 300(5628):2061–2065
Yildiz A, Tomishige M, Vale RD, Selvin PR (2004a) Kinesin walks hand-over-hand. Science 303(5658):676–678
Yildiz A, Park H, Safer D, Yang Z, Chen LQ, Selvin PR, Sweeney HL (2004b) Myosin VI steps via a hand-over-hand mechanism with its lever arm undergoing fluctuations when attached to actin. J Biol Chem 279(36):37223–37226
Young G, Kukura P (2019) Interferometric scattering microscopy. Annu Rev Phys Chem 70:301–322. https://doi.org/10.1146/annurev-physchem-050317-021247
Young G, Hundt N, Cole D, Fineberg A, Andrecka J, Tyler A, Olerinyova A, Ansari A, Marklund EG, Collier MP, Chandler SA, Tkachenko O, Allen J, Crispin M, Billington N, Takagi Y, Sellers JR, Eichmann C, Selenko P, Frey L, Riek R, Galpin MR, Struwe WB, Benesch JLP, Kukura P (2018) Quantitative mass imaging of single biological macromolecules. Science 360(6387):423–427

7 High-Speed Atomic Force Microscopy to Study Myosin Motility

Noriyuki Kodera and Toshio Ando

Abstract

High-speed atomic force microscopy (HS-AFM) is a unique tool that enables imaging of protein molecules during their functional activity at sub-100 ms temporal and submolecular spatial resolution. HS-AFM is suited for the study of highly dynamic proteins, including myosin motors. HS-AFM images of myosin V walking on actin filaments provide irrefutable evidence for the swinging lever arm motion propelling the molecule forward. Moreover, molecular behaviors that have not been noticed before are also displayed on the AFM movies. This chapter describes the principle, underlying techniques and performance of HS-AFM, filmed images of myosin V, and mechanistic insights into myosin motility provided from the filmed images.

Keywords

High-speed atomic force microscopy · Myosin ATPase · Molecular motor · Chemomechanical coupling · Single-molecule measurement

N. Kodera · T. Ando (✉)
Nano Life Science Institute (WPI NanoLSI), Kanazawa University, Kanazawa, Japan
e-mail: nkodera@staff.kanazawa-u.ac.jp; tando@staff.kanazawa-u.ac.jp

7.1 Introduction

Among a variety of many different proteins, myosins have been a special target of research, inspiring scientists to invent new measurement techniques or apply newly born techniques created for non-biological research fields. Successful use of these techniques in myosin motility studies has encouraged other biological fields to use them. Such techniques are typically represented by single-molecule biophysical techniques based on fluorescence and optical tweezers. The invention or exploitation of these techniques was stimulated by the early studies of *in vitro* myosin motility assays originated from naturally occurring cytoplasmic streaming in giant algal cells (Higashi-Fujime 1980; Sheetz and Spudich 1983). Then, myosin motility has been profoundly studied using single-molecule florescence microscopy and optical trap nanometry. The successful use of single-molecule fluorescence microscopy in turn stimulated the inventions of super-resolution fluorescence microscopy (e.g., Huang et al. 2009). Among diverse myosin superfamily proteins, class V myosin (M5) has remarkably contributed to the understanding of myosin motility as single M5 molecules undergoing unidirectional processive translocation can be tracked successively under these single-molecule biophysical measurements (Mehta et al. 1999; Sakamoto et al. 2000). From the single-molecule studies on M5 intensively

L. M. Coluccio (ed.), *Myosins*, Advances in Experimental Medicine and Biology 1239,
https://doi.org/10.1007/978-3-030-38062-5_7

conducted in the 2000s, the following fundamental characteristics of M5 motility have been established: (i) In every ATP hydrolysis cycle, M5 moves forward by ~36 nm (Mehta et al. 1999; Rief et al. 2000; Purcell et al. 2002; Veigel et al. 2002; Uemura et al. 2004; Clemen et al. 2005; Sakamoto et al. 2008), (ii) this large stride is made possible by the long lever arms of M5 (Purcell et al. 2002; Sakamoto et al. 2003, 2005), (iii) the two heads alternately switch between the leading and trailing roles so that M5 walks hand-over-hand (Yildiz et al. 2003; Forkey et al. 2003; Warshaw et al. 2005), and (iv) this style of movement is made possible by the intramolecular strain-mediated retardation of ADP release from the leading head (Sakamoto et al. 2008; Rosenfeld and Sweeney 2004; Veigel et al. 2005; Oguchi et al. 2008; Purcell et al. 2005; Forgacs et al. 2008). However, note that these optical techniques always observe optical markers attached to protein molecules. As such, the protein molecules themselves are invisible in the recorded data, even with super resolution. Despite these successful studies, the central issue of myosin motility, namely how the chemical energy of ATP is converted to the mechanical work to be executed by myosins, was not much elucidated through these single-molecule studies. Our understanding of this central issue has remained poor, and not much surpassed the level reached through long-term studies on muscle contraction with ensemble averaging techniques.

Atomic force microscopy (AFM) was invented (Binnig et al. 1986) to visualize atoms on solid surfaces. However, soon after, it started to be used to observe biological samples. Some AFM imaging studies were performed also for myosin II (M2) (Hallett et al. 1995; Zhang et al. 1997; Sheng et al. 2003; Taniguchi et al. 2003; Rigotti et al. 2005; Iwasaki et al. 2005; Kellermayer et al. 2018). The images of M2 were taken under ambient, non-physiological buffer or chemically-fixed conditions. In this regard, AFM was used in place of electron microscopy. AFM can also be used for force measurements to estimate the strength of intra- and inter-molecular bonds at the single-molecule level, and the elasticity of biological molecules and surfaces. AFM force measurements were performed for myosins and myosin-related proteins (Nakajima et al. 1997; Rief et al. 1997; Oberhauser et al. 2001; Schwaiger et al. 2002; Root et al. 2006; Decker and Kellermayer 2008; Karsai et al. 2011; Kiss et al. 2011; Kaiser et al. 2012; Baumann et al. 2017).

In a similar way that the development of single-molecule fluorescence microscopy was stimulated by the early *in vitro* myosin motility studies, the development of HS-AFM was initiated in 1993 under a stimulating influence of single-molecule myosin motility studies. In 2001, the diffusional motion of M5 molecules on mica was recorded with HS-AFM at 12.5 frames/s (fps) (Ando et al. 2001), but the HS-AFM instrumentation was not very sophisticated at that time. Through continuous improvements of the system, HS-AFM was established in 2008 (Ando et al. 2008). Finally, M5 molecules walking on actin filaments were filmed with HS-AFM in 2010 (Kodera et al. 2010). Remarkably, all characteristic features of M5 motility revealed collectively through numerous single molecule optical measurements (i–iv mentioned above) were visually displayed on the filmed HS-AFM images. Moreover, dynamic phenomena unrecognized before also appeared in the images. Thus, HS-AFM imaging was demonstrated to be able to make important discoveries even for proteins that had been extensively studied with other approaches.

7.2 High-Speed Atomic Force Microscopy

7.2.1 Operation Principle of AFM Imaging

AFM uses a micro cantilever with a sharp stylus tip attached to its free end. The cantilever, as a mechanical force sensor, responds to the interaction between the tip and sample surface. For the acquisition of sample height information over a rectangular area, the local tip-interaction point on the surface is successively shifted over the area by raster scanning of the sample stage relative to the tip. Among several imaging modes, the

tapping mode (Zhong et al. 1993), also called the amplitude modulation mode, is most suitable for fragile biological samples. In this mode, the cantilever is excited to oscillate in the Z-direction at or near its first resonant frequency. The oscillating tip intermittently taps the sample surface, resulting in amplitude reduction depending on the tapping strength. This intermittent tapping can avoid tip dragging across the sample and hence minimize sample deformation or dislocation in the lateral direction. The cantilever deflection is generally detected with an optical beam deflection (OBD) detector, in which a laser beam reflected back from the cantilever illuminates a position-sensitive photodetector. The laser spot on the photodetector moves up and down as the cantilever oscillates, and therefore, the cantilever deflection and oscillation amplitude can be measured from the photodetector output. During raster scanning, the sample stage is also moved in the Z-direction via feedback control so that the cantilever oscillation amplitude (and hence the tip-tapping force) is maintained constant at its set point value. Consequently, the three-dimensional (3D) movement of the sample stage approximately traces the sample surface, and hence, a topographical image of the sample can be constructed from the electric signal used to drive the scanner in the Z-direction.

7.2.2 Techniques Underlying HS-AFM

There are several devices in the feedback loop (Fig. 7.1). The input to this loop is a change of sample height under the cantilever tip caused by lateral scanning of the sample stage relative to the tip. First, the oscillating cantilever responds to the sample height change, resulting in a change of its amplitude. This amplitude change is detected by the OBD detector and the amplitude detector. The detected amplitude is compared to the set point amplitude to produce an error signal. This error signal is used to determine the output voltage from the proportional-integral-derivative (PID) feedback controller. This output voltage is sent to the Z-piezo driver to displace the Z-scanner, so that the cantilever oscillation amplitude is restored towards its set point value. This cycle is repeated to minimize the error signal. However, the feedback cycle is always delayed due to the chasing-after nature of feedback control. Moreover, the sample stage is continuously scanned in the lateral direction, independently of the feedback Z-scanning. When the lateral scanning is carried out too fast compared to the speed of feedback control, the error signal becomes large, resulting in an excessive tip force being exerted to the sample and hence in sample damage.

The operation principle of HS-AFM is basically the same as conventional slow AFM, but almost all components in HS-AFM systems are optimized for their fast responses to their respective input signals. Moreover, specialized devices are incorporated in some HS-AFM systems. As regards to the extent of optimization and the use of specialized devices, there are variations among laboratory-built and commercially available HS-AFM systems. Therefore, their speed and low-invasive performances are different. The descriptions below are mostly given for the HS-AFM system (Ando et al. 2008) that has demonstrated its capability to film walking M5 and many other protein molecules during their functional activity (Ando et al. 2014). We believe that commercial HS-AFM systems can also film walking M5 and other dynamic molecular processes.

- *Tiny cantilevers*. The response time of a cantilever is defined by $Q_c/(\pi f_c)$, where Q_c is the quality factor in water and f_c is the first resonant frequency in water. Tiny cantilevers of 7–10 μm long, 2 μm wide and ~100 nm thick are generally used for HS-AFM (Fig. 7.2a–c). These cantilevers made of silicon nitride or quartz have $Q_c = 1-2$ in water, $f_c = 400$ kHz − 1.2 MHz in water and a spring constant $k_c = 0.1$–0.2 N/m. Their response time ranges between 0.4 and 0.8 μs.
- *Scanner*. Faster HS-AFM systems scan the sample stage, rather than the cantilever chip because a simpler opto-mechanical design can be employed in the former system. The sample

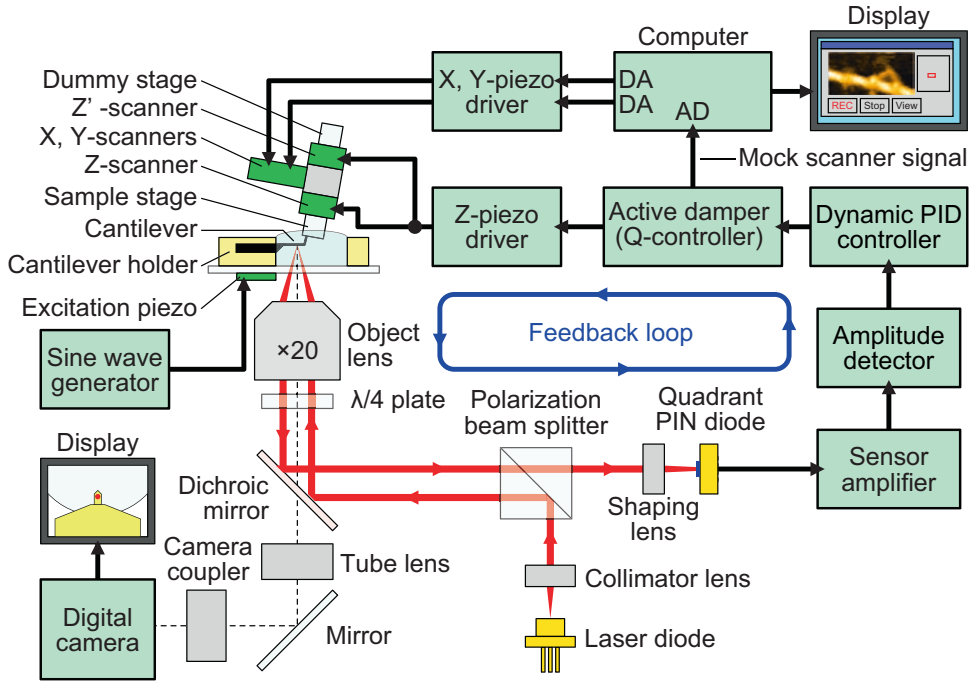

Fig. 7.1 Schematic of HS-AFM system. The system includes an inverted optical microscope. A cantilever chip is held in the holder so that its tip points upward (opposite to the way in conventional AFM). The sample stage, attached to the Z-scanner and facing downward, is placed over the cantilever. The cantilever immersed in a buffer solution is excited to oscillate with small amplitude (1–2 nm) at its first resonant frequency by the oscillation of the excitation piezo. The cantilever oscillation amplitude is maintained constant by feedback control. The scan signals for the X- and Y-scanner are output from the computer through the DA converters. The output from the active Q-control damper is recorded as the sample height through the AD converter. (*Source:* Adapted from Kodera and Ando 2014)

stage scanner is monolithically fabricated from a metallic block to minimize the number of resonant peaks. Different counter-balancing methods are employed for the X- and Z-scanners (Fig. 7.2d, e). In the X-scanner, a piezoactuator is held at both its ends by two identical flexure springs, each of which are attched to an identical mass, so that the center of mass of the X-scanner is hardly displaced. In the Z-scanner, two identical piezoactuators, each attached to an identical mass, are displaced simultaneously in the opposite direction to minimize the vibrations of their supporting base. The first resonance frequencies of the X-, Y- and Z-scanners are 60, 15 and 200 kHz, respectively, while their maximum strokes are 2 μm, 3 μm and 1μm at 100 V, respectively.

- *Active vibration damping of Z-scanner*. The Z-piezoactuator has a high quality factor (i.e., a sharp resonant peak at ~200 kHz), which generates undesirable ringing displacement of the Z-scanner when driven quickly. The quality factor is significantly reduced by an active vibration damping method (Kodera et al. 2005) that uses a mock Z-scanner (LRC circuit) characterized with the transfer function identical to that of the real Z-scanner.
- *Fast amplitude detectors*. To convert the cantilever deflection signal into an amplitude signal within a half or one cycle of cantilever oscillation, fast amplitude detectors based on

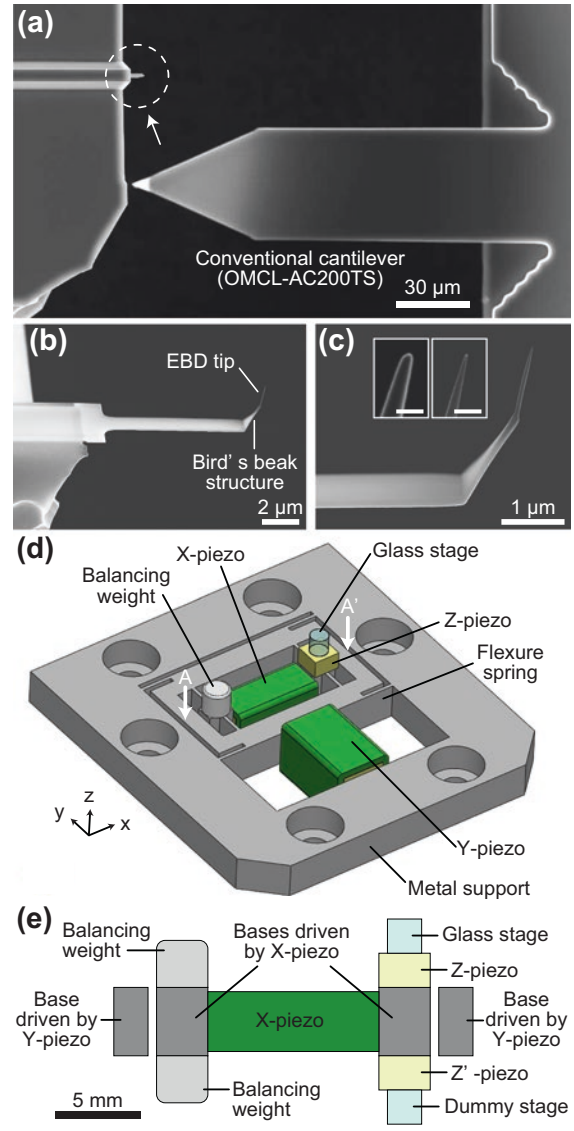

Fig. 7.2 Two key mechanical devices in HS-AFM. (**a**–**c**) SEM images showing small cantilever. (**a**) Size comparison between small cantilever (Olympus BL-AC10DS, encircled by dashed line) and conventional cantilever (Olympus OMCL-AC200TS). (**b**) Magnified side view of small cantilever. (**c**) Further magnified view around the electron-beam deposited (EBD) tip grown on the original bird beak-shaped tip of small cantilever. Insets show EBD tips before (left) and after (right) sharpening by plasma etching. Scale bars, 50 nm. (**d**–**e**) Schematic of high-speed scanner. (**d**) Three-dimensional view of the scanner. (**e**) Sectional view of the scanner along A-A' shown in (**d**)

peak-hold or Fourier methods are used, respectively (Ando et al. 2001, 2008).

- *Fast feedback controller*. The tip-tapping force can be reduced by the use of small free oscillation amplitude of the cantilever (A_0) and its set point amplitude (A_s) close to A_0 (more details are given in Sect. 7.2.3). However, under these conditions the tip tends to lose contact with the sample surface in the downhill region of the sample. This problem is overcome by a feedback controller referred to as the dynamic PID controller, which enables automatic gain adjustment during imaging (Kodera et al. 2006), making high-speed imaging compatible with low-invasive imaging, together with the drift compensator described below.
- *Drift compensator for cantilever excitation*. The cantilever is excited to oscillate by the oscillation of an excitation piezoactuator. However, the excitation power tends to decrease with time. The resulting decreasing oscillation amplitude is misinterpreted by the feedback control system as being caused by an increasing tip-sample interaction. Therefore, the sample stage is retracted from the tip to

restore the amplitude towards A_s. The difference between A_0 and A_s has to be set at a very small value (0.1–0.3 nm) to achieve low-invasive imaging. Therefore, under such setting the oscillating tip loses contact with the sample completely even when the amplitude reduction caused by a lowered excitation power (and hence the sample stage retraction caused by the misinterpretation of the amplitude reduction) exceeds only by 0.1–0.3 nm. The drift compensator (Kodera et al. 2006) controls the excitation power to maintain constant the time-averaged strength of tip-sample interaction. This strength can be detected by the amplitude measurement of a second harmonic oscillation component that appears as a consequence of distortion of sinusoidal oscillation caused by the tip-sample interaction. Thus, stable low-invasive imaging is possible.

For more details of these underlying techniques, see the reviews (Ando et al. 2008; Ando 2012).

7.2.3 Current Performance of HS-AFM

The structure and function of protein molecules should be preserved during their HS-AFM imaging. There are three issues to be considered to achieve this preservation: (i) the average amount of energy loss from the oscillating cantilever upon tip-sample interaction, (ii) excessive tip-force caused by feedback control error, and (iii) sample–substrate surface interactions. The third issue is described in Sect. 7.4. For the first issue, the cantilever free oscillation amplitude A_0 and set point amplitude A_s have to be set adequately. The average oscillation energy loss $<\Delta E>$ per each tip-sample contact is expressed as

$$\Delta E = \tfrac{1}{2} k_c \left(A_0^2 - A_s^2 \right) / Q_c . \qquad (7.1)$$

The value of $<\Delta E>$ is 5.2 $k_B T$ (k_B, Boltzmann constant; T, room temperature in kelvin) under the typical conditions used for successful imaging of active protein molecules (k_c = 0.1 N/m, Q_c = 1, A_0 = 1.5 nm, and A_s = 0.9 × A_0). This amount of energy is considered to be transferred into the sample at every tip-tapping event. However, this amount of transferred energy is partitioned into many degrees of freedom and dissipates quickly into the surrounding solution, explaining the retention of functional activity of proteins in the successful HS-AFM imaging studies carried out so far. Note that the tip-sample interaction force is not given by $k_c \times (A_0 - A_s) = 15$ pN, as the force is not a static force but dynamic. The magnitude of dynamic force is much larger than 15 pN, but the time during which the force acts on the sample is very short, ~100 ns. During this short contact period, the X-scanner is displaced only by ~0.05 nm even when imaging is carried out at the highest possible rate, 16 fps (described below). Thus, tip-dragging across the sample surface is negligibly small.

The second issue has to be considered because the extent of feedback error varies depending on the sample surface corrugation, even when the mean cantilever oscillation amplitude is maintained constant at A_s. An excessive dynamic force larger than the mean dynamic force is exerted at an uphill region of the sample. This force becomes larger with decreasing bandwidth of feedback control. The feedback bandwidth, f_B, is defined by the frequency of feedback Z-scanning at which π/4 phase delay occurs in tip tracing of the sample surface, and therefore, represents the speed performance of an AFM system. The feedback bandwidth is 110 kHz in the HS-AFM system used to film walking M5. Taking into account an adverse effect of excessive force on the sample, the highest possible imaging rate, R_{max}, is expressed as.

$$R_{max} = 2\lambda\theta_m f_B / (\pi N W), \qquad (7.2)$$

where W is the scan range in the X-direction, N is the number of scan lines, $1/\lambda$ is the spatial frequency of the sample surface corrugation to be imaged, and θ_m is the maximum possible phase delay in tracing the sample surface at which the resulting excessive tip-force does not disturb the biological function of the sample (Uchihashi

et al. 2012; Ando et al. 2013). θ_m depends on the sample fragility and is typically $\pi/9$ for proteins, according to previous imaging studies (Uchihashi et al. 2012). For example, under the conditions of $f_B = 110$ kHz, $W = 150$ nm, $N = 100$, $\theta_m = \pi/9$, and $\lambda = 10$ nm, R_{max} becomes 16 fps.

The spatial resolution of HS-AFM is comparable with that of conventional slow AFM, despite the high-bandwidth detection of cantilever oscillation amplitude and the fast scanning of the sample stage in HS-AFM. Spatial resolution of 2 nm for the lateral direction and 0.1 nm for the Z-direction can be achieved in the best case. The high spatiotemporal resolution and minimal invasiveness have opened up a new opportunity to directly visualize dynamic events of proteins, as reviewed (Ando 2012, Ando 2019; Ando et al. 2013, 2014; Dufrêne et al. 2017) and even dynamic phenomena on living cell surfaces (Yamashita et al. 2012; Watanabe et al. 2013; Shibata et al. 2015). Detailed protocols for HS-AFM imaging of protein molecules are described in (Uchihashi et al. 2012).

7.3 Myosin Studies with Conventional AFM

This section describes studies of myosins using conventional slow AFM. When this type of AFM is used as an imaging tool, only static images can be obtained. Therefore, the samples are often dried and imaged in air. AFM imaging has been carried out only for a few myosin systems; for example, titin-M2 filament complexes (Kellermayer et al. 2018), smooth muscle M2 filaments with non-phosphorylated and phosphorylated 20 kDa regulatory myosin light chains (Ip et al. 2007), and complexes of brain M5 and a SNARE component (Watanabe et al. 2005). The last study is described below.

Brain M5 transports synaptic vesicles and is involved in their Ca^{2+}-regulated exocytosis (e.g., Tilelli et al. 2003), although this issue is still in debate (Maschi et al. 2018). Biochemical analyses of murine brain M5 showed that syntaxin-1A, a t-SNARE involved in exocytosis, makes a complex with M5 in the presence of Ca^{2+} (> 0.3 μM) and ATP (Watanabe et al. 2005). In AFM images of this complex, syntaxin-1A appears to bind to a portion of the bifurcation of the two necks, suggesting that syntaxin-1A is an IQ motif-binding protein. Moreover, among six IQ-motifs on each neck domain Ca^{2+}-bound calmodulin (CaM) appears to dissociate from the sixth IQ motif (counted from the N-terminus).

Rather than imaging, slow AFM has been used more for single-molecule measurements of force-distance curves (simply referred to as "force curves") to study mechanical and structural properties of myosins and myosin-related proteins, although the tip-approach/retraction velocity (hence the force loading rate) is limited. HS-AFM has largely extended the loading rate up to the level of molecular dynamics simulations (Rico et al. 2013). For example, the following targets have been subjected to force curve measurements: UNC-45 chaperone–M2 interaction (Kaiser et al. 2012), mechanical force-based regulation of smooth muscle M2 light chain kinase (smMLCK) (Baumann et al. 2017), actin–M2 rigor bond (Nakajima et al. 1997), unzipping of M2 filaments (Decker and Kellermayer 2008), elasticity and uncoiling of M2 coiled-coil (Schwaiger et al. 2002; Root et al. 2006), and elastic properties of desmin protofibrils (Kiss et al. 2011), cardiac M2-binding protein-C (Karsai et al. 2011), and titin (e.g., Rief et al. 1997; Oberhauser et al. 2001). Some of these studies are described below.

The molecule chaperone UNC-45, a member of the UNC-45/Cro1/She4p family of proteins, is essential for proper folding and assembly of M2 into muscle thick filaments *in vivo* (Hellerschmied and Clausen 2014). The molecular chaperone activity of UNC-45 was observed for single molecules of skeletal muscle M2 subfragment-1 (S1) anchored onto a substrate surface through a linker (Hellerschmied and Clausen 2014). A surface-anchored single molecule of S1 was unfolded by pulling with the AFM tip. After the force was removed, the S1 was refolded only in the presence of UNC-45, indicating the chaperone activity of UNC-45 on the M2 head.

The study of smMLCK (Baumann et al. 2017) showed that when the molecule was stretched by forces applied to the N- and C-terminal sides in

the opposite direction, a region responsible for the auto-inhibition of smMLCK was released from the kinase core domain, thus permitting the kinase to bind to myosin regulatory light chain (RLC) without Ca^{2+}/CaM. This observation suggests that forces acting *in vivo* on smMLCK from actin bound to the N-terminus and from M2 bound to the C-terminus presumably regulate smMLCK, although Ca^{2+}/CaM is the major regulator. This force-dependent regulation of kinase activity is similar to that observed for titin kinase (Gautel 2011) and twitchin kinase (von Castelmur et al. 2012).

In another study (Nakajima et al. 1997), force curves were measured to estimate the recognition distance and magnitude of forces acting between surface-immobilized actin filaments and an AFM tip-attached single molecule of skeletal muscle heavy meromyosin (M2-HMM). The tail end of HMM was biotinylated using biotin-cadaverine and transglutaminase-catalysed amino exchange reaction, and attached specifically to the AFM tip through a UltraAvidin-coated fluorescent bead. From the measured force curves, values for various quantities are estimated: recognition distance between actin and a single M2 head (~5 nm at ionic strength of 0.05), the magnitudes of attractive force and force gradient exerted at this recognition distance (1.9 pN and 1.8 pN/nm, respectively), the rupture forces of a single rigor bond (14.8 ± 4 pN) and two-headed rigor bond (24.7 ± 1.4 pN) at a loading rate of ~300 pN/s, the lifetime of a single rigor bond (~12 ms) under the rupture force of 14.8 pN, and the effective rupture length (1.7–2.5 nm). The long recognition distance, which facilitates Brownian search of a M2 head for the binding site on actin, suggests that the mutual recognition occurs through an attractive electrostatic interaction. The number of effective electric charges involved in this recognition is also estimated as a product value of $N_m \times N_a = 16.3$, where N_m is the number of effective positive charges at the actin-binding site on a M2 head, while N_a is the number of effective negative charges at the M2-binding site on actin. The unusually long rupture length is consistent with the fact that actin-M2 head interfaces contain several bonds between flexible loop structures.

As exemplified above, the high precision AFM force-curve measurements at the single-molecule level are powerful in quantifying the structural and mechanical features of a single protein or its interaction with a counterpart. Nevertheless, the molecules under force are completely invisible. Unlike AFM force measurements, optical tweezers combined with AFM should allow for simultaneous force and topography measurement for a single molecule. Such a combined system exists, but this simultaneous measurement has never been reported.

7.4 Choice of Substrate Surfaces

The choice of substrate surfaces depends on proteins and dynamic phenomena to be visualized. The strength of sample-substrate surface interactions should be moderate. When the interaction is too strong, the protein structure is altered or the function is hampered. When too weak, protein molecules diffuse too fast on the surface to be imaged even with HS-AFM.

7.4.1 Bare Mica and Amino Silane-Coated Mica

Mica (natural muscovite or synthetic fluorophlogopite) is easily cleaved and its newly exposed surface is atomically flat over a large area. It has a net negative charge, conferring high hydrophilicity on the surface. The bare mica surface adsorbs most proteins by electrostatic interactions, and hence, nonspecifically. The electrostatic interaction can be controlled by the use of different ionic strengths, pH values, monovalent cations, and divalent cations such as Mg^{2+} (Yamamoto et al. 2010). For monovalent cations at a given concentration, the strength of electrostatic protein-mica interactions is reduced in the order of $Li^+ < Na^+ < K^+$. Divalent cations can mediate binding between negatively-charged proteins and the negatively-charged surface. The

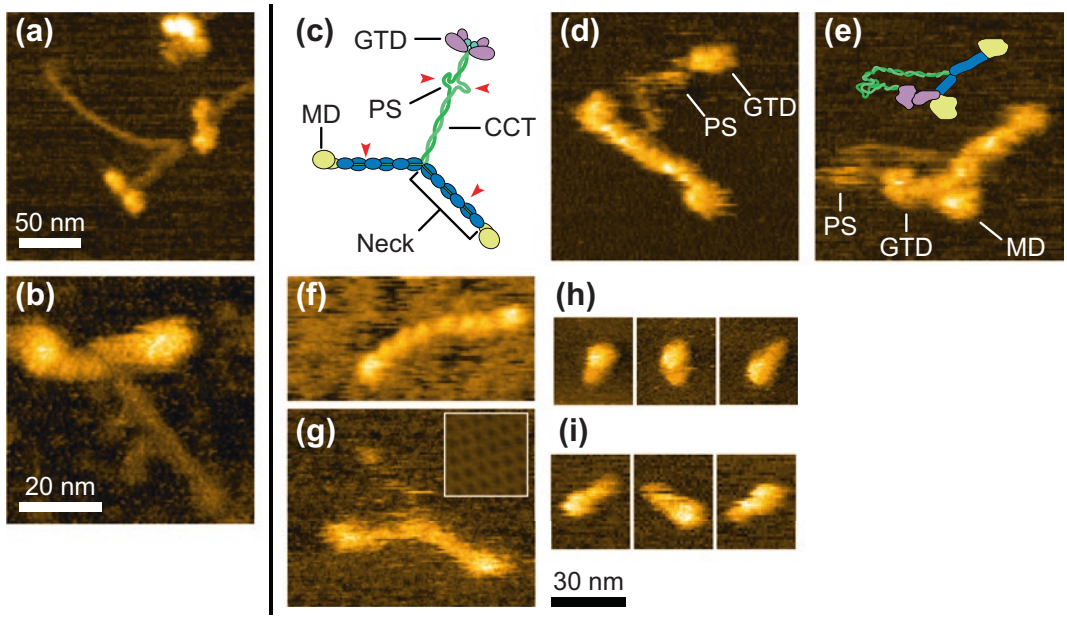

Fig. 7.3 HS-AFM images showing different forms of M2 (**a**–**b**) and M5 (**d**–**i**) on various substrates. (**a**) M2-full on bare mica. Frame rate, 10 fps. (**b**) M2-HMM on APTES mica. Frame rate, 3 fps. (**c**) Schematic of M5-full. MD, motor domain; CCT, coiled-coil tail domain; PS, PEST site; GTD, globular tail domain. Arrowheads indicate the PK proteolysis sites producing M5-HMM and M5-S1. (**d**) Extended form and (**e**) partially folded form of M5-full on bare mica. Frame rate, 5 fps. Molecular features seen in (**e**) are depicted by the schematic with the same color as (**c**). (**f**) M5-HMM on APTES mica. Frame rate, 10 fps. (**g**) M5-HHM with biotinylated CaMs immobilized on streptavidin 2D crystal. Frame rate, 2 fps. Inset shows a part of streptavidin 2D crystal. (**h**–**i**) M5-S1 on bare mica. Frame rate, 5 fps. M5-S1 with single CaM (**h**) and two CaMs (**i**)

charge polarity can be reversed by surface coating with aminosilane, *e.g.,* (3-aminopropyl) triethoxysilane (APTES). Various functional groups can be introduced to this surface.

When the electrostatic interaction of myosins with mica is too strong, the light chains or calmodulin (CaM) on the IQ motifs tend to dissociate from the heavy chain. When the interaction strength is optimized, typical structural features of full length M2 (M2-full) from rabbit skeletal muscle can been seen, including the ellipsoidal motor domains, the short neck regions and the long coiled-coil tail with a sharp kink at the border between subfragment-2 (S2) and light meromyosin (LMM) (Fig. 7.3a). In the case of full-length chick brain M5 (M5-full) in the presence of 1 mM EGTA and 100 mM KCl, extended (Fig. 7.3d) and partially folded (Fig. 7.3e) conformations are observed. In the latter, the globular distal tail domain appears to bind to the junction between the motor and lever arm domains, consistent with electron microscopy studies (Thirumurugan et al. 2006; Liu et al. 2006).

The heavy chain in each neck region of chick brain M5 contains six IQ motifs with different amino acid sequences, which are numbered 1–6 from the N-terminus. Five CaMs and either the 17 kDa essential light chain or the dynein 10 kDa light chain are bound to the six IQ motifs (Koide et al. 2006). Digestion of M5-full with proteinase K (PK) in the absence of Ca^{2+} predominantly yields tail-truncated M5-HMM. This cleavage specificity is similar to that of limited proteolysis of M2-full with trypsin or papain in the absence of Ca^{2+}. HS-AFM images of M2-HMM (Fig. 7.3b) and M5-HMM (Fig. 7.3f) on APTES-mica reveal detailed features of these molecules, as the molecules do not diffuse on this surface. The image of M5-HMM shows three consecutively aligned globular structures on each neck region, corresponding to three CaMs (one of

them may be either of the light chains). This appearance indicates that the other three CaMs (one of them may be either of the light chains) face mica, and thus, the six IQ motifs are alternately rotated by 180° (i.e., the even-numbered IQ motifs and the odd-numbered IQ motifs locate in the opposite sides around a heavy chain in the neck region). However, it has been suggested that one CaM molecule can bind to adjacent IQ sequences (i.e., bridging) (Martin and Bayley 2004). In the presence of Ca^{2+}, PK digests the neck region at a junction between IQ2 and IQ3, yielding S1 with IQ1 and IQ2 that contains only CaM (Koide et al. 2006). CaM on IQ1 does not dissociate, whereas CaM on IQ2 dissociates in the presence of a high concentration of Ca^{2+}, but the exposed IQ2 is refilled with exogenous CaM at a low concentration of Ca^{2+}, consistent with another study (Trybus et al. 1999). The AFM images of S1 (Fig. 7.3h) and CaM-refilled S1 (Fig. 7.3i) on bare mica show a similar appearance of the globular motor domain but different neck lengths. The proteolytic production of S1 with IQ1 and IQ2, and CaM release from IQ2 in the presence of Ca^{2+} are considered to be related to the motility inhibition by Ca^{2+} of M5-HMM as well as M5-full. That is, CaM release from IQ2 exposes IQ2 and an IQ2 − IQ3 junction, which would produce a floppy joint between the motor and neck domains, thus resulting in an inability of transmission of ATP-driven conformational changes in the motor domain to the long lever arm (or an inability of generating intramolecular tension). This view is not inconsistent with the observation that actin gliding by surface-immobilized S1 with only IQ1 is not regulated by Ca^{2+} (Trybus et al. 1999). Nevertheless, the mechanism of motility inhibition by Ca^{2+} for M5-HMM and extended M5-full (i.e., without association between the heads and the cargo-binding domain) is not yet fully understood.

7.4.2 Substrate Surfaces Without Non-specific Protein Binding

Compared to single proteins, it is more difficult to image protein systems containing multiple species interacting with each other, like actomyosins. Bare mica and aminosilane coated-mica are useless for imaging myosin motility, although the sliding motion of actin filaments over a mica surface densely coated with M5 can be observed (Ando et al. 2005). M5-HMM walking on actin filaments is only very rarely observed on bare mica by the addition of 300 mM KCl, which reduces mica−M5-HMM interactions. Even when observed, the number of observed steps is just 1–2 because the actin−M5-HMM interaction is also weakened and easily disrupted by the AFM tip.

The ideal assay conditions for observing dynamic intermolecular interactions between two different proteins would be as follows: (i) the substrate surface does not directly interact with the proteins, (ii) one protein is tethered onto the substrate surface through a linker, and (iii) another protein is completely free from the surface and only interacts with the tethered protein. The following two surfaces meet these conditions: streptavidin 2D crystals and mica-supported lipid bilayers of non-charged phospholipids with low fluidity. Streptavidin 2D crystals can be formed on a highly fluidic mica-supported lipid bilayer (mica-SLB) containing a biotin-lipid (Yamamoto et al. 2009, 2010). Biotinylated proteins can be specifically immobilized on this surface. For example, M5-HMM with biotinylated CaMs (Sakamoto et al. 2000; Yildiz et al. 2003) can be immobilized on the surface and imaged with HS-AFM (Fig. 7.3g). Although not yet attempted, conformational changes of this immobilized M5-HMM during ATP hydrolysis will be able to be captured by HS-AFM, as the motor domain is almost free from the surface. This surface also allows us to observe the motion of biotin-free myosins on surface-immobilized biotinylated actin filaments in a low ionic strength solution. Unidirectional processive movement of M5-HMM on actin filaments is observed using this assay system. However, actin-bound M5-HMM is almost free from the surface (i.e., not supported on the surface), and therefore, its high-resolution imaging is difficult. The surface of mica-SLB is flat enough. A low fluidity of lipid bilayers at room temperature can be afforded with lipids containing

saturated alkyl chains; molecules immobilized on this mica-SLB surface move very slowly (~1.5 nm^2/s) at room temperature (Yamamoto et al. 2010). Biotin-lipids, such as 1,2-dipalmitoyl -*sn*-glycero-3-phosphoethanolamine-*N*-(cap biotinyl) (biotin-cap DPPE), can be used to specifically tether biotinylated proteins through streptavidin with a low surface density. If necessary, electric charges can be introduced to these surfaces. In the case of streptavidin 2D crystal surface, positively or negatively charged biotin compounds can be partially bound to the surface. For mica-SLB, lipids with positively- or negatively-charged head groups can be used for this purpose. However, mica-SLB has a minor problem: the AFM tip is apt to be contaminated with lipids during imaging, resulting in noisy images.

7.5 HS-AFM Imaging of Walking M5-HMM

7.5.1 Unidirectional Processive Movement of M5-HMM

On the surface of uncharged mica-SLB containing biotin-cap DPPE and 1,2-dipalmitoyl-*sn*-glycero-3-phosphocholine (DPPC) at a weight ratio of 5:95, only biotinylated actin filaments are immobilized through streptavidin molecules sparsely attached to the surface (Fig. 7.4a). M5-HMM are never bound to the surface. Unidirectional processive movement of M5-HMM was successfully observed in this assay system. The mean velocities of this movement at different ATP concentrations are identical to those previously measured with single-molecule fluorescence microscopy under the same buffer solution condition (Forkey et al. 2003; Baker et al. 2004), indicating a negligible effect of the tip-sample interaction on the motor activity. However, the moving M5-HMM molecules are often oriented perpendicularly to the SLB surface. As such, their characteristic side view does not appear frequently (Fig. 7.4b). On mica-SLB surface containing a positively-charged lipid, 1,2-dipalmitoyl-3-trimethylammonium-propane (DPTAP) at 5% (weight ratio), the characteristic side view of M5-HMM molecules moving processively with discrete ~36-nm steps appear (Fig. 7.4c). Negatively-charged actin filaments are directly bound to this positively-charged surface even without streptavidin and diffuse slowly. M5-HMM molecules are also directly bound to the surface but diffuse very fast when actin filaments are absent. The mean velocities of unidirectional motion of M5-HMM at various ATP concentrations are retarded by 30% in the presence of DPTAP.

HS-AFM images captured under this nearly ideal condition exhibit unique structural features of two-headed bound M5-HMM in the presence of ATP (Fig. 7.4d). The junction between the neck and motor domains appears smooth in the leading head but is always V-shaped in the trailing head because the neck regions emerge from different parts of the respective motor domains. The short coiled-coil tail is mostly tilted towards the minus end of actin. These structural features, which are totally consistent with an electron microscopic observation (Walker et al. 2000; Burgess et al. 2002), can be used to determine the actin polarity when bound M5-HMM is stationary. In addition, the leading head always displays a straight conformation (slightly curved outwards), which agrees with the straight-neck model proposed for walking M5 (Forkey et al. 2003; Syed et al. 2006; Toprak et al. 2006), but disagrees with the bent-neck model (Walker et al. 2000; Burgess et al. 2002; Snyder et al. 2004; Oke et al. 2010). Despite this successful imaging showing these structural features and the unidirectional motion of M5-HMM, dynamic molecular processes occurring between two successive dwell states are not well resolved by the images captured at 7 fps (~150 ms/frame), as this process is complete within 10 ms (Dunn and Spudich 2007; Cappello et al. 2007).

7.5.2 Handover-Hand Movement of M5-HMM

Transient processes between two successive dwell states contain a forwardly biased diffusional process during which the detached head searches for its next binding site on an actin fila-

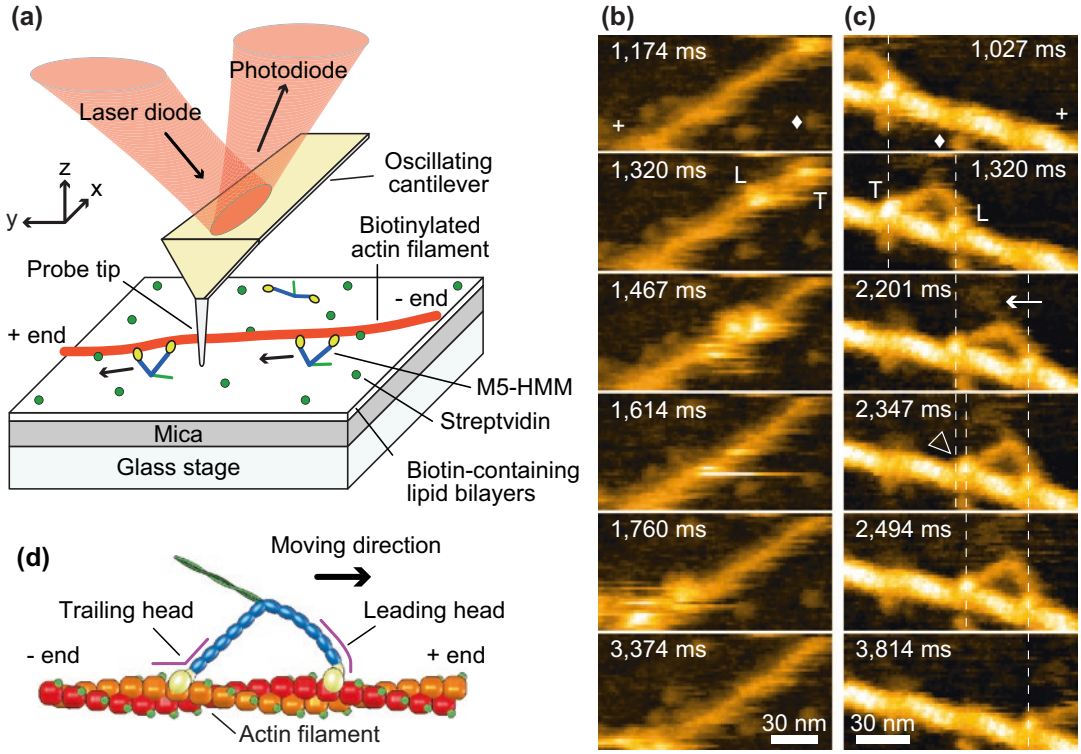

Fig. 7.4 Successive HS-AFM images showing unidirectional processive movement of M5-HMM along actin filaments observed in 1 μM ATP. (**a**) Schematic showing assay system used for HS-AFM imaging. (**b**, **c**) HS-AFM images of M5-HMM when DPTAP is absent (**b**) and present (**c**) in the mica-SLB surface. Frame rate, 7 fps. L and T represent the leading and trailing heads, respectively. Each white diamond indicates one of the streptavidin molecules attached to the mica-SLB surface, and each plus sign indicates the plus end of actin. The vertical dashed lines show the centers of mass of the motor domains. The arrow indicates the coiled-coil tail pointing to the minus end of actin. The open arrowhead indicates a foot sliding event observed in the trailing head. (**d**) Schematic explaining structural features of two-headed bound M5-HMM observed in the presence of nucleotides. (*Source:* Adapted from Ando et al. 2013)

ment (Dunn and Spudich 2007; Cappello et al. 2007; Shiroguchi and Kinosita 2007). This fast diffusional search can be slowed down by the placement of more streptavidin molecules on the SLB surface, which act as moderate obstacles to the walking of M5-HMM (Fig. 7.5a), as detailed below. With this means, transient processes are captured by HS-AFM imaging at 7 fps (Fig. 7.5b). Upon detachment of the trailing head from actin, the leading head spontaneously rotates from the reverse arrowhead (i.e., backwardly leaning) orientation towards the arrowhead (i.e., forwardly leaning) orientation. Before completing this rotation, the leading head is halted for a moment by colliding with a streptavidin molecule placed in the way of its natural path. In this halted state, the forwardly displaced trailing head is positioned most distant from the actin filament (thus, the two heads are aligned nearly straight, pointing in opposite directions), and slightly rotates around the neck-neck junction (the second frame in Fig. 7.5b). Then, the leading head overcomes the obstacle and further rotates forwards. Immediately after this, the trailing head is bound to a forward site of the actin filament to become a new leading head, completing one step. The observed rotation of the leading head is exactly the swinging lever arm motion itself initially proposed for the powerstroke of muscle M2 (Huxley 1969). Before completing a step, the detached trailing head never interacts with actin but passively moves forwards driven by the rotating leading head.

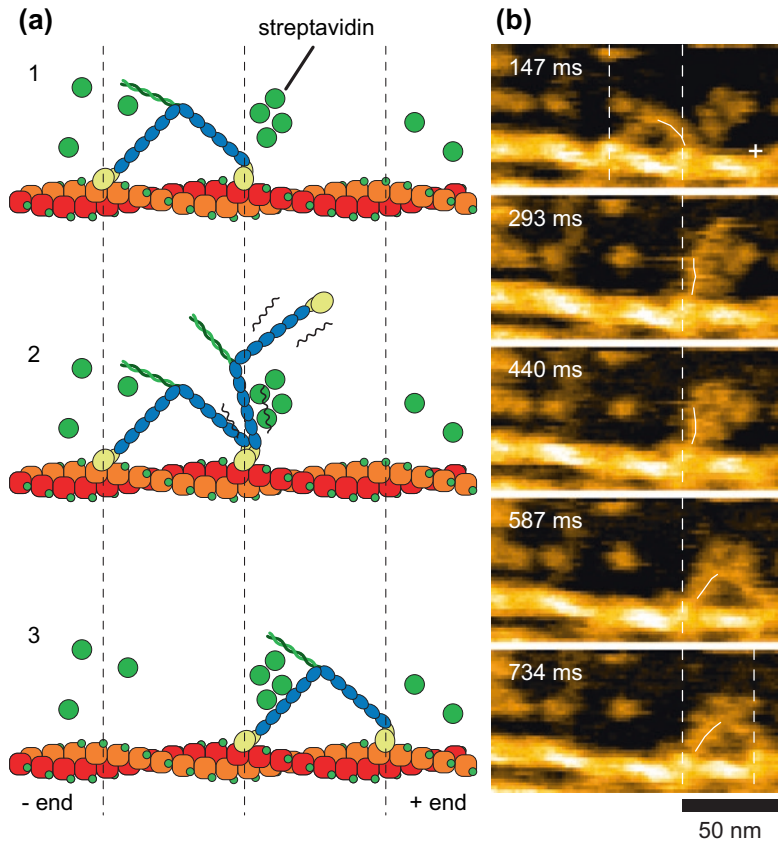

Fig. 7.5 Stepping behavior of M5-HMM visualized by HS-AFM. (**a**) Schematic explaining the HSAFM images shown in (**b**). (**b**) Successive HS-AFM images that resolved the stepping behavior of M5-HMM in 1 μM ATP. Frame rate, 7 fps. The swinging lever arm is highlighted with the thin white lines. The vertical dashed lines in (**a**) and (**b**) represent the centers of mass of the motor domains, and the plus sign indicates the plus end of actin. (*Source:* Adapted from Kodera et al. 2010)

This rules out some models of M5 motility such as the model of "biased head diffusion on actin" proposed for single-headed M5 (Okada et al. 2007). M5 strictly follows the hand-over-hand mechanism. In contrast, the other processive myosins VI and X, which function not only as cargo transporters but also as structural anchors in cells, are reported to move irregularly, namely by inchworm-like stepping, backward stepping, and forward hand-over-hand stepping (Yildiz et al. 2004; Sun et al. 2007, Sun et al. 2010; Nishikawa et al. 2010; Ricca and Rock 2010; Ikezaki et al. 2015).

7.5.3 Directional Rule

A "directional rule" was noticed from all HS-AFM images displaying unidirectionally moving M5-HMM molecules; there is a relationship between the moving direction and the direction from which M5-HMM is bound to an actin filament. M5-HMM molecules moving from the west to east are always bound to actin filaments from the north, while those moving from the east to west are bound to actin from the south (Fig. 7.6a). This rule is unrelated to the previously observed tendency of moderate left-handed spiral motion of walking M5 around a freely suspended actin filament (Ali et al. 2002), because this directional rule holds even in the absence of ATP, where the actin polarity can be judged from the above-mentioned structural features of two-headed bound M5-HMM. The directional rule suggests a geometry-specific positioning of the motor domain on an actin filament. As seen in AFM images of two-headed bound M5-HMM (e.g., Fig. 7.6a), the motor domain looks brighter than actin, meaning that the bound motor domain is taller than the top surface of the actin filament. Hence, as shown in Fig 7.6b, the directional rule indicates that the motor domains are bound to

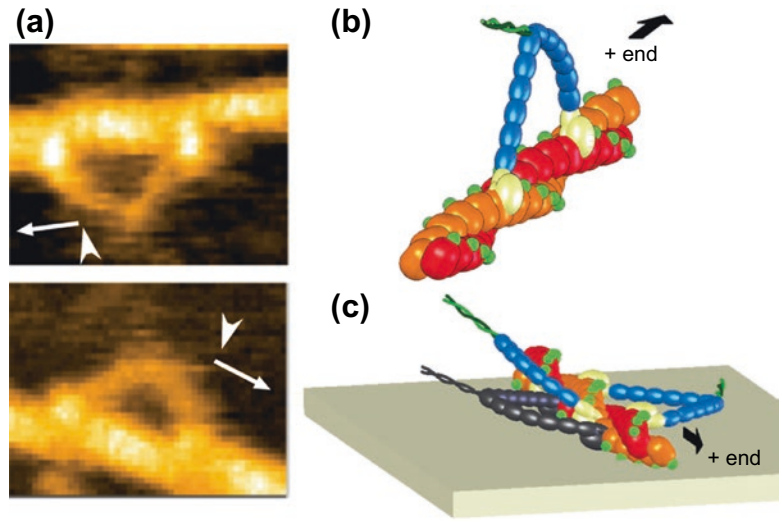

Fig. 7.6 Directional rule and its mechanism. (**a**) Typical HS-AFM images of two-headed bound M5-HMM showing the directional rule: there is a fixed relationship between the moving direction (arrows) and the direction (arrowheads) from which M5-HMM bind to an actin filament. (**b**) Schematic showing M5-HMM bound to actin at the left flanks of the motor domains. (**c**) Schematic showing the cause for the directional rule. In the M5-HMM shown in black, which does not follow the directional rule, the motor domains have to get into the narrow space between the actin filament and the substrate surface, which hardly occurs. (*Source:* Adapted from Ando et al. 2014)

actin at their left flank, provided that the M5-HMM molecule faces the advancing direction. If the actin filament shown in Fig. 7.6b is rotated clockwise about its long axis on the substrate surface, the outer surface of the motor domains would hit the substrate surface at some angle (Fig 7.6c). Thus, the directional rule originates from the steric hindrance effect of the surface, which is reinforced by a weak attractive surface−sample interaction. Nevertheless, a new view is derived here for a structural arrangement of naturally walking M5 (i.e., under no influence from the substrate surface). That is, when M5 stands on an actin filament and faces the advancing direction, the motor domains do not grasp the top surface of the actin filament but grasp the right flank of the filament, as shown in Fig 7.6b. Although not explicitly described before in electron microscopy 3D reconstruction studies of the actin-bound M5 head, this new view is consistent with the 3D structure of the binary complex (Volkmann et al. 2005). This directional rule would be consistently applied to other myosins, except myosin VI, for which a reversed directional rule holds.

7.5.4 Rare Molecular Events: Unwinding of Coiled-Coil Tail, Foot Stomp and Foot Sliding

In addition to molecular events constantly appearing in HS-AFM images, rarely appearing events can also provide new mechanistic insights into M5 motility. Constantly appearing events can be possibly detected by other methods, but rare events are often missed in observations with conventional methods as these methods detect molecular events indirectly. HS-AFM captured such rare events, as described below.

Two-headed bound M5-HMM in the presence of ADP occasionally undergoes unwinding of its coiled-coil tail, immediately after which the leading head rotates spontaneously from the reverse

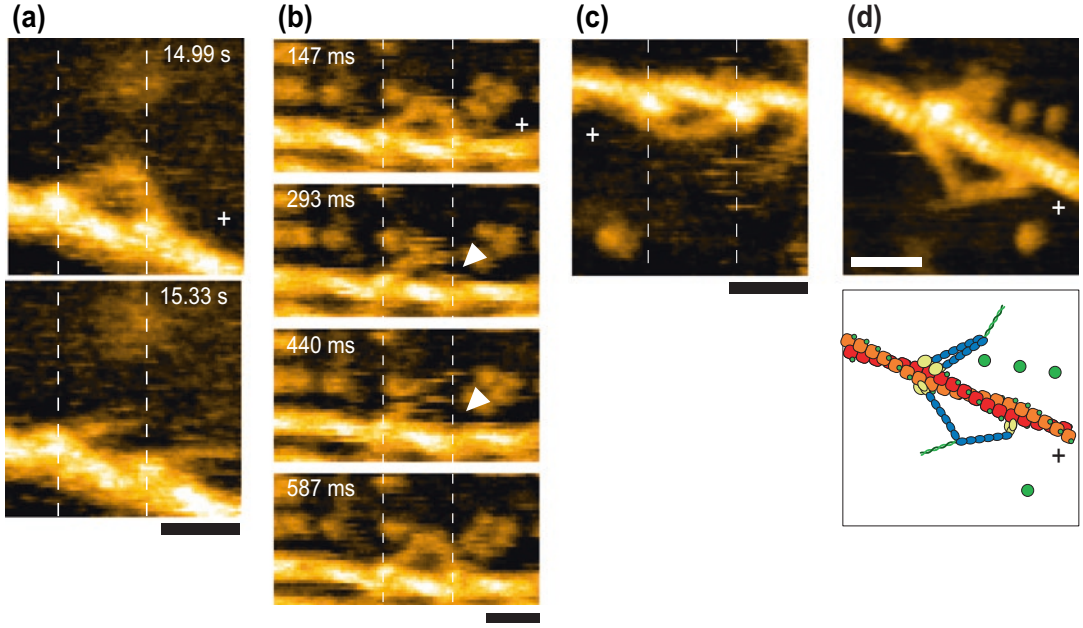

Fig. 7.7 Unique molecular behaviors of M5-HMM visualized by HS-AFM. (**a**) HS-AFM images before (upper panel) and after (lower panel) unwinding of coiled-coil tail observed in 50 μM ADP. (**b**) Successive HS-AFM images showing a foot stomp event that occurred at the leading-head (ATP, 1 μM; frame rate, 7 fps). The leading-head detachment is marked with the white arrowheads. (**c**) HS-AFM image showing the leading head with a sharply bent conformation observed in the NF condition. (**d**) HS-AFM image showing NF M5-HMM with heads bound to adjacent actin subunits (upper-positioned molecule in the upper panel) and its illustration (upper-positioned molecule in the lower panel). Note that the bottom-positioned molecule exceptionally does not follow the directional rule. Frame rate for (**b**–**d**), 3 fps. The vertical dashed lines represent the centers of mass of the motor domains, and the plus signs indicate the plus end of actin. Scale bar, 30 nm. (*Source:* Adapted from Kodera and Ando 2014)

arrowhead orientation to the arrowhead orientation (Fig. 7.7a), very much like the swinging lever arm motion (Fig. 7.5b). This unwinding is not an artifact arising from the AFM tip tapping. It has been noticed that M5-HMM specimens purified by co-pelleting with actin filaments contain a small fraction of single-headed species (Wang et al. 2000; Burgess et al. 2002), but the reason for this production has not been ascertained before. This unwinding of coiled-coil tail indicates that an unwinding force is exerted onto the tail from one or both of the heads. The trailing head is bound to actin in a natural arrowhead orientation, whereas the leading head is bound in a forced reverse-arrowhead orientation. This means that the leading head in the reverse-arrowhead orientation is pulled back by the trailing head at the neck–neck junction. Therefore, this unwinding force originates directly from the strained leading head and indirectly from the strong affinity of the motor domain for actin. The swinging lever arm-like motion of the leading head occurring immediately after the tail unwinding implies that the energy source for swinging lever arm motion in walking M5 in the presence of ATP is strain energy stored in the leading head in the reverse arrowhead orientation, not chemical energy liberated by ATP hydrolysis. Moreover, the strain energy is released upon trailing head detachment from actin and the following spontaneous rotation of the leading head.

The next rare event observed is “foot stomp”. That is, in the presence of ATP, the leading head briefly dissociates from actin and re-associates with the same actin filament, while the molecule remains at approximately the same position on the filament (Fig. 7.7b). Note that foot stomp is almost never observed with the trailing head. The

briefly detached leading head does not carry bound Pi because Pi has already been released from the leading head following its initial attachment to actin (De La Cruz et al. 1999; Olivares et al. 2006). Nevertheless, after this foot stomp, the molecule steps forwards propelled by the swinging lever arm motion of the leading head spontaneously occurring upon trailing head detachment from actin. Although not well documented, a foot-stomp-like behavior was previously suggested in fluorescence microscopy observations of walking M5 molecules (Syed et al. 2006; Shiroguchi and Kinosita 2007). The foot stomp was confirmed later by the observation of walking M5 by high-speed single-molecule polarized fluorescence microscopy (Beausang et al. 2013) and interferometric scattering microscopy (Andrecka et al. 2015). Thus, the foot stomp is an inherent behavior of this motor, although it is a rare event and only occurs at low ATP concentrations (Andrecka et al. 2015). Despite its rareness, the foot stomp has an interesting implication as to the chemo-mechanical coupling in M5.

These two rare events described above indicate the following three facts for the ADP-bound leading head. First, the ADP-bound leading head in the reverse arrowhead orientation can be formed even when the leading head does not perform a recovery stroke while it is in the actin-unbound state. Second, strain energy is stored in the actin-bound leading head formed in this way. Third, the stored strain energy can be used to swing the lever arm to bring the detached trailing head forwards. These three features are inconsistent with the well prevailing theory, which has advocated that the leading head can bind to actin after a recovery stroke caused by ATP hydrolysis into ADP − Pi and that the energy for mechanical work is supplied when Pi is released from the ADP − Pi-bound head. Therefore, this theory assumes that the ADP − Pi-bound head is in a high energy state. There is an observation (Sellers and Veigel 2010) that also seems inconsistent with this theory. That is, a single M5-S1 molecule bound to an actin filament in the presence of 100 μM ATP undergoes repeated transitions between an actin-bound pre–powerstroke and a post–powerstroke conformation at ~100 Hz under a certain backward load. However, it is not yet clear whether or not these repeated transitions are directly related to the above three facts of an ADP-bound leading head.

Although the same name (foot stomp) has been given to a different rare event, i.e., dislocation of either bound head on actin by ~ ± 5 nm without detaching from actin (See the red arrowhead in Fig. 7.4c), this event is referred to here as "foot sliding". Properties of foot stomping and foot sliding observed at 1 μM ATP are shown in Fig. 7.8. Foot sliding more frequently occurs at the leading head than at the trailing head (by a ratio of approximately 3:2; see Fig. 7.8c). The foot sliding is considered to be an annealing process in which the actin−head binding or the head separation becomes more stable. The asymmetric probability of foot sliding between the leading and trailing heads suggests their actin-affinity difference, consistent with a biochemically measured result (Olivares et al. 2006). The leading head binds to actin in the reverse arrowhead orientation, and hence, pays an energy cost by distorting the neck conformation, resulting in a lower affinity for actin.

7.5.5 Flexibility of Neck-Motor Domain Junction

Under the nucleotide-free (NF) condition, the leading head is often sharply bent (Fig. 7.7c). This conformation never occurs in the presence of ATP or in the presence of 1 mM ADP. Although not well resolved in AFM images (Fig. 7.7c), the sharp kink appears to occur at the neck−motor domain junction, as suggested by electron micrographs (Oke et al. 2010). In the kinked conformation, both heads have the forward leaning orientation around their motor domains, and thus both necks appear to emerge from the front of respective motor domains. The kink is likely to occur for the release of large strain accumulated in the neck, suggesting that the neck−motor domain junction in the NF head is stiffer than that in the nucleotide-bound head. This conjecture

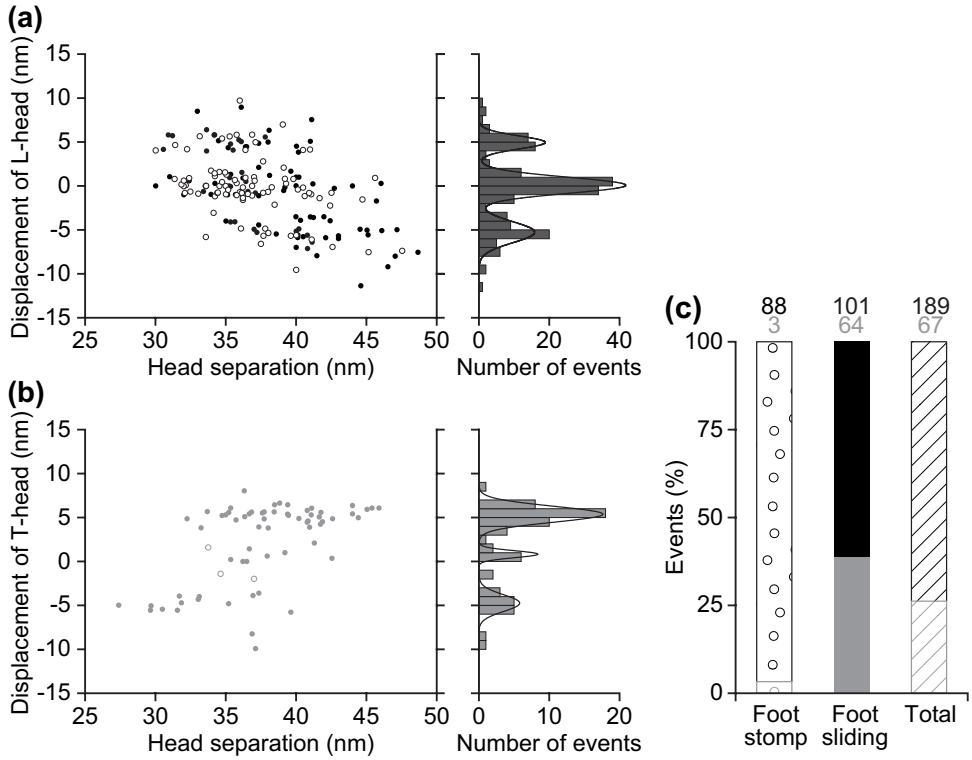

Fig. 7.8 Properties of foot stomping and foot sliding observed at 1 μM ATP. Displacement of motor domain of leading (**a**) and trailing (**b**) heads after foot stomping (open circles) and foot sliding (closed circles) as a function of head separation before foot stomping and sliding. Right-hand figures show the respective histograms of displacement. (**c**) Percentage of foot stomping and foot sliding events observed at the leading (black) and trailing head (gray), respectively. The numbers shown on each bar indicates the numbers of events observed at the leading head (black) and the trailing head (gray)

was confirmed by measurements of the arrowhead orientation angle between single-headed M5-HMM formed by unwinding of the coiled-coil tail and the bound actin filament (Fig. 7.9). The measured angle is distributed around ~34° in the NF solution (Fig. 7.9c). In the presence of ADP, the angle is distributed more widely and peaked at ~29° and ~51° (Fig. 7.9e). The proportion of these two Gaussian components is approximately 6 to 1. These two distinct angles are possibly relevant to the two different ADP-bound equilibrium states as reported for M2 (Geeves 1989; Geeves and Holmes 1999), M5 (Robblee et al. 2005; Hannemann et al. 2005; Oguchi et al. 2008; Jacobs et al. 2011), and myosin VI (Robblee et al. 2005). As revealed by these different angle distributions, the neck–motor domain junction is more flexible in the ADP-bound head than in the NF head. When both heads of NF M5-HMM are bound to actin in a nearly straight conformation, the leading head with a rigid hinge undergoes a large strain, and thus, tends to bend sharply to release the large strain. The rigid hinge in the NF state is consistent with the observation that both heads of M5-HMM can rarely bind to adjacent actin subunits despite their long necks, but this manner of binding occurs only in the NF condition (Fig. 7.7d). The flexibility of the neck-motor domain junction in ADP-bound head seems insufficient for two-heads binding to actin, as the leading head binding in the reverse arrowhead orientation requires the junction to bend by at least ~60°, even when the contribution of the long neck's flexibility is considered. However,

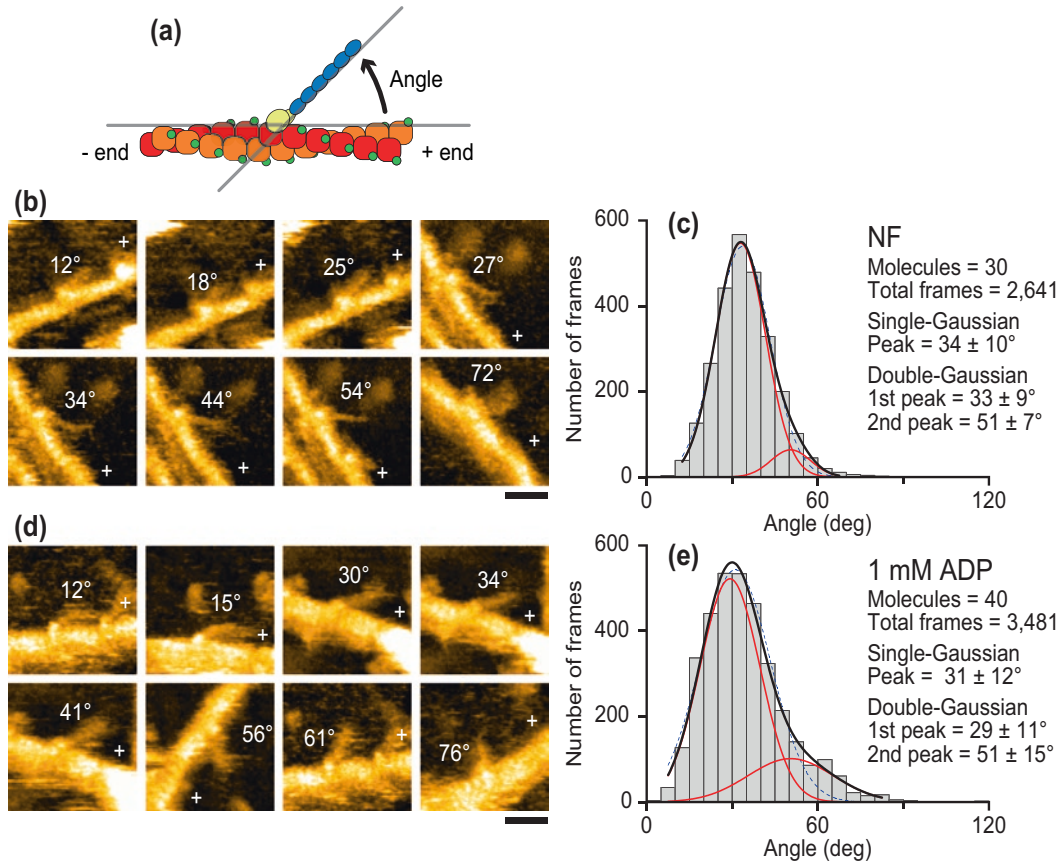

Fig. 7.9 Angle distributions of single-headed M5 bound to actin. (**a**) Schematic showing the angle measured. (**b**, **d**) AFM images of single-headed bound M5 in the NF (**b**) and 1 mM ADP (**d**) conditions. The plus ends of actin filaments are indicated with '+'. The measured angles are shown in the images. Frame rate, 3 fps; scale bar, 30 nm. (**c**, **e**) Histograms of angle measured for single-headed bound M5 in the NF (**c**) and 1 mM ADP (**e**) conditions. Broken lines, single-Gaussian fit results; black solid lines, double-Gaussian fit results; gray lines, Gaussian components in double-Gaussian fit. All values for peak angles represent mean ± s.d. (*Source:* Adapted from Kodera et al. 2010)

the hinge flexibility may depend on actin binding; an actin-unbound head with ADP is possibly more flexible than an actin-bound head with ADP. This actin binding dependence would facilitate two heads binding and at the same time guarantee the generation of a tensile force large enough for execution of mechanical work by the leading head. This possibility is proposed for M2 (Billington et al. 2014). Moreover, there is an additional possibility that the hinge of the ADP − Pi-bound head is more flexible than that of the ADP-bound head.

7.5.6 Asymmetry of ADP Dissociation Rate

As mentioned above, the leading head almost always (> 95%) takes a nearly straight conformation (slightly curved outward) in the presence of nucleotides. On the other hand, it takes two conformations (i.e., nearly straight and sharply bent conformations) under the NF condition, which alternate back and forth (Fig. 7.10a), indicating that they are in equilibrium. From the proportion (Fig. 7.10b) and the lifetime (Fig. 7.10c) of the

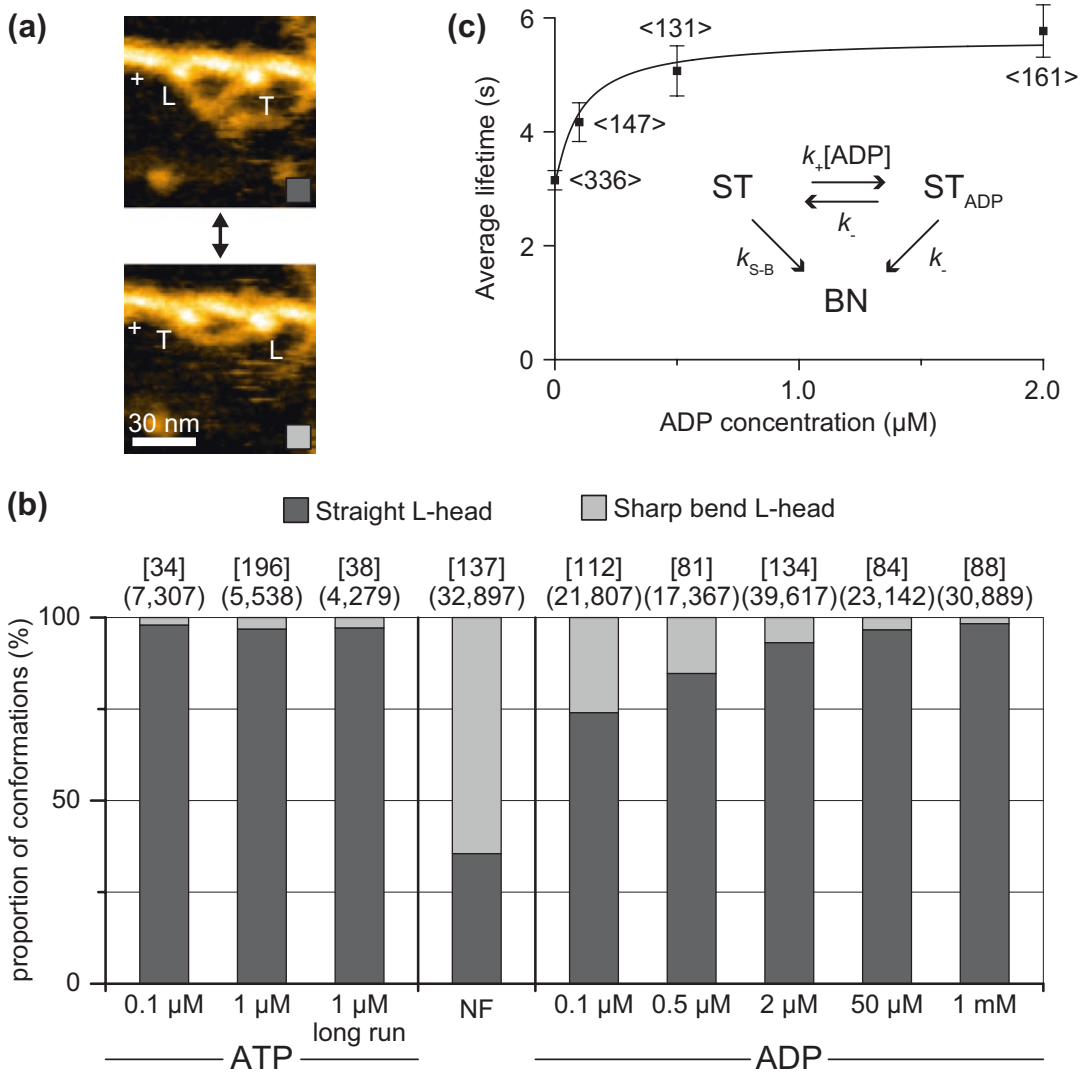

Fig. 7.10 Leading head conformations and their nucleotide dependence. (**a**) HS-AFM images showing a conformational change between straight (top panel) and sharp bent (bottom panel) conformations of the leading head in the presence of 0.1 μM ADP. The plus ends of actin filaments are indicated with '+'. Frame rate, 3 fps. L and T represent the leading and trailing heads, respectively. (**b**) Populations of straight and sharp bent conformations under different nucleotide conditions. The numbers in (frames) and [molecules] represent those of examined images and molecules, respectively. (**c**) Average lifetimes $\langle \tau_{ST} \rangle$ during which the leading head assumes the straight conformation in various ADP concentrations (the number of events used to obtain the average at each ADP concentration is shown in ⟨events⟩). The error bars indicate standard error. The line curve indicates the best fit result obtained by analyzing the data using the following equation: $\langle \tau_{ST} \rangle = n_{NF}/k_{S-B} + n_{ADP}/k_{-}$, where k_{S-B} represents the rate of spontaneous transition from the straight conformation to the sharply bent conformation in the NF leading head, k_{-} represents the ADP dissociation rate constant for the leading head, and n_{NF} and n_{ADP} are, respectively, the fractions of NF and ADP-bound leading heads under a given ADP concentration, which can be calculated using the ADP dissociation constant K_d of 0.075 μM estimated from the data shown in (**b**). (*Source:* Adapted from Kodera et al. 2010)

straight leading head as a function of ADP concentration, the following kinetic parameters for ADP binding and dissociation on the leading head are estimated: ADP dissociation constant $K_d = k_-/k_+ = 0.075 \pm 0.013$ μM, ADP dissociation rate constant, $k_- = 0.100 \pm 0.004$ s^{-1} and second-order ADP binding rate constant, $k_+ = 1.3 \pm 0.3$ μM^{-1} s^{-1}. The value of k_- is 70 times smaller than the corresponding rate for the trailing head estimated from the ATP concentration dependence of M5-HMM translocation velocity measured by HS-AFM ($k_- = 7.2 \pm 1.5$ s^{-1}) (Kodera et al. 2010). This asymmetry of k_- between the leading and trailing heads indicates strain-dependent ADP dissociation. The degree of this asymmetry observed by HS-AFM roughly agrees with previous biochemical measurements (Rosenfeld and Sweeney 2004). The ADP dissociation rate constant of 0.1 s^{-1} means that, on average, ADP is released from the leading head every 10 s. However, M5-HMM walks many steps during 10 s. Thus, the sequential events of ADP release, the subsequent ATP binding, and the resulting head dissociation take place solely at the trailing head, which is the basis underlying the processive hand-over-hand stroke generation. This mechanism was previously inferred from various indirect experiments (Rosenfeld and Sweeney 2004; Purcell et al. 2005; Veigel et al. 2005; Forgacs et al. 2008; Oguchi et al. 2008; Sakamoto et al. 2008). The value of k_+ is 10 times smaller than the corresponding value, 12.6 μM^{-1} s^{-1}, previously measured in a solution study on single-headed M5 (De La Cruz et al. 1999), suggesting that ADP binding is also strain-dependent.

Because ADP never dissociates from the leading head while M5-HMM is walking in the presence of ATP, the sharp kink of the leading head in the NF condition has no relevance to powerstroke generation. Moreover, the brief detachment of the leading head observed as a foot stomp in the presence of ATP is not caused by ATP binding to the head because the sharply kinked conformation is never observed before the brief detachment of the leading head.

7.6 Chemo-Mechanical Coupling in Myosins

The prevailing chemo-mechanical coupling mechanism in myosin motors has been modeled for M2 in the context of the swinging lever arm motion (Geeves and Holmes 1999). This model is based on a tight coupling among the structural, mechanical and nucleotide states in a myosin head (Fisher et al. 1995; Smith and Rayment 1996; Dominguez et al. 1998; Houdusse et al. 2000; Burgess et al. 2002; Coureux et al. 2003, 2004; Volkmann et al. 2005). Upon ATP hydrolysis into ADP–Pi, the actin-unbound head performs a recovery stroke (i.e., a conformational transition from the post-powerstroke to pre-powerstroke state), which facilitates its binding to actin in the reverse arrowhead orientation. Coupled to Pi release from the actin-bound head, a reversed conformational transition takes place from the pre-powerstroke to post-powerstroke state, resulting in the arrowhead orientation. This orientational change puts a strain on the head. The strained head swings its lever arm to release the strain. According to this scenario, the strain energy is supplied from ATP in the Pi-release step, and eventually used for the lever arm swing. As such, the ADP-bound head can no longer execute mechanical work once the strain energy is released by its detachment from actin.

However, the two phenomena appearing in HS-AFM images (i.e., unwinding of the coiled-coil tail in ADP and foot stomp in ATP) are inconsistent with this scenario. That is, the intramolecular strain energy responsible for the lever arm swing can be generated directly in the ADP-bound leading head (after foot stomping) (Fig. 7.7b). In addition, two-headed bound

M5-HMM with ADP alone can generate a sufficient magnitude of tensile force to cause occasional unwinding of the short coiled-coil tail, after which the lever arm swings (Fig. 7.7a). Not only by HS-AFM but also with other methods, it has been consistently observed that both ADP-bound heads of M5-HMM can bind to actin simultaneously without a recovery stoke (Walker et al. 2000; Rosenfeld and Sweeny 2004; Olivares et al. 2006), meaning that the head is floppy enough to bind to actin in the reverse arrowhead orientation. Of course, the efficiency of two-heads binding would be enhanced by the recovery stroke, meaning that a part of the ATP energy can be used to increase the efficiency of two heads binding. When bound to actin with two heads without a recovery stroke, strain energy is accumulated in the leading head. Using this strain energy (not derived from ATP), the leading head spontaneously swings its lever arm, when the trailing head is detached from actin upon ATP binding. This means that the head is stiff enough to swing the lever arm, although the floppiness or stiffness may differ between the actin-free and actin-bound head. Detailed discussions regarding this new model for chemo-mechanical coupling in myosin motors are described elsewhere (Ando et al. 2014; Kodera and Ando 2014).

7.7 Conclusion and Perspectives

One HS-AFM movie of walking M5-HMM molecules provided visual evidence for the swinging lever arm-based processive, hand-over-hand movement with a 36-nm advance for every ATPase cycle. This "all-in-one" measurement makes a stark contrast with previous single-molecule studies on this motor; these dynamic features of walking M5 were established collectively through numerous single-molecule fluorescence microscopy and optical tweezers measurements. HS-AFM can quickly corroborate or rule out previous views obtained through less direct approaches. Besides, HS-AFM can also uncover important phenomena that have not been exposed to measurements with other methods, as typically exemplified by the discoveries of foot stomp and unwinding of the coiled-coil tail of two-headed bound M5-HMM. These discoveries have cast doubt upon the prevailing view of the chemo-mechanical coupling in myosins. This central issue in myosin motility will be further resolved by more extensive studies from various approaches.

The success of HS-AFM imaging of walking M5-HMM has relied on the nature of this motor. Namely, the structural and elastic properties of M5 are fit for the ~36 nm separation between the two attached heads, which almost coincides with the half pitch of the actin helix. Therefore, M5-HMM walks along an actin filament approximately on a plane. This nature is suitable for HS-AFM that images the specimen in 2.5 dimensions. That is, only the space above the substrate surface can be imaged. For example, the processive movement of myosins VI and X, which have necks shorter than those of M5, draws spiral trajectories around an actin filament. Such translational motion makes it difficult for HS-AFM to trace the molecules successively for a long distance. We need a new imaging tool with high spatiotemporal resolution that allows us to directly observe myosin molecules moving on suspended actin filaments. As a suspended actin filament is very soft and fragile, it is largely deformed or broken by tip-contact. Scanning ion conductance microscopy (SICM) may become a good candidate for this type of imaging. SICM uses an electrolyte-filled pipette probe having a nanopore at the tip end, and measures an ion current flowing through the nanopore, driven by a bias voltage between an electrode inside the pipette and another electrode in the external bath solution (Hansma et al. 1989). The ionic current resistance between the pipette tip and sample surface increases (and hence the ion current is reduced) when the tip approaches the sample (a current blocking effect of the sample). This sensitivity of ion current to the tip−sample separation enables imaging of the sample surface without physical tip-sample contact. Currently, both spatial resolution and temporal resolution of SICM are far lower than those of HS-AFM, but attempts have

recently been made towards much higher spatio-temporal resolution (Ida et al. 2017; Watanabe and Ando 2017; Simeonov and Schaffer 2019; Watanabe et al. 2019). Once the resolution is significantly improved, this microscopy has a potential of enabling the observation of not only processive spiral movements of myosins but also dynamic structures and processes of M2 molecules in skinned muscle fibers.

Acknowledgements We thank Takayuki Uchihashi, Daisuke Yamamoto, Ryoki Ishikawa, Takeshi Sakamoto, Tatsuya Kinoshita and Hiroshi Koide for useful discussions and technical assistances. This work was supported by JSPS KAKENHI (JP22870011 and 24770149 to N.K; JP24227005, JP26119003 and 17H06121 to T.A.) and JST grant (JPMJPR13L4 and JPMJCR1762 to N.K.; JPMJCR13M1 to T.A.).

References

Ali MY, Uemura S, Adachi K, Itoh H, Kinosita K Jr, Ishiwata S (2002) Myosin V is a left-handed spiral motor on the right-handed actin helix. Nat Struct Biol 9:464–467. https://doi.org/10.1038/nsb803

Ando T (2012) High-speed atomic force microscopy coming of age. Nanotechnology 23:062001. https://doi.org/10.1088/0957-4484/23/6/062001

Ando T (2019) High-speed atomic force microscopy. Curr Opin Chem Biol 51:105–112

Ando T, Kodera N, Takai E, Maruyama D, Saito K, Toda A (2001) A high-speed atomic force microscope for studying biological macromolecules. Proc Natl Acad Sci U S A 98:12468–12472. https://doi.org/10.1073/pnas.211400898

Ando T, Kodera N, Uchihashi T, Miyagi A, Nakakita R, Yamashita H, Matada K (2005) High-speed atomic force microscopy for capturing dynamic behavior of protein molecules at work. e-J Surf Sci Nanotechnol 3:384–392. https://doi.org/10.1380/ejssnt.2005.384

Ando T, Uchihashi T, Fukuma T (2008) High-speed atomic force microscopy for nano-visualization of dynamic biomolecular processes. Prog Surf Sci 83:337–437. https://doi.org/10.1016/j.progsurf.2008.09.001

Ando T, Uchihashi T, Kodera N (2013) High-speed AFM and applications to biomolecular systems. Annu Rev Biophys 42:393–414. https://doi.org/10.1146/annurev-biophys-083012-130324

Ando T, Uchihashi T, Scheuring S (2014) Filming biomolecular processes by high-speed atomic force microscopy. Chem Rev 114:3120–3188. https://doi.org/10.1021/cr4003837

Andrecka J, Ortega Arroyo J, Takagi Y, de Wit G, Fineberg A, MacKinnon L, Young G, Sellers JR, Kukura P (2015) Structural dynamics of myosin 5 during processive motion revealed by interferometric scattering microscopy. eLife 4:e05413. https://doi.org/10.7554/eLife.05413

Baker JE, Krementsova EB, Kennedy GG, Armstrong A, Trybus KM, Warshaw DM (2004) Myosin V processivity: multiple kinetic pathways for head-to-head coordination. Proc Natl Acad Sci U S A 101:5542–5546. https://doi.org/10.1073/pnas.0307247101

Baumann F, Bauer MS, Rees M, Alexandrovich A, Gautel M, Pippig DA, Gaub HE (2017) Increasing evidence of mechanical force as a functional regulator in smooth muscle myosin light chain kinase. eLife 6:e26473. https://doi.org/10.7554/eLife.26473

Beausang JF, Shroder DY, Nelson PC, Goldman YE (2013) Tilting and wobble of myosin V by high-speed single-molecule polarized fluorescence microscopy. Biophys J 104:1263–1273. https://doi.org/10.1016/j.bpj.2013.01.057

Billington N, Revill DJ, Burgess SA, Chantler PD, Knight PJ (2014) Flexibility within the heads of muscle myosin-2 molecules. J Mol Biol 426:894–907. https://doi.org/10.1016/j.jmb.2013.11.028

Binnig G, Quate CF, Gerber C (1986) Atomic force microscope. Phys Rev Lett 56:930–933. https://doi.org/10.1103/PhysRevLett.56.930

Burgess S, Walker M, Wang F, Sellers JR, White HD, Knight PJ, Trinick J (2002) The prepower stroke conformation of myosin V. J Cell Biol 159:983–991. https://doi.org/10.1083/jcb.200208172

Cappello G, Pierobon P, Symonds C, Busoni L, Gebhardt JC, Rief M, Prost J (2007) Myosin V stepping mechanism. Proc Natl Acad Sci U S A 104:15328–15333. https://doi.org/10.1073/pnas.0706653104

Clemen AE, Vilfan M, Jaud J, Zhang J, Barmann M, Rief M (2005) Force-dependent stepping kinetics of myosin-V. Biophys J 88:4402–4410. https://doi.org/10.1529/biophysj.104.053504

Coureux PD, Wells AL, Menetrey J, Yengo CM, Morris CA, Sweeney HL, Houdusse A (2003) A structural state of the myosin V motor without bound nucleotide. Nature 425:419–423. https://doi.org/10.1038/nature01927

Coureux PD, Sweeney HL, Houdusse A (2004) Three myosin V structures delineate essential features of chemo-mechanical transduction. EMBO J 23:4527–4537. https://doi.org/10.1038/sj.emboj.7600458

De La Cruz EM, Wells AL, Rosenfeld SS, Ostap EM, Sweeney HL (1999) The kinetic mechanism of myosin V. Proc Natl Acad Sci U S A 96:13726–13731. https://doi.org/10.1073/pnas.96.24.13726

Decker B, Kellermayer MS (2008) Periodically arranged interactions within the myosin filament backbone revealed by mechanical unzipping. J Mol Biol 377:307–310. https://doi.org/10.1016/j.jmb.2008.01.023

Dominguez R, Freyzon Y, Trybus KM, Cohen C (1998) Crystal structure of a vertebrate smooth muscle myosin motor domain and its complex with the essential light chain: visualization of the pre-power stroke

state. Cell 94:559–571. https://doi.org/10.1016/s0092-8674(00)81598-6

Dufrêne YF, Ando T, Garcia R, Alsteens D, Martinez-Martin D, Engel A, Gerber C, Muller DJ (2017) Imaging modes of atomic force microscopy for application in molecular and cell biology. Nat Nanotechnol 12:295–307. https://doi.org/10.1038/nnano.2017.45

Dunn AR, Spudich JA (2007) Dynamics of the unbound head during myosin V processive translocation. Nat Struct Mol Biol 14:246–248. https://doi.org/10.1038/nsmb1206

Fisher AJ, Smith CA, Thoden JB, Smith R, Sutoh K, Holden HM, Rayment I (1995) X-ray structures of the myosin motor domain of Dictyostelium discoideum complexed with MgADP.BeFx and MgADP.AlF4. Biochemistry 34:8960–8972

Forgacs E, Cartwright S, Sakamoto T, Sellers JR, Corrie JE, Webb MR, White HD (2008) Kinetics of ADP dissociation from the trail and lead heads of actomyosin V following the power stroke. J Biol Chem 283:766–773. https://doi.org/10.1074/jbc.M704313200

Forkey JN, Quinlan ME, Shaw MA, Corrie JE, Goldman YE (2003) Three-dimensional structural dynamics of myosin V by single-molecule fluorescence polarization. Nature 422:399–404. https://doi.org/10.1038/nature01529

Gautel M (2011) Cytoskeletal protein kinases: titin and its relations in mechanosensing. Pflugers Arch 462:119–134. https://doi.org/10.1007/s00424-011-0946-1

Geeves MA (1989) Dynamic interaction between actin and myosin subfragment 1 in the presence of ADP. Biochemistry 28:5864–5871. https://doi.org/10.1021/bi00440a024

Geeves MA, Holmes KC (1999) Structural mechanism of muscle contraction. Annu Rev Biochem 68:687–728. https://doi.org/10.1146/annurev.biochem.68.1.687

Hallett P, Offer G, Miles MJ (1995) Atomic force microscopy of the myosin molecule. Biophys J 68:1604–1606. https://doi.org/10.1016/S0006-3495(95)80333-4

Hannemann DE, Cao W, Olivares AO, Robblee JP, De La Cruz EM (2005) Magnesium, ADP, and actin binding linkage of myosin V: evidence for multiple myosin V-ADP and actomyosin V-ADP states. Biochemistry 44:8826–8840. https://doi.org/10.1021/bi0473509

Hansma PK, Drake B, Marti O, Gould SA, Prater CB (1989) The scanning ion-conductance microscope. Science 243:641–643. https://doi.org/10.1126/science.2464851

Hellerschmied D, Clausen T (2014) Myosin chaperones. Curr Opin Struct Biol 25:9–15. https://doi.org/10.1016/j.sbi.2013.11.002

Higashi-Fujime S (1980) Active movement in vitro of bundle of microfilaments isolated from Nitella cell. J Cell Biol 87:569–578. https://doi.org/10.1083/jcb.87.3.569

Houdusse A, Szent-Gyorgyi AG, Cohen C (2000) Three conformational states of scallop myosin S1. Proc Natl Acad Sci U S A 97:11238–11243. https://doi.org/10.1073/pnas.200376897

Huang B, Bates M, Zhuang X (2009) Super-resolution fluorescence microscopy. Annu Rev Biochem 78:993–1016. https://doi.org/10.1146/annurev.biochem.77.061906.092014

Huxley HE (1969) The mechanism of muscular contraction. Science 164:1356–1365. https://doi.org/10.1126/science.164.3886.1356

Ida H, Takahashi Y, Kumatani A, Shiku H, Matsue T (2017) High speed scanning ion conductance microscopy for quantitative analysis of nanoscale dynamics of microvilli. Anal Chem 89:6015–6020. https://doi.org/10.1021/acs.analchem.7b00584

Ikezaki K, Komori T, Arai Y, Yanagida T (2015) Lever arm extension of myosin VI is unnecessary for the adjacent binding state. Biophysics 11:47–53. https://doi.org/10.2142/biophysics.11.47

Ip K, Sobieszek A, Solomon D, Jiao Y, Pare PD, Seow CY (2007) Physical integrity of smooth muscle myosin filaments is enhanced by phosphorylation of the regulatory myosin light chain. Cell Physiol Biochem 20:649–658. https://doi.org/10.1159/000107548

Iwasaki T, Washio M, Yamamoto K (2005) Atomic force microscopy of thermally treated myosin filaments. J Agric Food Chem 53:4589–4592. https://doi.org/10.1021/jf0500381

Jacobs DJ, Trivedi D, David C, Yengo CM (2011) Kinetics and thermodynamics of the rate-limiting conformational change in the actomyosin V mechanochemical cycle. J Mol Biol 407:716–730. https://doi.org/10.1016/j.jmb.2011.02.001

Kaiser CM, Bujalowski PJ, Ma L, Anderson J, Epstein HF, Oberhauser AF (2012) Tracking UNC-45 chaperone-myosin interaction with a titin mechanical reporter. Biophys J 102:2212–2219. https://doi.org/10.1016/j.bpj.2012.03.013

Karsai A, Kellermayer MS, Harris SP (2011) Mechanical unfolding of cardiac myosin binding protein-C by atomic force microscopy. Biophys J 101:1968–1977. https://doi.org/10.1016/j.bpj.2011.08.030

Kellermayer M, Sziklai D, Papp Z, Decker B, Lakatos E, Martonfalvi Z (2018) Topology of interaction between titin and myosin thick filaments. J Struct Biol 203:46–53. https://doi.org/10.1016/j.jsb.2018.05.001

Kiss B, Rohlich P, Kellermayer MS (2011) Structure and elasticity of desmin protofibrils explored with scanning force microscopy. J Mol Recognit 24:1095–1104. https://doi.org/10.1002/jmr.1158

Kodera N, Ando T (2014) The path to visualization of walking myosin V by high-speed atomic force microscopy. Biophys Rev 6:237–260. https://doi.org/10.1007/s12551-014-0141-7

Kodera N, Yamashita H, Ando T (2005) Active damping of the scanner for high-speed atomic force microscopy. Rev Sci Instrum 76:053708. https://doi.org/10.1063/1.1903123

Kodera N, Sakashita M, Ando T (2006) Dynamic proportional-integral-differential controller for high-speed atomic force microscopy. Rev Sci Instrum 77. https://doi.org/10.1063/1.2336113

Kodera N, Yamamoto D, Ishikawa R, Ando T (2010) Video imaging of walking myosin V by high-speed atomic force microscopy. Nature 468:72–76. https://doi.org/10.1038/nature09450

Koide H, Kinoshita T, Tanaka Y, Tanaka S, Nagura N, Meyer zu Horste G, Miyagi A, Ando T (2006) Identification of the single specific IQ motif of myosin V from which calmodulin dissociates in the presence of Ca2+. Biochemistry 45:11598–11604. https://doi.org/10.1021/bi0613877

Liu J, Taylor DW, Krementsova EB, Trybus KM, Taylor KA (2006) Three-dimensional structure of the myosin V inhibited state by cryoelectron tomography. Nature 442:208–211. https://doi.org/10.1038/nature04719

Martin SR, Bayley PM (2004) Calmodulin bridging of IQ motifs in myosin-V. FEBS Lett 567:166–170. https://doi.org/10.1016/j.febslet.2004.04.053

Maschi D, Gramlich MW, Klyachko VA (2018) Myosin V functions as a vesicle tether at the plasma membrane to control neurotransmitter release in central synapses. eLife 7:e39440. https://doi.org/10.7554/eLife.39440

Mehta AD, Rock RS, Rief M, Spudich JA, Mooseker MS, Cheney RE (1999) Myosin-V is a processive actin-based motor. Nature 400:590–593. https://doi.org/10.1038/23072

Nakajima H, Kunioka Y, Nakano K, Shimizu K, Seto M, Ando T (1997) Scanning force microscopy of the interaction events between a single molecule of heavy meromyosin and actin. Biochem Biophys Res Commun 234:178–182. https://doi.org/10.1006/bbrc.1997.6612

Nishikawa S, Arimoto I, Ikezaki K, Sugawa M, Ueno H, Komori T, Iwane AH, Yanagida T (2010) Switch between large hand-over-hand and small inchworm-like steps in myosin VI. Cell 142:879–888. https://doi.org/10.1016/j.cell.2010.08.033

Oberhauser AF, Hansma PK, Carrion-Vazquez M, Fernandez JM (2001) Stepwise unfolding of titin under force-clamp atomic force microscopy. Proc Natl Acad Sci U S A 98:468–472. https://doi.org/10.1073/pnas.021321798

Oguchi Y, Mikhailenko SV, Ohki T, Olivares AO, De La Cruz EM, Ishiwata S (2008) Load-dependent ADP binding to myosins V and VI: implications for subunit coordination and function. Proc Natl Acad Sci U S A 105:7714–7719. https://doi.org/10.1073/pnas.0800564105

Okada T, Tanaka H, Iwane AH, Kitamura K, Ikebe M, Yanagida T (2007) The diffusive search mechanism of processive myosin class-V motor involves directional steps along actin subunits. Biochem Biophys Res Commun 354:379–384. https://doi.org/10.1016/j.bbrc.2006.12.200

Oke OA, Burgess SA, Forgacs E, Knight PJ, Sakamoto T, Sellers JR, White H, Trinick J (2010) Influence of lever structure on myosin 5a walking. Proc Natl Acad Sci U S A 107:2509–2514. https://doi.org/10.1073/pnas.0906907107

Olivares AO, Chang W, Mooseker MS, Hackney DD, De La Cruz EM (2006) The tail domain of myosin Va modulates actin binding to one head. J Biol Chem 281:31326–31336. https://doi.org/10.1074/jbc.M603898200

Purcell TJ, Morris C, Spudich JA, Sweeney HL (2002) Role of the lever arm in the processive stepping of myosin V. Proc Natl Acad Sci U S A 99:14159–14164. https://doi.org/10.1073/pnas.182539599

Purcell TJ, Sweeney HL, Spudich JA (2005) A force-dependent state controls the coordination of processive myosin V. Proc Natl Acad Sci U S A 102:13873–13878. https://doi.org/10.1073/pnas.0506441102

Ricca BL, Rock RS (2010) The stepping pattern of myosin X is adapted for processive motility on bundled actin. Biophys J 99:1818–1826. https://doi.org/10.1016/j.bpj.2010.06.066

Rico F, Gonzalez L, Casuso I, Puig-Vidal M, Scheuring S (2013) High-speed force spectroscopy unfolds titin at the velocity of molecular dynamics simulations. Science 342:741–743. https://doi.org/10.1126/science.1239764

Rief M, Gautel M, Oesterhelt F, Fernandez JM, Gaub HE (1997) Reversible unfolding of individual titin immunoglobulin domains by AFM. Science 276:1109–1112. https://doi.org/10.1126/science.276.5315.1109

Rief M, Rock RS, Mehta AD, Mooseker MS, Cheney RE, Spudich JA (2000) Myosin-V stepping kinetics: a molecular model for processivity. Proc Natl Acad Sci U S A 97:9482–9486. https://doi.org/10.1073/pnas.97.17.9482

Rigotti DJ, Kokona B, Horne T, Acton EK, Lederman CD, Johnson KA, Manning RS, Kane SA, Smith WF, Fairman R (2005) Quantitative atomic force microscopy image analysis of unusual filaments formed by the Acanthamoeba castellanii myosin II rod domain. Anal Biochem 346:189–200. https://doi.org/10.1016/j.ab.2005.08.026

Robblee JP, Cao W, Henn A, Hannemann DE, De La Cruz EM (2005) Thermodynamics of nucleotide binding to actomyosin V and VI: a positive heat capacity change accompanies strong ADP binding. Biochemistry 44:10238–10249. https://doi.org/10.1021/bi050232g

Root DD, Yadavalli VK, Forbes JG, Wang K (2006) Coiled-coil nanomechanics and uncoiling and unfolding of the superhelix and alpha-helices of myosin. Biophys J 90:2852–2866. https://doi.org/10.1529/biophysj.105.071597

Rosenfeld SS, Sweeney HL (2004) A model of myosin V processivity. J Biol Chem 279:40100–40111. https://doi.org/10.1074/jbc.M402583200

Sakamoto T, Amitani I, Yokota E, Ando T (2000) Direct observation of processive movement by individual myosin V molecules. Biochem Biophys Res Commun 272:586–590. https://doi.org/10.1006/bbrc.2000.2819

Sakamoto T, Wang F, Schmitz S, Xu Y, Xu Q, Molloy JE, Veigel C, Sellers JR (2003) Neck length and processivity of myosin V. J Biol Chem 278:29201–29207. https://doi.org/10.1074/jbc.M303662200

Sakamoto T, Yildez A, Selvin PR, Sellers JR (2005) Step-size is determined by neck length in myo-

sin V. Biochemistry 44:16203–16210. https://doi.org/10.1021/bi0512086

Sakamoto T, Webb MR, Forgacs E, White HD, Sellers JR (2008) Direct observation of the mechanochemical coupling in myosin Va during processive movement. Nature 455:128–132. https://doi.org/10.1038/nature07188

Schwaiger I, Sattler C, Hostetter DR, Rief M (2002) The myosin coiled-coil is a truly elastic protein structure. Nat Mater 1:232–235. https://doi.org/10.1038/nmat776

Sellers JR, Veigel C (2010) Direct observation of the myosin-Va power stroke and its reversal. Nat Struct Mol Biol 17:590–595. https://doi.org/10.1038/nsmb.1820

Sheetz MP, Spudich JA (1983) Movement of myosin-coated fluorescent beads on actin cables in vitro. Nature 303:31–35. https://doi.org/10.1038/303031a0

Sheng S, Gao Y, Khromov AS, Somlyo AV, Somlyo AP, Shao Z (2003) Cryo-atomic force microscopy of unphosphorylated and thiophosphorylated single smooth muscle myosin molecules. J Biol Chem 278:39892–39896. https://doi.org/10.1074/jbc.M306094200

Shibata M, Uchihashi T, Ando T, Yasuda R (2015) Long-tip high-speed atomic force microscopy for nanometer-scale imaging in live cells. Sci Rep 5:8724. https://doi.org/10.1038/srep08724

Shiroguchi K, Kinosita K Jr (2007) Myosin V walks by lever action and Brownian motion. Science 316:1208–1212. https://doi.org/10.1126/science.1140468

Simeonov S, Schaffer TE (2019) High-speed scanning ion conductance microscopy for sub-second topography imaging of live cells. Nanoscale 11:8579–8587. https://doi.org/10.1039/c8nr10162k

Smith CA, Rayment I (1996) X-ray structure of the magnesium(II).ADP.vanadate complex of the Dictyostelium discoideum myosin motor domain to 1.9 A resolution. Biochemistry 35:5404–5417. https://doi.org/10.1021/bi952633+

Snyder GE, Sakamoto T, Hammer JA 3rd, Sellers JR, Selvin PR (2004) Nanometer localization of single green fluorescent proteins: evidence that myosin V walks hand-over-hand via telemark configuration. Biophys J 87:1776–1783. https://doi.org/10.1529/biophysj.103.036897

Sun Y, Schroeder HW 3rd, Beausang JF, Homma K, Ikebe M, Goldman YE (2007) Myosin VI walks "wiggly" on actin with large and variable tilting. Mol Cell 28:954–964. https://doi.org/10.1016/j.molcel.2007.10.029

Sun Y, Sato O, Ruhnow F, Arsenault ME, Ikebe M, Goldman YE (2010) Single-molecule stepping and structural dynamics of myosin X. Nat Struct Mol Biol 17:485–491. https://doi.org/10.1038/nsmb.1785

Syed S, Snyder GE, Franzini-Armstrong C, Selvin PR, Goldman YE (2006) Adaptability of myosin V studied by simultaneous detection of position and orientation. EMBO J 25:1795–1803. https://doi.org/10.1038/sj.emboj.7601060

Taniguchi M, Matsumoto O, Suzuki S, Nishino Y, Okuda A, Taga T, Yamane T (2003) MgATP-induced conformational changes in a single myosin molecule observed by atomic force microscopy: periodicity of substructures in myosin rods. Scanning 25:223–229. https://doi.org/10.1002/sca.4950250502

Thirumurugan K, Sakamoto T, Hammer JA 3rd, Sellers JR, Knight PJ (2006) The cargo-binding domain regulates structure and activity of myosin 5. Nature 442:212–215. https://doi.org/10.1038/nature04865

Tilelli CQ, Martins AR, Larson RE, Garcia-Cairasco N (2003) Immunohistochemical localization of myosin Va in the adult rat brain. Neuroscience 121:573–586. https://doi.org/10.1016/S0306-4522(03)00546-3

Toprak E, Enderlein J, Syed S, McKinney SA, Petschek RG, Ha T, Goldman YE, Selvin PR (2006) Defocused orientation and position imaging (DOPI) of myosin V. Proc Natl Acad Sci U S A 103:6495–6499. https://doi.org/10.1073/pnas.0507134103

Trybus KM, Krementsova E, Freyzon Y (1999) Kinetic characterization of a monomeric unconventional myosin V construct. J Biol Chem 274:27448–27456. https://doi.org/10.1074/jbc.274.39.27448

Uchihashi T, Kodera N, Ando T (2012) Guide to video recording of structure dynamics and dynamic processes of proteins by high-speed atomic force microscopy. Nat Protoc 7:1193–1206. https://doi.org/10.1038/nprot.2012.047

Uemura S, Higuchi H, Olivares AO, De La Cruz EM, Ishiwata S (2004) Mechanochemical coupling of two substeps in a single myosin V motor. Nat Struct Mol Biol 11:877–883. https://doi.org/10.1038/nsmb806

Veigel C, Wang F, Bartoo ML, Sellers JR, Molloy JE (2002) The gated gait of the processive molecular motor, myosin V. Nat Cell Biol 4:59–65. https://doi.org/10.1038/ncb732

Veigel C, Schmitz S, Wang F, Sellers JR (2005) Load-dependent kinetics of myosin-V can explain its high processivity. Nat Cell Biol 7:861–869. https://doi.org/10.1038/ncb1287

Volkmann N, Liu H, Hazelwood L, Krementsova EB, Lowey S, Trybus KM, Hanein D (2005) The structural basis of myosin V processive movement as revealed by electron cryomicroscopy. Mol Cell 19:595–605. https://doi.org/10.1016/j.molcel.2005.07.015

von Castelmur E, Strumpfer J, Franke B, Bogomolovas J, Barbieri S, Qadota H, Konarev PV, Svergun DI, Labeit S, Benian GM, Schulten K, Mayans O (2012) Identification of an N-terminal inhibitory extension as the primary mechanosensory regulator of twitchin kinase. Proc Natl Acad Sci U S A 109:13608–13613. https://doi.org/10.1073/pnas.1200697109

Walker ML, Burgess SA, Sellers JR, Wang F, Hammer JA 3rd, Trinick J, Knight PJ (2000) Two-headed binding of a processive myosin to F-actin. Nature 405:804–807. https://doi.org/10.1038/35015592

Wang F, Chen L, Arcucci O, Harvey EV, Bowers B, Xu Y, Hammer JA 3rd, Sellers JR (2000) Effect of ADP and ionic strength on the kinetic and motile properties of recombinant mouse myosin V. J Biol Chem 275:4329–4335. https://doi.org/10.1074/jbc.275.6.4329

Warshaw DM, Kennedy GG, Work SS, Krementsova EB, Beck S, Trybus KM (2005) Differential labeling of myosin V heads with quantum dots allows direct visualization of hand-over-hand processivity. Biophys J 88:L30–L32. https://doi.org/10.1529/biophysj.105.061903

Watanabe S, Ando T (2017) High-speed XYZ-nanopositioner for scanning ion conductance microscopy. Appl Phys Lett 111:113106. https://doi.org/10.1063/1.4993296

Watanabe M, Nomura K, Ohyama A, Ishikawa R, Komiya Y, Hosaka K, Yamauchi E, Taniguchi H, Sasakawa N, Kumakura K, Ushiki T, Sato O, Ikebe M, Igarashi M (2005) Myosin-Va regulates exocytosis through the submicromolar Ca2+−dependent binding of syntaxin-1A. Mol Biol Cell 16:4519–4530. https://doi.org/10.1091/mbc.e05-03-0252

Watanabe H, Uchihashi T, Kobashi T, Shibata M, Nishiyama J, Yasuda R, Ando T (2013) Wide-area scanner for high-speed atomic force microscopy. Rev Sci Instrum 84:053702. https://doi.org/10.1063/1.4803449

Watanabe S, Kitazawa S, Sun L, Kodera N, Ando T (2019) Development of high-speed ion conductance microscopy. Rev Sci Instrum 90(12):123704

Yamamoto D, Nagura N, Omote S, Taniguchi M, Ando T (2009) Streptavidin 2D crystal substrates for visualizing biomolecular processes by atomic force microscopy. Biophys J 97:2358–2367. https://doi.org/10.1016/j.bpj.2009.07.046

Yamamoto D, Uchihashi T, Kodera N, Yamashita H, Nishikori S, Ogura T, Shibata M, Ando T (2010) High-speed atomic force microscopy techniques for observing dynamic biomolecular processes. Methods Enzymol 475:541–564. https://doi.org/10.1016/S0076-6879(10)75020-5

Yamashita H, Taoka A, Uchihashi T, Asano T, Ando T, Fukumori Y (2012) Single-molecule imaging on living bacterial cell surface by high-speed AFM. J Mol Biol 422:300–309. https://doi.org/10.1016/j.jmb.2012.05.018

Yildiz A, Forkey JN, McKinney SA, Ha T, Goldman YE, Selvin PR (2003) Myosin V walks hand-over-hand: single fluorophore imaging with 1.5-nm localization. Science 300:2061–2065. https://doi.org/10.1126/science.1084398

Yildiz A, Park H, Safer D, Yang Z, Chen LQ, Selvin PR, Sweeney HL (2004) Myosin VI steps via a hand-over-hand mechanism with its lever arm undergoing fluctuations when attached to actin. J Biol Chem 279:37223–37226. https://doi.org/10.1074/jbc.C400252200

Zhang Y, Shao Z, Somlyo AP, Somlyo AV (1997) Cryo-atomic force microscopy of smooth muscle myosin. Biophys J 72:1308–1318. https://doi.org/10.1016/S0006-3495(97)78777-0

Zhong Q, Inniss D, Kjoller K, Elings VB (1993) Fractured polymer silica fiber surface studied by tapping mode atomic-force microscopy. Surf Sci 290:L688–L692. https://doi.org/10.1016/0039-6028(93)90582-5

8 How Myosin 5 Walks Deduced from Single-Molecule Biophysical Approaches

James R. Sellers and Yasuharu Takagi

Abstract

Myosin 5a is a two-headed myosin that functions as a cargo transporter in cells. To accomplish this task it has evolved several unique structural and kinetic features that allow it to move processively as a single molecule along actin filaments. A plethora of biophysical techniques have been used to elucidate the detailed mechanism of its movement along actin filaments *in vitro*. This chapter describes how this mechanism was deduced.

Keywords

Myosin · Kinetics · Mechanochemistry · Optical trapping · iSCAT · Single molecule

8.1 Introduction

Humans have three genes encoding for the myosin 5 heavy chain that give rise to the paralogs myosins 5a, 5b and 5c (Berg et al. 2001). Each of these myosins can be described as having four domains (Fig. 8.1). There is a motor domain that binds to actin and contains the catalytic site for ATP hydrolysis. This is followed by a "neck" domain consisting of a small globular region, termed the converter domain, from which emerges a single α-helical segment of the heavy chain that contains six IQ motifs, which bind calmodulin or calmodulin-family member light chains. This extended structure serves as a stiff lever arm to magnify ATP- and actin-dependent small conformational changes in the motor domain into larger scale movements that drive the translocation of the protein along actin filaments. The motor domain and the neck region are often referred to as the "head" of the myosin. Following the neck region, the heavy chain is composed of a long stretch of amino acids forming an interrupted coiled-coil domain by homo-dimerization with another myosin 5 heavy chain. This region is termed the "tail" or "stalk". The dimerization produces a molecule that has two motor domains, but, unlike class II myosins, the coiled-coil tail of myosin 5 does not self- associate into filaments. The last domain is the globular tail domain (GTD), which binds various cargo adapters in the cell and is involved in regulation of the enzymatic activity of the molecule through an autoinhibitory interaction with the motor domains (Thirumurugan et al. 2006; Liu et al. 2006).

The three myosin 5 paralogs appear to have non-redundant functions in the cell. The best

J. R. Sellers (✉) · Y. Takagi
Laboratory of Molecular Physiology, Cell and Developmental Biology Center, National Heart, Lung, and Blood Institute, National Institutes of Health, Bethesda, MD, USA
e-mail: sellersj@nhlbi.nih.gov

L. M. Coluccio (ed.), *Myosins*, Advances in Experimental Medicine and Biology 1239,
https://doi.org/10.1007/978-3-030-38062-5_8

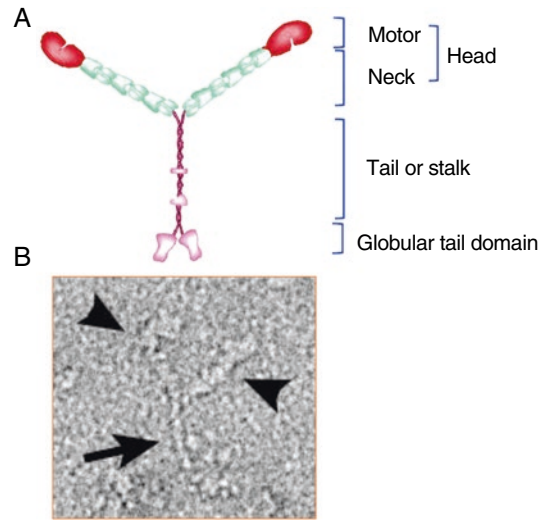

Fig. 8.1 A Myosin 5 structure. (**a**) Schematic of myosin 5 structure showing the four major domains. (**b**). Negatively-stained image of a full-length mouse myosin 5a molecule. This image was taken from Wang et al. 2004

characterized myosin 5 paralog with respect to its cellular function is myosin 5a, which will be the focus of this chapter (Hammer and Sellers 2012). Myosin 5a has two well characterized functions. It is involved in the later stages of melanosome transport in melanocytes and specifically helps to bring the melanosome to the tips of the dendritic processes where it can be phagocytized by the keratinocyte to facilitate skin pigmentation (Wu et al. 1998, 2012). The long-distance transport of melanosomes from their synthesis in the cell body into the dendritic tips of the cell is accomplished by the microtubule-dependent motors kinesin and dynein. In Purkinje neurons, myosin 5a is responsible for transporting endoplasmic reticulum into the dendritic spines (Wagner et al. 2011). Thus, myosin 5a is characterized as a cargo transporter. Mice that are lacking myosin 5a have pigment deficits in their coats and display severe ataxia (Mercer et al. 1991). Humans with point mutation have Griscelli's disease characterized by pigmentation defects and sometimes severe neurological defects depending on the location of the mutation (Pastural et al. 1997).

The discovery of myosin 5a in the early 1990's coincided with an amazing three decades of advancement in light microscopic techniques that allowed for the visualization and study of proteins at a single-molecule level. These include total *i*nternal *r*eflection *f*luorescence (TIRF) microscopy, super-resolution microscopy, *pol*arized *t*otal *i*nternal *r*eflection microscopy (polTIRF), *d*efocused *o*rientation and *p*osition *i*maging (DOPI) microscopy, optical trapping, *a*tomic *f*orce *m*icroscopy (AFM, high speed AFM) and *i*nterferometric light *scat*tering (iSCAT) microscopy. All of these techniques are described in detail in Chap. 6. TIRF microscopy allowed for the visualization of single fluorophores near the cover slip surface and, thus, allowed one to "see" single molecules of myosin 5. Super-resolution light microscopy allowed for precise localization of fluorophores at resolutions significantly higher (on the order of nanometers) than the diffraction barrier of light (250–300 nm). This technique was coined FIONA for *f*luorescence *i*maging at *o*ne *n*anometer *a*ccuracy and allowed one to follow the movement of myosin 5 along actin with high spatial resolution (Yildiz et al. 2003). Optical trapping allowed for the interrogation of the force dependent kinetics and mechanics of single myosin molecules. polTIRF and DOPI allowed for imaging the orientation and position of the probe attached to myosin while it is moving along actin filaments. Finally, iSCAT combined super-resolution localization precision with much higher sampling rates (Andrecka et al. 2016).

Many of these studies were carried out with myosin 5a purified from brain tissue, but during this time interval it became possible to use the baculovirus/Sf9 expression system (Wang et al. 2000) to produce recombinant myosin 5a. In this

system one could produce smaller, enzymatically-active fragments corresponding to single-headed subfragment-1 (S1) or double-headed heavy meromyosin (HMM) that had been produced by controlled proteolytic cleavage of skeletal muscle myosin 2 for many years and were so useful for biochemical and biophysical characterization of that myosin (Margossian and Lowey 1982). The use of the smaller fragments was important since full-length myosin 5a is auto inhibited by a conformational change whereby the globular tail domain folds back and directly interacts with its motor domain (Thirumurugan et al. 2006; Liu et al. 2006). The baculovirus/Sf9 system also allowed for the production of mutant myosin 5a fragments, such as ones with shorter or longer neck regions or those that were fused with green fluorescent protein or moieties to allow attachment of quantum dots (Qdots) or beads directly to the protein. These custom designed proteins were useful in addressing specific questions as will be seen below.

8.2 Thesis

It can be argued that myosin 5a is the best-characterized myosin with respect to its mechanochemical properties and that it is ideally suited for many single-molecule biophysical studies using the techniques just mentioned. Biochemical and biophysical studies by many investigators have arrived at a consensus viewpoint.

- Myosin 5a is a two-headed molecular motor that moves processively along actin filaments.
- It does so by alternating the positions of the two motor domains in a hand-over-hand manner.
- Each motor domain moves 72 nm during a stride, which results in incremental steps of 36 nm for the center of mass of the molecule.
- The neck domain acts as a lever arm to facilitate this movement.
- The kinetics of the two motor domains are gated to enhance the processivity.
- One ATP molecule is hydrolyzed per step.

This review will document the evidence to support each of these statements. It will show how a plethora of biochemical, structural and biophysical techniques were employed and will showcase how myosin 5a is almost uniquely suitable for such studies. The results will back the statement made earlier that myosin 5a is the best-understood cytoskeletal molecular motor. Note that this endeavor involved many excellent laboratories and the authors apologize to authors whose studies are not referenced. The work is presented thematically rather than historically so that some of the described experiments published in the last few years are presented alongside work that may date back to the early 1990s.

8.3 Myosin 5a Is a Two-Headed Motor

Myosin 5a was discovered independently in three laboratories at nearly the same time in yeast, chickens, and mice (Johnston et al. 1991; Espindola et al. 1992; Mercer et al. 1991). The protein was purified from chicken brain as a calmodulin-binding ATPase (Espindola et al. 1992). Subsequent cloning and sequencing of the cDNA encoding for this protein revealed it to be homologous to the yeast and mouse myosin 5 sequences reported earlier. Rotary-shadowing electron microscopy of the purified protein from chicken brain showed that, like the conventional class II myosins, myosin 5a also dimerized via a coiled-coil motif to form a two-headed motor protein, albeit with a shorter coiled-coil (Cheney et al. 1993). However, it had distinct features not found in class II myosins. The length of the head domain (including the neck) was 30 nm, consistent with the presence of six IQ motifs in the amino acid sequence. The coiled-coil regions terminated in large globular tail domains. The two-headed structure of myosin 5a was confirmed in negatively-stained images of protein either purified from myosin brain or from material that was produced by overexpression in Sf9 cells using the baculovirus infection system (Walker et al. 2000; Wang et al. 2004) (Fig. 8.1b).

8.4 Single Molecules of Myosin 5a Move Processively Along Actin Filaments In Vitro

Processivity for myosins is defined as the ability of single myosin molecules to take multiple ATP-dependent forward movements on actin during an attachment event. Members of the myosin superfamily can be broadly classified into two functional classes: nonprocessive and processive (De La Cruz and Ostap 2004). Examples of nonprocessive myosins include striated muscle myosin, which polymerizes into long bipolar filaments, and some single-headed myosins such as class I myosins.

To understand the mechanisms allowing for processivity, it is necessary to describe the actomyosin kinetic cycle. Figure 8.2 shows the minimal kinetic cycle that is used by all active myosins. Notice that myosin cycles between states that have a high affinity for actin (strongly-bound states) and ones that have only a weak affinity for actin (weakly-bound states). Also, note that the neck region moves from a pre-power stroke position to a post-power stroke position in order to propel the myosin along the actin filament. To describe the cycle, we start when myosin is bound to actin with no nucleotide present (AM). This is a high-affinity state. The position of the neck region is in the post-power stroke position. Upon binding of ATP, the actin affinity is dramatically reduced and M•ATP dissociates from actin. ATP hydrolysis occurs, but both products remain bound to the myosin (M•ADP•Pi). This is coupled to a conformational change that results in a rigid body movement of the neck region to the pre-power stroke state. The states shown in the brackets are all in rapid equilibrium and here the myosin with ATP or its hydrolysis products interact with actin only transiently. Pi is released when the myosin rebinds actin. Release of Pi from the motor is catalyzed by actin and the resulting M•ADP complex binds tightly to actin. The neck region undergoes a rigid body motion to produce a power stroke. It is debated whether this occurs upon Pi release, ADP release or in a conformational change preceding ADP release. Evidence will be presented for a two-step power stroke. The dissociation of ADP brings the cycle back to the AM complex, which will then bind ATP, thus restarting the cycle.

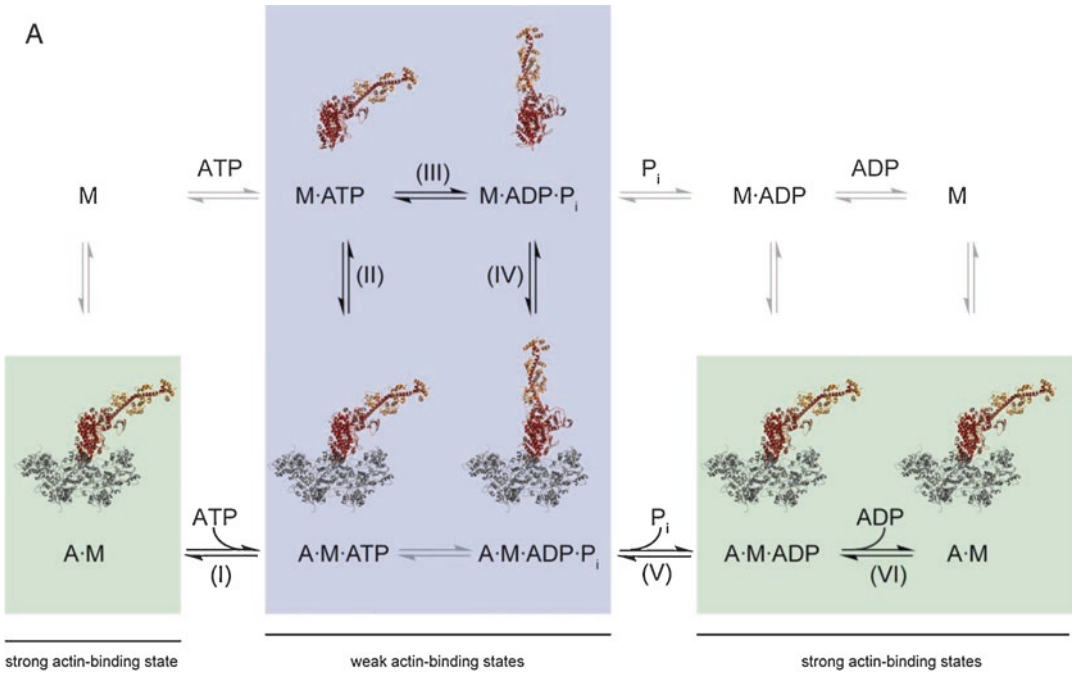

Fig. 8.2 Kinetic cycle for a single head of myosin 5a. See description in the text. From Heissler and Sellers 2016

An important concept in myosin kinetics is the duty ratio, which is the fractional time of the kinetic cycle that myosin spends strongly bound to actin. The duty ratio is essentially set by the ratio of the ADP-release time of AM compared to the overall cycle time. If Pi release is rate limiting, the steady-state intermediates (M•ATP and M•ADP•Pi) will bind weakly to actin, but if ADP release is rate limiting, the steady-state intermediate will be AM•ADP, where myosin and actin bind with high affinity.

Two primary features distinguish processive myosins from nonprocessive ones. First, to be processive as a single molecule, the presence of two motor domains (i.e., a dimeric myosin) is required to ensure that at least one of the motor domains is bound to actin while the other is searching for a new actin-binding site. Note that two heads are not sufficient for processive motion. For example, the two-headed skeletal muscle myosin 2 paralogs are not processive as single molecules. Second, the kinetics of ATP hydrolysis by the myosin must result in a high duty ratio. The two-headed skeletal muscle myosins are rate limited by Pi release from AM•ADP•Pi and have a low duty ratio (Bloemink and Geeves 2011). Thus, despite having two heads per molecule they are not processive. They have evolved to work in the context of a large filament array that is capable of rapidly shortening the sarcomere. De La Cruz et al. (1999) determined the kinetic mechanism of the single-headed recombinant S1-like fragment of chicken myosin 5a using steady-state and transient kinetic mechanisms. In marked contrast to the well-established kinetic mechanism for skeletal muscle myosin, they found that ADP release from the AM•ADP complex was rate limiting (~12 s^{-1}, which was equal to the steady state actin-activated ATPase rate) and that phosphate release was fast (at ~120 s^{-1}). This means that the steady-state intermediate for myosin 5a is AM•ADP. The calculated duty ratio for myosin 5a was 0.67 compared to values of 0.02–0.05 for nonprocessive motors such as fast skeletal muscle myosin. These kinetics help ensure that at least one of the two motor domains of myosin 5a is bound to actin at any given time.

A recombinant myosin 5a HMM was produced in Sf9 cells. This fragment was imaged by negative-stain electron microscopy (EM) when mixed with actin filaments in the presence of ATP (Walker et al. 2000). As expected for a processive motor, most of the molecules were bound to the actin filament via both of their heads with a relative constant separation of the two motors (Fig. 8.3a, b). Some molecules were bound via only one of the two heads and in these cases the neck region of the bound head could be seen in two positions representing the pre- and the post-power stroke states (Fig. 8.3c). When the attached head was in the post-power stroke position, the free head was in a position to bind to a new forward actin-binding site.

The technique of optical trapping of myosin is described in Chap. 6. The "three-bead" optical trapping geometry was first used to study single molecules of myosin 5a. Briefly, this technique involves creating two optical traps in a light microscope (Fig. 8.4A). One-micron-sized polystyrene beads are trapped and used to capture an actin filament between them creating a dumbbell-like structure. The suspended actin filament is brought in close contact to a larger silica bead that is stuck to the surface. Myosin 5a is sparsely bound to the surface and to the surface-attached bead. A myosin 5a molecule on the surface bead will interact with the suspended actin filament. The position of the trapped beads tethering the actin filament are typically monitored via a quadrant photodetector with nanometer spatial precision and millisecond temporal resolution. The beads fluctuate within the trap driven by thermal noise. When a surface-attached myosin binds the actin filament, the magnitude of the thermal noise is reduced since the myosin 5a motor domain acts as another spring in the system. When a single-headed S1 fragment of myosin 5a was used, only single attachments followed by dissociation events were seen (Fig. 8.4B) (Veigel et al. 2002). However, when a two-headed myosin 5a was used, most attachment events resulted in multiple discrete steps in which the molecule pulled the actin filament as the myosin underwent its consecutive power strokes (Fig. 8.4C). This demonstrated that myosin 5a was able to move

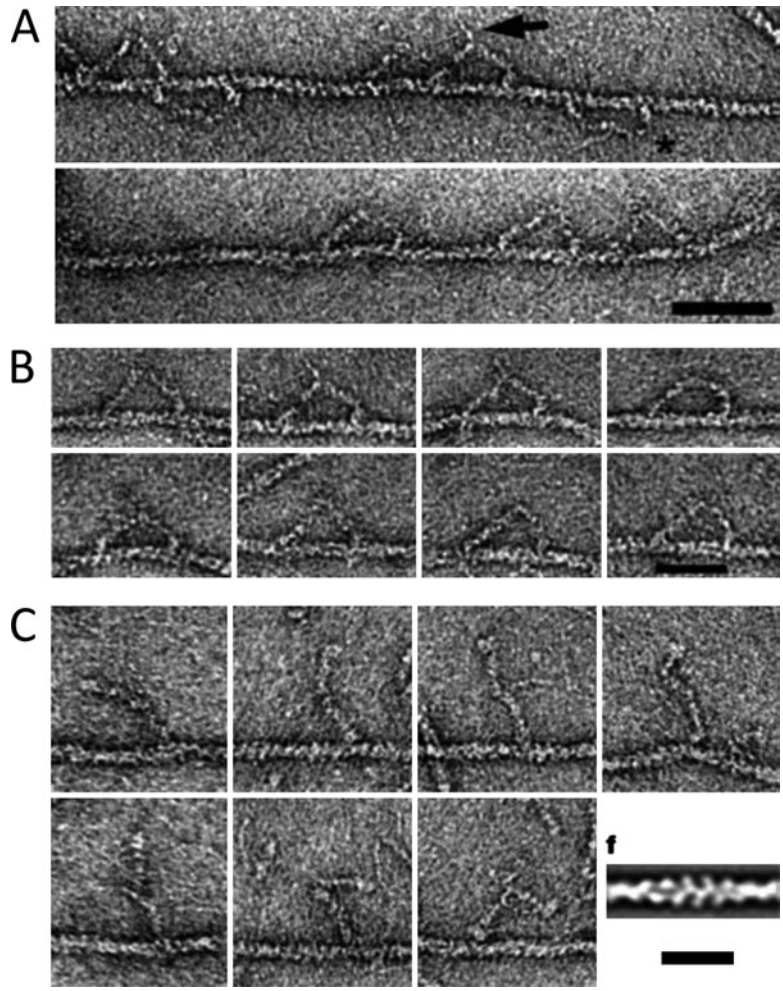

Fig. 8.3 EM of myosin 5a HMM bound to F-actin. (**a**). Several examples of myosin 5a HMM molecules bound to actin via two heads in the presence of 1 μM ATP. Myosin molecules would be walking towards the right. The arrow points to the coiled-coil tail fragment. (**b**). Galleries of single HMM molecules. (**c**). Examples of myosin 5a HMM bound to actin via a single head in the presence of 1 μM ATP. Note that progressing from the upper left-hand panel these images were chosen to simulate a possible walking cycle where the unattached head is unable to explore the forward binding sites on actin until the attached head undergoes its power stroke. Scale bar = 50 nm in A-B. All these images were taken from Walker et al. (2000)

processively (Mehta et al. 1999; Rief et al. 2000; Veigel et al. 2002). Each myosin power stroke incrementally pulled the trapped bead farther from the center of the trap and built up force. Once the force on the myosin was equal to the force that a myosin can exert there was a prolonged stall event and the myosin 5a would eventually dissociate from actin and, often, begin a new processive run. This peak force, called the stall force, was about 3 pN for myosin 5a (Mehta et al. 1999).

Another direct demonstration of a processive movement by myosin 5 was from Sakamoto et al. (Sakamoto et al. 2000), who visualized the movement of single fluorescently-labeled myosin 5a molecules on actin filaments bound to a coverslip surface using total internal fluorescence (TIRF) microscopy. Myosin was fluorescently-labeled by exchanging dye-labeled calmodulin subunits into the molecule. Similar results were later obtained by imaging myosin 5a fused at the N-terminus with green fluorescent protein (GFP) or labeled in various means with a quantum dot (QD) (Snyder et al. 2004; Warshaw et al. 2005). From these videos one could determine the velocity of movement and the characteristic run length. Typical values for the velocities were 0.5 to 1 μm/s and 0.7 to 1.5 μm for the run length (Bao et al. 2013; Hodges et al. 2007).

Using high speed atomic force microscopy (AFM), single molecules of myosin 5a could be imaged while attached to actin in the presence of ATP (Kodera et al. 2010). The two heads were bound at positions consistent with that seen by electron microscopy, and the molecule could be observed moving processively along actin (see

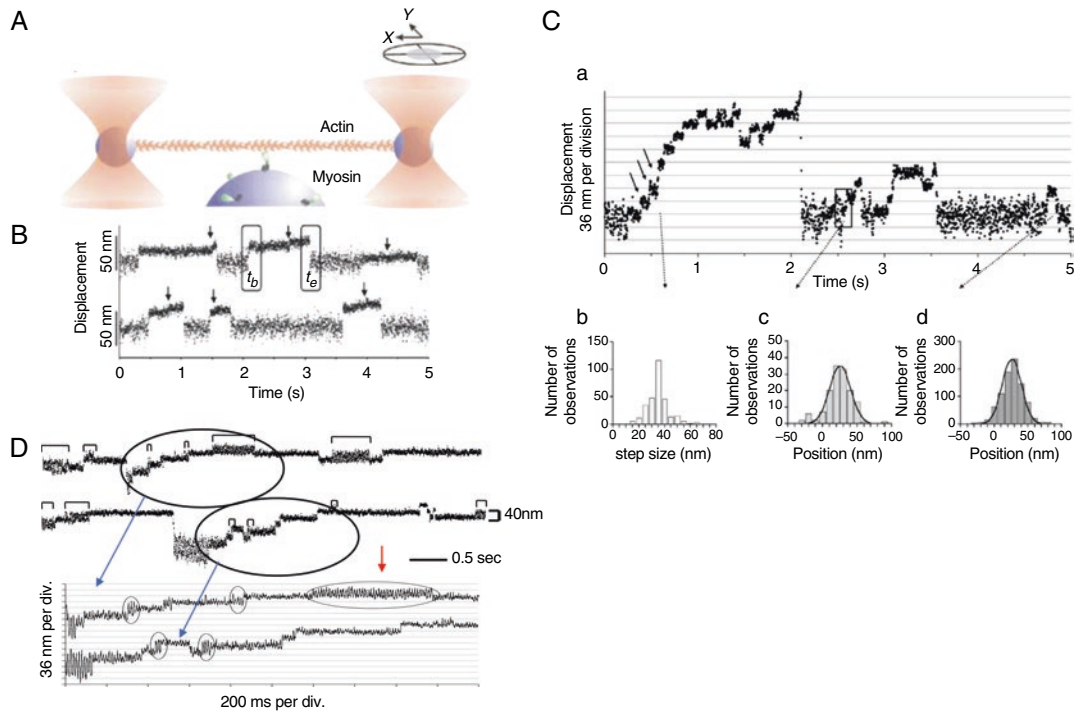

Fig. 8.4 Optical trapping of myosin 5a reveals details about the power stroke and stepping mechanism. (A). Schematic of the three-bead optical trapping geometry. See Chap. 6 for details of this technique. (**B**). Optical trapping of single-headed myosin 5a. Note that only single attachment/detachment cycles are observed. Arrows point to the presence of a second step of the power stroke, which will be described in Fig. 8.7. (**Ca**). Optical trapping record of a two-headed myosin 5 HMM. Note that abrupt forward movements followed by sustained dwell periods are observed as the myosin 5a processively pulls the actin filament away from the center of the trap. (**Cb**). Step-size histogram of the second to fourth steps in such processive runs. A mean value of 34.5 ± 0.6 nm was obtained. (**Cc**). Histogram of the first step in the staircases. Mean = 26.2 ± 2.3 nm (**Cd**). Histogram of single step events. Mean = 25.7 ± 0.6 nm. (**D**). Stiffness measurements of myosin 5a measured by driving one bead with a sinusoidal forcing function at a peak-to-peak amplitude of 250 nm. The position of each bead was monitored and the time dependence of the driven bead is shown for two records. Positional data from two areas are shown in expanded form below. Brackets illustrate regions of reduced stiffness consistent with the attachment of only one of the two heads of myosin 5a to actin that often transiently occur between stepping events. The red arrow in the lower panel demonstrates an area during stall that the myosin is bound via only one head for an extended period of time before returning to a two-head attached state. Figure taken from Veigel et al. (2002)

Chap. 7 for details of these experiments). The acquisition speed was not sufficiently high to follow the detached head as it transitioned to a new actin-binding site. However, if the surface was crowded by binding excess streptavidin, some images showed the restricted movement of the detached head as it tried to reposition itself in a forward-binding site.

The most recent confirmation that myosin 5a is a processive motor used a novel microscopic technique (iSCAT) (Andrecka et al. 2016) that is also described in Chap. 6. This technique used interferometric light scattering coupled with background subtraction to extract the small light scattering from a single myosin 5a molecule. Ortega et al. (Ortega et al. 2014) showed that single, unlabeled myosin 5a HMM molecules could be imaged and that these molecules moved processively along actin filaments. If a gold bead was attached to the motor domain of myosin 5a, the movement of the myosin could be tracked with very high spatial and temporal resolution due to the intense light scattering from the bead (Andrecka et al. 2015).

All of these techniques demonstrated that *in vitro* myosin 5a is a processive motor protein. This is consistent with the *in vivo* function of the protein as a cargo motor (Hammer and Sellers 2012). The ability of myosin 5a to function as a cargo motor could be simulated *in vitro* by attaching myosin 5a to micron-sized beads or lipid vesicles (Ali et al. 2008, 2016; Lombardo et al. 2017, 2019). Studies showed that even single molecules of myosin 5a could transport these artificial cargoes for distances approximately a micron in length and that if multiple myosin 5a motors were present on a bead, the run lengths were somewhat longer. More complex actin networks could be created *in vitro* where two actin filaments are crossed at various angles or even three-dimensional networks where actin filament meshworks were created by suspending actin filaments from different sized beads attached to the surface (Ali et al. 2007; Lombardo et al. 2019). Myosin 5 could switch from one filament track to another. Myosin 5 moves processively along single actin filament as well as bundles of actin filaments and can take occasional side steps from one filament to another (Bao et al. 2013).

8.5 Myosin 5a Takes 36-nm Steps and Moves in a "Hand-over-Hand" Mechanism Wherein the Two Motor Domains Alternate Being in the Leading and Trailing Positions

The actin filament is a polar biological polymer where one end, the + or barbed end, polymerizes faster than the other. In a muscle fiber the + ends are located at the Z-line. In the gliding actin *in vitro* motility assay, most myosins, including myosin 5a, propel actin filaments with the - end leading with myosin 6 being the only motor that moves actin in the opposite direction (Wells et al. 1999).

Several models might account for the ability of a two-headed myosin to move processively on actin filaments towards the + end (Fig. 8.5). The myosin might move in an "inchworm-like" manner where the rear motor domain detaches and rebinds to the actin subunit just behind the attached lead motor. The lead motor could then detach and reattach some distance forward to a new actin subunit. The cycle would then repeat itself. This mechanism would keep the two-headed molecule from dissociating from actin while moving forward and the same myosin head would always be in the leading position. A second model was proposed by Yanagida and co-workers in a series of papers (Watanabe et al. 2004; Tanaka et al. 2002). In this model, myosin would have a biased forward diffusion along an actin filament dwelling at certain locations before diffusing again, and there is not a tight coupling between ATP hydrolysis and movement. There is precedent for this type of diffusion of proteins along microtubules although it is not directional (Lu et al. 2009; Ali et al. 2007). The last model and the one where there is now general agreement is that myosin 5a moves in a hand-over-hand mechanism where the rear motor domain dissociates allowing the lever arm of the attached forward head to undergo its power stroke. This propels the detached head forward allowing it to reattach and become the new forward head. The dissociation of the rear head occurs when the ADP bound to that head dissociates allowing ATP to rapidly rebind which dramatically weakens the binding affinity of that head for actin.

The evidence to support the hand-over-hand model came from several methods. Negatively-stained EM images of myosin 5a HMM molecules interacting with actin in the presence of ATP showed that the two heads of myosin 5a were most often separated by 13 actin subunits, but head separations of 11 and 15 actin subunits were also observed (Fig. 8.3a) (Walker et al. 2000). Most doubly-attached myosins showed an obvious polarity with respect to the shape of their lever arms. In Fig. 8.3b, examples of symmetric molecules are shown in the left panel with asymmetric ones in the others. In some cases, both lever arms were curved, but this curvature was particularly obvious for the lead lever arms which appeared to have conformation similar to a telemark skier's stance (Fig. 8.3b). No images were seen of two myosin heads bound in close apposi-

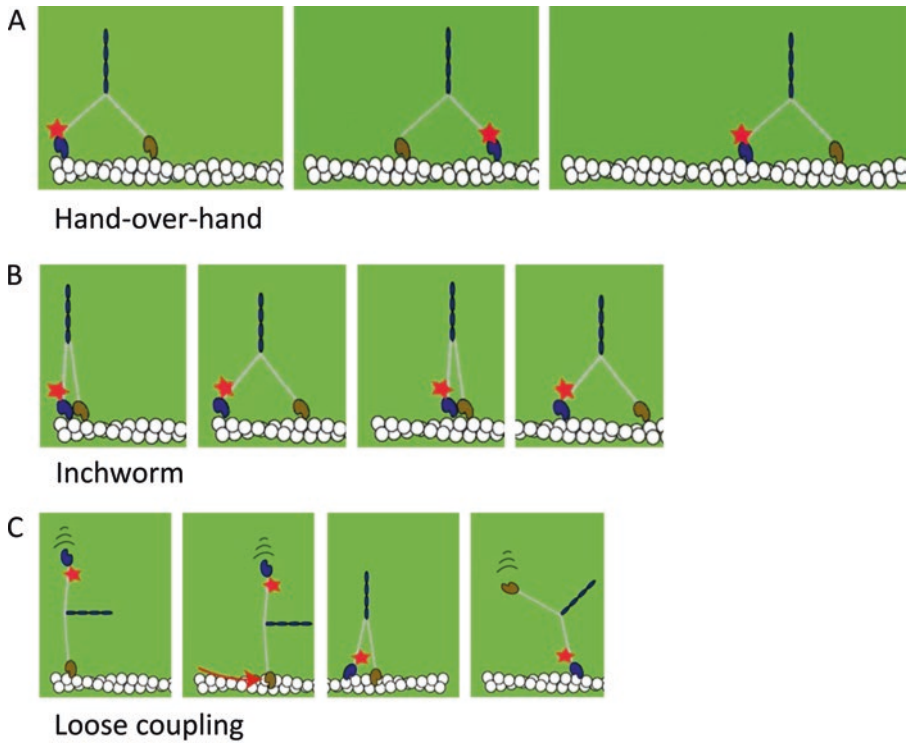

Fig. 8.5 Schematics depicting three possible stepping mechanisms. (**a**). *Hand-over-hand* mechanism in which the trail head detaches and becomes the new lead head. (**b**). *Inchworm* mechanism in which the forward head always steps before the trail head and the trail head always assumes a position behind the lead head when it transitions. (**c**). *Loose-coupling* mechanism where the movement of the molecule is not tightly coupled with ATP hydrolysis and where the ATP-containing head diffuses in a biased forward direction along the actin filament. The red star is used to mark one of the motors for clarity

tion as would be expected from an inchworm model. The converter region of myosin is a part of the neck region that undergoes the rigid body motion to produce a power stroke. Examination of image-averaged classes of the lead and trail myosin heads in the negatively-stained images and comparison to crystal structures of myosins in different nucleotide states showed that in most cases the two bound heads of myosin were in different conformational states as determined by the position of the converter domain, which was obvious even in EM images at 2-nm resolution (Fig. 8.6a) (Burgess et al. 2002). The lead heads appeared to be in a pre-power stroke state with the lever arm emerging from the back of the motor, whereas the trail head was in a post-power stroke state (Fig. 8.6a). In a small subset of attached myosins, the converter domain of the lead head lever emerged from the front of the motor and then bends strongly backward over the motor domains, indicating that in these myosins the lead head was in the post-power stroke position as was the trail head (Fig. 8.6b) (Oke et al. 2010). This occurred most commonly when the myosin heads were separated by 11 or 13 actin subunits and rarely in the case of heads separated by 15 subunits.

Some myosins were seen to be attached by only a single head (Fig. 8.3c). In these cases, the free head could be seen either in front of or behind the attached head depending on whether the attached head had yet undergone its power stroke, which could be determined since the polarity of the actin filament could be seen.

High speed AFM movies of myosin 5a moving on actin filaments showed that the trail head, upon detaching from actin, moved forward 72 nm to become the new lead head (Kodera et al. 2010).

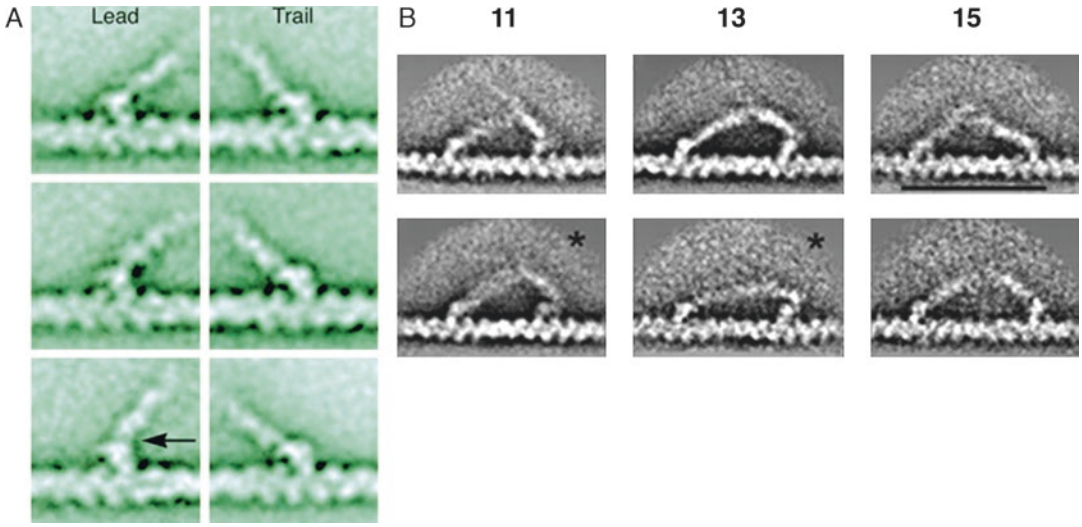

Fig. 8.6 Comparisons of the lead and trail myosin heads bound to actin. (**a**). Image averages of myosin 5a HMM heads bound to actin. It can be seen that the lever arm emerges from the front of the motor domain in the rear head and from the back of the motor domain in the lead head. The arrow marks the position of the pliant point. This figure was taken from Burgess et al. (2002). (**b**). Subclasses of myosin 5a HMM bound to actin with their motors 11, 13 and 15 actin subunits apart. The molecules in the upper row have straight lever arms and motor domains in the pre-power stroke conformation. The molecules in the lower row have curved lead lever arms. The two motors denoted with asterisks have post-power stroke lever arms. This figure is taken from Oke et al. (2010). Walking is toward the left in A and to the right in B

While the actual power stroke event was typically too fast to be observed with this technique, the movement of the head as it transitioned from the trail to lead position could be observed if the surface contained excess streptavidin molecules, which hindered the movement of the head.

Optical trapping of two-headed myosin 5a did not shed light on which of the three models for stepping was occurring, but it did show a discrete pattern of rapid forward movement followed by dwell periods whose lifetimes were a function of the ATP concentration (Fig. 8.4Ca) (Mehta et al. 1999; Rief et al. 2000; Veigel et al. 2002). A histogram of the step sizes during a processive run revealed a peak at ~36 nm (Fig. 8.4Cb), which is consistent with the spacing between two attached heads observed in the EM studies described above. The lifetimes of the dwell period at saturating ATP concentrations were consistent with ADP release from an AM•ADP complex being rate limiting. The stiffness of the acto-myosin interaction could be measured by driving one bead with a sinusoidal oscillation function at a defined rate and size while monitoring the position of both beads. Examination of the positional variation of the beads during stepping records showed evidence that myosin 5a was stably attached via two heads for most of the dwell period (Fig. 8.4D) (Veigel et al. 2002). At most transitions between steps the stiffness transiently dropped from a value of 0.35 to 0.18 $pN.nm^{-1}$, probably representing a short period where the myosin was attached to the actin via only one head. Occasionally during the stall periods, the stiffness levels fluctuated from the stiffness expected for a two-headed attachment to that which probably represented one head attachment (Fig. 8.4D, see red arrow).

Optical trapping of a single-headed myosin 5a S1 fragment, which only gave single interactions and no processive steps, allowed for the study of the power stroke or the working stroke (Veigel et al. 2002). This was determined to be 25 nm in magnitude and consisted of two separate mechanical phases as determined by ensemble averaging of the start and finish of many power stroke events (Fig. 8.7A, B). The first phase was 20 nm followed kinetically by a second phase of 5 nm.

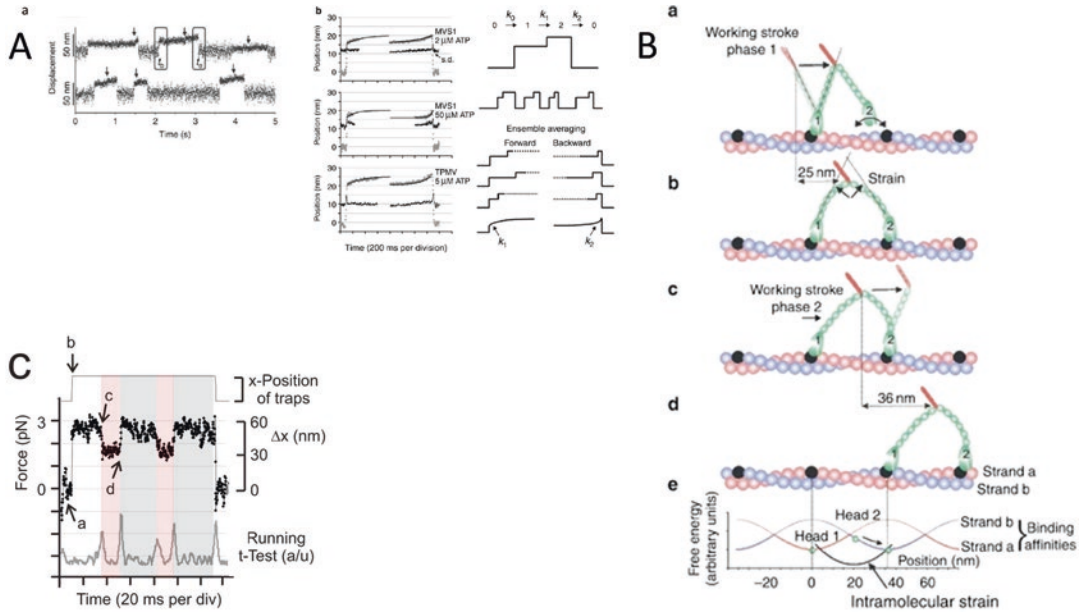

Fig. 8.7 The power stroke of myosin 5a occurs in two sub-steps and is reversible at high loads. Optical trapping of single-headed myosin 5a. (**Aa**). Note that at the end of the power stroke there is usually a further displacement denoted by arrows. (**Ab**). Examples of ensemble-averaged attachment events at three different ATP concentrations. Data points were synchronized to the beginning (t_b) and end (t_e) of each event. Right hand panels illustrate the method for the ensemble averaging. (**B**). Schematic showing the two phases of the power stroke. Figures taken from Veigel et al. (2002). See this paper for details on the methodology. (**C**). Displacements produced by bound myosin at different resisting forces (5 kHz sampling rate). In a typical binding event, initial binding and conformational change in the +Δx direction occurred around time point t_1 at <0.5 pN load and were not resolved separately. Load was applied at t_2 and at t_3a negative displacement occurred, consistent with a reversal of the power stroke followed by a positive displacement at t_4. This figure was taken from Sellers and Veigel (2010)

The larger first phase is likely due to a conformational change within myosin 5a between two AM•ADP states since the lifetime of this state is insensitive to the ATP concentration. The shorter, and subsequent, 5-nm displacement was probably linked to ADP release since its lifetime became shorter as the ATP concentration of the medium was increased. Thus, the working stroke is shorter than the step size (Veigel et al. 2002). If a load greater than 1.5 pN is applied to the optically-trapped myosin 5a S1 immediately after a binding event occurs, the position of the attached motor can sometimes be seen to fluctuate between two discrete levels which may represent the attached motor undergoing repeated power stroke/reversal of power stroke cycles (Fig. 8.7C) (Sellers and Veigel 2010). The presence of two AM•ADP states was also inferred by optical trapping studies with higher spatial and temporal resolution, which allowed for the detection of substrates during the time course of processive stepping (Uemura et al. 2004). The presence of the two-lead lever arm motor domains conformations (Figs. 8.3B, 8.6b) could also represent ADP-bound motors in different conformational states.

As described in the previous section, spots representing the fluorescence of single myosin 5a molecules moving along fixed actin filaments can be visualized using TIRF microscopy (Sakamoto et al. 2000). The use of TIRF microscopy combined with the super-resolution FIONA technique allowed for the visualization of the incremental stepping of the fluorescently-labeled myosin while moving processively (Yildiz et al. 2003). The spatial resolution of light microscopy is typically limited by the diffraction of light and is in the range of 250–300 nm depending on the

wavelength of the light and the numerical aperture of the objective. Thus, two fluorophores separated by distances less than this cannot be resolved and would appear as a single spot. Similarly, the image of a single fluorophore fills a spot of this size. Various super-resolution light microscopic methods have now been developed to "break" the diffraction barrier (Sydor et al. 2015). Of these, FIONA has been most useful in studying the function of molecular motors *in vitro* (Yildiz et al. 2003; Yildiz and Selvin 2005). The distribution of photons emitted by a fluorophore is called its point spread function. The FIONA technique fits the point spread function from a single fluorophore to a 2D Gaussian equation (Fig. 8.8a, b). The peak of the Gaussian distribution describes the location of the fluorophore to within a few nanometer resolution, and this resolution is increased as the number of collected photons increases. Yildiz et al. applied this technique to myosin 5a moving along actin (Yildiz et al. 2003). Myosin 5a was labeled by exchanging in a fluorescently-labeled calmodulin such that only one of the two heads was typically labeled. The molecules moved too fast at saturating ATP concentration and therefore subsaturating ATP concentrations were used in order to slow the stepping rate and allow for the collec-

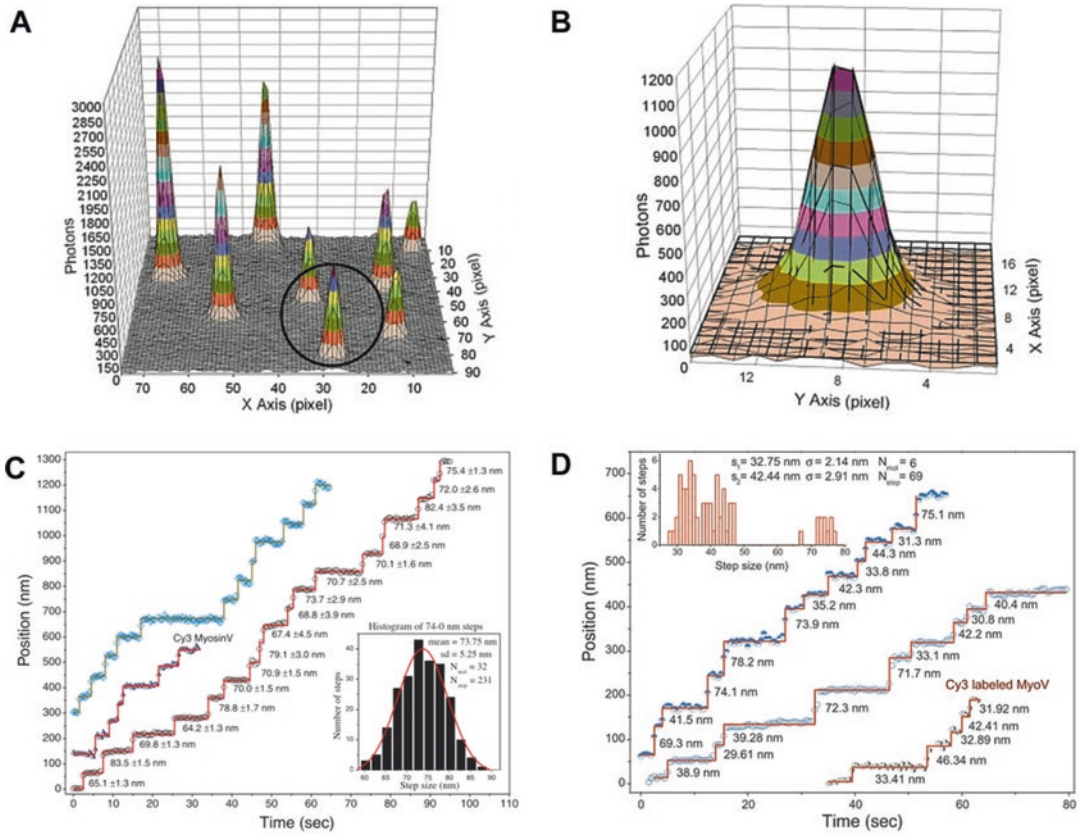

Fig. 8.8 Tracking the stepping of myosin 5a with FIONA. (**a**)**.** Field of fluorophores showing variable fluorescent intensities due to nonuniform illumination. (**b**)**.** A Gaussian curve-fit (solid lines) to the point spread function. (**c**). Stepping traces of three different myosin 5a molecules displaying 74 nm steps. The distribution of these steps is shown in the inset. (**d**). Stepping traces of three different myosin 5a molecules displaying alternating 42–33-nm steps with the distribution of step sizes shown in the inset. These step sizes indicate that the dye was 2–3 nm from the center of mass along the direction of motion. This figure was taken with permission from Yildiz et al. (2003)

tion of more photons per time point in order to increase the spatial resolution to the low nanometer levels. At sub-micromolar ATP concentrations, myosin 5a took one step every 2–10 s. The images were sampled at 0.3 Hz. The time and position records showed defined pauses in between large myosin stepping events that were too fast to measure (Fig. 8.8c).

The dwell periods in most of the traces were separated by 72-nm steps (Fig. 8.8c). This distance was consistent with the separation of the two heads by 36 nm observed by EM and the 36-nm step size distribution seen in optical-trapping studies since FIONA was measuring the stride length as a single-labeled head made its move. The 72-nm stride provided strong evidence for a hand-over-hand stepping mechanism where the two motors are separated by 36 nm when both were bound and where the labeled trail head detached and reattached at a position that is 36 nm in front of the original lead head. The movement of the unlabeled head was not detected in these traces; however, evidence for this movement was obtained by analyzing the dwell time histogram. The distribution was well fitted by a kinetic model for the probability of dwell times assuming that the stepping rate of the labeled head was the same as that of the unlabeled head.

If the myosin was moving in an inchworm-like manner, then a uniform 36-nm separation between dwells would be expected even for labeled single-headed myosins.

These data suggest that the exchanged calmodulin was likely on the IQ motif closest to the motor domain. Interestingly, some molecules displayed a more complex stepping pattern where alternating steps of 43 nm and 33 nm or 52 nm and 23 nm were observed (Fig. 8.7D). These were explained by assuming that the labeled calmodulin exchanged into an IQ position farther from the motor domain. In this case the longer step would represent the movement of the labeled head as it transitioned from the trail to the lead position. The shorter step would be obtained when the unlabeled head detached followed by a power stroke from the attached labeled head. This power stroke repositioned its labeled calmodulin by some lateral distance proportional to its vertical position in the lever arm. This was further evidence for a hand-over-hand mechanism.

Even stronger evidence for a hand-over-hand mechanism was obtained when the two heads of a single myosin 5a molecule were labeled with different color Qdots (Warshaw et al. 2005). In this elegant experiment, the stepping trace showed the two colors alternate in the lead position as the molecule moved forward (Fig. 8.9). Each individual head took 72-nm strides.

Using the high resolution iSCAT technique (See Chap. 6), Andrecka et al. examined the movement of myosin 5a HMM labeled at the N-terminus of one motor domain with a single gold bead. Given the large number of photons scattered by the gold bead, the authors were able to image the movement of single molecules of myosin 5a at speeds up to 1000 Hz with even better resolution than was obtained with QD-labeled myosin 5a at 60 Hz (Fig. 8.10a). At 100 Hz the localization precision was less than 1 nm (Fig. 8.10b). This methodology allowed for more detailed elucidation of the stepping mechanism than was previously possible with fluorescence or optical trapping. First, the overall size of the forward movement of the labeled head was 72 nm, consistent with the FIONA data discussed above. However, it was noticed that each dwell period showed an abrupt small backward movement (~5 nm) when the data were sampled at a rate of 100 Hz (Fig. 8.10b). Control experiments determined that this was likely a very small conformational change in the N-terminus of the myosin motor domain (where the gold bead was attached) when the unlabeled head made its stride. Examination of the dwell times before and after this event demonstrated that the two heads stepped with the same kinetics. In other words, the presence of a 20-nm gold bead, which was larger than the motor domain itself, had no effect on the stepping mechanics of that head.

When sampling at 1000 Hz, the position of the labeled unbound head could be followed as it made its transition from the trail to lead position (Fig. 8.11a) (Andrecka et al. 2015). The transition time from unbinding to binding was about 15 ms, consistent with values obtained by optical

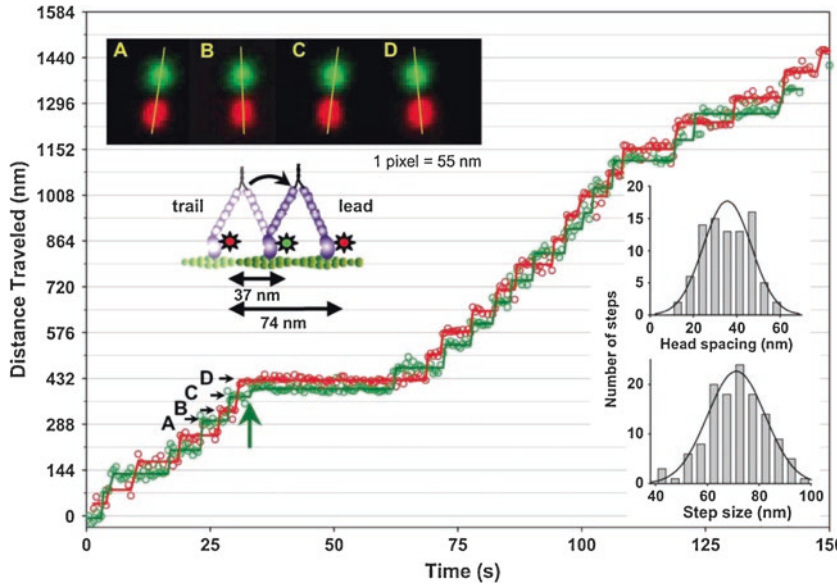

Fig. 8.9 Myosin 5a processive run with heads labeled with different colored Qdots. Green and red circles at the $Qdot_{565}$and the $Qdot_{655}$ positions, respectively determined by Gaussians fits of their point spread functions. Solid lines are the average Qdot positions between steps. Upper left inset are the averaged Qdot images for steps labeled A–D, with the red and green images offset by 12 pixels in the y-direction for clarity. The yellow lines connect the Qdot centers emphasizing alternating relative head position. Green arrow represents a sub-step. Lower right insets are histograms of inter-head spacing and stride size. Image taken from Warshaw et al. (2005) with permission

trapping (Veigel et al. 2002). Separate studies using dark field microscopy to study movement of a bead-labeled myosin (Dunn and Spudich 2007) or fast polTIRF to measure lever arm angles (Beausang et al. 2013) arrived at similar values. This was considerably slower than would be predicted if the reattachment event were purely diffusive as calculated by Kramer's first passage eq. (0.1 ms) or as modeled by molecular dynamics (Craig and Linke 2009). It was widely assumed that, following the power stroke of the attached head, the unbound head underwent random Brownian motion until it found the new forward actin-binding site (Dunn and Spudich 2007; Veigel et al. 2002; Walker et al. 2000). Instead, the iSCAT data showed that the movement of the free motor was rather constrained and that it spent most of its time in a position about 40 nm off axis (Fig. 8.11a–f) (Andrecka et al. 2015). From here the head made flickering attempts to find an actin-binding site located about 36 nm from the attached head. Furthermore, in each step the position of the unattached head was on the same side of the actin filament during a processive run. The "off track" position could either be on the right side or on the left side at the initiation of a run but did not change during a run on a single actin filament. This behavior argued against models where the unbound head diffused along the forward actin subunits before finding its high affinity binding site (Watanabe et al. 2010; Okada et al. 2007).

These data suggested that, rather than acting like a freely jointed swivel at the junction between the two lever arms, the unattached head maintains a rather constant angle between the two lever arms. In other words, the molecule behaves like a drawing compass. The angle between two myosin 5a heads bound to actin or deposited on an EM grid in the absence of actin was between 105 and 115° (Walker et al. 2000; Takagi et al. 2014; Andrecka et al. 2015). This angle would explain the off-actin localization of the head during the transition period and further suggested that the search for a forward binding site did not involve a random diffusion of the unattached head.

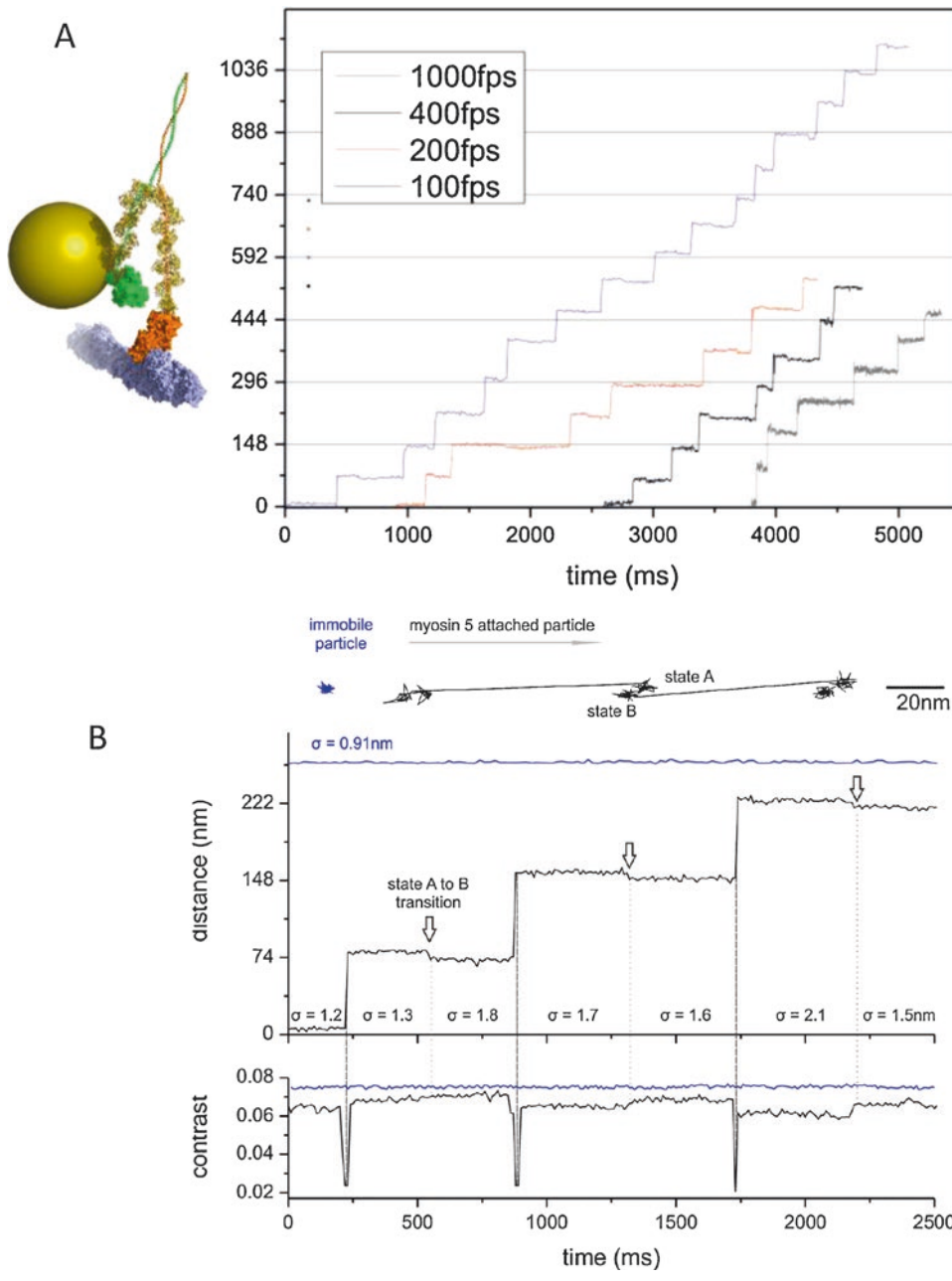

Fig. 8.10 High speed, high precision imaging of myosin 5a stepping using iSCAT. (**a**). Left, cartoon of myosin 5a HMM labeled at the amino terminus of one head with a 20-nm gold bead. Right, representative iSCAT stepping records of myosin 5a at four sampling speeds. (**b**). Upper panel, 2D trajectories for a 20-nm gold particle immobilized to the surface (blue) or attached to the amino-terminus of one head of myosin 5a. Arrow indicates the direction of travel. Middle panel, representative stepping trace at 100 Hz demonstrating two distinct states (A and B) during the dwell period following the stepping of the labeled head. This AB transition marks the movement of the gold bead on the labeled head at the time of stepping of the unlabeled head. Lower panel, corresponding iSCAT contrast time trace for the trajectories in the middle panel. A brief reduction in iSCAT contrast coincides with 74-nm strides taken by the labeled heads (red lines). Sampling rate was 100 Hz and the standard deviations (σ) of the bead positions are indicated. This figure is taken from Andrecka et al. (2015)

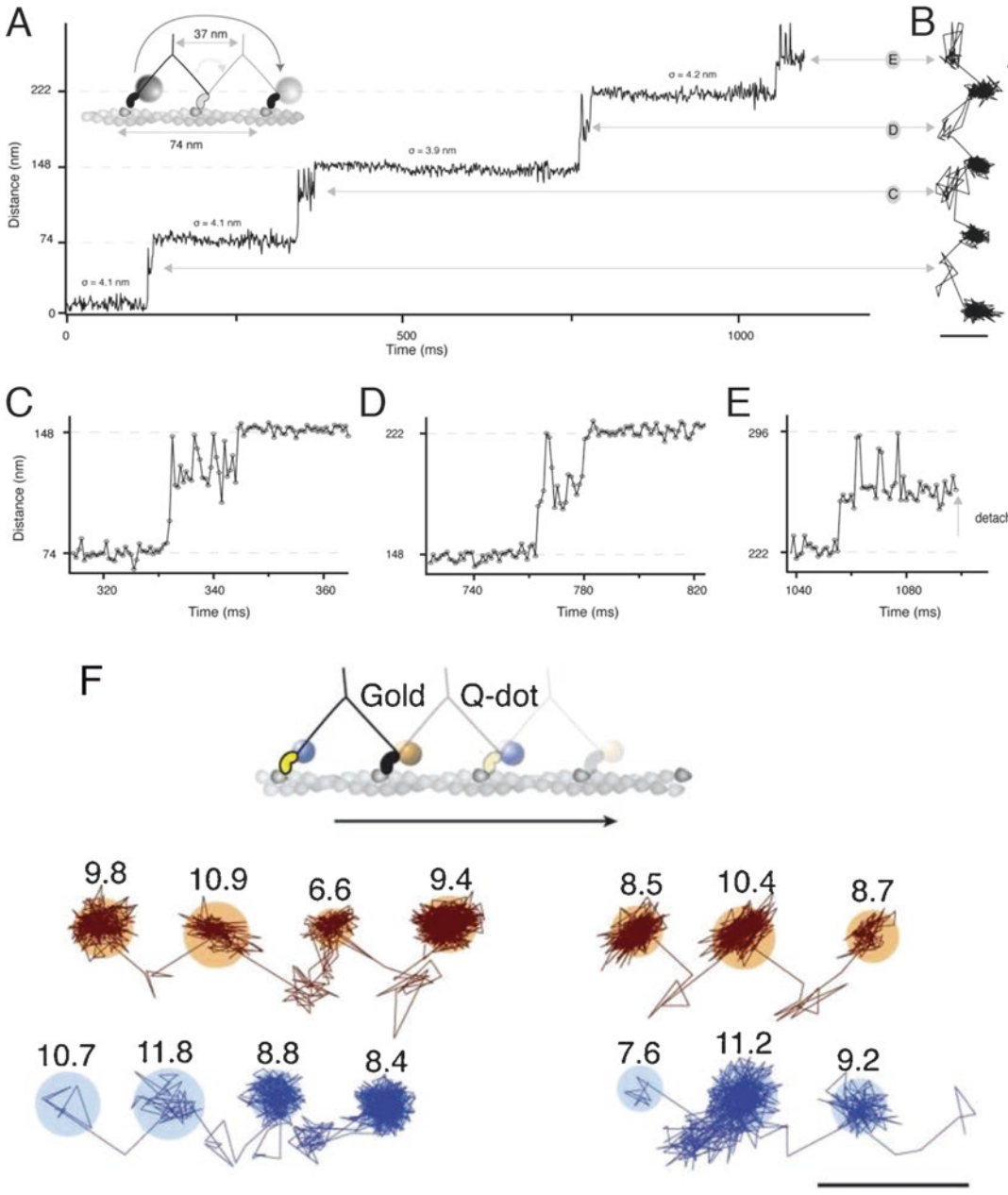

Fig. 8.11 iSCAT tracking of the unbound head of myosin 5a. (**a**). Distance traveled as a function of time for myosin 5a where a single head was labeled with a 20-nm gold bead. The lateral localization precision, σ, is given for each actin-attached period. Note that during each stepping event there is a brief transient period where the bead demonstrates larger fluctuations corresponding to its detachment time. (**b**)**.** Corresponding 2D trajectory with the arrow indicating direction of movement. (**c–e**). Expanded views of the transient states indicated in **a** and **b,** which are indicated by double-headed arrows. Scale bar: 50 nm. ATP concentration: 10 μM. Imaging speed: 1000 Hz. (**f**). Simultaneous measurement of scattering and fluorescence for a myosin 5a labeled with a 20-nm gold particle on one head and a Qdot on the other (see upper panel for schematic). Lower panel, the position of the gold bead is marked in gold and that of the Qdot in blue, labeled with the SD of the probe position. Note that the off state is on the same side of the actin filament for each label. Scale bar: 100 nm, Imaging speed: 500 Hz. Figure taken from Andrecka et al. (2015)

If myosin 5a walks in a hand-over-hand method it could either do so symmetrically or asymmetrically with regards to the movement of the two heads. An asymmetric mechanism would imply that when walking along an actin filament the two lever arms would alternate which side of the actin filament they occupy during the search period. One head would always have its off-actin position on the right side of the actin filament and the other would always have its off-actin position on the left. In a symmetric mechanism each time either head moves it would remain on the same side of actin filament in the unbound state. This was tested by attaching a fluorescent QD to one motor domain and a gold bead to the other (Andrecka et al. 2015). The position of the QD was followed by fluorescence while that of the gold bead by light scattering. The unbound state for both heads were on the same side of the actin filament showing that myosin 5a moves in a symmetric hand-over-hand mechanism (Fig. 8.11f). This suggests that a cargo attached to the tail region would rotate 180° with each step, which might complicate movement of cargo within the cell. It is likely that mechanisms have evolved to relieve the built-up torque that would result from such movement.

Myosin 5a is not a precise stepper. The detached head did not always bind to the 13th actin subunit (36 nm away) in front of the attached head. Electron microscopic images of myosin 5a bound to actin in the presence of ATP showed that the two heads could be separated by 11 or 15 actin monomers although the most favored separation was 13 actin subunits (Fig. 8.6) (Walker et al. 2000; Oke et al. 2010). This lack of fidelity is likely the explanation for the observations that beads coated with a single myosin 5a molecule spiraled around a suspended actin filament with a left-hand pitch of about 2 μm while moving on actin filaments (Ali et al. 2002) and that polTIRF measurements of myosin 5a molecules walking on actin showed a subpopulation of lever arm angles consistent with occasional azimuthal binding to an actin subunit other than the preferred 13th subunit (Lewis et al. 2012). polTIRF measures the angle that the dye that is rigidly attached to the lever arm makes with respect to the actin filament axis. These results could be explained if the motor mostly takes strides that result in a 13-actin subunit separation between the two heads, but occasionally takes short steps that result in an 11-actin subunit separation. Consistent with this, polarization studies where dyes were bound to actin filaments moving over myosin 5a bound to a surface also demonstrated that about 20% of the actin filaments exhibited a leftward spiral as they moved (Beausang et al. 2008).

8.6 The Neck Domain Acts as a Stiff Lever Arm

The length of the neck is one of the variabilities found amongst members of the myosin superfamily and is determined by the number of tandem IQ repeats in most myosins (Berg et al. 2001). Some myosins such as myosin 10 and myosin 7 also have a stable single α-helical (SAH) domain that contributes to the neck (Baboolal et al. 2009; Knight et al. 2005). The neck region of all members of class V myosins have six IQ motifs. In mouse, all six IQ motifs bind calmodulin as their light chain (Wang et al. 2000). Chicken myosin 5a has an essential light chain (ELC) bound to at least one of the IQ motifs in addition to calmodulin (Espindola et al. 2000).

The publication of the first crystal structure of skeletal muscle myosin S1 immediately suggested a mechanism for force generation and movement of actin (Rayment et al. 1993a, b). The neck region emanated from the motor domain opposite from the actin-binding region and it was hypothesized that it would be able to move as a rigid body to create the power stroke. Subsequent crystal structures in other nucleotide states and electron microscope images of various myosins bound to actin in the presence and absence of ATP confirmed this hypothesis (Sweeney and Houdusse 2010). Images of myosin 5a HMM bound to actin in the presence of ATP provided the first solid evidence for the power stroke that takes place on actin (Figs. 8.3 and 8.6) (Burgess et al. 2002; Walker et al. 2000). The neck region consisting of the converter region and the light chain bound IQ motifs moved as a rigid body

about a fixed pivot point in the base of the motor domain. The angle between the lever arm and the actin filaments was 129–143°in the lead heads and 39–49° in the trail heads. The stiffness of the lever arm from optical trap measurements was about 0.2 pN•nm^{-1} (Veigel et al. 2002).

As mentioned above, if myosin 5a were to walk along an actin filament in a straight line without major rotations around the filament, it would need to take 72-nm strides in order to match the periodic half repeat distance of the actin filament (36 nm), and this would require a longer neck than is found in class 2 myosins. Early EM images of myosin 5a bound to actin demonstrated that the neck region was relatively rigid whether the myosin was bound to actin via both heads or by only one head although some lead necks were clearly curved as if under strain (Fig. 8.3b) (Walker et al. 2000).

To address the importance of the long neck region several studies engineered myosin 5a HMM mutants containing fewer or larger numbers of IQ motifs. The six IQ motifs in myosin 5a are at intervals of 23–25-23-25-23 amino acids, respectively. Sakamoto et al. engineered molecules with 2, 4, 6, and 8 IQ motifs keeping these intervals intact (Sakamoto et al. 2003). In addition, they created a six-IQ HMM where the spacing between the 3rd and 4th IQ motifs was altered by the insertion of two alanine residues (HMM 2Ala-6IQ). Optical trapping experiments examining single (nonprocessive) attachments showed a linear increase in the power stroke as the number of IQs was increased (Fig. 8.12a) (Sakamoto et al. 2003). However, the HMM 2Ala-6IQ mutant had a shorter power stroke than would be predicted for a molecule with 3 IQ motifs suggesting that the spacing between IQ motifs was essential for maintaining lever arm rigidity. HMM-6IQ and HMM-8IQ showed robust processive movements, but HMM-4IQ was somewhat compromised and required lower ionic strengths in order to move processively. HMM-2IQ molecules exhibited short run lengths and then only if the ionic strength and ATP concentrations were lowered. Determining their step size via super-resolution imaging demonstrated a linear relationship between the neck length and the stride length (Sakamoto et al. 2005) (Fig. 8.12b). The distributions of stride sizes of the HMM-8IQ mutant were broad and could be fit best by several Gaussian functions indicating flexibility in sizes of the strides taken. Interestingly, in this unloaded assay the HMM-2Ala-6IQ mutant took 74-nm strides. Another study using optical trapping to study a different set of myosin 5a IQ mutants reached a similar conclusion with regards to neck length and step size (Purcell et al. 2002). This study found a broad distribution of step sizes for the myosin 4IQ mutants.

Examination of the myosin 5a HMM IQ mutants bound to actin in the presence of ATP revealed that the two heads of wild-type HMM-6IQ preferentially bound with 13 actin subunit separation, with some molecules separated by 11 or 15 subunits and a very small proportion by 9 subunits (Oke et al. 2010) (Fig. 8.13). HMM-8IQ preferred to bind with separations of 15 subunits but showed smaller populations separated by 13, 11, 17, and 9 subunits, respectively. HMM-4IQ predominantly bound with the two heads separated by 11 subunits but also showed smaller distributions at 13, 9 and 7. Thus, the length of the neck region determined the stepping distance of the molecule by altering the preferred actin subunit target. The myosin motor domain did not really discriminate among forward actin subunits to bind, but rather the length of the neck region dictates which actin subunit is most readily accessible. A test of this created a chimeric myosin 5a HMM mutant wherein a 17-nm stretch of SAH domain from *Dictyostelium* MyoM replaced IQ motifs 2–5 (Baboolal et al. 2009). This length of SAH domain was predicted to be of approxi-

Fig. 8.12 (continued) is proportional to the length of the neck region. Panels a, c and b, d show sample traces and power stroke histograms, respectively, for HMM-2IQ and HMM-8IQ mutants. Panel e shows the summary of the data for these and other mutants. These data are taken from Sakamoto et al. (2003). (**b**). Tracking of the stride length of GFP-tagged myosin 5a HMM-IQ mutants. Inset shows the summary of the data. Parts of this figure were taken from Sakamoto et al. (2005)

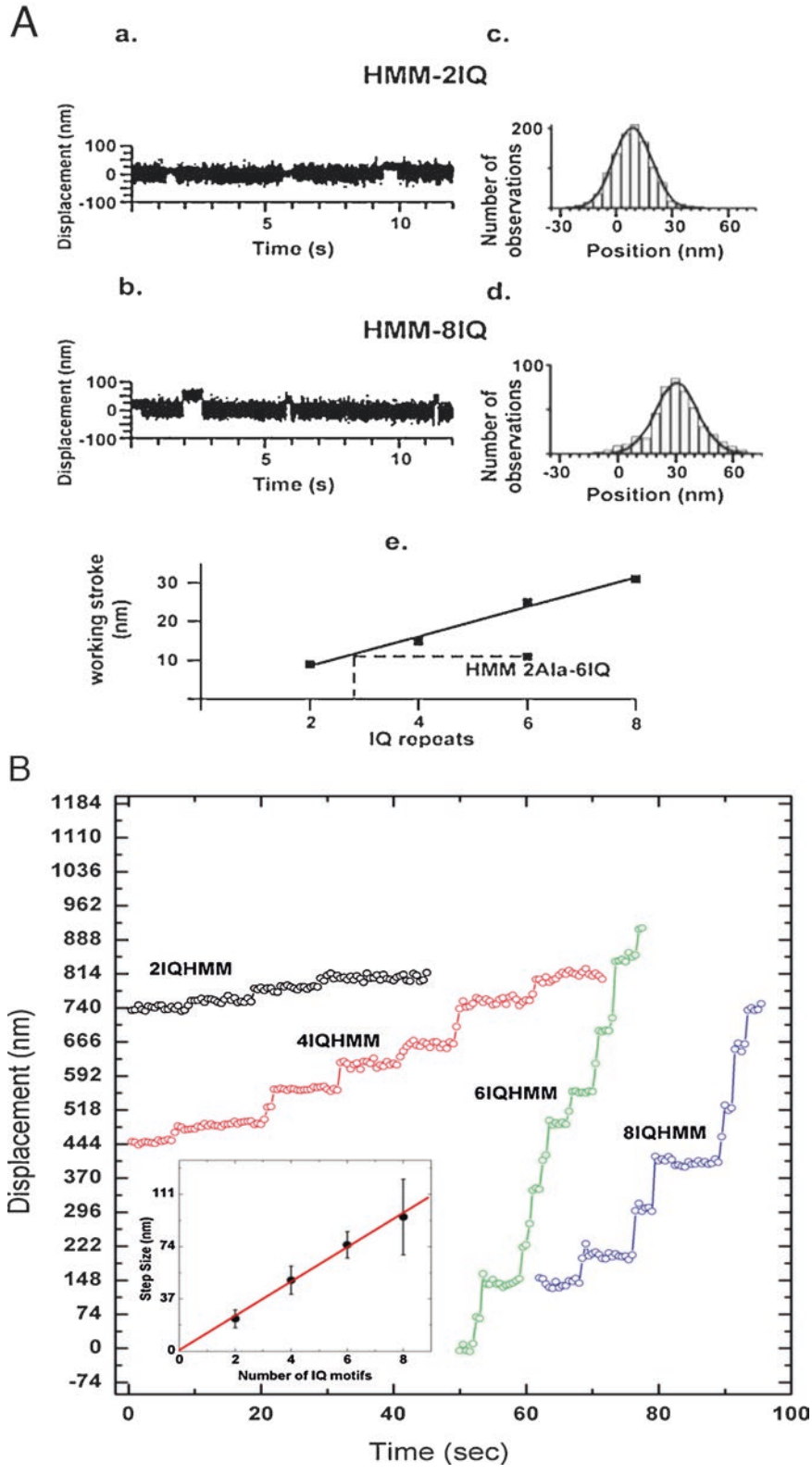

Fig. 8.12 The length of the neck determines the magnitude of the power stroke and step size. (**a**). Optical trapping studies of single interactions of myosin 5a HMM neck mutants demonstrate that the size of the power stroke

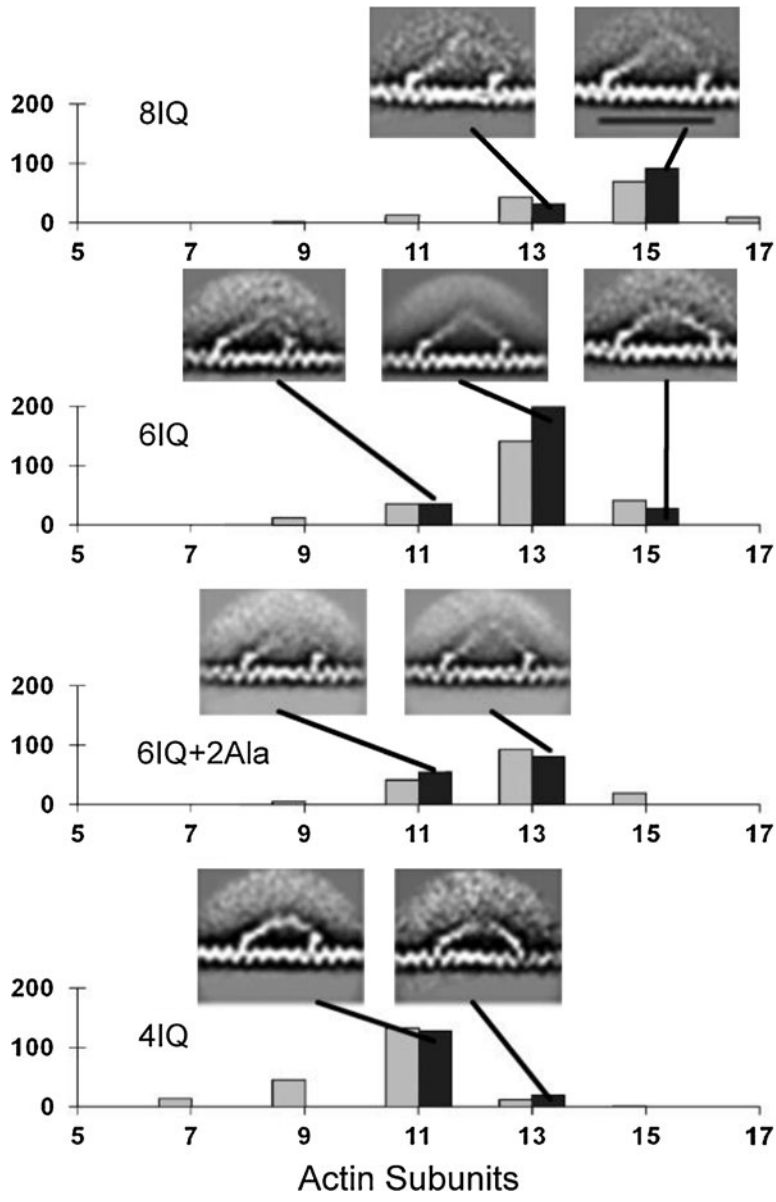

Fig. 8.13 Imaging the variable step size in myosin 5a HMM-IQ mutants. Histograms show head separation in raw images (gray bars) and image averages (black bars). Image averages documenting some of the classes are shown above the individual histograms. This image was taken from Oke et al. (2010)

mately the same length as that of the replaced four IQ motifs, and thus the molecule should have a neck length similar to that of a six-IQ myosin 5a. Electron microscopic images confirmed this prediction. Its stride length measured in single molecule stepping assays was 70 nm and it displayed a run length similar to that found with HMM-6IQ. The power stroke obtained from optical trapping assays (~22 nm) was only slightly lower than was found with HMM-6IQ (~25 nm). This demonstrated that the length of the neck was critical to precise stepping by myosin 5a and that SAH domains could function as part of a stiff lever arm.

Further evidence that the neck region acts as a stiff lever arm and undergoes a large rigid body motion to produce a power stroke was obtained using polTIRF, a technique that combined high resolution spatial imaging with fluorescence polarization to detect angle changes in a probe

located on one of the calmodulins in the neck region (Syed et al. 2006). For every 74-nm translocation of the labeled myosin head, the probe exhibited two reorientational motions that represented the orientation of the probe in the pre- and post-power stroke state. Myosin 5a would occasionally move from the top of the actin filament to a side position, which might have been in response to obstacles in its path. A subsequent study further defined the angle changes associated with the power stroke using DOPI (Toprak et al. 2006). The probe angle relative to the barbed end of the actin filament averaged 128° while the neck region was in the leading state and 57° when it was in the trailing state. This defined a lever arm rotation of 71°, which was consistent with a 37-nm forward step size of myosin V. Interestingly, when similar studies were carried out on a myosin 5a 4IQ mutant, the frequency of azimuthal movements was greatly increased and the data were consistent with most prominent head separations of 11 to 13 actin subunits for this mutant (Lewis et al. 2012). However, the data were also consistent with myosin 5a 4IQ taking a broader range of steps as suggested by optical-trapping studies (Purcell et al. 2005).

8.7 The Kinetics of the Two Motor Domains Are Gated to Enhance the Processivity

Assuming a duty ratio of 0.7 for a single motor domain of myosin 5a, one can calculate that a two-headed myosin 5a should take an average of 8 steps per encounter with actin, which would give rise to a run length of ~288 nm (Veigel et al. 2002). However, run length measurements for two-headed myosin 5a molecules are typically closer to 1000 nm (equaling nearly 30 steps) and some molecules move considerably farther (Bao et al. 2013; Hodges et al. 2007). To account for this discrepancy, it was proposed that the two heads of myosin 5a kinetically and mechanically gate each other's ATPase activity to increase the probability of forward processive stepping (Veigel et al. 2002). Evidence for this was that the attachment lifetimes of a single head of myosin 5a (S1) were dependent on the load applied by the trap during attachment (Veigel et al. 2005; Purcell et al. 2005). When the direction of the applied load opposed the power stroke, the lifetime of attachment increased and it decreased when the direction of the applied load was in the same direction as the power stroke (Fig. 8.14). In the context of a two-headed myosin 5a moving processively along actin this gives a method for load-dependent kinetic gating of the two motor domains. The trailing head would exert a resisting load on the lead head to delay its release of ATP products. At the same time the leading head would exert an assisting load on the trail head to increase its release of ADP and therefore shorten its attachment life time. Not only would this increase processivity, it also provides a strong mechanism for directionality since the lead head would remain in a strongly bound state with delayed product release as long as the trail head was still attached.

Unbinding studies of myosin 5a S1 molecules in the presence and absence of ADP showed evidence for a directional strain dependence (Oguchi et al. 2008). Myosin 5a S1 molecules were bound to an optically-trapped bead and allowed to attach to actin either in the absence or presence of ATP. The trap was then moved to apply a load. Myosin 5a S1 molecules dissociated from actin at lower applied forces if the force was in the direction of the power stroke (assisting load) in both the presence and absence of ADP. Conversely, if the applied force was in the opposite direction of power stroke (resisting load) then the force required for unbinding was greater.

Strain-dependent gating of ADP release from the rear head is probably the reason why most of the forward lever arms of myosin 5a seen in EM images of doubly-bound molecules were still in the pre-power stroke position (Fig. 8.6) (Burgess et al. 2002) (Oke et al. 2010; Walker et al. 2000). Only 7% of the wild-type HMM 6IQ molecules showed the post-power stroke lead head conformation. The percentage of the lead heads in the post-power stroke position is higher when the wild-type 6IQ myosin 5a was bound with its two motors separated by 11 actin subunits (45%) and was very small (2%) when the two motors were

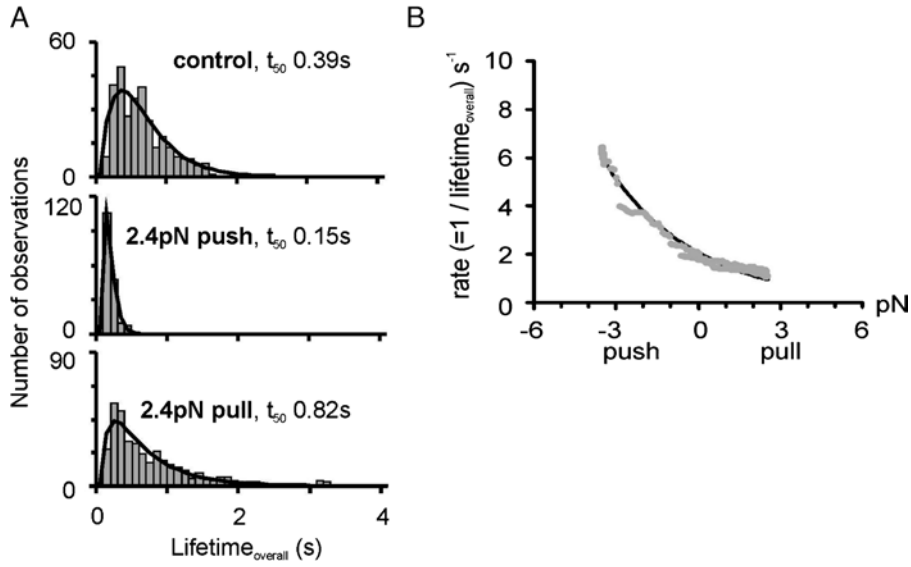

Fig. 8.14 Load dependence on the mechanics of single-headed fragments of myosin 5a. (a). Upon detection of a binding event the position of the laser tweezer was rapidly moved for a defined distance to apply a load to the bound head. The lifetimes of the attachment were plotted for different applied loads. (**b**). Summary plot demonstrating that the lifetime of attachment was prolonged for resisting loads (pull) and was decreased for assisting loads (push). These data were taken from Veigel et al. (2005)

separated by 13 actin subunits. This conformation was not detected when the heads were separated by 15 actin subunits. One explanation for this would be that the trail head in these images could have been in either the ADP-bound or the apo state. The second phase of the power stroke discussed earlier, which occurs upon release of ADP, could lessen the intramolecular strain on the lead head and allow it to attempt to undergo its power stroke. The study using neck length mutants showed a consistent pattern in accord with this (Oke et al. 2010). The most common head separation in the HMM-4IQ and HMM-8IQ mutants were 11 and 15 actin subunits, respectively. In both cases the percentage of lead motors in the post-power stroke position increased if the heads were separated by less than these characteristic amounts. It is reasonable to assume that ADP could only be lost from the lead head once the change from the pre- to post-power stroke occurred. Thus, strain exerted on the lead head by the attached rear head kinetically gated a structural transition likely coupled to the release of ADP.

Interestingly, a study of the force-dependent stepping of myosin 5a HMM showed little effect of resistive force on stepping rate until stall was reached (Clemen et al. 2005). The lack of force dependence of myosin 5a HMM versus the strong force dependence of myosin 5a S1 can be reconciled by considering the coupling of the two S1 molecules into a two-headed HMM. A modeling study suggested that internal conformational transitions with a two-headed HMM structure bound to actin via both heads would mostly be absorbed by the bending of the lever arms and will not act solely on the lead lever arm (Vilfan 2005). This study calculated that a conformational change of 5 nm within a single-headed construct would lead to only a 0.2-nm change in the center of mass of a two-headed molecule. The Clemen et al. paper also provided evidence that at high forces the search time of the unbound head increased (Clemen et al. 2005). At high resistive loads myosin 5a HMM took processive back steps even in the absence of ATP, but no such ATP-independent stepping occurred with high assistive loads (Gebhardt et al. 2006). This

implies that myosin 5a is a mechanical ratchet at high loads.

While the high-speed AFM movies of myosin 5a walking on actin showed some instances of transient lead head detachment (termed foot stomping) at low ATP concentrations (Kodera et al. 2003), iSCAT studies at saturating ATP concentrations found no events where the lead head detached from actin, and this only happened in 0.6% of the total events observed at 10 μM ATP (Andrecka et al. 2015).

Kinetic gating was tested in two studies by measuring the release of a fluorescent analog of ADP from A•MADP when chased by unlabeled nucleotide using stopped-flow kinetics (Forgacs et al. 2008; Rosenfeld and Sweeney 2004). Both studies showed a dramatic effect of strain on the release of ADP from the lead head if the trail head is still attached. The rate constant for ADP release from the lead head when it is under strain is up to 250 times slower than if there is no strain.

(3'-7-diethylaminocoumarin-3-carbonyl-amino)-3'-deoxyadenosine-5'-triphosphate) (deac-aminoATP) is a fluorescent analog of ATP whose fluorescence intensity increased 20–25 fold when bound to myosin 5a (Forgacs et al. 2006). This allowed for the simultaneous tracking of the position of a fluorescently-labeled myosin 5a HMM and of the intensity and position of deac-aminoATP (or products after hydrolysis) as it bound to and dissociated from myosin (Sakamoto et al. 2008). These experiments were carried out at sub-saturating concentrations of nucleotide using TIRF microscopy to detect the signal of the deac-amino nucleotide bound to myosin. Myosin 5a was extensively exchanged with labeled calmodulin subunits such that both neck regions were labeled and the observed steps were separated by 36 nm, consistent with the movement of the center of mass of the molecule (Fig. 8.15A). For each myosin protein step, two "steps", each separated by 18 nm, were observed for the position of the bound nucleotide. This was due to the dissociation of deac-aminoADP from the trail head which resulted in an 18-nm forward positioning of the localization of the nucleotide fluorescence. This interpretation was supported by the fact that the intensity of the nucleotide signal alternated between values representing one and two nucleotides bound (Fig. 8.15B). The nucleotide position always moved forward in the direction of stepping observed for the labeled myosin. Together this indicates that one ATP is used per step proving a tight coupling mechanism which was generally but not universally assumed (Okada et al. 2007; Sakamoto et al. 2000). Also, under these sub-saturating nucleotide conditions, ADP was always released from the trail head suggesting that the resisting load on the lead head effectively prevented its release of ADP before the trail head released its products, bound a new ATP and detached. Together this gating served to both increase processivity and to ensure directionality. The latter explains why reverse steps of myosin 5a are rarely observed in unloaded single-molecule stepping assays. Reverse steps are sometimes observed under high loads in the optical trap (Veigel et al. 2002; Mehta et al. 1998; Clemen et al. 2005; Kad et al. 2008).

The majority of the above studies support a simple mechanochemical scheme for the stepping of myosin 5a as shown in Fig. 8.16. In **panel 1**, myosin 5a is bound to actin via both heads spaced thirteen actin subunits (~72 nm) apart with ADP in both heads. The trail head is in the post-power stroke conformation whereas the lead head is in the pre-power stroke conformation. ADP release from the lead head is inhibited by internal strain exerted by the attached trail head. ADP dissociates from the trail head, perhaps accelerated by the internal strain exerted by the attached lead head (**panel 2**). ATP then rapidly binds to the apo-trail head resulting in fast dissociation from actin and ATP hydrolysis to the products ADP and Pi (**panel 3**). The attached head undergoes a power stroke which positions the unattached head in a forward position to begin a search for a new actin-binding site (**panel 4).** Not obvious in this 2D presentation is that the unattached head largely dwells in an off-axis position from which it transiently explores the forward actin-binding site (see Fig. 8.11) (Andrecka et al. 2016). The stiffness and length of the neck region places strong constraints on which actin subunits are sterically available for binding. In

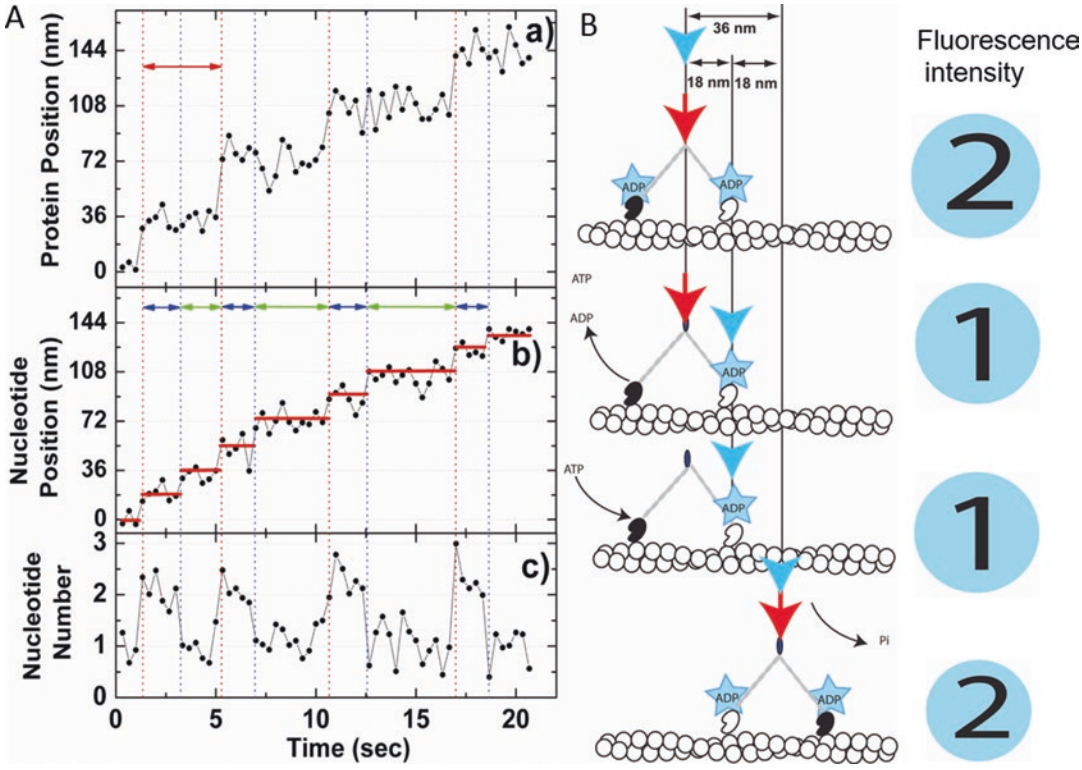

Fig. 8.15 Correlation between the movement of myosin 5a HMM and the binding/dissociation of deac-aminonucleotide. (**A**). Images of Alexa-Fluor-568-myosin 5a HM and deac-aminoATP fluorescence were acquired simultaneously and the positions were plotted versus time in panels Aa and Ab, respectively, for a single processive run. Panel Ac plots the intensity of the deac-aminonucleotide from this same record. (**B**). Schematic showing the relationship between myosin 5a movement and nucleotide binding/dissociation. This figure was taken from Sakamoto et al. (2008)

p**anel 5**, the previously unattached head finds a forward actin-binding site, which rapidly triggers the release of Pi to bring the molecule back to the nucleotide states in **panel 1** with a translocation of the center of mass of the myosin by 36 nm. One ATP molecule was consumed in this process. Note that the elapsed time between panels 3 and 5 is ~15 ms.

This scheme is overly simplistic since it does not show two strain-dependent conformational AM•ADP states as discussed in this chapter. Also, there is evidence from several studies of a branched pathway where ADP can sometimes be released from the trail head before the lead head has dissociated its bound Pi (Kad et al. 2008; Baker et al. 2004).

8.8 Conclusions

From this review, it is evident that application of a host of single-molecule biophysical techniques has elucidated the molecular basis for the movement of myosin 5a along actin filaments. This detailed knowledge of the structure, the kinetics of actomyosin interaction, the processive run length, the step size and the mechanical dependence of these parameters has made myosin 5a the best-characterized myosin. The data show that myosin 5a is a two-headed motor protein that moves processively along actin filaments, taking 36-nm steps in a symmetrical hand-over-hand mechanism. The molecule spends most of its time bound firmly to actin via both heads attached

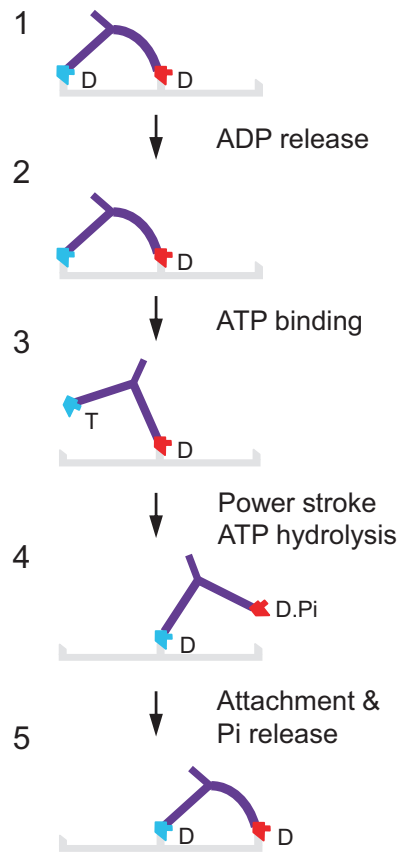

Fig. 8.16 Summary of the hand-over-hand myosin 5a stepping mechanism. **Panel 1**, myosin 5a is bound to actin (gray) via both heads spaced thirteen actin subunits (~36 nm) apart with ADP (D) in both heads. The trail head is in the post-power stroke conformation (blue motor) whereas the lead head is close to the pre-power stroke conformation (red motor). ADP release from the lead head is inhibited by internal strain exerted by the attached trail head that is shown by the lever curvature. **Panel 2**, ADP dissociates from the trail head, perhaps accelerated by the internal strain exerted by the attached lead head. **Panel 3**, ATP (T) rapidly binds to the apo-trail head resulting in fast dissociation from actin and hydrolysis of ATP to the products ADP and Pi. **Panel 4**, the attached head undergoes a power stroke which positions the unattached, pre-power stroke head in a forward position to begin a search for a new actin binding site. Not obvious in this 2D presentation is that the unattached head largely dwells in an off axis position from where it transiently explores the forward actin binding site. The stiffness and length of the neck region places strong constraints on which actin subunits are sterically available for binding. **Panel 5**, the previously unattached head finds a forward actin binding site which rapidly triggers the release of Pi to bring the molecule back to the nucleotide states in panel 1 with a translocation of the center of mass of the myosin by 36 nm. One ATP molecule is consumed in this process. Note that the elapsed time between panels 3 and 5 is ~15 ms

most commonly at 36 nm (13 actin subunits) apart. The kinetics of the two heads are gated by the internal strain that the trail head exerts upon the lead head resulting in extremely low probability that the lead head will detach before the trail head. These kinetics not only increase the processivity but also impart directionality, ensuring that the molecule moves forward. This forward motion is acquired by the ~25-nm power stroke taken by the still attached head upon ATP

binding and dissociation of the trail head from actin. This power stroke positions the unattached head predominately in an off-axis position from which it periodically samples the forward binding sites on the actin filament during a 10–15 ms search. The neck is a rigid lever arm in this regard and changing its length alters which forward actin subunit becomes the preferred target. For each step along actin, one ATP molecule is consumed.

The two other mammalian myosin 5 paralogs have not been as extensively studied, but there are some important differences in their kinetic and mechanical properties. Kinetic studies of myosin 5c S1 molecules predicted that it would not be a processive motor based on its low duty ratio (0.1) (Takagi et al. 2008; Watanabe et al. 2008). A subsequent study confirmed that it was not a processive motor when attempting to move along single actin filaments, but that it did move processively over fascin-bundled actin filaments (Sladewski et al. 2016). When myosin 5c molecules were coupled into small "teams", the run lengths increased (Krementsova et al. 2017; Gunther et al. 2014; Watanabe et al. 2006). Kinetic studies of myosin 5b S1 determined an intermediate duty ratio, but this was increased in the two-headed HMM molecule (Heissler et al. 2017). Single-molecule motility assays and optical trapping demonstrate that myosin 5b moved processively along single actin filaments (Gardini et al. 2018), as predicted before from a solution kinetics study. Its mechanical behavior, however, differed mechanically from that of myosin 5a in some respects. Unlike myosin 5a (Clemen et al. 2005), its run length is sensitive to both assistive and resistive force.

Myosins from class 6 and class 7 have also been shown to be processive if they are artificially dimerized via a leucine zipper coiled-coil. It will be interesting to apply these same techniques to these myosins to determine whether they have similar or novel mechanisms of stepping.

Acknowledgements JS would like to thank all his many collaborators who participated in studying the molecular mechanism of myosin 5a for their friendship, keen scientific insight and magnificent technical skills. It's been fun! Particularly, he would like to thank Claudia Veigel, Peter Knight, Justin Molloy, John Trinick (deceased), Stan Burgess, Philipp Kukura, Joanna Andrecka, Howard White, Fei Wang and Takeshi Sakamoto. The authors especially want to thank Peter Knight for his insightful comments on the manuscript and for preparing Fig. 8.16.

References

Ali MY, Uemura S, Adachi K, Itoh H, Kinosita K Jr, Ishiwata S (2002) Myosin V is a left-handed spiral motor on the right-handed actin helix. Nat Struct Biol 9(6):464–467

Ali MY, Krementsova EB, Kennedy GG, Mahaffy R, Pollard TD, Trybus KM, Warshaw DM (2007) From the cover: myosin Va maneuvers through actin intersections and diffuses along microtubules. Proc Natl Acad Sci U S A 104(11):4332–4336

Ali MY, Lu H, Bookwalter CS, Warshaw DM, Trybus KM (2008) Myosin V and Kinesin act as tethers to enhance each others' processivity 11. Proc Natl Acad Sci U S A 105(12):4691–4696

Ali MY, Vilfan A, Trybus KM, Warshaw DM (2016) Cargo transport by two coupled myosin Va motors on actin filaments and bundles. Biophys J 111(10):2228–2240. https://doi.org/10.1016/j.bpj.2016.09.046

Andrecka J, Ortega Arroyo J, Takagi Y, de Wit G, Fineberg A, MacKinnon L, Young G, Sellers JR, Kukura P (2015) Structural dynamics of myosin 5 during processive motion revealed by interferometric scattering microscopy. elife 4. https://doi.org/10.7554/eLife.05413

Andrecka J, Takagi Y, Mickolajczyk KJ, Lippert LG, Sellers JR, Hancock WO, Goldman YE, Kukura P (2016) Interferometric scattering microscopy for the study of molecular motors. Methods Enzymol 581:517–539. https://doi.org/10.1016/bs.mie.2016.08.016

Baboolal TG, Sakamoto T, Forgacs E, White HD, Jackson SM, Takagi Y, Farrow RE, Molloy JE, Knight PJ, Sellers JR, Peckham M (2009) The SAH domain extends the functional length of the myosin lever 2. Proc Natl Acad Sci U S A 106(52):22193–22198

Baker JE, Krementsova EB, Kennedy GG, Armstrong A, Trybus KM, Warshaw DM (2004) Myosin V processivity: multiple kinetic pathways for head-to-head coordination. Proc Natl Acad Sci U S A 101(15):5542–5546

Bao J, Huck D, Gunther LK, Sellers JR, Sakamoto T (2013) Actin structure-dependent stepping of myosin 5a and 10 during processive movement. PLoS ONE 8(9):e74936

Beausang JF, Schroeder HW III, Nelson PC, Goldman YE (2008) Twirling of actin by myosins II and V observed via polarized TIRF in a modified gliding assay 10. Biophys J 95(12):5820–5831

Beausang JF, Shroder DY, Nelson PC, Goldman YE (2013) Tilting and wobble of myosin V by high-

speed single-molecule polarized fluorescence microscopy. Biophys J 104(6):1263–1273. https://doi.org/10.1016/j.bpj.2013.01.057

Berg JS, Powell BC, Cheney RE (2001) A millennial myosin census. Mol Biol Cell 12(4):780–794

Bloemink MJ, Geeves MA (2011) Shaking the myosin family tree: biochemical kinetics defines four types of myosin motor. Semin Cell Dev Biol 22(9):961–967

Burgess S, Walker M, Wang F, Sellers JR, White HD, Knight PJ, Trinick J (2002) The prepower stroke conformation of myosin V. J Cell Biol 159(6):983–991

Cheney RE, O'Shea MK, Heuser JE, Coelho MV, Wolenski JS, Espreafico EM, Forscher P, Larson RE, Mooseker MS (1993) Brain myosin-V is a two-headed unconventional myosin with motor activity. Cell 75:13–23

Clemen AE, Vilfan M, Jaud J, Zhang J, Barmann M, Rief M (2005) Force-dependent stepping kinetics of myosin-V. Biophys J 88(6):4402–4410

Craig EM, Linke H (2009) Mechanochemical model for myosin V. Proc Natl Acad Sci U S A 106(43):18261–18266. https://doi.org/10.1073/pnas.0908192106

De La Cruz EM, Ostap EM (2004) Relating biochemistry and function in the myosin superfamily. Curr Opin Cell Biol 16(1):61–67

De La Cruz EM, Wells AL, Rosenfeld SS, Ostap EM, Sweeney HL (1999) The kinetic mechanism of myosin V. Proc Natl Acad Sci U S A 96(24):13726–13731

Dunn AR, Spudich JA (2007) Dynamics of the unbound head during myosin V processive translocation. Nat Struct Mol Biol 14(3):246–248

Espindola FS, Espreafico EM, Coelho MV, Martins AR, Costa FRC, Mooseker MS, Larson RE (1992) Biochemical and immunological characterization of p190-calmodulin complex from vertebrate brain: a novel calmodulin-binding myosin. J Cell Biol 118:359–368

Espindola FS, Suter DM, Partata LB, Cao T, Wolenski JS, Cheney RE, King SM, Mooseker MS (2000) The light chain composition of chicken brain myosin-Va: calmodulin, myosin-II essential light chains, and 8-kDa dynein light chain/PIN. Cell Motil Cytoskeleton 47(4):269–281

Forgacs E, Cartwright S, Kovacs M, Sakamoto T, Sellers JR, Corrie JE, Webb MR, White HD (2006) Kinetic mechanism of myosinV-S1 using a new fluorescent ATP analogue. Biochemistry 45(43):13035–13045

Forgacs E, Cartwright S, Sakamoto T, Sellers JR, Corrie JE, Webb MR, White HD (2008) Kinetics of ADP dissociation from the trail and lead heads of actomyosin V following the power stroke. J Biol Chem 283(2):766–773

Gardini L, Heissler SM, Arbore C, Yang Y, Sellers JR, Pavone FS, Capitanio M (2018) Dissecting myosin-5B mechanosensitivity and calcium regulation at the single molecule level. Nat Commun 9(1):2844. https://doi.org/10.1038/s41467-018-05251-z

Gebhardt JC, Clemen AE, Jaud J, Rief M (2006) Myosin-V is a mechanical ratchet. Proc Natl Acad Sci U S A 103(23):8680–8685

Gunther LK, Furuta K, Bao J, Urbanowski MK, Kojima H, White HD, Sakamoto T (2014) Coupling of two non-processive myosin 5c dimers enables processive stepping along actin filaments. Sci Rep 4:4907. https://doi.org/10.1038/srep04907

Hammer JA III, Sellers JR (2012) Walking to work: roles for class V myosins as cargo transporters. Nat Rev Mol Cell Biol 13(1):13–26

Heissler SM, Sellers JR (2016) Kinetic adaptations of myosins for their diverse cellular functions. Traffic 17(8):839–859

Heissler SM, Chinthalapudi K, Sellers JR (2017) Kinetic signatures of myosin-5B, the motor involved in microvillus inclusion disease. J Biol Chem 292(44):18372–18385. https://doi.org/10.1074/jbc.M117.801456

Hodges AR, Krementsova EB, Trybus KM (2007) Engineering the processive run length of myosin V. J Biol Chem 282(37):27192–27197

Johnston GC, Prendergast JA, Singer RA (1991) The Saccharomyces cerevisiae MYO2 gene encodes an essential myosin for vectorial transport of vesicles. J Cell Biol 113:539–552

Kad NM, Trybus KM, Warshaw DM (2008) Load and Pi control flux through the branched kinetic cycle of myosin V 9. J Biol Chem 283(25):17477–17484

Knight PJ, Thirumurugan K, Yu Y, Wang F, Kalverda AP, Stafford WF III, Sellers JR, Peckham M (2005) The predicted coiled-coil domain of myosin 10 forms a novel elongated domain that lengthens the head. J Biol Chem 280:34702–34708

Kodera N, Kinoshita T, Ito T, Ando T (2003) High-resolution imaging of myosin motor in action by a high-speed atomic force microscope. Adv Exp Med Biol 538:119–127

Kodera N, Yamamoto D, Ishikawa R, Ando T (2010) Video imaging of walking myosin V by high-speed atomic force microscopy. Nature 468(7320):72–76

Krementsova EB, Furuta K, Oiwa K, Trybus KM, Ali MY (2017) Small teams of myosin Vc motors coordinate their stepping for efficient cargo transport on actin bundles. J Biol Chem 292(26):10998–11008. https://doi.org/10.1074/jbc.M117.780791

Lewis JH, Beausang JF, Sweeney HL, Goldman YE (2012) The azimuthal path of myosin V and its dependence on lever-arm length. J Gen Physiol 139(2):101–120. https://doi.org/10.1085/jgp.201110715

Liu J, Taylor DW, Krementsova EB, Trybus KM, Taylor KA (2006) Three-dimensional structure of the myosin V inhibited state by cryoelectron tomography. Nature 442(7099):208–211

Lombardo AT, Nelson SR, Ali MY, Kennedy GG, Trybus KM, Walcott S, Warshaw DM (2017) Myosin Va molecular motors manoeuvre liposome cargo through suspended actin filament intersections in vitro. Nat Commun 8:15692. https://doi.org/10.1038/ncomms15692

Lombardo AT, Nelson SR, Kennedy GG, Trybus KM, Walcott S, Warshaw DM (2019) Myosin Va transport of liposomes in three-dimensional actin networks is modulated by actin filament density, position, and

polarity. Proc Natl Acad Sci U S A 116(17):8326–8335. https://doi.org/10.1073/pnas.1901176116

Lu H, Ali MY, Bookwalter CS, Warshaw DM, Trybus KM (2009) Diffusive movement of processive kinesin-1 on microtubules 4. Traffic 10(10):1429–1438

Margossian SS, Lowey S (1982) Preparation of myosin and its subfragments from rabbit skeletal muscle. Methods Enzymol 85:55–71

Mehta AD, Pullen KA, Spudich JA (1998) Single molecule biochemistry using optical tweezers. FEBS Lett 430(1–2):23–27

Mehta AD, Rock RS, Ridf M, Spudich JA, Mooseker MS, Cheney RE (1999) Myosin-V is a processive actin-based motor. Nature 400:590–593

Mercer JA, Seperack PK, Strobel MC, Copeland NG, Jenkins NA (1991) Novel myosin heavy chain encoded by murine dilute coat colour locus. Nature 349:709–713

Oguchi Y, Mikhailenko SV, Ohki T, Olivares AO, De La Cruz EM, Ishiwata S (2008) Load-dependent ADP binding to myosins V and VI: implications for subunit coordination and function. Proc Natl Acad Sci U S A 105(22):7714–7719. https://doi.org/10.1073/pnas.0800564105

Okada T, Tanaka H, Iwane AH, Kitamura K, Ikebe M, Yanagida T (2007) The diffusive search mechanism of processive myosin class-V motor involves directional steps along actin subunits. Biochem Biophys Res Commun 354(2):379–384

Oke OA, Burgess SA, Forgacs E, Knight PJ, Sakamoto T, Sellers JR, White H, Trinick J (2010) Influence of lever structure on myosin 5a walking 1. Proc Natl Acad Sci U S A 107(6):2509–2514

Ortega AJ, Andrecka J, Spillane KM, Billington N, Takagi Y, Sellers JR, Kukura P (2014) Label-free, all-optical detection, imaging and tracking of a single protein. Nano Lett 14(4):2065–2070

Pastural E, Barrat FJ, Dufourcq-Lagelouse R, Certain S, Sanal O, Jabado N, Seger R, Griscelli C, Fischer A, de Saint BG (1997) Griscelli disease maps to chromosome 15q21 and is associated with mutations in the myosin-Va gene. Nat Genet 16(3):289–292

Purcell TJ, Morris C, Spudich JA, Sweeney HL (2002) Role of the lever arm in the processive stepping of myosin V. Proc Natl Acad Sci U S A 99(22):14159–14164

Purcell TJ, Sweeney HL, Spudich JA (2005) A force-dependent state controls the coordination of processive myosin V. Proc Natl Acad Sci U S A 102(39):13873–13878

Rayment I, Holden HM, Whittaker M, Yohn CB, Lorenz M, Holmes KC, Milligan RA (1993a) Structure of the actin-myosin complex and its implications for muscle contraction. Science 261:58–65

Rayment I, Rypniewski WR, Schmidt-Bäse K, Smith R, Tomchick DR, Benning MM, Winkelmann DA, Wesenberg G, Holden HM (1993b) Three-dimensional structure of myosin subfragment-1: a molecular motor. Science 261:50–58

Rief M, Rock RS, Mehta AD, Mooseker MS, Cheney RE, Spudich JA (2000) Myosin-V stepping kinetics: a molecular model for processivity. Proc Natl Acad Sci U S A 97(17):9482–9486

Rosenfeld SS, Sweeney HL (2004) A model of myosin V processivity. J Biol Chem 279(40100):40111

Sakamoto T, Amitani I, Yokota E, Ando T (2000) Direct observation of processive movement by individual myosin V molecules. Biochem Biophys Res Commun 272(2):586–590

Sakamoto T, Wang F, Schmitz S, Xu YH, Xu Q, Molloy JE, Veigel C, Sellers JR (2003) Neck length and processivity of myosin V. J Biol Chem 278(31):29201–29207

Sakamoto T, Yildiz A, Selvin PR, Sellers JR (2005) Step-size is determined by neck length in myosin V. Biochemistry 44:16203–16210

Sakamoto T, Webb MR, Forgacs E, White HD, Sellers JR (2008) Direct observation of the mechanochemical coupling in myosin Va during processive movement. Nature 455(7209):128–132

Sellers JR, Veigel C (2010) Direct observation of the myosin-Va power stroke and its reversal 1. Nat Struct Mol Biol 17(5):590–595

Sladewski TE, Krementsova EB, Trybus KM (2016) Myosin Vc is specialized for transport on a secretory superhighway. Curr Biol 26(16):2202–2207. https://doi.org/10.1016/j.cub.2016.06.029

Snyder GE, Sakamoto T, Hammer JA III, Sellers JR, Selvin PR (2004) Nanometer localization of single green fluorescent proteins: evidence that myosin V walks hand-over-hand via telemark configuration. Biophys J 87(3):1776–1783

Sweeney HL, Houdusse A (2010) Structural and functional insights into the myosin motor mechanism 2. Annu Rev Biophys 39:539–557

Sydor AM, Czymmek KJ, Puchner EM, Mennella V (2015) Super-resolution microscopy: from single molecules to supramolecular assemblies. Trends Cell Biol 25(12):730–748. https://doi.org/10.1016/j.tcb.2015.10.004

Syed S, Snyder GE, Franzini-Armstrong C, Selvin PR, Goldman YE (2006) Adaptability of myosin V studied by simultaneous detection of position and orientation. EMBO J 25(9):1795–1803

Takagi Y, Yang Y, Fujiwara I, Jacobs D, Cheney RE, Sellers JR, Kovacs M (2008) Human myosin Vc is a low duty ratio, non-processive molecular motor. J Biol Chem

Takagi Y, Farrow RE, Billington N, Nagy A, Batters C, Yang Y, Sellers JR, Molloy JE (2014) Myosin-10 produces its power-stroke in two phases and moves processively along a single actin filament under low load. Proc Natl Acad Sci U S A 111(18):E1833–E1842. https://doi.org/10.1073/pnas.1320122111

Tanaka H, Homma K, Iwane AH, Katayama E, Ikebe R, Saito J, Yanagida T, Ikebe M (2002) The motor domain determines the large step of myosin-V. Nature 415(6868):192–195

Thirumurugan K, Sakamoto T, Hammer JA III, Sellers JR, Knight PJ (2006) The cargo-binding domain

regulates structure and activity of myosin 5. Nature 442(7099):212–215
Toprak E, Enderlein J, Syed S, McKinney SA, Petschek RG, Ha T, Goldman YE, Selvin PR (2006) Defocused orientation and position imaging (DOPI) of myosin V. Proc Natl Acad Sci U S A 103(17):6495–6499
Uemura S, Higuchi H, Olivares AO, De La Cruz EM, Ishiwata S (2004) Mechanochemical coupling of two substeps in a single myosin V motor. Nat Struct Mol Biol 11:877–883
Veigel C, Wang F, Bartoo ML, Sellers JR, Molloy JE (2002) The gated gait of the precessive molecular motor, myosin V. Nat Cell Biol 4:59–65
Veigel C, Schmitz S, Wang F, Sellers JR (2005) Load-dependent kinetics of myosin-V can explain its high processivity. Nat Cell Biol 7(9):861–869
Vilfan A (2005) Elastic lever-arm model for myosin V. Biophys J 88(6):3792–3805
Wagner W, Brenowitz SD, Hammer JA III (2011) Myosin-Va transports the endoplasmic reticulum into the dendritic spines of Purkinje neurons. Nat Cell Biol 13(1):40–48
Walker ML, Burgess SA, Sellers JR, Wang F, Hammer JA III, Trinick J, Knight PJ (2000) Two-headed binding of a processive myosin to F-actin. Nature 405:804–807
Wang F, Chen L, Arcucci O, Harvey EV, Bowers B, Xu Y, Hammer JA III, Sellers JR (2000) Effect of ADP and ionic strength on the kinetic and motile properties of recombinant mouse myosin V. J Biol Chem 275(6):4329–4335
Wang F, Thirumurugan K, Stafford WF, Hammer JA III, Knight PJ, Sellers JR (2004) Regulated conformation of myosin V. J Biol Chem 279(4):2333–2336
Warshaw DM, Kennedy GG, Work SS, Krementsova EB, Beck S, Trybus KM (2005) Differential labeling of myosin V heads with quantum dots allows direct visualization of hand-over-hand processivity. Biophys J 88(5):L30–L32
Watanabe TM, Tanaka H, Iwane AH, Maki-Yonekura S, Homma K, Inoue A, Ikebe R, Yanagida T, Ikebe M (2004) A one-headed class V myosin molecule develops multiple large (approximately 32-nm) steps successively. Proc Natl Acad Sci U S A 101(26):9630–9635
Watanabe S, Mabuchi K, Ikebe R, Ikebe M (2006) Mechanoenzymatic characterization of human myosin Vb. Biochemistry 45(8):2729–2738
Watanabe S, Watanabe TM, Sato O, Awata J, Homma K, Umeki N, Higuchi H, Ikebe R, Ikebe M (2008) Human myosin Vc is a low duty ratio nonprocessive motor. J Biol Chem 283(16):10581–10592
Watanabe TM, Iwane AH, Tanaka H, Ikebe M, Yanagida T (2010) Mechanical characterization of one-headed myosin-V using optical tweezers. PLoS ONE 5(8):e12224
Wells A, Lin AW, Chen LQ, Safer D, Cain SM, Hasson T, Carragher BO, Milligan RA, Sweeney HL (1999) Myosin VI is an actin-based motor that moves backwards. Nature 401:505–508
Wu X, Bowers B, Rao K, Wei Q, Hammer JA III (1998) Visualization of melanosome dynamics within wild-type and dilute melanocytes suggests a paradigm for myosin V function in vivo. J Cell Biol 143:1–20
Wu XS, Masedunskas A, Weigert R, Copeland NG, Jenkins NA, Hammer JA (2012) Melanoregulin regulates a shedding mechanism that drives melanosome transfer from melanocytes to keratinocytes. Proc Natl Acad Sci U S A 109(31):E2101–E2109. https://doi.org/10.1073/pnas.1209397109
Yildiz A, Selvin PR (2005) Fluorescence imaging with one nanometer accuracy: application to molecular motors. Acc Chem Res 38(7):574–582
Yildiz A, Forkey JN, McKinney SA, Ha T, Goldman YE, Selvin PR (2003) Myosin V walks hand-over-hand: single fluorophore imaging with 1.5-nm localization. Science 300(5628):2061–2065

How Actin Tracks Affect Myosin Motors

9

Alicja Santos, Yauhen Shauchuk, Urszula Cichoń, Kevin C. Vavra, and Ronald S. Rock

Abstract

Cellular organization through cytoskeletal trafficking is a process of fundamental importance. Highly specialized systems evolved that enable motors to identify and select the optimal tracks for motility. In this chapter, we examine the profound effect of actin filament networks on myosin motility patterns. We argue that the myosin classes have adaptations that allow them to detect local structural and chemical cues on actin. These cues are often arranged in a coherent manner on actin filament networks, allowing for directed transport over long distances. We identify a number of potentially important cues, ranging from the biochemical states of actin subunits all the way to multi-filament networks and bundles.

Keywords

Actin polymerization · Post-translational modifications · Actin-binding proteins · Actin networks · Actin filament crosslinkers

9.1 Introduction

Eukaryotic cells are intricately constructed. As membrane-bounded compartments evolved and the cytoplasm became more crowded, cytoskeletal transport systems emerged to handle the difficulty of organizing the cell and ensuring that components could meet at the right place and at the right time. These transport systems are not a luxury, but rather a brutal fact of life. Eukaryotic cells are so crowded that objects larger than a 50-nm diameter vesicle are essentially immobile by diffusion (Howard 2001). Compounding the issue, diffusion is a terrible transport mechanism over large cellular distances. First passage times by diffusion can reach eons in some cases (Howard 2001).

A remarkable feature of cellular organization is that it is spontaneous and robust. Even though there is no cellular architect with blueprints in hand, the cell manages to organize itself through a simple set of molecular interactions. But how simple can these systems be? One prevailing view is that the myosins, other motor proteins, and cytoskeletal filaments simply stir the pot. The motors have no role in defining the architecture;

A. Santos · U. Cichoń · K. C. Vavra · R. S. Rock (✉)
Department of Biochemistry and Molecular Biology, The University of Chicago, Chicago, IL, USA
e-mail: ucichon@uchicago.edu; rrock@uchicago.edu

Y. Shauchuk
Department of Biochemistry and Molecular Biology, The University of Chicago, Chicago, IL, USA

Faculty of Biotechnology, University of Wrocław, Wrocław, Poland
e-mail: eshauchuk@uchicago.edu

L. M. Coluccio (ed.), *Myosins*, Advances in Experimental Medicine and Biology 1239,
https://doi.org/10.1007/978-3-030-38062-5_9

instead, some type of molecular velcro captures the cargoes as they pass. Although seemingly simple, this mechanism is just diffusion all over again. Thus, it suffers from the same poor scaling of first passage times with distance. A second view uses a more clever myosin that picks the few actin filaments that lead to its delivery point. Tightly localized myosin activation is key here. It is true that directed motion has transport times that scale linearly with distance, a desirable feature. And indeed, myosins are carefully regulated, as noted throughout this book. However, even this myosin-centric regulatory system is insufficient. The myosins and their regulatory cofactors do not have a sense of vision, so they have no way to peer into the distance and pick only the actin filaments that lead to the cargo's programmed destination.

In this chapter, we argue for a central role of actin filament networks in organizing myosin traffic, enabling a complete cellular navigation system. The key advance is to recognize that not all actin filaments in the cell are alike. Actin filaments have different ages, are under the influence of different forces, have distinct cohorts of chemical modifications and actin-binding proteins, and exist in different network structures (Blanchoin et al. 2014). The myosins also have their own essential navigation adaptations, and have co-evolved to detect these actin network differences. While the myosins detect local actin features that are within reach (in the molecular recognition sense), those local actin features are tightly coupled to long-range information about where the filaments are headed.

To understand these actomyosin navigation systems, we need to define two key elements. First, actin filaments have structural or chemical diversity that myosin can recognize. The mechanism of recognition is typically through altered myosin kinetics and/or thermodynamics (*e.g.*, myosin affinity for actin, altered ADP release rates, etc.). Second, these different forms of actin must be spatially segregated in the cell, establishing distinct actin networks and cellular compartments. Uniform mixing of these actin types would only serve to globally up/down-regulate the myosin activity, but would not help to organize the cell.

This chapter will define the salient features of cellular actin (Fig. 9.1) and will describe molecular mechanisms for how myosins discriminate among the actin networks. In some cases, the actin structural features are well understood, but whether any myosins detect those features is still an open question. We will discuss the distinguishing features of actin in order of increasing molecular complexity, starting with intrinsic properties of actin, adding additional covalent modifications and actin-binding proteins, and ending with multifilament geometries and network architectures. Our focus is on vertebrate, nonmuscle systems. Muscle regulation through tropomyosin and troponin is extensively covered elsewhere. Although we will discuss the interplay between actin and myosin in terms of trafficking systems, keep in mind that the same molecular recognition principles also apply for systems that generate cytoskeletal tension or anchor organelles.

9.2 Actin Filament Structure

Actin is abundant in all eukaryotic cells and particularly prevalent in muscle, comprising about 20% of the total mass. Also present in non-muscle cells, actin forms a meshwork of filaments that serves as tracks for myosin-based transport. Actin takes two forms: monomeric, globular G-actin, and polymeric, filamentous F-actin. Actin filaments are chains of monomeric subunits lined up in a two-start helix with a pseudo repeat of 36 nm (Oda et al. 2009) (Fig. 9.1.2). Each actin filament is polar, with opposite "barbed" and "pointed" ends that are defined by the asymmetric arrowhead appearance when decorated with myosin fragments. The barbed end of the filament has the most rapid polymerization dynamics (Pollard and Borisy 2003). The length of the filaments, the architecture of their attachments, and force balance determine the dynamic shape of a cell.

The polymerization of actin filaments proceeds in three sequential phases: nucleation, elongation and steady state. The filaments start forming when the total concentration of G-actin exceeds the critical concentration (Cc) for assembly (Oosawa and Kasai 1962). The Cc

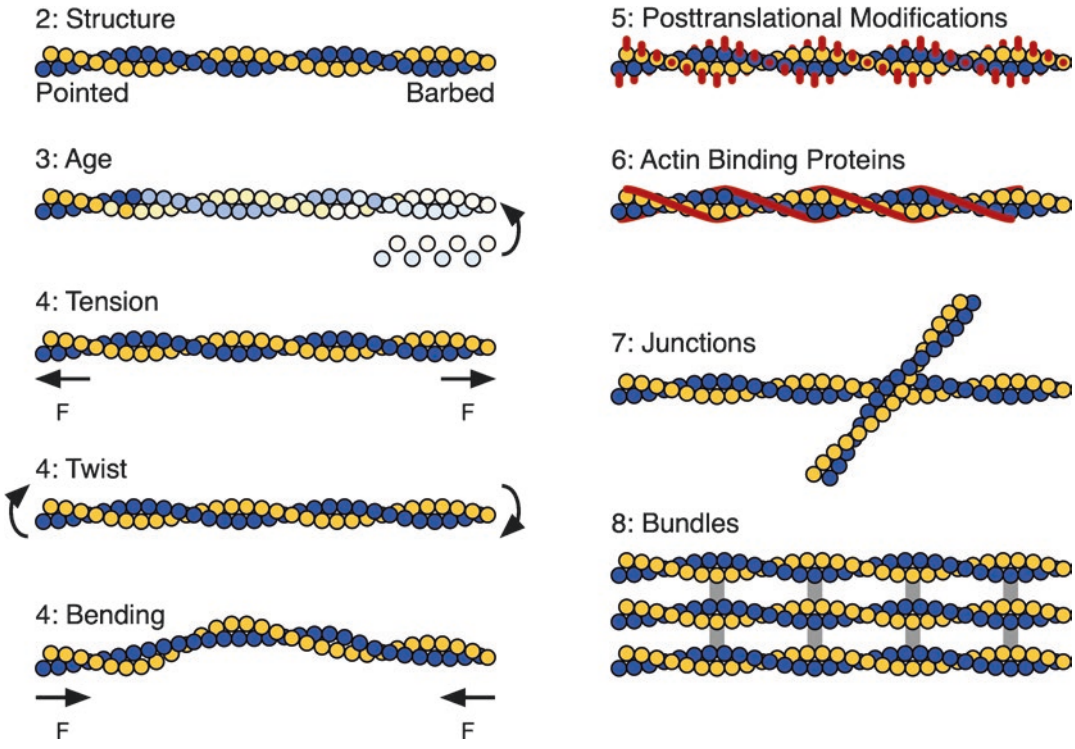

Fig. 9.1 A graphical table of contents for this chapter. Section 2 provides an overview of actin filament structure and polymerization. Section 3 considers actin filament age, where nucleotide state (ATP - > ADP•P_i - > ADP) serves as the clock. The filament is shown with light shades for the ATP state (young actin, at right), intermediate shades for ADP•P_i (middle-aged, middle), and dark shades for the ADP state (old, left). Section 4 examines mechanical perturbations on filaments from external forces and torques. Section 5 examines post-translational modifications and actin-isoform differences. These modifications are shown along the filament in red. Likewise, section 6 considers actin-binding proteins such as tropomyosins, also shown in red. Sections 7 and 8 examine multi-filament junctions and bundled assemblies

depends on the nucleotide bound by the monomer (ATP, ADP•P_i or ADP) and the type and concentration of ions in solution (Pollard and Cooper 1986; Pollard and Weeds 1984; Kang et al. 2012). The salt-dependent Cc in physiological condition has been attributed to binding of a divalent cation (*e.g.*, Mg^{2+}) at discrete sites (Frieden 1983; Estes et al. 1987). Early steps of actin polymerization require a conformational change in actin induced by an interaction with cations. At first a lag period can be distinguished, in which G-actin aggregates into short, unstable dimers. Once the oligomer reaches three subunits in length, it can act as a stable seed, or nucleus. With the nucleation step accomplished, the polymerization process enters the second phase: the filament rapidly elongates by the addition of actin monomers to both of its ends (Sept et al. 1999). The barbed end has a higher affinity for monomeric subunits and elongation progresses rapidly at that end. Thus, the barbed end is also the fast growing end. The pointed end is elongating as well, but at a significantly lower assembly rate, making it the slow growing end (Carlier 1991). As filaments expand, the G-actin monomers are used up in the local environment and their concentration decreases until a steady state is reached. This third phase of actin polymerization is called steady state because G-actin monomers exchange with subunits at the filament ends, but there is no net change in the total mass of filaments.

9.3 Actin Filament Age

The actin cytoskeleton is by no means a static structure in a living cell; the meshwork is constantly assembled, disassembled, and altered depending on the cellular needs. During elongation the actin filament undergoes nucleotide state changes, as the actin monomers in the chain progress from the ATP, to the ADP•P_i, and finally the ADP state. In general, the nucleotide state of each actin subunit depends upon when it was incorporated into the polymer, indicating how long ago that segment of the filament was built (Fig. 9.1.3). Monomers of actin that have the highest binding affinity to filamentous actin are in an ATP state, meaning that they have ATP bound in their nucleotide-binding pocket (Pollard and Cooper 1986; Carlier et al. 1987). The ATP-bound actin subunits newly incorporated into a filament create a so-called "ATP cap". This ATP cap is relatively short-lived. At typical filament growth rates of 10 monomers/s from 1 mM G-actin, the barbed end ATP cap has 30 monomers and is 100 nm long. The ATP is hydrolyzed to ADP•P_i within seconds, leaving the filament subunits with hydrolyzed nucleotide and its inorganic phosphate (P_i) still bound. Release of the P_i from F-actin is up to 100-fold slower (with half-life of ca. 350 s) and yields ADP actin that persists for the remaining lifetime of the filament. The process of ATP hydrolysis and P_i release is stochastic, meaning that there is no defined order for the monomers in the polymer to undergo these changes. In contrast, GTP hydrolysis and product release in microtubules is vectorial. As a result of the ATP hydrolysis and P_i release, most of the actin filament consists of ADP monomers after minutes from the moment of being incorporated into the polymer.

Although the nucleotide state of actin filaments in cells has not been experimentally determined, F-actin networks are enriched locally in ADP•P_i or ADP F-actin (Bindschadler et al. 2004). Actin networks that turnover in seconds, such as those found in dynamic regions of the cell, are enriched for ATP and ADP•P_i filaments (Melki et al. 1996). Other actin structures such as stress fibers have older filaments and are likely in the ADP state. These arguments match the localization of ADF/cofilin, which is typically excluded from the F-actin at the leading edge of migrating cells (Svitkina and Borisy 1999). Thus, old and new actin filaments are spatially segregated in cells, an important feature of any myosin navigation mechanism.

The nucleotide state of actin has structural implications to the entire filament that are still under investigation, with current progress by cryo-EM studies (Merino et al. 2018; Chou and Pollard 2019). Release of P_i closes the actin nucleotide-binding cleft, with an associated rotation of subdomain 2 (Isambert et al. 1995; Belmont et al. 1999). The DNase-I binding loop also folds into an alpha helix upon P_i release (Graceffa and Dominguez 2003). These structural changes also affect global actin filament stiffness (Chu and Voth 2005). Myosins could potentially recognize either the nucleotide-dependent conformational changes or the altered filament stiffness, and adjust their stepping kinetics in response.

Despite this circumstantial evidence that actin filament age might affect myosin motility, it was nevertheless a surprise that the effect was opposite for myosins that move in opposite directions. In single-molecule fluorescence motility assays, myosin-5 run lengths are enhanced 1.5× on young (ADP•P_i) actin, while myosin-6 run lengths are enhanced 3.6× on old (ADP) actin (Zimmermann et al. 2015). In this work, three approaches were used to obtain the desired actin nucleotide state. The first method is to use phalloidin and deliberately capture actin either in the ADP or ADP•P_i state. Phalloidin, a toxin from the mushroom *Amanita phalloides*, is commonly used to stabilize actin filaments. Phalloidin inhibits subunit dissociation at both ends of actin filaments (Coluccio and Tilney 1984). Moreover, phalloidin strongly inhibits the release of P_i, but without inhibiting ATP hydrolysis itself (Dancker and Hess 1990). Therefore, by using phalloidin in canonical single-molecule myosin motility assays, the actin is locked into whichever nucleotide state it was in at the time of phalloidin addition. If phalloidin is present at the nucleation/elongation phase, then the stabilized filament will

be in the ADP•P_i state. If, however, phalloidin is added after most filaments have assembled and aged, then the polymerized actin will be trapped in the ADP state. The second approach is to use capping protein in the single-molecule assays to stabilize actin filaments in the absence of phalloidin. Capping protein allows observations of myosin motility on freshly assembled filaments in the ADP•P_i state versus filaments aged to the ADP state, depending on how long the capped filament was incubated in the flow chamber before myosin motor was introduced. Finally, a motility assay with *de novo* assembled actin filaments allows myosin runs to be associated with a known actin age in a single experiment.

Intriguingly, previous reports found that the myosin-5 run length in untreated cells was 1.5-fold higher than in cells with blocked F-actin dynamics (Semenova et al. 2008). This difference is strikingly similar to what was found during *in vitro* motility assays on polymerizing actin under conditions where F-actin growth rates are also similar (20 monomers/s versus 10 monomers/s). The inherent ability of these myosins to discriminate filaments based on age is based on relatively subtle, but fundamental addition to the arsenal of myosin mechanisms developed to navigate actin networks. Further structural work is now needed to determine exactly how the information about actin nucleotide state (Merino et al. 2018; Chou and Pollard 2019) is transmitted to the myosins.

9.4 Actin Tension, Twist, and Curvature

Environmental forces can distort actin filaments in several ways. Tension tends to straighten and extend actin filaments; compression tends to bend and buckle them; and torques tend to twist them, altering their helical pitch (Fig. 9.1.4). Different myosins (and other proteins) can sense these structural changes in the actin filament to varying degrees.

Myosins are well known to be tension sensitive due to their intrinsic motor activity. A myosin that moves against a load is performing work, and that work is limited by the free energy of an ATP hydrolysis. As the load (and work) increases, the rates of the mechanical transitions slow until the myosin is "stalled" (Howard 2001). Depending on the details of the myosin, this approach to stall can happen through many potential mechanisms (Greenberg et al. 2016). Some of these lead to recruitment of myosins to regions of the cell with actin filament stresses in response (Effler et al. 2006; Ren et al. 2009; Luo et al. 2013).

However, myosins may also sense tension in the actin filament itself. The mechanical situation in this case is somewhat different. Instead of a force applied through a mechanically anchored myosin that stalls, here the tension is along the actin filament and does not involve the myosin. Either the actin filament under tension is not sliding past an anchored myosin, or the myosin is unanchored and free to move along with the filament. Galkin and coworkers have argued that tension on an actin filament can affect filament structure and dynamics in detectable ways (Galkin et al. 2012). And in fact, myosin S1 fragments, which lack anchoring tails and cannot experience load, can nevertheless identify actin filaments under tension. Uyeda and coworkers demonstrated such class-selective, tension-sensitive recruitment in cells. Myosin-2 S1 assembles at sites of actin filament tension, but myosin-1 S1 does not (Uyeda et al. 2011). This intrinsic tension-sensitivity could explain initial recruitment of unassembled myosin-2 s to actin filament networks under tension. Subsequent assembly of the myosin-2 s tails into bipolar thick filaments would then create contractile structures, without requiring *de novo* assembly of a thick filament for load sensing.

Actin filaments can also be twisted, which would alter their overall helical pitch. The most likely sources of actin filament twist are other myosin motors. For example, certain myosins walk processively along the long-pitch helix of actin (Hundt et al. 2016; Norstrom et al. 2010), which would twist the filament if the other end is anchored. However, it is currently unknown if other myosin classes would sense the twisted actin filaments. To discover twist-sensitive myosins, we would need to develop *in vitro* systems

to mechanically twist filaments (Tsuda et al. 1996), combined with single-molecule binding or motility assays.

Finally, actin filaments under compression can have curvature through buckling, a third type of structural distortion that can be used to identify F-actin. Myosin-1c and myosin-1d tend to curve actin filaments in one direction as they move, which may define cellular chirality (Pyrpassopoulos et al. 2012; Lebreton et al. 2018). Those bent filaments might recruit curvature-sensitive myosins. The actin branching and nucleating factor Arp2/3 tends to branch on the convex face of bent actin filaments (Risca et al. 2012), suggesting that structural differences in bent actin are sufficient to modulate protein binding. Further work along these lines is needed to identify curvature-sensitive myosin classes.

9.5 Actin Isoforms and Post-translational Modifications

Actin comes in three main isoforms: α, β, and γ. Muscle (skeletal, smooth, and cardiac) uses α-actin, while nonmuscle cells use the β- and γ-actins. Moreover, actin has post-translational modifications at as many as 94 sites (Varland et al. 2019). In recent years, arginylation at the N-terminus and methionine oxidation have emerged as two particularly important modifications to F-actin. Together, these actin variants have chemical diversity that might be recognized by the myosin classes (Fig. 9.1.5). In microtubule systems, post-translational modifications are believed to constitute a "microtubule code" that distinguishes microtubules from one another (Verhey and Gaertig 2007). We argue that a similar post-translational "actin code" might define F-actin networks in cells.

The actin isoforms are all highly similar, with most diversity concentrated at the N-terminus. However, even here, the sequence diversity is only in the pattern of negatively-charged Asp and Glu residues. Thus, all actin isoforms have a similar net charge at the N-terminus. After initial processing of the start-codon methionine, the β-actin N-terminus begins with Ac-DDD…, while the γ-actin N-terminus begins with Ac-EEE…. Likewise, the muscle α-actin isoforms begin with Ac-DDEE… (cardiac), Ac-DEDE… (skeletal), or Ac-EEED… (smooth) (Varland et al. 2019).

To date, only one study has searched for possible actin isoform effects on myosin motor activity. In work on myosin-5 by De La Cruz et al. (2000), skeletal muscle α-actin was compared to platelet β- and γ-actin (85% β, 15% γ). No major enzymatic rates were affected by the actin isoform. The only significant change was a twofold alteration in the ADP binding rate to the actomyosin (Cruz et al. 2000).

Although the β- and γ-actin isoforms have little chemical diversity and may be indistinguishable from myosin's perspective, they do differ in their ability to accept a specific post-translational modification, arginylation at the N-terminus (Karakozova et al. 2006). Only β-actin receives this particular modification. The process requires cleavage of the N-terminal Ac-D by an unknown peptidase, followed by R addition by the ATE1 enzyme. After arginylation, the N-terminal charge shifts from −3 to net neutral (Ac-DDD to RDD). Arginylated β-actin is concentrated at the leading edge of migrating cells (Pavlyk et al. 2018), and therefore arginylation may serve as a chemical signal to myosins (and other proteins) that the actin is at the leading edge. The reason that γ-actin is insignificantly arginylated is that any arginylated γ-actin is rapidly ubiquitinylated and degraded (Zhang et al. 2010).

Actin is also post-translationally modified through methionine oxidation. Oxidation can occur both through oxidative stress (Shartava et al. 1995; Farah et al. 2011) and through enzymatic addition by the enzyme MICAL. MICAL specifically oxidizes Met44 and Met47 on actin (Hung et al. 2011). MICAL modification tends to destabilize actin filaments, making them more susceptible to cofilin-mediated depolymerization (Grintsevich et al. 2016). Moreover, Met oxidation by MICAL directly alters filament structure (Grintsevich et al. 2017).

There are no known myosins that recognize either arginylation or MetO modification. However, given the location of these modifications at or near the myosin-binding site on actin, future work may uncover myosin regulation by these post-translational modifications. In particular, the N-terminus of actin interacts with loop-2 of myosin (Ecken et al. 2016), and myosin may detect the net charge at this site on actin (Cook et al. 1993). Because myosin loop-2 is a site with high local diversity among myosin classes, it seems likely that arginylation could control myosin traffic on β-actin, activating certain myosin classes while inhibiting others.

One potentially undesirable feature of diversity through isoforms and post-translational modifications is that it is possible to form mixed filaments with many different modifications present. Unless the modifications are added *in situ* to existing filaments in the cell, it is difficult to envision how these modifications would mark whole filaments to contribute to a global myosin navigation mechanism.

9.6 Actin-Binding Proteins

Until now, we have considered purely structural distortions of actin monomer interfaces within polymerized filaments or limited post-translational modifications such as addition of single atoms or residues, both of which provide relatively subtle molecular recognition cues that are nevertheless read by myosins. Next, we will examine actin-binding proteins (ABPs), which present far greater chemical and structural diversity to myosin.

There are currently over a hundred identified ABPs (Remedios et al. 2003a). A major subset of these bind to actin filaments rather than monomeric actin. Filament-binding ABPs establish actin networks with distinct identity and also promote filament polymerization, filament disassembly, or filament bundling (Remedios et al. 2003a). Potentially, any of these F-actin ABPs could modulate myosin function. But one family of ABPs in particular stands out in this regard, the tropomyosins (Tpms) (Ostap 2008; Manstein and Mulvihill 2016).

Tropomyosins form an extended, dimeric, and parallel coiled-coil that decorates the side of actin filaments (Gunning et al. 2008) (Fig. 9.1.6). In skeletal and cardiac muscle, tropomyosins combine with troponin to regulate contraction (Gordon et al. 2000). Tropomyosins are also widely expressed in nonmuscle cells, where they establish distinct actin compartments and play a role in cell shape and motility (Bryce et al. 2003). Mammalian cells have four Tpm genes (see Geeves et al. 2015 for current Tpm nomenclature) that are alternatively spliced to yield 40 isoforms with little, if any, functional redundancy (Gunning et al. 2008; Schevzov et al. 2005). Cancer cells typically down-regulate their high molecular-weight isoforms of Tpm, and when these isoforms are reintroduced into transformed cells, the growth, adhesion, and motility phenotypes are suppressed (O'Neill et al. 2008).

The 40 Tpm isoforms have distinct localization patterns in cells, a necessary condition if Tpms are to spatially regulate myosin activity across the cell (Gunning et al. 2008; Lin et al. 1988). Multiple mechanisms exist to establish the spatial organization of Tpms. In neuronal development, localized protein translation may be sufficient to direct distinct Tpm isoforms to the axon and growth cone (Gunning et al. 2008). Formin-nucleated actin filaments often recruit their own Tpms (Johnson et al. 2014). The Tpms also compete with the binding of other ABPs (*e.g.*, fimbrin, cofilin) in a manner that allows sorting among populations of actin filaments, even in purified systems with a limited number of components (Christensen et al. 2017). Even when competing only with other Tpm isoforms, the Tpms sort by isoform to distinct domains along actin filaments rather than mixing (Gateva et al. 2017). Moreover, regions of the cell undergoing rapid actin polymerization and depolymerization are often devoid of Tpms altogether (DesMarais et al. 2002). Unfortunately, our view of Tpm isoform distributions in the cell is incomplete due to a lack of imaging reagents. The extended Tpm structure spans up to seven actin subunits, which

means that the multiple splice-isoform junctions that form the unique epitopes are widely separated and cannot be identified by a single antibody.

Structurally, Tpm is in an ideal position on actin to regulate myosin activity. In muscle, tropomyosin is positioned such that it blocks myosin binding, and is shifted in a three-state mechanism that includes troponin (McKillop and Geeves 1993; Gordon et al. 2000). However, in nonmuscle systems, which lack troponin and use different Tpm isoforms, the Tpm is found in a variety of positions of similar energy on actin. Recent cryo-EM structures show that one Tpm shifts only slightly in response to nonmuscle myosin binding (Ecken et al. 2015, 2016; Manstein and Mulvihill 2016). Thus, rather than serving as a blunt on-off switch, the nonmuscle Tpms may also modulate myosins in a manner that depends on the details of the binding interface for each myosin class.

Mounting experimental evidence argues that the Tpms do indeed differentially regulate the myosin classes, including myosin-1, myosin-2, and myosin-5. The first such evidence in a reconstituted system showed that a series of expressed Tpm isoforms inhibit myosin-1 (Fanning et al. 1994). Consistent with this inhibition, myosin-1b localizes to dynamic actin filaments in cells that are devoid of Tpms. This myosin-1b localization depends on the myosin motor domain, because swapping the myosin-1b motor domain for that of nonmuscle myosin-2b allows the chimeric myosin to bind throughout the cell (Tang and Ostap 2001).

Nonmuscle myosin-2a (NM2A) motor activity is controlled by tropomyosin Tpm4.2, but in a more elaborate way. As mentioned briefly above, NM2A walks processively along an actin filament. The processive runs are short and composed of ~5.5-nm steps along an actin filament. When tropomyosin Tpm4.2 is purified and added to the actin dumbbell in the optical tweezers experiment, the NM2A takes slower steps and has enhanced processivity at high load (Hundt et al. 2016).

For certain myosin-5 motors, Tpms can control a switch from nonprocessive to processive behavior. This type of switch is ideal for directing motor traffic, because the myosin-5 molecules will move along the "correct", Tpm-decorated F-actin and effectively ignore the "incorrect", undecorated F-actin. The most striking example is the yeast (*S. cerevisiae*) class 5 myosin, Myo2p. This myosin-5 was confounding for some time because, unlike the vertebrate myosin-5 s, it was nonprocessive. However, Hodges and coworkers demonstrated that Myo2p is processive *in vitro* along Tpm1p-decorated F-actin (Hodges et al. 2012). This Tpm is found along yeast actin cables, demonstrating that single molecules rather than small teams of Myo2p are sufficient for transport along cables. Later work by the same group showed much the same behavior in vertebrate systems, where myosin-5a moves along Tpm3.1-actin while largely ignoring Tpm4.2-actin (Sckolnick et al. 2016; see also Barua et al. 2018).

9.7 Actin Filament Junctions

Next, we consider multiple actin filaments and the details of their spatial arrangement. At the point where two actin filaments intersect, myosin motors will often be found to switch from the first track to the second, with no discernible detachment between runs (Ali et al. 2007). Multifilament geometries add another layer of complexity, but must be included in the overall picture because such junctions are common in the cell. The tracks for myosin motors are actually actin networks, which are composed of a dense mix of single, branched and crosslinked filaments (Fig. 9.1.7).

Ali and colleagues used an *in vitro* motility assay to study the behavior of two motor proteins, myosin-5a and myosin-6, in the presence of actin crosses (Ali et al. 2007, 2013). The experimental setup consisted of a 2D mesh of actin immobilized on a coverslip. Actin filaments were labeled such that upper filaments could be distinguished from lower filaments. Myosin-5 and myosin-6 labeled with Qdots were added and tracked. The three possible outcomes at a junction were stopping, crossing over (continuing

straight), or turning onto the intersecting filament.

Of the myosin-5a molecules that encountered the intersection, most turned from the bottom to the top filament (a ratio of 3.2:1) (Ali et al. 2007). The direction of turns is dictated by the polarity of the top filament which is random, so left:right turns occur in a 1:1 ratio. The same ratio for myosin-6 was ~1.5:1, indicating less frequent turns at the junction (Ali et al. 2013). Track switches for both myosins occurred at intersection angles of up to 150°, which indicates considerable flexibility in both myosin-5a and myosin-6 while stepping. Surprisingly, these two myosin classes differ in their ability to turn at a junction. This ability to switch filaments is an excellent strategy for avoiding roadblocks and obstacles in the cell. Control of track switching is also a useful regulatory mechanism for myosin motility, as was observed for cargo transport in *Xenopus* melanophores (Snider et al. 2004).

Although these 2D networks were a significant technical advance, an even more realistic scenario is to consider 3D filament crosses and networks. To this end, the Warshaw group examined teams of myosin-5a motors conjugated to a liposome cargo. These myosin-coated liposomes were tested on filaments suspended between silicon beads to form a 3D actin network (Lombardo et al. 2017; Lombardo et al. 2019). Interestingly, although some myosin parameters (*e.g.*, speed) are comparable to results from single myosin studies, and turns onto the second filament at a junction were frequently observed, some new behaviors emerged. In particular, the 3D network allows myosin-liposomes to swing around the filament and effectively bypass some of the intersections. Although random filament networks constructed *in vitro* are a reasonable model system, in many cellular contexts the actin filaments will be ordered or partially ordered. Consider the effect of actin filament branching by the Arp2/3 complex (Volkmann et al. 2001). In 3D *in vitro* networks, Arp2/3 promotes directional movements of the myosin-5a liposome complexes and more effective overall transport (Lombardo et al. 2019). This phenomenon is likely the result of increased alignment of filament polarity for nearby filaments. This dense alignment allows more track switches and hence longer runs in cells (Snider et al. 2004). As we move to model systems that more closely resemble the cell, we have to consider teams of motors and branched, 3D networks. Both of these features lead to higher run lengths and more directed movement (Lombardo et al. 2017, 2019).

The switching behavior at actin filament junctions raises at least one fundamental question. Why would a single myosin bother with switching from one actin track to another without interruption? It could, after all, just detach, float around, and reattach to a new filament. Is there an important reason to maintain continuous contact with actin while switching in a cellular context? For a single myosin, perhaps not. However, for teams of myosins operating on a single vesicle, there are many more opportunities to engage in a tug-of-war. For these systems, perhaps it is important that the myosins do not let go when switching, or else they will lose the competition.

Although actin crosses seem to be an obstacle for myosin motility at first glance, they instead allow a more intricate form of motility regulation. These recent studies on myosins and crossed actin tracks appear to be one way to approach the question of emergent behavior in cellular transport, and will likely be a fruitful area of investigation.

9.8 Actin Crosslinking and Bundling

The final type of actin we will consider are F-actin bundles (Bartles 2000), a type of actin with a high degree of structural and functional diversity (Fig. 9.1.8). Actin bundles are formed from actin-binding proteins that can create crosslinks between two filaments with varying levels of spatial and directional organization and rigidity. These crosslinked actin networks are found in stress fibers and various cellular projections. Stress fibers are contractile structures formed through the interaction of bundled actin and myosin motors (Tojkander et al. 2012). Cellular projections, such as pseudopodia (Condeelis et al.

1988), lamellipodia (Small et al. 2002), filopodia (Faix and Rottner 2006), and phagocytotic cups (Gerisch 2010), also contain bundled actin. These projections require tight spatial and temporal control of actin polymerization and crosslinking (Lee et al. 1997; Rougerie et al. 2013; Johnson et al. 2015). Because a single actin filament is flexible and will buckle before distorting the plasma membrane, the cell crosslinks ten or more filaments into bundles for additional flexural rigidity (Mogilner and Rubinstein 2005).

On the macroscopic level, actin bundles can create stereocilia, which act as mechanosensors for hair cells within the ears that can change physical force into electrical signals (McGrath et al. 2017). Actin within stereocilia are crosslinked throughout the entire core, resulting in a stiff structure projecting from the cell (Tilney et al. 1980). Fascinatingly, stereocilia have an extremely long turnover time of the actin network (weeks vs. minutes (Loomis et al. 2003; Drummond et al. 2015)), indicating that the crosslinking of actin forms strong and very stable structures. Defects in the cytoskeletal network through mutations of hearing-related myosins and ABPs within stereocilia disrupt mechanotransduction and lead to hearing loss (Friedman et al. 1999; Pylypenko et al. 2015). These roles of actin within stereocilia highlight the importance of a regulated actin network in intricate structures in cells beyond skeletal muscle and cardiac tissue (Costa et al. 2004; Procaccio et al. 2006).

Crosslinking of actin filaments not only generates useful cellular structures, but it also provides a series of unique tracks that myosin motors can identify (Table 9.1) (Takatsuki et al. 2010). The key structural feature is the presence of multiple filaments in a small volume. A two-headed myosin that straddles two filaments can detect that it is walking on a bundle versus a single actin filament. Of particular interest is fascin, which creates parallel bundles with F-actin all oriented with the same polarity. Fascin is a highly selective crosslinker, in that it can only create a link between two actin filaments within 15° of each other (Courson and Rock 2010). In addition to orientation, different actin crosslinking proteins create different spacings between actin filaments, which is important in the building of structures and myosin movement on the bundles.

Table 9.1 Crosslinkers and their functions

Crosslinking protein	Crosslinking function	References
Alpha-actinin	Flexible	Sjöblom et al. (2008); Maruyama and Ebashi (1965); Djinović-Carugo et al. (1999); Courson and Rock (2010)
Dematin	Facilitates binding of spectrin + actin	Koshino et al. (2012)
Dynacortin	Parallel	Robinson et al. (2002)
Fascin	Parallel	DeRosier et al. (1977); Courson and Rock (2010); Jansen et al. (2011)
Filamin	Orient actin to form flexible, orthogonal-angled networks	Nakamura et al. (2011); Popowicz et al. (2006); Stossel et al. (2001)
Fimbrin	Parallel and anti-parallel	Bretscher (1981); Glenney et al. (1981); Skau et al. (2011); Klein et al. (2004)
Villin	Parallel; caps and severs	Khurana and George (2008)

Given the unique structural and functional features of actin bundles, how does a myosin tell that it is walking on a bundle rather than a single filament? Remarkably, the answer had nothing to do with the motor domain, but instead uncovered new functional roles for the myosin dimerization domain in the tail. Many of the discoveries about bundle-selective myosins are related to myosin-10, which has turned into one of the best model systems for myosin navigation in the cell. Myosin-10 is a motor protein that lives at the tips of filopodia (Berg and Cheney 2002), a cellular protrusion with a central core of a fascin-actin bundle (Wood and Martin 2002; Mattila and Lappalainen 2008; Kureishy et al. 2002; Faix and Rottner 2006; Vignjevic et al. 2006).

Myosin-10's specific localization was of particular interest because many cargo proteins known to bind to myosin-10, including VASP and

integrins, were colocalized at filopodial tips with the motor protein (Tokuo and Ikebe 2004; Zhang et al. 2004). To further determine how myosin-10 determines its target actin track, single-molecule microscopy studies were employed to discover the mechanism by which myosin-10 was able to determine its actin track. Myosin-10 HMM fragments moved processively on fascin-actin bundles, but were weakly processive at best on single actin filaments. Myosin-5, on the other hand, was equally processive on both bundles and single filaments. Importantly, other parallel actin bundles could substitute for fascin-actin bundles, demonstrating that the bundle is critical, not the presence of fascin in particular (Nagy et al. 2008). Thus, myosin-10 has a specialized function that enhances transport on bundled actin structures, unlike some other myosin classes. When combined with localized myosin-10 activation in cells (Baboolal et al. 2016), this myosin can achieve exceptionally precise filopodial tip localization.

Additional mechanistic work demonstrated that myosin-10 was straddling two filaments in a bundle (Nagy and Rock 2010; Ricca and Rock 2010). Moreover, chimera studies demonstrated that the dimerization domain in the myosin-10 tail was the key adaptation for selectivity. Replacing myosin-5's tail for that of myosin-10 converted myosin-5 into a bundle-selective motor. Likewise, insertion of flexible linkers into the tail abolished myosin-10's selectivity (Nagy and Rock 2010). Later structural work determined that the coiled-coil of myosin-10 is actually antiparallel (Lu et al. 2012), an unexpected orientation unlike that of myosin-5 (and other studied myosins). Although bundle selection in myosin-10 was initially controversial (Bao et al. 2013; Sun et al. 2010; Takagi et al. 2014), the field appears to be converging toward the view that myosin-10s with antiparallel coiled coils are bundle selective (Ropars et al. 2016; Vavra et al. 2016; Caporizzo et al. 2018). In this case, the details of the coiled coil dimerization domain had a significant impact on the ultimate function of the myosins.

So why is an antiparallel coiled-coil so critical for bundle selection? We believe that the antiparallel structure makes it difficult for myosin-10 to put both of its motor domains on the same filament. In a bundle, myosin-10 has more options that involve other filaments (Ropars et al. 2016; Nagy and Rock 2010; Vavra et al. 2016). We expect that other myosins may also be bundle selective, especially myosins such as myosin-7 and myosin-15 that are also found at bundled structures. In these cases, cargo adapters may serve as structural scaffolds that enforce an overall antiparallel structure of the myosin motor. As the myosin-10 story demonstrates, the diversity of actin and its bundling proteins can provide an efficient means for the identification of different compartments in the cell.

9.9 Conclusion and Perspective

As eukaryotic cells assumed more complex forms, the myosin motor family expanded to meet new transport, tension generating, and anchoring needs. Likewise, actin filament networks gained an enormous breadth of activities. Although *in vivo* imaging and *in vitro* reconstitution have answered many questions, we have much to learn about the complete set of myosin navigation strategies.

An analysis of sequence co-evolution is often the right approach to define potential mechanisms, but here there are additional challenges. The differences between actin filament networks are often established through an ever-expanding set of third parties that pull, distort, decorate, or bundle F-actin. Perhaps the best approach to discover how actin filaments affect myosins is use myosins themselves as imaging reagents in the cell. By mapping their movements, we can let the myosins tell us which actin they would like to use. We have been developing this approach to map cellular actin networks (Brawley and Rock 2009), as have others for actomyosin and other cytoskeletal motors (Sivaramakrishnan and Spudich 2009; Kapitein et al. 2013; Tee et al. 2015). Those efforts are in progress.

Further advances in this field will require us to identify understanding the diversity of actin networks and fully identifying the molecular recog-

nition mechanisms of the myosins. Despite our desire to simplify the system, ultimately there is no way to gloss over the molecular details of such an elegant control system. We hope that this chapter will stimulate further investigations into myosin navigation mechanisms and how the myosins decipher the hidden information encoded in actin networks.

Acknowledgements We thank members of the Rock lab and Annika Sääf for comments. This work was supported by a grant from the National Institutes of Health (GM124272).

References

Ali MY, Krementsova EB, Kennedy GG et al (2007) Myosin Va maneuvers through actin intersections and diffuses along microtubules. Proc Natl Acad Sci U S A 104:4332–4336

Ali MY, Previs SB, Trybus KM et al (2013) Myosin VI has a one track mind versus myosin Va when moving on actin bundles or at an intersection. Traffic 14:70–81

Baboolal TG, Mashanov GI, Nenasheva TA et al (2016) A combination of diffusion and active translocation localizes myosin 10 to the filopodial tip. J Biol Chem 291(43):22373–22385

Bao J, Huck D, Gunther LK et al (2013) Actin structure-dependent stepping of myosin 5a and 10 during processive movement. PLoS One 8:e74936

Bartles JR (2000) Parallel actin bundles and their multiple actin-bundling proteins. Curr Opin Cell Biol 12:72–78

Barua B, Sckolnick M, White HD et al (2018) Distinct sites in tropomyosin specify shared and isoform-specific regulation of myosins II and V. Cytoskeleton (Hoboken) 75:150–163

Belmont LD, Orlova A, Drubin DG, Egelman EH (1999) A change in actin conformation associated with filament instability after Pi release. Proc Natl Acad Sci U S A 96:29–34

Berg JS, Cheney RE (2002) Myosin-x is an unconventional myosin that undergoes intrafilopodial motility. Nat Cell Biol 4:246–250

Bindschadler M, Osborn EA, Dewey CF Jr, McGrath JL (2004) A mechanistic model of the actin cycle. Biophys J 86:2720–2739

Blanchoin L, Boujemaa-Paterski R, Sykes C, Plastino J (2014) Actin dynamics, architecture, and mechanics in cell motility. Physiol Rev 94:235–263

Brawley CM, Rock RS (2009) Unconventional myosin traffic in cells reveals a selective actin cytoskeleton. Proc Natl Acad Sci U S A 106:9685–9690

Bretscher A (1981) Fimbrin is a cytoskeletal protein that crosslinks F-actin in vitro. Proc Natl Acad Sci U S A 78:6849–6853

Bryce NS, Schevzov G, Ferguson V et al (2003) Specification of actin filament function and molecular composition by tropomyosin isoforms. Mol Biol Cell 14:1002–1016

Caporizzo MA, Fishman CE, Sato O et al (2018) The antiparallel dimerization of myosin X imparts bundle selectivity for processive motility. Biophys J 114:1400–1410

Carlier MF (1991) Nucleotide hydrolysis in cytoskeletal assembly. Curr Opin Cell Biol 3:12–17

Carlier MF, Pantaloni D, Korn ED (1987) The mechanisms of ATP hydrolysis accompanying the polymerization of Mg-actin and Ca-actin. J Biol Chem 262:3052–3059

Chou SZ, Pollard TD (2019) Mechanism of actin polymerization revealed by cryo-EM structures of actin filaments with three different bound nucleotides. Proc Natl Acad Sci U S A 116(10):4265–4274

Christensen JR, Hocky GM, Homa KE et al (2017) Competition between tropomyosin, fimbrin, and ADF/cofilin drives their sorting to distinct actin filament networks. Elife 6:e23152

Chu J-W, Voth GA (2005) Allostery of actin filaments: molecular dynamics simulations and coarse-grained analysis. Proc Natl Acad Sci U S A 102:13111–13116

Coluccio LM, Tilney LG (1984) Phalloidin enhances actin assembly by preventing monomer dissociation. J Cell Biol 99:529–535

Condeelis J, Hall A, Bresnick A et al (1988) Actin polymerization and pseudopod extension during amoeboid chemotaxis. Cell Motil Cytoskeleton 10:77–90

Cook KR, Root D, Miller C et al (1993) Enhanced stimulation of myosin subfragment 1 ATPase activity by addition of negatively charged residues to the yeast actin amino terminus. J Biol Chem 268:2410–2415

Costa CF, Rommelaere H, Waterschoot D et al (2004) Myopathy mutations in alpha-skeletal-muscle actin cause a range of molecular defects. J Cell Sci 117:3367–3377

Courson DS, Rock RS (2010) Actin cross-link assembly and disassembly mechanics for alpha-actinin and fascin. J Biol Chem 285:26350–26357

Dancker P, Hess L (1990) Phalloidin reduces the release of inorganic phosphate during actin polymerization. Biochim Biophys Acta 1035:197–200

de la Cruz EM, Wells AL, Sweeney HL, Ostap EM (2000) Actin and light chain isoform dependence of myosin V kinetics. Biochemistry 39:14196–14202

DeRosier D, Mandelkow E, Silliman A (1977) Structure of actin-containing filaments from two types of non-muscle cells. J Mol Biol 113:679–695

DesMarais V, Ichetovkin I, Condeelis J, Hitchcock-DeGregori SE (2002) Spatial regulation of actin dynamics: a tropomyosin-free, actin-rich compartment at the leading edge. J Cell Sci 115:4649–4660

Djinović-Carugo K, Young P, Gautel M, Saraste M (1999) Structure of the alpha-actinin rod: molecular basis for cross-linking of actin filaments. Cell 98:537–546

dos Remedios CG, Chhabra D, Kekic M et al (2003a) Actin binding proteins: regulation of cytoskeletal microfilaments. Physiol Rev 83:433–473

Drummond MC, Barzik M, Bird JE et al (2015) Live-cell imaging of actin dynamics reveals mechanisms of stereocilia length regulation in the inner ear. Nat Commun 6:6873

von der Ecken J, Heissler SM, Pathan-Chhatbar S et al (2016) Cryo-EM structure of a human cytoplasmic actomyosin complex at near-atomic resolution. Nature 534:724–728

von der Ecken J, Müller M, Lehman W et al (2015) Structure of the F-actin-tropomyosin complex. Nature 519:114–117

Effler JC, Kee Y-S, Berk JM et al (2006) Mitosis-specific mechanosensing and contractile-protein redistribution control cell shape. Curr Biol 16:1962–1967

Estes JE, Selden LA, Gershman LC (1987) Tight binding of divalent cations to monomeric actin. Binding kinetics support a simplified model. J Biol Chem 262:4952–4957

Faix J, Rottner K (2006) The making of filopodia. Curr Opin Cell Biol 18(1):18–25

Fanning AS, Wolenski JS, Mooseker MS, Izant JG (1994) Differential regulation of skeletal muscle myosin-II and brush border myosin-I enzymology and mechanochemistry by bacterially produced tropomyosin isoforms. Cell Motil Cytoskeleton 29:29–45

Farah ME, Sirotkin V, Haarer B et al (2011) Diverse protective roles of the actin cytoskeleton during oxidative stress. Cytoskeleton (Hoboken) 68:340–354

Frieden C (1983) Polymerization of actin: mechanism of the Mg2+−induced process at pH 8 and 20 degrees C. Proc Natl Acad Sci U S A 80:6513–6517

Friedman TB, Sellers JR, Avraham KB (1999) Unconventional myosins and the genetics of hearing loss. Am J Med Genet 89:147–157

Galkin VE, Orlova A, Egelman EH (2012) Actin filaments as tension sensors. Curr Biol 22:R96–R101

Gateva G, Kremneva E, Reindl T et al (2017) Tropomyosin isoforms specify functionally distinct actin filament populations in vitro. Curr Biol 27:705–713

Geeves MA, Hitchcock-DeGregori SE, Gunning PW (2015) A systematic nomenclature for mammalian tropomyosin isoforms. J Muscle Res Cell Motil 36:147–153

Gerisch G (2010) Self-organizing actin waves that simulate phagocytic cup structures. PMC Biophys 3:7

Glenney JR Jr, Kaulfus P, Matsudaira P, Weber K (1981) F-actin binding and bundling properties of fimbrin, a major cytoskeletal protein of microvillus core filaments. J Biol Chem 256:9283–9288

Gordon AM, Homsher E, Regnier M (2000) Regulation of contraction in striated muscle. Physiol Rev 80:853–924

Graceffa P, Dominguez R (2003) Crystal structure of monomeric actin in the ATP state. Structural basis of nucleotide-dependent actin dynamics. J Biol Chem 278:34172–34180

Greenberg MJ, Arpağ G, Tüzel E, Ostap EM (2016) A perspective on the role of myosins as mechanosensors. Biophys J 110:2568–2576

Grintsevich EE, Ge P, Sawaya MR et al (2017) Catastrophic disassembly of actin filaments via mical-mediated oxidation. Nat Commun 8:2183

Grintsevich EE, Yesilyurt HG, Rich SK et al (2016) F-actin dismantling through a redox-driven synergy between mical and cofilin. Nat Cell Biol 18:876–885

Gunning P, O'Neill G, Hardeman E (2008) Tropomyosin-based regulation of the actin cytoskeleton in time and space. Physiol Rev 88:1–35

Hodges AR, Krementsova EB, Bookwalter CS et al (2012) Tropomyosin is essential for processive movement of a class V myosin from budding yeast. Curr Biol 22:1410–1416

Howard J (2001) Mechanics of motor proteins and the cytoskeleton. Sinauer Associates, Inc., Sunderland

Hundt N, Steffen W, Pathan-Chhatbar S et al (2016) Load-dependent modulation of non-muscle myosin-2A function by tropomyosin 4.2. Sci Rep 6:20554

Hung R-J, Pak CW, Terman JR (2011) Direct redox regulation of F-actin assembly and disassembly by Mical. Science 334:1710–1713

Isambert H, Venier P, Maggs AC et al (1995) Flexibility of actin filaments derived from thermal fluctuations. Effect of bound nucleotide, phalloidin, and muscle regulatory proteins. J Biol Chem 270:11437–11444

Jansen S, Collins A, Yang C et al (2011) Mechanism of actin filament bundling by fascin. J Biol Chem 286:30087–30096

Johnson HE, King SJ, Asokan SB et al (2015) F-actin bundles direct the initiation and orientation of lamellipodia through adhesion-based signaling. J Cell Biol 208:443–455

Johnson M, East DA, Mulvihill DP (2014) Formins determine the functional properties of actin filaments in yeast. Curr Biol 24:1525–1530

Kang H, Bradley MJ, McCullough BR et al (2012) Identification of cation-binding sites on actin that drive polymerization and modulate bending stiffness. Proc Natl Acad Sci U S A 109:16923–16927

Kapitein LC, van BP, Lipka J et al (2013) Myosin-v opposes microtubule-based cargo transport and drives directional motility on cortical actin. Curr Biol 23(9):828–834

Karakozova M, Kozak M, Wong CCL et al (2006) Arginylation of beta-actin regulates actin cytoskeleton and cell motility. Science 313:192–196

Khurana S, George SP (2008) Regulation of cell structure and function by actin-binding proteins: Villin's perspective. FEBS Lett 582:2128–2139

Klein MG, Shi W, Ramagopal U et al (2004) Structure of the actin crosslinking core of fimbrin. Structure 12:999–1013

Koshino I, Mohandas N, Takakuwa Y (2012) Identification of a novel role for dematin in regulating red cell membrane function by modulating spectrin-actin interaction. J Biol Chem 287:35244–35250

Kureishy N, Sapountzi V, Prag S, Anilkumar N, Adams JC (2002) Fascins, and their roles in cell structure and function. Bioessays 24(4):350–361

Lebreton G, Géminard C, Lapraz F et al (2018) Molecular to organismal chirality is induced by the conserved myosin 1D. Science 362:949–952

Lee E, Shelden EA, Knecht DA (1997) Changes in actin filament organization during pseudopod formation. Exp Cell Res 235:295–299

Lin JJ, Hegmann TE, Lin JL (1988) Differential localization of tropomyosin isoforms in cultured nonmuscle cells. J Cell Biol 107:563–572

Lombardo AT, Nelson SR, Ali MY et al (2017) Myosin Va molecular motors manoeuvre liposome cargo through suspended actin filament intersections in vitro. Nat Commun 8:15692

Lombardo AT, Nelson SR, Kennedy GG et al (2019) Myosin Va transport of liposomes in three-dimensional actin networks is modulated by actin filament density, position, and polarity. Proc Natl Acad Sci U S A 116:8326–8335

Loomis PA, Zheng L, Sekerková G et al (2003) Espin cross-links cause the elongation of microvillus-type parallel actin bundles in vivo. J Cell Biol 163:1045–1055

Lu Q, Ye F, Wei Z et al (2012) Antiparallel coiled-coil-mediated dimerization of myosin X. Proc Natl Acad Sci U S A 109:17388–17393

Luo T, Mohan K, Iglesias PA, Robinson DN (2013) Molecular mechanisms of cellular mechanosensing. Nat Mater 12:1064–1071

Manstein DJ, Mulvihill DP (2016) Tropomyosin-mediated regulation of cytoplasmic myosins. Traffic 17(8):872–877

Maruyama K, Ebashi S (1965) Alpha-actinin, a new structural protein from striated muscle. II. Action on actin. J Biochem 58:13–19

Mattila PK, Lappalainen P (2008) Filopodia: Molecular architecture and cellular functions. Nat Rev Mol Cell Biol 9(6):446–454

McGrath J, Roy P, Perrin BJ (2017) Stereocilia morphogenesis and maintenance through regulation of actin stability. Semin Cell Dev Biol 65:88–95

McKillop DF, Geeves MA (1993) Regulation of the interaction between actin and myosin subfragment 1: evidence for three states of the thin filament. Biophys J 65:693–701

Melki R, Fievez S, Carlier MF (1996) Continuous monitoring of Pi release following nucleotide hydrolysis in actin or tubulin assembly using 2-amino-6-mercapto-7-methylpurine ribonucleoside and purine-nucleoside phosphorylase as an enzyme-linked assay. Biochemistry 35:12038–12045

Merino F, Pospich S, Funk J et al (2018) Structural transitions of F-actin upon ATP hydrolysis at near-atomic resolution revealed by cryo-EM. Nat Struct Mol Biol 25:528–537

Mogilner A, Rubinstein B (2005) The physics of filopodial protrusion. Biophys J 89:782–795

Nagy S, Ricca BL, Norstrom MF et al (2008) A myosin motor that selects bundled actin for motility. Proc Natl Acad Sci U S A 105:9616–9620

Nagy S, Rock RS (2010) A structured post-IQ domain governs selectivity of myosin X for fascin-actin bundles. J Biol Chem 285:26608–26617

Nakamura F, Stossel TP, Hartwig JH (2011) The filamins: organizers of cell structure and function. Cell Adhes Migr 5:160–169

Norstrom MF, Smithback PA, Rock RS (2010) Unconventional processive mechanics of non-muscle myosin IIB. J Biol Chem 285:26326–26334

Oda T, Iwasa M, Aihara T et al (2009) The nature of the globular- to fibrous-actin transition. Nature 457:441–445

O'Neill GM, Stehn J, Gunning PW (2008) Tropomyosins as interpreters of the signalling environment to regulate the local cytoskeleton. Semin Cancer Biol 18:35–44

Oosawa F, Kasai M (1962) A theory of linear and helical aggregates of macromolecules. J Mol Biol 4:10–21

Ostap EM (2008) Tropomyosins as discriminators of myosin function. In: Gunning P (ed) Tropomyosins. Landes Bioscience, pp 273–282

Pavlyk I, Leu NA, Vedula P et al (2018) Rapid and dynamic arginylation of the leading edge β-actin is required for cell migration. Traffic 19:263–272

Pollard TD, Borisy GG (2003) Cellular motility driven by assembly and disassembly of actin filaments. Cell 112:453–465

Pollard TD, Cooper JA (1986) Actin and actin-binding proteins. A critical evaluation of mechanisms and functions. Annu Rev Biochem 55:987–1035

Pollard TD, Weeds AG (1984) The rate constant for ATP hydrolysis by polymerized actin. FEBS Lett 170:94–98

Popowicz GM, Schleicher M, Noegel AA, Holak TA (2006) Filamins: promiscuous organizers of the cytoskeleton. Trends Biochem Sci 31:411–419

Procaccio V, Salazar G, Ono S et al (2006) A mutation of beta -actin that alters depolymerization dynamics is associated with autosomal dominant developmental malformations, deafness, and dystonia. Am J Hum Genet 78:947–960

Pylypenko O, Song L, Shima A et al (2015) Myosin VI deafness mutation prevents the initiation of processive runs on actin. Proc Natl Acad Sci U S A 112:E1201–E1209

Pyrpassopoulos S, Feeser EA, Mazerik JN et al (2012) Membrane-bound Myo1c powers asymmetric motility of actin filaments. Curr Biol 22(18):1688–1692

dos Remedios CG, Chhabra D, Kekic M et al (2003b) Actin binding proteins: regulation of cytoskeletal microfilaments. Physiol Rev 83:433–473

Ren Y, Effler JC, Norstrom M et al (2009) Mechanosensing through cooperative interactions between myosin II and the actin crosslinker cortexillin I. Curr Biol 19:1421–1428

Ricca BL, Rock RS (2010) The stepping pattern of myosin X is adapted for processive motility on bundled actin. Biophys J 99:1818–1826

Risca VI, Wang EB, Chaudhuri O et al (2012) Actin filament curvature biases branching direction. Proc Natl Acad Sci U S A 109:2913–2918

Robinson DN, Ocon SS, Rock RS, Spudich JA (2002) Dynacortin is a novel actin bundling protein that localizes to dynamic actin structures. J Biol Chem 277:9088–9095

Ropars V, Yang Z, Isabet T et al (2016) The myosin X motor is optimized for movement on actin bundles. Nat Commun 7:12456

Rougerie P, Miskolci V, Cox D (2013) Generation of membrane structures during phagocytosis and chemotaxis of macrophages: role and regulation of the actin cytoskeleton. Immunol Rev 256:222–239

Schevzov G, Vrhovski B, Bryce NS et al (2005) Tissue-specific tropomyosin isoform composition. J Histochem Cytochem 53:557–570

Sckolnick M, Krementsova EB, Warshaw DM, Trybus KM (2016) Tropomyosin isoforms bias actin track selection by vertebrate myosin Va. Mol Biol Cell 27:2889–2897

Semenova I, Burakov A, Berardone N et al (2008) Actin dynamics is essential for myosin-based transport of membrane organelles. Curr Biol 18:1581–1586

Sept D, Elcock AH, McCammon JA (1999) Computer simulations of actin polymerization can explain the barbed-pointed end asymmetry. J Mol Biol 294:1181–1189

Shartava A, Monteiro CA, Bencsath FA et al (1995) A posttranslational modification of beta-actin contributes to the slow dissociation of the spectrin-protein 4.1-actin complex of irreversibly sickled cells. J Cell Biol 128:805–818

Sivaramakrishnan S, Spudich JA (2009) Coupled myosin vi motors facilitate unidirectional movement on an f-actin network. J Cell Biol 187:53–60

Sjöblom B, Salmazo A, Djinović-Carugo K (2008) Alpha-actinin structure and regulation. Cell Mol Life Sci 65:2688–2701

Skau CT, Courson DS, Bestul AJ et al (2011) Actin filament bundling by fimbrin is important for endocytosis, cytokinesis, and polarization in fission yeast. J Biol Chem 286:26964–26977

Small JV, Stradal T, Vignal E, Rottner K (2002) The lamellipodium: where motility begins. Trends Cell Biol 12:112–120

Snider J, Lin F, Zahedi N et al (2004) Intracellular actin-based transport: how far you go depends on how often you switch. Proc Natl Acad Sci U S A 101:13204–13209

Stossel TP, Condeelis J, Cooley L et al (2001) Filamins as integrators of cell mechanics and signalling. Nat Rev Mol Cell Biol 2:138–145

Sun Y, Sato O, Ruhnow F et al (2010) Single-molecule stepping and structural dynamics of myosin x. Nat Struct Mol Biol 17:485–491

Svitkina TM, Borisy GG (1999) Arp2/3 complex and actin depolymerizing factor/cofilin in dendritic organization and treadmilling of actin filament array in lamellipodia. J Cell Biol 145:1009–1026

Takagi Y, Farrow RE, Billington N et al (2014) Myosin-10 produces its power-stroke in two phases and moves processively along a single actin filament under low load. Proc Natl Acad Sci U S A 111:E1833–E1842

Takatsuki H, Rice KM, Asano S et al (2010) Utilization of myosin and actin bundles for the transport of molecular cargo. Small 6:452–457

Tang N, Ostap EM (2001) Motor domain-dependent localization of myo1b (myr-1). Curr Biol 11:1131–1135

Tee YH, Shemesh T, Thiagarajan V et al (2015) Cellular chirality arising from the self-organization of the actin cytoskeleton. Nat Cell Biol 17:445–457

Tilney LG, Derosier DJ, Mulroy MJ (1980) The organization of actin filaments in the stereocilia of cochlear hair cells. J Cell Biol 86:244–259

Tojkander S, Gateva G, Lappalainen P (2012) Actin stress fibers–assembly, dynamics and biological roles. J Cell Sci 125:1855–1864

Tokuo H, Ikebe M (2004) Myosin X transports Mena/VASP to the tip of filopodia. Biochem Biophys Res Commun 319:214–220

Tsuda Y, Yasutake H, Ishijima A, Yanagida T (1996) Torsional rigidity of single actin filaments and actin-actin bond breaking force under torsion measured directly by in vitro micromanipulation. Proc Natl Acad Sci U S A 93:12937–12942

Uyeda TQP, Iwadate Y, Umeki N et al (2011) Stretching actin filaments within cells enhances their affinity for the myosin II motor domain. PLoS One 6:e26200

Varland S, Vandekerckhove J, Drazic A (2019) Actin post-translational modifications: the cinderella of cytoskeletal control. Trends Biochem Sci 44:502–516

Vavra KC, Xia Y, Rock RS (2016) Competition between coiled-coil structures and the impact on myosin-10 bundle selection. Biophys J 110:2517–2527

Verhey KJ, Gaertig J (2007) The tubulin code. Cell Cycle 6:2152–2160

Vignjevic D, Kojima S, Aratyn Y, Danciu O, Svitkina T, Borisy GG (2006) Role of fascin in filopodial protrusion. J Cell Biol 174(6):863–875

Volkmann N, Amann KJ, Stoilova-McPhie S et al (2001) Structure of Arp2/3 complex in its activated state and in actin filament branch junctions. Science 293:2456–2459

Wood W, Martin P (2002) Structures in focus—filopodia. Int J Biochem Cell Biol 34:726–730

Zhang F, Saha S, Shabalina SA, Kashina A (2010) Differential arginylation of actin isoforms is regulated by coding sequence-dependent degradation. Science 329:1534–1537

Zhang H, Berg JS, Li Z et al (2004) Myosin-X provides a motor-based link between integrins and the cytoskeleton. Nat Cell Biol 6:523–531

Zimmermann D, Santos A, Kovar DR, Rock RS (2015) Actin age orchestrates myosin-5 and myosin-6 run lengths. Curr Biol 25:2057–2062

Myosins in the Nucleus

10

Ivan V. Maly and Wilma A. Hofmann

Abstract

Although originally characterized as a cytoplasmic protein, myosin of various classes also performs key functions in the nucleus. We review the data concerning the nuclear localization, mechanism of entry, and functional interactions of myosin I, II, V, VI, X, XVI, and XVIII. To date, the first-characterized "nuclear myosin I" (or, in the prevailing nomenclature, myosin IC isoform B) remains the best-studied nuclear myosin, although results are rapidly accumulating that illuminate the roles of other myosin classes, and an outline of a unified picture of myosin functions in the nucleus is beginning to emerge. Reflecting the state of knowledge in this field, the review concentrates on the mechanisms mediating and regulating import of myosin IC into the nucleus and its role, alongside myosin V and VI, in transcription. Myosin functions in chromatin dynamics, epigenetic mechanisms, intranuclear motility, and nuclear export of RNA and protein are also addressed. Partners and regulators of myosin, such as nuclear actin, kinases, and phosphatases are briefly covered. Problem areas are identified and testable hypotheses are offered with an aim of focusing the research efforts on overcoming the gaps on the way toward a systems-level understanding of processes involving nuclear myosins and their place in cell physiology as a whole.

Keywords

Myosin · Nucleus · Nuclear myosin · Myosin IC · Nuclear actin · Localization · Transcription · Chromatin · Intranuclear motility · Nuclear export · Nuclear import · Nucleolus · RNA processing

10.1 Introduction

A growing number of myosin superfamily members have been demonstrated to localize to the nucleus and have specifically nuclear roles, such as intranuclear transport, chromatin dynamics, and functional participation in transcriptional complexes (de Lanerolle and Cole 2002; Hofmann et al. 2006a; Pederson and Singer 2006; de Lanerolle 2012; Sarshad and Percipalle 2014). The study of myosin in the nucleus has advanced from the initial controversy about its localization to the deployment of the modern approaches that resulted in an appreciation of its molecular diversity and polyfunctionality in the nuclei of various organisms. In the framework set by the

I. V. Maly · W. A. Hofmann (✉)
Department of Physiology and Biophysics, Jacobs School of Medicine and Biomedical Sciences, State University of New York, Buffalo, NY, USA
e-mail: ivanmaly@buffalo.edu; whofmann@buffalo.edu

L. M. Coluccio (ed.), *Myosins*, Advances in Experimental Medicine and Biology 1239,
https://doi.org/10.1007/978-3-030-38062-5_10

concept of nucleoskeleton, nuclear myosin is recognized alongside nuclear actin as an essential component of the genome-associated dynamic structural network (Simon and Wilson 2011; Xie and Percipalle 2018). Even though this is still a comparatively young field, much of the recent work already focuses on the place of the relatively well-established aspects of the molecular biology of nuclear myosin among the other pathways of regulation of nuclear functions in the cell and their perturbation in pathology (Li and Yang 2016; Maly and Hofmann 2018).

10.2 Localization to the Nucleus

10.2.1 Discovery and Initial Controversy

The notion of nuclear myosin can be traced to the 1964 work by Ohnishi, Kawamura, and Tanaka (Ohnishi et al. 1964), who used biochemical methods and fractionation to demonstrate the presence of a myosin-like nuclear ATPase activated by a nuclear protein that appeared similar to actin. In fact, the authors called these proteins "nuclear myosin" and "nuclear actin," but also expressed caution about their identification, which reflected the general state of the protein identification methodology at that time. In the two decades that followed, numerous new studies were published that employed other methods (Jockusch et al. 1973; Douvas et al. 1975; Hauser et al. 1975; Lestourgeon et al. 1975; Waldrop et al. 1976; De Martino et al. 1980; Stendahl et al. 1980; Herman and Pollard 1981; Perez et al. 1986; Oriatkina et al. 1989; Milankov and De Boni 1993), but caution and controversy remained attached to this work. Frequent negative results (Ostlund et al. 1974; Comings and Harris 1976; Fujiwara and Pollard 1976; Spyropoulos and Moens 1984; Mittal et al. 1987) were received as signs of irreproducibility of the nuclear localization of myosin. In retrospect, this stage of uncertainty in the study of nuclear myosin was an objective consequence of the contemporary state of the cell-biological methodology. In particular, the methods of the day did not possess the requisite molecular specificity and could not deal reliably with the diversity of the myosin subtypes, which remained hidden. Beginning with the emergence of modern molecular cell biology in the last decade of the twentieth century, the recognition of nuclear myosin went hand-in-hand with the characterization and appreciation of the diversity of myosin classes and isoforms.

10.2.2 Classes and Forms of Nuclear Myosin

10.2.2.1 Myosin IC

Myosin I was the first myosin class specifically demonstrated to be present in the nucleus. The class- and eventually isoform-specificity of this early definitive body of work finally resolved the remaining questions about the validity of the nuclear localization of myosin in the cell. The characterization of monoclonal antibodies against myosin IB (so designated in the nomenclature of the time) from *Acanthamoeba* led to a focus on the antibodies directed against the N-terminus of this protein (Hagen et al. 1986; Rimm and Pollard 1989). Application of this approach to metazoan myosin Iβ – now called myosin IC (Berg et al. 2001; Gillespie et al. 2001) – resulted in identification of a specific isoform that was given the name nuclear myosin I (NMI) (Nowak et al. 1997; Pestic-Dragovich et al. 2000). At the same time, evidence was obtained for the involvement of this isoform in transcription, giving rise to the new direction of functional studies of nuclear myosin, which will be detailed in a subsequent section.

Further work focusing on the N terminus demonstrated existence of three isoforms of myosin IC (Ihnatovych et al. 2012). Isoform A (full name "myosin IC isoform A") is marked by a 35-residue N-terminal sequence, and isoform B (i.e., NMI) – by a 16-residue sequence. Isoform C contains only the sequence that is common to all three isoforms. Isoform A is the last discovered isoform (Ihnatovych et al. 2012). It localizes to both the nucleus and the cytoplasm (Ihnatovych et al. 2012) and is strongly tissue-specific (Sielski et al. 2014). It is also characteristic of progressed

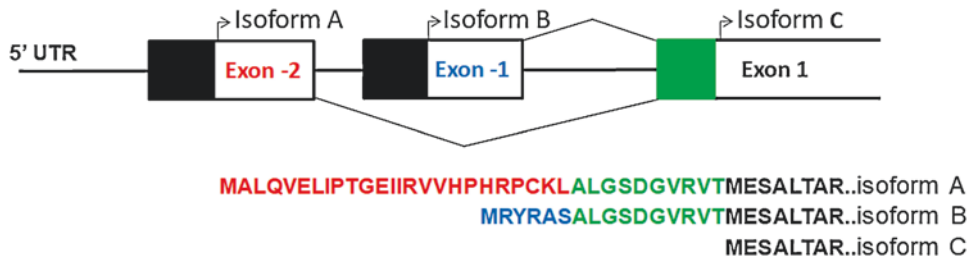

Fig. 10.1 Splicing variants of myosin IC

prostate cancer (Ihnatovych et al. 2014), where it contributes to secretion of matrix metalloproteases and to cell invasion (Maly et al. 2017). The original "nuclear" isoform (B) is actually similarly found in both the nucleus and the cytoplasm. In the cytoplasm, it has the ability to regulate plasma membrane tension, affecting the swelling responses to hypotonicity of the medium (Venit et al. 2016). The effect on the size of red blood cells in isoform B knock-out mice (Venit et al. 2013) can conceivably be related to this function, even though the other developmental defect – the one affecting bone density – remains entirely enigmatic. Isoform C is the original "cytoplasmic" myosin IC. Despite the fact that the commonly employed experimental methods of studying myosin IC do not differentiate between the isoforms, it is safe to assume, awaiting an experimental confirmation, that at least isoform C participates in the well-documented cytoplasmic functions of myosin IC, such as insulin-regulated vesicular transport of glucose transporter proteins (Bose et al. 2002, 2004), neuronal growth cone motility (Diefenbach et al. 2002), and organization of E-cadherin at cell-cell contacts (Tokuo and Coluccio 2013).

In the review of the various functions of myosin IC and its original "nuclear" isoform (B, i.e., NMI) it is important to keep in mind that gene knockdown techniques utilizing RNA interference have only been successful at targeting mRNA stretches from the main, shared sequence of all three isoforms, because the distinct N-terminal sequences are too short to be targeted with sufficient specificity. Less appreciated is the complication arising from a shared stretch on the C-terminal side of the lead peptides found in isoforms A and B, which arises from the first exon of the common myosin IC sequence and lies upstream from the isoform C translation start (Fig. 10.1). The stretch in question is long enough to be immunogenic. In our experience, the commonly used antibody against isoform B (NMI), which was developed before the discovery of isoform A, weakly but noticeably cross-reacts with isoform A. Therefore, in the current state of knowledge, the results that have arisen from antibody-based detection and functional blocking techniques targeted at isoform B may not be entirely specific with respect to isoform A. And even with this caveat, ruling in a role for isoform B with the existing methods does not rule out a role for isoform C, whose sequence is entirely shared with the other isoforms. The above pertains to the endogenous proteins; expression of genetically tagged isoforms from cDNA has served as a complementary method shedding light on their individual localization and function.

As the advancements in this field revealed (to be reviewed in mechanistic detail below), the nuclear localization signal (NLS) resides in the common sequence of all three isoforms and, on closer inspection, all three localize to the nucleus and the cytoplasm to some degree (Dzijak et al. 2012; Ihnatovych et al. 2012; Schwab et al. 2013). The significantly more pronounced nuclear accumulation of NMI/isoform B, however, has been quantitatively demonstrated in cultured human prostate cancer cells under resting conditions (Maly and Hofmann 2016). Further complicating the distinction between "nuclear" and "cytoplasmic" myosin IC is the fact that individual cells cultured in the same conditions can

display significantly different nucleocytoplasmic partitioning of each isoform (Dzijak et al. 2012; Maly and Hofmann 2016). At least isoforms B and C (Dzijak et al. 2012), and presumably also A, enter the nucleus with a delay, following reconstitution of the nuclear envelope after mitosis. However, the variability that is attributable to asynchronous cell division does not completely account for the diversity of the nucleocytoplasmic distributions.

The basic properties of myosin IC can be profitably revisited here insofar as they illuminate some aspects of the still-unresolved problems of the import of myosin IC into the nucleus and the mechanistic differences among the isoforms. So, it can be noted that the motor activity of myosin IC is sensitive to the free calcium concentration, with the kinetics pointing to regulation via calmodulin bound to the neck domain (Adamek et al. 2008). This fact, although it, to date, remains unconnected to the study of nuclear myosin, should be borne in mind when evaluating the molecular-biological context of the calcium- and calmodulin-regulated import of myosin into the nucleus, which will be reviewed below. Furthermore, it has been known for some time that the mechanochemical properties of myosin IC can be experimentally manipulated by fusions to its N-terminus, which, in the three-dimensional structure, is found sandwiched between the motor domain, the lever-arm helix, and the calmodulin bound to the neck region (Greenberg et al. 2015). The most recent work confirms (Zattelman et al. 2017) that the N-terminal extensions demarcating the three isoforms of myosin IC impact the kinetics of this molecular motor. While the distinction between the motor properties of the isoforms participating in the nuclear processes is itself a promising direction for future studies, the confirmed functional significance of the interactions of the N-terminus within the three-dimensional structure of the myosin IC-calmodulin complex is also highly suggestive with regard to the isoform differences in calmodulin-regulated nuclear import, to be reviewed below.

In addition to being expressed ubiquitously in mouse tissues (Kahle et al. 2007; Sielski et al. 2014), isoform B appears to be universal among vertebrates (Kahle et al. 2007). It is also found experimentally in the tunicate *Ciona intestinalis*, and bioinformatic analysis indicates that this isoform is as old as myosin IC itself and similarly specific to the Vertebrates-Tunicates clade of Chordata (Hofmann et al. 2009). However, a putative myosin heavy chain orthologous to human myosin I (named Atz-1) has been recently detected in the nuclei of *Caenorhabditis elegans* (Dawson et al. 2017). Intriguingly, the antibody against myosin IC isoform B also stains nuclei of the onion *Allium cepa* in a multifocal pattern resembling (Cruz and Moreno Diaz de la Espina 2009) the one that will be discussed in relation to the transcription processes in mammalian cells.

10.2.2.2 Other Nuclear Myosins

Myosin IA and IB Recent experiments, which will be reviewed in detail in connection with DNA repair, have demonstrated an intranuclear role for endogenous myosins IA and IB in *Drosophila* and the ability of full-length, tagged variants of these proteins to localize dynamically into the nucleus (Caridi et al. 2018). Further study of their import mechanism and its comparison to the longer-studied forms of nuclear myosin I would be of great interest.

Myosin II Muscle myosin II heavy chain localizes to nuclear pore complexes (Berrios et al. 1991), while the nuclei of myoblasts contain the embryonic isoform (Rodgers 2005). Smooth-muscle as well as non-muscle (Li and Sarna 2009; Xue et al. 2019) forms of myosin II have been implicated in transcription, as will be reviewed below.

Myosin V Myosin VA and VB have been localized to specific intranuclear compartments in distributions dependent on the phosphorylation status of the myosin, transcriptional status of the cell, and intracellular calcium (Pranchevicius et al. 2008; Lindsay and McCaffrey 2009). This work will be reviewed in connection with the respective molecular processes.

Myosin VI Myosin VI has been found in the nuclei of cultured human cells, including prostate cancer cells (Vreugde et al. 2006), simian cells infected with bronchitis virus (Emmott et al. 2010), and in rat skeletal muscle (Karolczak et al. 2013). Among its interaction partners in the latter system, proteins responsible for mRNA transport and maturation, as well as ribonuclear proteins, have been identified. Similar interaction partners, in addition to nucleolin, have been detected in neurosecretory PC12 cells, which also exhibit nuclear localization of this myosin (Majewski et al. 2018). Expression of myosin VI in these cells is important for proliferation and cell migration, but the contribution of the specifically nuclear localization to these processes remains to be established. Conceivably, the functions suggested for this myosin in transcription and RNA processing (to be reviewed below) may play some role.

Myosin X Myosin X localizes to the nuclei in *Xenopus* embryos (Woolner et al. 2008); the images reveal a very strong nuclear accumulation in interphase – almost to the exclusion of any visible cortical localization – and association with the spindle during cell division. However, the functions of this myosin that have been addressed to date relate only to the spindles and cell division (Weber et al. 2004; Woolner et al. 2008; Chan et al. 2014; Sandquist et al. 2018), and to filopodia and cell migration (Umeki et al. 2011; Tokuo et al. 2018; Bachg et al. 2019).

Myosin XVI Myosin XVIB, the principal form of myosin XVI, has been specifically localized to actin-rich euchromatin (Cameron et al. 2007). It is also found in nucleoli (Cameron et al. 2007), although in various tissue types, nuclear myosin XVI appears excluded from this nuclear compartment (Cameron et al. 2013). Overexpression of myosin XVIB has the effect of slowing the cells' progression through S-phase (Cameron et al. 2007). DNA replication inhibition, on the other hand, promotes export of myosin XVI from the nucleus and induces downregulation of its expression on the protein level (Cameron et al. 2013).

Myosin XVIIIB Myosin XVIIIB is distinguished by its large N- and C-terminal domains (Salamon et al. 2003). Upon differentiation of myotubes, it is upregulated and transitions from an exclusively cytoplasmic localization to accumulation in a subset of nuclei within the given fiber. While in non-muscle cells, myosin XVIIIB is involved in assembly of myosin II stacks as part of stress fibers (Jiu et al. 2019), and mutations in it have been implicated in the development of congenital myopathies, which can be accompanied by alterations of the sarcomere structure (Ajima et al. 2008; Alazami et al. 2015; Malfatti et al. 2015; Berger et al. 2017; Gurung et al. 2017), its functions in the nucleus remain to be investigated. In particular, it will be important to establish whether or not they could account for the tumor suppressor qualities of this protein, which have been documented for lung, colorectal, ovarian, and pancreatic cancers, as well as in melanoma (Nishioka et al. 2002; Yanaihara et al. 2004; Nakano et al. 2005; Bleeker et al. 2009). To date, the evidence concerning this function has pointed only at an action that is likely to be explained by the cytoplasmic functionality of myosin XVIIIB, as it localizes to stress fibers and affects anchorage-independent growth and cell motility (Nishioka et al. 2002; Edakuni et al. 2006; Ajima et al. 2007). The picture is far from complete, however, as indicated by the most recently demonstrated involvement of myosin XVIIIB in hepatocellular carcinoma, where it functions as an oncoprotein (Zhang et al. 2018).

10.2.3 Mechanism of Nuclear Localization

10.2.3.1 Myosin IC

Although it was initially determined that the unique N-terminus of isoform B of myosin IC was responsible for its nuclear localization (Pestic-Dragovich et al. 2000), a subsequent reanalysis of the problem by Dzijak et al. uncov-

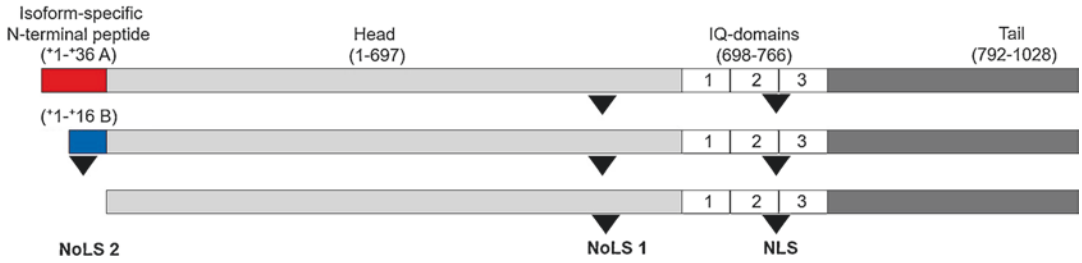

Fig. 10.2 Nuclear and nucleolar localization sequences in the primary structure of myosin IC isoforms

ered a novel NLS sequence in the second of the IQ domains in the neck region of the myosin IC structure (Dzijak et al. 2012). The capacity of this region to direct import to the nucleus has since been additionally confirmed (Schwab et al. 2013). The NLS discovered by Dzijak et al. (residues 754 through 766, Fig. 10.2) contains two clusters of basic amino acids, separated by a short stretch of non-polar residues, and does not function as a nuclear-retention signal. Instead, it is capable of binding importin 5, while importins 7 and β1 also can associate with myosin IC isoform B through an interaction localized to either its tail or neck region (Dzijak et al. 2012). At the same time, the import can be shown to be Ran-independent but sensitive to calmodulin. Overexpression of calmodulin suppresses the import, and the regulatory effect is mediated by the $IQ_{1–2}$ sequence, which is individually capable of associating with calmodulin (Dzijak et al. 2012). The authors of the study noted that the NLS belongs to the sequence that is not specific to isoform B, and succeeded in documenting the localization of isoform C, previously believed to be a cytoplasmic isoform, to the nucleus.

The results of Dzijak et al., in light of calcium-induced dissociation of calmodulin from $IQ_{1–2}$ of myosin IC (Gillespie and Cyr 2002; Houdusse et al. 2006), led to a hypothesis (Dzijak et al. 2012) whereby a calcium signal might dissociate the calmodulin obscuring the NLS and open it to the interaction with importins. Testing this model experimentally (Maly and Hofmann 2016), we were able to demonstrate by means of live-cell imaging that inducing an influx of calcium into the cell indeed leads to a rapid entry of myosin IC into the nucleus. This is seen in individual cells with both isoform C and isoform B, but quantification of the nucleocytoplasmic distributions in individual cells grown under the same conditions shows that only isoforms A and C display a significant shift toward the nuclear localization on the population level. Isoform B, in comparison, is markedly more accumulated in the nucleus under the population-level steady-state conditions, and induction of the calcium influx into the cells does not result in a significant additional shift in favor of the nuclear localization relative to the cytoplasmic one. In this regard isoform B behaves similarly to IQ → AA mutants that are defective for calmodulin binding. Such mutants accumulate in the nucleus in the steady state and do not respond to the calcium stimulus. The induced import can be blocked by inhibiting importin β (Maly and Hofmann 2016), further supporting the model whereby calmodulin and importin compete for access to the NLS, while calcium tips the scales in favor of the importin interaction (Fig. 10.3).

For the future elaboration of this model, it would be of interest to study the impact of the allosteric effect of actin binding, which, as the data suggest (Lieto-Trivedi and Coluccio 2008), leads to release of calmodulin from the second IQ domain of myosin IC. Conceivably, this mechanism could provide an additional pathway for the control of myosin IC localization to the nucleus, acting as a switch and enforcing reciprocal regulation of the cytoskeletal vs. nuclear accumulation and functions of this myosin.

The molecular basis for the difference in the nucleocytoplasmic distributions of the three isoforms of myosin IC remain unknown. It can be noted, however, that in the three-dimensional

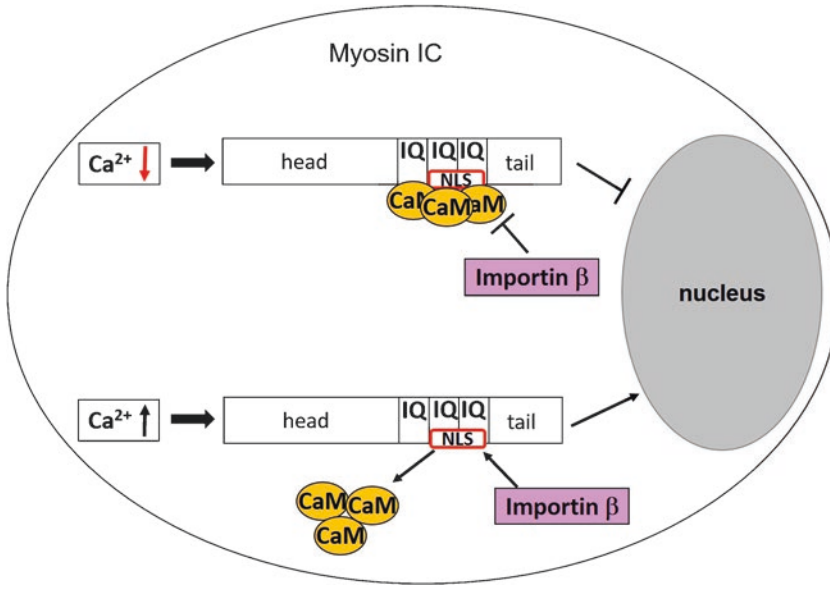

Fig. 10.3 Calcium regulation of myosin IC import into the nucleus

structure of myosin IC, the N-terminus is on the side of the globular head domain that faces the neck domain and interacts with calmodulin bound to the neck (Munnich et al. 2014). Hypothetically, therefore, the N-terminal sequence characterizing isoform B may interfere with calmodulin binding, thus exposing the NLS. The longer N-terminal sequence of isoform A could interfere with both calmodulin binding and the binding of importin β. This hypothesis requires testing. The exact mechanism and molecular-structural basis notwithstanding, the quantitative degree of differential localization visible as shifted proportions of cells with nuclear, cytoplasmic, and equal accumulation (Maly and Hofmann 2016) supports the original notion of importance of the unique N-terminal sequence for determining the nuclear localization of myosin IC isoforms (Pestic-Dragovich et al. 2000).

It is interesting to note that myosin VB was found to be more detectable in the nucleus after treatment of the cells with a cell-permeable calcium chelator (Lindsay and McCaffrey 2009). This might suggest that a mechanism opposite to the one established for myosin IC could be operable in the case of myosin VB. The result, however, was interpreted as arising, hypothetically, from calcium-dependent conformational changes in the myosin, which could regulate the accessibility of the epitope used for detection. The observed effect, however, deserves revisiting in a mechanistic study, in light of the new data on the calcium-dependent import of myosin IC, which shares with myosin VB certain features of the IQ domain architecture and calcium-dependent calmodulin binding (Trybus et al. 2007).

Most recently, a detailed investigation into the mechanism of the myosin IC entry (Nevzorov et al. 2018) has uncovered an unanticipated import pathway and clarified many additional aspects concerning the maintenance of this myosin's nucleocytoplasmic distribution. In this study, FRAP (fluorescence recovery after photobleaching) showed continuous shuttling of myosin IC isoform B into and out of the nucleus, which was significantly slower than that of actin. FLIP (fluorescence loss in photobleaching), at the same time, showed continuous export, which was limited to approximately half of the nuclear content of the isoform. The export signal was found to reside in the head domain, as evidenced by nuclear retention of the neck-and-tail construct. Mutations in the actin-binding sequence,

or in the second IQ domain, did not change the equally cytoplasmic and nuclear distribution of wild-type isoform B. At the same time, a mutation in the presumed NLS in the neck domain decreased the nuclear localization of the full-length isoform B – in agreement with the work already reviewed – but, remarkably, not of the neck-and-tail construct. It can be noted that this result may argue that in the absence of the export signal, the full level of nuclear accumulation can be reached by mechanisms that are independent of the NLS.

The new import pathway in the study by Nevzorov et al. was indicated by the finding that a point mutation in the pleckstrin homology (PH) phosphoinositide-binding domain resulted in a significant shift of isoform B toward cytoplasmic localization. This effect was also seen with isoform C. At the same time, it was found that the PH domain mediates binding of myosin IC to the endoplasmic reticulum (ER). The tail-and-neck construct is successfully imported into the nucleus in permeabilized cells that are supplied with an energy-regenerating mix, which argues in favor of a mechanism independent of any soluble macromolecular import factors. Supporting this notion, importin 5, 7, and β proved dispensable for import in knockdown experiments (Nevzorov et al. 2018). While obtained on isoform B, these results are in keeping with the lack of effect of the importin β inhibitor importazole on the steady-state distribution of isoform C (Maly and Hofmann 2016). In the latter experiments, importazole was only effective in preventing calcium-induced redistribution into the nucleus – of which isoform B was shown to be largely incapable in view of its approximately equally cytoplasmic and nuclear distribution at steady state (Maly and Hofmann 2016).

The combined evidence for the role of the head and PH domain is especially informative in juxtaposition with the earlier finding (Schwab et al. 2013) that the head-and-neck construct of myosin IC did not localize to the nucleus despite the presence of the neck-domain NLS, whereas mutations affecting actin binding led to the construct's accumulation in the nucleus. These results were obtained for all three of the isoforms on the background of unstimulated calcium signaling. Taken together, the data paint a somewhat complex but physiologically meaningful picture of the role of the multiple domains and sequences in orchestrating the localization of myosin IC to the nucleus that is balanced with its function in the cytoskeleton and regulated via intracellular calcium. In this picture, the tail, and likely specifically the PH domain, serves as an additional cytoplasmic-retention signal, presumably through its capacity for binding membrane lipids, that provides redundancy to the similar functionality of the head domain and actin-binding.

In the permeabilized model, the energy-independent binding to the ER membranes precedes the energy-dependent step of nuclear import (Nevzorov et al. 2018). It was further established that the delta-head construct of myosin IC binds chromatin independently of the integrity of its NLS sequence or PH domain. Both stretches, however, are involved in the construct's binding to PIP_2-containing lipid vesicles. Overall, the findings of Nevzorov et al. led to a model whereby myosin IC binds phosphoinositide-containing membranes of the ER prior to being transported via an active membrane-associated flow into the nucleus. According to the data, this mechanism appears to be responsible both for the post-mitotic entry into the nuclei of daughter cells and for the continued constitutive shuttling of myosin IC to the nucleus.

It has been argued that wild-type myosin IC (isoform B) is inaccessible to the conventional nuclear import factors, because fusing it with the SV40 NLS did not affect its nucleocytoplasmic distribution, whereas the same fusion drove the presumably solvable PH-domain mutant to the nucleus (Nevzorov et al. 2018). However, it should be noted that the results obtained with the SV40 NLS may also reflect the fact that the nearly full level of nuclear localization of isoform B is reached by the wild type, as far as cell population-level steady state is concerned (Maly and Hofmann 2016), whereas the PH-domain mutant is predominantly cytoplasmic (Nevzorov et al. 2018). In agreement with this view, individual cells that start with a predominantly cytoplasmic isoform B distribution are capable of

rapid calcium-induced and importin-dependent import (Maly and Hofmann 2016).

On the whole, the present state of knowledge in this field allows it to be posited that in addition to a constitutive phosphoinositide- and ER membrane-mediated import pathway (Nevzorov et al. 2018), an induced import pathway is operable that is mediated by importin β (Maly and Hofmann 2016). How the NLS sequence in the neck region of myosin IC switches from phosphoinositide binding – a function implicated by the experiments of Nevzorov et al. – to (possibly mediated) importin binding upon arrival of the calcium signal presents an interesting question for further studies. The first step toward illuminating this issue may be determining the role of calmodulin in the phosphoinositide-mediated pathway. Indeed, calcium is capable of releasing the calmodulin inhibition of lipid binding by myosin IC fragments containing the neck and tail (Tang et al. 2002; Hirono et al. 2004). This effect is in agreement with our observation that IQ mutants of isoform C may display significant plasma membrane-associated localization alongside their enhanced nuclear localization (Maly and Hofmann 2016). The relevance of such a mechanism of calmodulin-mediated regulation to nuclear import in general, and its implications for the distinction between the constitutive and induced pathways remain to be elucidated.

10.2.3.2 Other Myosins

Myosin IIA The NLS in myosin IIA in neurons is responsible for nuclear import of an apoptosis mediator, annexin 1, during oxygen deprivation and reoxygenation-induced cell injury (Zhao et al. 2015). This action complements annexin's myosin-driven mechanism of translocation across the cytoplasm, at the end of which the complex of the two proteins is recognized by importin β. A breaking report identifies the nuclear-targeting sequence of annexin 1 and a means to inhibit it as an experimental approach to the treatment of stroke (Li et al. 2019). The relationship of the identified sequence to the myosin-mediated import pathway remains, however, to be clarified. It would be of interest to assess generality of the combined mechanism of transport and nuclear entry, for instance, on the example of the recently discovered role of non-muscle myosin heavy chain IIA (Xu et al. 2016) in the nuclear translocation of CXCR4, a G protein-coupled receptor involved in renal carcinoma invasion (Bao et al. 2019). At the same time, non-muscle myosin heavy chain IIA binds the tumor suppressor menin in both the cytoplasm and the nucleus (Obungu et al. 2003). Menin is known to have its own nuclear-localization sequences, whose mutations are associated with endocrine neoplasia (Guru et al. 1998; La et al. 2006). Thus, the nuclear co-import of myosin IIA and its molecular partners may be driven by either side of the myosin-partner complex, and subject to compounded regulation. A further variation on the theme of co-import of myosin with other proteins in pathology is presented by the case of the CBF-SMMHC fusion in leukemia. Even though CBF itself is constitutively nuclear, the myosin tail domain contains a sequence that is instrumental in the nuclear entry of the fusion protein (Kummalue et al. 2002).

Myosin VI Potassium stimulation of rat pheochromocytoma PC12 cells causes enhanced nuclear localization of myosin VI (Majewski et al. 2018). A number of potential nuclear-localization sequences and a nuclear-export sequence have been identified bioinformatically in the head, neck, and tail regions of this protein (Vreugde et al. 2006; Majewski et al. 2018), and its accumulation in the nucleus has been shown to be sensitive to nuclear import and export inhibitors (Majewski et al. 2018). One of the putative NLS resides in the IQ domain of myosin VI, raising the possibility that a calcium-regulated mechanism might be operable in the case of this myosin class as well. Another, in the globular tail domain, contains the RRL protein interaction motif whose involvement in transcription will be reviewed below. Here it is of interest that this motif (and, presumably, the potential bipartite NLS) is obscured by an α-helix that is formed in a splicing isoform of myosin VI known as the "long" isoform (Wollscheid et al. 2016). Remarkably, this isoform is not localized to the

nucleus (Fili et al. 2017). This finding argues in favor of the role of the RRL-containing sequence as a critical NLS for myosin VI. At the same time, the "short" isoform that localizes to the nucleus (Fili et al. 2017) is specifically associated with ovarian cancer and responsible for migration of ovarian and breast cancer cells (Wollscheid et al. 2016). While myosin VI is also associated with aggressive prostate cancer and prostate cancer cell migration (Dunn et al. 2006), isoform specificity of its function in this malignancy remains to be elucidated.

Myosin X The mechanism of nuclear localization of myosin X has not yet been probed directly, but a number of molecular connections have been uncovered in the course of the investigations into this myosin's non-nuclear functions that can be seen as furnishing hypotheses concerning its entry into the nucleus. So, it has been noted that in *Xenopus* embryos, the nuclear accumulation of myosin X in interphase coincides with that of the spindle pole protein TPX2, which could be attributed to the two proteins' interaction through the MyTH4/FERM domain of myosin X (Woolner et al. 2008). It could, it was reasoned, therefore follow the regulated, cell cycle-dependent localization of TPX2, which is effected by the latter's interaction with importins and Ran (Gruss and Vernos 2004). At the same time, it was reported that the MyTH4/FERM cassette of myosin X itself can bind importin α (Woolner et al. 2008). Furthermore, the PH-domain cassette of myosin X has been demonstrated to target it to filopodia via phosphoinositide interactions (Umeki et al. 2011). It is conceivable that the phosphoinositide-mediated mechanism implicated in the nuclear import of myosin IC may be operable in the case of myosin X as well.

Myosin XVIB This myosin has also been demonstrated to possess a region in the tail that directs it to the nucleus (Cameron et al. 2007). Under the action mediated by this region, myosin XVIB achieves a predominantly nuclear localization in interphase. The minor isoform, myosin XVIA, does not have this region in its primary structure, and displays a negligible localization to the nucleus. Myosin XVIB, at the same time, is continuously shuttled in and out of the nucleus, and its level of nuclear accumulation is sensitive to inhibition of nuclear export. Remarkably, the head domain does not regulate the degree of retention of this myosin in the cytoplasm. The degree of nuclear localization of myosin XVI has – similarly to the reviewed case of myosin IC – been shown to vary within the cell population, and a shift in favor of more predominantly nuclear distribution could be seen with leptomycin B, an inhibitor of the export mediator CRM1 (Cameron et al. 2013). Residues 340–341 and 1061–1069 (which belong to the sequence common to both isoforms) were found to contain consensus leucine-rich nuclear motifs characteristic of the signals for CRM1-mediated nuclear protein export.

10.2.4 Nucleolar Localization

Myosin IC The molecular basis for the localization of nuclear myosin has also been studied on a finer level of localization to a major subnuclear compartment, the nucleolus. In the instance of myosin IC, it has been established that nucleolar targeting is attained through two sequences, termed nucleolar localization signals (NoLS), one of which resides in the head domain and the other in the N-terminal sequence that is specific to isoform B (Schwab et al. 2013). Both NoLS are necessary for localization to nucleoli, which explains the characteristic nucleolar localization of only one isoform, B. Moreover, this finding sheds light on the enigmatic specificity of the nuclear functions that distinguish the isoforms despite their largely identical primary structure, and specifically on the fact that unlike isoform B, which is essential for RNA polymerase I transcription (to be reviewed below), isoform A is not associated with this polymerase (Ihnatovych et al. 2012). Evidently, however, much more work is needed to fully explain the differences between the isoforms on the molecular level and

define the place of this complexity in the system-level regulation of the nuclear function.

The head-domain NoLS of myosin IC is comprised of amino acid residues 619–637 and contains two basic amino acid clusters, $R_{621}VRR_{624}$ and $R_{630}RK_{632}$ (Schwab et al. 2013). High basic amino acid content is a distinctive feature of NoLS found in other proteins (Scott et al. 2010). In the myosin IC head domain, both basic amino acid stretches are necessary for nucleolar localization (Schwab et al. 2013). Interestingly, when constructs (other than full-length myosin) are directed to the nucleolus by the head-domain NoLS alone, they localize exclusively to the granular component of this organelle and not to the fibrillar center or dense fibrillar component. In the isoform B specific N-terminal sequence, arginines at positions +2 and +4 (upstream of the beginning of the isoforms' common sequence) are involved in the nucleolar targeting, as part of the N-terminal NoLS. These residues are also responsible for directing a non-myosin construct bearing the sequence of the N-terminal NoLS to a perinucleolar localization pattern.

The significance of the distinct individual functions of the head-domain and isoform B specific NoLS for the sub-nuclear targeting of full-length myosin IC remains to be investigated, but they serve as an indication that the cooperative action of the two domains may resist a purely reductionist explanation. Several NoLS per protein are a common feature among the well-studied cases of nucleolar targeting (Hahn and Marsh 2007; Zhou et al. 2010; Kalt et al. 2012). The molecular basis for their action and for the necessity of more than one NoLS per protein remains insufficiently understood. Thus, further deciphering of the nucleolar targeting of myosin may shed light on this broader issue in nuclear biology. Another question that remains to be addressed is the functional or structural differences in the conditions that lead to the localization of isoform B to the fibrillar center and dense fibrillar component (Fomproix and Percipalle 2004; Kysela et al. 2005; Philimonenko et al. 2010), which is transcription-dependent and will be reviewed below in connection with that process.

Myosin V Isoforms of myosin V similarly display differential localization to the nucleolus (Lindsay and McCaffrey 2009). While both isoform A and isoform B are present in the nucleus, only B enters the nucleoli. An arginine-rich motif has been identified in the neck region of this isoform, which overlaps the calmodulin-binding IQ repeats. It was hypothesized, therefore, that calcium-regulated binding of calmodulin could regulate the accessibility of the NoLS and, consequently, targeting of myosin VB to the nucleolus. In light of the positive identification of a calcium-dependent mechanism of myosin IC import to the nucleus itself, it becomes imperative to revisit this hypothesis.

Myosin XVIB By comparison, nucleolar targeting of the nuclear isoform of myosin XVI – myosin XVIB – appears to be mediated by the N-terminal ankyrin-repeat domain that is characteristic of this myosin class. This notion is based on the observation that the N-terminus of myosin XVI is intrinsically capable of localizing to the nucleoli (Cameron et al. 2007). The mechanism of targeting in this case was seen as stemming from the ability of myosin XVI to bind protein phosphatase 1 catalytic subunit (Patel et al. 2001), believed to be analogous to ankyrin repeats-mediated binding by the myosin-targeting subunit (Hartshorne 1998), in view of the phosphatase's distribution to the nucleoli (Trinkle-Mulcahy et al. 2003). If so, the mechanism of the nucleolar targeting of myosin XVIB would be similar to the one that is known to be mediated by the ankyrin-repeat domain of IκB-α (Sachdev et al. 1998). The molecular partners involved in the nucleolar targeting of both myosin IC and XVIB remain to be identified. Despite the fact that in both cases, sequences preceding the head domain have been implicated, it appears unlikely that the interaction mechanisms mediated by them could be similar, given the great divergence between these myosin classes.

10.3 Molecular Partners of Myosin in the Nucleus

10.3.1 Nuclear Actin

Of all the functional partners of myosin, actin is certainly the best characterized. In addition to establishing the functions of these two proteins in the nucleus, studies continue to address the question of similarity and difference of their mode of interaction inside the nucleus relative to the paradigmatic modes they exhibit in the cytoplasm. Mechanisms involving nuclear actin are also a vibrant field on their own (Hofmann 2009; Belin and Mullins 2013; Virtanen and Vartiainen 2017; Plessner and Grosse 2019). Here, the current state of knowledge related to nuclear actin will be briefly reviewed as an introduction to the survey of its established interactions with nuclear myosin and to indicate its functions that remain unconnected to myosin, which may represent fruitful directions for researchers searching for novel system-level as well as molecular interactions in the nucleus.

Actin is co-transported into the nucleus with cofilin via an interaction with importin 9 (Dopie et al. 2012). Depleting importin 9 lowers the intranuclear content of actin and leads to inhibition of transcription. Transcriptional regulation through the levels of β-actin in the nucleus can also be under the control of growth factors, as demonstrated in experiments on mammary epithelial cells subjected to removal of serum (Spencer et al. 2011). Some of the latest results concerning the nucleocytoplasmic balance of actin come from work conducted on stem cells, which have been shown to be capable of fine-tuned transcription and epigenetic silencing that is orchestrated by mechanical forces (Le et al. 2016). In this system, morphogenetic lineage commitment depends on force-induced polymerization of actin in the cytoplasm that lowers the nuclear actin levels, leading to transcription inhibition and histone trimethylation in the facultative heterochromatin. The co-imported actin-depolymerizing protein cofilin plays its own role in transcription, being necessary for elongation by RNA polymerase II and associated with chromatin modifications (Obrdlik and Percipalle 2011). Most recently, intranuclear cofilin was found to be linked to malignancy in melanoma (Bracalente et al. 2018) and induced by oxidative DNA damage in medulloblastoma (Lewinska et al. 2019).

Polymeric nuclear actin (Belin et al. 2013; Plessner et al. 2015) has a number of particular functions. One established example is provided by intranuclear polymerization driven by formin, which can be induced by serum and mediates specific transcription factor activation (Baarlink et al. 2013). The large nuclei in *Xenopus* oocytes provide another revealing model (Bohnsack et al. 2006). These cells are naturally deficient in exportin 6, which normally mediates export of actin from the nucleus, and, as a result, accumulate large amounts of actin. An extensive intranuclear F-actin framework is responsible for maintaining the mechanical integrity of these uncommonly large pre-meiotic nuclei. It also prevents sedimentation of nucleoli and ribonucleoprotein aggregates (Feric and Brangwynne 2013). While *Xenopus* oocyte nuclei are unusual by virtue of their size, the functionality of F-actin in them presumably belongs to a continuum shared with normal-size nuclei and presents interest for probing its cooperation with nuclear myosin. One specific direction for this work may be elucidating how nuclear myosin affects the viscoelastic properties of the F-actin scaffold, which underlie the phenomenon of mechanical aging (Feric et al. 2015) that is so pronounced in the *Xenopus* oocyte model.

In addition to what has so far appeared as a passive mechanical role in supporting the intranuclear structures, actin polymerization has been implicated in intranuclear movement. HSP70 constructs have been seen to move in an actin depolymerization-sensitive manner toward nuclear speckles in the course of the gene activation following heat treatment (Khanna et al. 2014). Conversely, human immunodeficiency virus type 1 (HIV-1) provirus silencing by proximity to nuclear bodies can be relieved by their displacement powered by actin polymerization (Lusic et al. 2013). More instances of actin involvement in intranuclear movement, in which

the cooperation with myosin is firmly documented, will be reviewed in the corresponding section below.

Interestingly, depending on the conditions, the polymeric actin structures induced in the nucleus by heat shock may or may not include cofilin or accept traditional staining based on decoration with phalloidin (Serebryannyy et al. 2016c). Along with the requirement for certain novel actin probes in the cited work by Belin and Plessner, this recent finding strengthens the indication that the form of actin polymerization – or linear aggregation (Hill 1987) – in the nucleus is not necessarily identical, in all instances, to the form that is common in the cytoplasm. Furthermore, the study by Serebrannyy and colleagues showed that both the cofilin-containing rods and the ones that result from a polymerization-promoting mutation in actin are characteristic of intranuclear rod myopathy and perturb the spatial distribution of chromatin and RNA polymerase II.

Formin-mediated actin polymerization also participates in DNA repair (Belin et al. 2015). The nuclear content of formin 2 increases following DNA damage and, along with importin 9, this protein plays an important role in achieving an efficient clearance of double-stranded breaks. During this process, nuclear actin accepts phalloidin staining and forms long filaments in the nucleoplasm, short filaments associated with the nucleolus, and certain assemblies that can be described as dense clusters. Current research is clarifying the molecular mechanisms involved in the nuclear actin dependent DNA repair and suggests that it can be targeted as part of a combination chemotherapeutic regime (Pfitzer et al. 2019). The formin mDia2, by comparison, catalyzes formation of short, dynamic actin filaments in the interphase nucleus that position centromeric chromatin, facilitating association of the centromeric histone CENP-A (Liu et al. 2018).

Data show that actin need not acquire the polymeric form to perform some of its key functions in the nucleus. For example, the RNA polymerase II transcription elongation factor P-TEFb is recruited to the transcription complex through a mechanism that includes binding of its catalytic subunit, Cdk9, to G-actin (Qi et al. 2011). Furthermore, paradigmatic chromatin remodeling complexes such as SWI/SNF possess actin- and actin-related protein binding sites composed of their components' HSA domains, which can be essential in vivo (Szerlong et al. 2008). Remarkably, the bound actin in these complexes can be stoichiometrically monomeric (Klages-Mundt et al. 2018). At the same time, binding of monomeric actin to histone deacetylases plays an inhibitory role and couples the activity of these enzymes to the overall degree of polymerization of actin in the nucleus (Serebryannyy et al. 2016a). In connection with the chromatin dynamics functions of nuclear myosin, it is noteworthy that actin binds histone acetyltransferase PCAF, which facilitates RNA polymerase II transcription on chromatin (Obrdlik et al. 2008). This finding is especially suggestive of an actin-myosin interaction mechanism in light of the recruitment of this acetyltransferase by nuclear myosin, which will be reviewed in the section on chromatin dynamics.

The question of the polymeric vs. monomeric form of actin has been particularly intensely debated in connection with the function of actin in transcription. The results in this specific area, to date, have not been definitive. On the one hand, transcription by polymerase II is inhibited by actin-depolymerization agents *in vitro* (Wu et al. 2006). Also, the actin-polymerization activator N-WASP is part of the polymerase II transcription complex, and transcription is suppressed by its truncated version that is dominant-negative for Arp2/3-mediated actin polymerization (Wu et al. 2006). Moreover, the F-actin nucleator Arp2/3 is directly associated with RNA polymerase II (Yoo et al. 2007). On the other hand, WASP has a function in transcription that is independent of Arp2/3 activation (Sadhukhan et al. 2014). Additional contrarian evidence is represented by the facts that the association of actin with RNA polymerase II is insensitive to polymerization inhibitors (McDonald et al. 2006), and, moreover, experimentally driving the polymerization of nuclear actin disrupts RNA polymerase II transcription (Serebryannyy et al. 2016b). The collectively inconclusive, or non-

uniform, indications as to the polymerization state of actin involved in transcription are especially consequential for the unresolved question of the biophysical mode of the actin-myosin cooperation in this process, to which we will return in the following.

10.3.2 Myosin Regulators in the Nucleus

Besides actin, a range of other molecular partners of myosin, such as calmodulin, particular light chains, kinases, and phosphatases, have been found in the nucleus and implicated in a variety of nuclear functions. Some of these partners now have a comparatively well-established mechanism of interaction with nuclear myosin, which underlies their common function in the basic nuclear processes. These instances will be reviewed under the specific functional rubrics in the next section. Here we would like to collect a few instances where the studies of the dynamics and function of myosin-binding molecules in the nucleus have been fruitful but remain divorced from understanding the role of their interaction with nuclear myosin. It is hoped that this brief review of the apparently "orphaned" topics – as they may be viewed from the perspective of nuclear myosin biology – may stimulate the interest of myosin researchers.

Calmodulin, now firmly implicated in the regulation of import of myosin into the nucleus (reviewed above), is itself a nuclear protein with multiple roles that have been studied, to date, without regard to its interaction with nuclear myosin and the modulation or functional ramifications that it might bring. Since the early work on nuclear calmodulin, we know of its involvement in resistance to DNA damage (Chafouleas et al. 1984) and its ability to promote phosphorylation of nuclear proteins (Bachs and Carafoli 1987) and attenuate calcium-dependent induction of gene expression (White 1985). One well-researched direction is the role of calmodulin in signal propagation to the nucleus of neurons (Cohen et al. 2015). In this instance, calmodulin is shuttled to the nucleus in association with γ calmodulin-dependent kinase II in response to a cytoplasmic calcium signal mediated by influx through Ca_v1 channels in the plasma membrane. The translocation is followed by dissociation of the complex and release of the calcium-calmodulin, which is then able to activate the nuclear pools of other calmodulin-dependent kinases, leading to phosphorylation of the memory-associated transcription factor CREB. In light of the new data on nuclear myosin, one may begin to ask questions, for example, about the possibility that the calmodulin and myosin functionally recombine in the nucleus following their dissociation induced by the cytoplasmic calcium signal, with the CREB-mediated gene expression facilitated by the myosin interaction with the transcription machinery (the latter to be reviewed in the next section).

Skeletal muscle myosin light chain kinase (MLCK) is detectable in the nuclei of differentiated neurons (Pujol et al. 1993) as well as pluripotent stem cells (Al Madhoun et al. 2011). In stem cells, it is implicated in myogenic differentiation by phosphorylating the transcription factor MEF2C. In Schwann cells, on the other hand, nuclear MLCK plays the role of a negative regulator of myelination, downstream of cAMP signaling (Leitman et al. 2011). In light of the localization of myosin II to the nucleus (Berrios et al. 1991; Rodgers 2005) and its involvement in transcription processes in a manner regulated by light chain modifications, to be reviewed below (Li and Sarna 2009; Nevitt et al. 2018; Xue et al. 2019), these findings suggest a possibility that the other documented MLCK-dependent nuclear functions may also involve nuclear myosin, or otherwise intersect and cooperate with processes mediated by nuclear myosin. Recent work on myosin light chains in the nucleus adds impetus to follow up on the cited studies from the perspective of nuclear myosin biology. It has been found that phosphorylated myosin light chain 2 is elevated in the nuclei of cardiomyocytes subjected to ischemia and reperfusion *in vivo* and enhances the expression of NADPH oxidase 2 and H_2O_2 production in a MLCK-dependent manner (Zhang et al. 2015a). In cell culture under the hypoxia and reoxygenation conditions, phos-

phorylated myosin light chain 2 binds the NADPH oxidase 2 promoter and participates in formation of the preinitiation complex with RNA polymerase II and transcription factor IIB. Similar results have been obtained with non-muscle myosin light chain and xanthine oxidase transcription (Zhang et al. 2015b). At the same time, myosin light chain 5 is causally associated with distant metastasis in cervical cancer and promotes expression of the hypoxia-response factor HIF-1α by binding to its promoter (Zhang et al. 2017). HIF-1α, in turn, upregulates myosin light chain 5, which suggests formation of a molecular feedback loop favoring metastatic escape from the hypoxic niche.

The role of light chain phosphatase in nuclear functions of myosin has been documented in the comparatively well-studied case of ICAM-1 expression in the colon. Myosin light chain phosphatase inhibitor stimulated myosin II-modulated transcription of ICAM-1, an inflammation mediator, in colonic smooth muscle and was able to alleviate inflammation *in vivo* (Li and Sarna 2009). Additional results in need of follow-up from the perspective of nuclear myosin biology include the differential nuclear localization of the myosin light chain phosphatase catalytic subunit isoforms (Murata et al. 1997). The comparatively more nuclear isoform δ may conceivably be more closely associated with the nuclear functions of myosin. Interestingly, the myosin-binding subunit alone localizes predominantly to the nucleus, whereas its retention in the cytoplasm depends on its interaction with the δ isoform of the catalytic subunit (Eto et al. 2005). Thus, regulation of nuclear myosin by light chain phosphatases may be orchestrated on the molecular level in complex and unexpected ways.

10.4 Functions of Nuclear Myosin

10.4.1 Transcription

10.4.1.1 Polymerase II

Myosin IC The function of myosin IC isoform B (NMI) in transcription mediated by RNA polymerase II was the first to be demonstrated (Pestic-Dragovich et al. 2000). Subsequently, it was established that this isoform participates specifically in the synthesis of the first dinucleotide but not at the earlier steps of transcription initiation (Hofmann et al. 2006b). Myosin IC isoform B co-purifies with RNA polymerase II, yet it is not necessary for the formation of the pre-initiation complex (Hofmann et al. 2006b). The latter, however, depends on β-actin. Antibodies against β-actin block RNA polymerase II transcription, and this form of actin can be observed to be recruited to promoters of inducible genes (Hofmann et al. 2004). The notion of cooperation of NMI with nuclear actin has been supported by recent genome-wide analysis by means of chromatin immunoprecipitation and deep sequencing. It has been shown that promoter occupancies by β-actin and Pol II during *Drosophila* oogenesis are similarly distributed and co-vary under regulation of gene expression (Sokolova et al. 2018), while NMI is similarly present across the mammalian genome and displays occupancy peaks that are correlated with RNA polymerase II (Almuzzaini et al. 2015). Moreover, the latter study has demonstrated that genes selected from the top NMI binders display a drop in the promoter DNA association by actin and actin-binding core subunits of RNA polymerase II, Rpb6 and Rpb8, when NMI expression is silenced. These changes are accompanied by a decrease of promoter association with Ser5P RNA polymerase II, but not with the unphosphorylated form – a result indicative of involvement of NMI in activation of RNA polymerase II, or in retention of the activated form on the promoter.

As has been discussed in the section of this review devoted to the basic biology of nuclear actin, the state of actin polymerization that underlies this protein's functionality in RNA polymerase II transcription remains unclear, with some evidence for both polymeric, or polymerizing, actin and a monomeric functional form. Collectively, the observations to date suggest that the functions of myosin and actin in transcription are complementary, but it still remains to be elucidated whether the direct or mechanical interac-

tion between these proteins plays a role in RNA polymerase II transcription, which would be similar to their mutually dependent functionality in the cytoplasm. The data that have been obtained do not definitively rule out the early speculative model (de Lanerolle et al. 2005), whereby the association of myosin IC with DNA via its positively-charged lipid-binding tail domain and with the RNA polymerase complex via the actin-binding site on its motor head results in a propulsive force that assists the progression of the transcription machine. The possible spatial arrangements in the complex involving these molecules have recently been reviewed (Sarshad and Percipalle 2014).

Observations concerning the localization of NMI and actin in the nucleus comport with their role in RNA polymerase II transcription. NMI is colocalized with RNA polymerase II on the light-microscopic level and to within 100 nm on the electron-microscopic level (Pestic-Dragovich et al. 2000). The colocalization can be disrupted by RNA polymerase II and transcription inhibitors. Myosin IC isoform A behaves similarly (Ihnatovych et al. 2012). It is noteworthy that in stimulated lymphocytes, NMI becomes upregulated on both the mRNA and protein levels (Kysela et al. 2005). Together with actin, it also shifts from the condensed to the decondensed chromatin, as revealed by quantitative immunoelectron microscopy. Suggestively of their cooperative or complementary functions, NMI always resides in 30–50 nm clusters, while actin accumulates into similarly sized clusters only upon stimulation. These locations correlate with the ~80 nm transcription clusters, as identified by bromouridine pulsing and immunodetection (Kysela et al. 2005). Similarly, in the onion *Allium cepa*, NMI and β-actin (identified immunologically) localize to foci in the nucleoplasm whose number is sensitive to inhibition of RNA polymerase II-mediated transcription (Cruz and Moreno Diaz de la Espina 2009). Recently, the dynamic distribution of nuclear myosin was studied in human cells subjected to adenoviral infection (Fuchsova et al. 2015). In this system, formation of replication centers is accompanied by association of nuclear actin and myosin with clusters of viral DNA, where they colocalize with initiation-competent (Ser5P) RNA polymerase II. The process involves also other nuclear myosins, and certain differences between the localization of NMI, myosin V, and myosin VI have been noted, which present interest for future mechanistic research.

Myosin II Although antibodies against myosin II had no effect on transcription in the cited *in vitro* experiments (Hofmann et al. 2006b), smooth muscle myosin II has been found on the promoter of ICAM-1 in colonic smooth muscle cells (Li and Sarna 2009). The expression of this inflammation mediator is regulated through suppression of MLCK and elevation of myosin light chain phosphatase in the nucleus. This causes dephosphorylation of the 20-kD myosin light chain, which, in turn, promotes association of myosin II with transcription factor IIB. The nuclear activity of regulatory light chain 9 as a transcription factor can be enhanced by its methylation under the action of the nuclear enzyme N-terminal methyltransferase 1 (Nevitt et al. 2018). Interestingly, the alternative modification – acetylation by N-terminal acetyltransferase A – promotes the light chain's phosphorylation and such cytoplasmic functions as cell spreading and migration. It has also been established recently (Xue et al. 2019) that non-muscle myosin II binds nuclear Atoh1, a transcription factor driving neuronal differentiation of induced pluripotent stem cells, in a manner sensitive to the phosphorylation status of this factor. The experiments suggest that the promotion of the Atoh1 activity by myosin is dependent on the latter's calcium-regulated motor function. Thus, even though myosin II may not be part of the core transcription machinery, a picture is beginning to emerge in which this myosin's varied sub-classes play key roles in developmental and pathophysiological processes on the level of intranuclear transcription regulation.

Myosin VI Myosin VI associates with RNA polymerase II as well as intragenic and promoter regions in a transcription-dependent manner, and

its own downregulation suppresses the production of mRNA (Vreugde et al. 2006). Antibodies against this myosin have an inhibitory effect on transcription *in vitro*. The most recent data on dynamic localization of myosin VI in PC12 cells (Majewski et al. 2018) show that it colocalizes with active RNA polymerase II and active transcription sites, as well as with transcription factor SP1. It has also been established recently that the ability of myosin VI to bind DNA and associate with the RNA polymerase complex can be switched off by its acquiring an autoinhibitory conformation (Fili et al. 2017). The conformation, in turn, is prevented by NDP52, which is known to be an adhesion and autophagy-associated protein, but in this instance plays the role of a transcription activator and binds the RNA polymerase II complex together with myosin VI. The interaction is mediated by the RRL sequence in the cargo-binding domain of the myosin. Remarkably, this is the same sequence that is obscured in the non-nuclear splicing variant of myosin VI, reviewed in the section on nuclear localization mechanisms. The experiments also showed that association of myosin VI with DNA is a function of the same cargo-binding domain, while the association with the RNA polymerase II complex involves also the motor domain. NDP52 is capable of causing a four-fold increase in transcription activity. Furthermore, the C-terminal cargo-binding domain harbors a nuclear receptor binding sequence, which mediates interaction with estrogen receptor, and the myosin VI levels regulate expression of estrogen-dependent genes (Fili et al. 2017). It is likely that the previously documented interaction with androgen receptor, which appears to underlie the myosin VI function in promoting androgen-regulated expression (Loikkanen et al. 2009), is mediated similarly.

Regulated genes in T-helper cells present an interesting case (Zorca et al. 2015). In this system, RNA polymerase II is paused at the promoters, and recruitment of myosin VI is involved in the release of the pause. Global run-on sequencing showed that T-cell receptor (TCR) engagement results in a genome-wide decrease of paused RNA polymerase II, and its advancement to the gene body regions, in a myosin VI-dependent manner. In myosin-deficient cells, accumulation of the polymerase at the promoters is observed. One of the genes central to the T-helper differentiation is *TNF-α*. It was established by chromatin immunoprecipitation that a small quantity of myosin VI localizes to *TNF-α* in unstimulated cells. This quantity increases within 30 min after TCR stimulation, and decreases by 2 h. Interestingly, the expression of *TNF-α* is frequently monoallelic and, using immunofluorescence and RNA FISH methods, myosin VI puncta can be observed specifically at the active allele. The myosin-dependent mechanism of the pause release on the *TNF-α* locus could be narrowed down (Zorca et al. 2015) to the transition from the initiation-specific (Ferrai et al. 2010) phosphorylated form of RNA polymerase II–Ser5P–to Ser2P, which is characteristic of elongation. Furthermore, in T-helper cells from myosin VI +/− and −/− mice, similar amounts of *TNF-α* mRNA accumulate during the TCR-triggered differentiation process (7 days) as in +/+ cells, indicating that myosin VI functions in the rapid induction only. It is possible that other systems exhibiting the signaling-regulated Pol II pause release (Danko et al. 2013; Core and Lis 2008) follow a similar pattern of dependence on nuclear myosin VI in achieving their full dynamic range of transcription levels. The methods employed in the work of Zorca et al. appear to have a broad applicability, and further elucidation of the role of nuclear myosin in RNA polymerase II transcription mechanisms in a range of biological systems with regulated gene expression programs will represent an important advance for this field of study.

10.4.1.2 Polymerase I

The role of NMI in transcription by RNA polymerase I was initially demonstrated using a myosin motor inhibitor, microinjection of anti-NMI antibodies into the cell, and siRNA-mediated downregulation of the NMI expression (Fomproix and Percipalle 2004; Philimonenko et al. 2004; Percipalle et al. 2006). Subsequent work addressed the generality of this involvement for

the isoforms of myosin IC (Venit et al. 2013). In these experiments, knock-out of isoform B (i.e., NMI) alone was not seen to affect the levels of 45S pre-rRNA. At the same time, polymerase I transcription on the background of isoform-nonspecific shRNA knock-down could be rescued by a silent resistant mutant of isoform C. Collectively, these results are consistent with the conclusion (Venit et al. 2013) that isoform C can substitute for isoform B in Pol I transcription and does so in the knockout mouse. Isoform A, however, does not interact with Pol I (Ihnatovych et al. 2012). This raises the possibility that isoforms B and C may not be equally potent as factors in RNA polymerase I transcription, and also highlights the important unanswered question of the basic cell-physiological consequences of the tissue- and disease stage-specific expression of isoform A.

Interestingly, the N terminus of NMI appears immunologically accessible in association with rDNA promoters (Philimonenko et al. 2004), whereas the use of other antibodies against this protein inhibits elongation – but not initiation – of pre-rRNA transcription (Percipalle et al. 2006). Actin too enhances transcription by RNA polymerase I, and both actin and NMI are associated specifically with the transcription-competent fraction of the enzyme (Philimonenko et al. 2004). The association of NMI is mediated by the transcription initiation factor TIF-IA in a manner that is regulated by the factor's phosphorylation by RSK kinase (Philimonenko et al. 2004). In this connection, it can be noted that the phosphorylation of TIF-IA occurs downstream of the MAP kinase cascade and growth factor signaling (Zhao et al. 2003). NMI is also part of a chromatin remodeling complex that is essential for RNA polymerase I progression (Percipalle et al. 2006; Sarshad et al. 2013), as will be reviewed in the corresponding section below. NMI's expression level, motor function, and ability to bind actin and chromatin all impact rRNA synthesis by preventing stalling of RNA polymerase I at the promoter (Sarshad et al. 2013). Moreover, the experiments also showed that the motor function of NMI and polymerization competence of actin are required for the RNA polymerase I transcription activation (Ye et al. 2008). At the same time, it has been demonstrated *in vivo* that the capacity of the myosin for binding actin, and the myosin's calmodulin-binding domain are both critical to its association with the polymerase. In light of the recent work on the mechanism of myosin IC import into the nucleus and the function of calmodulin in its mechanical cycle (reviewed above), the question may be posed whether the observed lack of association of the mutants without the calmodulin-binding domain may be due to their suppressed motor function or exclusively to inability of the mutant to enter the nucleus.

Myosin VB can also be immunoprecipitated with RNA polymerase I and actin (Lindsay and McCaffrey 2009), pointing to the possibility of a diversity of nuclear myosins playing similar, but not necessarily identical, roles in rDNA transcription. Further broadening the range of processes involving these nuclear molecules, recent research has shown that human papillomavirus type 8 protein E7, an oncoprotein associated with skin carcinogenesis (Akgul et al. 2007), binds myosin IC and represses both RNA polymerase I activity and pre-rRNA production (Oswald et al. 2017). This finding raises the possibility that the basic function of nuclear myosins can be leveraged by parasites for redirecting the cell's resources to their proliferation needs.

The role of nuclear myosin in transcription mediated by RNA polymerase I is supported by its dynamic localization in the nucleus. It has been established that NMI and β-actin colocalize with RNA polymerase I and nascent pre-rRNA in nucleoli in a manner that is sensitive to transcription inhibition (Fomproix and Percipalle 2004; Percipalle et al. 2006; Ihnatovych et al. 2012). In stimulated lymphocytes, the characteristic accumulation of NMI in the dense fibrillar component of the nucleolus is enhanced concomitantly with the actin content of that compartment (Kysela et al. 2005). This is suggestive of the two proteins' complementary function, in view of the findings identifying the dense fibrillar component as the site of active rDNA transcription (Philimonenko et al. 2004; Raska et al. 2006). Supporting this notion is the fact that the localization of NMI to the dense fibrillar component is

disrupted upon inhibition of RNA polymerase I transcription, but not of RNA polymerases II and III (Philimonenko et al. 2010). Myosin VB (but not VA) colocalization with RNA polymerase I and actin in nucleoli is also sensitive to RNA polymerase I inhibitors (Lindsay and McCaffrey 2009). Similar results have been obtained on plant material, where NMI- as well as β actin-reactive foci are found in the nucleoli of the onion *Allium cepa*, and the number of such foci is reduced upon inhibition of RNA polymerase I transcription (Cruz and Moreno Diaz de la Espina 2009). The necessary counterexample is provided by myosin IC isoform A, which, in addition to not co-immunoprecipitating from nuclear extracts with RNA polymerase I, does not localize to the nucleoli of human cells despite its almost complete sequence identity with isoform B, i.e., NMI (Ihnatovych et al. 2012).

10.4.1.3 Polymerase III

Cavellan et al. described a 3 MDa complex involving NMI, chromatin remodeling factors WSTF and SNF2h, and other components (Cavellan et al. 2006). They called this complex B-WICH; its chromatin-remodeling functionality will be more fully reviewed in the next section. Of relevance here is its association with such RNA polymerase III transcripts as 5S rRNA and 7SL RNA (Cavellan et al. 2006). It has been recently established that B-WICH is able to promote binding of c-Myc, which enhances these genes' transcription (Sadeghifar et al. 2015). At the same time, the finding that β-actin is tightly bound to Pol III and necessary for reconstituting its activity *in vitro* (Hu et al. 2004) supports the notion that the involvement of actin and myosin in Pol III transcription may be at least broadly similar to the reviewed features of Pol I and Pol II transcription. Recent work (Wang et al. 2016) has established that the cytoskeletal protein filamin A associates with the Pol III transcription complex via its actin-binding domain, repressing transcription by means of decreasing Pol III promoter occupancy. Interestingly, both this repression mechanism and the association of B-WICH with transcripts, which was described in the original work of Cavellan et al., exclude tRNA genes. Thus, actin and myosin may act cooperatively, but only on a sub-class of Pol III genes.

10.4.2 Epigenetic Mechanisms and Chromatin Dynamics

Beyond participating in transcription, some of the best-understood functions of nuclear myosin are in the dynamics of chromatin and epigenetic modifications. A hypothesis about the role of nuclear actin and myosin in condensation of heterochromatin was put forward as early as 1976 (Comings and Okada 1976); however, the experiments with ATP-induced decondensation that were conducted to test at the time did not bear it out. This direction of inquiry has been re-focused with the advent of the modern molecular-biological methods, and a preliminary picture of the role of nuclear myosin in chromatin dynamics is now beginning to emerge. It was initially shown that NMI (myosin IC isoform B) is part of a macromolecular ensemble that includes the WSTF/SNF2h chromatin remodeling complex (Percipalle et al. 2006; Percipalle and Farrants 2006). The WSTF component of the complex has a role in RNA polymerase I transcription specifically on chromatin, as compared with naked DNA (Percipalle et al. 2006), which is achieved through enhanced association of histone acetyltransferases, including p300, and higher levels of acetylation of histone H3 at the rRNA promoter (Vintermist et al. 2011). Additional data (Sarshad et al. 2013) indicate that binding of NMI to SNF2h and to actin may be reciprocally regulated, while the rRNA gene occupancies of the three proteins (WSTF, SNF2h, and NMI) depend on the myosin motor function. It is also cell cycle-dependent, an effect that is mediated by phosphorylation of WSTF. Furthermore, the ability of NMI to bind actin and chromatin, its motor activity, and its expression all impinge on the H3K9 acetylation status at rDNA promoters, enabling the transition to transcription elongation and, ultimately, cell cycle progression (Sarshad et al. 2013). The acetylation is regulated by glycogen synthase kinase GSK3β by phosphorylating NMI on Ser-1020 (in the C-terminal tail

domain), which promotes the myosin's association with chromatin (Sarshad et al. 2014). The phosphorylation takes place on rDNA, with which the kinase associates selectively, and is characteristic of the G1 stage of the cell cycle. It also protects the myosin from polyubiquitination by the E3 ligase UBR5 and, consequently, from degradation. Interestingly, the leukemia-associated nuclear myosin fusion protein CBFβ-SMMHC similarly associates with ribosomal Pol I genes, through mitosis as well as the interphase. It regulates the ribosomal gene expression positively, apparently by shuttling its partner, the epigenetic repressor RUNX2, to the cytoplasm (Lopez-Camacho et al. 2014).

The role of NMI in chromatin dynamics has recently been probed also in connection with transcription by RNA polymerase II (Almuzzaini et al. 2015). It was determined that the myosin complex with the nucleosome remodeling protein SNF2h and WSTF assembles on polymerase II promoters as well. Functional myosin was also required for recruitment of actin, and negatively regulated the chromatin protection of DNA at the studied promoters. The same experiments showed that the occupancy by myosin correlates with the polymerase II promoters' histone H3 acetylation and trimethylation (Almuzzaini et al. 2015). This is suggestive in connection with the results obtained on rDNA, where NMI was found in a complex with histone acetyltransferase PCAF (Sarshad et al. 2013). On the polymerase II promoters, NMI positively regulated the recruitment of PCAF and histone methyltransferase Set1/Ash2 as well as the levels of specific acetylations and trimethylations (Almuzzaini et al. 2015).

10.4.3 RNA Processing

Myosin VA phosphorylated on Ser 1650 has been localized specifically to nuclear speckles containing the splicing factor SC35 (Pranchevicius et al. 2008). Upon inhibition of transcription, it redistributed to nucleoli and to aggregates outside the speckles. The transcription-dependent dynamic localization pattern could be seen as evidence for possible involvement of myosin VA in pre-mRNA processing. The colocalization with SC35 has also been recently shown for myosin VI (Majewski et al. 2018). At the same time, inhibition of transcription results in redistribution of myosin IC isoform A into nuclear speckles that contain U1 RNPs (Ihnatovych et al. 2012). This redistribution appears exquisitely specific with respect to the molecular structure of nuclear myosin, because isoform B (NMI), under the same conditions, similarly loses colocalization with RNA polymerase II but does not become accumulated in any speckled pattern. These findings remain in need of a follow-up and highlight the gap in our knowledge that concerns the potential role of nuclear myosin in RNA processing.

A different angle of approaching this problem might be through a further characterization of the functional parallels of the nuclear myosin localization to the dense fibrillar and granular components of the nucleolus. The descriptive aspects of this dynamic localization have been reviewed above in connection with rDNA transcription, but its possible relevance to pre-rRNA processing, which is structurally associated with these nucleolar compartments (Raska et al. 2006), remains to be investigated. A potential additional avenue for further research may be indicated by the work on myosin filament assembly in smooth muscle cells. The assembly was found to be facilitated by binding of smooth muscle myosin to a 38-kDa protein homologous to a subunit of pre-mRNA splicing factor 2 (Okagaki et al. 2000). At the same time, the 38-kDa protein was also reported to display a dynamic nuclear and cytoplasmic localization in the course of the smooth muscle cell differentiation. While it is difficult to predict the most fruitful direction of testing the long-standing hypothesis of myosin involvement in RNA processing, new studies are unquestionably needed to clarify this potentially important aspect of the nuclear myosin function.

10.4.4 Intranuclear Motility

Multiple lines of evidence confirm the role of myosins in intranuclear motility. One concerns the movement of double-strand DNA breaks,

which is an integral part of the repair mechanism. This movement has been studied in detail in *Drosophila* cells. The double-strand breaks in this system are translocated to the nuclear periphery (Chiolo et al. 2011) in the course of a process that requires SUMO ligases and inner nuclear membrane proteins (Ryu et al. 2015). Recently, it has been shown that the translocation is driven by myosins IA, IB, and V in the presence of F-actin (Caridi et al. 2018). The actin is nucleated by the Arp2/3 complex, and the myosin is recruited via the SUMO ligases Smc5/6. These findings were also generalizable to mouse cells. In human fibroblasts (Kulashreshtha et al. 2016), double-stranded breaks were found to initiate a signal via the phosphorylated histone H2AX and recruit myosin IC. The functionality of the motor domain of isoform B, specifically, is important for the relocation of the damaged chromosome territory in this experimental system.

Similar mechanisms are responsible for repositioning of active gene loci and interphase chromosome territories (Bridger 2011). Upon transcriptional activation, snRNA loci migrate to associate with Cajal bodies, a process marked by involvement of β-actin (Dundr et al. 2007). At the same time, quiescent cells exhibit a different chromosome territory organization than that of the interphase nuclei of actively proliferating cells (Mehta et al. 2010). Actin polymerization and myosin IC (earlier termed myosin I β) are involved in this process. Using an experimentally created fluorescently labeled locus, it was possible to show that its activation-induced relocation relied on actin polymerization and actin interaction with nuclear myosin IC (Chuang et al. 2006). Promyelocytic leukemia (PML) bodies move inside nuclei utilizing ATP through a process that is sensitive to an inhibitor of actin-dependent myosins (Muratani et al. 2002), which is indicative of a similar mechanism.

One of the models for studying the nuclear functions of myosins that has led to the recent advances in the study of the intranuclear motility mechanisms is the gene activation program induced by receptor engagement in T lymphocytes. The mechanistic details of RNA polymerase II transcription that involve myosin VI in this system have been reviewed above. Of interest in connection with the spectrum of myosin functions in intranuclear movements is the finding of transient homologous pairing of alleles of some of the induced genes, which occurs in the nuclei of T-cells at the early stages of this activation program (Zorca et al. 2015). The pairing is dependent on the transition of RNA polymerase II to elongation, and accompanies the switch from the predominantly monoallelic expression in the basal state to biallelic induced expression. It is sensitive to inhibition of actin polymerization, and depends on myosin VI expression and motor activity. The same dependence on myosin expression is displayed by the loci's acquisition of a peripheral localization in the nucleus. The findings concerning the myosin VI-dependent movements in the nuclei of developing T-cells appear to be an instance of migration of activated gene loci to the intranuclear sites known as "transcription factories" (Osborne et al. 2004), where they are believed to acquire transcription factors and machinery from pre-accumulated, shared pools. Myosin VI residence and functional importance in the transcription factories was first documented by Vreugde et al. (Vreugde et al. 2006). Deciphering further the role of nuclear myosin in the organization of the activated loci into the transcription foci is a promising direction for future work. Generality of this mechanism with respect to the genes and transcription activation programs, as well as to the classes of nuclear myosin, should be among the most urgent questions.

An additional example of intranuclear motility is provided by the movement of viral particles. Capsids of herpes simplex virus move inside nuclei in a manner that is sensitive to a myosin inhibitor (Forest et al. 2005). Both intranuclear pseudorabies virus (an alpha-herpesvirus) and herpes simplex virus infection induces actin polymerization in the nucleus, and the resulting actin filaments colocalize with the capsids on the electron microscopy level (Feierbach et al. 2006). The distribution of myosin VB, but not of NMI, correlates with them as well. The implications of these findings for the actin-myosin dependent transport, however, have been disputed (Bosse

and Enquist 2016) based on the lack of success in detecting nuclear F-actin in various infected cells, using an alternative to the method of fixation and phalloidin staining (Bosse et al. 2014). Enlargement of the intranuclear diffusion domains that is induced by infection is also capable of facilitating the movement of capsids (Bosse et al. 2015). The precise role of myosin and its contribution to the movement of viral particles will benefit from a quantitative evaluation using new methods such as super-resolution microscopy. One possibility for the synthesis of the diffusion-domain and myosin-driven models that could be tested is suggested by the finding that the herpesvirus replication domains themselves are subject to actin- and myosin-dependent intranuclear motility and coalescence as part of the virus's life cycle (Chang et al. 2011). The most recent results (Wilkie et al. 2018) offer a glimpse of how such a process involving the capsids, replication compartments, and myosin might unfold. In the experiments with cytomegalovirus, myosin VA has been found to be associated with the capsids and F-actin specifically at the edge of the replication domain, and its expression was responsible for efficient transport of the viral particles.

10.4.5 Nuclear Export

Actin and myosin were proposed to be functional components of the nuclear pore based on the results of experiments on isolated rat liver nuclei, in which the energy-dependent macromolecular transport was found to be sensitive to actin polymerization-perturbing drugs and anti-myosin antibodies (Schindler and Jiang 1986). The localization of actin to the nucleoplasmic filaments of the nuclear pore has also been observed by electron microscopy and immunogold labeling in anuran and urodelan amphibian species (Hofmann et al. 2001). The same work revealed binding of actin to eukaryotic initiation factor 5A, which, in turn, served as a nuclear export factor for HIV-1 RNA export. The localization of myosin to nuclear pores is also a general phenomenon. In *Drosophila*, it has been demonstrated by immuno-labeling on both the light and electron microscopy level (Berrios et al. 1991). In yeast, myosin-like proteins Mlp1 and Mlp2, which are themselves imported via an NLS in their C-terminal domain, decorate the nucleoplasmic basket of the nuclear pore and support specifically the active nuclear import of protein (Strambio-de-Castillia et al. 1999). Interestingly, the C-terminal domain of Mlp1 is also involved in the import of a shuttling ribonucleoprotein responsible for mRNA export (Green et al. 2003). The interaction is shown to be direct and, in light of the NLS localization to this domain, may be an example of a "piggy-back" or co-import. According to the most recent work on this system, deletions of Mlp1 and Mlp2 lead to intranuclear accumulation of polyadenylated RNA and inhibition of RNA synthesis (Tudek et al. 2018).

Another line of evidence for the involvement of myosin in nuclear export comes from the studies of export of ribosomal subunits. Small ribosomal subunits associate with NMI and actin at the periphery of the nucleolus and also at the nuclear pore, as demonstrated by immunogold labeling on the electron-microscopic level (Cisterna et al. 2006). The authors of the cited work estimated that as much as 10% of the small ribosomal subunits may be exported with participation of myosin, and proposed that this may represent a regulated export pathway to complement a diffusive constitutive one. The actin and myosin in these experiments were associated with the ribosomal protein S6, and prolonged application of anti-actin and anti-myosin antibodies to live cells resulted in accumulation of this protein in the nucleus, indicative of an export block. Ribosomal subunits at the same time accumulated in the granular component of the nucleolus, and there was evidence of overall RNA retention in the nucleus (Cisterna et al. 2009). The list of intranuclear ribosomal components associated with NMI was broadened in ultracentrifugation and immunoprecipitation experiments (Obrdlik et al. 2010), which also confirmed the myosin's association with actin-rich filaments of the nuclear pore basket. These findings lent additional weight to the model whereby nuclear myo-

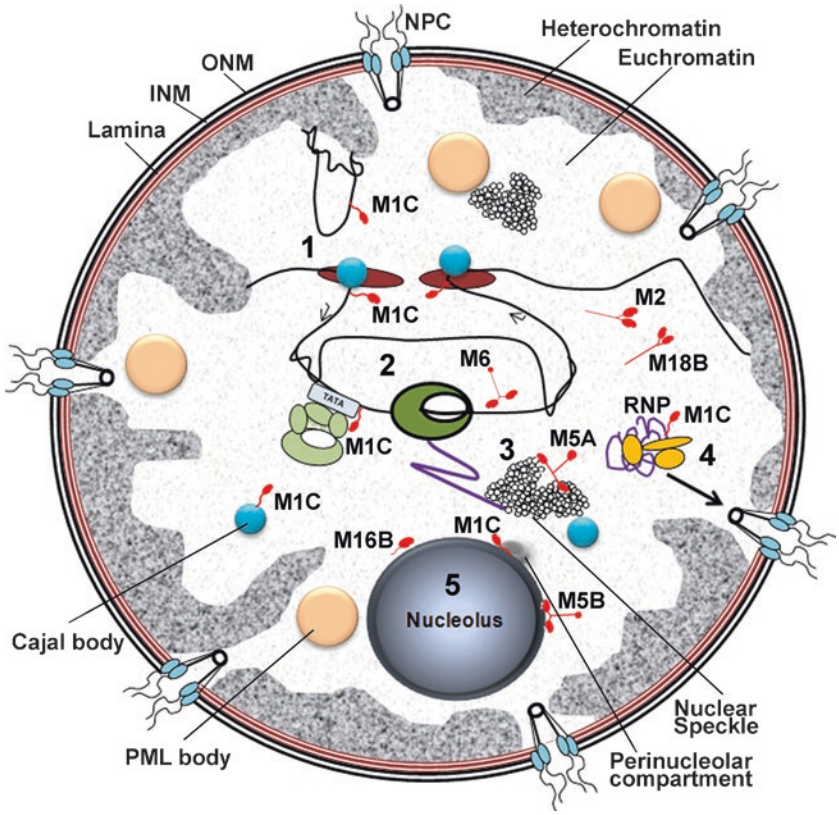

Fig. 10.4 Nuclear functions of myosin. The schematically depicted myosin classes and forms participate in the integrated processes of intranuclear motility (*1*, Sect. 10.4.4), Pol II transcription (*2*, Sect. 10.4.1), pre-mRNA processing (*3*, Sect 10.4.3), nuclear export (*4*, Sect. 10.4.5), and Pol I transcription and pre-rRNA processing (*5*, Sect. 10.4.1)

sin modulates export from the nucleus, even though certain questions remain unanswered to date, such as, for example, to what extent and by what biophysical mechanism the nuclear myosin drives the transport of RNA and ribonucleoproteins along the critical steps of the nuclear export pathway. The function of myosin in nuclear export, along with the integrated processes of transcription (Sect. 10.4.1), RNA processing (Sect 10.4.3), and intranuclear motility (Sect. 10.4.4) are summarized graphically in Fig. 10.4.

10.4.6 Pathology

Research work is underway to determine the contribution of nuclear myosins to pathological processes, especially in the area of cancer. It has long been known that smooth-muscle myosin heavy chain (SMMHC) forms a chimeric protein with core-binding factor β (CBFB) in acute myeloid leukemia (Liu et al. 1993), and that this chimera is capable of forming rod-like structures inside nuclei in cell culture experiments (Wijmenga et al. 1996). More recently, it has been shown that the chimeric protein exhibits a specifically nuclear localization in vivo and a microgranular intranuclear pattern (Zhao et al. 2006). The distinctive staining can be used for differential diagnosis of the myeloma subtype that is characterized by the chromosomal rearrangement that results in the fusion. The differentiation is valuable in the clinic, because the subtype in question responds well to established chemotherapy regimens. Moreover, studies on mouse models indicate that expression of CBFB-

SMMHC predisposes the animals to leukemia (Castilla et al. 1999; Kuo et al. 2006). CBFB-SMMHC acts in the nucleus through its binding partners, the transcription factor RUNX1 and histone deacetylase HDAC8. Small-molecule inhibitors of the RUNX1 interaction showed promise in experimental treatment of murine leukemia on the CBFB-SMMHC background (Richter et al. 2016).

Recent studies point to involvement of nuclear myosin in abnormal signal transduction to the nucleus in tumor cells. Recurrent lung cancer is often characterized (Godin-Heymann et al. 2007) by a mutation – T790M – in epidermal growth factor receptor (EGFR). In the nucleus, EGFR-T790M interacts with myosin heavy chain 9 (non-muscle myosin IIA) and β-actin to support proliferation and apoptosis resistance of cultured lung cancer cells, and this activity depends on the functionality of the myosin and its interaction with actin (Chiu et al. 2012). Furthermore, myosin VI has been shown to engage in a bidirectional interaction with p53, whereby p53 directly activates the myosin VI promoter and drives the protein's accumulation in the nucleus, while myosin VI participates in the accumulation of p53 induced by DNA damage and in the p53-dependent cell survival under these conditions (Jung et al. 2006). In conjunction with this work, the discovery of the calcium-regulated import of myosin IC into the nucleus of prostate cancer cells (Maly and Hofmann 2016) raises the possibility that nuclear myosin-mediated signal transduction may be a general feature of cells responding to the stress induced by the tumor microenvironment. Indeed, the response to such conditions is often characterized by elevated intracellular calcium concentration (Monteith et al. 2012; Cui et al. 2017; Maly and Hofmann 2018). Moreover, such regulation must be reciprocal with the cytoplasmic functions of the same myosin type, for example, the recently characterized function of myosin IC in prostate cancer cell invasion (Maly et al. 2017).

The nuclear myosin field has come a long way from the controversy about localization of the presumed cytoplasmic protein. Unraveling the molecular details of the nuclear myosin classes, functions, and intranuclear partners is an ongoing and flourishing enterprise. We have now come to the stage where systems-level questions are beginning to be formulated about the role of these multifunctional proteins in a variety of coordinated cell-physiological processes, such as signal transduction to the nucleus, in organism-level pathology, and also about the coordinated regulation of myosin's cytoplasmic and nuclear functions.

Acknowledgments Supported in part by the NCI of the National Institutes of Health under award number R21CA220155 to WAH.

References

Adamek N, Coluccio LM, Geeves MA (2008) Calcium sensitivity of the cross-bridge cycle of Myo1c, the adaptation motor in the inner ear. Proc Natl Acad Sci U S A 105(15):5710–5715. https://doi.org/10.1073/pnas.0710520105

Ajima R, Kajiya K, Inoue T, Tani M, Shiraishi-Yamaguchi Y, Maeda M, Segawa T, Furuichi T, Sutoh K, Yokota J (2007) HOMER2 binds MYO18B and enhances its activity to suppress anchorage independent growth. Biochem Biophys Res Commun 356(4):851–856. https://doi.org/10.1016/j.bbrc.2007.03.060

Ajima R, Akazawa H, Kodama M, Takeshita F, Otsuka A, Kohno T, Komuro I, Ochiya T, Yokota J (2008) Deficiency of Myo18B in mice results in embryonic lethality with cardiac myofibrillar aberrations. Genes Cells 13(10):987–999. https://doi.org/10.1111/j.1365-2443.2008.01226.x

Akgul B, Ghali L, Davies D, Pfister H, Leigh IM, Storey A (2007) HPV8 early genes modulate differentiation and cell cycle of primary human adult keratinocytes. Exp Dermatol 16(7):590–599. https://doi.org/10.1111/j.1600-0625.2007.00569.x

Al Madhoun AS, Mehta V, Li G, Figeys D, Wiper-Bergeron N, Skerjanc IS (2011) Skeletal myosin light chain kinase regulates skeletal myogenesis by phosphorylation of MEF2C. EMBO J 30(12):2477–2489. https://doi.org/10.1038/emboj.2011.153

Alazami AM, Kentab AY, Faqeih E, Mohamed JY, Alkhalidi H, Hijazi H, Alkuraya FS (2015) A novel syndrome of Klippel-Feil anomaly, myopathy, and characteristic facies is linked to a null mutation in MYO18B. J Med Genet 52(6):400–404. https://doi.org/10.1136/jmedgenet-2014-102964

Almuzzaini B, Sarshad AA, Farrants AK, Percipalle P (2015) Nuclear myosin 1 contributes to a chromatin landscape compatible with RNA polymerase II transcription activation. BMC Biol 13:35. https://doi.org/10.1186/s12915-015-0147-z

Baarlink C, Wang H, Grosse R (2013) Nuclear actin network assembly by formins regulates the SRF coactivator MAL. Science 340(6134):864–867. https://doi.org/10.1126/science.1235038

Bachg AC, Horsthemke M, Skryabin BV, Klasen T, Nagelmann N, Faber C, Woodham E, Machesky LM, Bachg S, Stange R, Jeong HW, Adams RH, Bahler M, Hanley PJ (2019) Phenotypic analysis of Myo10 knockout (Myo10(tm2/tm2)) mice lacking full-length (motorized) but not brain-specific headless myosin X. Sci Rep 9(1):597. https://doi.org/10.1038/s41598-018-37160-y

Bachs O, Carafoli E (1987) Calmodulin and calmodulin-binding proteins in liver cell nuclei. J Biol Chem 262(22):10786–10790

Bao Y, Wang Z, Liu B, Lu X, Xiong Y, Shi J, Li P, Chen J, Zhang Z, Chen M, Wang L, Wu Z (2019) A feed-forward loop between nuclear translocation of CXCR4 and HIF-1alpha promotes renal cell carcinoma metastasis. Oncogene 38(6):881–895. https://doi.org/10.1038/s41388-018-0452-4

Belin BJ, Mullins RD (2013) What we talk about when we talk about nuclear actin. Nucleus 4(4):291–297. https://doi.org/10.4161/nucl.25960

Belin BJ, Cimini BA, Blackburn EH, Mullins RD (2013) Visualization of actin filaments and monomers in somatic cell nuclei. Mol Biol Cell 24(7):982–994. https://doi.org/10.1091/mbc.E12-09-0685

Belin BJ, Lee T, Mullins RD (2015) DNA damage induces nuclear actin filament assembly by Formin-2 and Spire-(1/2) that promotes efficient DNA repair. [corrected]. Elife 4:e07735. https://doi.org/10.7554/eLife.07735

Berg JS, Powell BC, Cheney RE (2001) A millennial myosin census. Mol Biol Cell 12(4):780–794. https://doi.org/10.1091/mbc.12.4.780

Berger J, Berger S, Li M, Currie PD (2017) Myo18b is essential for sarcomere assembly in fast skeletal muscle. Hum Mol Genet 26(6):1146–1156. https://doi.org/10.1093/hmg/ddx025

Berrios M, Fisher PA, Matz EC (1991) Localization of a myosin heavy chain-like polypeptide to Drosophila nuclear pore complexes. Proc Natl Acad Sci U S A 88(1):219–223

Bleeker FE, Lamba S, Rodolfo M, Scarpa A, Leenstra S, Vandertop WP, Bardelli A (2009) Mutational profiling of cancer candidate genes in glioblastoma, melanoma and pancreatic carcinoma reveals a snapshot of their genomic landscapes. Hum Mutat 30(2):E451–E459. https://doi.org/10.1002/humu.20927

Bohnsack MT, Stuven T, Kuhn C, Cordes VC, Gorlich D (2006) A selective block of nuclear actin export stabilizes the giant nuclei of Xenopus oocytes. Nat Cell Biol 8(3):257–263. https://doi.org/10.1038/ncb1357

Bose A, Guilherme A, Robida SI, Nicoloro SM, Zhou QL, Jiang ZY, Pomerleau DP, Czech MP (2002) Glucose transporter recycling in response to insulin is facilitated by myosin Myo1c. Nature 420(6917):821–824. https://doi.org/10.1038/nature01246

Bose A, Robida S, Furcinitti PS, Chawla A, Fogarty K, Corvera S, Czech MP (2004) Unconventional myosin Myo1c promotes membrane fusion in a regulated exocytic pathway. Mol Cell Biol 24(12):5447–5458. https://doi.org/10.1128/MCB.24.12.5447-5458.2004

Bosse JB, Enquist LW (2016) The diffusive way out: Herpesviruses remodel the host nucleus, enabling capsids to access the inner nuclear membrane. Nucleus 7(1):13–19. https://doi.org/10.1080/19491034.2016.1149665

Bosse JB, Virding S, Thiberge SY, Scherer J, Wodrich H, Ruzsics Z, Koszinowski UH, Enquist LW (2014) Nuclear herpesvirus capsid motility is not dependent on F-actin. MBio 5(5):e01909–e01914. https://doi.org/10.1128/mBio.01909-14

Bosse JB, Hogue IB, Feric M, Thiberge SY, Sodeik B, Brangwynne CP, Enquist LW (2015) Remodeling nuclear architecture allows efficient transport of herpesvirus capsids by diffusion. Proc Natl Acad Sci U S A 112(42):E5725–E5733. https://doi.org/10.1073/pnas.1513876112

Bracalente C, Rinflerch AR, Ibanez IL, Garcia FM, Volonteri V, Galimberti GN, Klamt F, Duran H (2018) Cofilin-1 levels and intracellular localization are associated with melanoma prognosis in a cohort of patients. Oncotarget 9(35):24097–24108. https://doi.org/10.18632/oncotarget.25303

Bridger JM (2011) Chromobility: the rapid movement of chromosomes in interphase nuclei. Biochem Soc Trans 39(6):1747–1751. https://doi.org/10.1042/BST20110696

Cameron RS, Liu C, Mixon AS, Pihkala JP, Rahn RJ, Cameron PL (2007) Myosin16b: the COOH-tail region directs localization to the nucleus and overexpression delays S-phase progression. Cell Motil Cytoskeleton 64(1):19–48. https://doi.org/10.1002/cm.20162

Cameron RS, Liu C, Pihkala JP (2013) Myosin 16 levels fluctuate during the cell cycle and are downregulated in response to DNA replication stress. Cytoskeleton (Hoboken) 70(6):328–348. https://doi.org/10.1002/cm.21109

Caridi CP, D'Agostino C, Ryu T, Zapotoczny G, Delabaere L, Li X, Khodaverdian VY, Amaral N, Lin E, Rau AR, Chiolo I (2018) Nuclear F-actin and myosins drive relocalization of heterochromatic breaks. Nature 559(7712):54–60. https://doi.org/10.1038/s41586-018-0242-8

Castilla LH, Garrett L, Adya N, Orlic D, Dutra A, Anderson S, Owens J, Eckhaus M, Bodine D, Liu PP (1999) The fusion gene Cbfb-MYH11 blocks myeloid differentiation and predisposes mice to acute myelomonocytic leukaemia. Nat Genet 23(2):144–146. https://doi.org/10.1038/13776

Cavellan E, Asp P, Percipalle P, Farrants AK (2006) The WSTF-SNF2h chromatin remodeling complex interacts with several nuclear proteins in transcription. J Biol Chem 281(24):16264–16271. https://doi.org/10.1074/jbc.M600233200

Chafouleas JG, Bolton WE, Means AR (1984) Potentiation of bleomycin lethality by anticalmodulin

drugs: a role for calmodulin in DNA repair. Science 224(4655):1346–1348

Chan PC, Hsu RY, Liu CW, Lai CC, Chen HC (2014) Adducin-1 is essential for mitotic spindle assembly through its interaction with myosin-X. J Cell Biol 204(1):19–28. https://doi.org/10.1083/jcb.201306083

Chang L, Godinez WJ, Kim IH, Tektonidis M, de Lanerolle P, Eils R, Rohr K, Knipe DM (2011) Herpesviral replication compartments move and coalesce at nuclear speckles to enhance export of viral late mRNA. Proc Natl Acad Sci U S A 108(21):E136–E144. https://doi.org/10.1073/pnas.1103411108

Chiolo I, Minoda A, Colmenares SU, Polyzos A, Costes SV, Karpen GH (2011) Double-strand breaks in heterochromatin move outside of a dynamic HP1a domain to complete recombinational repair. Cell 144(5):732–744. https://doi.org/10.1016/j.cell.2011.02.012

Chiu HC, Chang TY, Huang CT, Chao YS, Hsu JT (2012) EGFR and myosin II inhibitors cooperate to suppress EGFR-T790M-mutant NSCLC cells. Mol Oncol 6(3):299–310. https://doi.org/10.1016/j.molonc.2012.02.001

Chuang CH, Carpenter AE, Fuchsova B, Johnson T, de Lanerolle P, Belmont AS (2006) Long-range directional movement of an interphase chromosome site. Curr Biol 16(8):825–831. https://doi.org/10.1016/j.cub.2006.03.059

Cisterna B, Necchi D, Prosperi E, Biggiogera M (2006) Small ribosomal subunits associate with nuclear myosin and actin in transit to the nuclear pores. FASEB J 20(11):1901–1903. https://doi.org/10.1096/fj.05-5278fje

Cisterna B, Malatesta M, Dieker J, Muller S, Prosperi E, Biggiogera M (2009) An active mechanism flanks and modulates the export of the small ribosomal subunits. Histochem Cell Biol 131(6):743–753. https://doi.org/10.1007/s00418-009-0583-3

Cohen SM, Li B, Tsien RW, Ma H (2015) Evolutionary and functional perspectives on signaling from neuronal surface to nucleus. Biochem Biophys Res Commun 460(1):88–99. https://doi.org/10.1016/j.bbrc.2015.02.146

Comings DE, Harris DC (1976) Nuclear proteins. II. Similarity of nonhistone proteins in nuclear sap and chromatin, and essential absence of contractile proteins from mouse liver nuclei. J Cell Biol 70(2 pt 1):440–452

Comings DE, Okada TA (1976) Fine structure of the heterochromatin of the kangaroo rat *Dipidomys ordii*, and examination of the possible role of actin and myosin in heterochromatin condensation. J Cell Sci 21(3):465–477

Core LJ, Lis JT (2008) Transcription regulation through promoter-proximal pausing of RNA polymerase II. Science 319(5871):1791–1792. https://doi.org/10.1126/science.1150843

Cruz JR, Moreno Diaz de la Espina S (2009) Subnuclear compartmentalization and function of actin and nuclear myosin I in plants. Chromosoma 118(2):193–207. https://doi.org/10.1007/s00412-008-0188-y

Cui C, Merritt R, Fu L, Pan Z (2017) Targeting calcium signaling in cancer therapy. Acta Pharm Sin B 7(1):3–17. https://doi.org/10.1016/j.apsb.2016.11.001

Danko CG, Hah N, Luo X, Martins AL, Core L, Lis JT, Siepel A, Kraus WL (2013) Signaling pathways differentially affect RNA polymerase II initiation, pausing, and elongation rate in cells. Mol Cell 50(2):212–222. https://doi.org/10.1016/j.molcel.2013.02.015

Dawson JA, Methven-Kelley C, Davis GM (2017) atz-1 influences meiosis to maintain germline chromosomal stability in Caenorhabditis elegans. Cell Biol Int 41(10):1160–1168. https://doi.org/10.1002/cbin.10821

de Lanerolle P (2012) Nuclear actin and myosins at a glance. J Cell Sci 125(Pt 21):4945–4949. https://doi.org/10.1242/jcs.099754

de Lanerolle P, Cole AB (2002) Cytoskeletal proteins and gene regulation: form, function, and signal transduction in the nucleus. Sci STKE 2002(139):pe30. https://doi.org/10.1126/stke.2002.139.pe30

De Martino C, Capanna E, Nicotra MR, Natali PG (1980) Immunochemical localization of contractile proteins in mammalian meiotic chromosomes. Cell Tissue Res 213(1):159–178

de Lanerolle P, Johnson T, Hofmann WA (2005) Actin and myosin I in the nucleus: what next? Nat Struct Mol Biol 12(9):742–746. https://doi.org/10.1038/nsmb983

Diefenbach TJ, Latham VM, Yimlamai D, Liu CA, Herman IM, Jay DG (2002) Myosin 1c and myosin IIB serve opposing roles in lamellipodial dynamics of the neuronal growth cone. J Cell Biol 158(7):1207–1217. https://doi.org/10.1083/jcb.200202028

Dopie J, Skarp KP, Rajakyla EK, Tanhuanpaa K, Vartiainen MK (2012) Active maintenance of nuclear actin by importin 9 supports transcription. Proc Natl Acad Sci U S A 109(9):E544–E552. https://doi.org/10.1073/pnas.1118880109

Douvas AS, Harrington CA, Bonner J (1975) Major nonhistone proteins of rat liver chromatin: preliminary identification of myosin, actin, tubulin, and tropomyosin. Proc Natl Acad Sci U S A 72(10):3902–3906

Dundr M, Ospina JK, Sung MH, John S, Upender M, Ried T, Hager GL, Matera AG (2007) Actin-dependent intranuclear repositioning of an active gene locus in vivo. J Cell Biol 179(6):1095–1103. https://doi.org/10.1083/jcb.200710058

Dunn TA, Chen S, Faith DA, Hicks JL, Platz EA, Chen Y, Ewing CM, Sauvageot J, Isaacs WB, De Marzo AM, Luo J (2006) A novel role of myosin VI in human prostate cancer. Am J Pathol 169(5):1843–1854. https://doi.org/10.2353/ajpath.2006.060316

Dzijak R, Yildirim S, Kahle M, Novak P, Hnilicova J, Venit T, Hozak P (2012) Specific nuclear localizing sequence directs two myosin isoforms to the cell nucleus in calmodulin-sensitive manner. PLoS One 7(1):e30529. https://doi.org/10.1371/journal.pone.0030529

Edakuni N, Ikuta K, Yano S, Nakataki E, Muguruma H, Uehara H, Tani M, Yokota J, Aizawa H, Sone S (2006) Restored expression of the MYO18B gene suppresses

orthotopic growth and the production of bloody pleural effusion by human malignant pleural mesothelioma cells in SCID mice. Oncol Res 16(5):235–243

Emmott E, Rodgers MA, Macdonald A, McCrory S, Ajuh P, Hiscox JA (2010) Quantitative proteomics using stable isotope labeling with amino acids in cell culture reveals changes in the cytoplasmic, nuclear, and nucleolar proteomes in Vero cells infected with the coronavirus infectious bronchitis virus. Mol Cell Proteomics 9(9):1920–1936. https://doi.org/10.1074/mcp.M900345-MCP200

Eto M, Kirkbride JA, Brautigan DL (2005) Assembly of MYPT1 with protein phosphatase-1 in fibroblasts redirects localization and reorganizes the actin cytoskeleton. Cell Motil Cytoskeleton 62(2):100–109. https://doi.org/10.1002/cm.20088

Feierbach B, Piccinotti S, Bisher M, Denk W, Enquist LW (2006) Alpha-herpesvirus infection induces the formation of nuclear actin filaments. PLoS Pathog 2(8):e85. https://doi.org/10.1371/journal.ppat.0020085

Feric M, Brangwynne CP (2013) A nuclear F-actin scaffold stabilizes ribonucleoprotein droplets against gravity in large cells. Nat Cell Biol 15(10):1253–1259. https://doi.org/10.1038/ncb2830

Feric M, Broedersz CP, Brangwynne CP (2015) Soft viscoelastic properties of nuclear actin age oocytes due to gravitational creep. Sci Rep 5:16607. https://doi.org/10.1038/srep16607

Ferrai C, Xie SQ, Luraghi P, Munari D, Ramirez F, Branco MR, Pombo A, Crippa MP (2010) Poised transcription factories prime silent uPA gene prior to activation. PLoS Biol 8(1):e1000270. https://doi.org/10.1371/journal.pbio.1000270

Fili N, Hari-Gupta Y, Dos Santos A, Cook A, Poland S, Ameer-Beg SM, Parsons M, Toseland CP (2017) NDP52 activates nuclear myosin VI to enhance RNA polymerase II transcription. Nat Commun 8(1):1871. https://doi.org/10.1038/s41467-017-02050-w

Fomproix N, Percipalle P (2004) An actin-myosin complex on actively transcribing genes. Exp Cell Res 294(1):140–148. https://doi.org/10.1016/j.yexcr.2003.10.028

Forest T, Barnard S, Baines JD (2005) Active intranuclear movement of herpesvirus capsids. Nat Cell Biol 7(4):429–431. https://doi.org/10.1038/ncb1243

Fuchsova B, Serebryannyy LA, de Lanerolle P (2015) Nuclear actin and myosins in adenovirus infection. Exp Cell Res 338(2):170–182. https://doi.org/10.1016/j.yexcr.2015.07.025

Fujiwara K, Pollard TD (1976) Fluorescent antibody localization of myosin in the cytoplasm, cleavage furrow, and mitotic spindle of human cells. J Cell Biol 71(3):848–875

Gillespie PG, Cyr JL (2002) Calmodulin binding to recombinant myosin-1c and myosin-1c IQ peptides. BMC Biochem 3:31

Gillespie PG, Albanesi JP, Bahler M, Bement WM, Berg JS, Burgess DR, Burnside B, Cheney RE, Corey DP, Coudrier E, de Lanerolle P, Hammer JA, Hasson T, Holt JR, Hudspeth AJ, Ikebe M, Kendrick-Jones J, Korn ED, Li R, Mercer JA, Milligan RA, Mooseker MS, Ostap EM, Petit C, Pollard TD, Sellers JR, Soldati T, Titus MA (2001) Myosin-I nomenclature. J Cell Biol 155(5):703–704. https://doi.org/10.1083/jcb.200110032

Godin-Heymann N, Bryant I, Rivera MN, Ulkus L, Bell DW, Riese DJ 2nd, Settleman J, Haber DA (2007) Oncogenic activity of epidermal growth factor receptor kinase mutant alleles is enhanced by the T790M drug resistance mutation. Cancer Res 67(15):7319–7326. https://doi.org/10.1158/0008-5472.CAN-06-4625

Green DM, Johnson CP, Hagan H, Corbett AH (2003) The C-terminal domain of myosin-like protein 1 (Mlp1p) is a docking site for heterogeneous nuclear ribonucleoproteins that are required for mRNA export. Proc Natl Acad Sci U S A 100(3):1010–1015. https://doi.org/10.1073/pnas.0336594100

Greenberg MJ, Lin T, Shuman H, Ostap EM (2015) Mechanochemical tuning of myosin-I by the N-terminal region. Proc Natl Acad Sci U S A 112(26):E3337–E3344. https://doi.org/10.1073/pnas.1506633112

Gruss OJ, Vernos I (2004) The mechanism of spindle assembly: functions of Ran and its target TPX2. J Cell Biol 166(7):949–955. https://doi.org/10.1083/jcb.200312112

Guru SC, Goldsmith PK, Burns AL, Marx SJ, Spiegel AM, Collins FS, Chandrasekharappa SC (1998) Menin, the product of the MEN1 gene, is a nuclear protein. Proc Natl Acad Sci U S A 95(4):1630–1634. https://doi.org/10.1073/pnas.95.4.1630

Gurung R, Ono Y, Baxendale S, Lee SL, Moore S, Calvert M, Ingham PW (2017) A Zebrafish model for a human myopathy associated with mutation of the unconventional myosin MYO18B. Genetics 205(2):725–735. https://doi.org/10.1534/genetics.116.192864

Hagen SJ, Kiehart DP, Kaiser DA, Pollard TD (1986) Characterization of monoclonal antibodies to Acanthamoeba myosin-I that cross-react with both myosin-II and low molecular mass nuclear proteins. J Cell Biol 103(6 Pt 1):2121–2128

Hahn MA, Marsh DJ (2007) Nucleolar localization of parafibromin is mediated by three nucleolar localization signals. FEBS Lett 581(26):5070–5074. https://doi.org/10.1016/j.febslet.2007.09.050

Hartshorne DJ (1998) Myosin phosphatase: subunits and interactions. Acta Physiol Scand 164(4):483–493. https://doi.org/10.1046/j.1365-201X.1998.00447.x

Hauser M, Beinbrech G, Groschel-Stewart U, Jockusch BM (1975) Localisation by immunological techniques of myosin in nuclei of lower eurkaryotes. Exp Cell Res 95(1):127–135

Herman IM, Pollard TD (1981) Electron microscopic localization of cytoplasmic myosin with ferritin-labeled antibodies. J Cell Biol 88(2):346–351

Hill TL (1987) Linear aggregation theory in cell biology. Springer series in molecular biology. Springer, New York

Hirono M, Denis CS, Richardson GP, Gillespie PG (2004) Hair cells require phosphatidylinositol

4,5-bisphosphate for mechanical transduction and adaptation. Neuron 44(2):309–320. https://doi.org/10.1016/j.neuron.2004.09.020

Hofmann WA (2009) Cell and molecular biology of nuclear actin. Int Rev Cell Mol Biol 273:219–263. https://doi.org/10.1016/S1937-6448(08)01806-6

Hofmann W, Reichart B, Ewald A, Muller E, Schmitt I, Stauber RH, Lottspeich F, Jockusch BM, Scheer U, Hauber J, Dabauvalle MC (2001) Cofactor requirements for nuclear export of Rev response element (RRE)- and constitutive transport element (CTE)-containing retroviral RNAs. An unexpected role for actin. J Cell Biol 152(5):895–910

Hofmann WA, Stojiljkovic L, Fuchsova B, Vargas GM, Mavrommatis E, Philimonenko V, Kysela K, Goodrich JA, Lessard JL, Hope TJ, Hozak P, de Lanerolle P (2004) Actin is part of pre-initiation complexes and is necessary for transcription by RNA polymerase II. Nat Cell Biol 6(11):1094–1101. https://doi.org/10.1038/ncb1182

Hofmann WA, Johnson T, Klapczynski M, Fan JL, de Lanerolle P (2006a) From transcription to transport: emerging roles for nuclear myosin I. Biochem Cell Biol 84(4):418–426. https://doi.org/10.1139/o06-069

Hofmann WA, Vargas GM, Ramchandran R, Stojiljkovic L, Goodrich JA, de Lanerolle P (2006b) Nuclear myosin I is necessary for the formation of the first phosphodiester bond during transcription initiation by RNA polymerase II. J Cell Biochem 99(4):1001–1009. https://doi.org/10.1002/jcb.21035

Hofmann WA, Richards TA, de Lanerolle P (2009) Ancient animal ancestry for nuclear myosin. J Cell Sci 122(Pt 5):636–643. https://doi.org/10.1242/jcs.030205

Houdusse A, Gaucher JF, Krementsova E, Mui S, Trybus KM, Cohen C (2006) Crystal structure of apo-calmodulin bound to the first two IQ motifs of myosin V reveals essential recognition features. Proc Natl Acad Sci U S A 103(51):19326–19331. https://doi.org/10.1073/pnas.0609436103

Hu P, Wu S, Hernandez N (2004) A role for beta-actin in RNA polymerase III transcription. Genes Dev 18(24):3010–3015. https://doi.org/10.1101/gad.1250804

Ihnatovych I, Migocka-Patrzalek M, Dukh M, Hofmann WA (2012) Identification and characterization of a novel myosin Ic isoform that localizes to the nucleus. Cytoskeleton (Hoboken) 69(8):555–565. https://doi.org/10.1002/cm.21040

Ihnatovych I, Sielski NL, Hofmann WA (2014) Selective expression of myosin IC Isoform A in mouse and human cell lines and mouse prostate cancer tissues. PLoS One 9(9):e108609. https://doi.org/10.1371/journal.pone.0108609

Jiu Y, Kumari R, Fenix AM, Schaible N, Liu X, Varjosalo M, Krishnan R, Burnette DT, Lappalainen P (2019) Myosin-18B promotes the assembly of myosin II stacks for maturation of contractile actomyosin bundles. Curr Biol 29(1):81–92. e85. https://doi.org/10.1016/j.cub.2018.11.045

Jockusch BM, Ryser U, Behnke O (1973) Myosin-like protein in Physarum nuclei. Exp Cell Res 76(2):464–466

Jung EJ, Liu G, Zhou W, Chen X (2006) Myosin VI is a mediator of the p53-dependent cell survival pathway. Mol Cell Biol 26(6):2175–2186. https://doi.org/10.1128/MCB.26.6.2175-2186.2006

Kahle M, Pridalova J, Spacek M, Dzijak R, Hozak P (2007) Nuclear myosin is ubiquitously expressed and evolutionary conserved in vertebrates. Histochem Cell Biol 127(2):139–148. https://doi.org/10.1007/s00418-006-0231-0

Kalt I, Levy A, Borodianskiy-Shteinberg T, Sarid R (2012) Nucleolar localization of GLTSCR2/PICT-1 is mediated by multiple unique nucleolar localization sequences. PLoS One 7(1):e30825. https://doi.org/10.1371/journal.pone.0030825

Karolczak J, Sobczak M, Majewski L, Yeghiazaryan M, Jakubiec-Puka A, Ehler E, Slawinska U, Wilczynski GM, Redowicz MJ (2013) Myosin VI in skeletal muscle: its localization in the sarcoplasmic reticulum, neuromuscular junction and muscle nuclei. Histochem Cell Biol 139(6):873–885. https://doi.org/10.1007/s00418-012-1070-9

Khanna N, Hu Y, Belmont AS (2014) HSP70 transgene directed motion to nuclear speckles facilitates heat shock activation. Curr Biol 24(10):1138–1144. https://doi.org/10.1016/j.cub.2014.03.053

Klages-Mundt NL, Kumar A, Zhang Y, Kapoor P, Shen X (2018) The nature of actin-family proteins in chromatin-modifying complexes. Front Genet 9:398. https://doi.org/10.3389/fgene.2018.00398

Kulashreshtha M, Mehta IS, Kumar P, Rao BJ (2016) Chromosome territory relocation during DNA repair requires nuclear myosin 1 recruitment to chromatin mediated by upsilon-H2AX signaling. Nucleic Acids Res 44(17):8272–8291. https://doi.org/10.1093/nar/gkw573

Kummalue T, Lou J, Friedman AD (2002) Multimerization via its myosin domain facilitates nuclear localization and inhibition of core binding factor (CBF) activities by the CBFbeta-smooth muscle myosin heavy chain myeloid leukemia oncoprotein. Mol Cell Biol 22(23):8278–8291. https://doi.org/10.1128/mcb.22.23.8278-8291.2002

Kuo YH, Landrette SF, Heilman SA, Perrat PN, Garrett L, Liu PP, Le Beau MM, Kogan SC, Castilla LH (2006) Cbf beta-SMMHC induces distinct abnormal myeloid progenitors able to develop acute myeloid leukemia. Cancer Cell 9(1):57–68. https://doi.org/10.1016/j.ccr.2005.12.014

Kysela K, Philimonenko AA, Philimonenko VV, Janacek J, Kahle M, Hozak P (2005) Nuclear distribution of actin and myosin I depends on transcriptional activity of the cell. Histochem Cell Biol 124(5):347–358. https://doi.org/10.1007/s00418-005-0042-8

La P, Desmond A, Hou Z, Silva AC, Schnepp RW, Hua X (2006) Tumor suppressor menin: the essential role of nuclear localization signal domains in coordinating gene expression. Oncogene 25(25):3537–3546. https://doi.org/10.1038/sj.onc.1209400

Le HQ, Ghatak S, Yeung CY, Tellkamp F, Gunschmann C, Dieterich C, Yeroslaviz A, Habermann B, Pombo A, Niessen CM, Wickstrom SA (2016) Mechanical regulation of transcription controls Polycomb-mediated gene silencing during lineage commitment. Nat Cell Biol 18(8):864–875. https://doi.org/10.1038/ncb3387

Leitman EM, Tewari A, Horn M, Urbanski M, Damanakis E, Einheber S, Salzer JL, de Lanerolle P, Melendez-Vasquez CV (2011) MLCK regulates Schwann cell cytoskeletal organization, differentiation and myelination. J Cell Sci 124(Pt 22):3784–3796. https://doi.org/10.1242/jcs.080200

Lestourgeon WM, Forer A, Yang YZ, Bertram JS, Pusch HP (1975) Contractile proteins. Major components of nuclear and chromosome non-histone proteins. Biochim Biophys Acta 379(2):529–552

Lewinska A, Klukowska-Rotzler J, Deregowska A, Adamczyk-Grochala J, Wnuk M (2019) c-Myc activation promotes cofilin-mediated F-actin cytoskeleton remodeling and telomere homeostasis as a response to oxidant-based DNA damage in medulloblastoma cells. Redox Biol 24:101163. https://doi.org/10.1016/j.redox.2019.101163

Li Q, Sarna SK (2009) Nuclear myosin II regulates the assembly of preinitiation complex for ICAM-1 gene transcription. Gastroenterology 137(3):1051–1060, 1060 e1051–1053. https://doi.org/10.1053/j.gastro.2009.03.040

Li YR, Yang WX (2016) Myosins as fundamental components during tumorigenesis: diverse and indispensable. Oncotarget 7(29):46785–46812. https://doi.org/10.18632/oncotarget.8800

Li X, Zheng L, Xia Q, Liu L, Mao M, Zhou H, Zhao Y, Shi J (2019) A novel cell-penetrating peptide protects against neuron apoptosis after cerebral ischemia by inhibiting the nuclear translocation of annexin A1. Cell Death Differ 26(2):260–275. https://doi.org/10.1038/s41418-018-0116-5

Lieto-Trivedi A, Coluccio LM (2008) Calcium, nucleotide, and actin affect the interaction of mammalian Myo1c with its light chain calmodulin. Biochemistry 47(38):10218–10226. https://doi.org/10.1021/bi8011059

Lindsay AJ, McCaffrey MW (2009) Myosin Vb localises to nucleoli and associates with the RNA polymerase I transcription complex. Cell Motil Cytoskeleton 66(12):1057–1072. https://doi.org/10.1002/cm.20408

Liu P, Tarle SA, Hajra A, Claxton DF, Marlton P, Freedman M, Siciliano MJ, Collins FS (1993) Fusion between transcription factor CBF beta/PEBP2 beta and a myosin heavy chain in acute myeloid leukemia. Science 261(5124):1041–1044

Liu C, Zhu R, Mao Y (2018) Nuclear actin polymerized by mDia2 confines centromere movement during CENP-A loading. iScience 9:314–327. https://doi.org/10.1016/j.isci.2018.10.031

Loikkanen I, Toljamo K, Hirvikoski P, Vaisanen T, Paavonen TK, Vaarala MH (2009) Myosin VI is a modulator of androgen-dependent gene expression. Oncol Rep 22(5):991–995

Lopez-Camacho C, van Wijnen AJ, Lian JB, Stein JL, Stein GS (2014) CBFbeta and the leukemogenic fusion protein CBFbeta-SMMHC associate with mitotic chromosomes to epigenetically regulate ribosomal genes. J Cell Biochem 115(12):2155–2164. https://doi.org/10.1002/jcb.24892

Lusic M, Marini B, Ali H, Lucic B, Luzzati R, Giacca M (2013) Proximity to PML nuclear bodies regulates HIV-1 latency in CD4+ T cells. Cell Host Microbe 13(6):665–677. https://doi.org/10.1016/j.chom.2013.05.006

Majewski L, Nowak J, Sobczak M, Karatsai O, Havrylov S, Lenartowski R, Suszek M, Lenartowska M, Redowicz MJ (2018) Myosin VI in the nucleus of neurosecretory PC12 cells: stimulation-dependent nuclear translocation and interaction with nuclear proteins. Nucleus 9(1):125–141. https://doi.org/10.1080/19491034.2017.1421881

Malfatti E, Bohm J, Lacene E, Beuvin M, Romero NB, Laporte J (2015) A premature stop codon in MYO18B is associated with severe nemaline myopathy with cardiomyopathy. J Neuromuscul Dis 2(3):219–227. https://doi.org/10.3233/JND-150085

Maly IV, Hofmann WA (2016) Calcium-regulated import of myosin IC into the nucleus. Cytoskeleton (Hoboken) 73(7):341–350. https://doi.org/10.1002/cm.21310

Maly IV, Hofmann WA (2018) Calcium and nuclear signaling in prostate cancer. Int J Mol Sci 19(4):pii: E1237. https://doi.org/10.3390/ijms19041237

Maly IV, Domaradzki TM, Gosy VA, Hofmann WA (2017) Myosin isoform expressed in metastatic prostate cancer stimulates cell invasion. Sci Rep 7(1):8476. https://doi.org/10.1038/s41598-017-09158-5

McDonald D, Carrero G, Andrin C, de Vries G, Hendzel MJ (2006) Nucleoplasmic beta-actin exists in a dynamic equilibrium between low-mobility polymeric species and rapidly diffusing populations. J Cell Biol 172(4):541–552. https://doi.org/10.1083/jcb.200507101

Mehta IS, Amira M, Harvey AJ, Bridger JM (2010) Rapid chromosome territory relocation by nuclear motor activity in response to serum removal in primary human fibroblasts. Genome Biol 11(1):R5. https://doi.org/10.1186/gb-2010-11-1-r5

Milankov K, De Boni U (1993) Cytochemical localization of actin and myosin aggregates in interphase nuclei in situ. Exp Cell Res 209(2):189–199. https://doi.org/10.1006/excr.1993.1301

Mittal B, Sanger JM, Sanger JW (1987) Visualization of myosin in living cells. J Cell Biol 105(4):1753–1760

Monteith GR, Davis FM, Roberts-Thomson SJ (2012) Calcium channels and pumps in cancer: changes and consequences. J Biol Chem 287(38):31666–31673. https://doi.org/10.1074/jbc.R112.343061

Munnich S, Taft MH, Manstein DJ (2014) Crystal structure of human myosin 1c – the motor in GLUT4 exocytosis: implications for Ca^{2+} regulation and 14-3-3 binding. J Mol Biol 426(10):2070–2081. https://doi.org/10.1016/j.jmb.2014.03.004

Murata K, Hirano K, Villa-Moruzzi E, Hartshorne DJ, Brautigan DL (1997) Differential localization of myosin and myosin phosphatase subunits in smooth muscle cells and migrating fibroblasts. Mol Biol Cell 8(4):663–673

Muratani M, Gerlich D, Janicki SM, Gebhard M, Eils R, Spector DL (2002) Metabolic-energy-dependent movement of PML bodies within the mammalian cell nucleus. Nat Cell Biol 4(2):106–110. https://doi.org/10.1038/ncb740

Nakano T, Tani M, Nishioka M, Kohno T, Otsuka A, Ohwada S, Yokota J (2005) Genetic and epigenetic alterations of the candidate tumor-suppressor gene MYO18B, on chromosome arm 22q, in colorectal cancer. Genes Chromosomes Cancer 43(2):162–171. https://doi.org/10.1002/gcc.20180

Nevitt C, Tooley JG, Schaner Tooley CE (2018) N-terminal acetylation and methylation differentially affect the function of MYL9. Biochem J 475(20):3201–3219. https://doi.org/10.1042/BCJ20180638

Nevzorov I, Sidorenko E, Wang W, Zhao H, Vartiainen MK (2018) Myosin-1C uses a novel phosphoinositide-dependent pathway for nuclear localization. EMBO Rep 19(2):290–304. https://doi.org/10.15252/embr.201744296

Nishioka M, Kohno T, Tani M, Yanaihara N, Tomizawa Y, Otsuka A, Sasaki S, Kobayashi K, Niki T, Maeshima A, Sekido Y, Minna JD, Sone S, Yokota J (2002) MYO18B, a candidate tumor suppressor gene at chromosome 22q12.1, deleted, mutated, and methylated in human lung cancer. Proc Natl Acad Sci U S A 99(19):12269–12274. https://doi.org/10.1073/pnas.192445899

Nowak G, Pestic-Dragovich L, Hozak P, Philimonenko A, Simerly C, Schatten G, de Lanerolle P (1997) Evidence for the presence of myosin I in the nucleus. J Biol Chem 272(27):17176–17181

Obrdlik A, Percipalle P (2011) The F-actin severing protein cofilin-1 is required for RNA polymerase II transcription elongation. Nucleus 2(1):72–79. https://doi.org/10.4161/nucl.2.1.14508

Obrdlik A, Kukalev A, Louvet E, Farrants AK, Caputo L, Percipalle P (2008) The histone acetyltransferase PCAF associates with actin and hnRNP U for RNA polymerase II transcription. Mol Cell Biol 28(20):6342–6357. https://doi.org/10.1128/MCB.00766-08

Obrdlik A, Louvet E, Kukalev A, Naschekin D, Kiseleva E, Fahrenkrog B, Percipalle P (2010) Nuclear myosin 1 is in complex with mature rRNA transcripts and associates with the nuclear pore basket. FASEB J 24(1):146–157. https://doi.org/10.1096/fj.09-135863

Obungu VH, Lee Burns A, Agarwal SK, Chandrasekharapa SC, Adelstein RS, Marx SJ (2003) Menin, a tumor suppressor, associates with nonmuscle myosin II-A heavy chain. Oncogene 22(41):6347–6358. https://doi.org/10.1038/sj.onc.1206658

Ohnishi T, Kawamura H, Tanaka Y (1964) Actin and myosin-like proteins in the calf thymus cell nucleus. J Biochem 56:6–15

Okagaki T, Nakamura A, Suzuki T, Ohmi K, Kohama K (2000) Assembly of smooth muscle myosin by the 38k protein, a homologue of a subunit of pre-mRNA splicing factor-2. J Cell Biol 148(4):653–663. https://doi.org/10.1083/jcb.148.4.653

Oriatkina TN, Zarembskaia OR, Goilo TA (1989) Identification of myosin-like proteins included in chromatin. Biokhimiia 54(6):933–939

Osborne CS, Chakalova L, Brown KE, Carter D, Horton A, Debrand E, Goyenechea B, Mitchell JA, Lopes S, Reik W, Fraser P (2004) Active genes dynamically colocalize to shared sites of ongoing transcription. Nat Genet 36(10):1065–1071. https://doi.org/10.1038/ng1423

Ostlund RE, Pastan I, Adelstein RS (1974) Myosin in cultured fibroblasts. J Biol Chem 249(12):3903–3907

Oswald E, Reinz E, Voit R, Aubin F, Alonso A, Auvinen E (2017) Human papillomavirus type 8 E7 protein binds nuclear myosin 1c and downregulates the expression of pre-rRNA. Virus Genes 53(6):807–813. https://doi.org/10.1007/s11262-017-1491-6

Patel KG, Liu C, Cameron PL, Cameron RS (2001) Myr 8, a novel unconventional myosin expressed during brain development associates with the protein phosphatase catalytic subunits 1alpha and 1gamma1. J Neurosci 21(20):7954–7968

Pederson T, Singer RH (2006) Nucleus and gene regulation. Curr Opin Cell Biol 18(3):229–230. https://doi.org/10.1016/j.ceb.2006.04.004

Percipalle P, Farrants AK (2006) Chromatin remodelling and transcription: be-WICHed by nuclear myosin 1. Curr Opin Cell Biol 18(3):267–274. https://doi.org/10.1016/j.ceb.2006.03.001

Percipalle P, Fomproix N, Cavellan E, Voit R, Reimer G, Kruger T, Thyberg J, Scheer U, Grummt I, Farrants AK (2006) The chromatin remodelling complex WSTF-SNF2h interacts with nuclear myosin 1 and has a role in RNA polymerase I transcription. EMBO Rep 7(5):525–530. https://doi.org/10.1038/sj.embor.7400657

Perez RA, Langford GM, Eckberg WR, Anderson WA (1986) Contractile proteins (actin, myosin) and tubulin are revealed within DNA-containing nucleocytoplasm in mature spermatozoa of Libinia emarginata L. J Submicrosc Cytol 18(3):471–480

Pestic-Dragovich L, Stojiljkovic L, Philimonenko AA, Nowak G, Ke Y, Settlage RE, Shabanowitz J, Hunt DF, Hozak P, de Lanerolle P (2000) A myosin I isoform in the nucleus. Science 290(5490):337–341

Pfitzer L, Moser C, Gegenfurtner F, Arner A, Foerster F, Atzberger C, Zisis T, Kubisch-Dohmen R, Busse J, Smith R, Timinszky G, Kalinina OV, Muller R, Wagner E, Vollmar AM, Zahler S (2019) Targeting actin inhibits repair of doxorubicin-induced DNA damage: a novel therapeutic approach for combination therapy. Cell Death Dis 10(4):302. https://doi.org/10.1038/s41419-019-1546-9

Philimonenko VV, Zhao J, Iben S, Dingova H, Kysela K, Kahle M, Zentgraf H, Hofmann WA, de Lanerolle P, Hozak P, Grummt I (2004) Nuclear actin and myosin I

are required for RNA polymerase I transcription. Nat Cell Biol 6(12):1165–1172. https://doi.org/10.1038/ncb1190

Philimonenko VV, Janacek J, Harata M, Hozak P (2010) Transcription-dependent rearrangements of actin and nuclear myosin I in the nucleolus. Histochem Cell Biol 134(3):243–249. https://doi.org/10.1007/s00418-010-0732-8

Plessner M, Grosse R (2019) Dynamizing nuclear actin filaments. Curr Opin Cell Biol 56:1–6. https://doi.org/10.1016/j.ceb.2018.08.005

Plessner M, Melak M, Chinchilla P, Baarlink C, Grosse R (2015) Nuclear F-actin formation and reorganization upon cell spreading. J Biol Chem 290(18):11209–11216. https://doi.org/10.1074/jbc.M114.627166

Pranchevicius MC, Baqui MM, Ishikawa-Ankerhold HC, Lourenco EV, Leao RM, Banzi SR, dos Santos CT, Roque-Barreira MC, Espreafico EM, Larson RE (2008) Myosin Va phosphorylated on Ser1650 is found in nuclear speckles and redistributes to nucleoli upon inhibition of transcription. Cell Motil Cytoskeleton 65(6):441–456. https://doi.org/10.1002/cm.20269

Pujol MJ, Bosser R, Vendrell M, Serratosa J, Bachs O (1993) Nuclear calmodulin-binding proteins in rat neurons. J Neurochem 60(4):1422–1428

Qi T, Tang W, Wang L, Zhai L, Guo L, Zeng X (2011) G-actin participates in RNA polymerase II-dependent transcription elongation by recruiting positive transcription elongation factor b (P-TEFb). J Biol Chem 286(17):15171–15181. https://doi.org/10.1074/jbc.M110.184374

Raska I, Shaw PJ, Cmarko D (2006) Structure and function of the nucleolus in the spotlight. Curr Opin Cell Biol 18(3):325–334. https://doi.org/10.1016/j.ceb.2006.04.008

Richter L, Wang Y, Hyde RK (2016) Targeting binding partners of the CBFbeta-SMMHC fusion protein for the treatment of inversion 16 acute myeloid leukemia. Oncotarget 7(40):66255–66266. https://doi.org/10.18632/oncotarget.11357

Rimm DL, Pollard TD (1989) Purification and characterization of an Acanthamoeba nuclear actin-binding protein. J Cell Biol 109(2):585–591

Rodgers BD (2005) Insulin-like growth factor-I down-regulates embryonic myosin heavy chain (eMyHC) in myoblast nuclei. Growth Horm IGF Res 15(6):377–383. https://doi.org/10.1016/j.ghir.2005.08.001

Ryu T, Spatola B, Delabaere L, Bowlin K, Hopp H, Kunitake R, Karpen GH, Chiolo I (2015) Heterochromatic breaks move to the nuclear periphery to continue recombinational repair. Nat Cell Biol 17(11):1401–1411. https://doi.org/10.1038/ncb3258

Sachdev S, Hoffmann A, Hannink M (1998) Nuclear localization of IkappaB alpha is mediated by the second ankyrin repeat: the IkappaB alpha ankyrin repeats define a novel class of cis-acting nuclear import sequences. Mol Cell Biol 18(5):2524–2534. https://doi.org/10.1128/mcb.18.5.2524

Sadeghifar F, Bohm S, Vintermist A, Ostlund Farrants AK (2015) The B-WICH chromatin-remodelling complex regulates RNA polymerase III transcription by promoting Max-dependent c-Myc binding. Nucleic Acids Res 43(9):4477–4490. https://doi.org/10.1093/nar/gkv312

Sadhukhan S, Sarkar K, Taylor M, Candotti F, Vyas YM (2014) Nuclear role of WASp in gene transcription is uncoupled from its ARP2/3-dependent cytoplasmic role in actin polymerization. J Immunol 193(1):150–160. https://doi.org/10.4049/jimmunol.1302923

Salamon M, Millino C, Raffaello A, Mongillo M, Sandri C, Bean C, Negrisolo E, Pallavicini A, Valle G, Zaccolo M, Schiaffino S, Lanfranchi G (2003) Human MYO18B, a novel unconventional myosin heavy chain expressed in striated muscles moves into the myonuclei upon differentiation. J Mol Biol 326(1):137–149

Sandquist JC, Larson ME, Woolner S, Ding Z, Bement WM (2018) An interaction between myosin-10 and the cell cycle regulator Wee1 links spindle dynamics to mitotic progression in epithelia. J Cell Biol 217(3):849–859. https://doi.org/10.1083/jcb.201708072

Sarshad AA, Percipalle P (2014) New insight into role of myosin motors for activation of RNA polymerases. Int Rev Cell Mol Biol 311:183–230. https://doi.org/10.1016/B978-0-12-800179-0.00004-0

Sarshad A, Sadeghifar F, Louvet E, Mori R, Bohm S, Al-Muzzaini B, Vintermist A, Fomproix N, Ostlund AK, Percipalle P (2013) Nuclear myosin 1c facilitates the chromatin modifications required to activate rRNA gene transcription and cell cycle progression. PLoS Genet 9(3):e1003397. https://doi.org/10.1371/journal.pgen.1003397

Sarshad AA, Corcoran M, Al-Muzzaini B, Borgonovo-Brandter L, Von Euler A, Lamont D, Visa N, Percipalle P (2014) Glycogen synthase kinase (GSK) 3beta phosphorylates and protects nuclear myosin 1c from proteasome-mediated degradation to activate rDNA transcription in early G1 cells. PLoS Genet 10(6):e1004390. https://doi.org/10.1371/journal.pgen.1004390

Schindler M, Jiang LW (1986) Nuclear actin and myosin as control elements in nucleocytoplasmic transport. J Cell Biol 102(3):859–862

Schwab RS, Ihnatovych I, Yunus SZ, Domaradzki T, Hofmann WA (2013) Identification of signals that facilitate isoform specific nucleolar localization of myosin IC. Exp Cell Res 319(8):1111–1123. https://doi.org/10.1016/j.yexcr.2013.02.008

Scott MS, Boisvert FM, McDowall MD, Lamond AI, Barton GJ (2010) Characterization and prediction of protein nucleolar localization sequences. Nucleic Acids Res 38(21):7388–7399. https://doi.org/10.1093/nar/gkq653

Serebryannyy LA, Cruz CM, de Lanerolle P (2016a) A role for nuclear actin in HDAC 1 and 2 regulation. Sci Rep 6:28460. https://doi.org/10.1038/srep28460

Serebryannyy LA, Parilla M, Annibale P, Cruz CM, Laster K, Gratton E, Kudryashov D, Kosak ST, Gottardi CJ, de Lanerolle P (2016b) Persistent nuclear actin filaments inhibit transcription by RNA polymerase II. J

Cell Sci 129(18):3412–3425. https://doi.org/10.1242/jcs.195867

Serebryannyy LA, Yuen M, Parilla M, Cooper ST, de Lanerolle P (2016c) The effects of disease models of nuclear actin polymerization on the nucleus. Front Physiol 7:454. https://doi.org/10.3389/fphys.2016.00454

Sielski NL, Ihnatovych I, Hagen JJ, Hofmann WA (2014) Tissue specific expression of myosin IC isoforms. BMC Cell Biol 15:8. https://doi.org/10.1186/1471-2121-15-8

Simon DN, Wilson KL (2011) The nucleoskeleton as a genome-associated dynamic 'network of networks'. Nat Rev Mol Cell Biol 12(11):695–708. https://doi.org/10.1038/nrm3207

Sokolova M, Moore HM, Prajapati B, Dopie J, Merilainen L, Honkanen M, Matos RC, Poukkula M, Hietakangas V, Vartiainen MK (2018) Nuclear actin is required for transcription during Drosophila oogenesis. iScience 9:63–70. https://doi.org/10.1016/j.isci.2018.10.010

Spencer VA, Costes S, Inman JL, Xu R, Chen J, Hendzel MJ, Bissell MJ (2011) Depletion of nuclear actin is a key mediator of quiescence in epithelial cells. J Cell Sci 124(Pt 1):123–132. https://doi.org/10.1242/jcs.073197

Spyropoulos B, Moens PB (1984) The synaptonemal complex: does it have contractile proteins? Can J Genet Cytol 26(6):776–781

Stendahl OI, Hartwig JH, Brotschi EA, Stossel TP (1980) Distribution of actin-binding protein and myosin in macrophages during spreading and phagocytosis. J Cell Biol 84(2):215–224

Strambio-de-Castillia C, Blobel G, Rout MP (1999) Proteins connecting the nuclear pore complex with the nuclear interior. J Cell Biol 144(5):839–855

Szerlong H, Hinata K, Viswanathan R, Erdjument-Bromage H, Tempst P, Cairns BR (2008) The HSA domain binds nuclear actin-related proteins to regulate chromatin-remodeling ATPases. Nat Struct Mol Biol 15(5):469–476. https://doi.org/10.1038/nsmb.1403

Tang N, Lin T, Ostap EM (2002) Dynamics of myo1c (myosin-ibeta) lipid binding and dissociation. J Biol Chem 277(45):42763–42768. https://doi.org/10.1074/jbc.M206388200

Tokuo H, Coluccio LM (2013) Myosin-1c regulates the dynamic stability of E-cadherin-based cell-cell contacts in polarized Madin-Darby canine kidney cells. Mol Biol Cell 24(18):2820–2833. https://doi.org/10.1091/mbc.E12-12-0884

Tokuo H, Bhawan J, Coluccio LM (2018) Myosin X is required for efficient melanoblast migration and melanoma initiation and metastasis. Sci Rep 8(1):10449. https://doi.org/10.1038/s41598-018-28717-y

Trinkle-Mulcahy L, Andrews PD, Wickramasinghe S, Sleeman J, Prescott A, Lam YW, Lyon C, Swedlow JR, Lamond AI (2003) Time-lapse imaging reveals dynamic relocalization of PP1gamma throughout the mammalian cell cycle. Mol Biol Cell 14(1):107–117. https://doi.org/10.1091/mbc.e02-07-0376

Trybus KM, Gushchin MI, Lui H, Hazelwood L, Krementsova EB, Volkmann N, Hanein D (2007) Effect of calcium on calmodulin bound to the IQ motifs of myosin V. J Biol Chem 282(32):23316–23325. https://doi.org/10.1074/jbc.M701636200

Tudek A, Schmid M, Makaras M, Barrass JD, Beggs JD, Jensen TH (2018) A Nuclear Export Block Triggers the Decay of Newly Synthesized Polyadenylated RNA. Cell Rep 24(9):2457–2467.e2457. https://doi.org/10.1016/j.celrep.2018.07.103

Umeki N, Jung HS, Sakai T, Sato O, Ikebe R, Ikebe M (2011) Phospholipid-dependent regulation of the motor activity of myosin X. Nat Struct Mol Biol 18(7):783–788. https://doi.org/10.1038/nsmb.2065

Venit T, Dzijak R, Kalendova A, Kahle M, Rohozkova J, Schmidt V, Rulicke T, Rathkolb B, Hans W, Bohla A, Eickelberg O, Stoeger T, Wolf E, Yildirim AO, Gailus-Durner V, Fuchs H, de Angelis MH, Hozak P (2013) Mouse nuclear myosin I knock-out shows interchangeability and redundancy of myosin isoforms in the cell nucleus. PLoS One 8(4):e61406. https://doi.org/10.1371/journal.pone.0061406

Venit T, Kalendova A, Petr M, Dzijak R, Pastorek L, Rohozkova J, Malohlava J, Hozak P (2016) Nuclear myosin I regulates cell membrane tension. Sci Rep 6:30864. https://doi.org/10.1038/srep30864

Vintermist A, Bohm S, Sadeghifar F, Louvet E, Mansen A, Percipalle P, Ostlund Farrants AK (2011) The chromatin remodelling complex B-WICH changes the chromatin structure and recruits histone acetyl-transferases to active rRNA genes. PLoS One 6(4):e19184. https://doi.org/10.1371/journal.pone.0019184

Virtanen JA, Vartiainen MK (2017) Diverse functions for different forms of nuclear actin. Curr Opin Cell Biol 46:33–38. https://doi.org/10.1016/j.ceb.2016.12.004

Vreugde S, Ferrai C, Miluzio A, Hauben E, Marchisio PC, Crippa MP, Bussi M, Biffo S (2006) Nuclear myosin VI enhances RNA polymerase II-dependent transcription. Mol Cell 23(5):749–755. https://doi.org/10.1016/j.molcel.2006.07.005

Waldrop FS, Puchtler H, Palmer GR (1976) Light microscopic demonstration of myoid material in nuclei. Histochemistry 46(3):237–243

Wang J, Zhao S, Wei Y, Zhou Y, Shore P, Deng W (2016) Cytoskeletal filamin A differentially modulates RNA polymerase III gene transcription in transformed cell lines. J Biol Chem 291(48):25239–25246. https://doi.org/10.1074/jbc.M116.735886

Weber KL, Sokac AM, Berg JS, Cheney RE, Bement WM (2004) A microtubule-binding myosin required for nuclear anchoring and spindle assembly. Nature 431(7006):325–329. https://doi.org/10.1038/nature02834

White BA (1985) Evidence for a role of calmodulin in the regulation of prolactin gene expression. J Biol Chem 260(2):1213–1217

Wijmenga C, Gregory PE, Hajra A, Schrock E, Ried T, Eils R, Liu PP, Collins FS (1996) Core binding factor beta-smooth muscle myosin heavy chain chimeric protein involved in acute myeloid leukemia forms unusual

nuclear rod-like structures in transformed NIH 3T3 cells. Proc Natl Acad Sci U S A 93(4):1630–1635

Wilkie AR, Sharma M, Pesola JM, Ericsson M, Fernandez R, Coen DM (2018) A role for myosin Va in human cytomegalovirus nuclear egress. J Virol 92(6). https://doi.org/10.1128/JVI.01849-17

Wollscheid HP, Biancospino M, He F, Magistrati E, Molteni E, Lupia M, Soffientini P, Rottner K, Cavallaro U, Pozzoli U, Mapelli M, Walters KJ, Polo S (2016) Diverse functions of myosin VI elucidated by an isoform-specific alpha-helix domain. Nat Struct Mol Biol 23(4):300–308. https://doi.org/10.1038/nsmb.3187

Woolner S, O'Brien LL, Wiese C, Bement WM (2008) Myosin-10 and actin filaments are essential for mitotic spindle function. J Cell Biol 182(1):77–88. https://doi.org/10.1083/jcb.200804062

Wu X, Yoo Y, Okuhama NN, Tucker PW, Liu G, Guan JL (2006) Regulation of RNA-polymerase-II-dependent transcription by N-WASP and its nuclear-binding partners. Nat Cell Biol 8(7):756–763. https://doi.org/10.1038/ncb1433

Xie X, Percipalle P (2018) An actin-based nucleoskeleton involved in gene regulation and genome organization. Biochem Biophys Res Commun 506(2):378–386. https://doi.org/10.1016/j.bbrc.2017.11.206

Xu Z, Li P, Wei D, Wang Z, Bao Y, Sun J, Qu L, Wang L (2016) NMMHC-IIA-dependent nuclear location of CXCR4 promotes migration and invasion in renal cell carcinoma. Oncol Rep 36(5):2681–2688. https://doi.org/10.3892/or.2016.5082

Xue Y, Zhan X, Sun S, Karuppagounder SS, Xia S, Dawson VL, Dawson TM, Laterra J, Zhang J, Ying M (2019) Synthetic mRNAs drive highly efficient iPS cell differentiation to dopaminergic neurons. Stem Cells Transl Med 8(2):112–123. https://doi.org/10.1002/sctm.18-0036

Yanaihara N, Nishioka M, Kohno T, Otsuka A, Okamoto A, Ochiai K, Tanaka T, Yokota J (2004) Reduced expression of MYO18B, a candidate tumor-suppressor gene on chromosome arm 22q, in ovarian cancer. Int J Cancer 112(1):150–154. https://doi.org/10.1002/ijc.20339

Ye J, Zhao J, Hoffmann-Rohrer U, Grummt I (2008) Nuclear myosin I acts in concert with polymeric actin to drive RNA polymerase I transcription. Genes Dev 22(3):322–330. https://doi.org/10.1101/gad.455908

Yoo Y, Wu X, Guan JL (2007) A novel role of the actin-nucleating Arp2/3 complex in the regulation of RNA polymerase II-dependent transcription. J Biol Chem 282(10):7616–7623. https://doi.org/10.1074/jbc.M607596200

Zattelman L, Regev R, Usaj M, Reinke PYA, Giese S, Samson AO, Taft MH, Manstein DJ, Henn A (2017) N-terminal splicing extensions of the human MYO1C gene fine-tune the kinetics of the three full-length myosin IC isoforms. J Biol Chem 292(43):17804–17818. https://doi.org/10.1074/jbc.M117.794008

Zhang YS, Liu B, Luo XJ, Li TB, Zhang JJ, Peng JJ, Zhang XJ, Ma QL, Hu CP, Li YJ, Peng J, Li Q (2015a) Nuclear cardiac myosin light chain 2 modulates NADPH oxidase 2 expression in myocardium: a novel function beyond muscle contraction. Basic Res Cardiol 110(4):38. https://doi.org/10.1007/s00395-015-0494-5

Zhang YS, Liu B, Luo XJ, Zhang JJ, Li NS, Ma QL, Jiang JL, Li YJ, Li Q, Peng J (2015b) A novel function of nuclear nonmuscle myosin regulatory light chain in promotion of xanthine oxidase transcription after myocardial ischemia/reperfusion. Free Radic Biol Med 83:115–128. https://doi.org/10.1016/j.freeradbiomed.2015.02.013

Zhang L, Huang ST, Feng YL, Wan T, Gu HF, Xu J, Yuan LJ, Zhou Y, Yu XJ, Huang L, Luo RZ, Jia WH, Zheng M (2017) The bidirectional regulation between MYL5 and HIF-1alpha promotes cervical carcinoma metastasis. Theranostics 7(15):3768–3780. https://doi.org/10.7150/thno.20796

Zhang Z, Zhu J, Huang Y, Li W, Cheng H (2018) MYO18B promotes hepatocellular carcinoma progression by activating PI3K/AKT/mTOR signaling pathway. Diagn Pathol 13(1):85. https://doi.org/10.1186/s13000-018-0763-3

Zhao J, Yuan X, Frodin M, Grummt I (2003) ERK-dependent phosphorylation of the transcription initiation factor TIF-IA is required for RNA polymerase I transcription and cell growth. Mol Cell 11(2):405–413

Zhao W, Claxton DF, Medeiros LJ, Lu D, Vadhan-Raj S, Kantarjian HM, Nguyen MH, Bueso-Ramos CE (2006) Immunohistochemical analysis of CBFbeta-SMMHC protein reveals a unique nuclear localization in acute myeloid leukemia with inv(16)(p13q22). Am J Surg Pathol 30(11):1436–1444. https://doi.org/10.1097/01.pas.0000213301.19273.66

Zhao Y, Wang J, Jiang H, Yu Z, Li X, Shi J (2015) Following OGD/R, annexin 1 nuclear translocation and subsequent induction of apoptosis in neurons are assisted by myosin IIA in a TRPM7 kinase-dependent manner. Mol Neurobiol 51(2):729–742. https://doi.org/10.1007/s12035-014-8781-y

Zhou G, Doci CL, Lingen MW (2010) Identification and functional analysis of NOL7 nuclear and nucleolar localization signals. BMC Cell Biol 11:74. https://doi.org/10.1186/1471-2121-11-74

Zorca CE, Kim LK, Kim YJ, Krause MR, Zenklusen D, Spilianakis CG, Flavell RA (2015) Myosin VI regulates gene pairing and transcriptional pause release in T cells. Proc Natl Acad Sci U S A 112(13):E1587–E1593. https://doi.org/10.1073/pnas.1502461112

Myosins in Cytokinesis

11

Thomas D. Pollard

Abstract

Nearly five decades of research have established myosin as the main motor responsible for cytokinesis in organisms on the branch of the phylogenetic tree that includes amoebas, fungi and animals. This research has grown to be more mechanistic over the past decade, so we now have computer simulations of physically reasonable models that explain how myosins contribute to the assembly and constriction of contractile rings that pinch dividing cells into two daughter cells. Isoforms of myosin-II, from the same family as muscle myosins, are the main myosins for cytokinesis, but other myosins contribute to cytokinesis in fission yeast. Progress has been made on how animal cells use Rho-GTPases to control the accumulation and activity of myosin-II at the site of cleavage, but the regulatory mechanisms are less clear in other systems.

Keywords

Cytokinesis · Myosin · Actin · Computer simulation

T. D. Pollard (✉)
Department of Molecular, Cellular and Developmental Biology, Department of Molecular Biophysics and Biochemistry, Department of Cell Biology, Yale University, New Haven, CT, USA
e-mail: thomas.pollard@yale.edu

11.1 Discovery of Myosin-II as the Motor for Cytokinesis

The concept that a tension-generating contractile ring of actin filaments and myosin-II produces the force for cytokinesis came from a series of crucial experiments in the decade beginning in 1967. Carter reported that a natural product called cytochalasin (cell relaxing) caused regression of the cleavage furrow in cultured mammalian cells (Carter 1967), suggesting that active tension produced the furrow. Rappaport (1967) showed that the cortex around the equator of echinoderm eggs generates enough tension to invaginate the plasma membrane into a cleavage furrow that divides the cell at the end of mitosis. The tension in the furrow was in the same range as contraction by an equivalent cross section of muscle, so he speculated that the mechanisms might be similar. Hiramoto (1975) later confirmed these observations. Next Schroeder (1970, 1972) used electron microscopy of thin sections of dividing Hela cells and echinoderm eggs to identify a thin layer of filaments on the cytoplasmic surface of plasma membrane in the cleavage furrow. He subsequently showed that they are actin filaments by decoration with myosin (Schroeder 1973). Like muscle, this ring of actin filaments maintains a constant volume as the cleavage furrow begins to constrict but then disassembles as cleavage progresses (Schroeder 1972). Fujiwara

L. M. Coluccio (ed.), *Myosins*, Advances in Experimental Medicine and Biology 1239,
https://doi.org/10.1007/978-3-030-38062-5_11

and Pollard (1976) used fluorescent antibodies to show that myosin-II concentrates in the cleavage furrow of Hela cells, and Mabuchi and Okuno (1977) blocked cytokinesis of echinoderm eggs by injecting antibodies to myosin-II. Together these studies established the textbook account of cytokinesis by the assembly and constriction of a contractile ring actin filaments and myosin-II around the equator (Fig. 11.1).

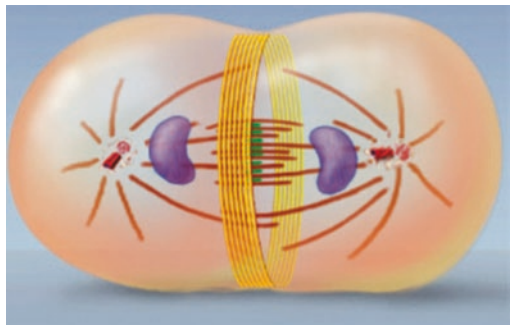

Fig. 11.1 Contractile ring model from "Cell Biology" (Pollard TD et al. 2017b). A ring of actin filaments (yellow) and myosin-II mini-filaments (rust) forms around the equator between the separated nuclei and produces force to invaginate the plasma membrane

11.2 Evolutionary Perspective

The evolutionary history of myosin genes (Odronitz and Kollmar 2007) (Fig. 11.2) explains why the mechanisms of cytokinesis differ in contemporary organisms. The primordial myosin gene appeared in an early eukaryote and encoded myosin-I with a single head, one or more light chains and short tails that typically interact with membranes. About 1 billion years ago the last eukaryotic common ancestor (LECA) also had a gene for myosin-V, a motor with two heads, multiple light chains and a tail including a coiled-coil and cargo-binding domains. The gene for myosin-II appeared on the branch leading to amoebas, fungi and animals (Odronitz and Kollmar 2007) and is not found in vast numbers of unicellular organisms, algae or plants. Consequently, these organisms do not have contractile rings and depend on membrane traffic and cell wall synthesis for cytokinesis, which may have also been true for LECA.

Myosin-II genes encode heavy chains that form dimers joined by long alpha-helical coiled-coil tails. The N-terminal catalytic domain is connected to the tail by a long alpha-helix associated with a pair of light chains. These myosins have short duty cycles (the fraction of force-producing states in the ATPase cycle associated

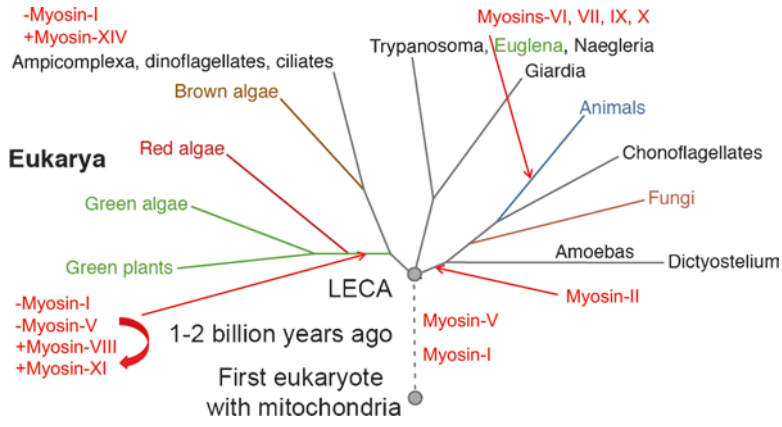

Fig. 11.2 Myosin phylogenetic tree. Myosin-I, followed by myosin-V arose during the billion years between the first eukaryote and LECA, the last eukaryotic common ancestor. Myosin-II appeared on the branch leading to amoebas, fungi and animals. Myosins VI, VII, IX and X evolved in animals. Myosin-I was lost, and myosin-V was replaced by myosins-VIII and -XI on the branch leading to algae and plants. Myosin-I was replaced by myosin-XIV in ampicomplexa. Based on the data of Odronitz and Kollmar (2007)

with actin filaments), so they work in parallel with each other to pull on an actin filament, as understood in detail for muscle contraction (Geeves and Holmes 1999). Vertebrates have three genes for nonmuscle myosin-II: MHY9 for NM2a, MHY10 for NM2b and MHY14 for NM2c with additional variation by tissue-specific, alternative splicing of two exons (Ma and Adelstein 2014). Each of these myosin-II isoforms is required for the normal development of the mouse, with the defects associated with the deletions of individual genes depending on their patterns of expression. The NM2 isoforms can substitute for each other when expressed from the native promoters.

11.3 Validation of the Role of Myosin-II in Cytokinesis

Both conditional and deletion mutations have been used to establish functions for myosins during cytokinesis. Temperature-sensitive mutations have allowed studies showing that the products of essential myosin-II genes are required for cytokinesis by fission yeast (Balasubramanian et al. 1998) and *C. elegans* (Davies et al. 2014). Deleting the gene for myosin-II shows that the protein is essential for cytokinesis in fission yeast (Kitayama et al. 1997) and that cytokinesis is severely compromised in *Dictyostelium*, which survives by cellular fragments pulling apart by amoeboid movement (DeLozanne and Spudich 1987). Depleting the regulatory light chain by RNAi showed that myosin-II is required for cytokinesis in *C. elegans* (Shelton et al. 1999).

The natural products cytochalasin (Carter 1967) and latrunculin (Spector et al. 1983) inhibit the polymerization of actin filaments and have been used in numerous studies showing the importance of actin filaments for cell division (Peterson and Mitchison 2002). Latrunculin has a much simpler mechanism of action (Fujiwara et al. 2018) than cytochalasin (Cooper 1987), an advantage for interpreting experiments.

Blebbistatin, a small molecule inhibitor of myosin-II, allows myosin-II and anillin to accumulate around the equator of mitotic vertebrate cells but reversibly blocks ingression of the cleavage furrow (Straight et al. 2003). Blebbistatin inhibits the myosin-actin ATPase cycle by stabilizing the myosin-ADP-P_i state detached from actin filaments (Kovacs et al. 2004). The drug is specific for myosin-II and has IC50's of 1 μM for skeletal muscle myosin-II, 6 μM for smooth muscle myosin-II, 4 μM for NM2a, 2 μM for NM2b and 2 μM for NM2c (Limouze et al. 2004, Zhang et al. 2017). The affinities for other myosins are much lower with IC50's of >150 μM for myosin-Ib, myosin-Va and myosin-X. These properties of blebbistatin showed that one or more myosin-II isoforms is required for constricting the contractile ring in animal cells. Note that blue light ($\lambda < 500$ nm) inactivates blebbistatin (Sakamoto et al. 2005), so routine imaging conditions for green fluorophores can inactivate blebbistatin. On the other hand, selective application of blue light can quickly reverse the effects of blebbistatin, allowing cytokinesis to continue after being inhibited by blebbistatin (Sakamoto et al. 2005).

11.4 Organization of Myosin-II During Cytokinesis

It was generally assumed that the myosin-II in the contractile ring was assembled into small bipolar filaments (Fig. 11.3a), because the purified protein spontaneously forms these structures from about 30 molecules under physiological conditions (Niederman and Pollard 1975). These filaments are often called "mini-filaments" to distinguish them from the thick filaments of 300 molecules of myosin-II in striated muscle. Both Schroeder (Schroeder 1973) and Sanger and Sanger (Sanger and Sanger 1980) observed in electron micrographs of thin sections rods that were consistent with myosin-II mini-filament bare zones among actin filaments decorated with myosin heads. After special conditions were discovered to preserve actin filaments in nonmuscle cells during preparation for electron microscopy (Maupin and Pollard 1983), micrographs of thin sections of contractile rings in Hela cells revealed not only actin filaments but some thicker rods the size of myosin-II mini-filaments (Maupin and

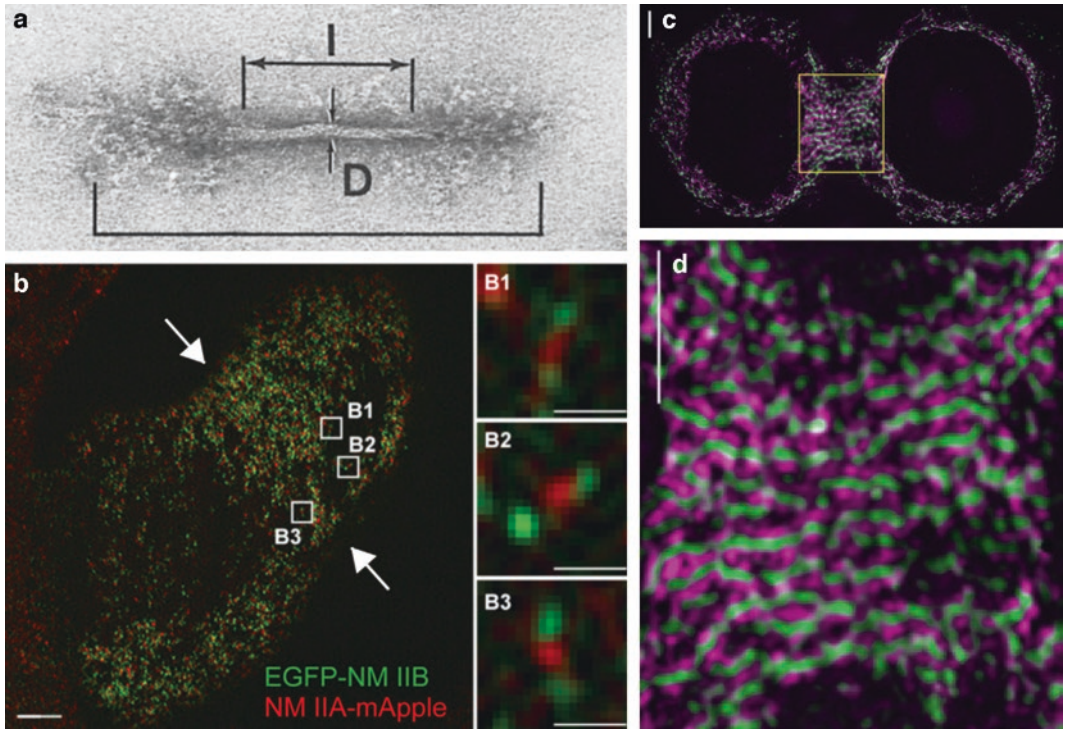

Fig. 11.3 Bipolar mini-filaments of myosin-II. (**a**) Electron micrograph of a negatively-stained bipolar mini-filament of human platelet myosin-II in 100 mM KCl, 1 mM $MgCl_2$, 10 mM imidazole, pH 7.0 (Niederman and Pollard 1975). I is the length of the bare zone (average = 173 nm), D is the diameter of the bare zone (average = 10.5 nm) and the brackets mark the length of the filament (average = 350 nm). (**b**) Myosin-II mini-filaments in a forming contractile ring (arrows) of a live LLC-Pk1 cell imaged by TIRF-structured illumination microscopy (Beach et al. 2014). The N-terminus of nonmuscle myosin-II was tagged with EGFP (green) and the C-terminus was tagged with mApple (red), so bipolar filaments appear as two green spots flanking a red spot in the central bare zone. Scale bars: 2 μm in main panel; 300 nm in insets. (**c, d**) Myosin-II mini-filaments in a live Hela cell with a deep cleavage furrow. The cell expressed non-muscle myosin-IIA with mEmerald on the N-terminus and mApple on the C-terminus and was imaged by structured illumination microscopy (Fenix et al. 2016). Scale bars: 2 μm

Pollard 1986). Electron microscopy of platinum replicas of the sea urchin egg contractile rings also showed bipolar myosin filaments closely associated with the circumferential ring of actin filaments (Henson et al. 2017).

Conventional fluorescence microscopy first showed rod-shaped clusters of myosin-II in isolated cleavage furrows from sea urchin eggs (Otto and Schroeder 1990). Optical sectioning by confocal fluorescence microscopy resolved the myosin-II in the cleavage furrow of Hela cells as diffraction-limited spots with fluorescence intensity judged to be greater than that expected for individual mini-filaments (Maupin et al. 1994). Tiny spots of myosin-II in the cortex of *C. elegans* embryos aggregate into larger actomyosin clusters that flow along the cortex toward the anterior pole (Munro et al. 2004) and subsequently assemble into the contractile ring (Werner et al. 2007; Reymann et al. 2016).

However, it took super-resolution fluorescence microscopy to show that myosin-II is organized into mini-filaments in forming (Fig. 11.3b) and mature (Fig. 11.3c, d) contractile rings of Hela cells (Fenix et al. 2016), LLC-Pk1 cells (Beach et al. 2014) and sea urchin embryos (Henson et al. 2017). These bipolar filaments align around the equator and associate laterally. The contractile ring filaments in LLC-Ptk1 cells are composed of a mixture of NM2a and NM2b. Myosin-II

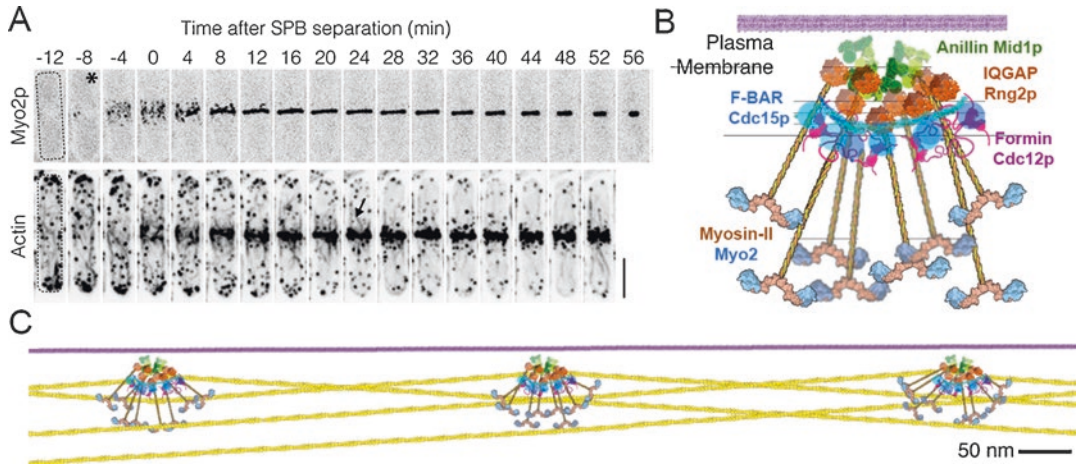

Fig. 11.4 Cytokinesis by fission yeast. (**a**) Reverse contrast fluorescence micrographs (maximum intensity projections of 18 confocal sections) showing the time course of contractile ring assembly from nodes containing Myo2 myosin-II (mEGFP-Myo2p) and from actin filaments (GFP-calponin homology domain) assembled by formin Cdc12p in nodes (Laplante et al. 2015a). Myo2p appears in nodes at time –8 min (asterisk) and actin filaments appear after time zero. The spots of actin filaments throughout the cortex are endocytic actin patches, which concentrate around the cleavage furrow at the end of cytokinesis. Bar is 5 μM. (**b**) Model of a cytokinetic node based on localization of the proteins by FPALM super-resolution microscopy (Laplante et al. 2015b; Laplante et al. 2016). (**c**) Schematic of three nodes associated with the plasma membrane and connected by actin filaments (Laplante et al. 2016). Myo2 molecules in the central node pull on oppositely polarized actin filaments from the lateral nodes to form a sarcomeric structure with the base of the central node equivalent to the bare zone of a bipolar filament of myosin-II

filaments in isolated cleavage furrows of sea urchin eggs are anchored independently of actin filaments (Otto and Schroeder 1990), but this has not been investigated in other animal cells.

In budding yeast, myosin-II (the product of the *myo1* gene) concentrates in the furrow between the mother and daughter cells on a scaffolding of septin filaments independent of actin filaments (Wloka et al. 2013). Electron micrographs of platinum replicas showed circumferential and radial septin filaments arranged in an hourglass fashion in the furrow (Ong et al. 2014) along with bumpy filaments that were absent in a strain with a *myo1*Δ deletion mutation. These may be myosin-II filaments, although they did not have bare zones like animal myosin-II mini-filaments.

Three myosins are located in the contractile rings of fission yeast. A conventional myosin-II called Myo2 (Myo2p heavy chain, Rlc1p regulatory light chain and Cdc4p essential light chain) has two heads and a coiled-coil tail about 85 nm long but does not seem to form bipolar filaments (Bezanilla and Pollard 2000; Lord and Pollard 2004; Pollard LW et al. 2017a; Friend et al. 2018). The intrinsically disordered N-terminal half of anillin Mid1p (Chatterjee and Pollard 2019) anchors the end of the Myo2 tail in cytokinetic nodes (Fig. 11.4b) by direct interactions and indirect interactions via IQGAP Rng2p (Motegi et al. 2004; Saha and Pollard 2012; Tebbs and Pollard 2013). Myp2 (Myp2p heavy chain, Rlc1p regulatory light chain and Cde4p essential light chain) is a genuine myosin-II based on the sequence of its catalytic domain but is unconventional, since its tail appears to fold back on itself in an antiparallel coiled-coil forming a molecule with a single head (Bezanilla et al. 1997). Myp2 joins the contractile ring after it assembles and is located further from the plasma membrane than Myo2 (Laplante et al. 2015a; McDonald et al. 2017). Its oligomeric state in the contractile ring is not known. In addition, one of two myosin-V isoforms, Myo51, is located between cytokinetic nodes (Wang et al. 2014) and contributes to assembly of the contractile ring (Laplante et al. 2015a).

11.5 The Role of Myosin-II in Assembling the Contractile Ring

Contractile ring assembly is best understood in fission yeast where the contractile ring proteins first accumulate at the cleavage site and then depend on force produced by myosin-II to condense into a compact structure (Fig. 11.4a). Computer simulations of a molecularly explicit model account for many of the observed details of the assembly of the contractile ring (Vavylonis et al. 2008). This model was based on a detailed time course of cytokinesis (Wu et al. 2003), quantitative measurements of the numbers of the participating proteins (Wu and Pollard 2005) and the biochemical properties of the proteins (Kovar et al. 2003; Lord and Pollard 2004; Andrianantoandro and Pollard 2006; Kovar et al. 2006). Preparation for cytokinesis starts during interphase, when two types of protein assemblies called nodes form on the inside of the plasma membrane and come together around the middle of the cell (Akamatsu et al. 2014). Already during interphase the contractile ring protein anillin Mid1p joins the nodes (Paoletti and Chang 2000) where its C-terminal lipid-binding domains (Sun et al. 2015) interact with the plasma membrane. As the cell enters mitosis, nodes accumulate Myo2 myosin-II, formin Cdc12 and other proteins anchored to the plasma membrane by anillin Mid1p and F-BAR protein Cdc15p (Fig. 11.4b) (Laplante et al. 2016). Formin Cdc12p polymerizes actin filaments that grow from the nodes in random directions, sometimes encountering a nearby node, where the myosin-II binds and pulls on the filament (Fig. 11.4c). This force slows polymerization of actin from the formin (Zimmermann et al. 2017), which facilitates the motion of the nodes towards each other. The stop and go motions of the nodes revealed that these connections break on average after about 20 s, a reaction that depends on severing of actin filaments by cofilin (Chen and Pollard 2011). Without severing, nodes form large clusters rather than rings. Simulations of this search-capture-pull and release model assemble nodes into a ring in the same time as live cells (Vavylonis et al. 2008). Key features of this mechanism include the initial placement of nodes around the equator of the cell (Martin and Berthelot-Grosjean 2009; Moseley et al. 2009), anchoring of both myosin-II and the barbed ends of actin filaments (by Cdc12p) to the plasma membrane and the release step, which serves as an error-correcting mechanism.

Contractile ring assembly by animal cells also proceeds in two steps, accumulation of the cytokinesis proteins around the equator followed by compaction into a narrower contractile ring (Green, et al. 2012). Both steps depend on the local accumulation of active RhoA-GTP on the cytoplasmic surface of plasma membrane in the plane between the nuclei being separated by the mitotic spindle (Basant and Glotzer 2018). In fact, local activation of RhoA can produce a membrane furrow anywhere on the surface of a cell at any time in the cell cycle (Wagner and Glotzer 2016). RhoA is positioned by a signaling pathway consisting of the centralspindlin complex (including a kinesin-6 microtubule motor) which localizes a guanine nucleotide exchange factor (GEF) called Ect-2 at the cleavage site where it activates RhoA by exchanging GDP for GTP (Basant and Glotzer 2018). RhoA-GTP stimulates contractile ring formation by activating both myosin-II and formins. Rho-kinase phosphorylates the regulatory light chain of myosin-II, which releases the myosin from auto-inhibition, allowing assembly into bipolar filaments, and stimulates its actin-activated ATPase. Active Rho-GTP also binds formins to release them from auto-inhibition, so they can nucleate and elongate actin filaments. The mechanism that positions Ect-2 at the cleavage site is still being investigated but involves overlapping anti-parallel microtubules from the poles of the mitotic spindle (Pollard and O'Shaughnessy 2019).

During the first step of contractile ring formation in *C. elegans* embryos, local RhoA activity positions contractile ring proteins including myosin-II, formin CYK1 and anillin in a broad, cortical band around the equator (Lewellyn et al. 2011). The physical interactions of these proteins with each other and the plasma membrane have

not been characterized. Myosin-II activity is not required for this initial step (Davies et al. 2014), although it may contribute to the initial flattening of the cell into a barrel shape. Vertebrate cells in culture also concentrate myosin-II and anillin in the cortex around the equator even in the presence of blebbistatin, so force produced by myosin is not required until the second step when a compact ring forms and invaginates the plasma membrane (Straight et al. 2003).

During the second step in *C. elegans* embryos the cortical sheet of actin filaments and myosin-II narrows into a ring and the furrow starts to invaginate (Reymann et al. 2016). This step depends on both the centralspindlin complex and active RhoA to localize myosin-II, formin CYK1 and actin filaments as well as a second master regulator called the chromosomal passenger complex, CPC (Lewellyn et al. 2011). A physical model based on an active nematic gel of actin filaments and myosin-II reproduces the alignment of the actin and myosin (Reymann et al. 2016) but does not consider the molecular details such as the organization of the proteins or their attachments to the plasma membrane.

11.6 Mechanisms of Force Production During Cleavage

Since the original suggestions by Rappaport (1967) and Schroeder (1975) sliding-filament models based on bipolar filaments of myosin-II have been considered the most likely mechanism to produce the force that constricts the contractile ring and invaginates the cleavage furrow (Fig. 11.5). Enough information is now available to test this hypothesis with computer simulations of mathematical models.

The most complete models of contractile ring constriction are based on data from fission yeast where information is available about the number

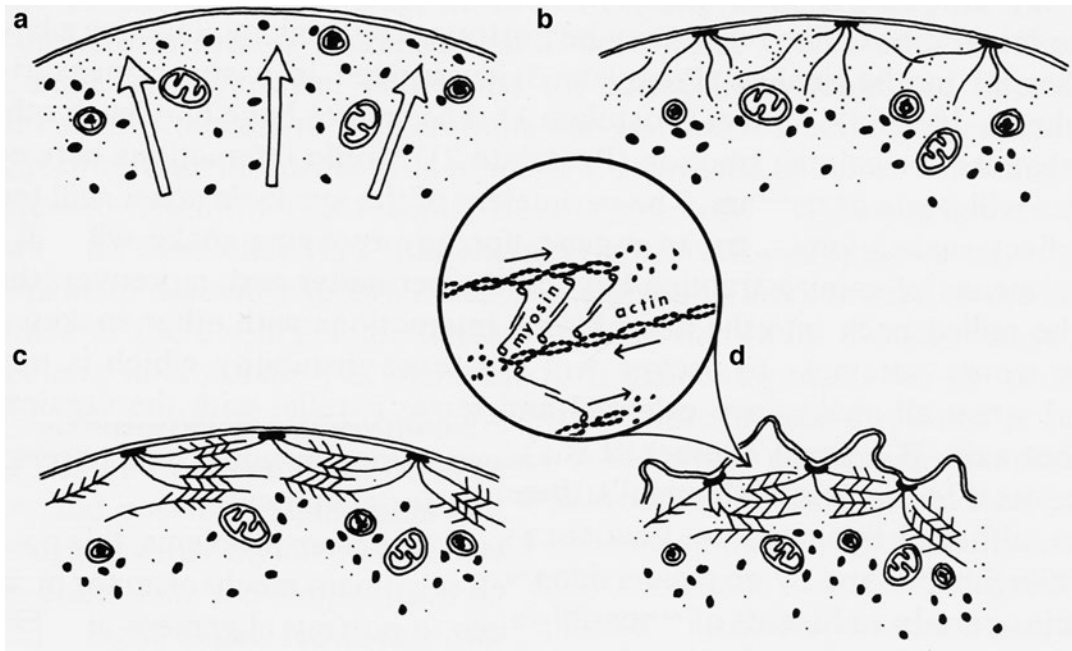

Fig. 11.5 The first published drawing of a sliding-filament model for cytokinesis (Schroeder 1975). (**a**) A signal (open arrows) arrives at the plasma membrane to assemble actin filaments. (**b**) Actin filaments assemble with their barbed ends attached to sites on the plasma membrane. (**c**) Myosin crosslinks antiparallel actin filaments. (**d**) A sliding filament mechanism pulls on actin filaments attached to the plasma membrane. The bipolar myosin filaments are represented by just two myosin molecules

of participating molecules (Wu and Pollard 2005), their turnover rates (Pelham and Chang 2002; Friend et al. 2018), and their organization (Laplante et al. 2015b). The original two-dimensional model (Stachowiak et al. 2014) assumed clusters of myosin-II Myo2 attached to the plasma membrane pulling on actin filaments anchored by their barbed ends by formins and crosslinked by alpha-actinin and included the observed rates of protein turnover. Simulations produced tension equal to that measured in yeast protoplasts from the indentation of the furrow and the membrane tension. Turnover of the actin and myosin on a time scale of tens of seconds was essential to avoid clustering of the myosin and loss of tension.

A more realistic second generation model (Wang et al. 2018) assumed Myo2 and formin Cdc12 in nodes (Fig. 11.4b), Myo2 applying force on adjacent nodes (Fig. 11.4c), myosins being concentrated in the ring as it constricts (Wu and Pollard 2005), actin being depleted from the ring in proportion to its circumference (Courtemanche et al. 2016) and clusters of Myp2 crosslinking actin filaments deeper in the cytoplasm (Laplante et al. 2015a; McDonald et al. 2017). Simulations of this model produced tension that increased as the ring constricted, as measured in dividing protoplasts, and showed that both Myo2 and Myp2 contribute about equally to tension generation as observed with measurements on protoplasts with mutations.

No molecularly explicit models are available of constriction of contractile rings in animal cells. However, simulations of continuum models of active gels of myosin and actin filaments reproduce many of the mechanical features of cytokinesis (Joanny et al. 2013; Turlier et al. 2014; Dorn et al. 2016).

11.7 Alternative Mechanisms of Contractile Ring Constriction

A number of observations raised questions about whether myosin-II alone is responsible for producing the forces for cytokinesis. For example, *C. elegans* embryos with a temperature-sensitive mutation of myosin-II can constrict their cleavage furrows slowly at the restrictive temperature (Davies et al. 2014). The mutant protein may have residual activity, but other myosins also might contribute and compensate for the loss of myosin-II activity. This is clearly the case in fission yeast, where conventional myosin-II Myo2 cooperates with myosin-V Myo51 to assemble the contractile ring and with unconventional myosin-II Myp2 to constrict the contractile ring (Laplante et al. 2015a). (Readers may be interested in letters discussing how to design and interpret these experiments (Laplante and Pollard 2017; Zambon et al. 2017). Such cooperation between myosins has not been explored in other cells.

A second class of question is whether myosin-II or other proteins might produce force by crosslinking shrinking actin filaments as proposed for budding yeast (Mendes Pinto et al. 2012; Mendes Pinto et al. 2013). For example, NM2 isoforms with the R709C mutation have low actin-activated ATPase and reduced or no ability to move actin filaments in a motility assay owing to prolonged attachment of the ADP-myosin intermediate to actin filaments (Ma and Adelstein 2014). However, cardiac myocytes depending on the R709C NM2c isoform divide normally. This led Ma et al. (Ma et al. 2012) to conclude that "R709C NM2b constricts the contractile ring by exerting tension during cytokinesis. These results support the idea that it is the structural (crosslinking actin-filaments) rather than the motor (translocating actin-filaments) properties of NM2 that are important for cytokinesis." Crosslinking by myosin-II filaments may contribute, but Osorio et al. find that the motor activity of myosin-II is essential to constrict the cleavage furrow of *C. elegans* embryos (Osorio et al. 2019).

A third type of question is whether forces other than contraction by actin and myosin filaments produce forces for cytokinesis. The answer is definitely "yes" in both budding yeast and fission yeast. Budding yeast form a furrow without the motor activity of myosin-II (Lord et al. 2005), although the tail of myosin-II is required in some way. Whether other myosins

contribute has not been investigated. Fission yeast requires a contractile ring of actin filaments and myosin to initiate but not to complete cytokinesis (Proctor et al. 2012). Instead, biosynthesis of the extracellular septum provides a major fraction of the force to overcome the turgor pressure. Tension in the contractile ring provides a feedback mechanism to the synthetic enzymes embedded in the plasma membrane that maintains the circular profile of the furrow (Thiyagarajan et al. 2015).

11.8 Contractile Ring Disassembly During Cleavage

Schroeder (Schroeder 1972) discovered that contractile rings of echinoderm eggs initially contract with constant volume (assessed by the area occupied by thin filaments in electron micrographs of thin sections) but subsequently lose volume in proportion to the declining circumference. Quantitative measurements with mEGFP-LifeAct showed that actin filaments in contractile rings of fission yeast also decline in proportion to their circumference (Courtemanche et al. 2016). The ratio of mEGFP-LifeAct to formins declines as contractile rings constrict in fission yeast cells, evidence that the filaments shorten progressively from about 1.5 μm to less than 0.4 μm (Courtemanche et al. 2016). On the other hand, both fission yeast (Wu and Pollard 2005) and *C. elegans* embryos (Khaliullin et al. 2018) concentrate myosin-II in their cleavage furrows as they constrict, which explains how rings produce more tension as constriction progresses (Wang et al. 2018). Nothing is known about the mechanisms maintaining the numbers of myosin-II in constricting rings.

11.9 Unanswered Questions

Although much progress has been made on understanding cytokinesis including the role of myosin-II and other myosins, many fundamental questions remain (Pollard 2017). In addition to the questions posed here, more work is needed on the mechanisms concentrating regulatory proteins such as RhoA at the cleavage site, anchoring contractile ring proteins to the plasma membrane, turning over contractile ring components and disassembling the contractile ring as it constricts. Clearly, much of fundamental interest is yet to be discovered.

Acknowledgements Research from the author's laboratory reported in this publication was supported by National Institute of General Medical Sciences of the National Institutes of Health under award number R01GM026132. The content is solely the responsibility of the authors and does not necessarily represent the official views of the National Institutes of Health.

References

Akamatsu MS, Berro J, Pu K-M, Tebbs IR, Pollard TD (2014) Cytokinetic nodes in fission yeast arise from two distinct types of nodes that merge during interphase. J Cell Biol 204:977–988

Andrianantoandro E, Pollard TD (2006) Mechanism of actin filament turnover by severing and nucleation at different concentrations of ADF/cofilin. Mol Cell 24(1):13–23

Balasubramanian MK, McCollum D, Chang L, Wong KC, Naqvi NI, He X, Sazer S, Gould KL (1998) Isolation and characterization of new fission yeast cytokinesis mutants. Genetics 149(3):1265–1275

Basant A, Glotzer M (2018) Spatiotemporal regulation of RhoA during cytokinesis. Curr Biol 28:R570–R580

Beach JR, Shao L, Remmert K, Li D, Betzig E, Hammer JA r (2014) Nonmuscle myosin II isoforms coassemble in living cells. Curr Biol 24:1160–1166

Bezanilla M, Pollard TD (2000) Myosin-II tails confer unique functions in *Schizosaccharomyces pombe*: characterization of a novel myosin-II tail. Mol Biol Cell 11(1):79–91

Bezanilla M, Forsburg SL, Pollard TD (1997) Identification of a second myosin-II in *Schizosaccharomyces pombe*: Myp2p is conditionally required for cytokinesis. Mol Biol Cell 8(12):2693–2705

Carter SB (1967) Effects of cytochalasins on mammalian cells. Nature 213:261–265

Chatterjee M, Pollard TD (2019) The functionally important N-terminal half of fission yeast Mid1p anillin is intrinsically disordered and undergoes phase separation. Biochemistry 58:3031–3041

Chen Q, Pollard TD (2011) Actin filament severing by cofilin is more important for assembly than constriction of the cytokinetic contractile ring. J Cell Biol 195:485–498

Cooper JA (1987) Effects of cytochalasin and phalloidin on actin. J Cell Biol 105:1473–1478

Courtemanche N, Pollard TD, Chen Q (2016) Avoiding artefacts when counting polymerized actin in live cells with Life Act fused to fluorescent proteins. Nat Cell Biol 18:676–683

Davies T, Jordan SN, Chand V, Sees JA, Laband K, Carvalho AX, Shirasu-Hiza M, Kovar DR, Dumont J, Canman JC (2014) High-resolution temporal analysis reveals a functional timeline for the molecular regulation of cytokinesis. Dev Cell 30:209–223

DeLozanne A, Spudich JA (1987) Disruption of the *Dictyostelium* myosin heavy chain gene by homologous recombination. Science 236:1086–1091

Dorn JF, Zhang L, Phi TT, Lacroix B, Maddox PS, Liu J, Maddox AS (2016) A theoretical model of cytokinesis implicates feedback between membrane curvature and cytoskeletal organization in asymmetric cytokinetic furrowing. Mol Biol Cell 27:1286–1299

Fenix A, Taneja N, Buttler CA, Lewis J, Van Engelenburg SB, Ohi R, Burnette DT (2016) Expansion and concatenation of nonmuscle myosin IIA filaments drive cellular contractile system formation during interphase and mitosis. Mol Biol Cell 27:1465–1478

Friend JE, Sayyad WA, Arasada R, McCormick CD, Heuser JE, Pollard TD (2018) Fission yeast Myo2: molecular organization and diffusion in the cytoplasm. Cytoskeleton 75:164–173

Fujiwara K, Pollard TD (1976) Fluorescent antibody localization of myosin in the cytoplasm, cleavage furrow, and mitotic spindle of human cells. J Cell Biol 71(3):848–875

Fujiwara I, Zweifel ME, Courtemanche N, Pollard TD (2018) Latrunculin A accelerates actin filament depolymerization in addition to sequestering actin monomers. Curr Biol 28:3183–3192

Geeves MA, Holmes KC (1999) Structural mechanism of muscle contraction. Annu Rev Biochem 68:687–728

Green RA, Paluch E, Oegema K (2012) Cytokinesis in animal cells. Annu Rev Cell Dev Biol 28:29–58

Henson JH, Ditzler CE, Germain A, Irwin PM, Vogt ET, Yang S, Wu X, Shuster CB (2017) The ultrastructural organization of actin and myosin II filaments in the contractile ring: new support for an old model of cytokinesis. Mol Biol Cell 28:613–623

Hiramoto Y (1975) Force exerted by the cleavage furrow of sea urchin eggs. Dev Growth Differ 17:27–38

Joanny JF, Kruse K, Ramaswamy S (2013) The actin cortex as an active wetting layer. Eur Phys J E Soft Matter 36:52–58

Khaliullin RN, Green RA, Shi LZ, Gomez-Cavazos JS, Berns MW, Desai A, Oegema K (2018) A positive-feedback-based mechanism for constriction rate acceleration during cytokinesis in Caenorhabditis elegans. elife 7:e36073

Kitayama C, Sugimoto A, Yamamoto M (1997) Type II myosin heavy chain encoded by the myo2 gene composes the contractile ring during cytokinesis in Schizosaccharomyces pombe. J Cell Biol 137(6):1309–1319

Kovacs M, Toth J, Hetenyi C, Malnasi-Csizmadia A, Sellers JR (2004) Mechanism of blebbistatin inhibition of myosin II. J Biol Chem 279:35557–35563

Kovar DR, Kuhn JR, Tichy AL, Pollard TD (2003) The fission yeast cytokinesis formin Cdc12p is a barbed end actin filament capping protein gated by profilin. J Cell Biol 161(5):875–887

Kovar DR, Harris ES, Mahaffy R, Higgs HN, Pollard TD (2006) Control of the assembly of ATP- and ADP-actin by formins and profilin. Cell 124(2):423–435

Laplante C, Pollard TD (2017) Response to Zambon et al. Curr Biol 27:R101–R102

Laplante C, Berro J, Karatekin E, Lee R, Hernandez-Leyva A, Pollard TD (2015a) Three myosins contribute uniquely to the assembly and constriction of the cytokinetic contractile ring in fission yeast. Curr Biol 25:1955–1965

Laplante C, Huang F, Bewersdorf J, Pollard TD (2015b) High-speed super-resolution imaging of live fission yeast cells. Methods Mol Biol 1369:45–57

Laplante C, Huang F, Tebbs IR, Bewersdorf J, Pollard TD (2016) Molecular organization of cytokinesis nodes and contractile rings by super-resolution fluorescence microscopy of live fission yeast. Proc Natl Acad Sci U S A 113:E5876–E5885

Lewellyn L, Carvalho A, Desai A, Maddox AS, Oegema K (2011) The chromosomal passenger complex and centralspindlin independently contribute to contractile ring assembly. J Cell Biol 193:155–169

Limouze J, Straight AF, Mitchison T, Sellers JR (2004) Specificity of blebbistatin, an inhibitor of myosin II. J Muscle Res Cell Motil 25:337–341

Lord M, Pollard TD (2004) UCS protein Rng3p activates actin filament gliding by fission yeast myosin-II. J Cell Biol 167(2):315–325

Lord M, Laves E, Pollard TD (2005) Cytokinesis depends on the motor domains of myosin-II in fission yeast but not in budding yeast. Mol Biol Cell 16(11):5346–5355

Ma X, Adelstein RS (2014) The role of vertebrate nonmuscle Myosin II in development and human disease. BioArchitecture 4:88–102

Ma X, Kovacs M, Conti MA, Wang A, Zhang Y, Sellers JR, Adelstein RS (2012) Nonmuscle myosin II exerts tension but does not translocate actin in vertebrate cytokinesis. Proc Natl Acad Sci U S A 109:4509–4514

Mabuchi I, Okuno M (1977) The effect of myosin antibody on the division of starfish blastomeres. J Cell Biol 74(1):251–263

Martin SG, Berthelot-Grosjean M (2009) Polar gradients of the DYRK-family kinase Pom1 couple cell length with the cell cycle. Nature 459:852–856

Maupin P, Pollard TD (1983) Improved preservation and staining of HeLa cell actin filaments, clathrin coated membranes and other cytoplasmic structures by tannic acid-glutaraldehyde-saponin fixation. J Cell Biol 96:51–62

Maupin P, Pollard TD (1986) Arrangement of actin filaments and myosin–like filaments in the contractile ring and of actin–like filaments in the mitotic spindle

of dividing HeLa cells. J Ultrastruct Mol Struct Res 94:92–103
Maupin P, Phillips CL, Adelstein RS, Pollard TD (1994) Differential localization of myosin-II isozymes in human cultured cells and blood cells. J Cell Sci 107:3077–3090
McDonald NA, Lind AL, Smith SE, Li R, Gould KL (2017) Nanoscale architecture of the Schizosaccharomyces pombe contractile ring. elife 6:e28865
Mendes Pinto I, Rubinstein B, Kucharavy A, Unruh JR, Li R (2012) Actin depolymerization drives actomyosin ring contraction during budding yeast cytokinesis. Dev Cell 22:1247–1260
Mendes Pinto I, Rubinstein B, Li R (2013) Force to divide: structural and mechanical requirements for actomyosin ring contraction. Biophys J 105:547–554
Moseley JB, Mayeux A, Paoletti A, Nurse P (2009) A spatial gradient coordinates cell size and mitotic entry in fission yeast. Nature 459:857–860
Motegi F, Mishra M, Balasubramanian MK, Mabuchi I (2004) Myosin-II reorganization during mitosis is controlled temporally by its dephosphorylation and spatially by Mid1 in fission yeast. J Cell Biol 165(5):685–695
Munro E, Jeremy Nance J, Priess JR (2004) Cortical flows powered by asymmetrical contraction transport PAR proteins to establish and maintain anterior-posterior polarity in the early *C. elegans* embryo. Dev Cell 7:413–424
Niederman R, Pollard TD (1975) Human platelet myosin. II. In vitro assembly and structure of myosin filaments. J Cell Biol 67:72–92
Odronitz F, Kollmar M (2007) Drawing the tree of eukaryotic life based on the analysis of 2,269 manually annotated myosins from 328 species. Genome Biol 8:R196
Ong K, Wloka C, Okada S, Svitkina T, Bi E (2014) Architecture and dynamic remodelling of the septin cytoskeleton during the cell cycle. Nat Commun 5:5698
Osorio DS, Chan FY, Saramago J, Leite J, Silva AM, Sobral AF, Gassmann R, Carvalho AX (2019) Crosslinking activity of n on-muscle myosin II is not sufficient for embryonic cytokinesis in C. elegans. Development 146(21):dev179150
Otto JJ, Schroeder TE (1990) Association of actin and myosin in the contractile ring. Ann N Y Acad Sci 582:179–184
Paoletti A, Chang F (2000) Analysis of mid1p, a protein required for placement of the cell division site, reveals a link between the nucleus and the cell surface in fission yeast. Mol Biol Cell 11(8):2757–2773
Pelham RJ, Chang F (2002) Actin dynamics in the contractile ring during cytokinesis in fission yeast. Nature 419:82–86
Peterson JR, Mitchison TJ (2002) Small molecules, big impact: a history of chemical inhibitors and the cytoskeleton. Chem Biol 9:1275–1285
Pollard TD (2017) Nine unanswered questions about cytokinesis. J Cell Biol 216:3007–3016
Pollard TD, O'Shaughnessy B (2019) Molecular mechanism of cytokinesis. Annu Rev Biochem 88:661–689
Pollard LW, Bookwalter CS, Tang Q, Krementsova EB, Trybus KM, Lowey S (2017a) Fission yeast myosin Myo2 is down-regulated in actin affinity by light chain phosphorylation. Proc Natl Acad Sci U S A 114:E7236–E7244
Pollard TD, Earnshaw WC, Lippincott-Schwartz J, Johnson G (2017b) Cell biology, 3rd edn. Elsevier, Philadelphia, p 882
Proctor SA, Minc N, Boudaoud A, Chang F (2012) Contributions of turgor pressure, the contractile ring, and septum assembly to forces in cytokinesis in fission yeast. Curr Biol 22:1601–1608
Rappaport R (1967) Cell division: direct measurement of maximum tension exerted by furrow of echinoderm eggs. Science 156(779):1241–1243
Reymann AC, Staniscia F, Erzberger A, Salbreux G, Grill SW (2016) Cortical flow aligns actin filaments to form a furrow. elife 5:e17807
Saha S, Pollard TD (2012) Characterization of structural and functional domains of anillin-related protein Mid1p that contribute to cytokinesis in fission yeast. Mol Biol Cell 23:3993–4007
Sakamoto T, Limouze J, Combs CA, Straight AF, Sellers JR (2005) Blebbistatin, a myosin II inhibitor, is photoinactivated by blue light. Biochemistry 44:584–588
Sanger JM, Sanger JW (1980) Banding and polarity of actin filaments in interphase and cleaving cells. J Cell Biol 86(2):568–575
Schroeder TE (1970) The contractile ring. I. Fine structure of dividing mammalian (HeLa) cells and the effects of cytochalasin B. Z Zellforsch Mikrosk Anat 109:431–449
Schroeder TE (1972) The contractile ring. II. Determining its brief existence, volumetric changes, and vital role in cleaving Arbacia eggs. J Cell Biol 53:419–434
Schroeder TE (1973) Actin in dividing cells: contractile ring filaments bind heavy meromyosin. Proc Natl Acad Sci U S A 70(6):1688–1692
Schroeder TE (1975) Dynamics of the contractile ring. Soc Gen Physiol Ser 30:305–334
Shelton CA, Carter JC, Ellis GC, Bowerman B (1999) The nonmuscle myosin regulatory light chain gene mlc-4 is required for cytokinesis, anterior-posterior polarity, and body morphology during Caenorhabditis elegans embryogenesis. J Cell Biol 146:439–451
Spector I, Shochet NR, Kashman Y, Groweiss A (1983) Latrunculins: novel marine toxins that disrupt microfilament organization in cultured cells. Science 219:493–495
Stachowiak MR, Laplante C, Chin HF, Guirao B, Karatekin E, Pollard TD, O'Shaughnessy B (2014) Mechanism of cytokinetic contractile ring constriction in fission yeast. Dev Cell 29:547–561
Straight AF, Cheung A, Limouze J, Chen I, Westwood NJ, Sellers JR, Mitchison TJ (2003) Dissecting temporal

and spatial control of cytokinesis with a myosin II inhibitor. Science 299:1743–1747

Sun L, Guan R, Lee IJ, Liu Y, Chen M, Wang J, Wu J-Q, Chen Z (2015) Mechanistic insights into the anchorage of the contractile ring by anillin and Mid1. Dev Cell 33:413–426

Tebbs IR, Pollard TD (2013) Separate roles of IQGAP Rng2p in forming and constricting the S. pombe cytokinetic contractile ring. Mol Biol Cell 24:1904–1917

Thiyagarajan S, Munteanu EL, Arasada R, Pollard TD, O'Shaughnessy B (2015) The fission yeast cytokinetic contractile ring regulates septum shape and closure. J Cell Sci 28:3672–3681

Turlier H, Audoly B, Prost J, Joanny JF (2014) Furrow constriction in animal cell cytokinesis. Biophys J 106:114–123

Vavylonis D, Wu J-Q, Hao S, O'Shaughnessy B, Pollard TD (2008) Assembly mechanism of the contractile ring for cytokinesis by fission yeast. Science 319:97–100

Wagner E, Glotzer M (2016) Local RhoA activation induces cytokinetic furrows independent of spindle position and cell cycle stage. J Cell Biol 213:641–649

Wang N, Lo Presti L, Zhu YH, Kang M, Wu Z, Martin SG, Wu JQ (2014) The novel proteins Rng8 and Rng9 regulate the myosin-V Myo51 during fission yeast cytokinesis. J Cell Biol 205:357–375

Wang S, Chin H, Thiyagarajan S, Karatekin E, Pollard TD, O'Shaughnessy B (2018) Two isoforms of myosin-II cooperate to organize the fission yeast cytokinetic ring for maximal tension production. Biophys J 114: 654a

Werner M, Munro E, Glotzer M (2007) Astral signals spatially bias cortical myosin recruitment to break symmetry and promote cytokinesis. Curr Biol 17(15):1286–1297

Wloka C, Vallen EA, Thé L, Fang X, Oh Y, Bi E (2013) Immobile myosin-II plays ascaffolding role during cytokinesis in budding yeast. J Cell Biol 200:271–286

Wu JQ, Pollard TD (2005) Counting cytokinesis proteins globally and locally in fission yeast. Science 310(5746):310–314

Wu JQ, Kuhn JR, Kovar DR, Pollard TD (2003) Spatial and temporal pathway for assembly and constriction of the contractile ring in fission yeast cytokinesis. Dev Cell 5(5):723–734

Zambon P, Palani S, Kamnev A, Balasubramanian MK (2017) Myo2p is the major motor involved in actomyosin ring contraction in fission yeast. Curr Biol 27:R99–R100

Zhang HM, Ji HH, Ni T, Ma RN, Wang A, Li XD (2017) Characterization of blebbistatin inhibition of smooth muscle myosin and nonmuscle myosin-2. Biochemistry 56:4235–4243

Zimmermann D, Homa KE, Hocky GM, Pollard LW, De La Cruz EM, Voth GA, Trybus KM, Kovar DR (2017) Mechanoregulated inhibition of formin facilitates contractile actomyosin ring assembly. Nat Commun 8:703

Myosins and Disease

12

Lynne M. Coluccio

Abstract

Myosins constitute a superfamily of actin-based molecular motor proteins that mediates a variety of cellular activities including muscle contraction, cell migration, intracellular transport, the formation of membrane projections, cell adhesion, and cell signaling. The 12 myosin classes that are expressed in humans share sequence similarities especially in the N-terminal motor domain; however, their enzymatic activities, regulation, ability to dimerize, binding partners, and cellular functions differ. It is becoming increasingly apparent that defects in myosins are associated with diseases including cardiomyopathies, colitis, glomerulosclerosis, neurological defects, cancer, blindness, and deafness. Here, we review the current state of knowledge regarding myosins and disease.

Keywords

Myosins · Disease · Cardiopmyopathy · Colitis · Glomerulosclerosis · Neurological defects · Cancer · Blindness · Deafness · Microvillous inclusion disease · Infectious disease

12.1 Myosin Superfamily

Myosins are actin-based motor molecules that use the energy from ATP hydrolysis to translocate actin filaments and to produce force. The human genome contains about 40 different myosin genes grouped into 12 subfamilies including myosins I, II, III, V, VI, VII, IX, X, XV, XVI, XVIII, and XIX (Foth et al. 2006). Although still a work in progress particularly for the myosin isoforms that were discovered more recently, there is abundant evidence that myosin malfunction results in human disease. Here, an overview of the myosins expressed in humans with respect to disease is presented. Note that the chapters in this volume pertaining to individual myosins address the role of that myosin in disease, e.g., the role of several myosins specifically in hearing is discussed in more detail in Chap. 13 (Friedman et al. 2020). Moreover, highly specific myosin inhibitors leading to the development of pharmacological agents to treat human diseases involving myosins are discussed in Chap. 5 (Manstein and Preller 2020). Other recent review articles that address myosins and disease include (Courson and Cheney 2015; Li and Yang 2016; Peckham 2016; Masters et al. 2017).

L. M. Coluccio (✉)
Department of Physiology & Biophysics, Boston University School of Medicine, Boston, MA, USA
e-mail: coluccio@bu.edu

L. M. Coluccio (ed.), *Myosins*, Advances in Experimental Medicine and Biology 1239,
https://doi.org/10.1007/978-3-030-38062-5_12

12.2 Myosins I

Class I myosins, which constitute a large and the most diverse class in the myosin superfamily, are monomeric membrane-associated motor proteins that interact with actin filaments to produce movement and force (Coluccio 2018). Eight myosin I isoforms divided into 4 subclasses are expressed in humans (subclass 1, MYO1E and MYO1F; subclass 2, MYO1A and MYO1B; subclass 3, MYO1C and MYO1H; and subclass 4, MYO1D and MYO1G) (Bähler et al. 1994; Morgan et al. 1994; Mooseker and Cheney 1995; Berg et al. 2001). Myosins I are ~110–140 kDa in size and have a motor domain of ~80 kDa with an ATP-binding site and an actin-binding site, a light chain-binding domain (LCBD) with 1–6 calmodulin-binding (IQ) sites, and a C-terminal tail (Coluccio 2018). There are both short-tailed (MYO1A, B, C, D, G, and H) and long-tailed (MYO1E and F) isoforms. All myosins I have a tail-homology 1 (TH1) domain containing a PH domain involved in membrane binding (Hokanson et al. 2006), whereas long-tailed myosins I contain a proline-rich TH2 domain, which might contain an ATP-insensitive actin-binding site, and a TH3 domain which is a src-homology domain.

Evidence from structural, kinetic, and single-molecule mechanical studies indicate that some class I myosins are strain sensors, i.e., their activity is regulated by load (for a review, see (Bloemink and Geeves 2011)). (i) Cryo-electron microscopy of MYO1A and MYO1C bound to F-actin shows that although the motor domain does not change its orientation relative to F-actin ± ADP, in ADP the LCBD swings through ~33° resulting in a ~50 Å movement (Jontes et al. 1995; Jontes and Milligan 1997; Batters et al. 2004). (ii) Optical trapping studies show that the mechanical interaction of single molecules of MYO1A, MYO1B, and MYO1C with F-actin occurs in two substeps, a first displacement associated with Pi release occurring within a millisecond after myosin I binding to F-actin followed by a second displacement associated with ADP release after a variable time delay with the amplitude of the second step corresponding to the movement of the LCBD observed in ADP by electron microscopy (Veigel et al. 1999; Batters et al. 2004). (iii) In transient kinetic studies the ATP-induced dissociation of MYO1B-actin, MYO1C-actin, and probably MYO1A is biphasic suggesting that myosin I exists in two forms, one competent to dissociate from actin and the other which must first isomerize before ATP binding (Jontes et al. 1997; Coluccio and Geeves 1999; Geeves et al. 2000; Batters et al. 2004). Isomerization of the nucleotide pocket is required both to bind ATP and to release ADP. (iv) The equilibrium constant for isomerization of the nucleotide pocket is small suggesting that there is a small free energy change. This is not compatible with a step linked to force generation. (v) The affinity of ADP for actin-myosin I is tight, and there is weak coupling between ADP and actin binding such that ADP remains tightly bound to myosin I in the presence of actin (Coluccio and Geeves 1999; Geeves et al. 2000). Together, the data suggest that like smooth muscle myosin, which is designed to bear tension (Cremo and Geeves 1998), some myosins I exhibit a strain-sensing ADP-release mechanism, which allows them to adapt to mechanical load (Coluccio and Geeves 1999; Geeves et al. 2000). Indeed, in single-molecule mechanical studies the rate of detachment of MYO1B from actin decreases 75-fold under tension of 2 pN or less, additional evidence that MYO1B is a low duty ratio motors, i.e., it spends most of their kinetic cycle unattached to actin but is converted to a high duty ratio motors under strain (Laakso et al. 2008). In the case of MYO1C, the force-sensitive transition in the ATPase cycle was found to be the isomerization that follows ATP binding rather than ADP release (Greenberg et al. 2012) suggesting that MYO1C may act as a tension sensor or slow transporter (Batters et al. 2004; Bloemink and Geeves 2011; Greenberg et al. 2012).

Class I myosins are implicated in multiple cellular functions including control of plasma membrane tension, tethering of membrane proteins, endocytosis, exocytosis, and cell-cell contact (McIntosh and Ostap 2016; Coluccio 2018). Recent studies implicate myosins in a variety of diseases including kidney disease and intestinal,

gastric, and prostate tumors (Mele et al. 2011; Mazzolini et al. 2012, 2013; Maly et al. 2017).

12.2.1 Myosin IA

The first myosin I to be discovered in higher organisms was MYO1A (previously the 110 K-calmodulin complex or brush border myosin I, BBMI). MYO1A is expressed predominantly in intestine (Hoshimaru and Nakanishi 1987) where it constitutes the lateral links that are seen between the core bundle of actin filaments and the microvillar membrane in electron micrographs of microvilli (Mukherjee and Staehelin 1971; Mooseker and Tilney 1975; Matsudaira and Burgess 1982). Reconstitution experiments using purified proteins showed that MYO1A binds in a helical fashion around the outside of actin filaments bundled by the two microvillar proteins villin and fimbrin (Coluccio and Bretscher 1989).

Early evidence of MYO1A's involvement in intracellular trafficking was gleaned from studies in cultured cells expressing truncated fragments of MYO1A. Expression in Caco-2 cells of a nonfunctional truncated MYO1A mutant was shown to affect the rate of transferrin recycling and the rate of transepithelial transport of dipeptidylpeptidase IV from the basolateral to the apical membrane (Durrbach et al. 2000).

Myo1a-null mice have shed light on the role of this myosin I in intestine. There are large extrusions of membranes at the tips of intestinal microvilli in *Myo1a*-knockout mice (Tyska et al. 2005). Less sucrose isomaltase is associated with the brush border membrane, and it is mistargeted to the basolateral membrane (Tyska et al. 2005). Moreover, cystic fibrosis transmembrane conductance regulator (CFTR) accumulates in subapical endosomes, redistributes to the basolateral domain, and is absent from the brush border membrane in *Myo1a*-null mice (Kravtsov et al. 2012). These data indicate that MYO1A mediates the association of some proteins with the apical membrane. Although the mice show no overt phenotype at the whole animal level (Tyska et al. 2005), they exhibit an increased sensitivity to dextran sulfate sodium-induced colitis (Hegan et al. 2015a).

Intestinal and Gastric Tumors *In vitro* studies indicate that MYO1A regulates the polarization and differentiation of colon cancer cells; moreover, the progression of tumors initiated by either genetic mutation or a pharmacological approach in *Myo1a*-null mice is accelerated, evidence that MYO1A inactivation mediates intestinal tumor progression (Mazzolini et al. 2012). Importantly, analysis of MYO1A protein in 155 colorectal patients showed that patients with low MYO1A tumor protein levels had shorter survival rates than patients with tumors having high levels of MYO1A, evidence that MYO1A is a tumor suppressor in human intestine (Mazzolini et al. 2012). MYO1A is also expressed at high levels in normal gastric mucosa and is frequently mutated in gastric tumors (Mazzolini et al. 2013).

Other Recently, four novel heterozygous sequence variants were identified by exome sequencing in different genes on chromosome 12, including *MYO1A*, that are shared among members of a Norwegian family with intermediate Charcot-Marie-Tooth disease (CMT), a common inherited neuropathy (Braathen et al. 2016). A clear link between MYO1A and CMT remains to be determined.

12.2.2 Myosin 1B

MYO1B, which is alternatively spliced to form three isoforms, is widely expressed (Ruppert et al. 1993). Splicing occurs within the IQ motifs in the neck domain leading to a deletion from MYO1B^{a} of 29-amino acids for MYO1B^{b} and twice the number of amino acids for MYO1B^{c} (Ruppert et al. 1993). As a result, MYO1B^{a} has 6 IQ domains, MYO1B^{b} has 5 IQ domains, and MYO1B^{c} has 4 IQ domains.

MYO1B associates with membrane and binds phosphatidylinositol 4,5-biphosphate (PIP_2) and phosphatidyl 3,4,5-triphosphate (PIP_3) specifically and with high affinity (Komaba and Coluccio 2010), and cells expressing exogenous

MYO1B exhibit increased cortical tension (Nambiar et al. 2009). MYO1B is associated with membranous subcellular compartments in many different cell types where it is implicated in intracellular trafficking (Raposo et al. 1999; Cordonnier et al. 2001; Salas-Cortes et al. 2005). In particular, by mediating the association of actin filaments with the *trans*-Golgi network, MYO1B may contribute to the formation of dynamic tubular membrane structures that form post-Golgi carriers (Almeida et al. 2011). Evidently, it also controls the formation of secretory granule biogenesis in neuroendocrine cells and in a model system of chromogranin A-expressing COS7 cells (Delestre-Delacour et al. 2017).

MYO1B interacts either directly or indirectly with the transmembrane tyrosine kinase receptors EPHB2, which bind ephrins to regulate processes such as cell repulsion, migration, proliferation, and cell-cell adhesion during embryogenesis (Prosperi et al. 2015; Kania and Klein 2016). It also mediates the interaction of amino acid transporters with the renal brush border membrane (Komaba and Coluccio 2015).

Cancer MYO1B is implicated in metastasis as its expression is increased in head and neck squamous cell carcinomas (HNSCC) (Ohmura et al. 2015), prostate cancer (Makowska et al. 2015), and melanoma (Singh et al. 2014). MYO1B depletion in human HNSCC cells inhibits protrusion formation and migration, and *MYO1B*-depleted human HNSCC cells metastasize to cervical lymph nodes less than control cells when implanted into nude mice, evidence that MYO1B mediates metastasis by enhancing cell migration (Ohmura et al. 2015).

MiRNA-363, which is upregulated in human papilloma virus-positive HNSCCs, targets the 3'UTR of *MYO1B* and downregulates *MYO1B* mRNA and MYO1B protein expression in HNSCC cells resulting in reduced motility (Chapman et al. 2015). Additionally, the passenger strand miRNA-145-3p targets MYO1B in HNSCC cells reducing *MYO1B* mRNA and protein levels and suppressing cancer cell proliferation (Yamada et al. 2017). Genome-wide gene expression analyses in HNSCC MYO1B-knockdown cells suggests that 54 genes are mediated by MYO1B (Yamada et al. 2017). Further analysis of these proteins might help to reveal the signaling pathways that involve MYO1B.

MYO1B is also highly expressed in metastatic prostate cancer cell lines (Makowska et al. 2015). Myo1b depletion in the prostate cancer cell line PC-3 significantly increases cell-spread area and reduces migration in a circular invasion assay that mimics 3D invasion suggesting that MYO1B supports metastasis of prostate cancer cells (Makowska et al. 2015). Together, the studies suggest that drugs targeting Myo1b may be effective against certain cancers.

A new report indicates that splicing of MYO1B is involved in gliomagenesis. Apparently, serine/arginine splicing factor 1 (SRSF1) is increased in glioma tissues and cells, and it promotes proliferation, survival, and invasion by specifically switching the alternate splicing of the *MYO1B* gene to the longest isoform, which is membrane-localized and has oncogenic properties (Zhou et al. 2019). The studies suggest that *MYO1B* splicing can serve as a prognosis factor for glioma.

12.2.3 Myosin 1C

MYO1C, whose motor domain is ~50% identical and ~72% similar to that of both MYO1A and MYO1B, was originally cloned from bovine adrenal gland (Zhu and Ikebe 1994). MYO1C exists as three isoforms: (i) MYO1C^{C}, or classical/cytoplasmic MYO1C, (ii) MYO1C^{B}, or nuclear myosin I, which has a 16-amino acid N-terminal region (NTR), and (iii) MYO1C^{A}, which has a 36-amino acid NTR (Ihnatovych et al. 2012). The NTRs affect the nucleotide-binding properties of MYO1C by affecting isomerization of the nucleotide pocket (Zattelman et al. 2017). Although MYO1C^{B} was the first myosin to be identified in the nucleus (Nowak et al. 1997; Pestic-Dragovich et al. 2000), and MYO1C^{C} localizes predominantly at the cell periphery and in punctae throughout the cyto-

plasm (Wagner et al. 1992; Ruppert et al. 1995), both MYO1C isoforms B and C locate in the cytoplasm *and* nuclei (Venit et al. 2013). The most recently discovered MYO1C^{A} also localizes to the nucleus (Ihnatovych et al. 2012). In fact, a nuclear localization-like sequence consisting of six positively-charged amino acid residues within the second IQ motif that directs the myosins to the nucleus via the importin-β import pathway is common to all three isoforms (Dzijak et al. 2012; Maly and Hofmann 2016). In addition, two nucleolar localization sequences, one in the motor domain common to the three MYO1C isoforms and one in the extended N-terminus of MYO1C^{B}, are both required for targeting of Myo1c^{B} to nucleoli (Schwab et al. 2013).

In reviewing the literature, it is not always clear which MYO1C isoform is being studied given that (i) the existence of three MYO1C isoforms was not known until recently, (ii) most available Myo1c antibodies recognize all three isoforms, (iii) the isoforms have overlapping localization patterns if not function, and (iv) the N-terminal sequence that distinguishes MYO1C^{B} from other MYO1C isoforms is too short to be targeted so siRNAs directed against MYO1C^{B} also affect the other isoforms (Maly et al. 2017). This is particularly true for the studies of MYO1C in the cytoplasm. As a result, the studies described under the MYO1C^{C} heading below may also be relevant to MYO1C^{B} or MYO1C^{A}. Thus, we use the designation MYO1C.

12.2.3.1 Myosin 1C^{C}

MYO1C localizes predominantly at the cell periphery and in punctae throughout the cytoplasm (Wagner et al. 1992; Ruppert et al. 1995), but it is also found in the nucleus (Venit et al. 2013). MYO1C is implicated in a variety of cellular processes including delivery of proteins to the cell surface, cell-cell contact, and cell migration. MYO1C mediates insulin-stimulated glucose uptake in adipocytes by promoting fusion of GLUT4-containing vesicles with the plasma membrane presumably by facilitating localized membrane remodeling (Bose et al. 2004). MYO1C also modulates insulin-stimulated glucose uptake in skeletal muscle cells (Toyoda et al. 2011) where it mediates tethering and efficient delivery of GLUT4 to the cell surface (Boguslavsky et al. 2012). In the kidney, MYO1C localizes at the podocyte membrane with Neph1, and MYO1C depletion or expression of MYO1C mutants leads to lower transepithelial resistance and increased permeability to bovine serum albumin, evidence that MYO1C is important to podocyte function (Arif et al. 2011).

Several reports indicate that MYO1C participates in cell migration, e. g., overexpression of MYO1C in 3 T3-L1 adipocytes results in extensive membrane ruffling (Bose et al. 2004). Moreover, MYO1C binds actin monomers *in vitro*, and overexpression of MYO1C tail or MYO1C depletion inhibits the accumulation of G-actin at the leading edge of migrating endothelial cells (Fan et al. 2012), evidence that MYO1C binds and transports G-actin to the leading edge where it assembles to promote cell migration. In lamellipodia and membrane ruffles of migrating N1 cells, MYO1C colocalizes with SH2-containing inositol phosphatase 2 (SHIP2), and MYO1C knockdown disrupts SHIP2 localization and reduces both PI(4,5)P2 staining and cell migration (Edimo et al. 2016). In endothelial cells, MYO1C colocalizes at the plasma membrane with the tyrosine kinase vascular endothelial growth factor receptor-2 (VEGFR2), which regulates angiogenic signal transduction, and is required for its delivery to the cell surface in response to VEGF (Tiwari et al. 2013). MYO1C depletion leads to reduced cell proliferation and migration demonstrating the importance of MYO1C in angiogenic signaling (Tiwari et al. 2013). MYO1C depletion in Crk$^{+/+}$ cells also reduces cell spreading (Oh et al. 2013), evidence of roles for MYO1C in both cell migration and spreading.

In HeLa cells depletion of MYO1C, which localizes with lipid rafts, or expression of a motor-dead MYO1C mutant redistributes lipid raft markers from the plasma membrane to intracellular membranes, evidence that MYO1C mediates cell migration and cell spreading by regulating recycling of lipid rafts (Brandstaetter et al. 2012). MYO1C localizes on membrane tubules emanating from the perinuclear recycling

compartment, and MYO1C depletion reduces the number of tubules, evidence that MYO1C promotes tubule formation (Brandstaetter et al. 2012). Cholesterol trafficking is also disturbed in MYO1C-depleted cells leading to the accumulation of autophagosomes and a deficiency in the ability to clear misfolded proteins from the cell (Brandstaetter et al. 2014).

Cancer The tumor suppressor gene *TP53*, which encodes p53, resides at chromosome 17p13.1 and is mutated in 40% of all tumors (Whibley et al. 2009). p53 inhibits tumor progression by acting on proteins that affect cell cycle arrest, DNA damage and repair, apoptosis, and anti-metastasis and anti-angiogenesis factors (Li and Yang 2016). Another commonly deleted region at 17p13.3, distal to the *TP53* locus, is also associated with tumor suppression (Guan et al. 2003; Konishi et al. 2003; Roncuzzi et al. 2005). Real-time qPCR analysis identified *MYO1C* and *Inpp5k* (inositol polyphosphate-5-phosphatase K) as two candidate tumor suppressor genes in this region. Both MYO1C and Inpp5k mRNA and protein are down regulated in human endometrial cancers (Hedberg Oldfors et al. 2015; Visuttijai et al. 2016). The significance of both proteins in tumorigenesis awaits further investigation.

Diabetes There is some preliminary evidence associating reduced MYO1C expression with the risk of diabetes. In proteomic studies MYO1C protein is reduced ~six-fold in diabetic vs. non-diabetic persons (Fang et al. 2015a). Insulin resistance in adipocytes, a major risk factor for type 2 diabetes, involves phosphorylation of insulin receptor substrate 1 (IRS-1) at serine 307 by tumor necrosis factor-α (TNF-α) acting through the IκB (IKK) complex thereby reducing insulin signaling (DiDonato et al. 1997). The IKK complex consists of the catalytic subunits IKK-α and IKK-β and the regulatory subunit nuclear factor κB essential modulator (NEMO)/IKK-γ (Senegas et al. 2015). MYO1C binds NEMO and is responsible for its targeting to membrane ruffles in response to insulin (Nakamori et al. 2006). Overexpression of dominant-negative MYO1C inhibits phosphorylation of IRS-1 at serine 307, evidence that MYO1C promotes the interaction of IRS-1 with NEMO and contributes to TNF-α-induced insulin resistance (Nakamori et al. 2006).

Other *MYO1C* has been identified as one of the top 30 genes in the NF-κB target gene network relevant to the immunopathogenesis of multiple sclerosis (Satoh 2014). In addition, patients with multiple sclerosis or another autoimmune disease, rheumatoid arthritis, have high levels of a MYO1C fragment in their blood serum vs. undetectable levels in control samples suggesting that MYO1C^{c} might serve as an autoimmune disease marker (Myronovkij et al. 2016). Also, MYO1C may participate in the entry of pathogens. MYO1C colocalizes with lipid raft-rich membrane sites to which *Salmonella* bacteria bind, and reduced expression of MYO1C decreases the number of macropinosomes and inhibits *Salmonella* entry (Brandstaetter et al. 2012). MYO1C has been implicated in adaptation in the inner ear (Holt et al. 2002; Stauffer et al. 2005), and six heterozygous missense mutations in MYO1C were identified in a group of 450 mostly European patients affected by bilateral sensorineural hearing loss (Zadro et al. 2009). Nevertheless, definitive proof that MYO1C mediates adaptation is lacking.

12.2.3.2 Myosin 1c^{B}

MYO1C^{B} is implicated in transcription, chromatin remodeling, and chromosomal movements. It colocalizes with actin and RNA polymerase II in the nucleus and with RNA polymerase I in nucleoli where it is involved in ribosomal RNA gene (rDNA) transcription initiation and regulation (Pestic-Dragovich et al. 2000; Fomproix and Percipalle 2004; Philimonenko et al. 2004; Hofmann et al. 2006b; Ye et al. 2008). Depletion of MYO1C^{B} inhibits polymerase I-mediated transcription in cultured cells and *in vitro* (Philimonenko et al. 2004). MYO1C^{B} interacts with initiation-competent polymerase I

complexes through the basal transcription factor TIF-1A, which must first be phosphorylated by ribosomal S6 kinase (RSK) (Philimonenko et al. 2004). Presumably, by binding actin through the motor domain and DNA through the tail domain, MYO1C^{B} generates the force required during transcription to pull the polymerase along an active gene (de Lanerolle et al. 2005; Hofmann et al. 2006a).

MYO1C^{B} shuttles in and out of the nucleus and the PH domain is critical, although insufficient, for nuclear targeting and import (Nevzorov et al. 2018). Evidently, the nuclear localization sequence (NLS) contributes to phosphoinositide binding (Nevzorov et al. 2018). Although how MYO1C^{B} is transported through the nuclear pore complex and how it is retained in the nucleus are not yet known, MYO1C^{B} might enter the nucleus by interacting with the endoplasmic reticulum, which forms a continuous membrane structure with the nuclear envelope, before diffusing into the nucleus, a mechanism employed by inner nuclear membrane proteins for import into the nucleus (Nevzorov et al. 2018).

Overexpression of a MYO1C^{B} motor domain mutant prevents the repositioning of chromosomes from the nuclear periphery to the interior during interphase (Chuang et al. 2006). The rapid repositioning of chromosomes following serum removal is also inhibited in primary fibroblasts expressing reduced amounts of MYO1C^{B} (Mehta et al. 2010). MYO1C^{B} is a component of the chromatin remodeling complex WICH, which contains Williams Syndrome transcription factor (WSTF) and the ATPase SNF2h as subunits and facilitates the post-initiation phase of polymerase I transcription on chromatin (Percipalle and Farrants 2006; Percipalle et al. 2006). HeLa cells depleted of MYO1C^{B} stalls polymerase I at the gene promoter (Sarshad et al. 2013). Presumably, MYO1C^{B} interacts with SNF2h to stabilize WICH at the gene promoter and to facilitate recruitment of the histone acetyl transferase PCAF, which maintains the levels of histone H3K9 acetylation required to activate transcription in order to allow cell cycle progression in late mitotic and interphase cells (Sarshad et al. 2013). At early G1, glycogen synthase kinase (GSK) 3β phosphorylates MYO1C^{B}, stabilizing MYO1C^{B} from degradation, and facilitating both the association of MYO1C^{B} with the rDNA chromatin and transcription activation at G1 (Sarshad et al. 2014). MYO1C^{B} also reportedly contributes to the maturation of pre-rRNA in nucleoli and accompanies rRNA transcripts to the nuclear pore basket where MYO1C^{B} associates with actin-rich pore-linked filaments to modulate transcript export from the nucleus (Obrdlik et al. 2010). A role for MYO1C^{B} in DNA repair is also possible as depletion of MYO1C^{B} or expression of a MYO1C^{B} motor-dead mutant prevents the relocation of certain gene-rich chromosome territories to newer positions within interphase nuclei during the DNA damage response (Kulashreshtha et al. 2016).

Immuno-depletion of MYO1C^{B} inhibits polymerase II-mediated transcription in HeLa cells and in an *in vitro* transcription system (Pestic-Dragovich et al. 2000; Hofmann et al. 2006b). It was shown to be required for formation of the first phosphodiester bond during transcription initiation (Hofmann et al. 2006b), and it may synergize with polymerase-associated actin to maintain active polymerase II at the promoter (Almuzzaini et al. 2015).

Most surprising, MYO1C^{B}-knockout mice do not show a phenotype related to a role in the nucleus suggesting that either MYO1C^{C} or another myosin I compensates (Venit et al. 2013). In particular, the reduction in polymerase I-mediated transcription that occurs in MYO1C^{B}-depleted U2OS cells is rescued by expression of RNAi-resistant MYO1C^{C}, evidence that MYO1C^{C} can functionally substitute for MYO1C^{B} (Venit et al. 2013). Furthermore, MYO1C^{C} binds polymerase II suggesting that it replaces MYO1C^{B} in polymerase II-mediated transcription (Venit et al. 2013). Conversely, MYO1C^{B} may function in cytoplasmic processes originally thought to be mediated by MYO1C^{C}. MYO1C^{B} localizes predominantly in the cytoplasm of HeLa cells, and MYO1C^{B}-depleted cells exhibit a 50% increase in elasticity of their plasma membrane as measured by atomic force

microscopy suggesting a role for MYO1C^{B} in maintenance of membrane tension (Venit et al. 2016).

Breast Cancer There is recent evidence that MYO1C^{B} plays a role in estrogen-responsive breast cancer. In mammary epithelial cells, which have the estrogen receptors ERα and ERβ, estrogens stimulate cell proliferation by modulating gene transcription (Hilton et al. 2017). Several actin-binding proteins and MYO1C^{B} were identified along with actin in ERα-containing multi-molecular complexes purified from nuclei of estrogen-treated breast cancer cells. The studies suggest that in breast cancer cells MYO1C^{B} plays a role in nuclear ERα actions by mediating assembly and/or stabilization of complexes containing ERα and actin early after activation by its ligand (Ambrosino et al. 2010).

12.2.3.3 Myosin 1c^{A}

MYO1C^{A}, which has a unique 36-amino acid N-terminal extension, localizes to the cytoplasm and to RNA polymerase II in the nucleus but not to nucleoli with polymerase I suggesting that MYO1C^{B} and MYO1C^{A} have distinct functions in the nucleus (Ihnatovych et al. 2012). MYO1C^{A} is unique amongst the isoforms in that it shows a tissue-specific expression pattern with high expression in adrenal gland, kidney, pancreas, and a subset of adipose tissues (Sielski et al. 2014).

Prostate Cancer While MYO1C^{A} is not expressed in normal prostate, recently MYO1C^{A} was shown to be expressed in metastatic prostate cancer cells (Ihnatovych et al. 2012; Saidova et al. 2018) where it associates with metalloprotease-containing exosomes and stimulates their secretion thereby facilitating cancer cell migration and metastasis (Maly et al. 2017). Interestingly, while MYO1C in general was found to contribute to both cell migration and cell invasion, isoform A specifically contributed only to invasion through extracellular matrix and not to migration unimpeded by extracellular matrix (Maly et al. 2017). These data suggest that MYO1C^{A} might be a target for detection or treatment of metastatic prostate cancer.

12.2.4 Myosin 1D

MYO1D is a widely expressed short-tailed class I myosin with two IQ domains that bind calmodulin (Bähler et al. 1994). Whereas the actin-activated ATPase activity of some myosins I increases in the presence of Ca^{2+} (Collins et al. 1990; Perreault-Micale et al. 2000; Lieto-Trivedi and Coluccio 2008), Ca^{2+} binding to the C-terminal Ca^{2+}-binding sites in the calmodulin molecule bound to the first IQ domain of MYO1D inhibits the actin-activated ATPase activity of MYO1D by ~75%, evidence that the regulation of class I myosins varies (Köhler et al. 2005).

MYO1D expression in rat is developmentally regulated with the highest expression in adult brain (Bähler et al. 1994). MYO1D controls left-right asymmetry in flies (Hozumi et al. 2006; Spéder et al. 2006) and zebrafish (Juan et al. 2018; Saydmohammed et al. 2018). *Situs invertus* is not observed in *Myo1d*-null mice, although they exhibit defects in rotational planar cell polarity of the cilia in the trachea, which rather than all bending in one direction, splay out in different directions due to disruption in the alignment of the central pair of microtubules in each cilium (Hegan et al. 2015c). *Myo1d*-null mice also exhibit defects in the positioning of cilia on ependymal epithelial cells of the brain ventricle, which results in clustering of cilia to one side of the cells, evidence that translational planar cell polarity is disrupted (Hegan et al. 2015c).

Myo1d and the Nervous System MYO1D is widely expressed with the highest expression in brain (Bähler et al. 1994), and its upregulation during development along with other major myelin proteins (Yamaguchi et al. 2008) suggests that MYO1D may contribute to nervous system development. Myo1d localizes in cell bodies and along dendrites of Purkinje cells with aspartoacylase, which binds MYO1D *in vitro* (Benesh et al. 2012). Mutations in aspartoacylase lead to

Canavan disease, a neurodegenerative disorder, probably due to defective myelin synthesis (Namboodiri et al. 2006). Reduced levels of NAA are also found in some regions of the brains of children diagnosed with autism spectrum disorder (Friedman et al. 2003; Levitt et al. 2003). Although a link between MYO1D and neurological disorders is possible, no such disorders were found in *Myo1d*-null rats (Hegan et al. 2015c). One possibility is that other class I myosins substitute for the lack of MYO1D.

Colitis Recent evidence from analysis of mice with mutant MYO1D generated by random germline mutagenesis indicates that MYO1D may protect from DSS-induced colitis (McAlpine et al. 2018). Mice with mutant MYO1D lose more weight than control mice, and their colons show histopathological changes following DSS treatment (McAlpine et al. 2018). Unlike MYO1A, which associates with the brush border membrane, MYO1D localizes primarily to the basolateral membrane (McAlpine et al. 2018). One idea, consistent with a role for MYO1D in intracellular trafficking as observed in MDCK cells (Huber et al. 2000), is that MYO1D mediates trafficking of adhesion molecules to the basolateral membrane, where they are necessary for the integrity of adherens and tight junctions, which are disrupted by DSS (McAlpine et al. 2018). Whether mutations in MYO1D in humans lead to susceptibility to colitis is unknown.

Cancer Recent studies have focused on whether MYO1D expression is modulated in prostate cancer. Epigenetic marks modify histones to silence or activate gene expression and can contribute to malignant transformation (Atlasi and Stunnenberg 2017). The trimethylated histone H3 at lysine 27 (H3K27me3) inactivates gene expression, and there are more H3K27me3-enriched genes in tumoral vs. normal prostatic tissues (Ngollo et al. 2017). One of the H3K27me3-enriched genes is *MYO1D* (Ngollo et al. 2017), although whether modification of MYO1D expression contributes to transformation awaits further investigation.

12.2.5 Myosin 1E

MYO1E, the first of the vertebrate long-tailed myosins I to be identified, was cloned from human liver and placenta cDNA libraries where it was called human myosin-IC (Bement et al. 1994b) and rat brain where it was called myr3 (Stöffler et al. 1995). The MYO1E tail domain contains a src-homology-3 (SH3) domain similar to that found in long-tailed myosins I from amoeboid cells. The tail domain likely regulates motor domain activity as antibodies directed against the tail increase the ATPase activity (Stöffler and Bähler 1998). In contrast, the actin-activated ATPase activity of MYO1E is inhibited 2-3-fold by micromolar amounts of Ca^{2+} which does not cause calmodulin dissociation (Stöffler and Bähler 1998).

MYO1E is widely expressed in humans with the highest levels in kidney, prostate, colon, liver, and ovary (Bement et al. 1994b). MYO1E binds synaptojanin-1 and dynamin, two proteins involved in clathrin-mediated endocytosis, through its SH3 domain, and inhibition of MYO1E in cultured fibroblasts leads to defects in endocytosis (Krendel et al. 2007). Myo1e is recruited to clathrin-coated pits in Swiss 3 T3 cells along with proteins that mediate actin assembly including WIP, WIRE and N-WASP, which initiate Arp2/3-mediated actin assembly, suggesting a role for MYO1E in coordinating actin assembly (Cheng et al. 2012). In support of this idea, MYO1E also localizes in fibroblasts to sites of actin assembly in lamellipodia (Gupta et al. 2013). In addition, MYO1E localizes in fibroblasts to actin-rich early adhesions with CARMIL, FHOD1, Arp3 and β3-integrin, and in *Myo1e*-knockdown cells, cell-matrix adhesions fail to mature, evidence of a role in adhesion formation (Gupta et al. 2013). MYO1E may also be critical to the immune response as the ability of macrophages and dendritic cells to stimulate antigen-specific CD4+ T-cell proliferation is impaired in murine MYO1E-deficient cells (Wenzel et al. 2015).

Glomerulosclerosis Mutations in MYO1E are associated with childhood familial focal

segmental glomerulosclerosis (FSCG) (Mele et al. 2011). In mouse kidneys MYO1E is expressed primarily in renal podocytes, which play a critical role in glomerular filtration (Krendel et al. 2009). MYO1E localizes in the foot processes of podocytes with actin and the tight junction protein ZO-1 at cell-cell junctions, or slit diaphragms, and the SH3 domain of MYO1E binds the C-terminus of ZO-1 *in vitro* (Pierchala et al. 2010; Bi et al. 2013), evidence that the actin cytoskeleton cooperates with junctional proteins at cell-cell contacts. The kidneys of podocyte-specific *Myo1e*-null mice show signs of renal injury such as thickened and closed capillary loops that are partially obstructed with extracellular material and defects in glomerular filtration resulting in proteinuria early in development, evidence of MYO1E's involvement in glomerular filtration (Krendel et al. 2009; Chase et al. 2012). Two MYO1E mutations, Ala159Pro, which lies in the switch-1 region of the motor domain, and Tyr695X, which leads to expression of a truncated fragment lacking the calmodulin-binding or tail domain, cause thickening and disorganization of the glomerular basement membrane and are associated with childhood-onset FSGS (Mele et al. 2011). Cultured podocytes expressing MYO1E Ala159Pro fail to assemble actin filaments along the junctions, and the junctions are small and fail to spread, evidence that MYO1E mediates the interaction of podocytes with the cell matrix (Bi et al. 2013).

Patients with X-linked Alport syndrome, an inherited nephropathy caused by mutation in COL4A5, the alpha chain of collagen IV, which is a component of the glomerular basement membrane, have more severe disease when they also have mutations in MYO1E (Lennon et al. 2015).

Cancer Increased MYO1E expression was linked to poor prognosis in a cohort of 134 patients with basal-like breast cancer, a subtype of breast cancer characterized by lack of expression of estrogen receptor, progesterone receptor, and human epidermal growth factor receptor 2 and a high expression of cytokeratins 5 and/or 17, characteristic of the basal/myoepithelial layer of normal breast epithelium (Hallett et al. 2012). The studies suggest that MYO1E expression could serve as a marker of invasive tumors, and they highlight the possibility that MYO1E may promote tumor formation. Indeed, studies with *Myo1e*-null mice crossed with the MMTV-PyMT mouse model for breast cancer indicate that Myo1e is a tumor promoter (Ouderkirk-Pecone et al. 2016). Tumor progression is delayed and cell proliferation is reduced in *Myo1e*KO/PyMT mice; moreover, the tumors that do form resemble papillary breast cancer, which is normally not invasive (Ouderkirk-Pecone et al. 2016). MYO1E's role in breast cancer may be related to its association with invadosomes, structures that are involved in degradation and invasion of the extracellular matrix (Arjonen et al. 2011; Shibue et al. 2012). MYO1E localizes in RSV-transformed BHK-21 fibroblasts via its TH2 domain to the actin-rich core of invadosomes, and expression of a dominant-negative form of MYO1E leads to mislocalization of newly formed invadosomes (Ouderkirk and Krendel 2014). Thus, inhibition or reduced expression of MYO1E could prevent metastasis of tumor cells.

Ketoids Single nucleotide polymorphisms (SNPs) in *MYO1E* are also associated with the formation of keloids, benign dermal tumors that occur 20 times more frequently in persons of African descent vs. Caucasians, suggesting that an altered cytoskeleton might contribute to enhanced migratory and invasive properties of fibroblasts (Velez Edwards et al. 2014).

12.2.6 Myosin 1F

MYO1F is a long-tailed myosin I that has a proline-rich TH2 domain and a TH3 domain containing a single SH3 domain in addition to the tail homology 1 domain found in all class I myosins (Krendel and Mooseker 2005). MYO1F was cloned from a mouse cochlear cDNA library and although it was originally reported to be widely expressed in mouse and human tissues (Crozet et al. 1997), a subsequent study showed that it is selectively expressed in the mammalian immune system, especially natural killer cells, macro-

phages, dendritic cells, and neutrophils (Kim et al. 2006).

Hearing MYO1F maps to human chromosomal region 19p13.2-p13.3n (Crozet et al. 1997) where the autosomal recessive nonsyndromic deafness locus DFNB15 is located (Chen et al. 2001a). MYO1F was also shown to be expressed in rodent inner ears (Dumont et al. 2002). Six heterozygous mutations in MYO1F were identified in a group of 450 mostly European patients affected by bilateral sensorineural hearing loss; four in the motor domain, one in TH1, and one in the TH1/SH3 domain (Zadro et al. 2009). One of these mutations, MYO1F I502V, which is located near the actin-binding site, was also identified in a Korean patient with hearing loss using targeted next-generation sequencing (Baek et al. 2012). Identification of MYO1F as an important determinant in hearing awaits further experimentation including its localization in cochlea and whether *Myo1f*-null mice have hearing loss.

Infectious Disease MYO1F is expressed predominantly in cells of the immune system (Kim et al. 2006). Initially, it was reported that MYO1F-deficient neutrophils exhibit both increased adhesion to integrins and reduced 2D migration due to increased exocytosis of β2 integrin-containing granules suggesting that MYO1F modulates cell adhesion and motility (Kim et al. 2006). In addition, it was reported that *Myo1f*-null mice fail to control infection with *Listeria* bacteria presumably due to impaired motility as a consequence of increased adhesion (Kim et al. 2006). However, in a subsequent study by another group, an increase in cell adhesion in MYO1F-depleted neutrophils was also noted, although migration in 2D culture was found to be normal (Salvermoser et al. 2018). Importantly, the extravasation of neutrophils into inflamed cremaster muscle in mice and neutrophil migration in 3D culture were significantly reduced in the absence of MYO1F (Salvermoser et al. 2018). Evidently, MYO1F-deficient neutrophils are unable to pass through 3D collagen networks a consequence of failure to deform their nuclei in order to pass through small holes. This has important implications for the extravasation of neutrophils as they migrate to sites of inflammation, and suggest that defects in MYO1F may result in immunological defects.

Cancer In The Cancer Genome Atlas (TCGA) data portal, mutations in *MYO1F* are reported in 352 cases, which include endometrial, skin, colon, stomach and many other types of cancers (Diquigiovanni et al. 2018). Furthermore, *de novo* gene co-expression network inference of tissue samples from 229 patients with head and neck squamous cell carcinomas identified *MYO1F* as one of the genes implicated in tumor progression (Sanati et al. 2018).

Leukemia Acute myeloid leukemia (AML) includes myeloid leukemia in which the cancer is in cells that produce neutrophils and monocytic leukemia, in which the cancer involves monocytes (AMoL). Rearrangements of the *mixed lineage leukemia* (*MLL)* gene at locus 11q23 that fuse the N-terminus of the histone methyltransferase MLL with partner genes that destroy the normal histone methyltransferase activity of MLL and replace it with heterologous functions of the fusion partner are often found in leukemias (Taki et al. 2005; Slany 2009; Duhoux et al. 2011). While the most frequent partner genes involved in infant AML code for nuclear proteins involved in chromatin remodeling associated with transcriptional elongation, in two infants with AMoL, the *MYO1F* gene was found to be fused to *MLL* (Taki et al. 2005; Duhoux et al. 2011). Cell transformation is associated with dimerization of MLL fusion proteins, so one idea is that the SH3 domain of MYO1F interacts with the proline-rich regions of MLL to mediate oligomerization of MLL-MYO1F (Taki et al. 2005; Duhoux et al. 2011). Although the studies provide the first clues to a role for MYO1F, linking MYO1F to leukemia will require considerably more investigation.

Colitis A new report provides evidence that MYO1F induces macrophage polarization to a proinflammatory phenotype by stimulating PI3K/Akt/STAT signaling (Piedra-Quintero et al. 2018). In a mouse model of colitis,

MYO1F depletion reduced epithelial damage and stimulated recovery (Piedra-Quintero et al. 2018). Assuming that MYO1F plays a similar role in humans, these studies suggest the possibility that therapies targeting MYO1F could be effective in treating inflammatory bowel disease.

Lymphoma VAV1 is a guanine nucleotide exchange factor (GEF) for Rho-family GTPases that is important in lymphocyte development and activation (Tybulewicz 2005). Recently, gene fusions of the protooncogene VAV1 in which the SH3 domain of MYO1F replaces the C-terminal SH3 domain of VAV1 have been associated with peripheral T-cell lymphomas, non-Hodgkin lymphomas that are often associated with poor prognosis (Abate et al. 2017). Jurkat cells, an immortalized line of human T-lymphocytes, expressing the VAV1-MYO1F fusion show increased VAV1 signaling (Abate et al. 2017). Normally, the C-terminus of VAV1 folds over the N-terminus, which contains the catalytic GEF and PH domains, and prevents access of effector factors to the catalytic domain; however, in the VAV1-MYO1F fusion protein, inhibition is lost leading to constitutive VAV1 signaling in hematopoietic tissue and disease (Abate et al. 2017). Further studies, e.g., with a larger cohort of patients, are needed.

Thyroid Cancer A mutation in the conserved ATP-binding region of MYO1F was detected in members of a family affected with familial non-medullary thyroid cancer (FNMTC) (Diquigiovanni et al. 2018). Transfection of this same Gly134Ser mutation into a stable rat thyroid cell line resulted in an increase in proliferation, number of colonies, and colony formation in soft agar, and greater invasion potential in wound-healing assays (Diquigiovanni et al. 2018). The total mitochondrial mass increased in the mutant cell line, and the mitochondria appeared more fragmented, consistent with the enrichment of mitochondria observed in tumors from patients carrying this mutation (Canzian et al. 1998). Several questions remain including what effect this mutation has on MYO1F motor activity, and why mutations in MYO1F, which is predominantly expressed in cells of the immune system, have a dramatic effect on motility of thyroid cells. One idea is that expression of MYO1F may compete with other myosins I that are expressed in these cell types.

Floating Harbor Syndrome In patients with Floating-Harbor Syndrome, a rare autosomal dominant genetic condition characterized by short stature, delayed bone development, expressive language impairment, unique facial appearance, and learning disabilities arising from mutations in SNF2-related CBP Activator Proteins (SRCAP), a large SWI/SNF-type chromatin remodeling ATPase (Hood et al. 2016), the *MYO1F* gene is hypomethylated. How epigenetic modification of *MYO1F* might lead to disease is currently unknown.

12.2.7 Myosin 1G

MYO1G localizes to chromosome 7p11.2-p13, and its motor domain is ~60% identical to that of *MYO1D* (Berg et al. 2001). A short-tailed myosin I, MYO1G is expressed specifically in hematopoietic tissues (Olety et al. 2010; Patino-Lopez et al. 2010). In macrophages MYO1G localizes at Fcγ-receptor phagocytic cups and mediates engulfment of large particles (Dart et al. 2012). In B lymphocytes MYO1G localizes to actin-based protrusions such as lamellipodia and filopodia (Maravillas-Montero et al. 2014). B cells from *Myo1g*-null mice exhibit defects in spreading, adhesion, and migration that affect their ability to phagocytose (Maravillas-Montero et al. 2014), most likely a consequence of disrupted trafficking of the adhesion protein CD44, whose recycling is mediated by MYO1G (Lopez-Ortega and Santos-Argumedo 2017).

MYO1G is also highly expressed in CD4 and CD8 T lymphocytes, whose function is to seek out foreign material marked by major histocompatibility complex molecules on antigen-

presenting cells (Gerard et al. 2014). Studies indicate that MYO1G is important for antigen detection. Isolated T cells from *Myo1g*-null mice have reduced membrane tension, move twice as fast as T cells from wild-type mice, and show altered migration patterns including making fewer changes in direction, which could compromise their ability to detect rare antigens (Gerard et al. 2014).

Cancer There is early evidence that MYO1G is required for cancer cell survival as MYO1G depletion in human MCF7 breast cancer (MCF7), cervical cancer (HeLa), and osteosarcoma (U-2-OS) cells destabilizes lysosomes, inhibits autophagic flux, and induces non-apoptotic cell death (Groth-Pedersen et al. 2012). Although the reason for these results is unclear, one possibility is that they may be due to the increase in actin stress fibers that follows treatment with MYO1G-specific siRNA, which could disrupt normal actin function. Further investigation including analysis of expression data in affected individuals and the use of mouse models is warranted.

Although additional studies are required, one possibility is that modification of the *MYO1G* gene can have profound effects on human health. Increased DNA methylation of CpG islands in the *MYO1G* gene in umbilical cord blood is found among infants born to maternal smokers (Joubert et al. 2012; Lee et al. 2015; Gonseth et al. 2016), and the modification persists at least until adolescence (Lee et al. 2015) suggesting that the *MYO1G* gene is sensitive to environmental exposure. Methylation can affect DNA structure or interfere with the binding of transcription factors to repress gene expression (Siegfried and Simon 2010), and changes in methylation have been associated with cancers and other diseases (Feinberg 2007).

12.2.8 Myosin 1H

MYO1H, coding for short-tailed myosin 1H, localizes to chromosome 12 and is ~50% identical to MYO1C (Berg et al. 2001). Little else, however, is known regarding the properties of this myosin.

Jaw Defects Evidence for a connection between MYO1H and jaw development is mounting. Initially, a marker flanking the *MYO1H* gene was found to be overrepresented in a group of 44 dental patients with mandibular prognathism (Tassopoulou-Fishell et al. 2012), where the lower jaw (mandible) protrudes beyond the upper jaw (maxilla) resulting in an extended chin and malocclusion. A second study associated MYO1H with horizontal maxillomandibular discrepancies (da Fontoura et al. 2015). Similarly, MYO1H was found to be associated with an increased risk for class III (SNB, sella-naison Point B, angle greater than 83°) mandibular prognathism (Cruz et al. 2017), and in a separate study targeted sequencing found a Pro100ILeu mutation in MYO1H to be significantly associated with mandibular prognathism (Sun et al. 2018). Polymorphism of the *MYO1H* gene was found in one study to be associated with an increased risk of mandibular retrognathism (Arun et al. 2016), where the mandible is usually positioned posterior to the maxilla.

The two MYO1H orthologs, *myo1ha* and *myo1hb*, in zebrafish are expressed primarily in jaw cartilage, and reduced expression of these orthologs results in severe jaw and tail defects (Sun et al. 2018). Together, the data implicate *MYO1H* as a contributory gene to jaw deformations by regulating maxillo-mandibular growth. Future studies should include the analysis of jaw development in *Myo1h*-null mice.

Respiration Defects MYO1H is broadly expressed in the central nervous system including the forebrain, midbrain, and lower medulla where the CO_2-sensitive Phox2b + neurons of the retrotrapezoid nucleus and the nucleus of the solitary tract (Spielmann et al. 2017), regions that play important roles in breathing, reside (Feldman et al. 2003). Mutations in *MYO1H* have been associated with a recessive form of central hypoventilation

with autonomic dysfunction (Spielmann et al. 2017). This hyperventilation phenotype was recapitulated in mice expressing mutated MYO1H, suggesting that MYO1H plays a role in in respiratory control (Spielmann et al. 2017).

12.3 Myosin II

Class II or "conventional" myosins are double-headed molecules that form bipolar filaments. According to the HUGO Gene Nomenclature Committee, the 15 genes coding for class II myosins in humans are designated as *MYH1, MYH2, MYH3, MYH4, MYH6, MYH7, MYH7B, MYH8, MYH9, MYH10, MYH11, MYH13, MYH14, MYH15,* and the pseudogene *MYH16*. They include genes coding for the myosin heavy chains that mediate (i) skeletal muscle contraction (*MYH1, MYH2, MYH3, MYH4, MYH7b, MYH8, MYH13,* and *MYH15)*, which are responsible for posture and locomotion; (ii) cardiac muscle contraction (*MYH6* and *MYH7*), which are responsible for beating of the heart; and (iii) smooth muscle contraction (*MYH11*), which is responsible for visceral activities such as maintenance of blood pressure; as well as the three myosin heavy chains (*MYH9*, *MYH10*, and *MYH14)* of non-muscle myosin IIA (NMIIA), IIB (NMIIB), and IIC (NMIIC), respectively, which are expressed in all eukaryotic cells where they mediate a number of cellular events including cytokinesis, cell migration, cell adhesion, and cell signaling (Simons et al. 1991; Berg et al. 2001; Marigo et al. 2004; Conti et al. 2008; Masters et al. 2017). As the nomenclature is confusing and changes are still being proposed (Mascarello et al. 2016), a list of the genes for human myosin II heavy chains, the currently approved names of the myosin heavy chain proteins along with synonyms, the names of the myosin II proteins, and the type of muscle fibers in which they are found are in Table 12.1 (Table 12.1).

To support such diverse functions, class II myosins are heterogenous in structure and function (Reggiani and Bottinelli 2008). Skeletal and cardiac muscles are referred to as striated or sarcomeric muscles because when magnified they exhibit alternating light and dark bands due to the arrangement of their thick myosin-containing and thin actin-containing filaments into units called sarcomeres. Different striated muscle fiber types have distinct myosin II isoforms (Schiaffino and Reggiani 2011; Schiaffino et al. 2015). There are three fast muscle isoforms: skeletal muscle myosin 2X/D is expressed predominantly in fast-twitch skeletal muscle type 2X fibers; skeletal muscle myosin 2A is expressed predominantly in fast-twitch oxidative glycolytic skeletal muscle type 2A fibers; and skeletal muscle myosin 2B is expressed predominantly in fast-twitch glycolytic skeletal muscle type 2B fibers. In addition, two other myosin II isoforms, embryonic myosin II and perinatal myosin II are expressed in developing muscle, whereas extraocular myosin II, slow tonic myosin II, and slow extraocular myosin II are expressed specifically in extraocular muscle (Rossi et al. 2010). There are two cardiac isoforms, β- and α-cardiac myosin II; β-cardiac muscle myosin II is also known as slow skeletal muscle myosin II. In contrast to striated/sarcomeric muscle, smooth muscle, as the name implies, does not have a striated appearance under the microscope as its contractile units are not regularly aligned into sarcomeres. There are four isoforms of smooth muscle myosin II (SM1A, SM1B, SM2A, and SM2B) generated by splicing at two alternate sites of a single gene, *MYH11* (Eddinger and Meer 2007).

The regulation of striated and smooth muscle also differs with skeletal muscle contraction regulated by the thin filament accessory proteins troponin and tropomyosin and smooth muscle contraction mediated by myosin light chain phosphorylation. Biochemical and mechanical properties indicate that class II myosins include fast movers (e.g., fast skeletal muscle myosin 2A), slow/efficient force holders (e.g., slow skeletal myosin II, β-cardiac myosin II), and strain sensors (NMIIA, NMIIB) (Bloemink and Geeves 2011).

The association of conventional myosin II with disease is the subject of several recent excellent review articles (Tajsharghi and Oldfors 2013; Ma and Adelstein 2014b; Marston 2018; Pecci et al. 2018; Trivedi et al. 2018).

Table 12.1 Myosin II genes in humans. Gene assignment is according to the HUGO Gene Nomenclature Committee. Approved names followed by synonyms in parentheses are found in the column labeled *Protein Name of Heavy Chain*

	Gene name	Protein name of heavy chain	Myosin protein name	Muscle fiber type
	Sarcomeric muscle myosins			
Skeletal muscle myosin II	*MYH1*	MYH1 (MyHC-2X/2D)	Skeletal muscle myosin 2X/2D	Type 2X muscle fibers in fast-twitch skeletal muscle
	MYH2	MYH2 (MyHC-2A)	Skeletal muscle myosin 2A	Type 2A muscle fibers in fast-twitch skeletal muscle
	MYH3	MYH3 (MyHC-EMB)	Embryonic myosin 2	Embryonic and fetal muscle; specialized muscles
	MYH4	MYH4 (MyHC-2B)	Skeletal muscle myosin 2B	Type 2B muscle fibers in fast-twitch skeletal muscle
	MYH7b (previouslyMYH14)	MYH7B (MyHC-7B)	Slow/tonic myosin 2	Slow/tonic extraocular muscles
	MYH8	MYH8 (MyHC-neo)	Neonatal/ perinatal myosin 2	Neonatal/perinatal skeletal muscle; specialized muscles
	MYH13	MYH13 (MyHC-EO)	Extraocular myosin 2	Extraocular muscle
	MYH15	MYH15 (MyHC-15)	Slow extraocular myosin 2	Extraocular muscle, slow B
	MYH16/pseudogene	MYH16- (MyHC-M)		
Cardiac myosin II	*MYH6*	MYH6 (MyHC-α-cardiac)	α-cardiac myosin 2	Atria, jaw muscles
	MYH7	MYH7; (MyHC/Slow skeletal/β-cardiac)	β-cardiac myosin 2; Slow skeletal myosin 2	Type 1 fibers in slow-twitch skeletal muscle; ventricles of the heart
	Non-sarcomeric muscle myosins			
Smooth muscle myosin II	*MYH11*	MYH11 (MyHC-smooth muscle); SMMHC	Smooth muscle myosin 2	Contractile units of smooth muscle cells
Non-muscle myosin II	*MYH9*	MYH9 (NMMHC-IIA)	NMIIA	Non-muscle cells
	MYH10	MYH10 (NMMHC-IIB)	NMIIB	Non-muscle cells
	MYH14	MYH14 (NMMHC-IIC)	NMIIC	Non-muscle cells

The Table is compiled from (Rossi et al. 2010; Schiaffino and Reggiani 2011; Schiaffino et al. 2015; Mascarello et al. 2016; Marston 2018)

12.3.1 Sarcomeric/Striated Muscle Myosin II

12.3.1.1 Skeletal Muscle Myosins II

Skeletal Muscle Myosin 2X/D (MYH1 Heavy Chain)

Myositis There is a strong selection pressure against mutations in *MYH1*, which codes for the heavy chain of skeletal muscle myosin 2X/D and is found in fast-twitch type 2X/D skeletal muscle fibers; however, recently, a Glu321Gly variant in the motor domain of MyHC-2X/D was found to be strongly associated with susceptibility in quarter horses to develop immune-mediated myositis under certain environmental conditions (Finno et al. 2018). In the absence of inflammation, type 2X myofibers were normal; however, in the presence of inflammation, myofibers in horses heterozygous or homozygous for the *MYH1* mutation

were subject to invasion and destruction by lymphocytes leading to gross muscle atrophy (Finno et al. 2018). This is the first reported disease-causing mutation in any species. Whether a similar situation occurs in humans carrying a mutation in this highly conserved amino acid in MyHC--2X/D is unknown.

Skeletal Muscle Myosin 2A (MYH2 Heavy Chain)

Hereditary Inclusion Body Myopathy A mutation in a highly conserved residue (Glu706Lys) in the SH1 helix of myosin heavy chain 2 (MYH2) or MyHC-2A, the heavy chain of skeletal muscle myosin 2A, which is found in fast-twitch (type 2A) skeletal muscle fibers, is associated with a rare autosomal dominant condition called hereditary inclusion body myopathy (Martinsson et al. 2000). Patients have congenital joint contractures that normalize during early childhood, and by age 40 the patients exhibit external opthalmoplegia (weakness of the eye muscles) and mostly proximal muscle weakness and atrophy (Martinsson et al. 1999). The muscles show rimmed vacuoles with filamentous inclusions, and in some patients the type 2A muscle fibers are frequently abnormal appearing small, infrequent and with abnormalities (Martinsson et al. 1999; Martinsson et al. 2000). The SH1 helix of the myosin motor domain is one of two helices that hold in place the converter region, which controls the position of the lever arm (Houdusse and Sweeney 2016). Thus, the Glu706Lys mutation in the SH1 helix is likely to result in a compromised myosin. In another study, five adults with generalized muscle weakness, extraocular muscle involvement, and relatively favorable prognosis were found to lack fast type 2A muscle fibers due to the total absence of fast myosin heavy chain 2A as a consequence of truncation mutations of the *MYH2* gene (Tajsharghi et al. 2010). Why the phenotype in patients missing one of the major muscle fiber types is mild is unknown.

Embryonic Myosin II (*MYH3/MyHC-EMB Heavy Chain)*

Freeman-Sheldon Syndrome and Sheldon-Hall Syndrome Mutations in *MYH3*, which codes for myosin heavy chain 3 (MYH3) or embryonic myosin heavy chain (MyHC-EMB), the heavy chain of embryonic myosin II, are responsible for Freeman-Sheldon syndrome (FSS; DA2A; "whistling face" syndrome), one of the most severe congenital contracture (i.e., arthrogryposis) syndromes, and one-third of all cases of Sheldon-Hall Syndrome (SHS; DA2B), the most common distal arthrogryposis, i.e., contractures affecting the hands (camptodactyly) and feet (clubfeet) (Toydemir et al. 2006). In addition to the hand and feet contractures in children with FSS and SHS, children afflicted with FSS have contractures of the mouth and face, resulting in a small mouth and pinched lips, and often develop scoliosis. Mutations responsible for both diseases localize primarily to the myosin motor domain, in the groove between the upper and lower 50-kDa domains in the case of FSS, and to surfaces that might interact with other proteins such as actin and troponin in the case of SHS, although two mutations in the myosin rod were found in patients with SHS indicating that mutations may affect either ATPase activity or filament formation (Toydemir et al. 2006). Three missense mutations, Thr178Ile, Arg672Cys, and Arg672His, account for 91% of FSS cases, with Thr178Ile, associated with the most severe phenotype (Beck et al. 2014). Analysis of Arg672Cys-containing muscle cells and myofibrils indicate that some myosin cross-bridges have greatly reduced detachment kinetics, which likely reduces filament sliding (Racca et al. 2015).

Perinatal Myosin II (*MYH8/MyHC-peri)*

Carney Complex Carney complex is a disease characterized by the presence of benign tumors (myxomas) in the heart, which can block blood flow causing serious complications or death, and in other parts of the body including endocrine tissues such as the pituitary, adrenal, and thyroid glands; patients also often exhibit pigment abnormalities (Wilkes et al. 2005). Although mutations in the *PRKAR1A* gene, which encodes for the R1α regulatory subunit of cyclic-AMP dependent protein kinase A, are the cause of Carney complex in most patients, a missense mutation (Arg674Gln) in the *MYH8* gene has been associ-

ated with cardiac myxomas (Dijkhuizen et al. 2001; Wilkes et al. 2005). One idea is that mutations in MYH8 could prevent the normal developmental switch from multipotent embryonic cardiac cells to non-proliferative mature cardiac cells (Wilkes et al. 2005).

Trismus-Pseudocamptodactyly Studies in mice indicate that expression of *MYH8*, which codes for myosin heavy chain 8 (MYH8) or neonatal myosin heavy chain (MyHC-neo) in fetal skeletal muscle, is transient, beginning during limb-bud development and declining after birth (Bandman 1985; Lyons et al. 1990; Weiss and Leinwand 1996; Machida et al. 2000; Sacks et al. 2003). Trismus-pseudocamptodactyly, a distal arthrogryposis characterized by contractures of facial muscles, has been linked to a substitution of glutamine at Arg674 in the motor domain of MYH8 in two small American families of Dutch descent (Veugelers et al. 2004). Arg674 is adjacent to the P-loop of the nucleotide pocket in the myosin motor domain suggesting that the enzymatic activity of the mutant myosin is disrupted.

12.3.1.2 Cardiac Muscle Myosins II

α-Cardiac Muscle Myosin II (*MYH6/MyHC-α-cardiac)*

Congenital Heart Defects *MYH6* codes for myosin heavy chain 6 (MYH6) or α-cardiac myosin heavy chain (α-cardiac MyHC), which is expressed at high levels in the developing atria. A mutation (Iso820Asn) in the neck region at the start of the IQ domain, which likely prevents light-chain binding to MYH6, is associated with an autosomal dominant form of atrial septal defect, one of the most common forms of congenital heart malformation (Ching et al. 2005). Further evidence that α-cardiac myosin II is required for atrial septum formation comes from studies showing that introduction of morpholinos against *MYH6* in the developing chick heart prevents the formation of the atrial septum (Ching et al. 2005). Subsequently, another study showed that mutations in MYH6 that disrupt myofibril formation (Ala230Pro; Ala1366Asp) or enhance myofibril assembly (His252Gln) cause a wide range of sporadic congenital heart defects (Granados-Riveron et al. 2010). Missense, in-frame deletion, premature stop, *de novo*, and heterozygous variants of *MYH6* are also associated with hypoplastic left heart syndrome (HLHS), a severe form of congenital heart disease that affects normal blood flow through the heart (Tomita-Mitchell et al. 2016).

A rare missense mutation in the converter region of MYH6, Arg721Trp, is associated in Icelandic patients with a high risk of sick sinus syndrome (SSS), or sinus node dysfunction, which is characterized by sinus bradycardia (slow heart rate), sinus arrest, and chronotropic incompetence (attenuated heart rate response to exercise) (Holm et al. 2011). The authors suggest that the Arg721Trp mutation may also be associated with several cardiovascular diseases including atrial fibrillation, atrioventricular block, and aortic stenosis. The same mutation is associated with coarctation of the aorta (CoA), a common birth defect defined by narrowing of the proximal descending aorta or aortic arch and a bicuspid aortic valve that causes neonatal heart failure or hypertension in adults (Bjornsson et al. 2018).

Cardiomyopathies Some mutations in cardiac muscle sarcomeric proteins affect heart development while others cause cardiomyopathies later in life. Although the majority of hypertrophic cardiomyopathy (HCM) cases, a disease of the left ventricles, are caused by mutations in β-cardiac myosin II and cardiac myosin-binding protein C (see below), mutations in MYH6 have also been associated with HCM and dilated cardiomyopathy (DCM) (Niimura et al. 2002; Carniel et al. 2005; Hershberger et al. 2010; Zhao et al. 2015). This suggests that MYH6, which is expressed predominantly in atria, may also be expressed in ventricles, or that events in the atria can affect ventricular function.

β-Cardiac Myosin II//Slow Skeletal Muscle Myosin II (MYH7)

The *MYH7* gene codes for myosin heavy chain 7 (MYH7) or the heavy chain of slow skeletal/β--cardiac myosin II, which is expressed in cardiac

ventricles and slow twitch (Type 1) skeletal muscle fibers and is associated with over 500 disease-causing mutations (Colegrave and Peckham 2014). *MYH7*-related disease can present as mild to fatal forms of cardiomyopathies and/or skeletal myopathies.

Cardiac Disease: Hypertrophic Cardiomyopathy
Missense mutations in *MYH7* and cardiac myosin-binding protein C (*MyBP-C*) account for 80% of HCM, the most common genetic form of inheritable heart disease, which is characterized by left ventricular hypertrophy, diastolic dysfunction, and hypercontractility often leading to sudden death, heart failure, and stroke (Geisterfer-Lowrance et al. 1996; Dadson et al. 2017).

Recently, Spudich proposed a model for how different myosin mutations associated with HCM could affect myosin structure and function (Spudich 2015). Many of the several hundred mutations in MYH7 that produce the same hypercontractile phenotype are located in the "myosin mesa", a relatively flat part of the surface of the myosin head, the converter region, or the proximal S2, which interfaces with the myosin mesa and the converter region (Colegrave and Peckham 2014; Spudich 2015; Homburger et al. 2016; Nag et al. 2017; Trivedi et al. 2018). The myosin mesa, which is adjacent to the actin-binding domain and contains multiple basic amino acids, may interact with myosin itself as myosin packs down on the surface of the thick filament forming the interacting-head motif (IHM), which does not bind actin (Wendt et al. 2001; Alamo et al. 2008; Jung et al. 2008). Under these conditions, the myosin is presumably trapped in a super-relaxed state (SRX) with very low basal activity (McNamara et al. 2015; Anderson et al. 2018). The HCM mutations in the converter domain cluster where the docked head contacts the converter domain of the free head (Marston 2018). Mutations in the myosin mesa, converter, or proximal S2 region of myosin could thus destabilize the interaction between myosin heads and make them available to interact with actin, thus accounting for the hyper-contractility that characterizes this disease (Nag et al. 2017; Trivedi et al. 2018). In support of this model, four HCM mutations, Arg249Gln, His251Asn, and Arg453Cys on the mesa and Asp906Gly on proximal S2, reportedly reduce the affinity of proximal S2 for sS1, a fragment representing the myosin motor domain without the regulatory light chain (Trivedi et al. 2018).

Examination of a newly solved high-resolution structure of the bovine β-cardiac myosin II sequestered state shows that 178 HCM mutations can affect either motor activity or the dysregulation of the sequestered state (Robert-Paganin et al. 2018). Some mutations can have dual effects, e. g., the Arg403Gln mutation reduces motor activity (Nag et al. 2015) and also weakens the IHM (Robert-Paganin et al. 2018). Importantly, the small molecule mavacamten inhibits the myosin ATPase and cardiomyocyte contractility *in vitro* and suppresses the development of ventricular hypertrophy in mice (Green et al. 2016) by stabilizing the IHM (Anderson et al. 2018).

Nearly 40% of the known mutations responsible for HCM are in myosin-binding protein C (MyBP-C) (Marston 2018). Mutations in MyBP-C may also lead to HCM by increasing the number of myosin molecules able to interact with actin (Trivedi et al. 2018). Cardiac MyBP-C is a long, flexible protein consisting of 11 domains, eight immunoglobulin domains, three fibronectin-3 family domains, a proline-alanine-rich domain, and a phosphorylatable M domain (Flashman et al. 2004). The C-terminal module anchors MyBP-C to the thick filament with the rest of the molecule extending away from the thick filament backbone (Marston 2018; Trivedi et al. 2018). In a model of IHM of the myosin molecule, MyBP-C appears to contact the mesa and light chains of the free head. Mutations in MyBP-C may weaken the IHM state resulting in an increase in the number of myosin heads available to interact with actin (Trivedi et al. 2018).

Cardiac Disease: Dilated Cardiomyopathy
Mutations in MYH7 account for 3–4% of familial DCM (McNally and Mestroni 2017), which is characterized by modest myocardial hypertrophy, thin-walled ventricles, and myocyte hypo-

plasia leading to heart failure due to reduced cardiac output (Seidman and Seidman 2001). Patients fatigue easily initially due to reduced systolic function then develop heart failure (Seidman and Seidman 2001). Two missense mutations, Ser532Pro, which is in the actin-binding domain, and Phe764Leu, which is in the converter region, cause DCM (Kamisago et al. 2000). Myosins purified from the hearts of mice expressing these mutants show reduced actin-activated ATPase activity and actin filament velocity in *in vitro* motility assays, suggesting that depressed motor function may be the root cause of the disease (Schmitt et al. 2006). Recombinant human β-cardiac sS1 containing these two mutations and three others that produce hypo-contractile DCM phenotypes, Ala223Thr, Arg237Trp, and Ile201Thr, were co-expressed with the essential light chain in the immortalized mouse myoblast cell line C_2C_{12} and purified, and individual events in the ATPase cycle were measured (Ujfalusi et al. 2018). No consistent effects of the mutations on rate constants for ATP binding, ATP hydrolysis, or ADP release or the affinity for ATP, ADP, or actin were observed, although four of the five mutations resulted in a reduced duty ratio, i.e., the percentage of time the myosin stays bound to actin vs. wild-type protein. A similar change in duty ratio was observed in single-molecule studies using Ala223Thr, Arg237Trp, and Ser532Pro (Liu et al. 2018a). These data suggest that the mutations may cause a deficit in force generation (Ujfalusi et al. 2018).

Laing Distal Myopathy The skeletal muscle disease Laing distal myopathy (LDM; MPD1), which initially causes weakness in the ankle extensors and toe and then long finger extensors and certain limb and neck muscles (Laing et al. 1995; Mastaglia et al. 2002; Lamont et al. 2006), is an autosomal dominant disease caused by mutations in the *MYH7* gene (Meredith et al. 2004). Six families with early onset distal myopathy were found to have five heterozygous mutations in the tail region of MYH7, two that introduce deletions, and three that introduce prolines, all of which are predicted to disrupt the coiled-coil structure of the myosin tail (Meredith et al. 2004). When expressed in myoblasts, however, two of the mutations, Arg1500Pro and Leu1706Pro, incorporated into thick filaments (Buvoli et al. 2012), although whether the filaments with mutant myosins function like wild-type filaments is unknown. Both mutants induce myosin aggregates in myoblasts, and the Leu1706Pro mutant accumulated in the sarcomeric bare zone suggesting that it affects the proper antiparallel arrangement of myosin molecules (Buvoli et al. 2012). Thus, *MYH7* mutations may result in muscle weakness by causing aggregation or subtle changes in sarcomere structure.

Myosin Storage Myopathy (MSM) Missense mutations in *MYH7* are responsible for the congenital skeletal muscle disease myosin storage myopathy (hyaline body myopathy) (Tajsharghi et al. 2003). Eight mutations all located at the distal tail of the myosin rod have been associated with MSM (Tajsharghi et al. 2003; Bohlega et al. 2004; Dye et al. 2006; Chai et al. 2007; Tajsharghi et al. 2007; Ortolano et al. 2011; Stalpers et al. 2011; Yuceyar et al. 2015). Patients can have no weakness to severe impairment of walking, and biopsies show subsarcolemmal hyaline bodies consisting of aggregated myosins in type 1 fibers (Tajsharghi and Oldfors 2013). Insight into how the mutations give rise to disease comes from studies in flies. Flies expressing one of the three mutant myosins, Leu1793Pro, Arg1845Trp, and Glu1883Lys, exhibit severe impairment of flight and jump ability and disrupted muscle ultrastructure and myosin aggregates as seen in human biopsies of afflicted patients (Viswanathan et al. 2017). Importantly, the mutant myosins exhibit a reduced ability to assemble into filaments and are more susceptible to controlled proteolysis indicating that the filaments are disordered, which could lead to muscle weakness.

Multi-Minicore Disease (MmD) Multi-minicore disease is a recessive congenital myopathy characterized by small areas or cores in skeletal muscle fibers of sarcomeric disorganization and lack of oxidative enzymes (Zorzato et al. 2007). Patients present with various pheno-

types; however, most have spinal rigidity, axial weakness, scoliosis, and respiratory impairment (Ferreiro et al. 2000; Jungbluth et al. 2000). Although multi-minicore disease has been associated with mutations in the skeletal muscle ryanodine receptor (*RYR1*) (Jungbluth et al. 2002; Jungbluth et al. 2004) and selenoprotein N (*SEPN1*) genes (Ferreiro et al. 2002), four patients with heterozygous missense mutations in the *MYH7* gene from two families reportedly show clinical features of skeletal myopathy with variable cardiac involvement (Cullup et al. 2012).

12.3.2 Non-sarcomeric Muscle Myosin II

12.3.2.1 Smooth Muscle Myosin II

Smooth Muscle Myosin II (MYH11)

Thoracic Aortic Aneurysm and Dissection (TAAD) and Patent Ductus Arteriosus (PDA) Mutations in the *MYH11* gene, which codes for myosin heavy chain 11 (MYH11) or smooth muscle myosin heavy chain (SMMHC), account for ~2% of non-syndromic TAAD (Pomianowski and Elefteriades 2013), an autosomal dominant disease in which the aorta becomes weakened and dilated forming a bulge, or aneurysm, leading in some cases to tearing (dissection) of the layers of the aorta, which disrupts normal blood flow. The condition can be life-threatening if the aneurysm bursts. Aortic tissues with heterozygous mutations in MYH11 are stiff, show large areas of degeneration, and they have both areas of reduced numbers of vascular smooth muscle cells and hyperplasia (Zhu et al. 2006; Pannu et al. 2007). In some cases, TAAD due to mutations in the *MYH11* gene is associated with patent ductus arteriosus (PDA) (Zhu et al. 2006; Pannu et al. 2007), a common congenital heart defect in which the ductus arteriosus fails to close following birth.

Rare variants in *MYH11* have been detected throughout the molecule; however, only a small number are associated with disease (Harakalova et al. 2013). The few *MYH11* mutations identified in familial TAAD patients with PDA are deletions and missense mutations in the coiled-coil tail region of the myosin heavy chain, which are likely to disrupt filament formation, and the missense variant Arg712Gln in the motor domain, which is expected to impair myosin motor function (Zhu et al. 2006; Pannu et al. 2007). A recurrent *MYH11* rare variant in the motor domain, Arg247Cys, found in patients with thoracic aortic disease but not in patients with familial TAAD, reduces myosin ATPase activity and motility *in vitro*, and *Myh11*$^{R247C/R247C}$ knock-in mice show reduced aortic contraction and in response to vascular injury increased smooth muscle cell proliferation (Kuang et al. 2012). *MYH11* mutations leading to aneurysms may be associated with upregulation of the transforming growth factor β (TGFβ) signaling pathway (Renard et al. 2013).

Patients with duplications of chromosomal 16p13.1 region, which contains 9 genes including *MYH11*, have increased *MYH11* mRNA levels in aortic tissue and an increased risk of thoracic aortic disease and neuropsychiatric conditions specifically, schizophrenia and attention-deficit disorder (Kuang et al. 2011). Insight into how increased expression leads to thoracic aorta disease comes from studies showing that overexpression of MYH11 in murine aortic smooth muscle cells results in ER stress and autophagy (Kwartler et al. 2014).

Cancer A pericentric inversion on chromosome 16 involving the transcription factor gene *CBFB* and *MYH11* results in the formation of an oncogenic fusion gene, *CBFB-MYH11,* which is associated with acute myelogenous leukemia subtype M4 with eosinophilia (Liu et al. 1993; Usuki et al. 1996). In mouse models CBFβ-SMMHC encoded by *CBFB-MYH11* is necessary, but not sufficient, to induce leukemia (Castilla et al. 1999). CBFβ binds the hematopoietic transcription factor RUNX1 (AML1) to regulate gene expression, and RUNX1 is required for *CBFB-MYH11*-induced leukemogenesis (Hyde et al. 2015). Evidently, RUNX1 binds chromodomain helicase DNA-binding protein 7 (CHD7), a chromatin remodeling factor that regulates transcription, and reduced expression of CHD7 delays

leukemogenesis by *CBFB-MYH11* by inhibiting proliferation of leukemia-initiating and leukemic cells (Zhen et al. 2017).

Missense mutations in MYH11 (Arg501Leu; Lys1044Asn) that result in unregulated myosins with constitutive motor activity are implicated in intestinal neoplasia, possibly by affecting the energy balance in cells or cell lineage decisions (Alhopuro et al. 2008). Moreover, colorectal cancers with lower expression of MYH11 reportedly correlate with poorer prognosis, suggesting a role for MYH11 in the prognosis of colorectal cancers (Wang et al. 2014).

Megacystis-Microcolon-Intestinal Hypoperistalsis Syndrome (MMIHS; Berdon syndrome) MMIHS, a rare congenital disease characterized by dilation of the bladder and microcolon, and lack of intestinal peristalsis, was associated with an homozygous mutation in MYH11 (Lys1200Ter) in one newborn (Gauthier et al. 2015) and compound heterozygous mutations (a 2-bp deletion in exon 22, and a 49-bp deletion in exon 49) in MYH11 in a second newborn (Yetman and Starr 2018). Similarly, *Myh11*-null mice have a thin-walled bladder and abnormal peristalsis and die after 3 days (Morano et al. 2000).

12.3.3 Non-muscle Myosins II

12.3.3.1 Non-muscle Myosin IIA (*MYH9, NMIIA*)

MYH9 Syndrome The *MYH9* gene product codes for myosin heavy chain 9 (MYH9) or NMMHC-IIA, the heavy chain of non-muscle myosin IIA (NMIIA), which is widely expressed. NMIIA is critical to early embryonic development in mice as *Myh9*-null mice fail to form E-cadherin-mediated cell-cell junctions and die by embryonic day 6.5 (Conti et al. 2004). Originally, five rare giant-platelet disorders, May-Hegglin anomaly, and Sebastian, Fechtner, Epstein and Alport-like syndromes with macrothrombocytopenia, were characterized as unrelated disorders; however, it was subsequently established that they are all caused by mutations in MYH9 and designated as *MYH9* syndrome (Kelley et al. 2000; Heath et al. 2001; Kunishima et al. 2001; Seri et al. 2003). Patients present with autosomal dominant macrothrombocytopenia with giant platelets and leukocyte inclusions due to aggregates of NMIIA and may develop late onset sensorineural hearing loss, cataracts, and nephritis (Seri et al. 2003). NMIIA is the only myosin II among three NMII isoforms (paralogs) expressed in the megakaryocytic and granulocytic lineages, so the late onset hearing, vision, and renal defects may be due to partial compensation by the other myosin II isoforms (Seri et al. 2003; Marigo et al. 2004).

Mutations are usually single amino acid substitutions. Commonly affected residues include Ser96 and Arg702 in the head domain, Arg1164, Asp1425, and Glu1841 in the coiled-coil region, and Arg1933 in the non-helical tailpiece at the C-terminus (Heath et al. 2001; Martignetti 2002; Pecci et al. 2018). Mutations in the head domain are associated with higher incidence of nephropathy than tail domain mutants (Pecci et al. 2014). The risk of developing one of the late-onset effects depends, however, on the specific mutation, e.g., patients with substitutions of Arg702 located in the short SH1 helix of the lower 50 kDa subdomain in the myosin head domain develop hearing defects before the age of 40 and kidney damage before the age of 45, whereas patients with mutations at the SH3/motor domain interface (Trp33, Val34, Asn93, Ala95, Ser96), coiled-coil region (Arg1165; Asp1424, Glu1841), or non-helical tailpiece (Arg1933∗) have less risk of developing hearing defects and nephropathy (Pecci et al. 2014).

Heterozygous expression of MYH9 Arg702Cys in mice causes macrothrombocytopenia reproducing the clinical phenotype of the human disease (Suzuki et al. 2013). Bleeding time and clot retraction are not different from that in wild-type animals, but proplatelet formation is abnormal. Platelets are formed from megakaryocytes in the bone marrow in a cytoskeletal-driven process whereby long branching processes called proplatelets are extended into blood vessels where they undergo fission to release platelets (Machlus and Italiano 2013). In the *Myh9*

Arg702Cys heterozygous mouse, the proplatelets are larger, consistent with thrombocytopenia and increased platelet size in patients with *MYH9* disorders (Zhang et al. 2012; Suzuki et al. 2013). Evidently, the observed defects are due to impaired actomyosin forces required to split platelets from proplatelets (Thon et al. 2012).

Insight into the pathogenesis of renal disease in *MYH9*-related disease comes from mice expressing the MYH9 missense mutations Arg702Cys, Asp1424Asn, or Glu1841Lys (Zhang et al. 2012; Cechova et al. 2018). The mice have severe focal segmental glomerulosclerosis and exhibit podocyte foot effacement, which is also observed in biopsy samples from patients with *MYH9*-related disease, suggesting that it may be responsible for the renal abnormalities (Zhang et al. 2012; Cechova et al. 2018).

Hearing Loss The hearing loss locus DFNA17 is associated with *MYH9* mutations (Lalwani et al. 2000). In mice NMIIA localizes to the stereocilia on the inner and outer hair cells of the sensory epithelium in the inner ear (Mhatre et al. 2006). Although why mutations in MYH9 cause hearing defects is currently unknown, localization of NMIIA to the stereocilia, which deflect in response to sound and vibration opening and closing transduction channels, suggests a role in mechanotransduction.

Cancer Increased expression of MYH9 has been linked to bladder cancer (Xiong et al. 2012), esophageal squamous cancer (Xia et al. 2012), non-small cell lung cancer (Katono et al. 2015), and gastric cancers (Liu et al. 2016) in agreement with studies showing that reduced expression of NMIIA in cultured human MCF-7 breast cancer cells inhibits invasion in *in vitro* assays (Derycke et al. 2011).

Myh9 was identified as a tumor suppresser using an *in vivo* RNAi-based screen for genes that upon repression predispose mice to squamous cell carcinomas (SCCs) (Schramek et al. 2014). Furthermore, knockout of *Myh9* expression in mice with tumor-susceptible backgrounds accelerated tumor development and malignant progression (Schramek et al. 2014). Interestingly, *Myh9* knockdown had little effect on tumor latency or multiplicity in mice carrying an epithelial-specific *Trp53* gain-of-function suggesting NMIIA's possible involvement in regulating posttranscriptional p53 stabilization and/or nuclear retention (Schramek et al. 2014). Analysis of hundreds of human tissues showed that 24% skin SCCs and 31% head and neck SCCs had weak or no NMIIA immunolabelling suggesting that *MYH9* is a tumor suppressor in humans (Schramek et al. 2014). In another study, conditional deletion of MYH9 in mouse heart and tongue epithelium had no effect on heart development but resulted in the development of SCC of the tongue (Conti et al. 2015). The tumors appeared during embryonic development, showed 100% penetrance, and did not show a change in TP53 stability (Conti et al. 2015). The authors speculate that the high penetrance of SCC in *Myh9*-depleted cells may be related to the role that NMIIA plays in cytokinesis and in karyokinesis by affecting microtubule dynamics (Ma et al. 2010; Schramek et al. 2014). Although functional loss of cadherin is responsible for most human invasive lobular carcinomas (ILCs), female mice with mammary-specific inactivation of E-cadherin are not prone to develop mammary tumors suggesting that mutations in other genes are required (Kas et al. 2017). Using an insertional mutagenesis screen in mice that also had mammary-specific inactivation of the cadherin gene *CDH1,* several genes involved in regulation of the actin cytoskeleton including *Myh9* were frequently mutated in ILC (Kas et al. 2017). The mutations in *Myh9* resulted in haploinsufficiency suggesting that dosage is important. Indeed, intraductal injection in mammary glands of female mice of CRISPR-Cas 9-encoding lentiviruses designed to cause hemizygous expression of Myh9 resulted in mammary tumors in 11/26 cases within 17 weeks suggesting that *Myh9* is a haplo-insufficient tumor suppressor in ILC development (Kas et al. 2017).

12.3.3.2 Nonmuscle Myosin IIB (*MYH10, NMIIB*)

Heart Disease The *MYH10* gene codes for myosin heavy chain 10 (MYH10) or NMMHC-

IIB, the heavy chain of non-muscle myosin IIB (NMIIB) (Simons et al. 1991). Mutations in *Myh10* in mice lead to abnormal heart development in which the heart develops outside of the body due to failure of ventral wall closure (Ma and Adelstein 2014a). A similar phenotype is found in the human syndrome Pentalogy of Cantrell (Ma and Adelstein 2014a), although whether mutations in *MYH10* are responsible is not yet known.

Pulmonary Disease Mice bearing a mutation in the *Myh10* gene that leads to a missense mutation (Leu458Arg) in NMMHC-IIB have recently been shown to exhibit cyanosis and respiratory distress due to a dramatic increase in matrix metalloproteinase 2 activity, which disrupts extracellular matrix remodeling in developing lungs (Kim et al. 2018). In healthy human lungs, NMIIB is expressed in smooth muscle cells and mesenchymal cells of the alveolar interstitium; however, NMIIB expression is strongly reduced in smooth muscle cells and moderately reduced in the alveolar interstitium of lung samples from emphysema patients (Kim et al. 2018). Further studies are required to establish a connection between NMIIB and pulmonary emphysema.

12.3.3.3 Non-muscle Myosin IIC (*MYH14, NMIIC*)

Hearing Loss The *MHY14* gene codes for myosin heavy chain 14 (MYH14) or NMMHC-IIC, the heavy chain of non-muscle myosin IIC (NMIIC) (Golomb et al. 2004). Four mutations (Ser7Ala, which introduces a stop codon in the motor domain; Gly376Cys, which introduces a mutation in the motor domain; and Arg726Ser and Leu976Phe, which introduce mutations in the tail domain) in MYH14 were initially associated with autosomal dominant non-syndromic hearing loss (ADNSHL), DFNA4, in Europeans with mild-to-moderate progressive hearing loss with postlingual onset (Donaudy et al. 2004). Another mutation in the tail, Ala1868Thr, was subsequently linked to ADNSHL in a Korean (Kim et al. 2016). Additional studies showed that two variants in MYH14, one a mutation in the motor domain (Asp191Gly) and one a mutation in exon 2 (Gln25∗), in a Korean family led to nonsyndromic severe sensorineural hearing loss with prelingual onset (Kim et al. 2017). Although its function in the inner ear is unknown, NMIIC localizes mainly in the organ of Corti, the stria vascularis, and the cells surrounding the scala media such as Hensen cells, Claudius cells, and the external sulcus cells (Lalwani et al. 2000), a localization pattern distinct from that of NMIIA, which localizes predominantly within the spiral ligament and sensory hair cells of the organ of Corti (Mhatre et al. 2006). Also in a Korean family, a mutation in the tail domain of MYH14, Gly2822Thr, was found to be responsible for peripheral neuropathy, myopathy, hoarseness, and hearing loss suggesting that mutations in *MYH14* might have a wider phenotypic spectrum (Choi et al. 2011).

Anorectal Malformations Whole-exome sequencing of the genomic DNA of 8 members of a Chinese family that included 2 siblings with anorectal malformations led to the identification of mutations in *MYH14* as the cause of the defect (Zhu et al. 2017). Localization studies in mice show that during embryonic development NMIIC localizes to the cloaca, which gives rise to the digestive and urinary tracts (Zhu et al. 2017). No defects in the hindgut were observed in *Myh14*-null mice (Ma et al. 2010). One possibility is that whereas in the case of the *Myh14*-null mouse, NMIIA and NMIIB may substitute for NMIIC as their expression overlaps with that of NMIIC in the region of cloacal development (Zhu et al. 2017), expression of a mutant NMIIC may act as a dominant negative.

Cancer NMMHC-IIC is alternatively spliced in loop 1 and loop 2 of the motor domain to form 4 splice variants: NMII0, NMIIC1, NMIIC2, and NMIIC1C2 (Ma and Adelstein 2014b). NMIIC0 contain no inserts at either position. NMIIC1 and NMIIC1C2 have an 8-amino acid insert at loop 1. In addition, NMIIC2 and NMIIC1C2 have a 33-amino acid insert in the loop 2 region. The isoforms differ primarily in the rates of ADP

release with NMIIC1C2 having a 5-7-fold increase in ADP affinity vs. NMIIC0 (Heissler and Manstein 2011). Accordingly, the actin-activated ATPase activity and *in vitro* motility of NMIIC2 and NMIIC1C2 are higher than those of NMIIC0 and NMIIC1 (Jana et al. 2009; Heissler and Manstein 2011).

There is some evidence that mislocalization of NMIIC1 during cytokinesis may lead to the development of breast cancer. NMIIC1 localizes to the midbody during abscission, the final step in cytokinesis, and is required in a number of tumor cell lines for cell division (Jana et al. 2006). BRCA2, a tumor suppressor whose mutation increases the risk of breast and ovarian cancer, functions in the repair of DNA double-strand breaks and also regulates cell division (Daniels et al. 2004; Jonsdottir et al. 2009). Phosphorylation of BRCA2 by mitotic polo-like kinase 1 (Plk1) results in localization of BRCA2 at the midbody where is associates with NMIIC1 to form a discrete ring-like structure (Takaoka et al. 2014). The MgATPase activity of NMIIC1 is stimulated by this interaction with BRCA2 and other components of the ring-like structure, and inhibition of this interaction interrupts cytokinesis (Takaoka et al. 2014). A missense mutation in the Plk1-binding site on BRCA2 is associated with hereditary breast cancer suggesting that disruption of the Plk1-BRCA2 interaction prevents phosphorylation of BRCA2, inhibits the MgATPase activity of NMIIC1, and interrupts cytokinesis, which may contribute to the cancer phenotype. Additional studies confirming these results are of great interest given their important implications.

Myotonic Dystrophy Type I Myotonic dystrophy type 1 (DM1), the most prevalent form of muscular dystrophy in adults, is caused by expansion of the CTG repeat in the 3′ untranslated region of DMPK, a protein kinase on chromosome 19q13.3 (Brook et al. 1992). Aberrant splicing of *MYH14,* also located on chromosome 19q13.3, has been observed in patients with DM1, suggesting that alterations of the *MYH14* gene could contribute to the pathogenesis of DM1 (Rinaldi et al. 2012).

12.4 Myosin III

Myosin III proteins are expressed predominantly in sensory cells where they localize to retinal photoreceptors in the eye and stereocilia on the hair cells of the inner ear (Dose et al. 2003; Schneider et al. 2006). Vertebrates express two genes coding for myosin 3: *Myo3a* codes for an N-terminal kinase domain followed by a motor domain, a neck region containing 2–4 IQ motifs, and a tail region containing two IQ motifs and two conserved domains 3THDI, which binds espin-1, and 3THDII, which binds actin; whereas *Myo3b* codes for a shorter molecule containing a kinase domain followed by a motor domain, neck domain with 2–3 IQ motifs, and tail region containing 3THDI (Dosé et al. 2008; Salles et al. 2009). There is no coiled-coil domain in the tail region suggesting that MYO3A is monomeric (Kambara et al. 2006). MYO3A is a high duty ratio motor (Kambara et al. 2006). Autophosphorylation of MYO3A significantly increases the probability of MYO3A dissociating from actin (Komaba et al. 2010).

Hearing Defects First identified in *Drosophila* as the gene (*ninaC*) responsible for the formation and function of photoreceptors in the eye (Montell and Rubin 1988), mutations in *MYO3* were subsequently associated with progressive nonsyndromic hearing loss (DFNB30) in an extended Israeli family (Walsh et al. 2002). A mouse model of DFNB30, $Myo3a^{KI/KI}$, carrying a nonsense mutation (Tyr1041X) equivalent to the nonsense allele (Tyr1042X) responsible for the most severe human phenotype was subsequently generated (Walsh et al. 2011). Hair cell degeneration and hearing loss in these mice progress with age, consistent with the phenotype of human DFNB30 (Walsh et al. 2011), and excellent support for the idea that mutations in MYO3A are responsible for hearing defects. Recently, a mutation in the motor domain of MYO3A protein (Leu697Trp) identified by whole-exome sequencing of samples from members of two unrelated families with autosomal dominant hearing loss and confirmed in 36 affected individuals was shown to lead to a reduction in ATPase activity and motil-

ity and an increase in actin affinity (Dantas et al. 2018). The authors suggest that the mutant molecule may act as a dominant negative and displace the wild-type protein.

In both outer and inner hair cells, MYO3A and MYO3B localize to the tips of stereocilia in a tip-to base gradient (Schneider et al. 2006; Merritt et al. 2012). Overexpression in COS7 cells of MYO3A but not MYO3B, induced the formation of filopodia (Merritt et al. 2012; Ebrahim et al. 2016). MYO3A and MYO3B presumably support the elongation of stereocilia by transporting the actin-bundling protein espin-1 to the plus ends of actin filaments (Salles et al. 2009; Merritt et al. 2012). When co-expressed in COS-7 cells with espin-1, MYO3A and MYO3B both produce longer filopodia than observed with expression of the motor domain only (Merritt et al. 2012; Ebrahim et al. 2016). Importantly, espin-1 is necessary for the normal staircase appearance of stereocilia (Ebrahim et al. 2016). The espin-1 paralog espin-like (ESPNL), which is found in developing stereocilia, is also transported by myosin III (Ebrahim et al. 2016).

Two actin-binding sites, one in the motor domain and one in the tail domain, are required for MYO3A's localization at filopodial tips (Les Erickson et al. 2003); however, MYO3B lacks an actin-binding site in the tail, yet its distribution in the hair bundle resembles that of MYO3A (Merritt et al. 2012). Apparently, MYO3B uses an actin-binding site in its espin-1 cargo to reach the tips of actin protrusions (Merritt et al. 2012). The stereocilia on the hair cells of mice lacking MYO3A and MYO3B are unusually tall and ungraded and the mice are profoundly deaf, whereas mice lacking MYO3B and losing MYO3A postnatally have normal hearing (Lelli et al. 2016). The results suggest that the two isoforms play redundant roles during early cochlear development by limiting the elongation of stereocilia but are not required for the formation of mature bundles (Lelli et al. 2016). In contract to studies in COS7 cells implicating myosin III in the transport of espin to the tips of filopodia, espin localizes at the tips of stereocilia from *Myo3a*$^{-/-}$*Myo3b*$^{-/-}$ mice (Lelli et al. 2016).

Whole-exome sequencing of genomic DNA from members of a family with post-lingual progressive nonsyndromic hearing loss identified the cause as a mutation (G488E) in the highly conserved switch-1 region of the motor domain of MYO3A (Grati et al. 2016). The mutant fails to accumulate at the tips of filopodia when expressed in COS7 cells but localizes at the tips of stereocilia in inner ear organ culture. One idea is that the mutant myosin can affect the position of the mechanoelectrical transduction (MET) complex which resides at the tips of stereocilia. In the hair cells of the inner ear, neighboring stereocilia are connected by fine filaments called tip links, which extend from the tip of each stereocilium to the side of its tallest neighbor (Pickles et al. 1984). Deflection of stereocilia in response to sound and pressure applies tension on the tip links opening mechanosensitive channels located at the lower end of each tip link and initiating auditory and vestibular perception (Assad et al. 1991; Beurg et al. 2009). MYO3A was found to interact with an isoform of protocadherin-15, a component of tip-link filaments (Pepermans et al. 2014; Grati et al. 2016). The authors suggest that the accumulation of mutant MYO3A at the tips of stereocilia could cause MET dysfunction (Grati et al. 2016).

Other In addition to sensory cells in the eye and ear, myosins III are expressed in lower levels in other tissues including brain (especially the olfactory bulb), pancreas, and intestine (Dosé et al. 2008; Katti et al. 2009). Modifications of the *MYO3A* gene have been associated with bladder cancer (Chung et al. 2011), colorectal cancer (Lascorz et al. 2010), and anxiety disorders (Unschuld et al. 2009)

12.5 Myosin V

Myosins V are double-headed motors that mediate membrane trafficking (Prekeris and Terrian 1997; Lapierre et al. 2001; Hales et al. 2002; Desnos et al. 2007; Swiatecka-Urban et al. 2007; Jacobs et al. 2009; Brozzi et al. 2012; Lombardo et al. 2017). Three myosins V, MYO5A, MYO5B,

and MYO5C, are expressed in almost all human cells (Rodriguez and Cheney 2002). The MYO5 heavy chain consists of a motor domain with ATP- and actin-binding sites, a neck region consisting of 6 IQ domains that bind calmodulin, a coiled-coil region that can dimerize, and a globular tail domain (GTD), which serves as an inhibitory domain that interacts with the head domain to regulate motor activity and is also involved in cargo binding (Mercer et al. 1991; Rodriguez and Cheney 2002; Wei et al. 2013; Zhang et al. 2016a). MYO5 assumes a compact, inactive conformation in the absence of Ca^{2+} and an active, extended conformation in the presence of Ca^{2+} (Wang et al. 2004). Most of the disease-causing mutations in MYO5 inhibit the folding of the GTD and thus impair proper function of MYO5 (Wei et al. 2013).

MYO5A (Mehta et al. 1999; Yildiz et al. 2003; Sakamoto et al. 2008) and to a lesser degree MYO5B (Heissler et al. 2017) are processive, i.e., they take multiple steps on an actin filament without detaching, whereas MYO5C is nonprocessive (Takagi et al. 2008). MYO5 walks in a coordinated hand-over-hand movement along actin filaments as observed with high-speed atomic force microscopy (Kodera et al. 2010). The activity of the two heads of a single MYO5 molecule are coordinated so that at least one head is always attached to an actin filament. Attachment of both heads to actin puts intramolecular strain on the leading head and inhibits its release of ADP so that the leading head stays attached to the filament while the trailing head detaches and rebinds at the front (Purcell et al. 2005; Veigel et al. 2005). This cycle is repeated over and over again. MYO5's long and relatively stiff neck region allows MYO5 to generate 36-nm steps, the same size as the actin helical repeat (Shiroguchi and Kinosita 2007).

MYO5A is expressed in high levels in brain and melanocytes, whereas MYO5B and MYO5C are more broadly expressed in non-neuronal cells with MYO5B abundant in kidney, liver, and placenta and MYO5C expressed in epithelial and glandular tissues like stomach, colon, pancreas, and lung as well as salivary, thyroid, prostate, and mammary glands (Rodriguez and Cheney 2002). All three isoforms interact through their tail regions with the Rab GTPases Rab10 and Rab8a, and MYO5A and MYO5B can bind to Rab 11 family members (Roland et al. 2007, 2009). Rab8a and Rab11a bind directly to MYO5B on recycling vesicles (Roland et al. 2011). It is estimated that >100 Myo5 molecules cluster on the surface of a vesicle to support vesicle movement along actin filaments (Miller and Sheetz 2000).

Defects in MYO5 lead to neurological defects, intestinal defects, cholestasis and cancer.

Griscelli Syndrome MYO5A was first identified as the gene whose defect is responsible for the *dilute* coat color in mice (Mercer et al. 1991). Mice carrying a mutation in the *dilute* gene have a light coat color due to the uneven distribution of pigment granules in developing hair shafts (Russell 1949), a consequence of reduced MYO5A-mediated melanosome transport in melanocytes (Provance et al. 1996), and they exhibit a neurological defect (Mercer et al. 1991). In humans, mutations in MYO5A lead to Griscelli syndrome, a rare autosomal recessive disorder characterized by diffuse skin pigmentation, silvery hair, an accumulation of melanosomes in melanocytes, and neurological defects that can include seizures and intellectual disabilities (Griscelli et al. 1978; Pastural et al. 1997; Anikster et al. 2002)

In melanocytes MYO5A transports melanosomes to the cell periphery along actin filaments by binding to the adaptor protein melanophilin and Rab27a (Strom et al. 2002; Wu et al. 2002). Defects in MYO5A thus result in the hypopigmentation observed in patients with Griscelli syndrome. MYO5A facilitates the transport of endoplasmic reticulum (Dekker-Ohno et al. 1996; Wagner et al. 2011) and mRNA-protein complexes (Yoshimura et al. 2006) into dendritic spines and mediates filopodia formation in neuronal growth cones (Wang et al. 1996), which may explain why mutations in MYO5A result in neurological defects.

Mutations in Rab27a lead to a second form of Griscelli syndrome (type 2), which is not associated with neurological defects but is associated with a severe immune disorder (Griscelli et al.

1978; Pastural et al. 1997; Anikster et al. 2002). The pigmentation defects in this second form of Griscelli syndrome are explained by defective melanosome transport (Hume et al. 2001; Wu et al. 2001). In the immune system Rab27 plays a role in cytotoxic T lymphocytes. Cytolytic granules are unable to fuse with the plasma membrane and to kill target cells in cytotoxic T lymphocytes from Griscelli syndrome type 2 patients (Haddad et al. 2001; Stinchcombe et al. 2001), which may be responsible for the immunological defects seen in these patients.

Microvillous Inclusion Disease (MVID) MVID is a rare but fatal congenital disorder leading to persistent diarrhea in newborns (Muller et al. 2008). The name MVID stems from the fact that the surface of intestinal enterocytes of affected individuals lack microvilli and exhibit secretory-like granules and vacuolar structures containing microvilli (Muller et al. 2008). Multiple mutations in MYO5B have been associated with MVID (Muller et al. 2008; Ruemmele et al. 2010; Szperl et al. 2011). The 62 mutations so far associated with MVID include large deletions, single nucleotide deletions, missense mutations, nonsense mutations, splicing mutations, and compound heterozygous mutations (Szperl et al. 2011; Dhekne et al. 2018). They are found in both the MYO5B motor domain, which contains the ATP-binding site and the actin-binding site, and the C-terminal tail, which is involved in cargo binding (Muller et al. 2008; Ruemmele et al. 2010; Dhekne et al. 2014; Knowles et al. 2014). In particular, a mutation in the MYO5B motor domain that is associated with MVID (Pro660Leu) is found in Navajo populations (Erickson et al. 2008). Mutations in the motor domain that are associated with MVID likely affect processivity or protein folding and stability (Heissler et al. 2017).

Depletion of MYO5B by RNA interference in cultured intestinal CaCo2 cells reproduces several of the disease phenotypes including loss of apical microvilli and the presence of large vacuoles lined by microvilli and subapical clusters of vesicles resembling secretory vesicles (Ruemmele et al. 2010). MYO5B-depleted CaCo2 cells have a modified distribution of endosomal and lysosomal markers and a disruption in cell polarity as evidenced by mislocalization of apical and basolateral transporters (Ruemmele et al. 2010; Thoeni et al. 2014). Studies of duodenal biopsy specimens from MVID patients show that the apical localization of several transporters including sodium hydrogen exchanger isoform 3 (NHE3; SLC9A3), sodium glucose cotransporter 1 (SGLT1; SLC5A1), and aquaporin water channel 7 (AQP7) is lost in intestinal cells, which may contribute to the severe diarrhea experienced by these patients (Engevik et al. 2018).

Tight junction integrity is affected by MYO5B depletion in cultured CaCo2-BBE cells and enterocytes from Navajo patients with MVID (Knowles et al. 2014). MYO5B mislocalizes and the normal accumulation of recycling endosomes positive for Rab11a and the Rab11a effector FIP5 in the apical cytoplasm of the cells is abolished in MVID enterocytes (Szperl et al. 2011). These data suggest that the defect is due to faulty trafficking from the apical recycling endosomal compartment to the apical membrane, which is regulated by MYO5B (Ameen and Salas 2000; Weisz and Rodriguez-Boulan 2009). Curiously, depletion of MYO5B in CaCo2-BBE cells, which are more polarized than the parental CaCo2 cells, does not lead to the formation of microvillous inclusions although rescue of MYO5B-depleted CaCo2-BBE cells with MYO5B P660L induced microvillous inclusions (Knowles et al. 2014). Interestingly, rescue experiments performed with CaCo2-BBE cells show that microvilli establishment requires the interaction of MYO5B with Rab8a, whereas loss of the MYO5B and Rab11a interaction results in the formation of microvillous inclusions (Knowles et al. 2014).

Recent mouse models of human MVID have been developed. Intestine-specific conditional *Myo5b*-deficient mouse models develop severe diarrhea shortly after tamoxifen treatment, and the enterocytes show reduced numbers of microvilli, microvillar inclusions, and subapical secretory granules, thus recapitulating the intestinal phenotype of human MVID (Carton-Garcia et al. 2015; Schneeberger et al. 2015). Apical trans-

porters (NHE3, SGLT1; and AQP7) and enzymes such as sucrase isomaltase and alkaline phosphatase are lost from the apical membranes of intestinal cells from *Myo5b*-null mice, consistent with studies in MVID patients (Engevik et al. 2018). These mouse models are expected to have an impact on understanding the molecular mechanism of this disease and the development of therapies.

Mutations in two other genes, syntaxin binding protein-2 (STXBP2) and syntaxin-3 (STX3), two proteins associated with the membrane fusion machinery, are also associated with MVID (Stepensky et al. 2013; Vogel et al. 2015; Dhekne et al. 2018). The overlap in symptoms among patients with MYO5B, STXBP2, and STX3 mutations suggest that these three proteins may cooperate to regulate protein trafficking to the apical brush border of enterocytes and exocytosis (Stepensky et al. 2013; Vogel et al. 2015).

One unresolved question is why defects in MYO5B, which as noted above is broadly expressed, lead to enterocyte-specific effects and not more global effects. One possibility is that loss or mutation of MYO5B is compensated for by the expression of MYO5A, which also binds to Rab8 and Rab11 (Roland et al. 2009; Knowles et al. 2014); however, MYO5A is unable to rescue MYO5B-depleted CaCo2-BBE cells. Another possibility is that trafficking in one polarized cell type is distinct from that of other cell types (Knowles et al. 2014).

Cancer Upregulation of MYO5A expression has been linked to cancer cell migration and metastasis. MYO5A expression is high in a number of human cancer cell lines including those derived from lung, colon, breast, and prostate, with the more highly metastatic cell lines containing higher levels of MYO5A than less metastatic cell lines (Lan et al. 2010). Similarly, metastatic colorectal cancer tissues have higher mRNA levels of *MYO5A* than nonmetastatic cancers suggesting a role for MYO5A in metastasis. MYO5A may promote tumor cell invasion. In cancer cell lines, the expression pattern of MYO5A mimics that of the transcriptional repressor Snail, which triggers epithelial-mesenchymal transition (Lan et al. 2010). Snail binds and activates the MYO5A promoter, and expression of MYO5A is reduced in Snail-depleted lung cancer A549 cells (Lan et al. 2010). In addition, MYO5A binds Bcl-xL, an anti-apoptotic protein that promotes invasion and metastasis (Du et al. 2007).

The disruption of cell polarity observed in intestinal cells with mutations in MYO5B (Muller et al. 2008) suggests that MYO5B may play a role in tumorigenesis as mammalian epithelial tissues lose polarity as they become malignant (Royer and Lu 2011). Histological examination of 70 normal and gastric cancer tissue samples showed that MYO5B expression is downregulated in gastric carcinomas vs. normal gastric tissues (Dong et al. 2012). Reduced expression correlated with nodal metastasis and cancer differentiation (Dong et al. 2012). In addition, reduced expression of MYO5B in AGS gastric cancer cells, which express MYO5B, causes the cells to become more invasive *in vitro* suggesting that MYO5B promotes cell migration (Dong et al. 2012). Further analysis showed that MYO5B is epigenetically silenced in gastric cancer cells by DNA methylation and histone modification (Dong et al. 2013).

Reduced MYO5B expression also correlates with shorter survival rates for colorectal cancer patients (Letellier et al. 2017). MYO5B is an effector of the Rab GTPases Rab8a, Rab10, and Rab11a, each of which is involved in regulating the recycling of proteins to the plasma membrane (Correia et al. 2008; Roland et al. 2007, 2009). Studies indicate that the gene expression signature of MYO5B or MYO5B and RAB8A may serve as a potential prognostic marker in colorectal cancer (Letellier et al. 2017).

An increase in MYO5C expression was identified in subtypes of pediatric acute lymphoblastic leukemia (ALL) by gene expression profiling; however, confirming and identifying a role for MYO5C in ALL awaits further investigation.

Cholestasis Recently, mutations in MYO5B have been associated with low gamma-glutamyltransferase cholestasis (Gonzales et al. 2016; Qiu et al. 2017). Liver samples taken by

biopsy showed an abnormal distribution of the bile salt export pump (BSEP) at canaliculi and a course granular dislocation of MYO5B, and the levels of total bile salts in the plasma were increased as observed in BSEP-deficient patients (Qiu et al. 2017). That the reduced bile secretion is likely a consequence of improper intracellular trafficking of BSEP to bile canaliculi is supported by *in vitro* studies. In polarized hepatic epithelial (WIF-B) cells, Rab11a and MYO5B are responsible for the trafficking of apical ATP-binding cassette (ABC) transporters like BSEP to the apical membrane to form bile canaliculi (Wakabayashi et al. 2005). Thus, MYO5B mutations may lead to cholestasis. Some patients with MVID also present with cholestasis (Girard et al. 2014).

12.6 Myosin VI

Myosin VI (MYO6) is the only myosin that moves toward the minus end of actin filaments (Wells et al. 1999). The MYO6 motor domain has two unique inserts: a 22-amino acid insert by the nucleotide-binding site near switch-1 that alters the rate of nucleotide association and dissociation and may be necessary for anchoring under high loads (Sweeney et al. 2007) and a 53-amino acids located between the converter region and the IQ region that binds calmodulin and redirects the lever arm to enable the motor to move toward the minus end of actin filaments (Wells et al. 1999; Menetrey et al. 2005; Menetrey et al. 2007). Indeed, removal of insert 2 causes MYO6 to move to the plus end of actin filaments (Bryant et al. 2007; Park et al. 2007).

Whether MYO6 exists as a monomer or dimer has been the subject of much debate. MYO6 purifies from cells as a monomer (Lister et al. 2004) and may serve in that state as an anchor (Altman et al. 2004). Upon cargo binding MYO6 dimerizes (Yu et al. 2009) and becomes a processive motor (Park et al. 2006). For processive movement the two heads of dimeric myosins must be coordinated so that the lead head stays bound to actin while the trail head is moving. The prevailing model is that MYO6 walks along actin by blocking ATP binding to the lead head (Sweeney et al. 2007; Pylypenko et al. 2011).

MYO6 has a short lever arm with one canonical IQ domain, but single molecules of dimeric MYO6 take large steps of 30–36 nm (Rock et al. 2001; Nishikawa et al. 2002). Evidently, cargo binding mediated by the C-terminus triggers dimerization of MYO6 and unfolding of a three-helix bundle in the proximal tail region that serves as a lever arm extension to support MYO6's large step size (Mukherjea et al. 2009). A single alpha helix (SAH) domain located in the N-terminal tail region may also contribute to the length of the lever arm (Spudich and Sivaramakrishnan 2010; Sweeney and Houdusse 2010). In addition to a PIP_2-binding motif (Spudich et al. 2007), the tail region of MYO6 contains a large insert before the CBD and a small insert in the CBD that generate alternatively spliced isoforms containing no insert, the large insert, the small insert, or both inserts (Buss et al. 2001; Dance et al. 2004). Isoforms containing the large insert are specifically found in polarized epithelia with apical microvilli and are targeted to clathrin-coated structures (Buss et al. 2001; Au et al. 2007; Wollscheid et al. 2016).

Recent structural evidence indicates that Ca^{2+} binding to calmodulin regulates MYO6 activity (Batters et al. 2016). In low Ca^{2+}, apo-calmodulin binds to both the IQ motif and a part of the cargo-binding domain (CBD) keeping MYO6 in an inactive form. High Ca^{2+} induces a major conformational change in calmodulin that releases the tail and increases lipid cargo binding. Importantly, although "primed" to bind cargo, MYO6 is not motile in the presence of Ca^{2+}, a likely consequence of a more flexible lever arm due to a conformational change in the second calmodulin. Presumably, a subsequent increase in Ca^{2+} would then be needed to effect motility. MYO6 regulation differs from that of myosin V where the CBD interacts with the head rather than the IQ domain (Liu et al. 2006; Thirumurugan et al. 2006).

MYO6 is involved in multiple functions including vesicle trafficking (Buss et al. 1998, 2001; Aschenbrenner et al. 2004; Bond et al. 2011; Tomatis et al. 2013), maintenance of Golgi morphology (Buss et al. 1998; Warner et al.

2003), and cell motility (Yoshida et al. 2004; Dunn et al. 2006), and multiple binding partners have been identified including the Golgi-associated protein optineurin (Sahlender et al. 2005), the adaptor protein Dab2 (Morris et al. 2002), the adaptor protein GAIP interacting protein C terminus (GIPC/synectin) (Naccache et al. 2006), and nuclear dot protein 52 (NDP52) (Morriswood et al. 2007), which shares 70% sequence identity with the transcription coactivator CoCoA (Yang et al. 2006). Binding is through the RRL or WWY motifs in the tail region (Tumbarello et al. 2013). Recently, a proximity labelling-based proteomics strategy identified MYO6 as a novel interactor with the LIFT (LARG-Induced F-actin for Tethering) complex, which controls endosome dynamics, and the DISP (DOCK7-Induced Septin disPlacement) complex, a regulator of the septin cytoskeleton (O'Loughlin et al. 2018).

Defects in MYO6 lead to cardiomyopathy, deafness, and cancer.

Familial Hypertrophic Cardiomyopathy As discussed above, although most familial cardiomyopathies are caused by mutations in sarcomeric proteins including the *MYH7* gene product, a missense mutation (His246Arg) in the motor domain of MYO6 has been linked to mild cardiac hypertrophy in a kindred with autosomal dominant sensorineural hearing loss (Mohiddin et al. 2004). Snell's waltzer mice also exhibit left ventricular hypertrophy (Hegan et al. 2015b).

Auditory and Vestibular Defects MYO6 is expressed at the base of the stereocilia on the hair cells of the sensory epithelium of the inner ear, on vesicles in the pericuticular necklace, an area of presumed membrane trafficking, and between the stereociliary membrane and the core bundle of actin filaments (Hasson et al. 1997; Rzadzinska et al. 2004). Missense, nonsense, splicing, and overexpression mutations including a Cys442Tyr mutation in a conserved cysteine residue in the MYO6 motor domain identified in an Italian family (Melchionda et al. 2001) and a nonsense mutation in MYO6 in a Brazilian family (Sampaio-Silva et al. 2018) are associated with autosomal dominant nonsyndromic hearing loss in humans, DFNA22.

Much of what is known regarding MYO6 function in the ear comes from mouse models. The *Myo6*-deficient Snell's waltzer (*sv*) mouse, which carries a spontaneous recessive mutation causing MYO6 deficiency by frameshift mutation, exhibits head tossing, circling, hyperactivity, and deafness due to degeneration of the sensory epithelium of the inner ear including the loss of inner and outer hair cells and supporting cells (Avraham et al. 1995). In neonatal *sv/sv* mice, the plasma membrane is detached from the base of stereociliary actin bundles resulting in fused stereocilia likely because the stereociliary membrane is not attached to the actin-rich cuticular plate in the absence of MYO6 (Self et al. 1999).

The stereocilia on the hair cells of the hearing- and balance-deficient tailchaser mouse, which carries a D179Y mutation in the transducer region of MYO6, are fused at the base and branched (Hertzano et al. 2008). The mutation prevents initiation of processive runs by allowing premature release of Pi from the head that is not attached to actin (Pylypenko et al. 2015). The impaired motor function, which affects MYO6 processivity, presumably results in the accumulation of MYO6 at the tips of stereocilia and the inability to transport cargo or to anchor the membrane of stereocilia to the core bundle of actin filaments.

Cancer MYO6 is implicated in intracellular trafficking and cell migration, and defects in these processes are linked to disease including cancer. Upregulation of MYO6 has been observed in human cancerous prostate specimens and breast cancer tissues using microarray analysis (Su et al. 2001). Curiously, although the most aggressive ovarian cancers exhibited the highest levels of MYO6 expression (Yoshida et al. 2004), the highest MYO6 expression levels were found in samples of prostate cancers of medium grade (Dunn et al. 2006). In a mouse model, reduced expression of MYO6 decreased metastasis of ovarian carcinoma cells inoculated intraperitoneally into nude mice (Yoshida et al. 2004). MYO6

depletion in LNCaP human prostate cancer cells impairs *in vitro* migration and soft-agar colony formation (Dunn et al. 2006), and reduced expression of MYO6 in two breast cancer cell lines inhibits cell viability and colony formation (Wang et al. 2015). Knockdown of *MYO6* expression also suppresses proliferation of melanoma cells *in vitro* (Li et al. 2015) consistent with the idea of MYO6 as a tumor promoter. MYO6 is also overexpressed in tongue squamous cell carcinoma, and reduced expression of *MYO6* in the human oral squamous cell carcinoma cell line CAL27 cells decreases cell proliferation and increases apoptosis suggesting that MYO6 promotes oral squamous cell carcinoma (Zhang et al. 2016b).

Several cancers express only the MYO6 non-insert splice form (Wollscheid et al. 2016), which localizes throughout the nucleus (Fili et al. 2017). In association with DNA and RNA polymerase II, MYO6 mediates transcription (Vreugde et al. 2006). MYO6 interacts with the androgen receptor (Loikkanen et al. 2009) and the estrogen receptor through a LxxLL nuclear receptor binding motif in the C-terminus (Fili et al. 2017). Evidently, MYO6 gets activated by NDP52, which unfolds MYO6 and enables recruitment of RNA polymerase II through actin (Fili et al. 2017). In support of this idea, estradiol-mediated promoter activity is significantly reduced in *MYO6*-depleted MCF-7 cells (Fili et al. 2017). The studies suggest a link between MYO6 and the regulation of hormone receptors.

Infectious Disease For the intestinal pathogen *Salmonella* to enter enterocytes, the bacteria must first inject into the cell a number of effector molecules that reorganize the actin cytoskeleton and induce membrane ruffling to support pathogen entry by macropinocytosis. The effector molecule SopE, a Rac1 and Cdc42 GEF, is critical for formation of membrane ruffles and uptake of the bacteria. Studies indicate that SopE activates RhoGTPases that recruit MYO6 to the membrane via PAK where it triggers PI3K signaling and the recruitment of PI(3)P-binding proteins that promote *Salmonella* uptake by marcopinocytosis (Brooks et al. 2017). Whether *MYO6* variants are associated with variable sensitivities to *Salmonella* infection, or whether myosin inhibitors can be used to fight bacterial infections is unknown.

12.7 Myosin VII

Two MYO7 isoforms are expressed in humans: a 250 kDa transcript called MYO7A and a shorter 240.8 kDa transcript called MYO7B (Bement et al. 1994a; Hasson et al. 1995). MYO7A contains a motor domain, a 5 IQ neck domain, a single α-helix domain, a myosin tail homology 4 (MyTH4) domain, and a protein 4.1, ezrin, radixin, moesin (FERM) domain followed by an SH3 domain and another MYTH4 and FERM domain (Chen et al. 1996). MYO7B lacks the SAH domain that follows the IQ domains in MYO7A (Chen et al. 2001b).

Monomeric MYO7A is a slow, high-duty ratio motor, well suited to serve as a transporter (Haithcock et al. 2011). Studies with *Drosophila* Myo7a indicate that in low Ca^{2+} the molecule folds back on itself so that the motor domain binds to the head-neck region thereby inhibiting motor activity (Umeki et al. 2009). Although a monomer *in vitro*, MYO7A dimerizes in the presence of its cargo molecule MyRip, (myosin-VIIa- and Rab-interacting protein) a Rab effector (El-Amraoui et al. 2002) that facilitates its interaction with vesicles, and can then move processively along actin filaments (Sakai et al. 2011). MYO7A is expressed in a variety of tissues although expression is highest in the testes, cochlea, and retina (Hasson et al. 1995). Mutations in MYO7A lead to Usher syndrome, a recessive genetic disorder characterized by deafness and progressive retinal degeneration, as well as nonsyndromic hearing loss, and cancer.

Purified MYO7B has a low basal ATPase activity that is activated by low concentrations of actin filaments. Its slow rate of ADP release means that it stays strongly bound to actin making it well suited to generate tension and to anchor membrane receptors to actin filaments (Henn and De La Cruz 2005). MYO7B is expressed primarily in the distal tips of apical

microvilli on intestinal and renal epithelial cells (Chen et al. 2001b). A complex of MYO7B, the actin-bundling protein harmonin, and the adaptor protein ankyrin repeat and SAM domain-containing protein 4B (ANKS4B) connects the actin bundles in microvilli with cadherins, which link adjacent microvilli (Li et al. 2016; Yu et al. 2017). Adhesion between the distal tips of microvilli is important for organizing the tight packing of microvilli (Crawley et al. 2014). Although perturbations in brush border structure and microvillar density lead to malabsorption and diarrhea (Khubchandani et al. 2011; Schneeberger et al. 2018), no direct link between mutations in MYO7B and disease has been identified.

Usher Syndrome 1B: Hearing Defects Hair cells on the sensory epithelia of the inner ear are responsible for hearing (cochlea) and balance (vestibular organs). On the apical surface of hair cells are hair bundles consisting of multiple well-organized actin-based stereocilia arranged by height. Extracellular tip links comprised of cadherin 23 and protocadherin 15, connect the side of the taller stereocilia, designated as the upper tip link density, to the tip of its neighboring shorter stereocilium (lower tip link density). In response to sound, movement or gravity, the hair bundles deflect toward the tallest stereocilia, which exerts tension on the tip links opening mechanotransduction channels located at the lower tip link density (Gillespie and Muller 2009; Kazmierczak and Muller 2012; Pan et al. 2018).

MYO7B is found in the hair bundles and cytoplasm of the sensory cells of the inner ear (Hasson et al. 1995; Lefevre et al. 2008; Grati and Kachar 2011). Mutations in the head and tail regions of MYO7A result in Usher syndrome 1B (USH1B), an autosomal recessive disorder with sensory impairment (Weil et al. 1995; Jacobson et al. 2011). Patients are borne deaf, have vestibular dysfunction, and develop progressive retinal degeneration leading to blindness (Smith et al. 1994). The genes, *USH1C* (harmonin) (Verpy et al. 2000), *CDH23* (cadherin 23) (Bolz et al. 2001; Bork et al. 2001), *PCDH15* (protocadherin 15) (Alagramam et al. 2001; Ahmed et al. 2006), *USH1G* (sans, scaffold protein containing ankyrin repeats and sam domain) (Weil et al. 2003), and *CIB2* (calcium- and integrin-binding protein 2) (Riazuddin et al. 2012), are also associated with Usher syndrome. A missense mutation in MYO7B, Arg502Pro, in a conserved actin-binding region of the motor domain called the activation loop (Varkuti et al. 2012) severely reduces motor activity (Xiong et al. 2018) and leads to recessive deafness in shaker-1 mice (Gibson et al. 1995). Shaker-1 homozygous mice exhibit hyperactivity, head tossing and circling due to vestibular defects (Gibson et al. 1995).

Insight into how mutations in MYO7A result in hearing and balance defects comes from the shaker-1 and other mouse models. During early development the hair bundles on the sensory cells of the cochlear and vestibular organs of USH1 mouse mutants are severely disorganized and fragmented, and the lateral links that connect stereocilia to each other along their shaft are sparse vs. wild-type mice (Boeda et al. 2002; Lefevre et al. 2008). At later stages of development stereocilia elongation and apical tip defects are observed (Lefevre et al. 2008). In $Myo7^{I487N/I487N}$ *ewaso* mice, which also have a mutation in the MYO7A motor domain and experience profound hearing loss and vestibular dysfunction including circling and star-gazing behavior, the outer hair cells of the cochlea degenerate, and the hair cells of the vestibular sensory epithelium have a highly disrupted staircase morphology (Miller et al. 2012).

In the mouse inner ear MYO7A localizes in stereocilia with its interacting protein sans at the upper tip link density along with the F-actin-bundling protein harmonin b (Boeda et al. 2002; El-Amraoui and Petit 2005; Grati and Kachar 2011). This complex is thought to anchor cadherin 23, a component of the tip links, to the actin filaments in the stereocilia and to exert tension on the tip link during mechanotransduction regulating transduction channels. Thus, mutations in *Myo7a* and other Usher genes would lead to defects in mechanotransduction. In support of this idea, studies with two mouse models for USH1 with defects in *Myo7a* show increased current, decreased sensitivity, and abnormal adaptation (Kros et al. 2002). Cochlear implantation at

an early age is common treatment for USH patients (Broomfield et al. 2013; Jatana et al. 2013). For further insight into the role of MYO7A in hearing, see (Cosgrove and Zallocchi 2014; Mathur and Yang 2015) and Chap. 13 by Friedman et al.

Usher Syndrome 1B: Vision Defects The outer retina of the eye consists of retinal pigment epithelial (RPE) cells and photoreceptors, ciliated cells whose outer segments are packed with membrane disks containing photopigments required for phototransduction. Rhodopsin is the photopigment for rods, photoreceptors that respond to very low light. Photopigments contain opsins, membrane-bound proteins that bind the chromophore retinal. The outer segment of photoreceptors is constantly being renewed with new disks added at the proximal end and old disks being shed at the distal end, which is in contact with RPE cells. The RPE cells phagocytose the outer segment disks and are involved in the regeneration of visual pigments. RPE cells are rich in melanosomes, which contain melanin, a pigment that reduces backscattered light and removes free radicals formed during phagocytosis of photoreceptor outer segments (Boulton and Dayhaw-Barker 2001; Strauss 2005).

MYO7A is expressed in the RPE and photoreceptor cells (El-Amraoui et al. 1996; Liu et al. 1999), and it participates in several events including (i) the transport of melanosomes into apical processes within the RPE (Liu et al. 1998), (ii) the normal phagocytosis of rod outer segment disks by the RPE (Gibbs et al. 2003), and (iii) opsin transport through the photoreceptor cilium (Liu et al. 1999) via an interaction with spectrin βV, which binds rhodopsin and the microtubule motors kinesin and dynein (Papal et al. 2013). Association of MYO7A with melanosomes is through the C-terminal FERM domain (Schwander et al. 2009).

An obvious defect in the retinas of shaker-1 mice is the mislocalization of melanosomes, which in the RPE do not extend into the apical processes that surround the tips of the photoreceptor outer segments as observed in wild-type animals (Liu et al. 1998). Evidently, MYO7A mediates melanosome trafficking by forming a complex with MyRip and Rab27a (Lopes et al. 2007; Sakai et al. 2011; Williams and Lopes 2011). Although shaker-1 mice housed under light intensities normally found in vivaria do not develop photoreceptor degeneration, in shaker-1 mice carrying the *Myo7a*$^{sh1\text{-}11J}$ allele, moderate light induces significant rod photoreceptor degeneration, a consequence of defective light-induced translocation from the outer to the inner segments of photoreceptors of the heterodimeric G-protein transducin, which mediates light/dark adaptation (Peng et al. 2011). This finding is in contrast to studies showing that the shaker-1 *Myo7*$^{ash1\text{-}4626SB}$ mouse has a lower amount of the retinoid isomerase RPE65 and thus protection from acute light damage (Lopes et al. 2011). In mice, MYO7B expression at wild-type levels was achieved in retinas *in vivo* using lentiviral-mediated gene transfer resulting in normal apical localization of melanosomes in RPE cells and distribution of opsin in photoreceptor cells (Hashimoto et al. 2007). These and other studies suggest the possibility of improving retinal activity by viral-mediated delivery of MYO7A in humans (Colella et al. 2013; Lopes and Williams 2015).

Nonsyndromic Deafness In addition to syndromic conditions such as Usher syndrome, mutations in MYO7A can cause dominant (DFNA11) (Liu et al. 1997b; Luijendijk et al. 2004) and recessive (DFNB2) (Liu et al. 1997a; Riazuddin et al. 2008) non-syndromic hearing loss. *Myo7a*$^{F947I/F947I}$ *dumbo* mice, which have a mutation between the coiled-coil region and the first MyTH4 domain in the C-terminus of MYO7A, have less hearing loss than *Myo7*$^{I487N/I487N}$ *ewaso* mice and no obvious vestibular dysfunction (Miller et al. 2012). The hair cells in the cochlea are disrupted but less than that of *Myo7*$^{I487N/I487N}$ *ewaso* mice, and the arrangement of vestibular hair bundles is only mildly affected. The *Myo7a*$^{F947I/F947I}$ *dumbo* mice may represent a possible mouse model for DFNB2 in humans. In transfected hair cells, MYO7A mutants associated with USH1B do not localize to stereocilia, whereas those associated with DFNB2 localize

correctly in the hair bundles (Riazuddin et al. 2008). Therefore, the DFNB2 mutants may retain some of their function and are thus associated with a milder phenotype (Riazuddin et al. 2008).

Cancer Recent evidence implicates MYO7A in the progression of melanoma (Liu et al. 2018b). MYO7A variant S1666C was found to be associated with an increased risk of malignant melanoma (Fernandez et al. 2009). Later studies show that MYO7A is highly expressed in mouse B16 melanoma cells, and *MYO7A* depletion inhibits colony formation in cultured B16 cells and also reduces tumor growth in a mouse xenograft model (Liu et al. 2018b).

12.8 Myosin IX

Two class IX myosins are expressed in mammals: MYO9A and MYO9B (previously known as myr7 and myr5, respectively). Class 9 myosins have a motor domain with an N-terminal extension similar to Ras-association domains and a large basic insert near loop 2 (50-20 kDa junction) that binds calmodulin (Liao et al. 2010). The light chain-binding region has 6 unevenly spaced IQ motifs in mammalian MYO9A and 4 evenly spaced IQ motifs in mammalian MYO9B. The tail region contains an atypical C1 domain, which contains a zinc-binding region, and a GAP (GTPase-activating protein) domain that catalyzes the inactivation of the small G-proteins RhoA, RhoB and RhoC (Reinhard et al. 1995; Wirth et al. 1996; Chieregatti et al. 1998; Gorman et al. 1999; Grewal et al. 1999).

MYO9B is single-headed but evidently moves processively toward the plus end of actin filaments taking several large steps before dissociating from the filament (Post et al. 1998; Inoue et al. 2002; Nishikawa et al. 2006; Liao et al. 2010). This requires a different mechanism of motility vs. the hand-over-hand movement associated with dimeric myosins, which requires one head to be attached to the actin filament at all times. Studies show that deletion of the large basic insert in the motor domain near loop 2 of *Caenorhabditis elegans* Myo9, which is closer to MYO9B than to MYO9A, leads to loss of processivity, evidence that this insertion acts as a tether to actin during the translocation of Myo9 (Elfrink et al. 2014).

The two myosin 9 isoforms differ in their expression and localization. MYO9A is largely expressed in the brain and testis with lower levels in adrenal gland, kidney, lung and spleen (Chieregatti et al. 1998; Gorman et al. 1999). *Myo9a*-deficient mice have severe hydrocephalus due to an accumulation of cerebral fluid in the brain as a consequence of aberrant cell morphology, tight junctions, and differentiation of the ependymal epithelial cells in the ventral caudal third ventricle and the aqueduct (Abouhamed et al. 2009). Treatment of the mice with a Rho kinase (ROCK) inhibitor reduced ventricle enlargement and rescued the defective maturation of the ependymal epithelial cells suggesting that unregulated Rho and Rho kinase activities contribute to hydrocephalus formation (Abouhamed et al. 2009; Bahler et al. 2011).

MYO9A is also expressed in the F-actin-rich belt of renal proximal tubule cells, and MYO9A-deficient mice develop renal disease as evidenced by proteinuria and polyuria (Thelen et al. 2015). The proximal portion of the nephron becomes dilated and fibrotic, and both albumin and its binding receptor megalin accumulate at the luminal surface of proximal tubule cells suggesting a defect in endocytosis, which may be due to downregulation of the murine Rho effector diaphanous-related formin-1 (mDia1).

MYO9B is expressed predominantly in the cells of the immune system including lymph nodes, thymus, macrophages and CDC4+ T cells (Wirth et al. 1996). *Myo9b*-null mice do not have an overt phenotype; however, macrophages isolated from *Myo9b*-null mice exhibit impaired motility and chemotaxis in *in vitro* assays due to the inability to form large lamellipodia as observed in wild-type cells (Hanley et al. 2010). The Rho inhibitor TAT-C3 increased the velocity of *Myo9b*-null cells but impaired tail retraction (Hanley et al. 2010). In addition, the accumulation of monocytes and macrophages in the peritoneum of *Myo9b*-null mice after intraperitoneal injection of the chemoattractant C5a was severely

diminished vs. wild-type animals, evidence that MYO9B is important for the immune response (Hanley et al. 2010). The studies reveal the RhoGAP Myo9b as a key signaling molecule in the formation of cell surface projections and motility in macrophages.

Hydrocephalus and Fetal Akinesia A nonsense mutation in *MYO9A* (c.1537C > T:p.(Arg513∗)) was identified in an infant with no observed movements (akinesia) and severe ventriculomegaly in both sides (Maddirevula et al. 2019). The enlarged brain ventricles are consistent with the hydrocephaly observed in *Myo9a*-knockout mice (Abouhamed et al. 2009).

Congenital Myasthenic Syndrome Missense biallelic mutations in the *MYO9B* gene were identified in two families afflicted with congenital myasthenic syndrome, a group of rare disorders due to defects in the structure and function of neuromuscular junctions (O'Connor et al. 2016). The idea that MYO9A is required for motor axon functionality is supported by reduced expression of two MYO9A orthologues in zebrafish which leads to shortened and abnormally branched axons and abnormal swimming (O'Connor et al. 2016).

Inflammatory Bowel Disease It has been proposed that gene polymorphisms are associated with inflammatory bowel disease (IBD). Some *MYO9B* gene polymorphisms were associated with an increased risk of IBD (*rs1457092*), Crohn's disease (CD) (*rs962917*), and ulcerative colitis (UC) (*rs962917*; *rs2305764*), and other polymorphisms were associated with a reduced risk of IBD (*rs1545620*) or UC (*rs2305764*) (Wang et al. 2016). However, these results are controversial as a meta-analysis found no significant association both in allele and genotype comparisons between *MYO9B* polymorphism (*rs2305764, rs2305767, rs1457092*) and CD in Caucasians (Chen et al. 2016b). Thus, more studies are needed. The rs2305767 polymorphism, one of the polymorphisms initially associated with a decreased risk of UC (Wang et al. 2016) was found to have a high association with Turner syndrome and predisposition to celiac disease (Villanueva-Ortega et al. 2017).

Other Autoimmune Diseases *MYO9B* gene polymorphisms have also been associated with systemic lupus erythematosus, rheumatoid arthritis, and type 1 diabetes in Spanish populations suggesting that MYO9B is a risk factor for autoimmune diseases (Sanchez et al. 2007; Santiago et al. 2008). In the mouse, experimental autoimmune encephalomyelitis (EAE), a model for multiple sclerosis, is characterized by an acute paralytic episode following an injection of myelin proteins followed by partial or total recovery (Miller et al. 2010). Initiation of EAE was delayed in *Myo9b*-null vs. wild-type mice, and fewer CD4+ T cells, including Th1 and Th17 subtypes, were found in the central nervous system; moreover, no recovery was observed (Liu et al. 2015b). The studies suggest that MYO9B is required for the normal development of EAE and that loss of MYO9B leads to defects in T-cell response.

12.9 Myosin X

MYO10 consists of a motor domain with nucleotide-binding and actin-binding sites, a LCBD, which binds three molecules of calmodulin, a single α-helix (SAH) region followed by a coiled-coil region involved in the formation of antiparallel dimers (Lu et al. 2012), a C-terminal tail domain that has 3 PEST sequences, which are rich in proline, glutamate, serine, and threonine and confer sensitivity to certain proteases, 3 pleckstrin homology (PH) domains, which bind phosphatidyl (3,4,5)-triphosphate (PIP_3), and a myosin tail homology 4 (MyTH4) and band 4.1, ezrin, radixin, merlin (FERM) domain responsible for binding to microtubules and integrins (Divito and Cheney 2008). Although full-length MYO10 (~237 kDa) is widely expressed in vertebrate tissues (Berg et al. 2000), a shorter version known as headless MYO10 (~165 kDa), which is missing most of the head domain, is expressed in neural stem cells, neurons, and astrocytes (Sousa et al. 2006; Raines et al. 2012).

MYO10 is thought to exist in the cytoplasm as a folded inactive monomer that unfolds and dimerizes upon contact with PIP_3 to act as a processive motor able to transport cargo (Umeki et al. 2011). Native MYO10 is difficult to isolate because it is found in low abundance, and when expressed in baculovirus, full-length MYO10 is mostly monomeric (Knight et al. 2005; Umeki et al. 2011), so some studies such as those designed to examine the mechanical interaction of MYO10 with actin filaments at the single-molecule level have used forced dimer constructs made, e.g., by adding a leucine zipper (Nagy et al. 2008; Takagi et al. 2014) or the coiled-coil region from myosin V (Sun et al. 2010) after the MYO10 coiled-coil region. These studies have shown that under low load MYO10 walks processively along single actin filaments (Takagi et al. 2014), on actin-fascin bundles (Ricca and Rock 2010; Lu et al. 2012; Ropars et al. 2016) or on both single filaments and bundles (Sun et al. 2010) depending on the construct. MYO10's interaction with actin occurs in two phases as first observed for myosin I: MYO10's 17-nm power stroke is composed of a 15-nm movement followed by a 2-nm movement (Takagi et al. 2014).

MYO10 localizes at the tips of filopodia, slender actin-rich membrane protrusions (Berg and Cheney 2002), and it mediates their formation as evidenced by *in vitro* studies showing that overexpression of MYO10 causes an increase in the number and length of filopdia, whereas reduced MYO10 expression leads to the loss of filopodia (Bohil et al. 2006; Tokuo et al. 2007; Watanabe et al. 2010). The mechanism of filament elongation involves transport of vasodilator-stimulated phosphoprotein, VASP, to the tips of filopodia, where VASP competes with actin capping protein to promote actin filament assembly and filopodia growth (Tokuo and Ikebe 2004). Integrins, cell surface proteins that mediate adhesion to the extracellular matix, are also actively transported to the tips of filopodia by MYO10, where they stabilize filopodia and support cell migration (Zhang et al. 2004). PIP_3 binding is required for the translocation of MYO10 to filopodial tips as mutation of the second PH domain, which specifically binds PIP_3, results in the intracellular localization of MYO10 and a reduction in the number and length of filopodia (Plantard et al. 2010).

Mice deficient in both full-length and headless MYO10 exhibit a white belly spot along with syndactyly and persistent hyaloid vasculature in the eye and have fewer live births with greater than half of the surviving pups exhibiting exencephaly, a defect in neural tube closure, results consistent with the idea that MYO10 performs critical functions during development (Heimsath et al. 2017).

Cancer Cancer cells spread by invading the surrounding tissue and establishing metastatic colonies. There is growing evidence that actin-rich protrusions like filopodia, filopodial-like protrusions, and invadopodia, membrane protrusions rich in matrix metalloproteases capable of digesting extracellular matrix, are used by cancer cells to invade adjacent tissues (Arjonen et al. 2011; Shibue et al. 2012). MYO10 localizes at the tips of invadopodia and is required for their formation, and MYO10 depletion reduces the number of long invadopodia (Schoumacher et al. 2010). MYO10 expression is increased in several different cancers including brain (Mischel et al. 2003), breast (Arjonen et al. 2014), lung (Bidkhori et al. 2013; Dvornikov et al. 2018; Wang et al. 2018), skin (Tokuo et al. 2018), and prostate cancer (Makowska et al. 2015) suggesting that MYO10 may be a potential therapeutic target for some cancers.

MYO10 is strongly expressed in aggressive breast cancers and is required for breast cancer cell invasion and dissemination in multiple cancer cell lines (Arjonen et al. 2014). In breast carcinomas, MYO10 is expressed at the invasive edges and correlates with the presence of TP53 mutations and poor prognosis (Arjonen et al. 2014). The proportion of cultured breast cancer cells expressing reduced amounts of MYO10 migrating through the membrane in transwell assays is significantly less than in control cells (Cao et al. 2014). The reduction in metastatic behavior as a consequence of reduced MYO10 expression many be due to a decrease in cell-substrate adhesion, which is required for filopo-

dia extension (Zhang et al. 2004). The FERM domain of MYO10 binds integrins through an NPXY motif and transports integrins within filopodia. The ability of Myo10 to transport β1 integrins is required for invasion (Arjonen et al. 2014), evidence that some integrins are important for cancer cell survival (Shibue et al. 2012). Indeed, altered expression of many different integrins correlates with increased tumor progression and poor prognosis in human cancer (Desgrosellier and Cheresh 2010). miRNA-340 is consistently expressed at a low level in human breast cancer cell lines and its overexpression inhibits breast cancer cell migration and invasion by regulating MYO10 expression (Chen et al. 2016a). The studies suggest that miRNA-340 may serve as a marker for breast cancer metastasis and prognosis.

Recent evidence indicates that MYO10 mediates melanoma initiation and metastasis. MYO10 depletion in cultured Melb-a mouse melanoblasts inhibits the formation of long protrusions by reducing the transportation of VASP to the leading edge of migrating cells (Tokuo et al. 2018). Furthermore, the ability of *MYO10*-depleted B16F1 mouse melanoma cells to form lung colonies after tail-vein injection is markedly decreased vs. control cells. Mice in which full-length but not headless *Myo10* is deleted exhibit with 100% penetrance a white spot on their belly caused by reduced melanoblast migration; other defects include syndactyly and persistent hyaloid vasculature in the eye (Tokuo et al. 2018). When crossed with mice that conditionally express in melanocytes the $BRAF^{V600E}$ mutation combined with Pten silencing the *Myo10*-null mice exhibit reduced melanoma development and metastasis vs. control mice resulting in an extended medial survival time (Tokuo et al. 2018). Importantly, examination of human melanoma samples showed that elevated expression of MYO10 is associated with low survival rates for melanoma patients (Tokuo et al. 2018).

Infectious Disease MYO10 may play a role in the budding of viral particles from target cells. Marburg virus, which causes hemorrhagic fever and is a close relative of the deadly Ebola virus, consists of a single strand of negative-sense RNA coding for seven structural proteins encapsulated by nucleoprotein that is embedded in matrix and surrounded by a membrane supplied by the host cell (Messaoudi et al. 2015). During infection, Marburg viruses attach to the cell surface and are taken up by macropinocytosis (Messaoudi et al. 2015). Viral and endosomal membranes fuse releasing the viral ribonucleocapsid into the cytoplasm where the negative-sense RNA genome undergoes transcription and replication (Messaoudi et al. 2015). After their formation in the perinuclear region of macrophages, nucleocapsids are transported to the cell surface where they are assembled; the matrix protein VP40 is important for virion assembly. In cells co-expressing VP40 and fluorescently-tagged MYO10, MYO10 is found at the tips of filopodia and along filopodia positive for VP40 (Kolesnikova et al. 2007). In cells expressing a putative dominant negative MYO10, both the number of VP40-enriched membrane protrusions at the cell surface and the amount of VP40 released decrease, evidence that MYO10 mediates the budding of virus particles (Kolesnikova et al. 2007).

The intracellular pathogenic bacteria *Shigella* and *Listeria*, which cause dysentery, spread in the colon from cell to cell through membrane protrusions. Once inside, these bacteria commandeer the host cell's actin machinery to form comet tails composed of microfilaments whose assembly propel the bacteria through the cytoplasm to the cell membrane where they form protrusions that are ingested by adjacent mucosal cells (Tilney and Portnoy 1989). In this way the bacteria evade the host's immune system while spreading from cell to cell. Myo10 is found near the rear of the bacteria and is a component of *Shigella*- and *Listeria*-induced protrusions. *Myo10*-depleted cells form the same number of protrusions as control cells; however, the protrusions are shorter and thicker, and the spread of bacteria from cell to cell is reduced by 80% (Bishai et al. 2013). The studies suggest that MYO10 might be an effective target for treatment against these pathogens.

Myo10 is also a key inducer of tunneling nanotubes (TNTs), actin-containing structures that facilitate the transfer of vesicles, organelles, genetic material, and pathogens between cells (Gousset et al. 2013). The transfer of the HIV viral protein Nef, which is critical to HIV pathogenesis and development of AIDS, depends on the presence of MYO10-dependent TNTs (Uhl et al. 2018). The studies suggest that insight into how TNTs are formed might lead to ways to control HIV infection.

12.10 Myosin XV

Humans have one gene encoding myosin 15A (*MYO15A*) and a myosin 15 pseudogene (*MYO15B*). *MYO15A* is alternatively spliced to form three isoforms. MYO15A isoform 1 encodes a 395-kDa polypeptide, the largest of the myosin heavy chains. It has a 133-kDa proline-rich N-terminal extension followed by a motor domain, 2–3 IQ domains, and a tail consisting of two sets of MYTH4 and FERM domains separated by an SH3 domain. The third potential IQ domain is noncanonical and binds neither calmodulin nor the regulatory or essential light chains (Bird et al. 2014). MYO15A isoform 2 is a 262-kDa polypeptide, which lacks the N-terminal extension (Liang et al. 1999; Fang et al. 2015b). MYO15A isoform 3 is recently discovered and has a novel 50-amino acid N-terminal domain (Rehman et al. 2016). In contrast, *MYO15B* is a transcribed pseudogene with a short, also proline-rich, N-terminal extension but with no similarity to the N-terminal extension of MYO15A, a motor domain missing the first N-terminal 66/204 residues, one apparent IQ domain, and a tail with 30% identity and 44% similarity to that of MYO15A (Boger et al. 2001). In addition to the deletion in the motor domain, amino acid substitutions in critical regions of the motor domain including the phosphate- and actin-binding regions indicate that this myosin is nonfunctional (Boger et al. 2001). One possibility is that MYO15B acts as a dominant negative protein to regulate endogenous myosin 15 function (Rehman et al. 2016).

In the mouse inner ear, *Myo15* is expressed at a low level making its isolation difficult so there are no reports of biochemical studies done with purified native full-length protein; however, an EGFP-tagged version of the myosin 15 isoform 2 motor domain and three predicted IQ motifs (EGFP-Myo15-3IQ) was successfully expressed in insect cells when coexpressed with the muscle-specific chaperone UNC45B, the chaperone heat-shock protein 90 (HSP90), and the regulatory light chain (RLC) and essential light chain (ELC) normally associated with myosin II (Bird et al. 2014). EGFP-Myo15-2IQ, whose ATPase activity is activated 67-fold by actin, is a barbed-end directed high-duty ratio motor with a power stroke of ~ 8 nm (Bird et al. 2014), consistent with the predicted step size for a myosin motor with a lever arm having two IQ domains (Warshaw 2004). Whether posttranslational modification such as phosphorylation regulates MYO15A activity as observed for smooth muscle myosin II (Sellers et al. 1981) is unknown. In addition, whether the tail regulates MYO15A activity awaits expression and purification of full-length MYO15a. Also, whether MYO15A dimerizes and how (no coiled-coil region associated with dimerization in other processive motors is present; Bird et al. 2014) to support processive movement on actin filaments has not been determined.

Myo15 is highly expressed in the ear and endocrine organs (Liang et al. 1999). On the hair cells of the cochlea and the vestibular organs, stereocilia, actin-rich protrusions that derive from microvilli, are precisely arranged in V- or W-shaped arrays according to height and cross-linked into bundles by extracellular filaments (Frolenkov et al. 2004). In response to sound waves, the stereocilia deflect opening mechano-electrical transduction (MET) channels that reside at the tips of the shorter stereocilia, thus initiating neurotransmission leading to hearing (Beurg et al. 2009). MYO15A isoform 1 localizes mainly to the tips of the shorter row stereocilia, and MYO15A isoform 2 localizes mainly to the tips of the taller stereocilia (Fang et al. 2015b). Mice engineered to express only MYO15A isoform 2 initially develop normal ste-

reociliary bundles; however, soon the shorter stereocilia, which house the active MET channels (Beurg et al. 2009), degenerate decreasing in both length and diameter, and the mice are profoundly deaf (Fang et al. 2015b). Thus, MYO15A isoform 1 is required for maintenance of stereocilia morphology and mechanotransduction of the shorter stereocilia (Fang et al. 2015b).

A mutation in an evolutionarily conserved cysteine residue in the motor domain of MYO15 is responsible for the shaker 2 (*sh2*) phenotype in mice, which is characterized by deafness and a vestibular defect that results in a head-tossing and circling phenotype (Probst et al. 1998; Wang et al. 1998). Shaker 2 mice have abnormally short stereocilia on the hair cells of the inner ear and do not develop the characteristic staircase arrangement of mature hair bundles, evidence that MYO15A is required for the graded growth of stereocilia (Probst et al. 1998; Belyantseva et al. 2003). Another spontaneous allele, shaker 2^J ($sh2^J$), in which the C-terminal FERM domain of MYO15A is missing, also causes congenital deafness and vestibular defects in mice (Anderson et al. 2000).

To drive stereocilia growth MYO15 interacts with two proteins, EPS8 (epidermal growth factor receptor kinase substrate 8) and the PDZ-containing protein whirlin, both of which localize to the tips of stereocilia with MYO15A (Belyantseva et al. 2005; Manor et al. 2011; Zampini et al. 2011). Indeed, MYO15A mediates their localization at the tips as both EPS8 and whirlin are absent from the stereocilia of shaker 2 mice, and transfection of tagged MYO15 isoform 2 into cultured hair cells from shaker 2 mice restores their normal localization and rescues stereocilia growth (Belyantseva et al. 2005; Manor et al. 2011).

Hearing Loss The shaker 2 mouse is a model for human DFNB3, one of the more common forms of severe to profound autosomal recessive nonsyndromic deafness, which was first identified in the village of Bengkala in Bali, Indonesia, where 2% of the population had hearing loss (Friedman et al. 1995). Subsequently, the locus was mapped to chromosome 17 (Liang et al. 1998) and then pathogenic variants were identified in *MYO15A* (Wang et al. 1998). Nearly 200 different mutations in *MYO15A* in humans including missense, frameshift, nonsense, splice-site, and in frame insertions or deletions, have now been linked to DFNB3 (Rehman et al. 2016). In addition to hearing loss, some patients state that they feel "inebriated" in the absence of visual cues (Anderson et al. 2000; Friedman et al. 2000) suggesting vestibular dysfunction. Despite MYO15's expression in other tissues, there is no evidence that mutations in MYO15A in humans are associated with syndromic deafness (Rehman et al. 2016), although it is possible that other phenotypes have been overlooked (Friedman and Riazuddin 2014).

12.11 Myosin XVI

Class XVI myosins were first identified in rat migrating neurons and astrocytes and originally designated as myr 8a (8th unconventional myosin from rat a; now MYO16A) and myr 8b (now MYO16B); MYO16B is the predominant form in the brain (Patel et al. 2001). Class XVI myosins contain a ~400 amino acid-long N-terminal extension ("ankyrin domain") comprised of two protein phosphatase catalytic subunit (PP1c)-binding sequence elements (the RxxQIKxY motif and the KVRF motif) and multiple (8) ankyrin/ankyrin-like repeats, followed by a motor domain with conserved ATP- and actin-binding sites, a single light chain-binding domain, and either a short positively-charged tail (MYO16A) or a longer (additional 590 amino acids) disordered neutral polyproline-rich tail (MYO16B) (Patel et al. 2001; Kengyel et al. 2015).

MYO16A has a heavy chain of ~149 kDa. Like MYO16B there are no coiled-coil motifs in the tail suggesting that the molecule is monomeric (Cameron et al. 2007). MYO16B, whose heavy chain is ~210.6 kDa, binds F-actin in an ATP-reversible fashion and immunoprecipitates with the protein catalytic subunits PP1α and PP1γ, suggesting that MYO16B may target protein phosphatase catalytic subunits to actin structures (Patel et al. 2001).

MYO16B, the predominant form in the brain, localizes to both the cytoplasm and the nucleus in cultured neurons and frozen sections of the brain (Patel et al. 2001; Cameron et al. 2007). The C-terminal extension of MYO16B directs it to the nucleus, where it colocalizes to a compartment containing profilin and filamentous actin (Cameron et al. 2007). MYO16 evidently regulates cell cycle progression. Rat2 cells (embryonic fibroblasts) express the most MYO16 during entry and progression through S-phase, whereas MYO16 expression is down regulated at the onset of M-phase (Cameron et al. 2013). Overexpression of MYO16 results in an increase in the number of cells in the G_1 and S phases of the cell cycle (Cameron et al. 2007), and cells expressing reduced amounts of MYO16 show aberrant cell shape and nuclear architecture, an increase in the fraction of cells at G_1 or G_2/M, and increased cell death (Cameron et al. 2013).

Schizophrenia There is evidence from studies of families from the European descent Afrikaner population from South Africa that variants in *MYO16* contribute to the genetic liability of schizophrenia (Rodriguez-Murillo et al. 2014); moreover, expression analysis of brain samples from control and schizophrenic patients shows that the expression of MYO16 in the frontal cortex of patients with schizophrenia was significantly elevated (Rodriguez-Murillo et al. 2014). Although confirmation of MYO16's role in schizophrenia awaits further studies, there is evidence that MYO16 is a member of the NYAP (neuronal tyrosine-phosphorylated adaptor for the PI 3-kinase) family of phosphoproteins, which are expressed in developing neurons (Yokoyama et al. 2011). When stimulated with contactin5, NYAPs are phosphorylated on tyrosine by Fyn, then interact with PI3K p85 to activate PI3K, Akt, and Rac1. NYAPs also interact with the WAVE complex, which mediates remodeling of the actin cytoskeleton. Mice deficient in MYO16 and the 2 other members of the NYAP family exhibit reduced brain size and total neuron length (Yokoyama et al. 2011).

Autism Initial studies implicate the association of MYO16 with neurocognitive developmental disorders. MYO16 has been identified as a binding partner of KIRREL3, a synaptic cell-adhesion molecule implicated in several neurodevelopmental conditions including intellectual disability and autism spectrum disorder (Liu et al. 2015a). Some partial colocalization of MYO16 and KIRREL3 was observed in the perinuclear region of cultured neuronal cells presumably corresponding to the Golgi complex and in punctae along the length of neurite processes identified as synaptic/secretory vesicles. The studies suggest that MYO16 may be a critical factor in the actin cytoskeleton associated with synaptic vesicles. A small number of patients with neurodevelopmental disorders have been found with deletions encompassing the *MYO16* gene. The availability of a *Myo16*-null mouse would help to address important questions regarding the role of MYO16 in the brain.

12.12 Myosin XVIII

Vertebrates including humans have two genes coding for myosin 18, *MYO18A* and *MYO18B* (Nishioka et al. 2002; Mori et al. 2003) (for recent reviews, see Chap. 19 (Taft and Latham 2020) and (Buschman and Field 2018)). Whereas Myo18A is expressed in most tissues (Furusawa et al. 2000), Myo18B expression is tissue specific with the highest amount expressed in cardiac and skeletal muscle (Salamon et al. 2003).

Myo18A is expressed in mice as three alternatively spliced isoforms, MYO18Aα (MysPDZ), MYO18Aβ (Mori et al. 2003), and MYO18Aδ (Horsthemke et al. 2019). MYO18Aα is expressed in most tissues, where it reportedly localizes at the endoplasmic reticulum and Golgi apparatus, MYO18Aβ is expressed in most hematopoietic cells such as bone marrow, spleen, and thymus (Furusawa et al. 2000; Mori et al. 2003), and MYO18Aδ is expressed in ventricular myocytes of the heart as well as skeletal muscle (Horsthemke et al. 2019).

Although both MYO18Aα and β isoforms have a motor domain, a single canonical IQ

motif, a less well conserved IQ motif, and a long coiled-coil tail, MYO18Aα (230kDA) also has a unique N-terminal domain consisting of a lysine- and glutamine (KE)-rich sequence followed by a PDZ domain, which mediates protein-protein interactions (Furusawa et al. 2000; Mori et al. 2003), whereas MYO18Aβ (190 kDa) has a short sequence before the motor domain but lacks the KE and PDZ domains (Furusawa et al. 2000; Mori et al. 2003). Rather than forming large bipolar filaments like myosin II, expressed full-length murine Myo18Aβ dimerizes forming ~65-nm long bipolar filaments with two heads at each end (Billington et al. 2015). MYO18Aγ has an alternative proline-rich N-terminus and a long serine-rich C-terminus (Horsthemke et al. 2019). Interestingly, purified MYO18Aβ co-assembles with MYH9 (NMIIA) *in vitro* and Myo18Aβ-MYH9 copolymers exist in cells suggesting the possibility that MYO18β regulates the assembly of MYH9 (Billington et al. 2015). There are conflicting reports regarding whether MYO18A binds actin in an ATP-reversible fashion (Mori et al. 2003; Isogawa et al. 2005; Guzik-Lendrum et al. 2013; Taft et al. 2013); however what does appear plausible is that class XVIII myosins are unlikely to operate as motors that translocate along actin filaments (Guzik-Lendrum et al. 2013).

MYO18Aα has also been reported to bind GOLPH3 through its PDZ module (Dippold et al. 2009; Taft et al. 2013), and MYO18Aα knockdown causes Golgi ribbons to compact into tight aggregates and Golgi-to-plasma membrane trafficking to decrease implicating MYO18Aα in Golgi morphology and trafficking (Dippold et al. 2009; Taft et al. 2013). However, another group subsequently reported that MYO18Aα is inactive even in the presence of GOLPH3; moreover, they found no evidence that MYO18Aα localizes to the Golgi or of Golgi defects in cells depleted of MYO18Aα (Bruun et al. 2017), evidence that more work must be done to reach a consensus regarding MYO18A at the Golgi.

In mouse heart, MYO18Aγ localizes to A bands and loss of function leads to disorganization of sarcomeres and embryonic lethality (Horsthemke et al. 2019). MYO18A is implicated in the assembly of lamellar actomyosin bundles in cooperation with the myotonic dystrophy kinase-related Rac/Cdc42-binding kinase (MRCK) and leucine-rich adaptor protein 1 (LURAP1; LRAP35a) (Tan et al. 2008). MYO18Aα also interacts via its C-terminal globular domains with the p21-activated kinase 2/PAK-interacting exchange factor-β/G-protein-coupled receptor kinase interactor 1 (PAK2/βPIX/GIT1) complex, and reduced expression of MYO18Aα in human epidermoid carcinoma A431 cells results in accumulation of the complex in focal adhesions and reduced cell migration (Hsu et al. 2010). Furthermore, disruption of the MYO18A-βPIX interaction impairs cell motility and also decreases Rac1 activity, evidence that the MYO18A-βPIX interaction is critical to adhesion and migration in epithelial cells (Hsu et al. 2014).

MYO18B (285 kDa) has a head, neck, and tail domain preceded by an N-terminal sequence that is unlike the N-terminal sequence in MYO18A (Nishioka et al. 2002). MYO18B is expressed primarily in cardiac and skeletal muscle cells where it localizes via its N-terminal extension to the Z-bands in skeletal muscle, and its deletion leads to embryonic lethality in mice due to defects in the myofibrils of cardiac myocytes (Ajima et al. 2008).

Cancer The expression level of several myosins including *MYO18A* is higher in the human prostate cancer cell line PC-3 vs. the less metastatic prostate cancer cell line LNCaP, and MYO18A depletion alters the actin cytoskeleton, reduces directional persistence in 2D migration assays indicating that the cells are less able to polarize, and decreases cell migration in 3D invasion assays, evidence that MYO18A supports tumor cell metastasis (Makowska et al. 2015).

Constitutive activation of protein tyrosine kinases including PDGFRB and FGFR1 is associated with the pathogenesis of chronic myeloproliferative neoplasm (MPN). In hematological malignancies *MYO18A* has been found as fusions with *FGFRI* leading to the 8p11 myeloproliferative syndrome (EMS) (Walz et al. 2005),

PDGFRB leading to eosinophilia-associated MPN (MPN-eo) (Walz et al. 2009), *MLL* leading to acute myeloid leukemia (AML) (Ussowicz et al. 2012), and *PDGFRB* leading to MPN without eosinophilia (Sheng et al. 2017).

MYO18B is frequently mutated, deleted, and methylated in ~50% human lung cancers (non-small cell lung carcinomas and small cell lung carcinomas) (Nishioka et al. 2002). Modification of the *MYO18B* gene is also observed in a considerable fraction of ovarian (Yanaihara et al. 2004) and colorectal (Nakano et al. 2005) cancer. These data suggest that MYO18B acts as a tumor suppressor in cancer development. Additional evidence for this comes from *in vitro* studies. Expression of Flag-tagged MYO18B in the non-small cell lung carcinoma cell line H322, which has undetectable levels of endogenous MYO18B, suppresses anchorage-independent growth (Nishioka et al. 2002). The mechanism may involve HOMER2, a protein that interacts with the C-terminus of MYO18B, co-localizes with MYO18B at membrane protrusions and stress fibers, and enhances the ability of MYO18B to suppress anchorage-independent growth of human lung cancer cells (Ajima et al. 2007).

Myopathies Mutations in *MYO18B* have been associated with human myopathies. Malfatti and colleagues reported that a premature stop mutation in *MYO18B* (c.6496G > T; p.Glu2166∗) in a Portuguese baby girl was associated with severe nemaline myopathy (NM), a rare and severe muscle disease characterized by the presence of nemaline bodies in muscle fibers (Malfatti et al. 2015). The child had dysmorphic features including enlargement of the skull, low-set ears, clinodactyly of the fourth and fifth fingers of the hands, and tendon contractures as well as cardiomyopathy, which is not typically associated with NM. A *MYO18B* missense mutation, c.6905C > A, which results in a premature stop codon, was also linked in two apparently unrelated patients to a novel syndrome of the bone disorder Klippel-Feil anomaly, myopathy, and distinctive dysmorphic facial features (Alazami et al. 2015). The studies are consistent with studies in zebrafish showing that loss of *myo18b* results in the complete lack of sarcomeric structure due to failure of thick and thin filaments to organize (Berger et al. 2017).

Viral Infection Although the mechanism is not yet known, there is evidence that MYO18A may mediate viral infections in humans. MYO18A associates with GOLPH3 at the Golgi and depletion of GOLPH3 or MYO18A in human fibroblasts reduces the release of hepatitis C virus (Bishe et al. 2012). Similarly, following infection of human fibroblasts with human cytomegalovirus (HCMV), MYO18A reportedly translocates from the plasma membrane to punctate structures adjacent to the Golgi region in the cytoplasm, where viral assembly occurs (Jean Beltran et al. 2016). Reduced expression of MYO18 significantly reduces virus production, evidence that MYO18A is necessary for efficient replication of HCMV.

12.13 Myosin XIX

Class XIX myosins are plus-end directed motors that have a 109-kDa heavy chain comprised of a motor domain, three IQ domains that bind the regulatory light chain (RLC) of smooth muscle/non-muscle myosin II, and a short tail (Quintero et al. 2009; Adikes et al. 2013; Lu et al. 2014). A fragment consisting of the MYO19 motor domain and 1 or 3 IQ domains expressed in baculovirus and purified from insect cells exhibits an actin-activated ATPase activity and high affinity for F-actin in the presence of ATP (Adikes et al. 2013). Kinetic studies including those showing a slow rate of ADP isomerization and ADP release indicate that MYO19 has a relatively high duty ratio and is likely to associate with other MYO19 molecules to support motility (Usaj and Henn 2017).

Class XIX myosins are expressed in multiple tissues where they interact directly with mitochondria through a ~150 amino acid MYO19-specific mitochondria outer membrane association (MyMOMA) domain in the tail and regulate mitochondria dynamics (Quintero et al. 2009). Two basic residues in this region, Arg882

and Lys883, are essential for mitochondrial localization, and their substitution with alanine leads to Myo19 localization at the endoplasmic reticulum (Hawthorne et al. 2016). Overexpression of MYO19 in A549 cells causes an 80% increase in average mitochondrial velocity, whereas expression of the MYO19 tail, predicted to act as a dominant negative, decreases mitochondrial runs in CAD cell neurites by 40% (Quintero et al. 2009). Reduced expression of MYO19 leads to an increase in the number of Hela cells that fail to divide and the abnormal asymmetrical distribution of mitochondria to the poles in dividing cells demonstrating that MYO19 is required for the regulated segregation of mitochondria during anaphase (Rohn et al. 2014).

During the response to glucose starvation, MYO19 localizes in U2OS cells with mitochondria in a motor-dependent manner to the tips of starvation-induced filopodia, and moves retrogradely during filopodia retraction (Shneyer et al. 2017). Reactive oxygen specifies (ROS) produce the same phenotype (Shneyer et al. 2017). MYO19 depletion reduces the number and length of filopodia, evidence that MYO19 plays a role in the formation of filopodia induced by starvation (Shneyer et al. 2016). Evidently, MYO19 promotes the localization of mitochondria to the tips of growing filopodia where they are needed to produce the ATP required for rapid actin assembly (Shneyer et al. 2016).

Cancer MYO19 is one of the least well-studied myosins, and little is known regarding its role in human health; however, initial reports implicate MYO19 in cancer. In two families *MYO19* was identified as a candidate gene on chromosome 17q for familial glioma, a rare but fatal cancer (Jalali et al. 2015). In another study, *MYO19* fused *SKA2* (spindle and kinetochore-associated complex subunit 2) (SKA2-MYO19) is one of 27 fusion genes identified by paired-end RNA sequencing in breast cancer samples (Edgren et al. 2011).

Other As perturbations in mitochondrial dynamics are linked to neurodegenerative diseases including Parkinson's disease, Alzheimer's disease, and Huntington's disease (Chen and Chan 2009; Federico et al. 2012), it is possible that future studies will show that mutations in *MYO19* are associated with neurological disorders.

Acknowledgements I am grateful for the many helpful comments of Drs. Robert Adelstein, Thomas Friedman, Michael Geeves, Wilma Hofmann, Carlo Reggiani, and Hiroshi Tokuo on early versions of the text. The support of NIH grant GM111615 is greatly appreciated.

References

Abate F, da Silva-Almeida AC, Zairis S, Robles-Valero J, Couronne L, Khiabanian H, Quinn SA, Kim MY, Laginestra MA, Kim C, Fiore D, Bhagat G, Piris MA, Campo E, Lossos IS, Bernard OA, Inghirami G, Pileri S, Bustelo XR, Rabadan R, Ferrando AA, Palomero T (2017) Activating mutations and translocations in the guanine exchange factor VAV1 in peripheral T-cell lymphomas. Proc Natl Acad Sci U S A 114(4):764–769. https://doi.org/10.1073/pnas.1608839114

Abouhamed M, Grobe K, San IV, Thelen S, Honnert U, Balda MS, Matter K, Bahler M (2009) Myosin IXa regulates epithelial differentiation and its deficiency results in hydrocephalus. Mol Biol Cell 20(24):5074–5085. https://doi.org/10.1091/mbc.E09-04-0291

Adikes RC, Unrath WC, Yengo CM, Quintero OA (2013) Biochemical and bioinformatic analysis of the myosin-XIX motor domain. Cytoskeleton (Hoboken) 70(5):281–295. https://doi.org/10.1002/cm.21110

Ahmed ZM, Goodyear R, Riazuddin S, Lagziel A, Legan PK, Behra M, Burgess SM, Lilley KS, Wilcox ER, Riazuddin S, Griffith AJ, Frolenkov GI, Belyantseva IA, Richardson GP, Friedman TB (2006) The tip-link antigen, a protein associated with the transduction complex of sensory hair cells, is protocadherin-15. J Neurosci 26:7022–7034

Ajima R, Kajiya K, Inoue T, Tani M, Shiraishi-Yamaguchi Y, Maeda M, Segawa T, Furuichi T, Sutoh K, Yokota J (2007) HOMER2 binds MYO18B and enhances its activity to suppress anchorage independent growth. Biochem Biophys Res Commun 356(4):851–856. https://doi.org/10.1016/j.bbrc.2007.03.060

Ajima R, Akazawa H, Kodama M, Takeshita F, Otsuka A, Kohno T, Komuro I, Ochiya T, Yokota J (2008) Deficiency of Myo18B in mice results in embryonic lethality with cardiac myofibrillar aberrations. Genes Cells 13(10):987–999. https://doi.org/10.1111/j.1365-2443.2008.01226.x

Alagramam KN, Yuan H, Kuehn MH, Murcia CL, Wayne S, Srisailpathy CR, Lowry RB, Knaus R, Van Laer L, Bernier FP, Schwartz S, Lee C, Morton CC, Mullins RF, Ramesh A, Van Camp G, Hageman GS, Woychik RP, Smith RJ (2001) Mutations in the novel protocad-

herin PCDH15 cause Usher syndrome type 1F. Hum Mol Genet 10(16):1709–1718

Alamo L, Wriggers W, Pinto A, Bartoli F, Salazar L, Zhao FQ, Craig R, Padron R (2008) Three-dimensional reconstruction of tarantula myosin filaments suggests how phosphorylation may regulate myosin activity. J Mol Biol 384(4):780–797. https://doi.org/10.1016/j.jmb.2008.10.013

Alazami AM, Kentab AY, Faqeih E, Mohamed JY, Alkhalidi H, Hijazi H, Alkuraya FS (2015) A novel syndrome of Klippel-Feil anomaly, myopathy, and characteristic facies is linked to a null mutation in MYO18B. J Med Genet 52(6):400–404. https://doi.org/10.1136/jmedgenet-2014-102964

Alhopuro P, Phichith D, Tuupanen S, Sammalkorpi H, Nybondas M, Saharinen J, Robinson JP, Yang Z, Chen LQ, Orntoft T, Mecklin JP, Jarvinen H, Eng C, Moeslein G, Shibata D, Houlston RS, Lucassen A, Tomlinson IP, Launonen V, Ristimaki A, Arango D, Karhu A, Sweeney HL, Aaltonen LA (2008) Unregulated smooth-muscle myosin in human intestinal neoplasia. Proc Natl Acad Sci U S A 105(14):5513–5518. https://doi.org/10.1073/pnas.0801213105

Almeida CG, Yamada A, Tenza D, Louvard D, Raposo G, Coudrier E (2011) Myosin 1b promotes the formation of post-Golgi carriers by regulating actin assembly and membrane remodelling at the trans-Golgi network. Nat Cell Biol 13(7):779–789. https://doi.org/10.1038/ncb2262 ncb2262 [pii]

Almuzzaini B, Sarshad AA, Farrants AK, Percipalle P (2015) Nuclear myosin 1 contributes to a chromatin landscape compatible with RNA polymerase II transcription activation. BMC Biol 13:35. https://doi.org/10.1186/s12915-015-0147-z

Altman D, Sweeney HL, Spudich JA (2004) The mechanism of myosin VI translocation and its load-induced anchoring. Cell 116(5):737–749

Ambrosino C, Tarallo R, Bamundo A, Cuomo D, Franci G, Nassa G, Paris O, Ravo M, Giovane A, Zambrano N, Lepikhova T, Janne OA, Baumann M, Nyman TA, Cicatiello L, Weisz A (2010) Identification of a hormone-regulated dynamic nuclear actin network associated with estrogen receptor alpha in human breast cancer cell nuclei. Mol Cell Proteomics 9(6):1352–1367. https://doi.org/10.1074/mcp.M900519-MCP200

Ameen NA, Salas PJ (2000) Microvillus inclusion disease: a genetic defect affecting apical membrane protein traffic in intestinal epithelium. Traffic 1(1):76–83

Anderson DW, Probst FJ, Belyantseva IA, Fridell RA, Beyer L, Martin DM, Wu D, Kachar B, Friedman TB, Raphael Y, Camper SA (2000) The motor and tail regions of myosin XV are critical for normal structure and function of auditory and vestibular hair cells. Hum Mol Genet 9(12):1729–1738

Anderson RL, Trivedi DV, Sarkar SS, Henze M, Ma W, Gong H, Rogers CS, Gorham JM, Wong FL, Morck MM, Seidman JG, Ruppel KM, Irving TC, Cooke R, Green EM, Spudich JA (2018) Deciphering the super relaxed state of human beta-cardiac myosin and the mode of action of mavacamten from myosin molecules to muscle fibers. Proc Natl Acad Sci U S A 115(35):E8143–E8152. https://doi.org/10.1073/pnas.1809540115

Anikster Y, Huizing M, Anderson PD, Fitzpatrick DL, Klar A, Gross-Kieselstein E, Berkun Y, Shazberg G, Gahl WA, Hurvitz H (2002) Evidence that Griscelli syndrome with neurological involvement is caused by mutations in RAB27A, not MYO5A. Am J Hum Genet 71(2):407–414. https://doi.org/10.1086/341606

Arif E, Wagner MC, Johnstone DB, Wong HN, George B, Pruthi PA, Lazzara MJ, Nihalani D (2011) Motor protein Myo1c is a podocyte protein that facilitates the transport of slit diaphragm protein Neph1 to the podocyte membrane. Mol Cell Biol 31(10):2134–2150. https://doi.org/10.1128/MCB.05051-11

Arjonen A, Kaukonen R, Ivaska J (2011) Filopodia and adhesion in cancer cell motility. Cell Adhes Migr 5(5):421–430. https://doi.org/10.4161/cam.5.5.17723

Arjonen A, Kaukonen R, Mattila E, Rouhi P, Hognas G, Sihto H, Miller BW, Morton JP, Bucher E, Taimen P, Virtakoivu R, Cao Y, Sansom OJ, Joensuu H, Ivaska J (2014) Mutant p53-associated myosin-X upregulation promotes breast cancer invasion and metastasis. J Clin Invest 124(3):1069–1082. https://doi.org/10.1172/JCI67280

Arun RM, Lakkakula BV, Chitharanjan AB (2016) Role of myosin 1H gene polymorphisms in mandibular retrognathism. Am J Orthod Dentofac Orthop 149(5):699–704. https://doi.org/10.1016/j.ajodo.2015.10.028

Aschenbrenner L, Naccache SN, Hasson T (2004) Uncoated endocytic vesicles require the unconventional myosin, Myo6, for rapid transport through actin barriers. Mol Biol Cell 15(5):2253–2263. https://doi.org/10.1091/mbc.e04-01-0002

Assad JA, Shepherd GM, Corey DP (1991) Tip-link integrity and mechanical transduction in vertebrate hair cells. Neuron 7(6):985–994

Atlasi Y, Stunnenberg HG (2017) The interplay of epigenetic marks during stem cell differentiation and development. Nat Rev Genet 18(11):643–658. https://doi.org/10.1038/nrg.2017.57

Au JS, Puri C, Ihrke G, Kendrick-Jones J, Buss F (2007) Myosin VI is required for sorting of AP-1B-dependent cargo to the basolateral domain in polarized MDCK cells. J Cell Biol 177(1):103–114. jcb.200608126 [pii] https://doi.org/10.1083/jcb.200608126

Avraham KB, Hasson T, Steel KP, Kingsley DM, Russell LB, Mooseker MS, Copeland NG, Jenkins NA (1995) The mouse Snell's waltzer deafness gene encodes an unconventional myosin required for structural integrity of inner ear hair cells. Nat Genet 11(4):369–375

Baek JI, Oh SK, Kim DB, Choi SY, Kim UK, Lee KY, Lee SH (2012) Targeted massive parallel sequencing: the effective detection of novel causative mutations associated with hearing loss in small families. Orphanet J Rare Dis 7:60. https://doi.org/10.1186/1750-1172-7-60

Bähler M, Kroschewski R, Stöffler HE, Behrmann T (1994) Rat myr 4 defines a novel subclass of myosin I: identification, distribution, localization, and mapping

of calmodulin-binding sites with differential calcium sensitivity. J Cell Biol 126(2):375–389
Bahler M, Elfrink K, Hanley PJ, Thelen S, Xu Y (2011) Cellular functions of class IX myosins in epithelia and immune cells. Biochem Soc Trans 39(5):1166–1168. https://doi.org/10.1042/BST0391166
Bandman E (1985) Continued expression of neonatal myosin heavy chain in adult dystrophic skeletal muscle. Science (New York, NY) 227(4688):780–782
Batters C, Arthur CP, Lin A, Porter J, Geeves MA, Milligan RA, Molloy JE, Coluccio LM (2004) Myo1c is designed for the adaptation response in the inner ear. EMBO J 23:1433–1440
Batters C, Brack D, Ellrich H, Averbeck B, Veigel C (2016) Calcium can mobilize and activate myosin-VI. Proc Natl Acad Sci U S A 113(9):E1162–E1169. https://doi.org/10.1073/pnas.1519435113
Beck AE, McMillin MJ, Gildersleeve HI, Shively KM, Tang A, Bamshad MJ (2014) Genotype-phenotype relationships in Freeman-Sheldon syndrome. Am J Med Genet A 164A(11):2808–2813. https://doi.org/10.1002/ajmg.a.36762
Belyantseva IA, Boger ET, Friedman TB (2003) Myosin XVa localizes to the tips of inner ear sensory cell stereocilia and is essential for staircase formation of the hair bundle. Proc Natl Acad Sci U S A 100(24):13958–13963
Belyantseva IA, Boger ET, Naz S, Frolenkov GI, Sellers JR, Ahmed ZM, Griffith AJ, Friedman TB (2005) Myosin-XVa is required for tip localization of whirlin and differential elongation of hair-cell stereocilia. Nat Cell Biol 7:148–156
Bement WM, Hasson T, Wirth JA, Cheney RE, Mooseker MS (1994a) Identification and overlapping expression of multiple unconventional myosin genes in vertebrate cell types [published erratum appears in Proc Natl Acad Sci U S A 1994 Nov 22;91(24):11767]. Proc Natl Acad Sci U S A 91(14):6549–6553
Bement WM, Wirth JA, Mooseker MS (1994b) Cloning and mRNA expression of human unconventional myosin-IC. A homologue of amoeboid myosins-I with a single IQ motif and an SH3 domain. J Mol Biol 243(2):356–363
Benesh AE, Fleming JT, Chiang C, Carter BD, Tyska MJ (2012) Expression and localization of myosin-1d in the developing nervous system. Brain Res 1440:9–22. https://doi.org/10.1016/j.brainres.2011.12.054
Berg JS, Cheney RE (2002) Myosin-X is an unconventional myosin that undergoes intrafilopodial motility. Nat Cell Biol 4(3):246–250. https://doi.org/10.1038/ncb762 ncb762 [pii]
Berg JS, Derfler BH, Pennisi CM, Corey DP, Cheney RE (2000) Myosin-X, a novel myosin with pleckstrin homology domains, associates with regions of dynamic actin. J Cell Sci 113(Pt 19):3439–3451
Berg JS, Powell BC, Cheney RE (2001) A millennial myosin census. Mol Biol Cell 12(4):780–794
Berger J, Berger S, Li M, Currie PD (2017) Myo18b is essential for sarcomere assembly in fast skeletal muscle. Hum Mol Genet 26(6):1146–1156. https://doi.org/10.1093/hmg/ddx025
Beurg M, Fettiplace R, Nam J-H, Ricci AJ (2009) Localization of inner hair cell mechanotransducer channels using high speed imaging. Nat Neurosci 12:553–558
Bi J, Chase SE, Pellenz CD, Kurihara H, Fanning AS, Krendel M (2013) Myosin 1e is a component of the glomerular slit diaphragm complex that regulates actin reorganization during cell-cell contact formation in podocytes. Am J Physiol Renal Physiol 305(4):F532–F544. https://doi.org/10.1152/ajprenal.00223.2013
Bidkhori G, Narimani Z, Hosseini Ashtiani S, Moeini A, Nowzari-Dalini A, Masoudi-Nejad A (2013) Reconstruction of an integrated genome-scale co-expression network reveals key modules involved in lung adenocarcinoma. PLoS One 8(7):e67552. https://doi.org/10.1371/journal.pone.0067552
Billington N, Beach JR, Heissler SM, Remmert K, Guzik-Lendrum S, Nagy A, Takagi Y, Shao L, Li D, Yang Y, Zhang Y, Barzik M, Betzig E, Hammer JA 3rd, Sellers JR (2015) Myosin 18A coassembles with nonmuscle myosin 2 to form mixed bipolar filaments. Curr Biol 25(7):942–948. https://doi.org/10.1016/j.cub.2015.02.012
Bird JE, Takagi Y, Billington N, Strub MP, Sellers JR, Friedman TB (2014) Chaperone-enhanced purification of unconventional myosin 15, a molecular motor specialized for stereocilia protein trafficking. Proc Natl Acad Sci U S A 111(34):12390–12395. https://doi.org/10.1073/pnas.1409459111
Bishai EA, Sidhu GS, Li W, Dhillon J, Bohil AB, Cheney RE, Hartwig JH, Southwick FS (2013) Myosin-X facilitates Shigella-induced membrane protrusions and cell-to-cell spread. Cell Microbiol 15(3):353–367. https://doi.org/10.1111/cmi.12051
Bishe B, Syed GH, Field SJ, Siddiqui A (2012) Role of phosphatidylinositol 4-phosphate (PI4P) and its binding protein GOLPH3 in hepatitis C virus secretion. J Biol Chem 287(33):27637–27647. https://doi.org/10.1074/jbc.M112.346569
Bjornsson T, Thorolfsdottir RB, Sveinbjornsson G, Sulem P, Norddahl GL, Helgadottir A, Gretarsdottir S, Magnusdottir A, Danielsen R, Sigurdsson EL, Adalsteinsdottir B, Gunnarsson SI, Jonsdottir I, Arnar DO, Helgason H, Gudbjartsson T, Gudbjartsson DF, Thorsteinsdottir U, Holm H, Stefansson K (2018) A rare missense mutation in MYH6 associates with non-syndromic coarctation of the aorta. Eur Heart J 39(34):3243–3249. https://doi.org/10.1093/eurheartj/ehy142
Bloemink MJ, Geeves MA (2011) Shaking the myosin family tree: biochemical kinetics defines four types of myosin motor. Semin Cell Dev Biol 22(9):961–967. https://doi.org/10.1016/j.semcdb.2011.09.015
Boeda B, El-Amraoui A, Bahloul A, Goodyear R, Daviet L, Blanchard S, Perfettini I, Fath KR, Shorte S, Reiners J, Houdusse A, Legrain P, Wolfrum U, Richardson G, Petit C (2002) Myosin VIIa, harmonin and cadherin 23,

three Usher I gene products that cooperate to shape the sensory hair cell bundle. EMBO J 21(24):6689–6699

Boger ET, Sellers JR, Friedman TB (2001) Human myosin XVBP is a transcribed pseudogene. J Muscle Res Cell Motil 22(5):477–483

Boguslavsky S, Chiu T, Foley KP, Osorio-Fuentealba C, Antonescu CN, Bayer KU, Bilan PJ, Klip A (2012) Myo1c binding to submembrane actin mediates insulin-induced tethering of GLUT4 vesicles. Mol Biol Cell 23(20):4065–4078. https://doi.org/10.1091/mbc.E12-04-0263

Bohil AB, Robertson BW, Cheney RE (2006) Myosin-X is a molecular motor that functions in filopodia formation. Proc Natl Acad Sci U S A 103(33):12411–12416

Bohlega S, Abu-Amero SN, Wakil SM, Carroll P, Al-Amr R, Lach B, Al-Sayed Y, Cupler EJ, Meyer BF (2004) Mutation of the slow myosin heavy chain rod domain underlies hyaline body myopathy. Neurology 62(9):1518–1521

Bolz H, von Brederlow B, Ramirez A, Bryda EC, Kutsche K, Nothwang HG, Seeliger M, del CSCM, Vila MC, Molina OP, Gal A, Kubisch C (2001) Mutation of CDH23, encoding a new member of the cadherin gene family, causes Usher syndrome type 1D. Nat Genet 27(1):108–112. https://doi.org/10.1038/83667

Bond LM, Peden AA, Kendrick-Jones J, Sellers JR, Buss F (2011) Myosin VI and its binding partner optineurin are involved in secretory vesicle fusion at the plasma membrane. Mol Biol Cell 22(1):54–65. https://doi.org/10.1091/mbc.E10-06-0553

Bork JM, Peters LM, Riazuddin S, Bernstein SL, Ahmed ZM, Ness SL, Polomeno R, Ramesh A, Schloss M, Srisailpathy CR, Wayne S, Bellman S, Desmukh D, Ahmed Z, Khan SN, Kaloustian VM, Li XC, Lalwani A, Riazuddin S, Bitner-Glindzicz M, Nance WE, Liu XZ, Wistow G, Smith RJ, Griffith AJ, Wilcox ER, Friedman TB, Morell RJ (2001) Usher syndrome 1D and nonsyndromic autosomal recessive deafness DFNB12 are caused by allelic mutations of the novel cadherin-like gene CDH23. Am J Hum Genet 68(1):26–37. https://doi.org/10.1086/316954

Bose A, Robida S, Furcinitti PS, Chawla A, Fogarty K, Corvera S, Czech MP (2004) Unconventional myosin Myo1c promotes membrane fusion in a regulated exocytic pathway. Mol Cell Biol 24(12):5447–5458

Boulton M, Dayhaw-Barker P (2001) The role of the retinal pigment epithelium: topographical variation and ageing changes. Eye (Lond) 15(Pt 3):384–389. https://doi.org/10.1038/eye.2001.141

Braathen GJ, Hoyer H, Busk OL, Tveten K, Skjelbred CF, Russell MB (2016) Variants in the genes DCTN2, DNAH10, LRIG3, and MYO1A are associated with intermediate Charcot-Marie-Tooth disease in a Norwegian family. Acta Neurol Scand 134(1):67–75. https://doi.org/10.1111/ane.12515

Brandstaetter H, Kendrick-Jones J, Buss F (2012) Myo1c regulates lipid raft recycling to control cell spreading, migration and Salmonella invasion. J Cell Sci 125(Pt 8):1991–2003. https://doi.org/10.1242/jcs.097212

Brandstaetter H, Kishi-Itakura C, Tumbarello DA, Manstein DJ, Buss F (2014) Loss of functional MYO1C/myosin 1c, a motor protein involved in lipid raft trafficking, disrupts autophagosome-lysosome fusion. Autophagy 10(12):2310–2323. https://doi.org/10.4161/15548627.2014.984272

Brook JD, McCurrach ME, Harley HG, Buckler AJ, Church D, Aburatani H, Hunter K, Stanton VP, Thirion JP, Hudson T et al (1992) Molecular basis of myotonic dystrophy: expansion of a trinucleotide (CTG) repeat at the 3′ end of a transcript encoding a protein kinase family member. Cell 69(2):385

Brooks AB, Humphreys D, Singh V, Davidson AC, Arden SD, Buss F, Koronakis V (2017) MYO6 is targeted by Salmonella virulence effectors to trigger PI3-kinase signaling and pathogen invasion into host cells. Proc Natl Acad Sci U S A 114(15):3915–3920. https://doi.org/10.1073/pnas.1616418114

Broomfield SJ, Bruce IA, Henderson L, Ramsden RT, Green KM (2013) Cochlear implantation in children with syndromic deafness. Int J Pediatr Otorhinolaryngol 77(8):1312–1316. https://doi.org/10.1016/j.ijporl.2013.05.022

Brozzi F, Diraison F, Lajus S, Rajatileka S, Philips T, Regazzi R, Fukuda M, Verkade P, Molnar E, Varadi A (2012) Molecular mechanism of myosin Va recruitment to dense core secretory granules. Traffic 13(1):54–69. https://doi.org/10.1111/j.1600-0854.2011.01301.x

Bruun K, Beach JR, Heissler SM, Remmert K, Sellers JR, Hammer JA (2017) Re-evaluating the roles of myosin 18Aalpha and F-actin in determining Golgi morphology. Cytoskeleton (Hoboken) 74(5):205–218. https://doi.org/10.1002/cm.21364

Bryant Z, Altman D, Spudich JA (2007) The power stroke of myosin VI and the basis of reverse directionality. Proc Natl Acad Sci U S A 104(3):772–777. https://doi.org/10.1073/pnas.0610144104

Buschman MD, Field SJ (2018) MYO18A: an unusual myosin. Adv Biol Regul 67:84–92. https://doi.org/10.1016/j.jbior.2017.09.005

Buss F, Kendrick-Jones J, Lionne C, Knight AE, Cote GP, Paul Luzio J (1998) The localization of myosin VI at the golgi complex and leading edge of fibroblasts and its phosphorylation and recruitment into membrane ruffles of A431 cells after growth factor stimulation. J Cell Biol 143(6):1535–1545

Buss F, Arden SD, Lindsay M, Luzio JP, Kendrick-Jones J (2001) Myosin VI isoform localized to clathrin-coated vesicles with a role in clathrin-mediated endocytosis. EMBO J 20(14):3676–3684

Buvoli M, Buvoli A, Leinwand LA (2012) Effects of pathogenic proline mutations on myosin assembly. J Mol Biol 415(5):807–818. https://doi.org/10.1016/j.jmb.2011.11.042

Cameron RS, Liu C, Mixon AS, Pihkala JP, Rahn RJ, Cameron PL (2007) Myosin16b: The COOH-tail region directs localization to the nucleus and overexpression delays S-phase progression. Cell Motil Cytoskeleton 64(1):19–48. https://doi.org/10.1002/cm.20162

Cameron RS, Liu C, Pihkala JP (2013) Myosin 16 levels fluctuate during the cell cycle and are downregulated in response to DNA replication stress. Cytoskeleton (Hoboken) 70(6):328–348. https://doi.org/10.1002/cm.21109

Canzian F, Amati P, Harach HR, Kraimps JL, Lesueur F, Barbier J, Levillain P, Romeo G, Bonneau D (1998) A gene predisposing to familial thyroid tumors with cell oxyphilia maps to chromosome 19p13.2. Am J Hum Genet 63(6):1743–1748. https://doi.org/10.1086/302164

Cao R, Chen J, Zhang X, Zhai Y, Qing X, Xing W, Zhang L, Malik YS, Yu H, Zhu X (2014) Elevated expression of myosin X in tumours contributes to breast cancer aggressiveness and metastasis. Br J Cancer 111(3):539–550. https://doi.org/10.1038/bjc.2014.298

Carniel E, Taylor MR, Sinagra G, Di Lenarda A, Ku L, Fain PR, Boucek MM, Cavanaugh J, Miocic S, Slavov D, Graw SL, Feiger J, Zhu XZ, Dao D, Ferguson DA, Bristow MR, Mestroni L (2005) Alpha-myosin heavy chain: a sarcomeric gene associated with dilated and hypertrophic phenotypes of cardiomyopathy. Circulation 112(1):54–59. https://doi.org/10.1161/CIRCULATIONAHA.104.507699

Carton-Garcia F, Overeem AW, Nieto R, Bazzocco S, Dopeso H, Macaya I, Bilic J, Landolfi S, Hernandez-Losa J, Schwartz S Jr, Ramon y CS, van Ijzendoorn SC, Arango D (2015) Myo5b knockout mice as a model of microvillus inclusion disease. Sci Rep 5:12312. https://doi.org/10.1038/srep12312

Castilla LH, Garrett L, Adya N, Orlic D, Dutra A, Anderson S, Owens J, Eckhaus M, Bodine D, Liu PP (1999) The fusion gene Cbfb-MYH11 blocks myeloid differentiation and predisposes mice to acute myelomonocytic leukaemia. Nat Genet 23(2):144–146. https://doi.org/10.1038/13776

Cechova S, Dong F, Chan F, Kelley MJ, Ruiz P, Le TH (2018) MYH9 E1841K mutation augments proteinuria and podocyte injury and migration. J Am Soc Nephrol 29(1):155–167. https://doi.org/10.1681/ASN.2015060707

Chai J, Liu C, Lai P, Yee W (2007) C.P.1.15 Myosin storage myopathy with a novel slow-skeletal myosin (MYH7) mutation in a Chinese patient. Neuromuscul Disord 17(9–10):838

Chapman BV, Wald AI, Akhtar P, Munko AC, Xu J, Gibson SP, Grandis JR, Ferris RL, Khan SA (2015) MicroRNA-363 targets myosin 1B to reduce cellular migration in head and neck cancer. BMC Cancer 15:861. https://doi.org/10.1186/s12885-015-1888-3

Chase SE, Encina CV, Stolzenburg LR, Tatum AH, Holzman LB, Krendel M (2012) Podocyte-specific knockout of myosin 1e disrupts glomerular filtration. Am J Physiol Renal Physiol 303(7):F1099–F1106. https://doi.org/10.1152/ajprenal.00251.2012

Chen H, Chan DC (2009) Mitochondrial dynamics–fusion, fission, movement, and mitophagy–in neurodegenerative diseases. Hum Mol Genet 18(R2):R169–R176. https://doi.org/10.1093/hmg/ddp326

Chen ZY, Hasson T, Kelley PM, Schwender BJ, Schwartz MF, Ramakrishnan M, Kimberling WJ, Mooseker MS, Corey DP (1996) Molecular cloning and domain structure of human myosin-VIIa, the gene product defective in Usher syndrome 1B. Genomics 36(3):440–448

Chen AH, Stephan DA, Hasson T, Fukushima K, Nelissen CM, Chen AF, Jun AI, Ramesh A, Van Camp G, Smith RJ (2001a) MYO1F as a candidate gene for nonsyndromic deafness, DFNB15. Arch Otolaryngol Head Neck Surg 127(8):921–925

Chen ZY, Hasson T, Zhang DS, Schwender BJ, Derfler BH, Mooseker MS, Corey DP (2001b) Myosin-VIIb, a novel unconventional myosin, is a constituent of microvilli in transporting epithelia. Genomics 72(3):285–296. https://doi.org/10.1006/geno.2000.6456

Chen CP, Sun ZL, Lu X, Wu WX, Guo WL, Lu JJ, Han C, Huang JQ, Fang Y (2016a) MiR-340 suppresses cell migration and invasion by targeting MYO10 in breast cancer. Oncol Rep 35(2):709–716. https://doi.org/10.3892/or.2015.4411

Chen YQ, Zhang L, Lv XY, Wang HZ (2016b) Lack of association between MYO9B gene polymorphisms and susceptibility to coeliac disease in caucasians: evidence from a meta-analysis. Immunol Investig 45(5):396–405. https://doi.org/10.3109/08820139.2016.1156692

Cheng J, Grassart A, Drubin DG (2012) Myosin 1E coordinates actin assembly and cargo trafficking during clathrin-mediated endocytosis. Mol Biol Cell 23(15):2891–2904. https://doi.org/10.1091/mbc.E11-04-0383

Chieregatti E, Gartner A, Stoffler HE, Bahler M (1998) Myr 7 is a novel myosin IX-RhoGAP expressed in rat brain. J Cell Sci 111(Pt 24):3597–3608

Ching YH, Ghosh TK, Cross SJ, Packham EA, Honeyman L, Loughna S, Robinson TE, Dearlove AM, Ribas G, Bonser AJ, Thomas NR, Scotter AJ, Caves LS, Tyrrell GP, Newbury-Ecob RA, Munnich A, Bonnet D, Brook JD (2005) Mutation in myosin heavy chain 6 causes atrial septal defect. Nat Genet 37(4):423–428. https://doi.org/10.1038/ng1526

Choi BO, Kang SH, Hyun YS, Kanwal S, Park SW, Koo H, Kim SB, Choi YC, Yoo JH, Kim JW, Park KD, Choi KG, Kim SJ, Zuchner S, Chung KW (2011) A complex phenotype of peripheral neuropathy, myopathy, hoarseness, and hearing loss is linked to an autosomal dominant mutation in MYH14. Hum Mutat 32(6):669–677. https://doi.org/10.1002/humu.21488

Chuang CH, Carpenter AE, Fuchsova B, Johnson T, de Lanerolle P, Belmont AS (2006) Long-range directional movement of an interphase chromosome site. Curr Biol 16(8):825–831. https://doi.org/10.1016/j.cub.2006.03.059

Chung W, Bondaruk J, Jelinek J, Lotan Y, Liang S, Czerniak B, Issa JP (2011) Detection of bladder cancer using novel DNA methylation biomarkers in urine sediments. Cancer epidemiology, biomarkers & prevention: a publication of the American Association for Cancer Research, cosponsored by the American

Society of Preventive. Oncology 20(7):1483–1491. https://doi.org/10.1158/1055-9965.EPI-11-0067

Colegrave M, Peckham M (2014) Structural implications of beta-cardiac myosin heavy chain mutations in human disease. Anat Rec (Hoboken) 297(9):1670–1680. https://doi.org/10.1002/ar.22973

Colella P, Sommella A, Marrocco E, Di Vicino U, Polishchuk E, Garcia Garrido M, Seeliger MW, Polishchuk R, Auricchio A (2013) Myosin7a deficiency results in reduced retinal activity which is improved by gene therapy. PLoS One 8(8):e72027. https://doi.org/10.1371/journal.pone.0072027

Collins K, Sellers JR, Matsudaira P (1990) Calmodulin dissociation regulates brush border myosin I (110-kD-calmodulin) mechanochemical activity in vitro. J Cell Biol 110(4):1137–1147

Coluccio LM (2018) Structure and function of mammalian class I myosins. In: Broadbent D (ed) Myosin. Nova Science Publishers, Inc

Coluccio LM, Bretscher A (1989) Reassociation of microvillar core proteins: making a microvillar core in vitro. J Cell Biol 108(2):495–502

Coluccio LM, Geeves MA (1999) Transient kinetic analysis of the 130-kDa myosin I (myr 1 gene product) from rat liver: a myosin I designed for maintenance of tension? J Biol Chem 274:21575–21580

Conti MA, Even-Ram S, Liu C, Yamada KM, Adelstein RS (2004) Defects in cell adhesion and the visceral endoderm following ablation of nonmuscle myosin heavy chain II-A in mice. J Biol Chem 279(40):41263–41266. https://doi.org/10.1074/jbc.C400352200

Conti MA, Kawamoto S, Adelstein RS (2008) Nonmuscle myosin II. In: Proteins and cell regulation, vol 7. Springer, Dordrecht, pp 223–264

Conti MA, Saleh AD, Brinster LR, Cheng H, Chen Z, Cornelius S, Liu C, Ma X, Van Waes C, Adelstein RS (2015) Conditional deletion of nonmuscle myosin II-A in mouse tongue epithelium results in squamous cell carcinoma. Sci Rep 5:14068. https://doi.org/10.1038/srep14068

Cordonnier MN, Dauzonne D, Louvard D, Coudrier E (2001) Actin filaments and Myosin I alpha cooperate with microtubules for the movement of lysosomes. Mol Biol Cell 12(12):4013–4029

Correia SS, Bassani S, Brown TC, Lise MF, Backos DS, El-Husseini A, Passafaro M, Esteban JA (2008) Motor protein-dependent transport of AMPA receptors into spines during long-term potentiation. Nat Neurosci 11(4):457–466. https://doi.org/10.1038/nn2063

Cosgrove D, Zallocchi M (2014) Usher protein functions in hair cells and photoreceptors. Int J Biochem Cell Biol 46:80–89. https://doi.org/10.1016/j.biocel.2013.11.001

Courson DS, Cheney RE (2015) Myosin-X and disease. Exp Cell Res 334(1):10–15. https://doi.org/10.1016/j.yexcr.2015.03.014

Crawley SW, Shifrin DA Jr, Grega-Larson NE, McConnell RE, Benesh AE, Mao S, Zheng Y, Zheng QY, Nam KT, Millis BA, Kachar B, Tyska MJ (2014) Intestinal brush border assembly driven by protocadherin-based intermicrovillar adhesion. Cell 157(2):433–446. https://doi.org/10.1016/j.cell.2014.01.067

Cremo CR, Geeves MA (1998) Interaction of actin and ADP with the head domain of smooth muscle myosin: implications for strain-dependent ADP release in smooth muscle. Biochemistry 37(7):1969–1978

Crozet F, el Amraoui A, Blanchard S, Lenoir M, Ripoll C, Vago P, Hamel C, Fizames C, Levi-Acobas F, Depetris D, Mattei MG, Weil D, Pujol R, Petit C (1997) Cloning of the genes encoding two murine and human cochlear unconventional type I myosins. Genomics 40(2):332–341

Cruz CV, Mattos CT, Maia JC, Granjeiro JM, Reis MF, Mucha JN, Vilella B, Ruellas AC, Luiz RR, Costa MC, Vieira AR (2017) Genetic polymorphisms underlying the skeletal Class III phenotype. Am J Orthod Dentofac Orthop 151(4):700–707. https://doi.org/10.1016/j.ajodo.2016.09.013

Cullup T, Lamont PJ, Cirak S, Damian MS, Wallefeld W, Gooding R, Tan SV, Sheehan J, Muntoni F, Abbs S, Sewry CA, Dubowitz V, Laing NG, Jungbluth H (2012) Mutations in MYH7 cause Multi-minicore Disease (MmD) with variable cardiac involvement. Neuromuscul Disord 22(12):1096–1104. https://doi.org/10.1016/j.nmd.2012.06.007

da Fontoura CS, Miller SF, Wehby GL, Amendt BA, Holton NE, Southard TE, Allareddy V, Moreno Uribe LM (2015) Candidate gene analyses of skeletal variation in malocclusion. J Dent Res 94(7):913–920. https://doi.org/10.1177/0022034515581643

Dadson K, Hauck L, Billia F (2017) Molecular mechanisms in cardiomyopathy. Clin Sci (Lond) 131(13):1375–1392. https://doi.org/10.1042/CS20160170

Dance AL, Miller M, Seragaki S, Aryal P, White B, Aschenbrenner L, Hasson T (2004) Regulation of myosin-VI targeting to endocytic compartments. Traffic 5(10):798–813. https://doi.org/10.1111/j.1600-0854.2004.00224.x

Daniels MJ, Wang Y, Lee M, Venkitaraman AR (2004) Abnormal cytokinesis in cells deficient in the breast cancer susceptibility protein BRCA2. Science (New York, NY) 306(5697):876–879. https://doi.org/10.1126/science.1102574

Dantas VGL, Raval MH, Ballesteros A, Cui R, Gunther LK, Yamamoto GL, Alves LU, Bueno AS, Lezirovitz K, Pirana S, Mendes BCA, Yengo CM, Kachar B, Mingroni-Netto RC (2018) Characterization of a novel MYO3A missense mutation associated with a dominant form of late onset hearing loss. Sci Rep 8(1):8706. https://doi.org/10.1038/s41598-018-26818-2

Dart AE, Tollis S, Bright MD, Frankel G, Endres RG (2012) The motor protein myosin 1G functions in FcgammaR-mediated phagocytosis. J Cell Sci 125(Pt 24):6020–6029. https://doi.org/10.1242/jcs.109561

de Lanerolle P, Johnson T, Hofmann WA (2005) Actin and myosin I in the nucleus: what next? Nat Struct Mol Biol 12:742–746

Dekker-Ohno K, Hayasaka S, Takagishi Y, Oda S, Wakasugi N, Mikoshiba K, Inouye M, Yamamura H

(1996) Endoplasmic reticulum is missing in dendritic spines of Purkinje cells of the ataxic mutant rat. Brain Res 714(1–2):226–230

Delestre-Delacour C, Carmon O, Laguerre F, Estay-Ahumada C, Courel M, Elias S, Jeandel L, Rayo MV, Peinado JR, Sengmanivong L, Gasman S, Coudrier E, Anouar Y, Montero-Hadjadje M (2017) Myosin 1b and F-actin are involved in the control of secretory granule biogenesis. Sci Rep 7(1):5172. https://doi.org/10.1038/s41598-017-05617-1

Derycke L, Stove C, Vercoutter-Edouart AS, De Wever O, Dolle L, Colpaert N, Depypere H, Michalski JC, Bracke M (2011) The role of non-muscle myosin IIA in aggregation and invasion of human MCF-7 breast cancer cells. Int J Dev Biol 55(7–9):835–840. https://doi.org/10.1387/ijdb.113336ld

Desgrosellier JS, Cheresh DA (2010) Integrins in cancer: biological implications and therapeutic opportunities. Nat Rev Cancer 10(1):9–22. https://doi.org/10.1038/nrc2748

Desnos C, Huet S, Fanget I, Chapuis C, Bottiger C, Racine V, Sibarita JB, Henry JP, Darchen F (2007) Myosin va mediates docking of secretory granules at the plasma membrane. J Neurosci 27(39):10636–10645. https://doi.org/10.1523/JNEUROSCI.1228-07.2007

Dhekne HS, Hsiao NH, Roelofs P, Kumari M, Slim CL, Rings EH, van Ijzendoorn SC (2014) Myosin Vb and Rab11a regulate phosphorylation of ezrin in enterocytes. J Cell Sci 127(Pt 5):1007–1017. https://doi.org/10.1242/jcs.137273

Dhekne HS, Pylypenko O, Overeem AW, Ferreira RJ, van der Velde KJ, Rings E, Posovszky C, Swertz MA, Houdusse A, van ISCD (2018) MYO5B, STX3, and STXBP2 mutations reveal a common disease mechanism that unifies a subset of congenital diarrheal disorders: a mutation update. Hum Mutat 39(3):333–344. https://doi.org/10.1002/humu.23386

DiDonato JA, Hayakawa M, Rothwarf DM, Zandi E, Karin M (1997) A cytokine-responsive IkappaB kinase that activates the transcription factor NF-kappaB. Nature 388(6642):548–554. https://doi.org/10.1038/41493

Dijkhuizen T, de Jong B, Meuzelaar JJ, Molenaar WM, van den Berg E (2001) No cytogenetic evidence for involvement of gene(s) at 2p16 in sporadic cardiac myxomas: cytogenetic changes in ten sporadic cardiac myxomas. Cancer Genet Cytogenet 126(2):162–165

Dippold HC, Ng MM, Farber-Katz SE, Lee SK, Kerr ML, Peterman MC, Sim R, Wiharto PA, Galbraith KA, Madhavarapu S, Fuchs GJ, Meerloo T, Farquhar MG, Zhou H, Field SJ (2009) GOLPH3 bridges phosphatidylinositol-4- phosphate and actomyosin to stretch and shape the Golgi to promote budding. Cell 139(2):337–351. https://doi.org/10.1016/j.cell.2009.07.052

Diquigiovanni C, Bergamini C, Evangelisti C, Isidori F, Vettori A, Tiso N, Argenton F, Costanzini A, Iommarini L, Anbunathan H, Pagotto U, Repaci A, Babbi G, Casadio R, Lenaz G, Rhoden KJ, Porcelli AM, Fato R, Bowcock A, Seri M, Romeo G, Bonora E (2018) Mutant MYO1F alters the mitochondrial network and induces tumor proliferation in thyroid cancer. Int J Cancer. https://doi.org/10.1002/ijc.31548

Divito MM, Cheney RE (2008) Myosin X. Proteins. Cell Regul 7:403–419

Donaudy F, Snoeckx R, Pfister M, Zenner HP, Blin N, Di Stazio M, Ferrara A, Lanzara C, Ficarella R, Declau F, Pusch CM, Nurnberg P, Melchionda S, Zelante L, Ballana E, Estivill X, Van Camp G, Gasparini P, Savoia A (2004) Nonmuscle myosin heavy-chain gene MYH14 is expressed in cochlea and mutated in patients affected by autosomal dominant hearing impairment (DFNA4). Am J Hum Genet 74(4):770–776. https://doi.org/10.1086/383285

Dong W, Chen X, Chen P, Yue D, Zhu L, Fan Q (2012) Inactivation of MYO5B promotes invasion and motility in gastric cancer cells. Dig Dis Sci 57(5):1247–1252. https://doi.org/10.1007/s10620-011-1989-z

Dong W, Wang L, Shen R (2013) MYO5B is epigenetically silenced and associated with MET signaling in human gastric cancer. Dig Dis Sci 58(7):2038–2045. https://doi.org/10.1007/s10620-013-2600-6

Dose AC, Hillman DW, Wong C, Sohlberg L, Lin-Jones J, Burnside B (2003) Myo3A, one of two class III myosin genes expressed in vertebrate retina, is localized to the calycal processes of rod and cone photoreceptors and is expressed in the sacculus. Mol Biol Cell 14(3):1058–1073. https://doi.org/10.1091/mbc.E02-06-0317

Dosé A, Lin-Jones J, Burnside B (2008) Class III Myosins. In: Proteins and cell regulation, vol 7. Springer, Dordrecht, pp 265–287

Du YC, Lewis BC, Hanahan D, Varmus H (2007) Assessing tumor progression factors by somatic gene transfer into a mouse model: Bcl-xL promotes islet tumor cell invasion. PLoS Biol 5(10):e276. https://doi.org/10.1371/journal.pbio.0050276

Duhoux FP, Ameye G, Libouton JM, Bahloula K, Iossifidis S, Chantrain CF, Demoulin JB, Poirel HA (2011) The t(11;19)(q23;p13) fusing MLL with MYO1F is recurrent in infant acute myeloid leukemias. Leuk Res 35(9):e171–e172. https://doi.org/10.1016/j.leukres.2011.04.022

Dumont RA, Zhao YD, Holt JR, Bahler M, Gillespie PG (2002) Myosin-I isozymes in neonatal rodent auditory and vestibular epithelia. J Assoc Res Otolaryngol 3(4):375–389. https://doi.org/10.1007/s101620020049

Dunn TA, Chen S, Faith DA, Hicks JL, Platz EA, Chen Y, Ewing CM, Sauvageot J, Isaacs WB, De Marzo AM, Luo J (2006) A novel role of myosin VI in human prostate cancer. Am J Pathol 169(5):1843–1854. https://doi.org/10.2353/ajpath.2006.060316

Durrbach A, Raposo G, Tenza D, Louvard D, Coudrier E (2000) Truncated brush border myosin I affects membrane traffic in polarized epithelial cells. Traffic 1:411–424

Dvornikov D, Schneider MA, Ohse S, Szczygiel M, Titkova I, Rosenblatt M, Muley T, Warth A, Herth FJ, Dienemann H, Thomas M, Timmer J, Schilling M, Busch H, Boerries M, Meister M, Klingmuller U (2018) Expression ratio of the TGFbeta-inducible gene MYO10 is prognostic for overall survival of squamous cell lung cancer patients and predicts chemotherapy response. Sci Rep 8(1):9517. https://doi.org/10.1038/s41598-018-27912-1

Dye DE, Azzarelli B, Goebel HH, Laing NG (2006) Novel slow-skeletal myosin (MYH7) mutation in the original myosin storage myopathy kindred. Neuromuscul Disord 16(6):357–360. https://doi.org/10.1016/j.nmd.2006.03.011

Dzijak R, Yildirim S, Kahle M, Novak P, Hnilicova J, Venit T, Hozak P (2012) Specific nuclear localizing sequence directs two myosin isoforms to the cell nucleus in calmodulin-sensitive manner. PLoS One 7(1):e30529. https://doi.org/10.1371/journal.pone.0030529

Ebrahim S, Avenarius MR, Grati M, Krey JF, Windsor AM, Sousa AD, Ballesteros A, Cui R, Millis BA, Salles FT, Baird MA, Davidson MW, Jones SM, Choi D, Dong L, Raval MH, Yengo CM, Barr-Gillespie PG, Kachar B (2016) Stereocilia-staircase spacing is influenced by myosin III motors and their cargos espin-1 and espin-like. Nat Commun 7:10833. https://doi.org/10.1038/ncomms10833

Eddinger TJ, Meer DP (2007) Myosin II isoforms in smooth muscle: heterogeneity and function. Am J Physiol Cell Physiol 293(2):C493–C508. https://doi.org/10.1152/ajpcell.00131.2007

Edgren H, Murumagi A, Kangaspeska S, Nicorici D, Hongisto V, Kleivi K, Rye IH, Nyberg S, Wolf M, Borresen-Dale AL, Kallioniemi O (2011) Identification of fusion genes in breast cancer by paired-end RNA-sequencing. Genome Biol 12(1):R6. https://doi.org/10.1186/gb-2011-12-1-r6

Edimo WE, Ramos AR, Ghosh S, Vanderwinden JM, Erneux C (2016) The SHIP2 interactor Myo1c is required for cell migration in 1321 N1 glioblastoma cells. Biochem Biophys Res Commun. https://doi.org/10.1016/j.bbrc.2016.05.154

El-Amraoui A, Petit C (2005) Usher I syndrome: unravelling the mechanisms that underlie the cohesion of the growing hair bundle in inner ear sensory cells. J Cell Sci 118(Pt 20):4593–4603. https://doi.org/10.1242/jcs.02636

El-Amraoui A, Sahly I, Picaud S, Sahel J, Abitbol M, Petit C (1996) Human Usher 1B/mouse shaker-1: the retinal phenotype discrepancy explained by the presence/absence of myosin VIIA in the photoreceptor cells. Hum Mol Genet 5(8):1171–1178

El-Amraoui A, Schonn JS, Kussel-Andermann P, Blanchard S, Desnos C, Henry JP, Wolfrum U, Darchen F, Petit C (2002) MyRIP, a novel Rab effector, enables myosin VIIa recruitment to retinal melanosomes. EMBO Rep 3(5):463–470. https://doi.org/10.1093/embo-reports/kvf090

Elfrink K, Liao W, Pieper U, Oeding SJ, Bahler M (2014) The loop2 insertion of type IX myosin acts as an electrostatic actin tether that permits processive movement. PLoS One 9(1):e84874. https://doi.org/10.1371/journal.pone.0084874

Engevik AC, Kaji I, Engevik MA, Meyer AR, Weis VG, Goldstein A, Hess MW, Muller T, Koepsell H, Dudeja PK, Tyska M, Huber LA, Shub MD, Ameen N, Goldenring JR (2018) Loss of MYO5B leads to reductions in Na(+) absorption with maintenance of CFTR-dependent Cl(−) secretion in enterocytes. Gastroenterology. https://doi.org/10.1053/j.gastro.2018.08.025

Erickson RP, Larson-Thome K, Valenzuela RK, Whitaker SE, Shub MD (2008) Navajo microvillous inclusion disease is due to a mutation in MYO5B. Am J Med Genet A 146A(24):3117–3119. https://doi.org/10.1002/ajmg.a.32605

Fan Y, Eswarappa SM, Hitomi M, Fox PL (2012) Myo1c facilitates G-actin transport to the leading edge of migrating endothelial cells. J Cell Biol 198(1):47–55. https://doi.org/10.1083/jcb.201111088

Fang L, Kojima K, Zhou L, Crossman DK, Mobley JA, Grams J (2015a) Analysis of the human proteome in subcutaneous and visceral fat depots in diabetic and non-diabetic patients with morbid obesity. J Proteomics Bioinform 8(6):133–141. https://doi.org/10.4172/jpb.1000361

Fang Q, Indzhykulian AA, Mustapha M, Riordan GP, Dolan DF, Friedman TB, Belyantseva IA, Frolenkov GI, Camper SA, Bird JE (2015b) The 133-kDa N-terminal domain enables myosin 15 to maintain mechanotransducing stereocilia and is essential for hearing. elife 4. https://doi.org/10.7554/eLife.08627

Federico A, Cardaioli E, Da Pozzo P, Formichi P, Gallus GN, Radi E (2012) Mitochondria, oxidative stress and neurodegeneration. J Neurol Sci 322(1–2):254–262. https://doi.org/10.1016/j.jns.2012.05.030

Feinberg AP (2007) Phenotypic plasticity and the epigenetics of human disease. Nature 447(7143):433–440. https://doi.org/10.1038/nature05919

Feldman JL, Mitchell GS, Nattie EE (2003) Breathing: rhythmicity, plasticity, chemosensitivity. Annu Rev Neurosci 26:239–266. https://doi.org/10.1146/annurev.neuro.26.041002.131103

Fernandez LP, Milne RL, Pita G, Floristan U, Sendagorta E, Feito M, Aviles JA, Martin-Gonzalez M, Lazaro P, Benitez J, Ribas G (2009) Pigmentation-related genes and their implication in malignant melanoma susceptibility. Exp Dermatol 18(7):634–642. https://doi.org/10.1111/j.1600-0625.2009.00846.x

Ferreiro A, Estournet B, Chateau D, Romero NB, Laroche C, Odent S, Toutain A, Cabello A, Fontan D, dos Santos HG, Haenggeli CA, Bertini E, Urtizberea JA, Guicheney P, Fardeau M (2000) Multi-minicore disease–searching for boundaries: phenotype analysis of 38 cases. Ann Neurol 48(5):745–757

Ferreiro A, Quijano-Roy S, Pichereau C, Moghadaszadeh B, Goemans N, Bonnemann C, Jungbluth H, Straub

V, Villanova M, Leroy JP, Romero NB, Martin JJ, Muntoni F, Voit T, Estournet B, Richard P, Fardeau M, Guicheney P (2002) Mutations of the selenoprotein N gene, which is implicated in rigid spine muscular dystrophy, cause the classical phenotype of multiminicore disease: reassessing the nosology of early-onset myopathies. Am J Hum Genet 71(4):739–749. https://doi.org/10.1086/342719

Fili N, Hari-Gupta Y, Dos Santos A, Cook A, Poland S, Ameer-Beg SM, Parsons M, Toseland CP (2017) NDP52 activates nuclear myosin VI to enhance RNA polymerase II transcription. Nat Commun 8(1):1871. https://doi.org/10.1038/s41467-017-02050-w

Finno CJ, Gianino G, Perumbakkam S, Williams ZJ, Bordbari MH, Gardner KL, Burns E, Peng S, Durward-Akhurst SA, Valberg SJ (2018) A missense mutation in MYH1 is associated with susceptibility to immune-mediated myositis in Quarter Horses. Skelet Muscle 8(1):7. https://doi.org/10.1186/s13395-018-0155-0

Flashman E, Redwood C, Moolman-Smook J, Watkins H (2004) Cardiac myosin binding protein C: its role in physiology and disease. Circ Res 94(10):1279–1289. https://doi.org/10.1161/01.RES.0000127175.21818.C2

Fomproix N, Percipalle P (2004) An actin-myosin complex on actively transcribing genes. Exp Cell Res 294(1):140–148. https://doi.org/10.1016/j.yexcr.2003.10.028

Foth BJ, Goedecke MC, Soldati D (2006) New insights into myosin evolution and classification. Proc Natl Acad Sci U S A 103:3681–3686

Friedman TB, Riazuddin S (2014) Nonsyndromic deafness: it ain't necessarily so. In: Popper A, Fay R (eds) Perspectives on auditory research. Springer Verlag, New York, pp 149–161

Friedman TB, Liang Y, Weber JL, Hinnant JT, Barber TD, Winata S, Arhya IN, Asher JH Jr (1995) A gene for congenital, recessive deafness DFNB3 maps to the pericentromeric region of chromosome 17. Nat Genet 9(1):86–91. https://doi.org/10.1038/ng0195-86

Friedman TB, Hinnant JT, Fridell RA, Wilcox ER, Raphael Y, Camper SA (2000) DFNB3 families and Shaker-2 mice: mutations in an unconventional myosin, myo 15. Adv Otorhinolaryngol 56:131–144

Friedman SD, Shaw DW, Artru AA, Richards TL, Gardner J, Dawson G, Posse S, Dager SR (2003) Regional brain chemical alterations in young children with autism spectrum disorder. Neurology 60(1):100–107

Friedman TB, Belyantseva I, Frolenkov G (2020) Chapter 13: Myosins and hearing. In: Coluccio LM (ed) Myosins: a superfamily of molecular motors, 2nd edn. Springer, Cham

Frolenkov GI, Belyantseva IA, Friedman TB, Griffith AJ (2004) Genetic insights into the morphogenesis of inner ear hair cells. Nat Rev 5:489–498

Furusawa T, Ikawa S, Yanai N, Obinata M (2000) Isolation of a novel PDZ-containing myosin from hematopoietic supportive bone marrow stromal cell lines. Biochem Biophys Res Commun 270(1):67–75. https://doi.org/10.1006/bbrc.2000.2377

Gauthier J, Ouled Amar Bencheikh B, Hamdan FF, Harrison SM, Baker LA, Couture F, Thiffault I, Ouazzani R, Samuels ME, Mitchell GA, Rouleau GA, Michaud JL, Soucy JF (2015) A homozygous loss-of-function variant in MYH11 in a case with megacystis-microcolon-intestinal hypoperistalsis syndrome. Eur J Hum Genet 23(9):1266–1268. https://doi.org/10.1038/ejhg.2014.256

Geeves MA, Perreault-Micale C, Coluccio LM (2000) Kinetic analyses of a truncated mammalian myosin I suggest a novel isomerization event preceding nucleotide binding. J Biol Chem 275:21624–21630

Geisterfer-Lowrance AA, Christe M, Conner DA, Ingwall JS, Schoen FJ, Seidman CE, Seidman JG (1996) A mouse model of familial hypertrophic cardiomyopathy. Science (New York, NY) 272(5262):731–734

Gerard A, Patino-Lopez G, Beemiller P, Nambiar R, Ben-Aissa K, Liu Y, Totah FJ, Tyska MJ, Shaw S, Krummel MF (2014) Detection of rare antigen-presenting cells through T cell-intrinsic meandering motility, mediated by Myo1g. Cell 158(3):492–505. https://doi.org/10.1016/j.cell.2014.05.044

Gibbs D, Kitamoto J, Williams DS (2003) Abnormal phagocytosis by retinal pigmented epithelium that lacks myosin VIIa, the Usher syndrome 1B protein. Proc Natl Acad Sci U S A 100(11):6481–6486. https://doi.org/10.1073/pnas.1130432100

Gibson F, Walsh J, Mburu P, Varela A, Brown KA, Antonio M, Beisel KW, Steel KP, Brown SD (1995) A type VII myosin encoded by the mouse deafness gene shaker-1. Nature 374(6517):62–64

Gillespie PG, Muller U (2009) Mechanotransduction by hair cells: models, molecules, and mechanisms. Cell 139(1):33–44. https://doi.org/10.1016/j.cell.2009.09.010

Girard M, Lacaille F, Verkarre V, Mategot R, Feldmann G, Grodet A, Sauvat F, Irtan S, Davit-Spraul A, Jacquemin E, Ruemmele F, Rainteau D, Goulet O, Colomb V, Chardot C, Henrion-Caude A, Debray D (2014) MYO5B and bile salt export pump contribute to cholestatic liver disorder in microvillous inclusion disease. Hepatology 60(1):301–310. https://doi.org/10.1002/hep.26974

Golomb E, Ma X, Jana SS, Preston YA, Kawamoto S, Shoham NG, Goldin E, Conti MA, Sellers JR, Adelstein RS (2004) Identification and characterization of nonmuscle myosin II-C, a new member of the myosin II family. J Biol Chem 279(4):2800–2808

Gonseth S, de Smith AJ, Roy R, Zhou M, Lee ST, Shao X, Ohja J, Wrensch MR, Walsh KM, Metayer C, Wiemels JL (2016) Genetic contribution to variation in DNA methylation at maternal smoking-sensitive loci in exposed neonates. Epigenetics 11(9):664–673. https://doi.org/10.1080/15592294.2016.1209614

Gonzales E, Taylor SA, Davit-Spraul A, Thebaut A, Thomassin N, Guettier C, Whitington PF, Jacquemin E (2016) MYO5B mutations cause cholestasis with normal serum gamma-glutamyl transferase activity in children without microvillous inclusion disease. Hepatology. https://doi.org/10.1002/hep.28779

Gorman SW, Haider NB, Grieshammer U, Swiderski RE, Kim E, Welch JW, Searby C, Leng S, Carmi R, Sheffield VC, Duhl DM (1999) The cloning and developmental expression of unconventional myosin IXA (MYO9A) a gene in the Bardet-Biedl syndrome (BBS4) region at chromosome 15q22-q23. Genomics 59(2):150–160. https://doi.org/10.1006/geno.1999.5867

Gousset K, Marzo L, Commere PH, Zurzolo C (2013) Myo10 is a key regulator of TNT formation in neuronal cells. J Cell Sci 126(Pt 19):4424–4435. https://doi.org/10.1242/jcs.129239

Granados-Riveron JT, Ghosh TK, Pope M, Bu'Lock F, Thornborough C, Eason J, Kirk EP, Fatkin D, Feneley MP, Harvey RP, Armour JA, David Brook J (2010) Alpha-cardiac myosin heavy chain (MYH6) mutations affecting myofibril formation are associated with congenital heart defects. Hum Mol Genet 19(20):4007–4016. https://doi.org/10.1093/hmg/ddq315

Grati M, Kachar B (2011) Myosin VIIa and sans localization at stereocilia upper tip-link density implicates these Usher syndrome proteins in mechanotransduction. Proc Natl Acad Sci U S A 108(28):11476–11481. https://doi.org/10.1073/pnas.1104161108

Grati M, Yan D, Raval MH, Walsh T, Ma Q, Chakchouk I, Kannan-Sundhari A, Mittal R, Masmoudi S, Blanton SH, Tekin M, King MC, Yengo CM, Liu XZ (2016) MYO3A causes human dominant deafness and interacts with protocadherin 15-CD2 Isoform. Hum Mutat 37(5):481–487. https://doi.org/10.1002/humu.22961

Green EM, Wakimoto H, Anderson RL, Evanchik MJ, Gorham JM, Harrison BC, Henze M, Kawas R, Oslob JD, Rodriguez HM, Song Y, Wan W, Leinwand LA, Spudich JA, McDowell RS, Seidman JG, Seidman CE (2016) A small-molecule inhibitor of sarcomere contractility suppresses hypertrophic cardiomyopathy in mice. Science (New York, NY) 351(6273):617–621. https://doi.org/10.1126/science.aad3456

Greenberg MJ, Lin T, Goldman YE, Shuman H, Ostap EM (2012) Myosin IC generates power over a range of loads via a new tension-sensing mechanism. Proc Natl Acad Sci U S A 109(37):E2433–E2440. https://doi.org/10.1073/pnas.1207811109

Grewal PK, Jones AM, Maconochie M, Lemmers RJ, Frants RR, Hewitt JE (1999) Cloning of the murine unconventional myosin gene Myo9b and identification of alternative splicing. Gene 240(2):389–398

Griscelli C, Durandy A, Guy-Grand D, Daguillard F, Herzog C, Prunieras M (1978) A syndrome associating partial albinism and immunodeficiency. Am J Med 65(4):691–702

Groth-Pedersen L, Aits S, Corcelle-Termeau E, Petersen NH, Nylandsted J, Jaattela M (2012) Identification of cytoskeleton-associated proteins essential for lysosomal stability and survival of human cancer cells. PLoS One 7(10):e45381. https://doi.org/10.1371/journal.pone.0045381

Guan XY, Sham JS, Tai LS, Fang Y, Li H, Liang Q (2003) Evidence for another tumor suppressor gene at 17p13.3 distal to TP53 in hepatocellular carcinoma. Cancer Genet Cytogenet 140(1):45–48

Gupta P, Gauthier NC, Cheng-Han Y, Zuanning Y, Pontes B, Ohmstede M, Martin R, Knolker HJ, Dobereiner HG, Krendel M, Sheetz M (2013) Myosin 1E localizes to actin polymerization sites in lamellipodia, affecting actin dynamics and adhesion formation. Biol Open 2(12):1288–1299. https://doi.org/10.1242/bio.20135827

Guzik-Lendrum S, Heissler SM, Billington N, Takagi Y, Yang Y, Knight PJ, Homsher E, Sellers JR (2013) Mammalian myosin-18A, a highly divergent myosin. J Biol Chem 288(13):9532–9548. https://doi.org/10.1074/jbc.M112.441238

Haddad EK, Wu X, Hammer JA 3rd, Henkart PA (2001) Defective granule exocytosis in Rab27a-deficient lymphocytes from Ashen mice. J Cell Biol 152(4):835–842

Haithcock J, Billington N, Choi K, Fordham J, Sellers JR, Stafford WF, White H, Forgacs E (2011) The kinetic mechanism of mouse myosin VIIA. J Biol Chem 286(11):8819–8828. https://doi.org/10.1074/jbc.M110.163592

Hales CM, Vaerman JP, Goldenring JR (2002) Rab11 family interacting protein 2 associates with Myosin Vb and regulates plasma membrane recycling. J Biol Chem 277(52):50415–50421. https://doi.org/10.1074/jbc.M209270200

Hallett RM, Dvorkin-Gheva A, Bane A, Hassell JA (2012) A gene signature for predicting outcome in patients with basal-like breast cancer. Sci Rep 2:227. https://doi.org/10.1038/srep00227

Hanley PJ, Xu Y, Kronlage M, Grobe K, Schon P, Song J, Sorokin L, Schwab A, Bahler M (2010) Motorized RhoGAP myosin IXb (Myo9b) controls cell shape and motility. Proc Natl Acad Sci U S A 107(27):12145–12150. 0911986107 [pii] https://doi.org/10.1073/pnas.0911986107

Harakalova M, van der Smagt J, de Kovel CG, Van't Slot R, Poot M, Nijman IJ, Medic J, Joziasse I, Deckers J, Roos-Hesselink JW, Wessels MW, Baars HF, Weiss MM, Pals G, Golmard L, Jeunemaitre X, Lindhout D, Cuppen E, Baas AF (2013) Incomplete segregation of MYH11 variants with thoracic aortic aneurysms and dissections and patent ductus arteriosus. Eur J Hum Genet 21(5):487–493. https://doi.org/10.1038/ejhg.2012.206

Hashimoto T, Gibbs D, Lillo C, Azarian SM, Legacki E, Zhang XM, Yang XJ, Williams DS (2007) Lentiviral gene replacement therapy of retinas in a mouse model for Usher syndrome type 1B. Gene Ther 14(7):584–594. https://doi.org/10.1038/sj.gt.3302897

Hasson T, Heintzelman MB, Santos-Sacchi J, Corey DP, Mooseker MS (1995) Expression in cochlea and retina of myosin VIIa, the gene product defective in Usher syndrome type 1B. Proc Natl Acad Sci U S A 92(21):9815–9819

Hasson T, Gillespie PG, Garcia JA, MacDonald RB, Zhao Y, Yee AG, Mooseker MS, Corey DP (1997) Unconventional myosins in inner-ear sensory epithelia. J Cell Biol 137(6):1287–1307

Hawthorne JL, Mehta PR, Singh PP, Wong NQ, Quintero OA (2016) Positively charged residues within the MYO19 MyMOMA domain are essential for proper localization of MYO19 to the mitochondrial outer membrane. Cytoskeleton (Hoboken) 73(6):286–299. https://doi.org/10.1002/cm.21305

Heath KE, Campos-Barros A, Toren A, Rozenfeld-Granot G, Carlsson LE, Savige J, Denison JC, Gregory MC, White JG, Barker DF, Greinacher A, Epstein CJ, Glucksman MJ, Martignetti JA (2001) Nonmuscle myosin heavy chain IIA mutations define a spectrum of autosomal dominant macrothrombocytopenias: May-Hegglin anomaly and Fechtner, Sebastian, Epstein, and Alport-like syndromes. Am J Hum Genet 69(5):1033–1045. https://doi.org/10.1086/324267

Hedberg Oldfors C, Dios DG, Linder A, Visuttijai K, Samuelson E, Karlsson S, Nilsson S, Behboudi A (2015) Analysis of an independent tumor suppressor locus telomeric to Tp53 suggested Inpp5k and Myo1c as novel tumor suppressor gene candidates in this region. BMC Genet 16(1):80. https://doi.org/10.1186/s12863-015-0238-4

Hegan PS, Kravtsov DV, Caputo C, Egan ME, Ameen NA, Mooseker MS (2015a) Restoration of cytoskeletal and membrane tethering defects but not defects in membrane trafficking in the intestinal brush border of mice lacking both myosin Ia and myosin VI. Cytoskeleton (Hoboken) 72(9):455–476. https://doi.org/10.1002/cm.21238

Hegan PS, Lanahan AA, Simons M, Mooseker MS (2015b) Myosin VI and cardiomyopathy: Left ventricular hypertrophy, fibrosis, and both cardiac and pulmonary vascular endothelial cell defects in the Snell's waltzer mouse. Cytoskeleton (Hoboken) 72(8):373–387. https://doi.org/10.1002/cm.21236

Hegan PS, Ostertag E, Geurts AM, Mooseker MS (2015c) Myosin Id is required for planar cell polarity in ciliated tracheal and ependymal epithelial cells. Cytoskeleton (Hoboken) 72(10):503–516. https://doi.org/10.1002/cm.21259

Heimsath EG Jr, Yim YI, Mustapha M, Hammer JA, Cheney RE (2017) Myosin-X knockout is semi-lethal and demonstrates that myosin-X functions in neural tube closure, pigmentation, hyaloid vasculature regression, and filopodia formation. Sci Rep 7(1):17354. https://doi.org/10.1038/s41598-017-17638-x

Heissler SM, Manstein DJ (2011) Comparative kinetic and functional characterization of the motor domains of human nonmuscle myosin-2C isoforms. J Biol Chem 286(24):21191–21202. https://doi.org/10.1074/jbc.M110.212290

Heissler SM, Chinthalapudi K, Sellers JR (2017) Kinetic signatures of myosin-5B, the motor involved in microvillus inclusion disease. J Biol Chem 292(44):18372–18385. https://doi.org/10.1074/jbc.M117.801456

Henn A, De La Cruz EM (2005) Vertebrate myosin VIIb is a high duty ratio motor adapted for generating and maintaining tension. J Biol Chem 280(47):39665–39676. https://doi.org/10.1074/jbc.M507667200

Hershberger RE, Norton N, Morales A, Li D, Siegfried JD, Gonzalez-Quintana J (2010) Coding sequence rare variants identified in MYBPC3, MYH6, TPM1, TNNC1, and TNNI3 from 312 patients with familial or idiopathic dilated cardiomyopathy. Circ Cardiovasc Genet 3(2):155–161. https://doi.org/10.1161/CIRCGENETICS.109.912345

Hertzano R, Shalit E, Rzadzinska AK, Dror AA, Song L, Ron U, Tan JT, Shitrit AS, Fuchs H, Hasson T, Ben-Tal N, Sweeney HL, de Angelis MH, Steel KP, Avraham KB (2008) A Myo6 mutation destroys coordination between the myosin heads, revealing new functions of myosin VI in the stereocilia of mammalian inner ear hair cells. PLoS Genet 4(10):e1000207. https://doi.org/10.1371/journal.pgen.1000207

Hilton HN, Clarke CL, Graham JD (2017) Estrogen and progesterone signalling in the normal breast and its implications for cancer development. Mol Cell Endocrinol. https://doi.org/10.1016/j.mce.2017.08.011

Hofmann WA, Johnson T, Klapczynski M, Fan JL, de Lanerolle P (2006a) From transcription to transport: emerging roles for nuclear myosin I. Biochem Cell Biol 84(4):418–426. https://doi.org/10.1139/o06-069

Hofmann WA, Vargas GM, Ramchandran R, Stojiljkovic L, Goodrich JA, de Lanerolle PA (2006b) Nuclear myosin I is necessary for the formation of the first phosphodiester bond during transcription initiation by RNA polymerase II. J Cell Biochem 99:1001–1009

Hokanson DE, Laakso JM, Lin T, Sept D, Ostap EM (2006) Myo1c binds phosphoinositides through a putative pleckstrin homology domain. Mol Biol Cell 17:4856–4865

Holm H, Gudbjartsson DF, Sulem P, Masson G, Helgadottir HT, Zanon C, Magnusson OT, Helgason A, Saemundsdottir J, Gylfason A, Stefansdottir H, Gretarsdottir S, Matthiasson SE, Thorgeirsson GM, Jonasdottir A, Sigurdsson A, Stefansson H, Werge T, Rafnar T, Kiemeney LA, Parvez B, Muhammad R, Roden DM, Darbar D, Thorleifsson G, Walters GB, Kong A, Thorsteinsdottir U, Arnar DO, Stefansson K (2011) A rare variant in MYH6 is associated with high risk of sick sinus syndrome. Nat Genet 43(4):316–320. https://doi.org/10.1038/ng.781

Holt JR, Gillespie SKH, Provance DW, Shah K, Shokat KM, Corey DP, Mercer JA, Gillespie PG (2002) A chemical-genetic strategy implicates myosin-1c in adaptation by hair cells. Cell 108(3):371–381

Homburger JR, Green EM, Caleshu C, Sunitha MS, Taylor RE, Ruppel KM, Metpally RP, Colan SD, Michels M, Day SM, Olivotto I, Bustamante CD, Dewey FE, Ho CY, Spudich JA, Ashley EA (2016) Multidimensional structure-function relationships in human beta-cardiac myosin from population-scale genetic variation. Proc Natl Acad Sci U S A 113(24):6701–6706. https://doi.org/10.1073/pnas.1606950113

Hood RL, Schenkel LC, Nikkel SM, Ainsworth PJ, Pare G, Boycott KM, Bulman DE, Sadikovic B (2016) The defining DNA methylation signature of Floating-

Harbor Syndrome. Sci Rep 6:38803. https://doi.org/10.1038/srep38803

Horsthemke M, Nutter LMJ, Bachg AC, Skryabin BV, Honnert U, Zobel T, Bogdan S, Stoll M, Seidl MD, Müller FU, Ravens U, Unger A, Linke WA, van Gorp PRR, de Vries AAF, Bähler M, Hanley PJ (2019) A novel isoform of myosin 18A (Myo18Aγ) is an essential sarcomeric protein in mouse heart. J Biol Chem 294(18):7202–7218

Hoshimaru M, Nakanishi S (1987) Identification of a new type of mammalian myosin heavy chain by molecular cloning. Overlap of its mRNA with preprotachykinin B mRNA. J Biol Chem 262(30):14625–14632

Houdusse A, Sweeney HL (2016) How myosin generates force on actin filaments. Trends Biochem Sci 41(12):989–997. https://doi.org/10.1016/j.tibs.2016.09.006

Hozumi S, Maeda R, Taniguchi K, Kanai M, Shirakabe S, Sasamura T, Spéder P, Noselli S, Aigaki T, Murakami R, Matsuno K (2006) An unconventional myosin in *Drosophila* reverses the default handedness in visceral organs. Nature 440:798–802

Hsu RM, Tsai MH, Hsieh YJ, Lyu PC, Yu JS (2010) Identification of MYO18A as a novel interacting partner of the PAK2/betaPIX/GIT1 complex and its potential function in modulating epithelial cell migration. Mol Biol Cell 21(2):287–301. https://doi.org/10.1091/mbc.E09-03-0232

Hsu RM, Hsieh YJ, Yang TH, Chiang YC, Kan CY, Lin YT, Chen JT, Yu JS (2014) Binding of the extreme carboxyl-terminus of PAK-interacting exchange factor beta (betaPIX) to myosin 18A (MYO18A) is required for epithelial cell migration. Biochim Biophys Acta 1843(11):2513–2527. https://doi.org/10.1016/j.bbamcr.2014.06.023

Huber LA, Fialka I, Paiha K, Hunziker W, Sacks DB, Bähler M, Way M, Gagescu R, Gruenberg J (2000) Both calmodulin and the unconventional myosin Myr4 regulate membrane trafficking along the recycling pathway of MDCK cells. Traffic 1:494–503

Hume AN, Collinson LM, Rapak A, Gomes AQ, Hopkins CR, Seabra MC (2001) Rab27a regulates the peripheral distribution of melanosomes in melanocytes. J Cell Biol 152(4):795–808

Hyde RK, Zhao L, Alemu L, Liu PP (2015) Runx1 is required for hematopoietic defects and leukemogenesis in Cbfb-MYH11 knock-in mice. Leukemia 29(8):1771–1778. https://doi.org/10.1038/leu.2015.58

Ihnatovych I, Migocka-Patrzalek M, Dukh M, Hofmann WA (2012) Identification and characterization of a novel myosin Ic isoform that localizes to the nucleus. Cytoskeleton (Hoboken) 69(8):555–565. https://doi.org/10.1002/cm.21040

Inoue A, Saito J, Ikebe R, Ikebe M (2002) Myosin IXb is a single-headed minus-end-directed processive motor. Nat Cell Biol 4(4):302–306

Isogawa Y, Kon T, Inoue T, Ohkura R, Yamakawa H, Ohara O, Sutoh K (2005) The N-terminal domain of MYO18A has an ATP-insensitive actin-binding site. Biochemistry 44(16):6190–6196. https://doi.org/10.1021/bi0475931

Jacobs DT, Weigert R, Grode KD, Donaldson JG, Cheney RE (2009) Myosin Vc is a molecular motor that functions in secretory granule trafficking. Mol Biol Cell 20(21):4471–4488. https://doi.org/10.1091/mbc.E08-08-0865

Jacobson SG, Cideciyan AV, Gibbs D, Sumaroka A, Roman AJ, Aleman TS, Schwartz SB, Olivares MB, Russell RC, Steinberg JD, Kenna MA, Kimberling WJ, Rehm HL, Williams DS (2011) Retinal disease course in Usher syndrome 1B due to MYO7A mutations. Invest Ophthalmol Vis Sci 52(11):7924–7936. https://doi.org/10.1167/iovs.11-8313

Jalali A, Amirian ES, Bainbridge MN, Armstrong GN, Liu Y, Tsavachidis S, Jhangiani SN, Plon SE, Lau CC, Claus EB, Barnholtz-Sloan JS, Il'yasova D, Schildkraut J, Ali-Osman F, Sadetzki S, Johansen C, Houlston RS, Jenkins RB, Lachance D, Olson SH, Bernstein JL, Merrell RT, Wrensch MR, Davis FG, Lai R, Shete S, Aldape K, Amos CI, Muzny DM, Gibbs RA, Melin BS, Bondy ML (2015) Targeted sequencing in chromosome 17q linkage region identifies familial glioma candidates in the Gliogene Consortium. Sci Rep 5:8278. https://doi.org/10.1038/srep08278

Jana SS, Kawamoto S, Adelstein RS (2006) A specific isoform of nonmuscle myosin II-C is required for cytokinesis in a tumor cell line. J Biol Chem 281(34):24662–24670. https://doi.org/10.1074/jbc.M604606200

Jana SS, Kim KY, Mao J, Kawamoto S, Sellers JR, Adelstein RS (2009) An alternatively spliced isoform of non-muscle myosin II-C is not regulated by myosin light chain phosphorylation. J Biol Chem 284(17):11563–11571. https://doi.org/10.1074/jbc.M806574200

Jatana KR, Thomas D, Weber L, Mets MB, Silverman JB, Young NM (2013) Usher syndrome: characteristics and outcomes of pediatric cochlear implant recipients. Otol Neurotol 34(3):484–489. https://doi.org/10.1097/MAO.0b013e3182877ef2

Jean Beltran PM, Mathias RA, Cristea IM (2016) A portrait of the human organelle proteome in space and time during cytomegalovirus infection. Cell Syst 3(4):361–373 e366. https://doi.org/10.1016/j.cels.2016.08.012

Jonsdottir AB, Vreeswijk MP, Wolterbeek R, Devilee P, Tanke HJ, Eyfjord JE, Szuhai K (2009) BRCA2 heterozygosity delays cytokinesis in primary human fibroblasts. Cell Oncol 31(3):191–201. https://doi.org/10.3233/CLO-2009-0465

Jontes JD, Milligan RA (1997) Brush border myosin-I structure and ADP-dependent conformational changes revealed by cryoelectron microscopy and image analysis. J Cell Biol 139(3):683–693

Jontes JD, Wilson-Kubalek EM, Milligan RA (1995) A 32 degree tail swing in brush border myosin I on ADP release [see comments]. Nature 378(6558):751–753

Jontes JD, Milligan RA, Pollard TD, Ostap EM (1997) Kinetic characterization of brush border myosin-I ATPase. Proc Natl Acad Sci U S A 94(26):14332–14337

Joubert BR, Haberg SE, Nilsen RM, Wang X, Vollset SE, Murphy SK, Huang Z, Hoyo C, Midttun O, Cupul-Uicab LA, Ueland PM, Wu MC, Nystad W, Bell DA, Peddada SD, London SJ (2012) 450K epigenome-wide scan identifies differential DNA methylation in newborns related to maternal smoking during pregnancy. Environ Health Perspect 120(10):1425–1431. https://doi.org/10.1289/ehp.1205412

Juan T, Geminard C, Coutelis JB, Cerezo D, Poles S, Noselli S, Furthauer M (2018) Myosin1D is an evolutionarily conserved regulator of animal left-right asymmetry. Nat Commun 9(1):1942. https://doi.org/10.1038/s41467-018-04284-8

Jung HS, Komatsu S, Ikebe M, Craig R (2008) Head-head and head-tail interaction: a general mechanism for switching off myosin II activity in cells. Mol Biol Cell 19(8):3234–3242. https://doi.org/10.1091/mbc.E08-02-0206

Jungbluth H, Sewry C, Brown SC, Manzur AY, Mercuri E, Bushby K, Rowe P, Johnson MA, Hughes I, Kelsey A, Dubowitz V, Muntoni F (2000) Minicore myopathy in children: a clinical and histopathological study of 19 cases. Neuromuscul Disord 10(4–5):264–273

Jungbluth H, Muller CR, Halliger-Keller B, Brockington M, Brown SC, Feng L, Chattopadhyay A, Mercuri E, Manzur AY, Ferreiro A, Laing NG, Davis MR, Roper HP, Dubowitz V, Bydder G, Sewry CA, Muntoni F (2002) Autosomal recessive inheritance of RYR1 mutations in a congenital myopathy with cores. Neurology 59(2):284–287

Jungbluth H, Davis MR, Muller C, Counsell S, Allsop J, Chattopadhyay A, Messina S, Mercuri E, Laing NG, Sewry CA, Bydder G, Muntoni F (2004) Magnetic resonance imaging of muscle in congenital myopathies associated with RYR1 mutations. Neuromuscul Disord 14(12):785–790. https://doi.org/10.1016/j.nmd.2004.08.006

Kambara T, Komaba S, Ikebe M (2006) Human myosin III is a motor having an extremely high affinity for actin. J Biol Chem 281(49):37291–37301. M603823200 [pii] https://doi.org/10.1074/jbc.M603823200

Kamisago M, Sharma SD, DePalma SR, Solomon S, Sharma P, McDonough B, Smoot L, Mullen MP, Woolf PK, Wigle ED, Seidman JG, Seidman CE (2000) Mutations in sarcomere protein genes as a cause of dilated cardiomyopathy. N Engl J Med 343(23):1688–1696. https://doi.org/10.1056/NEJM200012073432304

Kania A, Klein R (2016) Mechanisms of ephrin-Eph signalling in development, physiology and disease. Nat Rev Mol Cell Biol 17(4):240–256. https://doi.org/10.1038/nrm.2015.16

Kas SM, de Ruiter JR, Schipper K, Annunziato S, Schut E, Klarenbeek S, Drenth AP, van der Burg E, Klijn C, Ten Hoeve JJ, Adams DJ, Koudijs MJ, Wesseling J, Nethe M, Wessels LFA, Jonkers J (2017) Insertional mutagenesis identifies drivers of a novel oncogenic pathway in invasive lobular breast carcinoma. Nat Genet 49(8):1219–1230. https://doi.org/10.1038/ng.3905

Katono K, Sato Y, Jiang SX, Kobayashi M, Nagashio R, Ryuge S, Fukuda E, Goshima N, Satoh Y, Saegusa M, Masuda N (2015) Prognostic significance of MYH9 expression in resected non-small cell lung cancer. PLoS One 10(3):e0121460. https://doi.org/10.1371/journal.pone.0121460

Katti C, Dalal JS, Dose AC, Burnside B, Battelle BA (2009) Cloning and distribution of myosin 3B in the mouse retina: differential distribution in cone outer segments. Exp Eye Res 89(2):224–237. S0014-4835(09)00074-8 [pii]. https://doi.org/10.1016/j.exer.2009.03.011

Kazmierczak P, Muller U (2012) Sensing sound: molecules that orchestrate mechanotransduction by hair cells. Trends Neurosci 35(4):220–229. https://doi.org/10.1016/j.tins.2011.10.007

Kelley MJ, Jawien W, Ortel TL, Korczak JF (2000) Mutation of MYH9, encoding non-muscle myosin heavy chain A, in May-Hegglin anomaly. Nat Genet 26(1):106–108. https://doi.org/10.1038/79069

Kengyel A, Becsi B, Konya Z, Sellers JR, Erdodi F, Nyitrai M (2015) Ankyrin domain of myosin 16 influences motor function and decreases protein phosphatase catalytic activity. Eur Biophys J 44(4):207–218. https://doi.org/10.1007/s00249-015-1015-z

Khubchandani SR, Vohra P, Chitale AR, Sidana P (2011) Microvillous inclusion disease–an ultrastructural diagnosis: with a review of the literature. Ultrastruct Pathol 35(2):87–91. https://doi.org/10.3109/01913123.2010.537438

Kim SV, Mehal WZ, Dong X, Heinrich V, Pypaert M, Mellman I, Dembo M, Mooseker MS, Wu D, Flavell RA (2006) Modulation of cell adhesion and motility in the immune system by Myo1f. Science (New York, NY) 314:136–139

Kim SJ, Lee S, Park HJ, Kang TH, Sagong B, Baek JI, Oh SK, Choi JY, Lee KY, Kim UK (2016) Genetic association of MYH genes with hereditary hearing loss in Korea. Gene 591(1):177–182. https://doi.org/10.1016/j.gene.2016.07.011

Kim BJ, Kim AR, Han JH, Lee C, Oh DY, Choi BY (2017) Discovery of MYH14 as an important and unique deafness gene causing prelingually severe autosomal dominant nonsyndromic hearing loss. J Gene Med 19(4). https://doi.org/10.1002/jgm.2950

Kim HT, Yin W, Jin YJ, Panza P, Gunawan F, Grohmann B, Buettner C, Sokol AM, Preussner J, Guenther S, Kostin S, Ruppert C, Bhagwat AM, Ma X, Graumann J, Looso M, Guenther A, Adelstein RS, Offermanns S, Stainier DYR (2018) Myh10 deficiency leads to defective extracellular matrix remodeling and pulmonary disease. Nat Commun 9(1):4600. https://doi.org/10.1038/s41467-018-06833-7

Knight PJ, Thirumurugan K, Xu Y, Kalverda AP, Stafford WFI, Sellers JR, Peckham M (2005) The predicted coiled-coil domain of myosin 10 forms a novel elon-

gated domain that lengthens the head. J Biol Chem 280(41):34702–34708
Knowles BC, Roland JT, Krishnan M, Tyska MJ, Lapierre LA, Dickman PS, Goldenring JR, Shub MD (2014) Myosin Vb uncoupling from RAB8A and RAB11A elicits microvillus inclusion disease. J Clin Invest 124(7):2947–2962. https://doi.org/10.1172/JCI71651
Kodera N, Yamamoto D, Ishikawa R, Ando T (2010) Video imaging of walking myosin V by high-speed atomic force microscopy. Nature 468(7320):72–76. https://doi.org/10.1038/nature09450
Köhler D, Struchholz S, Bähler M (2005) The two IQ-motifs and Ca^{2+}/calmodulin regulate the rat myosin 1d ATPase activity. FEBS J 272:2189–2197
Kolesnikova L, Bohil AB, Cheney RE, Becker S (2007) Budding of Marburgvirus is associated with filopodia. Cell Microbiol 9(4):939–951. https://doi.org/10.1111/j.1462-5822.2006.00842.x
Komaba S, Coluccio LM (2010) Localization of myosin 1b to actin protrusions requires phosphoinositide binding. J Biol Chem 285(36):27686–27693. M109.087270 [pii] https://doi.org/10.1074/jbc.M109.087270
Komaba S, Coluccio LM (2015) Myosin 1b regulates amino acid transport by associating transporters with the apical plasma membrane of kidney cells. PLoS One 10(9):e0138012. https://doi.org/10.1371/journal.pone.0138012
Komaba S, Watanabe S, Umeki N, Sato O, Ikebe M (2010) Effect of phosphorylation in the motor domain of human myosin IIIA on its ATP hydrolysis cycle. Biochemistry 49(17):3695–3702. https://doi.org/10.1021/bi902211w
Konishi H, Sugiyama M, Mizuno K, Saito H, Yatabe Y, Takahashi T, Osada H, Takahashi T (2003) Detailed characterization of a homozygously deleted region corresponding to a candidate tumor suppressor locus at distal 17p13.3 in human lung cancer. Oncogene 22(12):1892–1905. https://doi.org/10.1038/sj.onc.1206304
Kravtsov DV, Caputo C, Collaco A, Hoekstra N, Egan ME, Mooseker MS, Ameen NA (2012) Myosin Ia is required for CFTR brush border membrane trafficking and ion transport in the mouse small intestine. Traffic 13(7):1–11. https://doi.org/10.1111/j.1600-0854.2012.01368.x
Krendel M, Mooseker MS (2005) Myosins: tails (and heads) of functional diversity. Physiology (Bethesda) 20:239–251. 20/4/239 [pii] https://doi.org/10.1152/physiol.00014.2005
Krendel MO, Emily K, Mooseker MS (2007) Myosin 1E interacts with synaptojanin-1 and dynamin and is involved in endocytosis. FEBS Lett 581:644–650
Krendel M, Kim SV, Willinger T, Wang T, Kashgarian M, Flavell RA, Mooseker MS (2009) Disruption of Myosin 1e promotes podocyte injury. J Am Soc Nephrol 20(1):86–94. ASN.2007111172 [pii] https://doi.org/10.1681/ASN.2007111172
Kros CJ, Marcotti W, van Netten SM, Self TJ, Libby RT, Brown SD, Richardson GP, Steel KP (2002) Reduced climbing and increased slipping adaptation in cochlear hair cells of mice with Myo7a mutations. Nat Neurosci 5(1):41–47
Kuang SQ, Guo DC, Prakash SK, McDonald ML, Johnson RJ, Wang M, Regalado ES, Russell L, Cao JM, Kwartler C, Fraivillig K, Coselli JS, Safi HJ, Estrera AL, Leal SM, LeMaire SA, Belmont JW, Milewicz DM, Gen TACI (2011) Recurrent chromosome 16p13.1 duplications are a risk factor for aortic dissections. PLoS Genet 7(6):e1002118. https://doi.org/10.1371/journal.pgen.1002118
Kuang SQ, Kwartler CS, Byanova KL, Pham J, Gong L, Prakash SK, Huang J, Kamm KE, Stull JT, Sweeney HL, Milewicz DM (2012) Rare, nonsynonymous variant in the smooth muscle-specific isoform of myosin heavy chain, MYH11, R247C, alters force generation in the aorta and phenotype of smooth muscle cells. Circ Res 110(11):1411–1422. https://doi.org/10.1161/CIRCRESAHA.111.261743
Kulashreshtha M, Mehta IS, Kumar P, Rao BJ (2016) Chromosome territory relocation during DNA repair requires nuclear myosin 1 recruitment to chromatin mediated by Upsilon-H2AX signaling. Nucleic Acids Res 44(17):8272–8291. https://doi.org/10.1093/nar/gkw573
Kunishima S, Matsushita T, Kojima T, Amemiya N, Choi YM, Hosaka N, Inoue M, Jung Y, Mamiya S, Matsumoto K, Miyajima Y, Zhang G, Ruan C, Saito K, Song KS, Yoon HJ, Kamiya T, Saito H (2001) Identification of six novel MYH9 mutations and genotype-phenotype relationships in autosomal dominant macrothrombocytopenia with leukocyte inclusions. J Hum Genet 46(12):722–729. https://doi.org/10.1007/s100380170007
Kwartler CS, Chen J, Thakur D, Li S, Baskin K, Wang S, Wang ZV, Walker L, Hill JA, Epstein HF, Taegtmeyer H, Milewicz DM (2014) Overexpression of smooth muscle myosin heavy chain leads to activation of the unfolded protein response and autophagic turnover of thick filament-associated proteins in vascular smooth muscle cells. J Biol Chem 289(20):14075–14088. https://doi.org/10.1074/jbc.M113.499277
Laakso JM, Lewis JH, Shuman H, Ostap EM (2008) Myosin I can act as a molecular force sensor. Science (New York, NY) 321(5885):133–136
Laing NG, Laing BA, Meredith C, Wilton SD, Robbins P, Honeyman K, Dorosz S, Kozman H, Mastaglia FL, Kakulas BA (1995) Autosomal dominant distal myopathy: linkage to chromosome 14. Am J Hum Genet 56(2):422–427
Lalwani AK, Goldstein JA, Kelley MJ, Luxford W, Castelein CM, Mhatre AN (2000) Human nonsyndromic hereditary deafness DFNA17 is due to a mutation in nonmuscle myosin MYH9. Am J Hum Genet 67(5):1121–1128. https://doi.org/10.1016/S0002-9297(07)62942-5
Lamont PJ, Udd B, Mastaglia FL, de Visser M, Hedera P, Voit T, Bridges LR, Fabian V, Rozemuller A, Laing NG (2006) Laing early onset distal myopathy: slow myosin defect with variable abnormalities on muscle

biopsy. J Neurol Neurosurg Psychiatry 77(2):208–215. https://doi.org/10.1136/jnnp.2005.073825

Lan L, Han H, Zuo H, Chen Z, Du Y, Zhao W, Gu J, Zhang Z (2010) Upregulation of myosin Va by Snail is involved in cancer cell migration and metastasis. Int J Cancer 126(1):53–64. https://doi.org/10.1002/ijc.24641

Lapierre LA, Kumar R, Hales CM, Navarre J, Bhartur SG, Burnette JO, Provance DW Jr, Mercer JA, Bahler M, Goldenring JR (2001) Myosin vb is associated with plasma membrane recycling systems. Mol Biol Cell 12(6):1843–1857

Lascorz J, Forsti A, Chen B, Buch S, Steinke V, Rahner N, Holinski-Feder E, Morak M, Schackert HK, Gorgens H, Schulmann K, Goecke T, Kloor M, Engel C, Buttner R, Kunkel N, Weires M, Hoffmeister M, Pardini B, Naccarati A, Vodickova L, Novotny J, Schreiber S, Krawczak M, Broring CD, Volzke H, Schafmayer C, Vodicka P, Chang-Claude J, Brenner H, Burwinkel B, Propping P, Hampe J, Hemminki K (2010) Genome-wide association study for colorectal cancer identifies risk polymorphisms in German familial cases and implicates MAPK signalling pathways in disease susceptibility. Carcinogenesis 31(9):1612–1619. https://doi.org/10.1093/carcin/bgq146

Lee KW, Richmond R, Hu P, French L, Shin J, Bourdon C, Reischl E, Waldenberger M, Zeilinger S, Gaunt T, McArdle W, Ring S, Woodward G, Bouchard L, Gaudet D, Smith GD, Relton C, Paus T, Pausova Z (2015) Prenatal exposure to maternal cigarette smoking and DNA methylation: epigenome-wide association in a discovery sample of adolescents and replication in an independent cohort at birth through 17 years of age. Environ Health Perspect 123(2):193–199. https://doi.org/10.1289/ehp.1408614

Lefevre G, Michel V, Weil D, Lepelletier L, Bizard E, Wolfrum U, Hardelin JP, Petit C (2008) A core cochlear phenotype in USH1 mouse mutants implicates fibrous links of the hair bundle in its cohesion, orientation and differential growth. Development 135(8):1427–1437. https://doi.org/10.1242/dev.012922

Lelli A, Michel V, Boutet de Monvel J, Cortese M, Bosch-Grau M, Aghaie A, Perfettini I, Dupont T, Avan P, El-Amraoui A, Petit C (2016) Class III myosins shape the auditory hair bundles by limiting microvilli and stereocilia growth. J Cell Biol 212(2):231–244. https://doi.org/10.1083/jcb.201509017

Lennon R, Stuart HM, Bierzynska A, Randles MJ, Kerr B, Hillman KA, Batra G, Campbell J, Storey H, Flinter FA, Koziell A, Welsh GI, Saleem MA, Webb NJ, Woolf AS (2015) Coinheritance of COL4A5 and MYO1E mutations accentuate the severity of kidney disease. Pediatr Nephrol 30(9):1459–1465. https://doi.org/10.1007/s00467-015-3067-9

Les Erickson F, Corsa AC, Dose AC, Burnside B (2003) Localization of a class III myosin to filopodia tips in transfected HeLa cells requires an actin-binding site in its tail domain. Mol Biol Cell 14(10):4173–4180. E02-10-0656 [pii] https://doi.org/10.1091/mbc.E02-10-0656

Letellier E, Schmitz M, Ginolhac A, Rodriguez F, Ullmann P, Qureshi-Baig K, Frasquilho S, Antunes L, Haan S (2017) Loss of Myosin Vb in colorectal cancer is a strong prognostic factor for disease recurrence. Br J Cancer 117(11):1689–1701. https://doi.org/10.1038/bjc.2017.352

Levitt JG, O'Neill J, Blanton RE, Smalley S, Fadale D, McCracken JT, Guthrie D, Toga AW, Alger JR (2003) Proton magnetic resonance spectroscopic imaging of the brain in childhood autism. Biol Psychiatry 54(12):1355–1366

Li YR, Yang WX (2016) Myosins as fundamental components during tumorigenesis: diverse and indispensable. Oncotarget 7(29):46785–46812. https://doi.org/10.18632/oncotarget.8800

Li H, Zhou F, Wang H, Lin D, Chen G, Zuo X, Sun L, Zhang X, Yang S (2015) Knockdown of myosin VI by lentivirus-mediated short hairpin RNA suppresses proliferation of melanoma. Mol Med Rep 12(5):6801–6806. https://doi.org/10.3892/mmr.2015.4261

Li J, He Y, Lu Q, Zhang M (2016) Mechanistic basis of organization of the Harmonin/USH1C-Mediated Brush Border Microvilli Tip-Link Complex. Dev Cell 36(2):179–189. https://doi.org/10.1016/j.devcel.2015.12.020

Liang Y, Wang A, Probst FJ, Arhya IN, Barber TD, Chen KS, Deshmukh D, Dolan DF, Hinnant JT, Carter LE, Jain PK, Lalwani AK, Li XC, Lupski JR, Moeljopawiro S, Morell R, Negrini C, Wilcox ER, Winata S, Camper SA, Friedman TB (1998) Genetic mapping refines DFNB3 to 17p11.2, suggests multiple alleles of DFNB3, and supports homology to the mouse model shaker-2. Am J Hum Genet 62(4):904–915. https://doi.org/10.1086/301786

Liang Y, Wang A, Belyantseva IA, Anderson DW, Probst FJ, Barber TD, Miller W, Touchman JW, Jin L, Sullivan SL, Sellers JR, Camper SA, Lloyd RV, Kachar B, Friedman TB, Fridell RA (1999) Characterization of the human and mouse unconventional myosin XV genes responsible for hereditary deafness DFNB3 and shaker 2. Genomics 61(3):243–258. https://doi.org/10.1006/geno.1999.5976

Liao W, Elfrink K, Bahler M (2010) Head of myosin IX binds calmodulin and moves processively toward the plus-end of actin filaments. J Biol Chem 285(32):24933–24942. https://doi.org/10.1074/jbc.M110.101105

Lieto-Trivedi A, Coluccio LM (2008) Calcium, nucleotide, and actin affect the interaction of mammalian Myo1c with its light chain calmodulin. Biochemistry 47:10218–10226

Lister I, Schmitz S, Walker M, Trinick J, Buss F, Veigel C, Kendrick-Jones J (2004) A monomeric myosin VI with a large working stroke. EMBO J 23(8):1729–1738. https://doi.org/10.1038/sj.emboj.7600180

Liu P, Tarle SA, Hajra A, Claxton DF, Marlton P, Freedman M, Siciliano MJ, Collins FS (1993) Fusion

between transcription factor CBF beta/PEBP2 beta and a myosin heavy chain in acute myeloid leukemia. Science (New York, NY) 261(5124):1041–1044

Liu XZ, Walsh J, Mburu P, Kendrick-Jones J, Cope MJ, Steel KP, Brown SD (1997a) Mutations in the myosin VIIA gene cause non-syndromic recessive deafness. Nat Genet 16(2):188–190. https://doi.org/10.1038/ng0697-188

Liu XZ, Walsh J, Tamagawa Y, Kitamura K, Nishizawa M, Steel KP, Brown SD (1997b) Autosomal dominant non-syndromic deafness caused by a mutation in the myosin VIIA gene. Nat Genet 17(3):268–269. https://doi.org/10.1038/ng1197-268

Liu X, Ondek B, Williams DS (1998) Mutant myosin VIIa causes defective melanosome distribution in the RPE of shaker-1 mice. Nat Genet 19(2):117–118. https://doi.org/10.1038/470

Liu X, Udovichenko IP, Brown SD, Steel KP, Williams DS (1999) Myosin VIIa participates in opsin transport through the photoreceptor cilium. J Neurosci 19(15):6267–6274

Liu J, Taylor DW, Krementsova EB, Trybus KM, Taylor KA (2006) Three-dimensional structure of the myosin V inhibited state by cryoelectron tomography. Nature 442(7099):208–211. https://doi.org/10.1038/nature04719

Liu YF, Sowell SM, Luo Y, Chaubey A, Cameron RS, Kim HG, Srivastava AK (2015a) Autism and intellectual disability-associated KIRREL3 interacts with neuronal proteins MAP 1B and MYO16 with potential roles in neurodevelopment. PLoS One 10(4):e0123106. https://doi.org/10.1371/journal.pone.0123106

Liu Z, Xu Y, Zhang X, Song J, Sorokin L, Bahler M (2015b) The motorized RhoGAP myosin IXb (Myo9b) in leukocytes regulates experimental autoimmune encephalomyelitis induction and recovery. J Neuroimmunol 282:25–32. https://doi.org/10.1016/j.jneuroim.2015.03.014

Liu T, Ye Y, Zhang X, Zhu A, Yang Z, Fu Y, Wei C, Liu Q, Zhao C, Wang G (2016) Downregulation of non-muscle myosin IIA expression inhibits migration and invasion of gastric cancer cells via the cJun Nterminal kinase signaling pathway. Mol Med Rep 13(2):1639–1644. https://doi.org/10.3892/mmr.2015.4742

Liu C, Kawana M, Song D, Ruppel KM, Spudich JA (2018a) Controlling load-dependent kinetics of beta-cardiac myosin at the single-molecule level. Nat Struct Mol Biol 25(6):505–514. https://doi.org/10.1038/s41594-018-0069-x

Liu Y, Wei X, Guan L, Xu S, Yuan Y, Lv D, He X, Zhan J, Kong Y, Guo J, Zhang H (2018b) Unconventional myosin VIIA promotes melanoma progression. J Cell Sci 131(4). https://doi.org/10.1242/jcs.209924

Loikkanen I, Toljamo K, Hirvikoski P, Vaisanen T, Paavonen TK, Vaarala MH (2009) Myosin VI is a modulator of androgen-dependent gene expression. Oncol Rep 22(5):991–995

Lombardo AT, Nelson SR, Ali MY, Kennedy GG, Trybus KM, Walcott S, Warshaw DM (2017) Myosin Va molecular motors manoeuvre liposome cargo through suspended actin filament intersections in vitro. Nat Commun 8:15692. https://doi.org/10.1038/ncomms15692

Lopes VS, Williams DS (2015) Gene therapy for the retinal degeneration of usher syndrome caused by mutations in MYO7A. Cold Spring Harb Perspect Med 5(6). https://doi.org/10.1101/cshperspect.a017319

Lopes VS, Ramalho JS, Owen DM, Karl MO, Strauss O, Futter CE, Seabra MC (2007) The ternary Rab27a-Myrip-Myosin VIIa complex regulates melanosome motility in the retinal pigment epithelium. Traffic 8(5):486–499. https://doi.org/10.1111/j.1600-0854.2007.00548.x

Lopes VS, Gibbs D, Libby RT, Aleman TS, Welch DL, Lillo C, Jacobson SG, Radu RA, Steel KP, Williams DS (2011) The Usher 1B protein, MYO7A, is required for normal localization and function of the visual retinoid cycle enzyme, RPE65. Hum Mol Genet 20(13):2560–2570. https://doi.org/10.1093/hmg/ddr155

Lopez-Ortega O, Santos-Argumedo L (2017) Myosin 1g contributes to CD44 adhesion protein and lipid rafts recycling and controls CD44 capping and cell migration in B lymphocytes. Front Immunol 8:1731. https://doi.org/10.3389/fimmu.2017.01731

Lu Q, Ye F, Wei Z, Wen Z, Zhang M (2012) Antiparallel coiled-coil-mediated dimerization of myosin X. Proc Natl Acad Sci U S A 109(43):17388–17393. https://doi.org/10.1073/pnas.1208642109

Lu Z, Ma XN, Zhang HM, Ji HH, Ding H, Zhang J, Luo D, Sun Y, Li XD (2014) Mouse myosin-19 is a plus-end-directed, high-duty ratio molecular motor. J Biol Chem 289(26):18535–18548. https://doi.org/10.1074/jbc.M114.569087

Luijendijk MW, Van Wijk E, Bischoff AM, Krieger E, Huygen PL, Pennings RJ, Brunner HG, Cremers CW, Cremers FP, Kremer H (2004) Identification and molecular modelling of a mutation in the motor head domain of myosin VIIA in a family with autosomal dominant hearing impairment (DFNA11). Hum Genet 115(2):149–156. https://doi.org/10.1007/s00439-004-1137-3

Lyons GE, Ontell M, Cox R, Sassoon D, Buckingham M (1990) The expression of myosin genes in developing skeletal muscle in the mouse embryo. J Cell Biol 111(4):1465–1476

Ma X, Adelstein RS (2014a) A point mutation in Myh10 causes major defects in heart development and body wall closure. Circ Cardiovasc Genet 7(3):257–265. https://doi.org/10.1161/CIRCGENETICS.113.000455

Ma X, Adelstein RS (2014b) The role of vertebrate nonmuscle Myosin II in development and human disease. BioArchitecture 4(3):88–102. https://doi.org/10.4161/bioa.29766

Ma X, Jana SS, Conti MA, Kawamoto S, Claycomb WC, Adelstein RS (2010) Ablation of nonmuscle myosin II-B and II-C reveals a role for nonmuscle myosin II in cardiac myocyte karyokinesis. Mol Biol Cell 21(22):3952–3962. https://doi.org/10.1091/mbc.E10-04-0293

Machida S, Matsuoka R, Noda S, Hiratsuka E, Takagaki Y, Oana S, Furutani Y, Nakajima H, Takao A, Momma K (2000) Evidence for the expression of neonatal skeletal myosin heavy chain in primary myocardium and cardiac conduction tissue in the developing chick heart. Dev Dyn 217(1):37–49. https://doi.org/10.1002/(SICI)1097-0177(200001)217:1<37::AID-DVDY4>3.0.CO;2-3

Machlus KR, Italiano JE Jr (2013) The incredible journey: From megakaryocyte development to platelet formation. J Cell Biol 201(6):785–796. https://doi.org/10.1083/jcb.201304054

Maddirevula S, Alzahrani F, Al-Owain M, Al Muhaizea MA, Kayyali HR, AlHashem A, Rahbeeni Z, Al-Otaibi M, Alzaidan HI, Balobaid A, El Khashab HY, Bubshait DK, Faden M, Yamani SA, Dabbagh O, Al-Mureikhi M, Jasser AA, Alsaif HS, Alluhaydan I, Seidahmed MZ, Alabbasi BH, Almogarri I, Kurdi W, Akleh H, Qari A, Al Tala SM, Alhomaidi S, Kentab AY, Salih MA, Chedrawi A, Alameer S, Tabarki B, Shamseldin HE, Patel N, Ibrahim N, Abdulwahab F, Samira M, Goljan E, Abouelhoda M, Meyer BF, Hashem M, Shaheen R, AlShahwan S, Alfadhel M, Ben-Omran T, Al-Qattan MM, Monies D, Alkuraya FS (2019) Autozygome and high throughput confirmation of disease genes candidacy. Genet Med 21(3):736–742. https://doi.org/10.1038/s41436-018-0138-x

Makowska KA, Hughes RE, White KJ, Wells CM, Peckham M (2015) Specific myosins control actin organization, cell morphology, and migration in prostate cancer cells. Cell Rep. https://doi.org/10.1016/j.celrep.2015.11.012

Malfatti E, Bohm J, Lacene E, Beuvin M, Romero NB, Laporte J (2015) A premature stop codon in MYO18B is associated with severe nemaline myopathy with cardiomyopathy. J Neuromuscul Dis 2(3):219–227. https://doi.org/10.3233/JND-150085

Maly IV, Hofmann WA (2016) Calcium-regulated import of myosin IC into the nucleus. Cytoskeleton (Hoboken) 73(7):341–350. https://doi.org/10.1002/cm.21310

Maly IV, Domaradzki TM, Gosy VA, Hofmann WA (2017) Myosin isoform expressed in metastatic prostate cancer stimulates cell invasion. Sci Rep 7(1):8476. https://doi.org/10.1038/s41598-017-09158-5

Manor U, Disanza A, Grati M, Andrade L, Lin H, Di Fiore PP, Scita G, Kachar B (2011) Regulation of stereocilia length by myosin XVa and whirlin depends on the actin-regulatory protein Eps8. Curr Biol 21(2):167–172. S0960-9822(10)01714-8 [pii] https://doi.org/10.1016/j.cub.2010.12.046

Manstein D, Preller M (2020) Chapter 5: Small molecule effectors of myosin function. In: Coluccio LM (ed) Myosins: a superfamily of molecular motors, 2nd edn. Springer, Cham

Maravillas-Montero JL, Lopez-Ortega O, Patino-Lopez G, Santos-Argumedo L (2014) Myosin 1g regulates cytoskeleton plasticity, cell migration, exocytosis, and endocytosis in B lymphocytes. Eur J Immunol 44(3):877–886. https://doi.org/10.1002/eji.201343873

Marigo V, Nigro A, Pecci A, Montanaro D, Di Stazio M, Balduini CL, Savoia A (2004) Correlation between the clinical phenotype of MYH9-related disease and tissue distribution of class II nonmuscle myosin heavy chains. Genomics 83(6):1125–1133. https://doi.org/10.1016/j.ygeno.2003.12.012

Marston S (2018) The molecular mechanisms of mutations in actin and myosin that cause inherited myopathy. Int J Mol Sci 19(7). https://doi.org/10.3390/ijms19072020

Martignetti J (2002) Five (un)easy pieces: the MYH9-related giant platelet syndromes. Haematologica 87(9):897–898

Martinsson T, Darin N, Kyllerman M, Oldfors A, Hallberg B, Wahlstrom J (1999) Dominant hereditary inclusion-body myopathy gene (IBM3) maps to chromosome region 17p13.1. Am J Hum Genet 64(5):1420–1426. https://doi.org/10.1086/302375

Martinsson T, Oldfors A, Darin N, Berg K, Tajsharghi H, Kyllerman M, Wahlstrom J (2000) Autosomal dominant myopathy: missense mutation (Glu-706 → Lys) in the myosin heavy chain IIa gene. Proc Natl Acad Sci U S A 97(26):14614–14619. https://doi.org/10.1073/pnas.250289597

Mascarello F, Toniolo L, Cancellara P, Reggiani C, Maccatrozzo L (2016) Expression and identification of 10 sarcomeric MyHC isoforms in human skeletal muscles of different embryological origin. Diversity and similarity in mammalian species. Ann Anat 207:9–20. https://doi.org/10.1016/j.aanat.2016.02.007

Mastaglia FL, Phillips BA, Cala LA, Meredith C, Egli S, Akkari PA, Laing NG (2002) Early onset chromosome 14-linked distal myopathy (Laing). Neuromuscul Disord 12(4):350–357

Masters TA, Kendrick-Jones J, Buss F (2017) Myosins: domain organisation, motor properties, physiological roles and cellular functions. Handb Exp Pharmacol 235:77–122. https://doi.org/10.1007/164_2016_29

Mathur P, Yang J (2015) Usher syndrome: hearing loss, retinal degeneration and associated abnormalities. Biochim Biophys Acta 1852(3):406–420. https://doi.org/10.1016/j.bbadis.2014.11.020

Matsudaira PT, Burgess DR (1982) Organization of the cross-filaments in intestinal microvilli. J Cell Biol 92(3):657–664

Mazzolini R, Dopeso H, Mateo-Lozano S, Chang W, Rodrigues P, Bazzocco S, Alazzouzi H, Landolfi S, Hernandez-Losa J, Andretta E, Alhopuro P, Espin E, Armengol M, Tabernero J, Ramon y CS, Kloor M, Gebert J, Mariadason JM, Schwartz S Jr, Aaltonen LA, Mooseker MS, Arango D (2012) Brush border Myosin Ia has tumor suppressor activity in the intestine. Proc Natl Acad Sci U S A 109(5):1530–1535. https://doi.org/10.1073/pnas.1108411109

Mazzolini R, Rodrigues P, Bazzocco S, Dopeso H, Ferreira AM, Mateo-Lozano S, Andretta E, Woerner SM, Alazzouzi H, Landolfi S, Hernandez-Losa J, Macaya I, Suzuki H, Ramon y CS, Mooseker MS, Mariadason JM, Gebert J, Hofstra RM, Reventos

J, Yamamoto H, Schwartz S Jr, Arango D (2013) Brush border myosin Ia inactivation in gastric but not endometrial tumors. Int J Cancer 132(8):1790–1799. https://doi.org/10.1002/ijc.27856

McAlpine W, Wang KW, Choi JH, San Miguel M, McAlpine SG, Russell J, Ludwig S, Li X, Tang M, Zhan X, Choi M, Wang T, Bu CH, Murray AR, Moresco EMY, Turer EE, Beutler B (2018) The class I myosin MYO1D binds to lipid and protects against colitis. Dis Model Mech 11(9). https://doi.org/10.1242/dmm.035923

McIntosh BB, Ostap EM (2016) Myosin-I molecular motors at a glance. J Cell Sci 129(14):2689–2695. https://doi.org/10.1242/jcs.186403

McNally EM, Mestroni L (2017) Dilated cardiomyopathy: genetic determinants and mechanisms. Circ Res 121(7):731–748. https://doi.org/10.1161/CIRCRESAHA.116.309396

McNamara JW, Li A, Dos Remedios CG, Cooke R (2015) The role of super-relaxed myosin in skeletal and cardiac muscle. Biophys Rev 7(1):5–14. https://doi.org/10.1007/s12551-014-0151-5

Mehta AD, Rock RS, Rief M, Spudich JA, Mooseker MS, Cheney RE (1999) Myosin-V is a processive actin-based motor. Nature 400(6744):590–593

Mehta IS, Amira M, Harvey AJ, Bridger JM (2010) Rapid chromosome territory relocation by nuclear motor activity in response to serum removal in primary human fibroblasts. Genome Biol 11(1):R5. https://doi.org/10.1186/gb-2010-11-1-r5

Melchionda S, Ahituv N, Bisceglia L, Sobe T, Glaser F, Rabionet R, Arbones ML, Notarangelo A, Di Iorio E, Carella M, Zelante L, Estivill X, Avraham KB, Gasparini P (2001) MYO6, the human homologue of the gene responsible for deafness in Snell's waltzer mice, is mutated in autosomal dominant nonsyndromic hearing loss. Am J Hum Genet 69(3):635–640. https://doi.org/10.1086/323156

Mele C, Iatropoulos P, Donadelli R, Calabria A, Maranta R, Cassis P, Buelli S, Tomasoni S, Piras R, Krendel M, Bettoni S, Morigi M, Delledonne M, Pecoraro C, Abbate I, Capobianchi MR, Hildebrandt F, Otto E, Schaefer F, Macciardi F, Ozaltin F, Emre S, Ibsirlioglu T, Benigni A, Remuzzi G, Noris M, PodoNet C (2011) MYO1E mutations and childhood familial focal segmental glomerulosclerosis. N Engl J Med 365(4):295–306. https://doi.org/10.1056/NEJMoa1101273

Menetrey J, Bahloul A, Wells AL, Yengo CM, Morris CA, Sweeney HL, Houdusse A (2005) The structure of the myosin VI motor reveals the mechanism of directionality reversal. Nature 435(7043):779–785. https://doi.org/10.1038/nature03592

Menetrey J, Llinas P, Mukherjea M, Sweeney HL, Houdusse A (2007) The structural basis for the large powerstroke of myosin VI. Cell 131(2):300–308. https://doi.org/10.1016/j.cell.2007.08.027

Mercer JA, Seperack PK, Strobel MC, Copeland NG, Jenkins NA (1991) Novel myosin heavy chain encoded by murine dilute coat colour locus [published erratum appears in Nature 1991 Aug 8;352(6335):547]. Nature 349(6311):709–713

Meredith C, Herrmann R, Parry C, Liyanage K, Dye DE, Durling HJ, Duff RM, Beckman K, de Visser M, van der Graaff MM, Hedera P, Fink JK, Petty EM, Lamont P, Fabian V, Bridges L, Voit T, Mastaglia FL, Laing NG (2004) Mutations in the slow skeletal muscle fiber myosin heavy chain gene (MYH7) cause laing early-onset distal myopathy (MPD1). Am J Hum Genet 75(4):703–708. https://doi.org/10.1086/424760

Merritt RC, Manor U, Salles FT, Grati M, Dose AC, Unrath WC, Quintero OA, Yengo CM, Kachar B (2012) Myosin IIIB uses an actin-binding motif in its espin-1 cargo to reach the tips of actin protrusions. Curr Biol 22(4):320–325. https://doi.org/10.1016/j.cub.2011.12.053

Messaoudi I, Amarasinghe GK, Basler CF (2015) Filovirus pathogenesis and immune evasion: insights from Ebola virus and Marburg virus. Nat Rev Microbiol 13(11):663–676. https://doi.org/10.1038/nrmicro3524

Mhatre AN, Li Y, Atkin G, Maghnouj A, Lalwani AK (2006) Expression of Myh9 in the mammalian cochlea: localization within the stereocilia. J Neurosci Res 84(4):809–818. https://doi.org/10.1002/jnr.20993

Miller KE, Sheetz MP (2000) Characterization of myosin V binding to brain vesicles. J Biol Chem 275(4):2598–2606

Miller SD, Karpus WJ, Davidson TS (2010) Experimental autoimmune encephalomyelitis in the mouse. Current protocols in immunology/edited by John E Coligan [et al] Chapter 15:Unit 15 11. https://doi.org/10.1002/0471142735.im1501s88

Miller KA, Williams LH, Rose E, Kuiper M, Dahl HH, Manji SS (2012) Inner ear morphology is perturbed in two novel mouse models of recessive deafness. PLoS One 7(12):e51284. https://doi.org/10.1371/journal.pone.0051284

Mischel PS, Shai R, Shi T, Horvath S, Lu KV, Choe G, Seligson D, Kremen TJ, Palotie A, Liau LM, Cloughesy TF, Nelson SF (2003) Identification of molecular subtypes of glioblastoma by gene expression profiling. Oncogene 22(15):2361–2373. https://doi.org/10.1038/sj.onc.1206344

Mohiddin SA, Ahmed ZM, Griffith AJ, Tripodi D, Friedman TB, Fananapazir L, Morell RJ (2004) Novel association of hypertrophic cardiomyopathy, sensorineural deafness, and a mutation in unconventional myosin VI (MYO6). J Med Genet 41(4):309–314

Montell C, Rubin GM (1988) The Drosophila ninaC locus encodes two photoreceptor cell specific proteins with domains homologous to protein kinases and the myosin heavy chain head. Cell 52(5):757–772

Mooseker MS, Cheney RE (1995) Unconventional myosins. Annu Rev Cell Dev Biol 11:633–675

Mooseker MS, Tilney LG (1975) Organization of an actin filament-membrane complex. Filament polarity and membrane attachment in the microvilli of intestinal epithelial cells. J Cell Biol 67(3):725–743

Morano I, Chai GX, Baltas LG, Lamounier-Zepter V, Lutsch G, Kott M, Haase H, Bader M (2000) Smooth-muscle contraction without smooth-muscle myosin. Nat Cell Biol 2(6):371–375. https://doi.org/10.1038/35014065

Morgan NS, Skovronsky DM, Artavanis-Tsakonas S, Mooseker MS (1994) The molecular cloning and characterization of *Drosophila melanogaster* myosin-IA and myosin-IB. J Mol Biol 239(3):347–356

Mori K, Furusawa T, Okubo T, Inoue T, Ikawa S, Yanai N, Mori KJ, Obinata M (2003) Genome structure and differential expression of two isoforms of a novel PDZ-containing myosin (MysPDZ) (Myo18A). J Biochem 133(4):405–413

Morris SM, Arden SD, Roberts RC, Kendrick-Jones J, Cooper JA, Luzio JP, Buss F (2002) Myosin VI binds to and localises with Dab2, potentially linking receptor-mediated endocytosis and the actin cytoskeleton. Traffic 3(5):331–341

Morriswood B, Ryzhakov G, Puri C, Arden SD, Roberts R, Dendrou C, Kendrick-Jones J, Buss F (2007) T6BP and NDP52 are myosin VI binding partners with potential roles in cytokine signalling and cell adhesion. J Cell Sci 120(Pt 15):2574–2585. https://doi.org/10.1242/jcs.007005

Mukherjea M, Llinas P, Kim H, Travaglia M, Safer D, Menetrey J, Franzini-Armstrong C, Selvin PR, Houdusse A, Sweeney HL (2009) Myosin VI dimerization triggers an unfolding of a three-helix bundle in order to extend its reach. Mol Cell 35(3):305–315. S1097-2765(09)00505-X [pii]. https://doi.org/10.1016/j.molcel.2009.07.010

Mukherjee TM, Staehelin LA (1971) The fine structural organization of the brush border of intestinal epithelial cells. J Cell Sci 8:573–599

Muller T, Hess MW, Schiefermeier N, Pfaller K, Ebner HL, Heinz-Erian P, Ponstingl H, Partsch J, Rollinghoff B, Kohler H, Berger T, Lenhartz H, Schlenck B, Houwen RJ, Taylor CJ, Zoller H, Lechner S, Goulet O, Utermann G, Ruemmele FM, Huber LA, Janecke AR (2008) MYO5B mutations cause microvillus inclusion disease and disrupt epithelial cell polarity. Nat Genet 40(10):1163–1165. ng.225 [pii] https://doi.org/10.1038/ng.225

Myronovkij S, Negrych N, Nehrych T, Redowicz MJ, Souchelnytskyi S, Stoika R, Kit Y (2016) Identification of a 48 kDa form of unconventional myosin 1c in blood serum of patients with autoimmune diseases. Biochem Biophys Rep 5:175–179

Naccache SN, Hasson T, Horowitz A (2006) Binding of internalized receptors to the PDZ domain of GIPC/synectin recruits myosin VI to endocytic vesicles. Proc Natl Acad Sci U S A 103(34):12735–12740. https://doi.org/10.1073/pnas.0605317103

Nag S, Sommese RF, Ujfalusi Z, Combs A, Langer S, Sutton S, Leinwand LA, Geeves MA, Ruppel KM, Spudich JA (2015) Contractility parameters of human beta-cardiac myosin with the hypertrophic cardiomyopathy mutation R403Q show loss of motor function. Sci Adv 1(9):e1500511. https://doi.org/10.1126/sciadv.1500511

Nag S, Trivedi DV, Sarkar SS, Adhikari AS, Sunitha MS, Sutton S, Ruppel KM, Spudich JA (2017) The myosin mesa and the basis of hypercontractility caused by hypertrophic cardiomyopathy mutations. Nat Struct Mol Biol 24(6):525–533. https://doi.org/10.1038/nsmb.3408

Nagy S, Ricca BL, Norstrom MF, Courson DS, Brawley CM, Smithback PA, Rock RS (2008) A myosin motor that selects bundled actin for motility. Proc Natl Acad Sci U S A 105(28):9616–9620. https://doi.org/10.1073/pnas.0802592105

Nakamori Y, Emoto M, Fukuda N, Taguchi A, Okuya S, Tajiri M, Miyagishi M, Taira K, Wada Y, Tanizawa Y (2006) Myosin motor Myo1c and its receptor NEMO/IKK-gamma promote TNF-alpha-induced serine307 phosphorylation of IRS-1. J Cell Biol 173(5):665–671. https://doi.org/10.1083/jcb.200601065

Nakano T, Tani M, Nishioka M, Kohno T, Otsuka A, Ohwada S, Yokota J (2005) Genetic and epigenetic alterations of the candidate tumor-suppressor gene MYO18B, on chromosome arm 22q, in colorectal cancer. Genes Chromosomes Cancer 43(2):162–171. https://doi.org/10.1002/gcc.20180

Nambiar R, McConnell RE, Tyska MJ (2009) Control of cell membrane tension by myosin-I. Proc Natl Acad Sci U S A 106(29):11972–11977

Namboodiri AM, Peethambaran A, Mathew R, Sambhu PA, Hershfield J, Moffett JR, Madhavarao CN (2006) Canavan disease and the role of N-acetylaspartate in myelin synthesis. Mol Cell Endocrinol 252(1–2):216–223. https://doi.org/10.1016/j.mce.2006.03.016

Nevzorov I, Sidorenko E, Wang W, Zhao H, Vartiainen MK (2018) Myosin-1C uses a novel phosphoinositide-dependent pathway for nuclear localization. EMBO Rep. https://doi.org/10.15252/embr.201744296

Ngollo M, Lebert A, Daures M, Judes G, Rifai K, Dubois L, Kemeny JL, Penault-Llorca F, Bignon YJ, Guy L, Bernard-Gallon D (2017) Global analysis of H3K27me3 as an epigenetic marker in prostate cancer progression. BMC Cancer 17(1):261. https://doi.org/10.1186/s12885-017-3256-y

Niimura H, Patton KK, McKenna WJ, Soults J, Maron BJ, Seidman JG, Seidman CE (2002) Sarcomere protein gene mutations in hypertrophic cardiomyopathy of the elderly. Circulation 105(4):446–451

Nishikawa S, Homma K, Komori Y, Iwaki M, Wazawa T, Hikikoshi Iwane A, Saito J, Ikebe R, Katayama E, Yanagida T, Ikebe M (2002) Class VI myosin moves processively along actin filaments backward with large steps. Biochem Biophys Res Commun 290(1):311–317. https://doi.org/10.1006/bbrc.2001.6142

Nishikawa M, Nishikawa S, Inoue A, Iwane AH, Yanagida T, Ikebe M (2006) A unique mechanism for the processive movement of single-headed myosin-IX. Biochem Biophys Res Commun 343(4):1159–1164. https://doi.org/10.1016/j.bbrc.2006.03.057

Nishioka M, Kohno T, Tani M, Yanaihara N, Tomizawa Y, Otsuka A, Sasaki S, Kobayashi K, Niki T, Maeshima A, Sekido Y, Minna JD, Sone S, Yokota J (2002) MYO18B, a candidate tumor suppressor gene at chromosome 22q12.1, deleted, mutated, and methylated in human lung cancer. Proc Natl Acad Sci U S A 99(19):12269–12274. https://doi.org/10.1073/pnas.192445899

Nowak G, Pestic-Dragovich L, Hozák P, Philimonenko A, Simerly C, Schatten G, de Lanerolle PA (1997) Evidence for the presence of myosin I in the nucleus. J Biol Chem 272:17176–17181

O'Loughlin T, Masters TA, Buss F (2018) The MYO6 interactome reveals adaptor complexes coordinating early endosome and cytoskeletal dynamics. EMBO Rep 19(4). https://doi.org/10.15252/embr.201744884

Obrdlik A, Louvet E, Kukalev A, Naschekin D, Kiseleva E, Fahrenkrog B, Percipalle P (2010) Nuclear myosin 1 is in complex with mature rRNA transcripts and associates with the nuclear pore basket. FASEB J 24(1):146–157. https://doi.org/10.1096/fj.09-135863

O'Connor E, Topf A, Muller JS, Cox D, Evangelista T, Colomer J, Abicht A, Senderek J, Hasselmann O, Yaramis A, Laval SH, Lochmuller H (2016) Identification of mutations in the MYO9A gene in patients with congenital myasthenic syndrome. Brain J Neurol 139(Pt 8):2143–2153. https://doi.org/10.1093/brain/aww130

Oh H, Kim H, Shin B, Lee KH, Yeo MG, Song WK (2013) Interaction of crk with Myosin-1c participates in fibronectin-induced cell spreading. Int J Biol Sci 9(8):778–791. https://doi.org/10.7150/ijbs.6459

Ohmura G, Tsujikawa T, Yaguchi T, Kawamura N, Mikami S, Sugiyama J, Nakamura K, Kobayashi A, Iwata T, Nakano H, Shimada T, Hisa Y, Kawakami Y (2015) Aberrant myosin 1b expression promotes cell migration and lymph node metastasis of HNSCC. Mol Cancer Res 13(4):721–731. https://doi.org/10.1158/1541-7786.MCR-14-0410

Olety B, Wälte M, Honnert U, Schillers H, Bähler M (2010) Myo1g is a haematopoietic specific myosin that localises to the plasma membrane and regulates cell elasticity. FEBS Lett 584:493–499

Ortolano S, Tarrio R, Blanco-Arias P, Teijeira S, Rodriguez-Trelles F, Garcia-Murias M, Delague V, Levy N, Fernandez JM, Quintans B, Millan BS, Carracedo A, Navarro C, Sobrido MJ (2011) A novel MYH7 mutation links congenital fiber type disproportion and myosin storage myopathy. Neuromuscul Disord 21(4):254–262. https://doi.org/10.1016/j.nmd.2010.12.011

Ouderkirk JL, Krendel M (2014) Myosin 1e is a component of the invadosome core that contributes to regulation of invadosome dynamics. Exp Cell Res 322(2):265–276. https://doi.org/10.1016/j.yexcr.2014.01.015

Ouderkirk-Pecone JL, Goreczny GJ, Chase SE, Tatum AH, Turner CE, Krendel M (2016) Myosin 1e promotes breast cancer malignancy by enhancing tumor cell proliferation and stimulating tumor cell dedifferentiation. Oncotarget. https://doi.org/10.18632/oncotarget.10139

Pan B, Akyuz N, Liu XP, Asai Y, Nist-Lund C, Kurima K, Derfler BH, Gyorgy B, Limapichat W, Walujkar S, Wimalasena LN, Sotomayor M, Corey DP, Holt JR (2018) TMC1 forms the pore of mechanosensory transduction channels in vertebrate inner ear hair cells. Neuron 99(4):736–753 e736. https://doi.org/10.1016/j.neuron.2018.07.033

Pannu H, Tran-Fadulu V, Papke CL, Scherer S, Liu Y, Presley C, Guo D, Estrera AL, Safi HJ, Brasier AR, Vick GW, Marian AJ, Raman CS, Buja LM, Milewicz DM (2007) MYH11 mutations result in a distinct vascular pathology driven by insulin-like growth factor 1 and angiotensin II. Hum Mol Genet 16(20):2453–2462. https://doi.org/10.1093/hmg/ddm201

Papal S, Cortese M, Legendre K, Sorusch N, Dragavon J, Sahly I, Shorte S, Wolfrum U, Petit C, El-Amraoui A (2013) The giant spectrin betaV couples the molecular motors to phototransduction and Usher syndrome type I proteins along their trafficking route. Hum Mol Genet 22(18):3773–3788. https://doi.org/10.1093/hmg/ddt228

Park H, Ramamurthy B, Travaglia M, Safer D, Chen LQ, Franzini-Armstrong C, Selvin PR, Sweeney HL (2006) Full-length myosin VI dimerizes and moves processively along actin filaments upon monomer clustering. Mol Cell 21(3):331–336. https://doi.org/10.1016/j.molcel.2005.12.015

Park H, Li A, Chen LQ, Houdusse A, Selvin PR, Sweeney HL (2007) The unique insert at the end of the myosin VI motor is the sole determinant of directionality. Proc Natl Acad Sci U S A 104(3):778–783. https://doi.org/10.1073/pnas.0610066104

Pastural E, Barrat FJ, Dufourcq-Lagelouse R, Certain S, Sanal O, Jabado N, Seger R, Griscelli C, Fischer A, de Saint Basile G (1997) Griscelli disease maps to chromosome 15q21 and is associated with mutations in the myosin-Va gene. Nat Genet 16(3):289–292

Patel KG, Liu C, Cameron PL, Cameron RS (2001) Myr 8, a novel unconventional myosin expressed during brain development associates with the protein phosphatase catalytic subunits 1alpha and 1gamma1. J Neurosci 21 (\):7954–7968

Patino-Lopez G, Aravind L, Dong X, Kruhlak MJ, Ostap EM, Shaw S (2010) Myosin 1G is an abundant class I myosin in lymphocytes whose localization at the plasma membrane depends on its ancient divergent pleckstrin homology (PH) domain (Myo1PH). J Biol Chem 285(12):8675–8686. M109.086959 [pii] https://doi.org/10.1074/jbc.M109.086959

Pecci A, Klersy C, Gresele P, Lee KJ, De Rocco D, Bozzi V, Russo G, Heller PG, Loffredo G, Ballmaier M, Fabris F, Beggiato E, Kahr WH, Pujol-Moix N, Platokouki H, Van Geet C, Noris P, Yerram P, Hermans C, Gerber B, Economou M, De Groot M, Zieger B, De Candia E, Fraticelli V, Kersseboom R, Piccoli GB, Zimmermann S, Fierro T, Glembotsky AC, Vianello F, Zaninetti C, Nicchia E, Guthner C, Baronci C, Seri M, Knight PJ, Balduini CL, Savoia

A (2014) MYH9-related disease: a novel prognostic model to predict the clinical evolution of the disease based on genotype-phenotype correlations. Hum Mutat 35(2):236–247. https://doi.org/10.1002/humu.22476

Pecci A, Ma X, Savoia A, Adelstein RS (2018) MYH9: Structure, functions and role of non-muscle myosin IIA in human disease. Gene 664:152–167. https://doi.org/10.1016/j.gene.2018.04.048

Peckham M (2016) How myosin organization of the actin cytoskeleton contributes to the cancer phenotype. Biochem Soc Trans 44(4):1026–1034. https://doi.org/10.1042/BST20160034

Peng YW, Zallocchi M, Wang WM, Delimont D, Cosgrove D (2011) Moderate light-induced degeneration of rod photoreceptors with delayed transducin translocation in shaker1 mice. Invest Ophthalmol Vis Sci 52(9):6421–6427. https://doi.org/10.1167/iovs.10-6557

Pepermans E, Michel V, Goodyear R, Bonnet C, Abdi S, Dupont T, Gherbi S, Holder M, Makrelouf M, Hardelin JP, Marlin S, Zenati A, Richardson G, Avan P, Bahloul A, Petit C (2014) The CD2 isoform of protocadherin-15 is an essential component of the tip-link complex in mature auditory hair cells. EMBO Mol Med 6(7):984–992. https://doi.org/10.15252/emmm.201403976

Percipalle P, Farrants AK (2006) Chromatin remodelling and transcription: be-WICHed by nuclear myosin 1. Curr Opin Cell Biol 18(3):267–274. https://doi.org/10.1016/j.ceb.2006.03.001

Percipalle P, Fomproix N, Cavellan E, Voit R, Reimer G, Kruger T, Thyberg J, Scheer U, Grummt I, Farrants AK (2006) The chromatin remodelling complex WSTF-SNF2h interacts with nuclear myosin 1 and has a role in RNA polymerase I transcription. EMBO Rep 7(5):525–530. https://doi.org/10.1038/sj.embor.7400657

Perreault-Micale C, Shushan AD, Coluccio LM (2000) Truncation of a mammalian myosin I results in loss of Ca^{2+}-sensitive motility. J Biol Chem 275:21618–21623

Pestic-Dragovich L, Stojiljkovic L, Philimonenko AA, Nowak G, Ke Y, Settlage RE, Shabanowitz J, Hunt DF, Hozak P, de Lanerolle P (2000) A myosin I isoform in the nucleus. Science (New York, NY) 290(5490):337–341

Philimonenko VV, Zhao J, Iben S, Dingova H, Kysela K, Hozak P, Grummt I (2004) Nuclear actin and myosin I are required for RNA polymerase I transcription. Nat Cell Biol 6:1165–1172

Pickles JO, Comis SD, Osborne MP (1984) Cross-links between stereocilia in the guinea pig organ of Corti, and their possible relation to sensory transduction. Hear Res 15:103–112

Piedra-Quintero ZL, Serrano C, Villegas-Sepulveda N, Maravillas-Montero JL, Romero-Ramirez S, Shibayama M, Medina-Contreras O, Nava P, Santos-Argumedo L (2018) Myosin 1F regulates M1-Polarization by stimulating intercellular adhesion in macrophages. Front Immunol 9:3118. https://doi.org/10.3389/fimmu.2018.03118

Pierchala BA, Munoz MR, Tsui CC (2010) Proteomic analysis of the slit diaphragm complex: CLIC5 is a protein critical for podocyte morphology and function. Kidney Int 78(9):868–882. https://doi.org/10.1038/ki.2010.212

Plantard L, Arjonen A, Lock JG, Nurani G, Ivaska J, Stromblad S (2010) PtdIns(3,4,5)P is a regulator of myosin-X localization and filopodia formation. J Cell Sci 123(Pt 20):3525–3534. 123/20/3525 [pii] https://doi.org/10.1242/jcs.069609

Pomianowski P, Elefteriades JA (2013) The genetics and genomics of thoracic aortic disease. Ann Cardiothorac Surg 2(3):271–279. https://doi.org/10.3978/j.issn.2225-319X.2013.05.12

Post PL, Bokoch GM, Mooseker MS (1998) Human myosin-IXb is a mechanochemically active motor and a GAP for rho. J Cell Sci 111(Pt 7):941–950

Prekeris R, Terrian DM (1997) Brain myosin V is a synaptic vesicle-associated motor protein: evidence for a Ca^{2+}-dependent interaction with the synaptobrevin-synaptophysin complex. J Cell Biol 137(7):1589–1601

Probst FJ, Fridell RA, Raphael Y, Saunders TL, Wang A, Liang Y, Morell RJ, Touchman JW, Lyons RH, Noben-Trauth K, Friedman TB, Camper SA (1998) Correction of deafness in shaker-2 mice by an unconventional myosin in a BAC transgene. Science (New York, NY) 280(5368):1444–1447

Prosperi MT, Lepine P, Dingli F, Paul-Gilloteaux P, Martin R, Loew D, Knolker HJ, Coudrier E (2015) Myosin 1b functions as an effector of EphB signaling to control cell repulsion. J Cell Biol 210(2):347–361. https://doi.org/10.1083/jcb.201501018

Provance DW Jr, Wei M, Ipe V, Mercer JA (1996) Cultured melanocytes from dilute mutant mice exhibit dendritic morphology and altered melanosome distribution. Proc Natl Acad Sci U S A 93(25):14554–14558

Purcell TJ, Sweeney HL, Spudich JA (2005) A force-dependent state controls the coordination of processive myosin V. Proc Natl Acad Sci U S A 102(39):13873–13878. https://doi.org/10.1073/pnas.0506441102

Pylypenko O, Song L, Squires G, Liu X, Zong AB, Houdusse A, Sweeney HL (2011) Role of insert-1 of myosin VI in modulating nucleotide affinity. J Biol Chem 286(13):11716–11723. https://doi.org/10.1074/jbc.M110.200626

Pylypenko O, Song L, Shima A, Yang Z, Houdusse AM, Sweeney HL (2015) Myosin VI deafness mutation prevents the initiation of processive runs on actin. Proc Natl Acad Sci U S A 112(11):E1201–E1209. https://doi.org/10.1073/pnas.1420989112

Qiu YL, Gong JY, Feng JY, Wang RX, Han J, Liu T, Lu Y, Li LT, Zhang MH, Sheps JA, Wang NL, Yan YY, Li JQ, Chen L, Borchers CH, Sipos B, Knisely AS, Ling V, Xing QH, Wang JS (2017) Defects in myosin VB are associated with a spectrum of previously undiagnosed low gamma-glutamyltransferase cholestasis. Hepatology 65(5):1655–1669. https://doi.org/10.1002/hep.29020

Quintero OA, DiVito MM, Adikes RC, Kortan MB, Case LB, Lier AJ, Panaretos NS, Slater SQ, Rengarajan

M, Feliu M, Cheney RE (2009) Human Myo19 is a novel myosin that associates with mitochondria. Curr Biol 19(23):2008–2013. https://doi.org/10.1016/j.cub.2009.10.026

Racca AW, Beck AE, McMillin MJ, Korte FS, Bamshad MJ, Regnier M (2015) The embryonic myosin R672C mutation that underlies Freeman-Sheldon syndrome impairs cross-bridge detachment and cycling in adult skeletal muscle. Hum Mol Genet 24(12):3348–3358. https://doi.org/10.1093/hmg/ddv084

Raines AN, Nagdas S, Kerber ML, Cheney RE (2012) Headless Myo10 is a negative regulator of full-length Myo10 and inhibits axon outgrowth in cortical neurons. J Biol Chem 287(30):24873–24883. https://doi.org/10.1074/jbc.M112.369173

Raposo G, Cordonnier MN, Tenza D, Menichi B, Dürrbach A, Louvard D, Coudrier E (1999) Association of myosin I alpha with endosomes and lysosomes in mammalian cells. Mol Biol Cell 10(5):1477–1494

Reggiani C, Bottinelli R (2008) Myosin II: Sarcomeric myosins, the motors of contraction in cardiac and skeletal muscles. In: Coluccio LM (ed) Proteins and cell regulation, vol 7. Myosins: a superfamily of molecular motors. Springer, Dordrecht, pp 125–170

Rehman AU, Bird JE, Faridi R, Shahzad M, Shah S, Lee K, Khan SN, Imtiaz A, Ahmed ZM, Riazuddin S, Santos-Cortez RL, Ahmad W, Leal SM, Riazuddin S, Friedman TB (2016) Mutational Spectrum of MYO15A and the Molecular Mechanisms of DFNB3 Human Deafness. Hum Mutat 37(10):991–1003. https://doi.org/10.1002/humu.23042

Reinhard J, Scheel AA, Diekmann D, Hall A, Ruppert C, Bähler M (1995) A novel type of myosin implicated in signalling by rho family GTPases. EMBO J 14(4):697–704

Renard M, Callewaert B, Baetens M, Campens L, MacDermot K, Fryns JP, Bonduelle M, Dietz HC, Gaspar IM, Cavaco D, Stattin EL, Schrander-Stumpel C, Coucke P, Loeys B, De Paepe A, De Backer J (2013) Novel MYH11 and ACTA2 mutations reveal a role for enhanced TGFbeta signaling in FTAAD. Int J Cardiol 165(2):314–321. https://doi.org/10.1016/j.ijcard.2011.08.079

Riazuddin S, Nazli S, Ahmed ZM, Yang Y, Zulfiqar F, Shaikh RS, Zafar AU, Khan SN, Sabar F, Javid FT, Wilcox ER, Tsilou E, Boger ET, Sellers JR, Belyantseva IA, Riazuddin S, Friedman TB (2008) Mutation spectrum of MYO7A and evaluation of a novel nonsyndromic deafness DFNB2 allele with residual function. Hum Mutat 29(4):502–511. https://doi.org/10.1002/humu.20677

Riazuddin S, Belyantseva IA, Giese AP, Lee K, Indzhykulian AA, Nandamuri SP, Yousaf R, Sinha GP, Lee S, Terrell D, Hegde RS, Ali RA, Anwar S, Andrade-Elizondo PB, Sirmaci A, Parise LV, Basit S, Wali A, Ayub M, Ansar M, Ahmad W, Khan SN, Akram J, Tekin M, Riazuddin S, Cook T, Buschbeck EK, Frolenkov GI, Leal SM, Friedman TB, Ahmed ZM (2012) Alterations of the CIB2 calcium- and integrin-binding protein cause Usher syndrome type 1J and nonsyndromic deafness DFNB48. Nat Genet 44(11):1265–1271. https://doi.org/10.1038/ng.2426

Ricca BL, Rock RS (2010) The stepping pattern of myosin X is adapted for processive motility on bundled actin. Biophys J 99(6):1818–1826. S0006-3495(10)00836-2 [pii]. https://doi.org/10.1016/j.bpj.2010.06.066

Rinaldi F, Terracciano C, Pisani V, Massa R, Loro E, Vergani L, Di Girolamo S, Angelini C, Gourdon G, Novelli G, Botta A (2012) Aberrant splicing and expression of the non muscle myosin heavy-chain gene MYH14 in DM1 muscle tissues. Neurobiol Dis 45(1):264–271. https://doi.org/10.1016/j.nbd.2011.08.010

Robert-Paganin J, Auguin D, Houdusse A (2018) Hypertrophic cardiomyopathy disease results from disparate impairments of cardiac myosin function and auto-inhibition. Nat Commun 9(1):4019. https://doi.org/10.1038/s41467-018-06191-4

Rock RS, Rice SE, Wells AL, Purcell TJ, Spudich JA, Sweeney HL (2001) Myosin VI is a processive motor with a large step size. Proc Natl Acad Sci U S A 98(24):13655–13659. https://doi.org/10.1073/pnas.191512398

Rodriguez OC, Cheney RE (2002) Human myosin-Vc is a novel class V myosin expressed in epithelial cells. J Cell Sci 115(Pt 5):991–1004

Rodriguez-Murillo L, Xu B, Roos JL, Abecasis GR, Gogos JA, Karayiorgou M (2014) Fine mapping on chromosome 13q32-34 and brain expression analysis implicates MYO16 in schizophrenia. Neuropsychopharmacology 39(4):934–943. https://doi.org/10.1038/npp.2013.293

Rohn JL, Patel JV, Neumann B, Bulkescher J, McHedlishvili N, McMullan RC, Quintero OA, Ellenberg J, Baum B (2014) Myo19 ensures symmetric partitioning of mitochondria and coupling of mitochondrial segregation to cell division. Curr Biol 24(21):2598–2605. https://doi.org/10.1016/j.cub.2014.09.045

Roland JT, Kenworthy AK, Peranen J, Caplan S, Goldenring JR (2007) Myosin Vb interacts with Rab8a on a tubular network containing EHD1 and EHD3. Mol Biol Cell 18(8):2828–2837. https://doi.org/10.1091/mbc.E07-02-0169

Roland JT, Lapierre LA, Goldenring JR (2009) Alternative splicing in class V myosins determines association with Rab10. J Biol Chem 284(2):1213–1223. https://doi.org/10.1074/jbc.M805957200

Roland JT, Bryant DM, Datta A, Itzen A, Mostov KE, Goldenring JR (2011) Rab GTPase-Myo5B complexes control membrane recycling and epithelial polarization. Proc Natl Acad Sci U S A 108(7):2789–2794. https://doi.org/10.1073/pnas.1010754108

Roncuzzi L, Brognara I, Baiocchi D, Amadori D, Gasperi-Campani A (2005) Loss of heterozygosity at 17p13.3-ter, distal to TP53, correlates with negative hormonal phenotype in sporadic breast cancer. Oncol Rep 14(2):471–474

Ropars V, Yang Z, Isabet T, Blanc F, Zhou K, Lin T, Liu X, Hissier P, Samazan F, Amigues B, Yang ED, Park H, Pylypenko O, Cecchini M, Sindelar CV, Sweeney HL, Houdusse A (2016) The myosin X motor is optimized for movement on actin bundles. Nat Commun 7:12456. https://doi.org/10.1038/ncomms12456

Rossi AC, Mammucari C, Argentini C, Reggiani C, Schiaffino S (2010) Two novel/ancient myosins in mammalian skeletal muscles: MYH14/7b and MYH15 are expressed in extraocular muscles and muscle spindles. J Physiol 588(Pt 2):353–364. https://doi.org/10.1113/jphysiol.2009.181008

Royer C, Lu X (2011) Epithelial cell polarity: a major gatekeeper against cancer? Cell Death Differ 18(9):1470–1477. https://doi.org/10.1038/cdd.2011.60

Ruemmele FM, Muller T, Schiefermeier N, Ebner HL, Lechner S, Pfaller K, Thoni CE, Goulet O, Lacaille F, Schmitz J, Colomb V, Sauvat F, Revillon Y, Canioni D, Brousse N, de Saint-Basile G, Lefebvre J, Heinz-Erian P, Enninger A, Utermann G, Hess MW, Janecke AR, Huber LA (2010) Loss-of-function of MYO5B is the main cause of microvillus inclusion disease: 15 novel mutations and a CaCo-2 RNAi cell model. Hum Mutat 31(5):544–551. https://doi.org/10.1002/humu.21224

Ruppert C, Kroschewski R, Bähler M (1993) Identification, characterization and cloning of myr 1, a mammalian myosin-I. J Cell Biol 120(6):1393–1403

Ruppert C, Godel J, Müller RT, Kroschewski R, Reinhard J, Bähler M (1995) Localization of the rat myosin I molecules myr 1 and myr 2 and in vivo targeting of their tail domains. J Cell Sci 108(Pt 12):3775–3786

Russell ES (1949) A quantitative histological study of the pigment found in the coat-color mutants of the house mouse; the nature of the effects of genic substitution in five major allelic series. Genetics 34(2):146–166

Rzadzinska AK, Schneider ME, Davies C, Riordan GP, Kachar B (2004) An actin molecular treadmill and myosins maintain stereocilia functional architecture and self-renewal. J Cell Biol 164(6):887–897. https://doi.org/10.1083/jcb.200310055

Sacks LD, Cann GM, Nikovits W Jr, Conlon S, Espinoza NR, Stockdale FE (2003) Regulation of myosin expression during myotome formation. Development 130(15):3391–3402

Sahlender DA, Roberts RC, Arden SD, Spudich G, Taylor MJ, Luzio JP, Kendrick-Jones J, Buss F (2005) Optineurin links myosin VI to the Golgi complex and is involved in Golgi organization and exocytosis. J Cell Biol 169(2):285–295. https://doi.org/10.1083/jcb.200501162

Saidova AA, Potashnikova DM, Tvorogova AV, Maly IV, Hofmann WA, Vorobjev IA (2018) Specific and reliable detection of Myosin 1C isoform A by RTqPCR in prostate cancer cells. PeerJ 6:e5970. https://doi.org/10.7717/peerj.5970

Sakai T, Umeki N, Ikebe R, Ikebe M (2011) Cargo binding activates myosin VIIA motor function in cells. Proc Natl Acad Sci U S A 108(17):7028–7033. https://doi.org/10.1073/pnas.1009188108

Sakamoto T, Webb MR, Forgacs E, White HD, Sellers JR (2008) Direct observation of the mechanochemical coupling in myosin Va during processive movement. Nature 455(7209):128–132. https://doi.org/10.1038/nature07188

Salamon M, Millino C, Raffaello A, Mongillo M, Sandri C, Bean C, Negrisolo E, Pallavicini A, Valle G, Zaccolo M, Schiaffino S, Lanfranchi G (2003) Human MYO18B, a novel unconventional myosin heavy chain expressed in striated muscles moves into the myonuclei upon differentiation. J Mol Biol 326(1):137–149. https://doi.org/10.1016/s0022-2836(02)01335-9

Salas-Cortes L, Ye F, Tenza D, Claire W, Theos A, Louvard D, Raposo G, Coudrier E (2005) Myosin 1b modulates the morphology and the protein transport within multi-vesicular sorting endosomes. J Cell Sci 118:4823–4832

Salles FT, Merritt JRC, Manor U, Dougherty GW, Sousa AD, Moore JE, Yengo CM, Dosé AC, Kachar B (2009) Myosin IIIa boosts elongation of stereocilia by transporting espin 1 to the plus ends of actin filaments. Nat Cell Biol. 15 Mar 09 on line

Salvermoser M, Pick R, Weckbach LT, Zehrer A, Lohr P, Drechsler M, Sperandio M, Soehnlein O, Walzog B (2018) Myosin 1f is specifically required for neutrophil migration in 3D environments during acute inflammation. Blood 131(17):1887–1898. https://doi.org/10.1182/blood-2017-10-811851

Sampaio-Silva J, Batissoco AC, Jesus-Santos R, Abath-Neto O, Scarpelli LC, Nishimura PY, Galindo LT, Bento RF, Oiticica J, Lezirovitz K (2018) Exome sequencing identifies a novel nonsense mutation of MYO6 as the cause of deafness in a Brazilian family. Ann Hum Genet 82(1):23–34. https://doi.org/10.1111/ahg.12213

Sanati N, Iancu OD, Wu G, Jacobs JE, McWeeney SK (2018) Network-based predictors of progression in head and neck squamous cell carcinoma. Front Genet 9:183. https://doi.org/10.3389/fgene.2018.00183

Sanchez E, Alizadeh BZ, Valdigem G, Ortego-Centeno N, Jimenez-Alonso J, de Ramon E, Garcia A, Lopez-Nevot MA, Wijmenga C, Martin J, Koeleman BP (2007) MYO9B gene polymorphisms are associated with autoimmune diseases in Spanish population. Hum Immunol 68(7):610–615. https://doi.org/10.1016/j.humimm.2007.03.006

Santiago JL, Martinez A, Nunez C, de la Calle H, Fernandez-Arquero M, de la Concha EG, Urcelay E (2008) Association of MYO9B haplotype with type 1 diabetes. Hum Immunol 69(2):112–115. https://doi.org/10.1016/j.humimm.2008.01.003

Sarshad A, Sadeghifar F, Louvet E, Mori R, Bohm S, Al-Muzzaini B, Vintermist A, Fomproix N, Ostlund AK, Percipalle P (2013) Nuclear myosin 1c facilitates the chromatin modifications required to activate rRNA gene transcription and cell cycle progression. PLoS Genet 9(3):e1003397. https://doi.org/10.1371/journal.pgen.1003397

Sarshad AA, Corcoran M, Al-Muzzaini B, Borgonovo-Brandter L, Von Euler A, Lamont D, Visa N,

Percipalle P (2014) Glycogen synthase kinase (GSK) 3beta phosphorylates and protects nuclear myosin 1c from proteasome-mediated degradation to activate rDNA transcription in early G1 cells. PLoS Genet 10(6):e1004390. https://doi.org/10.1371/journal.pgen.1004390

Satoh J (2014) Molecular network of ChIP-Seq-based NF-kappaB p65 target genes involves diverse immune functions relevant to the immunopathogenesis of multiple sclerosis. Mult Scler Relat Disord 3(1):94–106. https://doi.org/10.1016/j.msard.2013.04.005

Saydmohammed M, Yagi H, Calderon M, Clark MJ, Feinstein T, Sun M, Stolz DB, Watkins SC, Amack JD, Lo CW, Tsang M (2018) Vertebrate myosin 1d regulates left-right organizer morphogenesis and laterality. Nat Commun 9(1):3381. https://doi.org/10.1038/s41467-018-05866-2

Schiaffino S, Reggiani C (2011) Fiber types in mammalian skeletal muscles. Physiol Rev 91(4):1447–1531. https://doi.org/10.1152/physrev.00031.2010

Schiaffino S, Rossi AC, Smerdu V, Leinwand LA, Reggiani C (2015) Developmental myosins: expression patterns and functional significance. Skelet Muscle 5:22. https://doi.org/10.1186/s13395-015-0046-6

Schmitt JP, Debold EP, Ahmad F, Armstrong A, Frederico A, Conner DA, Mende U, Lohse MJ, Warshaw D, Seidman CE, Seidman JG (2006) Cardiac myosin missense mutations cause dilated cardiomyopathy in mouse models and depress molecular motor function. Proc Natl Acad Sci U S A 103(39):14525–14530. https://doi.org/10.1073/pnas.0606383103

Schneeberger K, Vogel GF, Teunissen H, van Ommen DD, Begthel H, El Bouazzaoui L, van Vugt AH, Beekman JM, Klumperman J, Muller T, Janecke A, Gerner P, Huber LA, Hess MW, Clevers H, van Es JH, Nieuwenhuis EE, Middendorp S (2015) An inducible mouse model for microvillus inclusion disease reveals a role for myosin Vb in apical and basolateral trafficking. Proc Natl Acad Sci U S A 112(40):12408–12413. https://doi.org/10.1073/pnas.1516672112

Schneeberger K, Roth S, Nieuwenhuis EES, Middendorp S (2018) Intestinal epithelial cell polarity defects in disease: lessons from microvillus inclusion disease. Dis Model Mech 11(2). https://doi.org/10.1242/dmm.031088

Schneider ME, Dosé AC, Salles FT, Change W, Erickson FL, Burnside B, Kachar B (2006) A new compartment at stereocilia tips defined by spatial and temporal patterns of myosin IIIa expression. J Neurosci 26(40):10243–10252

Schoumacher M, Goldman RD, Louvard D, Vignjevic DM (2010) Actin, microtubules, and vimentin intermediate filaments cooperate for elongation of invadopodia. J Cell Biol 189(3):541–556. https://doi.org/10.1083/jcb.200909113

Schramek D, Sendoel A, Segal JP, Beronja S, Heller E, Oristian D, Reva B, Fuchs E (2014) Direct in vivo RNAi screen unveils myosin IIa as a tumor suppressor of squamous cell carcinomas. Science (New York, NY) 343(6168):309–313. https://doi.org/10.1126/science.1248627

Schwab RS, Ihnatovych I, Yunus SZ, Domaradzki T, Hofmann WA (2013) Identification of signals that facilitate isoform specific nucleolar localization of myosin IC. Exp Cell Res 319(8):1111–1123. https://doi.org/10.1016/j.yexcr.2013.02.008

Schwander M, Lopes V, Sczaniecka A, Gibbs D, Lillo C, Delano D, Tarantino LM, Wiltshire T, Williams DS, Muller U (2009) A novel allele of myosin VIIa reveals a critical function for the C-terminal FERM domain for melanosome transport in retinal pigment epithelial cells. J Neurosci 29(50):15810–15818. https://doi.org/10.1523/JNEUROSCI.4876-09.2009

Seidman JG, Seidman C (2001) The genetic basis for cardiomyopathy: from mutation identification to mechanistic paradigms. Cell 104(4):557–567. S0092-8674(01)00242-2 [pii]

Self T, Sobe T, Copeland NG, Jenkins NA, Avraham KB, Steel KP (1999) Role of myosin VI in the differentiation of cochlear hair cells. Dev Biol 214(2):331–341. https://doi.org/10.1006/dbio.1999.9424

Sellers JR, Pato MD, Adelstein RS (1981) Reversible phosphorylation of smooth muscle myosin, heavy meromyosin, and platelet myosin. J Biol Chem 256(24):13137–13142

Senegas A, Gautheron J, Maurin AG, Courtois G (2015) IKK-related genetic diseases: probing NF-kappaB functions in humans and other matters. Cell Mol Life Sci 72(7):1275–1287. https://doi.org/10.1007/s00018-014-1793-y

Seri M, Pecci A, Di Bari F, Cusano R, Savino M, Panza E, Nigro A, Noris P, Gangarossa S, Rocca B, Gresele P, Bizzaro N, Malatesta P, Koivisto PA, Longo I, Musso R, Pecoraro C, Iolascon A, Magrini U, Rodriguez Soriano J, Renieri A, Ghiggeri GM, Ravazzolo R, Balduini CL, Savoia A (2003) MYH9-related disease: May-Hegglin anomaly, Sebastian syndrome, Fechtner syndrome, and Epstein syndrome are not distinct entities but represent a variable expression of a single illness. Medicine (Baltimore) 82(3):203–215. https://doi.org/10.1097/01.md.0000076006.64510.5c

Sheng G, Zeng Z, Pan J, Kou L, Wang Q, Yao H, Wen L, Ma L, Wu D, Qiu H, Chen S (2017) Multiple MYO18A-PDGFRB fusion transcripts in a myeloproliferative neoplasm patient with t(5;17)(q32;q11). Mol Cytogenet 10:4. https://doi.org/10.1186/s13039-017-0306-8

Shibue T, Brooks MW, Inan MF, Reinhardt F, Weinberg RA (2012) The outgrowth of micrometastases is enabled by the formation of filopodium-like protrusions. Cancer Discov 2(8):706–721. https://doi.org/10.1158/2159-8290.CD-11-0239

Shiroguchi K, Kinosita K Jr (2007) Myosin V walks by lever action and Brownian motion. Science (New York, NY) 316(5828):1208–1212

Shneyer BI, Usaj M, Henn A (2016) Myo19 is an outer mitochondrial membrane motor and effector of starvation-induced filopodia. J Cell Sci 129(3):543–556. https://doi.org/10.1242/jcs.175349

Shneyer BI, Usaj M, Wiesel-Motiuk N, Regev R, Henn A (2017) ROS induced distribution of mitochondria to filopodia by Myo19 depends on a class specific tryptophan in the motor domain. Sci Rep 7(1):11577. https://doi.org/10.1038/s41598-017-11002-9

Siegfried Z, Simon I (2010) DNA methylation and gene expression. Wiley Interdiscip Rev Syst Biol Med 2(3):362–371. https://doi.org/10.1002/wsbm.64

Sielski NL, Ihnatovych I, Hagen JJ, Hofmann WA (2014) Tissue specific expression of myosin IC isoforms. BMC Cell Biol 15:8. https://doi.org/10.1186/1471-2121-15-8

Simons M, Wang M, McBride OW, Kawamoto S, Yamakawa K, Gdula D, Adelstein RS, Weir L (1991) Human nonmuscle myosin heavy chains are encoded by two genes located on different chromosomes. Circ Res 69(2):530–539

Singh CK, George J, Nihal M, Sabat G, Kumar R, Ahmad N (2014) Novel downstream molecular targets of SIRT1 in melanoma: a quantitative proteomics approach. Oncotarget 5(7):1987–1999

Slany RK (2009) The molecular biology of mixed lineage leukemia. Haematologica 94(7):984–993. https://doi.org/10.3324/haematol.2008.002436

Smith RJ, Berlin CI, Hejtmancik JF, Keats BJ, Kimberling WJ, Lewis RA, Moller CG, Pelias MZ, Tranebjaerg L (1994) Clinical diagnosis of the Usher syndromes. Usher Syndrome Consortium. Am J Med Genet 50(1):32–38. https://doi.org/10.1002/ajmg.1320500107

Sousa AD, Berg JS, Robertson BW, Meeker RB, Cheney RE (2006) Myo10 in brain: developmental regulation, identification of a headless isoform and dynamics in neurons. J Cell Sci 119(Pt 1):184–194

Spéder P, Ádám G, Noselli S (2006) Type 1D unconventional myosin controls left-right asymmetry in *Drosophila*. Nature 440:803–807

Spielmann M, Hernandez-Miranda LR, Ceccherini I, Weese-Mayer DE, Kragesteen BK, Harabula I, Krawitz P, Birchmeier C, Leonard N, Mundlos S (2017) Mutations in MYO1H cause a recessive form of central hypoventilation with autonomic dysfunction. J Med Genet 54(11):754–761. https://doi.org/10.1136/jmedgenet-2017-104765

Spudich JA (2015) The myosin mesa and a possible unifying hypothesis for the molecular basis of human hypertrophic cardiomyopathy. Biochem Soc Trans 43(1):64–72. https://doi.org/10.1042/BST20140324

Spudich JA, Sivaramakrishnan S (2010) Myosin VI: an innovative motor that challenged the swinging lever arm hypothesis. Nat Rev Mol Cell Biol 11(2):128–137. https://doi.org/10.1038/nrm2833

Spudich G, Chibalina MV, Au JS, Arden SD, Buss F, Kendrick-Jones J (2007) Myosin VI targeting to clathrin-coated structures and dimerization is mediated by binding to Disabled-2 and PtdIns(4,5)P2. Nat Cell Biol 9(2):176–183. https://doi.org/10.1038/ncb1531

Stalpers X, Verrips A, Braakhekke J, Lammens M, van den Wijngaard A, Mostert A (2011) Scoliosis surgery in a patient with "de novo" myosin storage myopathy. Neuromuscul Disord 21(11):812–815. https://doi.org/10.1016/j.nmd.2011.05.005

Stauffer EA, Scarborough JD, Hirono M, Miller ED, Shah K, Mercer JA, Holt JR, Gillespie PG (2005) Fast adaptation in vestibular hair cells requires myosin-1c activity. Neuron 47(4):541–553

Stepensky P, Bartram J, Barth TF, Lehmberg K, Walther P, Amann K, Philips AD, Beringer O, Zur Stadt U, Schulz A, Amrolia P, Weintraub M, Debatin KM, Hoenig M, Posovszky C (2013) Persistent defective membrane trafficking in epithelial cells of patients with familial hemophagocytic lymphohistiocytosis type 5 due to STXBP2/MUNC18-2 mutations. Pediatr Blood Cancer 60(7):1215–1222. https://doi.org/10.1002/pbc.24475

Stinchcombe JC, Barral DC, Mules EH, Booth S, Hume AN, Machesky LM, Seabra MC, Griffiths GM (2001) Rab27a is required for regulated secretion in cytotoxic T lymphocytes. J Cell Biol 152(4):825–834

Stöffler HE, Bähler M (1998) The ATPase activity of Myr3, a rat myosin I, is allosterically inhibited by its own tail domain and by Ca^{2+} binding to its light chain calmodulin. J Biol Chem 273(23):14605–14611

Stöffler HE, Ruppert C, Reinhard J, Bähler M (1995) A novel mammalian myosin I from rat with an SH3 domain localizes to Con A-inducible, F-actin-rich structures at cell-cell contacts. J Cell Biol 129(3):819–830

Strauss O (2005) The retinal pigment epithelium in visual function. Physiol Rev 85(3):845–881. https://doi.org/10.1152/physrev.00021.2004

Strom M, Hume AN, Tarafder AK, Barkagianni E, Seabra MC (2002) A family of Rab27-binding proteins. Melanophilin links Rab27a and myosin Va function in melanosome transport. J Biol Chem 277(28):25423–25430. https://doi.org/10.1074/jbc.M202574200

Su AI, Welsh JB, Sapinoso LM, Kern SG, Dimitrov P, Lapp H, Schultz PG, Powell SM, Moskaluk CA, Frierson HF Jr, Hampton GM (2001) Molecular classification of human carcinomas by use of gene expression signatures. Cancer Res 61(20):7388–7393

Sun Y, Sato O, Ruhnow F, Arsenault ME, Ikebe M, Goldman YE (2010) Single-molecule stepping and structural dynamics of myosin X. Nat Struct Mol Biol 17(4):485–491. https://doi.org/10.1038/nsmb.1785

Sun R, Wang Y, Jin M, Chen L, Cao Y, Chen F (2018) Identification and functional studies of MYO1H for mandibular prognathism. J Dent Res 97:1501–1509. https://doi.org/10.1177/0022034518784936

Suzuki N, Kunishima S, Ikejiri M, Maruyama S, Sone M, Takagi A, Ikawa M, Okabe M, Kojima T, Saito H, Naoe T, Matsushita T (2013) Establishment of mouse model of MYH9 disorders: heterozygous R702C mutation provokes macrothrombocytopenia with leukocyte inclusion bodies, renal glomerulosclerosis and hearing disability. PLoS One 8(8):e71187. https://doi.org/10.1371/journal.pone.0071187

Sweeney HL, Houdusse A (2010) Myosin VI rewrites the rules for myosin motors. Cell 141(4):573–582. https://doi.org/10.1016/j.cell.2010.04.028

Sweeney HL, Park H, Zong AB, Yang Z, Selvin PR, Rosenfeld SS (2007) How myosin VI coordinates its heads during processive movement. EMBO J 26(11):2682–2692. https://doi.org/10.1038/sj.emboj.7601720

Swiatecka-Urban A, Talebian L, Kanno E, Moreau-Marquis S, Coutermarsh B, Hansen K, Karlson KH, Barnaby R, Cheney RE, Langford GM, Fukuda M, Stanton BA (2007) Myosin Vb is required for trafficking of the cystic fibrosis transmembrane conductance regulator in Rab11a-specific apical recycling endosomes in polarized human airway epithelial cells. J Biol Chem 282(32):23725–23736. https://doi.org/10.1074/jbc.M608531200

Szperl AM, Golachowska MR, Bruinenberg M, Prekeris R, Thunnissen AM, Karrenbeld A, Dijkstra G, Hoekstra D, Mercer D, Ksiazyk J, Wijmenga C, Wapenaar MC, Rings EH, van ISC (2011) Functional characterization of mutations in the myosin Vb gene associated with microvillus inclusion disease. J Pediatr Gastroenterol Nutr 52(3):307–313. https://doi.org/10.1097/MPG.0b013e3181eea177

Taft MH, Latham SL (2020) Chapter 19: Myosin XVIII. In: Coluccio LM (ed) Myosins: a superfamily of molecular motors, 2nd edn. Springer, Cham

Taft MH, Behrmann E, Munske-Weidemann LC, Thiel C, Raunser S, Manstein DJ (2013) Functional characterization of human myosin-18A and its interaction with F-actin and GOLPH3. J Biol Chem 288(42):30029–30041. https://doi.org/10.1074/jbc.M113.497180

Tajsharghi H, Oldfors A (2013) Myosinopathies: pathology and mechanisms. Acta Neuropathol 125(1):3–18. https://doi.org/10.1007/s00401-012-1024-2

Tajsharghi H, Thornell LE, Lindberg C, Lindvall B, Henriksson KG, Oldfors A (2003) Myosin storage myopathy associated with a heterozygous missense mutation in MYH7. Ann Neurol 54(4):494–500. https://doi.org/10.1002/ana.10693

Tajsharghi H, Oldfors A, Macleod DP, Swash M (2007) Homozygous mutation in MYH7 in myosin storage myopathy and cardiomyopathy. Neurology 68(12):962. https://doi.org/10.1212/01.wnl.0000257131.13438.2c

Tajsharghi H, Hilton-Jones D, Raheem O, Saukkonen AM, Oldfors A, Udd B (2010) Human disease caused by loss of fast IIa myosin heavy chain due to recessive MYH2 mutations. Brain 133(Pt 5):1451–1459. https://doi.org/10.1093/brain/awq083

Takagi Y, Yang Y, Fujiwara I, Jacobs D, Cheney RE, Sellers JR, Kovacs M (2008) Human myosin Vc is a low duty ratio, nonprocessive molecular motor. J Biol Chem 283(13):8527–8537. https://doi.org/10.1074/jbc.M709150200

Takagi Y, Farrow RE, Billington N, Nagy A, Batters C, Yang Y, Sellers JR, Molloy JE (2014) Myosin-10 produces its power-stroke in two phases and moves processively along a single actin filament under low load. Proc Natl Acad Sci U S A 111(18):E1833–E1842. https://doi.org/10.1073/pnas.1320122111

Takaoka M, Saito H, Takenaka K, Miki Y, Nakanishi A (2014) BRCA2 phosphorylated by PLK1 moves to the midbody to regulate cytokinesis mediated by nonmuscle myosin IIC. Cancer Res 74(5):1518–1528. https://doi.org/10.1158/0008-5472.CAN-13-0504

Taki T, Akiyama M, Saito S, Ono R, Taniwaki M, Kato Y, Yuza Y, Eto Y, Hayashi Y (2005) The MYO1F, unconventional myosin type 1F, gene is fused to MLL in infant acute monocytic leukemia with a complex translocation involving chromosomes 7, 11, 19 and 22. Oncogene 24(33):5191–5197. https://doi.org/10.1038/sj.onc.1208711

Tan I, Yong J, Dong JM, Lim L, Leung T (2008) A tripartite complex containing MRCK modulates lamellar actomyosin retrograde flow. Cell 135(1):123–136. https://doi.org/10.1016/j.cell.2008.09.018

Tassopoulou-Fishell M, Deeley K, Harvey EM, Sciote J, Vieira AR (2012) Genetic variation in myosin 1H contributes to mandibular prognathism. Am J Orthod Dentofac Orthop 141(1):51–59. https://doi.org/10.1016/j.ajodo.2011.06.033

Thelen S, Abouhamed M, Ciarimboli G, Edemir B, Bahler M (2015) Rho GAP myosin IXa is a regulator of kidney tubule function. Am J Physiol Renal Physiol 309(6):F501–F513. https://doi.org/10.1152/ajprenal.00220.2014

Thirumurugan K, Sakamoto T, Hammer JA 3rd, Sellers JR, Knight PJ (2006) The cargo-binding domain regulates structure and activity of myosin 5. Nature 442(7099):212–215. https://doi.org/10.1038/nature04865

Thoeni CE, Vogel GF, Tancevski I, Geley S, Lechner S, Pfaller K, Hess MW, Muller T, Janecke AR, Avitzur Y, Muise A, Cutz E, Huber LA (2014) Microvillus inclusion disease: loss of Myosin vb disrupts intracellular traffic and cell polarity. Traffic 15(1):22–42. https://doi.org/10.1111/tra.12131

Thon JN, Macleod H, Begonja AJ, Zhu J, Lee KC, Mogilner A, Hartwig JH, Italiano JE Jr (2012) Microtubule and cortical forces determine platelet size during vascular platelet production. Nat Commun 3:852. https://doi.org/10.1038/ncomms1838

Tilney LG, Portnoy DA (1989) Actin filaments and the growth, movement, and spread of the intracellular bacterial parasite, Listeria monocytogenes. J Cell Biol 109(4 Pt 1):1597–1608

Tiwari A, Jung JJ, Inamdar SM, Nihalani D, Choudhury A (2013) The myosin motor Myo1c is required for VEGFR2 delivery to the cell surface and for angiogenic signaling. Am J Phys Heart Circ Phys 304(5):H687–H696. https://doi.org/10.1152/ajpheart.00744.2012

Tokuo H, Ikebe M (2004) Myosin X transports Mena/VASP to the tip of filopodia. Biochem Biophys Res Commun 319(1):214–220. https://doi.org/10.1016/j.bbrc.2004.04.167 S0006291X04008484 [pii]

Tokuo H, Mabuchi K, Ikebe M (2007) The motor activity of myosin-X promotes actin fiber convergence at the cell periphery to initiate filopodia formation. J Cell Biol 179(2):229–238. jcb.200703178 [pii] https://doi.org/10.1083/jcb.200703178

Tokuo H, Bhawan J, Coluccio LM (2018) Myosin X is required for efficient melanoblast migration and mela-

noma initiation and metastasis. Sci Rep 8(1):10449. https://doi.org/10.1038/s41598-018-28717-y

Tomatis VM, Papadopulos A, Malintan NT, Martin S, Wallis T, Gormal RS, Kendrick-Jones J, Buss F, Meunier FA (2013) Myosin VI small insert isoform maintains exocytosis by tethering secretory granules to the cortical actin. J Cell Biol 200(3):301–320. https://doi.org/10.1083/jcb.201204092

Tomita-Mitchell A, Stamm KD, Mahnke DK, Kim MS, Hidestrand PM, Liang HL, Goetsch MA, Hidestrand M, Simpson P, Pelech AN, Tweddell JS, Benson DW, Lough JW, Mitchell ME (2016) Impact of MYH6 variants in hypoplastic left heart syndrome. Physiol Genomics 48(12):912–921. https://doi.org/10.1152/physiolgenomics.00091.2016

Toydemir RM, Rutherford A, Whitby FG, Jorde LB, Carey JC, Bamshad MJ (2006) Mutations in embryonic myosin heavy chain (MYH3) cause freeman-sheldon syndrome and sheldon-hall syndrome. Nat Genet 38(5):561–565. https://doi.org/10.1038/ng1775

Toyoda T, An D, Witczak CA, Koh HJ, Hirshman MF, Fujii N, Goodyear LJ (2011) Myo1c regulates glucose uptake in mouse skeletal muscle. J Biol Chem 286(6):4133–4140. https://doi.org/10.1074/jbc.M110.174938

Trivedi DV, Adhikari AS, Sarkar SS, Ruppel KM, Spudich JA (2018) Hypertrophic cardiomyopathy and the myosin mesa: viewing an old disease in a new light. Biophys Rev 10:27–48. https://doi.org/10.1007/s12551-017-0274-6

Tumbarello DA, Kendrick-Jones J, Buss F (2013) Myosin VI and its cargo adaptors – linking endocytosis and autophagy. J Cell Sci 126(Pt 12):2561–2570. https://doi.org/10.1242/jcs.095554

Tybulewicz VL (2005) Vav-family proteins in T-cell signalling. Curr Opin Immunol 17(3):267–274. https://doi.org/10.1016/j.coi.2005.04.003

Tyska MJ, Mackey AT, Huang J-D, Copeland NG, Jenkins NA, Mooseker MS (2005) Myosin-1a is critical for normal brush border structure and composition. Mol Biol Cell 16:2443–2457

Uhl J, Gujarathi S, Waheed AA, Gordon A, Freed EO, Gousset K (2018) Myosin-X is essential to the intercellular spread of HIV-1 Nef through tunneling nanotubes. J Cell Commun Signal. https://doi.org/10.1007/s12079-018-0493-z

Ujfalusi Z, Vera CD, Mijailovich SM, Svicevic M, Yu EC, Kawana M, Ruppel KM, Spudich JA, Geeves MA, Leinwand LA (2018) Dilated cardiomyopathy myosin mutants have reduced force-generating capacity. J Biol Chem 293(23):9017–9029. https://doi.org/10.1074/jbc.RA118.001938

Umeki N, Jung HS, Watanabe S, Sakai T, Li XD, Ikebe R, Craig R, Ikebe M (2009) The tail binds to the head-neck domain, inhibiting ATPase activity of myosin VIIA. Proc Natl Acad Sci U S A 106(21):8483–8488. https://doi.org/10.1073/pnas.0812930106

Umeki N, Jung HS, Sakai T, Sato O, Ikebe R, Ikebe M (2011) Phospholipid-dependent regulation of the motor activity of myosin X. Nat Struct Mol Biol 18(7):783–788. https://doi.org/10.1038/nsmb.2065

Unschuld PG, Ising M, Specht M, Erhardt A, Ripke S, Heck A, Kloiber S, Straub V, Brueckl T, Muller-Myhsok B, Holsboer F, Binder EB (2009) Polymorphisms in the GAD2 gene-region are associated with susceptibility for unipolar depression and with a risk factor for anxiety disorders. Am J Med Genet B Neuropsychiatr Genet 150B(8):1100–1109. https://doi.org/10.1002/ajmg.b.30938

Usaj M, Henn A (2017) Kinetic adaptation of human Myo19 for active mitochondrial transport to growing filopodia tips. Sci Rep 7(1):11596. https://doi.org/10.1038/s41598-017-11984-6

Ussowicz M, Jaskowiec A, Meyer C, Marschalek R, Chybicka A, Szczepanski T, Haus O (2012) A three-way translocation of MLL, MLLT11, and the novel reciprocal partner gene MYO18A in a child with acute myeloid leukemia. Cancer Genet 205(5):261–265. https://doi.org/10.1016/j.cancergen.2012.02.006

Usuki K, Nakatsu M, Kitazume K, Endo M, Osawa M, Iki S, Arai M, Urabe A (1996) CBFB/MYH11 fusion transcripts in a case of acute myelogenous leukemia (M1) with partial deletion of the long arm of chromosome 16. Intern Med 35(4):327–330

Varkuti BH, Yang Z, Kintses B, Erdelyi P, Bardos-Nagy I, Kovacs AL, Hari P, Kellermayer M, Vellai T, Malnasi-Csizmadia A (2012) A novel actin binding site of myosin required for effective muscle contraction. Nat Struct Mol Biol 19(3):299–306. https://doi.org/10.1038/nsmb.2216

Veigel C, Coluccio LM, Jontes JD, Sparrow JC, Milligan RA, Molloy JE (1999) The motor protein myosin-I produces its working stroke in two steps [see comments]. Nature 398(6727):530–533

Veigel C, Schmitz S, Wang F, Sellers JR (2005) Load-dependent kinetics of myosin-V can explain its high processivity. Nat Cell Biol 7(9):861–869. https://doi.org/10.1038/ncb1287

Velez Edwards DR, Tsosie KS, Williams SM, Edwards TL, Russell SB (2014) Admixture mapping identifies a locus at 15q21.2-22.3 associated with keloid formation in African Americans. Hum Genet 133(12):1513–1523. https://doi.org/10.1007/s00439-014-1490-9

Venit T, Dzijak R, Kalendova A, Kahle M, Rohozkova J, Schmidt V, Rulicke T, Rathkolb B, Hans W, Bohla A, Eickelberg O, Stoeger T, Wolf E, Yildirim AO, Gailus-Durner V, Fuchs H, de Angelis MH, Hozak P (2013) Mouse nuclear myosin I knock-out shows interchangeability and redundancy of myosin isoforms in the cell nucleus. PLoS One 8(4):e61406. https://doi.org/10.1371/journal.pone.0061406

Venit T, Kalendova A, Petr M, Dzijak R, Pastorek L, Rohozkova J, Malohlava J, Hozak P (2016) Nuclear myosin I regulates cell membrane tension. Sci Rep 6:30864. https://doi.org/10.1038/srep30864

Verpy E, Leibovici M, Zwaenepoel I, Liu XZ, Gal A, Salem N, Mansour A, Blanchard S, Kobayashi I, Keats BJ, Slim R, Petit C (2000) A defect in harmonin, a PDZ domain-containing protein expressed in

the inner ear sensory hair cells, underlies Usher syndrome type 1C. Nat Genet 26(1):51–55. https://doi.org/10.1038/79171

Veugelers M, Bressan M, McDermott DA, Weremowicz S, Morton CC, Mabry CC, Lefaivre JF, Zunamon A, Destree A, Chaudron JM, Basson CT (2004) Mutation of perinatal myosin heavy chain associated with a Carney complex variant. N Engl J Med 351(5):460–469. https://doi.org/10.1056/NEJMoa040584

Villanueva-Ortega E, Ahedo B, Fonseca-Sanchez MA, Perez-Duran J, Garibay-Nieto N, Macias-Galaviz MT, Trujillo-Cabrera Y, Garcia-Latorre E, Queipo G (2017) Analysis of PTPN22, ZFAT and MYO9B polymorphisms in Turner Syndrome and risk of autoimmune disease. Int J Immunogenet 44(4):153–157. https://doi.org/10.1111/iji.12323

Visuttijai K, Pettersson J, Mehrbani Azar Y, van den Bout I, Orndal C, Marcickiewicz J, Nilsson S, Hornquist M, Olsson B, Ejeskar K, Behboudi A (2016) Lowered expression of tumor suppressor candidate MYO1C stimulates cell proliferation, suppresses cell adhesion and activates AKT. PLoS One 11(10):e0164063. https://doi.org/10.1371/journal.pone.0164063

Viswanathan MC, Tham RC, Kronert WA, Sarsoza F, Trujillo AS, Cammarato A, Bernstein SI (2017) Myosin storage myopathy mutations yield defective myosin filament assembly in vitro and disrupted myofibrillar structure and function in vivo. Hum Mol Genet 26(24):4799–4813. https://doi.org/10.1093/hmg/ddx359

Vogel GF, Klee KM, Janecke AR, Muller T, Hess MW, Huber LA (2015) Cargo-selective apical exocytosis in epithelial cells is conducted by Myo5B, Slp4a, Vamp7, and Syntaxin 3. J Cell Biol 211(3):587–604. https://doi.org/10.1083/jcb.201506112

Vreugde S, Ferrai C, Miluzio A, Hauben E, Marchisio PC, Crippa MP, Bussi M, Biffo S (2006) Nuclear myosin VI enhances RNA polymerase II-dependent transcription. Mol Cell 23(5):749–755. https://doi.org/10.1016/j.molcel.2006.07.005

Wagner MC, Barylko B, Albanesi JP (1992) Tissue distribution and subcellular localization of mammalian myosin I. J Cell Biol 119(1):163–170

Wagner W, Brenowitz SD, Hammer JA 3rd (2011) Myosin-Va transports the endoplasmic reticulum into the dendritic spines of Purkinje neurons. Nat Cell Biol 13(1):40–48. https://doi.org/10.1038/ncb2132

Wakabayashi Y, Dutt P, Lippincott-Schwartz J, Arias IM (2005) Rab11a and myosin Vb are required for bile canalicular formation in WIF-B9 cells. Proc Natl Acad Sci U S A 102(42):15087–15092. https://doi.org/10.1073/pnas.0503702102

Walsh T, Walsh V, Vreugde S, Hertzano R, Shahin H, Haika S, Lee MK, Kanaan M, King MC, Avraham KB (2002) From flies' eyes to our ears: mutations in a human class III myosin cause progressive nonsyndromic hearing loss DFNB30. Proc Natl Acad Sci U S A 99(11):7518–7523

Walsh VL, Raviv D, Dror AA, Shahin H, Walsh T, Kanaan MN, Avraham KB, King MC (2011) A mouse model for human hearing loss DFNB30 due to loss of function of myosin IIIA. Mamm Genome 22(3–4):170–177. https://doi.org/10.1007/s00335-010-9310-6

Walz C, Chase A, Schoch C, Weisser A, Schlegel F, Hochhaus A, Fuchs R, Schmitt-Graff A, Hehlmann R, Cross NC, Reiter A (2005) The t(8;17)(p11;q23) in the 8p11 myeloproliferative syndrome fuses MYO18A to FGFR1. Leukemia 19(6):1005–1009. https://doi.org/10.1038/sj.leu.2403712

Walz C, Haferlach C, Hanel A, Metzgeroth G, Erben P, Gosenca D, Hochhaus A, Cross NC, Reiter A (2009) Identification of a MYO18A-PDGFRB fusion gene in an eosinophilia-associated atypical myeloproliferative neoplasm with a t(5;17)(q33-34;q11.2). Genes Chromosomes Cancer 48(2):179–183. https://doi.org/10.1002/gcc.20629

Wang FS, Wolenski JS, Cheney RE, Mooseker MS, Jay DG (1996) Function of myosin-V in filopodial extension of neuronal growth cones. Science (New York, NY) 273(5275):660–663

Wang A, Liang Y, Fridell RA, Probst FJ, Wilcox ER, Touchman JW, Morton CC, Morell RJ, Noben-Trauth K, Camper SA, Friedman TB (1998) Association of unconventional myosin MYO15 mutations with human nonsyndromic deafness DFNB3. Science (New York, NY) 280:1447–1451

Wang F, Thirumurugan K, Stafford WF, Hammer JA 3rd, Knight PJ, Sellers JR (2004) Regulated conformation of myosin V. J Biol Chem 279(4):2333–2336. https://doi.org/10.1074/jbc.C300488200 C300488200 [pii]

Wang RJ, Wu P, Cai GX, Wang ZM, Xu Y, Peng JJ, Sheng WQ, Lu HF, Cai SJ (2014) Down-regulated MYH11 expression correlates with poor prognosis in stage II and III colorectal cancer. Asian Pac J Cancer Prev 15(17):7223–7228

Wang H, Wang B, Zhu W, Yang Z (2015) Lentivirus-mediated knockdown of myosin VI inhibits cell proliferation of breast Cancer cell. Cancer Biother Radiopharm 30(8):330–335. https://doi.org/10.1089/cbr.2014.1759

Wang MJ, Xu XL, Yao GL, Yu Q, Zhu CF, Kong ZJ, Zhao H, Tang LM, Qin XH (2016) MYO9B gene polymorphisms are associated with the risk of inflammatory bowel diseases. Oncotarget 7(37):58862–58875. https://doi.org/10.18632/oncotarget.11186

Wang X, Li J, Xu X, Zheng J, Li Q (2018) miR-129 inhibits tumor growth and potentiates chemosensitivity of neuroblastoma by targeting MYO10. Biomed Pharmacother 103:1312–1318. https://doi.org/10.1016/j.biopha.2018.04.153

Warner CL, Stewart A, Luzio JP, Steel KP, Libby RT, Kendrick-Jones J, Buss F (2003) Loss of myosin VI reduces secretion and the size of the Golgi in fibroblasts from Snell's waltzer mice. EMBO J 22(3):569–579. https://doi.org/10.1093/emboj/cdg055

Warshaw DM (2004) Lever arms and necks: a common mechanistic theme across the myosin superfamily. J Muscle Res Cell Motil 25(6):467–474. https://doi.org/10.1007/s10974-004-1767-z

Watanabe TM, Tokuo H, Gonda K, Higuchi H, Ikebe M (2010) Myosin-X induces filopodia by multiple elongation mechanism. J Biol Chem 285(25):19605–19614. https://doi.org/10.1074/jbc.M109.093864

Wei Z, Liu X, Yu C, Zhang M (2013) Structural basis of cargo recognitions for class V myosins. Proc Natl Acad Sci U S A 110(28):11314–11319. https://doi.org/10.1073/pnas.1306768110

Weil D, Blanchard S, Kaplan J, Guilford P, Gibson F, Walsh J, Mburu P, Varela A, Levilliers J, Weston MD et al (1995) Defective myosin VIIA gene responsible for Usher syndrome type 1B. Nature 374(6517):60–61. https://doi.org/10.1038/374060a0

Weil D, El-Amraoui A, Masmoudi S, Mustapha M, Kikkawa Y, Laine S, Delmaghani S, Adato A, Nadifi S, Zina ZB, Hamel C, Gal A, Ayadi H, Yonekawa H, Petit C (2003) Usher syndrome type I G (USH1G) is caused by mutations in the gene encoding SANS, a protein that associates with the USH1C protein, harmonin. Hum Mol Genet 12(5):463–471

Weiss A, Leinwand LA (1996) The mammalian myosin heavy chain gene family. Annu Rev Cell Dev Biol 12:417–439

Weisz OA, Rodriguez-Boulan E (2009) Apical trafficking in epithelial cells: signals, clusters and motors. J Cell Sci 122(Pt 23):4253–4266. 122/23/4253 [pii] https://doi.org/10.1242/jcs.032615

Wells AL, Lin AW, Chen LQ, Safer D, Cain SM, Hasson T, Carragher BO, Milligan RA, Sweeney HL (1999) Myosin VI is an actin-based motor that moves backwards [see comments]. Nature 401(6752):505–508

Wendt T, Taylor D, Trybus KM, Taylor K (2001) Three-dimensional image reconstruction of dephosphorylated smooth muscle heavy meromyosin reveals asymmetry in the interaction between myosin heads and placement of subfragment 2. Proc Natl Acad Sci U S A 98(8):4361–4366

Wenzel J, Ouderkirk JL, Krendel M, Lang R (2015) Class I myosin Myo1e regulates TLR4-triggered macrophage spreading, chemokine release, and antigen presentation via MHC class II. Eur J Immunol 45(1):225–237. https://doi.org/10.1002/eji.201444698

Whibley C, Pharoah PD, Hollstein M (2009) p53 polymorphisms: cancer implications. Nat Rev Cancer 9(2):95–107. https://doi.org/10.1038/nrc2584

Wilkes D, McDermott DA, Basson CT (2005) Clinical phenotypes and molecular genetic mechanisms of Carney complex. Lancet Oncol 6(7):501–508. https://doi.org/10.1016/S1470-2045(05)70244-8

Williams DS, Lopes VS (2011) The many different cellular functions of MYO7A in the retina. Biochem Soc Trans 39(5):1207–1210. https://doi.org/10.1042/BST0391207

Wirth JA, Jensen KA, Post PL, Bement WM, Mooseker MS (1996) Human myosin-IXb, an unconventional myosin with a chimerin-like rho/rac GTPase-activating protein domain in its tail. J Cell Sci 109(Pt 3):653–661

Wollscheid HP, Biancospino M, He F, Magistrati E, Molteni E, Lupia M, Soffientini P, Rottner K, Cavallaro U, Pozzoli U, Mapelli M, Walters KJ, Polo S (2016) Diverse functions of myosin VI elucidated by an isoform-specific alpha-helix domain. Nat Struct Mol Biol 23(4):300–308. https://doi.org/10.1038/nsmb.3187

Wu X, Rao K, Bowers MB, Copeland NG, Jenkins NA, Hammer JA 3rd (2001) Rab27a enables myosin Va-dependent melanosome capture by recruiting the myosin to the organelle. J Cell Sci 114(Pt 6):1091–1100

Wu X, Wang F, Rao K, Sellers JR, Hammer JA 3rd (2002) Rab27a is an essential component of melanosome receptor for myosin Va. Mol Biol Cell 13(5):1735–1749. https://doi.org/10.1091/mbc.01-12-0595

Xia ZK, Yuan YC, Yin N, Yin BL, Tan ZP, Hu YR (2012) Nonmuscle myosin IIA is associated with poor prognosis of esophageal squamous cancer. Dis Esophagus 25(5):427–436. https://doi.org/10.1111/j.1442-2050.2011.01261.x

Xiong D, Ye YL, Chen MK, Qin ZK, Li MZ, Zhang H, Xu LH, Xu ZZ, Zeng MS (2012) Non-muscle myosin II is an independent predictor of overall survival for cystectomy candidates with early-stage bladder cancer. Oncol Rep 28(5):1625–1632. https://doi.org/10.3892/or.2012.1965

Xiong A, Haithcock J, Liu Y, Eusner L, McConnell M, White HD, Belknap B, Forgacs E (2018) The shaker-1 mouse myosin VIIa deafness mutation results in a severely reduced rate of the ATP hydrolysis step. J Biol Chem 293(3):819–829. https://doi.org/10.1074/jbc.M117.810119

Yamada Y, Koshizuka K, Hanazawa T, Kikkawa N, Okato A, Idichi T, Arai T, Sugawara S, Katada K, Okamoto Y, Seki N (2017) Passenger strand of miR-145-3p acts as a tumor-suppressor by targeting MYO1B in head and neck squamous cell carcinoma. Int J Oncol. https://doi.org/10.3892/ijo.2017.4190

Yamaguchi Y, Miyagi Y, Baba H (2008) Two-dimensional electrophoresis with cationic detergents: a powerful tool for the proteomic analysis of myelin proteins. Part 2: analytical aspects. J Neurosci Res 86(4):766–775. https://doi.org/10.1002/jnr.21549

Yanaihara N, Nishioka M, Kohno T, Otsuka A, Okamoto A, Ochiai K, Tanaka T, Yokota J (2004) Reduced expression of MYO18B, a candidate tumor-suppressor gene on chromosome arm 22q, in ovarian cancer. Int J Cancer 112(1):150–154. https://doi.org/10.1002/ijc.20339

Yang CK, Kim JH, Stallcup MR (2006) Role of the N-terminal activation domain of the coiled-coil coactivator in mediating transcriptional activation by beta-catenin. Mol Endocrinol 20(12):3251–3262. https://doi.org/10.1210/me.2006-0200

Ye J, Zhao J, Hoffmann-Rohrer U, Grummt I (2008) Nuclear myosin I acts in concert with polymeric actin to drive RNA polymerase I transcription. Genes Dev 22(3):322–330. https://doi.org/10.1101/gad.455908

Yetman AT, Starr LJ (2018) Newly described recessive MYH11 disorder with clinical overlap of Multisystemic smooth muscle dysfunction and Megacystis microcolon hypoperistalsis syndromes.

Am J Med Genet A 176(4):1011–1014. https://doi.org/10.1002/ajmg.a.38647

Yildiz A, Forkey JN, McKinney SA, Ha T, Goldman YE, Selvin PR (2003) Myosin V walks hand-over-hand: single fluorophore imaging with 1.5-nm localization. Science (New York, NY) 300(5628):2061–2065. https://doi.org/10.1126/science.1084398

Yokoyama K, Tezuka T, Kotani M, Nakazawa T, Hoshina N, Shimoda Y, Kakuta S, Sudo K, Watanabe K, Iwakura Y, Yamamoto T (2011) NYAP: a phosphoprotein family that links PI3K to WAVE1 signalling in neurons. EMBO J 30(23):4739–4754. https://doi.org/10.1038/emboj.2011.348

Yoshida H, Cheng W, Hung J, Montell D, Geisbrecht E, Rosen D, Liu J, Naora H (2004) Lessons from border cell migration in the Drosophila ovary: A role for myosin VI in dissemination of human ovarian cancer. Proc Natl Acad Sci U S A 101(21):8144–8149. https://doi.org/10.1073/pnas.0400400101

Yoshimura A, Fujii R, Watanabe Y, Okabe S, Fukui K, Takumi T (2006) Myosin-Va facilitates the accumulation of mRNA/protein complex in dendritic spines. Curr Biol 16(23):2345–2351. https://doi.org/10.1016/j.cub.2006.10.024

Yu C, Feng W, Wei Z, Miyanoiri Y, Wen W, Zhao Y, Zhang M (2009) Myosin VI undergoes cargo-mediated dimerization. Cell 138(3):537–554

Yu IM, Planelles-Herrero VJ, Sourigues Y, Moussaoui D, Sirkia H, Kikuti C, Stroebel D, Titus MA, Houdusse A (2017) Myosin 7 and its adaptors link cadherins to actin. Nat Commun 8:15864. https://doi.org/10.1038/ncomms15864

Yuceyar N, Ayhan O, Karasoy H, Tolun A (2015) Homozygous MYH7 R1820W mutation results in recessive myosin storage myopathy: scapuloperoneal and respiratory weakness with dilated cardiomyopathy. Neuromuscul Disord 25(4):340–344. https://doi.org/10.1016/j.nmd.2015.01.007

Zadro C, Alemanno MS, Bellacchio E, Ficarella R, Donaudy F, Melchionda S, Zalante L, Rabionet R, Hilgert N, Estivill X, Van Camp G, Gasparini P, Carella M (2009) Are Myo1C and Myo1F associated with hearing loss? Biochim Biophys Acta 1792:27–32

Zampini V, Ruttiger L, Johnson SL, Franz C, Furness DN, Waldhaus J, Xiong H, Hackney CM, Holley MC, Offenhauser N, Di Fiore PP, Knipper M, Masetto S, Marcotti W (2011) Eps8 regulates hair bundle length and functional maturation of mammalian auditory hair cells. PLoS Biol 9(4):e1001048. https://doi.org/10.1371/journal.pbio.1001048

Zattelman L, Regev R, Usaj M, Reinke PYA, Giese S, Samson AO, Taft MH, Manstein DJ, Henn A (2017) N-terminal splicing extensions of the human MYO1C gene fine-tune the kinetics of the three full-length myosin IC isoforms. J Biol Chem 292(43):17804–17818. https://doi.org/10.1074/jbc.M117.794008

Zhang H, Berg JS, Li Z, Wang Y, Lang P, Sousa AD, Bhaskar A, Cheney RE, Stromblad S (2004) Myosin-X provides a motor-based link between integrins and the cytoskeleton. Nat Cell Biol 6(6):523–531. https://doi.org/10.1038/ncb1136 ncb1136 [pii]

Zhang Y, Conti MA, Malide D, Dong F, Wang A, Shmist YA, Liu C, Zerfas P, Daniels MP, Chan CC, Kozin E, Kachar B, Kelley MJ, Kopp JB, Adelstein RS (2012) Mouse models of MYH9-related disease: mutations in nonmuscle myosin II-A. Blood 119(1):238–250. https://doi.org/10.1182/blood-2011-06-358853

Zhang WB, Yao LL, Li XD (2016a) The globular tail domain of Myosin-5a functions as a dimer in regulating the motor activity. J Biol Chem 291(26):13571–13579. https://doi.org/10.1074/jbc.M116.724328

Zhang X, Huang Z, Hu Y, Liu L (2016b) Knockdown of Myosin 6 inhibits proliferation of oral squamous cell carcinoma cells. J Oral Pathol Med 45(10):740–745. https://doi.org/10.1111/jop.12448

Zhao Y, Feng Y, Zhang YM, Ding XX, Song YZ, Zhang AM, Liu L, Zhang H, Ding JH, Xia XS (2015) Targeted next-generation sequencing of candidate genes reveals novel mutations in patients with dilated cardiomyopathy. Int J Mol Med 36(6):1479–1486. https://doi.org/10.3892/ijmm.2015.2361

Zhen T, Kwon EM, Zhao L, Hsu J, Hyde RK, Lu Y, Alemu L, Speck NA, Liu PP (2017) Chd7 deficiency delays leukemogenesis in mice induced by Cbfb-MYH11. Blood 130(22):2431–2442. https://doi.org/10.1182/blood-2017-04-780106

Zhou X, Wang R, Li X, Yu L, Hua D, Sun C, Shi C, Luo W, Rao C, Jiang Z, Feng Y, Wang Q, Yu S (2019) Splicing factor SRSF1 promotes gliomagenesis via oncogenic splice-switching of MYO1B. J Clin Invest 129(2):676–693. https://doi.org/10.1172/JCI120279

Zhu T, Ikebe M (1994) A novel myosin I from bovine adrenal gland. FEBS Lett 339(1–2):31–36

Zhu L, Vranckx R, Khau Van Kien P, Lalande A, Boisset N, Mathieu F, Wegman M, Glancy L, Gasc JM, Brunotte F, Bruneval P, Wolf JE, Michel JB, Jeunemaitre X (2006) Mutations in myosin heavy chain 11 cause a syndrome associating thoracic aortic aneurysm/aortic dissection and patent ductus arteriosus. Nat Genet 38(3):343–349. https://doi.org/10.1038/ng1721

Zhu Z, Peng L, Chen G, Jiang W, Shen Z, Du C, Zang R, Su Y, Xie H, Li H, Xia Y, Tang W (2017) Mutations of MYH14 are associated to anorectal malformations with recto-perineal fistulas in a small subset of Chinese population. Clin Genet 92(5):503–509. https://doi.org/10.1111/cge.12993

Zorzato F, Jungbluth H, Zhou H, Muntoni F, Treves S (2007) Functional effects of mutations identified in patients with multiminicore disease. IUBMB Life 59(1):14–20. https://doi.org/10.1080/15216540601187803

Myosins and Hearing

13

Thomas B. Friedman, Inna A. Belyantseva, and Gregory I. Frolenkov

Abstract

Hearing loss is both genetically and clinically heterogeneous, and pathogenic variants of over a hundred different genes are associated with this common neurosensory disorder. A relatively large number of these "deafness genes" encode myosin super family members. The evidence that pathogenic variants of human MYO3A, MYO6, MYO7A, MYO15A, MYH14 and MYH9 are associated with deafness ranges from moderate to definitive. Additional evidence for the involvement of these six myosins for normal hearing also comes from animal models, usually mouse or zebra fish, where mutations of these genes cause hearing loss and from biochemical, physiological and cell biological studies of their roles in the inner ear. This chapter focuses on these six genes for which evidence of a causative role in deafness is substantial.

Keywords

MYO3A · MYO6 · MYO7A · MYO15A · MYH14 · MYH9 · Deafness · Stereocilia · Hair cells · Hearing · Usher syndrome · Retinitis pigmentosa · Harmonin · Shaker 2 mouse · Whirler mouse · Helio gene-gun

13.1 Introduction

Hearing loss is one of the most common neurosensory disorders. Pathogenic variants of 142 human genes have been reported to be associated with deafness (DiStefano et al. 2019). Nine of these "deafness genes" encode myosin family members reported to be necessary for normal hearing (Table 13.1). Rare variants of additional "deafness genes" likely remain to be discovered, as there are hundreds of syndromes that include deafness as one feature for which the underlying biological causes have not been reported. The requirement of such a large number of genes for hearing isn't surprising, given the structural and physiological complexity of the inner ear (Frolenkov et al. 2004; Griffith and Friedman 2016; Velez-Ortega and Frolenkov 2019).

Despite annotations as of January 2020 in the UCSC Genome Browser indicating an involvement with human deafness, the hypothesis that heterozygous variants of *MYO1A* are a primary

T. B. Friedman (✉) · I. A. Belyantseva
Laboratory of Molecular Genetics, National Institute on Deafness and Other Communication Disorders, Porter Neuroscience Research Center, National Institutes of Health, Bethesda, MD, USA
e-mail: friedman@nidcd.nih.gov; belyants@nidcd.nih.gov

G. I. Frolenkov
Department of Physiology, University of Kentucky College of Medicine, Lexington, KY, USA
e-mail: gregory.frolenkov@uky.edu

L. M. Coluccio (ed.), *Myosins*, Advances in Experimental Medicine and Biology 1239,
https://doi.org/10.1007/978-3-030-38062-5_13

Table 13.1 Human myosins reported necessary for hearing and the strength of genetic evidence

Myosin gene[a]	Inheritance	Hearing loss	Strength of evidence[b]
MYO1A	AD	Moderate to profound	Refuted
MYO1C	AD	Moderate	Disputed
MYO1F	AD	Moderate	Disputed
MYO3A	AR	Profound	Strong
MYO6	AD	Profound	Definitive
MYO6	AR	Profound	Not available
MYO7A	AR	Profound, Usher syndrome type 1	Definitive
MYO7A	AD	Post-lingual, moderate, progressive nonsyndromic hearing loss	Definitive
MYO7A	AR	Profound, nonsyndromic deafness	Not available
MYO15A	AR	Profound	Definitive
MYH14	AD	Profound	Moderate
MYH9	AD	Profound	Definitive

Mode of inheritance, *AR* autosomal recessive hearing loss, *AD* autosomal dominant hearing loss

[a]For mouse models, see the Jackson Laboratory Mouse Genome Informatics at http://www.informatics.jax.org

[b]Definitions and assignment of evidence strength reported in (DiStefano et al. 2019); refuted, original claim demonstrated to be proven wrong or where "significance evidence outweigh[ed] evidence supporting the claim."; disputed, insufficient or conflicting evidence; moderate, evidence is "promising"; strong or definitive classification required replication in two or more studies

cause of neurosensory hearing loss has been refuted (Eisenberger et al. 2014; Patton et al. 2017). Additionally, causal relationships for variants of *MYO1C* and *MYO1F* in human deafness are also disputed (DiStefano et al. 2019). It remains possible that variants of *MYO1A*, *MYO1C* and *MYO1F* may have reduced penetrance for deafness, could be genetic modifiers of a major "deafness gene" or may increase risk of hearing loss due to loud noise or ototoxic agents (Patton et al. 2017). However, in light of the concerns about the current evidence supporting *MYO1A*, *MYO1C* and *MYO1F* in human deafness, the focus of this chapter is limited to six different *bona fide* "deafness genes" encoding myosins, where the evidence ranges from moderate to definitive that variants of *MYO3A*, *MYO6*, *MYO7A*, *MYO15A*, *MYH14* and *MYH9* are pathogenic (DiStefano et al. 2019). Additional evidence for the crucial involvement of these six different myosins for hearing comes from animal models, usually mouse or zebra fish, that recapitulate the human hearing loss phenotype or from protein partners of these myosins, such as whirlin, ESPN, EPS8, GPSM2 and $G\alpha_{i3}$, that are also required for normal hearing (Mauriac et al. 2017).

13.2 Mechanisms of Sound Transduction

Hair cells in the inner ear detect sound, gravity and head movement. A conversion of sound stimuli into electrical signals that are further transmitted to the brain occurs in stereocilia, which protrude from the apical surface of hair cells in the inner ear (Fig. 13.1). During development, stereocilia are derived from microvilli that become long, thick, and mechanically rigid structures because of crosslinking of actin filaments by espins, fascin and plastin/fimbrin (Drummond et al. 2015; Frolenkov et al. 2004; Narayanan et al. 2015; Tilney et al. 1992; Velez-Ortega and Frolenkov 2019; Zhang et al. 2012). In all mammalian species that have been studied, including mouse and human, hair cells must last a lifetime for normal hearing. Unlike some birds and fish, there is little or no neurogenesis in the postnatal mammalian inner ear and hair cells are not replaced when they die.

Stereocilia are organized in an evolutionarily conserved staircase-like architecture in rows of increasing height. Each stereocilium in a bundle is anchored to its hair cell by a rootlet structure embedded in the cuticular plate (Fig. 13.1) (Kitajiri et al. 2010; Katsuno et al. 2019). The number of stereocilia in a bundle and their dimensions are variable for each inner ear sensory organ. The elongation of stereocilia to a predetermined length and width and the dynamic maintenance processes for this complex cellular architecture depend on the position of stereocilia within a bundle and the location of a hair cell

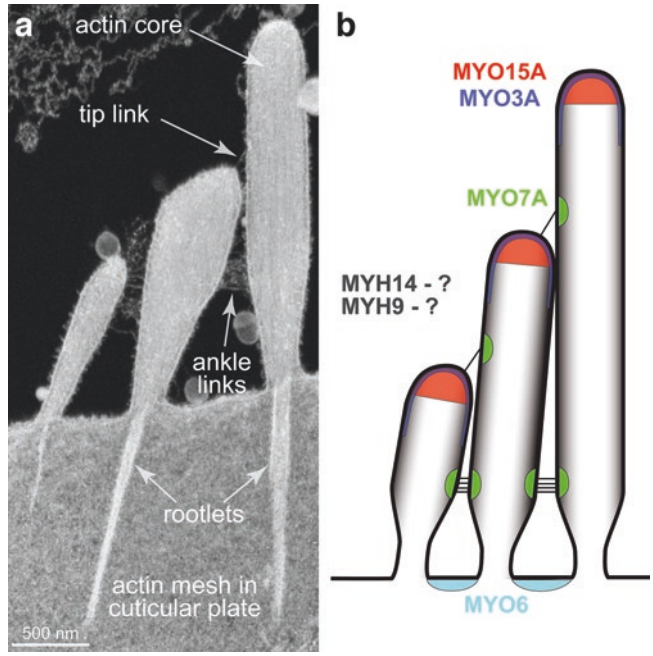

Fig. 13.1 Mammalian auditory hair cell stereocilia and reported localization of deafness-related myosins. (**a**) An inner hair cell from a postnatal day 6 mouse at the middle of the apical turn of the cochlea. Maximum intensity projection of a stack of backscattered scanning electron microscopy images obtained in 20 nm serial sectioning using a focused ion beam (FIB-SEM). The total thickness of the stack was 200 nm and, therefore, only one stereocilium from each row within a hair bundle is present. Relevant structures are indicated by arrows. (**b**) Schematic localization of the myosins of interest in the stereocilia bundle. (Note that MYO15A and MYO3A overlap at the tips of stereocilia. For simplicity, differences in localization of the different MYO15 and MYO7A isoforms are not shown.)

within a specific inner ear sensory organ (reviewed in (Velez-Ortega and Frolenkov 2019; Wagner and Shin 2019)). Many of the myosin superfamily members contribute to stereocilia development, maintenance or both (Fig. 13.1B. Yet, a multitude of studies point to the alternative isoforms of MYO15 in consort with its protein partners as the maestros of stereocilia elongation and maintenance.

13.3 MYO3A

To date, 22 recessive variants (mutations) have been reported for the human *MYO3A* gene that are associated with nonsyndromic progressive hearing loss. The initial report was of three different variants of *MYO3A* segregating with variable age-dependent hearing loss in a single large consanguineous Israeli family that defined the 13-cM *DFNB30* locus on chromosome 10p (Walsh et al. 2002). MYO3A has 33 exons and encodes a protein of 1660 residues (largest isoform), although there are smaller alternative splice isoforms of *MYO3A*. Additionally, two heterozygous missense variant in the motor domain of *MYO3A* were reported to be co-segregating as a dominant trait with post-lingual progressive deafness in three affecteds of a single family (Grati et al. 2016). The mechanism by which a missense mutation in the motor domain of MYO3A would cause a progressive hearing loss inherited as a dominant trait is not known, although the authors provide some interesting speculation about the function of MYO3A at the tips of stereocilia near the mechanotransduction channel in partnership with protocadherin-CD2 (Grati et al. 2016; Dantas et al. 2018). Moreover, Grati et al. (2016) identified an interaction of MYO3A with the cytosolic tail of protocadherin

15-CD2 (Ahmed et al. 2006; Pepermans et al. 2014), indicating a possible involvement of MYO3A in the positioning and/or maintenace of the mechanotransduction channel complex at stereocilia tips of mature hair cells. Additionally, in mouse, MYO3A and MYO3B play reducndant roles in hair bundle morphogenesis by limiting elongation of stereocilia (Lelli et al. 2016).

Previous to 2002, *MYO3A* was known to be expressed in the retina and pancreas (Dose and Burnside 2000). In vertebrate photoreceptors, MYO3A is involved in the development and conservation of calyceal processes (Lin-Jones et al. 2004) as well as in arrestin translocation into microvilli (Lee and Montell 2004). In the inner ear, *MYO3A* mRNA is expressed in inner and outer hair cells (Walsh et al. 2002). MYO3A protein was immunolocalized at the surface of stereocilia near the tips with some uncertainties as to whether it is present at the very tip of the tallest stereocilia row (Ebrahim et al. 2016; Schneider et al. 2006). MYO3A partners with the ankyrin repeat-containing alternative splice isoform 1 of espin, which is transported by MYO3A along F-actin to the tips of stereocilia where it is involved in stereocilia length regulation (Salles et al. 2009). Pathogenic variants of espin are also associated with recessively inherited deafness DFNB36 in human (Naz et al. 2004) and in the jerker mouse (Sekerkova et al. 2011). The authors reported that stereocilia of the jerker mouse are 30–60% thinner probably due to 50–85% fewer actin filaments. Stereocilia of the jerker mouse were also shorter indicating that espin is required for the differential elongation, crosslinking and subsequent maintenance of the F-actin core (Sekerkova et al. 2011).

13.4 MYO6

The orthologs of human and mouse *MYO6* genes have been identified in organisms as diverse as *Drosophila melanogaster* and *Caenorhabditis elegans* (Avraham et al. 1997). A null mutation of mouse *Myo6* was found to be the cause of congenital deafness of the Snell's waltzer ($Myo6^{SV}$) mouse. Western blot analysis of proteins in the homozygous $Myo6^{SV}$ deaf mouse showed no detectable myosin 6 protein, and in the inner ear rapid progressive loss of hair cells was reported (Avraham et al. 1995). In human, DFNB37 and DFNA22 hearing loss are associated with a total of 73 rare pathogenic variants of *MYO6* (as of 2019) segregating either as a recessive trait or a dominant trait, respectively (Ahmed et al. 2003b; Melchionda et al. 2001).

For many years it was assumed that all myosins moved toward the plus end of F-actin. However, MYO6 moves on F-actin in the opposite direction towards the 'minus' end of F-actin. The reversal of direction was attributed to 53 unique amino acid residues inserted into the converter domain of MYO6. When this unique sequence was or was not inserted into the MYO5 lever arm and attached to the MYO6 motor domain, this chimeric myosin became either a minus-end or plus-end directed motor, respectively (Park et al. 2007; Wells et al. 1999).

Immunofluorescence localization of MYO6 revealed signals predominantly in hair cells that were enriched at the apical cell surface near the taper of stereocilia (Avraham et al. 1995, 1997; Hasson 2003; Hasson and Mooseker 1994). In the absence of functional MYO6, adjacent stereocilia fuse with one another suggesting that MYO6 may anchor the plasma membrane to the actin-rich cytoskeleton structure at the base of the stereocilia bundle that is known as the cuticular plate (Fig. 13.1), thereby preventing closely apposed stereocilia membranes from coalescing. When mouse green fluorescent protein tagged (GFP)-MYO6 was gene-gun transfected into hair cells, GFP-MYO6 was localized to the cuticular plate and at the base of stereocilia, but was not detected in the stereocilia core even when overexpressed (Belyantseva et al. 2005).

13.5 MYO7A

MYO7A is a big gene on chromosome 11q13.5 that has 48 exons encoding a full-length protein of 2215 residues. There are a variety of alternatively spliced *MYO7A* transcripts encoding shorter isoforms. The Human Gene Mutation

Database (professional version; HGMD (http://www.hgmd.cf.ac.uk/ac/index.php) entry for the *MYO7A* gene lists 559 pathogenic mutations. A few rare variants cause either nonsyndromic deafness inherited as a dominant trait (DFNA11; OMIM 601317) characterized by a progressive loss of hearing or recessively inherited deafness that is often congenital and profound (DFNB2; OMIM 600060). The majority of mutations of *MYO7A* reported to date cause deafness, vestibular dysfunction and progressive loss of vision due to retinitis pigmentosa, which is referred to as Usher syndrome, *USH1B* (Liu et al. 1997a; Weil et al. 1995, 1997). There are presently seven additional genes for which pathogenic variants are associated with Usher syndrome, but the only member of the myosin superfamily involved with Usher syndrome is *MYO7A*.

Protein truncating variants and splice site mutations of *MYO7A* are often associated with Usher syndrome while some variants that retain residual MYO7A function, due to, for example, an amino acid substitutions or a leaky splice site mutation, are associated with normal vision but deafness (Ahmed et al. 2002, 2003a; Astuto et al. 2002; Bork et al. 2001). Experimental data supporting this idea that residual function of MYO7A is sufficient for retinal function are hard to acquire as there are no simple or quick functional assays for MYO7A. One measure of residual function was based on the *in vivo* localization of endogenous MYO7A to stereocilia, which is recapitulated by GFP-tagged MYO7A gene gunned into hair cells *in vitro*. A few missense variants of MYO7A located in the tail domain of a GFP-tagged MYO7A were compared to wild-type, which is a test of the ability of mutant MYO7A to move on actin filaments of hair cell stereocilia (Belyantseva et al. 2005; Riazuddin et al. 2008).

In the retina, wild-type MYO7A is reported to be localized in the connecting cilium of photoreceptor cells and is proposed to have a role in the transport of opsin (Liu et al. 1997a, b). In the mammalian inner ear, MYO7A was first localized along the length of stereocilia (Hasson et al. 1997). However, subsequent studies (Grati and Kachar 2011) used a different antibody, perhaps more specific or a lower affinity, or specific to an alternative splice isoform of MYO7A, and reported that MYO7A concentrates at the upper end of the tip links, the extracellular filaments that "pull" the mechanotransduction channels open during sound-induced deflections of the stereocilia bundle. Therefore, MYO7A may modulate mechano-electrical transduction (MET) in the hair cells. Indeed, there are several reports demonstrating that mutations and/or deletions in *MYO7A* and its molecular partners, for example, harmonin, affect the tension within the MET machinery (Corns et al. 2018; Grillet et al. 2009; Kros et al. 2002). In addition to the tip link region, MYO7A was reported to be localized near the base of stereocilia (Senften et al. 2006). At this location, MYO7A seems to be an essential component of the complex that forms ankle links (Michalski et al. 2007), the links between stereocilia at the base of the hair bundle. These links assemble early in postnatal development and disappear by the time of the onset of hearing in rodents (Goodyear et al. 2005). Yet, they play a crucial role in hair bundle structure through largely unknown mechanisms. One possibility is that the ankle links hold the hair bundle together while stereocilia rootlets are being formed during the first two postnatal weeks (Kitajiri et al. 2010). Finally, in wild-type auditory hair cells, MYO7A was proposed to be present at the tips of mature stereocilia of the shorter row, but absent from the tips of developing stereocilia of the shorter row (Prosser et al. 2008). At this location, MYO7A may interact with twinfillin-2 and limit the growth of stereocilia, thereby contributing to the characteristic staircase shape of hair cell bundles (Rzadzinska et al. 2009).

13.6 MYO15

The deaf shaker 2 mouse moves in tight circles indicative of a vestibular disorder (Snell and Law 1939) and was mapped to mouse chromosome 11qB2 suggesting that mutations in the same gene cause the shaker 2 phenotype and DFNB3 human deafness that was genetically mapped to chromosome 17p11.2 (Friedman et al. 1995;

Winata et al. 1995). Subsequently, the DFNB3 and shaker 2 genes were identified and found to encode a hitherto novel myosin, MYO15, the largest mammalian myosin heavy chain (Probst et al. 1998; Wakabayashi et al. 1998; Wang et al. 1998). A recessive variant of mouse *Myo15* causes deafness and vestibular dysfunction (the shaker 2 phenotype). This was directly demonstrated by showing that a bacterial artificial chromosome (BAC) containing the wild-type mouse *Myo15* gene results in wild-type hearing when introduced into a homozygous shaker 2 oocyte and the mouse was allowed to develop. All progeny of such females are expected to be deaf and circle, but a normal hearing mouse was produced as a result of the rescue by a wild-type *Myo15* gene encoded in the BAC (Probst et al. 1998).

Expression data indicate that *Myo15* mRNA and protein are present in a limited subset of neurosensory cells in the inner ear. Surprisingly, *MYO15A* is also expressed in several neuroendocrine cells and endocrine tumors of the gut and pancreas (Lloyd et al. 2001). This observation raised the possibility that deafness DFNB3 may not be nonsyndromic, but rather one feature of a syndrome. This question remains unanswered for lack of detailed clinical data from deaf individuals with biallelic recessive variants of *MYO15A*.

In the mouse inner ear, MYO15 protein is localized at the tips of stereocilia (Belyantseva et al. 2003). Many, but not all, of the deafness-causing mutations of mouse *Myo15* result in hair cells with abnormally short stereocilia bundles that lack the characteristic mature staircase architecture required for normal hearing and subsequently die (Anderson et al. 2000; Belyantseva et al. 2003; Probst et al. 1998). Some of the details of how MYO15 precisely regulates elongation of stereocilia have been reported and depend on an understanding of the alternative splice isoforms of the gene encoding MYO15 (Belyantseva et al. 2005).

The human *MYO15A* gene and the mouse *Myo15* gene are comprised of 67 exons and encode three major alternative splice isoforms (Rehman et al. 2016). The longest mouse *Myo15* isoform consists of a long N-terminal extension that precedes the motor domain and is predicted to be intrinsically unstructured (Uversky 2002). When the giant exon 2 encoding the N-terminal extension with proline-rich protein sequence is included, MYO15 has 3493 residues (395 kilodalton). *Myo15* isoform 2 does not include the giant exon 2 sequence and encodes 2306 residues (260 kilodaltons). A recently discovered additional exon of mouse *Myo15* located downstream of the giant exon 2 encodes 50 unique residues and is evolutionarily conserved, but has no predicted domains or motifs and is the first exon of a novel isoform 3 (Rehman et al. 2016). During development, MYO15 isoform 2 is necessary for programmed differential elongation of the stereocilia (Belyantseva et al. 2003), while isoform 1, which is predominantly expressed after birth, is necessary for maintenance of the shorter row mechanosensitive stereocilia (Fang et al. 2015). The function of isoform 3 of MYO15 is not yet known (Rehman et al. 2016). Transcripts of human and mouse *MYO15A*/*Myo15* genes have additional alternative exon splicing that generates further diversity, but their functional significance is also unknown. For example, alternatively spliced micro exon 8 encodes two amino acids that are inserted into the motor domain corresponding to loop 1 of non-muscle and smooth muscle myosin II. *In vitro,* these surface loops, when present, increase the actin-activated MgATPase activity and motility (Murphy and Spudich 1999; Spudich 1994).

There is an unprocessed, expressed pseudogene named MYO15B (formerly MYO15BP) with some sequence similarity to MYO15A. MYO15B is an evolutionary relic expressed in brain, colon, small intestine, mammary gland, stomach, kidney, spleen, lymph node, uterus, thymus and rectum (Boger et al. 2001). Variants of the *MYO15B* pseudogene should not be confused with deafness-causing variants of *MYO15A*. There are now hundreds of recessive pathogenic mutations of human *MYO15A* associated with profound, congenital deafness and some variants in exon 2 are associated with moderate to severe progressive deafness (Rehman et al. 2016), a phenotype recapitulated in a mutant *Myo15* mouse model devoid of isoform 1 but expressing isoform 2

(Fang et al. 2015). Pathogenic variants of human *MYO15* are distributed across the entire gene. Engineered mouse models are required to determine how these particular mutations, including the missense mutations of the tail domain, alter localization of MYO15 at stereocilia tips, perturb the process of stereocilia elongation or interfere with long-term maintenance of stereocilia (Fang et al. 2015).

Confocal microscopy images revealed that MYO15 is localized at stereocilia tips just under the plasma membrane (Belyantseva et al. 2003), overlapping with the barbed ends of the actin filaments, the sites of active actin polymerization (Belyantseva et al. 2003, 2005; Rzadzinska et al. 2004; Schneider et al. 2002; Tilney et al. 1981). MYO15 is not required for the emergence, initial elongation or increase in thickness of nascent stereocilia, but is required for the graded elongation of stereocilia to form the mature staircase architecture of the bundle (Belyantseva et al. 2005). Excessive amount of MYO15, when overexpressed as GFP- MYO15, does not cause overelongation of the wild-type mouse stereocilia bundles indicating that elongation and thickening of stereocilia during development is a tightly regulated process (Belyantseva et al. 2003). Although MYO15 is not endogenously expressed in COS-7 cells, GFP-MYO15 localizes to the filopodia tips in these cells (Belyantseva et al. 2003), but unlike MYO10 (Bohil et al. 2006), wild-type MYO15 has little or no ability to enhance the formation of filopodia. The concentration after photobleaching of MYO15 at the filopodia tips of COS7 cells and simultaneous movement of MYO15 and whirlin speckles along the filopodia in live COS7 cells suggest that MYO15 moves toward the plus end of F-actin and is able to transport protein partners to the tips of both filopodia and stereocilia (Belyantseva et al. 2003, 2005).

The kinetics of MYO15 make it especially suited to deliver proteins to the tips of actin-based cellular protrusions such as filopodia or hair-cell stereocilia and to be a barbed-end directed myosin (Bird et al. 2014), and as expected from other observations (Belyantseva et al. 2005) has high duty-ratio kinetics and thus spends most of its time bound to actin, although the affinity for actin is low by comparison to MYO5A and MYO6 (Bird et al. 2014). The weak affinity of MYO15 for actin was speculated to be an adaptation for motility with cargo only where the actin concentration is high, such as the core of hair cell stereocilia (Bird et al. 2014).

Downstream of the motor domain are two consensus IQ domains (IQXXXRGXXXR). Using an UNC-45 and HSP90AA1 chaperone-assisted purification protocol, soluble and functional mouse MYO15 motor domain protein was obtained. Unexpectedly, the first two IQ domains were found to bind regulatory (RLC, MYL12B) light chain and essential light chain (ELC) that are normally partners of class II myosins (Bird et al. 2014). MYO15 also has a third IQ domain that is highly divergent from the sequence of the canonical IQ. A light chain that binds the third IQ has not been identified, but it is known not to bind calmodulin, RLC or ELC (Bird et al. 2014).

The large tail domain of MYO15 has two pairs of MyTh4/FERM domains, a SH3 domain and a C-terminal PDZ-ligand (Hung and Sheng 2002; Liang et al. 1999). The PDZ domain-containing whirlin protein binds the PDZ-ligand of MYO15 (Belyantseva et al. 2005). The binding partners and functions of the SH3, FERM and MyTh4 domains in the tail of MYO15 are not known, but may regulate motor function (Bird et al. 2014).

MYO15 and whirlin, a scaffolding protein, are partners of a complex at stereocilia tips necessary for elongation of stereocilia and staircase formation (Belyantseva et al. 2005). Variants of human *WHRN*, encoding whirlin, are associated with Usher syndrome type 2 (Ebermann et al. 2007) or nonsyndromic deafness DFNB31 and deafness and circling in the whirler mouse. Deaf adult homozygous whirler mice also have abnormally short and thick stereocilia similar to the shaker 2 mouse (Mburu et al. 2003; Mogensen et al. 2007). The tips of short stereocilia of homozygous whirler mice have no whirlin, and the short stereocilia of the shaker 2 mice have no whirlin or MYO15 at stereocilia tips. However, MYO15 is present at the tips of the short stereocilia of whirler mice and thus whirlin is not necessary for MYO15 targeting to the tips of stereocilia, and MYO15 alone (without whirlin) is not sufficient

for stereocilia elongation (Belyantseva et al. 2005). Interestingly, Helios gene gun-transfected GFP-MYO15 (wild-type) into stunted shaker 2 cochlear and vestibular stereocilia recruits endogenous whirlin to stereocilia tips (Belyantseva et al. 2005), which re-initiates the developmentally programmed elongation of stereocilia and rescues the staircase architecture of the stereocilia bundles (Belyantseva et al. 2005).

These data support the conclusion that MYO15 transports whirlin to stereocilia tips (Belyantseva et al. 2003). The short stereocilia phenotype, vestibular dysfunction and deafness of homozygous whirler mice can be partially corrected with gene therapy using a variety of adeno-associated viral vectors encoding whirlin cDNA injected into the inner ear of neonatal pups (Chien et al. 2016; Isgrig et al. 2017, 2019) suggesting the possibility that one day gene therapy may restore some hearing in individuals with DFNB31 and DFNB3 deafness as well as other inherited forms of hearing loss.

At least in cochlear outer hair cells, MYO15 is not required for mechanotransduction or adaptation. Young postnatal shaker 2 outer hair cells have "wild-type" mechano-electrical transduction current in the absence of functional MYO15 (Stepanyan et al. 2006; Stepanyan and Frolenkov 2009). Thus, hair cell morphogenesis and the formation of the mechanotransduction complex at the tips of stereocilia occur independently of MYO15-directed stereocilia elongation. However, MET currents in cochlear inner hair cells of the same shaker 2 mice do not have adaptation (Stepanyan and Frolenkov 2009) and, therefore, we cannot rule out a possibility that different types of hair cells may have some differences in the molecular composition of their MET machineries. MYO15 may be involved in transporting these differentially expressed MET component to the tips of stereocilia.

13.7 MYH14 and MYH9

The phenotype of autosomal dominant nonsyndromic deafness (DFNA) is usually bilateral and progressive. Genetic linkage analyses identified the *DFNA4A* locus on chromosome 19q (Donaudy et al. 2004) and the *DFNA17* locus on chromosome 22q (Lalwani et al. 2000), which were mapped in a few large multigeneration families. The underlying genes in which dominant pathogenic variants were associated with DFNA4A and DFNA17 progressive hearing loss are *MYH14* (myosin heavy chain 14) and *MYH9*, respectively, and the variants were not identified in hundreds of healthy control individuals (Dantas et al. 2014; Hildebrand et al. 2006). In addition to nonsyndromic deafness DFNA17 associated with heterozygous variants of *MYH9*, numerous heterozygous variants of *MYH9* have been reported to be associated with Fechtner syndrome, May-Hegglin syndrome and Sebastian syndrome, three syndromes characterized by various degrees of sensorineural deafness, cataracts and nephritis (Balduini et al. 2011; Heath et al. 2001; Kunishima et al. 2001). In a genotype-phenotype study of numerous variants of *MYH9*, pathogenic variants in the motor domain were associated with severe thrombocytopenia, nephritis and deafness (Pecci et al. 2008). In mouse, a homozygous deletion of *Myh9* is embryonic lethal (Matsushita et al. 2004; Parker et al. 2006). Heterozygotes are viable and had a hearing loss in one study (Matsushita et al. 2004), but had normal hearing in another study (Parker et al. 2006).

A dominant variant of *MYH14* was also associated with progressive muscle atrophy of the lower limbs and progressive sensorineural hearing loss (Choi et al. 2011). Since variants of both *MYH14* and *MYH9* have been associated with syndromic forms of deafness, it seems plausible that subtle forms of these other clinical features may have been overlooked when families were ascertained and initially presumed to have dominantly-inherited nonsyndromic deafness DFNA4A and DFNA17. Alternatively, it seems more likely that there is a highly variable range of clinical features due to different dominant variants of *MYH9*. The functions of *MYH14* and *MYH9* in the auditory system remain to be elucidated, although this class of non-muscle heavy chains have been actively studied by biophysicists and known to power cell migration, cytokinesis and morphogenetic processes (Melli et al. 2018).

13.8 Summary

Variants *MYO3A*, *MYO6*, *MYO7A*, *MYO15A*, *MYH14* and *MYH9* are associated with human hearing loss. Mutant mouse and zebra fish models of some of these six different myosins recapitulate the human deafness phenotype, providing a window into inner ear pathogenesis but also their wild-type functions. In the future, rare variants of other myosin superfamily members may eventually be demonstrated to have critical roles in sound transduction. For example, MYO10 and MYO18 are both expressed in the inner ear according to RNAseq data available on the gEAR Portal (https://umgear.org/). However, variants of these two myosin genes have not been reported to be associated with hearing loss in human or animal models.

The cellular structures that hair cells depend upon for mechanotransduction of sound require several different myosins to build and then maintain them. For those motor domains of "deafness myosins" that have been purified, each has unique motor domain kinetics, and each one has a unique intracellular localization, data consistent with distinctly different functions for each myosin in the auditory system. If ototoxic agents, inner ear infections and damaging levels of sound can be avoided, a wild-type peripheral auditory epithelium has an extraordinary ability to endure for a person's lifetime, in part because of the diverse functions of several myosins.

Acknowledgements This research was supported (in part) by the Intramural Research Program of the NIH, National Institute on Deafness and Other Communication Disorders to T.B.F and by R01DC014658, R01DC012564, and S10OD025130 grants to G.I.F. We thank Dr. Mhamed Grati for his critique of this chapter.

References

Ahmed ZM, Goodyear R, Riazuddin S, Lagziel A, Legan PK, Behra M, Burgess SM, Lilley KS, Wilcox ER, Riazuddin S, Griffith AJ, Frolenkov GI, Belyantseva IA, Richardson GP, Friedman TB (2006) The tip-link antigen, a protein associated with the transduction complex of sensory hair cells, is protocadherin-15. J Neurosci 26:7022–7034

Ahmed ZM, Smith TN, Riazuddin S, Makishima T, Ghosh M, Bokhari S, Menon PS, Deshmukh D, Griffith AJ, Riazuddin S, Friedman TB, Wilcox ER (2002) Nonsyndromic recessive deafness DFNB18 and Usher syndrome type IC are allelic mutations of USHIC. Hum Genet 110(6):527–531. https://doi.org/10.1007/s00439-002-0732-4

Ahmed ZM, Morell RJ, Riazuddin S, Gropman A, Shaukat S, Ahmad MM, Mohiddin SA, Fananapazir L, Caruso RC, Husnain T, Khan SN, Riazuddin S, Griffith AJ, Friedman TB, Wilcox ER (2003a) Mutations of MYO6 are associated with recessive deafness, DFNB37. Am J Hum Genet 72(5):1315–1322. https://doi.org/10.1086/375122

Ahmed ZM, Riazuddin S, Riazuddin S, Wilcox ER (2003b) The molecular genetics of Usher syndrome. Clin Genet 63(6):431–444

Anderson DW, Probst FJ, Belyantseva IA, Fridell RA, Beyer L, Martin DM, Wu D, Kachar B, Friedman TB, Raphael Y, Camper SA (2000) The motor and tail regions of myosin XV are critical for normal structure and function of auditory and vestibular hair cells. Hum Mol Genet 9(12):1729–1738. https://doi.org/10.1093/hmg/9.12.1729

Astuto LM, Bork JM, Weston MD, Askew JW, Fields RR, Orten DJ, Ohliger SJ, Riazuddin S, Morell RJ, Khan S, Riazuddin S, Kremer H, van Hauwe P, Moller CG, Cremers CW, Ayuso C, Heckenlively JR, Rohrschneider K, Spandau U, Greenberg J, Ramesar R, Reardon W, Bitoun P, Millan J, Legge R, Friedman TB, Kimberling WJ (2002) CDH23 mutation and phenotype heterogeneity: a profile of 107 diverse families with Usher syndrome and nonsyndromic deafness. Am J Hum Genet 71(2):262–275. https://doi.org/10.1086/341558

Avraham KB, Hasson T, Steel KP, Kingsley DM, Russell LB, Mooseker MS, Copeland NG, Jenkins NA (1995) The mouse Snell's waltzer deafness gene encodes an unconventional myosin required for structural integrity of inner ear hair cells. Nat Genet 11(4):369–375. https://doi.org/10.1038/ng1295-369

Avraham KB, Hasson T, Sobe T, Balsara B, Testa JR, Skvorak AB, Morton CC, Copeland NG, Jenkins NA (1997) Characterization of unconventional MYO6, the human homologue of the gene responsible for deafness in Snell's waltzer mice. Hum Mol Genet 6(8):1225–1231. https://doi.org/10.1093/hmg/6.8.1225

Balduini CL, Pecci A, Savoia A (2011) Recent advances in the understanding and management of MYH9-related inherited thrombocytopenias. Br J Haematol 154(2):161–174. https://doi.org/10.1111/j.1365-2141.2011.08716.x

Belyantseva IA, Boger ET, Friedman TB (2003) Myosin XVa localizes to the tips of inner ear sensory cell stereocilia and is essential for staircase formation of the hair bundle. Proc Natl Acad Sci U S A 100(24):13958–13963. https://doi.org/10.1073/pnas.2334417100

Belyantseva IA, Boger ET, Naz S, Frolenkov GI, Sellers JR, Ahmed ZM, Griffith AJ, Friedman TB (2005) Myosin-XVa is required for tip localization of whir-

lin and differential elongation of hair-cell stereocilia. Nat Cell Biol 7(2):148–156. https://doi.org/10.1038/ncb1219

Bird JE, Takagi Y, Billington N, Strub MP, Sellers JR, Friedman TB (2014) Chaperone-enhanced purification of unconventional myosin 15, a molecular motor specialized for stereocilia protein trafficking. Proc Natl Acad Sci U S A 111(34):12390–12395. https://doi.org/10.1073/pnas.1409459111

Boger ET, Sellers JR, Friedman TB (2001) Human myosin XVBP is a transcribed pseudogene. J Muscle Res Cell Motil 22(5):477–483

Bohil AB, Robertson BW, Cheney RE (2006) Myosin-X is a molecular motor that functions in filopodia formation. Proc Natl Acad Sci U S A 103(33):12411–12416. https://doi.org/10.1073/pnas.0602443103

Bork JM, Peters LM, Riazuddin S, Bernstein SL, Ahmed ZM, Ness SL, Polomeno R, Ramesh A, Schloss M, Srisailpathy CR, Wayne S, Bellman S, Desmukh D, Ahmed Z, Khan SN, Kaloustian VM, Li XC, Lalwani A, Riazuddin S, Bitner-Glindzicz M, Nance WE, Liu XZ, Wistow G, Smith RJ, Griffith AJ, Wilcox ER, Friedman TB, Morell RJ (2001) Usher syndrome 1D and nonsyndromic autosomal recessive deafness DFNB12 are caused by allelic mutations of the novel cadherin-like gene CDH23. Am J Hum Genet 68(1):26–37. https://doi.org/10.1086/316954

Chien WW, Isgrig K, Roy S, Belyantseva IA, Drummond MC, May LA, Fitzgerald TS, Friedman TB, Cunningham LL (2016) Gene therapy restores hair cell stereocilia morphology in inner ears of deaf whirler mice. Mol Ther 24(1):17–25. https://doi.org/10.1038/mt.2015.150

Choi BO, Kang SH, Hyun YS, Kanwal S, Park SW, Koo H, Kim SB, Choi YC, Yoo JH, Kim JW, Park KD, Choi KG, Kim SJ, Zuchner S, Chung KW (2011) A complex phenotype of peripheral neuropathy, myopathy, hoarseness, and hearing loss is linked to an autosomal dominant mutation in MYH14. Hum Mutat 32(6):669–677. https://doi.org/10.1002/humu.21488

Corns LF, Johnson SL, Roberts T, Ranatunga KM, Hendry A, Ceriani F, Safieddine S, Steel KP, Forge A, Petit C, Furness DN, Kros CJ, Marcotti W (2018) Mechanotransduction is required for establishing and maintaining mature inner hair cells and regulating efferent innervation. Nat Commun 9(1):4015. https://doi.org/10.1038/s41467-018-06307-w

Dantas VG, Lezirovitz K, Yamamoto GL, Moura de Souza CF, Ferreira SG, Mingroni-Netto RC (2014) c.G2114A MYH9 mutation (DFNA17) causes nonsyndromic autosomal dominant hearing loss in a Brazilian family. Genet Mol Biol 37(4):616–621. https://doi.org/10.1590/S1415-47572014005000025

Dantas VGL, Raval MH, Ballesteros A, Cui R, Gunther LK, Yamamoto GL, Alves LU, Bueno AS, Lezirovitz K, Pirana S, Mendes BCA, Yengo CM, Kachar B, Mingroni-Netto RC (2018) Characterization of a novel MYO3A missense mutation associated with a dominant form of late onset hearing loss. Sci Rep 8:8706

DiStefano MT, Hemphill SE, Oza AM, Siegert RK, Grant AR, Hughes MY, Cushman BJ, Azaiez H, Booth KT, Chapin A, Duzkale H, Matsunaga T, Shen J, Zhang W, Kenna M, Schimmenti LA, Tekin M, Rehm HL, Tayoun ANA, Amr SS, ClinGen Hearing Loss Clinical Domain Working G (2019) ClinGen expert clinical validity curation of 164 hearing loss gene-disease pairs. Genet Med. https://doi.org/10.1038/s41436-019-0487-0

Donaudy F, Snoeckx R, Pfister M, Zenner HP, Blin N, Di Stazio M, Ferrara A, Lanzara C, Ficarella R, Declau F, Pusch CM, Nurnberg P, Melchionda S, Zelante L, Ballana E, Estivill X, Van Camp G, Gasparini P, Savoia A (2004) Nonmuscle myosin heavy-chain gene MYH14 is expressed in cochlea and mutated in patients affected by autosomal dominant hearing impairment (DFNA4). Am J Hum Genet 74(4):770–776. https://doi.org/10.1086/383285

Dose AC, Burnside B (2000) Cloning and chromosomal localization of a human class III myosin. Genomics 67(3):333–342. https://doi.org/10.1006/geno.2000.6256

Drummond MC, Barzik M, Bird JE, Zhang DS, Lechene CP, Corey DP, Cunningham LL, Friedman TB (2015) Live-cell imaging of actin dynamics reveals mechanisms of stereocilia length regulation in the inner ear. Nat Commun 6:6873. https://doi.org/10.1038/ncomms7873

Ebermann I, Scholl HP, Charbel Issa P, Becirovic E, Lamprecht J, Jurklies B, Millan JM, Aller E, Mitter D, Bolz H (2007) A novel gene for Usher syndrome type 2: mutations in the long isoform of whirlin are associated with retinitis pigmentosa and sensorineural hearing loss. Hum Genet 121(2):203–211. https://doi.org/10.1007/s00439-006-0304-0

Ebrahim S, Avenarius MR, Grati M, Krey JF, Windsor AM, Sousa AD, Ballesteros A, Cui R, Millis BA, Salles FT, Baird MA, Davidson MW, Jones SM, Choi D, Dong L, Raval MH, Yengo CM, Barr-Gillespie PG, Kachar B (2016) Stereocilia-staircase spacing is influenced by myosin III motors and their cargos espin-1 and espin-like. Nat Commun 7:10833. https://doi.org/10.1038/ncomms10833

Eisenberger T, Di Donato N, Baig SM, Neuhaus C, Beyer A, Decker E, Murbe D, Decker C, Bergmann C, Bolz HJ (2014) Targeted and genomewide NGS data disqualify mutations in MYO1A, the "DFNA48 gene", as a cause of deafness. Hum Mutat 35(5):565–570. https://doi.org/10.1002/humu.22532

Fang Q, Indzhykulian AA, Mustapha M, Riordan GP, Dolan DF, Friedman TB, Belyantseva IA, Frolenkov GI, Camper SA, Bird JE (2015) The 133-kDa N-terminal domain enables myosin 15 to maintain mechanotransducing stereocilia and is essential for hearing. elife 4. https://doi.org/10.7554/eLife.08627

Friedman TB, Liang Y, Weber JL, Hinnant JT, Barber TD, Winata S, Arhya IN, Asher JH Jr (1995) A gene for congenital, recessive deafness DFNB3 maps to the pericentromeric region of chromosome 17. Nat Genet 9(1):86–91. https://doi.org/10.1038/ng0195-86

Frolenkov GI, Belyantseva IA, Friedman TB, Griffith AJ (2004) Genetic insights into the morphogenesis of inner ear hair cells. Nat Rev Genet 5(7):489–498. https://doi.org/10.1038/nrg1377

Goodyear RJ, Marcotti W, Kros CJ, Richardson GP (2005) Development and properties of stereociliary link types in hair cells of the mouse cochlea. J Comp Neurol 485(1):75–85. https://doi.org/10.1002/cne.20513

Grati M, Kachar B (2011) Myosin VIIa and sans localization at stereocilia upper tip-link density implicates these Usher syndrome proteins in mechanotransduction. Proc Natl Acad Sci U S A 108(28):11476–11481. https://doi.org/10.1073/pnas.1104161108

Grati M, Yan D, Raval MH, Walsh T, Ma Q, Chakchouk I, Kannan-Sundhari A, Mittal R, Masmoudi S, Blanton SH, Tekin M, King MC, Yengo CM, Liu XZ (2016) MYO3A causes human dominant deafness and interacts with protocadherin 15-CD2 isoform. Hum Mutat 37(5):481–487. https://doi.org/10.1002/humu.22961

Griffith AJ, Friedman TB (2016) Hereditary hearing loss. In: Wackym PA, James B, Snow J (eds) Ballenger's otorhinolaryngology head and neck surgery, 18th edn. People's Medical Publishing House-USA, Shelton

Grillet N, Xiong W, Reynolds A, Kazmierczak P, Sato T, Lillo C, Dumont RA, Hintermann E, Sczaniecka A, Schwander M, Williams D, Kachar B, Gillespie PG, Muller U (2009) Harmonin mutations cause mechanotransduction defects in cochlear hair cells. Neuron 62(3):375–387. https://doi.org/10.1016/j.neuron.2009.04.006

Hasson T (2003) Myosin VI: two distinct roles in endocytosis. J Cell Sci 116(Pt 17):3453–3461. https://doi.org/10.1242/jcs.00669

Hasson T, Mooseker MS (1994) Porcine myosin-VI: characterization of a new mammalian unconventional myosin. J Cell Biol 127(2):425–440. https://doi.org/10.1083/jcb.127.2.425

Hasson T, Gillespie PG, Garcia JA, MacDonald RB, Zhao Y, Yee AG, Mooseker MS, Corey DP (1997) Unconventional myosins in inner-ear sensory epithelia. J Cell Biol 137(6):1287–1307. https://doi.org/10.1083/jcb.137.6.1287

Heath KE, Campos-Barros A, Toren A, Rozenfeld-Granot G, Carlsson LE, Savige J, Denison JC, Gregory MC, White JG, Barker DF, Greinacher A, Epstein CJ, Glucksman MJ, Martignetti JA (2001) Nonmuscle myosin heavy chain IIA mutations define a spectrum of autosomal dominant macrothrombocytopenias: May-Hegglin anomaly and Fechtner, Sebastian, Epstein, and Alport-like syndromes. Am J Hum Genet 69(5):1033–1045. https://doi.org/10.1086/324267

Hildebrand MS, de Silva MG, Gardner RJ, Rose E, de Graaf CA, Bahlo M, Dahl HH (2006) Cochlear implants for DFNA17 deafness. Laryngoscope 116(12):2211–2215. https://doi.org/10.1097/01.mlg.0000242089.72880.f8

Hung AY, Sheng M (2002) PDZ domains: structural modules for protein complex assembly. J Biol Chem 277(8):5699–5702. https://doi.org/10.1074/jbc.R100065200

Isgrig K, Shteamer JW, Belyantseva IA, Drummond MC, Fitzgerald TS, Vijayakumar S, Jones SM, Griffith AJ, Friedman TB, Cunningham LL, Chien WW (2017) Gene therapy restores balance and auditory functions in a mouse model of Usher syndrome. Mol Ther 25(3):780–791. https://doi.org/10.1016/j.ymthe.2017.01.007

Isgrig K, McDougald DS, Zhu J, Wang HJ, Bennett J, Chien WW (2019) AAV2.7m8 is a powerful viral vector for inner ear gene therapy. Nat Commun 10(1):427. https://doi.org/10.1038/s41467-018-08243-1

Katsuno T, Belyantseva IA, Cartegena-Rivera AX, Ohta K, Crump SM, Petralia RS, Ono K, Tona R, Imtiaz A, Rehman A, Kiyonari H, Kaneko M, Wang Y-X, Abe T, Ikeya M, Fenollar-Ferrer C, Riordan GP, Wilson E, Fitzgerald TS, Segawa K, Omori K, Ito J, Frolenkov GI, Friedman TB, Kitajiri S-i (2019) TRIOBP-5 sculpts stereocilia rootlets and stiffens supporting cells enabling hearing. JCI Insight 4. https://doi.org/10.1172/jci.insight.128561

Kitajiri S, Sakamoto T, Belyantseva IA, Goodyear RJ, Stepanyan R, Fujiwara I, Bird JE, Riazuddin S, Riazuddin S, Ahmed ZM, Hinshaw JE, Sellers J, Bartles JR, Hammer JA 3rd, Richardson GP, Griffith AJ, Frolenkov GI, Friedman TB (2010) Actin-bundling protein TRIOBP forms resilient rootlets of hair cell stereocilia essential for hearing. Cell 141(5):786–798. https://doi.org/10.1016/j.cell.2010.03.049

Kros CJ, Marcotti W, van Netten SM, Self TJ, Libby RT, Brown SD, Richardson GP, Steel KP (2002) Reduced climbing and increased slipping adaptation in cochlear hair cells of mice with Myo7a mutations. Nat Neurosci 5(1):41–47. https://doi.org/10.1038/nn784

Kunishima S, Matsushita T, Kojima T, Amemiya N, Choi YM, Hosaka N, Inoue M, Jung Y, Mamiya S, Matsumoto K, Miyajima Y, Zhang G, Ruan C, Saito K, Song KS, Yoon HJ, Kamiya T, Saito H (2001) Identification of six novel MYH9 mutations and genotype-phenotype relationships in autosomal dominant macrothrombocytopenia with leukocyte inclusions. J Hum Genet 46(12):722–729. https://doi.org/10.1007/s100380170007

Lalwani AK, Goldstein JA, Kelley MJ, Luxford W, Castelein CM, Mhatre AN (2000) Human nonsyndromic hereditary deafness DFNA17 is due to a mutation in nonmuscle myosin MYH9. Am J Hum Genet 67(5):1121–1128. https://doi.org/10.1016/S0002-9297(07)62942-5

Lee SJ, Montell C (2004) Light-dependent translocation of visual arrestin regulated by the NINAC myosin III. Neuron 43(1):95–103. https://doi.org/10.1016/j.neuron.2004.06.014

Lelli A, Michel V, Boutet de Monvel J, Cortese M, Bosch-Grau M, Aghaie A, Perfettini I, Dupont T, Avan P, El-Amraoui A, Petit C (2016) Class III myosins shape the auditory hair bundles by limiting microvilli and stereocilia growth. J Cell Biol 212:231–244

Liang Y, Wang A, Belyantseva IA, Anderson DW, Probst FJ, Barber TD, Miller W, Touchman JW, Jin L, Sullivan SL, Sellers JR, Camper SA, Lloyd RV, Kachar B,

Friedman TB, Fridell RA (1999) Characterization of the human and mouse unconventional myosin XV genes responsible for hereditary deafness DFNB3 and shaker 2. Genomics 61(3):243–258. https://doi.org/10.1006/geno.1999.5976

Lin-Jones J, Parker E, Wu M, Dose A, Burnside B (2004) Myosin 3A transgene expression produces abnormal actin filament bundles in transgenic Xenopus laevis rod photoreceptors. J Cell Sci 117(Pt 24):5825–5834. https://doi.org/10.1242/jcs.01512

Liu X, Vansant G, Udovichenko IP, Wolfrum U, Williams DS (1997a) Myosin VIIa, the product of the Usher 1B syndrome gene, is concentrated in the connecting cilia of photoreceptor cells. Cell Motil Cytoskeleton 37(3):240–252. https://doi.org/10.1002/(SICI)1097-0169(1997)37:3<240::AID-CM6>3.0.CO;2-A

Liu XZ, Walsh J, Mburu P, Kendrick-Jones J, Cope MJ, Steel KP, Brown SD (1997b) Mutations in the myosin VIIA gene cause non-syndromic recessive deafness. Nat Genet 16(2):188–190. https://doi.org/10.1038/ng0697-188

Lloyd RV, Vidal S, Jin L, Zhang S, Kovacs K, Horvath E, Scheithauer BW, Boger ET, Fridell RA, Friedman TB (2001) Myosin XVA expression in the pituitary and in other neuroendocrine tissues and tumors. Am J Pathol 159(4):1375–1382. https://doi.org/10.1016/S0002-9440(10)62524-2

Matsushita T, Hayashi H, Kunishima S, Hayashi M, Ikejiri M, Takeshita K, Yuzawa Y, Adachi T, Hirashima K, Sone M, Yamamoto K, Takagi A, Katsumi A, Kawai K, Nezu T, Takahashi M, Nakashima T, Naoe T, Kojima T, Saito H (2004) Targeted disruption of mouse ortholog of the human MYH9 responsible for macrothrombocytopenia with different organ involvement: hematological, nephrological, and otological studies of heterozygous KO mice. Biochem Biophys Res Commun 325(4):1163–1171. https://doi.org/10.1016/j.bbrc.2004.10.147

Mauriac SA, Hien YE, Bird JE, Carvalho SD, Peyroutou R, Lee SC, Moreau MM, Blanc JM, Geyser A, Medina C, Thoumine O, Beer-Hammer S, Friedman TB, Ruttiger L, Forge A, Nurnberg B, Sans N, Montcouquiol M (2017) Defective Gpsm2/Galphai3 signalling disrupts stereocilia development and growth cone actin dynamics in Chudley-McCullough syndrome. Nat Commun 8:14907. https://doi.org/10.1038/ncomms14907

Mburu P, Mustapha M, Varela A, Weil D, El-Amraoui A, Holme RH, Rump A, Hardisty RE, Blanchard S, Coimbra RS, Perfettini I, Parkinson N, Mallon AM, Glenister P, Rogers MJ, Paige AJ, Moir L, Clay J, Rosenthal A, Liu XZ, Blanco G, Steel KP, Petit C, Brown SD (2003) Defects in whirlin, a PDZ domain molecule involved in stereocilia elongation, cause deafness in the whirler mouse and families with DFNB31. Nat Genet 34(4):421–428. https://doi.org/10.1038/ng1208

Melchionda S, Ahituv N, Bisceglia L, Sobe T, Glaser F, Rabionet R, Arbones ML, Notarangelo A, Di Iorio E, Carella M, Zelante L, Estivill X, Avraham KB, Gasparini P (2001) MYO6, the human homologue of the gene responsible for deafness in Snell's waltzer mice, is mutated in autosomal dominant nonsyndromic hearing loss. Am J Hum Genet 69(3):635–640. https://doi.org/10.1086/323156

Melli L, Billington N, Sun SA, Bird JE, Nagy A, Friedman TB, Takagi Y, Sellers JR (2018) Bipolar filaments of human nonmuscle myosin 2-A and 2-B have distinct motile and mechanical properties. elife 7. https://doi.org/10.7554/eLife.32871

Michalski N, Michel V, Bahloul A, Lefevre G, Barral J, Yagi H, Chardenoux S, Weil D, Martin P, Hardelin JP, Sato M, Petit C (2007) Molecular characterization of the ankle-link complex in cochlear hair cells and its role in the hair bundle functioning. J Neurosci 27(24):6478–6488. https://doi.org/10.1523/JNEUROSCI.0342-07.2007

Mogensen MM, Rzadzinska A, Steel KP (2007) The deaf mouse mutant whirler suggests a role for whirlin in actin filament dynamics and stereocilia development. Cell Motil Cytoskeleton 64(7):496–508. https://doi.org/10.1002/cm.20199

Murphy CT, Spudich JA (1999) The sequence of the myosin 50-20K loop affects Myosin's affinity for actin throughout the actin-myosin ATPase cycle and its maximum ATPase activity. Biochemistry 38(12):3785–3792. https://doi.org/10.1021/bi9826815

Narayanan P, Chatterton P, Ikeda A, Ikeda S, Corey DP, Ervasti JM, Perrin BJ (2015) Length regulation of mechanosensitive stereocilia depends on very slow actin dynamics and filament-severing proteins. Nat Commun 6:6855. https://doi.org/10.1038/ncomms7855

Naz S, Griffith AJ, Riazuddin S, Hampton LL, Battey JF Jr, Khan SN, Riazuddin S, Wilcox ER, Friedman TB (2004) Mutations of ESPN cause autosomal recessive deafness and vestibular dysfunction. J Med Genet 41(8):591–595. https://doi.org/10.1136/jmg.2004.018523

Park H, Li A, Chen LQ, Houdusse A, Selvin PR, Sweeney HL (2007) The unique insert at the end of the myosin VI motor is the sole determinant of directionality. Proc Natl Acad Sci U S A 104(3):778–783. https://doi.org/10.1073/pnas.0610066104

Parker LL, Gao J, Zuo J (2006) Absence of hearing loss in a mouse model for DFNA17 and MYH9-related disease: the use of public gene-targeted ES cell resources. Brain Res 1091(1):235–242. https://doi.org/10.1016/j.brainres.2006.03.032

Patton J, Brewer C, Chien WW, Johnston JJ, Griffith AJ, Biesecker LG (2017) A genotypic ascertainment approach to refute the association of *MYO1A* variants with non-syndromic deafness. Eur J Hum Genet 25:147–149

Pecci A, Panza E, Pujol-Moix N, Klersy C, Di Bari F, Bozzi V, Gresele P, Lethagen S, Fabris F, Dufour C, Granata A, Doubek M, Pecoraro C, Koivisto PA, Heller PG, Iolascon A, Alvisi P, Schwabe D, De Candia

E, Rocca B, Russo U, Ramenghi U, Noris P, Seri M, Balduini CL, Savoia A (2008) Position of nonmuscle myosin heavy chain IIA (NMMHC-IIA) mutations predicts the natural history of MYH9-related disease. Hum Mutat 29(3):409–417. https://doi.org/10.1002/humu.20661

Pepermans E, Michel V, Goodyear R, Bonnet C, Abdi S, Dupont T, Gherbi S, Holder M, Makrelouf M, Hardelin JP, Marlin S, Zenati A, Richardson G, Avan P, Bahloul A, Petit C (2014) The CD2 isoform of protocadherin-15 is an essential component of the tip-link complex in mature auditory hair cells. EMBO Mol Med 6:984–992

Probst FJ, Fridell RA, Raphael Y, Saunders TL, Wang A, Liang Y, Morell RJ, Touchman JW, Lyons RH, Noben-Trauth K, Friedman TB, Camper SA (1998) Correction of deafness in shaker-2 mice by an unconventional myosin in a BAC transgene. Science 280(5368):1444–1447

Prosser HM, Rzadzinska AK, Steel KP, Bradley A (2008) Mosaic complementation demonstrates a regulatory role for myosin VIIa in actin dynamics of stereocilia. Mol Cell Biol 28:1702–1712

Rehman AU, Bird JE, Faridi R, Shahzad M, Shah S, Lee K, Khan SN, Imtiaz A, Ahmed ZM, Riazuddin S, Santos-Cortez RL, Ahmad W, Leal SM, Riazuddin S, Friedman TB (2016) Mutational spectrum of MYO15A and the molecular mechanisms of DFNB3 human deafness. Hum Mutat 37(10):991–1003. https://doi.org/10.1002/humu.23042

Riazuddin S, Nazli S, Ahmed ZM, Yang Y, Zulfiqar F, Shaikh RS, Zafar AU, Khan SN, Sabar F, Javid FT, Wilcox ER, Tsilou E, Boger ET, Sellers JR, Belyantseva IA, Riazuddin S, Friedman TB (2008) Mutation spectrum of MYO7A and evaluation of a novel nonsyndromic deafness DFNB2 allele with residual function. Hum Mutat 29(4):502–511. https://doi.org/10.1002/humu.20677

Rzadzinska AK, Nevalainen EM, Prosser HM, Lappalainen P, Steel KP (2009) MyosinVIIa interacts with Twinfilin-2 at the tips of mechanosensory stereocilia in the inner ear. PLoS One 4:e7097

Rzadzinska AK, Schneider ME, Davies C, Riordan GP, Kachar B (2004) An actin molecular treadmill and myosins maintain stereocilia functional architecture and self-renewal. J Cell Biol 164(6):887–897. https://doi.org/10.1083/jcb.200310055

Salles FT, Merritt RC Jr, Manor U, Dougherty GW, Sousa AD, Moore JE, Yengo CM, Dose AC, Kachar B (2009) Myosin IIIa boosts elongation of stereocilia by transporting espin 1 to the plus ends of actin filaments. Nat Cell Biol 11(4):443–450. https://doi.org/10.1038/ncb1851

Schneider ME, Belyantseva IA, Azevedo RB, Kachar B (2002) Rapid renewal of auditory hair bundles. Nature 418(6900):837–838. https://doi.org/10.1038/418837a

Schneider ME, Dose AC, Salles FT, Chang W, Erickson FL, Burnside B, Kachar B (2006) A new compartment at stereocilia tips defined by spatial and temporal patterns of myosin IIIa expression. J Neurosci 26(40):10243–10252. https://doi.org/10.1523/JNEUROSCI.2812-06.2006

Sekerkova G, Richter CP, Bartles JR (2011) Roles of the espin actin-bundling proteins in the morphogenesis and stabilization of hair cell stereocilia revealed in CBA/CaJ congenic jerker mice. PLoS Genet 7(3):e1002032. https://doi.org/10.1371/journal.pgen.1002032

Senften M, Schwander M, Kazmierczak P, Lillo C, Shin JB, Hasson T, Geleoc GS, Gillespie PG, Williams D, Holt JR, Muller U (2006) Physical and functional interaction between protocadherin 15 and myosin VIIa in mechanosensory hair cells. J Neurosci 26(7):2060–2071. https://doi.org/10.1523/JNEUROSCI.4251-05.2006

Snell GD, Law LW (1939) A linkage between the shaker-2 and wavy-2 in the house mouse. J Hered 30:447

Spudich JA (1994) How molecular motors work. Nature 372(6506):515–518. https://doi.org/10.1038/372515a0

Stepanyan R, Frolenkov GI (2009) Fast adaptation and Ca2+ sensitivity of the mechanotransducer require myosin-XVa in inner but not outer cochlear hair cells. J Neurosci 29(13):4023–4034. https://doi.org/10.1523/JNEUROSCI.4566-08.2009

Stepanyan R, Belyantseva IA, Griffith AJ, Friedman TB, Frolenkov GI (2006) Auditory mechanotransduction in the absence of functional myosin-XVa. J Physiol 576(Pt 3):801–808. https://doi.org/10.1113/jphysiol.2006.118547

Tilney LG, Bonder EM, DeRosier DJ (1981) Actin filaments elongate from their membrane-associated ends. J Cell Biol 90(2):485–494. https://doi.org/10.1083/jcb.90.2.485

Tilney LG, Tilney MS, DeRosier DJ (1992) Actin filaments, stereocilia, and hair cells: how cells count and measure. Annu Rev Cell Biol 8:257–274. https://doi.org/10.1146/annurev.cb.08.110192.001353

Uversky VN (2002) What does it mean to be natively unfolded? Eur J Biochem 269(1):2–12

Velez-Ortega AC, Frolenkov GI (2019) Building and repairing the stereocilia cytoskeleton in mammalian auditory hair cells. Hear Res 376:47–57. https://doi.org/10.1016/j.heares.2018.12.012

Wagner EL, Shin JB (2019) Mechanisms of hair cell damage and repair. Trends Neurosci. https://doi.org/10.1016/j.tins.2019.03.006

Wakabayashi Y, Takahashi Y, Kikkawa Y, Okano H, Mishima Y, Ushiki T, Yonekawa H, Kominami R (1998) A novel type of myosin encoded by the mouse deafness gene shaker-2. Biochem Biophys Res Commun 248(3):655–659. https://doi.org/10.1006/bbrc.1998.8976

Walsh T, Walsh V, Vreugde S, Hertzano R, Shahin H, Haika S, Lee MK, Kanaan M, King MC, Avraham KB (2002) From flies' eyes to our ears: mutations in a human class III myosin cause progressive nonsyndromic hearing loss DFNB30. Proc Natl Acad Sci U S A 99(11):7518–7523. https://doi.org/10.1073/pnas.102091699

Wang A, Liang Y, Fridell RA, Probst FJ, Wilcox ER, Touchman JW, Morton CC, Morell RJ, Noben-Trauth K, Camper SA, Friedman TB (1998) Association of unconventional myosin MYO15 mutations with human nonsyndromic deafness DFNB3. Science 280(5368):1447–1451

Weil D, Blanchard S, Kaplan J, Guilford P, Gibson F, Walsh J, Mburu P, Varela A, Levilliers J, Weston MD et al (1995) Defective myosin VIIA gene responsible for Usher syndrome type 1B. Nature 374(6517):60–61. https://doi.org/10.1038/374060a0

Weil D, Kussel P, Blanchard S, Levy G, Levi-Acobas F, Drira M, Ayadi H, Petit C (1997) The autosomal recessive isolated deafness, DFNB2, and the Usher 1B syndrome are allelic defects of the myosin-VIIA gene. Nat Genet 16(2):191–193. https://doi.org/10.1038/ng0697-191

Wells AL, Lin AW, Chen LQ, Safer D, Cain SM, Hasson T, Carragher BO, Milligan RA, Sweeney HL (1999) Myosin VI is an actin-based motor that moves backwards. Nature 401(6752):505–508. https://doi.org/10.1038/46835

Winata S, Arhya IN, Moeljopawiro S, Hinnant JT, Liang Y, Friedman TB, Asher JH Jr (1995) Congenital nonsyndromal autosomal recessive deafness in Bengkala, an isolated Balinese village. J Med Genet 32(5):336–343. https://doi.org/10.1136/jmg.32.5.336

Zhang DS, Piazza V, Perrin BJ, Rzadzinska AK, Poczatek JC, Wang M, Prosser HM, Ervasti JM, Corey DP, Lechene CP (2012) Multi-isotope imaging mass spectrometry reveals slow protein turnover in hair-cell stereocilia. Nature 481(7382):520–524. https://doi.org/10.1038/nature10745

The Actomyosin Systems in Apicomplexa

14

Karine Frénal, Aarti Krishnan, and Dominique Soldati-Favre

Abstract

The phylum of Apicomplexa groups obligate intracellular parasites that exhibit unique classes of unconventional myosin motors. These parasites also encode a limited repertoire of actins, actin-like proteins, actin-binding proteins and nucleators of filamentous actin (F-actin) that display atypical properties. In the last decade, significant progress has been made to visualize F-actin and to unravel the functional contribution of actomyosin systems in the biology of *Toxoplasma* and *Plasmodium*, the most genetically-tractable members of the phylum. In addition to assigning specific roles to each myosin, recent biochemical and structural studies have begun to uncover mechanistic insights into myosin function at the atomic level. In several instances, the myosin light chains associated with the myosin heavy chains have been identified, helping to understand the composition of the motor complexes and their mode of regulation. Moreover, the considerable advance in proteomic methodologies and especially in assignment of posttranslational modifications is offering a new dimension to our understanding of the regulation of actin dynamics and myosin function. Remarkably, the actomyosin system contributes to three major processes in *Toxoplasma gondii*: (i) organelle trafficking, positioning and inheritance, (ii) basal pole constriction and intravacuolar cell-cell communication and (iii) motility, invasion, and egress from infected cells. In this chapter, we summarize how the actomyosin system harnesses these key events to ensure successful completion of the parasite life cycle.

Keywords

Toxoplasma · Plasmodium · Actomyosin system · Motility · Invasion · Organelle inheritance · Basal pole constriction · Cell-cell communication

K. Frénal (✉)
Microbiologie Fondamentale et Pathogénicité, UMR 5234, University of Bordeaux and CNRS, Bordeaux Cedex, France

Department of Microbiology and Molecular Medicine, Faculty of Medicine, University of Geneva, Geneva, Switzerland
e-mail: karine.frenal@u-bordeaux.fr

A. Krishnan · D. Soldati-Favre
Department of Microbiology and Molecular Medicine, Faculty of Medicine, University of Geneva, Geneva, Switzerland
e-mail: aarti.krishnan@unige.ch; dominique.soldati-favre@unige.ch

L. M. Coluccio (ed.), *Myosins*, Advances in Experimental Medicine and Biology 1239,
https://doi.org/10.1007/978-3-030-38062-5_14

14.1 Introduction

14.1.1 The Phylum of Apicomplexa

The phylum Apicomplexa is composed of obligate intracellular parasites and comprises several pathogens of medical and veterinary significance such as *Plasmodium*, responsible for malaria, *Toxoplasma*, the agent of opportunistic toxoplasmosis, or *Cryptosporidium*, responsible for the diarrheal cryptosporidiosis. Apicomplexans are single-celled eukaryotes of the infrakingdom Alveolate, which also includes ciliates and dinoflagellate algae (Gould et al. 2008). Although these protists are very diverse in their shape and lifestyle, they are unified by a common structural feature: the presence of a pellicle composed of the external plasma membrane (PM) under which lies membranous sacs termed alveoli or inner membrane complex (IMC) (Fig. 14.1a). On the cytoplasmic face of the IMC, a meshwork of intermediate filament-like proteins connects the pellicle to the cortical microtubules that constitute the cytoskeleton of the parasite (Harding and Meissner 2014). Most Apicomplexans possess a non-photosynthetic relic plastid named the "apicoplast" that originates from secondary endosymbiosis of a red alga (van Dooren and Striepen 2013) (Fig. 14.1a). This organelle fulfils metabolic functions that are critical for parasite survival. Apicomplexans are further characterized by the presence of an apical complex composed of cytoskeletal elements, the apical polar rings, and two sets of secretory organelles, the micronemes and rhoptries, which play a critical role in gliding motility and during the invasion process and egress from infected cells (Hu et al. 2006; Frénal et al. 2017a). In the subclass of Coccidia, which comprises, among others, *Toxoplasma gondii*, *Eimeria,* and *Cryptosporidium* species, the conoid and the pre-conoidal ring are additional cytoskeletal elements of the apical complex (Fig. 14.1a). The conoid is an organelle found at the apex of these parasites and composed of α-tubulin-rich spiraling fibers named conoid fibers (Hu et al. 2002). The conoid is retracted in intracellular parasites and protrudes beyond the IMC in extracellular parasites upon an increase in intracellular calcium, although its function remains unknown (Monteiro et al. 2001).

In this chapter, we will focus on the two most studied and tractable parasites of the phylum, *Toxoplasma* and *Plasmodium.* Studies on *T. gondii* are mainly carried out on the fast-replicative stage, the tachyzoite, whose lytic cycle is depicted in Fig. 14.1b. Studies on human malaria parasite *P. falciparum* predominantly focus on erythrocytic stages, whereas *P. berghei*, a rodent model of malaria offers the possibility to investigate the full life cycle of the parasite taking place between the murine intermediate host and the *Anopheles* mosquito vector, the definitive host (Fig. 14.1c).

14.1.2 Parasite Lifestyle

The apicomplexan motile stages, also called zoites, exhibit a unique form of substrate-dependent locomotion. In contrast to other protozoans, they do not rely on specific attributes such as flagella or amoeboid movement. Instead, they use gliding motility powered by an actomyosin system, termed glideosome, to actively penetrate into their host cell (invasion), exit from the infected cell (egress), and cross biological barriers. This molecular machine is located within the pellicle in the space between the plasma membrane and the IMC (Frénal et al. 2017a). Following an increase in intracellular calcium, exocytosis of microneme content occurs at the apical pole of the parasite leading to the insertion of micronemal adhesins into the parasite plasma membrane. During motility, these adhesins can bind to host receptors at the surface of target cells and the rearward translocation of these adhesin-receptor complexes by the glideosome propels the parasite forward. During invasion, apical microneme secretion induces the reorientation of the parasite, placing the apex of the parasite in juxtaposition with the host cell plasma membrane (Fig. 14.1b). Subsequently, rhoptry discharge occurs, releasing rhoptry neck (RONs) and rhoptry bulb proteins (ROPs) into the host cells. A complex of RONs (RON2/4/5) inserted within the host cell plasma membrane and inter-

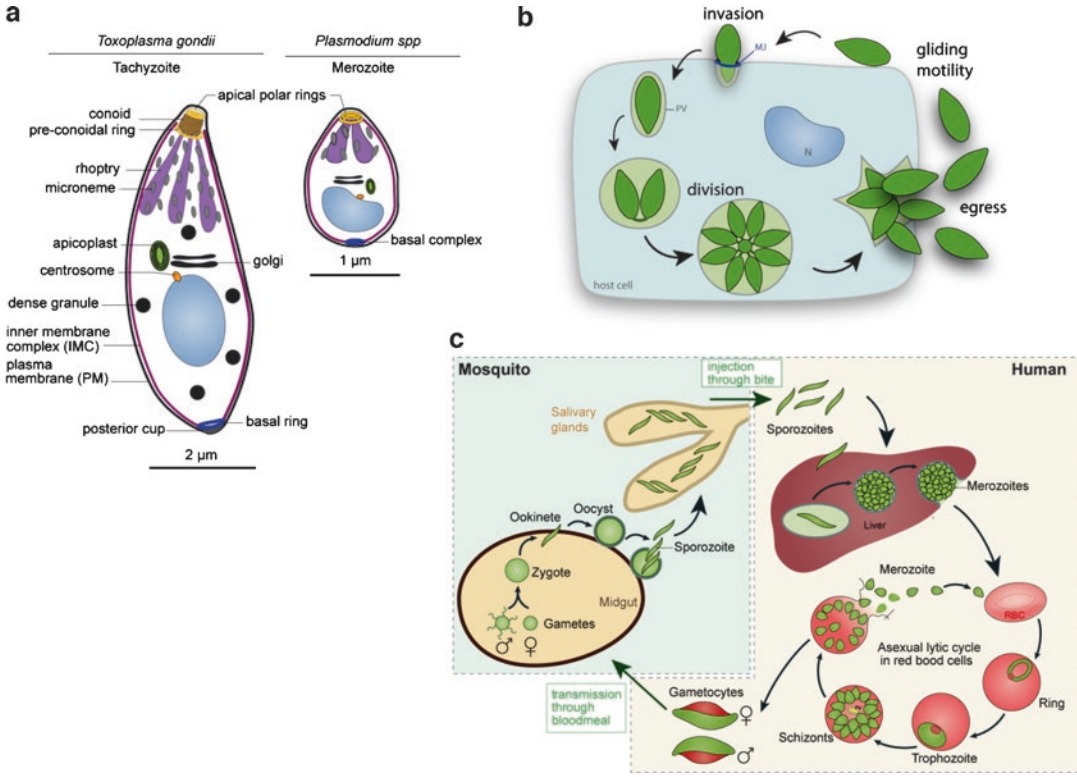

Fig. 14.1 Example of zoites in *Toxoplasma gondii* and *Plasmodium species* and their life cycle. (**a**) Schematic representation of *Toxoplasma gondii* tachyzoite (left panel), a member of the coccidian sub-group of Apicomplexa and *Plasmodium* merozoite, belonging to the haemosporida sub-group (right panel). The main difference resides in the presence of the conoid, a structure composed of tubulin, located at the apex of the Coccidians. The zoites harbor three types of secretory organelles, the micronemes, rhoptries, and dense granules and a non-photosynthetic plastic-like organelle, the apicoplast. Mitochondrion and endoplasmic reticulum are not represented but are present in these zoites. (**b**) Lytic cycle of *Toxoplasma gondii*. The fast replicative tachyzoite is capable of entering virtually any nucleated cell. Within the host cell, the parasite divides by endodyogeny within a parasitophorous vacuole and after several rounds of replication, will eventually egress from the infected cell, lysing it, and glide to invade a neighboring cell. *N* nucleus, *PV* parasitophorous vacuole, *MJ* moving junction. (**c**). Life cycle of *Plasmodium falciparum* taking place between the definitive host, the *Anopheles* mosquito, and the intermediate host, the human. Infection of the human starts through the bite of an infected female mosquito, which injects sporozoites into the dermis. The sporozoites migrate to the liver and invade hepatocytes where they divide and produce thousands of merozoites that are released into the bloodstream. There, the merozoites infect erythrocytes (*RBC*, red blood cells). The parasites undergo repeated asexual cycles within the RBC, where they progress from rings to trophozoites and schizonts and are eventually released as merozoites. Some parasites will develop into gametocytes, the sexual forms that circulate in the bloodstream, prior to being taken up by the mosquito. The sexual cycle takes place within its midgut, leading to the formation of motile but non-invasive ookinetes, which migrate through the midgut and develop into oocysts in the epithelium. Maturation of the oocyst produce sporozoites that migrate to the salivary glands where they are ready to infect subsequent hosts through the mosquito bite

acting with the microneme protein AMA1 (apical membrane antigen 1) at the parasite plasma membrane forms the moving junction that supports the motility-driven progression of the parasite into the target cell (Harvey et al. 2014; Bichet et al. 2014). At the same time, the parasite induces the formation of a non-fusogenic parasitophorous vacuole membrane (PVM), which is derived from the invagination of the host-cell plasma membrane (Mordue et al. 1999). Once intracellular, tachyzoites secrete effectors from the secretory organelles named dense granules that ensure

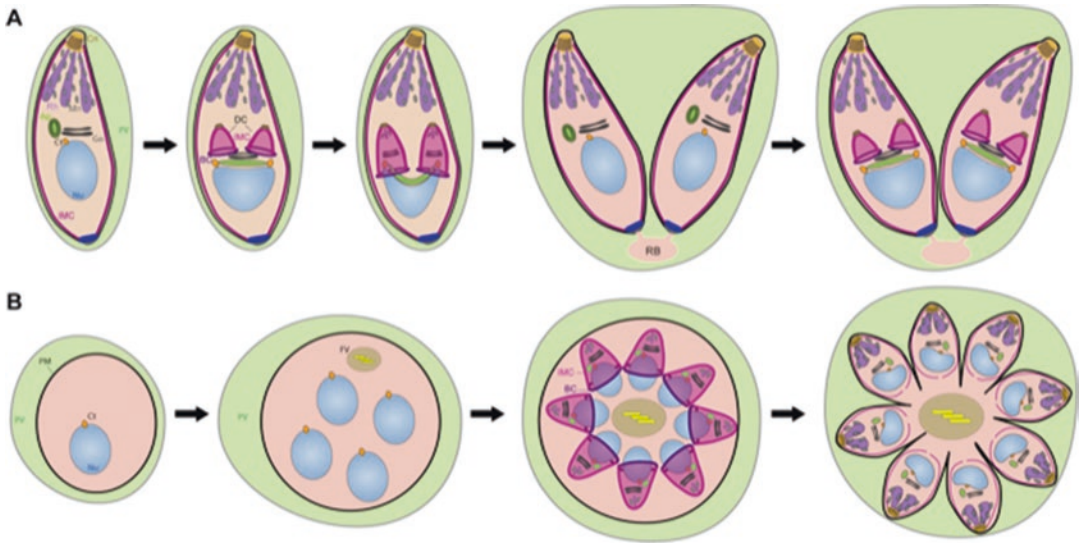

Fig. 14.2 Endodyogeny of *Toxoplasma gondii* tachyzoite and schizogony of *Plasmodium*. (**a**) Scheme of tachyzoites dividing by endodyogeny during which two daughter cells grow inside the mother cell. The scheme highlights particularly the division of the apicoplast that is associated to centrosomes during its inheritance into the daughter cell. The apicoplast is first elongated, then forms a U-shape before being incorporated in the two developing progenies. *Cn* conoid, *Rh* rhoptries, *Mn* micronemes, *Ap* apicoplast, *Go* Golgi apparatus, *Ct* centrosome, *Nu* nucleus, *IMC* inner membrane complex, *BC* basal complex, *DC* daughter cells, *PV* parasitophorous vacuole, *RB* residual body. (**b**) Scheme of the schizogony process, the mode of division of *Plasmodium* species, taking place in the erythrocytes. During this process, the nucleus divides several times and the other organelles are also dividing and/or synthesized *de novo*. All the organelles are then packaged into the IMC at the same time before the segmentation of the individual merozoites. *PM* plasma membrane, *PV* parasitophorous vacuole, *FV* food vacuole

their safe replication by participating in the modification of the parasitophorous vacuole (PV), recruitment of host endoplasmic reticulum and mitochondria, and subversion of host cellular functions (Mercier and Cesbron-Delauw 2015; Hakimi et al. 2017).

Within the PV, *T. gondii* tachyzoites divide synchronously by endodyogeny, a process during which two daughter cells develop within the mother cell and consume it (Francia and Striepen 2014) (Fig. 14.2a). During this replication, some organelles are made *de novo* such as the IMC, micronemes, and rhoptries, whereas others, including the mitochondrion and the apicoplast, are inherited (Nishi et al. 2008). For the segregation of the apicoplast, the positioning of the centrosome is crucial since the ends of the apicoplast have been shown to be tightly associated to the centrosomes during its elongation and incorporation into the daughter cells (Striepen et al. 2000). At each round of division, the basal pole of the parasites constricts and the parasites remain associated through the residual body and adopt an organization in rosettes. After several rounds of replication, the tachyzoites actively egress from the infected cell using the gliding motility and lyse the PVM and host-cell PM through the action of at least one perforin (PLP1) secreted by the micronemes (Kafsack et al. 2009).

In contrast to *Toxoplasma*, *Plasmodium* undergoes schizogony in the erythrocytic stage, a process wherein the components of the daughter cells (such as mitochondrion, apicoplast, nucleus, and secretory organelles) are produced in the same cytoplasm before being encapsulated simultaneously within the forming daughter cells (Fig. 14.2b). Cytokinesis then occurs and produces individual invasive merozoites released in the bloodstream that are able to infect new erythrocytes (Francia and Striepen 2014).

Use of drugs, such as the actin-depolymerizing agent cytochalasin D, revealed that actin does not play a crucial cytoskeletal role during apicomplexan division (Jacot et al. 2013; Frénal et al. 2017b). In contrast, actin polymerization and the connected myosin functions are critical for several steps of the parasite lytic cycle. In the following sections, we will review the role of the actomyosin system for organelle positioning and inheritance, basal complex constriction and intravacuolar cell-cell connection, and gliding motility.

14.2 Myosin Heavy Chain and Actin Features in Apicomplexa

14.2.1 Overview of the Evolution and Classification of Protozoan Myosin Motors

Myosin motors, one of the largest protein families in eukaryotes, are involved in a multitude of cellular functions. Several comprehensive phylogenetic analyses of myosin heavy chains, progressively updated with newly sequenced genomes, have led to the classification and reconstruction of the evolutionary history of these proteins (Richards and Cavalier-Smith 2005; Foth et al. 2006; Odronitz and Kollmar 2007; Sebé-Pedrós et al. 2014). Foth et al. established the first phylogenetic analysis including myosin sequences from numerous protozoa, such as seven members of Apicomplexa, the ciliate *Tetrahymena thermophila* as well as five members of the Kinetoplastida phylum (*Leishmania* and *Trypanosoma* species), and those from metazoans, fungi, and plants (Foth et al. 2006) (Table 14.1). This analysis led to the discovery of six novel classes of unconventional myosins, three of them restricted to the alveolates (classes XXII, XXIII, XXIV), one of which is found only in trypanosomatids (class XXI). Interestingly, characterization of this broader repertoire of myosin heavy chains identified protein domains, such as FYVE, WW, UBA, ATS1-like and WD40, within the tails that were not previously associated with myosins. In addition, apicomplexan myosins, previously restricted to class XIV, were placed into several classes encompassing myosins from other systematic lineages (classes VI, XXII, XXIII, XXIV), while the class XIV was found to no longer accommodate only apicomplexan myosins but also myosins of *T. thermophila*.

Subsequent phylogenetic analyses have extended and modified the myosin classification described above. Odronitz et al. used 2269 myosin motor domains from 328 organisms to build a new eukaryotic tree of life (Odronitz and Kollmar 2007). This resulted in the definition of 35 myosin classes and some re-classifications. Of relevance concerning the protists, a new class XIII was attributed to myosins specific to the kinetoplastida and exhibiting SH3-like, coiled-coil, and UBA domains, and finally, five new classes were composed solely of apicomplexan myosins.

A more recent study used an expanded taxon sampling in which all major eukaryotic supergroups were represented to define 31 myosin classes (Sebé-Pedrós et al. 2014). With regard to the protozoan myosins, some interesting aspects of this study need to be mentioned. Some alveolate sequences that were previously grouped within myosin class VI (Foth et al. 2006) are now accommodated within myosin class XXIII. Eighteen myosins from the alveolate *T. thermophila* and *Paramecium tetraurelia* are grouped again within the alveolate-specific myosin class XIV (Sebé-Pedrós et al. 2014), and interestingly, several of them contain the protein domain combination MyTH4/FERM. They constitute the only example of bikonts harboring these domains. Recently, the classification from Foth et al. has been updated to include sequences of two recently sequenced Alveolates, the related photosynthetic chromerids, *Chromera velia* and *Vitrella brassicaformis* (Mueller et al. 2017) (Table 14.1). We have chosen to use this latest phylogeny to describe the apicomplexan myosin heavy chains in the following sections.

Table 14.1 Overview of the repertoire of myosin heavy chains in Apicomplexa

Class	Gene name	Gene ID	№ of IQ motifs	MW (kDa)	Localization	Cellular function	Fitness	Coccidia	Cryptosporidia	Haemosporida	Piroplasmida	Gregarines	Chromerids
XIV a	MyoA	TGME49_235470	1	93	Inner membrane complex	Gliding/ Invasion/ Egress	-3.09	●	●	●	●	●	○
	MyoD	TGME49_263180	0	91	Plasma membrane	n.d.	1.56	●	○	○	○	○	○
XIV b	MyoB/C	TGME49_255190	0–1	133	Basal ring	Gliding/ Invasion/ Egress	2.25	●	○	○	○	●	○
	MyoE	TGME49_239560	1	93	Conoid	n.d.	0.11	◐	○	○	○	○	○
XIV c	MyoH	TGME49_243250	6–8	170	Conoid/ Cytoplasm	Gliding/ Invasion/ Egress	-3.94	●	●	○	●	○	○
XIV e	MyoL	TGME49_291020	4	278	Conoid/ Cytoplasm	n.d.	-1.83	●	○	○	○	○	○
XXII	MyoF	TGME49_278870	3–6	216	Apicoplast, juxanuclear region, cytoplasm, daughter cells	Organellar inheritance	-3.55	●	●	●	●	●	●
XXIII	MyoG	TGME49_314780	1	227	Cytoplasm/ Pellicle	n.d.	0.54	●	○	○	○	○	○
XXIV	MyoI	TGME49_230980	2	201	Residual body	Intravacuolar parasite communication	0.21	◐	○	○	○	○	●
VI-like	MyoJ	TGME49_257470	0	274	Posterior cup/ daughter cells	Basal constriction	-3.01	●	●	●	○	○	●
	MyoK	TGME49_206415	2–3	263	Centrosome	n.d.	-2.78	◐	●	●	○	○	●
XIV c	MyoB	PBANKA_1103300	1	93	Apical ring	n.d.	D	○	○	●	○	○	○
	MyoE	PBANKA_0613900	0	255	Basal 'cap'	n.d.	n.d.	○	○	●	○	○	○

● *Present*
○ *Absent*
D : *dispensable*
n.d. : *no data*

The myosin classification is based on the review from Mueller et al. (2017). The GeneID corresponds to the accession numbers of EuPathDB. The number of IQ motifs has been predicted by SMART (Letunic and Bork 2018). The references for the localization and cellular functions are cited in the text. The fitness scores are from the CRISPR-Cas9 genome wide screen performed on *T. gondii* (Sidik et al. 2016) and the PlasmoGEM database established for the erythrocytic stages of *Plasmodium berghei* in mice (Bushell et al. 2017). Conservation within the Apicomplexa phylum was performed by a BLAST search. The genes written in purple are specific to *Plasmodium* species

14.2.2 Repertoire of Myosin Heavy Chains in Apicomplexa

Among the apicomplexans, *T. gondii* has the largest repertoire of myosin heavy chains with 11 isoforms, while *P. falciparum* genome encodes six, two of them, PfMyoB and PfMyoE, being specific to the malaria parasites (Table 14.1). All apicomplexan myosin heavy chains are unconventional and two of them are conserved across the phylum, namely the class XIV MyoA and the class XXVII MyoF, with the latter having also orthologs in the chromerids (Mueller et al. 2017). All the myosin heavy chains have been localized in *T. gondii* tachyzoites (Fig. 14.3) and *P. berghei* blood stages and their essentiality evaluated by the generation of knockout, when possible (Wall et al. 2019; Herm-Götz et al. 2006; Andenmatten et al. 2013; Frénal et al. 2014, 2017b), or knockdown (Meissner et al. 2002; Siden-Kiamos et al. 2011; Jacot et al. 2013; Graindorge et al. 2016) cell lines. Out of the 11 myosin heavy chains expressed by the tachyzoite, only two, TgMyoF and TgMyoH, have been completely refractory to deletion and thus are considered indispensable for parasite survival. The other nine motors have been individually deleted with no or very mild impact on tachyzoite fitness, except for TgMyoA. Interestingly, although the class VI-like TgMyoJ and the class XXIV TgMyoI are dispensable for tachyzoite growth *in vitro*, their deletion uncovered their respective function in basal complex constriction and in intravacuolar parasite connection allowing diffusion of soluble molecules and synchronized division (Frénal et al. 2017b). Deletion of the highly conserved TgMyoA showed a strong defect on the parasite lytic cycle being critical for gliding motility (Andenmatten et al. 2013). However, it was impossible to delete *TgMyoA* in a background lacking *TgMyoC* indicating that these two motors fulfil overlapping functions (Egarter et al. 2014).

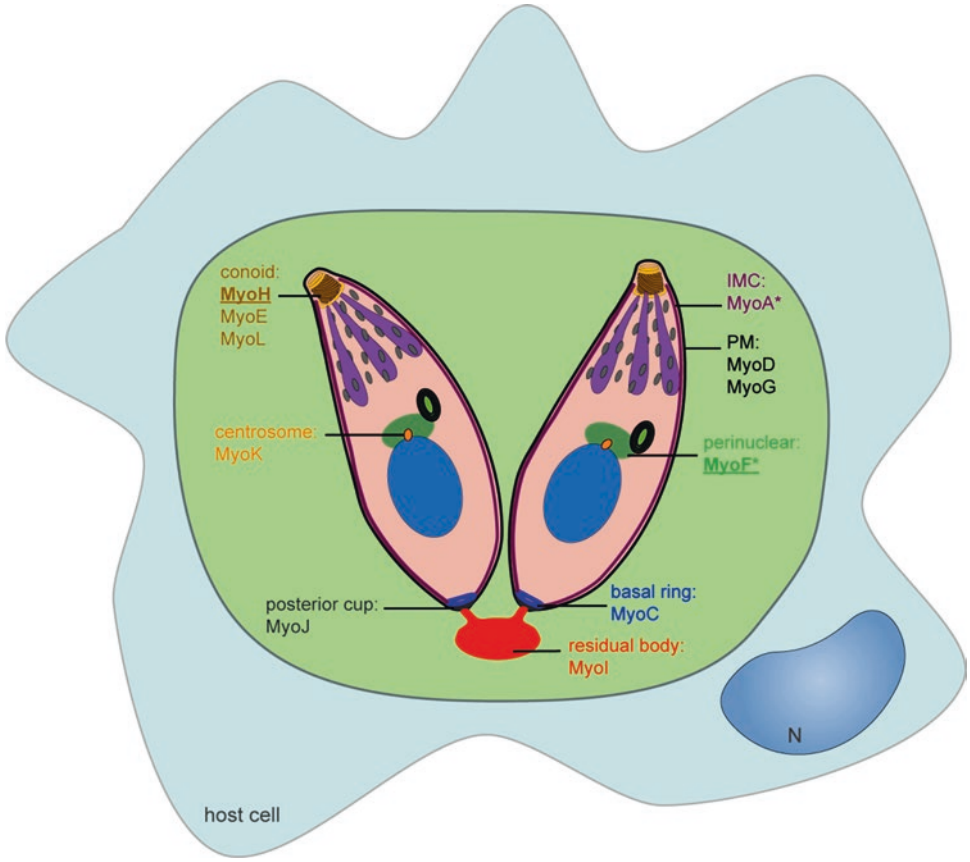

Fig. 14.3 Localization of the *Toxoplasma gondii* myosins. Scheme of a parasitophorous vacuole containing two tachyzoites connected by the residual body showing the localization of the 11 myosins expressed by this parasite. The dense granule, mitochondria and endoplasmic reticulum are not represented but are present in these zoites. The bold and underlined myosins are the ones found essential for the survival of the tachyzoite. The asterisks indicate the myosins conserved across the Apicomplexa

In *Plasmodium* species that lack an ortholog of TgMyoC, MyoA is likely essential for all motile stages of the life cycle as is the case for the *P. berghei* ookinete (Siden-Kiamos et al. 2011). Moreover, in *P. berghei*, out of the five other myosin heavy chains, PbMyoF and PbMyoK are likely essential for the blood stages since their deletion was unsuccessful (Wall et al. 2019). However, PbMyoB, PbMyoE, and PbMyoJ were shown to be dispensable for these asexual stages while the class XIV PbMyoE appeared critical for motility of the mosquito salivary gland sporozoites (Wall et al. 2019).

For *Toxoplasma,* the experimental results of the individual deletions (Frénal et al. 2017b) are in accordance with the recently-published genome-wide loss-of-function screen performed on *T. gondii* using the CRISPR/Cas9 technology (Sidik et al. 2016), except for the class VI-like TgMyoK, which presents a fitness defect not detected in the phenotyping of the knockout strain (Frénal et al. 2017b) (Table 14.1). Likewise, the fitness data collected for *P. berghei* are in agreement for PbMyoA and PbMyoB, but a discrepancy exists for PbMyoK, which appears dispensable in the large *in vivo* genetic screen performed in the mouse model (Bushell et al. 2017) (Table 14.1). The individual role of each myosin heavy chain will be discussed in detail below.

14.2.3 Unusual Features of Apicomplexan Actin

Actin, one of the most abundant and conserved proteins in eukaryotic cells, exists in a monomeric globular state (G-actin) and a polymerized filamentous state (F-actin). It plays fundamental roles in many cellular processes such as muscle contraction, cell division, and cell motility (Dominguez and Holmes 2011; Pollard 2016).

The apicomplexans possess a single gene coding for actin (ACT1), except for the *Plasmodium* species, which also encode a second isoform (ACT2) mainly expressed in the gametocytes and mosquito stages (Deligianni et al. 2011) (Table 14.2). PfACT2 plays a critical role in gametogenesis and its deletion cannot be complemented by PfACT1 (Deligianni et al. 2011; Vahokoski et al. 2014). Actin filaments cannot be readily observed in the parasites. It appears to be mainly globular (Dobrowolski et al. 1997; Schmitz et al. 2005), and the generated filaments tend to be short and unstable (Schmitz et al. 2005; Sahoo et al. 2005). The inherent instability of apicomplexan F-actin resides both in its amino acid sequence, which is distant from other eukaryotic actins (Schüler et al. 2005a; Skillman et al. 2011; Pospich et al. 2017; Douglas et al. 2018), and in its regulation by a limited and divergent set of actin-binding proteins (ABPs) compared to most eukaryotic cells (Baum et al. 2006; Schüler and Matuschewski 2006) (Table 14.2). Yet, actin filaments are essential for parasite growth (Skillman et al. 2011) and especially for motility (Egarter et al. 2014; Drewry and Sibley 2015), suggesting a tight spatial and temporal regulation of the polymerization process within the parasites.

Actin dynamics have been carefully examined *in vitro* with recombinant TgACT1 and PfACT1 purified from the baculovirus insect cell expression system. TgACT1 polymerization was reported to follow an unconventional isodesmic model in which each monomer has the same assembly/disassembly rate in the polymer. Consequently, the polymerization rate is slow without a lag phase or critical concentration, and increases proportionally to the number of actin molecules (Skillman et al. 2013). In contrast, PfACT1 polymerization is reported to follow a classical nucleation-elongation model in which a slow nucleation step precedes a more rapid polymerization phase after reaching a critical concentration (Kumpula et al. 2017). Although the critical concentration and the polymerization rate of PfACT1 are similar to the canonical actin, structural and biochemical studies demonstrated that its depolymerization is faster, likely due to the inherent instability of the filaments (Vahokoski et al. 2014; Pospich et al. 2017). Indeed, despite a conserved location of the monomer interface, substitution of several residues in PfACT1 compared to rabbit actin weaken the interaction within the filament (Pospich et al. 2017; Kumpula et al. 2019). Interestingly, point mutations generated in both *Toxoplasma* and *Plasmodium* to stabilize F-actin revealed that filament instability is in fact essential for the survival of these parasites (Skillman et al. 2011; Douglas et al. 2018).

14.2.4 A Large Pool of Globular Actin

Actin turnover is fine-tuned by actin-binding proteins (ABPs). Searches across the sequenced genomes revealed that the apicomplexans have a limited repertoire of actin regulators, ten times smaller than most eukaryotes (Gordon and Sibley 2005; Schüler and Matuschewski 2006). These ABPs include a monomer-binding profilin (PRF), a F-actin-binding coronin (COR), filament-severing actin-depolymerizing factors (ADFs), and F-actin-capping proteins (CPs) (Table 14.2). The apicomplexans lack one of the main regulators of actin dynamics, the actin-related protein-2/3 (ARP2/3) complex, which mediates nucleation and branching of actin filaments, and possess instead two formins (FRM1 and FRM2). A third formin (FRM3) is found in the parasites of the coccidian sub-group of Apicomplexa.

As discussed above, the vast majority of actin is not incorporated into filaments but rather maintained in its globular form. Unexpectedly, ADF and PRF have been identified as the main contributors of the maintenance of this actin pool. Indeed, in contrast to most eukaryotic ADF, api-

Table 14.2 Actin, actin-related and actin-binding proteins in *Toxoplasma gondii* and *Plasmodium berghei*

	Class	Gene name	Gene ID	MW (kDa)	Localization	FS (Tg)	Ess (Pb)	Seq Sim. (Tg)	Seq Sim. (Pb)	PDB entry
Filament forming	Actin	ACT1	TGME49_209030 PBANKA_1459300	42	Cytoplasm	–4.50	E	84%	82%	4CBU 4CBW
		ACT2	PBANKA_1030100	43	cytoplasm (gametocyte)		D	NA	76%	4CBX
	Actin-like	ALP1	TGME49_219280 PBANKA_0936900	46	Cytoplasm	–2.53	S	39%	49%	
		ALP2a	TGME49_248890 PBANKA_0943300	61	NA	–4.54	S	27%	20%	
		ALP2b	PBANKA_1104800	65	NA		n.d.	NA	n.d.	
		ALP3	TGME49_221410 PBANKA_0212300	52	NA	–1.50	D	23%	36%	
		ALP5a	PBANKA_0811800	68	NA		n.d.	NA	n.d.	
		ALP5b	PBANKA_1007500	48	NA		n.d.	NA	n.d.	
		ALP8	TGME49_294850	49	NA	0.59		25%	NA	
		ALP9a	TGME49_234670	72	NA	–2.59		24%	NA	
		ALP9b	TGME49_269240	58	NA	–0.37		n.d.	NA	
	Actin-related	ARP1	TGME49_248630 PBANKA_0209300	42	NA	–1.82	n.d.	53%	63%	
		ARP4a	TGME49_253040 PBANKA_1020600	77	NA	–4.16	E	34%	36%	
		ARP4b	TGME49_258050	60	NA	–4.44		27%	NA	
		ARP6	TGME49_257710 PBANKA_0616800	67	NA	–5.04	D	20%	40%	
F-actin binding	Coronin	COR	TGME49_216970 PBANKA_1464100	68	Cytoplasm	0.71	n.d.	24%	21%	2AQ5
F-actin capping	Capping protein	CPa	TGME49_208390 PBANKA_1233900	47	NA	0.09	E	15%	19%	2B0R
		CPb	TGME49_219290 PBANKA_1232400	36	NA	–1.30	D	29%	25%	
G-actin sequestering	Profilin	PRF	TGME49_293690 PBANKA_0833000	18	Cytoplasm	–4.58	S	16%	18%	2JKF 2KJG 3NEC
	Cofilin/ ADF	ADF1	TGME49_220400 PBANKA_1137500	13	Cytoplasm	–4.23	n.d.	27%	21%	3Q2B 2XF1 2L72
		ADF2	PBANKA_1103100	14	NA		E	NA	25%	2XFA
	Cyclase-associated protein	CAP	TGME49_310030 PBANKA_0208000	225	NA	1.17	n.d.	NA	NA	
F-actin nucleators	Formins	FRM1	TGME49_206430 PBANKA_1245300	547	Apical pole	–3.24	n.d.	n.d.	n.d.	
		FRM2	TGME49_206580 PBANKA_1434600	492	Cytoplasm, juxtanuclear region	–1.12	n.d.	n.d.	n.d.	
		FRM3	TGME49_213370	299	Residual body	–2.79		n.d.	NA	

E: Essential
S: slow
D: dispensable
n.d.: no data

Similarity with (BLAST-pairwise)
Oryctolagus cuniculus (rabbit)
TgACT1

The GeneID corresponds to the accession numbers of EuPathDB. The references for the localization are cited in the text. The fitness scores are from the CRISPR-Cas9 genome wide screen performed on *T. gondii* (Sidik et al. 2016) and the PlasmoGEM database established for the erythrocytic stages of *Plasmodium berghei* in mice (Bushell et al. 2017). The sequence similarity (Seq. Sim.) is denoted as a percentage relative to the counterpart in the rabbit *Oryctolagus cuniculus (grey) or TgACT1 (blue)*. The solved structures of the proteins can be accessed via the RCSB Protein Data Bank (PDB). The genes in purple are specific to *Plasmodium* species

complexan ADF (or ADF1 in *Plasmodia*) does not contain the typical F-actin-binding site and therefore prevents actin polymerization by sequestering G-actin (Schüler et al. 2005b; Mehta and Sibley 2010; Singh et al. 2011; Yadav et al. 2011; Baroni et al. 2018). Likewise, PRF appeared to sequester actin monomers and prevent their incorporation into filaments (Skillman et al. 2012), while in other eukaryotes, the presence of PRF usually enhances the polymerization rate of the formin nucleators by increasing the local concentration of ATP-actin in the vicinity of the growing filaments (Pollard 2016). Despite divergence in the amino acids sequences, the apicomplexan PRF shares an overall common structure with mammalian PRFs with the exception of an additional region composed of an acidic loop and a β-hairpin (Kursula et al. 2008; Kucera et al. 2010). This flexible region is a key determinant for interaction with actin but also serves as a recognition pattern in TgPRF to elicit the Toll-like receptor 11 (TLR11) innate immune response

(Kucera et al. 2010; Moreau et al. 2017; Kadirvel and Anishetty 2018).

Another protein that has the capacity to bind G-actin and to regulate F-actin disassembly is the cyclase-associated protein or CAP (Table 14.2). In Apicomplexa, this protein harbors only a CARP domain able to interact and sequester G-actin and to promote the nucleotide exchange from ADP to ATP (Hliscs et al. 2010; Makkonen et al. 2013). CAP thus contributes to the abundant pool of G-actin, is important for the growth of tachyzoites, and appeared dispensable for the erythrocytic stages of malaria parasites but essential for oocyst development in the mosquito midgut (Hliscs et al. 2010; Hunt et al. 2019).

In the absence of ARP2/3 complex, the formins are the sole identified nucleators of F-actin in Apicomplexa. Formins are very large multidomain proteins (>300 kDa) that interact with the barbed end of an actin filament, wherein actin nucleation activity is achieved by the formin homology 2 (FH2) domain (Pollard 2016). It was indeed confirmed, in both *Toxoplasma* and *Plasmodium*, that all the formins expressed were able to bind ACT1 and were potent nucleators of filamentous actin through their FH2 domain (Baum et al. 2008; Daher et al. 2010, 2012; Skillman et al. 2012). In both parasites, formins have been localized in subcellular locations where actomyosin systems participate for critical functions: PfFRM1 and TgFRM1 at the apical pole for motility, TgFRM2 in the cytoplasm at the apical juxtanuclear region involved in organelle positioning and inheritance, and TgFRM3 in the residual body implicated in cell-cell communication (Baum et al. 2008; Jacot et al. 2016; Stortz et al. 2018; Tosetti et al. 2019).

Growth of actin filaments is regulated by their polymerization but also by F-actin-binding proteins such as CPs, a family of proteins that binds the barbed end of F-actin and prevents the exchange with new subunits (Cooper and Sept 2008) and COR, a protein known to stabilize and bundle newly-formed filaments (de Hostos 1999). CPs have been investigated in *P. berghei,* and although their sequences differ from the mammalian counterparts, their folding and biochemical properties are preserved. Remarkably, the length of rabbit actin filaments was significantly decreased by the addition of the heterodimer PbCPα/β (Ganter et al. 2009). *In vivo*, PbCPα/β disruption has a strong impact on the malaria life cycle blocking the transmission of the parasites to a new host as described below (Ganter et al. 2009). In contrast, COR was shown to bind F-actin and increase its polymerization and cross-linking in Apicomplexa (Salamun et al. 2014; Olshina et al. 2015).

Overall, the intrinsic features of apicomplexan actin and ABPs contribute to the maintenance of a heterogeneous mixture of sequestered free G-actin and short filaments in these parasites. A fine-tuned coordination and regulation between the actin polymerization process and the action of ABPs is therefore needed to achieve specific and vital functions. The process is tightly regulated in time and space during parasite division but also during motility when actin filaments are crucial for the survival of the obligate intracellular parasites. All the ABPs have a critical role in the parasites' life cycle and their specific contribution to the regulation of the different actomyosin systems will be discussed below.

14.3 Actomyosin Systems in Apicomplexa

14.3.1 Actin Polymerization Occurs at Specific Locations

After decades of great limitation in visualization of actin filaments, unexpectedly, antibodies raised against *Plasmodium* ACT1 that preferentially recognized F-actin allowed for the observation of actin concentrated near the nucleus, at the periphery of motile parasites (ookinetes, sporozoites and merozoites), and at the moving junction during merozoite invasion (Siden-Kiamos et al. 2012; Angrisano et al. 2012). In gametocytes, the sexual stages of the malaria parasite, super-resolution and immuno-electron microscopy revealed the presence of an actin cytoskeleton underneath the IMC, along the

microtubules with accumulation at the two poles of the parasite (Hliscs et al. 2015). Gametocytes express both ACT1 and ACT2, so it remains to be determined which one constitutes the observed actin cytoskeleton. More recently, actin chromobodies designed to visualize eukaryotic F-actin have been expressed in *T. gondii* and *P. falciparum* and revealed that polymerized actin is located in distinct subcellular compartments and at specific time points of the lytic cycle. In *P. falciparum*, they confirmed all the previous observations (Stortz et al. 2018). In *T. gondii* intracellular tachyzoites, F-actin was found at the apical perinuclear region, close to the apicoplast. In addition, an extensive F-actin network was stained in the residual body, which connects the basal pole of intravacuolar tachyzoites and organizes them into a rosette within the parasitophorous vacuole (Periz et al. 2017; Tosetti et al. 2019) (Fig. 14.2a, c). Remarkably, in extracellular tachyzoites, a ring of F-actin appears to be produced apically and to translocate to the rear of the parasite, co-localizing with the moving junction. Consequently, an accumulation of F-actin is observed as a dot at the basal pole of the parasites immediately after activation of motility (Tosetti et al. 2019).

Conditional knockout of TgACT1 and PfACT1 has recently been generated in *T. gondii* tachyzoites and *P. falciparum* erythrocytic stages, respectively (Andenmatten et al. 2013; Egarter et al. 2014; Drewry and Sibley 2015; Periz et al. 2017). As expected, absence of actin in both parasites is lethal, but the establishment of a dimerizable Cre-recombinase strategy that efficiently excises the loxP sites flanking the actin gene allowed scrutinizing all aspects of the parasite life cycle and dissecting the cellular functions for which actin is required. The localization of F-actin in both *T. gondii* and *P. falciparum* are in accordance with the location of the formins expressed by these parasites. The composition and role of the corresponding actomyosin systems are discussed below.

14.3.2 Contribution of Actomyosin Systems to Cell Division Processes

14.3.2.1 Intravacuolar Connection and Cell-Cell Communication

While *in vitro* cultures of *T. gondii* are asynchronous, the division of tachyzoites within a given parasitophorous vacuole is highly synchronized. The class XXIV TgMyoI, a fairly large myosin (approximately 200 kDa) with two predicted IQ motifs in its neck and no domain identified in its tail, was shown to be responsible for this phenomenon. TgMyoI localizes to the residual body and seems to be associated with the F-actin network, and importantly, TgFRM3 is present at the same location (Frénal et al. 2017b; Periz et al. 2017; Das et al. 2017; Tosetti et al. 2019). Knockout of TgMyoI or TgFRM3 had no impact on the fitness of the tachyzoites. Yet, the parasites appeared disorganized within the PV, failed to organize in rosettes, and divided in an asynchronous manner (Frénal et al. 2017b; Tosetti et al. 2019). The same phenotype was also observed in actin-depleted tachyzoites (TgACT1-cKO) (Periz et al. 2017). It was therefore hypothesized that an actomyosin system could be involved in the formation and/or maintenance of a basal connection between the parasites within the vacuole. Fluorescence recovery after photobleaching (FRAP) experiments performed on wild-type, TgMyoI-KO, TgFRM3-KO and TgACT1-cKO parasites demonstrated that soluble proteins from the cytoplasm but also from the nucleus were able to diffuse between the parasites of the same vacuole only when TgMyoI, TgFRM3 or TgACT1 were expressed (Frénal et al. 2017b; Periz et al. 2017; Tosetti et al. 2019).

These experiments identified the presence of an actomyosin system in the residual body, composed of TgMyoI that likely moves along actin filaments assembled by TgFRM3. This complex is involved in the formation and maintenance of a cytoplasmic connection between intravacuolar parasites allowing the diffusion of soluble proteins and metabolites to ensure a tightly synchro-

nized division. Electron microscopy and 3D reconstruction revealed the presence of a tubular mitochondrion within the connection, passing through the basal complex and shared between intracellular parasites (Frénal et al. 2017b). This observation raises the possibility that diffusion or exchanges could occur between parasites through the mitochondrion as well. In addition, it has been shown that vesicles are also exchanged between the parasites along the actin filaments (Periz et al. 2017). It remains to be determined whether this transport is TgMyoI-dependent. Considering the extensive filamentous network present in the residual body, it is likely that ABPs influence the dynamics and structure of the network. Deletion of TgCAP, which modulates actin turnover through its G-actin sequestering activity, has a strong impact on the structure of the intravacuolar cell-cell connection and the arrangement in rosette of the parasites (Hunt et al. 2019). In this mutant, although the parasites are still connected and able to divide synchronously, the connections are really long, tubular, and not organized around a residual body. The endoplasmic reticulum was also observed within the connections suggesting a possible exchange of material through this organelle, just like the mitochondrion. However, diffusion of reporter protein was observed only between parasites in close proximity. These results open the question on the nature of the material that ensures synchronicity within the PV.

Of relevance, MyoI and FRM3 are only present in the genome of a few coccidians that divide by endodyogeny ensuring the communication that naturally exists in the other apicomplexans that divide by schizogony in the cytoplasm of the same cell (Tables 14.1 and Fig. 14.2c, d). Interestingly, this connection is not maintained in the bradyzoite stage, a latent and encysted form of *T. gondii* that grows slowly and asynchronously (Frénal et al. 2017b).

14.3.2.2 Basal Pole Constriction and Cytokinesis

At the end of cell division, the basal pole of the daughter cells constricts. In *T. gondii*, the class VI-like TgMyoJ has been associated with this process (Frénal et al. 2017b). MyoJ is a large myosin (approximately 270 kDa), but no IQ motif or other domains have been identified (Table 14.1). The protein is found in most apicomplexans and the chromerids (Foth et al. 2006; Mueller et al. 2017). It localizes at a ring-shaped structure at the basal end of the IMC in the developing daughter cells (Frénal et al. 2017b). At the end of division, this structure will constrict and form the posterior cup of the mature parasite (Hu 2008) (Fig. 14.2c). TgMyoJ colocalizes with the CaM-like protein centrin 2 (TgCEN2) at the posterior cup. In the absence of TgMyoJ, tachyzoites display an enlarged posterior pole and a loss of TgCEN2 staining. However, no problem in cytokinesis was observed in these parasites, which only exhibit a modest fitness defect in *in vitro* culture but in contrast a clear loss of virulence in the mouse model of infection (Frénal et al. 2017b). Conversely, depletion of TgCEN2 impacts the basal pole constriction although TgMyoJ remains associated with the enlarged basal cup. These results indicate that TgMyoJ and TgCEN2 play a role in the constriction of the tachyzoite basal pole, but it is not clear yet if they are directly associated with one another (Frénal et al. 2017b). One possibility is that TgCEN2 could act as a light chain for TgMyoJ.

Intriguingly, although loss of basal pole constriction has been observed in TgACT1-depleted tachyzoites demonstrating that it is an actin-dependent process (Periz et al. 2017), none of the three formins expressed by the parasites seems to be involved in this process (Tosetti et al. 2019). This suggests that either an unknown nucleator acts at the basal cup or that some F-actin can be formed in the absence of polymerizing factors possibly following the isodesmic model identified *in vitro* with recombinant TgACT1 (Skillman et al. 2013). This hypothesis is yet to be tested.

In *T. gondii*, depletion of TgACT1 (or TgMyoJ) does not affect the cytokinesis process that occurs naturally, releasing individual parasites during egress. In contrast, in *P. falciparum*, PfACT1 depletion leads to a cytokinesis defect with conjoined merozoites that egress from the infected erythrocytes (Das et al. 2017). The same phenotype was also observed in PfFRM2 depleted

parasites, indicating that PfACT1 and PfFRM2 participate in cytokinesis of malaria schizonts (Das et al. 2017; Stortz et al. 2018). A defect in proper parasite segmentation has also been reported with the depletion of the newly identified basal complex protein PfCINCH (coordinator of nascent cell detachment). Interestingly, co-immunoprecipitation experiments performed on *P. falciparum* schizonts with PfCINCH identified several new proteins of the basal complex and pulled-down PfMyoJ suggesting that in malaria parasites, a basal actomyosin system is responsible for constriction of the schizont basal pole, but also cytokinesis prior egress (Rudlaff et al. 2019). As in *T. gondii*, PbMyoJ was successfully deleted in *P. berghei* without noticeable impact on its life cycle (Wall et al. 2019). Its endogenous tagging allowed its detection only in mature oocysts when sporozoites are formed. PbMyoJ localizes at the junction between the sporozoites and the residual bodies, consistent with a basal localization but remains associated with the oocyst body upon egress of the sporozoites (Wall et al. 2019). So far, it remains enigmatic how these different components contribute to the segregation of the schizonts, but these studies pave the way to a better understanding of the contractile ring, and the constriction and cytokinesis processes in Apicomplexa.

14.3.3 Contribution of Actomyosin to Organelle Positioning and Inheritance

Besides MyoA, the second myosin strictly conserved across the Apicomplexa is the class XXII MyoF, which interestingly also has orthologs in the chromerids *C. velia* and *V. brassicaformis* (Foth et al. 2006; Mueller et al. 2017). The function of MyoF has been characterized in *T. gondii* tachyzoites. TgMyoF possesses six predicted IQ motifs and a tail domain with seven WD40 and a coiled-coil domain suggesting that the protein might function as a dimer. Homology was found between TgMyoF and class V myosins that function as cargo transporters, moving organelles within the organism (Hammer and Sellers 2012; Heaslip et al. 2016). No myosin light chain has been found associated with TgMyoF so far (Table 14.3). TgMyoF localizes in the cytoplasm of the parasites, particularly concentrated in the juxtanuclear region and in the vicinity of the dividing apicoplast (Jacot et al. 2013), where the actin nucleator TgFRM2 is also located (Tosetti et al. 2019). Taking advantage of the possibility that TgMyoF could form a dimer, its function was tackled by disrupting this dimer *via* overexpression of the tail of TgMyoF, with the aim to generate a non-functional heterodimer having a dominant-negative effect. TgMyoF was thus found to be essential for the survival of the tachyzoites and a severe defect in apicoplast inheritance was detected as well as a loss of the close positioning of the centrosomes on one side of the nucleus (Jacot et al. 2013). The same phenotype was also observed with the inducible knockout and knockdown of TgMyoF subsequently generated (Jacot et al. 2013; Heaslip et al. 2016). Concordantly, a defect in apicoplast inheritance was observed in TgACT1-depleted parasites as well as in the TgFRM2-KO strain (Periz et al. 2017; Tosetti et al. 2019). The same phenotype is also observed in the intraerythrocytic stages of *P. falciparum* depleted in PfACT1 or in PfFRM2 confirming the conservation of the machinery in Apicomplexa (Das et al. 2017; Stortz et al. 2018). In addition, PbMyoF is also likely essential in *P. berghei* since the attempts to delete the gene have been unsuccessful so far (Wall et al. 2019).

The primary function of MyoF is likely to maintain the positioning of the centrosomes during cell division. As a consequence of their mispositioning in TgMyoF mutants, the daughter cells grow in opposite directions within the mother parasite instead of growing side-by-side, and the recruitment and association of the apicoplast by the centrosomes are lost (Striepen et al. 2000; Jacot et al. 2013). Some rhoptry organelles also fail to be encapsulated in the progenies and enlarged residual bodies containing apicoplasts and rhoptries were observed. However, enough rhoptries are still accurately targeted to the apical pole and no defect in invasion was recorded in TgMyoF mutants (Jacot et al. 2013). TgMyoF

Table 14.3 Myosin light chains in *Toxoplasma gondii*

Gene name	Associated mysoin	Gene ID	FS (Tg)	MW (kDa)	Localization
MLC1	MyoA – MyoB/C MyoH	TGME49_257680	-2.70	24	Inner membrane complex
MLC2	MyoD	TGME49_297470	0.78	41	Plasma membrane
MLC3	-	TGME49_250840	-1.91	100	Conoid
MLC4	-	TGME49_294390	0.38	19	Endoplasmic reticulum
MLC5	MyoH	TGME49_311260	-0.33	14	Conoid
MLC7	MyoH	TGME49_315780	-0.12	23	Conoid
ELC1a	MyoA – MyoB/C	TGME49_269438	1.09	8	Inner membrane complex
ELC1b	MyoA – MyoB/C	TGME49_269442	0.11	10	Inner membrane complex
ELC2	MyoA	TGME49_305050	1.57	15	Inner membrane complex
CAM1	MyoH	TGME49_246930	1.09	19	Conoid
CAM2	MyoH	TGME49_262010	-0.81	15	Conoid
CAM3	MyoH	TGME49_226040	-3.25	19	Conoid

The GeneID corresponds to the accession numbers of EuPathDB. The fitness scores are from the CRISPR-Cas9 genome wide screen performed on *T. gondii* (Sidik et al. 2016). The references for the localization are cited in the text

was also identified as the motor responsible for the directed movement of the dense granules, in agreement with the fact that this movement is an actin-dependent process (Heaslip et al. 2016). TgCAP has been shown to regulate the trafficking of the dense granules, given that the deletion of this ABP causes the organelles to move further distances and at higher speeds (Hunt et al. 2019). These findings support the fact that TgMyoF might function as class V myosin motors transporting organelles inside cells (Hammer and Sellers 2012). TgMyoF has been also found associated with the acylated protein ARO (armadillo-repeat only) anchored at the surface of the rhoptries and whose depletion leads to the dispersion of mature rhoptry organelles in the cytoplasm, preventing the invasion process to occur (Mueller et al. 2013). Yet, apical rhoptry positioning does not appear to be an actin-dependent process since these organelles are not impacted in the absence of TgACT1 (Egarter et al. 2014; Drewry and Sibley 2015). TgMyoF might play a role in tethering the newly-made rhoptries to the apical part of the developing daughter cells, where they are actually found to accumulate, in addition to the vicinity of the apicoplast (Jacot et al. 2013). Such a tethering function of myosin class Va has been observed for melanosomes in mouse melanocytes for their long-distance transport on microtubules (Hammer and Sellers 2012). We might hypothesize that rhoptries made *de novo* are first tethered by TgMyoF and then transported longer distances by microtubule-binding motor(s), explaining why some rhoptries are found lost in the residual body while most of them are still accurately transported and anchored to the apical pole (Lentini et al. 2019). Alternatively, the rhoptries observed in the residual body might be the ones of the mother that were not properly recycled during the cell division process.

Interestingly, TgMyoF is also found in chromerids, which possess a photosynthetic plastid. It is likely that the function of TgMyoF in positioning of the centrosomes and inheritance of the plastid is conserved in these organisms.

14.3.4 Vital Contribution of the Actomyosin System to Motility

MyoA has been identified in *T. gondii* as the motor responsible for the motility of the tachyzoite, powering the movement within the glideosome complex (Meissner et al. 2002). Conditional depletion of this motor clearly demonstrated its critical role for invasion of and egress from the host cell as well as virulence in mice. In *P. berghei*, a promoter-swap strategy has been used to down-regulate PbMyoA in the motile ookinete stage (Siden-Kiamos et al. 2011). This demonstrated the essential role of the protein for motility since no sign of productive gliding locomotion was recorded. As a consequence, the formation of oocysts was completely abolished and no sporozoite were found to be transmitted from the mosquito to a new host.

MyoA belongs to the class XIV myosins and is conserved across the phylum Apicomplexa (Table 14.1). It is one of the smallest myosins (93 kDa), exhibiting a short neck domain with degenerated IQ motifs and no tail (Heintzelman and Schwartzman 1997; Herm-Götz et al. 2002). Moreover, MyoA lacks two key conserved residues in the motor domain, one in the actin-binding surface loop and one in the pivot-point for the motion of the lever arm.

TgMyoA was the first apicomplexan motor that has been directly purified from the parasites for biochemical and biophysical characterization (Herm-Götz et al. 2002). TgMyoA is a monomeric and plus-end-directed motor and despite its unusual features, it exhibits the kinetic properties and velocity of a fast myosin such as the conventional skeletal muscle myosins designed to generate movement rather than force. TgMyoA is non-processive and likely functions in the context of large motor arrays. MyoA localizes to the periphery of the tachyzoites and all motile stages of *Plasmodium*, in tight association with the membrane, a localization dependent on a dibasic motif (two arginines) conserved across the phylum (Hettmann et al. 2000; Green et al. 2017). One myosin light chain (MLC) and one essential light chain (ELC) have been associated with TgMyoA and PfMyoA (Nebl et al. 2011; Williams et al. 2015; Bookwalter et al. 2017; Green et al. 2017) (Table 14.3). TgMLC1, named MyoA-tail interacting protein (MTIP) in *Plasmodia*, is conserved throughout the phylum and is unusual, presenting a long N-terminal extension of 70 residues preceding the CaM-like domain composed of degenerated EF-hands (Herm-Götz et al. 2002; Bergman et al. 2003). The solved structures of the CaM-like domain of TgMLC1 and PfMTIP bound to the neck of MyoA revealed a conserved clamping conformation of the EF-hands around the posterior region of the neck and a buried electrostatic surface between the two proteins as found for other myosin heavy/light chain interaction previously determined (Bosch et al. 2007; Powell et al. 2017). However, this binding is not influenced by the presence of calcium (Green et al. 2006; Bookwalter et al. 2014). In addition, dissection of TgMLC1 mutants in *T. gondii* identified the N-terminal extension as responsible for the localization of TgMyoA at the IMC, thus substituting for the role of the myosin heavy chain tail that TgMyoA lacks (Frénal et al. 2010). Upstream of the MLC1/MTIP binding site, one essential light chain has been identified first in *T. gondii* and very recently in *Plasmodium* species (Nebl et al. 2011; Bookwalter et al. 2017; Green et al. 2017). Surprisingly, the sequence identity between TgELC and PfELC is low (approximately 20%) and prevented the identification of PfELC based on homology search (Bookwalter et al. 2017; Green et al. 2017). In fact, in *T. gondii*, two ELCs, named TgELC1 and TgELC2, compete for the same binding site on the neck of TgMyoA, but TgELC1 is likely and predominantly bound since it was the only one identified by mass spectrometry following co-immunoprecipitation of the glideosome (Nebl et al. 2011; Williams et al. 2015). TgELC1 and TgELC2 are individually

dispensable but cannot be deleted at the same time. Indeed, their contribution to the glideosome complex is essential since their disruption totally destabilizes TgMyoA (Williams et al. 2015). The same is true for the myosin light chain. When TgMLC1 is depleted in tachyzoites or when PbMTIP is depleted in *P. berghei* ookinetes, TgMyoA and PbMyoA are also fully depleted (Sebastian et al. 2012; Egarter et al. 2014). Therefore, the myosin light chain MTIP/MLC1 is essential in both species.

Until recently, it had not been possible to produce soluble and functional apicomplexan myosins from heterologous expression systems, which hampered structural assessment of the unusual features of MyoA and its bound light chains. Remarkably, in 2014, Bookwalter et al. identified the ortholog of the striated muscle myosin-specific co-chaperone of the UCS protein family, Unc45b, in the *T. gondii* genome (Bookwalter et al. 2014). They succeeded in producing soluble and functional TgMyoA/TgMLC1 and TgMyoA/TgMLC1/TgELC1 complexes by co-expressing these proteins in the presence of the co-chaperone TgUNC. This not only led to the determination of the kinetics of the motor in the presence of its light chains in both *T. gondii* (Bookwalter et al. 2014) and *P. falciparum* (Bookwalter et al. 2017) but also to structural insight of TgMyoA bound to its light chains (Powell et al. 2017, 2018). In both parasites, it was elegantly demonstrated with the *in vitro* motility assay that the binding of ELC in addition to MLC/MTIP doubles the speed of the actin movement (Bookwalter et al. 2014, 2017). ELC binds upstream of MLC to the neck domain of MyoA but also to the converter of the head domain (Powell et al. 2017). With the two bound light chains, the length and stability of the lever arm is increased and optimized for force transduction. Interestingly, binding of ELC and MLC is cooperative and requires first binding of MLC to MyoA (Bookwalter et al. 2017; Powell et al. 2017). This could be due to the fact that TgMyoA needs TgMLC1 for its localization *in vivo* (Frénal et al. 2010), a possible pre-requisite for the binding of TgELC1.

The crystal structure of TgMyoA solved in complex with the CaM-like domain of TgMLC1 was an important step forward. It revealed that mutations of the key residues implicated in binding to actin and in the function of the motor domain are a clear adaptation to the divergent TgACT1 and create new interactions that maintain and possibly enhance the transduction of the force from the active site to the lever arm (Powell et al. 2018). These results unravel the mystery of MyoA being a *bona fide* fast motor despite its unusual features.

It remains to be determined how the function of the motor is regulated. Calcium seems to regulate the assembly of the motor complex since the cooperative binding of the light chains to MyoA is further increased in the presence of calcium (Powell et al. 2017). Phosphorylation of TgMyoA and PfMyoA appear to modulate rather than activate the motor since phospho-mimetic mutants enhanced the affinity for actin filaments and the speed of their displacement *in vitro* (Bookwalter et al. 2017; Powell et al. 2018). *In vivo*, some phosphorylation sites on TgMyoA seem to be important for the activation of the motility while no site on TgMLC1 was found to be critical to modulate gliding (Jacot et al. 2014; Gaji et al. 2015).

Unexpectedly, the gene coding for *TgMyoA* has been successfully deleted in *T. gondii* tachyzoites (Andenmatten et al. 2013). Parasites could be maintained in culture although their lytic cycle was severely impacted with a strong defect in motility, invasion, and egress. The isolation of this mutant raised the question of how some motility can still be achieved without TgMyoA. The identification of a second glideosome complex similar to the initial one but located at the basal ring of the parasite, which includes the class XIV TgMyoC instead of TgMyoA, raised the possibility of a functional complementation between the complexes, especially because TgMyoC shares the two light chains TgMLC1 and TgELC1 with TgMyoA (Frénal et al. 2014). Indeed, in the absence of TgMyoA, a relocalization of TgMyoC along the pellicle was observed, highlighting the plasticity and adaptation of the parasite to ensure comple-

tion of the vital step of host cell invasion (Frénal et al. 2014, 2017b). Accordingly, parasite clones with a simultaneous deletion of *MyoA* and *MyoB/C* could not be isolated (Egarter et al. 2014). In contrast to MyoA, MyoC is not conserved across the Apicomplexa, especially in *Plasmodium* species (Table 14.1). In these parasites, MyoA is therefore likely essential for motility as in *P. berghei* ookinete wherein down-regulation of PbMyoA completely abrogated gliding and blocked the life-cycle progression of the parasite into the mosquito vector (Siden-Kiamos et al. 2011).

A third motor from the class XIV, TgMyoH, has been found to be crucially involved in motility of the tachyzoites (Graindorge et al. 2016). TgMyoH is located in the conoid, at the apex of the parasites, and its conditional depletion led to a severe defect in motility, invasion, and egress from the infected cells. Invasion experiments demonstrated that, in contrast to wild-type parasites that completed invasion, TgMyoH-depleted parasites were attached to the surface of the host cell by their tip, forming a moving junction that cannot be translocated along the parasite body. In the same experiment, TgMyoA-depleted parasites were engaged in the penetration into the host cell, but most of them stopped at the level where the IMC starts. These results indicate that a relay of myosins is involved in the translocation of the adhesins along the parasites with TgMyoH initiating the process at the apex until the edge of the IMC, then TgMyoA along the pellicle and finally TgMyoC at the basal ring (Fig. 14.3). Noteworthy in this context, in the absence of TgMyoC, TgMyoA is additionally found at the basal ring (Frénal et al. 2014). The precise role of TgMyoC is therefore unknown, but it might be involved in the parasite twisting motion observed at the very end of the invasion process that enables sealing of the PV (Pavlou et al. 2018).

TgMyoH belongs to class XIV and orthologs are found in other coccidians such as *Eimeria* and *Cryptosporidium* that harbor a conoid but also in piroplasma such as *Theileria* and *Babesia* that do not (Table 14.1) (Mueller et al. 2017). However, no direct ortholog has been identified in *Plasmodium* species. Its sequence predicts a neck region with eight IQ motifs and a tail harboring three α-tubulin suppressor 1 (ATS1) or RCC1 (Regulator of chromosome condensation 1) domains. These domains target TgMyoH to the apex of the parasite, linking directly or not TgMyoH to the conoid fibers (Graindorge et al. 2016). Six CaM-containing domain proteins have been found associated with TgMyoH (Graindorge et al. 2016; Long et al. 2017). Four of them, TgMLC5, TgCaM1, TgCaM2, and TgCaM3, are only associated with TgMyoH, since their apical localization is disrupted when TgMyoH is down-regulated, but no difference in the localization of the two others, TgMLC1 and TgMLC7, was observed. In addition to TgMLC1, only TgCaM3 appears essential for tachyzoite survival (Long et al. 2017) (Table 14.3). The function of this protein is not dependent on the presence of calcium, suggesting a structural role of TgCaM3 in the neck domain of TgMyoH, in contrast to TgCaM1 and TgCaM2, which might have a regulatory role since their function is calcium-dependent (Long et al. 2017).

While no direct ortholog of TgMyoH has been found in *Plasmodium* species, PbMyoB, which was characterized in *P. berghei*, might be a functional homolog (Yusuf et al. 2015). PbMyoB, like TgMyoH, belongs to myosin class XIVc, but it is significantly smaller since it exhibits a shorter neck with one predicted IQ motif and no tail (Foth et al. 2006). PbMyoB has been localized at the extreme apical pole, likely at the apical polar rings, of all the motile forms of the parasite (merozoite, ookinete and sporozoite). Its associated light chain, PbMLC-B, is quite atypical being very long (652 aa) and possessing two coiled-coil domains, similar to TgMLC3, which is also found at the apex of the tachyzoite (Graindorge et al. 2016). Functional studies would be needed to determine the role of this complex in *Plasmodium,* although PbMyoB appeared dispensable both in the high throughput knockout screen of *P. berghei* genes (Bushell et al. 2017) as well as a specific reverse genetics approach (Wall et al. 2019). In contrast, PbMyoE is found at the basal pole of the motile ookinete and sporozoite (Table 14.1), and its deletion severely impacts the motility of the sporozoite (Wall et al. 2019).

In line with the role of myosin motors, TgACT1 and PfACT1 have been shown to be essential for gliding motility. *T. gondii* tachyzoites are severely impaired in their motility, invasion capacity and exit from the infected cell (Egarter et al. 2014; Drewry and Sibley 2015). In contrast, although invasion of the erythrocyte by *P. falciparum* merozoites is completely abolished in the absence of actin, egress is not (Das et al. 2017). For both parasites, egress involves the rupture the parasitophorous vacuole membrane and the host cell plasma membrane, which is assisted by the release of perforins from the micronemes (Kafsack et al. 2009; Garg et al. 2013). While the tachyzoite needs to impose an additional mechanical pressure on the membranes applied by its motility to exit the cell (Meissner et al. 2002; Plattner et al. 2008; Frénal et al. 2010; Mehta and Sibley 2011; Graindorge et al. 2016; Jacot et al. 2016), the schizonts activate parasite and host proteases that destabilize the cytoskeleton of the red blood cell, and it is not clear that motility is required (Millholland et al. 2011). The actin depletion performed in *Plasmodium* indicates that motility is absolutely required during invasion for the moving junction to progress backward along the parasite but not for egress, for which the destabilization of the erythrocyte cytoskeleton and then the curling of the red blood cell membrane might be sufficient to eject the merozoites into the bloodstream (Das et al. 2017).

14.4 ABPs Regulate the Function of the Actomyosin Systems

ABPs that influence actin turnover have obvious impacts on the function of the actomyosin systems. The two main actin monomer-sequestering proteins, ADF and PRF, have been shown to have a strong impact on motility, invasion, and egress of *T. gondii* and *P. berghei* (Plattner et al. 2008; Mehta and Sibley 2011; Moreau et al. 2017). In addition, depletion of TgADF and TgPRF also revealed a defect in the inheritance of the plastid-like apicoplast in daughter cells (Jacot et al. 2013). Contrastingly, the G-actin-sequestering protein TgCAP, which is also critical for gliding motility, invasion, and egress of *T. gondii*, as well as for dense-granule trafficking and parasite connection, has no influence on apicoplast inheritance (Hunt et al. 2019). These observations reflect the different spatial requirements for actin turnover within the parasite. In *Plasmodium*, PbCAP has an essential role only in the oocyst stage within the mosquito (Hliscs et al. 2010). In the absence of PbCAP, maturation of the oocysts is compromised and no sporozoites are formed, preventing transmission of parasites from the mosquito to a new host.

The growth of actin filaments is regulated by capping proteins. The heterodimer PbCPα/β has the ability to decrease the length of rabbit actin filaments *in vitro* (Ganter et al. 2009). *In vivo*, disruption of PbCPβ had no impact on the erythrocytic cycle of the parasite, but in the *Anopheles* mosquito vector, the sporozoites displayed a strong defect in motility preventing them from colonizing the salivary glands and therefore blocking transmission of the parasites to a new host (Ganter et al. 2009). Unexpectedly, PbCPα appears to be essential alone in the erythrocytic cycle likely working as a homodimer, but its precise role has not been assessed yet (Ganter et al. 2015). One hypothesis for the split role of these dimers is the environment-dependent function with PbCPα/β working at ambient temperature in the mosquito while the PbCPα homodimer could be adapted to the warm-blooded host.

Actin polymerization is also regulated by coronin (COR). Both TgCOR and PfCOR are able to bind F-actin and increase its polymerization and bundling *in vitro* (Salamun et al. 2014; Olshina et al. 2015). Deletion of TgCOR revealed that this protein is not essential in tachyzoites with only a modest effect on the invasion and egress steps of the lytic cycle (Salamun et al. 2014). Yet, interestingly, TgCOR is cytosolic but strikingly relocalizes to the posterior pole in motile parasites, independently of actin dynamics but concomitantly to microneme secretion (Salamun et al. 2014). This suggests that TgCOR could play a role in endocytosis and membrane

recycling linked to the microneme exocytosis to eliminate excessive accumulation of membranes at the posterior pole and preserve the pellicle integrity. A relocalization from the periphery to the rear of the parasite has also been observed in the sporozoite of *P. berghei* during motility, but this time in an actin-dependent manner occurring downstream of the calcium-signaling cascade leading to microneme secretion (Bane et al. 2016). Sporozoites lacking PbCOR are impaired in motility and in their ability to colonize the salivary glands of the *Anopheles* mosquito (Bane et al. 2016). Recently, PfCOR has also been associated with artemisinin resistance. Indeed, long-term *in vitro* culture of *P. falciparum* cell lines under dihydroartemisinin selection allowed the isolation of mutants presenting several point mutations in the beta-propeller region of PfCOR (Demas et al. 2018). After *PfKelch13*, *PfCOR* is the second gene demonstrated to confer reduced artemisinin susceptibility and the conservation of the beta-propeller motif in the two proteins suggests a common mechanism of resistance and the possible emergence of PfCOR mutants in nature.

14.5 Conclusion

Over the last decade, a big step forward has been made in elucidating the role of myosin heavy chains, visualizing actin filaments, and characterizing regulatory ABPs in *Toxoplasma* and *Plasmodium*. This led to the identification of actomyosin systems serving three major processes in these parasites; (i) organelle trafficking, positioning and inheritance, (ii) basal pole constriction and intravacuolar cell-cell connection and (iii) motility, invasion, and egress. Until recently, it was really challenging to purify soluble and functional apicomplexan myosin heavy chains from heterologous systems. The identification of the *T. gondii* homolog of a myosin-specific co-chaperone of the UCS (UNC-45/CRO1/She4p) family changed this and has been a key factor in producing TgMyoA and its light chains from the baculovirus/*Sf9* insect cell expression system (Bookwalter et al. 2014). This allowed in-depth biochemical and structural characterization of TgMyoA/TgMLC1 and TgMyoA/TgMLC1/TgELC1 complexes uncovering mechanistic and regulatory aspects of these interactions (Bookwalter et al. 2014; Powell et al. 2017, 2018). Functional study of the chaperone TgUNC in *T. gondii* tachyzoites demonstrated that it is indeed a *bona fide* myosin chaperone in the parasite (Frénal et al. 2017b). All 11 myosin heavy chains expressed were destabilized upon depletion of TgUNC, and the phenotype of its down-regulation is a combination of the phenotypes of each myosin heavy chain described previously.

The repertoire of myosin heavy chains has been localized in both *Toxoplasma* and *Plasmodium,* and all the essential motors have been functionally characterized in *T. gondii* (Wall et al. 2019; Jacot et al. 2013; Graindorge et al. 2016; Frénal et al. 2017b). It remains now to assess the function of the myosin heavy chains in *Plasmodium* and to identify the components of the different actomyosin systems, especially the proteins of the basal complex that could be involved in the constriction and cytokinesis of the parasites, a process shared by all the parasites of the phylum. To understand the function and regulation of the myosin heavy chains, it also remains to identify the associated myosin light chains (MLCs). Several of them have been localized in *T. gondii* (Polonais et al. 2011) (Table 14.3) but not yet demonstrated as being associated with a motor. The limited repertoire of classical MLCs suggests that some other EF-hand-containing proteins could act as myosin light chains. Three calmodulins (TgCAM1–3) have been identified as light chains for TgMyoH (Long et al. 2017), and it might be worth exploring the possibility that some centrins could also play this role, especially TgCEN2, which shares the same function as TgMyoJ in the basal complex constriction.

A better understanding of the dynamics of the actomyosin system has been provided by the biochemical and functional characterization of ABPs that unraveled unusual features of these proteins compared to other eukaryotes. The genome of *Toxoplasma* and *Plasmodium* further encodes a

large repertoire of actin-like and actin-related proteins that has not yet been explored, with several of them being likely critical for the survival of the parasites as suggested by the genome wide screens (Table 14.2). Characterization of these proteins should provide new insights on the contribution of actomyosin systems to the diverse cellular functions of the parasite.

References

Andenmatten N, Egarter S, Jackson AJ et al (2013) Conditional genome engineering in *Toxoplasma gondii* uncovers alternative invasion mechanisms. Nat Methods 10:125–127. https://doi.org/10.1038/nmeth.2301

Angrisano F, Riglar DT, Sturm A et al (2012) Spatial localisation of actin filaments across developmental stages of the malaria parasite. PLoS One 7:e32188. https://doi.org/10.1371/journal.pone.0032188

Bane KS, Lepper S, Kehrer J et al (2016) The actin filament-binding protein coronin regulates motility in *Plasmodium* Sporozoites. PLoS Pathog 12:e1005710. https://doi.org/10.1371/journal.ppat.1005710

Baroni L, Pereira LM, Maciver SK, Yatsuda AP (2018) Functional characterisation of the actin-depolymerising factor from the apicomplexan *Neospora caninum* (NcADF). Mol Biochem Parasitol 224:26–36. https://doi.org/10.1016/j.molbiopara.2018.07.008

Baum J, Papenfuss AT, Baum B et al (2006) Regulation of apicomplexan actin-based motility. Nat Rev Microbiol 4:621–628. https://doi.org/10.1038/nrmicro1465

Baum J, Tonkin CJ, Paul AS et al (2008) A malaria parasite formin regulates actin polymerization and localizes to the parasite-erythrocyte moving junction during invasion. Cell Host Microbe 3:188–198. https://doi.org/10.1016/j.chom.2008.02.006

Bergman LW, Kaiser K, Fujioka H et al (2003) Myosin A tail domain interacting protein (MTIP) localizes to the inner membrane complex of *Plasmodium* sporozoites. J Cell Sci 116:39–49

Bichet M, Joly C, Henni AH et al (2014) The toxoplasma-host cell junction is anchored to the cell cortex to sustain parasite invasive force. BMC Biol 12:773. https://doi.org/10.1186/s12915-014-0108-y

Bookwalter CS, Kelsen A, Leung JM et al (2014) A *Toxoplasma gondii* class XIV myosin, expressed in Sf9 cells with a parasite co-chaperone, requires two light chains for fast motility. J Biol Chem 289:30832–30841. https://doi.org/10.1074/jbc.M114.572453

Bookwalter CS, Tay CL, McCrorie R et al (2017) Reconstitution of the core of the malaria parasite glideosome with recombinant *Plasmodium* class XIV myosin A and *Plasmodium* actin. J Biol Chem 292:19290–19303. https://doi.org/10.1074/jbc.M117.813972

Bosch J, Turley S, Roach CM et al (2007) The closed MTIP-myosin A-tail complex from the malaria parasite invasion machinery. J Mol Biol 372:77–88. https://doi.org/10.1016/j.jmb.2007.06.016

Bushell E, Gomes AR, Sanderson T et al (2017) Functional profiling of a plasmodium genome reveals an abundance of essential genes. Cell 170:260–272.e8. https://doi.org/10.1016/j.cell.2017.06.030

Cooper JA, Sept D (2008) New insights into mechanism and regulation of actin capping protein. Int Rev Cell Mol Biol 267:183–206. https://doi.org/10.1016/S1937-6448(08)00604-7

Daher W, Plattner F, Carlier M-F, Soldati-Favre D (2010) Concerted action of two formins in gliding motility and host cell invasion by *Toxoplasma gondii*. PLoS Pathog 6:e1001132. https://doi.org/10.1371/journal.ppat.1001132

Daher W, Klages N, Carlier M-F, Soldati-Favre D (2012) Molecular characterization of *Toxoplasma gondii* formin 3, an actin nucleator dispensable for tachyzoite growth and motility. Eukaryot Cell 11:343–352. https://doi.org/10.1128/EC.05192-11

Das S, Lemgruber L, Tay CL et al (2017) Multiple essential functions of *Plasmodium falciparum* actin-1 during malaria blood-stage development. BMC Biol 15:70. https://doi.org/10.1186/s12915-017-0406-2

de Hostos EL (1999) The coronin family of actin-associated proteins. Trends Cell Biol 9:345–350

Deligianni E, Morgan RN, Bertuccini L et al (2011) Critical role for a stage-specific actin in male exflagellation of the malaria parasite. Cell Microbiol 13:1714–1730. https://doi.org/10.1111/j.1462-5822.2011.01652.x

Demas AR, Sharma AI, Wong W et al (2018) Mutations in *Plasmodium falciparum* actin-binding protein coronin confer reduced artemisinin susceptibility. Proc Natl Acad Sci U S A 115:12799–12804. https://doi.org/10.1073/pnas.1812317115

Dobrowolski JM, Niesman IR, Sibley LD (1997) Actin in the parasite *Toxoplasma gondii* is encoded by a single copy gene, ACT1 and exists primarily in a globular form. Cell Motil Cytoskeleton 37:253–262. https://doi.org/10.1002/(SICI)1097-0169(1997)37:3<253::AID-CM7>3.0.CO;2-7

Dominguez R, Holmes KC (2011) Actin structure and function. Annu Rev Biophys 40:169–186. https://doi.org/10.1146/annurev-biophys-042910-155359

Douglas RG, Nandekar P, Aktories J-E et al (2018) Intersubunit interactions drive divergent dynamics in mammalian and *Plasmodium* actin filaments. PLoS Biol 16:e2005345. https://doi.org/10.1371/journal.pbio.2005345

Drewry LL, Sibley LD (2015) *Toxoplasma* actin is required for efficient host cell invasion. MBio 6:e00557. https://doi.org/10.1128/mBio.00557-15

Egarter S, Andenmatten N, Jackson AJ et al (2014) The toxoplasma Acto-MyoA motor complex is important but not essential for gliding motility and host cell invasion. PLoS One 9:e91819. https://doi.org/10.1371/journal.pone.0091819

Foth BJ, Goedecke MC, Soldati D (2006) New insights into myosin evolution and classification. Proc Natl Acad Sci 103:3681–3686. https://doi.org/10.1073/pnas.0506307103

Francia ME, Striepen B (2014) Cell division in apicomplexan parasites. Nat Rev Microbiol 12:125–136. https://doi.org/10.1038/nrmicro3184

Frénal K, Polonais V, Marq J-B et al (2010) Functional dissection of the apicomplexan glideosome molecular architecture. Cell Host Microbe 8:343–357. https://doi.org/10.1016/j.chom.2010.09.002

Frénal K, Marq J-B, Jacot D et al (2014) Plasticity between MyoC- and MyoA-glideosomes: an example of functional compensation in *Toxoplasma gondii* invasion. PLoS Pathog 10:e1004504. https://doi.org/10.1371/journal.ppat.1004504

Frénal K, Dubremetz J-F, Lebrun M, Soldati-Favre D (2017a) Gliding motility powers invasion and egress in Apicomplexa. Nat Rev Microbiol 15:645–660. https://doi.org/10.1038/nrmicro.2017.86

Frénal K, Jacot D, Hammoudi P-M et al (2017b) Myosin-dependent cell-cell communication controls synchronicity of division in acute and chronic stages of *Toxoplasma gondii*. Nat Commun 8:15710. https://doi.org/10.1038/ncomms15710

Gaji RY, Johnson DE, Treeck M et al (2015) Phosphorylation of a myosin motor by TgCDPK3 facilitates rapid initiation of motility during *Toxoplasma gondii* egress. PLoS Pathog 11:e1005268. https://doi.org/10.1371/journal.ppat.1005268

Ganter M, Schüler H, Matuschewski K (2009) Vital role for the *Plasmodium* actin capping protein (CP) beta-subunit in motility of malaria sporozoites. Mol Microbiol 74:1356–1367. https://doi.org/10.1111/j.1365-2958.2009.06828.x

Ganter M, Rizopoulos Z, Schüler H, Matuschewski K (2015) Pivotal and distinct role for Plasmodium actin capping protein alpha during blood infection of the malaria parasite. Mol Microbiol 96:84–94. https://doi.org/10.1111/mmi.12922

Garg S, Agarwal S, Kumar S et al (2013) Calcium-dependent permeabilization of erythrocytes by a perforin-like protein during egress of malaria parasites. Nat Commun 4:1736. https://doi.org/10.1038/ncomms2725

Gordon JL, Sibley LD (2005) Comparative genome analysis reveals a conserved family of actin-like proteins in apicomplexan parasites. BMC Genomics 6:179. https://doi.org/10.1186/1471-2164-6-179

Gould SB, Tham W-H, Cowman AF et al (2008) Alveolins, a new family of cortical proteins that define the protist infrakingdom Alveolata. Mol Biol Evol 25:1219–1230. https://doi.org/10.1093/molbev/msn070

Graindorge A, Frénal K, Jacot D et al (2016) The conoid associated motor MyoH is indispensable for *Toxoplasma gondii* entry and exit from host cells. PLoS Pathog 12:e1005388. https://doi.org/10.1371/journal.ppat.1005388

Green JL, Martin SR, Fielden J et al (2006) The MTIP-myosin A complex in blood stage malaria parasites. J Mol Biol 355:933–941. https://doi.org/10.1016/j.jmb.2005.11.027

Green JL, Wall RJ, Vahokoski J et al (2017) Compositional and expression analyses of the glideosome during the *Plasmodium* life cycle reveal an additional myosin light chain required for maximum motility. J Biol Chem 292:17857–17875. https://doi.org/10.1074/jbc.M117.802769

Hakimi M-A, Olias P, Sibley LD (2017) *Toxoplasma* effectors targeting host signaling and transcription. Clin Microbiol Rev 30:615–645. https://doi.org/10.1128/CMR.00005-17

Hammer JA, Sellers JR (2012) Walking to work: roles for class V myosins as cargo transporters. Nat Rev Mol Cell Biol 13:13–26. https://doi.org/10.1038/nrm3248

Harding CR, Meissner M (2014) The inner membrane complex through development of *Toxoplasma gondii* and *Plasmodium*. Cell Microbiol 16:632–641. https://doi.org/10.1111/cmi.12285

Harvey KL, Yap A, Gilson PR et al (2014) Insights and controversies into the role of the key apicomplexan invasion ligand, apical membrane antigen 1. Int J Parasitol 44:853–857. https://doi.org/10.1016/j.ijpara.2014.08.001

Heaslip AT, Nelson SR, Warshaw DM (2016) Dense granule trafficking in *Toxoplasma gondii* requires a unique class 27 myosin and actin filaments. Mol Biol Cell 27:2080–2089. https://doi.org/10.1091/mbc.E15-12-0824

Heintzelman MB, Schwartzman JD (1997) A novel class of unconventional myosins from *Toxoplasma gondii*. J Mol Biol 271:139–146. https://doi.org/10.1006/jmbi.1997.1167

Herm-Götz A, Weiss S, Stratmann R et al (2002) *Toxoplasma gondii* myosin A and its light chain: a fast, single-headed, plus-end-directed motor. EMBO J 21:2149–2158. https://doi.org/10.1093/emboj/21.9.2149

Herm-Götz A, Delbac F, Weiss S et al (2006) Functional and biophysical analyses of the class XIV *Toxoplasma gondii* myosin D. J Muscle Res Cell Motil 27:139–151. https://doi.org/10.1007/s10974-005-9046-1

Hettmann C, Herm A, Geiter A et al (2000) A dibasic motif in the tail of a class XIV apicomplexan myosin is an essential determinant of plasma membrane localization. Mol Biol Cell 11:1385–1400. https://doi.org/10.1091/mbc.11.4.1385

Hliscs M, Sattler JM, Tempel W et al (2010) Structure and function of a G-actin sequestering protein with a vital role in malaria oocyst development inside the mosquito vector. J Biol Chem 285:11572–11583. https://doi.org/10.1074/jbc.M109.054916

Hliscs M, Millet C, Dixon MW et al (2015) Organization and function of an actin cytoskeleton in *Plasmodium falciparum* gametocytes. Cell Microbiol 17:207–225. https://doi.org/10.1111/cmi.12359

Hu K (2008) Organizational changes of the daughter basal complex during the parasite replication of *Toxoplasma gondii*. PLoS Pathog 4:e10. https://doi.org/10.1371/journal.ppat.0040010

Hu K, Roos DS, Murray JM (2002) A novel polymer of tubulin forms the conoid of *Toxoplasma gondii*. J Cell Biol 156:1039–1050. https://doi.org/10.1083/jcb.200112086

Hu K, Johnson J, Florens L et al (2006) Cytoskeletal components of an invasion machine – the apical complex of *Toxoplasma gondii*. PLoS Pathog 2:e13. https://doi.org/10.1371/journal.ppat.0020013

Hunt A, Russell MRG, Wagener J et al (2019, October 2) Differential requirements for cyclase-associated protein (CAP) in actin-dependent processes of Toxoplasma gondii. Elife 8:pii: e50598. https://doi.org/10.7554/eLife.50598.001

Jacot D, Daher W, Soldati-Favre D (2013) *Toxoplasma gondii* myosin F, an essential motor for centrosomes positioning and apicoplast inheritance. EMBO J 32:1702–1716. https://doi.org/10.1038/emboj.2013.113

Jacot D, Frénal K, Marq J-B et al (2014) Assessment of phosphorylation in *Toxoplasma* glideosome assembly and function. Cell Microbiol 16:1518–1532. https://doi.org/10.1111/cmi.12307

Jacot D, Tosetti N, Pires I et al (2016) An Apicomplexan actin-binding protein serves as a connector and lipid sensor to coordinate motility and invasion. Cell Host Microbe 20:731–743. https://doi.org/10.1016/j.chom.2016.10.020

Kadirvel P, Anishetty S (2018) Potential role of salt-bridges in the hinge-like movement of apicomplexa specific β-hairpin of *Plasmodium* and *Toxoplasma* profilins: a molecular dynamics simulation study. J Cell Biochem 119:3683–3696. https://doi.org/10.1002/jcb.26579

Kafsack BFC, Pena JDO, Coppens I et al (2009) Rapid membrane disruption by a perforin-like protein facilitates parasite exit from host cells. Science 323:530–533. https://doi.org/10.1126/science.1165740

Kucera K, Koblansky AA, Saunders LP et al (2010) Structure-based analysis of *Toxoplasma gondii* profilin: a parasite-specific motif is required for recognition by toll-like receptor 11. J Mol Biol 403:616–629. https://doi.org/10.1016/j.jmb.2010.09.022

Kumpula E-P, Pires I, Lasiwa D et al (2017) Apicomplexan actin polymerization depends on nucleation. Sci Rep 7:12137. https://doi.org/10.1038/s41598-017-11330-w

Kumpula E-P, Lopez AJ, Tajedin L et al (2019) Atomic view into *Plasmodium* actin polymerization, ATP hydrolysis, and fragmentation. PLoS Biol 17:e3000315. https://doi.org/10.1371/journal.pbio.3000315

Kursula I, Kursula P, Ganter M et al (2008) Structural basis for parasite-specific functions of the divergent profilin of *Plasmodium falciparum*. Structure 16:1638–1648. https://doi.org/10.1016/j.str.2008.09.008

Lentini G, Dubois DJ, Maco B et al (2019) The roles of CEN2 and DLC8a in apical secretory organelles discharge of *Toxoplasma gondii*. Traffic 20:583–600. https://doi.org/10.1111/tra.12673

Letunic I, Bork P (2018) 20 years of the SMART protein domain annotation resource. Nucleic Acids Res 46(D1)D493–D496. https://doi.org/10.1093/nar/gkx922

Long S, Brown KM, Drewry LL et al (2017) Calmodulin-like proteins localized to the conoid regulate motility and cell invasion by *Toxoplasma gondii*. PLoS Pathog 13:e1006379. https://doi.org/10.1371/journal.ppat.1006379

Makkonen M, Bertling E, Chebotareva NA et al (2013) Mammalian and malaria parasite cyclase-associated proteins catalyze nucleotide exchange on G-actin through a conserved mechanism. J Biol Chem 288:984–994. https://doi.org/10.1074/jbc.M112.435719

Mehta S, Sibley LD (2010) *Toxoplasma gondii* actin depolymerizing factor acts primarily to sequester G-actin. J Biol Chem 285:6835–6847. https://doi.org/10.1074/jbc.M109.068155

Mehta S, Sibley LD (2011) Actin depolymerizing factor controls actin turnover and gliding motility in *Toxoplasma gondii*. Mol Biol Cell 22:1290–1299. https://doi.org/10.1091/mbc.E10-12-0939

Meissner M, Schlüter D, Soldati D (2002) Role of *Toxoplasma gondii* myosin A in powering parasite gliding and host cell invasion. Science 298:837–840. https://doi.org/10.1126/science.1074553

Mercier C, Cesbron-Delauw M-F (2015) *Toxoplasma* secretory granules: one population or more? Trends Parasitol 31:60–71. https://doi.org/10.1016/j.pt.2014.12.002

Millholland MG, Chandramohanadas R, Pizzarro A et al (2011) The malaria parasite progressively dismantles the host erythrocyte cytoskeleton for efficient egress. Mol Cell Proteomics 10:M111.010678. https://doi.org/10.1074/mcp.M111.010678

Monteiro VG, de Melo EJ, Attias M, de Souza W (2001) Morphological changes during conoid extrusion in *Toxoplasma gondii* tachyzoites treated with calcium ionophore. J Struct Biol 136:181–189. https://doi.org/10.1006/jsbi.2002.4444

Mordue DG, Håkansson S, Niesman I, Sibley LD (1999) *Toxoplasma gondii* resides in a vacuole that avoids fusion with host cell endocytic and exocytic vesicular trafficking pathways. Exp Parasitol 92:87–99

Moreau CA, Bhargav SP, Kumar H et al (2017) A unique profilin-actin interface is important for malaria parasite motility. PLoS Pathog 13:e1006412. https://doi.org/10.1371/journal.ppat.1006412

Mueller C, Klages N, Jacot D et al (2013) The *Toxoplasma* protein ARO mediates the apical positioning of rhoptry organelles, a prerequisite for host cell invasion. Cell Host Microbe 13:289–301. https://doi.org/10.1016/j.chom.2013.02.001

Mueller C, Graindorge A, Soldati-Favre D (2017) Functions of myosin motors tailored for parasitism. Curr Opin Microbiol 40:113–122. https://doi.org/10.1016/j.mib.2017.11.003

Nebl T, Prieto JH, Kapp E et al (2011) Quantitative in vivo analyses reveal calcium-dependent phos-

phorylation sites and identifies a novel component of the toxoplasma invasion motor complex. PLoS Pathog 7:e1002222. https://doi.org/10.1371/journal.ppat.1002222

Nishi M, Hu K, Murray JM, Roos DS (2008) Organellar dynamics during the cell cycle of *Toxoplasma gondii*. J Cell Sci 121:1559–1568. https://doi.org/10.1242/jcs.021089

Odronitz F, Kollmar M (2007) Drawing the tree of eukaryotic life based on the analysis of 2,269 manually annotated myosins from 328 species. Genome Biol 8:R196. https://doi.org/10.1186/gb-2007-8-9-r196

Olshina MA, Angrisano F, Marapana DS et al (2015) *Plasmodium falciparum* coronin organizes arrays of parallel actin filaments potentially guiding directional motility in invasive malaria parasites. Malar J 14:280. https://doi.org/10.1186/s12936-015-0801-5

Pavlou G, Biesaga M, Touquet B et al (2018) *Toxoplasma* parasite twisting motion mechanically induces host cell membrane fission to complete invasion within a protective vacuole. Cell Host Microbe 24:81–96.e5. https://doi.org/10.1016/j.chom.2018.06.003

Periz J, Whitelaw J, Harding C et al (2017) *Toxoplasma gondii* F-actin forms an extensive filamentous network required for material exchange and parasite maturation. Elife 6:pii: e24119. https://doi.org/10.7554/eLife.24119

Plattner F, Yarovinsky F, Romero S et al (2008) *Toxoplasma* profilin is essential for host cell invasion and TLR11-dependent induction of an interleukin-12 response. Cell Host Microbe 3:77–87. https://doi.org/10.1016/j.chom.2008.01.001

Pollard TD (2016) Actin and actin-binding proteins. Cold Spring Harb Perspect Biol 8. https://doi.org/10.1101/cshperspect.a018226

Polonais V, Javier Foth B, Chinthalapudi K et al (2011) Unusual anchor of a motor complex (MyoD-MLC2) to the plasma membrane of *Toxoplasma gondii*. Traffic 12:287–300. https://doi.org/10.1111/j.1600-0854.2010.01148.x

Pospich S, Kumpula E-P, von der Ecken J et al (2017) Near-atomic structure of jasplakinolide-stabilized malaria parasite F-actin reveals the structural basis of filament instability. Proc Natl Acad Sci U S A 114:10636–10641. https://doi.org/10.1073/pnas.1707506114

Powell CJ, Jenkins ML, Parker ML et al (2017) Dissecting the molecular assembly of the *Toxoplasma gondii* MyoA motility complex. J Biol Chem 292:19469–19477. https://doi.org/10.1074/jbc.M117.809632

Powell CJ, Ramaswamy R, Kelsen A et al (2018) Structural and mechanistic insights into the function of the unconventional class XIV myosin MyoA from *Toxoplasma gondii*. Proc Natl Acad Sci U S A 115:E10548–E10555. https://doi.org/10.1073/pnas.1811167115

Richards TA, Cavalier-Smith T (2005) Myosin domain evolution and the primary divergence of eukaryotes. Nature 436:1113–1118. https://doi.org/10.1038/nature03949

Rudlaff RM, Kraemer S, Streva VA, Dvorin JD (2019) An essential contractile ring protein controls cell division in Plasmodium falciparum. Nat Commun 10:2181. https://doi.org/10.1038/s41467-019-10214-z

Sahoo N, Beatty W, Heuser J et al (2005) Unusual kinetic and structural properties control rapid assembly and turnover of actin in the parasite *Toxoplasma gondii*. MBoC 17:895–906. https://doi.org/10.1091/mbc.e05-06-0512

Salamun J, Kallio JP, Daher W et al (2014) Structure of *Toxoplasma gondii* coronin, an actin-binding protein that relocalizes to the posterior pole of invasive parasites and contributes to invasion and egress. FASEB J 28:4729–4747. https://doi.org/10.1096/fj.14-252569

Schmitz S, Grainger M, Howell S et al (2005) Malaria parasite actin filaments are very short. J Mol Biol 349:113–125. https://doi.org/10.1016/j.jmb.2005.03.056

Schüler H, Matuschewski K (2006) Regulation of apicomplexan microfilament dynamics by a minimal set of actin-binding proteins. Traffic 7:1433–1439. https://doi.org/10.1111/j.1600-0854.2006.00484.x

Schüler H, Mueller A-K, Matuschewski K (2005a) Unusual properties of *Plasmodium falciparum* actin: new insights into microfilament dynamics of apicomplexan parasites. FEBS Lett 579:655–660. https://doi.org/10.1016/j.febslet.2004.12.037

Schüler H, Mueller A-K, Matuschewski K (2005b) A *Plasmodium* actin-depolymerizing factor that binds exclusively to actin monomers. MBoC 16:4013–4023. https://doi.org/10.1091/mbc.e05-02-0086

Sebastian S, Brochet M, Collins MO et al (2012) A *Plasmodium* calcium-dependent protein kinase controls zygote development and transmission by translationally activating repressed mRNAs. Cell Host Microbe 12:9–19. https://doi.org/10.1016/j.chom.2012.05.014

Sebé-Pedrós A, Grau-Bové X, Richards TA, Ruiz-Trillo I (2014) Evolution and classification of myosins, a paneukaryotic whole-genome approach. Genome Biol Evol 6:290–305. https://doi.org/10.1093/gbe/evu013

Siden-Kiamos I, Ganter M, Kunze A et al (2011) Stage-specific depletion of myosin a supports an essential role in motility of malarial ookinetes. Cell Microbiol 13:1996–2006. https://doi.org/10.1111/j.1462-5822.2011.01686.x

Siden-Kiamos I, Louis C, Matuschewski K (2012) Evidence for filamentous actin in ookinetes of a malarial parasite. Mol Biochem Parasitol 181:186–189. https://doi.org/10.1016/j.molbiopara.2011.11.002

Sidik SM, Huet D, Ganesan SM et al (2016) A genome-wide CRISPR screen in *Toxoplasma* identifies essential Apicomplexan genes. Cell 166:1423–1435.e12. https://doi.org/10.1016/j.cell.2016.08.019

Singh BK, Sattler JM, Chatterjee M et al (2011) Crystal structures explain functional differences in the two actin depolymerization factors of the malaria parasite. J Biol Chem 286:28256–28264. https://doi.org/10.1074/jbc.M111.211730

Skillman KM, Diraviyam K, Khan A et al (2011) Evolutionarily divergent, unstable filamentous actin is essential for gliding motility in Apicomplexan parasites. PLoS Pathog 7:e1002280. https://doi.org/10.1371/journal.ppat.1002280

Skillman KM, Daher W, Ma CI et al (2012) *Toxoplasma gondii* profilin acts primarily to sequester G-actin while formins efficiently nucleate actin filament formation *in Vitro*. Biochemistry 51:2486–2495. https://doi.org/10.1021/bi201704y

Skillman KM, Ma CI, Fremont DH et al (2013) The unusual dynamics of parasite actin result from isodesmic polymerization. Nat Commun 4:2285. https://doi.org/10.1038/ncomms3285

Stortz JF, Del Rosario M, Singer M et al (2018) Formin-2 drives polymerisation of actin filaments enabling segregation of apicoplasts and cytokinesis in *Plasmodium falciparum*. Elife. 2019 Jul 19;8. pii: e49030. https://doi.org/10.7554/eLife.49030.005

Striepen B, Crawford MJ, Shaw MK et al (2000) The plastid of *Toxoplasma gondii* is divided by association with the centrosomes. J Cell Biol 151:1423–1434. https://doi.org/10.1083/jcb.151.7.1423

Tosetti N, Dos Santos Pacheco N, Soldati-Favre D, Jacot D (2019) Three F-actin assembly centers regulate organelle inheritance, cell-cell communication and motility in *Toxoplasma gondii*. Elife 8:pii: e42669. https://doi.org/10.7554/eLife.42669

Vahokoski J, Bhargav SP, Desfosses A et al (2014) Structural differences explain diverse functions of *Plasmodium* actins. PLoS Pathog 10:e1004091. https://doi.org/10.1371/journal.ppat.1004091

van Dooren GG, Striepen B (2013) The algal past and parasite present of the apicoplast. Annu Rev Microbiol 67:271–289. https://doi.org/10.1146/annurev-micro-092412-155741

Wall RJ, Zeeshan M, Katris NJ et al (2019) Systematic analysis of *Plasmodium* myosins reveals differential expression, localization and function in invasive and proliferative parasite stages. Cell Microbiol 21(10):e13082

Williams MJ, Alonso H, Enciso M et al (2015) Two essential light chains regulate the MyoA lever arm to promote toxoplasma gliding motility. MBio 6:e00845–e00815. https://doi.org/10.1128/mBio.00845-15

Yadav R, Pathak PP, Shukla VK et al (2011) Solution structure and dynamics of ADF from *Toxoplasma gondii*. J Struct Biol 176:97–111. https://doi.org/10.1016/j.jsb.2011.07.011

Yusuf NA, Green JL, Wall RJ et al (2015) The *Plasmodium* class XIV myosin, MyoB, has a distinct subcellular location in invasive and motile stages of the malaria parasite and an unusual light chain. J Biol Chem 290:12147–12164. https://doi.org/10.1074/jbc.M115.637694

15 Approaches to Identify and Characterise MYO6-Cargo Interactions

Thomas O'Loughlin, John Kendrick-Jones, and Folma Buss

Abstract

Given the prevalence and importance of the actin cytoskeleton and the host of associated myosin motors, it comes as no surprise to find that they are linked to a plethora of cellular functions and pathologies. Although our understanding of the biophysical properties of myosin motors has been aided by the high levels of conservation in their motor domains and the extensive work on myosin in skeletal muscle contraction, our understanding of how the nonmuscle myosins participate in such a wide variety of cellular processes is less clear. It is now well established that the highly variable myosin tails are responsible for targeting these myosins to distinct cellular sites for specific functions, and although a number of adaptor proteins have been identified, our current understanding of the cellular processes involved is rather limited. Furthermore, as more adaptor proteins, cargoes and complexes are identified, the importance of elucidating the regulatory mechanisms involved is essential. Ca^{2+}, and now phosphorylation and ubiquitination, are emerging as important regulators of cargo binding, and it is likely that other post-translational modifications are also involved. In the case of myosin VI (MYO6), a number of immediate binding partners have been identified using traditional approaches such as yeast two-hybrid screens and affinity-based pull-downs. However, these methods have only been successful in identifying the cargo adaptors, but not the cargoes themselves, which may often comprise multi-protein complexes. Furthermore, motor-adaptor-cargo interactions are dynamic by nature and often weak, transient and highly regulated and therefore difficult to capture using traditional affinity-based methods. In this chapter we will discuss the various approaches including functional proteomics that have been used to uncover and characterise novel MYO6-associated proteins and complexes and how this work contributes to a fuller understanding of the targeting and function(s) of this unique myosin motor.

Keywords

Myosin VI · Cargo adaptor proteins · BioID · Functional proteomics

T. O'Loughlin · F. Buss (✉)
Cambridge Institute for Medical Research, University of Cambridge, The Keith Peters Building, Cambridge, UK
e-mail: to277@cam.ac.uk; fb207@cam.ac.uk

J. Kendrick-Jones
MRC Laboratory of Molecular Biology, Cambridge, UK
e-mail: jkj@mrc-lmb.cam.ac.uk

L. M. Coluccio (ed.), *Myosins*, Advances in Experimental Medicine and Biology 1239,
https://doi.org/10.1007/978-3-030-38062-5_15

15.1 Motor-Cargo Interactions Determine Cellular Functions

In eukaryotes, diversification has given rise to a multitude of novel myosin classes, a total which currently stands at 31 (Foth et al. 2006; Goodson and Dawson 2006; Sebe-Pedros et al. 2014). Humans express up to 40 different myosin genes belonging to 12 classes: I, II, III, V, VI, VII, IX, X, XV, XVI, XVIII and XIX, and any given cell is thought to express 10 or more separate myosin genes at any one given time (Bement et al. 1994; Foth et al. 2006; Goodson and Dawson 2006). Following their discovery there has been rapid progress in characterising these so-called unconventional myosins, which are now known to be the drivers of intracellular motility and force generation and are responsible for vesicle trafficking, organelle distribution, cell morphology, plasma membrane dynamics, cell migration, and many other dynamic cellular processes.

In order to carry out this wide array of cellular processes, which require motility and force, specific myosins with the appropriate properties must be targeted with high precision within the relevant cell, and switched on and off in response to appropriate cues. To achieve this, cells have evolved to express a variety of different myosins with different kinetic and binding characteristics and also multiple mechanisms by which they can regulate and alter the properties of the relevant genes and their protein products: for example, tissue expression levels and splicing at the DNA/mRNA level or autoinhibition and post-translational modifications at the protein level. These mechanisms allow the exquisite tuning of the myosin motor activity, its cargo binding and its localisation in order to produce the required cellular responses. Naturally, defects in these regulatory processes are linked to a plethora of pathologies ranging from cardiomyopathy to neurodegeneration and cancer.

Whilst the function of a myosin is inextricably linked to its motor properties and its highly conserved N-terminal motor domain, it is the C-termini, or in some cases the N-terminal extensions, which are thought to generate the bulk of the functional diversity amongst this protein family. There is very little sequence conservation found in the tail regions among the different classes of myosins, although they often contain common protein-binding domains such as SH3 or FERM domains. Indeed, these regions often mediate cargo binding and are thus required for targeting of the myosin to its appropriate cellular location, making them a critical determinant of myosin function. In this chapter we describe the approaches and methods employed to identify the proteins and complexes that associate with the cargo-binding domains of myosins, focusing on MYO6, and how these interactions with different cargo adaptor proteins determine the cellular functions of this motor.

15.2 MYO6 – Motor Properties and Domain Organisation

Within the myosin superfamily, MYO6 is unique, as it moves in the direction opposite to all the other myosins, i.e., toward the minus end of actin filaments (Wells et al. 1999). This specialised feature of MYO6 may explain the many proposed functions of this myosin in a wide array of processes including endocytosis, secretion and maintenance of Golgi morphology, receptor trafficking and signalling, autophagy and actin cytoskeletal organisation. These roles underlie a number of phenotypes observed in flies, in the MYO6-null *Snell's waltzer* mouse or in humans harbouring mutations in the *MYO6* gene. For example, the *Snell's waltzer* mouse displays deafness, astrogliosis and proteinuria, and mutations in the human gene are linked to deafness and hypertrophic cardiomyopathy (Avraham et al. 1995; Gotoh et al. 2010; Melchionda et al. 2001; Osterweil et al. 2005; Aabo et al. 1995; Mohiddin et al. 2004). Furthermore, overexpression of MYO6 is a hallmark of a number of cancers including prostate cancer (Naora and Montell 2005; Dunn et al. 2006).

MYO6 has a number of specialised structural and functional adaptations not found in the other classes of myosins (see Fig. 15.1). Crystal structures of the MYO6 motor domain and neck have

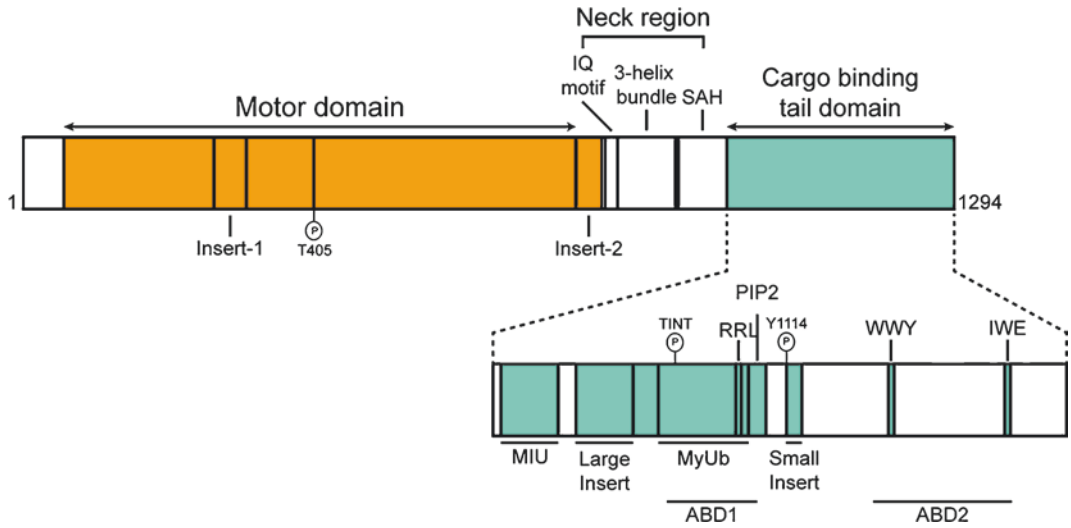

Fig. 15.1 MYO6 domain structure. Schematic diagram of MYO6 domain organisation and regulatory elements. MYO6 is composed of a motor domain (orange), a neck region (grey) and a cargo-binding tail domain (green). The motor contains two unique inserts: insert-1, which modulates nucleotide binding, and insert-2, which confers MYO6 with its reverse directionality. The neck region contains a single canonical IQ motif that binds to calmodulin and a three-helix bundle and single stable alpha-helix (SAH), which may act to extend the lever arm. The tail domain is composed of two protein interaction motifs, the RRL and WWY, a PIP2 lipid-binding motif and two ubiquitin-binding domains (MIU and MyUb). In addition, tissue-specific splicing at two sites gives rise to a large and small insertion in the cargo-binding tail region, which regulates cargo binding and subcellular targeting. Phosphorylation at T405 in the motor domain modulates Pi release and phosphorylation sites in the tail (e.g., TINT or Y1114) might regulate cargo binding. Furthermore, within the tail there are two adaptor-binding domains, ABD1 and ABD2

revealed the presence of two unique inserts (Menetrey et al. 2005, 2007; Sweeney and Houdusse 2010). The first unique insert, insert-1, is close to the motor's nucleotide-binding pocket. This insert forms an extra loop and appears to perturb nucleotide accessibility to the ATP-binding pocket and may explain why MYO6 has such a slow rate of ADP release and weak affinity for ATP (Menetrey et al. 2005; De La Cruz et al. 2001; Pylypenko et al. 2011; Zimmermann et al. 2015). This slow rate of ADP release means that MYO6 has a high duty ratio (spending ~80% of its ATPase cycle bound to actin), which may allow it to function as a slow processive motor under cellular conditions that promote dimerization or multimerization. Insert-1 has also been proposed to respond to strain, a potential key factor in gating the heads of MYO6 for processive movement, blocking ATP binding to the leading head and preventing its dissociation from actin (Altman et al. 2004; Sweeney et al. 2007). It should be stressed that most of the kinetic studies on MYO6 outlined above have been carried out on truncated MYO6 molecules artificially forced to dimerise by the inclusion of either leucine zippers or coiled-coil regions. Further experiments using native MYO6 in combination with different membranes or cargo adaptor proteins will reveal the kinetic properties of MYO6 under physiological conditions.

The second unique insert, insert-2, is responsible for the reverse reposition of the lever arm at the end of the power stroke. Insert-2, also called the 'reverse gear', comprises 53 amino acids and is found between the converter region in the motor domain and the lever arm. This insert binds a non-exchangeable 'structural' calmodulin and is responsible for repositioning the lever arm by ~120° at the end of the power stroke to generate the reverse directionality of MYO6 (Bahloul et al. 2004; Park et al. 2007; Menetrey et al. 2007). A second calmodulin is bound to a short

lever arm through a single canonical IQ motif. This calmodulin not only determines the rigidity of the lever arm, but may also operate as a calcium sensory mechanism that controls motor domain-tail interactions and thereby coordinates motor activity with cargo binding. Upon Ca^{2+} binding a lobe of the second calmodulin is released from the lever arm and now binds to a site at the beginning of the tail domain. This destabilises the lever arm, which impairs MYO6 movement, while simultaneously promotes a "primed" conformation in the tail that allows cargo binding. Cargo attachment restores the lever arm and thereby promotes MYO6 translocation along the actin track (Batters et al. 2016).

The proximal MYO6 tail contains a three-helix bundle that can extend by unfolding and thus may function as a lever arm extension to allow for the large 36-nm steps observed for MYO6 dimers (Rock et al. 2001; Mukherjea et al. 2009). This domain is followed by a region with alternating acidic and basic amino acids predicted by Lister et al. 2004 to be a single alpha-helical domain and has now been confirmed to be a single stabilised helical domain (SAH domain) (Lister et al. 2004; Batchelor et al. 2018). Although there have been numerous speculations that the SAH domain might function as a lever arm extension or might induce MYO6 to dimerise (Rock et al. 2001; Yildiz et al. 2004; Sweeney et al. 2007), the precise function(s) of this MYO6 domain remain(s) to be shown.

At the C-terminus of the MYO6 tail is the cargo-binding domain (CBD), which undergoes tissue-specific splicing at two sites giving rise to four different MYO6 variants. The presence of a large insert (LI) (12–32 amino acids), a small insert (SI) (9 amino acids), or no insert (NI) (or both) in the cargo-binding region regulates adaptor binding and subcellular targeting (Buss et al. 2001; Dance et al. 2004). The MYO6 isoform containing the large insert LI is expressed in tissues such as kidney, liver and intestine, which contain polarized epithelial cells with apical microvilli. In these cell types the LI isoform of MYO6 is localized along the length and at the base of microvilli. MYO6 is important for maintenance of brush border structure and specifically has been shown to facilitate movement of receptors down the microvillus and subsequent uptake via clathrin-mediated endocytosis (Biemesderfer et al. 2002; Hegan et al. 2012; Buss et al. 2001; Ameen and Apodaca 2007). The SI MYO6 isoform is found in testis and brain, where it has been shown to regulate exocytosis in neurosecretory cells (Tomatis et al. 2013). In contrast, the no-insert NI splice variant is widely expressed in most cell types and tissues and mediates the function(s) of this myosin isoform in a wide variety of different cellular processes.

In addition to the tissue-specific expression of the four different MYO6 splice variants, the relative expression levels of MYO6 adaptor proteins are also crucial determinants that control motor–cargo interactions, MYO6 cellular localisation and physiological function (Dance et al. 2004). A series of interactions between the unique MYO6 CBD and multiple cargo adaptors have been identified, which include disabled-2 (DAB2), GAIP-interacting protein C-terminus (GIPC1), target of Myb 1 (TOM1), lemur tyrosine kinase 2 (LMTK2), Synapse associated protein 97 (SAP97), otoferlin, optineurin (OPTN), TAX1 binding protein 1 (TAX1BP1) and nuclear dot protein 52 (NDP52), Phospholipase C (PLCδ3), kinase anchoring protein 9 (AKAP9) and RNA polymerase II (RNAPII) (Bunn et al. 1999; Morris et al. 2002a; Sahlender et al. 2005; Chibalina et al. 2007; Morriswood et al. 2007; Tumbarello et al. 2012; Sakurai et al. 2011; Roux et al. 2009; Karolczak et al. 2015; Vreugde et al. 2006) (summarised in Table 15.1).

Interestingly, so far adaptor protein binding has only been reported in the MYO6 CBD, which is composed of two subdomains containing two distinct protein-binding motifs, the adaptor-binding domains 1 and 2 (ABD1 and ABD2), which are located within the first and second subdomains, respectively (Fig. 15.1) (Spudich et al. 2007). The ABD1 contains the $RRL^{1116–1118}$ motif and the ABD2 the $WWY^{1201–1203}$ motif. In addition, the tail also has a phosphatidylinositol 4,5-bisphosphate (PIP2) binding $motif^{1122–1131}$, which aids recruitment of the motor to membranes along with its binding partners (Spudich et al. 2007). Finally, recent work has identified

Table 15.1 Known MYO6 adaptor proteins and their proposed function(s)

Binding partner(s)	General properties	Interaction motif	MYO6-partner function(s)	Reference(s)
DAB2	Clathrin-associated sorting protein	WWY	Endocytosis	Morris and Cooper (2001); Morris et al. (2002a, b)
GIPC1	Membrane and receptor binding Present on RAB5 endosomes	RRL	Receptor trafficking and signalling	Bunn et al. (1999); Aschenbrenner et al. (2003); Varsano et al. (2006)
TOM1/L2	ESCRT-0-like Present on RAB5 endosomes	WWY	Cargo delivery from endocytic to autophagic pathway	Tumbarello et al. (2012)
LMTK2	Serine/Threonine kinase Present on RAB5/11 and EEA1 endosomes	WWY	Receptor recycling	Chibalina et al. (2007)
OPTN	Selective autophagy receptor and regulator of secretion	RRL	Polarised secretion and exocytic vesicle fusion at the plasma membrane Autophagy, xenophagy and mitophagy	Sahlender et al. (2005); Chibalina et al. (2010); Bond et al. (2011); Tumbarello et al. (2012, 2015)
TAX1BP1 & NDP52	Selective autophagy receptor	RRL	Autophagy, xenophagy and mitophagy	Morriswood et al. (2007); Tumbarello et al. (2012, 2015)
LRCH3	Leucine rich repeats and Calponin-Homology domain-containing protein Regulation of septin cytoskeleton	WWY/ RRL	Regulation of septin cytoskeleton	O'Loughlin et al. (2018)
SAP97	Synapse-associated protein Membrane-associated guanylate kinase Trafficking of receptors and ion channels	N/A	AMPAR receptor trafficking	Wu et al. (2002); Osterweil et al. (2005); Nash et al. (2009)
Phospholipase Cδ3	Enzyme regulating phosphoinositide metabolism	N/A	Maintenance of microvilli stability	Sakurai et al. (2011)
Otoferlin	Ca^{2+} sensor regulating vesicle fusion	N/A	Membrane trafficking in inner hair cells	Heidrych et al. (2009)
AKAP9	Regulator of protein kinase A signalling	N/A	Regulation of protein kinase A signalling and MYO6 phosphorylation	Karolczak et al. (2015)
RNAPII	Catalyses transcription of DNA to mRNA	N/A	Regulation of RNAPII-dependent gene transcription	Vreugde et al. (2006)

two distinct ubiquitin-binding sites in the tail; a Motif Interacting with Ubiquitin (MIU)$^{990–1014}$ and a MYO6 Ubiquitin-Binding Domain (MyUb)$^{998–1025}$ (He et al. 2016; Penengo et al. 2006). The MyUb site appears to be able to bind K11, K29 and K63-linked ubiquitin chains and to a lesser extent K48-linked chains, while MIU has a specific role in binding to K11 chains. There are now structural data on the cargo-binding tail domain (CBD) of MYO6 with and without these binding partners, which show that the MyUB domain overlaps with the ABD1 containing the RRL motif (Yu et al. 2009; He et al. 2016; Shang et al. 2017). Thus, MYO6 may bind directly to

adaptor proteins such as GIPC1, optineurin, NDP52, TAX1BP1 through the MyUb/ABD1 (Sahlender et al. 2005; Morriswood et al. 2007; Tumbarello et al. 2012) or indirectly to ubiquitylated binding partners as point mutations in the MyUb ubiquitin-binding site does impact on MYO6 interaction with optineurin (He et al. 2016). A further mechanism to control motor-cargo interaction is provided by the large insert in the LI MYO6 isoform, which is located just before the MyUb/ABD1. In the NMR structure this insert forms a single amphipathic α-helix (named the α-2 linker), which generates a unique clathrin-binding site. This helix appears to sterically hinder the binding of adaptor proteins to the RRL motif in the ABD1 (Wollscheid et al. 2016). Finally, adaptor binding to the different sites in the CBD is not mutually exclusive and simultaneous binding of NDP52 to the RRL motif in ABD1 and TOM1 to the WWY motif in ABD2 has been demonstrated *in vitro* (Arden et al. 2016). ABD1 and ABD2 are located on different subdomains of the CBD connected by a large unstructured region, which may increase flexibility to allow adaptor binding to the RRL and the WWY motifs simultaneously.

15.3 Approaches to Identify Motor-Cargo Complexes

Over the years a variety of approaches has been used to identify motor-cargo complexes. The first direct binding partners of myosin motor proteins were identified with the help of traditional methods such as yeast two-hybrid screens. More recently, various affinity-based purification techniques such as native co-immunoprecipitation or pull-down assays with the cargo-binding tail domain in combination with mass spectrometry have identified several motor-adaptor complexes (Hartman et al. 2011; Finan et al. 2011). Although these methods have been successful in uncovering a number of direct binding partners for MYO6 (Morris et al. 2002a; Sahlender et al. 2005), in many cases the organelle anchors, the cargoes themselves or the regulatory component(s) of the motor-cargo complex were still unknown. In addition, due to the dynamic nature of motor proteins, their adaptor-cargo interactions are weak, transient, and highly regulated, thus the larger complexes they associate with are often inaccessible or undetected.

15.3.1 Yeast Two-Hybrid Screens

Yeast two-hybrid screens have been extensively used as a tool to identify and characterise macromolecular interactions. Initially described by Field and Song in 1989 (Fields and Song 1989), the yeast two-hybrid screen is an *in vivo* system that identifies interacting proteins by the reconstitution of active transcription factor dimers. For example, the plasmid encoding the protein of interest (the Bait) is attached to a DNA-binding domain, while the plasmid of a second protein (the Prey) is attached to an activating domain, and when the two fusion proteins interact, an active transcription factor dimer is formed, resulting in the expression of a specific reporter gene. This system can be used to characterise and map the interacting domains of two proteins known to bind to each other, or it can be used to perform a library screen to identify new binding partners (Mehla et al. 2015). Using this procedure, optineurin, NDP52, TAX1BP1, DAB2 and GIPC were identified as MYO6 adaptors in screens using a human umbilical vein epithelial cell (HUVEC) cDNA library or GIPC1 screening with a rat brain cDNA library (Sahlender et al. 2005; Morriswood et al. 2007; Bunn et al. 1999; Morris et al. 2002a).

15.3.2 Affinity Columns Using the Myosin-CBD

In more recent work Finan et al. (2011) used an affinity-based approach to identify cargo interactions with the *Drosophila* homologue of MYO6 (Jaguar). In these experiments they ran a *Drosophila melanogaster* embryonic extract over a column constructed with the cargo-binding domain of Jaguar and identified the retained proteins by mass spectrometry (MS). Their results

revealed numerous putative MYO6/Jaguar-binding partners, both known and unknown, including Kermit and CG3529, the *Drosophila* homologues of GIPC1 and TOM1. The authors validated various interactions including one between Jaguar and a novel interactor, cornetto, and showed that this interaction had a role in the secretion of the lipidated morphogen Hedgehog (Finan et al. 2011). In this study the interaction with TOM1 was not further investigated; however, it was later demonstrated that the MYO6-TOM1 interaction was conserved in mammalian cells, where it participates in the delivery of endocytic cargo to autophagosomes (Tumbarello et al. 2012). This affinity-binding approach identified other novel and functionally important MYO6/Jaguar interactors, which are also conserved in mammals. This includes the seven proteins (CG7611, CG31357, CG3295, CG6617, RanBP9, Yippee and Muskelin), which together form the evolutionarily conserved CTLH (C-terminal to LisH) complex. In yeast this complex functions as an E3 ubiquitin ligase that regulates degradation of enzymes of the gluconeogenesis pathway (Regelmann et al. 2003). Although this complex is conserved in mammals, its function is currently unclear (Kobayashi et al. 2007). Intriguingly, muskelin, a component of the CTLH complex, was identified as interacting indirectly with MYO6 in neurons, hinting at the tantalising possibility that an interaction between MYO6 and the CTLH complex is conserved in mammals (Heisler et al. 2011).

15.3.3 Immunoprecipitation of Motor-Cargo Complexes

Affinity-based identification of motor-cargo complexes can also be performed using conventional immunoprecipitation of the endogenous protein from cell lysates using affinity-purified antibodies specific to a desired myosin motor followed by identification of co-immunoprecipitated (bound) proteins by mass spectrometry (ten Have et al. 2011). Where an antibody against the protein of interest (POI) is available, the endogenous protein can be immunoprecipitated directly. In the absence of a specific antibody, the full-length myosin motor or the CBD can be expressed with an epitope tag such as GFP or FLAG, which can be used to purify the tagged motor along with its bound cargo complexes. A myriad of commercially available antibodies exists targeting a growing list of epitope tags. Alternatively, single-chain antibodies such as high-affinity camelid antibodies, called nanobodies, can be used. These antibodies are devoid of light chains and contain a single antigen-binding variable domain that specifically binds to its target (Rothbauer et al. 2008). Several of these antibodies have been described and characterised including nanobodies targeting GFP. The simplicity of these antibodies allows them to be readily expressed and purified from *E. coli* before conjugation to beads (Rothbauer et al. 2006, 2008). After pull-down of the tagged myosin from a cell extract, on-bead protease digestion can be performed and the myosin and its adaptor proteins released for identification by mass spectrometry.

The yield of co-immunoprecipitated proteins is likely to depend on the procedure and buffer conditions used for cell lysis, so to preserve lower affinity weak interactions, different protocols and buffer conditions with varying amounts of detergent and/or salt should be tested.

15.3.4 In Situ Proximity Labelling

As discussed in the previous sections, a significant number of motor-adaptor interactions have been identified using traditional approaches such as yeast two-hybrid assays or immunoprecipitation. However, due to the dynamic nature of motor proteins, their adaptor-cargo interactions are weak, transient, and highly regulated, thus the larger complexes they associate with are often undetected. In order to develop a clearer picture of the functions and cargoes of MYO6, we have applied proximity-based proteomic strategies with the aim of establishing a more complete motor-cargo interactome.

One such strategy is BioID (biotin identification), which utilises a mutated form of the *E. coli* enzyme BirA, a biotin ligase that binds to

biotin and ATP and catalyses the formation of "active" biotinoyl-5′-AMP (bioAMP). A single amino acid mutation (R118G) in the active site of the BirA enzyme reduces its affinity for bioAMP by two orders of magnitude and this causes premature release of the molecule (Kwon and Beckett 2000). This activated biotin can then diffuse and conjugate to any protein (or more specifically to primary amines, mostly lysines) within a radius of ~10 to 20 nm (Choi-Rhee et al. 2004). When the mutant BirA (BirA∗) is genetically fused to a protein of interest and assuming BirA∗ doesn't disrupt correct localisation, it allows it to label physiologically relevant interacting and vicinal proteins (Roux et al. 2012). Utilising the high affinity interaction between biotin and streptavidin it is possible to pull down and then isolate and identify these proteins (Fig. 15.2). The advantage of this technique is that the labelling occurs inside liv-

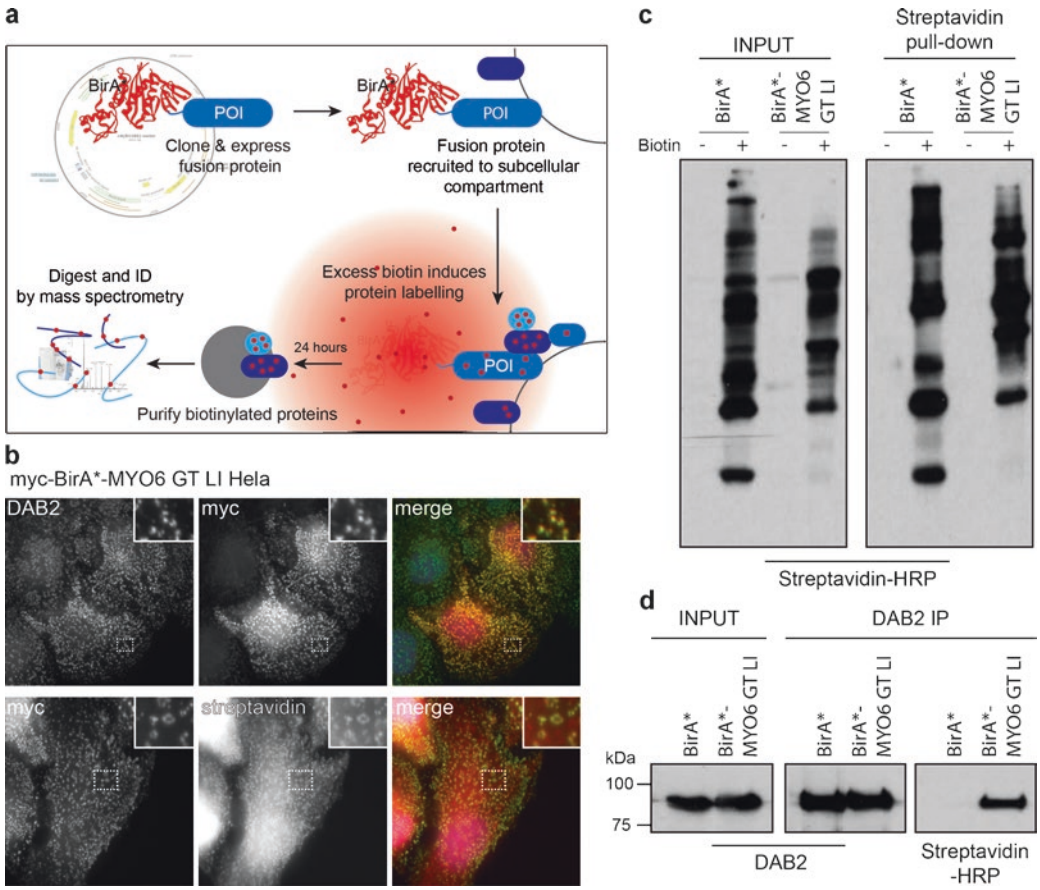

Fig. 15.2 The promiscuous biotin ligase BirA*. (**a**) Schematic cartoon of BirA∗ workflow. BirA∗ fusion proteins are cloned, expressed and recruited to the relevant subcellular compartment. Addition of excess biotin to the culture medium induces biotinylation of proximal proteins. After 24 h cells are lysed and labelled proteins are purified using streptavidin resin. Purified proteins can then be identified by mass spectrometry (or western blotting with specific antibodies). (**b**) Immunofluorescence microscopy of Hela cells transfected with myc-tagged BirA∗-MYO6 GT LI and treated with 50 μM biotin for 24 h. Cells were immunostained with myc (red) and DAB2 antibodies (green) (upper panels) or a myc antibody (green) and streptavidin (red) to visualise biotinylated proteins. Scale bar, 10 μm. (**c**) Lysates and streptavidin pull downs from Hela cells transfected with BirA∗ or BirA∗-MYO6 GT LI and treated −/+ 50 μM biotin for 24 h. Samples were analysed by western blot with streptavidin-HRP. (D) DAB2 immunoprecipitates from Hela cells transfected with BirA∗ and BirA∗-MYO6 GT LI and treated with 50 μM biotin for 24 h. Samples were analysed by western blot with a DAB2 antibody and streptavidin-HRP as indicated

ing cells and will not be disrupted even under harsh lysis conditions.

15.3.4.1 Limitations of BioID

Range

First of all, one of the primary concerns with BioID is its labelling radius. Recent studies have used BioID to look at the architecture of the nuclear pore complexes and, as a large amount of structural data exists for these proteins, it was possible to infer range from the data (Kim et al. 2014). These experiments showed that BirA∗ was likely to have a labelling radius of ~10 nm. As negative-stain electron microscopy indicates that MYO6 is ~15–20 nm long depending on its conformation (Lister et al. 2004), this range is possibly insufficient for BirA∗ fused to the N-terminus of MYO6 to reach the C-terminal end. Therefore, potential range limitations should certainly be considered when opting to use this method. Using small targeting and protein interaction domains, like the MYO6 CBD, have proven to be an effective way to avoid these problems (O'Loughlin et al. 2018). In addition, the use of a long flexible linker between the BirA∗-tag and fusion protein can also help increase the range by allowing the BirA∗ tag flexibility and freedom to diffuse (O'Loughlin et al. 2018; Kim et al. 2016).

Kinetics

Another issue is the kinetics of the BirA∗ enzyme. The initial MYO6 CBD-BioID pull downs were performed after a 24-h labelling period and more recent studies have reduced the labelling time to approximately 16 h, which is in line with other studies (O'Loughlin et al. 2018). Nevertheless, many cellular processes occur on second and minute timescales and will be largely lost to the background over a 16–24-h period. This timeframe also implies that BioID will enrich for proteins with longer half-lives, which can be biotinylated over a longer period. Similarly, the size of the protein and its composition (e.g., lysine abundance) will also affect labelling. These points emphasize that while BioID may be good to enrich weak and transient interactions by labelling proteins over a large timescale, this will also skew the data toward long-lived or lysine-abundant proteins. Likewise, even though the range might be insufficient for N-terminal BirA∗-MYO6 full-length to biotinylate proteins bound to the C-terminal tail domain, proteins in proximity to the motor domain (e.g., actin and actin-associated proteins) and possibly the neck (e.g., light chains) should be close enough. However, as the rate of turnover of actin and actin-associated proteins is often very high due to the dynamic nature of actin filaments, the biotinylated proteins are likely to be lost very quickly. Therefore, to avoid overlooking potentially interesting partners, it is worthwhile using alternative methods in parallel.

In recent years orthogonal proximity-based labelling approaches have been developed, which utilise peroxidases with much more rapid labelling kinetics (see review by (Kim and Roux 2016). These enzymes require peroxide (H_2O_2) and a biotin-phenol substrate but, much like BioID, ultimately lead to the conjugation of biotin moieties onto proteins in the immediate vicinity, which can then be purified using streptavidin-based technologies without fear of disrupting the interaction with harsh lysis conditions. The major benefit of these systems is that they only require a one-minute labelling period prior to cell lysis and therefore can, in theory, be used to capture transient events occurring on those timescales. The first of these approaches, APEX, which utilises an ascorbate peroxidase, has been used to map the mitochondria and cilia proteome (Hung et al. 2014; Mick et al. 2015; Rhee et al. 2013), while another system using horseradish peroxidase has been used for mapping the extracellular space at the neuronal synapse (Martell et al. 2016). Unfortunately, both these enzymes require the use of peroxide, which is toxic to living systems. Recently, a new generation of proximity-labelling enzymes, TurboID (35 kD) and miniTurboID (27kD) have been developed, which show much improved catalytic efficiency and are comparable to the APEX enzyme (Branon et al. 2018). TurboID has been shown to generate nearly as much biotinylated product within 10 min using the same non-toxic

biotin as the original BioID enzyme is able to generate in 18 h (Branon et al. 2018). These approaches could be used to capture transient interactions in short-lived cellular processes such as responses to mitogenic or pathogenic stimuli.

Non-specific Biotinylation

Another major consideration is the selection of appropriate controls. For the identification of the MYO6 interactome, BirA∗-MYO6 tail fusions were compared against a large number of BirA∗ only controls (O'Loughlin et al. 2018). False positives can also arise as highly abundant proteins are likely to be biotinylated by BirA∗, and subsequently enriched, solely on account of their prevalence and can hinder statistical approaches. In our studies (O'Loughlin et al. 2018), we chose to perform quantitative SILAC experiments using targeted mutations in the known tail domain binding motifs of MYO6. However, this approach may not be feasible for every protein due to a lack of knowledge regarding binding sites. Software available online at CRAPome.org was used to compare the average spectral counts from a pre-selected number of control experiments (> 10) to the spectral counts of the BirA∗-MYO6 tail experiments. These comparisons generated a confidence score, FC-A or SAINT, which was used as a guide for follow-up experiments (O'Loughlin et al. 2018).

Cellular Targeting of BirA∗ Fusion Constructs

To achieve target-specific proximity labelling it is important to ensure that the large size of the 37 kDa BirA∗ tag does not disrupt the appropriate localisation of the bait. Since BioID labels in a proximity-dependent fashion, maintaining the correct proximity of a protein to its interactors is likely to be critical for specific labelling (Fig. 15.2b). In our experience, the best datasets we generated were those where the fusion protein showed strong localisation to the correct compartment (e.g. MYO6 GT NI/LI) and likewise point mutations in MYO6 leading to disrupted cellular localisation led to loss of a number of its binding partners (O'Loughlin et al. 2018). Nevertheless, BioID has been used to study cytosolic proteins such as kinases involved in hippo signalling, indicating that a diffuse localisation doesn't necessarily exclude a protein from generating quality data (Couzens et al. 2013). Of note, our experience has suggested that proteins that show good localisation with a GFP tag also work well with BirA∗. Taken together, despite these limitations, BioID is clearly an extremely powerful tool to identify novel myosin-cargo interactions as well as protein interactions generally.

15.4 MYO6 Adaptor Proteins

15.4.1 DAB2

DAB2 was one of the first MYO6 binding partners identified, and it interacts directly with the $WWY^{1201–1203}$ motif in the MYO6 ABD2 through its C-terminal domain (Morris et al. 2002a). DAB2 is a clathrin- and cargo-binding endocytic adaptor protein containing a phosphotyrosine-interacting domain that binds to the F*X*NP*X*Y endocytic motif found in the cytoplasmic domains of cell surface receptors such as the lipoprotein receptors, megalin and integrins. It also contains motifs that enable binding to different components of the endocytic machinery including AP-2, clathrin and EH (EPS15 Homology) domain-containing proteins and as such is able to link cargo recruitment and clathrin coat formation (Mishra et al. 2002; Morris and Cooper 2001; Teckchandani et al. 2012). DAB2 also facilitates the endocytosis of the RAS-activating GRB2/SOS1 signalling complex and thereby regulates RAS/MAPK downstream signalling. DAB2 is thus a multi-modular scaffold protein with a variety of signalling roles in cell growth, trafficking and differentiation (Finkielstein and Capelluto 2016). Expression of DAB2 is downregulated in a large variety of different cancer types, suggesting that it has additional functions as a tumour suppressor (Zhang et al. 2014).

The C-terminal domain of DAB2 binds to two distinct sites in the MYO6 ABD2, the $WWY^{1201–1203}$ motif and the $IWE^{1261–1263}$ motif, which are located on opposite faces of the central beta sheet within the

MYO6 CBD (Yu et al. 2009). Both of these sites are essential for MYO6 binding to DAB2, and a single point mutation in the WWY or the IWE motif inhibits DAB2 binding and MYO6 targeting to clathrin-coated structures (Spudich et al. 2007; Arden et al. 2016; Yu et al. 2009). Binding of DAB2 has been suggested to induce dimerization of MYO6, highlighting a novel cargo-dependent mechanism to regulate monomer-dimer conversion of this myosin (Yu et al. 2009). The crystal structure of the MYO6-DAB2 complex indicates that DAB2 may induce MYO6 dimerization by binding to the WWY motif on one MYO6 monomer and the IWE motif on another monomer. A second DAB2 monomer binds to the same sites in the reverse orientation thereby stabilising the MYO6 dimer.

Recruitment of MYO6 to clathrin-coated structures at the plasma membrane not only involves binding to DAB2 but also requires the phospholipid-binding domain$^{1122–1131}$, which associates with PI(4,5)P2, and the LI, which contains a recently identified clathrin-binding site (Spudich et al. 2007; Buss et al. 2001; Wollscheid et al. 2016). Functional proteomics and *in situ* proximity labelling, identified 16 indirect binding partners that selectively interact with the MYO6 LI isoform, which include proteins involved in clathrin-mediated endocytosis such as FCHO2 (FCH domain only protein 2), adaptor protein-2 (AP-2), PICALM (phosphatidylinositol binding clathrin assembly protein), ITSN1 (endocytic scaffold protein intersectin1), EPS15L1 (epidermal growth factor receptor substrate 15-like 1) and SYNJ1 (synaptojanin 1) (O'Loughlin et al. 2018). Interestingly, the MYO6-null *Snell's waltzer* mouse shows perturbed apical endocytosis in tissues normally expressing the LI isoform of MYO6. This results in reduced uptake of cystic fibrosis transmembrane conductance regulator (CFTR) in enterocytes and induces proteinuria linked to defective uptake of the lipoprotein receptor-related protein megalin in the kidney. Both of these phenotypes are shared with DAB2-null mice (Ameen and Apodaca 2007; Collaco et al. 2010; Gotoh et al. 2010; Morris et al. 2002b).

15.4.2 GIPC1

In many different cell types MYO6 is present on a subset of peripheral endosomes underneath the plasma membrane. GIPC1 is important for the recruitment of MYO6 to these endosomes, which are positive for the GTPase RAB5 and the RAB5 effector APPL1 (Adaptor protein Phosphotyrosine interacting with PH domain and Leucine Zipper 1) (Naccache et al. 2006; Dance et al. 2004; Aschenbrenner et al. 2003). APPL1 is able to bind directly to RAB5 and membranes through its N-terminal PH and BAR domains but also to signalling molecules or the tails of cell surface receptors through a C-terminal PTB domain. The latter interactions endow APPL1 with important functions in linking receptor trafficking to different signalling events in the early endocytic pathway (Lin et al. 2006; Mitsuuchi et al. 1999; Varsano et al. 2006).

GIPC1 binds directly to the RRL motif in MYO6 ABD1 and through its PDZ domain to the extreme COOH-terminus of APPL1 (Bunn et al. 1999; Shang et al. 2017; Spudich et al. 2007; Lin et al. 2006; Varsano et al. 2006). In the absence of cargo, GIPC1 forms an antiparallel autoinhibited dimer that is unable to bind to MYO6 or transmembrane proteins. Binding to cargo, i.e., receptor proteins, releases the autoinhibition and allows interaction of GIPC1 with MYO6, which results in the formation of high-order oligomers of GIPC1 and MYO6 and increases the efficiency of transport through the assembly of MYO6 clusters/arrays on the membrane (Shang et al. 2017).

GIPC1 was initially identified as an interactor of RGS-GAIP, a GTPase-activating protein (GAP) for the G protein coupled receptor subunit Gαi (De Vries et al. 1998). Subsequent work has shown that it can interact with the cytoplasmic tails of a plethora of receptor tyrosine kinases (RTKs), G protein coupled receptors (GPCRs) and other transmembrane proteins regulating their signalling and trafficking within the endocytic system (Katoh 2013). Some of these functions require a GIPC1-APPL1 complex involved in, for example, tropomyosin-related kinase A (TrkA) or lysophosphatidic acid receptor (LPAR1) signalling and trafficking. Indeed,

depletion of GIPC1 leads to delays in sorting and maturation of this population of peripheral endosomes and depletion of GIPC1 or APPL1 modulates endosomal signalling events (Lin et al. 2006; Varsano et al. 2006, 2012).

In a similar way, the recruitment of MYO6 has been suggested to mediate the transport of these APPL1-positive endosomes through the cortical actin network as defects have been observed in retrograde endosome movement in the presence of non-motile MYO6 mutants (Aschenbrenner et al. 2003, 2004; Naccache et al. 2006). Furthermore, depletion of MYO6 causes accelerated maturation and release of these APPL1-positive endosomes from their cortical localisation and subsequent accumulation in the perinuclear region (Masters et al. 2017). Together, this suggests that the PDZ-containing GIPC1 is likely to function as an adaptor to target PDZ-binding motif-containing cargoes to MYO6, mediating their subsequent trafficking and signalling.

Functional proteomic screens identified 27 high-confidence GIPC1-interacting proteins, 15 of which were mutual interactors with MYO6. This included known links such as with APPL1/2 in addition to a number of novel shared associations including GULP1, SIPA1L1/3 and FMNL3 (O'Loughlin et al. 2018). Of particular interest were the GIPC1 interactors LARG, SH3BP4 and CARD10, which were also identified with extremely high confidence in MYO6 complexes. Leukaemia-Associated RhoGEF (LARG) was originally discovered as a MLL (mixed lineage leukaemia) fusion protein and the possible cause of acute myeloid leukaemia (Kourlas et al. 2000). It contains an N-terminal PDZ domain, a regulator of G protein signalling-like (RGSL) domain, a Dbl homology (DH) domain and a pleckstrin homology (PH) domain and functions as a guanine nucleotide exchange factor (GEF) for RHO GTPases downstream of G protein-coupled receptors (GPCR) (Fukuhara et al. 2000). GNA12/13 (guanine nucleotide binding protein subunit 12/13) has been shown to bind to the RGSL domain of LARG and to stimulate its RHOA GEF activity and conversely the RGSL domain functions as a GAP (Rho GTPase activating protein) toward GNA12/13, thereby creating a negative feedback loop to shut off the signalling process (Suzuki et al. 2003).

Src Homology 3 domain Binding Protein 4 (SH3BP4) is a relatively uncharacterised protein, which contains three NPF (asparagine-proline-phenylalanine) motifs, known to bind to EH (EPS15 homology) domains, as well as a clathrin-binding site (LIDL), an SH3 domain and an AP-2 binding site (WRSF) (Kim and Kim 2013). These sites, unsurprisingly, allow SH3BP4 to bind to EPS15, clathrin, dynamin and AP-2, respectively and, given the critical importance of those proteins in endocytosis, it follows that SH3BP4 is also a regulator of this process, specifically in the uptake of transferrin receptor (TfR) into clathrin-coated pits (Tosoni et al. 2005). SH3BP4 has also been found to participate in receptor recycling (Francavilla et al. 2013) and has been implicated in autophagy and mTOR signalling through an interaction between its SH3 domain and the GTPase Rag (Kim et al. 2012). Our data have indicated that LARG and SH3BP4 form a protein complex with MYO6 and GIPC1, which might modulate actin organisation in the cell periphery to regulate receptor trafficking (O'Loughlin et al. 2018).

Caspase Activated and Recruitment Domain 10 (CARD10), also known as CARMA3, belongs to the CARMA protein family, which also contains CARD11 and CARD14 (CARMA1 and 2, respectively). These proteins all contain an N-terminal CARD domain followed by a PDZ domain, an SH3 domain and a membrane-associated guanylate kinase (MAGUK) domain and are all implicated in NF-κB signalling (Blonska and Lin 2011).

15.4.3 TOM1/L2

The second direct binding partner of MYO6 found on APPL1-positive endosomes is TOM1 and the related TOM1L2. This interaction was first found in *Drosophila*, where the fly homologue of TOM1/L2, named CG3529, was identified as a Jaguar (*Drosophila* MYO6) binding protein using affinity chromatography (Finan

et al. 2011). Co-immunoprecipitation confirmed that the interaction between MYO6 and TOM1/L2 is conserved in mammalian cells (Tumbarello et al. 2012). TOM1 and TOM1L2 both contain a ubiquitin-binding GAT (GGA and TOM1) domain and a VHS (VPS27-HRS-STAM) domain, which are common to many endocytic trafficking proteins including the endosomal sorting complex required for transport type-0 (ESCRT-0) and its subunits HRS and STAM1/2 (Shiba et al. 2004; Seroussi et al. 1999). These proteins are involved in the recognition of ubiquitinated cargo and promote their sorting into intraluminal vesicles leading to degradation. In mammalian cells, TOM1/TOM1L2 are able to bind to ESCRT-0 component HRS, but only the more divergent family member TOM1L1 is able to bind ESCRT-I component TSG101 (Puertollano 2005). TOM1 is recruited to endosomes through its interactions with TOLLIP (Toll interacting protein) and ZYVE16 (endofin) and these can in turn bind clathrin to bring it to these sites (Seet and Hong 2005; Yamakami et al. 2003). In addition, recent work has shown that TOM1 can bind to PI5P on signalling endosomes through its VHS domain and, as a PI5P effector, can regulate endosomal maturation (Boal et al. 2015). Overall, the precise function of TOM1 is currently unclear, but it may participate in modulating IL-1β and TNF-α signalling and receptor trafficking (Yamakami and Yokosawa 2004; Brissoni et al. 2006). Likewise, the role of the MYO6-TOM1/TOM1L2 interaction has also not yet been fully established, but it has been shown to be required for autophagosome maturation and fusion with lysosomes possibly through delivery of endocytic cargoes (Tumbarello et al. 2012).

15.4.4 LRCH3

In situ proximity labelling identified LRCH1, LRCH3 and DOCK7 as a MYO6-associated protein complex (O'Loughlin et al. 2018). LRCH1 and LRCH3 belong to the Leucine Rich repeats/Calponin Homology domain (LRCH) family of proteins, which in mammals are almost entirely uncharacterised. LRCH3 specifically was shown to be a direct MYO6-binding partner. These proteins comprise a series of N-terminal leucine rich repeats (LRRs) (20–29 residue motifs), which are involved in protein-protein interactions, and a C-terminal calponin homology (CH) domain that can directly bind to actin. Interestingly, LRCH1 and LRCH3 also bind directly to DOCK7 (Dedicator Of CytoKinesis 7), which had previously been suggested to be a direct MYO6-binding partner (Majewski et al. 2012). DOCK7 belongs to the DOCK180 family of GEFs, which activate RhoGTPases by catalysing the loading of GTP onto the GTPases through a DOCK homology region (DHR)-2 domain (Cote and Vuori 2002). DOCK7 has been identified as a GEF for membrane localised CDC42 (Cell Division control protein 42) and RAC1 (Ras-related C3 toxin substrate-1), which are two crucial regulators of the actin cytoskeleton (Zhou et al. 2013). Although DOCK7 is expressed in a variety of cell types and tissues, it functions predominantly in the nervous system and is required for Schwann cell migration, myelination and neuritogenesis (Tai et al. 2014; Watabe-Uchida et al. 2006; Yamauchi et al. 2008, 2011). In the adrenal medulla-derived PC12 cell line, DOCK7 and RAC1 activity are important for neurite outgrowth in response to nerve growth factor (NGF) stimulation (Majewski et al. 2012; Sobczak et al. 2016).

MYO6, LRCH3 and DOCK7 form a tripartite complex, the DISP (DOCK7-Induced Septin dis-Placement) complex, in which LRCH3 forms the indirect link between MYO6 and DOCK7. LRCH3 binds to the MYO6 CBD via the WWY motif in ABD2 and to a lesser extent to the RRL motif in ABD1. BioID data (O'Loughlin et al. 2018) revealed a complex between LRCH3 and the septins, in particular SEPT7, but also SEPT8, SEPT9, and SEPT10. Septins are a large enigmatic family of GTPases with phospholipid-binding activity, which can form heteromeric complexes and assemble to form large structures such as filaments, rings and cages (Weirich et al. 2008). Due to their propensity to form filaments and other oligomers, they have been described as the fourth member of the cytoskeleton family (Mostowy and Cossart 2012). Indeed, septins

share an intimate relationship with the other major elements of the cytoskeleton; for example, they have been shown to interact with distinct actin filament structures, with microtubules and with membranes with specific lipid compositions (Bowen et al. 2011; Sellin et al. 2011; Kinoshita et al. 2002). When LRCH3 and the DOCK7 DHR-2 domain are overexpressed, the septins are displaced from actin filaments and form characteristic septin rings in the cytosol. Since the dynamic actin filament assemblies present in membrane ruffles are devoid of septins, the tripartite MYO6-LRCH3-DOCK7 DISP complex may regulate the removal of septin structures from these actin filaments to enable actin filament reorganisation through DOCK7-stimulated RAC1 and CDC42 GTPase activities (O'Loughlin et al. 2018).

15.4.5 LMTK2

The transmembrane serine/threonine kinase, lemur tyrosine kinase 2 (LMTK2), is the first transmembrane protein and kinase that has been identified as a direct MYO6-binding partner. At present it is not known whether MYO6 regulates trafficking of this kinase or whether MYO6 activity is modulated by LMTK2-dependent phosphorylation. LMTK2 is present on RAB5-positive endosomes in the early endocytic pathway, where it appears to mediate sorting of receptors from early endosomes to the recycling compartment (Chibalina et al. 2007). This kinase is phosphorylated and regulated by cyclin-dependent kinase-5 (CDK5) (Kesavapany et al. 2003) and has been shown to directly bind to the MYO6 CBD through the WWY motif in the ABD2. Little is known about the function of the LMTK2-MYO6 complex although it has been shown that LMTK2 phosphorylates the cystic fibrosis transmembrane conductance regulator (CFTR), potentially regulating the MYO6-dependent endocytosis of this receptor (Luz et al. 2014; Wang and Brautigan 2006). Both LMTK2 and MYO6 have been identified as prostate cancer-associated genes indicating a possible role in the progression of this pathology (Eeles et al. 2008; Shah and Bradbury 2015). Interestingly, LMTK2 has also been linked to neurodegeneration, and early studies have suggested that it might be a promising therapeutic target (Rattray 2012; Bencze et al. 2018).

15.4.6 Optineurin

Optineurin is a multifunctional protein that was identified in a yeast 2-hybrid screen as a MYO6-binding partner. Optineurin has been implicated in many different signalling pathways and cellular processes including autophagy, Golgi maintenance, membrane trafficking and the inflammatory response. Mutations in optineurin are associated with a variety of different human pathologies such as primary open angle glaucoma, Paget's disease of the bone, amyotrophic lateral sclerosis (ALS) and frontotemporal dementia (FTD) (Rezaie et al. 2002; Albagha et al. 2010; Maruyama et al. 2010; Pottier et al. 2015). Optineurin is a highly conserved protein with substantial homology to the NF-kB essential modulator (NEMO), and has been shown to be a negative regulator of NF-kB signalling (Nakazawa et al. 2016). Optineurin contains two distinct ubiquitin-binding domains, a UBAN and a C-terminal zinc finger domain (ZF), one leucine zipper, several coiled-coil domains, a NEMO-like domain and a LC3-interacting region (LIR) (Ryan and Tumbarello 2018). MYO6 either binds directly to the UBAN domain of optineurin through its ABD1/MyUb domain (Sahlender et al. 2005) or indirectly to ubiquitinated optineurin (He et al. 2016). Phosphorylation of MYO6 in the CBD at TINT$^{1096–1100}$ may regulate this interaction, as phosphomimetic mutations of the TINT motif to EINE has been shown to inhibit binding of MYO6 to optineurin (Sahlender et al. 2005). Binding to optineurin or optineurin oligomers (Ying et al. 2010) may induce dimerization of MYO6 allowing processive movement of this monomeric myosin in cells when attached to this binding partner (Phichith et al. 2009). The diverse cellular processes that involve optineurin are mediated by a large number of interacting proteins, which include not only MYO6, but also TBK1 (kinase), CYLD

(deubiquitinating enzyme), HACE1 (ubiquitin ligase), RAB8 and RAB1A (RabGTPases) among others. The MYO6-optineurin complex regulates protein secretion, which is consistent with previous observations that in *Snell's waltzer* (MYO6 KO) fibroblasts, exocytosis of a secreted form of alkaline phosphatase (SEAP) is impaired (Warner et al. 2003). Likewise, depletion of MYO6 causes a reduction in vesicular stomatitis virus G protein (VSV-G) delivery to the basolateral membrane in polarised MDCK cells (Au et al. 2007). These phenotypes were later determined to be the result of the interaction between the RRL motif in the CBD of MYO6 and optineurin, together with the small GTPase RAB8, as depletion of optineurin also leads to a decrease in both SEAP and VSV-G secretion in different systems (Chibalina et al. 2008; Sahlender et al. 2005). The effects of MYO6 and optineurin on secretion appear to be the result of defects in secretory vesicle fusion at the plasma membrane (Bond et al. 2011). This deficiency in secretion results in defects in directed cell migration due to problems with polarised EGFR delivery to the leading edge of the migratory cell (Chibalina et al. 2010). Related to its function in vesicle trafficking, the MYO6-optineurin complex also plays an important role in autophagy, a lysosomal degradation pathway for the removal of protein aggregates, intracellular bacteria and damaged organelles. Similarly to TAX1BP1 and NDP52, optineurin is also an autophagy receptor, involved in the clearance of *Salmonella enterica* (Wild et al. 2011) and the removal of damaged mitochondria (Wong and Holzbaur 2014). In this process, optineurin recognises and binds to ubiquitinated substrates through its UBAN domain and recruits microtubule-associated light chain 3(LC3)-containing membranes for phagophore formation through its LIR domain.

15.4.7 TAX1BP1 and NDP52

TAX1BP1 and NDP52 bind directly to MYO6 and link this myosin to the autophagy pathway (Tumbarello et al. 2012). TAX1BP1 and NDP52 as well as optineurin are selective autophagy receptors on account of their abilities to bind both ubiquitinated cargo via their ubiquitin binding domains (UBD) and LC3. These autophagy receptors recruit LC3-associated autophagosomal membranes to ubiquitinated cargo, promoting its engulfment by an autophagosome and subsequent degradation. Selective autophagy is responsible for the controlled degradation of a growing list of cytosolic components that are too large to be degraded by the proteasome including protein aggregates, invading pathogens and damaged organelles such as mitochondria. In addition, it is a homeostatic pathway that maintains cell survival and growth under adverse conditions such as starvation and also acts a cellular defense mechanism to thwart invading pathogens. NDP52 and TAX1BP1 have similar structures and contain an N-terminal SKICH domain, then a non-canonical LC3 binding domain (named LIR), followed by a coiled-coil domain and C-terminal zinc finger domains. TAX1BP1 is a paralogue NDP52, but it may have a predominant role in vertebrates, since a genomic and phylogenetic survey revealed that TAX1BP1 preserves the ancestral features and can be found in all vertebrates, whereas functional NDP52 is lost from Xenopus and mice (Tumbarello et al. 2015). In TAX1BP1 and NDP52 the ubiquitin and MYO6 binding sites are in the same C-terminal zinc finger domains and completely overlap. Interestingly, at least in TAX1BP1, MYO6 binding affinity is stronger and blocks ubiquitin binding (Tumbarello et al. 2015). These results suggest a model whereby these adaptor proteins may have dual roles in autophagy; initially, they identify and bind selective ubiquitinated cargo to initiate autophagosome formation without MYO6 involvement. Then, in the late steps of autophagosomal maturation and fusion with the lysosome they function together with MYO6 (Tumbarello et al. 2012, 2015). Recent data have indicated that ubiquitin may regulate TAX1BP1 and MYO6 binding and form a ternary complex (Kruppa et al. 2018). These adaptor proteins and optineurin have all been shown to bind directly to the MYO6 ABD1 containing the RRL$^{107–1109}$ motif *in vitro* (Tumbarello et al. 2015; Sahlender et al. 2005; Arden et al. 2016). In addition,

TAX1BP1 and also optineurin have been shown to interact indirectly with the MYO6 MyUB$^{1071–1122}$ region via ubiquitin chains (Kruppa et al. 2018; He et al. 2016; Tumbarello et al. 2015).

TAX1BP1, NDP52 and optineurin also have been found to have important roles in the autophagy-dependent clearance of *Salmonella enterica*, in a process termed xenophagy. They recognise ubiquitinated *Salmonella* that have escaped the vacuole into the cytosol and prevent their proliferation by targeting them for destruction (Thurston et al. 2009, 2012; Wild et al. 2011; Ravenhill et al. 2019). In functional studies, depletion of MYO6 leads to autophagosome accumulation and increased *Salmonella* proliferation (Tumbarello et al. 2012, 2015). MYO6 was also found to participate in the mitophagy pathway wherein damaged mitochondria are ubiquitinated by the E3 ligase parkin and degraded by autophagy. MYO6 is recruited to the ubiquitinated damaged mitochondria but, surprisingly, its recruitment is not dependent on the autophagy adaptors TAX1BP1, NDP52 and optineurin. Instead, recruitment may involve direct binding of MYO6 to ubiquitinated proteins on the outer mitochondrial membrane. The recruitment of MYO6 to the surface of these damaged mitochondria induces the assembly of cross-linked actin filament cages, which isolate these dysfunctional mitochondria and prevent their refusion with their functional neighbours (Kruppa et al. 2018). In addition to this novel role in segregating damaged mitochondria, MYO6, together with the autophagy receptors, also plays more traditional roles in the later stages of the mitophagy pathway to ensure mitophagosome maturation and lysosome fusion (Kruppa et al. 2018; Lazarou et al. 2015; Heo et al. 2015).

15.4.8 SAP97

Synapse associated protein 97 (SAP97) is an example of a tissue-specific binding partner of MYO6. Although SAP97 is widely expressed in multiple cell types and tissues, the interaction between MYO6 and SAP97 has only been demonstrated in neuronal systems so far (Wu et al. 2002). SAP97 is a member of the membrane-associated guanylate kinase (MAGUK) family typically involved in the targeting, trafficking and organisation of receptors, membrane ion channels and adhesion molecules at the cell surface. It is present both pre- and post-synaptically in different neuronal tissues and is able to bind to both α-amino-3-hydroxy-5-methyl-4-isoxazolepropionic acid (AMPA) and *N*-methyl-D-aspartate (NMDA) glutamate receptors, as well as potassium channels, to promote their trafficking and organisation and therefore ensure synaptic transmission (Fourie et al. 2014). Structure-function analysis of SAP97 suggests that it acts as a modular scaffolding protein to assemble AMPA receptor complexes to promote dendrite growth (Zhang et al. 2015). MYO6 forms a complex with SAP97, AP-2 and the AMPA receptor subunits GluA1 and GluA2 and regulates activity-dependent trafficking of the receptors in the brain (Osterweil et al. 2005; Wu et al. 2002). Although the exact binding site of SAP97 in the MYO6 CBD is not known, the C-terminal region of the CBD$^{1126–1262}$ containing the ABD2 with the WWY$^{1201–1203}$ binding motif was shown to interact with the N-terminal region$^{1–104}$ of SAP97 (Nash et al. 2009). In complex with SAP97, MYO6 appears to play a central role in endocytosis and recycling of AMPA receptors in neuronal cells and its absence in the *Snell's waltzer* mouse leads to a decrease in synaptic number, abnormal synaptic structures and profound astrogliosis (Osterweil et al. 2005; Wu et al. 2002; Nash et al. 2009).

15.4.9 Phospholipase C

Phospholipase C (PLCδ3) is a key enzyme in phosphoinositide metabolism, hydrolyzing phosphatidylinositol 4,5-bisphosphate (PIP2) to generate inositol 1,4,5-trisphosphate (IP3) and diacylglycerol. PLCδ3-KO mice display no obvious phenotype and so the physiological function(s) of this isoform of PLC remain(s) unknown. MYO6 was identified in a yeast two-hybrid screen as a PLCδ3-binding partner, however, the exact binding domains have not been

determined since the whole MYO6 tail from the IQ motif to the CBD and the C2 and PH domain of PLCδ3 was involved in these binding studies (Sakurai et al. 2011). Interestingly, depletion of PLCδ3 or the loss of MYO6 causes similar defects in microvilli morphology in polarised intestinal cells suggesting that a functional complex of MYO6-PLCδ3 is important for the maintenance and stabilisation of microvilli structure in the small intestine (Sakurai et al. 2011; Hegan et al. 2012).

15.4.10 Otoferlin

Otoferlin is a MYO6-binding partner at the ribbon synapse in inner ear hair cells. Loss of otoferlin causes a recessive form of congenital deafness, since this transmembrane protein functions as a putative Ca^{2+} sensor in synaptic exocytosis in auditory and vestibular hair cells. Mutations in both proteins, MYO6 and otoferlin, lead to deafness in humans, suggesting a complementary role for these proteins in the recycling of synaptic vesicles at the inner hair cell ribbon synapse (Melchionda et al. 2001; Yasunaga et al. 1999; Heidrych et al. 2009; Roux et al. 2009). In addition, recent studies have shown that in mature inner hair cells otoferlin not only binds to MYO6 but also to AP-2 and together they are involved in the clathrin-mediated endocytosis of Ca^{2+} -regulated vesicles to maintain the integrity and function of these mature hair cells (Duncker et al. 2013).

15.4.11 AKAP9

Kinase-anchoring protein 9 (AKAP9) was identified as a MYO6-binding partner in myogenic cells, binding within the MYO6 CBD (Karolczak et al. 2015). AKAP9 is a regulator of the cAMP-dependent protein kinase (PKA), which was shown to phosphorylate the MYO6 CBD. It was postulated that the MYO6-AKAK9 complex might have functional regulatory relevance by linking MYO6 with the cAMP-dependent PKA signalling pathway, which is vital for myoblast differentiation and possibly also for neuromuscular junction development (Karolczak et al. 2015).

15.4.12 RNAPII

Another MYO6-binding partner is RNA polymerase II (RNAPII), which is involved in the transcription of DNA into mRNA in the nucleus. Whether MYO6 is present in the nucleus has been a controversial subject; however, there were early indications that MYO6 might form a nuclear complex with RNAPII and might regulate RNAPII-dependent transcription (Vreugde et al. 2006). More recent results have demonstrated that the MYO6 adaptor protein NDP52 forms an active complex with nuclear MYO6 to promote RNAPII transcription (Fili et al. 2017) and further studies have suggested that MYO6 may interact with a host of nuclear receptors to drive the target genes involved in, for example, cell proliferation (Fili et al. 2017).

15.5 Regulation of MYO6- Cargo Interactions

Recent results indicate that the interaction of MYO6 with cargo is regulated by autoinhibition by a folded/unfolded tail regulatory mechanism similar to that originally identified in nonmuscle myosin II (Craig et al. 1983) and now also observed in the myosins of class V, VII and X (Thirumurugan et al. 2006; Lu et al. 2006; Umeki et al. 2009). A similar mechanism operates in MYO6: in the absence of Ca^{2+} the tail of MYO6 binds to the neck region to create a folded, inhibited form, which unfolds on Ca^{2+} binding to allow cargo binding and subsequent active translocation (Batters et al. 2016). Additional post-translational modifications such as phosphorylation play an important role in regulating MYO6 adaptor protein interactions. So far, two phosphorylation sites, $TINT^{1096–1100}$ and $DYD^{1145–1147}$, have been identified in the CBD. Mutating the TINT to EINE, thus mimicking the phosphorylated states, has been shown to inhibit binding to optineurin (Sahlender et al.

2005). Furthermore, the tyrosine in the DYD motif in the MYO6 CBD, which is only present in the small insert isoform, is a predicted phosphorylation site for the src kinase. This SI isoform mediates tethering of secretory granules to the actin cortex in neurosecretory cells in a DYD motif-dependent manner, suggesting that the different splice isoforms of MYO6 confer different regulatory mechanisms (Tomatis et al. 2013).

15.6 Outlook

It is clear that MYO6 has multiple binding partners involved in different pathways at different cellular locations and in different tissues (Fig. 15.3); however, in many cases it is unclear what the precise function of MYO6 is at these sites. In particular, the breadth of MYO6-binding partners observed on early endosomes is intrigu-

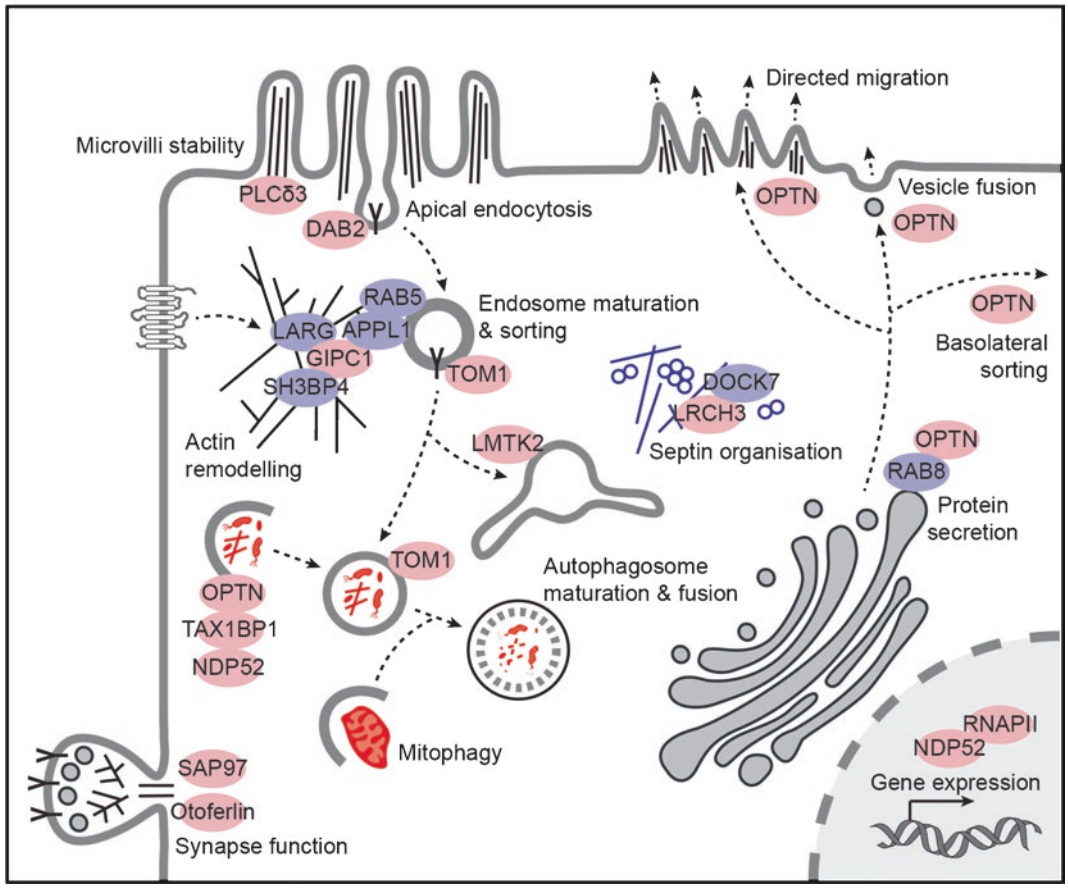

Fig. 15.3 Cellular functions of MYO6. Schematic cartoon illustrating known MYO6-binding partners and highlighting proposed cellular functions and locations. MYO6 is linked to apical endocytosis in polarised epithelia through an interaction with DAB2, in early endosome sorting and trafficking through interactions with GIPC, TOM1 and LMTK2, in autophagy through OPTN, TAX1BP1 and NDP52 and in synapse function involving SAP97 and otoferlin. MYO6 also has multiple functions in the secretory pathway including secretion and maintaining Golgi morphology through an interaction with OPTN. Finally, MYO6 has a range of specialised functions including roles in stereocilia morphology, cytokinesis, directed cell migration, synaptic transmission, dendritic spine morphology and neurite outgrowth. (Adapted from Tumbarello et al. 2013)

ing. Do these partners link MYO6 to distinct maturation stages, sorting steps or signalling platforms on these peripheral membrane components? Likewise, the multitude of selective autophagy receptors interacting with MYO6 comes as a surprise. Do the other selective autophagy receptors such as SQSTM1/p62 and NBR1 also interact with MYO6, or do optineurin, TAX1BP1 and NDP52 link MYO6 to specific autophagic cargoes? Thus, it is unclear whether the full repertoire of MYO6 adaptors and their cargoes has been identified, but it is obvious that the functions of the many known interactors and their interactions with MYO6 have yet to be clearly established.

Another crucial question is whether MYO6 exists as a processive dimer or as a monomeric tether to carry out its multiple functions in the cell. Initial studies showed that full-length MYO6 expressed and purified from baculovirus/insect cells is monomeric and undergoes single independent actin binding events indicative of a non-processive motor (Lister et al. 2004). Further research has shown that MYO6 can be dimerised by cargo binding, although not through interactions with the myosin cargo-binding tail, but through interactions with dimeric cargo or monomeric cargo binding to two tail domains (Phichith et al. 2009; Shang et al. 2017; Yu et al. 2009). So, it is currently unclear whether MYO6 exists as a dimer or a monomer or functions processively as a transporter or as an anchor *in vivo*. Indeed, it may be that MYO6 can perform all of these functions depending on its bound cargo, cellular location and the participation of regulatory mechanisms, emphasising their importance for its function(s). In addition, we need to understand how MYO6 is precisely regulated within the cell, how its activity is coordinated with the vast array of other motors in the cell, and the mechanisms by which it recognises and selects specific cargo, delivers it to specific locations and releases it with the appropriate kinetics.

References

Aabo S, Olsen JE, Threlfall EJ, Brown DJ (1995) Characterization of non-virulence plasmids with homology to the virulence plasmid of Salmonella dublin. Res Microbiol 146(9):751–759. https://doi.org/10.1016/0923-2508(96)81071-0. [pii]

Albagha OM, Visconti MR, Alonso N, Langston AL, Cundy T, Dargie R, Dunlop MG, Fraser WD, Hooper MJ, Isaia G, Nicholson GC, del Pino Montes J, Gonzalez-Sarmiento R, di Stefano M, Tenesa A, Walsh JP, Ralston SH (2010) Genome-wide association study identifies variants at CSF1, OPTN and TNFRSF11A as genetic risk factors for Paget's disease of bone. Nat Genet 42(6):520–524. https://doi.org/10.1038/ng.562

Altman D, Sweeney HL, Spudich JA (2004) The mechanism of myosin VI translocation and its load-induced anchoring. Cell 116(5):737–749

Ameen N, Apodaca G (2007) Defective CFTR apical endocytosis and enterocyte brush border in myosin VI-deficient mice. Traffic 8(8):998–1006. TRA587 [pii]. https://doi.org/10.1111/j.1600-0854.2007.00587.x

Arden SD, Tumbarello DA, Butt T, Kendrick-Jones J, Buss F (2016) Loss of cargo binding in the human myosin VI deafness mutant (R1166X) leads to increased actin filament binding. Biochem J 473(19):3307–3319. https://doi.org/10.1042/BCJ20160571

Aschenbrenner L, Lee T, Hasson T (2003) Myo6 facilitates the translocation of endocytic vesicles from cell peripheries. Mol Biol Cell 14(7):2728–2743

Aschenbrenner L, Naccache SN, Hasson T (2004) Uncoated endocytic vesicles require the unconventional myosin, Myo6, for rapid transport through actin barriers. Mol Biol Cell 15(5):2253–2263. https://doi.org/10.1091/mbc.e04-01-0002

Au JS, Puri C, Ihrke G, Kendrick-Jones J, Buss F (2007) Myosin VI is required for sorting of AP-1B-dependent cargo to the basolateral domain in polarized MDCK cells. J Cell Biol 177(1):103–114

Avraham KB, Hasson T, Steel KP, Kingsley DM, Russell LB, Mooseker MS, Copeland NG, Jenkins NA (1995) The mouse Snell's waltzer deafness gene encodes an unconventional myosin required for structural integrity of inner ear hair cells. Nat Genet 11(4):369–375. https://doi.org/10.1038/ng1295-369

Bahloul A, Chevreux G, Wells AL, Martin D, Nolt J, Yang Z, Chen LQ, Potier N, Van Dorsselaer A, Rosenfeld S, Houdusse A, Sweeney HL (2004) The unique insert in myosin VI is a structural calcium-calmodulin binding site. Proc Natl Acad Sci U S A 101(14):4787–4792. https://doi.org/10.1073/pnas.0306892101

Batchelor M, Wolny M, Kurzawa M, Dougan L, Knight PJ, Peckham M (2018) Determining stable single alpha helical (SAH) domain properties by

circular dichroism and atomic force microscopy. Methods Mol Biol 1805:185–211. https://doi.org/10.1007/978-1-4939-8556-2_10

Batters C, Brack D, Ellrich H, Averbeck B, Veigel C (2016) Calcium can mobilize and activate myosin-VI. Proc Natl Acad Sci U S A 113(9):E1162–E1169. https://doi.org/10.1073/pnas.1519435113

Bement WM, Hasson T, Wirth JA, Cheney RE, Mooseker MS (1994) Identification and overlapping expression of multiple unconventional myosin genes in vertebrate cell types. Proc Natl Acad Sci U S A 91(14):6549–6553. https://doi.org/10.1073/pnas.91.14.6549

Bencze J, Morotz GM, Seo W, Bencs V, Kalman J, Miller CCJ, Hortobagyi T (2018) Biological function of Lemur tyrosine kinase 2 (LMTK2): implications in neurodegeneration. Mol Brain 11(1):20. https://doi.org/10.1186/s13041-018-0363-x

Biemesderfer D, Mentone SA, Mooseker M, Hasson T (2002) Expression of myosin VI within the early endocytic pathway in adult and developing proximal tubules. Am J Physiol Renal Physiol 282(5):F785–F794. https://doi.org/10.1152/ajprenal.00287.2001

Blonska M, Lin X (2011) NF-kappaB signaling pathways regulated by CARMA family of scaffold proteins. Cell Res 21(1):55–70. https://doi.org/10.1038/cr.2010.182

Boal F, Mansour R, Gayral M, Saland E, Chicanne G, Xuereb JM, Marcellin M, Burlet-Schiltz O, Sansonetti PJ, Payrastre B, Tronchere H (2015) TOM1 is a PI5P effector involved in the regulation of endosomal maturation. J Cell Sci 128(4):815–827. https://doi.org/10.1242/jcs.166314

Bond LM, Peden AA, Kendrick-Jones J, Sellers JR, Buss F (2011) Myosin VI and its binding partner optineurin are involved in secretory vesicle fusion at the plasma membrane. Mol Biol Cell 22 (1):54–65. mbc.E10-06-0553 [pii]. https://doi.org/10.1091/mbc.E10-06-0553

Bowen JR, Hwang D, Bai X, Roy D, Spiliotis ET (2011) Septin GTPases spatially guide microtubule organization and plus end dynamics in polarizing epithelia. J Cell Biol 194(2):187–197. https://doi.org/10.1083/jcb.201102076

Branon TC, Bosch JA, Sanchez AD, Udeshi ND, Svinkina T, Carr SA, Feldman JL, Perrimon N, Ting AY (2018) Efficient proximity labeling in living cells and organisms with TurboID. Nat Biotechnol 36(9):880–887. https://doi.org/10.1038/nbt.4201

Brissoni B, Agostini L, Kropf M, Martinon F, Swoboda V, Lippens S, Everett H, Aebi N, Janssens S, Meylan E, Felberbaum-Corti M, Hirling H, Gruenberg J, Tschopp J, Burns K (2006) Intracellular trafficking of interleukin-1 receptor I requires Tollip. Curr Biol 16(22):2265–2270. https://doi.org/10.1016/j.cub.2006.09.062

Bunn RC, Jensen MA, Reed BC (1999) Protein interactions with the glucose transporter binding protein GLUT1CBP that provide a link between GLUT1 and the cytoskeleton. Mol Biol Cell 10(4):819–832

Buss F, Arden SD, Lindsay M, Luzio JP, Kendrick-Jones J (2001) Myosin VI isoform localized to clathrin-coated vesicles with a role in clathrin-mediated endocytosis. EMBO J 20(14):3676–3684

Chibalina MV, Seaman MN, Miller CC, Kendrick-Jones J, Buss F (2007) Myosin VI and its interacting protein LMTK2 regulate tubule formation and transport to the endocytic recycling compartment. J Cell Sci 120(Pt 24):4278–4288

Chibalina MV, Roberts RC, Arden SD, Kendrick-Jones J, Buss F (2008) Rab8-optineurin-myosin VI: analysis of interactions and functions in the secretory pathway. Methods Enzymol 438:11–24. S0076-6879(07)38002-6 [pii]. https://doi.org/10.1016/S0076-6879(07)38002-6

Chibalina MV, Poliakov A, Kendrick-Jones J, Buss F (2010) Myosin VI and optineurin are required for polarised EGFR delivery and directed migration. Traffic. TRA1101 [pii]. https://doi.org/10.1111/j.1600-0854.2010.01101.x

Choi-Rhee E, Schulman H, Cronan JE (2004) Promiscuous protein biotinylation by Escherichia coli biotin protein ligase. Protein Sci 13(11):3043–3050. https://doi.org/10.1110/ps.04911804

Collaco A, Jakab R, Hegan P, Mooseker M, Ameen N (2010) Alpha-AP-2 directs myosin VI-dependent endocytosis of cystic fibrosis transmembrane conductance regulator chloride channels in the intestine. J Biol Chem 285(22):17177–17187. https://doi.org/10.1074/jbc.M110.127613

Cote JF, Vuori K (2002) Identification of an evolutionarily conserved superfamily of DOCK180-related proteins with guanine nucleotide exchange activity. J Cell Sci 115(Pt 24):4901–4913

Couzens AL, Knight JD, Kean MJ, Teo G, Weiss A, Dunham WH, Lin ZY, Bagshaw RD, Sicheri F, Pawson T, Wrana JL, Choi H, Gingras AC (2013) Protein interaction network of the mammalian Hippo pathway reveals mechanisms of kinase-phosphatase interactions. Sci Signal 6(302):rs15. https://doi.org/10.1126/scisignal.2004712

Craig R, Smith R, Kendrick-Jones J (1983) Light-chain phosphorylation controls the conformation of vertebrate non-muscle and smooth muscle myosin molecules. Nature 302(5907):436–439

Dance AL, Miller M, Seragaki S, Aryal P, White B, Aschenbrenner L, Hasson T (2004) Regulation of myosin-VI targeting to endocytic compartments. Traffic 5(10):798–813. https://doi.org/10.1111/j.1600-0854.2004.00224.x

De La Cruz EM, Ostap EM, Sweeney HL (2001) Kinetic mechanism and regulation of myosin VI. J Biol Chem 276(34):32373–32381. https://doi.org/10.1074/jbc.M104136200

De Vries L, Lou X, Zhao G, Zheng B, Farquhar MG (1998) GIPC, a PDZ domain containing protein, interacts specifically with the C terminus of RGS-GAIP. Proc Natl Acad Sci U S A 95(21):12340–12345. https://doi.org/10.1073/pnas.95.21.12340

Duncker SV, Franz C, Kuhn S, Schulte U, Campanelli D, Brandt N, Hirt B, Fakler B, Blin N, Ruth P, Engel J, Marcotti W, Zimmermann U, Knipper

M (2013) Otoferlin couples to clathrin-mediated endocytosis in mature cochlear inner hair cells. J Neurosci 33(22):9508–9519. https://doi.org/10.1523/JNEUROSCI.5689-12.2013

Dunn TA, Chen S, Faith DA, Hicks JL, Platz EA, Chen Y, Ewing CM, Sauvageot J, Isaacs WB, De Marzo AM, Luo J (2006) A novel role of myosin VI in human prostate cancer. Am J Pathol 169(5):1843–1854. doi:169/5/1843 [pii]

Eeles RA, Kote-Jarai Z, Giles GG, Olama AA, Guy M, Jugurnauth SK, Mulholland S, Leongamornlert DA, Edwards SM, Morrison J, Field HI, Southey MC, Severi G, Donovan JL, Hamdy FC, Dearnaley DP, Muir KR, Smith C, Bagnato M, Ardern-Jones AT, Hall AL, O'Brien LT, Gehr-Swain BN, Wilkinson RA, Cox A, Lewis S, Brown PM, Jhavar SG, Tymrakiewicz M, Lophatananon A, Bryant SL, Collaborators UKGPCS, British Association of Urological Surgeons' Section of O, Collaborators UKPS, Horwich A, Huddart RA, Khoo VS, Parker CC, Woodhouse CJ, Thompson A, Christmas T, Ogden C, Fisher C, Jamieson C, Cooper CS, English DR, Hopper JL, Neal DE, Easton DF (2008) Multiple newly identified loci associated with prostate cancer susceptibility. Nat Genet 40(3):316–321. https://doi.org/10.1038/ng.90

Fields S, Song O (1989) A novel genetic system to detect protein-protein interactions. Nature 340(6230):245–246. https://doi.org/10.1038/340245a0

Fili N, Hari-Gupta Y, Dos Santos A, Cook A, Poland S, Ameer-Beg SM, Parsons M, Toseland CP (2017) NDP52 activates nuclear myosin VI to enhance RNA polymerase II transcription. Nat Commun 8(1):1871. https://doi.org/10.1038/s41467-017-02050-w

Finan D, Hartman MA, Spudich JA (2011) Proteomics approach to study the functions of Drosophila myosin VI through identification of multiple cargo-binding proteins. Proc Natl Acad Sci U S A 108(14):5566–5571. https://doi.org/10.1073/pnas.1101415108

Finkielstein CV, Capelluto DG (2016) Disabled-2: a modular scaffold protein with multifaceted functions in signaling. BioEssays 38(Suppl 1):S45–S55. https://doi.org/10.1002/bies.201670907

Foth BJ, Goedecke MC, Soldati D (2006) New insights into myosin evolution and classification. Proc Natl Acad Sci U S A 103(10):3681–3686. https://doi.org/10.1073/pnas.0506307103

Fourie C, Li D, Montgomery JM (2014) The anchoring protein SAP97 influences the trafficking and localisation of multiple membrane channels. Biochim Biophys Acta 1838(2):589–594. https://doi.org/10.1016/j.bbamem.2013.03.015

Francavilla C, Rigbolt KT, Emdal KB, Carraro G, Vernet E, Bekker-Jensen DB, Streicher W, Wikstrom M, Sundstrom M, Bellusci S, Cavallaro U, Blagoev B, Olsen JV (2013) Functional proteomics defines the molecular switch underlying FGF receptor trafficking and cellular outputs. Mol Cell 51(6):707–722. https://doi.org/10.1016/j.molcel.2013.08.002

Fukuhara S, Chikumi H, Gutkind JS (2000) Leukemia-associated Rho guanine nucleotide exchange factor (LARG) links heterotrimeric G proteins of the G(12) family to Rho. FEBS Lett 485(2–3):183–188

Goodson HV, Dawson SC (2006) Multiplying myosins. Proc Natl Acad Sci U S A 103(10):3498–3499. https://doi.org/10.1073/pnas.0600045103

Gotoh N, Yan Q, Du Z, Biemesderfer D, Kashgarian M, Mooseker MS, Wang T (2010) Altered renal proximal tubular endocytosis and histology in mice lacking myosin-VI. Cytoskeleton (Hoboken) 67(3):178–192. https://doi.org/10.1002/cm.20435

Hartman MA, Finan D, Sivaramakrishnan S, Spudich JA (2011) Principles of unconventional myosin function and targeting. Annu Rev Cell Dev Biol 27:133–155. https://doi.org/10.1146/annurev-cellbio-100809-151502

He F, Wollscheid HP, Nowicka U, Biancospino M, Valentini E, Ehlinger A, Acconcia F, Magistrati E, Polo S, Walters KJ (2016) Myosin VI contains a compact structural motif that binds to ubiquitin chains. Cell Rep 14(11):2683–2694. https://doi.org/10.1016/j.celrep.2016.01.079

Hegan PS, Giral H, Levi M, Mooseker MS (2012) Myosin VI is required for maintenance of brush border structure, composition, and membrane trafficking functions in the intestinal epithelial cell. Cytoskeleton (Hoboken) 69(4):235–251. https://doi.org/10.1002/cm.21018

Heidrych P, Zimmermann U, Kuhn S, Franz C, Engel J, Duncker SV, Hirt B, Pusch CM, Ruth P, Pfister M, Marcotti W, Blin N, Knipper M (2009) Otoferlin interacts with myosin VI: implications for maintenance of the basolateral synaptic structure of the inner hair cell. Hum Mol Genet 18(15):2779–2790. https://doi.org/10.1093/hmg/ddp213

Heisler FF, Loebrich S, Pechmann Y, Maier N, Zivkovic AR, Tokito M, Hausrat TJ, Schweizer M, Bahring R, Holzbaur EL, Schmitz D, Kneussel M (2011) Muskelin regulates actin filament- and microtubule-based GABA(A) receptor transport in neurons. Neuron 70(1):66–81. https://doi.org/10.1016/j.neuron.2011.03.008

Heo J-M, Ordureau A, Paulo Joao A, Rinehart J, Harper JW (2015) The PINK1-PARKIN mitochondrial ubiquitylation pathway drives a program of OPTN/NDP52 recruitment and TBK1 activation to promote mitophagy. Mol Cell 60(1):7–20. https://doi.org/10.1016/j.molcel.2015.08.016

Hung V, Zou P, Rhee HW, Udeshi ND, Cracan V, Svinkina T, Carr SA, Mootha VK, Ting AY (2014) Proteomic mapping of the human mitochondrial intermembrane space in live cells via ratiometric APEX tagging. Mol Cell 55(2):332–341. https://doi.org/10.1016/j.molcel.2014.06.003

Karolczak J, Sobczak M, Skowronek K, Redowicz MJ (2015) A kinase anchoring protein 9 is a novel myosin VI binding partner that links myosin VI with the PKA pathway in myogenic cells. Biomed Res Int 2015:816019. https://doi.org/10.1155/2015/816019

Katoh M (2013) Functional proteomics, human genetics and cancer biology of GIPC family members. Exp Mol Med 45:e26. https://doi.org/10.1038/emm.2013.49

Kesavapany S, Lau KF, Ackerley S, Banner SJ, Shemilt SJ, Cooper JD, Leigh PN, Shaw CE, McLoughlin DM, Miller CC (2003) Identification of a novel, membrane-associated neuronal kinase, cyclin-dependent kinase 5/p35-regulated kinase. J Neurosci 23(12):4975–4983

Kim YM, Kim DH (2013) dRAGging amino acid-mTORC1 signaling by SH3BP4. Mol Cells 35(1):1–6. https://doi.org/10.1007/s10059-013-2249-1

Kim DI, Roux KJ (2016) Filling the void: proximity-based labeling of proteins in living cells. Trends Cell Biol 26(11):804–817. https://doi.org/10.1016/j.tcb.2016.09.004

Kim YM, Stone M, Hwang TH, Kim YG, Dunlevy JR, Griffin TJ, Kim DH (2012) SH3BP4 is a negative regulator of amino acid-Rag GTPase-mTORC1 signaling. Mol Cell 46(6):833–846. https://doi.org/10.1016/j.molcel.2012.04.007

Kim DI, Birendra KC, Zhu W, Motamedchaboki K, Doye V, Roux KJ (2014) Probing nuclear pore complex architecture with proximity-dependent biotinylation. Proc Natl Acad Sci U S A 111(24):E2453–E2461. https://doi.org/10.1073/pnas.1406459111

Kim DI, Jensen SC, Noble KA, Kc B, Roux KH, Motamedchaboki K, Roux KJ (2016) An improved smaller biotin ligase for BioID proximity labeling. Mol Biol Cell 27(8):1188–1196. https://doi.org/10.1091/mbc.E15-12-0844

Kinoshita M, Field CM, Coughlin ML, Straight AF, Mitchison TJ (2002) Self- and actin-templated assembly of mammalian septins. Dev Cell 3(6):791–802

Kobayashi N, Yang J, Ueda A, Suzuki T, Tomaru K, Takeno M, Okuda K, Ishigatsubo Y (2007) RanBPM, Muskelin, p48EMLP, p44CTLH, and the armadillo-repeat proteins ARMC8alpha and ARMC8beta are components of the CTLH complex. Gene 396(2):236–247. https://doi.org/10.1016/j.gene.2007.02.032

Kourlas PJ, Strout MP, Becknell B, Veronese ML, Croce CM, Theil KS, Krahe R, Ruutu T, Knuutila S, Bloomfield CD, Caligiuri MA (2000) Identification of a gene at 11q23 encoding a guanine nucleotide exchange factor: evidence for its fusion with MLL in acute myeloid leukemia. Proc Natl Acad Sci U S A 97(5):2145–2150. https://doi.org/10.1073/pnas.040569197

Kruppa AJ, Kishi-Itakura C, Masters TA, Rorbach JE, Grice GL, Kendrick-Jones J, Nathan JA, Minczuk M, Buss F (2018) Myosin VI-dependent actin cages encapsulate Parkin-positive damaged mitochondria. Dev Cell 44(4):484–499. e486. https://doi.org/10.1016/j.devcel.2018.01.007

Kwon K, Beckett D (2000) Function of a conserved sequence motif in biotin holoenzyme synthetases. Protein Sci 9(8):1530–1539. https://doi.org/10.1110/ps.9.8.1530

Lazarou M, Sliter DA, Kane LA, Sarraf SA, Wang C, Burman JL, Sideris DP, Fogel AI, Youle RJ (2015) The ubiquitin kinase PINK1 recruits autophagy receptors to induce mitophagy. Nature 524(7565):309–314. https://doi.org/10.1038/nature14893

Lin DC, Quevedo C, Brewer NE, Bell A, Testa JR, Grimes ML, Miller FD, Kaplan DR (2006) APPL1 associates with TrkA and GIPC1 and is required for nerve growth factor-mediated signal transduction. Mol Cell Biol 26(23):8928–8941

Lister I, Schmitz S, Walker M, Trinick J, Buss F, Veigel C, Kendrick-Jones J (2004) A monomeric myosin VI with a large working stroke. EMBO J 23(8):1729–1738. https://doi.org/10.1038/sj.emboj.76001807600180. [pii]

Lu H, Krementsova EB, Trybus KM (2006) Regulation of myosin V processivity by calcium at the single molecule level. J Biol Chem 281(42):31987–31994. https://doi.org/10.1074/jbc.M605181200

Luz S, Cihil KM, Brautigan DL, Amaral MD, Farinha CM, Swiatecka-Urban A (2014) LMTK2-mediated phosphorylation regulates CFTR endocytosis in human airway epithelial cells. J Biol Chem 289(21):15080–15093. https://doi.org/10.1074/jbc.M114.563742

Majewski L, Sobczak M, Havrylov S, Jozwiak J, Redowicz MJ (2012) Dock7: a GEF for Rho-family GTPases and a novel myosin VI-binding partner in neuronal PC12 cells. Biochem Cell Biol 90(4):565–574. https://doi.org/10.1139/o2012-009

Martell JD, Yamagata M, Deerinck TJ, Phan S, Kwa CG, Ellisman MH, Sanes JR, Ting AY (2016) A split horseradish peroxidase for the detection of intercellular protein-protein interactions and sensitive visualization of synapses. Nat Biotechnol 34(7):774–780. https://doi.org/10.1038/nbt.3563

Maruyama H, Morino H, Ito H, Izumi Y, Kato H, Watanabe Y, Kinoshita Y, Kamada M, Nodera H, Suzuki H, Komure O, Matsuura S, Kobatake K, Morimoto N, Abe K, Suzuki N, Aoki M, Kawata A, Hirai T, Kato T, Ogasawara K, Hirano A, Takumi T, Kusaka H, Hagiwara K, Kaji R, Kawakami H (2010) Mutations of optineurin in amyotrophic lateral sclerosis. Nature 465(7295):223–226. nature08971 [pii]. https://doi.org/10.1038/nature08971

Masters TA, Tumbarello DA, Chibalina MV, Buss F (2017) MYO6 regulates spatial organization of signaling endosomes driving AKT activation and actin dynamics. Cell Rep 19(10):2088–2101. https://doi.org/10.1016/j.celrep.2017.05.048

Mehla J, Caufield JH, Uetz P (2015) Mapping protein-protein interactions using yeast two-hybrid assays. Cold Spring Harb Protoc 2015(5):442–452. https://doi.org/10.1101/pdb.prot086157

Melchionda S, Ahituv N, Bisceglia L, Sobe T, Glaser F, Rabionet R, Arbones ML, Notarangelo A, Di Iorio E, Carella M, Zelante L, Estivill X, Avraham KB, Gasparini P (2001) MYO6, the human homologue of the gene responsible for deafness in Snell's waltzer mice, is mutated in autosomal dominant nonsyndromic hearing loss. Am J Hum Genet 69(3):635–640. https://doi.org/10.1086/323156

Menetrey J, Bahloul A, Wells AL, Yengo CM, Morris CA, Sweeney HL, Houdusse A (2005) The structure of the

myosin VI motor reveals the mechanism of directionality reversal. Nature 435(7043):779–785. https://doi.org/10.1038/nature03592

Menetrey J, Llinas P, Mukherjea M, Sweeney HL, Houdusse A (2007) The structural basis for the large powerstroke of myosin VI. Cell 131(2):300–308. https://doi.org/10.1016/j.cell.2007.08.027

Mick DU, Rodrigues RB, Leib RD, Adams CM, Chien AS, Gygi SP, Nachury MV (2015) Proteomics of primary cilia by proximity labeling. Dev Cell 35(4):497–512. https://doi.org/10.1016/j.devcel.2015.10.015

Mishra SK, Keyel PA, Hawryluk MJ, Agostinelli NR, Watkins SC, Traub LM (2002) Disabled-2 exhibits the properties of a cargo-selective endocytic clathrin adaptor. EMBO J 21(18):4915–4926. https://doi.org/10.1093/emboj/cdf487

Mitsuuchi Y, Johnson SW, Sonoda G, Tanno S, Golemis EA, Testa JR (1999) Identification of a chromosome 3p14.3-21.1 gene, APPL, encoding an adaptor molecule that interacts with the oncoprotein-serine/threonine kinase AKT2. Oncogene 18(35):4891–4898

Mohiddin SA, Ahmed ZM, Griffith AJ, Tripodi D, Friedman TB, Fananapazir L, Morell RJ (2004) Novel association of hypertrophic cardiomyopathy, sensorineural deafness, and a mutation in unconventional myosin VI (MYO6). J Med Genet 41(4):309–314

Morris SM, Cooper JA (2001) Disabled-2 colocalizes with the LDLR in clathrin-coated pits and interacts with AP-2. Traffic 2(2):111–123

Morris SM, Arden SD, Roberts RC, Kendrick-Jones J, Cooper JA, Luzio JP, Buss F (2002a) Myosin VI binds to and localises with Dab2, potentially linking receptor-mediated endocytosis and the actin cytoskeleton. Traffic 3(5):331–341

Morris SM, Tallquist MD, Rock CO, Cooper JA (2002b) Dual roles for the Dab2 adaptor protein in embryonic development and kidney transport. EMBO J 21(7):1555–1564. https://doi.org/10.1093/emboj/21.7.1555

Morriswood B, Ryzhakov G, Puri C, Arden SD, Roberts R, Dendrou C, Kendrick-Jones J, Buss F (2007) T6BP and NDP52 are myosin VI binding partners with potential roles in cytokine signalling and cell adhesion. J Cell Sci 120(Pt 15):2574–2585. jcs.007005 [pii]. https://doi.org/10.1242/jcs.007005

Mostowy S, Cossart P (2012) Septins: the fourth component of the cytoskeleton. Nat Rev Mol Cell Biol 13(3):183–194. https://doi.org/10.1038/nrm3284

Mukherjea M, Llinas P, Kim H, Travaglia M, Safer D, Menetrey J, Franzini-Armstrong C, Selvin PR, Houdusse A, Sweeney HL (2009) Myosin VI dimerization triggers an unfolding of a three-helix bundle in order to extend its reach. Mol Cell 35(3):305–315. https://doi.org/10.1016/j.molcel.2009.07.010

Naccache SN, Hasson T, Horowitz A (2006) Binding of internalized receptors to the PDZ domain of GIPC/synectin recruits myosin VI to endocytic vesicles. Proc Natl Acad Sci U S A 103(34):12735–12740. 0605317103 [pii]. https://doi.org/10.1073/pnas.0605317103

Nakazawa S, Oikawa D, Ishii R, Ayaki T, Takahashi H, Takeda H, Ishitani R, Kamei K, Takeyoshi I, Kawakami H, Iwai K, Hatada I, Sawasaki T, Ito H, Nureki O, Tokunaga F (2016) Linear ubiquitination is involved in the pathogenesis of optineurin-associated amyotrophic lateral sclerosis. Nat Commun 7:12547. https://doi.org/10.1038/ncomms12547

Naora H, Montell DJ (2005) Ovarian cancer metastasis: integrating insights from disparate model organisms. Nat Rev Cancer 5(5):355–366. https://doi.org/10.1038/nrc1611

Nash JE, Appleby VJ, Corre SA, Wu H, Fitzjohn SM, Garner CC, Collingridge GL, Molnar E (2009) Disruption of the interaction between myosin VI and SAP97 is associated with a reduction in the number of AMPARs at hippocampal synapses. J Neurochem 112(3):677–690. https://doi.org/10.1111/j.1471-4159.2009.06480

O'Loughlin T, Masters TA, Buss F (2018) The MYO6 interactome reveals adaptor complexes coordinating early endosome and cytoskeletal dynamics. EMBO Rep 19(4). https://doi.org/10.15252/embr.201744884

Osterweil E, Wells DG, Mooseker MS (2005) A role for myosin VI in postsynaptic structure and glutamate receptor endocytosis. J Cell Biol 168(2):329–338. jcb.200410091 [pii]. https://doi.org/10.1083/jcb.200410091

Park H, Li A, Chen LQ, Houdusse A, Selvin PR, Sweeney HL (2007) The unique insert at the end of the myosin VI motor is the sole determinant of directionality. Proc Natl Acad Sci U S A 104(3):778–783. https://doi.org/10.1073/pnas.0610066104

Penengo L, Mapelli M, Murachelli AG, Confalonieri S, Magri L, Musacchio A, Di Fiore PP, Polo S, Schneider TR (2006) Crystal structure of the ubiquitin binding domains of rabex-5 reveals two modes of interaction with ubiquitin. Cell 124(6):1183–1195. S0092-8674(06)00195-4 [pii]. https://doi.org/10.1016/j.cell.2006.02.020

Phichith D, Travaglia M, Yang Z, Liu X, Zong AB, Safer D, Sweeney HL (2009) Cargo binding induces dimerization of myosin VI. Proc Natl Acad Sci U S A 106(41):17320–17324. https://doi.org/10.1073/pnas.0909748106

Pottier C, Bieniek KF, Finch N, van de Vorst M, Baker M, Perkersen R, Brown P, Ravenscroft T, van Blitterswijk M, Nicholson AM, DeTure M, Knopman DS, Josephs KA, Parisi JE, Petersen RC, Boylan KB, Boeve BF, Graff-Radford NR, Veltman JA, Gilissen C, Murray ME, Dickson DW, Rademakers R (2015) Whole-genome sequencing reveals important role for TBK1 and OPTN mutations in frontotemporal lobar degeneration without motor neuron disease. Acta Neuropathol 130(1):77–92. https://doi.org/10.1007/s00401-015-1436-x

Puertollano R (2005) Interactions of TOM1L1 with the multivesicular body sorting machinery. J Biol Chem 280(10):9258–9264. https://doi.org/10.1074/jbc.M412481200

Pylypenko O, Song L, Squires G, Liu X, Zong AB, Houdusse A, Sweeney HL (2011) Role of insert-1 of myosin VI in modulating nucleotide affinity. J Biol Chem 286(13):11716–11723. https://doi.org/10.1074/jbc.M110.200626

Rattray M (2012) New insights on regulation of LMTK2, a membrane kinase integrating pathways central to neurodegeneration. J Neurochem 121(3):327–328. https://doi.org/10.1111/j.1471-4159.2012.07654.x

Ravenhill BJ, Boyle KB, von Muhlinen N, Ellison CJ, Masson GR, Otten EG, Foeglein A, Williams R, Randow F (2019) The cargo receptor NDP52 initiates selective autophagy by recruiting the ULK complex to cytosol-invading bacteria. Mol Cell 74(2):320–329. e326. https://doi.org/10.1016/j.molcel.2019.01.041

Regelmann J, Schule T, Josupeit FS, Horak J, Rose M, Entian KD, Thumm M, Wolf DH (2003) Catabolite degradation of fructose-1,6-bisphosphatase in the yeast Saccharomyces cerevisiae: a genome-wide screen identifies eight novel GID genes and indicates the existence of two degradation pathways. Mol Biol Cell 14(4):1652–1663. https://doi.org/10.1091/mbc.e02-08-0456

Rezaie T, Child A, Hitchings R, Brice G, Miller L, Coca-Prados M, Heon E, Krupin T, Ritch R, Kreutzer D, Crick RP, Sarfarazi M (2002) Adult-onset primary open-angle glaucoma caused by mutations in optineurin. Science 295(5557):1077–1079. https://doi.org/10.1126/science.1066901

Rhee HW, Zou P, Udeshi ND, Martell JD, Mootha VK, Carr SA, Ting AY (2013) Proteomic mapping of mitochondria in living cells via spatially restricted enzymatic tagging. Science 339(6125):1328–1331. https://doi.org/10.1126/science.1230593

Rock RS, Rice SE, Wells AL, Purcell TJ, Spudich JA, Sweeney HL (2001) Myosin VI is a processive motor with a large step size. Proc Natl Acad Sci U S A 98(24):13655–13659. https://doi.org/10.1073/pnas.191512398

Rothbauer U, Zolghadr K, Tillib S, Nowak D, Schermelleh L, Gahl A, Backmann N, Conrath K, Muyldermans S, Cardoso MC, Leonhardt H (2006) Targeting and tracing antigens in live cells with fluorescent nanobodies. Nat Methods 3(11):887–889. https://doi.org/10.1038/nmeth953

Rothbauer U, Zolghadr K, Muyldermans S, Schepers A, Cardoso MC, Leonhardt H (2008) A versatile nanotrap for biochemical and functional studies with fluorescent fusion proteins. Mol Cell Proteomics 7(2):282–289. https://doi.org/10.1074/mcp.M700342-MCP200

Roux I, Hosie S, Johnson SL, Bahloul A, Cayet N, Nouaille S, Kros CJ, Petit C, Safieddine S (2009) Myosin VI is required for the proper maturation and function of inner hair cell ribbon synapses. Hum Mol Genet 18(23):4615–4628. ddp429 [pii]. https://doi.org/10.1093/hmg/ddp429

Roux KJ, Kim DI, Raida M, Burke B (2012) A promiscuous biotin ligase fusion protein identifies proximal and interacting proteins in mammalian cells. J Cell Biol 196(6):801–810. jcb.201112098 [pii]. https://doi.org/10.1083/jcb.201112098

Ryan TA, Tumbarello DA (2018) Optineurin: a coordinator of membrane-associated cargo trafficking and autophagy. Front Immunol 9:1024. https://doi.org/10.3389/fimmu.2018.01024

Sahlender DA, Roberts RC, Arden SD, Spudich G, Taylor MJ, Luzio JP, Kendrick-Jones J, Buss F (2005) Optineurin links myosin VI to the Golgi complex and is involved in Golgi organization and exocytosis. J Cell Biol 169(2):285–295

Sakurai K, Hirata M, Yamaguchi H, Nakamura Y, Fukami K (2011) Phospholipase Cdelta3 is a novel binding partner of myosin VI and functions as anchoring of myosin VI on plasma membrane. Adv Enzym Regul 51(1):171–181. https://doi.org/10.1016/j.advenzreg.2010.09.014

Sebe-Pedros A, Grau-Bove X, Richards TA, Ruiz-Trillo I (2014) Evolution and classification of myosins, a paneukaryotic whole-genome approach. Genome Biol Evol 6(2):290–305. https://doi.org/10.1093/gbe/evu013

Seet LF, Hong W (2005) Endofin recruits clathrin to early endosomes via TOM1. J Cell Sci 118(Pt 3):575–587. https://doi.org/10.1242/jcs.01628

Sellin ME, Holmfeldt P, Stenmark S, Gullberg M (2011) Microtubules support a disk-like septin arrangement at the plasma membrane of mammalian cells. Mol Biol Cell 22(23):4588–4601. https://doi.org/10.1091/mbc.E11-09-0754

Seroussi E, Kedra D, Kost-Alimova M, Sandberg-Nordqvist AC, Fransson I, Jacobs JF, Fu Y, Pan HQ, Roe BA, Imreh S, Dumanski JP (1999) TOM1 genes map to human chromosome 22q13.1 and mouse chromosome 8C1 and encode proteins similar to the endosomal proteins HGS and STAM. Genomics 57(3):380–388. https://doi.org/10.1006/geno.1998.5739

Shah K, Bradbury NA (2015) Lemur tyrosine kinase 2, a novel target in prostate cancer therapy. Oncotarget 6(16):14233–14246. https://doi.org/10.18632/oncotarget.3899

Shang G, Brautigam CA, Chen R, Lu D, Torres-Vazquez J, Zhang X (2017) Structure analyses reveal a regulated oligomerization mechanism of the PlexinD1/GIPC/myosin VI complex. elife 6. https://doi.org/10.7554/eLife.27322

Shiba Y, Katoh Y, Shiba T, Yoshino K, Takatsu H, Kobayashi H, Shin HW, Wakatsuki S, Nakayama K (2004) GAT (GGA and Tom1) domain responsible for ubiquitin binding and ubiquitination. J Biol Chem 279(8):7105–7111. https://doi.org/10.1074/jbc.M311702200

Sobczak M, Chumak V, Pomorski P, Wojtera E, Majewski L, Nowak J, Yamauchi J, Redowicz MJ (2016) Interaction of myosin VI and its binding partner DOCK7 plays an important role in NGF-stimulated protrusion formation in PC12 cells. Biochim Biophys Acta 1863(7 Pt A):1589–1600. https://doi.org/10.1016/j.bbamcr.2016.03.020

Spudich G, Chibalina MV, Au JS, Arden SD, Buss F, Kendrick-Jones J (2007) Myosin VI targeting to clathrin-coated structures and dimerization is mediated by binding to Disabled-2 and PtdIns(4,5)P2. Nat Cell Biol 9(2):176–183. ncb1531 [pii]. https://doi.org/10.1038/ncb1531

Suzuki N, Nakamura S, Mano H, Kozasa T (2003) Galpha 12 activates Rho GTPase through tyrosine-phosphorylated leukemia-associated RhoGEF. Proc Natl Acad Sci U S A 100(2):733–738. https://doi.org/10.1073/pnas.0234057100

Sweeney HL, Houdusse A (2010) Structural and functional insights into the Myosin motor mechanism. Annu Rev Biophys 39:539–557. https://doi.org/10.1146/annurev.biophys.050708.133751

Sweeney HL, Park H, Zong AB, Yang Z, Selvin PR, Rosenfeld SS (2007) How myosin VI coordinates its heads during processive movement. EMBO J 26(11):2682–2692. https://doi.org/10.1038/sj.emboj.7601720

Tai Y, Janas JA, Wang CL, Van Aelst L (2014) Regulation of chandelier cell cartridge and Bouton development via DOCK7-mediated ErbB4 activation. Cell Rep 6(2):254–263. https://doi.org/10.1016/j.celrep.2013.12.034

Teckchandani A, Mulkearns EE, Randolph TW, Toida N, Cooper JA (2012) The clathrin adaptor Dab2 recruits EH domain scaffold proteins to regulate integrin beta1 endocytosis. Mol Biol Cell 23(15):2905–2916. https://doi.org/10.1091/mbc.E11-12-1007

ten Have S, Boulon S, Ahmad Y, Lamond AI (2011) Mass spectrometry-based immuno-precipitation proteomics – the user's guide. Proteomics 11(6):1153–1159. https://doi.org/10.1002/pmic.201000548

Thirumurugan K, Sakamoto T, Hammer JA 3rd, Sellers JR, Knight PJ (2006) The cargo-binding domain regulates structure and activity of myosin 5. Nature 442(7099):212–215. https://doi.org/10.1038/nature04865

Thurston TL, Ryzhakov G, Bloor S, von Muhlinen N, Randow F (2009) The TBK1 adaptor and autophagy receptor NDP52 restricts the proliferation of ubiquitin-coated bacteria. Nat Immunol 10(11):1215–1221. ni.1800 [pii]. https://doi.org/10.1038/ni.1800

Thurston TL, Wandel MP, von Muhlinen N, Foeglein A, Randow F (2012) Galectin 8 targets damaged vesicles for autophagy to defend cells against bacterial invasion. Nature 482(7385):414–418. https://doi.org/10.1038/nature10744

Tomatis VM, Papadopulos A, Malintan NT, Martin S, Wallis T, Gormal RS, Kendrick-Jones J, Buss F, Meunier FA (2013) Myosin VI small insert isoform maintains exocytosis by tethering secretory granules to the cortical actin. J Cell Biol 200(3):301–320. https://doi.org/10.1083/jcb.201204092

Tosoni D, Puri C, Confalonieri S, Salcini AE, De Camilli P, Tacchetti C, Di Fiore PP (2005) TTP specifically regulates the internalization of the transferrin receptor. Cell 123(5):875–888. https://doi.org/10.1016/j.cell.2005.10.021

Tumbarello DA, Waxse BJ, Arden SD, Bright NA, Kendrick-Jones J, Buss F (2012) Autophagy receptors link myosin VI to autophagosomes to mediate Tom1-dependent autophagosome maturation and fusion with the lysosome. Nat Cell Biol 14(10):1024–1035. https://doi.org/10.1038/ncb2589

Tumbarello DA, Kendrick-Jones J, Buss F (2013) Myosin VI and its cargo adaptors – linking endocytosis and autophagy. J Cell Sci 126(Pt 12):2561–2570. https://doi.org/10.1242/jcs.095554

Tumbarello DA, Manna PT, Allen M, Bycroft M, Arden SD, Kendrick-Jones J, Buss F (2015) The autophagy receptor TAX1BP1 and the molecular motor myosin VI are required for clearance of Salmonella Typhimurium by Autophagy. PLoS Pathog 11(10):e1005174. https://doi.org/10.1371/journal.ppat.1005174

Umeki N, Jung HS, Watanabe S, Sakai T, Li XD, Ikebe R, Craig R, Ikebe M (2009) The tail binds to the head-neck domain, inhibiting ATPase activity of myosin VIIA. Proc Natl Acad Sci U S A 106(21):8483–8488. https://doi.org/10.1073/pnas.0812930106

Varsano T, Dong MQ, Niesman I, Gacula H, Lou X, Ma T, Testa JR, Yates JR 3rd, Farquhar MG (2006) GIPC is recruited by APPL to peripheral TrkA endosomes and regulates TrkA trafficking and signaling. Mol Cell Biol 26(23):8942–8952

Varsano T, Taupin V, Guo L, Baterina OY Jr, Farquhar MG (2012) The PDZ protein GIPC regulates trafficking of the LPA1 receptor from APPL signaling endosomes and attenuates the cell's response to LPA. PLoS One 7(11):e49227. https://doi.org/10.1371/journal.pone.0049227

Vreugde S, Ferrai C, Miluzio A, Hauben E, Marchisio PC, Crippa MP, Bussi M, Biffo S (2006) Nuclear myosin VI enhances RNA polymerase II-dependent transcription. Mol Cell 23(5):749–755. S1097-2765(06)00482-5 [pii]. https://doi.org/10.1016/j.molcel.2006.07.005

Wang H, Brautigan DL (2006) Peptide microarray analysis of substrate specificity of the transmembrane Ser/Thr kinase KPI-2 reveals reactivity with cystic fibrosis transmembrane conductance regulator and phosphorylase. Mol Cell Proteomics 5(11):2124–2130. https://doi.org/10.1074/mcp.M600188-MCP200

Warner CL, Stewart A, Luzio JP, Steel KP, Libby RT, Kendrick-Jones J, Buss F (2003) Loss of myosin VI reduces secretion and the size of the Golgi in fibroblasts from Snell's waltzer mice. EMBO J 22(3):569–579

Watabe-Uchida M, John KA, Janas JA, Newey SE, Van Aelst L (2006) The Rac activator DOCK7 regulates neuronal polarity through local phosphorylation of stathmin/Op18. Neuron 51(6):727–739. https://doi.org/10.1016/j.neuron.2006.07.020

Weirich CS, Erzberger JP, Barral Y (2008) The septin family of GTPases: architecture and dynamics. Nat Rev Mol Cell Biol 9(6):478–489. https://doi.org/10.1038/nrm2407

Wells AL, Lin AW, Chen LQ, Safer D, Cain SM, Hasson T, Carragher BO, Milligan RA, Sweeney HL (1999) Myosin VI is an actin-based motor that moves backwards. Nature 401(6752):505–508

Wild P, Farhan H, McEwan DG, Wagner S, Rogov VV, Brady NR, Richter B, Korac J, Waidmann O, Choudhary C, Dotsch V, Bumann D, Dikic I (2011) Phosphorylation of the autophagy receptor optineurin restricts Salmonella growth. Science 333(6039):228–233. science.1205405 [pii]. https://doi.org/10.1126/science.1205405

Wollscheid HP, Biancospino M, He F, Magistrati E, Molteni E, Lupia M, Soffientini P, Rottner K, Cavallaro U, Pozzoli U, Mapelli M, Walters KJ, Polo S (2016) Diverse functions of myosin VI elucidated by an isoform-specific alpha-helix domain. Nat Struct Mol Biol 23(4):300–308. https://doi.org/10.1038/nsmb.3187

Wong YC, Holzbaur EL (2014) Optineurin is an autophagy receptor for damaged mitochondria in parkin-mediated mitophagy that is disrupted by an ALS-linked mutation. Proc Natl Acad Sci U S A 111(42):E4439–E4448. https://doi.org/10.1073/pnas.1405752111

Wu H, Nash JE, Zamorano P, Garner CC (2002) Interaction of SAP97 with minus-end-directed actin motor myosin VI. Implications for AMPA receptor trafficking. J Biol Chem 277(34):30928–30934. https://doi.org/10.1074/jbc.M203735200

Yamakami M, Yokosawa H (2004) Tom1 (target of Myb 1) is a novel negative regulator of interleukin-1- and tumor necrosis factor-induced signaling pathways. Biol Pharm Bull 27(4):564–566

Yamakami M, Yoshimori T, Yokosawa H (2003) Tom1, a VHS domain-containing protein, interacts with tollip, ubiquitin, and clathrin. J Biol Chem 278(52):52865–52872. https://doi.org/10.1074/jbc.M306740200

Yamauchi J, Miyamoto Y, Chan JR, Tanoue A (2008) ErbB2 directly activates the exchange factor Dock7 to promote Schwann cell migration. J Cell Biol 181(2):351–365. https://doi.org/10.1083/jcb.200709033

Yamauchi J, Miyamoto Y, Hamasaki H, Sanbe A, Kusakawa S, Nakamura A, Tsumura H, Maeda M, Nemoto N, Kawahara K, Torii T, Tanoue A (2011) The atypical Guanine-nucleotide exchange factor, dock7, negatively regulates schwann cell differentiation and myelination. J Neurosci 31(35):12579–12592. https://doi.org/10.1523/JNEUROSCI.2738-11.2011

Yasunaga S, Grati M, Cohen-Salmon M, El-Amraoui A, Mustapha M, Salem N, El-Zir E, Loiselet J, Petit C (1999) A mutation in OTOF, encoding otoferlin, a FER-1-like protein, causes DFNB9, a nonsyndromic form of deafness. Nat Genet 21(4):363–369. https://doi.org/10.1038/7693

Yildiz A, Park H, Safer D, Yang Z, Chen LQ, Selvin PR, Sweeney HL (2004) Myosin VI steps via a hand-over-hand mechanism with its lever arm undergoing fluctuations when attached to actin. J Biol Chem 279(36):37223–37226. https://doi.org/10.1074/jbc.C400252200

Ying H, Shen X, Park B, Yue BY (2010) Posttranslational modifications, localization, and protein interactions of optineurin, the product of a glaucoma gene. PLoS One 5(2):e9168. https://doi.org/10.1371/journal.pone.0009168

Yu C, Feng W, Wei Z, Miyanoiri Y, Wen W, Zhao Y, Zhang M (2009) Myosin VI undergoes cargo-mediated dimerization. Cell 138(3):537–548. S0092-8674(09)00633-3 [pii]. https://doi.org/10.1016/j.cell.2009.05.030

Zhang Z, Chen Y, Tang J, Xie X (2014) Frequent loss expression of dab2 and promotor hypermethylation in human cancers: a meta-analysis and systematic review. Pak J Med Sci 30(2):432–437

Zhang L, Hsu FC, Mojsilovic-Petrovic J, Jablonski AM, Zhai J, Coulter DA, Kalb RG (2015) Structure-function analysis of SAP97, a modular scaffolding protein that drives dendrite growth. Mol Cell Neurosci 65:31–44. https://doi.org/10.1016/j.mcn.2015.02.011

Zhou Y, Johnson JL, Cerione RA, Erickson JW (2013) Prenylation and membrane localization of Cdc42 are essential for activation by DOCK7. Biochemistry 52(25):4354–4363. https://doi.org/10.1021/bi301688g

Zimmermann D, Santos A, Kovar DR, Rock RS (2015) Actin age orchestrates myosin-5 and myosin-6 run lengths. Curr Biol 25(15):2057–2062. https://doi.org/10.1016/j.cub.2015.06.033

Class IX Myosins: Motorized RhoGAP Signaling Molecules

16

Peter J. Hanley, Veith Vollmer, and Martin Bähler

Abstract

Class IX myosins are simultaneously motor and signaling molecules. In addition to myosin class-specific functions of the tail region, they feature unique motor properties. Within their motor region they contain a long insertion with a calmodulin- and a F-actin-binding site. The rate-limiting step in the ATPase cycle is ATP hydrolysis rather than, typical for other myosins, the release of either product. This means that class IX myosins spend a large fraction of their cycle time in the ATP-bound state, which is typically a low F-actin affinity state. Nevertheless, class IX myosins in the ATP-bound state stochastically switch between a low and a high F-actin affinity state. Single motor domains even show characteristics of processive movement towards the plus end of actin filaments. The insertion thereby acts as an actin tether. The motor domain transports as intramolecular cargo a signaling Rho GTPase-activating protein domain located in the tail region. Rho GTPase-activating proteins catalyze the conversion of active GTP-bound Rho to inactive GDP-bound Rho by stimulating GTP hydrolysis. In cells, Rho activity regulates actin cytoskeleton organization and actomyosin II contractility. Thus, class IX myosins regulate cell morphology, cell migration, cell-cell junctions and membrane trafficking. These cellular functions affect embryonic development, adult organ homeostasis and immune responses. Human diseases associated with mutations in the two class IX myosins, Myo9a and Myo9b, have been identified, including hydrocephalus and congenital myasthenic syndrome in connection with Myo9a and autoimmune diseases in connection with Myo9b.

Keywords

Myosin IX · Myo9 · HUM-7 · myr 5 · myr 7 · Myo9a · Myo9b · RhoGAP · Atypical C1 domain · IQ-motif · Calmodulin

16.1 Introduction

Class IX myosins are motorized signaling molecules that regulate the organization of the actin cytoskeleton on which the motor domain depends for directed motility or force generation. Classification of myosin motor proteins is based on motor domain phylogeny. During evolution the last holozoan ancestor acquired in a burst of myosin inventions seven new myosin classes, including amongst others class IX (Kollmar and

P. J. Hanley · V. Vollmer · M. Bähler (✉)
Institute of Molecular Cell Biology, Westfalian Wilhelms University Münster, Münster, Germany
e-mail: baehler@uni-muenster.de

L. M. Coluccio (ed.), *Myosins*, Advances in Experimental Medicine and Biology 1239,
https://doi.org/10.1007/978-3-030-38062-5_16

Mühlhausen 2017). Since then class IX myosin has undergone processes of both duplications and losses. Invertebrate model organisms have either a single myosin 9 such as *Caenorhabditis elegans* or none such as *Drosophila melanogaster*. Nevertheless, the genomes of a variety of other insects and even diptera contain a gene encoding for a class IX myosin. Vertebrates on the other hand harbor either two class IX myosin genes, Myo9a and Myo9b, as is the case for mammals, or four, Myo9a-d, as in bony fishes, e.g., zebrafish *Danio rerio*. Individual members of class IX myosins were initially named HUM-7 (Myo9 from *C. elegans*), myr 5 (Myo9b from rat) and myr 7 (Myo9a from rat). Studies on class IX myosins have focused until now on Myo9 from *C. elegans* and Myo9a/b from mammals.

16.2 Myosin IX Domain Structure

Class IX myosins encompass in addition to their myosin motor domain several motifs and domains that are present also in other proteins (Fig.16.1). At the N-terminus there is a Ras-association (RA) domain. This domain adopts a similar folding topology to RA domains in Ras-effector proteins that associate with active GTP-bound Ras. However, the RA domain in class IX myosins is unable to associate with Ras (Kalhammer et al. 1997). In accordance with this finding, modeling of the RA domain demonstrated a different surface shape and charge at the presumed Ras contact site. The conserved myosin head region follows the RA domain. Noteworthy, at the position of loop 2 the head region contains a unique long insertion of about 145 or more residues. This insertion contains at its N-terminus a highly conserved calmodulin-binding site (Liao et al. 2010; Saczko-Brack et al. 2016). Furthermore, this insertion interacts with actin filaments (Struchholz et al. 2009). Apart from this unique insertion, the head region of class IX myosins conforms to other myosin heads. Following the head region class IX myosins contain a light chain-binding region with 4–6 IQ-motifs, each of which can bind the Ca^{2+}-sensor protein calmodulin. The binding of calmodulin to the IQ motifs allows for the formation of a rigid lever arm, the length of which determines the step size during force production or motility. The associated light chains have additionally a regulatory function. The light chain-binding or neck region connects to an extended tail region. The tail region contains one or two atypical C1 domains. The structure of C1 domains is determined by the coordination of two zinc ions (Reinhard et al. 1995). Atypical C1 domains are distinguished from typical C1 domains in that they do not bind diacylglycerol and phorbol esters. Furthermore, the tail region encompasses C-terminal to the single or second C1 domain, a Rho GTPase activating protein (RhoGAP) domain that catalyzes GTP hydrolysis by small monomeric GTPases of the Rho subfamily, switching them from the active GTP-bound "on" state to the inactive GDP-bound "off" state. In addition to these domains shared by all class IX myosins there exist a number of alternatively-spliced sequences that contain no known motifs or functions.

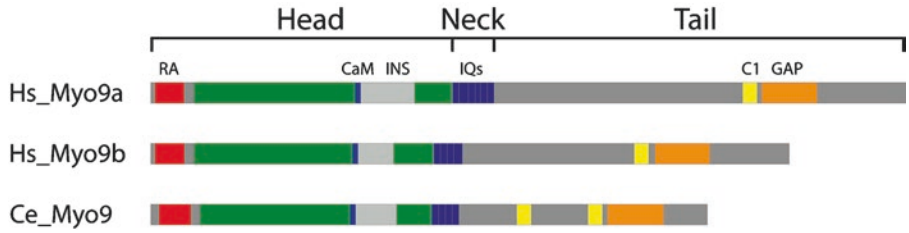

Fig. 16.1 Schematic bar diagrams of the domain organizations of mammalian and invertebrate class IX myosins. Hs: *Homo sapiens*; Ce: *Caenorhabditis elegans*; RA: Ras association motif (red); CaM: calmodulin (blue); INS: loop2 insertion (light grey); IQ: IQ-motif (blue); C1: atypical C1 zinc-ion binding domain (yellow); GAP: Rho GTPase-activating protein (orange)

16.3 Myosin IX Motor Properties

Class IX myosins are active motors that show actin-activated ATPase activity and when adsorbed in an oriented manner to a surface induce gliding of actin filaments by plus-end directed motion (Post et al. 1998, 2002; Inoue et al. 2002; O'Connell and Mooseker 2003; Liao et al. 2010; Saczko-Brack et al. 2016). Kinetic analysis of the ATPase cycle of rat and human Myo9b revealed unique properties. Unlike in other myosins, the rate-limiting step in the ATPase cycle of rat and human Myo9b was found to be ATP hydrolysis (Nalavadi et al. 2005; Kambara and Ikebe 2006). The ATP-bound state of myosins generally has a weak affinity for F-actin but not so for Myo9b. In the ATP-bound state a subpopulation of Myo9b still demonstrated a remarkably high affinity for F-actin. Curiously, Myo9b in the ATP-bound state demonstrated a stochastic interconversion between states of weak and high F-actin affinity (Nalavadi et al. 2005). The high affinity for F-actin in the ATP-bound state seems to be due to the unique insertion in the head region that can associate with actin filaments (Nalavadi et al. 2005; Struchholz et al. 2009). Although class IX myosins are single-headed and spend most of their cycling time in an ATP-bound weak F-actin affinity state, it was reported by different groups that class IX myosins show characteristics of a processive motor that takes multiple successive steps along F-actin without dissociating (Post et al. 2002; Inoue et al. 2002; Nishikawa et al. 2006; Liao et al. 2010; Elfrink et al. 2014). Processive movement of Myo9 from *C. elegans* requires the unique insertion that serves as an actin tether (Elfrink et al. 2014). This mechanism differs from the hand-over-hand movement by the other processive myosins that are all double-headed and for which ADP release is the rate-limiting step in the ATPase cycle. To explain processive movement of single-headed Myo9, a Brownian ratchet model has been proposed that involves an active role of actin (Xie 2010). Alternatively, a Brownian motor model similar to that proposed for the single-headed kinesin KIF1A might apply to the processive movement of Myo9 along F-actin (Okada and Hirokawa 2000; Okada et al. 2003; Nitta et al. 2004). More work will be needed to elucidate whether class IX myosins function as processive motors *in vivo*.

The ATPase- and motor activities of class IX myosins are regulated by binding of Ca^{2+} ions to calmodulin. Actin gliding velocity by full-length Myo9b was decreased in the presence of Ca^{2+} ions, whereas steady-state ATPase activity of truncated Myo9 and Myo9a motor constructs was increased (Post et al. 1998; Liao et al. 2010; Saczko-Brack et al. 2016). These differences might be explained by the use of different constructs. More detailed studies are needed on the regulation of class IX myosin motor activities by Ca^{2+} ions and the tail region.

Structural studies revealed that human Myo9a in the nucleotide-free state is able to cross-link actin filaments into parallel bundles forming a lattice with a 36-nm interval along the actin filaments, matching the length of the actin helical repeat. The insertion formed a second actin-binding site that could adopt three different conformations. It bound either to the same filament as the head region or in two different orientations to a neighboring filament (Saczko-Brack et al. 2016).

16.4 Myosin IX RhoGAP Activity and Tail Properties

The RhoGAP domains of both mammalian Myo9a and Myo9b were shown *in vitro* and *in vivo* to activate GTP hydrolysis preferentially of RhoA (Reinhard et al. 1995; Müller et al. 1997; Chieregatti et al. 1998; Yi et al. 2016). For Myo9 from *C. elegans* RhoGAP activity was demonstrated genetically (Wallace et al. 2018). Furthermore, *in vitro* Myo9b was shown to activate the closely related GTPases RhoA, RhoB and RhoC to a comparable extent (Graf et al. 2000). Mutation of a single arginine residue that is conserved in many GAPs for small monomeric GTPases, the so-called arginine finger (Scheffzek et al. 1998), abolished GAP activity (Müller et al. 1997). More recently, it was shown that mutation of a second arginine residue also abolishes GAP

activity. Determination of the Myo9b RhoGAP structure in complex with RhoA-GDP and magnesium fluoride revealed that this arginine residue substitutes for the canonical asparagine residue at this position in other GAPs (Yi et al. 2016). The RhoGAP domain of Myo9b was found to interact with the cytosolic region of the single transmembrane receptor Robo1 that becomes activated by the secreted glycoprotein SLIT. This interaction inhibits the GAP activity (Kong et al. 2015).

The function of the atypical C1 domain that is located just N-terminal to the GAP domain remains to be determined. At least *in vitro*, it does not affect GAP activity (unpublished observation, K. Uhlenbrock and M. Bähler).

The tail regions of both Myo9a and Myo9b become phosphorylated at multiple sites (Daub et al. 2008; Dephoure et al. 2008; Huttlin et al. 2010; Gnad et al. 2011; Rigbolt et al. 2011; Lundby et al. 2012; Zhou et al. 2013; Bian et al. 2014). However, so far it is not known whether phosphorylation of the tail region plays any regulatory role.

A PDZ-binding motif that interacts with a PDZ-like domain in the F11 protein of Vaccinia virus was discovered at the very C-terminus of Myo9a. This interaction promotes viral spread through the inhibition of RhoA activity by the recruitment of Myo9a and its RhoGAP domain (Handa et al. 2013). Several additional binding partners for class IX myosins have been identified, e.g., JNK and ezrin; however, the physiological significance of these interactions is currently not known.

16.5 Myosin IX in Diseases

Mutations in class IX myosins have been implicated in a number of human diseases. A human fetus with hydrocephalus and akinesia was found to carry a homozygous nonsense mutation in Myo9a (Maddirevula et al. 2019). In line with this finding, formation of postnatal hydrocephalus was also observed in Myo9a-deficient mice (Abouhamed et al. 2009). Furthermore, Myo9a was associated with congenital myasthenic syndrome, which might be caused by impaired vesicular transport (O'Connor et al. 2016, 2018; Yiş et al. 2017). Myo9a-deficient mice additionally develop bilateral renal disease, characterized by dilation of proximal tubules, calyceal dilation, and thinning of the parenchyma and fibrosis. These structural changes were accompanied by polyuria and low-molecular-weight proteinuria (Thelen et al. 2015). For the second class IX myosin, Myo9b, it is somewhat controversial whether certain variants are linked to increased risk for intestinal bowel diseases such as celiac disease, Crohn's disease, ulcerative colitis and pancreatitis (Wang et al. 2016; Li et al. 2016; Chen et al. 2016; Nijmeijer et al. 2013). Mice deficient for Myo9b show impaired intestinal barrier function and superficial ulceration in the ileum (Hegan et al. 2016). These mice also show altered innate and adaptive immune responses, as well as altered bone characteristics (Hanley et al. 2010; Xu et al. 2014; Liu et al. 2015; Moalli et al. 2018; McMichael et al. 2017; Kim et al. 2018). More diseases linked to altered class IX myosins are likely to be discovered in the future.

16.6 Myo9 in *C. elegans* Development

Myo9 regulates embryonic morphogenesis in *C. elegans* (Wallace et al. 2018). It integrates signals from the cell surface receptor Sax-3/ROBO to negatively modulate RHO-1/RhoA signaling, leading to decreased actomyosin contractility and cell migration. This affects cell migrations required for epiboly and the timing of epidermal morphogenesis. Myo9 also functions in postembryonic axonal guidance.

16.7 Myosin IXa in Epithelia

Myo9a localizes in epithelial cells along the actin belt of cell junctions and in the cytosol (Abouhamed et al. 2009; Omelchenko and Hall 2012; Thelen et al. 2015) (Fig. 16.2). Mice deficient for Myo9a develop postnatally in the brain stenosis of the ventral caudal 3rd ventricle and

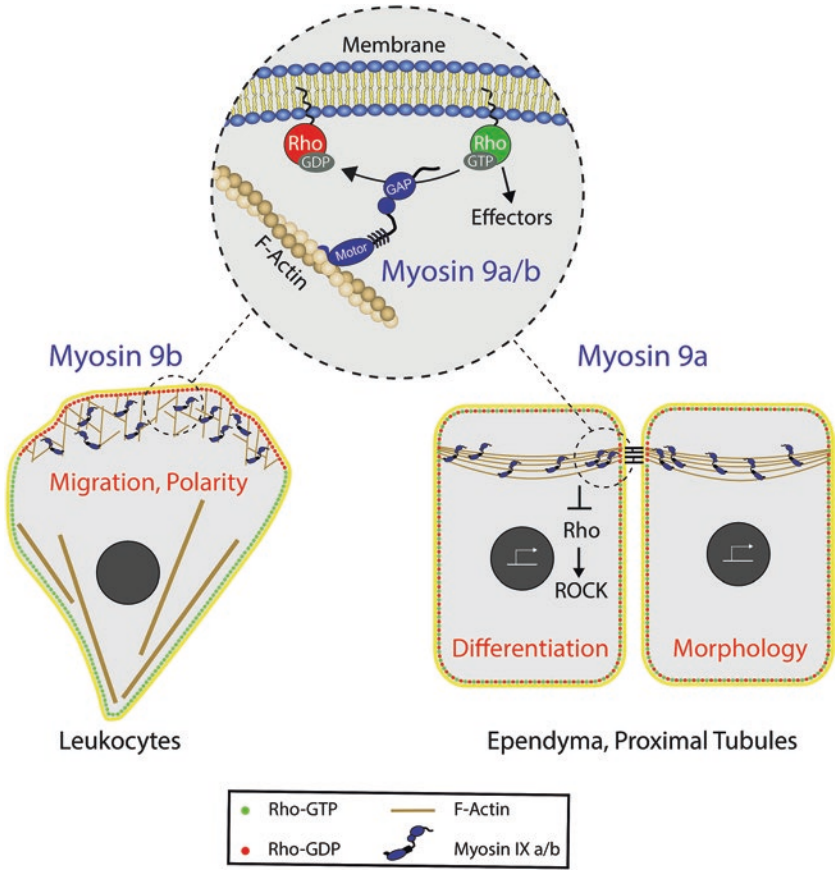

Fig. 16.2 Graphical illustration of the functions of the two mammalian class IX myosins. Class IX myosins produce directional force along actin filaments. In their tail region they contain a GTPase-activating protein (GAP) domain that catalyzes the inactivation of the small monomeric G-protein RhoA. Myo9a localizes in epithelial cells to areas of cell-cell contact that are connected to an F-actin belt. It regulates the morphology and differentiation of ependymal and proximal tubule epithelial cells. The differentiation is regulated through Rho and Rho-kinase signaling. Myo9b localizes to dynamic F-actin at the extending cell front where it negatively regulates Rho signaling. Thereby it controls the cell polarity and migration of leukocytes

the aqueduct (Abouhamed et al. 2009). The ventricle and the aqueduct are lined by multiciliated epithelial cells, the ependyma, that separate cerebrospinal fluid from nervous tissue. Lack of Myo9a reduced the maturation of ependymal cells, perturbed their cell shape and cell-cell contacts so that cells delaminated. Inhibition of Rho-kinase (ROCK) attenuated hydrocephalus formation and rescued the maturation of ependymal cells, indicating that Myo9a regulates, at least in part, Rho-ROCK signaling (Abouhamed et al. 2009). Defects were also observed for the proximal tubules in the kidney when Myo9a was lost (Thelen et al. 2015). The epithelial cells forming the proximal tubules appeared flattened and correspondingly the tubules were dilated. The amount of albumin and megalin, a receptor for albumin, appeared to be increased at the apical surface of the epithelial cells, indicative of impaired membrane trafficking. Downregulation of Myo9a in different epithelial cell lines mimicked largely the *in vivo* observations (Abouhamed et al. 2009; Thelen et al. 2015; Omelchenko and Hall 2012). Downregulation of Myo9a in Caco-2 cells resulted in a modest increase in Rho-ROCK signaling (Abouhamed et al. 2009). Staining for the differentiation marker DPPIV was reduced. The regular cell shape was lost and the cells

appeared more flattened. Moreover, Rho-dependent as well as independent gene transcription was altered in Myo9a knock-down Caco-2 cells. In bronchial epithelial 16HBE cells the knock-down of Myo9a even led to cell scattering due to a defect in junction formation because of increased Rho-activity at nascent cell-cell contacts (Omelchenko and Hall 2012). However, cell scattering was not observed either in Caco-2 or LLC-PK1 cells when Myo9a was downregulated (Abouhamed et al. 2009; Thelen et al. 2015). Upon downregulation of Myo9a in the pig proximal tubule epithelial cell line LLC-PK1, the cells altered their cell shape and started to grow on top of each other without losing cell-cell junctions (Thelen et al. 2015). The knockdown cells showed in accordance with the *in vivo* findings increased binding of albumin to cell surface receptors. Myo9a might have comparable functions in neurons in that it regulates synaptic cell-cell contacts, membrane trafficking and cell morphology (Folci et al. 2016; O'Connor et al. 2018). Further work will be needed to elucidate the exact molecular mechanisms of how Myo9a motor, RhoGAP and possibly unknown activities are regulated and how they in turn affect epithelial and neuronal cell shape, cell-cell junctions, membrane trafficking and cell fate.

16.8 Myosin IXb in Cell Migration

In mammals Myo9b is widely expressed in many tissues during development and in the adult. It is well expressed in leukocytes (Reinhard et al. 1995; Wirth et al. 1996; Chieregatti et al. 1998) and regulates their motility (Fig. 16.2). The chemotactic migration of mouse dendritic cells (DCs), T cells and peritoneal macrophages that lack Myo9b was impaired (Hanley et al. 2010; Xu et al. 2014; Moalli et al. 2018). Myo9b-deficient peritoneal macrophages showed *in vitro* severe defects in morphological polarization, motility and chemotaxis (Hanley et al. 2010). In an *in vivo* experimental model of complement C5a-induced peritonitis, recruitment of mononuclear phagocytes in Myo9b−/− mice was reduced in comparison to wild-type mice. Similarly, the motility of Myo9b−/− DCs was reduced both in collagen gel matrices *in vitro* and *in vivo* (Xu et al. 2014). In the absence of Myo9b the accumulation of $CD8^+$ T cells in non-lymphoid tissues is strongly impaired as Myo9b is required for T-cell crossing of basement membranes (Moalli et al. 2018). Myo9b regulates cell migration not only in leukocytes but also in Caco-2 epithelial cells and the lung cancer cell line H1299 (Chandhoke and Mooseker 2012; Kong et al. 2015; Yi et al. 2016). On a molecular level the loss of Myo9b in leukocytes leads to increased RhoA activity. This in turn increases acto-myosin II contractility and decreases the activity of the actin-depolymerizing factor cofilin. To migrate, cells need to polarize into a front and a back. The driving force for front extension is provided by actin polymerization that can be induced by the Rho subfamily small monomeric GTPases Cdc42 and Rac. The back is retracted through acto-myosin II contraction induced by RhoA activity. Myo9b accumulates at sites of polymerizing actin filaments such as in extending lamellipodia and at the tips of filopodia (van den Boom et al. 2007). Recruitment to these sites requires the motor activity of Myo9b that carries the RhoGAP domain as intramolecular cargo. The proposed working model for how Myo9b regulates cell migration is as follows: (i) activation of Cdc42 and/or Rac induces actin filament polymerization; (ii) actin polymerization allows for the recruitment of Myo9b; (iii) Rho activity is locally inhibited by the RhoGAP domain of Myo9b preventing acto-myosin II contractility. Acto-myosin II contraction is induced only at the sides and back of the cells. This scenario would allow for extension at the front and retraction of the back.

16.9 Myo9b in Phagocytosis

Myo9b could play a role in various actin-dependent processes, such as phagocytosis. The binding of ligand-coated particles to phagocytic receptors triggers actin polymerization and engulfment of the particle by the formation of membrane cups. Using antibody staining of fixed cells, Myo9b was observed to be enriched at

early phagosomes induced by particles opsonized with IgG (Diakonova et al. 2002). The uptake of dextran, *E. coli* or ovalbumin by bone marrow-derived mouse dendritic cells was not altered when Myo9b was ablated (Xu et al. 2014). Interestingly, Myo9b-knockout cells of the macrophage-differentiated human myeloid cell line U937 showed differential impairment of particle uptake (Haney et al. 2018). Whereas Myo9b knockout strongly reduced the uptake of 1.3 µm amine-modified beads and 0.3–4 µm carboxylate-modified beads, it weakly reduced the uptake of IgG-opsonized red blood cells (RBCs) and did not affect the uptake of C3b-opsonized RBCs, zymosan (yeast) or myelin.

16.10 Perspectives

Although single-headed *C. elegans* Myo9 and mammalian Myo9b are able to move processively under certain conditions by means of an actin filament tether in loop 2 *in vitro*, it remains to be seen whether class IX myosins move processively *in vivo*. The stochastic switching between an actin-binding and non-binding population needs to be analyzed further to understand the control of motor properties. Class IX myosins are multidomain proteins and several domains have no defined functions so far, such as the RA domain, the calmodulin bound to the loop 2 insertion or the C1 domain(s) in the tail region. Additional functional motifs may be present in the tail region and remain to be identified. If and how the different activities of class IX myosins could be regulated is currently not resolved. Current information concerning regulation is restricted to the expression of class IX myosins (Ma et al. 2017; Kong et al. 2015). Although a number of physiological functions related to negative regulation of Rho activity have been identified for class IX myosins, it is likey that additional Rho-dependent and possibly Rho-independent physiological functions will be discovered in the future. In species that contain more than a single class IX myosin the functional diffferences and potential redundancies need to be addressed in more detail in the future.

Acknowledgements M.B. acknowledges the support by the "Deutsche Forschungsgemeinschaft" grant BA1354/14-1.

References

Abouhamed M, Grobe K, San IV, Thelen S, Honnert U, Balda MS, Matter K, Bähler M (2009) Myosin IXa regulates epithelial differentiation and its deficiency results in hydrocephalus. Mol Biol Cell 20(24):5074–5085

Bian Y, Song C, Cheng K, Dong M, Wang F, Huang J, Sun D, Wang L, Ye M, Zou H (2014) An enzyme assisted RP-RPLC approach for in-depth analysis of human liver phosphoproteome. J Proteome 96:253–262

Chandhoke SK, Mooseker MS (2012) A role for myosin IXb, a motor-RhoGAP chimera, in epithelial wound healing and tight junction regulation. Mol Biol Cell 23(13):2468–2480

Chen YQ, Zhang L, Lv XY, Wang HZ (2016) lack of association between myo9b gene polymorphisms and susceptibility to coeliac disease in caucasians: evidence from a meta-analysis. Immunol Investig 45(5):396–405

Chieregatti E, Gärtner A, Stöffler HE, Bähler M (1998) Myr 7 is a novel myosin IX-RhoGAP expressed in rat brain. J Cell Sci 111(Pt 24):3597–3608

Daub H, Olsen JV, Bairlein M, Gnad F, Oppermann FS, Körner R, Greff Z, Kéri G, Stemmann O, Mann M (2008) Kinase-selective enrichment enables quantitative phosphoproteomics of the kinome across the cell cycle. Mol Cell 31(3):438–448

Dephoure N, Zhou C, Villén J, Beausoleil SA, Bakalarski CE, Elledge SJ, Gygi SP (2008) A quantitative atlas of mitotic phosphorylation. Proc Natl Acad Sci U S A 105(31):10762–10767

Diakonova M, Bokoch G, Swanson JA (2002) Dynamics of cytoskeletal proteins during Fcgamma receptor-mediated phagocytosis in macrophages. Mol Biol Cell 13(2):402–411

Elfrink K, Liao W, Pieper U, Oeding SJ, Bähler M (2014) The loop2 insertion of type IX myosin acts as an electrostatic actin tether that permits processive movement. PLoS One 9(1):e84874

Folci A, Murru L, Vezzoli E, Ponzoni L, Gerosa L, Moretto E, Longo F, Zapata J, Braida D, Pistillo F, Bähler M, Francolini M, Sala M, Bassani S (2016) Myosin IXa binds AMPAR and regulates synaptic structure, LTP, and cognitive function. Front Mol Neurosci 9:1

Gnad F, Gunawardena J, Mann M (2011) PHOSIDA 2011: the posttranslational modification database. Nucleic Acids Res 39(Database):D253–D260

Graf B, Bähler M, Hilpelä P, Böwe C, Adam T (2000) Functional role for the class IX myosin myr5 in epithelial cell infection by Shigella flexneri. Cell Microbiol 2(6):601–616

Handa Y, Durkin CH, Dodding MP, Way M (2013) Vaccinia virus F11 promotes viral spread by acting as

a PDZ-containing scaffolding protein to bind myosin-9A and inhibit RhoA signaling. Cell Host Microbe 14(1):51–62

Haney MS, Bohlen CJ, Morgens DW, Ousey JA, Barkal AA, Tsui CK, Ego BK, Levin R, Kamber RA, Collins H, Tucker A, Li A, Vorselen D, Labitigan L, Crane E, Boyle E, Jiang L, Chan J, Rincón E, Greenleaf WJ, Li B, Snyder MP, Weissman IL, Theriot JA, Collins SR, Barres BA, Bassik MC (2018) Identification of phagocytosis regulators using magnetic genome-wide CRISPR screens. Nat Genet 50(12):1716–1727

Hanley PJ, Xu Y, Kronlage M, Grobe K, Schön P, Song J, Sorokin L, Schwab A, Bähler M (2010) Motorized RhoGAP myosin IXb (Myo9b) controls cell shape and motility. Proc Natl Acad Sci U S A 107(27):12145–12150

Hegan PS, Chandhoke SK, Barone C, Egan M, Bähler M, Mooseker MS (2016) Mice lacking myosin IXb, an inflammatory bowel disease susceptibility gene, have impaired intestinal barrier function and superficial ulceration in the ileum. Cytoskeleton (Hoboken) 73(4):163–179

Huttlin EL, Jedrychowski MP, Elias JE, Goswami T, Rad R, Beausoleil SA, Villén J, Haas W, Sowa ME, Gygi SP (2010) A tissue-specific atlas of mouse protein phosphorylation and expression. Cell 143(7):1174–1189

Inoue A, Saito J, Ikebe R, Ikebe M (2002) Myosin IXb is a single-headed minus-end-directed processive motor. Nat Cell Biol 4(4):302–306

Kalhammer G, Bähler M, Schmitz F, Jöckel J, Block C (1997) Ras-binding domains: predicting function versus folding. FEBS Lett 414(3):599–602

Kambara T, Ikebe M (2006) A unique ATP hydrolysis mechanism of single-headed processive myosin, myosin IX. J Biol Chem 281(8):4949–4957

Kim DG, Jeong YH, McMichael BK, Bähler M, Bodnyk K, Sedlar R, Lee BS (2018) Relationships of bone characteristics in MYO9B deficient femurs. J Mech Behav Biomed Mater 84:99–107

Kollmar M, Mühlhausen S (2017) Myosin repertoire expansion coincides with eukaryotic diversification in the Mesoproterozoic era. BMC Evol Biol 17(1):211

Kong R, Yi F, Wen P, Liu J, Chen X, Ren J, Li X, Shang Y, Nie Y, Wu K, Fan D, Zhu L, Feng W, Wu JY (2015) Myo9b is a key player in SLIT/ROBO-mediated lung tumor suppression. J Clin Invest 125(12):4407–4420

Li P, Yang XK, Wang X, Zhao MQ, Zhang C, Tao SS, Zhao W, Huang Q, Li LJ, Pan HF, Ye DQ (2016) A meta-analysis of the relationship between MYO9B gene polymorphisms and susceptibility to Crohn's disease and ulcerative colitis. Hum Immunol 77(10):990–996

Liao W, Elfrink K, Bähler M (2010) Head of myosin IX binds calmodulin and moves processively toward the plus-end of actin filaments. J Biol Chem 285(32):24933–24942

Liu Z, Xu Y, Zhang X, Song J, Sorokin L, Bähler M (2015) The motorized RhoGAP myosin IXb (Myo9b) in leukocytes regulates experimental autoimmune encephalomyelitis induction and recovery. J Neuroimmunol 282:25–32

Lundby A, Secher A, Lage K, Nordsborg NB, Dmytriyev A, Lundby C, Olsen JV (2012) Quantitative maps of protein phosphorylation sites across 14 different rat organs and tissues. Nat Commun 3:876

Ma D, Zheng B, Suzuki T, Zhang R, Jiang C, Bai D, Yin W, Yang Z, Zhang X, Hou L, Zhan H, Wen JK (2017) Inhibition of KLF5-Myo9b-RhoA pathway-mediated podosome formation in macrophages ameliorates abdominal aortic aneurysm. Circ Res 120(5):799–815

Maddirevula S, Alzahrani F, Al-Owain M, Al Muhaizea MA, Kayyali HR, AlHashem A, Rahbeeni Z, Al-Otaibi M, Alzaidan HI, Balobaid A, El Khashab HY, Bubshait DK, Faden M, Yamani SA, Dabbagh O, Al-Mureikhi M, Jasser AA, Alsaif HS, Alluhaydan I, Seidahmed MZ, Alabbasi BH, Almogarri I, Kurdi W, Akleh H, Qari A, Al Tala SM, Alhomaidi S, Kentab AY, Salih MA, Chedrawi A, Alameer S, Tabarki B, Shamseldin HE, Patel N, Ibrahim N, Abdulwahab F, Samira M, Goljan E, Abouelhoda M, Meyer BF, Hashem M, Shaheen R, AlShahwan S, Alfadhel M, Ben-Omran T, Al-Qattan MM, Monies D, Alkuraya FS (2019) Autozygome and high throughput confirmation of disease genes candidacy. Genet Med 21(3):736–742

McMichael BK, Jeong YH, Auerbach JA, Han CM, Sedlar R, Shettigar V, Bähler M, Agarwal S, Kim DG, Lee BS (2017) The RhoGAP Myo9b promotes bone growth by mediating osteoblastic responsiveness to IGF-1. J Bone Miner Res 32(10):2103–2115

Moalli F, Ficht X, Germann P, Vladymyrov M, Stolp B, de Vries I, Lyck R, Balmer J, Fiocchi A, Kreutzfeldt M, Merkler D, Iannacone M, Ariga A, Stoffel MH, Sharpe J, Bähler M, Sixt M, Diz-Muñoz A, Stein JV (2018) The Rho regulator Myosin IXb enables nonlymphoid tissue seeding of protective $CD8^+$ T cells. J Exp Med 215(7):1869–1890

Müller RT, Honnert U, Reinhard J, Bähler M (1997) The rat myosin myr 5 is a GTPase-activating protein for Rho in vivo: essential role of arginine 1695. Mol Biol Cell 8(10):2039–2053

Nalavadi V, Nyitrai M, Bertolini C, Adamek N, Geeves MA, Bähler M (2005) Kinetic mechanism of myosin IXB and the contributions of two class IX-specific regions. J Biol Chem 280(47):38957–38968

Nijmeijer RM, van Santvoort HC, Zhernakova A, Teller S, Scheiber JA, de Kovel CG, Besselink MG, Visser JT, Lutgendorff F, Bollen TL, Boermeester MA, Rijkers GT, Weiss FU, Mayerle J, Lerch MM, Gooszen HG, Akkermans LM, Wijmenga C, Dutch Pancreatitis Study Group (2013) Association analysis of genetic variants in the myosin IXB gene in acute pancreatitis. PLoS One 8(12):e85870

Nishikawa M, Nishikawa S, Inoue A, Iwane AH, Yanagida T, Ikebe M (2006) A unique mechanism for the processive movement of single-headed myosin-IX. Biochem Biophys Res Commun 343(4):1159–1164

Nitta R, Kikkawa M, Okada Y, Hirokawa N (2004) KIF1A alternately uses two loops to bind microtubules. Science 305(5684):678–683

O'Connell CB, Mooseker MS (2003) Native Myosin-IXb is a plus-, not a minus-end-directed motor. Nat Cell Biol 5(2):171–172

O'Connor E, Töpf A, Müller JS, Cox D, Evangelista T, Colomer J, Abicht A, Senderek J, Hasselmann O, Yaramis A, Laval SH, Lochmüller H (2016) Identification of mutations in the MYO9A gene in patients with congenital myasthenic syndrome. Brain 139(Pt 8):2143–2153

O'Connor E, Phan V, Cordts I, Cairns G, Hettwer S, Cox D, Lochmüller H, Roos A (2018) MYO9A deficiency in motor neurons is associated with reduced neuromuscular agrin secretion. Hum Mol Genet 27(8):1434–1446

Okada Y, Hirokawa N (2000) Mechanism of the single-headed processivity: diffusional anchoring between the K-loop of kinesin and the C terminus of tubulin. Proc Natl Acad Sci U S A 97(2):640–645

Okada Y, Higuchi H, Hirokawa N (2003) Processivity of the single-headed kinesin KIF1A through biased binding to tubulin. Nature 424(6948):574–577

Omelchenko T, Hall A (2012) Myosin-IXA regulates collective epithelial cell migration by targeting RhoGAP activity to cell-cell junctions. Curr Biol 22(4):278–288

Post PL, Bokoch GM, Mooseker MS (1998) Human myosin-IXb is a mechanochemically active motor and a GAP for rho. J Cell Sci 111(Pt 7):941–950

Post PL, Tyska MJ, O'Connell CB, Johung K, Hayward A, Mooseker MS (2002) Myosin-IXb is a single-headed and processive motor. J Biol Chem 277(14):11679–11683

Reinhard J, Scheel AA, Diekmann D, Hall A, Ruppert C, Bähler M (1995) A novel type of myosin implicated in signalling by rho family GTPases. EMBO J 14(4):697–704

Rigbolt KT, Prokhorova TA, Akimov V, Henningsen J, Johansen PT, Kratchmarova I, Kassem M, Mann M, Olsen JV, Blagoev B (2011) System-wide temporal characterization of the proteome and phosphoproteome of human embryonic stem cell differentiation. Sci Signal 4(164):rs3

Saczko-Brack D, Warchol E, Rogez B, Kröss M, Heissler SM, Sellers JR, Batters C, Veigel C (2016) Self-organization of actin networks by a monomeric myosin. Proc Natl Acad Sci U S A 113(52):E8387–E8395

Scheffzek K, Ahmadian MR, Wittinghofer A (1998) GTPase-activating proteins: helping hands to complement an active site. Trends Biochem Sci 23(7):257–262

Struchholz S, Elfrink K, Pieper U, Kalhammer G, Honnert U, Grützner A, Linke WA, Liao W, Bähler M (2009) Functional role of the extended loop 2 in the myosin 9b head for binding F-actin. J Biol Chem 284(6):3663–3671

Thelen S, Abouhamed M, Ciarimboli G, Edemir B, Bähler M (2015) Rho GAP myosin IXa is a regulator of kidney tubule function. Am J Physiol Ren Physiol 309(6):F501–F513

van den Boom F, Düssmann H, Uhlenbrock K, Abouhamed M, Bähler M (2007) The Myosin IXb motor activity targets the myosin IXb RhoGAP domain as cargo to sites of actin polymerization. Mol Biol Cell 18(4):1507–1518

Wallace AG, Raduwan H, Carlet J, Soto MC (2018) The RhoGAP HUM-7/Myo9 integrates signals to modulate RHO-1/RhoA during embryonic morphogenesis in *Caenorhabditis elegans*. Development 145(23):dev168724

Wang MJ, Xu XL, Yao GL, Yu Q, Zhu CF, Kong ZJ, Zhao H, Tang LM, Qin XH (2016) MYO9B gene polymorphisms are associated with the risk of inflammatory bowel diseases. Oncotarget 7(37):58862–58875

Wirth JA, Jensen KA, Post PL, Bement WM, Mooseker MS (1996) Human myosin-IXb, an unconventional myosin with a chimerin-like rho/rac GTPase-activating protein domain in its tail. J Cell Sci 109(Pt 3):653–661

Xie P (2010) A model for processive movement of single-headed myosin-IX. Biophys Chem 151(1–2):71–80

Xu Y, Pektor S, Balkow S, Hemkemeyer SA, Liu Z, Grobe K, Hanley PJ, Shen L, Bros M, Schmidt T, Bähler M, Grabbe S (2014) Dendritic cell motility and T cell activation requires regulation of Rho-cofilin signaling by the Rho-GTPase activating protein myosin IXb. J Immunol 192(8):3559–3568

Yi F, Kong R, Ren J, Zhu L, Lou J, Wu JY, Feng W (2016) Noncanonical Myo9b-RhoGAP accelerates RhoA GTP hydrolysis by a Dual-Arginine-finger mechanism. J Mol Biol 428(15):3043–3057

Yiş U, Becker K, Kurul SH, Uyanik G, Bayram E, Haliloğlu G, Polat Aİ, Ayanoğlu M, Okur D, Tosun AF, Serdaroğlu G, Yilmaz S, Topaloğlu H, Anlar B, Cirak S, Engel AG (2017) Genetic Landscape of congenital myasthenic syndromes from Turkey: Novel mutations and clinical insights. J Child Neurol 32(8):759–765

Zhou H, Di Palma S, Preisinger C, Peng M, Polat AN, Heck AJ, Mohammed S (2013) Toward a comprehensive characterization of a human cancer cell phosphoproteome. J Proteome Res 12(1):260–271

Myosin X

17

Hiroshi Tokuo

Abstract

Myosin X (Myo10), an actin-based molecular motor, induces filopodia formation and controls cell migration in vitro. In the 25 years since Myo10 was first identified, it has been implicated in several different functions in different cell types including phagocytosis in macrophages, axon outgrowth in neurons, cell-cell adhesion in epithelial and endothelial cells, podosome formation in osteoclasts, spindle-pole positioning in meiosis and mitosis of cultured cells, migration of melanocytes and cranial neural crest cells, and invadopodia formation in cancer cells. Recently, the availability of Myo10-knockout (Myo10KO) mice has allowed for tremendous progress toward understanding the biological function of Myo10 *in vivo*.

In this chapter, I address the structure of the Myo10 gene; the molecular structure of Myo10 protein with its multiple domains, e.g., PH, MyTH4, and FERM domains; the regulation of actin structures induced in cells by Myo10; the expression and function of Myo10 *in vitro* and *in vivo*; and the role of Myo10 in cancer. Previous reviews on Myo10 include Divito MM, Cheney RE, (Myosins: a superfamily of molecular motors chapter 14 MYOSIN X. In: Proteins and cell regulation, vol 7. Springer, Dordrecht, 2008) and Kerber ML, Cheney RE (J Cell Sci 124:3733–3741).

Keywords

Filopodia · Pseudopod · Podosome · Invadopodia · Migration · Cancer · Melanoma · Pleckstrin homology domain · MyTH4 and FERM domains · Tunneling nanotube

17.1 Introduction

Myo10 was first identified in 1994 in the sensory epithelia of the inner ear of bullfrogs using a PCR screen with primers based on regions of high amino acid homology among motor domains of myosins known at that time (Solc et al. 1994). By 2000 the full-length cDNA sequences of mouse, human, and cow Myo10 had been determined along with the first information regarding its molecular structure, its wide expression in tissues, and its localization in dynamic actin-rich regions of the cell including membrane ruffles, lamellipodia, and the tips of filopodia (Berg et al. 2000; Yonezawa et al. 2000). The following year, an expressed and purified Myo10 construct representing the head domain and coiled-coil domain of Myo10 was shown to bind to actin filaments

H. Tokuo (✉)
Department of Physiology & Biophysics, Boston University School of Medicine, Boston, MA, USA
e-mail: tokuo@bu.edu

L. M. Coluccio (ed.), *Myosins*, Advances in Experimental Medicine and Biology 1239,
https://doi.org/10.1007/978-3-030-38062-5_17

and to hydrolyze ATP, the first demonstration of Myo10's motor activity (Homma et al. 2001). In 2002, expression of exogenous full-length Myo10 was shown to exhibit both forward and rearward movements within filopodia of HeLa cells and to increase both the number and the average length of the filopodia in COS-7 cells (Berg and Cheney 2002). Subsequent studies focused on revealing the identification of its binding partners including phospholipids (Umeki et al. 2011), Mena/VASP (Mammalian enabled/vasodilator-stimulated phosphoprotein) (Tokuo and Ikebe 2004), microtubules (Weber et al. 2004) and integrins (Zhang et al. 2004) in order to gain insight into its cellular functions.

17.2 Gene Structure of Myo10

The class X myosin gene (*MYO10*) is found exclusively in vertebrates and gives rise to the alternatively-spliced proteins full-length Myo10 and headless Myo10 (Sousa et al. 2006). Figure 17.1a shows the genomic structure of mouse *Myo10* and the Myo10KO mouse *Myo10*$^{tm2(KOMP)Wtsi}$, which will be discussed in

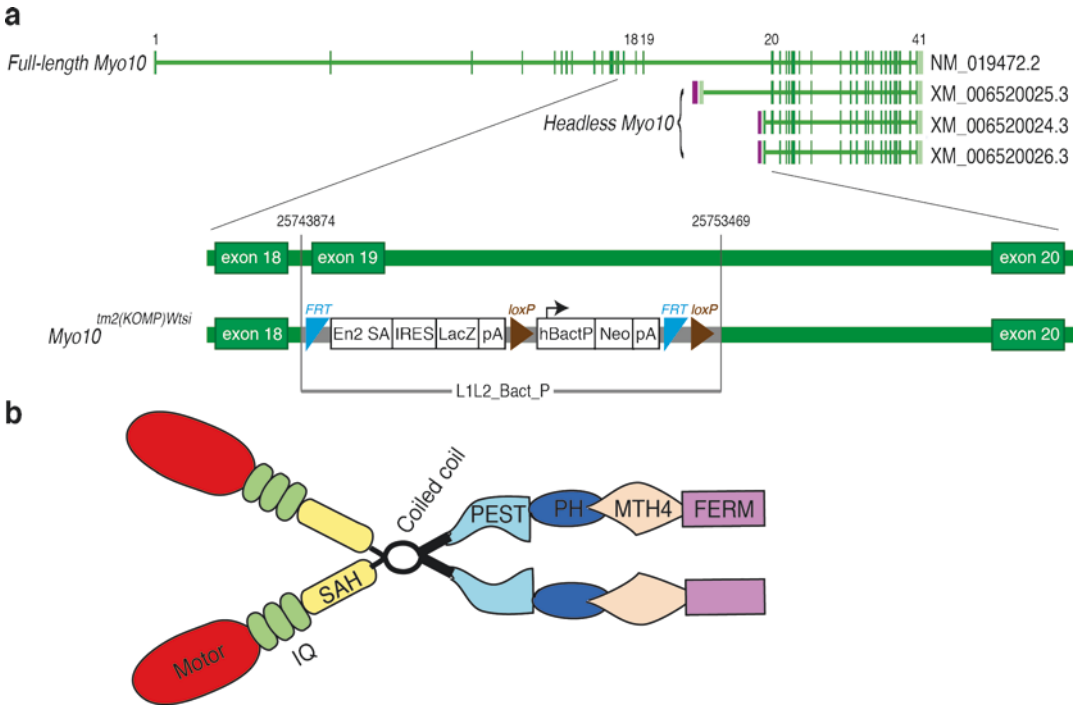

Fig. 17.1 Genomic structure and protein expression of Myo10. (**a**) Allele structure of mouse *full-length Myo10* and three variants formed by alternative splicing referred to as "*headless Myo10*" (top) with magnification of the lesion from exon 18–20. Vertical lines on the schematic gene represent exons, and purple lines represent first exons specific for *headless Myo10*. Below is the genomic structure of *Myo10*$^{tm2(KOMP)Wtsi}$ in Myo10KO mice in which the *lacZ* and *neomycin (neo)* expression cassette was inserted between exon 18 and exon 20 (Genome Build GRCm38) resulting in the removal of functionally critical exon 19 and a portion of intron 19 (Tokuo et al. 2018). (**b**) Schematic diagram of a dimerized Myo10 molecule showing its N-terminal motor domain, followed by a neck domain with IQ region, SAH domain, and coiled coil, and tail domain with PEST, PH, MTH4 and FERM domains

Sect. 17.5.1. This Myo10KO strategy is useful in identifying and confirming the expression of splice variants because it deletes full-length, but not headless, Myo10. We detected headless and full-length Myo10 in immunoblots of brain lysates from control mice, but only headless Myo10 in brain lysates from Myo10KO mice, evidence that the *Myo10*$^{tm2(KOMP)Wtsi}$ allele knocks out full-length, but not headless, Myo10.

17.3 Structural, Biochemical and Biomechanical Properties of Myo10

The ~237-kDa Myo10 heavy chain consists of a head, neck, and tail domain (Berg et al. 2000). The Myo10 head, or motor, domain has a nucleotide-binding site and an actin-binding site and is responsible for its actin-activated ATPase activity. The neck, or IQ domain, binds three molecules of calmodulin or calmodulin-like protein (Rogers and Strehler 2001; Caride et al. 2010) and consists of a single α-helix (SAH) region (Knight et al. 2005) followed by a coiled-coil region involved in dimerization (Lu et al. 2012). A carboxy-terminal (C-terminal) tail domain, which is primarily involved in cargo binding, consists of four parts: three PEST sequences, which are rich in the amino acids proline, glutamate, serine, and threonine and confer sensitivity to certain proteases, three pleckstrin homology (PH) domains, a Myosin Tail Homology 4 (MyTH4) domain, and a band 4.1, Ezrin, Radixin, Merlin (FERM) domain (Berg et al. 2000) (Fig. 17.1b).

Myo10 exists as both a monomer and a dimer in the cytoplasm. The coiled-coil region following the SAH domain is involved in dimerization and was shown by nuclear magnetic resonance (NMR) spectroscopy to adopt an anti-parallel conformation (Lu et al. 2012). This finding led to the prediction that each of the two heads of dimeric Myo10 could bind to two parallel actin filaments and thus support the movement of Myo10 along actin bundles as well as single filaments (Lu et al. 2012). Previously, a forced dimer of Myo10 heavy meromyosin (HMM) consisting of the motor, neck, coiled-cold and leucine zipper had been shown to move processively on actin filaments bundled with fascin (Nagy et al. 2008), although in another report using a different forced Myo10 HMM dimer, no selectivity for bundles was observed (Sun et al. 2010). Subsequently, full-length Myo10 molecules (anti-parallel dimers) labeled at the N-terminus with the GFP derivative mWasabi were shown to take 36-nm steps in the forward direction on single actin filaments and steps as large as 52–57nm along fascin-actin bundles (Ropars et al. 2016). The SAH domain and following α-helical domain form a long α-helix that lengthens the Myo10 lever arm and contributes to its ability to take particularly large steps (Ropars et al. 2016). Importantly, Myo10 moves along fascin-actin bundles at a rate nearly twice the rate of on a single actin filament due to an ~two-fold increase in the rate of transition between Pi and ADP release (Ropars et al. 2016).

17.3.1 Monomer-to-Dimer Transition of Myo10 Supports Filopodia Formation

Strikingly, in live-cell imaging studies Myo10 exhibits both forward and rearward movements within filopodia (Berg and Cheney 2002). The speed of the forward movement as determined by total internal reflection fluorescence (TIRF) microscopy is ~600 nm/s in living cells (Kerber et al. 2009), very close to that reported in one recent study tracking full-length Myo10 on fascin bundles (Ropars et al. 2016) and somewhat larger that the 340–780 nm/s reported for movement of a forced dimer of Myo10 heavy meromyosin consisting of the motor, neck, coiled-coil and leucine zipper on artificial actin bundles (Nagy et al. 2008). The rearward movement of Myo10 in filopodia is slow at 10–20 nm/s (Berg and Cheney 2002) and closely matches the rate of the retrograde flow of actin in filopodia. Importantly, only dimerized Myo10 exhibits intrafilopodial motility, suggesting that dimerization of Myo10 is necessary for its proper movement in cells. Moreover, the dimers must form

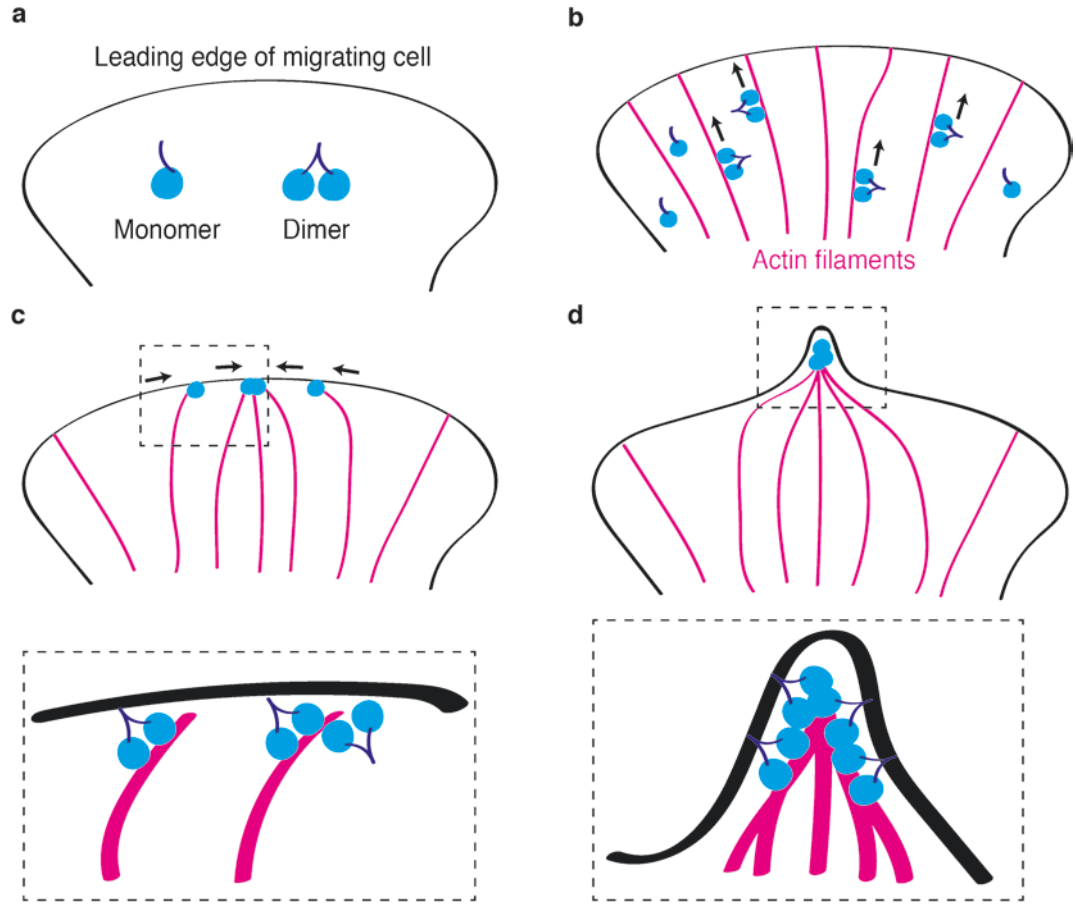

Fig. 17.2 Model of filopodia initiation by dimerization of Myo10. (**a**) Myo10 is present in the cytosol as both a monomer and a dimer. (**b**) Once Myo10 dimerizes to form a two-headed structure, it moves to the tips of the actin filaments. (**c**) The tips of actin filaments move laterally along the leading edge powered by Myo10. (**d**) The lateral drift induces a convergence of the barbed ends of the actin filaments, thereby inducing the formation of microspikes, which develop further into full-length filopodia by actin assembly (Tokuo et al. 2007)

through an antiparallel coiled-coil dimerization or else localization at the tips of filopodia and filopodia induction are compromised (Lu et al. 2012).

Using a dimer-inducing technique we found that when expressed in cells, dimerized tail-less Myo10 induces short unstable filopodia, or microspikes, which may be an initial step in filopodia formation, evidence that the monomer-to-dimer transition of Myo10 induces filopodia in cultured cells (Tokuo et al. 2007). From these results, we advocate a model in which Myo10 exists as both a monomer and a dimer in cells. Although monomeric Myo10 does not localize at the leading edge of migrating cells, after dimerization, Myo10 moves toward the tips of actin filaments at the leading edge, presumably by walking toward the barbed ends of actin filaments (Fig. 17.2). The tips of actin filaments move laterally along the leading edge supported by the mechanical activity of Myo10. Finally, clustering of Myo10 causes convergence of actin filaments into parallel bundles to form the base of the filopodia. This convergence of actin filaments into bundles is likely supported by the structure and flexibility of the Myo10 lever arm, which may facilitate parallel actin filaments being brought together (Ropars et al. 2016).

17.3.2 PH Domains

Pleckstrin Homology (PH) domains are regions of ~120 amino acids with sequence similarity to two regions in pleckstrin (Haslam et al. 1993; Shaw 1993; Mayer et al. 1993), a major substrate of protein kinase C in platelets. This domain, the 11th most common domain in the human proteome, was first recognized for its ability to bind phosphoinositides with high affinity and specificity, although it is now understood that not all PH domains share this property.

Myo10 contains three PH domains. The first PH domain (PH1) is split by the insertion of a second PH domain (PH2). The amino acid sequences of PH1 and PH2 are most similar to that of the PH domain in protein kinase B homologs from *Dictyostelium*, but the sequence of the C-terminal half of the third PH domain (PH3) diverges from that of other PH domains (Berg et al. 2000). PH2 and PH3 contain several residues also found in other proteins that bind phosphatidylinositol lipids phosphorylated by phosphatidylinositol-3-kinase (PI3K) (Rameh et al. 1997; Isakoff et al. 1998).

In a lipid pull-down assay using purified PH domains of Myo10, PH2, but not PH1 or PH3, specifically bound to phosphatidylinositol (3,4,5)-triphosphate (PIP3). Deletion of PH2 or point mutations in PH2 (Lys 1215 to Ala and Lys 1216 to Ala) in full-length Myo10 results in significantly less Myo10 at the tips of filopodia and fewer filopodia (Plantard et al. 2010). These results suggest that PIP3 binding to the PH2 domain of Myo10 is involved in Myo10 trafficking and regulation of filopodia formation. PIP3 binding to the PH domain of Myo10 is also essential for axon development (Yu et al. 2012).

The Arg at position 1231 in Myo10, which is within PH2, corresponds to a conserved residue in the β2 strand of PH domain-containing proteins such as GTPase-activating protein (Gap1) and Bruton's tyrosine kinese (Btk), which is critical for binding to lipid products of PI3K (Salim et al. 1996; Fukuda and Mikoshiba 1996). Insight into the importance of Arg 1231 in Myo10 comes from studies examining phagocytosis in macrophages. Expression of Myo10 tail in macrophages inhibits phagocytosis by a dominant-negative effect; however, expression of Myo10 tail in which Arg 1231 was mutated to Cys (Myo10 tail^{R1231C}) did not change phagocytosis indicating that Arg 1231 is required for the inhibition of phagocytosis by the Myo10 tail (Cox et al. 2002).

17.3.3 MyTH4 and FERM Domains

The myosin tail homology 4 (MyTH4) domain was first named to distinguish it from tail homology domains 1–3 in myosins-I (Hammer 1994). In addition to Myo10, MyTH4 was identified in vertebrate Myo7 (Chen et al. 1996) and Myo15 (Wang et al. 1998). The name of the FERM domain (F for 4.1 protein, E for ezrin, R for radixin, and M for moesin) reflects the initial identification of this domain in a family of peripheral membrane proteins that functions as membrane-cytoskeleton linkers (Chishti et al. 1998). Dozens of FERM domains are encoded by multiple genes in the human genome (Frame et al. 2010). In the myosin superfamily, only Myo7, Myo10, and Myo15 include this domain in the C-terminal tail; these myosins constitute the MyTH4-FERM subfamily of unconventional myosins. The FERM domain consists of three lobes, and lobes F2 and F3 in the FERM domain of Myo10 are required for interaction and relocalization of beta-integrins (Zhang et al. 2004).

MyTH4 and FERM always appear in tandem in Myo7, Myo10, and Myo15. The MyTH4-FERM myosins have conserved physiological functions with all involved in forming actin-rich membrane protrusions: Myo7 in microvilli, Myo10 in filopodia, and Myo15 in stereocilia. Both the FERM domain and the MyTH4 domain are required for the cellular functions of Myo10: deletion of either domain decreases the ability of Myo10 to form filopodia (Bohil et al. 2006; Tokuo et al. 2007; Watanabe et al. 2010).

Myo10 is speculated to exist primarily as a folded monomer in the cytoplasm with its head bound to the PH and FERM domains in the tail; however, association with PIP3 results in its unfolding and dimerization to promote its activ-

ity as a processive motor able to transport cargo (Umeki et al. 2011). This interaction also recruits Myo10 to the cell membrane of the leading edge for filopodia formation (Plantard et al. 2010).

The MyTH4-FERM tandem of Myo10 binds to microtubules, but the individual domains do not (Weber et al. 2004), and binding of Myo10 to deleted in colorectal cancer (DCC) or neogenin also requires a covalent connection between MyTH4 and FERM domains (Zhu et al. 2007). By crystal structure analysis, the MyTH4 and FERM domains interact with each other and form an integral structural supramodule (Wei et al. 2011).

The interaction of Myo10 with microtubules was first identified in 2004 (Weber et al. 2004) as an important factor for nuclear anchoring, spindle assembly, and spindle-F-actin association during meiosis in *Xenopus laevis*. These observations were also confirmed in mitosis of mammalian cells (Toyoshima and Nishida 2007), and the interaction of Myo10 with adducin-1 was found to be essential for mitotic spindle assembly (Chan et al. 2014). Studies of X-ray structures identified specific residues (Lys1645 and Lys1650) within the MyTH4 domain that are essential for direct binding to the acidic C-terminal tail of tubulin (Hirano et al. 2011; Wei et al. 2011; Wu et al. 2011). A double-point mutation in MyTH4 (Lys1645 to Asp and Lys1650 to Asp) in full-length Myo10, which specifically disrupts microtubule binding without altering the interaction of Myo10 with the FERM domain-binding cargo (Hirano et al. 2011), could not rescue the spindle orientation defect resulting from Myo10 knockdown (kd) (Kwon et al. 2015). These results suggest that direct binding of Myo10 to microtubules controls the proper positioning of centrosomes toward retraction fibers and subcortical actin.

17.4 Regulation of Actin Structures by Myo10

17.4.1 Filopodia

Myo10, which specifically localizes to the tips of filopodia, was first identified as an inducer of filopodia (Berg et al. 2000). Filopodia are actin-rich, finger-like protrusions found at the leading edge of cells and believed to modulate numerous cellular processes including cell migration, wound healing closure, adhesion to the extracellular matrix and other substrates, guidance towards chemoattractants and other guidance cues, neuronal growth-cone path finding, and embryonic development in many organs (Mattila and Lappalainen 2008).

Many studies have reported that Myo10 promotes filopodia formation by delivering specific cargos to the cell periphery, e.g., Mena and VASP, which bind to the tail domain of Myo10 (Tokuo and Ikebe 2004; Lin et al. 2013). Myo10-mediated delivery of VASP to filopodial tips would support filopodia elongation as VASP competes with capping protein at the plus end of actin filaments and induces clustering of actin filaments (Applewhite et al. 2007). Myo10 transports integrins to the tips of filopodia for supporting cell attachment to the extracellular matrix (ECM) and promoting filopodia extension (Zhang et al. 2004). In neurites, full-length Myo10 interacts with the netrin receptor DCC to enhance the formation of filopodia, whereas headless Myo10 interacts preferentially with the DCC-related protein neogenin, which could inhibit filopodia formation induced by DCC and Myo10 signaling and axon growth (Zhu et al. 2007). In endothelial cells, Myo10 mediates the transport of VE-cadherin to cell edges and filopodia to support the formation of cell-cell junctions (Almagro et al. 2010).

17.4.2 Podosomes and Invadopodia

In addition to filopodia formation, Myo10 mediates the formation of other actin-based structures such as the adhesive structures podosomes and invadopodia (Schoumacher et al. 2010). Podosomes are found on the ventral side of a variety of cells including osteoclasts, macrophages, and endothelial cells. Myo10 localizes in the podosomal ring of osteoclasts between actin and microtubules and participates in osteoclast attachment and podosome

positioning by directly linking actin to microtubules.

Invasive cancer cells display membrane protrusions called invadopodia, which resemble podosomes. They are primary sites of rapid actin polymerization and major sites of matrix degradation. Invadopodia contain several proteases such as membrane-type 1 matrix metalloproteinase (MT1-MMP) and seprase, which are used for degrading the basement membrane. Myo10 localizes to invadopodia, and Myo10 knockdown in a breast cancer cell line reduces invadopodia formation (Schoumacher et al. 2010).

Both podosomes and invadopodia are cell matrix adhesion sites that connect the cortical actin cytoskeleton within the cell to the ECM. Although many of the same proteins are found in both podosomes and invadopodia including integrin, talin, and paxillin, their structures and dynamics differ. The ability to degrade ECM in order to move through tissue barriers is a hallmark of invasive tumors. At the subcellular level, ECM-degrading activity occurs at the tips of invadopodia where Myo10 accumulates.

17.4.3 Tunneling Nanotubes (TNTs)

In 2004, Ruston and colleagues discovered thin structures connecting single cells over long distances *in vitro* and named them tunneling nanotubes (TNTs) (Appenzeller et al. 2004). TNTs hover above the cell culture substrate and contain a straight, continuous actin rod enclosed in a lipid bilayer. Since then, TNTs have been noted in many different cell types and shown to act as conduits for the intercellular transfer of cellular compounds (Appenzeller et al. 2004; Gurke et al. 2008), transmission of depolarization signals (Wang et al. 2010, 2012; Wittig et al. 2012), spreading of pathogens (Onfelt et al. 2006; Sowinski et al. 2008), and transfer of proteins implicated in disease such as prions, misfolded huntingtin, and pathological Tau protein assemblies (Gousset et al. 2009; Costanzo et al. 2013; Tardivel et al. 2016). In 2013, Myo10 was first reported as a key regulator for TNT formation by interacting with several transmembrane proteins (Gousset et al. 2013). Thus, it is probable that Myo10 plays a significant role in the induction of TNT and in TNT-mediated biological and pathological functions.

17.4.4 Pseudopods

Pseudopods ("false feet") are large dynamic protrusions found at the front of migrating cells. The term is used broadly to describe actin-rich membrane protrusions without the defined geometry of lamellipodia or filopodia. Thus, the definition of pseudopod varies among cell types. In macrophages, pseudopods are defined as the leading protrusions of phagocytic cups, Myo10 was identified as essential for pseudopod extension during phagocytosis (Cox et al. 2002).

Pseudopods support cancer cell migration and metastasis. Multiple filopodia are induced at the front of pseudopods where they pull on collagen fibrils resulting in a change in the position of both the fibrils and filopodia (Starke et al. 2013). Multiple Myo10-positive filopodia were observed at the front of pseudopods protruding from migrating mouse melanoma cells cultured in 3D collagen matrices. The number of cells with long pseudopods was less in Myo10-kd vs. control cells (Tokuo et al. 2018). These results suggest that Myo10 plays important roles in pseudopod formation, which drives cell migration.

17.5 Expression and Function of Myo10

Myo10 protein expression is observed in all vertebrate tissues (Berg et al. 2000; Yonezawa et al. 2000; Yonezawa et al. 2003), and the functional importance of this motor protein has been found in several different cells and tissues including phagocytic cup formation in leukocytes (Cox et al. 2002), nuclear anchoring and spindle assembly during meiosis in *Xenopus laevis* (Weber et al. 2004), orientation of the mitotic spindle in cultured cells (Toyoshima and Nishida 2007), endothelial cell migration and angiogenesis (Pi et al.

2007), axonal path-finding regulated by netrin (Zhu et al. 2007), migration of cranial neural crest cells in *Xenopus* (Nie et al. 2009; Hwang et al. 2009), sealing zone patterning (McMichael et al. 2010) and differentiation (Tasca et al. 2017) in osteoclasts, barrier formation at tight junctions in polarized epithelial cells (Liu et al. 2012), axon outgrowth in cortical neurons (Raines et al. 2012), cell-to-cell spreading of *Shigella* by membrane protrusions (Bishai et al. 2013), dendritic spine development by VASP transport (Lin et al. 2013), and leukocyte extravasation through cultured endothelial cells (Kroon et al. 2018). Most recently, diminished filopodia formation was detected in isolated macrophages from Myo10KO mice (Horsthemke et al. 2017) and in retinal angiogenesis in the eyes of Myo10KO mice (Heimsath et al. 2017).

17.5.1 Myo10 Functions *In Vivo*

The ability to knockout specific genes in mice has been instrumental in elucidating gene function *in vivo*. The Sanger Mouse Genetics Project generated Myo10KO (*Myo10*$^{tm2(KOMP)Wtsi}$; *Myo10*$^{tm2/tm2}$) mice in 2013. After crossing heterozygous *Myo10*$^{+/tm2}$ mice with each other, we obtained *Myo10*$^{tm2/tm2}$ pups at almost the same rate as observed with the Myo10KO mice *Myo10*$^{tm1d/tm1d}$, *Myo10*$^{tm1a/tm1a}$ and *Myo10*$^{m1J/m1J}$, in which both full-length and headless Myo10 were deleted (total-KO) (Heimsath et al. 2017). A white spot on the belly was observed with 100% penetrance in *Myo10*$^{tm2/tm2}$ mice, the same rate as in total-KO mice. The number of melanocytes in the white patches of the *Myo10*$^{tm2/tm2}$ mice was significantly reduced vs. dark patches on wild-type mice, evidence that depletion of Myo10 in the melanocyte lineage reduces the number of melanocytes in the white belly spots resulting in a pigmentation defect. *Myo10*$^{tm2/tm2}$ mice also exhibit syndactyly in the form of webbed digits in the forelimbs or hind legs, with a slightly higher rate than that observed in total-KO mice. The International Mouse Phenotyping Consortium (IMPC) reported that *Myo10*$^{tm2/tm2}$ mice had persistent hyaloid vasculature, fused cornea and lens, corneal opacity, and an abnormal pupil light response. These abnormal phenotypes in eyes are similar to those found in the total-KO mice, which exhibited persistent hyaloid vasculature (Heimsath et al. 2017). Other phenotypes related to the *Myo10*$^{tm2(KOMP)Wtsi}$ allele including fused phalanges are described on the IMPC website (http://www.mousephenotype.org/data/genes/MGI:107716).

These findings suggest that the phenotype of the full-length Myo10 only KO mouse (*Myo10*$^{tm2/tm2}$) is nearly identical as that of the total KO mouse. This observation is understandable because most tissues express only full-length Myo10, whereas neuronal cells (neural stem cells, neurons, and astrocytes) express both full-length and headless Myo10 (Sousa et al. 2006; Raines et al. 2012). Thus, the difference between the total Myo10 KO mouse and the full-length only Myo10 KO mouse is due to depleted expression of headless Myo10 in neuronal cells. One idea is that headless Myo10 is a negative regulator of full-length Myo10 (Raines et al. 2012), but whether headless Myo10 plays other functions is unknown.

17.5.2 Myo10 in Melanoblast Migration

Studies of naturally occurring mutations that lead to white belly spots in mice have significantly increased our understanding of melanoblast (precursors to melanocytes) migration including the identification of molecules essential for melanoblast migration. To investigate the effects of *Myo10* loss on melanoblast function, we reduced Myo10 expression in the mouse melanoblast cell line Melb-a with short hairpin RNA (shRNA). Melb-a cells retain the character of melanoblasts versus that of mature melanocytes or melanoma cells (Sviderskaya et al. 1995). The number of cells with long pseudopods was significantly lower in Myo10kd vs. control cells cultured on collagen matrices, and the migration rate of Myo10kd cells was slower than control cells (Tokuo et al. 2018). These results are consistent with studies show-

ing that Myo10kd inhibits migration of breast cancer cells (Cao et al. 2014). Together, the studies indicate that long pseudopods play a major role in the migration of melanoblasts and that Myo10 is required for pseudopod formation.

17.6 Myo10 in Cancer

Recently, Myo10 was found to play important roles in a variety of cancers, e.g., increased MYO10 expression correlates with aggressiveness and metastasis of breast cancer (Cao et al. 2014; Arjonen et al. 2014); expression of MYO10 is up-regulated and contributes to lung adenocarcinoma metastasis (Bidkhori et al. 2013); the *MYO10* gene is a target of microRNA-124, which is suppressed in aggressive non-small cell lung cancer (Sun et al. 2015) and also a target of microRNA-340, which impedes the metastasis of breast cancer (Chen et al. 2016); MYO10 expression is higher in prostate cancer than in normal tissue; and MYO10kd reduces the migratory speed and directional persistence of a prostate cancer cell line (Makowska et al. 2015).

17.6.1 Myo10 in a Mouse Melanoma Model

Melanoblast migration in development correlates well with melanoma metastasis, and past migratory behavior in melanoblasts may incline primary melanomas to form remote metastases (Gupta et al. 2005; Uong and Zon 2010; Strizzi et al. 2011). Thus, Myo10 may function in melanoma metastasis as well as melanoblast migration.

To study this, we employed a mouse melanoma induction model consisting of mice with melanocyte-specific expression of activated Braf, a proto-oncogene, combined with silencing of the Pten tumor suppressor gene (Tyr-CreER/BrafCA/PtenKO); all Tyr-CreER/BrafCA/PtenKO mice develop melanoma (Dankort et al. 2009). When Myo10KO mice were crossed with Tyr-CreER/BrafCA/PtenKO mice, tumor formation was delayed, the average tumor volumes were markedly reduced, lymph node metastasis was significantly decreased, and the medial survival time was significantly extended in Tyr-CreER/BrafCA/PtenKO/Myo10KO mice vs. Tyr-CreER/BrafCA/PtenKO/Myo10 wild type mice (Tokuo et al. 2018), evidence that Myo10 is involved in melanoma initiation and development.

17.6.2 Myo10 in Human Melanoma

Using the PROGgeneV2 prognostic biomarker identification tool (Goswami and Nakshatri 2014), we found in studies designed to investigate the role of Myo10 in human melanoma patients that the amount of *MYO10* mRNA was significantly higher in malignant melanoma than in benign nevi and that elevated expression of the *MYO10* gene was associated with inferior survival outcomes (Tokuo et al. 2018). We also investigated MYO10 protein expression in human melanoma and nevi using a tissue microarray and found that MYO10 staining intensity was significantly higher in melanoma lesions than in nevi, consistent with the results showing that *MYO10* mRNA expression is higher in melanoma vs. benign nevi. These results suggest that the Myo10 expression level correlates with melanocytic neoplastic progression in humans and overall survival of melanoma patients.

17.7 Summary and Perspectives

Myo10 has been studied in many types of cells and organs, and regulation of actin-based protrusions is the main physiological function of this interesting motor protein. These findings are now confirmed in Myo10KO mice, which will continue to provide opportunities for in-depth analyses of the biological and pathological functions of Myo10 *in vivo*. For example, the function of headless Myo10 *in vivo* should be investigated by comparing neuronal function in *total Myo10* KO mice vs. *full-length Myo10 only* KO mice to give new insights into motor domain regulations. Also, in particular, human diseases (including

cancer) related to MYO10 should be reconstructed in mice and challenged for the development of new therapies.

Acknowledgements I am grateful to Lynne M. Coluccio for her helpful comments and suggestions. I apologize for not citing all the relevant references because of space limitation. The work in the author's laboratory is supported by NIH R01 GM111615 to L.M.C., the Boston University Clinical and Translational Science Institute (1UL1TR001430) and NIH R03 DC009887 to H.T.

References

Almagro S, Durmort C, Chervin-Petinot A, Heyraud S, Dubois M, Lambert O, Maillefaud C, Hewat E, Schaal JP, Huber P, Gulino-Debrac D (2010) The motor protein myosin-X transports VE-cadherin along filopodia to allow the formation of early endothelial cell-cell contacts. Mol Cell Biol 30(7):1703–1717. https://doi.org/10.1128/MCB.01226-09

Appenzeller J, Lin YM, Knoch J, Avouris P (2004) Band-to-band tunneling in carbon nanotube field-effect transistors. Phys Rev Lett 93(19):196805. https://doi.org/10.1103/PhysRevLett.93.196805

Applewhite DA, Barzik M, Kojima S, Svitkina TM, Gertler FB, Borisy GG (2007) Ena/VASP proteins have an anti-capping independent function in filopodia formation. Mol Biol Cell 18(7):2579–2591

Arjonen A, Kaukonen R, Mattila E, Rouhi P, Hognas G, Sihto H, Miller BW, Morton JP, Bucher E, Taimen P, Virtakoivu R, Cao Y, Sansom OJ, Joensuu H, Ivaska J (2014) Mutant p53-associated myosin-X upregulation promotes breast cancer invasion and metastasis. J Clin Invest 124(3):1069–1082. https://doi.org/10.1172/JCI67280

Berg JS, Cheney RE (2002) Myosin-X is an unconventional myosin that undergoes intrafilopodial motility. Nat Cell Biol 4(3):246–250

Berg JS, Derfler BH, Pennisi CM, Corey DP, Cheney RE (2000) Myosin-X, a novel myosin with pleckstrin homology domains, associates with regions of dynamic actin. J Cell Sci 113(Pt 19):3439–3451

Bidkhori G, Narimani Z, Hosseini Ashtiani S, Moeini A, Nowzari-Dalini A, Masoudi-Nejad A (2013) Reconstruction of an integrated genome-scale co-expression network reveals key modules involved in lung adenocarcinoma. PLoS One 8(7):e67552. https://doi.org/10.1371/journal.pone.0067552

Bishai EA, Sidhu GS, Li W, Dhillon J, Bohil AB, Cheney RE, Hartwig JH, Southwick FS (2013) Myosin-X facilitates Shigella-induced membrane protrusions and cell-to-cell spread. Cell Microbiol 15(3):353–367. https://doi.org/10.1111/cmi.12051

Bohil AB, Robertson BW, Cheney RE (2006) Myosin-X is a molecular motor that functions in filopodia formation. Proc Natl Acad Sci U S A 103(33):12411–12416

Cao R, Chen J, Zhang X, Zhai Y, Qing X, Xing W, Zhang L, Malik YS, Yu H, Zhu X (2014) Elevated expression of myosin X in tumours contributes to breast cancer aggressiveness and metastasis. Br J Cancer 111(3):539–550. https://doi.org/10.1038/bjc.2014.298

Caride AJ, Bennett RD, Strehler EE (2010) Kinetic analysis reveals differences in the binding mechanism of calmodulin and calmodulin-like protein to the IQ motifs of myosin-10. Biochemistry 49(37):8105–8116. https://doi.org/10.1021/bi100644q

Chan PC, Hsu RY, Liu CW, Lai CC, Chen HC (2014) Adducin-1 is essential for mitotic spindle assembly through its interaction with myosin-X. J Cell Biol 204(1):19–28. https://doi.org/10.1083/jcb.201306083

Chen ZY, Hasson T, Kelley PM, Schwender BJ, Schwartz MF, Ramakrishnan M, Kimberling WJ, Mooseker MS, Corey DP (1996) Molecular cloning and domain structure of human myosin-VIIa, the gene product defective in usher syndrome 1B. Genomics 36(3):440–448. https://doi.org/10.1006/geno.1996.0489

Chen CP, Sun ZL, Lu X, Wu WX, Guo WL, Lu JJ, Han C, Huang JQ, Fang Y (2016) MiR-340 suppresses cell migration and invasion by targeting MYO10 in breast cancer. Oncol Rep 35(2):709–716. https://doi.org/10.3892/or.2015.4411

Chishti AH, Kim AC, Marfatia SM, Lutchman M, Hanspal M, Jindal H, Liu SC, Low PS, Rouleau GA, Mohandas N, Chasis JA, Conboy JG, Gascard P, Takakuwa Y, Huang SC, Benz EJ Jr, Bretscher A, Fehon RG, Gusella JF, Ramesh V, Solomon F, Marchesi VT, Tsukita S, Tsukita S, Hoover KB et al (1998) The FERM domain: a unique module involved in the linkage of cytoplasmic proteins to the membrane. Trends Biochem Sci 23(8):281–282

Costanzo M, Abounit S, Marzo L, Danckaert A, Chamoun Z, Roux P, Zurzolo C (2013) Transfer of polyglutamine aggregates in neuronal cells occurs in tunneling nanotubes. J Cell Sci 126(Pt 16):3678–3685. https://doi.org/10.1242/jcs.126086

Cox D, Berg JS, Cammer M, Chinegwundoh JO, Dale BM, Cheney RE, Greenberg S (2002) Myosin X is a downstream effector of PI(3)K during phagocytosis. Nat Cell Biol 4(7):469–477

Dankort D, Curley DP, Cartlidge RA, Nelson B, Karnezis AN, Damsky WE Jr, You MJ, DePinho RA, McMahon M, Bosenberg M (2009) Braf(V600E) cooperates with Pten loss to induce metastatic melanoma. Nat Genet 41(5):544–552. https://doi.org/10.1038/ng.356

Divito MM, Cheney RE (2008) Myosins: a superfamily of molecular motors chapter 14 MYOSIN X. In: Proteins and cell regulation, vol 7. Springer, Dordrecht

Frame MC, Patel H, Serrels B, Lietha D, Eck MJ (2010) The FERM domain: organizing the structure and function of FAK. Nat Rev Mol Cell Biol 11(11):802–814. https://doi.org/10.1038/nrm2996

Fukuda M, Mikoshiba K (1996) Structure-function relationships of the mouse Gap1m. Determination of the inositol 1,3,4,5-tetrakisphosphate-binding domain. J Biol Chem 271(31):18838–18842

Goswami CP, Nakshatri H (2014) PROGgeneV2: enhancements on the existing database. BMC Cancer 14:970. https://doi.org/10.1186/1471-2407-14-970

Gousset K, Schiff E, Langevin C, Marijanovic Z, Caputo A, Browman DT, Chenouard N, de Chaumont F, Martino A, Enninga J, Olivo-Marin JC, Mannel D, Zurzolo C (2009) Prions hijack tunnelling nanotubes for intercellular spread. Nat Cell Biol 11(3):328–336. https://doi.org/10.1038/ncb1841

Gousset K, Marzo L, Commere PH, Zurzolo C (2013) Myo10 is a key regulator of TNT formation in neuronal cells. J Cell Sci 126(Pt 19):4424–4435. https://doi.org/10.1242/jcs.129239

Gupta PB, Kuperwasser C, Brunet JP, Ramaswamy S, Kuo WL, Gray JW, Naber SP, Weinberg RA (2005) The melanocyte differentiation program predisposes to metastasis after neoplastic transformation. Nat Genet 37(10):1047–1054. https://doi.org/10.1038/ng1634

Gurke S, Barroso JF, Hodneland E, Bukoreshtliev NV, Schlicker O, Gerdes HH (2008) Tunneling nanotube (TNT)-like structures facilitate a constitutive, actomyosin-dependent exchange of endocytic organelles between normal rat kidney cells. Exp Cell Res 314(20):3669–3683. https://doi.org/10.1016/j.yexcr.2008.08.022

Hammer JA 3rd (1994) The structure and function of unconventional myosins: a review. J Muscle Res Cell Motil 15(1):1–10

Haslam RJ, Koide HB, Hemmings BA (1993) Pleckstrin domain homology. Nature 363(6427):309–310. https://doi.org/10.1038/363309b0

Heimsath EG Jr, Yim YI, Mustapha M, Hammer JA, Cheney RE (2017) Myosin-X knockout is semi-lethal and demonstrates that myosin-X functions in neural tube closure, pigmentation, hyaloid vasculature regression, and filopodia formation. Sci Rep 7(1):17354. https://doi.org/10.1038/s41598-017-17638-x

Hirano Y, Hatano T, Takahashi A, Toriyama M, Inagaki N, Hakoshima T (2011) Structural basis of cargo recognition by the myosin-X MyTH4-FERM domain. EMBO J 30(13):2734–2747. https://doi.org/10.1038/emboj.2011.177

Homma K, Saito J, Ikebe R, Ikebe M (2001) Motor function and regulation of myosin X. J Biol Chem 276(36):34348–34354

Horsthemke M, Bachg AC, Groll K, Moyzio S, Muther B, Hemkemeyer SA, Wedlich-Soldner R, Sixt M, Tacke S, Bahler M, Hanley PJ (2017) Multiple roles of filopodial dynamics in particle capture and phagocytosis and phenotypes of Cdc42 and Myo10 deletion. J Biol Chem 292(17):7258–7273. https://doi.org/10.1074/jbc.M116.766923

Hwang YS, Luo T, Xu Y, Sargent TD (2009) Myosin-X is required for cranial neural crest cell migration in Xenopus laevis. Dev Dyn 238(10):2522–2529

Isakoff SJ, Cardozo T, Andreev J, Li Z, Ferguson KM, Abagyan R, Lemmon MA, Aronheim A, Skolnik EY (1998) Identification and analysis of PH domain-containing targets of phosphatidylinositol 3-kinase using a novel in vivo assay in yeast. EMBO J 17(18):5374–5387. https://doi.org/10.1093/emboj/17.18.5374

Kerber ML, Cheney RE (2011) Myosin-X: a MyTH-FERM myosin at the tips of filopodia. J Cell Sci 124(Pt 22):3733–3741. https://doi.org/10.1242/jcs.023549

Kerber ML, Jacobs DT, Campagnola L, Dunn BD, Yin T, Sousa AD, Quintero OA, Cheney RE (2009) A novel form of motility in filopodia revealed by imaging myosin-X at the single-molecule level. Curr Biol 19(11):967–973

Knight PJ, Thirumurugan K, Xu Y, Wang F, Kalverda AP, Stafford WF 3rd, Sellers JR, Peckham M (2005) The predicted coiled-coil domain of myosin 10 forms a novel elongated domain that lengthens the head. J Biol Chem 280(41):34702–34708

Kroon J, Schaefer A, van Rijssel J, Hoogenboezem M, van Alphen F, Hordijk P, Stroes ESG, Stromblad S, van Rheenen J, van Buul JD (2018) Inflammation-sensitive myosin-X functionally supports leukocyte extravasation by Cdc42-mediated ICAM-1-rich endothelial Filopodia formation. J Immunol 200(5):1790–1801. https://doi.org/10.4049/jimmunol.1700702

Kwon M, Bagonis M, Danuser G, Pellman D (2015) Direct microtubule-binding by Myosin-10 orients centrosomes toward retraction fibers and subcortical actin clouds. Dev Cell 34(3):323–337. https://doi.org/10.1016/j.devcel.2015.06.013

Lin WH, Hurley JT, Raines AN, Cheney RE, Webb DJ (2013) Myosin X and its motorless isoform differentially modulate dendritic spine development by regulating trafficking and retention of vasodilator-stimulated phosphoprotein. J Cell Sci 126(Pt 20):4756–4768. https://doi.org/10.1242/jcs.132969

Liu KC, Jacobs DT, Dunn BD, Fanning AS, Cheney RE (2012) Myosin-X functions in polarized epithelial cells. Mol Biol Cell 23(9):1675–1687. https://doi.org/10.1091/mbc.E11-04-0358

Lu Q, Ye F, Wei Z, Wen Z, Zhang M (2012) Antiparallel coiled-coil-mediated dimerization of myosin X. Proc Natl Acad Sci U S A 109(43):17388–17393. https://doi.org/10.1073/pnas.1208642109

Makowska KA, Hughes RE, White KJ, Wells CM, Peckham M (2015) Specific Myosins control actin organization, cell morphology, and migration in prostate Cancer cells. Cell Rep 13(10):2118–2125. https://doi.org/10.1016/j.celrep.2015.11.012

Mattila PK, Lappalainen P (2008) Filopodia: molecular architecture and cellular functions. Nat Rev Mol Cell Biol 9(6):446–454. https://doi.org/10.1038/nrm2406

Mayer BJ, Ren R, Clark KL, Baltimore D (1993) A putative modular domain present in diverse signaling proteins. Cell 73(4):629–630

McMichael BK, Cheney RE, Lee BS (2010) Myosin X regulates sealing zone patterning in osteoclasts through linkage of podosomes and microtubules. J Biol Chem 285(13):9506–9515. https://doi.org/10.1074/jbc.M109.017269

Nagy S, Ricca BL, Norstrom MF, Courson DS, Brawley CM, Smithback PA, Rock RS (2008) A myosin motor

that selects bundled actin for motility. Proc Natl Acad Sci U S A 105(28):9616–9620
Nie S, Kee Y, Bronner-Fraser M (2009) Myosin-X is critical for migratory ability of Xenopus cranial neural crest cells. Dev Biol 335(1):132–142
Onfelt B, Nedvetzki S, Benninger RK, Purbhoo MA, Sowinski S, Hume AN, Seabra MC, Neil MA, French PM, Davis DM (2006) Structurally distinct membrane nanotubes between human macrophages support long-distance vesicular traffic or surfing of bacteria. J Immunol 177(12):8476–8483
Pi X, Ren R, Kelley R, Zhang C, Moser M, Bohil AB, Divito M, Cheney RE, Patterson C (2007) Sequential roles for myosin-X in BMP6-dependent filopodial extension, migration, and activation of BMP receptors. J Cell Biol 179(7):1569–1582
Plantard L, Arjonen A, Lock JG, Nurani G, Ivaska J, Stromblad S (2010) PtdIns(3,4,5)P(3) is a regulator of myosin-X localization and filopodia formation. J Cell Sci 123(Pt 20):3525–3534. https://doi.org/10.1242/jcs.069609
Raines AN, Nagdas S, Kerber ML, Cheney RE (2012) Headless Myo10 is a negative regulator of full-length Myo10 and inhibits axon outgrowth in cortical neurons. J Biol Chem 287(30):24873–24883. https://doi.org/10.1074/jbc.M112.369173
Rameh LE, Arvidsson A, Carraway KL 3rd, Couvillon AD, Rathbun G, Crompton A, VanRenterghem B, Czech MP, Ravichandran KS, Burakoff SJ, Wang DS, Chen CS, Cantley LC (1997) A comparative analysis of the phosphoinositide binding specificity of pleckstrin homology domains. J Biol Chem 272(35):22059–22066
Rogers MS, Strehler EE (2001) The tumor-sensitive calmodulin-like protein is a specific light chain of human unconventional myosin X. J Biol Chem 276(15):12182–12189
Ropars V, Yang Z, Isabet T, Blanc F, Zhou K, Lin T, Liu X, Hissier P, Samazan F, Amigues B, Yang ED, Park H, Pylypenko O, Cecchini M, Sindelar CV, Sweeney HL, Houdusse A (2016) The myosin X motor is optimized for movement on actin bundles. Nat Commun 7:12456. https://doi.org/10.1038/ncomms12456
Salim K, Bottomley MJ, Querfurth E, Zvelebil MJ, Gout I, Scaife R, Margolis RL, Gigg R, Smith CI, Driscoll PC, Waterfield MD, Panayotou G (1996) Distinct specificity in the recognition of phosphoinositides by the pleckstrin homology domains of dynamin and Bruton's tyrosine kinase. EMBO J 15(22):6241–6250
Schoumacher M, Goldman RD, Louvard D, Vignjevic DM (2010) Actin, microtubules, and vimentin intermediate filaments cooperate for elongation of invadopodia. J Cell Biol 189(3):541–556. https://doi.org/10.1083/jcb.200909113
Shaw G (1993) Identification of novel pleckstrin homology (PH) domains provides a hypothesis for PH domain function. Biochem Biophys Res Commun 195(2):1145–1151. https://doi.org/10.1006/bbrc.1993.2164
Solc CK, Derfler BH, Duyk GM, Corey DP (1994) Molecular cloning of myosins from the bullfrog saccular macula: a candidate for the hair cell adaptation motor. Aud Neurosci 1:63–75
Sousa AD, Berg JS, Robertson BW, Meeker RB, Cheney RE (2006) Myo10 in brain: developmental regulation, identification of a headless isoform and dynamics in neurons. J Cell Sci 119(Pt 1):184–194
Sowinski S, Jolly C, Berninghausen O, Purbhoo MA, Chauveau A, Kohler K, Oddos S, Eissmann P, Brodsky FM, Hopkins C, Onfelt B, Sattentau Q, Davis DM (2008) Membrane nanotubes physically connect T cells over long distances presenting a novel route for HIV-1 transmission. Nat Cell Biol 10(2):211–219. https://doi.org/10.1038/ncb1682
Starke J, Maaser K, Wehrle-Haller B, Friedl P (2013) Mechanotransduction of mesenchymal melanoma cell invasion into 3D collagen lattices: filopod-mediated extension-relaxation cycles and force anisotropy. Exp Cell Res 319(16):2424–2433. https://doi.org/10.1016/j.yexcr.2013.04.003
Strizzi L, Hardy KM, Kirsammer GT, Gerami P, Hendrix MJ (2011) Embryonic signaling in melanoma: potential for diagnosis and therapy. Lab Investig 91(6):819–824. https://doi.org/10.1038/labinvest.2011.63
Sun Y, Ai X, Shen S, Lu S (2015) NF-kappaB-mediated miR-124 suppresses metastasis of non-small-cell lung cancer by targeting MYO10. Oncotarget 6(10):8244–8254. https://doi.org/10.18632/oncotarget.3135
Sviderskaya EV, Wakeling WF, Bennett DC (1995) A cloned, immortal line of murine melanoblasts inducible to differentiate to melanocytes. Development 121(5):1547–1557
Tardivel M, Begard S, Bousset L, Dujardin S, Coens A, Melki R, Buee L, Colin M (2016) Tunneling nanotube (TNT)-mediated neuron-to neuron transfer of pathological Tau protein assemblies. Acta Neuropathol Commun 4(1):117. https://doi.org/10.1186/s40478-016-0386-4
Tasca A, Astleford K, Lederman A, Jensen ED, Lee BS, Gopalakrishnan R, Mansky KC (2017) Regulation of osteoclast differentiation by myosin X. Sci Rep 7(1):7603. https://doi.org/10.1038/s41598-017-07855-9
Tokuo H, Ikebe M (2004) Myosin X transports Mena/VASP to the tip of filopodia. Biochem Biophys Res Commun 319(1):214–220
Tokuo H, Mabuchi K, Ikebe M (2007) The motor activity of myosin-X promotes actin fiber convergence at the cell periphery to initiate filopodia formation. J Cell Biol 179(2):229–238. https://doi.org/10.1083/jcb.200703178
Tokuo H, Bhawan J, Coluccio LM (2018) Myosin X is required for efficient melanoblast migration and melanoma initiation and metastasis. Sci Rep 8(1):10449. https://doi.org/10.1038/s41598-018-28717-y
Toyoshima F, Nishida E (2007) Integrin-mediated adhesion orients the spindle parallel to the substratum in an EB1- and myosin X-dependent manner. EMBO J 26(6):1487–1498

Umeki N, Jung HS, Sakai T, Sato O, Ikebe R, Ikebe M (2011) Phospholipid-dependent regulation of the motor activity of myosin X. Nat Struct Mol Biol 18(7):783–788. https://doi.org/10.1038/nsmb.2065

Uong A, Zon LI (2010) Melanocytes in development and cancer. J Cell Physiol 222(1):38–41. https://doi.org/10.1002/jcp.21935

Wang A, Liang Y, Fridell RA, Probst FJ, Wilcox ER, Touchman JW, Morton CC, Morell RJ, Noben-Trauth K, Camper SA, Friedman TB (1998) Association of unconventional myosin MYO15 mutations with human nonsyndromic deafness DFNB3. Science 280(5368):1447–1451

Wang X, Veruki ML, Bukoreshtliev NV, Hartveit E, Gerdes HH (2010) Animal cells connected by nanotubes can be electrically coupled through interposed gap-junction channels. Proc Natl Acad Sci U S A 107(40):17194–17199. https://doi.org/10.1073/pnas.1006785107

Wang X, Bukoreshtliev NV, Gerdes HH (2012) Developing neurons form transient nanotubes facilitating electrical coupling and calcium signaling with distant astrocytes. PLoS One 7(10):e47429. https://doi.org/10.1371/journal.pone.0047429

Watanabe TM, Tokuo H, Gonda K, Higuchi H, Ikebe M (2010) Myosin-X induces filopodia by multiple elongation mechanism. J Biol Chem 285(25):19605–19614. https://doi.org/10.1074/jbc.M109.093864

Weber KL, Sokac AM, Berg JS, Cheney RE, Bement WM (2004) A microtubule-binding myosin required for nuclear anchoring and spindle assembly. Nature 431(7006):325–329

Wei Z, Yan J, Lu Q, Pan L, Zhang M (2011) Cargo recognition mechanism of myosin X revealed by the structure of its tail MyTH4-FERM tandem in complex with the DCC P3 domain. Proc Natl Acad Sci U S A 108(9):3572–3577. https://doi.org/10.1073/pnas.1016567108

Wittig D, Wang X, Walter C, Gerdes HH, Funk RH, Roehlecke C (2012) Multi-level communication of human retinal pigment epithelial cells via tunneling nanotubes. PLoS One 7(3):e33195. https://doi.org/10.1371/journal.pone.0033195

Wu L, Pan L, Wei Z, Zhang M (2011) Structure of MyTH4-FERM domains in myosin VIIa tail bound to cargo. Science 331(6018):757–760. https://doi.org/10.1126/science.1198848

Yonezawa S, Kimura A, Koshiba S, Masaki S, Ono T, Hanai A, Sonta S, Kageyama T, Takahashi T, Moriyama A (2000) Mouse myosin X: molecular architecture and tissue expression as revealed by northern blot and in situ hybridization analyses. Biochem Biophys Res Commun 271(2):526–533

Yonezawa S, Yoshizaki N, Sano M, Hanai A, Masaki S, Takizawa T, Kageyama T, Moriyama A (2003) Possible involvement of myosin-X in intercellular adhesion: importance of serial pleckstrin homology regions for intracellular localization. Develop Growth Differ 45(2):175–185

Yu H, Wang N, Ju X, Yang Y, Sun D, Lai M, Cui L, Sheikh MA, Zhang J, Wang X, Zhu X (2012) PtdIns (3,4,5) P3 recruitment of Myo10 is essential for axon development. PLoS One 7(5):e36988. https://doi.org/10.1371/journal.pone.0036988

Zhang H, Berg JS, Li Z, Wang Y, Lang P, Sousa AD, Bhaskar A, Cheney RE, Stromblad S (2004) Myosin-X provides a motor-based link between integrins and the cytoskeleton. Nat Cell Biol 6(6):523–531. https://doi.org/10.1038/ncb1136

Zhu XJ, Wang CZ, Dai PG, Xie Y, Song NN, Liu Y, Du QS, Mei L, Ding YQ, Xiong WC (2007) Myosin X regulates netrin receptors and functions in axonal path-finding. Nat Cell Biol 9(2):184–192

Myosin XVI

18

Beáta Bugyi and András Kengyel

Abstract

Myosin XVI (Myo16), a vertebrate-specific motor protein, is a recently discovered member of the myosin superfamily. The detailed functionality regarding myosin XVI requires elucidating or clarification; however, it appears to portray an important role in neural development and in the proper functioning of the nervous system. It is expressed in the largest amount in neural tissues in the late embryonic-early postnatal period, specifically the time in which neuronal cell migration and dendritic elaboration coincide. The impaired expression of myosin XVI has been found lurking in the background of several neuropsychiatric disorders including autism, schizophrenia and/or bipolar disorders.

Two principal isoforms of class XVI myosins have been thus far described: Myo16a, the tailless cytoplasmic isoform and Myo16b, the full-length molecule featuring both cytoplasmic and nuclear localization. Both isoforms contain a class-specific N-terminal ankyrin repeat domain that binds to the protein phosphatase catalytic subunit. Myo16b, the predominant isoform, exhibits a diverse function. In the cytoplasm, it participates in the reorganization of the actin cytoskeleton through activation of the PI3K pathway and the WAVE-complex, while in the nucleus it may possess a role in cell cycle regulation. Based on the sequence, myosin XVI may have a compromised ATPase activity, implying a potential stationary role.

Keywords

Myosin · Ankyrin repeat · Nucleus · Cell cycle · Neural development

18.1 Introduction

Myosins are a large and diverse superfamily of actin-based motor proteins participating in various cellular processes such as cell division, cell motility, polarity formation or cargo transport (Berg et al. 2001; Mermall 1998; Schliwa and Woehlke 2003). Unconventional myosins do not form filaments. They function as monomers or dimers and are specialized in support of various functions. Several unconventional myosins have been described in their portrayal of an integral role regarding neural development or in the proper operation of the nervous system. In reference to this category, one is identified as myosin XVI, a recently discovered and lesser known member of the myosin superfamily.

B. Bugyi · A. Kengyel (✉)
Department of Biophysics, University of Pécs, Medical School, Pécs, Hungary
e-mail: andras.kengyel@aok.pte.hu

L. M. Coluccio (ed.), *Myosins*, Advances in Experimental Medicine and Biology 1239,
https://doi.org/10.1007/978-3-030-38062-5_18

Myosin XVI was first described in 2001 when Patel and colleagues were searching for motor proteins in migrating granule neurons and type 1 astrocytes. The PCR-based screening identified among the known motor protein types, a sequence, which was not homologous with any other formerly described myosin class with exception of the conserved motor domain. Initially, it was denoted as myr8, named for the eighth unconventional myosin in rat, and later it was designated as the novel myosin class XVI (Patel et al. 2001).

18.2 Evolution and Genetics of Myosin XVI

Factually, the cDNA of Myo16 was first isolated from size-fractionated human cDNA library in a search for clones encoding large proteins, as KIAA0865, without noting it encodes a myosin (Nagase et al. 1998). The systematic characterization in the expression of unconventional myosin-encoding genes in the developing nervous system of zebrafish identified Myo16 (Sittaramane and Chandrasekhar 2008). Orthologues were predicted in vertebrates, yet not in consideration of the lower species. Consistently, phylogenetic analysis implicates Myo16 as appearing relatively late during evolution, and, significantly, it is found only in vertebrates. Currently, Myo16 is the only vertebrate-specific myosin, and the *MYO16* gene is conserved in Euteleostomi (Odronitz and Kollmar 2007). Based on a recent classification according to the head domain sequence, Myo16 is aligned to the group of myosin III-like proteins, which are characterized by specific N-terminal extensions. In respect to the phylogenetic tree, the closest relatives of myosin XVI are myosin III and myosin IX, both of which comprise an N-terminal domain specialized for different functions (Sebé-Pedrós et al. 2014).

18.3 Domain Organization and Sequence Characteristics of Myosin XVI

The genomic region of *MYO16* spans ~362 kb in the 16q12.5 chromosome region among rats and ~660 kb in the 13q33.3 chromosome among humans. The principal isoform in both species is composed of 34 coding exons with the size ranging from 66 to 1296 bp (Cameron et al. 2007). Based on sequence analysis, two splice variants of rat Myo16 were found and named Myo16a and Myo16b (Table 18.1). The sequences diverge at the exon 30/intron boundary. They have identical N-terminal regions up to 1321 residues. While Myo16a ends at Gly^{1322}, Myo16b possesses an additional ~600 aa long C-terminus.

In addition to the conventional motor domain and a short neck region, both Myo16 isoforms

Table 18.1 Myo16 isoforms

Human isoform (Accession number)	Rat synonyms (Accession number)	Other names	Amino acid length (*hs/rn*)	Molecular weight[a] (kDa) (*hs/rn*)	Remark
Myo16a (NA)	**myr8a** (EDM08807.1)	Myr 8 CRA_b	1329/1322	150.25/148.78	Tailless cytoplasmic isoform
Myo16b isoform 1 (NP_001185879.1)	[Predicted: myosin XVI isoform X1] (XP_008769606.1)	NA	1880/1934	208.84/213.41	Transcript variant with 22 amino acid N- terminal extension
Myo16b isoform 2 (NP_055826.1)	**myr8b** (NP_620248.1)	Myr 8 CRA_a; KIAA0865; NYAP3	1858/1912	206.13/210.56	Predominant isoform

hs Homo sapiens, *rn Rattus norvegicus*, *NA* not applicable
[a]Calculated with ProtParam (https://web.expasy.org/protparam/)

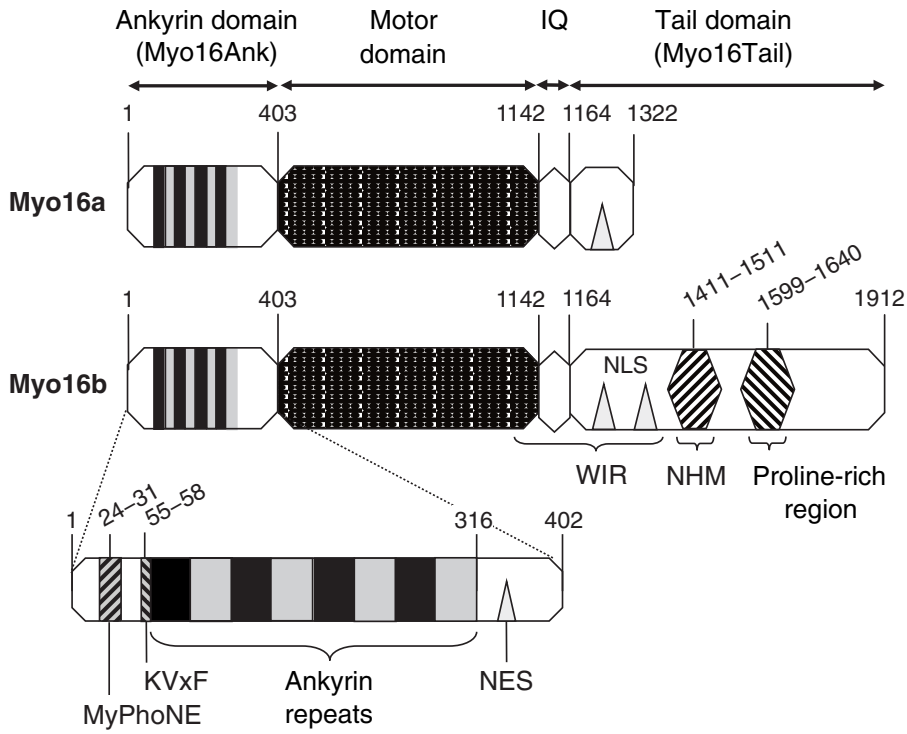

Fig. 18.1 Schematic structure of Myo16 isoforms. Numbers represent the amino acid residues corresponding to *Rattus norvegicus* Myo16 (NP_620248.1). *NLS* nuclear localization signal, *WIR* WAVE1 interacting region, *NHM* NYAP homology motif, *MyPhoNE* myosin phosphatase N-terminal element, *NES* nuclear export signal

contain an N-terminal extension, the often referred to ankyrin repeat domain (Myo16Ank) (Patel et al. 2001). In Myo16b, the neck region is followed by a ~750 amino acid long extension, the commonly referred to tail domain (Myo16Tail). In contrast, Myo16a has only a relatively short C-terminal tail region (Fig. 18.1).

Myo16Ank is a structural element specific to class XVI myosins. It is a large, ~40 kDa N-terminal domain preceding the motor domain. It contains eight ankyrin repeats, which is unique among myosin families; however, it is one of the most common sequential motifs in different proteins (Sedgwick and Smerdon 1999). The ankyrin repeats consist of several tandemly-organized ankyrin motifs of 30 to 33 amino acid and express a ß-hairpin–loop–helix–loop structure. The ankyrin repeats form an interacting interface. Thus, these domains typically participate in protein-protein interactions; however, they do not bind selectively to a class of proteins. Rather there is an immense diversity among partner proteins and the interaction is target specific (Li et al. 2006).

Sequence analysis reveals the N-terminal of Myo16 consists of a MyPhoNE (myosin phosphatase N-terminal element) sequence motif having the consensus of RxxQ[VIL][KR]x[YW] (Table 18.2). Downstream, immediately preceding the first ankyrin repeat, the [RK][VI]x[FW] motif can be found. These sequence elements are known to be among the conserved binding sites of the regulatory subunits of myosin phosphatase for PP1c (protein phosphatase 1 catalytic subunit) (Hartshorne et al. 1998). Comprehensively, Myo16Ank exhibits a high similarity with the N-terminal structure of the large target (also known as: regulatory) subunit of myosin phosphatase (myosin phosphatase target subunit 1, MYPT1).

The ~90 kDa motor domain of Myo16, which is the most conserved segment, shows ~50%

Table 18.2 Sequence comparison of Myo16 from different species

	PP1c binding regions		NYAP homology motif	
	MyPhoNE			
consensus	Rx$_2$Q[VIL][KR]x[YW]	[RK][VI]x[FW]	Yx$_2$M	Yx$_2$M
	**:*::.*	:: *	****	****
hs	RCEQIKAY	KVHF	YIEM	YEEM
mm	RCEQIKAY	KVRF	YIEM	YEEM
rn	RCEQIKAY	KVRF	YIEM	YEEM
gg	RCDQIKAY	RVRF	YIEM	YEEM
xt	RCDQIKAY	KVHF	YIEM	YEEM
dr	RCEQLRVY	KISF	YIEM	YEEM

	Motor domain					IQ motif
	Purine binding loop	P-loop	Switch I	Switch II	DLLAK motif	
consensus	NPx$_6$Y	GE[SR]G[SA]GKT	LEAFGHAKTx$_2$N[ND]NSSR	DxGFE	Dx$_{16}$DLLAK	[ILV]Qx$_3$RG x$_3$[RK]
	:*:**	** ****:	:******:* :. .*	******	* ***:*	*: ****:* :***
hs	NPYKELPIY	GERGSGKS	LEAFGHAKTTLNDLSSC	DIFGFE	Dx$_{16}$DLLAK	IITCQKVIRGFLAR
mm	NPFKELPIY	GERGSGKT	VEAFGHAKTTLNNVSSC	DIFGFE	Dx$_{16}$DLLAK	IITCQKVIRGFLAR
rn	NPFKELPIY	GERGSGKT	LEAFGHAKTTLNNVSSC	DIFGFE	Dx$_{16}$DLLAK	IVTCQKVIRGFLAR
gg	NPFKELPIY	GESGSGKT	LEAFGHAKTPLSDFSSC	DIFGFE	Dx$_{16}$DLLAK	IITCQKVVRGFLAR
xt	NPYKNLPIY	GESGSGKT	LEAFGHARTSINNSSSR	DIFGFE	Dx$_{16}$DLLAK	IILCQKVIRRFLAR
dr	NPYKDLPIY	GESGSGKS	LEAFGHAKTQMNTSGSR	DIFGFE	Dx$_{16}$DLLTK	IIICQKVMRGWLAR

Sequence alignment were made by Clustal X (Larkin et al. 2007)
Accession numbers are *Homo sapiens (hs)*: Q9Y6X6, *Mus musculus (mm)*: Q5DU14, *Rattus norvegicus (rn)*: Q9ERC1, *Gallus gallus (gg)*: XP_416950.3, *Xenopus tropicalis (xt)*: F6TDT5, *Danio rerio (dr)*: F1QE80. Highlighted the terminal arginine-cysteine replacement in switch I. Consensus sequences and conservations are indicated: fully conserved (∗), strongly similar (:), weakly similar (.)

homology with other myosin motor domains within a species. It contains the purine-binding loop (NPxxxxxxY), the P-loop (GE[SR]G[SA]GKT), switch I (LEAFGHAKTxxN[ND]NSSR) and switch II (DxxGFE) motifs, which are responsible for forming the ATP-binding pocket (Bement et al. 1994). These regions follow the respective consensus sequences and are well-conserved, except for switch I, in which the terminal arginine is changed to cysteine in mammalian and avian orthologues of Myo16. Arginine and glutamine residues in switch I and switch II, respectively, form a salt-bridge important for the ATPase activity of the motor. The substitution was intended to occur during the evolution of vertebrate taxon and to correlate with differences in neurogenesis (Cameron et al. 2007).

The motor domain is followed by a short neck region containing a single IQ motif ([ILV]QxxxRGxxx[RK]), which is a predicted light chain-binding site. However, the identity of the light chain of Myo16 needs further clarification. The conserved sequence motifs are summarized in Table 18.2.

Myo16a isoform has only a short tail domain, meanwhile, Myo16b isoform has an additional ~600 amino acid extension on its C-terminus. Predictably, the Myo16Tail is considerably disordered, lacking a secondary structure (predicted with IUPred (Dosztányi et al. 2005)). The C-terminal tail domain is typically the most diverse region of the myosin molecules and is often responsible for their specific function. The proximal region of Myo16Tail contains a recently identified NHM (NYAP homology motif) with two phosphotyrosine sites (Tyr1416 and Tyr1441 in mouse) (Yokoyama et al. 2011). The NHM is the identifying signature among the NYAP-family proteins, which are neuronal tyrosine phosphorylated adaptors for the PI3K (phosphoinositide-3 kinase). The C-terminal part of Myo16Tail contains proline-rich sequences with ~18% of proline residues. The poly-proline motifs can serve ligands in support of proteins

involved in the regulation of the actin cytoskeleton (reviewed in (Holt and Koffer 2001)). These include the small actin-binding protein profilin, EVH1 (Ena/Vasp homology 1), SH3 (Src-homology 3) and WW domain proteins. The strength of the interaction is dependent upon the characteristic of the poly-L-proline helix (*cis/trans*) and the number of proline residues, while specificity is provided by incorporated non-proline residues (Holt and Koffer 2001; Petrella et al. 1996).

18.4 Basic Functions and Regulation of Myosin XVI

18.4.1 Actin Binding and ATP Hydrolysis

The ability of Myo16 to bind actin and to hydrolyze ATP, basic features of myosin proteins, currently defies clarification. Early studies by Patel and colleagues suggested Myo16 interacts with actin filaments. The interaction of Myo16b with actin filaments was investigated in high-speed (100.000 *g*) co-sedimentation assays by implementing postnatal day 8 rat brain detergent-soluble lysate and platelet actin (Patel et al. 2001). In the presence of ATP (with or without actin), only a small fraction of Myo16b sedimented. In contrast, upon hexokinase addition to deplete ATP, the majority of Myo16b co-sedimented with actin filaments. This indicates Myo16b interacts with actin filaments in an ATP-dependent manner. However, the direct or indirect nature of the interaction remains to be clarified. In the analysis regarding the sequence of the ATP-binding pocket, the arginine residue in the switch-1 region, which stabilizes the closed conformation of the ATP-binding pocket (Geeves and Holmes 1999), is substituted by a cysteine in all mammalian and avian Myo16 isoforms (Table 18.2) (Cameron et al. 2007). This alteration may lead to a reduced ATPase activity of Myo16 and the elimination of the actin activation, as shown in other myosins (Onishi et al. 2002; Shimada et al. 1997).

18.4.2 Regulation

Based on sequence analysis, the motor domain contains an aspartate in the position 16 residues upstream from the conserved DLLAK motif (Table 18.2). Thus, Myo16 follows the TEDS rule and bears a negative charge on the surface loop in contact with actin. Since acidic amino acids can mimic phosphorylated residues, this implies that the enzymatic and mechanochemical activity of the Myo16 motor domain may be independent of head phosphorylation (Bement and Mooseker 1995; Patel et al. 2001). Although the motor activity and its regulation of Myo16 have not yet been directly measured, the potential regulatory role of the Myo16Ank domain was formerly described (Kengyel et al. 2015). Using skeletal and non-muscle myosin II (heavy meromyosin or full-length myosin) as a model system, Myo16Ank was found to bind to the motor domain of myosin II and markedly increase its steady-state ATPase activity. Another possible regulatory mechanism to be considered is the backfolding of the tail domain to the N-terminal of the molecule rendering the motor inactive. This type of autoregulation was described by several other myosins originating from different classes, including IIa, V, VI, VII and X (Milton et al. 2011; Umeki et al. 2011; Wang et al. 2004; Yang et al. 2009). In support of this mode of regulation, recent experiments have proven that isolated Myo16Ank and Myo16Tail are able to bind with a micromolar affinity assuming a regulatory function by backfolding of the tail to the N-terminus of Myo16 (Kengyel et al. 2017).

18.5 Expression and Localization Pattern of MYOSIN XVI

18.5.1 Tissue-Specific Localization

Myo16 is expressed predominantly throughout the nervous system, but it also can be found among peripheral tissues. The first Northern-blot analysis demonstrated how Myo16b, the prevalent isoform, is dominantly expressed in the cerebellum and neocortex in the hippocampal

neurons of embryonic and adult brain in rats and mice. Myo16b expression correlates with brain development, peaking at the first and second postnatal weeks (Patel et al. 2001; Yokoyama et al. 2011), the time which coincides with neuronal cell migration, axonal extension, dendritic elaboration and the increase in synaptic densities of the neocortex (Semplea et al. 2013). In the cerebellum of P10 rats, Myo16 was localized to the migrating granule neurons in the external granule layer and, in a lesser amount, among the Purkinje cells. In adult cerebellum Myo16 was found in a reduced amount; principally occurring in the Purkinje cells, in the elongated processes of the glia cells and in the granule neurons of the inner granule layer (Patel et al. 2001). Using primary neuronal cell cultures from rat, Myo16 was found in different cell types, including type-1 astrocytes, cerebellar granule neurons and hippocampal neurons. Interestingly, when isolated from the cortex of E18.5 Whistar rat, Myo16 was found in cortical neurons but not in astrocytes (Yokoyama et al. 2011).

In addition to the nervous system, Myo16b expression was found among peripheral tissues: in the bladder, lung, kidney and in lesser amount in thymus, adrenal, skeletal and cardiac muscle. However, it remains to be substantiated whether Myo16 is expressed in the non-neural tissues or in the associated neuronal tissue (Patel et al. 2001).

18.5.2 Intracellular Localization

Immunofluorescence labeling of the endogenous proteins in model cell lines, including COS7 and Rat2, suggests that Myo16a, the tailless, short isoform, localizes nearly exclusively to the cytoplasm in an overlapping manner of Myo16b, even though Myo16a contains a predicted nuclear localization signal (NLS) on its short tail domain (Cameron et al. 2007). Meanwhile, both cytoplasmic and nuclear localization of Myo16b is observed (Cameron et al. 2007, 2013; Patel et al. 2001). Myo16b is also present in the cytoplasm of neuronal cells, where it is distributed in soluble and membrane-associated fractions (Patel et al. 2001; Yokoyama et al. 2011). In Purkinje cells Myo16 accumulates in the dendritic spines (Roesler et al. 2019). The cytoplasmic fraction of full length EGFP-Myo16b colocalizes with neither actin filaments nor microtubules in COS7 cells. In contrast, the cytoplasmic fraction of isolated Myo16Tail domain distributed mostly along the plasma membrane and to the filopodial and lamellipodial structures, where it colocalizes with actin filaments (Cameron et al. 2007).

Immunofluorescence of endogenous Myo16b and transient transfection of EGFP-Myo16b in unsynchronized COS7 cells reflect nearly an equal distribution of Myo16b between the nucleus and cytoplasm, yet predominantly nuclear or cytoplasmic localization was also observed in a lesser degree (Cameron et al. 2007, 2013). The nuclear localization can also be detected *in vivo* in the mouse cerebellum (P23, P31) (Cameron et al. 2007; Patel et al. 2001). However, the pathways regulating the intracellular localization as well as the nuclear export and import of Myo16b remain elusive.

Truncated forms of Myo16b including its isolated ankyrin repeats (1–352) and C-terminal region (1616–1912) localized preferentially in the nucleus, even though these regions do not possess any obvious classical nuclear localization signals. Interestingly, Myo16b with a motor domain disrupted at either the ATP-, actin- or light-chain binding sites, shows exclusive cytoplasmic localization (Cameron et al. 2007). Two nuclear localization signals found on its C-terminal domain are predicted in Myo16. Myo16a containing only the first NLS remains in the cytoplasm, meanwhile the C-terminal fragment of Myo16b lacking both NLSs can migrate into the nucleus (Cameron et al. 2007). These results suggest that the NLSs are non-functional and indicate that the nuclear import of Myo16 is governed by an atypical localization mechanism.

Myo16 contains a leucine-rich nuclear export signal (NES) between the ankyrin repeats and the motor domain ($Lx_{2,3}$[LIVFM]x_2Lx[LI]) (Fukuda et al. 1997). Blocking the interaction between the NES and the export receptor CRM1 by

Leptomycin B leads to the nuclear accumulation of Myo16b, indicating that its nuclear export is regulated by signaling through the leucine-rich NES region. Additionally, truncating the ankyrin repeats results in an increase in the nuclear abundance of Myo16-ΔAnk, suggesting that Myo16Ank might play a role in the nuclear export process (Cameron et al. 2007).

These observations suggest that the distribution of Myo16b within the cell may have complex regulation through the Myo16Ank, Myo16Tail and/or the motor domain.

18.6 Cellular Functions of Myosin XVI

The sequence characteristics and the localization pattern of myosin XVI highlight its complex and multi-faceted roles in the regulation of cell functionality, which has just begun to emerge. Myo16 interacts with cytoplasmic components including signaling cascade molecules, therefore, it participates in the control of actin cytoskeleton remodeling in an indirect manner (Yokoyama et al. 2011). Characteristic of motor proteins, Myo16 associates with actin in an ATP-dependent fashion in brain lysates (Patel et al. 2001). On the other hand, the consensus switch-1 nucleotide-binding pocket sequence suggests compromised ATPase activity (Cameron et al. 2007). Therefore, it awaits further investigation and evidence as to whether Myo16 has a direct mode of action via its motor activity on actin arrays. Moreover, additional levels of functional complexity arise from its presence in the nucleus.

18.6.1 Cytoplasmic Function: Activation of the WAVE1 Complex Through the PI3K Pathway

Exploring the cytoplasmic functions of Myo16b was promoted by the identification of Myo16b as a member of the NYAP family of molecular adaptor proteins, designated as NYAP3 (Yokoyama et al. 2011). NYAP phosphoproteins (NYAP 1–3) were identified in Src non-receptor tyrosine kinase family substrate screening using a human hippocampus cDNA library. NYAPs are characterized by a ~100 amino acid region containing conserved tyrosine residues and a proline-rich stretch termed NYAP homology motif (NHM). The C-terminal region of Myo16b, downstream to its motor domain, possesses the NHM (Fig. 18.1). Myo16b was shown to be directly phosphorylated by the Src tyrosine kinase family member Fyn at tyrosine residues in the NHM. The phosphotyrosines of Myo16b are in two YxxM motifs which are identical from zebrafish to the human protein, suggesting a conserved function (Table 18.2). Myo16b phosphorylation is induced by Contactin5, a glycosylphosphatidylinositol (GPI) anchored membrane protein. Contactins, members of the immunoglobulin (Ig) superfamily, are expressed exclusively in the nervous system and can activate Src tyrosine kinases, such as Lyn directly, or, as in the case of Fyn, indirectly through receptor protein tyrosine phosphatase PTPα (Kasahara et al. 2002; Zeng et al. 1999). The YxxM is a consensus motif for the binding of the SH2 domain of the phosphoinositide 3-kinase (PI3K) p85 regulatory subunit. Indeed, co-immunoprecipitation and pull down analysis revealed a direct interaction between phosphorylated Myo16b and the PI3K p85 subunit. The absence of NYAPs compromised the membrane localization of PI3K, including the activation of its downstream effectors Akt and Rac1. Comprehensively, the data demonstrate that Myo16b is involved in the regulation of PI3K activity, which is a key regulatory pathway in neuronal functioning (Gross and Bassell 2014; Sánchez-Alegría et al. 2018).

Myo16b interacts with the Sra1 and Nap1 components of the WAVE1 regulatory complex as indicated by proteomic analysis and experimental data (Yokoyama et al. 2011). The WAVE1 interacting region (WIR) identified between the motor domain and the NHM differs from that of PI3K, which led to a proposal in which Myo16b, in the formation of a ternary complex with PI3K and WAVE1 regulatory complex, bridges PI3K and WAVE1. The

WAVE1 regulatory complex is activated by Rac1 and drives Arp2/3 complex-dependent actin filament dynamics. In Myo16 knockout (KO) or knockdown mice, a faster F-actin turnover rate was observed in the postsynaptic dendritic spines of the Purkinje cells, and the area of the presynaptic axon terminals and the number of synaptic vesicles per terminal was dramatically reduced. This underlies the role of Myo16 in the regulation of WAVE1-Arp2/3-mediated actin dynamics both at the postsynaptic and presynaptic side (Roesler et al. 2019). Transfection of HeLa cells with Myo16Tail (containing the WAVE1-binding and the NHM motifs) resulted in the collapse of actin filaments and the disappearance of stress fibers. These effects on the remodeling of the actin cytoskeleton rely on the simultaneous interaction of Myo16b with both PI3K and WAVE1 complex (Yokoyama et al. 2011). Thus, Myo16b is involved in the indirect regulation of actin cytoskeleton dynamics through the PI3K pathway (Fig. 18.2).

The PI3K pathway is established as an essential pathway in support of neuronal development, synapse formation, dendritic spine development, neuronal plasticity and memory formation. Mutations/dysregulation of PI3K signal transduction are implicated in brain disorders and mental diseases such as autism, epilepsy, schizophrenia or Alzheimer's disease. From another perspective, PI3K is a central signaling node in neurons and beneficial for various aspects of neuronal physiology, metabolism, tissue homeostasis or control of gene expression (Gross and Bassell 2014; Sánchez-Alegría et al. 2018; Zang et al. 2016). Altogether, the role of Myo16b as an activator of this pathway emphasizes its relevance in proper neuronal functioning.

In addition to the above interaction, Myo16b also co-immunoprecipitated with GRAF (GTPase regulator associated with focal adhesion kinase) and ACOT9 (Acyl-CoA thioesterase) in HEK293T cells (Yokoyama et al. 2011). Thus, Myo16b may be involved in the regulation of the curvature and composition of the neural membrane (Poupon et al. 1999; Taylor et al. 1999). Interacting partners of Myo16b are summarized in Table 18.3.

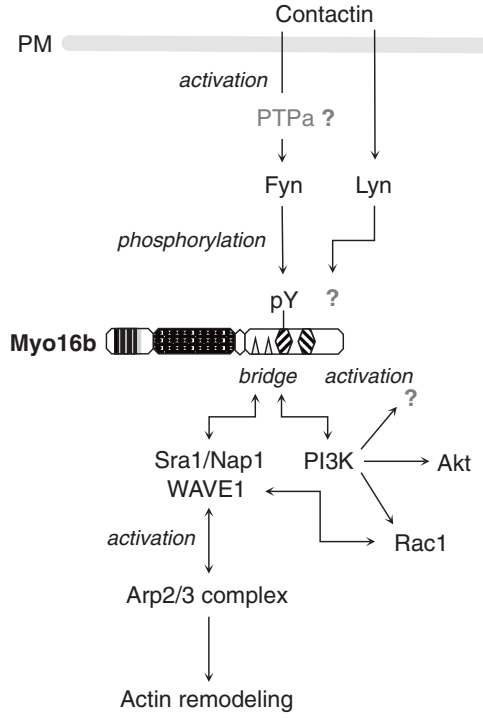

Fig. 18.2 Cytoplasmic interactions and functions of Myo16b. Myo16b is phosphorylated in a Contactin-dependent manner by Fyn at tyrosine residues at the conserved YxxM motif in the NHM. Contactin can also activate Lyn directly. Phosphorylated Myo16b interacts with the p85 subunit of PI3K via the NHM. The association results in the activation of the PI3K pathway, including downstream effectors of Akt and Rac1. Considering that PI3K is a central signaling node, its interaction with Myo16b may have effects on other downstream effectors. Myo16b also recruits the WAVE1 complex by binding to its Sra1 and Nap1 components. By the simultaneous interactions, Myo16b bridges the PI3K and WAVE1 complex and thereby may facilitate Rac1-dependent WAVE1 complex activation. WAVE1, in turn, activates the Arp2/3 complex machinery leading to actin cytoskeleton reorganization. *PM* plasma membrane, *pY* phosphotyrosine. Myo16b is depicted as in Fig. 18.1

18.6.2 Nuclear Function: Cell Cycle Regulation and Involvement in DNA Stress Response

Beyond its cytoplasmic functions, nuclear functioning of Myo16b is implicated in studies using cellular model systems including COS7, Rat2 and HeLa (Cameron et al. 2007, 2013; Yokoyama et al. 2011). The tail region (1322–1912) of EGFP-Myo16b was found to colocalize with

Table 18.3 Interacting partners of Myo16b

Partner	Interacting region	Method	Potential functional significance	References
Actin	Motor	Cosedimentation (rat brain P8)	Direct or indirect ATP dependent binding	Patel et al. (2001)
Fyn	NHM	Phosphorylation screening	Tyrosine-phosphorylation	Yokoyama et al. (2011)
PI3K	NHM	Co-IP (HEK293H, mouse brain P1)	Signaling to the actin cytoskeleton	Yokoyama et al. (2011)
WAVE1-Sra1	WIR	Co-IP (HEK293H, mouse brain P1)	Signaling to the actin cytoskeleton Arp2/3 complex activity	Yokoyama et al. (2011)
WAVE1-Nap1	WIR	Co-IP (HEK293H, mouse brain P1)	Signaling to the actin cytoskeleton Arp2/3 complex activity	Yokoyama et al. (2011)
GRAF	(NA)	Co-IP (HEK293H)	Membrane curvature	Yokoyama et al. (2011)
ACOT9	(NA)	Co-IP (HEK293H)	Membrane composition	Yokoyama et al. (2011)
PCNA	Myo16Tail	Colocalization, co-IP	DNA replication, repair, cell cycle control, chromatin remodeling	Cameron et al. (2007)
Cyclin A	Myo16Tail	Colocalization	Cell cycle regulation	Cameron et al. (2007)
PP1c α, γ	Myo16Ank	Co-IP (rat cerebellum P10)	Targeted dephosphorylation in protein phosphatase complex	Patel et al. (2001)
PP1c α, δ	Myo16Ank	SPR (recombinant proteins)	Targeted dephosphorylation in protein phosphatase complex	Kengyel et al. (2015)
KIRREL3	(NA)	Y2H, co-IP (HEK293H), IF colocalization (rat PNC)	Synaptic cell-adhesion	Liu et al. (2013)
Neurexin 1α	(NA)	Y2H, co-IP	Synaptic organization	Nakayama (2002)

PI3K phosphoinositide 3-kinase, *NHM* NYAP homology motif, *WIR* WAVE1 interacting region, *GRAF* GTPase regulator associated with focal adhesion kinase, *ACOT9* Acyl-CoA thioesterase, *PCNA* proliferating cell nuclear antigen, *PP1c* protein phosphatase catalytic subunit, *KIRREL* Kin of IRRE-like protein 3, *P8* postnatal day 8, *Co-IP* co-immunoprecipitation, *Y2H* yeast-two-hybrid screen, *IF* immunofluorescence, *SPR* surface plasmon resonance, *PNC* primary neuronal cell, *NA* not applicable

nuclear actin and profilin-associated structures in transiently-transfected COS7 cells (Cameron et al. 2007). The functional consequence and the nature (manifested through direct or indirect binding) of this coincidental localization is unknown. In respect to this, the proline-rich C-terminal tail of Myo16b can serve as a potential profilin-interacting segment. However, no direct interaction between recombinantly produced Myo16Tail and profilin 1 isoform was found in steady-state anisotropy measurements (Kengyel et al. 2017).

The level of nuclear Myo16b is regulated in a cell cycle stage dependent fashion. Both Myo16b mRNA and protein expression levels increase in late G1 and peak in S phase followed by a decline at the onset of M phase in Rat2 cells. During mitosis, in prophase, Myo16b shows a predominant localization at the non-chromosomal nuclear territory, while from metaphase to telophase it distributes throughout the cytoplasm (Cameron et al. 2007, 2013). The stability of Myo16b is sensitive to inhibitors of the 26S proteasome suggesting a possible degradation pathway (Cameron et al. 2013). As a functional consequence of its cell cycle dependent level, Myo16b negatively affects cell cycle progression. Transient overexpression of Myo16b delays progression through the S phase. In contrast, depletion of Myo16 by shRNAi leads to an increased fraction of cells in the G2/M phases (Cameron et al. 2007, 2013). Inducers of DNA damage that impair replication fork progression (hydroxyurea, aphidicolin, UV irradiation and various chemical inducers) downregulate Myo16b

expression and induce its cytoplasmic accumulation (Cameron et al. 2013). The replication stress induced alterations in Myo16b level and distribution were found to be reversible.

The nuclear localization of transiently transfected EGFP-Myo16Tail and endogenous Myo16b in COS7 cells is coincidental to proliferating cell nuclear antigen (PCNA) and cyclin A when examined by immunofluorescence microscopy (Table 18.3), albeit only a partial accumulation of PCNA and cyclin A was detected in the detergent-resistant fraction of the core nuclear matrix enriched in EGFP-Myo16Tail. Moreover, Myo16Tail seems to be essential for the nuclear appearance of PCNA, as in the case in which Myo16 exhibited predominant cytoplasmic localization, PCNA was absent from the nucleus (Cameron et al. 2007). Altogether, these results indicate that Myo16b can be involved in the proper order and direction of cell cycle progression.

18.6.3 Interaction with PP1c Subunits

The N-terminal extension of Myo16 (Myo16Ank) containing the MyPhoNE element, the KVxF consensus motif, eight ankyrin repeats and a PKC phosphorylation site, shows ~50% sequence similarity with the target/regulatory subunit (MYPT1) of myosin phosphatase (Kengyel et al. 2015). MYPT1 binds the protein phosphatase type 1 catalytic subunit (PP1c) through its N-terminal region. The binding enhances the dephosphorylation activity of the catalytic subunit towards the specific target, which is the myosin regulatory light chain (RLC). Consistently with the predicted N-terminal sequence similarity, *in vivo* co-immunoprecipitation in extracts prepared from postnatal rat cerebellum has shown that Myo16 associates with the catalytic subunits PP1cα and PP1cγ (Patel et al. 2001). Corroborating this, *in vitro* surface plasmon resonance experiments have shown that the recombinant fragment of Myo16Ank binds strongly with submicromolar affinity to PP1cα and also to PP1cδ (Table 18.3). Despite the similarity to MYPT1 and the affinity to PP1c subunits, the binding of Myo16Ank to PP1c does not enhance the dephosphorylation of the myosin RLC, but rather the phosphatase activity of the PP1c subunits markedly decreases in the presence of Myo16Ank. This suggests that Myo16Ank competes for the RLC binding site on PP1c (Kengyel et al. 2015).

PP1c has been described both in the functioning of the actin cytoskeleton as well as in nuclear processes, including gene transcription and cell cycle regulation (Rebelo et al. 2015), in which Myo16b likely plays a role. There is no evidence yet as to whether Myo16b may function as a regulatory subunit of PP1c, thus participating in selective dephosphorylation. PP1c is abundantly found in the nucleus; however, it lacks any nuclear localization sequence. Therefore, a potential role for Myo16b was thought to be the transportation of the PP1c subunits into the nucleus during interphase (Cameron et al. 2007).

Additionally, PP1c localizes to dendritic spines and is involved in the control of synaptic plasticity and memory formation. Distinctly, PP1c activation positively correlates with long-term depression (Gao et al. 2018). These underline the importance of the interaction between Myo16b and PP1c in the proper operation of the nervous system.

18.7 The Role of Myosin XVI in the Background of Human Diseases

Taking into consideration that Myo16 is expressed mostly in neural tissues and in the largest amount during brain development, Myo16 is likely to participate in the normal functioning of the brain. Recently, several human neurological disorders were associated to the genetic locus within or adjacent to *MYO16*.

18.7.1 Schizophrenia

Schizophrenia is caused by multiple genetic and environmental factors, and several unconventional myosins have thus far been associated with

schizophrenia. These include Myo5b, Myo18b and/or Myo9b, which are often associated with other neuropsychiatric disorders (Chen et al. 2013; Huang et al. 2010; Jungerius et al. 2008).

The fine mapping of chromosome 13q32–34 revealed a significant association between single nuclear polymorphism (SNP) within the Myo16 encoding region in schizophrenia patients. Three of the four SNPs associated with this disease were located within intron 3 of the *MYO16* gene (Rodriguez-Murillo et al. 2014). The main SNP (rs9583277) is a potential trans-acting expression activated trait locus for MAP3K13, a protein kinase which can phosphorylate the protein kinase MAP2K7, which has been recently implicated in schizophrenia (Winchester et al. 2012). The effect of these SNPs on the function of Myo16 remains as of yet, unknown.

Expression analysis in the frontal cortex revealed an increased level of Myo16 expression among schizophrenia patients compared with a control patient group suggesting that variations in the *MYO16* gene may contribute to the genetic liability to schizophrenia (Rodriguez-Murillo et al. 2014).

18.7.2 Autism

Autism spectrum disorder (ASD) refers to a group of neurodevelopmental diseases characterized by impaired social behavior and communication skills. ASD has multiple causes with both genetic and environmental factors playing a role; however, studies suggest it originates from a disorder in the early development of the neural system. Several genes have thus far been linked to autism (Inui et al. 2017).

In a recent study, 24 SNPs were identified in association with ASD, several of them were found on chromosome 13q33.3, between *MYO16* and *IRS2* (insulin receptor substrate) genes but only in families in which only males were affected. None of these SNPs associated with ASD in families in which both males and females were affected (Chang et al. 2013).

It was also shown using yeast-two-hybrid screening that Myo16 interacts with neurexin 1-α (Nakayama 2002), a pre-synaptic membrane adhesion protein, which plays a key role in complex with neuroligin in synaptogenesis, the process initiated prior to birth and continuing into adulthood, which has an important role in the cognitive process. The neurexin-neuroligin complex facilitates axo-dendritic contact and stabilizes synapses, and malfunction of these proteins are believed to be associated with autism (Patel et al. 2015).

Myo16 interacts with the Ig-like extracellular domain of the synaptic adhesion protein Kin of IRRE-like protein 3 (KIRREL3) in yeast-two-hybrid screens, and the interaction was confirmed with co-immunoprecipitation and colocalization studies (Table 18.3) (Liu et al. 2013). KIRREL3, a synaptic molecule of the immunoglobulin superfamily, may play a potential role in neuronal development as disruption leads to intellectual disability (Bhalla et al. 2008).

In various studies, genetic analysis of at least five patients with neurodevelopmental disorders showed a deletion of 6 to 25 genes on chromosome 13 in the region including *MYO16* (Liu et al. 2013). These patients express different neurological symptoms including developmental delay, autism and intellectual disability. Despite the several associations, animal tests have not proven the connection between impaired Myo16 function and ASD yet. The behaviour of Myo16 KO mice shows no abnormalities in motor- and social interaction-tests, which are typically altered in the mouse model of ASD (Roesler et al. 2019).

18.7.3 Bipolar Disorder

Bipolar II (BP-II) disorder is defined by mood swings between depressive and hypomanic episodes. The hereditary appearance of bipolar disorder suggests a genetic etiology, however the genetic etiology is complex and multifactorial (Barnett and Smoller 2009).

In a recent genome-wide association study, several SNPs were identified in the background of the II-type bipolar disorder. Two of the reported seven replicated susceptible loci of BP-II are

found in *MYO16* (Kao et al. 2016). The involvement of Myo16 in bipolar disorder is not surprising given its connection with schizophrenia since the two neuropsychiatric disorders often share a common pathophysiology (Konopaske et al. 2014).

18.8 Summary

Since the vertebrate-specific class XVI myosin was discovered, several *in vitro* and *in vivo* studies have been performed to enlighten the biochemical nature and physiological role of this unusual motor protein. The peak expression of myosin XVI in neural tissues in the late embryonic-early postnatal time period suggests it is central to neuronal development. This hypothesis is strengthened by the genetic analysis of patients afflicted with neuropsychiatric disorders, in which the deletion of *MYO16* gene, nuclear polymorphism in or adjacent to the *MYO16* gene, or altered expression pattern of Myo16 protein were found. Since these disorders are usually multi-etiological, the impaired expression or functionality of myosin XVI may not be the sole cause, however, it can exacerbate the pathological status.

Myosin XVI appears not to be a vital protein, yet its deficiency leads to severe conditions. The cerebellar structure of Myo16 KO mice did not reveal gross abnormalities (Roesler et al. 2019). KO mice in which all three NYAP-proteins including Myo16b were missing appear healthy and fertile; however, they show a clear reduction in brain size and weight especially in the cortex and striatum, which was the possible consequence of neurite hypotrophy (Yokoyama et al. 2011). Additionally, in patients suffering from ASD, in which (among others) the deletion of *MYO16* gene was found, different neurological symptoms were present with developmental delay and intellectual disability (Liu et al. 2013).

The physiological role of myosin XVI is still not well understood, although its cellular function appears to be quite diverse, possessing distinct interactions in the cytoplasm and in the nucleus. One concern is that the majority of the experiments were performed in fibroblast-derived cell cultures (COS7, Rat2). Nonetheless, the evidence supports the idea that myosin XVI plays a key role in cell cycle regulation, actin cytoskeleton remodeling through the PI3K signal transduction pathway, and dephosphorylation processes. This functional diversity is connected to the unique structural elements of myosin XVI, such as the ankyrin repeat domain (Myo16Ank) and the disordered tail domain (Myo16Tail).

Myo16Ank can bind to different PP1c isoforms and thus may participate either in the targeted dephosphorylation of proteins not yet identified or in the transport of PP1c subunits to the nucleus. The long and likely disordered Myo16Tail offers a large binding surface in support of several protein complexes, which is regulated through the phosphorylation of the NHM motif. Based on the sequence, myosin XVI may have a reduced ATPase activity implying a potential stationary role in which the tail domain may serve as an interacting interface, by corralling the PI3K and the WAVE1-complex in close proximity (Cameron et al. 2007; Yokoyama et al. 2011).

Acknowledgement The present scientific contribution is dedicated to the 650th anniversary of the foundation of the University of Pécs, Hungary. This work was supported by OTKA grant, K 12794 "Molecular Mechanisms Underlying the Function of Myosin 16b" from the Hungarian Scientific Research Fund. The work was supported by EFOP-3.6.2-16-2017-00006. The authors thank Jon E. Marquette for proofreading the manuscript.

References

Barnett JH, Smoller JW (2009) The genetics of bipolar disorder. Neuroscience 164:331–343. https://doi.org/10.1016/j.neuroscience.2009.03.080

Bement WM, Mooseker MS (1995) TEDS rule: A molecular rationale for differential regulation of myosins by phosphorylation of the heavy chain head. Cell Motil Cytoskeleton 31:87–92. https://doi.org/10.1002/cm.970310202

Bement WM, Hasson T, Wirth JA, Cheney RE, Mooseker MS (1994) Identification and overlapping expression of multiple unconventional myosin genes in vertebrate cell types. Proc Natl Acad Sci USA 91:6549–6553

Berg JS, Powell BC, Cheney RE (2001) A millennial myosin census. Mol Biol Cell 12:780–794

Bhalla K, Luo Y, Buchan T, Beachem MA, Guzauskas GF, Ladd S, Bratcher SJ, Schroer RJ, Balsamo J, Dupont BR, Lilien J, Srivastava AK (2008) Alterations in CDH15 and KIRREL3 in patients with mild to severe intellectual disability. Am J Hum Genet 83:703–713. https://doi.org/10.1016/j.ajhg.2008.10.020

Cameron RS, Liu C, Mixon AS, Pihkala JPS, Rebecca J, Cameron PL, Rahn RJ, Cameron PL (2007) Myosin16b: the COOH-tail region directs localization to the nucleus and overexpression delays S-phase progression. Cell Motil Cytoskeleton 64:19–48. https://doi.org/10.1002/cm.20162

Cameron RS, Liu C, Pihkala JPS (2013) Myosin 16 levels fluctuate during the cell cycle and are downregulated in response to DNA replication stress. Cytoskeleton 70:328–348. https://doi.org/10.1002/cm.21109

Chang S-CC, Pauls DL, Lange C, Sasanfar R, Santangelo SL (2013) Sex-specific association of a common variant of the XG gene with autism spectrum disorders. Am J Med Genet B Neuropsychiatr Genet 162:742–750. https://doi.org/10.1002/ajmg.b.32165

Chen Y, Tian L, Zhang F, Liu C, Lu T, Ruan Y, Li K, Lv L, Zhang D, Yue W (2013) Myosin Vb gene is associated with schizophrenia in Chinese Han population. Psychiatry Res 207:13–18. https://doi.org/10.1016/j.psychres.2013.02.026

Dosztányi Z, Csizmok V, Tompa P, Simon I (2005) IUPred: web server for the prediction of intrinsically unstructured regions of proteins based on estimated energy content. Bioinformatics 21:3433–3434. https://doi.org/10.1093/bioinformatics/bti541

Fukuda M, Asano S, Nakamura T, Adachi M, Yoshida M, Yanagida M, Nishida E (1997) CRM1 is responsible for intracellular transport mediated by the nuclear export signal. Nature 390:308–311. https://doi.org/10.1038/36894

Gao J, Hu X-D, Yang H, Xia H (2018) Distinct roles of protein phosphatase 1 bound on neurabin and spinophilin and its regulation in AMPA receptor trafficking and LTD induction. Mol Neurobiol 55:7179–7186. https://doi.org/10.1007/s12035-018-0886-2

Geeves MA, Holmes KC (1999) Structural mechanism of muscle contraction. Annu Rev Biochem 68:687–728. https://doi.org/10.1146/annurev.biochem.68.1.687

Gross C, Bassell GJ (2014) Neuron-specific regulation of class I PI3K catalytic subunits and their dysfunction in brain disorders. Front Mol Neurosci 7(1–8). https://doi.org/10.3389/fnmol.2014.00012

Hartshorne DJ, Ito M, Erdodi F, Erdödi F, Erdodi F (1998) Myosin light chain phosphatase: subunit composition, interactions and regulation. J Muscle Res Cell Motil 19:325–341

Holt MR, Koffer A (2001) Cell motility: proline-rich proteins promote protrusions. Trends Cell Biol 11:38–46

Huang J, Perlis RH, Lee PH, Rush AJ, Fava M, Sachs GS, Lieberman J, Hamilton SP, Sullivan P, Sklar P, Purcell S, Smoller JW (2010) Cross-disorder genome-wide analysis of schizophrenia, bipolar disorder, and depression. Am J Psychiatry 167:1254–1263. https://doi.org/10.1016/j.psychres.2013.02.026

Inui T, Kumagaya S, Myowa-yamakoshi M (2017) Neurodevelopmental hypothesis about the etiology of autism spectrum disorders. Front Hum Neurosci 11:1–19. https://doi.org/10.3389/fnhum.2017.00354

Jungerius BJ, Bakker SC, Monsuur AJ, Sinke RJ, Kahn RS, Wijmenga C (2008) Is MYO9B the missing link between schizophrenia and celiac disease? Am J Med Genet B Neuropsychiatr Genet 147B:351–355. https://doi.org/10.1002/ajmg.b.30605

Kao C-F, Chen H-W, Chen H-C, Yang J-H, Huang M-C, Chiu Y-H, Lin S-K, Lee Y-C, Liu C-M, Chuang L-C, Chen C-H, Wu J-Y, Lu R-B, Kuo P-H (2016) Identification of susceptible loci and enriched pathways for bipolar II disorder using genome-wide association studies. Int J Neuropsychopharmacol 19:pyw064. https://doi.org/10.1093/ijnp/pyw064

Kasahara K, Watanabe K, Kozutsumi Y, Oohira A, Yamamoto T, Sanai Y (2002) Association of GPI-anchored protein TAG-1 with src-family kinase Lyn in lipid rafts of cerebellar granule cells. Neurochem Res 27:823–829

Kengyel A, Bécsi B, Kónya Z, Sellers JR, Erdődi F, Nyitrai M (2015) Ankyrin domain of myosin 16 influences motor function and decreases protein phosphatase catalytic activity. Eur Biophys J 44:207–218. https://doi.org/10.1007/s00249-015-1015-z

Kengyel A, Telek E, Konya Z, Becsi B, Erdodi F, Nyitrai M (2017) Interactions and functions of myosin 16 domains. Biophys J 112:267a

Konopaske GT, Lange N, Coyle JT, Benes FM (2014) Prefrontal cortical dendritic spine pathology in schizophrenia and bipolar disorder. JAMA Psychiat 71:1323. https://doi.org/10.1001/jamapsychiatry.2014.1582

Larkin MA, Blackshields G, Brown NP, Chenna R, McGettigan PA, McWilliam H, Valentin F, Wallace IM, Wilm A, Lopez R, Thompson JD, Gibson TJ, Higgins DG (2007) Clustal W and Clustal X version 2.0. Bioinformatics 23:2947–2948. https://doi.org/10.1093/bioinformatics/btm404

Li J, Mahajan A, Tsai MD (2006) Ankyrin repeat: a unique motif mediating protein-protein interactions. Biochemistry 45:15168–15178

Liu YF, Sowell SM, Luo Y, Chaubey A, Cameron RS, Kim H-G, Srivastava AK (2013) Autism and intellectual disability-associated KIRREL3 interacts with neuronal proteins MAP1B and MYO16 with potential roles in neurodevelopment. PLoS One 84:487–492. https://doi.org/10.1371/journal.pone.0123106

Mermall V (1998) Unconventional myosins in cell movement, membrane traffic, and signal transduction. Science 279:527–533. https://doi.org/10.1126/science.279.5350.527

Milton DL, Schneck AN, Ziech DA, Ba M, Facemyer KC, Halayko AJ, Baker JE, Gerthoffer WT, Cremo CR (2011) Direct evidence for functional smooth muscle myosin II in the 10S self-inhibited monomeric conformation in airway smooth muscle cells. Proc Natl Acad Sci USA 108:1421–1426. https://doi.org/10.1073/pnas.1011784108

Nagase T, Ishikawa K, Suyama M, Kikuno R, Hirosawa M, Miyajima N, Tanaka A, Kotani H, Nomura N, Ohara O (1998) Prediction of the coding sequences of unidentified human genes. XII. The complete sequences of 100 new cDNA clones from brain which code for large proteins in vitro. DNA Res 5:355–364

Nakayama M (2002) Protein-protein interactions between large proteins: two-hybrid screening using a functionally classified library composed of long cDNAs. Genome Res 12:1773–1784. https://doi.org/10.1101/gr.406902

Odronitz F, Kollmar M (2007) Drawing the tree of eukaryotic life based on the analysis of 2,269 manually annotated myosins from 328 species. Genome Biol 8:R196. https://doi.org/10.1186/gb-2007-8-9-r196

Onishi H, Ohki T, Mochizuki N, Morales MF (2002) Early stages of energy transduction by myosin: roles of Arg in Switch I, of Glu in Switch II, and of the salt-bridge between them. Proc Natl Acad Sci USA 99(24):15339–15344

Patel KG, Liu C, Cameron PL, Cameron RS (2001) Myr 8, A novel unconventional myosin expressed during brain development associates with the protein phosphatase catalytic subunits 1α and 1γ1. J Neurosci 21:7954–7968. https://doi.org/10.1523/JNEUROSCI.21-20-07954.2001

Patel S, Roncaglia P, Lovering RC (2015) Using gene ontology to describe the role of the neurexin-neuroligin-SHANK complex in human, mouse and rat and its relevance to autism using gene ontology to describe the role of the neurexin-neuroligin-SHANK complex in human, mouse and rat and its relev. BMC Bioinforma. https://doi.org/10.1186/s12859-015-0622-0

Petrella EC, Machesky LM, Kaiser DA, Pollard TD (1996) Structural requirements and thermodynamics of the interaction of proline peptides with profilin. Biochemistry 35:16535–16543. https://doi.org/10.1021/bi961498d

Poupon V, Bègue B, Gagnon J, Dautry-Varsat A, Cerf-Bensussan N, Benmerah A (1999) Molecular cloning and characterization of MT-ACT48, a novel mitochondrial acyl-CoA thioesterase. J Biol Chem 274:19188–19194

Rebelo S, Santos M, Martins F, da Cruz e Silva EF, da Cruz e Silva OAB (2015) Protein phosphatase 1 is a key player in nuclear events. Cell Signal 27:2589–2598. https://doi.org/10.1016/j.cellsig.2015.08.007

Rodriguez-Murillo L, Xu B, Roos JL, Abecasis GR, Gogos J a, Karayiorgou M (2014) Fine mapping on chromosome 13q32-34 and brain expression analysis implicates MYO16 in schizophrenia. Neuropsychopharmacology 39:934–943. https://doi.org/10.1038/npp.2013.293

Roesler MK, Lombino FL, Freitag S, Schweizer M, Hermans-Borgmeyer I, Schwarz JR, Kneussel M, Wagner W (2019) Myosin XVI regulates actin cytoskeleton dynamics in dendritic spines of Purkinje cells and affects presynaptic organization. Front Cell Neurosci 13

Sánchez-Alegría K, Flores-León M, Avila-Muñoz E, Rodríguez-Corona N, Arias C (2018) PI3K signaling in neurons: a central node for the control of multiple functions. Int J Mol Sci 19. https://doi.org/10.3390/ijms19123725

Schliwa M, Woehlke G (2003) Molecular motors. Nature 422:759–765

Sebé-Pedrós A, Grau-Bové X, Richards TA, Ruiz-Trillo I (2014) Evolution and classification of myosins, a paneukaryotic whole genome approach. Genome Biol Evol 6:290–305. https://doi.org/10.1093/gbe/evu013

Sedgwick SG, Smerdon SJ (1999) The ankyrin repeat: a diversity of interactions on a common structural framework. Trends Biochem Sci 24:311–316

Semplea BD, Blomgrenb K, Gimlina K, Ferrieroe DM, Noble-Haeusslein LJ (2013) Brain development in rodents and humans: identifying benchmarks of maturation and vulnerability to injury across species. Prog Neurobiol 0:1–16. https://doi.org/10.1016/j.pneurobio.2013.04.001.Brain

Shimada T, Sasaki N, Ohkura R, Sutoh K (1997) Alanine scanning mutagenesis of the switch I region in the ATPase site of dictyostelium discoideum Myosin II. Biochemistry 36:14037–14043. https://doi.org/10.1021/bi971837i

Sittaramane V, Chandrasekhar A (2008) Expression of unconventional myosin genes during neuronal development in zebrafish. Gene Expr Patterns 8:161–170. https://doi.org/10.1016/j.gep.2007.10.010

Taylor JM, Macklem MM, Parsons JT (1999) Cytoskeletal changes induced by GRAF, the GTPase regulator associated with focal adhesion kinase, are mediated by Rho. J Cell Sci 112(Pt 2):231–242

Umeki N, Jung HS, Sakai T, Sato O, Ikebe R, Ikebe M (2011) Phospholipid-dependent regulation of the motor activity of myosin X. Nat Struct Mol Biol 18:783–788. https://doi.org/10.1038/nsmb.2065

Wang F, Thirumurugan K, Stafford WF, Hammer JA, Knight PJ, Sellers JR (2004) Regulated conformation of myosin V. J Biol Chem 279:2333–2336. https://doi.org/10.1074/jbc.C300488200

Winchester CL, Ohzeki H, Vouyiouklis DA, Thompson R, Penninger JM, Yamagami K, Norrie JD, Hunter R, Pratt JA, Morris BJ (2012) Converging evidence that sequence variations in the novel candidate gene MAP2K7 (MKK7) are functionally associated with schizophrenia. Hum Mol Genet 21:4910–4921. https://doi.org/10.1093/hmg/dds331

Yang Y, Baboolal TG, Siththanandan V, Chen M, Walker ML, Knight PJ, Peckham M, Sellers JR (2009) A FERM domain autoregulates Drosophila myosin 7a activity. Proc Natl Acad Sci 106:4189–4194. https://doi.org/10.1073/pnas.0808682106

Yokoyama K, Tezuka T, Kotani M, Nakazawa T, Hoshina N, Shimoda Y, Kakuta S, Sudo K, Watanabe K,

Iwakura Y, Yamamoto T (2011) NYAP: a phosphoprotein family that links PI3K to WAVE1 signalling in neurons. EMBO J 30:4739–4754. https://doi.org/10.1038/emboj.2011.348

Zang X, Mo X, Fu Z, Wang L, Zhou K, Yu D, Huang H (2016) Brain development and Akt signaling: the crossroads of signaling pathway and neurodevelopmental diseases. J Mol Neurosci 61:379–384. https://doi.org/10.1007/s12031-016-0872-y

Zeng L, D'Alessandri L, Kalousek MB, Vaughan L, Pallen CJ (1999) Protein tyrosine phosphatase α (Ptpα) and contactin form a novel neuronal receptor complex linked to the intracellular tyrosine kinase Fyn. J Cell Biol 147:707–714. https://doi.org/10.1083/jcb.147.4.707

Myosin XVIII

19

Manuel H. Taft and Sharissa L. Latham

Abstract

Class XVIII myosins represent a branch of the myosin family tree characterized by the presence of large N- and C-terminal extensions flanking a generic myosin core. These myosins display the highest sequence similarity to conventional class II muscle myosins and are compatible with but not restricted to myosin-2 contractile structures. Instead, they fulfill their functions at diverse localities, such as lamella, actomyosin bundles, the Golgi apparatus, focal adhesions, the cell membrane, and within sarcomeres. Sequence comparison of active-site residues and biochemical data available thus far indicate that this myosin class lacks active ATPase-driven motor activity, suggesting that its members function as structural myosins. An emerging body of evidence indicates that this structural capability is essential for the organization, maturation, and regulation of the contractile machinery in both muscle and nonmuscle cells. This is supported by the clear association of myosin-18A (Myo18A) and myosin-18B (Myo18B) dysregulation with diseases such as cancer and various myopathies.

Keywords

Myosin-18 · Golgi · GOLPH3 · Transport · Surfactant protein A receptor · Cancer · Tumor suppressor · Sarcomere · Myofibrillogenesis

19.1 Introduction

The class XVIII myosin family encompasses two distinct myosins known as Myo18A and Myo18B, which are synthesized from two different genes. These are amongst the most recently identified myosins with the mouse Myo18A gene discovered as recently as the year 2000 through a gene expression screen of bone marrow stromal cells (Furusawa et al. 2000). Originally named MysPDZ due to the presence of a PDZ domain within its unique ~400 amino acid N-terminal extension, this protein was later renamed Myo18A following the identification of other PDZ-myosins in ver-

M. H. Taft (✉)
Institute for Biophysical Chemistry, Hannover Medical School, Hannover, Germany
e-mail: Taft.Manuel@mh-hannover.de

S. L. Latham
The Kinghorn Cancer Centre, Garvan Institute of Medical Research, Darlinghurst, NSW, Australia

St Vincent's Clinical School, Faculty of Medicine, UNSW Sydney, Darlinghurst, NSW, Australia
e-mail: s.latham@garvan.org.au

L. M. Coluccio (ed.), *Myosins*, Advances in Experimental Medicine and Biology 1239,
https://doi.org/10.1007/978-3-030-38062-5_19

tebrates and *Drosophila*. Together, these myosins constituted the new myosin XVIII class (Yamashita et al. 2000; Berg et al. 2001). The second family member, Myo18B, was first reported in 2001 following partial annotation of the human *MYO18B* gene (Berg et al. 2001). Phylogenetic analysis suggests that *MYO18B*, which is exclusively found in vertebrates, is likely derived from duplication of the *MYO18A* gene, which is found in both invertebrates and vertebrates (Salamon et al. 2003). At the protein level, Myo18A and Myo18B share ~40% identity and are distinguished from other classes by their large N-terminal and C-terminal extensions, which flank either side of a generic myosin core structure. While the literature demonstrates unique roles for these two proteins at specific subcellular localities, it remains unclear whether they have distinct or overlapping functions at sites where they both localize, such as stress fibers in nonmuscle cells and sarcomeric structures in striated muscle.

19.2 Myosin-18A

19.2.1 *MYO18A* Gene Architecture and RNA Expression Across Cell Lines and Tissues

Myo18A, located on mouse chromosome 11 and arm q11.2 of chromosome 17 in humans (*MYO18A*), was first discovered in 2000 in a gene expression screen of bone marrow stromal cells, where it was found to be upregulated in cell lines with increased hematopoietic supportive ability (Furusawa et al. 2000). In mouse, the ORF encodes for two splice isoforms that produce long (Myo18Aα) and short (Myo18Aβ) versions of the protein, which consist of 2035 amino acids (230 kDa) and 1719 amino acids (196 kDa), respectively. The human homologues display similar dimensions with Myo18Aα comprising 2054 amino acids (~233 kDa) and Myo18Aβ comprising 1723 amino acids (~196 kDa) (Fig. 19.1). The central part of Myo18Aα (residues 405–1972) exhibits homology to generic

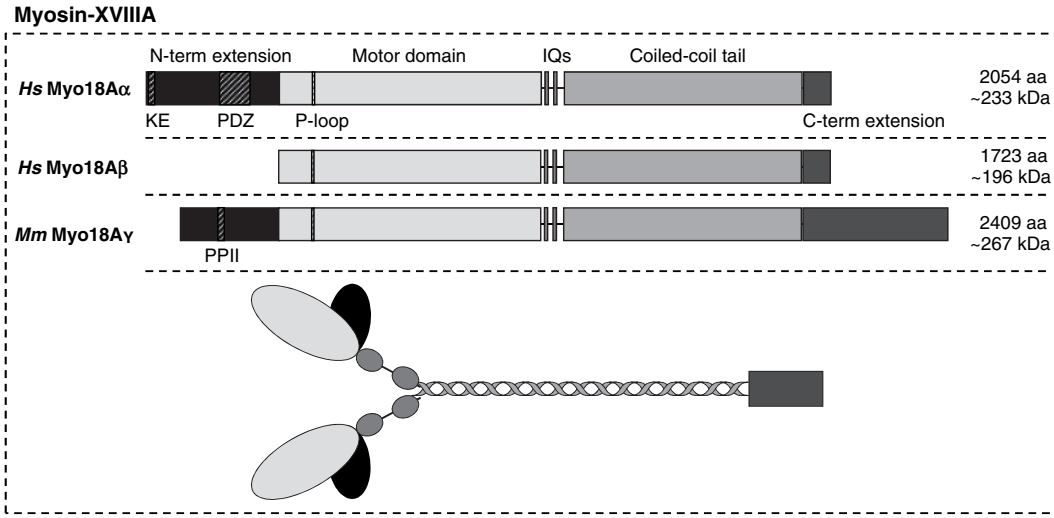

Fig. 19.1 Schematic representation of the domain structure of human (*Hs, Homo sapiens*) and mouse (*Mm, Mus musculus*) Myosin-18A splice isoforms. These construct diagrams illustrate the large N-terminal and C-terminal extensions characteristic of class XVIII myosins, which flank the generic myosin core containing a motor domain, neck region, and coiled-coil tail domain. Specifically for Myo18A, splice isoforms are distinguished by the presence of a KE-rich region, PDZ domain, or PPII (polyproline II helix) domain within the N-terminal extension. Like myosin-2 motors, this protein forms homotypic dimers via the tail domain. The precise structure and organization of the N-terminal and C-terminal extensions remain to be resolved

myosins and displays the highest similarity with conventional muscle myosin-2, as both have extended coiled-coil regions in the C-terminal half of the protein. Further examination of the domain structure and SMART-based sequence analysis reveals the existence of a region rich in lysine and glutamate residues (KE motif) and a PDZ domain inside the long N-terminal extension (Fig. 19.1). Whilst a few other myosin classes described thus far also contain additional domains at the N- or C-terminus (e.g., myosin class III, IX, XV, and XVI (Odronitz and Kollmar 2007)), the presence of the PDZ domain is unique and prompted Furusawa et al. to give this novel myosin the name MysPDZ, which denoted "Myosin containing a PDZ domain" (Furusawa et al. 2000). An independent study also identified Myo18A in a human peripheral blood cDNA library during a screen for novel interaction partners of the cytosolic tyrosine kinase JAK3. Accordingly, this protein was designated as MAJN (molecule associated with Jak3 N-terminal) (Ji et al. 2000).

When mRNA expression levels were examined, ubiquitous expression of Myo18A was detected in all tissues and cell lines tested (Furusawa et al. 2000). However, a longer transcript with a size of 10 kb was enriched in heart and skeletal muscle. The normal 7.5-kb Myo18Aα transcript was found in most tissues (brain, thymus, lung, liver, etc.) and a shorter transcript of 7 kb, later identified as Myo18Aβ, was observed in hematopoietic cell lines (Furusawa et al. 2000; Mori et al. 2003). The long transcript has not been explicitly studied further; however, the larger size and muscle expression profile indicate that it could in fact be the recently identified Myo18Aγ splice isoform (Horsthemke et al. 2019). In addition to these splice isoforms, which have been verified at both the RNA and protein levels, a short version of Myo18A has also been identified in a macrophage cell line, where it is tyrosine-phosphorylated after CSF-1 stimulation (Cross et al. 2004). Intriguingly, this protein had a molecular weight of only 110 kDa (p110 myosin 18A), and peptide analysis suggests that the protein boundaries span from the middle of the motor domain to the end of the coiled-coil region. The lack of evidence for an alternative translational start within the *Myo18A* mRNA suggests that this protein results from post-translational cleavage of one of the higher molecular mass isoforms.

19.2.2 Myo18A Biochemistry: Protein Domain Architecture and Functional Properties

Myo18A has a complex domain architecture that comprises a number of different elements with various functions. In the Myo18Aα splice isoform, the N-terminal extension has thus far been shown to contain two distinct functional regions: a KE motif (containing 11 lysine and 3 glutamate residues within a stretch of twenty amino acids) located at the far N-terminus and a PDZ domain that is found in the middle of the N-terminal extension (Fig. 19.1) (Furusawa et al. 2000). Myo18Aγ comprises a polyproline II helix (PPII) of yet unknown function in its N-terminal extension whereas Myo18Aβ completely lacks this domain. The molecular function of the Myo18Aα N-terminal extension has been investigated in two studies to date. Isogawa et al. utilized GFP-tagged deletion constructs of human Myo18A to characterize actin-binding properties in lysates of HeLa cells that overexpress the respective proteins (Isogawa et al. 2005). The N-terminal extension construct displayed a strong, ATP-independent interaction with actin in cosedimentation assays, and this result was validated with bacterially-expressed deletion constructs. Analysis of a selection of purified truncation and mutation constructs in these assays localized the actin-binding interface to the middle of the N-terminal extension, outside of the KE motif and PDZ domain. Through a series of cosedimentation affinity assays, it was shown that a recombinant human Myo18A protein construct spanning from the N-terminus to the start of the PDZ domain weakly interacted with actin (K_A of 6.5 μM), whilst a construct encompassing the whole N-terminal extension had a six-fold enhanced actin affinity with a K_A of 1 μM (Taft et al. 2013). Actin affinity is further enhanced five-fold by the direct binding to GOLPH3, a phosphoprotein of the Golgi membrane (cf. 19.2.3.). These data demonstrate that

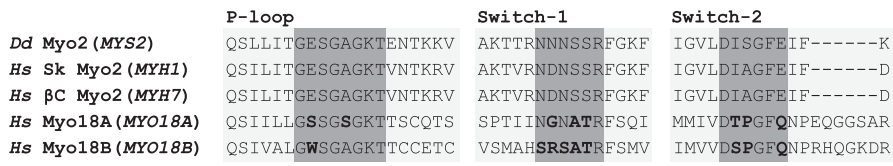

Fig. 19.2 Alignment of *Hs* Myosin-18A and *Hs* Myosin-18B P-loop, switch-1, and switch-2 sequences with *Dictyostelium discoideum* (*Dd*) myosin-2, *Hs* skeletal muscle myosin-2, and *Hs* β-cardiac muscle myosin-2. Conserved sequence motifs are defined in dark grey regions, while deviations in Myo18A and Myo18A are shown in bold

the N-terminal extension combines at least two functional modules that mediate actin binding, are dependent from one another, and can be regulated by binding of an interaction partner, GOLPH3.

The adjacent structural element in the domain architecture of Myo18A is its motor domain. A fundamental feature of the myosin family is the inherent ability of their motor domains to hydrolyze ATP and to convert the resulting energy into force and directed movement along actin filaments (Geeves et al. 2005; Bloemink and Geeves 2011). The basic structural elements in the motor domain known to be essential for the enzymatic activity of myosins are the P-loop, switch-1, and switch-2 (Preller and Manstein 2013; Geeves 2016). Sequence alignments with other myosin motor domains show that these three aforementioned motifs are modified in Myo18A (Fig. 19.2). Most strikingly, two highly conserved serine residues in switch-1, which usually coordinate the γ-phosphate of ATP and Mg^{2+} for efficient catalysis, are mutated to alanine and threonine. In addition, the salt bridge between an arginine in switch-1 and a glutamate in switch-2 cannot be formed due to a glutamate-to-glutamine exchange in Myo18A. As the salt bridge has been shown to be essential for ATPase activity and motor function of myosins (Onishi et al. 1998; Furch et al. 1999), the sequence variations found in Myo18A raise the question of whether this myosin can function as an active motor. To date, three studies have addressed this question, none of which could demonstrate motor function or ATPase activity for class XVIII myosins. The first study by Guzik-Lendrum et al. assessed the biochemical properties of the sole *Drosophila melanogaster* (*Dm*) class XVIII myosin (Myo18), which has the highest homology to mammalian Myo18A (Guzik-Lendrum et al. 2011). They purified motor domain constructs with and without the PDZ domain using the baculovirus/*Sf*9 insect cell system and found that neither of the constructs exhibits ATPase activity or can even bind ATP. Actin-binding affinity of the Myo18 motor domain was demonstrated and quantified with cosedimentation assays (K_D ~1 μM) and optical trap studies showed the existence of short-lived actin interactions. The functional properties of mouse Myo18A were subsequently studied by the same group with purified S1 constructs, which display weak ATP and ADP affinities (~80 and ~100 μM) (Guzik-Lendrum et al. 2013). Furthermore, the long (Myo18Aα) and short (Myo18Aβ) isoforms exhibit actin-binding affinities of ~5 and ~50 μM, and no regulation of the actin interaction by nucleotide binding or light chain phosphorylation was found. In line with the previous study, no ATPase activity or motor function was detected for mouse Myo18A, and negative-stain electron microscopy revealed no structural changes of the S1 conformation associated with changes in the nucleotide state (ATP, ADP, or rigor). The third study sought to understand the molecular function of human Myo18A and its interaction with nucleotides, actin, and GOLPH3 (Taft et al. 2013). Nucleotide and actin affinities of motor domain constructs produced with the baculovirus/*Sf*9 insect cell system were found to be 10–100 times higher for the human protein compared to its mouse homologue. In line with the mouse protein, human Myo18A does not exhibit ATPase activity. Intriguingly, in the ADP state, the human Myo18A motor domain displays the highest actin affinity and the most complete binding to actin. Negative-stain elec-

tron microscopy revealed the typical arrowhead pattern of myosin bound to actin. In contrast to generic myosins, the decoration was not only complete and well-ordered in the absence of nucleotide and in the presence of ADP but also in the presence of excess ATP.

The myosin motor domain adjoins to the light chain-binding domain, which binds the essential light chain (ELC) and regulatory light chain (RLC) of conventional class II muscle myosins. In the case of unconventional myosins, which contain one or more IQ motifs, this region mediates the interaction with calmodulin (CaM) or CaM-like light chains (Odronitz and Kollmar 2007). Initial examination of the Myo18A domain structure suggested the presence of one IQ motif following the motor domain (Furusawa et al. 2000; Mori et al. 2003). However, subsequent analysis proposed the existence of two IQ motifs based on comprehensive alignments of Myo18A sequences across subclasses and phyla with myosin-2 (Guzik-Lendrum et al. 2013). This was experimentally confirmed by the co-purification of S1 and HMM mouse Myo18A constructs along with both ELC and RLC. Whilst it had already previously been shown that overexpressed Myo18A binds to and co-purifies with RLC in COS7 cells (Tan et al. 2008), the ability of Myo18A to bind both ELC and RLC of the nonmuscle myosin-2 (NM2) system suggests a role for Myo18A in NM2-dependent cellular structures and processes.

The C-terminal end of the light chain-binding domain leads over to the "bend" motif (WPWW/WQWW/WPWM), which is followed by a highly conserved tryptophan residue located eight residues further, where the coiled-coil domain of class II myosins starts. According to sequence analyses, the coiled-coil domain in human Myo18A encompasses amino acids 1253-1966 (Fig. 19.1). This strongly suggests that the protein exists and functions inside cells as a dimer of two heavy chains, which has been confirmed for human and mouse Myo18A by chemical cross-linking of HMM constructs and by co-immunoprecipitation (Mori et al. 2005; Isogawa et al. 2005), and for mouse Myo18A HMM by negative-stain electron microscopy (Guzik-Lendrum et al. 2013). When purified untruncated mouse Myo18Aβ protein was subjected to electron microscopy, the formation of unusual short and condensed antiparallel dimers was observed (Billington et al. 2015). In addition, Myo18Aβ has been shown to co-assemble with NM2A to form mixed bipolar filaments, where its incorporation reduces the average filament length (from 310 to 220 nm).

So far, the C-terminal extension is the least-characterized domain of Myo18A. Extending from residue 1972 to the C-terminus, this domain of 83 amino acids is predicted not to form coiled-coil structures. It appears reasonable that this domain provides Myo18A with additional binding motifs for protein-protein interactions. In line with this, it has been shown that the C-terminal extension of Myo18A directly interacts with the C-terminal last 8 residues of the Rho GTPase activator βPIX (PAK-interacting exchange factor-β) (cf. 19.2.4) (Hsu et al. 2010). No additional direct binding partner of the C-terminal extension has been described yet.

19.2.3 The Role of Myo18A at the Golgi

The Golgi apparatus is a membranous system essential for the intracellular sorting and transport of proteins and is known to connect to both the microtubule and the actin cytoskeletons (reviewed in (Gurel et al. 2014)). The phospholipid phosphatidylinositol-4-phosphate (PI4P) is enriched in Golgi membranes and directly binds to a few proteins containing pleckstrin homology (PH) domains (Dowler et al. 2000; Levine and Munro 2002). An *in vitro* lipid-binding screen identified the Golgi phosphoprotein GOLPH3 as a direct binding partner for PI4P, which was subsequently shown to localize to the Golgi membrane (Dippold et al. 2009). It was observed that latrunculin B-induced actin depolymerization and GOLPH3 knockdown both result in rapid Golgi compaction. In search of an interaction partner that can mediate the connection between GOLPH3 and the actin cytoskeleton, immunoprecipitation studies using HeLa cell

lysates and mass spectrometry identified a ~250-kDa putative interaction partner to be Myo18A. Whilst a direct interaction between Myo18A and GOLPH3 was validated by reciprocal co-immunoprecipitation of both proteins from cell lysates by specific antibodies, other Golgi-localized myosins (NM2B, myosin-6) were shown not to interact with GOLPH3 (Dippold et al. 2009). Further mapping the interaction region, pulldown experiments with bacterially-expressed domains of Myo18A showed direct binding between GOLPH3 and the N-terminal extension and motor/IQ domains of Myo18A. As both domains interact with GOLPH3 independently of each other, bipartite binding can be assumed. It should be noted that the expression of myosin motor domains in bacteria does not produce functional protein as a certain setup of chaperones is needed for proper folding (McNally et al. 1991). In cellular studies utilizing siRNA-mediated knockdown of GOLPH3, Myo18A localization to the Golgi was abolished. Further, a functional Myo18A/GOLPH3 complex is needed for normal *trans*-Golgi appearance and efficient tubule and vesicle budding, as well as directed vesicle trafficking away from the Golgi ribbon (Dippold et al. 2009). To understand whether active force generation by Myo18A is required for its cellular function, a Myo18A construct with ATP-binding pocket mutations (G520S/K521A in the P-loop) was utilized to rescue the Myo18A-knockdown phenotype of condensed Golgi. The fact that this rescue failed prompted the authors to suggest that force generation via the Myo18A motor is needed to stretch and shape the Golgi. This interpretation is additionally backed up by a study by Tan et al., where overexpression of a similar ATP-binding pocket mutation (G520D/K521E) in Myo18A generates a dominant-negative phenotype similar to the depletion of Myo18A (cf. 19.2.4) (Tan et al. 2008). However, the fact that Myo18A function can be altered by mutations in the active site is in contrast with the aforementioned biochemical studies that could not detect any ATPase or motor function for Myo18A from different species (cf. 19.2.2). There are at least three possible explanations for this obvious contradiction. Firstly, it is possible that inside the cell, Myo18A actually functions as a molecular motor either activated by thus far unidentified binding partners or by other mechanisms such as posttranslational modifications, the binding of metabolites, or the performance of specific chaperones. Secondly, the mutations that have been introduced in the center of the Myo18A globular motor domain could impair its proper folding and as such, lead to decreased protein stability and the observed phenotypes. Thirdly, the mutations may not deactivate motor function but rather interfere with the proper discrimination of the nucleotide state, which is shown to regulate the actin-binding properties of human Myo18A (Taft et al. 2013). Additionally, this could also affect the functional competence of mixed bipolar filaments of Myo18A and NM2A, which have been detected inside living cells (Billington et al. 2015), where NM2A provides the motor activity for the mixed myosin filaments.

Independent of the exact mechanism of how Myo18A performs its function at the Golgi, further studies by the same group support its interaction with GOLPH3 and its participation in maintaining Golgi morphology and function. In secretory tissues, a GOLPH3 paralogue, GOLPH3L, was identified that antagonizes GOLPH3 function as it binds to the Golgi membrane via PI4P interaction and supports anterograde trafficking without binding to Myo18A (Ng et al. 2013). Accordingly, GOLPH3L blocks PI4P for GOLPH3 binding and thereby suppresses Myo18A-mediated anchoring of the Golgi to the actin cytoskeleton. In a subsequent study it was shown that the nuclear DNA-PK protein kinase is activated by doxorubicin-induced DNA damage to phosphorylate GOLPH3, which leads to an increased interaction with Myo18A (Farber-Katz et al. 2014). The enhanced interaction impairs vesicle trafficking from the Golgi membrane to the plasma membrane and thus induces fragmentation of the Golgi as a result of DNA damage. It has previously been described that GOLPH3 is an oncogene that is frequently overexpressed and amplified in human cancers

(Scott et al. 2009; Buschman et al. 2015; Buschman and Field 2018). GOLPH3 acts as an oncogenic factor by increasing cell migration. Overexpression of GOLPH3 and siRNA-mediated knockdown of both GOLPH3 and Myo18A show that the entire PI4P/GOLPH3/Myo18A/F-actin complex is necessary and sufficient to promote Golgi reorientation towards the leading edge via the actin cytoskeleton and as such is able to enhance directional cell migration (Xing et al. 2016).

Although a plethora of experimental evidence speaks in favor of a direct role of the Myo18A/GOLPH3 complex in the maintenance of Golgi morphology and function, a recent study provides data that question the previous results (Bruun et al. 2017). Here, Hammer and coworkers used immunofluorescence studies with specific antibodies and overexpression of GFP-tagged proteins and found no proof of Myo18A localization to the Golgi or an impact of reduced Myo18A levels on Golgi morphology. As their study focuses on Myo18Aα, the authors consider that unknown splice variants of Myo18A may facilitate the Golgi-shaping via GOLPH3. However, based on their experimental results, they assume that global F-actin disassembly is the major reason for the observed Golgi morphology.

19.2.4 Myo18A Has Multiple Roles in Focal Adhesions, Stress Fibers and Lamellipodia

Myo18A has biochemically been defined as an actin-binding protein that comprises four actin-binding sites per heavy chain dimer (Taft et al. 2013). On the cellular level, a few studies have analyzed its localization and role in the context of different actin structures, specifically focal adhesions, actin stress fibers and lamellar actomyosin bundles. Characterization of the subcellular distribution of overexpressed EYFP-tagged Myo18A protein and deletion constructs in fibroblasts revealed that the KE motif mediates actin fiber co-distribution, whilst the PDZ domain controls the localization of Myo18A to the inner surface of the cell membrane (Mori et al. 2005). FRAP experiments revealed random and rapid short-range movement of punctate structures in the cytoplasm. The cellular function of Myo18A has also been assessed in the context of lamellar actomyosin bundles (Tan et al. 2008). Here, a tripartite complex of Myo18A with the myosin light chain kinase MRCK (myotonic dystrophy-related Cdc42-binding kinase) and the leucine-rich adapter protein LRAP35a was shown to co-localize with lamellar actomyosin filaments. In this protein complex, LRAP35a binds and activates MRCK and simultaneously binds to Myo18A, which directs the complex to actomyosin bundles. The activated MRCK subsequently phosphorylates the RLC, which is bound to Myo18A. In parallel, MRCK also phosphorylates NM2A and thereby initiates actomyosin assembly in the lamella to enable cell protrusion and cell migration. The results of this study are in line with the findings of Billington et al., who applied TIRF-SIM microscopy of fluorescently-tagged Myo18Aα and Myo18Aβ in combination with NM2A and found that these myosins co-assemble in living cells (Billington et al. 2015). These results were further confirmed with antibodies specific for Myo18A and NM2A. Thus, Myo18A can incorporate into NM2 filaments and might regulate the assembly and functional properties of structures like actomyosin bundles and stress fibers. In addition, a direct interaction of Myo18A with the PAK2/βPIX/GIT1 (p21-activated kinase 2/PAK-interacting exchange factor-β/G protein-coupled receptor kinase-interactor 1) complex was established in a proteomics approach that sought to identify new proteins that interact with PAK2 in human epidermoid carcinoma cells (Hsu et al. 2010). The interaction of Myo18A with PAK2 is indirect and mediated via βPIX/GIT1 to direct the whole complex to lamellipodia and membrane ruffles. Myo18A-depleted cells display decreased cell migration, an enlarged morphology, and also increased actin stress fiber density and focal adhesion formation. It appears that Myo18A is essential for lamellipodia targeting of the complex, as Myo18A depletion and

disruption of its interaction with βPIX both induce accumulation of the complex at focal adhesions and decrease cell migration (Hsu et al. 2010, 2014).

19.2.5 Membrane Proteins Identified as Myo18A

A striking feature of Myo18A is its implication in binding of surfactant protein A (SPA) at the cell surface. Chroneos and coworkers identified Myo18A as SPA-receptor 210 (SP-R210) using mass spectrometry and antibodies specific for the C-terminus of Myo18A (Yang et al. 2005). They showed that Myo18A overexpression in COS-1 cells enables SPA binding and that SP-R210-directed antibodies detect bacterially-expressed Myo18A domains that correspond to the region encompassing the IQ motifs and the first half of the coiled-coil domain. Intriguingly, these antibodies block the binding of SPA to macrophages (Yang et al. 2005) as well as T-cell-mediated immune responses (Samten et al. 2008). Further, the stable expression of the C-terminal domain of Myo18A in macrophages is also shown to induce a dominant-negative inhibition of SP-R210 protein expression (Szeliga et al. 2005; Yang et al. 2015). In addition, a single study by a different group applied mass spectrometry supported by immunoblotting with a Myo18A-specific antibody and identified CD245, a surface antigen of peripheral blood lymphocytes, as Myo18A (De Masson et al. 2016). In line with the aforementioned studies, both the long and the short isoforms (230 and 190 kDa) were detected, and the authors suggest a mechanism for Myo18A recruitment-mediated activation of NK cell cytotoxicity. Although the results of these studies were substantiated with numerous independent experiments, these findings raise a number of obvious questions. Myo18A does not contain transmembrane domains and has exclusively been detected in the cytosolic compartment of cells in all other studies. Further, it is completely unclear how Myo18A is externalized to the cell surface as a Golgi/ER-mediated process should have been detected in other studies. Future research may shed light on this unique role for Myo18A and unravel the underlying cellular and functional mechanisms.

19.2.6 Participation of Myo18A in Muscle Development and Integrity

A central feature of the other class XVIII myosin, Myo18B, is its implication in the process of striated muscle maturation (cf. 19.3.2). Initial evidence indicating that Myo18A likewise contributes to muscle development stems from studies in *Drosophila* and zebrafish. The sole class XVIII myosin in *Drosophila*, Myo18, was shown to localize to cell-cell contacts in myocytes during myoblast fusion (Bonn et al. 2013). The protein Rolling Pebbles 7, which is an integral part of a protein complex at myoblast fusion pores, was identified as a direct interaction partner essential for Myo18 localization to these sites. A possible role of Myo18 at these sites is to organize the actin cytoskeleton to widen the fusion pore. As deficiency of Myo18 does not impact muscle development, it can be speculated that other myosins have redundant functions in *Drosophila*. In mature muscles, *Drosophila* Myo18 localizes adjacent to the Z-disc but does not directly co-localize with Z-disc markers, implying an additional role not connected to myoblast development. Two studies shed light on the participation of Myo18A in myofiber integrity in zebrafish. It was found that both Myo18Aα and Myo18Aβ are expressed in somite borders during zebrafish development (Cao et al. 2014). Knockdown of Myo18A or overexpression of the PDZ module was shown to disrupt myofiber integrity. Accordingly, it was suggested that Myo18A mediates adhesion of myofibers to the cell membrane, permitting their stable attachment to the extracellular matrix. In a follow-up study by the same group, yeast two-hybrid screening and co-immunoprecipitation identified p190Rho-guanine nucleotide exchange factor (p190RhoGEF) and Golgin45 as novel binding

partners for the PDZ module of Myo18A during zebrafish development (Cao et al. 2016). These experiments also confirmed the direct interaction of Myo18A with LURAP (LRAP35A, (Tan et al. 2008)). Knockdown of Myo18A alone or in combination with the aforementioned three binding partners severely disrupts myofiber integrity during development supposedly via a combined effect on the localization of dystrophin via a Myo18A-mediated impact on the actin cytoskeleton and/or via Myo18A-mediated support of Golgi morphology and trafficking (Cao et al. 2016).

A recent study identified a new class XVIII myosin isoform in mouse myocytes and human heart, termed Myo18Aγ (Horsthemke et al. 2019). Myo18A-directed antibodies were used to define the Myo18A isoform expression pattern in mouse ventricular myocytes and detected a protein of a molecular mass of ~267 kDa, which is not compatible with either Myo18Aα or Myo18Aβ. RNA-Seq confirmed that this protein constitutes a novel isoform of Myo18A, which has not been described previously. This isoform comprises an alternate N-terminal extension, as well as an extended C-terminus (Fig. 19.1). Overexpression of EYFP-tagged Myo18Aγ led to its accumulation within the A-band of sarcomeres in mouse ventricular myocytes whilst *Myo18A*-knockout mice displayed disorganized sarcomeres.

19.2.7 Disease Implications of Myo18A in Cancer and Virus Transport

In terms of disease, Myo18A has predominantly been investigated in cancer, where it is described to be part of fusion genes. However, it is also proposed to play a role in virus assembly and secretion.

An exon array analysis study identified alternative splicing of *MYO18A* in non-small cell lung cancer, which caused in-frame variations in the protein sequence (Langer et al. 2010). Further, the *MYO18A* gene was identified as a partner in the three-way chromosomal translocation of stem cell leukemia-lymphoma syndrome (Walz et al. 2005). Here, exon 32 of *MYO18A* is fused with exon 9 of *FGFR1* (fibroblast growth factor receptor 1), which creates a constitutively-active tyrosine kinase that stimulates cell growth and proliferation. This leads to thrombocytopenia with decreased number and size of megakaryocytes and increased monocyte, eosinophil, and basophil cell numbers, establishing an unusual myelodysplastic/myeloproliferative disease (Walz et al. 2005). An additional fusion gene, *MYO18A-PDGFRB* (platelet-derived growth factor receptor beta), was detected by long-distance inverse PCR in eosinophilia-associated atypical myeloproliferative neoplasms (Walz et al. 2009). Fusion of exon 40 of *MYO18A* with exon 10 of *PDGFRB* creates a large protein (2661 aa) that retains most of Myo18A (98%) and contains the C-terminal 59% of PDGFRB. The proposed activation mechanism is based on the dimerization or oligomerization of the PDGFRB part by the Myo18A coiled-coil domain. In addition, a three-way translocation of the highly promiscuous oncogene *MLL*, a histone methyltransferase, and the reciprocal partner gene *MYO18A* was described in acute myeloid leukemia (Ussowicz et al. 2012). As the fusion gene is in frame, it translates into a functional fusion protein that encompasses the N-terminal 362 amino acids of Myo18A and the C-terminal 2607 amino acids (of 3969) of MLL, producing a chimeric protein that preserves methyltransferase activity and contains the N-terminal PDZ domain of Myo18A. However, the consequence of this fusion on the localization, regulation, or activity of the resulting protein is not yet known. An additional cancer-related role for Myo18A, not linked to gene fusion events, was proposed for its abundance in prostate cancer cell lines (Peckham 2016). Here, increased levels of four unconventional myosins, Myo1b, Myo9b, Myo10, and Myo18A, were reported (Makowska et al. 2015). Conversely, knockdown of Myo18A results in reorganization of long NM2A-rich stress fibers. This is in line with the previously reported ability of Myo18A to form mixed filaments with NM2A

(Billington et al. 2015). The re-organized stress fibers, depleted of Myo18A, locate along the length of prostate cancer cells, which results in reduced directionality persistence in cell migration (Makowska et al. 2015). These findings suggest a contribution of increased Myo18A levels to prostate cancer metastasis.

Using a systems biology approach to follow the fate of organelles during human cytomegalovirus (HCMV) infection, Myo18A was found to localize to the plasma membrane in primary human fibroblasts (Jean Beltran et al. 2016). Following viral infection, Myo18A is translocated to the viral assembly complex and supports virus production by an as of yet unknown mechanism. The authors speculate that a Myo18A-mediated tethering of virus-loaded vesicles to NM2-containing myosin filaments provides the molecular basis for vesicle movement. A role for Myo18A in the virus secretion process was described for the hepatitis C virus (Bishé et al. 2012). Silencing of GOLPH3 or Myo18A inhibits hepatitis C virus secretion and leads to virion accumulation inside the cell. These findings are in line with a role of Myo18A in Golgi budding via GOLPH3 interaction (Dippold et al. 2009) and in virus secretion pathways (Jean Beltran et al. 2016).

19.3 Myosin-18B

19.3.1 Molecular and Cell Biology

The existence of a second class XVIII myosin family member, Myo18B, was first reported by Berg et al. in 2001 following partial annotation of the human *MYO18B* gene (Berg et al. 2001). *MYO18B* maps on human chromosome 22q12.1 between the *GRK3* and *SEZ6L* genes, in an area of ~322 kb (25,742,133 – 26,063,847) and produces an mRNA transcript of 8577 bp from 43 coding exons and a 5′ non-coding exon (NCBI, NM_032608.6). The 7704 bp ORF encodes for a 2567-amino acid protein with a molecular mass of ~285 kDa that shares ~90% identity with the ~288 kDa homologue produced in mouse (Nishioka et al. 2002; Salamon et al. 2003). According to the NCBI database, an additional 7707-bp mRNA transcript has been curated for the human *MYO18B gene*, which lacks the 5′ non-coding region and includes three nucleotides that encode an additional glutamine residue at position 1020 within the protein sequence [NCBI, NM_001318245.1]. However, no data are currently available to validate or differentiate the occurrence or function of these two proteins.

Northern blot and PCR analyses have demonstrated that unlike Myo18A, which is ubiquitously expressed in most mammalian cells and tissues, Myo18B transcript expression is highly tissue specific. The highest level of expression is observed in cardiac and skeletal striated muscles, although Myo18B contributes as little as 0.005% of the total mRNA content in skeletal muscle (Nishioka et al. 2002; Salamon et al. 2003; Ajima et al. 2008). In addition, Myo18B mRNA is also found at low levels in other organs and tissues, including the testis, bone marrow, thymus, mammary glands, lungs (both fibroblastic and epithelial cell types), kidney, pancreas, placenta, prostate and brain. Whilst BLAST analyses have indicated that three potential splice isoforms exist in murine and human tissues, there is currently no experimental evidence demonstrating that *MYO18B* is susceptible to alternative mRNA splicing (Salamon et al. 2003).

Myo18B comprises a central region with a generic myosin configuration (Fig. 19.3). Within this core structure is a 767-amino acid motor domain (residues 565-1332), which encompasses both nucleotide- and actin-binding sites. Sequence analysis reveals that much like Myo18A, with which it shares ~40% protein identity, Myo18B also harbors amino acid substitutions in evolutionarily-conserved residues within the P-loop, switch-1, and switch-2; the regions essential for generating ATP-dependent force and movement along actin filaments (Fig. 19.2). Whilst these alignments indicate that Myo18B lacks motor ATPase activity, the precise function of the motor domain remains to be deciphered through biochemical analyses. Following the motor domain is a 69-amino acid neck region

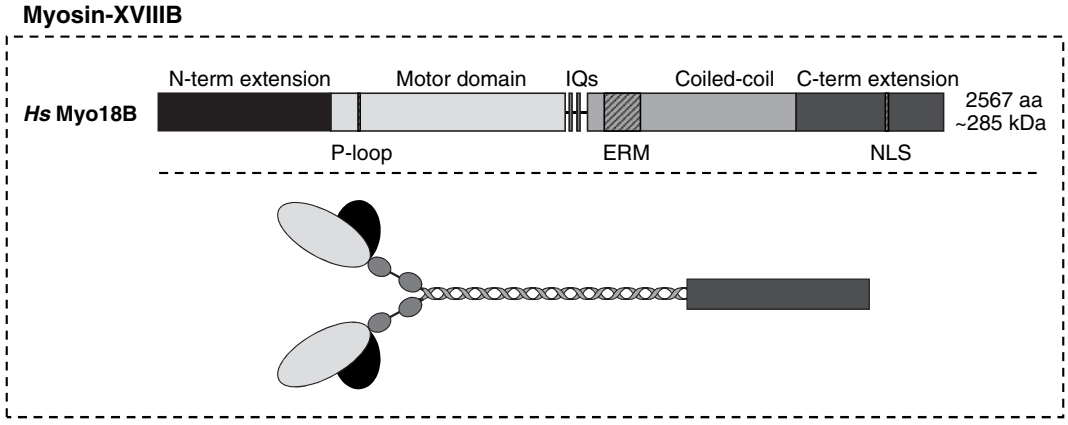

Fig. 19.3 Schematic representation of the domain structure of human Myosin-18B illustrating the 564-amino acid N-terminal extension, generic motor domain, neck region containing two myosin light chain binding IQ motifs, coiled-coil tail domain predicted to enable dimerization, and C-terminal extension, which contains a putative nuclear localization sequence (NLS) at residues 2377–2387

(residues 1333-1402), which contains two myosin light chain-binding IQ motifs stretching from amino acids 1343-1353 (FQAACKGFLSR) and 1369-1379 (IQKNVAVFLAV). At the present time, there is no information available regarding the interaction of Myo18B with either ELC or RLC. The generic region is completed with a coiled-coil tail domain between residues 1403-2085, which is essential in other myosins, including Myo18A, for heavy chain dimerization. Exhaustive domain analyses predict that this tail region also incorporates an ERM (ezrin-radixin-moesin) domain for plasma membrane interactions (residues 1458-1576), an AAA domain for association with chaperone-like ATPase proteins (residues 1434-1917 amino acids), and a putative A-motif for nucleotide binding at position 1818-1825 (Salamon et al. 2003). However, the functional capabilities of each of these proposed domains remains to be assessed. Flanking the core region are large N-terminal and C-terminal extensions, which encompass 564 and 480 amino acids, respectively. Unlike the Myo18Aα N-terminal extension, which contains a well-defined KE-rich region and a PDZ domain, the N-terminal extension of Myo18B does not resemble any known protein sequence. With the exception of a putative nuclear localization sequence (NLS) at residues 2377-2387, the C-terminal extension also bares no similarity with known protein domains (Salamon et al. 2003).

Whilst the biochemical properties of Myo18B remain to be elucidated, cellular localization studies and experiments with truncated overexpression constructs provide some insight into the function of this unique protein. Using overexpression constructs as well as N-terminal- and C-terminal-specific antibodies, this protein has been localized to a number of specific sites within both nonmuscle and muscle cell types (c.f. 19.3.2). In nonmuscle cells specifically, Myo18B has been shown to localize in a punctate pattern throughout the cytoplasm, in membrane protrusions, and within stress fibers (Inoue et al. 2006; Ajima et al. 2007; Jiu et al. 2019). In this last locality, Myo18B is thought to assemble into a compact configuration at the end of NM2 bipolar bundles, where it aids in the fusion and coalescence of adjacent myosin stacks to facilitate actomyosin bundle maturation (Jiu et al. 2019). This is evident in CRISPR/Cas9-mediated *MYO18B* knockout osteosarcoma cells, where a subset of stress fibers known as transverse arcs are unable to assemble into thick mature ventral stress fibers. Defective stress fiber maturation in these cells leads to abnormal morphogenesis, contractility, and reduced migration. Utilizing a series of over-

expression domain constructs, both the N-terminal extension and coiled-coil tail domains were identified as being essential for the integration of Myo18B within stress fibers. The N-terminal extension alone localizes to stress fibers and actin bundles (Ajima et al. 2008; Jiu et al. 2019), suggesting that this unique protein domain may harbor essential actin-interaction sites, as seen within the N-terminal extension of Myo18A (Isogawa et al. 2005; Taft et al. 2013). Punctate and cytoplasmic localization of an overexpression construct lacking the N-terminal extension further supports the pivotal role for the N-terminus in mediating actin interactions. Unlike the N-terminus, deletion of the C-terminal extension has no effect on stress fiber localization and overexpression of a C-terminal deletion construct is able to rescue the CRISPR/Cas9-mediated *MYO18B*-knockout phenotype in osteosarcoma cells. Interestingly, Myo18A overexpression is shown to partially rescue the *Myo18B*-knockout phenotype, although it is not intrinsically upregulated to compensate for reduced Myo18B protein levels.

Aside from actin, two other interaction partners have been identified and validated for Myo18B through yeast two-hybrid screening studies. In the first study, Sug1, a component of the 19S regulatory complex of the 26S proteasome was identified and the interaction was validated in COS-7 and C2C12 cells (Inoue et al. 2006). Colocalization analysis in HeLa cells revealed that cytoplasmic punctate Myo18B staining in nonmuscle cells partially overlaps with Sug1 staining. Accordingly, it was validated that Myo18B is susceptible to polyubiquitination and Sug1-mediated proteasomal degradation, although the precise mechanisms and physiological relevance of these findings remain undetermined. In a second report, the C-terminal tail of Myo18B was found to interact with the C-terminal half of Homer2, a post-synaptic adaptor protein, at membrane protrusions and stress fibers (Ajima et al. 2007). Expression of Homer2 was shown to enhance the ability of Myo18B to suppress anchorage-independent growth (cf. 19.3.3); however, the precise mechanisms mediating this effect are unresolved.

19.3.2 Myo18B in Striated Muscle Development and Assembly

In accordance with the strong expression profile of *MYO18B* in cardiac and skeletal muscles, a considerable portion of the literature on Myo18B is specifically focused on understanding its function in striated muscle tissues. At the level of the gene, *MYO18B* is distinct from many other human sarcomeric myosin genes, as it does not map to chromosomes 14 and 17, where cardiac and skeletal myosin heavy chain genes are clustered, but instead localizes to chromosome 22 (Salamon et al. 2003). Gene expression profiling studies in mice reveal that *Myo18B* expression is upregulated following the onset of myogenic differentiation, the process by which myotubes mature from myoblast precursors under the control of myocyte enhancer factor-2 (MEF2) transcription factors (Salamon et al. 2003; Ajima et al. 2008). A single study in Atlantic cod also indicates that the expression of this gene in skeletal muscle is linked to the transcription pattern of clock genes (Lazado et al. 2014). In the immortalized C2C12 mouse myoblast cell line, expression peaks at differentiation day 3 and remains constant throughout myotube maturation (Salamon et al. 2003). In mouse embryos, this translates to strong expression of *MYO18B* mRNA in heart tissue at embryonic days 9.5–11.5 and within myotomes and muscle mass at embryonic day 13.5 (Ajima et al. 2008).

Whilst a number of studies have reported that Myo18B adopts a regularly-spaced striated distribution pattern within sarcomeric structures in mature myocytes, its precise subcellular distribution throughout differentiation and within sarcomeres remains controversial. The first study examining Myo18B localization by Salamon et al. utilizing stable c-myc-tagged overexpression constructs and an N-terminal rabbit polyclonal antibody reported several distinct localization patterns. Specifically, Myo18B was observed in the cytoplasm in undifferentiated myoblasts, within the nucleus in undifferentiated myoblasts and select differentiated myotubes, and was prominently incorporated into A-bands within mature sarcomeric structures (Salamon

et al. 2003). However, a follow-up study utilizing two antibodies raised against C-terminal residues (amino acids 2448-2518) found no indication of Myo18B within the nucleus and observed that it localized with α-actinin at Z-discs rather than with muscle myosin-2 in A-bands (Ajima et al. 2008). Aspects of both of these initial studies were reproduced in a third publication assessing GFP-tagged Myo18B localization in zebrafish. In this instance, Berger et al. reported that exogenous Myo18B is integrated into sarcomeric A-bands 3 days post fertilization (dpf), where it alternates with α-actinin (Berger et al. 2017). They also report that they do not observe a nuclear localization pattern for Myo18B; however, it is unclear if their analysis adequately assesses localization in undifferentiated myoblasts.

Regardless of the discrepancies in localization analyses, these studies firmly demonstrate that Myo18B is an essential component of muscle contractile machinery. In mice, homozygous knockout of *Myo18B* was found to be embryonically lethal with major defects evident at embryonic day 10.5 (Ajima et al. 2008). Knockout embryos had severe cardiac defects, including dilated pericardial cavities and internal hemorrhage or resorption, and ultrastructural analysis revealed severe abnormalities in the organization and alignment of myosin thick and actin thin filaments in muscle tissue. This gave the first indication that Myo18B is required for the development and maintenance of myofibril structure. Two recent studies linking mutations in the zebrafish *myo18B* gene with defective muscle integrity, cardiac deformities and reduced motile capacity have further demonstrated the essential role for Myo18B in sarcomere assembly (Berger et al. 2017; Gurung et al. 2017). In this model organism, *myo18B* is expressed exclusively in fast-twitch muscle fibres 1 dpf, is found within the fin and heart 2 dpf, and is present in the head and extraocular muscles 3 dpf. Accordingly, mechanical force measurements in zebrafish baring allelic deletions and mutations in *myo18B* reveal that this protein is essential for force generation in fast-twitch muscles and not slow-twitch musculature (Berger et al. 2017). Ultrastructural analysis of fast-twitch muscle tissue in these mutant fish (3 dpf) by transmission electron microscopy demonstrates that the registered alignment of thick and thin filaments into sarcomeric structures does not occur in the absence of functional Myo18B.

To date, two studies have implicated *MYO18B* mutations in human myopathies. In the first instance, Malfatti et al. reported that a homozygous missense mutation in *MYO18B* (c.6496G > T, p.Glu2166∗) was linked with nemaline myopathy, a rare and severe congenital muscle disorder characterized by the presence of nemaline bodies (rods) within patient skeletal muscle (Malfatti et al. 2015). In this instance, mRNA expression was not affected by the mutation; however, the resulting protein was truncated within the C-terminal extension and the full-length protein could not be detected with a C-terminal antibody. The patients presented with dysmorphic features, clinodactyly, severe hypotonia, muscle weakness, and cardiomyopathy. In the second published case study, two patients presenting with a novel form of Klippel-Feil anomaly that included myopathy and distinct facial features were found to have the same homozygous nonsense mutation in *MYO18B* (c.6905C > A), which induced a premature stop codon at residue 2302 (Alazami et al. 2015). This mutation induced nonsense-mediated mRNA decay with almost no *MYO18B* mRNA identified in patient lymphoblastic cells. Consistent with the mouse and zebrafish models of Myo18B knockdown and knockout, ultrastructural analysis revealed that loss of functional Myo18B in these patients culminated in an apparent loss of thick and thin filament banding in muscle biopsies, further demonstrating the essential role for Myo18B in sarcomere assembly.

19.3.3 *MYO18B* in Cancer Progression

Initial studies characterizing the *MYO18B* gene in cancer stemmed from the observation that allelic losses on chromosome 22q are frequently

detected in human tumors. This suggested that an essential tumor suppressor gene is present within this chromosomal region. A series of studies by the work group of Jun Yokota demonstrated that *MYO18B* is effectively inactivated in lung, ovarian, and colorectal cell lines and primary tumor samples by homozygous deletions, mutations, and/or epigenetic silencing (Nishioka et al. 2002; Tani et al. 2004; Yanaihara et al. 2004; Nakano et al. 2005). Specifically, hypermethylation of CpG sites in the *MYO18B* promoter region and deacetylation of histone H3 and histone H4 all significantly inactivate *MYO18B* in these cancer subsets. In accordance with the initial hypothesis that *MYO18B* functions as a tumor suppressor gene, Myo18B overexpression or restoration was also found to impede tumor progression by suppressing anchorage-independent growth.

The tumor suppressive role for Myo18B is further supported by the handful of studies that have identified *MYO18B* mutations in various cancers. This includes patients with melanoma and pancreatic ductal adenocarcinoma (Bleeker et al. 2009), two siblings with familial lung cancer (Kukita et al. 2016), and a single patient with neuroendocrine cancer (Bhatla et al. 2016). Two additional reports further strengthen the link between *MYO18B* epigenetic modifications and cancer. Specifically, reduced *MYO18B* expression due to hypermethylation was linked to a reduced response to platinum-based chemotherapies in ovarian cancer cases (Tomar et al. 2017), and increased *MYO18B* expression due to hypomethylation in T-cell acute leukemia was associated with better patient prognosis (Haider et al. 2019). Both reports support a tumor suppressive role for *MYO18B* in cancer.

To date, a single study published in 2018 by Zhang et al. has reported a tumor promoting role for *MYO18B* in hepatocellular carcinoma progression (Zhang et al. 2018). Specifically, increased *MYO18B* expression in a large TCGA (The Cancer Genome Atlas) cohort and an independent validation cohort correlated with advanced disease and worse overall survival. In support of this, Myo18B knockdown by siRNA reduced cell proliferation, decreased tumor colony formation over time, slowed 2D-wound healing, and significantly decreased 3D-invasion in Transwell assays. This is in line with the effect of CRISPR/Cas9-mediated Myo18B knockout in osteosarcoma cells, which significantly impaired the ability for cells to undergo 3D-invasive migration, likely due to the defective maturation of NM2 stress fibers (Jiu et al. 2019). In the case of hepatocellular carcinoma cells, it was shown that Myo18B knockdown significantly affected signaling components essential for proliferation, apoptosis, and migrations. Specifically, knockdown suppressed the phosphorylation of PI3K, AKT, and mTOR, and resulted in an evident decrease in p70S6K expression.

19.3.4 *MYO18B* in Other Disease Contexts

In addition to the role of *MYO18B* in cancer and myopathies, this gene has also been linked to other diseases. One of the most significant findings was a report by Ludwig et al., which found that single nucleotide polymorphisms in *MYO18B* are indicative and causative of mathematical disability (Ludwig et al. 2013). The authors reported that people carrying a *MYO18B* risk-genotype displayed significantly lower depth in an area of the brain involved in numerical processing, the intraparietal sulcus (IPS). These results have however been questioned by a follow-up study, which reports that no link between *MYO18B* and mathematical disability could be found in four independent validation cohorts (Pettigrew et al. 2015). In addition, *MYO18B* single nucleotide variants have also been associated with schizophrenia in a genome-wide association study (Takata et al. 2013), and a heterozygous variant in *MYO18B* was identified in a single case of infant death, where the fetus had significant deformities, which included a muscle phenotype (Armes et al. 2018).

19.4 Perspectives

In the 20 years since class XVIII myosins were first discovered, there have been significant advances in resolving their functions at both the molecular and cellular levels. However, it is clear that we have only just begun to unravel the properties of members of this new branch within the myosin family, characterized by their unique N- and C-terminal extensions, as well as their apparent lack of active ATPase-driven motor function. A number of obvious questions remain to be addressed. This includes whether the two proteins in this family, Myo18A and Myo18B, have overlapping functions within common subcellular localities. This has been addressed in a single study by Jiu et al., where overexpression of Myo18A could slightly compensate for Myo18B knockout in stress fiber maturation; however, knockout did not induce an intrinsic compensatory increase in Myo18A (Jiu et al. 2019). With regard to surfactant protein A receptor, it is important to address how this cytoplasmic soluble protein is translocated and anchored to the plasma membrane. Further, does the PDZ domain, which is known to mediate membrane association, play a role in this function? With regard to Myo18B, it is clear that an in-depth biochemical analysis of the protein's subdomains is required to completely understand the function of Myo18B in stress fiber maturation and sarcomere assembly. Furthermore, as a putative NLS has been identified within the C-terminal extension and a nuclear localization has been reported in myocytes, it would be of great interest to resolve whether Myo18B has a nuclear function. Whilst Salamon et al. proposed that Myo18B may function as a transcriptional regulator of myogenic differentiation (Salamon et al. 2003), this remains to be resolved in follow-up studies.

References

Ajima R, Kajiya K, Inoue T et al (2007) HOMER2 binds MYO18B and enhances its activity to suppress anchorage independent growth. Biochem Biophys Res Commun 356:851–856. https://doi.org/10.1016/j.bbrc.2007.03.060

Ajima R, Akazawa H, Kodama M et al (2008) Deficiency of Myo18B in mice results in embryonic lethality with cardiac myofibrillar aberrations. Genes Cells 13:987–999. https://doi.org/10.1111/j.1365-2443.2008.01226.x

Alazami AM, Kentab AY, Faqeih E et al (2015) A novel syndrome of Klippel-Feil anomaly, myopathy, and characteristic facies is linked to a null mutation in *MYO18B*. J Med Genet 52:400–404. https://doi.org/10.1136/jmedgenet-2014-102964

Armes JE, Williams M, Price G et al (2018) Application of whole genome sequencing technology in the investigation of genetic causes of Fetal, perinatal, and early infant death. Pediatr Dev Pathol 21:54–67. https://doi.org/10.1177/1093526617715528

Berg JS, Powell BC, Cheney RE (2001) A millennial myosin census. Mol Biol Cell 12:780–794

Berger J, Berger S, Li M, Currie PD (2017) Myo18b is essential for sarcomere assembly in fast skeletal muscle. Hum Mol Genet 26:ddx025. https://doi.org/10.1093/hmg/ddx025

Bhatla T, Dandekar S, Lu BY et al (2016) Genomic characterization of poorly differentiated neuroendocrine carcinoma in a Pediatric patient. J Pediatr Hematol Oncol 38:e21–e25. https://doi.org/10.1097/MPH.0000000000000463

Billington N, Beach JR, Heissler SM et al (2015) Myosin 18A coassembles with nonmuscle myosin 2 to form mixed bipolar filaments. Curr Biol 25:942–948. https://doi.org/10.1016/j.cub.2015.02.012

Bishé B, Syed GH, Field SJ, Siddiqui A (2012) Role of phosphatidylinositol 4-phosphate (PI4P) and its binding protein GOLPH3 in hepatitis C virus secretion. J Biol Chem 287:27637–27647. https://doi.org/10.1074/jbc.M112.346569

Bleeker FE, Lamba S, Rodolfo M et al (2009) Mutational profiling of cancer candidate genes in glioblastoma, melanoma and pancreatic carcinoma reveals a snapshot of their genomic landscapes. Hum Mutat 30:E451–E459. https://doi.org/10.1002/humu.20927

Bloemink MJ, Geeves MA (2011) Shaking the myosin family tree: biochemical kinetics defines four types of myosin motor. Semin Cell Dev Biol 22:961–967

Bonn BR, Rudolf A, Hornbruch-Freitag C et al (2013) Myosin heavy chain-like localizes at cell contact sites during Drosophila myoblast fusion and interacts in vitro with rolling pebbles 7. Exp Cell Res 319:402–416. https://doi.org/10.1016/j.yexcr.2012.12.005

Bruun K, Beach JR, Heissler SM et al (2017) Re-evaluating the roles of myosin 18Aα and F-actin in determining Golgi morphology. Cytoskeleton (Hoboken) 74:205–218. https://doi.org/10.1002/cm.21364

Buschman MD, Field SJ (2018) MYO18A: an unusual myosin. Adv Biol Regul 67:84–92. https://doi.org/10.1016/j.jbior.2017.09.005

Buschman MD, Xing M, Field SJ (2015) The GOLPH3 pathway regulates Golgi shape and function and is activated by DNA damage. Front Neurosci 9:362. https://doi.org/10.3389/fnins.2015.00362

Cao J, Li S, Shao M et al (2014) The PDZ-containing unconventional myosin XVIIIA regulates embryonic muscle

integrity in zebrafish. J Genet Genomics 41:417–428. https://doi.org/10.1016/j.jgg.2014.06.008

Cao J-M, Cheng X-N, Li S-Q et al (2016) Identification of novel MYO18A interaction partners required for myoblast adhesion and muscle integrity. Sci Rep 6:36768. https://doi.org/10.1038/srep36768

Cross M, Csar XF, Wilson NJ et al (2004) A novel 110 kDa form of myosin XVIIIA (MysPDZ) is tyrosine-phosphorylated after colony-stimulating factor-1 receptor signalling. Biochem J 380:243–253. https://doi.org/10.1042/BJ20031978

De Masson A, Giustiniani J, Marie-Cardine A et al (2016) Identification of CD245 as myosin 18A, a receptor for surfactant a: a novel pathway for activating human NK lymphocytes. Oncoimmunology 5:e1127493. https://doi.org/10.1080/2162402X.2015.1127493

Dippold HC, Ng MM, Farber-Katz SE et al (2009) GOLPH3 bridges phosphatidylinositol-4- phosphate and actomyosin to stretch and shape the Golgi to promote budding. Cell 139:337–351. https://doi.org/10.1016/j.cell.2009.07.052

Dowler S, Currie RA, Campbell DG et al (2000) Identification of pleckstrin-homology-domain-containing proteins with novel phosphoinositide-binding specificities. Biochem J 351:19. https://doi.org/10.1042/0264-6021:3510019

Farber-Katz SE, Dippold HC, Buschman MD et al (2014) DNA Damage Triggers Golgi Dispersal via DNA-PK and GOLPH3. Cell 156:413–427. https://doi.org/10.1016/j.cell.2013.12.023

Furch M, Fujita-Becker S, Geeves MA et al (1999) Role of the salt-bridge between switch-1 and switch-2 of Dictyostelium myosin. J Mol Biol 290:797–809

Furusawa T, Ikawa S, Yanai N, Obinata M (2000) Isolation of a novel PDZ-containing myosin from hematopoietic supportive bone marrow stromal cell lines. Biochem Biophys Res Commun 270:67–75. https://doi.org/10.1006/bbrc.2000.2377

Geeves MA (2016) Review: the ATPase mechanism of myosin and actomyosin. Biopolymers 105:483–491. https://doi.org/10.1002/bip.22853

Geeves MA, Fedorov R, Manstein DJ (2005) Molecular mechanism of actomyosin-based motility. Cell Mol Life Sci 62:1462–1477. https://doi.org/10.1007/s00018-005-5015-5

Gurel PS, Hatch AL, Higgs HN (2014) Connecting the cytoskeleton to the endoplasmic reticulum and Golgi. Curr Biol 24:R660–R672. https://doi.org/10.1016/j.cub.2014.05.033

Gurung R, Ono Y, Baxendale S et al (2017) A zebrafish model for a human myopathy associated with mutation of the unconventional myosin MYO18B. Genetics 205:725–735. https://doi.org/10.1534/genetics.116.192864

Guzik-Lendrum S, Nagy A, Takagi Y et al (2011) Drosophila melanogaster myosin-18 represents a highly divergent motor with actin tethering properties. J Biol Chem 286:21755–21766

Guzik-Lendrum S, Heissler SM, Billington N et al (2013) Mammalian myosin-18A, a highly divergent myosin. J Biol Chem 288:9532–9548. https://doi.org/10.1074/jbc.M112.441238

Haider Z, Larsson P, Landfors M et al (2019) An integrated transcriptome analysis in T-cell acute lymphoblastic leukemia links DNA methylation subgroups to dysregulated *TAL1* and ANTP homeobox gene expression. Cancer Med 8:311–324. https://doi.org/10.1002/cam4.1917

Horsthemke M, Nutter LMJ, Bachg AC et al (2019) A novel isoform of myosin 18A (Myo18Aγ) is an essential sarcomeric protein in mouse heart. J Biol Chem 294:7202–7218. https://doi.org/10.1074/jbc.RA118.004560

Hsu R-M, Tsai M-H, Hsieh Y-J et al (2010) Identification of MYO18A as a novel interacting partner of the PAK2/betaPIX/GIT1 complex and its potential function in modulating epithelial cell migration. Mol Biol Cell 21:287–301. https://doi.org/10.1091/mbc.E09-03-0232

Hsu R-M, Hsieh Y-J, Yang T-H et al (2014) Binding of the extreme carboxyl-terminus of PAK-interacting exchange factor β (βPIX) to myosin 18A (MYO18A) is required for epithelial cell migration. Biochim Biophys Acta, Mol Cell Res 1843:2513–2527. https://doi.org/10.1016/j.bbamcr.2014.06.023

Inoue T, Kon T, Ajima R et al (2006) MYO18B interacts with the proteasomal subunit Sug1 and is degraded by the ubiquitin-proteasome pathway. Biochem Biophys Res Commun 342:829–834. https://doi.org/10.1016/j.bbrc.2006.02.025

Isogawa Y, Kon T, Inoue T et al (2005) The N-terminal domain of MYO18A has an ATP-insensitive actin-binding site. Biochemistry 44:6190–6196

Jean Beltran PM, Mathias RA, Cristea IM (2016) A portrait of the human organelle proteome in space and time during cytomegalovirus infection. Cell Syst 3:361–373.e6. https://doi.org/10.1016/j.cels.2016.08.012

Ji H, Zhai Q, Zhu J et al (2000) A novel protein MAJN binds to Jak3 and inhibits apoptosis induced by IL-2 deprival. Biochem Biophys Res Commun 270:267–271. https://doi.org/10.1006/bbrc.2000.2413

Jiu Y, Kumari R, Fenix AM et al (2019) Myosin-18B promotes the assembly of myosin II stacks for maturation of contractile Actomyosin bundles. Curr Biol 29:81–92.e5. https://doi.org/10.1016/j.cub.2018.11.045

Kukita Y, Okami J, Yoneda-Kato N et al (2016) Homozygous inactivation of *CHEK2* is linked to a familial case of multiple primary lung cancer with accompanying cancers in other organs. Mol Case Stud 2:a001032. https://doi.org/10.1101/mcs.a001032

Langer W, Sohler F, Leder G et al (2010) Exon array analysis using re-defined probe sets results in reliable identification of alternatively spliced genes in non-small cell lung cancer. BMC Genomics 11:676. https://doi.org/10.1186/1471-2164-11-676

Lazado CC, Nagasawa K, Babiak I et al (2014) Circadian rhythmicity and photic plasticity of myosin gene transcription in fast skeletal muscle of Atlantic cod (Gadus morhua). Mar Genomics 18:21–29. https://doi.org/10.1016/j.margen.2014.04.011

Levine TP, Munro S (2002) Targeting of Golgi-specific pleckstrin homology domains involves both PtdIns 4-kinase-dependent and -independent components. Curr Biol 12:695–704

Ludwig KU, Sämann P, Alexander M et al (2013) A common variant in Myosin-18B contributes to mathematical abilities in children with dyslexia and intraparietal sulcus variability in adults. Transl Psychiatry 3:e229. https://doi.org/10.1038/tp.2012.148

Makowska KA, Hughes RE, White KJ et al (2015) Specific Myosins control actin organization, cell morphology, and migration in prostate Cancer cells. Cell Rep 13:2118–2125. https://doi.org/10.1016/j.celrep.2015.11.012

Malfatti E, Böhm J, Lacène E et al (2015) A premature stop codon in MYO18B is associated with severe Nemaline myopathy with cardiomyopathy. J Neuromuscul Dis 2:219–227. https://doi.org/10.3233/JND-150085

McNally E, Sohn R, Frankel S, Leinwand L (1991) Expression of myosin and actin in Escherichia coli. Methods Enzymol 196:368–389

Mori K, Furusawa T, Okubo T et al (2003) Genome structure and differential expression of two isoforms of a novel PDZ-containing myosin (MysPDZ) (Myo18A). J Biochem 133:405–413

Mori K, Matsuda K, Furusawa T et al (2005) Subcellular localization and dynamics of MysPDZ (Myo18A) in live mammalian cells. Biochem Biophys Res Commun 326:491–498

Nakano T, Tani M, Nishioka M et al (2005) Genetic and epigenetic alterations of the candidate tumor-suppressor gene MYO18B, on chromosome arm 22q, in colorectal cancer. Genes Chromosomes Cancer 43:162–171. https://doi.org/10.1002/gcc.20180

Ng MM, Dippold HC, Buschman MD et al (2013) GOLPH3L antagonizes GOLPH3 to determine Golgi morphology. Mol Biol Cell 24:796–808. https://doi.org/10.1091/mbc.e12-07-0525

Nishioka M, Kohno T, Tani M et al (2002) MYO18B, a candidate tumor suppressor gene at chromosome 22q12.1, deleted, mutated, and methylated in human lung cancer. Proc Natl Acad Sci U S A 99:12269–12274. https://doi.org/10.1073/pnas.192445899

Odronitz F, Kollmar M (2007) Drawing the tree of eukaryotic life based on the analysis of 2,269 manually annotated myosins from 328 species. Genome Biol 8:R196

Onishi H, Kojima S, Katoh K et al (1998) Functional transitions in myosin: formation of a critical salt-bridge and transmission of effect to the sensitive tryptophan. Proc Natl Acad Sci U S A 95:6653–6658

Peckham M (2016) How myosin organization of the actin cytoskeleton contributes to the cancer phenotype. Biochem Soc Trans 44:1026–1034. https://doi.org/10.1042/BST20160034

Pettigrew KA, Fajutrao Valles SF, Moll K et al (2015) Lack of replication for the myosin-18B association with mathematical ability in independent cohorts. Genes Brain Behav 14:369–376. https://doi.org/10.1111/gbb.12213

Preller M, Manstein DJ (2013) Myosin structure, allostery, and mechano-chemistry. Structure 21:1911–1922. https://doi.org/10.1016/j.str.2013.09.015

Salamon M, Millino C, Raffaello A et al (2003) Human MYO18B, a novel unconventional myosin heavy chain expressed in striated muscles moves into the myonuclei upon differentiation. J Mol Biol 326:137–149

Samten B, Townsend JC, Sever-Chroneos Z et al (2008) An antibody against the surfactant protein a (SP-A)-binding domain of the SP-A receptor inhibits T cell-mediated immune responses to Mycobacterium tuberculosis. J Leukoc Biol 84:115–123. https://doi.org/10.1189/jlb.1207835

Scott KL, Kabbarah O, Liang M-C et al (2009) GOLPH3 modulates mTOR signalling and rapamycin sensitivity in cancer. Nature 459:1085–1090. https://doi.org/10.1038/nature08109

Szeliga J, Jordan J, Yang C-H et al (2005) Bacterial expression of recombinant MyoXVIIIA domains. Anal Biochem 346:179–181. https://doi.org/10.1016/j.ab.2005.07.021

Taft MH, Behrmann E, Munske-Weidemann L-C et al (2013) Functional characterization of human Myosin-18A and its interaction with F-actin and GOLPH3. J Biol Chem 288:30029–30041. https://doi.org/10.1074/jbc.M113.497180

Takata A, Iwayama Y, Fukuo Y et al (2013) A population-specific uncommon variant in GRIN3A associated with schizophrenia. Biol Psychiatry 73:532–539. https://doi.org/10.1016/j.biopsych.2012.10.024

Tan I, Yong J, Dong JM et al (2008) A tripartite complex containing MRCK modulates lamellar actomyosin retrograde flow. Cell 135:123–136. https://doi.org/10.1016/j.cell.2008.09.018

Tani M, Ito J, Nishioka M et al (2004) Correlation between histone acetylation and expression of the MYO18B gene in human lung cancer cells. Genes Chromosomes Cancer 40:146–151. https://doi.org/10.1002/gcc.20027

Tomar T, Alkema NG, Schreuder L et al (2017) Methylome analysis of extreme chemoresponsive patients identifies novel markers of platinum sensitivity in high-grade serous ovarian cancer. BMC Med 15:116. https://doi.org/10.1186/s12916-017-0870-0

Ussowicz M, Jaśkowiec A, Meyer C et al (2012) A three-way translocation of MLL, MLLT11, and the novel reciprocal partner gene MYO18A in a child with acute myeloid leukemia. Cancer Genet 205:261–265. https://doi.org/10.1016/j.cancergen.2012.02.006

Walz C, Chase A, Schoch C et al (2005) The t(8;17)(p11;q23) in the 8p11 myeloproliferative syndrome fuses MYO18A to FGFR1. Leuk Off J Leuk Soc Am Leuk Res Fund UK 19:1005–1009. https://doi.org/10.1038/sj.leu.2403712

Walz C, Haferlach C, Hänel A et al (2009) Identification of a MYO18A-PDGFRB fusion gene in an eosinophilia-associated atypical myeloproliferative neoplasm with a t(5;17)(q33-34;q11.2). Genes Chromosomes Cancer 48:179–183. https://doi.org/10.1002/gcc.20629

Xing M, Peterman MC, Davis RL et al (2016) GOLPH3 drives cell migration by promoting Golgi reorientation and directional trafficking to the leading edge. Mol Biol Cell 27:3828–3840. https://doi.org/10.1091/mbc.E16-01-0005

Yamashita RA, Sellers JR, Anderson JB (2000) Identification and analysis of the myosin superfamily in Drosophila: a database approach. J Muscle Res Cell Motil 21:491–505

Yanaihara N, Nishioka M, Kohno T et al (2004) Reduced expression ofMYO18B, a candidate tumor-suppressor gene on chromosome arm 22q, in ovarian cancer. Int J Cancer 112:150–154. https://doi.org/10.1002/ijc.20339

Yang C-H, Szeliga J, Jordan J et al (2005) Identification of the surfactant protein A receptor 210 as the unconventional myosin 18A. J Biol Chem 280:34447–34457. https://doi.org/10.1074/jbc.M505229200

Yang L, Carrillo M, Wu YM et al (2015) SP-R210 (Myo18A) isoforms as intrinsic modulators of macrophage priming and activation. PLoS One 10:e0126576. https://doi.org/10.1371/journal.pone.0126576

Zhang Z, Zhu J, Huang Y et al (2018) MYO18B promotes hepatocellular carcinoma progression by activating PI3K/AKT/mTOR signaling pathway. Diagn Pathol 13:85. https://doi.org/10.1186/s13000-018-0763-3

Myosin XIX

20

Jennifer L. Bocanegra, Rebecca Adikes, and Omar A. Quintero

Abstract

The birth of widely available genomic databases at the turn of the millennium led to the identification of many previously unknown myosin genes and identification of novel classes of myosin, including MYO19. Further sequence analysis has revealed the unique evolutionary history of class XIX myosins. MYO19 is found in species ranging from vertebrates to some unicellular organisms, while it has been lost from some lineages containing traditional experimental model organisms. Unique sequences in the motor domain suggest class-specific mechanochemistry that may relate to its cellular function as a mitochondria-associated motor. Work over the past 10 years has demonstrated that MYO19 is an actin-activated ATPase capable of actin-based transport, and investigation of some of the conserved differences within the motor domain indicate their importance in MYO19 motor activity. The cargo-binding MyMOMA tail domain contains two distinct mechanisms of interaction with mitochondrial outer membrane components, and perturbation of MYO19 expression leads to alterations in mitochondrial movement and dynamics that impact cell function. This chapter summarizes the current state of the field and highlights potential new directions of inquiry.

Keywords

Actin · Myosin · Mitochondria · Motility

20.1 Introduction

Myosin-XIX (MYO19) was discovered as a consequence of early genome sequencing initiatives cataloging myosin sequences in common research organisms: human, mouse, *C. elegans, D. melanogaster, A. thaliana, S. cerevisiae, S. pombe, and D. discoideum* (Berg et al. 2001). At the time, it was one of 9 uncharacterized myosins predicted by sequence analysis. Fourteen uncharacterized myosins in total were identified as members of a superfamily of 39 human myosin genes. As it shared at most ~35% sequence identity with other myosin motor domains and

Authors Jennifer L. Bocanegra and Rebecca C. Adikes have equally contributed to this chapter.

J. L. Bocanegra
Department of Biochemistry, University of Washington, Seattle, WA, USA

R. Adikes
Department of Biochemistry and Cell Biology, Stony Brook University, Stony Brook, NY, USA

O. A. Quintero (✉)
Department of Biology, University of Richmond, Richmond, VA, USA
e-mail: oquinter@richmond.edu

L. M. Coluccio (ed.), *Myosins*, Advances in Experimental Medicine and Biology 1239,
https://doi.org/10.1007/978-3-030-38062-5_20

phylogenetic analysis indicated that it did not group with other known classes, it was suggested that it might represent a novel class and was not assigned a class designation.

Early reports indicated that it was vertebrate-specific (Quintero et al. 2009), as orthologs could be identified in mouse, chicken, *Xenopus,* and zebrafish. As more species were sequenced, the evolutionary history of MYO19 gained more resolution. MYO19 is found in species ranging from vertebrates to unicellular holozoans (Sebe-Pedros et al. 2014). It is also found in platyhelminths, arthropods, mollusks, annelids, echinoderms, cnidarians, hemichordates, and chordates (Kollmar and Muhlhausen 2017; Odronitz and Kollmar 2007) (Fig. 20.1). Expressed sequence tag analysis, northern blot analysis, and western blot analysis all indicate that MYO19 is expressed at varying levels across many tissue and cell types (Quintero et al. 2009). With respect to experimental approaches, it is in some ways unfortunate that MYO19 has been lost from lineages leading to two common model systems (Fig. 20.1), as studies in whole organisms like flies and roundworms could greatly enhance our knowledge of the role of MYO19 in the physiological function of particular tissues and organs.

20.2 Sequence and Structure

Full-length MYO19 protein consists of an N-terminal motor domain, a neck region containing three IQ motifs and a short MYO19-specific mitochondrial outer membrane association (MyMOMA) tail domain (Fig. 20.2). Most orthologs are ~1000 amino acids in length with human MYO19 consisting of 970 amino acids. The motor domain of MYO19 contains a Walker-A ATPase domain. The P-loop, switch I, and switch II motifs in myosin motors are responsible for coordinating to the phosphates of ATP (Smith and Rayment 1996) and (along with other regions of the motor domain) participating in the mechanochemical linkage between ATP hydrolysis, actin binding, lever arm position, and force generation (Cope et al. 1996). MYO19 has a number of class-specific differences in its motor domain hypothesized to impact motor activity (Adikes et al. 2013), and one of the most well-conserved is at the amino acid position following the P-loop. While most other myosins have a valine or glutamic acid immediately following the P-loop, the most common residue at that position among MYO19 paralogs is the bulkier tryptophan. Echinoderms, cnidarians, hemichordates and chordates all contain tryptophan at that position, while a subset of class XIX myosins from arthropods contain a phenylalanine at this position, which is also bulky (Fig. 20.1). Based on its size and position, interactions between the ring structure of the side-chain and the ring structure of the nucleotide could influence nucleotide binding or nucleotide release. Platyhelminthes (E), mollusks (V), annelids (V) and a subset of arthropods (C or E) have residues more commonly found in other myosins at that position. Other well-conserved differences exist within the core of the MYO19 motor domain, such as the GNAKT motif in switch I. This residue is often a lysine in many myosin families, but it is much more variable across MYO19 orthologs. Cysteine often exists in that position in mammalian MYO19, whereas in other lineages, glutamine, alanine, or glycine are present. As the functional significance is difficult to predict from sequence analysis and modeling, biochemical and kinetic analyses may be required to reveal the role that such class-specific structures play in myosin function. It remains to be seen whether individual amino acids contribute significantly to the mechanochemical properties of MYO19, or if the suite of conserved differences function as an ensemble to influence the properties of the motor.

Potentially significant conserved differences exist within the MYO19 motor domain that are distinct from other myosin classes. MYO19 contains the actin-binding interface loops and subdomains, loop 2, loop 3, loop 4, helix-turn-helix and hypertrophic cardiomyopathy (HCM) loop. The net charges of each of these loops differ from those found in other myosins, and these differences have been hypothesized to influence the high affinity of Myo19 for actin (Adikes et al. 2013). Additionally, the converter domain contains two short insertions totaling 30–35 amino

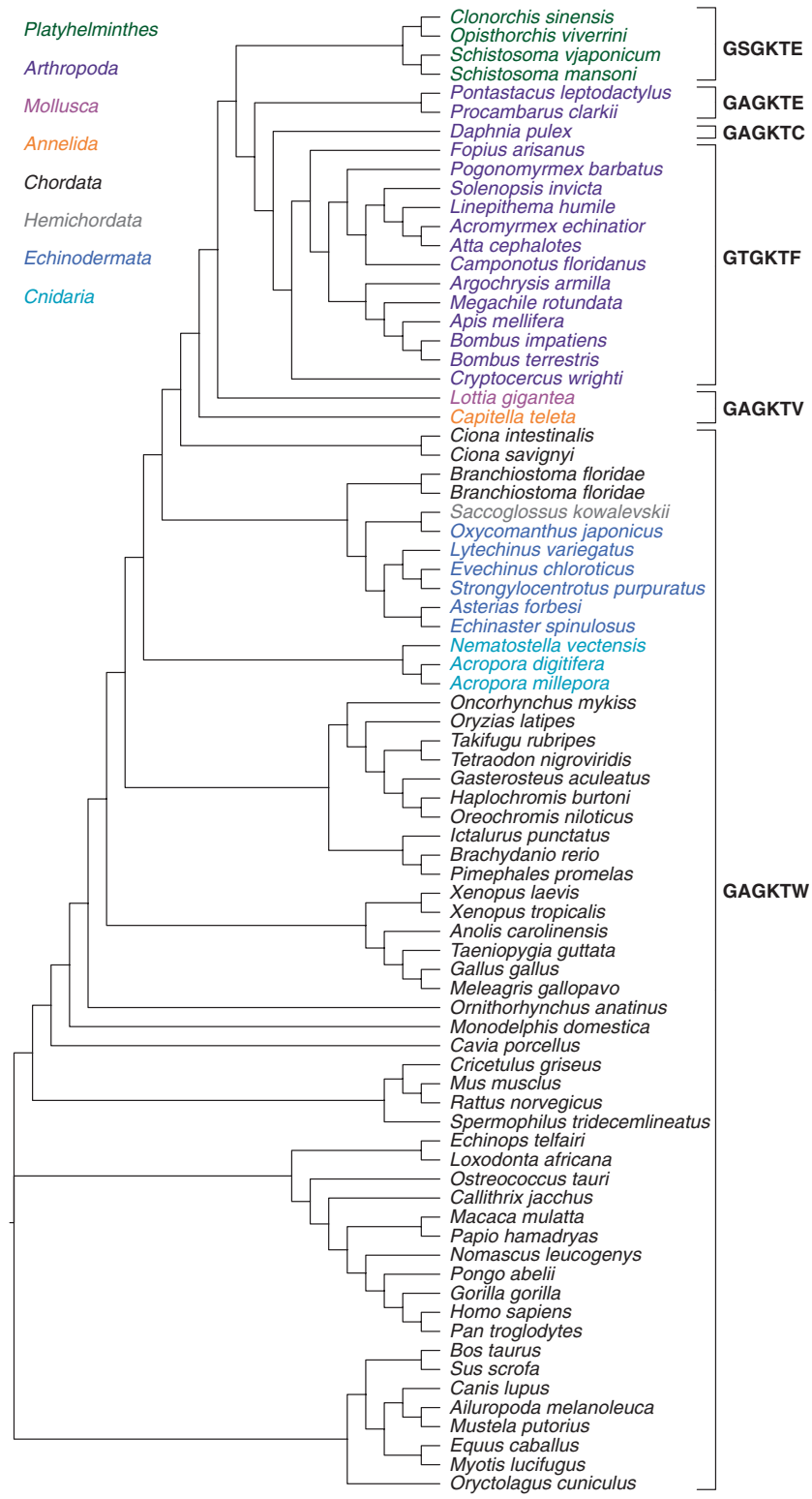

Fig. 20.1 Myosin XIX orthologs have been identified in many species. An unrooted phylogenetic tree of 78 Myo19 orthologs from invertebrates, including flatworms *Platyhelminthes* (green), arthropods *Arthropoda* (purple), mollusks *Mollusca* (light purple), annelids *Annelida* (orange), echinoderms *Echinodermata* (blue) and *Cnidaria* (cyan), to hemichordates *Hemichordata* (grey) and chordates *Chordata* (black). The sequence for the P-Loop is shown to the right for each species; most contain a bulky W or F immediately following the P-Loop (69/78)

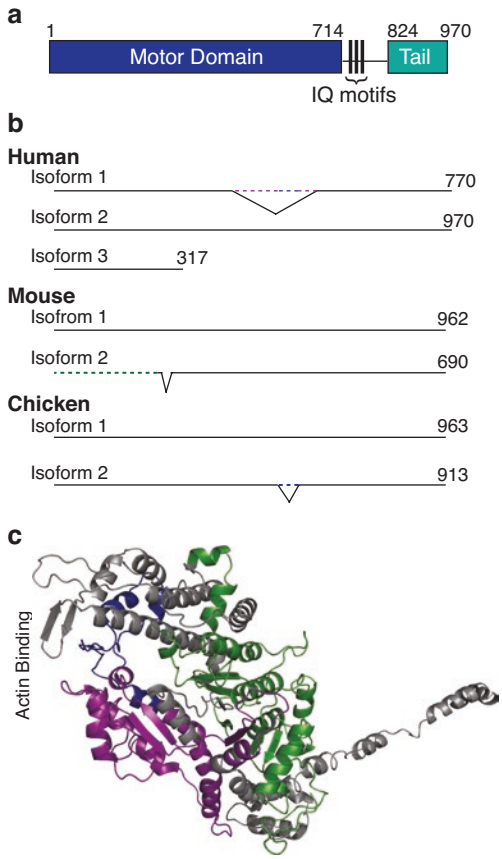

Fig. 20.2 Structural architecture of Myosin XIX. (**a**) Human MYO19 consists of a motor domain, neck region with three IQ motifs, and a short tail domain. (**b**) Some data exist indicating that certain species may contain multiple splice isoforms of MYO19, including human, mouse, and chicken. (**c**) A Phyre-threaded model (Kelley et al. 2015) where the regions of the motor domain excluded from various isoforms are highlighted: human isoform 1 (purple and blue), mouse isoform 2 (green) and chicken isoform 2 (blue). The expression patterns and potential functional roles of these truncated isoforms remain to be elucidated

acids. These insertions are located approximately within the converter domain itself, while the "reverse gear" insertion in MYO6 is located after the converter (Adikes et al. 2013; Menetrey et al. 2005). Studies using recombinant MYO19 in *in vitro* gliding assays indicate that unlike MYO6 (Wells et al. 1999), MYO19 is a plus-end directed motor (Lu et al. 2014). Threaded models indicate that the MYO19 insertions may be located in close proximity to the end of the relay helix, potentially influencing the coordination of ATP hydrolysis and lever-arm position (Lu et al. 2014), but such hypotheses will need to be examined through structural studies.

The Myo19 neck contains three IQ motifs (Quintero et al. 2009), and when recombinant human MYO19 was generated in the presence of calmodulin, MYO19 co-purified with calmodulin at the stoichiometries expected for the number of IQ motifs present in the construct (Adikes et al. 2013). However, the consensus sequences of the MYO19 IQ motifs (IQ1, AXXIQXXWRR; IQ2, AAXXIQAAXRSWLXIXXH; IQ3, AAXXIKXXWXXWRXXLA) (Lu et al. 2014) indicate that they are divergent from calmodulin-binding IQ motifs found in other myosins (IQXXXRGXXXR) (Cheney and Mooseker 1992). When MYO19 expressed in Sf9 cells is mixed with kidney extract, MYO19 copurifies with other regulatory light chains such as RLC9, RLC12a or RLC12b. Coexpression assays demonstrate that IQ motifs 1 and 3 have a higher affinity for RLC9, while IQ motif 2 binds RLC9 and RLC12b approximately equally (Lu et al. 2014). Taken together, these data indicate that the IQ motif occupancy may depend on the light-chain expression profile of the cell type and tissue where MYO19 is expressed.

The most C-terminal region of the full-length MYO19 protein consists of a sequence of ~150 amino acids that is enriched for basic residues. Sequence analysis was not particularly useful in identifying the function of this domain, as homology searches did not identify other proteins or genes in the database with similar sequences (Quintero et al. 2009). However, this region, known as the **MY**O19-specific **m**itochondria **o**uter **m**embrane **a**ssociation domain (MyMOMA), is well conserved within the MYO19 family (Adikes et al. 2013). In addition to contributing to the overall high pI of the MyMOMA domain (~9.1 in human MYO19), many of the basic residues are conserved across species and have been shown to play a role in the interaction with mitochondrial membranes (Bocanegra et al. 2019; Hawthorne et al. 2016; Shneyer et al. 2016).

Of interesting note, according to NCBI databases, MYO19 may have multiple isoforms in

human, mouse, and chicken (Fig. 20.2). In addition to a full-length isoform containing a complete motor domain, neck and tail, the other isoforms lack some region of the motor domain. Which region is missing varies from species to species. In humans and chicken, the region encompassing loop 2 is missing, while the isoform in mice lacks the N-terminal half of the motor domain (Fig. 20.2). There is experimental evidence for alternative splicing leading to other myosins with altered motor domain structures that are expressed in cells and tissues (Sousa et al. 2006); however, data do not yet exist on whether MYO19 alternate splice-forms are expressed, and their cellular roles have yet to be determined.

20.3 Motor Domain Biochemistry

In addition to sequence homology of the core motor domain to other members of the myosin superfamily, the motor domain of MYO19 also contains enzymatic activity that is a hallmark of most of the members of the myosin superfamily – an actin-activated ATPase activity (Adikes et al. 2013). The intrinsic *in vitro* ATPase activity in the absence of actin is relatively low (~0.03 s^{-1}, Table 20.1), as has been demonstrated by multiple research groups (Adikes et al. 2013; Lu et al. 2014; Usaj and Henn 2017). The maximal rate of actin-activated ATPase activities reported varies slightly from 2.7 to 4.2 s^{-1} for constructs containing all 3 IQ-motifs, an increase of more than 50-fold (Adikes et al. 2013; Lu et al. 2014; Usaj and Henn 2017). These differences may be due to the experimental conditions, the species of the myosin, the expression system, and/or the purification methods used. Some variability in maximal steady-state ATPase rate would be expected due to the number of IQ motifs present in the construct (Adikes et al. 2013; Lu et al. 2014). The concentration of actin at which MYO19 displayed half its maximal ATPase activity, K_{ATPase}, ranged from 12 to 20 μM. Lu et al. also demonstrated a mild sensitivity of motor activity of the 1-IQ construct to ionic strength and that the presence of RLC9 and RLC12b as regulatory light-chains enhanced the steady-state ATPase rate of the 3-IQ construct. However, phosphorylation of RLC9 or RLC12b did not seem to impact the ATPase activity or gliding velocity of MYO19 constructs. MYO19 ATPase activity and actin gliding velocity were strongly inhibited by increasing concentrations of ADP, a property of high duty ratio motors where ADP release is the rate-limiting step (Lu et al. 2014).

MYO19 is capable of translocating actin filaments *in vitro* at velocities ranging from 50 to 200 nm/s (Adikes et al. 2013; Lu et al. 2014). This four-fold difference in apparent rate may be due to the method used to attach the motor domain to the coverslip. While Adikes et al. used antibodies to the most-C-terminal portion of their construct to capture MYO19 on the coverslip surface, Lu et al. biotinylated their construct and then used biotinylated BSA and streptavidin to attach the motor to the coverslip. Lu et al. also

Table 20.1 Kinetic parameters of the MYO19 motor domain measured *in vitro*

	V_0 (s^{-1})	V_{max} (s^{-1})	K_{ATPase} (μM)	Velocity (nm/s)
Human MYO19-1IQ (Adikes et al. 2013)	0.034 ± 0.002	2.2 ± 0.2	20.1 ± 3.7	
Human MYO19-3IQ (Adikes et al. 2013; Ušaj and Henn 2017)	0.03 ± 0.01, 0.06 ± 0.02	2.7 ± 0.2, 3.1 ± 0.1	26.5 ± 5.4, 11.6 ± 1.2	218 ± 39, na
Human MYO19-3IQ^{W140V} (Shneyer et al. 2017)	0.10 ± 0.05	4.1 ± 0.4	56.7 ± 10.9	
Mouse MYO19-1IQ (Lu et al. 2014)	0.032 ± 0.001	6.75 ± 0.33	15.2 ± 4.0	27.1 ± 1.2
Mouse MYO19-3IQ (Lu et al. 2014)	0.035 ± 0.001	4.20 ± 0.72	20.0 ± 6.8	46.8 ± 4.7

These data are summarized from (Adikes et al. 2013; Lu et al. 2014; Shneyer et al. 2017; Usaj and Henn 2017)
V_0 indicates the rate of intrinsic ATPase activity, V_{max} is the maximal actin-activated ATPase rate, K_{ATPase} is the actin concentration at which the ATPase rate is 50% of the maximal value, and Velocity is the rate at which actin filaments were translocated in *in vitro* gliding assays

demonstrated that the directionality of MYO19 was towards the plus-end of actin and that samples with high MYO19 motor density tended to shred the actin filaments, lending evidence to the hypothesis that MYO19 is a high-duty ratio motor (Lu et al. 2014).

Adikes et al. used actin-cosedimentation assays to indicate that MYO19 populates high actin affinity states during its ATPase cycle as measured under steady-state conditions. MYO19 has a K_{actin} for cosedimentation lower than the K_{ATPase} for ATPase rate, which is a property of high duty ratio motors (Howard 2001). They also hypothesized that MYO19 might be a high duty ratio motor, suggesting that amino acid differences near the P-loop and in the actin-binding loops might contribute to the particular mechanochemical properties of MYO19 (Adikes et al. 2013).

Some of the first evidence describing the amino acid sequences responsible for MYO19's high duty ratio came from two reports by the Henn research group using the sequence for the human MYO19 motor domain expressed in suspension cultures of HEK293 cells (Shneyer et al. 2017; Usaj and Henn 2017). ATP binding to the acto-MYO19 motor domain involves an isomerization step from a "closed" to an "open" state prior to ATP binding and actin dissociation. Transient kinetic analysis also demonstrated that MYO19 has a very high affinity for ADP, which contributes to ADP release as a component of the rate-limiting steps for ATP hydrolysis and product release. Phosphate release was shown to be sufficiently rapid to not contribute to limiting the ATPase cycle when actin is present. Kinetic models that incorporated the measured steady-state and transient kinetic parameters also indicated that MYO19 is a high duty ratio motor where continuous movement along actin filaments might require assembly of monomeric motors into functional ensembles as would occur when multiple motors are bound to a single cargo (Usaj and Henn 2017). Mutation of the class XIX-specific tryptophan, W140, to valine resulted in a 25% increase in the maximal steady-state actin-activated ATPase rate, with changes to individual kinetic parameters. $MYO19^{W140V}$ showed a four-fold decrease in the second-order association rate constant of ATP for acto-MYO19, a ten-fold decrease in ADP affinity, a five-fold increase in K_{ATPase}, and a lower duty ratio, indicating that W140 is involved in establishing the enzymatic activities that relate to particular cellular roles in mitochondrial transport (Shneyer et al. 2017).

20.4 MyMOMA Domain Biochemistry

The initial identification of mitochondria as the cargo of MYO19 was demonstrated via immunostaining of primate cells for endogenous MYO19 using an antibody generated against a short peptide sequence found C-terminal to the third IQ motif (Quintero et al. 2009). Ectopic expression of human MYO19 truncations revealed that the C-terminal ~150 amino acids were necessary and sufficient for GFP-tagged MYO19 constructs to localize to mitochondria, as constructs containing the motor domain and IQ motifs failed to localize to mitochondria, while constructs consisting of the tail domain did localize to mitochondria. Quintero et al. demonstrated that the interaction between MYO19 and the mitochondrial outer membrane was unlikely to be via a C-terminal α-helical transmembrane insertion, as constructs tagged with GFP at the C-terminus localized to mitochondria (Quintero et al. 2009). FRAP analysis revealed that mitochondria-localizing MYO19 constructs that contained the MyMOMA domain exchanged extremely slowly with other cellular pools, suggesting a strong interaction between MYO19 and the mitochondrial outer membrane. Additionally, endogenous MYO19 could be released from mitochondria-enriched fractions by treatment with high pH buffer, indicating that the mechanism of binding was at least partially based on electrostatic interactions (Hawthorne et al. 2016; Shneyer et al. 2016).

The ~150 amino acids C-terminal to the third IQ motif make up the MyMOMA domain, and in addition to having a high pI of approximately 9.1 (human), there are many well-conserved basic

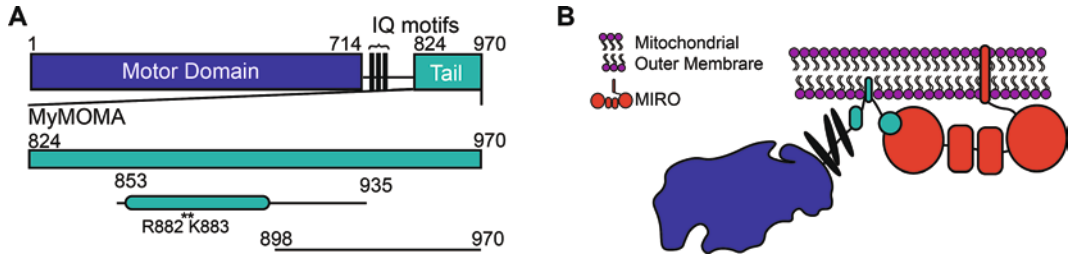

Fig. 20.3 The MyMOMA domain of the MYO19 tail facilitates mitochondrial interactions. (**a**) The ~150 amino acids C-terminal to the third IQ motif make up the MyMOMA domain. The region encompassing resides 853–935 localizes to mitochondria. A putative monotopic α-helical insertion motif lies within amino acids 860–890 (teal domain). Additionally, R882 and K883 are important in establishing the membrane specificity of MYO19 binding. The region encompassing residues 898–970 has been shown to interact with MIRO proteins. (**b**) Schematic of MYO19 mitochondrial interactions: insertion of the central region of MyMOMA into the mitochondrial outer membrane and C-terminal region interaction with MIRO

residues within this domain (Hawthorne et al. 2016) (Fig. 20.3). Using sequence analysis to identify regions of low conservation within the tail, Hawthorne et al. generated truncation constructs of the MYO19 tail in an attempt to identify the minimal region necessary for mitochondrial localization. Constructs containing amino acids 853–935 of human MYO19 were able to localize to mitochondria (Hawthorne et al. 2016). In addition, these constructs also displayed slow FRAP recovery kinetics, similar to constructs containing the full MyMOMA domain. Sequential mutation of amino acids that are well-conserved in mouse and human revealed that amino acids R882 and K883 are important in establishing the membrane specificity of MYO19 binding, as their paired mutation to alanine results in an interesting phenotype where GFP-tagged MYO19$^{RK882\text{-}883AA}$ constructs localized to the endoplasmic reticulum rather than to mitochondrial membranes (Hawthorne et al. 2016).

Shneyer and colleagues verified that MYO19 resides on the cytosol-facing side of the mitochondrial outer membrane, as treatment of isolated mitochondria with proteases resulted in the digestion of MYO19 in the absence of detergent (Shneyer et al. 2016). These assays also indicated that the C-terminus of MYO19 is accessible to the cytosol consistent with monotopic insertion of MYO19 into the mitochondrial outer membrane. Using proteomics and sequence analysis approaches, they were able to predict a putative monotopic α-helical insertion motif within amino acids 860–890 of the human MYO19 sequence. Expression of MYO19$^{860–890}$-GFP resulted in mitochondrial localization, and expression of constructs lacking this sequence displayed significantly reduced mitochondrial localization. Mutation of R882 and K883 to serine in this construct also resulted in a switch to ER localization (Shneyer et al. 2016). Peptides matching this sequence (851–895) incubated with small unilamellar liposomes with similar lipid composition to the mitochondrial outer membrane displayed similar binding characteristics to what was observed with the GFP-tagged constructs in cells and what was observed with endogenous MYO19 in cell-based assays – resistance to high salt extraction and strong affinity for binding the membranes.

Recent reports suggest a connection between MYO19 and MIRO proteins (Bocanegra et al. 2019; Lopez-Domenech et al. 2018; Oeding et al. 2018). MIRO1 and MIRO2 are a divergent family of small GTPases found on the mitochondrial outer membrane (Reis et al. 2009). They have been shown to play roles in microtubule-based mitochondrial traffic (Babic et al. 2015; Fransson et al. 2006; Russo et al. 2009) and in mitochondrial fission/fusion dynamics (Misko et al. 2010). Multiple groups have demonstrated potential MYO19/MIRO interactions using promiscuous biotinylation/proteomics approaches (Bocanegra et al. 2019; Oeding et al. 2018). Embryonic fibroblasts derived from MIRO1/MIRO2 double-knockout mice show significantly decreased

levels of MYO19 (Lopez-Domenech et al. 2018) as do cultured mammalian cells knocked down for MIRO1 and MIRO2 via shRNA (Oeding et al. 2018). This loss of MYO19 levels is likely due to degradation of MYO19 via ubiquitination and proteasome-mediated degradation. The MIRO-interacting region is contained within the C-terminal ~72 amino acids (based on human sequence) and is distinct from the monotopic membrane insertion (Oeding et al. 2018). Ectopic expression of MIRO constructs enhances localization of fluorescently tagged MYO19$^{898–970}$ constructs, although inconsistencies exist between published reports as to whether the N-terminal GTPase domain of MIRO is sufficient to mislocalize MYO19$^{898–970}$ constructs (Bocanegra et al. 2019; Oeding et al. 2018). FRAP kinetics indicate that the MIRO/MYO19$^{898–970}$ interaction exchanges faster than the interaction of the mitochondrial outer membrane with the monotopic insertion motif, and MIRO interaction may be dependent on the nucleotide state of the N-terminal MIRO domain (Bocanegra et al. 2019). Well-conserved basic residues on MYO19 and acidic residues on MIRO may be involved in mediating MYO19/MIRO interactions. Constructs lacking the MIRO-interacting region but still containing the membrane-insertion motif were likely able to localize at the membrane when overexpressed, saturating proteasome-mediated degradation pathways, which allowed for the slower membrane insertion events to occur. Bocanegra and colleagues hypothesized that MIRO interactions provide an initial, weak interaction between MYO19 and the mitochondrial outer membrane, which then facilitates membrane insertion (Bocanegra et al. 2019).

20.5 MYO19 and Cell Physiology

20.5.1 Ectopic Expression of MYO19 Influences Mitochondrial Motility and Shape

The majority of MYO19 immunofluorescence signal colocalizes with mitochondria under typical cell culture conditions (Quintero et al. 2009). Ectopic expression of fluorescently-tagged MYO19 results in a variety of phenotypes depending on the construct being expressed, expression level of the tagged protein, and the cell type in which the protein is expressed (Adikes et al. 2013; Hawthorne et al. 2016; Lopez-Domenech et al. 2018; Oeding et al. 2018; Quintero et al. 2009; Rohn et al. 2014; Shneyer et al. 2016, 2017). Expression of full-length GFP-MYO19 in A549 pulmonary epithelial cells results in mitochondrial localization of the GFP-fluorescence and increased dynamics of the mitochondrial network (Quintero et al. 2009). The increase in mitochondrial dynamics was shown to be actin-dependent as treatment with actin-depolymerizing drugs halted mitochondrial movements. Expression of constructs lacking the motor domain or constructs containing a putative rigor-binding mutant did not lead to increased mitochondrial motility, indicating that motor activity plays a role in the observed phenotype (Adikes et al. 2013; Quintero et al. 2009). In some instances, expression of constructs lacking the motor domain behaved in an dominant-negative fashion, interfering with MYO19 function (Oeding et al. 2018; Shneyer et al. 2016).

Under conditions where mitochondrial motility was enhanced, many of the mitochondria moved with a leading end, and the leading end was wider than the trailing end; this shape distortion was also shown to be actin-dependent (Quintero et al. 2009). As the tadpole-shaped moving mitochondria resembled polymerization-induced *Listeria* motility, Quintero and colleagues attempted to address whether MYO19-mediated mitochondrial motility was driven by polymerization-mediated pushing, but no obvious actin accumulations associating with mitochondria were observed via the currently-available technology – wide-field epi-fluorescence (Quintero et al. 2009). Refinement of fluorescence microscopy approaches led to the discovery of mitochondria-associated actin clouds that influence the organelle sizes present in the mitochondrial network (Moore et al. 2016). A more careful investigation of the geometry of the actin associated with mitochondria during

MYO19-mediated motility using modern imaging approaches is now possible and worth investigating.

Certain stress conditions result in additional cellular localizations of MYO19 (Shneyer et al. 2016, 2017). Glucose starvation and oxidative stress result in the formation of actin-filled protrusions known as filopodia. MYO19 localizes to a subset of these structures in stressed U-2OS osteosarcoma cells. MYO19 localized more strongly to filopodia induced by cells ectopically expressing an unregulated GFP-mDia2 than to filopodia induced by GFP-MYO10 expression (Shneyer et al. 2017). Motor activity is necessary for tip-localization of fluorescently-tagged MYO19 as rigor mutation or the W140V mutation, which decreases the duty ratio, did not localize to filopodial tips (Shneyer et al. 2017). Mitochondria markers colocalize with MYO19 at stress-induced filopodial tips, suggesting that MYO19 might be transporting mitochondria to actin-protrusions (Shneyer et al. 2016). It remains to be seen if MYO19 is involved in the potential organelle transport between cells via tunneling nanotubes (Babenko et al. 2018; Sartori-Rupp et al. 2019), another actin-rich cellular protrusion capable of connecting two different cells.

20.5.2 Depletion of MYO19 Protein Reveals Cellular Function(s)

Loss of MYO19 leads to observable phenotypes in mitochondrial position and distribution, and in some instances altered cellular physiology. Interfering RNA approaches revealed a less dispersed mitochondrial distribution in HeLa cells (Oeding et al. 2018) and hTert-RPE1 cells (Capmany et al. 2019), but not in U2-OS cells (Shneyer et al. 2016). Knockdown of MYO19 also led to decreased numbers of filopodia in HeLa cells (Rohn et al. 2011) as well as decreased filopodial number and inhibition of MYO19 transport into stress-induced filopodia in U2-OS cells (Shneyer et al. 2016).

A siRNA screen of the "actinome" identified MYO19 as a novel regulator of cell division in HeLa cells as MYO19 knockdown led to an increase in the percentage of multinucleate cells (Rohn et al. 2011). Closer investigation revealed that in addition to an increase in the percentage of multinucleate cells present in a population, MYO19 knockdown resulted in an increase in the population of cells failing at cytokinesis (Rohn et al. 2014) (Fig. 20.4). The cytokinesis failure/multinucleate cell phenotype could be phenocopied by inhibiting mitochondrial fission via treatment with the drug mDivI. Additionally, the cytokinesis phenotype in MYO19 siRNA cell samples could be partially rescued by knockdown of a component of the mitochondrial fusion machinery, MFN2. Taken together, these data suggest that the mitochondrial particle size present in the network was interfering with cytokinesis, potentially via physical interference with the cytokinetic ring closure.

A second phenotype was observed in MYO19 siRNA-treated cells that did complete cytokinesis – there was an asymmetry in the mitochondrial dosage of each daughter cell (Rohn et al. 2014) (Fig. 20.4). This asymmetry was unlikely due to mitochondrial network particle size as cotreatment with siRNA targeting MFN2 did not rescue the asymmetry in mitochondrial inheritance between daughter cells. However, ectopic expression of mouse GFP-MYO19 refractory to the MYO19 siRNA did rescue the asymmetry in mitochondrial distribution between daughter cells, supporting the hypothesis that MYO19 motor activity contributes to the proper spatial arrangement necessary for symmetric partitioning of mitochondria during mitosis. Asymmetric mitochondrial distribution was also observed in MEF isolated from MIRO1/2 double knockout mice (Lopez-Domenech et al. 2018), which have diminished levels of MYO19. Ectopic expression of MYO19 also rescued the asymmetry in mitochondrial distribution in these cells as well. The long-term consequence of uneven mitochondrial distribution into daughter cells following cell division has yet to be investigated. It has not yet been determined whether there is a specific subset of mitochondria whose motility is being mediated via MYO19 during cell division (Katajisto et al. 2015).

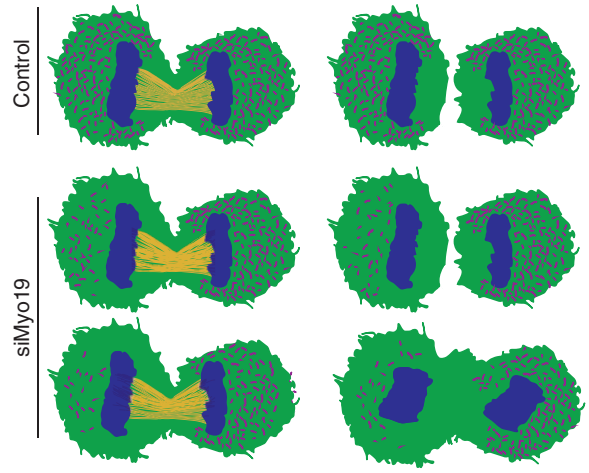

Fig. 20.4 Loss of MYO19 leads to cytokinetic failure and asymmetric inheritance of mitochondria. Summary of results from Rohn et al. (2011, 2014). MYO19 knockdown leads to an increase in multinucleate cells due to cells failing cytokinesis. Additionally, many cells are unable to distribute mitochondria equally between daughter cells, leading to asymmetric inheritance of mitochondria

20.6 Future Directions and Connections to Health and Physiology

Little is known about the physiology and pathological consequences associated with MYO19 function. It is interesting to note that *MYO19* has been identified as a potential gene associated with skeletal muscle development. One study looking at genetic differences among horse breeds suggested that variants of *MYO19* could play a role in muscle development in halter horses (Avila et al. 2018). Additionally, two individual studies, one on thoroughbred horses and another on young human males, analyzed transcriptome data before and after a period of extended high intensity training and found *MYO19* to be significantly upregulated (Bryan et al. 2017; Miyamoto-Mikami et al. 2018). This suggests a potential physiological role in mammals that is worthy of investigation.

Due to the large amounts of sequencing data currently available, new areas of research are being defined. Examination of MYO19 sequence variations in different types of cancers revealed that MYO19 sequence differences are highly represented in certain cancers (Hudson et al. 2010), namely gall bladder/cholangiocarcinoma (31/71 donors affected), melanoma (two studies: 32/100 and 56/183), pulmonary carcinoma (45/170), and leiomyosarcoma (14/67). Gene fusions are a well-known mechanism for oncogene activation in some cancers. Using RNA sequencing, Edgren et al. found a fusion between MYO19 and the spindle- and kinetochore-associated complex subunit 2 (SKA2) in breast cancer cell lines (Edgren et al. 2011), suggesting that *SKA2-MYO19* could play a role in oncogene activation. Additional case- and genome-wide association studies have identified *MYO19* as a potential gene involved in ovarian cancer, pancreatic ductal adenocarcinoma, and breast cancer, among others (Choi et al. 2015; Kohutek et al. 2017; Novak et al. 2015; Permuth et al. 2016; Zhang et al. 2017). Copy number variations in chromosome 17q where *MYO19* is deleted has also been linked to cancer (Jalali et al. 2015), as well as neurological and psychiatric diseases such as epilepsy (Catarino et al. 2011), ADHD (Martin et al. 2014), autism, schizophrenia (Moreno-De-Luca et al. 2010), and developmental disorders (Hinkes et al. 2012; Roberts et al. 2014; Sandbacka et al. 2013; Tsuiko et al. 2016). Although the particular MYO19 misfunction caused by these mutations or the physiological consequence is not readily

apparent, the high frequency of MYO19 mutations in multiple pathophysiologies warrants further investigation. As future researchers combine traditional cell biological approaches with modern informatic and quantitative methods, our deeper understanding of this unique and interesting myosin class will illuminate our understanding of cell physiology, motor protein function, and motor protein evolution.

Acknowledgements Myosin XIX studies by OAQ began as part of his NIH-IRACDA-funded postdoctoral fellowship with Richard Cheney at the University of North Carolina, Chapel Hill. OAQ is grateful to Richard Cheney and the greater cytoskeleton community at UNC. Additionally, the work was supported by The Franklin & Marshall College Department of Biology, The Whitman Summer Fellows Program at the MBL, Mount Holyoke College Department of Biology, and The Pennsylvania State University College of Medicine Department of Cellular & Molecular Physiology during OAQ's appointments at each of those institutions. The studies were also supported by Ernest Everett Just Endowed Research Fellowship, Robert Day Allen Fellowship, and The Laura & Arthur Colwin Endowed Summer Research Fellowship from the MBL, as well as K01CA160667 & R15GM119077 from NIH. OAQ would like to thank Margaret Titus (University of Minnesota) and Christopher Yengo (Penn State College of Medicine) for their mentorship in the marvelous world of myosins, and the 60+ undergraduate researchers who have made discovery-based science a joy to share.

References

Adikes RC, Unrath WC, Yengo CM, Quintero OA (2013) Biochemical and bioinformatic analysis of the myosin-XIX motor domain. Cytoskeleton (Hoboken) 70(5):281–295

Avila F, Mickelson JR, Schaefer RJ, McCue ME (2018) Genome-wide signatures of selection reveal genes associated with performance in American quarter horse subpopulations. Front Genet 9:249

Babenko VA, Silachev DN, Popkov VA, Zorova LD, Pevzner IB, Plotnikov EY, Sukhikh GT, Zorov DB (2018) Miro1 enhances mitochondria transfer from Multipotent Mesenchymal Stem Cells (MMSC) to neural cells and improves the efficacy of cell recovery. Molecules 23(3)

Babic M, Russo GJ, Wellington AJ, Sangston RM, Gonzalez M, Zinsmaier KE (2015) Miro's N-terminal GTPase domain is required for transport of mitochondria into axons and dendrites. J Neurosci 35(14):5754–5771

Berg JS, Powell BC, Cheney RE (2001) A millennial myosin census. Mol Biol Cell 12(4):780–794

Bocanegra JL, Fujita BM, Melton NR, Cowan JM, Schinski EL, Tamir TY, Major MB, Quintero OA (2019) The MyMOMA domain of MYO19 encodes for distinct Miro-dependent and Miro-independent mechanisms of interaction with mitochondrial membranes. Cytoskeleton (Hoboken), Sep 3. https://doi.org/10.1002/cm.21560

Bryan K, McGivney BA, Farries G, McGettigan PA, McGivney CL, Gough KF, MacHugh DE, Katz LM, Hill EW (2017) Equine skeletal muscle adaptations to exercise and training: evidence of differential regulation of autophagosomal and mitochondrial components. BMC Genomics 18(1):595

Capmany A, Latge B, Schauer K (2019) Analysis of organelle positioning using patterned microdevices. Curr Protoc Cell Biol 82(1):e77

Catarino CB, Kasperaviciute D, Thom M, Cavalleri GL, Martinian L, Heinzen EL, Dorn T, Grunwald T, Chaila E, Depondt C et al (2011) Genomic microdeletions associated with epilepsy: not a contraindication to resective surgery. Epilepsia 52(8):1388–1392

Cheney RE, Mooseker MS (1992) Unconventional myosins. Curr Opin Cell Biol 4(1):27–35

Choi YJ, Jung SH, Kim MS, Baek IP, Rhee JK, Lee SH, Hur SY, Kim TM, Chung YJ, Lee SH (2015) Genomic landscape of endometrial stromal sarcoma of uterus. Oncotarget 6(32):33319–33328

Cope MJ, Whisstock J, Rayment I, Kendrick-Jones J (1996) Conservation within the myosin motor domain: implications for structure and function. Structure 4(8):969–987

Edgren H, Murumagi A, Kangaspeska S, Nicorici D, Hongisto V, Kleivi K, Rye IH, Nyberg S, Wolf M, Borresen-Dale AL et al (2011) Identification of fusion genes in breast cancer by paired-end RNA-sequencing. Genome Biol 12(1):R6

Fransson S, Ruusala A, Aspenstrom P (2006) The atypical Rho GTPases Miro-1 and Miro-2 have essential roles in mitochondrial trafficking. Biochem Biophys Res Commun 344(2):500–510

Hawthorne JL, Mehta PR, Singh PP, Wong N, Quintero OA (2016) Positively charged residues within the MYO19 MyMOMA domain are essential for proper localization of MYO19 to the mitochondrial outer membrane. Cytoskeleton 73(6):286–299

Hinkes B, Hilgers KF, Bolz HJ, Goppelt-Struebe M, Amann K, Nagl S, Bergmann C, Rascher W, Eckardt KU, Jacobi J (2012) A complex microdeletion 17q12 phenotype in a patient with recurrent de novo membranous nephropathy. BMC Nephrol 13:27

Howard J (2001) Mechanics of motor proteins and the cytoskeleton. Sinauer Associates, Sunderland, MA, pp 229–244

Hudson TJ, Anderson W, Artez A, Barker AD, Bell C, Bernabe RR, Bhan MK, Calvo F, Eerola I et al (2010) International network of cancer genome projects. Nature 464(7291):993–998

Jalali A, Amirian ES, Bainbridge MN, Armstrong GN, Liu Y, Tsavachidis S, Jhangiani SN, Plon SE, Lau CC, Claus EB et al (2015) Targeted sequencing in chromosome 17q linkage region identifies familial glioma candidates in the Gliogene Consortium. Sci Rep 5:8278

Katajisto P, Dohla J, Chaffer CL, Pentinmikko N, Marjanovic N, Iqbal S, Zoncu R, Chen W, Weinberg RA, Sabatini DM (2015) Stem cells. Asymmetric apportioning of aged mitochondria between daughter cells is required for stemness. Science 348(6232):340–343

Kelley LA, Mezulis S, Yates CM, Wass MN, Sternberg MJ (2015) The Phyre2 web portal for protein modeling, prediction and analysis. Nat Protoc 10(6):845–858

Kohutek ZA, Rosati LM, Hong J, Poling J, Attiyeh MA, Makohon-Moore A, Herman JM, Iacobuzio-Donahue CA (2017) An unusual genomic variant of pancreatic ductal adenocarcinoma with an indolent clinical course. Cold Spring Harb Mol Case Stud 3(4)

Kollmar M, Muhlhausen S (2017) Myosin repertoire expansion coincides with eukaryotic diversification in the Mesoproterozoic era. BMC Evol Biol 17(1):211

Lopez-Domenech G, Covill-Cooke C, Ivankovic D, Halff EF, Sheehan DF, Norkett R, Birsa N, Kittler JT (2018) Miro proteins coordinate microtubule- and actin-dependent mitochondrial transport and distribution. EMBO J 37(3):321–336

Lu Z, Ma XN, Zhang HM, Ji HH, Ding H, Zhang J, Luo D, Sun Y, Li XD (2014) Mouse myosin-19 is a plus-end-directed, high-duty ratio molecular motor. J Biol Chem 289(26):18535–18548

Martin J, Cooper M, Hamshere ML, Pocklington A, Scherer SW, Kent L, Gill M, Owen MJ, Williams N, O'Donovan MC, et al (2014) Biological overlap of attention-deficit/hyperactivity disorder and autism spectrum disorder: evidence from copy number variants. J Am Acad Child Adolesc Psychiatry 53(7):761–770. e26

Menetrey J, Bahloul A, Wells AL, Yengo CM, Morris CA, Sweeney HL, Houdusse A (2005) The structure of the myosin VI motor reveals the mechanism of directionality reversal. Nature 435(7043):779–785

Misko A, Jiang S, Wegorzewska I, Milbrandt J, Baloh RH (2010) Mitofusin 2 is necessary for transport of axonal mitochondria and interacts with the Miro/Milton complex. J Neurosci 30(12):4232–4240

Miyamoto-Mikami E, Tsuji K, Horii N, Hasegawa N, Fujie S, Homma T, Uchida M, Hamaoka T, Kanehisa H, Tabata I et al (2018) Gene expression profile of muscle adaptation to high-intensity intermittent exercise training in young men. Sci Rep 8(1):16811

Moore AS, Wong YC, Simpson CL, Holzbaur EL (2016) Dynamic actin cycling through mitochondrial subpopulations locally regulates the fission-fusion balance within mitochondrial networks. Nat Commun 7:12886

Moreno-De-Luca D, SGENE Consortium S, Mulle JG, Simons Simplex Collection Genetics Consortium, Kaminsky EB, Sanders SJ, GeneStar MSM, Adam MP, Pakula AT et al (2010) Deletion 17q12 is a recurrent copy number variant that confers high risk of autism and schizophrenia. Am J Hum Genet 87(5):618–630

Novak AJ, Asmann YW, Maurer MJ, Wang C, Slager SL, Hodge LS, Manske M, Price-Troska T, Yang ZZ, Zimmermann MT et al (2015) Whole-exome analysis reveals novel somatic genomic alterations associated with outcome in immunochemotherapy-treated diffuse large B-cell lymphoma. Blood Cancer J 5:e346

Odronitz F, Kollmar M (2007) Drawing the tree of eukaryotic life based on the analysis of 2,269 manually annotated myosins from 328 species. Genome Biol 8(9):R196

Oeding SJ, Majstrowicz K, Hu XP, Schwarz V, Freitag A, Honnert U, Nikolaus P, Bahler M (2018) Identification of Miro as a mitochondrial receptor for myosin XIX. J Cell Sci

Permuth JB, Pirie A, Ann Chen Y, Lin HY, Reid BM, Chen Z, Monteiro A, Dennis J, Mendoza-Fandino G, AOCS Study Group et al (2016) Exome genotyping arrays to identify rare and low frequency variants associated with epithelial ovarian cancer risk. Hum Mol Genet 25(16):3600–3612

Quintero OA, DiVito MM, Adikes RC, Kortan MB, Case LB, Lier AJ, Panaretos NS, Slater SQ, Rengarajan M, Feliu M et al (2009) Human Myo19 is a novel myosin that associates with mitochondria. Curr Biol 19(23):2008–2013

Reis K, Fransson A, Aspenstrom P (2009) The Miro GTPases: at the heart of the mitochondrial transport machinery. FEBS Lett 583(9):1391–1398

Roberts JL, Gandomi SK, Parra M, Lu I, Gau CL, Dasouki M, Butler MG (2014) Clinical report of a 17q12 microdeletion with additionally unreported clinical features. Case Rep Genet 2014:264947

Rohn JL, Sims D, Liu T, Fedorova M, Schock F, Dopie J, Vartiainen MK, Kiger AA, Perrimon N, Baum B (2011) Comparative RNAi screening identifies a conserved core metazoan actinome by phenotype. J Cell Biol 194(5):789–805

Rohn JL, Patel JV, Neumann B, Bulkescher J, McHedlishvili N, McMullan RC, Quintero OA, Ellenberg J, Baum B (2014) Myo19 ensures symmetric partitioning of mitochondria and coupling of mitochondrial segregation to cell division. Curr Biol 24(21):2598–2605

Russo GJ, Louie K, Wellington A, Macleod GT, Hu F, Panchumarthi S, Zinsmaier KE (2009) Drosophila Miro is required for both anterograde and retrograde axonal mitochondrial transport. J Neurosci 29(17):5443–5455

Sandbacka M, Laivuori H, Freitas E, Halttunen M, Jokimaa V, Morin-Papunen L, Rosenberg C, Aittomaki K (2013) TBX6, LHX1 and copy number variations in the complex genetics of Mullerian aplasia. Orphanet J Rare Dis 8:125

Sartori-Rupp A, Cordero Cervantes D, Pepe A, Gousset K, Delage E, Corroyer-Dulmont S, Schmitt C, Krijnse-Locker J, Zurzolo C (2019) Correlative cryo-electron microscopy reveals the structure of TNTs in neuronal cells. Nat Commun 10(1):342

Sebe-Pedros A, Grau-Bove X, Richards TA, Ruiz-Trillo I (2014) Evolution and classification of myosins, a paneukaryotic whole-genome approach. Genome Biol Evol 6(2):290–305

Shneyer BI, Usaj M, Henn A (2016) Myo19 is an outer mitochondrial membrane motor and effector of starvation-induced filopodia. J Cell Sci 129(3):543–556

Shneyer BI, Usaj M, Wiesel-Motiuk N, Regev R, Henn A (2017) ROS induced distribution of mitochondria to filopodia by Myo19 depends on a class specific tryptophan in the motor domain. Sci Rep 7(1):11577

Smith CA, Rayment I (1996) Active site comparisons highlight structural similarities between myosin and other P-loop proteins. Biophys J 70(4):1590–1602

Sousa AD, Berg JS, Robertson BW, Meeker RB, Cheney RE (2006) Myo10 in brain: developmental regulation, identification of a headless isoform and dynamics in neurons. J Cell Sci 119(Pt 1):184–194

Tsuiko O, Noukas M, Zilina O, Hensen K, Tapanainen JS, Magi R, Kals M, Kivistik PA, Haller-Kikkatalo K, Salumets A et al (2016) Copy number variation analysis detects novel candidate genes involved in follicular growth and oocyte maturation in a cohort of premature ovarian failure cases. Hum Reprod 31(8):1913–1925

Usaj M, Henn A (2017) Kinetic adaptation of human Myo19 for active mitochondrial transport to growing filopodia tips. Sci Rep 7(1):11596

Wells AL, Lin AW, Chen LQ, Safer D, Cain SM, Hasson T, Carragher BO, Milligan RA, Sweeney HL (1999) Myosin VI is an actin-based motor that moves backwards. Nature 401(6752):505–508

Zhang F, Chen X, Wei K, Liu D, Xu X, Zhang X, Shi H (2017) Identification of key transcription factors associated with lung squamous cell carcinoma. Med Sci Monit 23:172–206

Index

L. M. Coluccio (ed.), *Myosins*, Advances in Experimental Medicine and Biology 1239,
https://doi.org/10.1007/978-3-030-38062-5